



# NOVEL DIAGNOSTIC AND THERAPEUTIC STRATEGIES FOR RETINAL DISEASES

EDITED BY: Shaochong Zhang, Haijiang Lin and Hetian Lei  
PUBLISHED IN: *Frontiers in Medicine*



# frontiers

## Frontiers eBook Copyright Statement

The copyright in the text of individual articles in this eBook is the property of their respective authors or their respective institutions or funders. The copyright in graphics and images within each article may be subject to copyright of other parties. In both cases this is subject to a license granted to Frontiers.

The compilation of articles constituting this eBook is the property of Frontiers.

Each article within this eBook, and the eBook itself, are published under the most recent version of the Creative Commons CC-BY licence.

The version current at the date of publication of this eBook is CC-BY 4.0. If the CC-BY licence is updated, the licence granted by Frontiers is automatically updated to the new version.

When exercising any right under the CC-BY licence, Frontiers must be attributed as the original publisher of the article or eBook, as applicable.

Authors have the responsibility of ensuring that any graphics or other materials which are the property of others may be included in the CC-BY licence, but this should be checked before relying on the CC-BY licence to reproduce those materials. Any copyright notices relating to those materials must be complied with.

Copyright and source acknowledgement notices may not be removed and must be displayed in any copy, derivative work or partial copy which includes the elements in question.

All copyright, and all rights therein, are protected by national and international copyright laws. The above represents a summary only. For further information please read Frontiers' Conditions for Website Use and Copyright Statement, and the applicable CC-BY licence.

ISSN 1664-8714

ISBN 978-2-83250-327-0

DOI 10.3389/978-2-83250-327-0

## About Frontiers

Frontiers is more than just an open-access publisher of scholarly articles: it is a pioneering approach to the world of academia, radically improving the way scholarly research is managed. The grand vision of Frontiers is a world where all people have an equal opportunity to seek, share and generate knowledge. Frontiers provides immediate and permanent online open access to all its publications, but this alone is not enough to realize our grand goals.

## Frontiers Journal Series

The Frontiers Journal Series is a multi-tier and interdisciplinary set of open-access, online journals, promising a paradigm shift from the current review, selection and dissemination processes in academic publishing. All Frontiers journals are driven by researchers for researchers; therefore, they constitute a service to the scholarly community. At the same time, the Frontiers Journal Series operates on a revolutionary invention, the tiered publishing system, initially addressing specific communities of scholars, and gradually climbing up to broader public understanding, thus serving the interests of the lay society, too.

## Dedication to Quality

Each Frontiers article is a landmark of the highest quality, thanks to genuinely collaborative interactions between authors and review editors, who include some of the world's best academicians. Research must be certified by peers before entering a stream of knowledge that may eventually reach the public - and shape society; therefore, Frontiers only applies the most rigorous and unbiased reviews. Frontiers revolutionizes research publishing by freely delivering the most outstanding research, evaluated with no bias from both the academic and social point of view. By applying the most advanced information technologies, Frontiers is catapulting scholarly publishing into a new generation.

## What are Frontiers Research Topics?

Frontiers Research Topics are very popular trademarks of the Frontiers Journals Series: they are collections of at least ten articles, all centered on a particular subject. With their unique mix of varied contributions from Original Research to Review Articles, Frontiers Research Topics unify the most influential researchers, the latest key findings and historical advances in a hot research area! Find out more on how to host your own Frontiers Research Topic or contribute to one as an author by contacting the Frontiers Editorial Office: [frontiersin.org/about/contact](https://frontiersin.org/about/contact)



# NOVEL DIAGNOSTIC AND THERAPEUTIC STRATEGIES FOR RETINAL DISEASES

Topic Editors:

**Shaochong Zhang**, Shenzhen Eye Hospital, China

**Haijiang Lin**, Massachusetts Eye & Ear Infirmary, Harvard Medical School

**Hetian Lei**, Shenzhen Eye Hospital, China

**Citation:** Zhang, S., Lin, H., Lei, H., eds. (2022). Novel Diagnostic and Therapeutic Strategies for Retinal Diseases. Lausanne: Frontiers Media SA.

doi: 10.3389/978-2-83250-327-0

# Table of Contents

- 07** *Proteomics of Vitreous Humor Reveals PPARA, RXR, and LXR Are Possible Upstream Regulators of Proliferative Diabetic Retinopathy*  
Siyan Li, Enzhong Jin, Xuan Shi, Yi Cai, Hui Zhang and Mingwei Zhao
- 14** *Beyond the Visual Acuity: Assessing the Visual Function in mCNV Patients After Anti-VEGF Treatment*  
Songshan Li, Limei Sun, Xiujuan Zhao, Zhaotian Zhang, Xiaoling Luo and Xiaoyan Ding
- 23** *Microvasculature Features of Vogt-Koyanagi-Harada Disease Revealed by Widefield Swept-Source Optical Coherence Tomography Angiography*  
Xiaoyuan Ye, Haiping Zhang, Peng Xiao, Gengyuan Wang, Xiaoqing Hu, Chun Yan, Fan Li, Yixin Hu, Lishi Su, Jiawen Luo, Jin Yuan, Feng Wen and Wei Chi
- 34** *Elevated NLRP3 Inflammasome Levels Correlate With Vitamin D in the Vitreous of Proliferative Diabetic Retinopathy*  
Li Lu, Gaocheng Zou, Li Chen, Qianyi Lu, Mian Wu and Chunxia Li
- 45** *Long-Term Retinal Neurovascular and Choroidal Changes After Panretinal Photocoagulation in Diabetic Retinopathy*  
Tian Huang, Xiaoli Li, Jie Xie, Liang Zhang, Guanrong Zhang, Aiping Zhang, Xiangting Chen, Ying Cui and Qianli Meng
- 56** *Efficacy of Conbercept in the Treatment of Choroidal Neovascularization Secondary to Pathologic Myopia*  
Hui Lu, Tao Yue, Na Liu, Zuo-Fen Wang, Gai-Xia Zhai, Dong-Ming Mi, Jing Zhang and Shao-Peng Wang
- 62** *Effects of the Pars Plana Vitrectomy on the Chronic Total Rhegmatogenous Retinal Detachment in the Young Adults*  
Jinguo Yu, Xingxing Hu, Jiangkai Zhang, Han Han, Bo Huang, Rodrigo Brant, Cheng Zhang and Hua Yan
- 68** *Clinical Characteristics of Pediatric Coats' Disease With Retinal Cyst Using Wide-Angle Fluorescein Angiography*  
Jing-Hua Liu, Guangda Deng, Jing Ma, Liang Li, Yuxin Fang, Songfeng Li and Hai Lu
- 76** *Ellipsoid Zone and External Limiting Membrane-Related Parameters on Spectral Domain-Optical Coherence Tomography and Their Relationships With Visual Prognosis After Successful Macular Hole Surgery*  
Jiarui Yang, Huaqin Xia, Yushi Liu, Xinglin Wang, Hao Yuan, Qingyi Hou, Yimeng Ge, Yi Ding, Yuexin Wang, Changguan Wang and Xuemin Li
- 84** *Factors for Visual Acuity Improvement After Anti-VEGF Treatment of Wet Age-Related Macular Degeneration in China: 12 Months Follow up*  
Yan Lu, Wenzhi Huang, Yuehong Zhang, Xiongfei Huang, Xu Zhang, Haizhi Ma, Guoliang Ren, Feng Shi, Lihui Kuang, Shigang Yan, Shuke Luo, Junyan Zhang, Jingfang He, Weizhong Yang, Zongyin Gao and Yunxia Leng

- 94 ***Dysregulated Serum Lipid Metabolism Promotes the Occurrence and Development of Diabetic Retinopathy Associated With Upregulated Circulating Levels of VEGF-A, VEGF-D, and PlGF***  
Xinyuan Zhang, Bingjie Qiu, Qiyun Wang, Sobha Sivaprasad, Yanhong Wang, Lin Zhao, Rui Xie, Lei Li and Wenting Kang
- 104 ***Choroidal Neovascularization in Pediatric Patients: Analysis of Etiologic Factors, Clinical Characteristics and Treatment Outcomes***  
Ting Zhang, You Wang, Wenjia Yan, Yafen Liu, Jinglin Lu, Limei Sun, Songshan Li, Li Huang, Zhaotian Zhang and Xiaoyan Ding
- 113 ***Retinal Nerve Fibre Layer Thickness Change Following Femtosecond Laser-Assisted in situ Keratomileusis***  
Yang Jiang, Zhonghai Wang, Ying Li, Yong Li and Thomas Chengxuan Lu
- 117 ***Evaluation of Choroidal Thickness Using Optical Coherent Tomography: A Review***  
Rui Xie, Bingjie Qiu, Jay Chhablani and Xinyuan Zhang
- 128 ***Sustained Release of Gas6 via mPEG-PLGA Nanoparticles Enhances the Therapeutic Effects of MERTK Gene Therapy in RCS Rats***  
Shen Wu, Yingyan Mao, Qian Liu, Xuejing Yan, Jingxue Zhang and Ningli Wang
- 142 ***Comparison of Intraocular Cytokine Levels of Choroidal Neovascularization Secondary to Different Retinopathies***  
Chenyi Liu, Shian Zhang, Xinyi Deng, Yijing Chen, Lijun Shen, Liang Hu and Jianbo Mao
- 149 ***Peroxisome Proliferator-Activated Receptor  $\alpha$  Activation Protects Retinal Ganglion Cells in Ischemia-Reperfusion Retinas***  
Fei Yao, Xuan Zhang, Xueyan Yao, Xiaohua Ren, Xiaobo Xia, Jian Jiang and Lexi Ding
- 161 ***Axl Is Essential for in-vitro Angiogenesis Induced by Vitreous From Patients With Proliferative Diabetic Retinopathy***  
Wenyi Wu, Huizuo Xu, Zhishang Meng, Jianxi Zhu, Siqi Xiong, Xiaobo Xia and Hetian Lei
- 170 ***Erratum: Axl Is Essential for in-vitro Angiogenesis Induced by Vitreous From Patients With Proliferative Diabetic Retinopathy***  
Frontiers Production Office
- 171 ***Serum Sodium Concentration and Increased Risk for Primary Epiretinal Membrane***  
Can Can Xue, Jing Cui, Xiao Bo Zhu, Jie Xu, Chun Zhang, Dong Ning Chen, Ya Xing Wang and Jost B. Jonas
- 180 ***Targeting Pyroptotic Cell Death Pathways in Retinal Disease***  
Mary Zhao, Siqi Li and Joanne A. Matsubara
- 192 ***Choroidal Morphologic and Vascular Features in Patients With Myopic Choroidal Neovascularization and Different Levels of Myopia Based on Image Binarization of Optical Coherence Tomography***  
Xinglin Wang, Jiarui Yang, Yushi Liu, Luling Yang, Huaqin Xia, Xiaotong Ren, Qingyi Hou, Yimeng Ge, Changguan Wang and Xuemin Li
- 201 ***The Role of Internal Limiting Membrane as a Biomarker in the Evolution of Myopic Traction Maculopathy***  
Dong Fang, Jindi Su, Lu Chen and Shaochong Zhang

- 210 ***Novel Findings of Retinal and Choroidal Features Utilizing Optical Coherence Tomography Angiography Analysis in Patients With Autoimmune Posterior Uveitis***  
Junhui Shen, Jinfeng Kong, Si Chen, Xin Liu, Yan Teng, Hailan Wu, Lijuan Wang, Manman Wu, Zhaoan Su and Lei Feng
- 219 ***Adalimumab in Vogt-Koyanagi-Harada Disease Refractory to Conventional Therapy***  
Shizhao Yang, Tianyu Tao, Zhaohao Huang, Xiuxing Liu, He Li, Lihui Xie, Feng Wen, Wei Chi and Wenru Su
- 228 ***Case Report: Associated Ocular Adverse Reactions With Inactivated COVID-19 Vaccine in China***  
Kunpeng Pang, Lijie Pan, Hui Guo and Xinyi Wu
- 234 ***Commentary: Case report: Associated Ocular Adverse Reactions With Inactivated COVID-19 Vaccine in China***  
Yusuke Kameda, Yutaka Kaneko, Megumi Sugai, Karin Ishinabe and Nichika Fukuoka
- 237 ***Study of the Biological Developmental Characteristics of the Eye in Children After Laser Surgery for the Treatment of Retinopathy of Prematurity***  
Xianlu Zeng, Miaohong Chen, Lei Zheng, Ruyin Tian, Yi Chen, Honghui He, Jian Zeng, Jicang He and Guoming Zhang
- 245 ***Treat-and-Extend vs. Pro Re Nata Regimen of Ranibizumab for Diabetic Macular Edema—A Two-Year Matched Comparative Study***  
Tso-Ting Lai, Ta-Ching Chen, Chang-Hao Yang, Chung-May Yang, Tzyy-Chang Ho and Yi-Ting Hsieh
- 254 ***A Comparison of Face-Down Positioning and Adjustable Positioning After Pars Plana Vitrectomy for Macular Hole Retinal Detachment in High Myopia***  
Yan Gao, Ting Ruan, Nan Chen, Bin Yu, Xiaoli Xing, Qing Du, Yan Qi and Jun Li
- 264 ***Screening of Common Retinal Diseases Using Six-Category Models Based on EfficientNet***  
Shaojun Zhu, Bing Lu, Chenghu Wang, Maonian Wu, Bo Zheng, Qin Jiang, Ruili Wei, Qixin Cao and Weihua Yang
- 273 ***Predicting Optical Coherence Tomography-Derived High Myopia Grades From Fundus Photographs Using Deep Learning***  
Zhenquan Wu, Wenjia Cai, Hai Xie, Shida Chen, Yanbing Wang, Baiying Lei, Yingfeng Zheng and Lin Lu
- 282 ***Air Tamponade for Rhegmatogenous Retinal Detachment With Inferior Breaks After 25-Gauge Pars Plana Vitrectomy: Technique and Outcome***  
Peiyang Shen, Xiangbin Kong, Lijun Zhou, Peng Su, Xiaohe Lu and Mingguang He
- 289 ***Clinical Relevance of Body Fluid Volume Status in Diabetic Patients With Macular Edema***  
Jie Yao, Qingsheng Peng, Yuanhong Li, Anyi Liang, Jianteng Xie, Xuenan Zhuang, Ruoyu Chen, Yesheng Chen, Zicheng Wang, Liang Zhang and Dan Cao

- 298** *Chaperonin-Containing TCP1 Subunit 5 Protects Against the Effect of Mer Receptor Tyrosine Kinase Knockdown in Retinal Pigment Epithelial Cells by Interacting With Filamentous Actin and Activating the LIM-Kinase 1/Cofilin Pathway*  
Lujia Feng, Haichun Li, Yong Du, Ting Zhang, Yingting Zhu, Zhidong Li, Ling Zhao, Xing Wang, Gongpei Wang, Linbin Zhou, Zhaorong Jiang, Zheng Liu, Zhancong Ou, Yuwen Wen and Yehong Zhuo
- 313** *Blue Light Induces RPE Cell Necroptosis, Which Can Be Inhibited by Minocycline*  
Weilin Song, Ruilin Zhu, Wenna Gao, Chen Xing and Liu Yang
- 327** *Cytomegalovirus-Immune Recovery Retinitis After Initiation of Highly Active Antiretroviral Therapy: A Case Series*  
Yiwen Qian, Luoziyi Wang, Jing Jiang, Jinshan Suo, Huan Weng, Xin Che, Hongzhou Lu and Zhiliang Wang
- 335** *Differences in Vitreous Protein Profiles in Patients With Proliferative Diabetic Retinopathy Before and After Ranibizumab Treatment*  
Xinping She, Chen Zou and Zhi Zheng
- 347** *Optical Coherence Tomography Biomarkers in Predicting Treatment Outcomes of Diabetic Macular Edema After Dexamethasone Implants*  
Yu-Te Huang, Yen-Chieh Chang, Ping-Ping Meng, Chun-Ju Lin, Chun-Ting Lai, Ning-Yi Hsia, Huan-Sheng Chen, Peng-Tai Tien, Henry Bair, Jane-Ming Lin, Wen-Lu Chen and Yi-Yu Tsai
- 357** *Uveal Effusion Syndrome: Clinical Characteristics, Outcome of Surgical Treatment, and Histopathological Examination of the Sclera*  
Nan Zhou, Lihong Yang, Xiaolin Xu and Wenbin Wei
- 372** *A Novel Role of IL13R $\alpha$ 2 in the Pathogenesis of Proliferative Vitreoretinopathy*  
Hui Qi, Lijun Dong, Dong Fang, Lu Chen, Yun Wang, Ning Fan, Xingxing Mao, Wenyi Wu, Xiaohe Yan, Guoming Zhang, Shaochong Zhang and Hetian Lei
- 382** *Inner Retinal Layer Hyperreflectivity Is an Early Biomarker for Acute Central Retinal Artery Occlusion*  
Daniel A. Wenzel, Sven Poli, Maria Casagrande, Vasyl Druchkiv, Martin S. Spitzer, Karl Ulrich Bartz-Schmidt, Carsten Grohmann and Maximilian Schultheiss





# Proteomics of Vitreous Humor Reveals PPARA, RXR, and LXR Are Possible Upstream Regulators of Proliferative Diabetic Retinopathy

Siyan Li<sup>††</sup>, Enzhong Jin<sup>††</sup>, Xuan Shi<sup>1</sup>, Yi Cai<sup>1</sup>, Hui Zhang<sup>2</sup> and Mingwei Zhao<sup>1\*</sup>

<sup>1</sup> Department of Ophthalmology, Peking University People's Hospital, Eye Diseases and Optometry Institute, Beijing Key Laboratory of Diagnosis and Therapy of Retinal and Choroid Diseases, College of Optometry, Peking University Health Science Center, Beijing, China, <sup>2</sup> Department of Ophthalmology, Beijing Jingmei Group General Hospital, Beijing, China

## OPEN ACCESS

### Edited by:

Shaochong Zhang,  
Sun Yat-sen University, China

### Reviewed by:

Qing Chang,  
Fudan University, China  
Xu Xun,  
Shanghai General Hospital, China

### \*Correspondence:

Mingwei Zhao  
zhaomingwei64@163.com

<sup>††</sup>These authors have contributed  
equally to this work and share first  
authorship

### Specialty section:

This article was submitted to  
Ophthalmology,  
a section of the journal  
Frontiers in Medicine

Received: 14 June 2021

Accepted: 19 July 2021

Published: 17 August 2021

### Citation:

Li S, Jin E, Shi X, Cai Y, Zhang H and  
Zhao M (2021) Proteomics of Vitreous  
Humor Reveals PPARA, RXR, and LXR  
Are Possible Upstream Regulators of  
Proliferative Diabetic Retinopathy.  
Front. Med. 8:724695.  
doi: 10.3389/fmed.2021.724695

**Purpose:** To investigate the key regulators of the disease by comparing the abundance of vitreous proteins between the patients with proliferative diabetic retinopathy (PDR) and the controls with idiopathic epiretinal membrane (iERM).

**Methods:** Vitreous humor (VH) samples were derived from patients with PDR or iERM through the pars plana vitrectomy. The VH proteins were identified by liquid chromatography tandem mass spectrometry (LC-MS/MS) analysis. MaxQuant software and Metascape were applied to explore the enrichment of differentially expressed proteins in biological processes, cellular components, and molecular functions. Enrichr online tool and Gene Set Enrichment Analysis (GSEA) were performed to detect upstream transcriptional regulators of the highly expressed proteins.

**Results:** The present study collected 8 vitreous humor samples from 5 PDR eyes and 3 iERM eyes and identified 88 highly expressed proteins in PDR patients. We validated our highly expressed proteome was able to distinguish the PDR patients from the non-PDR patients by using the VH proteomics data from a previous study. The majority of highly expressed proteins were involved in complement and coagulation cascades, regulating exocytosis, and hemostasis. Using the Gene Set Enrichment Analysis (GSEA), we identified that transcription factors (TFs) PPAR- $\alpha$ , RXR, LXR regulate these proteins.

**Conclusions:** In this study, we identified a highly expressed proteome in VH of PDR patients. The role of the complement and coagulation system, regulating exocytosis, and hemostasis has been of great significance to PDR. Nuclear receptors PPARA, RXR, LXR were possible upstream regulators of disease progression and required further study.

**Keywords:** proliferative diabetic retinopathy, proteomics, vitreous humor, transcription factors, mass spectrometry

## INTRODUCTION

Diabetic retinopathy (DR) has become the most prevalent cause of blindness among adults aged 20–74 and the major complication of patients with either type of diabetes (1). In the early, non-proliferative stage of the disease, DR begins with abnormal microvascular changes, which are characterized by microaneurysms, increased vascular permeability, capillary closures.

With increasing duration, these microangiopathies can lead to neovascularization, indicates a proliferative stage developed. Proliferative diabetic retinopathy (PDR) is characterized by retinal neovascularization due to retinal ischemia. The overgrowth of the neovascular tufts toward the vitreous leading vitreous hemorrhage and fibrovascular membranes (FVMs) formation. In the severe stage of PDR, the FVMs can cause tractional retinal detachment and result in devastating vision impairment.

The progressive course of DR is often irreversible. Laser photocoagulation, intravitreal anti-vascular endothelial growth factor (VEGF) agents, and vitreoretinal surgery are classic treatments of the disease (2). Even if many patients have received proper treatment, it cannot deter the advancement of the disease. New therapeutic strategies are being explored in numerous ongoing trials, but most target the advanced stages of the disease. The complexity of pathophysiological mechanisms and molecular events contributing to DR creates obstacles in finding effective intervention in the very early stage.

The vitreous humor (VH) contains a variety of soluble proteins and has a close relationship with the progress of DR. Besides, the VH is the first site in the eye where anti-VEGF agents exert their curative effects. Many studies have demonstrated that label-free quantitative proteomics analysis is capable of detecting proteins in the VH and provided quantitatively mapped proteome changes of the VH in the DR patients (3). However, these data have not been fully used for further analysis and research to understand the complexity of pathophysiological mechanisms and molecular events contributing to the disease. In the present study, we firstly performed label-free quantitative proteomics analysis to identify the differentially expressed proteins between patients with PDR and patients with idiopathic epiretinal membrane (iERM). We determined 88 highly expressed proteins in PDR and found they can also distinguish PDR patients from non-PDR by using the previous VH protein profiles. Then we analyzed the upstream regulators of these proteins by combining our data with previous proteomics data. Using the Gene Set Enrichment Analysis (GSEA), we identified that transcription factors (TFs) including PPAR- $\alpha$ , RXR and LXR regulate these proteins.

## MATERIALS AND METHODS

This was a cross-sectional, observational study of consecutive PDR patients who underwent surgical treatment at the Department of Ophthalmology, Peking University People's Hospital, Beijing, China, between March 2019 and December 2019. Patients in the control group underwent vitreoretinal surgery due to iERM. This study was approved by the Clinic Institutional Review Board of Peking University People's Hospital and complied with the Declaration of Helsinki. Written informed consent was obtained from all patients before enrollment in the present study. All patients underwent comprehensive preoperative eye examinations by the recruiting surgeons. Clinical data, including the medical history and treatment of diabetes mellitus, were collected. Each patient underwent

eye examinations including visual acuity, intraocular pressure, axial length, slit-lamp biomicroscopy, dilated fundoscopic examination, and optical coherence tomography before and after surgery.

VH samples (up to 200  $\mu$ L) were collected before conventional three-port pars plana vitrectomy without artificial humor infusion. A 25-gauge trocar was introduced into the inferior temporal sclera, and a closed infusion tube was inserted. The stopcock of the vitrector aspiration line was opened, and a 5 mL sterile syringe was attached. By active cutting combined with syringe suction, 100–200  $\mu$ L vitreous was aspirated into the syringe, the aspiration line was closed, and the infusion was initiated to stabilize the intraocular pressure. The samples were transferred into sterile 1.5 mL microcentrifuge tubes, snap-frozen, and stored at  $-80^{\circ}\text{C}$  until further analysis.

VH samples were centrifuged at 20,000 g for 15 min at  $48^{\circ}\text{C}$  to remove cells or cell debris. Nanodrop determined the concentration of protein. For liquid chromatography tandem mass spectrometry (LC-MS/MS) analysis, samples were separated by a 120 min gradient elution at a flow rate of 0.300  $\mu$ L/min with the Thermo Ultimate 3000 nano-UPLC system which was directly interfaced with the Thermo Fusion LUMOS mass spectrometer. The analytical column was an Acclaim PepMap RSLC column (75  $\mu$ m ID, 250 mm length, C18). Mobile phase A consisted of 0.1% formic acid, and mobile phase B consisted of 100% acetonitrile and 0.1% formic acid. The Fusion LUMOS mass spectrometer was operated in the data-dependent acquisition mode using Xcalibur 4.1.50 software, and there is a single full-scan mass spectrum in the Orbitrap (375–1,500 m/z, 60,000 resolution) followed by data-dependent MS/MS scans. The MS/MS spectra from each LC-MS/MS run were searched against the selected database using the software Proteome Discovery (version 2.2).

Label-free quantification was performed using MaxQuant software (version 1.5.3.30), and the iFOT (defined as iBAQ/iBAQ<sub>total</sub>) values were used to quantify protein expression. The cutoff of the false discovery rate for peptide and protein identification was set to 0.05. Gene ontology (GO) analysis was applied to explore the possible biological functions of the differentially expressed proteins via Metascape (4); *p*-values of Fisher's exact test were calculated to measure the significance of enriched ontology terms and pathways.

TFs and target genes of each TF were extracted from ChIP-seq data in the ChEA database (5). TFs that regulate highly expressed proteins were enriched using the Enrichr online tool (6). The predicted regulating TFs were validated in an external validation set (7). Gene Set Enrichment Analysis (GSEA) was applied to quantify the activity of each candidate TF in different samples using the GSEAPy package (<https://github.com/zqfang/GSEAPy>).

## RESULTS

### Patient Information

A total of eight patients (8 eyes) was recruited in our study, including 5 PDR eyes and 3 non-diabetic eyes (control). Three eyes underwent vitreoretinal surgery due to tractional retinal

detachment, and 2 eyes due to persistent vitreous hemorrhage. Three non-diabetic eyes underwent surgery due to iERM. The two groups were well-balanced for demographics. The VH protein concentrations were not significantly different among the two groups. The characteristics of the PDR and control patients were summarized in **Table 1**.

After proteome profiling, differentially expressed proteins were identified between PDR and control group as shown in **Figure 1** proteomic analysis identified 239 and 218 intravitreal proteins by LC/MS-MS in PDR and control group. Among these proteins, 50 proteins were detected only in the PDR group, and 29 proteins were detected only in the control group. Among the total 268 proteins, 189 proteins were detected in both groups, 88 proteins were significantly highly expressed in PDR patients,

and 68 proteins were significantly low expressed in PDR patients. We defined those 88 highly expressed proteins as the highly expressed proteome.

We used the VH proteomics data from a previous quantitative proteomics analysis study as an independent validation set to validate the highly expressed proteome is specific in PDR patients (7). The highly expressed proteome in our cohort remained highly expressed in PDR patients in the independent cohort ( $P = 9.4E-9$ , **Figure 2A**). **Figure 2B** shows the ROC curve and AUC which examine the performance of the mean Z-score of the highly expressed proteome to separate PDR patients from the non-PDR patients.

## Gene Ontology Enrichment Analysis

Gene enrichment analysis was performed to identify the enrichment of differentially expressed proteins in biological processes, cellular components, and molecular functions. The results demonstrated that the majority of highly expressed proteins were involved in complement and coagulation cascades, regulating exocytosis, and hemostasis (**Figure 3A**). Conversely, the low expressed proteins were mainly associated with the regulation of insulin-like growth factor transport and uptake by insulin-like growth factor Bi (**Figure 3B**).

## Enrichr Analysis and TFs Identification

We analyzed the upstream TFs which promote the expression of these PDR-related proteins in the ChEA database. As the result, most of the highly expressed proteins were regulated by peroxisome proliferative-activated receptor alpha (PPAR- $\alpha$ ), retinoid-X receptor (RXR), Liver X receptor (LXR), forkhead activin signal transducer 1 (FOXH1), octamer-binding transcription factor 4 (OCT4), RELA/transcription factor p65, early growth response 1 (EGR1), estrogen receptor 1 (ESR1),

**TABLE 1** | Data for patients with proliferative diabetic retinopathy or idiopathic epiretinal membrane.

Characteristics	Idiopathic epiretinal membrane group (n = 3)	Proliferative diabetic retinopathy group (n = 5)
Age (year)	63 $\pm$ 10.61	60.4 $\pm$ 9.71
Sex, male/female	2/1	3/2
Diabetes duration (year)	–	14.1 $\pm$ 10.70
Macular edema	–	2
Vitreous hemorrhage	–	3
Traction membrane	–	3
Proliferative membrane	–	3
Tractional retinal detachment	–	2
Retinal laser frequency	–	1.6 $\pm$ 1.36
Insulin	–	4
Hypoglycemic drugs	–	2

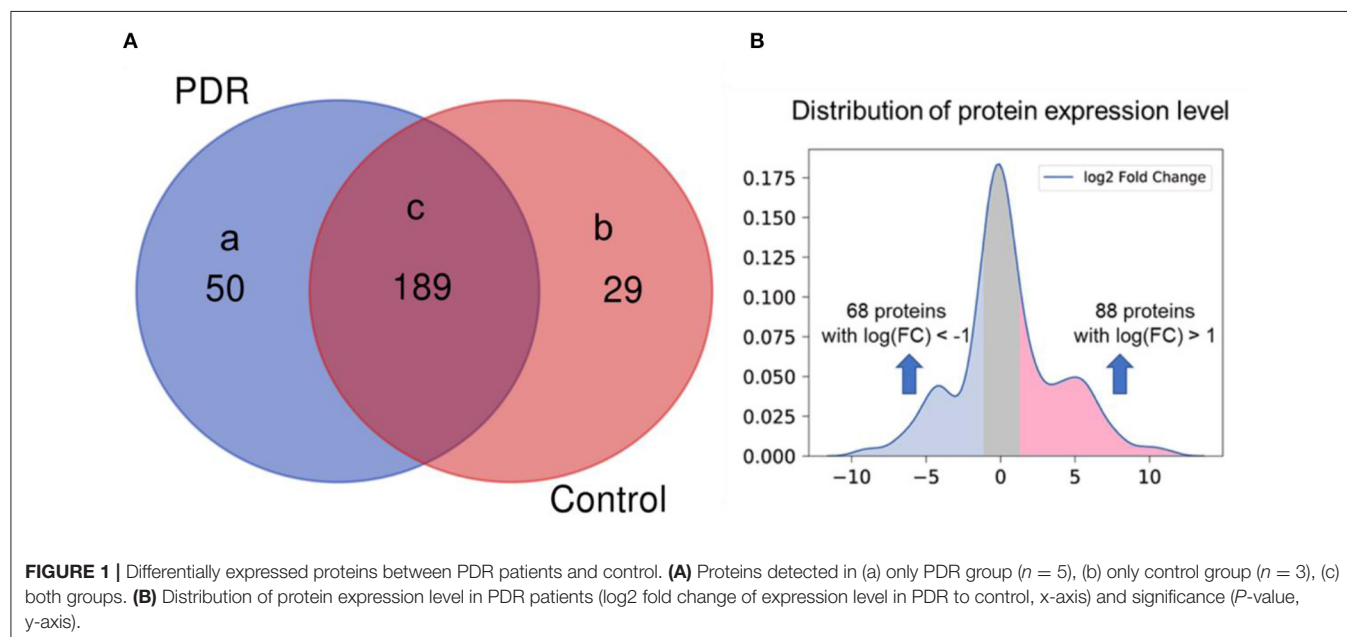
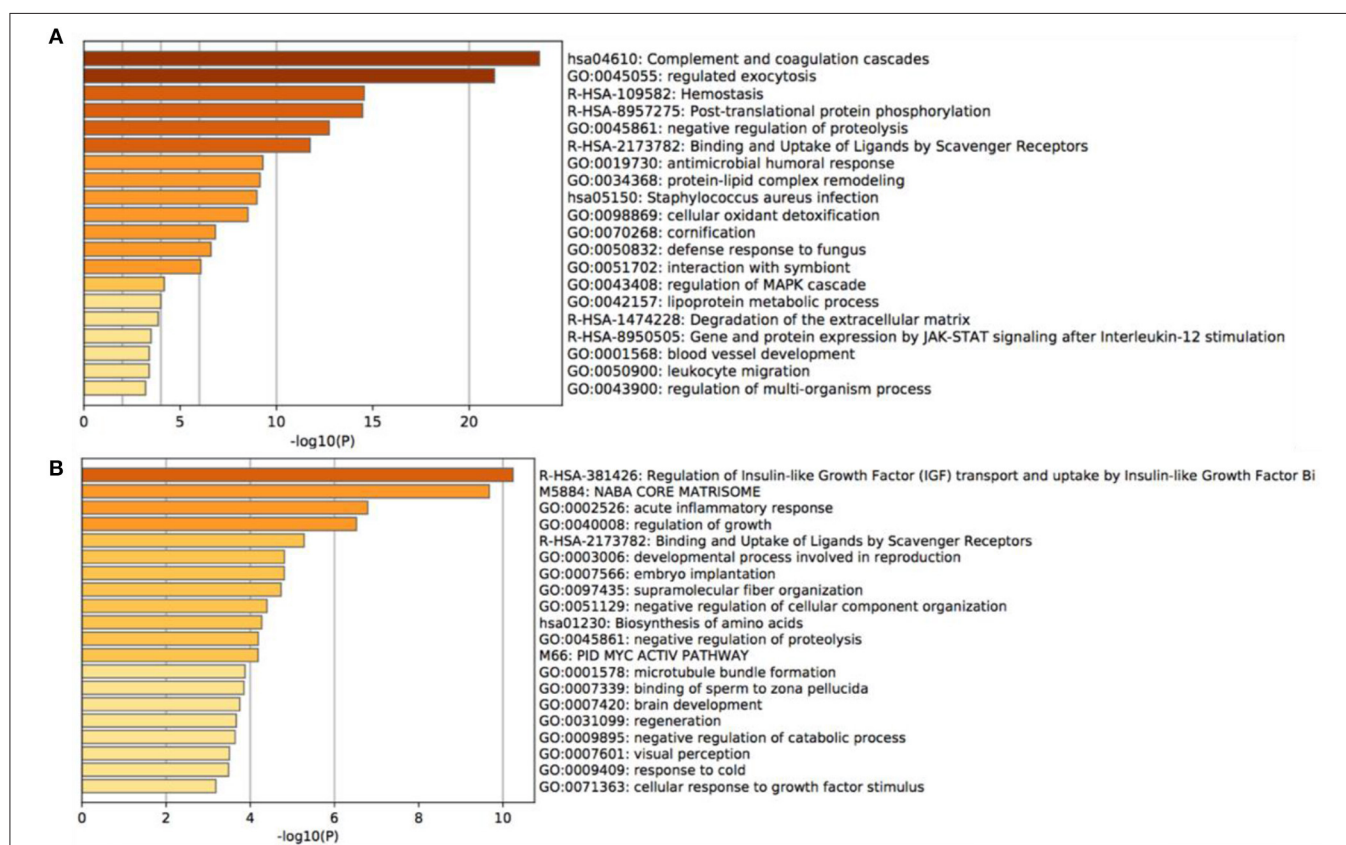
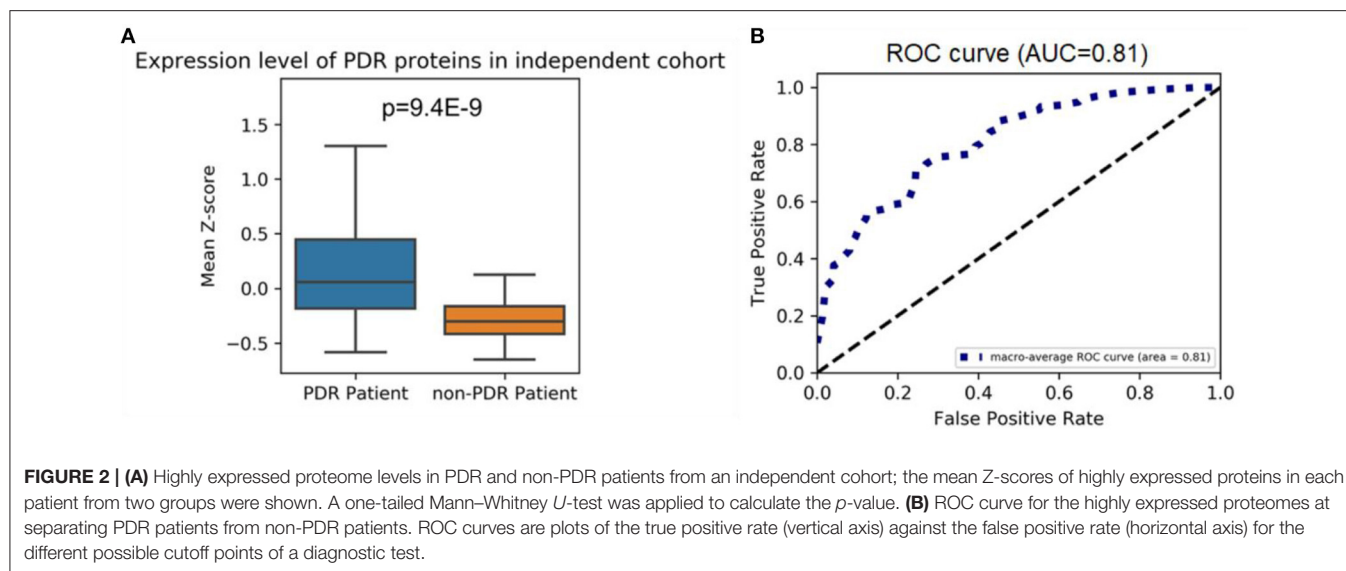


**FIGURE 1** | Differentially expressed proteins between PDR patients and control. **(A)** Proteins detected in (a) only PDR group (n = 5), (b) only control group (n = 3), (c) both groups. **(B)** Distribution of protein expression level in PDR patients (log2 fold change of expression level in PDR to control, x-axis) and significance (P-value, y-axis).

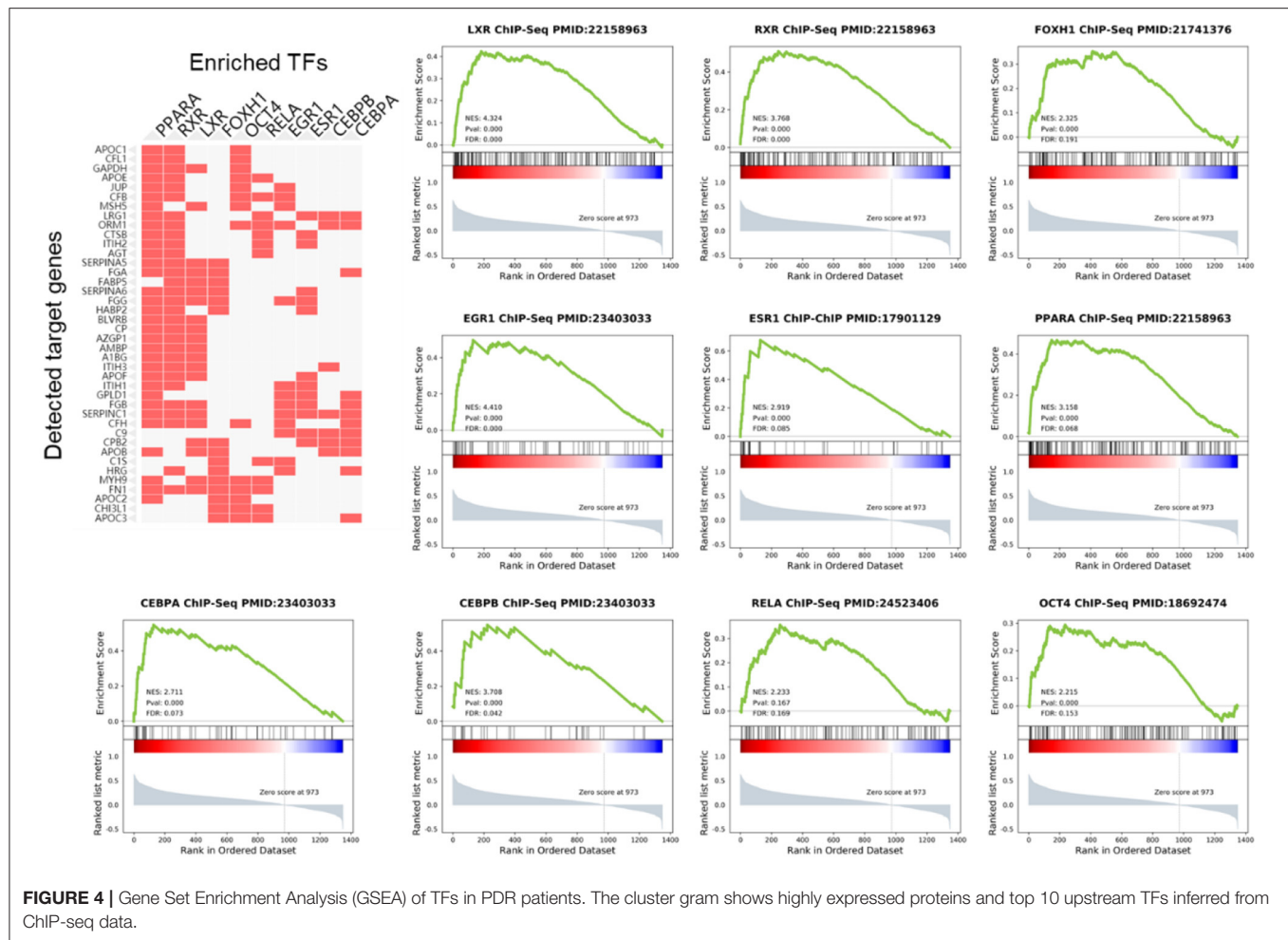


enhancer-binding protein  $\alpha$  (CEBPA), and enhancer-binding protein  $\beta$  (CEBPB) (Figure 4).

Using GSEA in the previous PDR/non-PDR proteome study (7), we identified target genes of TFs including PPARA,

RXR, LXR, FOXH1, OCT4, RELA, EGR1, ESR1, CEBPA, and CEBPB were significantly up-regulated in the proteome data of PDR patients in the independent cohort. We reanalyzed the transcriptome of vascular endothelial cells obtained from FVMs





in a previous study (8), and consistently, the results demonstrated that gene targets of these TFs were also up-regulated in the PDR related vascular endothelial cells (**Figure 5**).

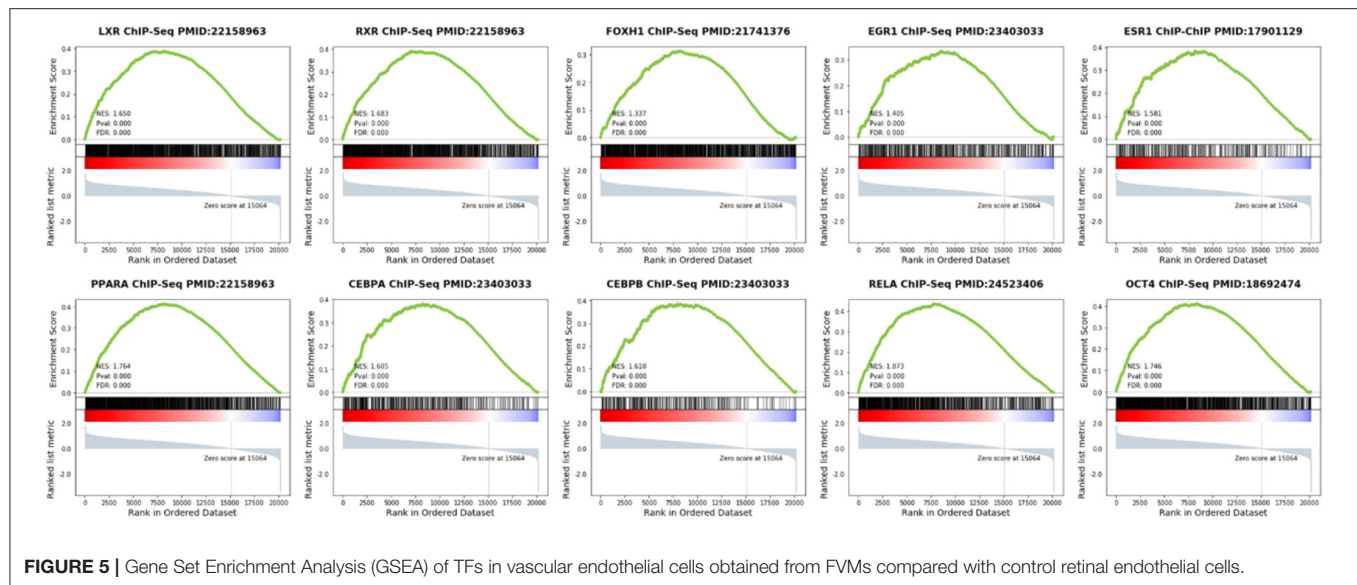
## DISCUSSION

We performed label-free quantitative proteomics analysis to compare the vitreous humor (VH) of PDR patients and iERM patients, and identified proteins explicitly expressed within the PDR patients. A few proteomics studies focused on the VH in DR, but most of them did not compare PDR patients and non-DR patients. Li et al. conducted the proteomic analysis on VH from PDR patients and idiopathic macular hole patients and identified 52 proteins over-expressed in PDR patients out of 610 proteins (3). In this study, though the number of proteins we demonstrated was less than them, more highly expressed proteins (88 proteins) were identified compared with iERM. Since the collection of an ordinary person's VH is unethical, we suggest iERM patients are more suitable as controls. The highly expressed collection of proteins can also properly separate PDR patients from non-PDR patients in the most extensive VH proteomics analysis by far (7), suggesting amounts of proteins in the

vitreous humor of diabetic retinopathy patients might indicate the progress of proliferation. It can be used to understand the comprehensive molecular pathogenesis of PDR and help with individualized treatment.

We performed Gene enrichment analysis to identify the enrichment of differentially expressed proteins in biological processes, cellular components, and molecular functions. We noticed that the proteins up-regulated in the PDR samples most significantly were attributed to complement and coagulation cascades. The role of the complement and coagulation system in angiogenesis has become of prime importance. Previous studies indicated that the complement components were present in the early stages of the DR (9–11). Indeed, the proteomics profile of our enriched results indicated the abundance of cascade components increased dramatically in the proliferative stage. Our results suggest that the role of the complement system might be an important mediator of DR pathogenesis. Previous research demonstrated prolonged exposure to elevated glucose alters the exocytosis in retinal neurons, which contributes to the pathogenesis of DR (12). Notably, we demonstrated that the 27 highly expressed proteins (including CAT, CHI3L1, FABP, CTSB, etc.) were functionally involved in the regulation of exocytosis. These results suggest that exocytosis is the major pathologic event





in PDR, and future researches need to focus on the exocytosis mechanism in the development of PDR.

Presently, there are already some proteomics researches on PDR, however, these data have not been fully used for further analysis and research. Since we found the highly expressed proteome in our cohort remained highly expressed in PDR patients in the largest-scale cohort (7), we sought to determine the upstream regulator of these proteins. Therefore, enrichment analysis was performed by the Enrichr online tool, and we identified the top 10 TFs including PPARA, RXR, LXR, FOXH1, OCT4, RELA, EGR1, ESR1, CEBPA, and CEBPB regulated these highly expressed proteins. Then, GSEA analysis was performed to elucidate the target genes regulated by these identified TFs in PDR patients. Our results showed that the expression of these genes was elevated in PDR. We demonstrated that the target genes of the top 10 TFs were overexpressed in FVMs. Therefore, our results highlighted these TFs play an important role in the pathogenesis of PDR. The highly expressed proteins in VH might be released from FVMs in PDR. The present study is the first to utilize bioinformatics tools based on previous proteomics data of VH in PDR.

Among those transcription factors, PPARA, RXR, and LXR are nuclear receptors deserving more concern. PPARA, also known as PPAR $\alpha$ , is one of the three subtypes of peroxisome proliferator-activated receptors (PPARs). It plays a crucial role in the regulation of ketogenesis, lipid transport, lipogenesis, cholesterol metabolism, fatty acid transport, and oxidation (13). For PPARs to induce gene expression, they must also interact with their co-activator, the retinoid-X receptor (RXR) (14). Previous studies related to decreased PPARA expression in diabetic retinas contributed to retinal inflammation and neovascularization in DR (15). Cells treated with RXR agonists were demonstrated to prevent the effect of high glucose (16). Besides, activation of LXR was reported to prevent inflammation and the formation of diabetes-induced acellular capillaries (17). All these studies revealed the upregulation

of PPARA/RXR/LXR contributed to DR progression delay by playing a protective role in the retina. However, in the current study, we found that highly expressed proteins were regulated by PPARA/RXR/LXR, suggesting that these TFs might be activated in the stage of PDR. Compared with a study of saliva samples collected from DR patients, the differentially expressed proteins also indicated increased LXR/RXR activation (13). Our study provided the evidence for the first time that PPARA/RXR/LXR was activation in PDR. There should be careful consideration of the use of PPARA/RXR/LXR agonists recommended by previous studies. The comprehensive mechanism, as well as for drug instructions, needs to be explored by future studies.

The primary limitations of this study were the scale of the enrolled patients and the number of proteins we identified, which limited the available pool of data to analyze. Non-DR patients with iERM were enrolled as controls, but they were not disease-free status. Some iERM-related proteins in the VH might have affected the differentiation from the PDR group.

## CONCLUSIONS

In this study, we identified a highly expressed proteome in VH of PDR patients. The role of the complement and coagulation system, regulating exocytosis, and hemostasis has been of great significance to PDR. Nuclear receptors PPARA, RXR, LXR were possible upstream regulators of disease progression and required further study.

## DATA AVAILABILITY STATEMENT

The data presented in the study are deposited in the ProteomeXchange repository with accession number PXD027556, and the iProX repository with accession number IPX0003325000.

## ETHICS STATEMENT

The studies involving human participants were reviewed and approved by The Ethics Committee of Peking University People's Hospital. The patients/participants provided their written informed consent to participate in this study.

## AUTHOR CONTRIBUTIONS

SL and MZ conceived the study and wrote the paper with input from all authors. SL and EJ designed the research and performed the research. SL, EJ, and XS collected the samples and data. SL,

XS, and HZ analyzed the data. All authors contributed to the article and approved the submitted version.

## FUNDING

This work was funded by National Natural Science Foundation of China (Grant no. 81800850).

## ACKNOWLEDGMENTS

The authors would like to thank Chunyu Yu and Xiaohui Zhang for their grateful technical support.

## REFERENCES

- Fong DS, Aiello L, Gardner TW, King GL, Blankenship G, Cavallerano JD, et al. Retinopathy in Diabetes. *Diabetes Care*. (2004) 27(suppl 1):s84–s7. doi: 10.2337/diacare.27.2007.S84
- Mohamed Q, Gillies MC, Wong TY. Management of diabetic retinopathy: a systematic review. *JAMA*. (2007) 298:902–16. doi: 10.1001/jama.298.8.902
- Li J, Lu Q, Lu P. Quantitative proteomics analysis of vitreous body from type 2 diabetic patients with proliferative diabetic retinopathy. *BMC Ophthalmol*. (2018) 18:151. doi: 10.1186/s12886-018-0821-3
- Zhou Y, Zhou B, Pache L, Chang M, Khodabakhshi AH, Tanasechuk O, et al. Metascape provides a biologist-oriented resource for the analysis of systems-level datasets. *Nat Commun*. (2019) 10:1523. doi: 10.1038/s41467-019-09234-6
- Lachmann A, Xu H, Krishnan J, Berger SI, Mazloom AR, Ma'ayan A. ChEA: transcription factor regulation inferred from integrating genome-wide ChIP-X experiments. *Bioinformatics*. (2010) 26:2438–44. doi: 10.1093/bioinformatics/btq466
- Kuleshov MV, Jones MR, Rouillard AD, Fernandez NF, Duan Q, Wang Z, et al. Enrichr: a comprehensive gene set enrichment analysis web server 2016 update. *Nucleic Acids Res*. (2016) 44:W90–7. doi: 10.1093/nar/gkw377
- Loukovaara S, Nurkkala H, Tamene F, Gucciardo E, Liu X, Repo P, et al. Quantitative proteomics analysis of vitreous humor from diabetic retinopathy patients. *J Proteome Res*. (2015) 14:5131–43. doi: 10.1021/acs.jproteome.5b00900
- Lam JD, Oh DJ, Wong LL, Amarnani D, Park-Windhol C, Sanchez AV, et al. Identification of RUNX1 as a mediator of aberrant retinal angiogenesis. *Diabetes*. (2017) 66:1950–6. doi: 10.2337/db16-1035
- Yanai R, Thanos A, Connor KM. Complement involvement in neovascular ocular diseases. *Adv Exp Med Biol*. (2012) 946:161–83. doi: 10.1007/978-1-4614-0106-3\_10
- Huang C, Fisher KP, Hammer SS, Busik JV. Extracellular vesicle-induced classical complement activation leads to retinal endothelial cell damage via MAC deposition. *Int J Mol Sci*. (2020) 21:1693. doi: 10.3390/ijms21051693
- Shahulhameed S, Vishwakarma S, Chhablani J, Tyagi M, Pappuru RR, Jakati S, et al. A systematic investigation on complement pathway activation in diabetic retinopathy. *Front Immunol*. (2020) 11:154. doi: 10.3389/fimmu.2020.00154
- Baptista FI, Castilho ÁF, Gaspar JM, Liberal JT, Aveleira CA, Ambrósio AF. Long-term exposure to high glucose increases the content of several exocytotic proteins and of vesicular GABA transporter in cultured retinal neural cells. *Neurosci Lett*. (2015) 602:56–61. doi: 10.1016/j.neulet.2015.06.044
- Chee CS, Chang KM, Loke MF, Angela Loo VP, Subrayan V. Association of potential salivary biomarkers with diabetic retinopathy and its severity in type-2 diabetes mellitus: a proteomic analysis by mass spectrometry. *PeerJ*. (2016) 4:e2022. doi: 10.7717/peerj.2022
- Treacy MP, Hurst TP. The case for intraocular delivery of PPAR agonists in the treatment of diabetic retinopathy. *BMC Ophthalmol*. (2012) 12:46. doi: 10.1186/1471-2415-12-46
- Hu Y, Chen Y, Ding L, He X, Takahashi Y, Gao Y, et al. Pathogenic role of diabetes-induced PPAR- $\alpha$  down-regulation in microvascular dysfunction. *Proc Natl Acad Sci USA*. (2013) 110:15401–6. doi: 10.1073/pnas.1307211110
- Chai D, Wang B, Shen L, Pu J, Zhang X-k, He B. RXR agonists inhibit high-glucose-induced oxidative stress by repressing PKC activity in human endothelial cells. *Free Radic Biol Med*. (2008) 44:1334–47. doi: 10.1016/j.freeradbiomed.2007.12.022
- Hammer SS, Beli E, Kady N, Wang Q, Wood K, Lydic TA, et al. The mechanism of diabetic retinopathy pathogenesis unifying key lipid regulators, sirtuin 1 and liver X receptor. *EBioMedicine*. (2017) 22:181–90. doi: 10.1016/j.ebiom.2017.07.008

**Conflict of Interest:** The authors declare that the research was conducted in the absence of any commercial or financial relationships that could be construed as a potential conflict of interest.

**Publisher's Note:** All claims expressed in this article are solely those of the authors and do not necessarily represent those of their affiliated organizations, or those of the publisher, the editors and the reviewers. Any product that may be evaluated in this article, or claim that may be made by its manufacturer, is not guaranteed or endorsed by the publisher.

Copyright © 2021 Li, Jin, Shi, Cai, Zhang and Zhao. This is an open-access article distributed under the terms of the Creative Commons Attribution License (CC BY). The use, distribution or reproduction in other forums is permitted, provided the original author(s) and the copyright owner(s) are credited and that the original publication in this journal is cited, in accordance with accepted academic practice. No use, distribution or reproduction is permitted which does not comply with these terms.



# Beyond the Visual Acuity: Assessing the Visual Function in mCNV Patients After Anti-VEGF Treatment

Songshan Li, Limei Sun, Xiujuan Zhao, Zhaotian Zhang, Xiaoling Luo and Xiaoyan Ding\*

State Key Laboratory of Ophthalmology, Retina Division, Zhongshan Ophthalmic Center, Sun Yat-sen University, Guangzhou, China

**Purpose:** To investigate visual function and vision-related quality of life (VR-QoL) changes in patients with myopic choroidal neovascularization (mCNV) after ranibizumab treatment.

**Methods:** Quantitatively evaluate the objective tests of visual function (visual acuity, microperimetry, and metamorphopsia by m-Charts) before and after 3+prn (pro re nata) ranibizumab treatment for 1 year. The National Eye Institute 25-Item Visual Function Questionnaire (VFQ-25) was performed to evaluate the VR-QoL.

**Results:** A total of 57 eyes of 57 patients were included in this study. The median average metamorphopsia score was 0.65 before treatment and improved to 0.45 after treatment ( $p = 0.0003$ ). There was also a significant difference in the average threshold, macular integrity, and proportion of patients with stable fixation by the microperimetry ( $p < 0.000$ ,  $p < 0.0001$ , and  $p = 0.03$ , respectively). After treatment, the VR-QoL composite, general vision subscale, and vision-related mental health subscale score were increased with borderline or statistical significance ( $p = 0.088$ ,  $p = 0.0038$ , and  $p = 0.012$ , respectively). Subgroup analysis demonstrated parallel improvement of the VR-QoL score, metamorphopsia, average macular threshold, and fixation stability in patients with or without visual acuity increase. By multiple linear regression analysis, the VFQ-25 score after anti-VEGF treatment was only associated with the baseline VFQ-25 score and macular integrity. Improvements in the VFQ-25 score were only associated with changes in the metamorphopsia score.

**Conclusions:** Integral lifting in several aspects of visual function was observed in mCNV after ranibizumab treatment. Macular integrity and metamorphopsia, but not visual acuity, were associated with VR-QoL.

**Keywords:** myopic choroidal neovascularization, visual function, metamorphopsia, microperimetry, mCNV

## INTRODUCTION

Myopic choroidal neovascularization (mCNV) is one of the most common vision-threatening complications of pathological myopia, affecting 5–11% of patients with pathological myopia and 0.04–0.05% of the general population (1). It is particularly prevalent among young and middle-aged Asians (2). Vision-related quality of life (VR-QoL) is significantly compromised in mCNV patients (3, 4), probably caused by not only the decrease in visual acuity (VA) but also the presence of metamorphopsia, scotomata, and fixation ability (5, 6). To date, VA is the standard, most common

## OPEN ACCESS

### Edited by:

Haijiang Lin,  
Massachusetts Eye and Ear Infirmary  
and Harvard Medical School,  
United States

### Reviewed by:

Suyan Li,  
First People's Hospital of  
Xuzhou, China  
Han Zhang,  
The First Affiliated Hospital of China  
Medical University, China

### \*Correspondence:

Xiaoyan Ding  
dingxiaoyan@gzoc.com

### Specialty section:

This article was submitted to  
Ophthalmology,  
a section of the journal  
Frontiers in Medicine

**Received:** 14 May 2021

**Accepted:** 26 July 2021

**Published:** 31 August 2021

### Citation:

Li S, Sun L, Zhao X, Zhang Z, Luo X  
and Ding X (2021) Beyond the Visual  
Acuity: Assessing the Visual Function  
in mCNV Patients After Anti-VEGF  
Treatment. *Front. Med.* 8:709584.  
doi: 10.3389/fmed.2021.709584

way to evaluate visual function in mCNV. In most clinical studies, it is even the only way to assess the visual function (7, 8). VR-QoL and other aspects of visual function, including the fixation ability, metamorphopsia, and scotomata, are barely studied.

To date, several quantifiable measurements have been developed for a wide recognition of the total visual ability and subjective perception of VR-QoL, including microperimetry, contrast sensitivity, metamorphopsia, and the 25-item National Eye Institute Visual Function Questionnaire (VFQ-25). The macular sensitivity measured by microperimetry has been used for the assessment of macular function in several diseases and showed correlation with the VA or VFQ-25 in several diseases (9, 10). Some studies in wet age-related macular degeneration (wAMD) demonstrated the discrepancy between VA and other visual functions. Tran et al. reported severe impairment of macular sensitivity by microperimetry in AMD patients with good central visual acuity (11). Discrepant changes of VA and metamorphopsia improvement were also reported after treatment in wAMD or after surgery in patients with macular holes (12, 13).

In patients with mCNV, VA improved about 13–15 Early Treatment Diabetic Retinopathy Study (ETDRS) letters 1 year after a scheduled anti-VEGF treatment (7, 8, 14). Without treatment, VA may drop to 20/200 or worse within 5 years in patients with mCNV (15, 16). However, very few studies paid attention to changes in other aspects of visual function impairment except VA. In the limited studies, the improvement of macular sensitivity or fixation ability was noticed after bevacizumab or photodynamic therapy but failed to correlate the improvement with patient-reported outcomes (5, 17, 18). It was observed in the MYRROR study (VEGF trap-eye in choroidal neovascularization secondary to pathologic myopia, NCT01249664) that more than 10% mCNV patients did not achieve substantial VA improvement ( $\geq 5$  letters) after 12 months of anti-VEGF treatment (7), while the changes in VR-QoL and other aspects of visual function in these patients remain unknown.

During anti-VEGF treatment, monitoring visual function and VR-QoL not limited to the VA could be helpful for recognizing the entire picture of the disease and for assessing the benefits of anti-VEGF therapy. Therefore, the purpose of this study was to investigate visual functional improvements and VR-QoL changes during anti-VEGF treatment in patients with mCNV. Indicators in addition to VA were prospected for visual function assessment.

## METHODS

### Patients

This retrospective case series was conducted in Zhongshan Ophthalmic Center, Sun Yat-Sen University with the permission of the Institutional Review Board (2015MEKY053). All investigations followed the tenets of the Declaration of Helsinki. A total of 57 eyes of 57 patients with active unilateral mCNV were enrolled in this study from March 2014 to July 2018, including 20 patients who participated in a previous published study (SMILE: a single blind clinical trial “Treatment and assessment Strategy for Myopic CNV with LucEntis: a single-center,

prospective randomized controlled study,” NCT03042871) (14). The inclusion criteria were as follows: (1) unilateral active subfoveal or juxtafoveal CNV associated with high myopia (spherical equivalence  $< -6.0$  D or axial length  $> 26$  mm) confirmed by fundus fluorescein angiography (FFA) with a hyperfluorescent CNV network on early frames and leakage on late frames; (2) patients with baseline best-corrected visual acuity (BCVA) in the affected eye from 24 to 73 ETDRS letters; and (3) patients who received 3+prn (pro re neta) intravitreal ranibizumab treatments for 12 months. The exclusion criteria were as follows: (1) presence of other ocular diseases or evidence of any condition other than CNV associated with high myopia that affected the VA for both eyes (including moderate to dense lens opacity); (2) any anti-VEGF therapy performed within the last 6 months; (3) previous photodynamic therapy (PDT); (4) intraocular surgery performed within the last 3 months; and (5) pregnancy or severe systemic conditions, including uncontrolled systemic hypertension, or any history of thromboembolic or ischemic cardiovascular diseases. The retreatment was administered in patients who met any of the following criteria: (a) reduction of BCVA  $> 5$  letters from the previous visit; (b) increase in central retinal thickness (CRT)  $> 50 \mu\text{m}$  from the previous visit; new or persistent cystic retinal changes, subretinal fluid or pigment epithelial detachment; and (c) new or persistent bleeding or leakage in FFA or fundus examination.

BCVA, optical coherence tomography (OCT), and FFA were measured before and after 12-month ranibizumab treatments. Quantitative evaluation of metamorphopsia using m-Charts (Inami Co., Tokyo, Japan) and macular function assessed by microperimetry (MAIA, Centervue, Italy) were performed on each patient. The m-Charts were used to analyze the metamorphopsia score by quantifying the minimum visual angle (from 0 to 2 degrees) of a dotted straight line for patients to recognize the distortion. The measurement was conducted in a bright light at a distance of 30 cm. Both vertical and horizontal metamorphopsia scores were measured and repeated three times. The mean m-Charts value was used in the statistical analysis. Microperimetry was performed using a macular integrity assessment (MAIA) by an expert 4-2 examination covering 10 degrees of diameter of the macular area. The examination included 37 measurement points in three circles with 2, 6, and 10 degrees of diameter, respectively. The stimulus was Goldman III in magnitude and lasted 200 ms. The illumination of the stimulus was distributed from 0 to 36 dB. The results of average threshold of macular sensitivity, macular integrity index, P1, P2, 63% bivariate contour ellipse area (BCEA), and 95% BCEA were analyzed and classified. Fixation stability was classified according to Fujii et al. (19): (1) If P1 is  $\geq 75\%$ , the fixation was classified as “stable”; (2) if P1  $< 75\%$  but P2 is  $\geq 75\%$ , the fixation was classified as “relatively unstable”; and (3) if P2  $< 75\%$ , the fixation was classified as “unstable.” VR-QoL, using the National Eye Institute 25-Item Visual Function Questionnaire (VFQ-25), was reported in all patients before and 12 months after 3+prn intravitreal ranibizumab treatment. The composite score and the score of each subscale were calculated followed the specifications of the National Eye Institute (20).



**TABLE 1** | Demographic and baseline characters.

Characteristics	Mean $\pm$ SD	Median of total	Min of total	Max of total
<i>n</i>	57			
Male/female	24/33			
Age(year)	50.51 $\pm$ 13.80	53	20	76
BCVA (ETDRS)	51.89 $\pm$ 14.89	52	24	73
Axial length (mm)	28.65 $\pm$ 1.40	28.77	26.16	32.01
Spherical equivalent	-11.76 $\pm$ 5.03	-10.75	-21.25	-6.25
CNV location (subfoveal/juxtafoveal)	47/10			

**TABLE 2** | Functional visual performance before and after anti-VEGF treatment.

Characteristics	Baseline	After treatment	<i>P</i>
	Mean $\pm$ SD (median)	Mean $\pm$ SD (median)	
BCVA (ETDRS)	51.89 $\pm$ 14.89 (52)	62.95 $\pm$ 14.52 (66)	<b>&lt;0.0001</b>
CRT ( $\mu$ m)	261.6 $\pm$ 85.7 (257.5)	215.9 $\pm$ 70.1 (210.5)	<b>&lt;0.0001</b>
Average metamorphopsia score	0.90 $\pm$ 0.70 (0.65)	0.58 $\pm$ 0.55 (0.45)	<b>0.0003*</b>
Macular integrity	94.65 $\pm$ 17.03 (100)	82.81 $\pm$ 25.43 (97.6)	<b>&lt;0.0001*</b>
Average threshold	18.50 $\pm$ 5.99 (19.3)	22.42 $\pm$ 5.11 (23.6)	<b>&lt;0.0001</b>
P1	45.14 $\pm$ 30.17 (43)	63.25 $\pm$ 28.58 (70)	<b>&lt;0.0001*</b>
P2	72.60 $\pm$ 26.27 (84)	84.32 $\pm$ 28.58 (91)	<b>0.0006*</b>
Unstable/Relatively unstable/Stable	21 (36.8%)/23 (40.4%)/13 (22.8%)	14 (24.6%)/18 (31.6%)/25 (43.9%)	<b>0.03<sup>#</sup></b>
Area of 63% BCEA (mm <sup>2</sup> )	12.74 $\pm$ 13.13 (7.35)	6.92 $\pm$ 7.46 (3.90)	<b>0.0003*</b>
Area of 95% BCEA (mm <sup>2</sup> )	38.17 $\pm$ 39.36 (22.15)	21.31 $\pm$ 24.40 (11.60)	<b>0.0007*</b>

\*Wilcoxon matched-pairs signed rank test.

<sup>#</sup>Chi-square test for trend.

## Statistical Analysis

Statistical analysis was performed using GraphPad (GraphPad Software, CA, USA) or SPSS (SPSS Inc., Chicago, IL, USA). Shapiro–Wilk test was used to test for the normality distribution. Comparisons of the continuous variables were performed using the two-tailed Student's *t*-test or the Mann–Whitney test when appropriate. Paired two-tailed Student's *t*-tests or Wilcoxon matched-pairs signed rank tests were used for paired data. Analysis of the dichotomous variables was performed using the chi-square test (or Fisher's exact test when appropriate). To determine the factors that might be correlated with the VA and the VR-QoL score, multiple linear regression analyses by the stepwise methods were conducted. Three dependent variables were used: the final BCVA after 12 months of treatment, the final composite VR-QoL score, and the improvement of the composite VR-QoL score. According to the reported possible prognostic factors, the independent variables included gender, age, BCVA, macular integrity, average threshold, P1, P2, 63% BCEA area, 95% BCEA area, composite VR-QoL score, and average metamorphopsia score (3, 9, 10, 20). The level of significance was set at  $p < 0.05$ .

## RESULTS

### Demographics

A total of 57 eyes in 57 patients were enrolled in this study. Overall, 33/57 (57.9%) of the patients were female, and the mean

age was 50.51  $\pm$  13.80 years old (range: 20–76 years). The average spherical equivalent refractive error was -11.76  $\pm$  5.03 D, and the mean axial length was 28.65  $\pm$  1.40 mm. The average baseline BCVA was 51.89  $\pm$  14.89 ETDRS letters. mCNV was located subfoveally in 82.5% (47/57) patients. The other 17.5% (10/57) was juxtafoveal CNV (Table 1).

### VA and Structural Improvement in Patients With mCNV Before and After Treatment

After 12-month 3+prn intravitreal ranibizumab (IVR) treatments, the average BCVA increased from 51.89  $\pm$  14.89 to 62.95  $\pm$  14.52 letters ( $p < 0.0001$ ). Of these, more than 5-letter improvements were found in 66.7% (38/57) patients. The central retinal thickness (CRT) decreased from 261.6  $\pm$  85.7 to 215.9  $\pm$  70.1  $\mu$ m ( $p < 0.0001$ ) (Table 2).

### Functional Visual Performance in Patients With mCNV Before and After Treatment

The functional visual changes following IVR treatments are summarized in Table 2. The mean average metamorphopsia score was 0.90  $\pm$  0.70 (median 0.65) before treatment and improved to 0.58  $\pm$  0.55 (median 0.45) after treatment ( $p = 0.0003$ ). There was also a significant difference in the average threshold (18.50  $\pm$  5.99 median 19.3 to 22.42  $\pm$  5.11 median 23.6,  $p < 0.0001$ ) and macular integrity (94.65  $\pm$  17.03 median 100 to 82.81  $\pm$  25.43 median 97.6,  $p < 0.0001$ ) by the microperimetry. Fixation was significantly more stable in P1, P2, 63% area of



**TABLE 3 |** Subjective QoL score by VFQ25 before and after anti-VEGF treatment.

Subscales	Baseline	After	P
General health	40.35 ± 19.91	44.02 ± 17.63	0.58
General vision	26.93 ± 17.21	35.36 ± 17.47	<b>0.0038</b>
Ocular pain	72.37 ± 17.56	74.33 ± 16.59	0.45
Near activities	66.52 ± 23.01	71.27 ± 24.42	0.11
Distance activities	71.42 ± 21.02	74.25 ± 18.10	0.21
Vision related social functioning	86.18 ± 19.86	86.38 ± 16.22	0.84
Vision related mental health	47.48 ± 19.97	53.24 ± 21.09	<b>0.012</b>
Vision related role difficulties	52.63 ± 25.52	53.79 ± 22.73	0.84
Vision related dependency	59.94 ± 24.11	62.80 ± 25.22	0.43
Driving	62.30 ± 39.58	66.67 ± 39.09	0.39
Color vision	91.07 ± 16.81	92.41 ± 15.01	0.81
Peripheral vision	82.14 ± 21.17	78.57 ± 21.55	0.10
Composite score	65.42 ± 14.05	68.12 ± 14.28	0.088

**TABLE 4 |** Visual function and VR-QoL parameters in BCVA improved subgroup and BCVA sustained subgroup.

Parameters	BCVA changes ≤ 5 letters n = 19	BCVA changes > 5 letters n = 38	P
Baseline BCVA	55.58 ± 16.13 (52)	50.05 ± 14.08 (48.5)	0.189
Final BCVA	57.11 ± 16.15 (59)	65.87 ± 12.88 (69)	<b>0.03</b>
P (baseline vs. final)	0.093	<b>&lt;0.0001</b>	
Baseline Macular integrity	88.22 ± 26.96 (100)	97.86 ± 7.33 (100)	0.139*
Final integrity	84.54 ± 29.10 (100)	81.95 ± 23.76 (96.15)	0.229*
P (baseline vs. final)	0.285*	<b>&lt;0.0001*</b>	
Baseline average threshold	18.97 ± 6.99 (19.8)	18.27 ± 5.51 (19.1)	0.683
Final average threshold	21.93 ± 5.57 (22.5)	22.66 ± 4.93 (23.85)	0.614
P (baseline vs. final)	<b>0.001</b>	<b>&lt;0.0001</b>	
Baseline P1	48.74 ± 31.51 (46)	43.34 ± 29.73 (41)	0.559*
Final P1	68.00 ± 31.12 (86)	60.87 ± 27.34 (62.00)	0.334*
P (baseline vs. final)	<b>0.005*</b>	<b>0.004*</b>	
Baseline P2	74.16 ± 27.97 (84)	71.82 ± 25.73 (83.5)	0.703*
Final P2	86.79 ± 16.93 (96.00)	83.08 ± 17.87 (86.00)	0.278*
P (baseline vs. final)	<b>0.010*</b>	<b>0.017*</b>	
Baseline 63%BCEA area	14.58 ± 17.85 (6.65)	11.96 ± 10.77 (7.80)	0.955*
Final 63%BCEA area	5.95 ± 7.59 (2.3)	7.41 ± 7.45 (6.2)	0.184*
P (baseline vs. final)	<b>0.009*</b>	<b>0.012*</b>	
Baseline 95%BCEA area	43.68 ± 53.47 (19.95)	35.86 ± 32.28 (23.40)	0.947*
Final 95%BCEA area	17.78 ± 22.71 (6.8)	23.08 ± 25.30 (17.60)	0.190*
P (baseline vs. final)	<b>0.010*</b>	<b>0.024*</b>	
Baseline metamorphopsia score	0.91 ± 0.71 (0.60)	0.89 ± 0.70 (0.70)	0.946*
Final metamorphopsia score	0.64 ± 0.64 (0.50)	0.55 ± 0.51 (0.425)	0.858*
P (baseline vs. final)	<b>0.016*</b>	<b>0.010*</b>	
Baseline composite score	65.60 ± 16.09 (70.45)	65.33 ± 13.14 (65.42)	0.946
Final composite score	67.48 ± 15.19 (65.79)	68.44 ± 14.00 (67.625)	0.813
P (baseline vs. final)	0.479	0.103	
Baseline vision subscale score	25.26 ± 16.11 (20)	27.76 ± 17.89 (20)	0.610
Final vision subscale score	33.68 ± 17.71 (40)	36.22 ± 17.54 (40)	0.612
P (baseline vs. final)	<b>0.011</b>	<b>0.003</b>	
Baseline mental health subscale score	46.38 ± 19.13 (43.75)	48.03 ± 20.61 (43.75)	0.772
Final mental health subscale score	51.64 ± 20.71 (56.25)	54.05 ± 21.51 (56.25)	0.689
P (baseline vs. final)	0.186	<b>0.034</b>	

\*Wilcoxon matched-pairs signed rank test or Mann-Whitney test.

BCEA, and 95% area of BCEA after treatment, when compared with those at baseline (details in **Table 2**). The proportion of patients with normal fixation stability also increased from 22.8% (13/57) to 43.9% (25/57) ( $p = 0.03$ ).

### Changes of VR-QoL in Patients With mCNV Before and After Treatment

The changes of VR-QoL measured using the VFQ-25 questionnaire are summarized in **Table 3**. After IVR treatment, most subscale scores and the composite score were numerically increased, except for the “peripheral vision subscale.” Although no statistical significance was observed ( $p = 0.088$ ), the composite score modestly increased from  $65.42 \pm 14.05$  to  $68.12 \pm 14.28$ . The “general vision subscale” and the “vision related mental health subscale” significantly increased after treatment ( $26.93 \pm 17.21$  to  $35.36 \pm 17.47$ ,  $p = 0.0038$  and  $47.48 \pm 19.97$  to  $53.24 \pm 21.09$ ,  $p = 0.012$ , respectively).

### Parallel Improvement of VR-QoL in Subgroups With/Without VA Improvement

As mentioned above, not all patients gained significant VA improvement after the treatment. Among the 57 patients, two-thirds (38/57, 66.7%) showed a BCVA improvement of more than 5 ETDRS letters (mean  $\pm$  SD,  $15.82 \pm 7.81$  letters) and were subdivided into group A, and the other one-third (19/57, 33.3%) of patients were subdivided into group B [with BCVA improvement  $\leq 5$  ETDRS letters (mean  $\pm$  SD,  $1.53 \pm 3.75$  letters)]. No patients experienced a VA loss of more than 5 ETDRS letters. The average injection number was  $3.31 \pm 0.69$  in group A, while it was  $3.61 \pm 0.91$  in group B ( $p = 0.17$ ). The median age was 53.5 years old (range: 23–76 years) in group A and 50 years old (range: 20–71 years) in group B ( $p = 0.42$ ). In addition, no statistical difference was found about the sex between the two subgroups (male/female, 14/24 in group A and 10/9 in group B,  $p = 0.27$ ).

The changes of VR-QoL before and after treatment between the two subgroups were then analyzed (**Table 4**). The composite score increased from  $65.33 \pm 13.14$  to  $68.44 \pm 14.00$ , and

the score of vision subscale statistically increased from  $27.76 \pm 17.89$  to  $36.22 \pm 17.54$  ( $p = 0.003$ ) in group A. Despite poor improvement of VA, the patients in group B gained parallel improvement in VR-QoL compared with group A. The composite score increased from  $65.60 \pm 16.09$  to  $67.48 \pm 15.19$ , and the score of vision subscale increased from  $25.26 \pm 16.11$  to  $33.68 \pm 17.71$  ( $p = 0.011$ ). Furthermore, the change of vision subscale before and after treatment was comparable between the two subgroups ( $p = 0.976$ , **Table 5**).

### Parallel Resolution of Metamorphopsia in Subgroups With/Without VA Improvement

We then analyzed the metamorphopsia evaluation with or without BCVA improvement after ranibizumab treatment (**Table 4**). The average m-Charts score significantly improved from  $0.89 \pm 0.70$  (median 0.70) to  $0.55 \pm 0.51$  (median 0.425) ( $p = 0.010$ ) in group A and from  $0.91 \pm 0.71$  (median 0.60) to  $0.64 \pm 0.64$  (median 0.50) in group B ( $p = 0.016$ ). The resolution of metamorphopsia was also comparable in the two subgroups ( $p = 0.79$ ).

### Visual Function by Microperimetry in Subgroups With/Without VA Improvement

Visual function parameters measured using microperimetry were also compared between groups A and B (**Table 4**). In group B, the macular integrity did not dramatically change after 3+prn IVR. In the BCVA improved subgroup, the macular integrity improved statistically from  $97.86 \pm 7.33$  (median 100) to  $81.95 \pm 23.76$  (median 96.15) ( $p < 0.0001$ ). However, the average macular threshold in groups A ( $18.27 \pm 5.51$  to  $22.66 \pm 4.93$ ,  $p < 0.0001$ ) and B ( $18.97 \pm 6.99$  to  $21.93 \pm 5.57$ ,  $p = 0.001$ ) both significantly increased. All parameters focusing on the macular fixation stability, including P1, P2, 63% BCEA area, and 95% BCEA area, were all significantly ameliorated no matter the VA improvement or not. No statistical difference could be detected between the two subgroups (**Table 4**; **Figures 1, 2**).

Comparing changes of vision function between groups A and B, a board line difference was found only in the change of macular

**TABLE 5 |** Visual function and VR-QoL changes in BCVA improved subgroup and BCVA sustained subgroup.

	BCVA change $\leq 5$	BCVA change $> 5$	P
n	19	38	
BCVA	$1.53 \pm 3.75$ (1.0)	$15.82 \pm 7.81$ (14.0)	<b>&lt;0.0001</b>
Macular integrity	$-3.68 \pm 24.62$ (−0.2)	$-15.91 \pm 24.44$ (−2.55)	0.06*
Average threshold	$2.96 \pm 3.27$ (2.1)	$4.39 \pm 4.25$ (4.1)	0.81
P1	$19.26 \pm 25.53$ (19.00)	$17.53 \pm 33.01$ (14.50)	0.79*
P2	$12.63 \pm 20.75$ (9.0)	$11.26 \pm 24.10$ (3.0)	0.45*
63% BCEA area	$-8.27 \pm 13.56$ (−3.45)	$-4.55 \pm 11.03$ (−1.90)	0.46*
95% BCEA area	$-24.80 \pm 40.69$ (−10.20)	$-12.78 \pm 33.13$ (−5.00)	0.36*
Average metamorphopsia score	$-0.27 \pm 0.44$ (−0.2)	$-0.34 \pm 0.68$ (−0.18)	0.79*
General vision subscale	$8.42 \pm 15.37$ (0.0)	$8.24 \pm 22.98$ (0.0)	0.976
Mental health subscale	$5.26 \pm 16.70$ (6.25)	$5.57 \pm 15.36$ (6.25)	0.945
Composite score	$1.88 \pm 11.36$ (2.42)	$2.40 \pm 8.73$ (3.52)	0.521

\*Mann–Whitney test.

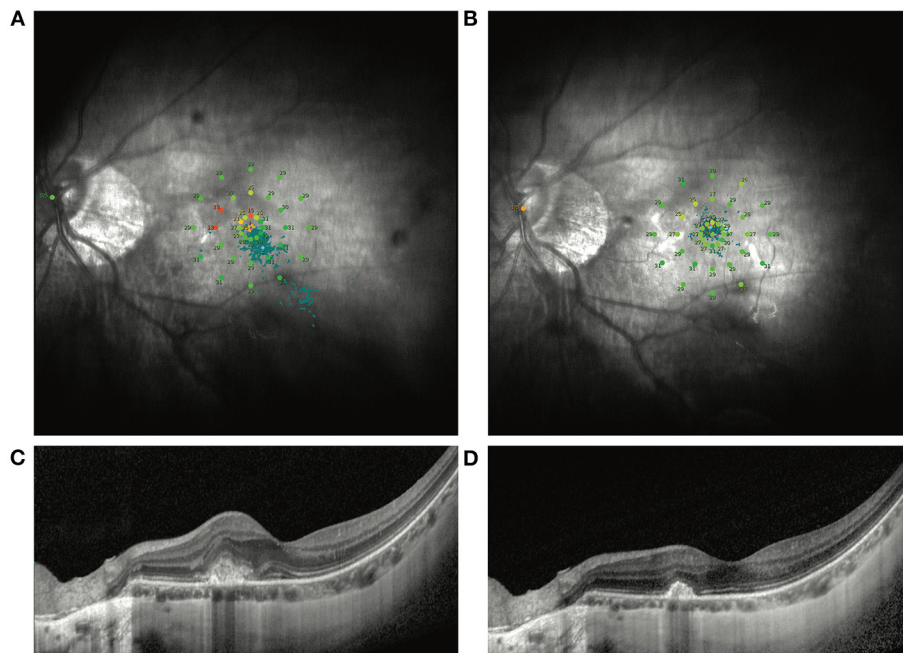


**FIGURE 1 |** Representative MP1 findings in an mCNV patient without VA improvement after ranibizumab treatment. **(A)** Shows the image of the MP1 before ranibizumab treatment in an mCNV patient with baseline BCVA as 67 ETDRS letters. After treatment, the VA increased by only 1 ETDRS letter. Nevertheless, the macular sensitivity and fixation improved dramatically by MP1 **(B)**. OCT images also show the remission of the CNV lesion in the macular **(C,D)**.

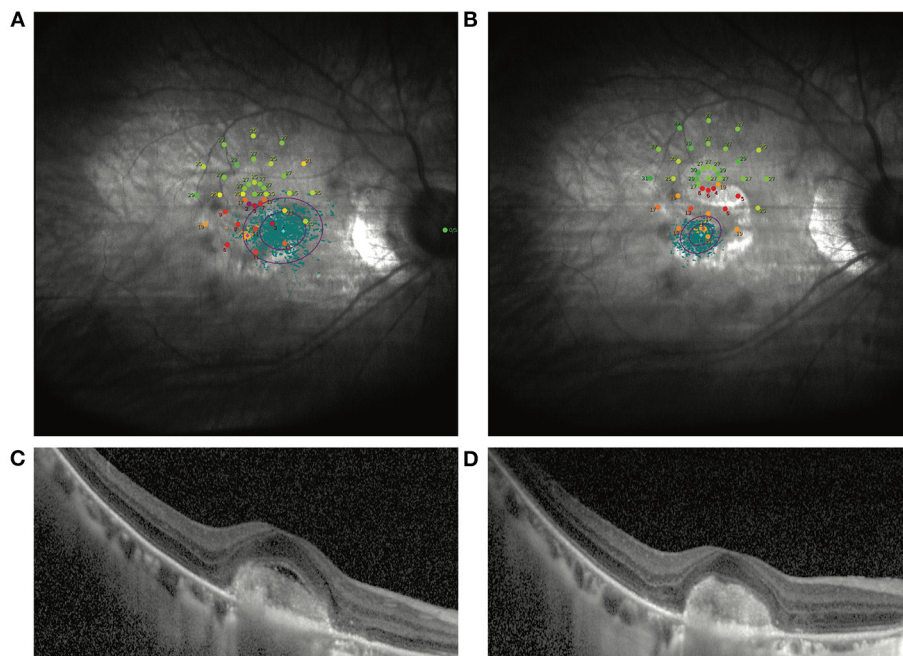


**FIGURE 2 |** Another representative patient without VA improvement after ranibizumab treatment. **(A)** Shows the image of the MP1 before ranibizumab treatment in an mCNV patient with baseline BCVA as 35 ETDRS letters. After treatment, the VA increased by 3 ETDRS letters. Nevertheless, the macular sensitivity and fixation improved dramatically by MP1 **(B)**. OCT images also show the remission of the CNV lesion in the macular **(C,D)**.

**TABLE 6 |** Multiple linear regression model to evaluate the factors associated with the final BCVA.

Characters	Beta	P
Baseline BCVA	0.789	<b>&lt;0.0001</b>
Gender		0.403
Age		0.966
Macular integrity		0.317
Average threshold		0.058
P1		0.111
P2		0.131
63% BCEA area		0.160
95% BCEA area		0.205
Average metamorphopsia score		0.159
Composite VFQ-25 score		0.968

$R = 0.789, p < 0.0001.$

integrity ( $p = 0.06$ ). The improvement of average threshold and retinal fixation were comparable regardless of whether BCVA improved or sustained.

## Multiple Regression Analysis for the Visual Functional Performance After the Treatment

According to the reported possible prognostic factors, age, sex, baseline BCVA, final macular integrity, final average threshold, final P1, final P2, final 63% BCEA area, final 95% BCEA area, final average metamorphopsia score, and final composite VFQ-25 score were included in the multiple linear regression analysis to identify the possible factors that might have influenced the final BCVA. Among these factors, the final BCVA after anti-VEGF treatment correlated only with baseline BCVA ( $R = 0.789, p < 0.0001$ ) (Table 6).

We then determined which parameter correlated with the final composite VFQ-25 score. The baseline composite VFQ-25 score and macular integrity were both significantly correlated with the final composite VFQ-25 score, with the betas equal to 0.666 and  $-0.335$ , respectively, in a model including gender, age, baseline VFQ-25 composite score, final BCVA, final macular integrity, final average threshold, final P1, final P2, final 63% BCEA area, final 95% BCEA area, and final average metamorphopsia score ( $R = 0.830, p < 0.0001$ ) (Table 7).

The change of average metamorphopsia score was the only factor that correlated with the change of the composite VFQ-25 score, with  $\beta = -0.284$  and  $p = 0.039$ , respectively, in a model including gender, age, the change of macular integrity, the change of average threshold, the change of P1, the change of P2, the change of 63% BCEA area, the change of 95% BCEA area, and the change of BCVA ( $R = 0.284, p = 0.039$ ) (Table 8).

## DISCUSSION

In the present study, patients with mCNV underwent a wide range of visual function tests that included microperimetry,

**TABLE 7 |** Multiple linear regression model to evaluate the factors associated with the final composite VFQ-25 score.

Characters	Beta	P
Baseline composite VFQ-25 score	0.666	<b>&lt;0.0001</b>
Macular integrity	$-0.335$	<b>&lt;0.0001</b>
Gender		0.433
Age		0.960
Average threshold		0.308
P1		0.834
P2		0.766
63% BCEA area		0.465
95% BCEA area		0.654
Average metamorphopsia score		0.092
Composite VFQ-25 score		0.721

$R = 0.830, p < 0.0001.$

**TABLE 8 |** Multiple linear regression model to evaluate the factors associated with the change of VR-QoL score.

Characters	beta	P
Gender		0.913
Age		0.091
Change of macular integrity		0.057
Change of average threshold		0.679
Change of P1		0.808
Change of P2		0.338
Change of 63%BCEA area		0.524
Change of 95%BCEA area		0.469
Change of average metamorphopsia score	$-0.284$	<b>0.039</b>
Change of BCVA		0.962

$R = 0.284, p = 0.039.$

m-Charts, VA, as well as subjective judgment of the VR-QoL by VFQ-25 before and after 3+prn anti-VEGF treatments for 1 year. Based on the findings of this retrospective study in mCNV, comprehensive visual function measured by fixation ability, whole macular sensitivity, macular integrity, and the metamorphopsia improved dramatically after anti-VEGF treatment, suggesting the integral lifting in several aspects of visual function. Interestingly, the promotion could still be observed in macular average sensitivity, fixation ability, the metamorphopsia score, and the VFQ-25 score in patients with BCVA improvement  $\leq 5$  ETDRS letters. That is, even when VA did not improve dramatically after anti-VEGF treatment, these patients nevertheless benefited from anti-VEGF treatment.

VA, especially BCVA in distance, has been considered the gold standard for the assessment of visual function in macular disease, including AMD and mCNV (7, 8, 21). Nevertheless, BCVA only represents the acuity of macular fovea. Surprisingly, as the most commonly used measurement, distance visual acuity failed to correlate with patient-reported visual impairment scores in several diseases as well as in our current study (11–13).



However, the metamorphopsia score (22) and general retinal sensitivity (23) correlated with patient-reported VR-QoL in wAMD patients or patients with retinitis pigmentosa. In the present study, we showed that the VR-QoL VFQ-25 score after anti-VEGF treatment was only associated with the baseline VFQ-25 score and macular integrity. Improvements in the VFQ-25 score were associated with changes in the metamorphopsia score. By contrast, no correlation was observed between the BCVA and the VR-QoL.

Microperimetry and m-Charts were widely used in the macular function assessment in AMD and other ocular disease but were barely reported in mCNV (11, 24). The visual function development in mCNV patients with limited BCVA changes was also ignored previously. VA is an important indicator, reflecting part of the visual function. On the other hand, microperimetry and m-Charts are distinct and irreplaceable for quantitative measurement of metamorphopsia, fixation, and general macular sensitivity. As the inexpensive and quickly conducted examination, microperimetry and m-Charts could be examined to obtain a comprehensive understanding of visual function especially in patients with limited or no VA improvement after treatment.

Limitations of this study included the retrospective nature and the relatively limited sample size, possibly explaining the negative results of the change of the VFQ-25 composite score before and after treatment. Twenty patients in the study were also included in a prospective single-blind clinical trial, the SMILE study (NCT03042871). Similar including criteria were used in these two studies to limit the selection bias. Additionally, economic burden may limit the practical application of the multiple examination of visual function in the real world. Furthermore, only 1-year results after the anti-VEGF treatment were analyzed in this study. Future studies with longer follow-up would be greatly beneficial to determining the long-term visual functional improvement.

In conclusion, VA is not the only part that should be noticed following the treatment of mCNV. The severity of macular integrity, macular sensitivity, fixation, and metamorphopsia should also be paid attention after anti-VEGF treatment, especially in patients with limited BCVA gain, whose

visual function could still improve. Macular integrity and metamorphopsia, but not VA, were associated with reported VR-QoL, suggesting that VA is far from sufficient for the assessment of visual function. Microperimetry and m-Charts serve as important supplements to measure mCNV treatment responses.

## DATA AVAILABILITY STATEMENT

The raw data are available from the corresponding author by request.

## ETHICS STATEMENT

The studies involving human participants were reviewed and approved by Institutional Review Board of Zhongshan Ophthalmic Center, Sun Yat-Sen University. The patients/participants provided their written informed consent to participate in this study.

## AUTHOR CONTRIBUTIONS

XD supervised the project. SL and XD developed the original idea and wrote the manuscript. SL and LS conducted the statistical analysis. SL, XZ, ZZ, and XL collected the data. All authors contributed to the article and approved the submitted version.

## FUNDING

This study was supported in part by grants from the Fundamental Research Funds of State Key Laboratory of Ophthalmology, research funds of Sun Yat-sen University (15ykjc22d; Guangzhou, Guangdong, China) (18zxxt73; Guangzhou, Guangdong, China), Science and Technology Program Guangdong, China (2016A020215096; Guangzhou, Guangdong, China) (2018A030310230; Guangzhou, Guangdong, China), and the grant from the National Natural Science Foundation of China (31800873). The sponsors and funding organizations had no role in the design or conduct of this research.

## REFERENCES

- Wong TY, Ferreira A, Hughes R, Carter G, Mitchell P. Epidemiology and disease burden of pathologic myopia and myopic choroidal neovascularization: an evidence-based systematic review. *Am J Ophthalmol.* (2014) 157:9–25.e12. doi: 10.1016/j.ajo.2013.08.010
- Soubrane G. Choroidal neovascularization in pathologic myopia: recent developments in diagnosis and treatment. *Surv Ophthalmol.* (2008) 53:121–38. doi: 10.1016/j.survophthal.2007.12.004
- Amoaku WM, Gale RP, Lotery AJ, Menon G, Sivaprasad S, Petrillo J, et al. Treatment satisfaction and well-being in patients with myopic choroidal neovascularization treated with ranibizumab in the REPAIR study. *PLoS ONE.* (2015) 10:e0128403. doi: 10.1371/journal.pone.0128403
- Virgili G, Parravano M, Viola F, Varano M. Vision-related quality of life in patients treated for myopic choroidal neovascularization: a post hoc analysis of the OLIMPIC study. *Eur J Ophthalmol.* (2019) 30:1069–75. doi: 10.1177/1120672119853745
- Yodoi Y, Tsujikawa A, Nakanishi H, Otani A, Tamura H, Ojima Y, et al. Central retinal sensitivity after intravitreal injection of bevacizumab for myopic choroidal neovascularization. *Am J Ophthalmol.* (2009) 147:816–824.e1. doi: 10.1016/j.ajo.2008.11.020
- Gaucher D, Chartier C, Cohen S-Y, Malecaze F, Souied EH, Weber M, et al. High myopic patients: a survey of their history, feelings, beliefs and needs. *J Fr Ophthalmol.* (2016) 39:12–9. doi: 10.1016/j.jfo.2015.04.019
- Ikuno Y, Ohno-Matsui K, Wong TY, Korobelnik JF, Vittori R, Li T, et al. Intravitreal aflibercept injection in patients with myopic choroidal neovascularization: the MYRROR study. *Ophthalmology.* (2015) 122:1220–27. doi: 10.1016/j.ophtha.2015.01.025
- Wolf S, Balciunienė VJ, Laganovska G, Menchini U, Ohno-Matsui K, Sharma T, et al. RADIANCE: a randomized controlled study of ranibizumab in patients with choroidal neovascularization secondary to pathologic myopia. *Ophthalmology.* (2014) 121:682–92.e2. doi: 10.1016/j.ophtha.2013.10.023
- Okada K, Yamamoto S, Mizunoya S, Hoshino A, Arai M, Takatsuna Y. Correlation of retinal sensitivity measured with fundus-related



- microperimetry to visual acuity and retinal thickness in eyes with diabetic macular edema. *Eye*. (2006) 20:805–9. doi: 10.1038/sj.eye.6702014
10. Forshaw TRJ, Parpounas AK, Sørensen TL. Correlation of macular sensitivity measures and visual acuity to vision-related quality of life in patients with age-related macular degeneration. *BMC Ophthalmol*. (2021) 21:149. doi: 10.1186/s12886-021-01901-x
  11. Tran B-K, Herborn CP. Discrepancy between visual acuity and microperimetry in AMD patients: visual acuity appears as an inadequate parameter to test macular function. *Klin Monatsbl Augenheilkd*. (2015) 232:529–32. doi: 10.1055/s-0035-1545779
  12. Nowomiejska K, Oleszczuk A, Brzozowska A, Grzybowski A, Ksiązek K, Maciejewski R, et al. M-charts as a tool for quantifying metamorphopsia in age-related macular degeneration treated with the bevacizumab injections. *BMC Ophthalmol*. (2013) 13:13. doi: 10.1186/1471-2415-13-13
  13. Wada I, Yoshida S, Kobayashi Y, Zhou Y, Ishikawa K, Nakao S, et al. Quantifying metamorphopsia with M-CHARTS in patients with idiopathic macular hole. *Clin Ophthalmol Auckl NZ*. (2017) 11:1719–26. doi: 10.2147/OPTH.S144981
  14. Li S, Ding X, Sun L, Zhao X, Zhang A, Lyu C, et al. Two different initial treatment regimens of ranibizumab in myopic choroidal neovascularization: 12-month results from a randomized controlled study. *Clin Experiment Ophthalmol*. (2019) 47:250–8. doi: 10.1111/ceo.13424
  15. Yoshida T, Ohno-Matsui K, Yasuzumi K, Kojima A, Shimada N, Futagami S, et al. Myopic choroidal neovascularization: a 10-year follow-up. *Ophthalmology*. (2003) 110:1297–305. doi: 10.1016/S0161-6420(03)00461-5
  16. Shih Y-F, Ho T-C, Hsiao CK, Lin LL-K. Visual outcomes for high myopic patients with or without myopic maculopathy: a 10 year follow up study. *Br J Ophthalmol*. (2006) 90:546–50. doi: 10.1136/bjo.2005.081992
  17. Oshima Y, Harino S, Tano Y. Scanning laser ophthalmoscope microperimetric assessment in patients with successful laser treatment for juxtafoveal choroidal neovascularization. *Retina Phila Pa*. (1998) 18:109–17. doi: 10.1097/00006982-199818020-00003
  18. Rinaldi M, Semeraro F, Chiosi F, Russo A, Romano MR, Savastano MC, et al. Reduced-fluence verteporfin photodynamic therapy plus ranibizumab for choroidal neovascularization in pathologic myopia. *Graefes Arch Clin Exp Ophthalmol Albrecht Von Graefes Arch Klin Exp Ophthalmol*. (2017) 255:529–39. doi: 10.1007/s00417-016-3498-4
  19. Fujii GY, De Juan E, Humayun MS, Sunness JS, Chang TS, Rossi JV. Characteristics of visual loss by scanning laser ophthalmoscope microperimetry in eyes with subfoveal choroidal neovascularization secondary to age-related macular degeneration. *Am J Ophthalmol*. (2003) 136:1067–78. doi: 10.1016/S0002-9394(03)00663-9
  20. Orr P, Rentz AM, Margolis MK, Revicki DA, Dolan CM, Colman S, et al. Validation of the National Eye Institute Visual Function Questionnaire-25 (NEI VFQ-25) in age-related macular degeneration. *Invest Ophthalmol Vis Sci*. (2011) 52:3354–9. doi: 10.1167/iovs.10-5645
  21. Busbee BG, Ho AC, Brown DM, Heier JS, Suñer IJ, Li Z, et al. Twelve-month efficacy and safety of 0.5 mg or 2.0 mg ranibizumab in patients with subfoveal neovascular age-related macular degeneration. *Ophthalmology*. (2013) 120:1046–1056. doi: 10.1016/j.ophtha.2012.10.014
  22. Xu K, Gupta V, Bae S, Sharma S. Metamorphopsia and vision-related quality of life among patients with age-related macular degeneration. *Can J Ophthalmol J Can Ophthalmol*. (2018) 53:168–72. doi: 10.1016/j.cjco.2017.08.006
  23. Sugawara T, Sato E, Baba T, Hagiwara A, Tawada A, Yamamoto S. Relationship between vision-related quality of life and microperimetry-determined macular sensitivity in patients with retinitis pigmentosa. *Jpn J Ophthalmol*. (2011) 55:643–6. doi: 10.1007/s10384-011-0080-9
  24. Murakami T, Okamoto F, Sugiura Y, Okamoto Y, Hiraoka T, Oshika T. Changes in metamorphopsia and optical coherence tomography findings after successful retinal detachment surgery. *Retina Phila Pa*. (2018) 38:684–91. doi: 10.1097/IAE.0000000000001588

**Conflict of Interest:** The authors declare that the research was conducted in the absence of any commercial or financial relationships that could be construed as a potential conflict of interest.

**Publisher's Note:** All claims expressed in this article are solely those of the authors and do not necessarily represent those of their affiliated organizations, or those of the publisher, the editors and the reviewers. Any product that may be evaluated in this article, or claim that may be made by its manufacturer, is not guaranteed or endorsed by the publisher.

Copyright © 2021 Li, Sun, Zhao, Zhang, Luo and Ding. This is an open-access article distributed under the terms of the Creative Commons Attribution License (CC BY). The use, distribution or reproduction in other forums is permitted, provided the original author(s) and the copyright owner(s) are credited and that the original publication in this journal is cited, in accordance with accepted academic practice. No use, distribution or reproduction is permitted which does not comply with these terms.



# Microvasculature Features of Vogt-Koyanagi-Harada Disease Revealed by Widefield Swept-Source Optical Coherence Tomography Angiography

## OPEN ACCESS

### Edited by:

Hetian Lei,  
Shenzhen Eye Hospital, China

### Reviewed by:

Han Zhang,  
The First Affiliated Hospital of China  
Medical University, China

Qianli Meng,  
Guangdong Provincial People's  
Hospital, China

Xiaorong Li,  
Tianjin Medical University Eye  
Hospital, China

### \*Correspondence:

Jin Yuan  
yuanjin@cornea@126.com  
Feng Wen  
wenfeng208@foxmail.com  
Wei Chi  
chiwei@mail.sysu.edu.cn

†These authors have contributed  
equally to this work

### Specialty section:

This article was submitted to  
Ophthalmology,  
a section of the journal  
Frontiers in Medicine

Received: 02 June 2021

Accepted: 16 September 2021

Published: 14 October 2021

### Citation:

Ye X, Zhang H, Xiao P, Wang G, Hu X,  
Yan C, Li F, Hu Y, Su L, Luo J, Yuan J,  
Wen F and Chi W (2021)  
Microvasculature Features of  
Vogt-Koyanagi-Harada Disease  
Revealed by Widefield Swept-Source  
Optical Coherence Tomography  
Angiography. *Front. Med.* 8:719593.  
doi: 10.3389/fmed.2021.719593

Xiaoyuan Ye<sup>1†</sup>, Haiping Zhang<sup>2,3†</sup>, Peng Xiao<sup>1</sup>, Gengyuan Wang<sup>1</sup>, Xiaoqing Hu<sup>1</sup>,  
Chun Yan<sup>1</sup>, Fan Li<sup>1</sup>, Yixin Hu<sup>1</sup>, Lishi Su<sup>1</sup>, Jiawen Luo<sup>1</sup>, Jin Yuan<sup>1\*</sup>, Feng Wen<sup>1\*</sup> and  
Wei Chi<sup>1\*</sup>

<sup>1</sup> State Key Laboratory of Ophthalmology, Zhongshan Ophthalmic Center, Sun Yat-sen University, Guangzhou, China, <sup>2</sup> Tianjin Aier Eye Hospital, Tianjin, China, <sup>3</sup> Aier Eye Institute, Changsha, China

**Background:** Vogt-Koyanagi-Harada (VKH) disease is a multisystem autoimmune disorder which could induce bilateral panuveitis involving the posterior pole and peripheral fundus. Optical coherence tomography angiography (OCTA) provides several advantages over traditional fluorescence angiography for revealing pathological abnormalities of the retinal vasculature. Until recently, however, the OCTA field of view (FOV) was limited to  $6 \times 6 \text{ mm}^2$  scans.

**Purpose:** This study examined retinal vasculature and choriocapillaris abnormalities across multiple regions of the retina ( $15 \times 9 \text{ mm}^2$  wide field, macular, peripapillary regions) among acute and convalescent VKH patients using a novel widefield swept-source OCTA (WSS-OCTA) device and assessed correlations between imaging features and best-corrected visual acuity (BCVA).

**Methods:** Twenty eyes of 13 VKH disease patients in the acute phase, 30 eyes of 17 patients in the convalescent phase, and 30 eyes of 15 healthy controls (HCs) were included in this study. Vascular length density (VLD) in superficial and deep vascular plexuses (SVP, DVP), vascular perfusion density (VPD) in SVP, DVP, and choriocapillaris (CC), and flow voids (FV) in CC were measured across multiple retinal regions via WSS-OCTA (PLEX Elite 9000, Carl Zeiss Meditec Inc., USA) using the  $15 \times 9 \text{ mm}^2$  scan pattern centered on the fovea and quantified by ImageJ.

**Results:** Compared to HCs, acute phase VKH patients exhibited significantly reduced SVP-VLD, SVP-VPD, and CC-VPD across multiple retinal regions (all  $p < 0.01$ ). Notably, the FV area was more extensive in VKH patients, especially those in the acute phase ( $p < 0.01$ ). These changes were reversed in the convalescent phase. Stepwise multiple linear regression analysis demonstrated that macular DVP-VLD and macular CC-VPD were the best predictive factors for BCVA in the acute and convalescent VKH groups.

**Conclusion:** The wider field of SS-OCAT provides more comprehensive and detailed images of the microvasculature abnormalities characterizing VKH disease.

The quantifiable and layer-specific information from OCTA allows for the identification of sensitive and specific imaging markers for prognosis and treatment guidance, highlighting WSS-OCTA as a promising modality for the clinical management of VKH disease.

**Keywords:** Vogt-Koyanagi-Harada disease, widefield swept-source optical coherence tomography angiography, vascular length density, vascular perfusion density, flow voids

## INTRODUCTION

Vogt-Koyanagi-Harada (VKH) disease is a multisystemic autoimmune disorder primarily afflicting pigmented tissues. In Asia, VKH disease is a relatively common vision-threatening disorder (1). The classic clinical characteristics are bilateral panuveitis, hypoacusis, meningitis, and cutaneous involvement such as poliosis, vitiligo, and alopecia (2). While the precise mechanisms underlying targeted pigmented tissue attack are still uncertain, it is likely that aberrant T cell-mediated inflammation contributes to disease initiation and maintenance (3, 4). Ophthalmic manifestations could involve the choroidal stroma, retinal pigment epithelium, and outer retina at the posterior pole and peripheral fundus. Inflammation of the choroidal stroma and retinal pigment epithelium layer (RPE) results in a series of changes, including choroidal depigmentation, sunset glow fundus (SGF), subretinal neovascularization, and even exudative retinal detachment (5–7). The clinical course of ophthalmic manifestations can be divided into four stages, prodromal, uveitic, chronic, and chronic recurrent, according to findings from multimodal ocular vascular imaging, traditional indocyanine green angiography (ICGA), fluorescein angiography (FA), and optical coherence tomography (OCT) (5). Injection of fluorescent dye into the circulation reveals characteristic vascular patterns that provide clues to disease progression (8). However, fluorescent imaging modalities (ICGA and FA) do not allow for quantitative analysis of retinal and choroidal blood flow characteristics. Moreover, there are inherent risks from intravenous administration of these dyes.

Optical coherence tomography angiography (OCTA) permits non-invasive, detailed, and depth-resolved imaging of the chorioretinal microvasculature in disease states such as diabetic retinopathy, age-related macular degeneration, retinal vein occlusion, and uveitis (9–15). In addition, several OCTA studies have documented changes in the chorioretinal microvasculature associated with VKH disease (16–24). However, traditional OCTA images provide a limited field-of-view, necessitating montage imaging. Further, the aforementioned OCTA studies analyzed limited vascular features.

The introduction of swept-source technology to OCTA has substantially expanded the potential field of view (FOV), which is particularly advantageous for disorders such as VKH disease afflicting broad regions of the retina. In this study, we enrolled VKH patients in acute and convalescent phases and used the newest PLEX Elite 9000 swept-source OCTA (SS-OCTA) system to capture widefield ( $15 \times 9 \text{ mm}^2$ ) OCTA images of the chorioretinal microvasculature in macular and peripapillary regions to provide a more detailed description of disease

progression and identify signs indicative of visual dysfunction and recovery.

## MATERIALS AND METHODS

### Study Population

This cross-sectional, observational study, included 20 eyes of 13 patients with acute VKH disease, 30 eyes of 17 VKH disease patients in the convalescent stage, and 30 eyes of 15 age-matched healthy volunteers without any ophthalmological and/or systemic disorders examined at the Zhongshan Ophthalmic Center from November 2019 to December 2020. Patients were diagnosed based on revised diagnostic criteria established by the First International Workshop on Vogt-Koyanagi-Harada (VKH) disease (25), and grouped according to disease stage. Patients initially diagnosed or receiving systemic corticosteroids for <2 weeks were considered in the acute stage. Among these patients, those with severe exudative retinal detachment, severe anterior chamber inflammation, or vitreous opacity were excluded, and the rest were allocated to the acute stage group. Alternatively, patients receiving systemic corticosteroids for over 3 months and showing no signs of acute ocular inflammation such as choroiditis, serous retinal detachment, disc edema, or exudative retinal detachment were included in the convalescent stage group.

All procedures were performed in compliance with the tenets of the Declaration of Helsinki, and the study was approved by the Ethics Committee of Zhongshan Ophthalmic Center (Guangzhou, China 2019KYPJ127). Written informed consent was obtained from each participant. The following data were collected for all participants: age, sex, best-corrected visual acuity (BCVA) as measured using a Snellen chart, and bilateral intraocular pressure. Patients also received slit-lamp microscopy, indirect fundus ophthalmoscopy, and FA examinations.

### Optical Coherence Tomography Angiography Acquisition

All widefield swept-source OCTA (WSS-OCTA) images were acquired using a PLEX Elite 9000 SS-OCTA device (Carl Zeiss Meditec Inc., USA) that simultaneously assesses the fundus with a central wavelength of 1,060 nm (1,000–1,100 nm full bandwidth) and operates at 100,000 A-scans per second. The system also includes an active eye-tracking system. For each eye, OCTA scans of  $15 \times 9 \text{ mm}^2$  centered on the fovea were performed after pupil dilation. All images were collected by the same experienced technician (Hu). Images with either substantial motion artifact or incorrect segmentation were excluded. Representative pictures are presented in **Figure 1**. To



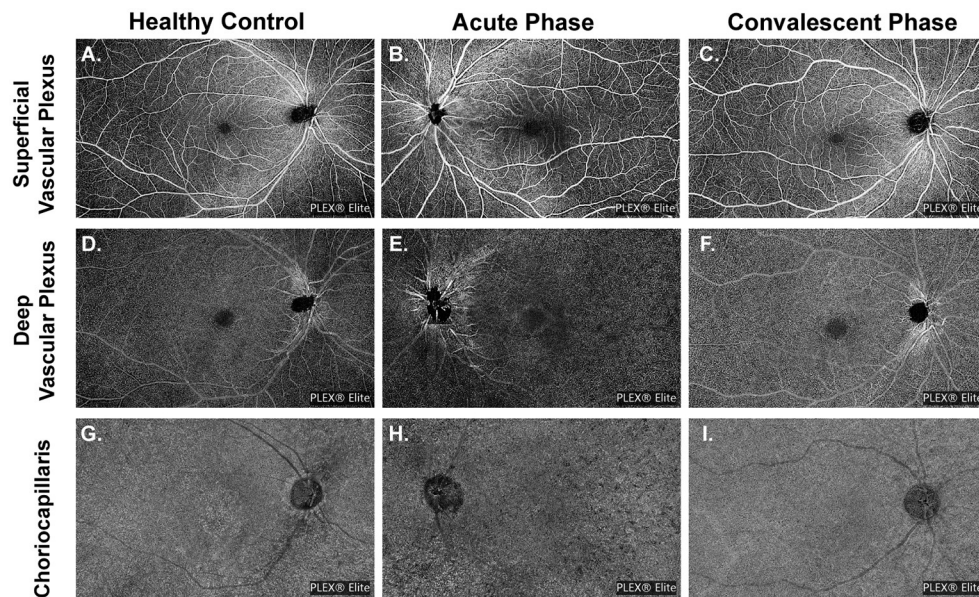


**FIGURE 1** | Demonstration of representative images of different slabs in three groups. **(A,D,G)** Slabs are from a healthy volunteer (No. 14, the right eye). **(B,E,H)** Slabs are from a patient with acute VKH disease (No. 12, the left eye). **(C,F,I)** Slabs are from a patient with quiescent VKH disease (No. 17, the right eye).

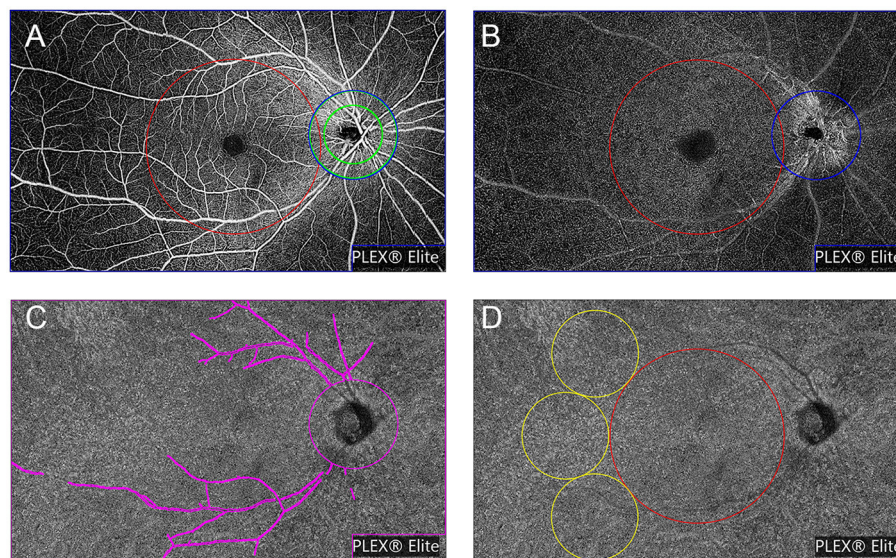
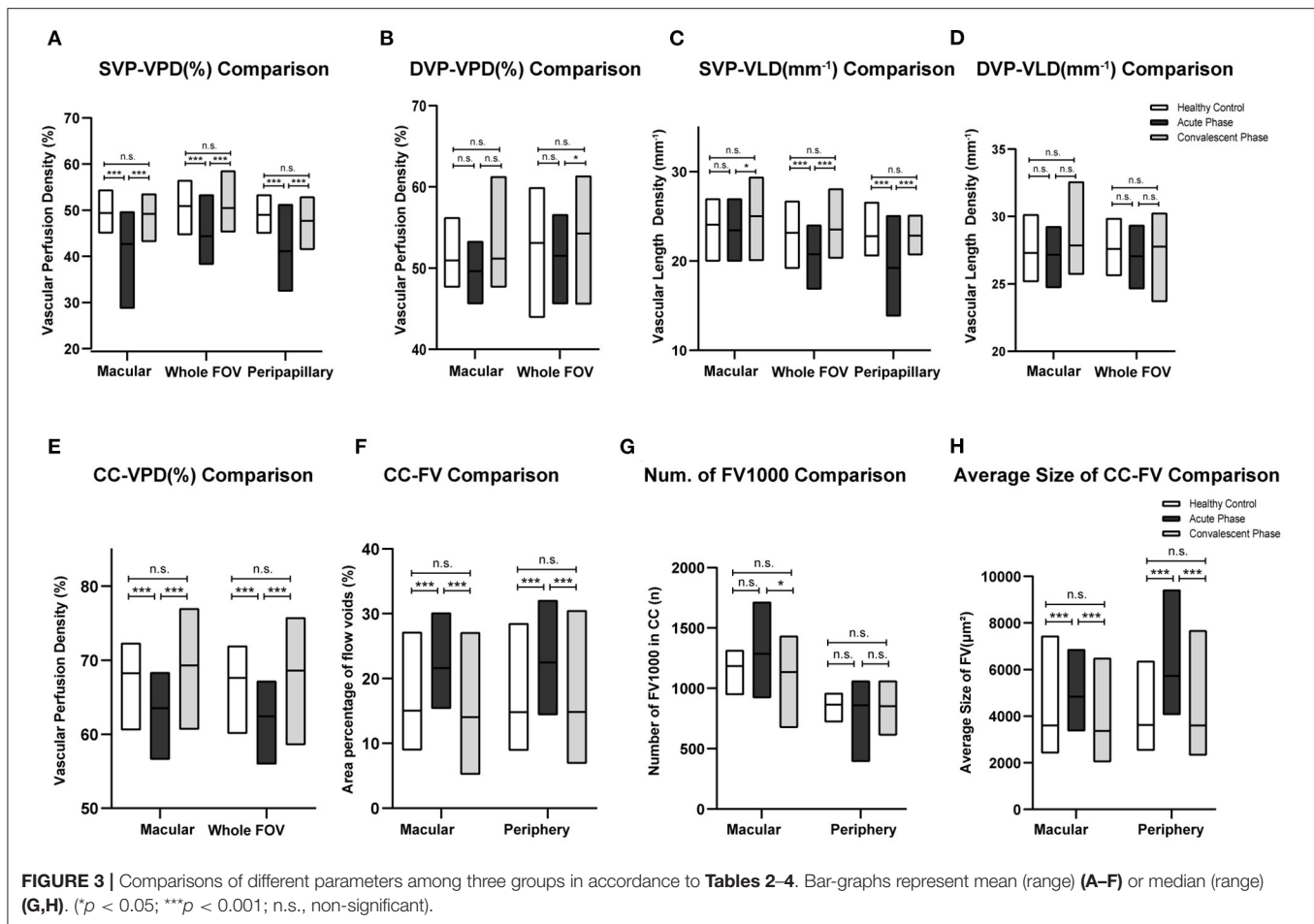


**FIGURE 2** | Representation of the regions used to explore OCTA parameters, slabs are from a healthy volunteer (No. 13, the right eye). OCTA parameters were investigated in different regions of the superficial vascular plexus (SVP) slab **(A)** and deep vascular plexus (DVP) slab **(B)**: (1) the macular region (red circle with a diameter of 6 mm centered at the fovea); (2) the peripapillary region (a 500  $\mu\text{m}$ -wide ring of 2 mm inner diameter and 3 mm outer diameter centered at the optic nerve head) (green annulus); and (3) the whole field of view (FOV) with optic papilla area (a 3 mm diameter circle) and the image label “PLEX® Elite” excluded (cropped) (blue polygon shape). **(C)** Representation of whole FOV removing the large retinal vessel mask used to explore OCTA parameters in choriocapillaris slab (shown in magenta). **(D)** Representation of regions to explore flow voids metrics: (1) the macular region (shown in red) and (2) the peripheral region (three 3 mm-diameter circles next to the macular region) (shown in yellow).

quantify the foveal avascular zone (FAZ), vascular length density (VLD), vascular perfusion density (VPD), and flow voids (FV) across regions and layers, all images were first segmented using built-in software. Segmentation lines defining the inner limiting

membrane (ILM), inner plexiform layer (IPL), outer plexiform layer (OPL), and RPE were automatically delineated in each B-scan. Any notable segmentation error was manually corrected. Image slabs were generated to reveal the superficial retinal



vascular plexus (SVP) (from the ILM to the outer boundary of IPL), the deep retinal vascular plexus (DVP) (from the outer boundary of IPL to the outer boundary of OPL), and the choriocapillaris (CC) (derived from a 10  $\mu\text{m}$  slab 31–40  $\mu\text{m}$  below the RPE) as previously described (26). Projection artifacts caused by the overlying retinal circulation were removed using built-in software.

## Image Processing and Measurements of the Parameters

All images were checked independently by two trained graders (Ye and Zhang). The OCTA slabs were processed and analyzed according to the procedure used in previous works (16, 27–30). Each OCTA slab was loaded into ImageJ (National Institutes of Health, Bethesda, Maryland, USA; <https://imagej.net/Welcome>) to measure FAZ, VLD or VPD, and FV parameters as follows. The area and perimeter of the FAZ from the SVP slab were measured by two trained graders by manually outlining the FAZ border in ImageJ and measuring the area and length. The Acircularity Index (AI), defined as the ratio of the FAZ perimeter to the perimeter of a circle with equal area (16), was introduced to describe the acircularity of FAZ shape. “Vascular Perfusion Density” is defined as the fraction of area covered by vessels in an enface slab view (more specifically, the ratio of the vessel area to the total region of interest or ROI), and ranges from

0 (no perfusion) to 1 (fully perfused). The procedure for VPD quantification was as follows. First, images were converted to 8-bit format. Second, the ROI tool in ImageJ was used to select the target regions for analysis, which included the macular region (a 6 mm diameter circle centered at the fovea), the peripapillary area (a 500  $\mu\text{m}$ -wide ring of 2 mm inner diameter and 3 mm outer diameter centered at the optic nerve head), and the whole field of view (whole FOV) with optic papilla area (a 3 mm diameter circle) and the image label “PLEX® Elite” excluded (cropped). Next, images were binarized using commands “Huang’s fuzzy” for SVP and DVP slabs or “Phansalkar method” with radius = 15 for CC slabs (27). Finally, the fractional area of vessels within the ROI (or the perfusion density) was measured. To remove large vessel projection artifacts within the 15  $\times$  9 mm<sup>2</sup> CC slab, we obtained a large retinal vessel mask from the SVP slab by applying “Default” threshold and then used the ImageJ “wand tool” to select the region representing the large vessels. The superficial retinal vessels were successively masked from the CC slab and then the CC slab was binarized using the “Phansalkar method.” Detailed procedures are provided in **Figure 2**.

“Vascular Length Density” is defined as the vessel length per unit area (31). As far as we know the VPD algorithm is greatly influenced by large blood vessels, and has low sensitivity for detecting capillary changes. Alternatively, the VLD algorithm can more sensitively detect changes in small blood



**TABLE 1 |** Demographic and clinical characteristics of study groups.

	Healthy controls	Acute phase	Convalescent phase	p-Value
Number of eyes/individuals	30/15	20/13	30/17	
Age (years)	34 (26–58)	34 (27–53)	36 (29–43)	0.971*
Sex, male/female	5/10	8/5	9/8	0.302 <sup>†</sup>
BCVA (LogMAR)	NA	0.60 ± 0.35 (0.20–1.30)	0.42 ± 0.28 (0.00–0.92)	0.012 <sup>‡</sup>
FAZ (mm <sup>2</sup> )	0.409 ± 0.090 (0.253–0.568)	0.334 ± 0.116 (0.168–0.543)	0.347 ± 0.110 (0.184–0.518)	0.055 <sup>§</sup>
AI	1.133 ± 0.048 (1.062–1.201)	1.122 ± 0.047 (1.050–1.182)	1.133 ± 0.034 (1.080–1.195)	0.869 <sup>§</sup>

BCVA, best-corrected visual acuity; FAZ, foveal avascular zone; AI, acircularity index. Data are presented as Mean ± SD (range) or Median (P25–P75), unless otherwise indicated.

\*Kruskal–Wallis test.

<sup>†</sup>Chi-square test.

<sup>‡</sup>Student t-test.

<sup>§</sup>One-way ANOVA.

**TABLE 2 |** The vascular perfusion density (VPD) measurements in different slabs and regions.

VPD (%)	Healthy controls	Acute phase	Convalescent phase	p	p <sup>a</sup>	p <sup>b</sup>	p <sup>c</sup>
<b>SVP</b>							
Macular	49.41 ± 2.55, (48.46–50.36)	42.70 ± 5.14, (40.30–45.11)	49.24 ± 2.39, (48.35–50.13)	<0.001*	<0.001	0.907	<0.001
Whole FOV	50.95 ± 3.52, (49.64–52.27)	44.41 ± 4.48, (42.31–46.51)	50.46 ± 3.98, (49.35–51.58)	<0.001*	<0.001	1.000	<0.001
Peripapillary	49.04 ± 2.53, (48.10–49.99)	41.15 ± 5.73, (38.47–43.83)	47.72 ± 2.60, (46.75–48.69)	<0.001 <sup>†</sup>	<0.001	0.484	<0.001
<b>DVP</b>							
Macular	50.93 ± 2.24, (50.10–51.77)	49.63 ± 2.38, (48.52–49.66)	51.17 ± 2.96, (50.10–52.28)	0.101*	0.251	1.000	0.123
Whole FOV	53.10 ± 3.59, (51.76–54.44)	51.52 ± 3.38, (49.94–53.10)	54.25 ± 4.32, (52.64–55.86)	0.054*	0.474	0.746	0.048
<b>CC</b>							
Macular	68.23 ± 2.67, (67.24–69.23)	63.53 ± 2.83, (62.21–64.86)	69.30 ± 4.34, (67.68–70.92)	<0.001*	<0.001	0.069	<0.001
Whole FOV	67.59 ± 2.62, (66.61–68.57)	62.42 ± 3.01, (61.01–63.83)	68.61 ± 4.61, (66.89–70.33)	<0.001*	<0.001	0.083	<0.001

VPD, vascular perfusion density; SVP, superficial vascular plexus; DVP, deep vascular plexus; CC, choriocapillaris; FOV, field of view. Data are presented as mean ± SD, (95%CI).

\*One-Way ANOVA followed by Bonferroni post-hoc test.

<sup>†</sup>Kruskal–Wallis test followed by Bonferroni post-hoc test.

p<sup>a</sup>: p-value between Healthy Controls and Acute VKH patients.

p<sup>b</sup>: p-value between Healthy Controls and VKH patients in convalescent phase.

p<sup>c</sup>: p-value between Acute VKH patients and VKH patients in convalescent phase.

vessels and capillaries. To calculate VLD, we binarized the slab using the “Huang’s fuzzy” command and then skeletonized the binary image, followed by measurement of vessel length in the ROI and calculation of VLD as described previously (31, 32). Choriocapillaris flow voids (CC-FV), also termed flow deficit in other studies, is defined as the area lacking flow or with flow below the detectable threshold of OCTA (28, 29). Flow voids were calculated in the macular region (a 6 mm-diameter circle centered at the fovea) and the peripheral region (three 3 mm-diameter circles next to the macular region). Flow void metrics, including total flow void area fraction (ROI area divided by total

flow void area), number of FV, and average size of FV, were calculated for FV area > 1,000 μm<sup>2</sup> (FV1,000) using the “Analyze Particles” function in ImageJ (30).

## Statistical Analysis

All statistical analyses were conducted using SPSS software 22 (SPSS Inc., Chicago, IL). Continuous variables were first tested for normality using the Shapiro–Wilk test and then for homogeneity of variance. Normally distributed variables are presented as mean ± standard deviation (SD) and variables following a skewed distribution as median and 25th percentile to

**TABLE 3 |** The vascular length density (VLD) measurements in different slabs and regions.

VLD (mm <sup>-1</sup> )	Healthy controls	Acute phase	Convalescent phase	<i>p</i>	<i>p</i> <sup>a</sup>	<i>p</i> <sup>b</sup>	<i>p</i> <sup>c</sup>
<b>SVP</b>							
Macular	24.07 ± 1.91, (23.36–24.79)	21.88 ± 2.54, (20.69–23.07)	24.69 ± 2.04, (23.93–25.45)	0.013*	0.692	0.17	0.013
Whole FOV	23.15 ± 1.88, (22.45–23.85)	20.07 ± 1.91, (19.87–21.66)	23.54 ± 1.54, (22.96–24.11)	<0.001*	<0.001	1	<0.001
Peripapillary	22.79 ± 1.37, (22.28–23.30)	19.21 ± 2.94, (17.84–20.59)	22.84 ± 1.35, (22.34–23.35)	<0.001*	<0.001	1	<0.001
<b>DVP</b>							
Macular	27.29 ± 1.13, (26.87–27.71)	27.16 ± 1.30, (26.55–27.76)	27.86 ± 1.68, (27.23–28.48)	0.157*	1	0.36	0.263
Whole FOV	27.60 ± 1.01, (27.22–27.97)	27.05 ± 1.35, (26.41–27.68)	27.77 ± 1.71, (27.13–28.41)	0.19*	0.52	1	0.224

VPD, vascular perfusion density; SVP, superficial vascular plexus; DVP, deep vascular plexus; CC, choriocapillaris; FOV, field of view. Data are presented as mean ± SD, (95%CI).

\*One-Way ANOVA followed by Bonferroni post-hoc test.

*p*<sup>a</sup>: *p*-value between Healthy Controls and Acute VKH patients.

*p*<sup>b</sup>: *p*-value between Healthy Controls and VKH patients in convalescent phase.

*p*<sup>c</sup>: *p*-value between Acute VKH patients and VKH patients in convalescent phase.

**TABLE 4 |** The flow void parameters in CC slab.

Flow voids	Healthy controls	Acute phase	Convalescent phase	<i>p</i>	<i>p</i> <sup>a</sup>	<i>p</i> <sup>b</sup>	<i>p</i> <sup>c</sup>
<b>Macular (6 × 6 mm<sup>2</sup>)</b>							
Flow void area (%)	14.80 ± 3.84, (13.54–16.54)	21.61 ± 3.80, (19.82–23.39)	14.86 ± 5.87, (11.89–16.19)	<0.001*	<0.001	1.000	<0.001
Number of FV1,000 ( <i>n</i> )	1182.00 (1140.25–1246.25)	1285.00 (1204.00–1335.00)	1211.50 (973.50–1273.25)	0.007 <sup>†</sup>	0.092	0.635	0.004
Average size (μm <sup>2</sup> )	3332.50 (2911.75–3687.25)	4901.50 (3998.00–5332.50)	3316.00 (2466.50–3940.00)	<0.001 <sup>†</sup>	<0.001	1.000	<0.001
<b>Periphery</b>							
Flow void area (%)	15.04 ± 4.03, (13.37–16.24)	22.49 ± 4.49, (20.39–24.59)	14.04 ± 5.98, (12.67–18.84)	<0.001*	<0.001	1.000	<0.001
Number of FV1,000 ( <i>n</i> )	868.00 (834.75–921.50)	907.50 (835.50–964.25)	901.50 (710.50–953.25)	0.513 <sup>†</sup>	1.000	1.000	1.000
Average size (μm <sup>2</sup> )	3397.00 (3070.75–3948.00)	5607.50 (4450.50–6625.50)	3548.00 (2726.25–4208.00)	<0.001 <sup>†</sup>	<0.001	1.000	<0.001

FV1,000, flow void area >1,000 μm<sup>2</sup>. Data are presented as mean ± SD, (95%CI) or median (P25–P75).

\*One-Way ANOVA followed by Bonferroni post-hoc test.

<sup>†</sup> Kruskal-Wallis test followed by Bonferroni post-hoc test.

*p*<sup>a</sup>: *p*-value between healthy controls and acute VKH patients.

*p*<sup>b</sup>: *p*-value between healthy controls and VKH patients in convalescent phase.

*p*<sup>c</sup>: *p*-value between acute VKH patients and VKH patients in convalescent phase.

75th percentile range (P25–P75). Means of parametric datasets were compared by one-way analysis of variance (ANOVA) and non-parametric datasets by the Kruskal–Wallis test, followed by *post-hoc* Bonferroni test or Student *t*-test for pair-wise comparisons. Correlations between parametric variables and logMAR BCVA were analyzed using Pearson Correlation analysis. Stepwise multiple linear regression analysis was run to detect the significant predictors of BCVA. A *p* < 0.05 was considered statistically significant for all tests.

## RESULTS

### Study Population Characteristics

Twenty eyes of 13 patients in the acute phase of VKH disease, 30 eyes of 17 patients in the convalescent phase of VKH disease, and 30 eyes of 15 age-matched healthy controls (HCs) were included in this study. Images of 10 eyes with VKH disease were excluded due to significant motion artifacts or incorrect segmentation. Best-corrected visual acuity of the HCs was not

available. The demographic and clinical characteristics of study groups are summarized in **Table 1**.

## Widefield OCTA Parameters of Each Group FAZ and AI

The FAZ was smaller in eyes of patients with acute or convalescent VKH disease compared to control eyes, while AI was smaller in acute VKH disease eyes than convalescent VKH disease or control eyes. However, neither difference reached statistical significance ( $p = 0.055$  and  $0.0869$ , respectively) (**Table 1**).

## Vascular Perfusion Density and Vascular Length Density

The VPD of the SVP (SVP-VPD) was significantly lower in the peripapillary region, macular region, and whole FOV of acute VKH disease patients compared to HCs and convalescent VKH disease patients (all  $p < 0.001$ ). The same tendency was observed in CC and DVP slabs of the macular region and whole FOV scans. The CC-VPD was also significantly lower in acute VKH disease patients compared to convalescent patients and HCs (both  $p < 0.001$ ). DVP-VPD was also lower in acute phase patients compared to convalescent patients within whole FOV ( $p < 0.05$ ). Compared to HCs, convalescent VKH patients exhibited slightly decreased SVP-VPD and modest increased CC-VPD and DVP-VPD in multiple regions but without statistical significance (**Table 2**) and (**Figures 3A,B**). Group differences in VLD roughly mirrored those of VPD, albeit with a few notable differences. In contrast to VPD differences between HCs and convalescent VKH patients, the SVP-VLD of convalescent VKH patients was slightly greater in three regions compared to HCs, but again without reaching statistical significance (**Table 3**) and (**Figures 3C,D**).

## Flow Voids in Choriocapillaris

Acute-stage VKH patients exhibited significantly larger FV area fractions and average FV sizes in both macular and peripheral retinal regions compared to convalescent-stage patients and HCs (all  $p < 0.001$ ). Compared to HCs, convalescent-stage patients exhibited a smaller FV area fraction but larger numbers of FV1,000 (single flow void area  $>1\,000\ \mu\text{m}^2$ ) and larger mean FV1,000 area size in the peripheral region; however, these differences did not reach statistical significance. Details of these comparisons are presented in **Table 4** and (**Figures 3E-H**).

## Correlations Between OCTA Parameters and BCVA

To identifying those parameters most strongly associated with BCVA and thus of potential prognostic or diagnostic utility, we conducted Pearson correlation analysis (**Table 5**). There were strong negative correlations between BCVA and macular DVP-VLD in patients with acute VKH. While at convalescent stage, macular SVP-VPD and parameters in CC have a stronger correlation with BCVA. Stepwise multiple linear regression analysis demonstrated that macular DVP-VLD and macular CC-VPD were the best predictive factors for BCVA in the acute and convalescent VKH groups (**Table 6**).

**TABLE 5 |** Correlation of best-corrected visual acuity with the parameters of VKH patients in acute phase and convalescent phase.

BCVA (LogMAR)	Acute phase		Convalescent phase	
	<i>r</i>	<i>p</i> -value	<i>r</i>	<i>p</i> -value
<b>SVP-VPD</b>				
Macular	0.298	0.201	−0.445*	0.014
Whole FOV	−0.143	0.549	−0.340	0.066
Peripapillary	0.049	0.837	0.076	0.692
<b>SVP-VLD</b>				
Macular	0.381	0.098	−0.210	0.265
Whole FOV	−0.089	0.709	−0.240	0.201
Peripapillary	0.193	0.415	0.275	0.141
<b>DVP-VPD</b>				
Macular	−0.367	0.112	0.088	0.644
Whole FOV	−0.132	0.580	−0.353	0.055
<b>DVP-VLD</b>				
Macular	−0.500*	0.025	0.060	0.752
Whole FOV	−0.154	0.516	−0.303	0.104
<b>CC-VPD</b>				
Macular	−0.243	0.301	−0.441*	0.015
Whole FOV	−0.370	0.108	−0.373*	0.042
<b>Macular CC-FV</b>				
Flow void area (%)	0.235	0.319	0.414*	0.023
<b>Peripheral CC-FV</b>				
Flow void area (%)	0.149	0.532	0.365*	0.047

*r*, Pearson correlation coefficient. VPD, vascular perfusion density; VLD, vascular length density; SVP, superficial vascular plexus; DVP, deep vascular plexus; CC, choriocapillaris; FV, flow voids; FOV, field of view. \* $p < 0.05$ .

## DISCUSSION

Vogt-Koyanagi-Harada disease is a multisystemic autoimmune disorder that attacks tissues containing melanin, and thus mainly damages the RPE and choroid in the eyes (2). Acute uveitic phase is characterized by acute, bilateral and diffuse uveitis; hyperemia and edema of the optic disk; choroidal thickening and serous retinal detachment (33, 34). As the disease progresses, there can be signs of SGF or RPE clumping/migration, Dalen-Fuchs nodules or multifocal chorioretinal atrophy (34). Multiple imaging modalities have been used to examine the choroidal features in different stages of VKH disease. On fluorescein fundus angiography (FFA), the retina exhibited disseminated spotted choroidal hyperfluorescence and choroidal hypofluorescence in both acute and chronic uveitic stages (35), while ICGA showed hypofluorescent dark dots during initial acute VKH uveitis episodes that usually resolved after therapy (36). Laser speckle flowgraphy (LSFG), which can non-invasively visualize the hemodynamics of choroidal circulation, revealed inflammation-related impairment in choroidal blood flow velocity at the macula that was again improved by systemic corticosteroid therapy (37).

Optical coherence tomography angiography is a new non-invasive imaging technique that can detect the movement of erythrocytes within blood vessels (9). Compared to spectral-domain OCT (SD-OCT), swept-source OCT (SS-OCT) is able

**TABLE 6 |** Stepwise Multiple Linear Regression Analysis for the Predictors of LogMAR BCVA.

Model summary (acute phase)		$R^2$	Adjusted $R^2$	P-value
		0.250	0.209	0.025
Variable	Unstandardized coefficients		Standardized coefficients	
	B	Std. error	Beta	
(Constant)	4.675	1.638		0.011
Macular DVP-VLD	-0.148	0.060	-0.500	0.025
Model summary (convalescent phase)		$R^2$	Adjusted $R^2$	P-value
		0.425	0.358	0.030
Variable	Unstandardized coefficients		Standardized coefficients	
	B	Std. error	Beta	
(Constant)	5.309	1.141		0.000
Macular SVP-VPD	-0.033	0.020	-0.261	0.113
Macular CC-VPD	-0.028	0.011	-0.415	0.014
Whole FOV DVP-VPD	-0.025	0.011	-0.356	0.030

VPD, vascular perfusion density; VLD, vascular length density; SVP, superficial vascular plexus; DVP, deep vascular plexus; CC, choriocapillaris; FV, flow voids; FOV, field of view;  $R^2$ , regression coefficient; Std. error, standard error.

to incorporate longer wavelengths (1,040 to 1,060 nm) and to simultaneously provide images of the vitreous, retina, and choroid (9), yielding high-resolution near-complete images of choroidal anatomy and CC perfusion (38). Therefore, SS-OCTA is a better imaging modality tool for detailed chorioretinal angiography than SD-OCTA.

Flow voids appear as dark foci in the OCTA CC slab and multiple studies have demonstrated that most FV revealed by OCTA correspond to hypofluorescent spots on ICGA images (19, 24, 39–42) and hyporeflective spots on enhanced-depth imaging (EDI)-OCT (43). Aggarwal et al. reported that the CC FV on OCTA images reflected true CC ischemia instead of a shadowing effect from overlying subretinal fluid and RPE detachment as was observed in central serous chorioretinopathy (19). Thus, hypoperfusion spots in CC may be attributed to choroidal granulomas (24, 39) or blood flow perturbation caused by choroidal vessel inflammation (39).

In our study, VKH disease patients demonstrated increased CC-FV and FV average size during the acute phase but not the convalescent phase, consistent with previous studies reporting that systemic corticosteroids can mitigate FV (17, 22, 24, 40). Indeed, the CC-FV observed in convalescent-stage VKH disease patients did not differ significantly from those measured in HCs. Further, the CC-FV area fraction and CC-VPD correlated strongly with logMAR BCVA during the convalescent phase. The CC-VPD was also dramatically reduced during the acute stage but fully restored during the convalescent phase, in contrast to several previous reports (21–23, 44). We speculate that this reflects effective recovery of CC blood flow after appropriate treatment. These positive correlations strongly suggest that choroidal granulomas and persistent inflammation contribute to the vision impairment in VKH disease. Consistent with

this notion, Wintergerst et al. reported a case of acute VKH syndrome with massively hypoperfusion in Sattler's layer on OCTA that fully resolved after 4 weeks of treatment concomitant with improved BCVA (20). However, that study was the first to use SS-OCTA for evaluation of CC abnormalities in VKH, so differences in detection device, retinal region, and (or) retinal stratification may have accounted for changes between pre- and post-treatment.

Luo et al. divided acute VKH patients into two subgroups (1 and 2) according to choroid flow area (21), while in the current study we did not observe the subgroup 1 showing significantly enhanced capillary signals, possibly due to the small sample size. Moreover, perfusion density in the CC and flow void size were correlated with visual acuity in our study, suggesting that higher perfusion density [or greater flow area as described by Luo et al. (21)] predict better visual outcome.

In addition to CC, OCTA also allows visualization and quantitative analyses of retinal vessel morphology and perfusion in SVP and DVP slabs. Many researches have revealed a decrease of vascular density when inflammation occurs in fundus, such as Behçet Uveitis (10) and retinal vasculitis (45). Correspondingly, SVP-VPD was markedly reduced in acute VKH disease patients, and a similar trend was also found for the DVP (but did not reach significance). Previous studies have reported similar findings for the SVP, while others have found greater changes in the DVP (16, 23). Different stratification methods may account for these discrepancies. Compared to VPD, the alteration in VLD was relative mild. The SVP-VLD of convalescent VKH disease patients was slightly increased compared to HCs. Though these values were not statistically significant, based on the fact that a minority of VKH patients will develop macular choroidal neovascularization (46), the difference suggests that

flow through small blood vessels and capillaries may increase during the convalescent phase as a compensatory mechanism against ischemia caused by inflammation.

A classic manifestation of acute VKH disease revealed by fundus photography is hyperemia and by FFA, hyperfluorescence around the optic disc (35). Surprisingly, however, we found that the peripapillary region VPD was lower among acute VKH disease patients. Therefore, we suggest that inflammation may also affect small vessels near the optic disc. Indeed, peripapillary blood flow is also reduced in patients with optic neuritis (47–49). However, we cannot exclude possible papilledema as eyes afflicted with optic neuritis also showed decreased blood flow (48). Further studies are awaited.

In the current study, logMAR BCVA was strongly correlated with DVP-VLD despite the insignificant changes in DVP among acute VKH disease patients compared to convalescent patients and controls. This may be due to enhanced importance of the DVP for outer retina perfusion when the choroid is ischemic (23). Pearson correlation analysis showed parameters in CC slab correlate best with BCVA and stepwise multiple linear regression analysis demonstrated that macular CC-VPD were the best predictive factors for BCVA in the convalescent VKH group. The results indicated a more significant role of CC slab than SVP/DVP in convalescent VKH disease.

Limitations of this study include the modest sample size and grouping based mainly on manifestations in the eye rather than more extensive clinical features. Further, patients received different treatment regimens. Manual correction for inaccuracies of retinochoroidal layer segmentation in images acquired using PLEX 9000 OCTA (performed in this study) may lead to errors in vessel density and perfusion calculations.

To the best of our knowledge, this is the first study to apply a SS-OCTA device to capture widefield  $15 \times 9 \text{ mm}^2$  images revealing microvasculature changes associated with VKH disease. The large imaging field avoids potential mistakes of montage pictures thus allow for better simultaneous observation of macular and peripapillary areas in fundus thereby mitigating the many potential errors inherent in analysis of montages. We explore the peripapillary microvasculature for the first time. Besides, we also calculate the total length of blood vessel per unit area (vessel length density) in the retina of VKH patients, which

offers a fresh perspective to explore vascular changes in VKH disease. Further studies are needed to confirm our results.

In conclusion, the quantifiable and layer-specific characteristics of wider field SS-OCTA enable better evaluation of the microvasculature features of VKH disease and identification of superior markers for prognosis and treatment guidance.

## DATA AVAILABILITY STATEMENT

The raw data supporting the conclusions of this article will be made available by the authors, without undue reservation.

## ETHICS STATEMENT

The studies involving human participants were reviewed and approved by Guangzhou, China 2019KYPJ127, Medical Ethics Committee of Zhongshan Ophthalmic Center, Sun Yat-sen University (Guangzhou, China). Written informed consent to participate in this study was provided by the participants' legal guardian/next of kin.

## AUTHOR CONTRIBUTIONS

WC, JY, FW, XY, and HZ contributed to conception and design of the study. XH, LS, and JL conducted the OCTA imaging. XY, HZ, PX, and GW processed the images and organized the database. XY, HZ, and FL performed the statistical analysis. XY, HZ, CY, and YH wrote the first draft of the manuscript. JY and WC wrote sections of the manuscript. All authors contributed to manuscript revision, read, and approved the submitted version.

## FUNDING

This work was supported by National Natural Science Foundation of China (no. 82070950) and Science and Technology Program of Guangzhou of WC (no. 201804010415).

## ACKNOWLEDGMENTS

We would like to acknowledge the assistance of Guandi Chen at Zhongshan Ophthalmic Center for her contribution to assisting in examining the patients and providing images.

## REFERENCES

- Du L, Kijlstra A, Yang P. Vogt-Koyanagi-Harada disease: novel insights into pathophysiology, diagnosis and treatment. *Prog Retin Eye Res.* (2016) 52:84–111. doi: 10.1016/j.preteyeres.2016.02.002
- Greco A, Fusconi M, Gallo A, Turchetta R, Marinelli C, Macri GF, et al. Vogt-Koyanagi-Harada syndrome. *Autoimmun Rev.* (2013) 12:1033–8. doi: 10.1016/j.autrev.2013.01.004
- Bordaberry MF. Vogt-Koyanagi-Harada disease: diagnosis and treatments update. *Curr Opin Ophthalmol.* (2010) 21:430–5. doi: 10.1097/ICU.0b013e32833eb78c
- Fang W, Yang P. Vogt-koyanagi-harada syndrome. *Curr Eye Res.* (2008) 33:517–23. doi: 10.1080/02713680802233968
- Moorthy RS, Inomata H, Rao NA. Vogt-Koyanagi-Harada syndrome. *Surv Ophthalmol.* (1995) 39:265–92. doi: 10.1016/S0039-6257(05)80105-5
- Magliyah MS, Al-Fakhri AS, Al-Dhibi HA. Proliferative retinopathy as a feature of Vogt Koyanagi Harada Disease: a report of two cases. *BMC Ophthalmol.* (2020) 20:470. doi: 10.1186/s12886-020-01736-y
- Ipek SC, Ayhan Z, Emre S, Saatci AO. Favorable clinical outcome with intravitreal aflibercept treatment in a case with bilateral choroidal neovascular membrane and quiescent Vogt-Koyanagi-Harada syndrome. *GMS Ophthalmol Cases.* (2020) 10:Doc23. doi: 10.3205/oc000150
- Agrawal R, Li LK, Nakhate V, Khandelwal N, Mahendradas P. Choroidal vascularity index in Vogt-Koyanagi-Harada disease: an EDI-OCT derived tool for monitoring disease progression. *Transl Vis Sci Technol.* (2016) 5:7. doi: 10.1167/tvst.5.4.7



9. Lains I, Wang JC, Cui Y, Katz R, Vingopoulos F, Staurengi G, et al. Retinal applications of swept source optical coherence tomography (OCT) and optical coherence tomography angiography (OCTA). *Prog Retin Eye Res.* (2021) 2021:100951. doi: 10.1016/j.preteyeres.2021.100951
10. Khairallah M, Abroug N, Khohtali S, Mahmoud A, Jelliti B, Coscas G, et al. UVEITIS. *Retina.* (2017) 37:1678–91. doi: 10.1097/IAE.0000000000001418
11. Toto L, Borrelli E, Di Antonio L, Carpineto P, Mastropasqua R. Retinal vascular. Plexuses' changes in dry age-related macular degeneration, evaluated by means of optical coherence tomography angiography. *Retina.* (2016) 36:1566–72. doi: 10.1097/IAE.0000000000000962
12. Arrigo A, Aragona E, Bordato A, Amato A, Borghesan F, Bandello F, et al. Quantitative OCTA parameter variations after treatment of macular neovascularization secondary to age-related macular degeneration. *Retina.* (2020) 41:1463–9. doi: 10.1097/IAE.0000000000003065
13. Bae K, Bang SK, Kang SW, Kim ES, Yu SY. Gap in capillary perfusion and burden of treatment in branch retinal vein occlusion: a wide-field optical coherence tomography angiography study. *Retina.* (2020) 41:1227–35. doi: 10.1097/IAE.0000000000003006
14. Kawai K, Uji A, Murakami T, Kadamoto S, Oritani Y, Dodo Y, et al. Image evaluation of artificial intelligence supported optical coherence tomography angiography imaging using OCT-HS100 device in diabetic retinopathy. *Retina.* (2020) 41:1730–8. doi: 10.1097/IAE.0000000000003101
15. Borrelli E, Sacconi R, Brambati M, Bandello F, Querques G. In vivo rotational three-dimensional OCTA analysis of microaneurysms in the human diabetic retina. *Sci Rep.* (2019) 9:16789. doi: 10.1038/s41598-019-53357-1
16. Karaca I, Yilmaz SG, Afrashi F, Nalçacı S. Assessment of macular capillary perfusion in patients with inactive Vogt-Koyanagi-Harada disease: an optical coherence tomography angiography study. *Graefes Arch Clin Exp Ophthalmol.* (2020) 258:1181–90. doi: 10.1007/s00417-020-04676-x
17. Vingopoulos F, Cui Y, Katz R, Le R, Zhu Y, Wang JC, et al. Widefield swept-source OCTA in Vogt-Koyanagi-Harada disease. *Ophthalmic Surg Lasers Imaging Retina.* (2020) 51:407–12. doi: 10.3928/23258160-20200702-06
18. Fan S, Lin D, Hu J, Cao J, Wu K, Li Y, et al. Evaluation of microvasculature alterations in convalescent Vogt-Koyanagi-Harada disease using optical coherence tomography angiography. *Eye (Lond).* (2020). doi: 10.1038/s41433-020-01210-5
19. Aggarwal K, Agarwal A, Deokar A, Mahajan S, Singh R, Bansal R, et al. Distinguishing features of acute Vogt-Koyanagi-Harada disease and acute central serous chorioretinopathy on optical coherence tomography angiography and en face optical coherence tomography imaging. *J Ophthalmic Inflamm Infect.* (2017) 7:3. doi: 10.1186/s12348-016-0122-z
20. Wintergerst MWM, Herrmann P, Finger RP. Optical coherence tomography angiography for evaluation of Sattler's layer in Vogt-Koyanagi-Harada disease. *Ophthalmic Surg Lasers Imaging Retina.* (2018) 49:639–42. doi: 10.3928/23258160-20180803-14
21. Luo K, Cai H, Hu Y, Jin C, Gan X, Deng Y, et al. Distinguishing microvasculature features of vogt-koyanagi-harada in patients in acute and convalescent phases using optical coherence tomography angiography. *Ocul Immunol Inflamm.* (2020) 29:465–71. doi: 10.1080/09273948.2019.1695856
22. Khan HA, Iqbal F, Shahzad MA, Khan QA, Rashid F, Sharjeel M, et al. Textural properties of choriocapillaris on OCTA in healed inflammatory choriocapillaropathies. *Ophthalmic Surg Lasers Imaging Retina.* (2019) 50:566–72. doi: 10.3928/23258160-20190905-05
23. Liang A, Zhao C, Jia S, Gao F, Han X, Pei M, et al. Retinal microcirculation defects on OCTA correlate with active inflammation and vision in Vogt-Koyanagi-Harada disease. *Ocul Immunol Inflamm.* (2020) 2020:1–7. doi: 10.1080/09273948.2020.1751212
24. Aggarwal K, Agarwal A, Mahajan S, Invernizzi A, Mandadi SKR, Singh R, et al. The role of optical coherence tomography angiography in the diagnosis and management of acute Vogt-Koyanagi-Harada disease. *Ocul Immunol Inflamm.* (2018) 26:142–53. doi: 10.1080/09273948.2016.1195001
25. Read RW, Holland GN, Rao NA, Tabbara KF, Ohno S, Arellanes-Garcia L, et al. Revised diagnostic criteria for Vogt-Koyanagi-Harada disease: report of an international committee on nomenclature. *Am J Ophthalmol.* (2001) 131:647–52. doi: 10.1016/S0002-9394(01)00925-4
26. Zheng F, Chua J, Ke M, Tan B, Yu M, Hu Q, et al. Quantitative OCT angiography of the retinal microvasculature and choriocapillaris in highly myopic eyes with myopic macular degeneration. *Br J Ophthalmol.* (2021). doi: 10.1136/bjophthalmol-2020-317632
27. Hong J, Ke M, Tan B, Lau A, Wong D, Yao X, et al. Effect of vessel enhancement filters on the repeatability of measurements obtained from widefield swept-source optical coherence tomography angiography. *Sci Rep.* (2020) 10:22179. doi: 10.1038/s41598-020-79281-3
28. Ji YS, Alagorie AR, Byon I, Sadda SR. Impact of scan tilt on quantitative assessments using optical coherence tomography angiography. *Transl Vis Sci Technol.* (2020) 9:46. doi: 10.1167/tvst.9.7.46
29. Ledesma-Gil G, Fernández-Avellaneda P, Spaide RF. Swept source optical coherence tomography angiography imaging of the choriocapillaris. *Retina.* (2021) 41:https://journals.lww.com/retinajournal/toc/2021/070001373--8. doi: 10.1097/IAE.0000000000003109
30. Borrelli E, Uji A, Toto L, Viggiano P, Evangelista F, Mastropasqua R. In vivo mapping of the choriocapillaris in healthy eyes: a widefield swept-source OCT angiography study. *Ophthalmol Retina.* (2019) 3:979–84. doi: 10.1016/j.oret.2019.05.026
31. Uji A, Balasubramanian S, Lei J, Baghdasaryan E, Al-Sheikh M, Sadda SR. Impact of multiple en face image averaging on quantitative assessment from optical coherence tomography angiography images. *Ophthalmology.* (2017) 124:944–52. doi: 10.1016/j.ophtha.2017.02.006
32. Dhiman R, Chawla R, Azad SV, Kumar P, Gupta V, Kumar A, et al. Peripapillary retinal and choroidal perfusion in nonarteritic ischemic optic neuropathy using optical coherence tomography angiography. *Optom Vis Sci.* (2020) 97:583–90. doi: 10.1097/OPX.0000000000001550
33. Sakata VM, da Silva FT, Hirata CE, de Carvalho JE, Yamamoto JH. Diagnosis and classification of Vogt-Koyanagi-Harada disease. *Autoimmun Rev.* (2014) 13:550–5. doi: 10.1016/j.autrev.2014.01.023
34. Yang P, Zhong Y, Du L, Chi W, Chen L, Zhang R, et al. Development and evaluation of diagnostic criteria for Vogt-Koyanagi-Harada disease. *JAMA Ophthalmol.* (2018) 136:1025–31. doi: 10.1001/jamaophthalmol.2018.2664
35. Arellanes-Garcia L, Hernandez-Barrios M, Fromow-Guerra J, Cervantes-Fanning P. Fluorescein fundus angiographic findings in Vogt-Koyanagi-Harada syndrome. *Int Ophthalmol.* (2007) 27:155–61. doi: 10.1007/s10792-006-9027-4
36. Herbot CP, Mantovani A, Bouchenaki N. Indocyanine green angiography in Vogt-Koyanagi-Harada disease: angiographic signs and utility in patient follow-up. *Int Ophthalmol.* (2007) 27:173–82. doi: 10.1007/s10792-007-9060-y
37. Hirose S, Saito W, Yoshida K, Saito M, Dong Z, Namba K, et al. Elevated choroidal blood flow velocity during systemic corticosteroid therapy in Vogt-Koyanagi-Harada disease. *Acta Ophthalmol.* (2008) 86:902–7. doi: 10.1111/j.1755-3768.2008.01384.x
38. Chu Z, Weinstein JE, Wang RK, Pepple KL. Quantitative analysis of the choriocapillaris in uveitis using en face swept-source optical coherence tomography angiography. *Am J Ophthalmol.* (2020) 218:17–27. doi: 10.1016/j.ajo.2020.05.006
39. Pichi F, Smith SD, Neri P, Woodstock E, Hay S, Parrulli S, et al. Choroidal granulomas visualized by swept-source optical coherence tomography angiography. *Retina (Philadelphia, Pa).* (2020) 41:602–9. doi: 10.1097/IAE.0000000000002864
40. Erba S, Govetto A, Scialdone A, Casalino G. Role of optical coherence tomography angiography in Vogt-Koyanagi-Harada disease. *GMS Ophthalmol Cases.* (2021) 11:Doc06. doi: 10.3205/oc000179
41. Cennamo G, Romano MR, Iovino C, de Crecchio G, Cennamo G. Optical coherence tomography angiography in incomplete acute Vogt-Koyanagi-Harada disease. *Int J Ophthalmol.* (2017) 10:661–2. doi: 10.18240/ijo.2017.04.27
42. Giannakouras P, Andreanos K, Giavi B, Diagourtas A. Optical coherence tomography angiography: employing a novel technique for investigation in Vogt-Koyanagi-Harada disease. *Case Rep Ophthalmol.* (2017) 8:362–9. doi: 10.1159/000477611
43. Pichi F, Aggarwal K, Neri P, Salvetti P, Lembo A, Nucci P, et al. Choroidal biomarkers. *Indian J Ophthalmol.* (2018) 66:1716–26. doi: 10.4103/ijo.IJO\_893\_18
44. Liang A, Jia S, Gao F, Han X, Pei M, Qu Y, et al. Decrease of choriocapillary vascular density measured by optical coherence tomography angiography in Vogt-Koyanagi-Harada disease. *Graefes Arch Clin Exp Ophthalmol.* (2021). doi: 10.1007/s00417-021-05238-5. [Epub ahead of print].

45. Tian M, Tappeiner C, Zinkernagel MS, Huf W, Wolf S, Munk MR. Evaluation of vascular changes in intermediate uveitis and retinal vasculitis using swept-source wide-field optical coherence tomography angiography. *Br J Ophthalmol*. (2019) 103:1289–95. doi: 10.1136/bjophthalmol-2018-313078
46. Yang P, Ye Z, Xu J, Du L, Zhou Q, Qi J, et al. Macular abnormalities in Vogt-Koyanagi-Harada disease. *Ocul Immunol Inflamm*. (2019) 27:1195–202. doi: 10.1080/09273948.2019.1624781
47. Lee GI, Park KA, Oh SY, Min JH, Kim BJ. Peripapillary and parafoveal microvascular changes in eyes with optic neuritis and their fellow eyes measured by optical coherence tomography angiography: an exploratory study. *Acta Ophthalmol*. (2020) 99:288–298. doi: 10.1111/aos.14577
48. Fard MA, Jalili J, Sahraian A, Khojasteh H, Hejazi M, Ritch R, et al. Optical coherence tomography angiography in optic disc swelling. *Am J Ophthalmol*. (2018) 191:116–23. doi: 10.1016/j.ajo.2018.04.017
49. Fard MA, Yadegari S, Ghahvechian H, Moghimi S, Soltani-Moghaddam R, Subramanian PS. Optical Coherence tomography angiography of a pale optic disc in demyelinating optic neuritis and ischemic optic neuropathy. *J Neuroophthalmol*. (2019) 39:339–44. doi: 10.1097/WNO.0000000000000075

**Conflict of Interest:** The authors declare that the research was conducted in the absence of any commercial or financial relationships that could be construed as a potential conflict of interest.

The reviewer XL declared a shared affiliation with one of the authors, HZ, to the handling editor at time of review.

**Publisher's Note:** All claims expressed in this article are solely those of the authors and do not necessarily represent those of their affiliated organizations, or those of the publisher, the editors and the reviewers. Any product that may be evaluated in this article, or claim that may be made by its manufacturer, is not guaranteed or endorsed by the publisher.

Copyright © 2021 Ye, Zhang, Xiao, Wang, Hu, Yan, Li, Hu, Su, Luo, Yuan, Wen and Chi. This is an open-access article distributed under the terms of the Creative Commons Attribution License (CC BY). The use, distribution or reproduction in other forums is permitted, provided the original author(s) and the copyright owner(s) are credited and that the original publication in this journal is cited, in accordance with accepted academic practice. No use, distribution or reproduction is permitted which does not comply with these terms.



# Elevated NLRP3 Inflammasome Levels Correlate With Vitamin D in the Vitreous of Proliferative Diabetic Retinopathy

Li Lu<sup>1†</sup>, Gaocheng Zou<sup>1†</sup>, Li Chen<sup>2</sup>, Qianyi Lu<sup>3</sup>, Mian Wu<sup>4\*</sup> and Chunxia Li<sup>5\*</sup>

## OPEN ACCESS

### Edited by:

Haijiang Lin,  
Massachusetts Eye & Ear Infirmary,  
Harvard Medical School,  
United States

### Reviewed by:

Romina Mayra Lasagni Vitar,  
San Raffaele Hospital (IRCCS), Italy  
Xiaodong Sun,  
Shanghai First People's  
Hospital, China

### \*Correspondence:

Mian Wu  
wumian320@163.com  
Chunxia Li  
cx\_li1964@outlook.com

<sup>†</sup>These authors have contributed  
equally to this work and share first  
authorship

### Specialty section:

This article was submitted to  
Ophthalmology,  
a section of the journal  
Frontiers in Medicine

**Received:** 05 July 2021

**Accepted:** 20 September 2021

**Published:** 15 October 2021

### Citation:

Lu L, Zou G, Chen L, Lu Q, Wu M and  
Li C (2021) Elevated NLRP3  
Inflammasome Levels Correlate With  
Vitamin D in the Vitreous of  
Proliferative Diabetic Retinopathy.  
Front. Med. 8:736316.  
doi: 10.3389/fmed.2021.736316

<sup>1</sup> Department of Ophthalmology, The First Affiliated Hospital of University of Science and Technology of China, Hefei, China,  
<sup>2</sup> Department of Clinical laboratory, The First Affiliated Hospital of University of Science and Technology of China, Hefei,  
China, <sup>3</sup> Department of Ophthalmology, The First Affiliated Hospital of Soochow University, Suzhou, China, <sup>4</sup> Department of  
Endocrinology and Metabolism, The Affiliated Suzhou Hospital of Nanjing Medical University, Suzhou Municipal Hospital,  
Suzhou, China, <sup>5</sup> Department of Ophthalmology, Shanghai TCM-Integrated Hospital, Shanghai University of TCM, Shanghai,  
China

**Purpose:** This study aims to determine vitamin D concentrations in the vitreous and serum, as well as the expression levels of NLRP3 inflammasome pathway in the vitreous of patients with proliferative diabetic retinopathy (PDR). In addition, we investigated the possible correlation between NLRP3 inflammasome levels and vitamin D concentrations.

**Methods:** We obtained vitreous samples before vitrectomy from 55 PDR patients, 25 non-diabetic patients with idiopathic macular hole (IMH), and 10 non-proliferative diabetic retinopathy (NPDR) patients. We also collected serum samples from the same patients. Enzyme-linked immunosorbent assay (ELISA) was used to examine NLRP3 inflammasome pathway proteins, including NLRP3, caspase-1, IL-1 $\beta$ , and VEGF. In addition, vitamin D concentrations were analyzed in Roche Cobas 6000's module e601 platform using electrochemiluminescence immune assay.

**Results:** The levels of NLRP3 inflammasome pathway and VEGF increased dramatically in PDR vitreous. However, vitamin D concentrations in vitreous and serum followed the opposite trend. Meanwhile, vitreous and serum vitamin D concentrations were significantly negatively correlated with vitreous NLRP3 expression in PDR patients. Moreover, serum and vitreous vitamin D concentrations were positively correlated and demonstrated discriminatory ability in DR. The subgroup analysis of PDR group revealed that eyes with tractional retinal detachment (TRD) had higher NLRP3 inflammasome pathway and VEGF levels but lower vitamin D concentrations. Conversely, eyes that received preoperative pan-retinal photocoagulation (PRP) exhibited lower levels of NLRP3 inflammasome pathway, but vitamin D concentrations were irrelevant to laser treatment.

**Conclusions:** Our results demonstrate a strong correlation between increased NLRP3 inflammasome pathway and decreased vitamin D concentrations in the vitreous of

PDR patients, which may be linked to PDR pathogenesis. In addition, vitamin D supplementation may play a key role in preventing, treating, and improving PDR prognosis due to its inhibitory impact on NLRP3 inflammasome pathway and VEGF.

**Keywords:** proliferative diabetic retinopathy (PDR), vitamin D, NLRP3 inflammasome, VEGF, vitrectomy

## INTRODUCTION

Diabetic retinopathy (DR) is the most frequent microvascular complication of diabetes, causing blindness and vision impairment in the working-age population worldwide (1). About 35% of diabetes patients suffer from DR, 6.8% have diabetic macular edema, 7.0% have proliferative diabetic retinopathy (PDR), and 10.2% have vision-threatening DR (2). Notably, China has the highest number of diabetes mellitus (DM) patients globally, with about 116.4 million cases, implying a sizable burden of DR (3). Numerous sophisticated treatments, including anti-vascular endothelial growth factor (VEGF) therapy and vitrectomy, can minimize the vision loss of severe DR patients. However, DR pathogenesis, particularly proliferative diabetic retinopathy (PDR), remains unclear.

Much DR pathogenesis is attributed to the aberrant production of reactive oxygen species (ROS) and chronic inflammation (4, 5). Recently, our research group and Chaurasia et al. demonstrated that ROS/TXNIP/NLRP3 inflammasome pathway is a major mechanism in DR and that NLRP3 inflammasome is involved in vascular impairment in the advanced stages of the disease (6, 7). NLRP3 inflammasome is the best-characterized inflammasome, including sensor protein NLRP3, adaptor protein apoptosis-associated speck-like protein (ASC), and proinflammatory caspase, procaspase-1 (8). Upon recognition and activation by danger signals, NLRP3 inflammasome mediates caspase-1 activation, cleaving proIL-1 $\beta$ , and proIL-18 into their active forms (9–11). Furthermore, Loukovaara et al. discovered that caspase-1 and IL-18 levels were significantly higher in the vitreous of PDR eyes than non-proliferative diabetic retinopathy (NPDR) eyes (12), confirming the dominating role of NLRP3 in PDR pathogenesis.

In addition, our previous research found that 1,25-dihydroxy vitamin D was able to confer protection of retinal structure and function by down-regulating ROS and suppressing inflammation and apoptosis (7). The antioxidant and anti-inflammatory properties of vitamin D have been the focus of recent diabetes research (13, 14). In addition, several clinical and epidemiological studies reported an inverse relationship between retinopathy severity and serum vitamin D concentrations, with vitamin D deficiency serving as an independent determinant of DR (15–18). Therefore, based on our prior work and other studies stated above, we hypothesize that NLRP3 levels and vitamin D concentrations in vitreous fluid may be correlated and hold a critical function in DR pathogenesis.

To further investigate this issue, we conducted this study to compare NLRP3 and vitamin D levels in vitreous fluid of patients with or without PDR and analyze their relationship. Meanwhile, we evaluated the association between vitreous vitamin D concentration and serum vitamin D concentration.

As a result, this study may provide advanced evidence for vitamin D as a considerable potential target for DR prevention and treatment.

## MATERIALS AND METHODS

### Participants

This retrospective study was conducted following the Declaration of Helsinki and approved by the First Affiliated Hospital of University of Science and Technology of China. All participants underwent preoperative examinations, including eye examination, history taking, physiological, and laboratory blood tests. DR was diagnosed by a retinal specialist based on ICO Guidelines for Diabetic Eye Care (19). Before surgery, we excluded participants with repeated vitrectomy, vitamin D supplementation, or anti-VEGF therapy, and endocrine or digestive diseases that could affect vitamin D concentrations. In addition to main diseases of each group, we excluded patients with other ophthalmological diseases (glaucoma, serious cataract, age-related macular degeneration, rhegmatogenous retinal detachment, etc.). Finally, we excluded eyes with recent vitreous hemorrhage (<1 month) to avoid possible interference of intravitreal hemoglobin.

The study recruited 90 eyes of 90 inpatients from the ophthalmology department of the First Affiliated Hospital of University of Science and Technology of China, between June 2019 and September 2019. After that, the patients were divided into three groups: the control group (25 eyes of 25 patients with idiopathic macular hole), NPDR group (10 eyes of 10 patients with NPDR), and PDR group (55 eyes of 55 patients with PDR). None of these control patients had any severe systemic medical problems, including diabetes, while all patients in NPDR and PDR groups had type 2 diabetes (T2DM). The demographic details of patients are summarized in **Table 1**.

### Vitrectomy and Biological Samples Collection

The patient's blood and vitreous samples were collected during the same period of hospitalization. All patients among the three groups underwent a 23-gauge standard three-port pars plana vitrectomy without an infusion of artificial fluid using CONSTELLATION Vision System (Alcon Laboratories, Inc., Fort Worth, TX, USA). The vitreous fluid (0.3–0.5 mL) was collected by manual aspiration into a syringe via the vitrectomy with the cutting function activated (12). Vitreous samples were immediately centrifuged at 13,000 rpm for 5 min at 4°C in sterile 1.5 mL Eppendorf tubes. Supernatants were rapidly collected and stored at –80°C until the assay was performed (20). After fasting overnight for at least 10 h, blood samples of patients were taken by aseptic vein puncture and submitted for testing.

**TABLE 1 |** Systemic and ocular characteristics of participants.

	Control (n = 25)	NPDR (n = 10)	PDR (n = 55)	P-value		
				P <sup>a</sup>	P <sup>b</sup>	P <sup>c</sup>
Patient characteristics						
Age (years)	61.68±10.63	65.50 ± 9.30	51.07 ± 11.50	>0.99	<0.01	<0.01
Female/male (n)	16/9	5/5	28/27	0.9519	0.9519	0.1365
Duration of diabetes (years)	–	12.6 ± 5.89	13.0 ± 6.46	–	–	0.856
HbA1c (%)	5.27 ± 0.35	5.97 ± 0.48	7.82 ± 1.55	0.1801	<0.0001	0.0041
Body mass index (kg/m2)	23.67 ± 3.28	22.98 ± 2.41	23.74 ± 2.68	>0.99	>0.99	>0.99
TC (mmol/L)	4.52 ± 0.71	5.49 ± 0.59	4.99 ± 1.14	0.1272	0.0113	0.2515
TG (mmol/L)	1.76 ± 0.71	2.12 ± 2.23	1.71 ± 1.14	>0.99	0.9274	>0.99
HDL (mmol/L)	1.13 ± 0.20	1.025 ± 0.24	1.05 ± 0.28	0.6994	0.4579	>0.99
LDL (mmol/L)	2.25 ± 0.66	2.72 ± 0.70	2.47 ± 0.73	0.2083	0.7058	0.7588
Systolic BP (mmHg)	136.10 ± 20.49	147.30 ± 12.89	140.90 ± 19.60	0.1062	0.8543	0.3714
Diastolic BP (mmHg)	82.08 ± 8.36	80.20 ± 7.42	83.20 ± 13.10	>0.99	>0.99	>0.99
Ocular characteristics						
Vitreous hemorrhage	–	0/10	55/55	–	–	<0.01
Tractional retinal detachment	–	0/10	21/55	–	–	<0.01
Previous laser treatment	–	6/10	28/55	–	–	0.7359
(Non-PRP/IRP/PRP)	–	4/3/3	27/9/19	–	–	
Epiretinal fibrosis	–	–	41/55	–	–	–
silicon oil filling	–	–	21/55	–	–	–
Operated eye (right/left)	8/17	5/5	20/35	0.9519	0.9519	0.1365
NLRP3 (ng/mL)	0.03 ± 0.00	0.04 ± 0.00	0.05 ± 0.01	0.0615	<0.0001	0.0174
Caspase-1 (pg/mL)	15.48 ± 3.8	12.38 ± 2.97	44.52 ± 12.32	>0.99	<0.0001	<0.0001
IL-1β (pg/mL)	8.72 ± 5.22	11.07 ± 3.56	29.03 ± 6.17	>0.99	<0.0001	<0.0001
VEGF (pg/mL)	30.98 ± 5.88	56.31 ± 11.36	350.54 ± 81.03	0.2610	<0.0001	0.0007
SVD (ng/mL)	19.83 ± 4.51	17.74 ± 4.47	14.46 ± 5.73	>0.99	<0.0001	0.1603
VVD (ng/mL)	21.83 ± 3.95	16.86 ± 2.40	18.21 ± 2.91	0.0049	0.0008	>0.99

<sup>a</sup>*P*, Control vs. NPDR; <sup>b</sup>*P*, Control vs. PDR; <sup>c</sup>*P*, NPDR vs. PDR.

Data are displayed either as mean ± SD or numbers of subjects. *P* ≤ 0.05 is considered statistically significant. PDR, proliferative diabetic retinopathy; TC, total cholesterol; TG, triglyceride; HDL, high-density lipoprotein; LDL, low-density lipoprotein; PRP, pan-retinal photocoagulation; IRP, incomplete retinal laser photocoagulation; IL-1β, interleukin-1β; VEGF, vascular endothelial growth factor; SVD, serum 25 (OH) D; VVD, vitreous 25 (OH) D.

## Laboratory Assessments

The blood samples of subjects underwent the following tests: HbA1c, triglyceride (TG), total cholesterol (TC), high-density lipoprotein cholesterol (HDL-C), and low-density lipoprotein cholesterol (LDL-C) using an automatic biochemical analyzer (FUJI DRI-CHEM 4000i, Fuji, Japan). In addition, all participants were evaluated clinically and in the laboratory according to established procedures.

## Measurement of NLRP3 Inflammasome Pathway and VEGF by Enzyme-Linked Immunosorbent Assay (ELISA)

The vitreous NLRP3 levels were measured using a commercially available ELISA kit (Cusabio, Wuhan, China), following the manufacturer's instructions. Moreover, IL-1β, caspase-1, and VEGF levels in the vitreous fluid were also determined using ELISA following the manufacturer's instructions (R&D Systems, Minneapolis, MN, USA).

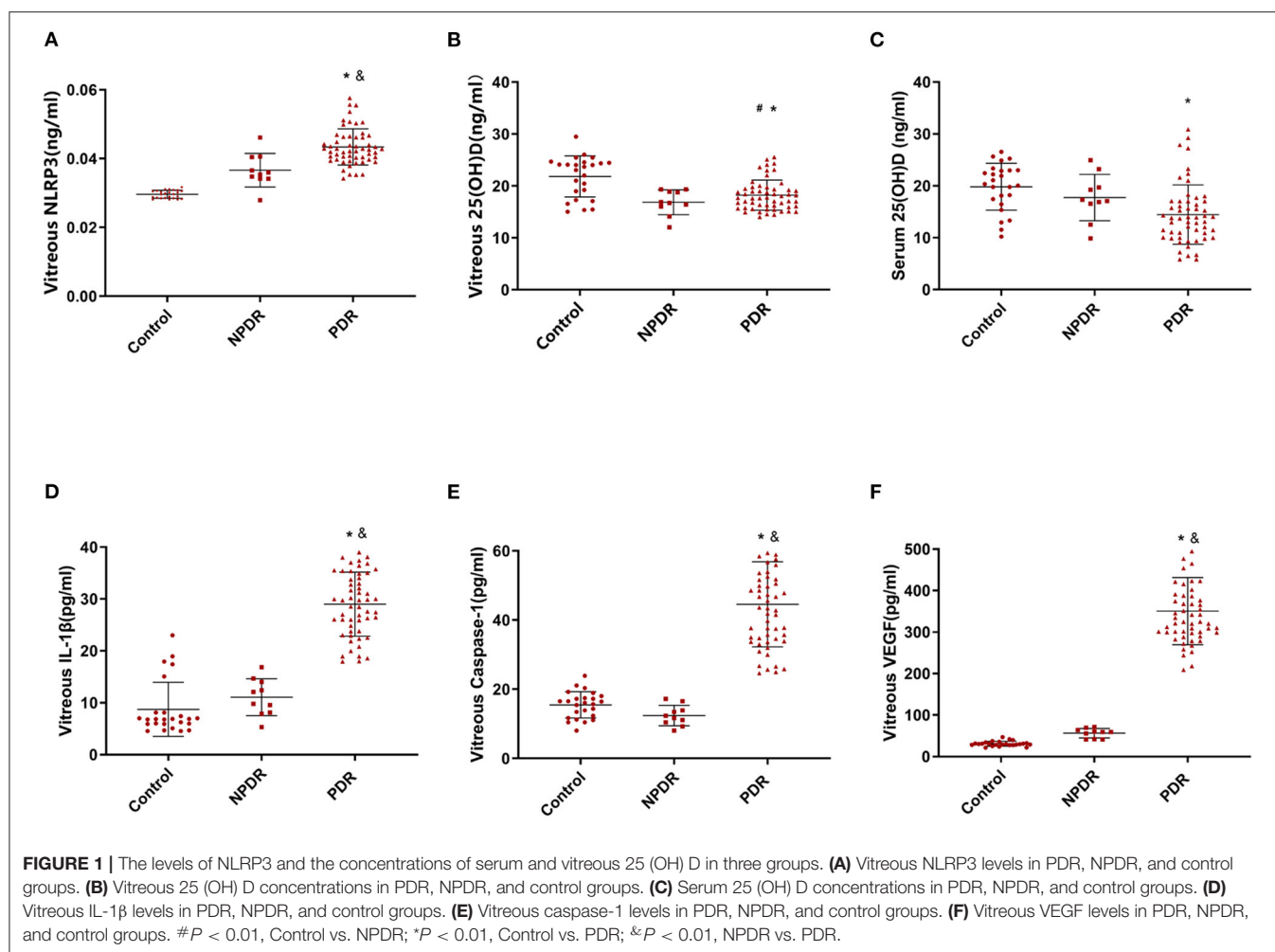
## 25 (OH) D Measurements

Vitreous and serum 25 (OH) D concentrations were determined using Roche Cobas electrochemiluminescence immunoassay. The samples were processed in a single batch in duplicate on each analyzer according to manufacturer's instructions. A total of 200 μL of each vitreous or serum sample was used per assay without dilution. The calibration curves were constructed using calibrators provided in the kits. Roche Cobas Vitamin D total assay had a measurement range of 2.9–63.4 ng/mL (21).

## Statistical Analysis

GraphPad Prism 7.0 Software (GraphPad, San Diego, CA, USA) was deployed to accomplish all data analysis and graph drawing. The measurement data were presented as mean ± SD. The Mann–Whitney *U*-test was employed to compare the parameters of the two groups. The Kruskal–Wallis test followed by Dunns was employed to compare the three groups among each other. Spearman correlation coefficients were used to determine





correlations. A receiver-operating characteristic (ROC) curve was used to estimate the predictive value of the vitreous or serum 25 (OH) D concentrations. For all comparisons, a value of  $P < 0.05$  was considered statistically significant.

## RESULTS

### Patients Characteristics

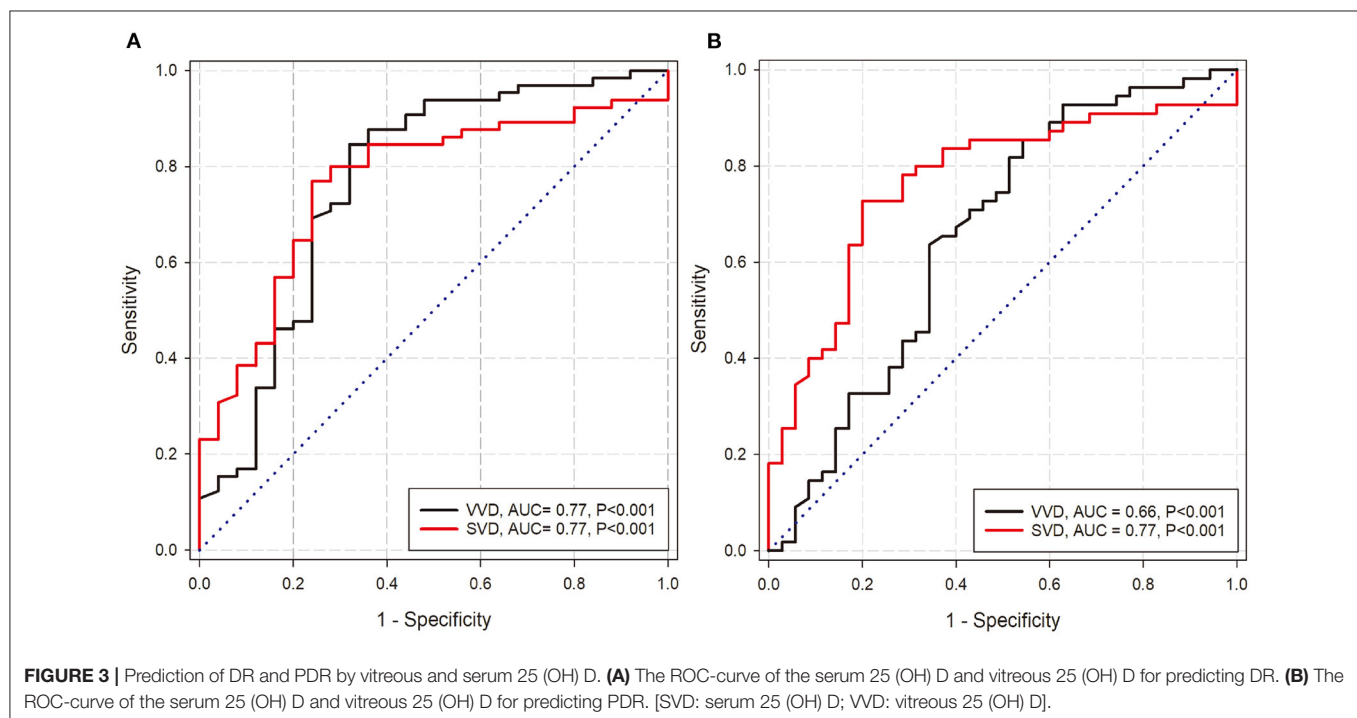
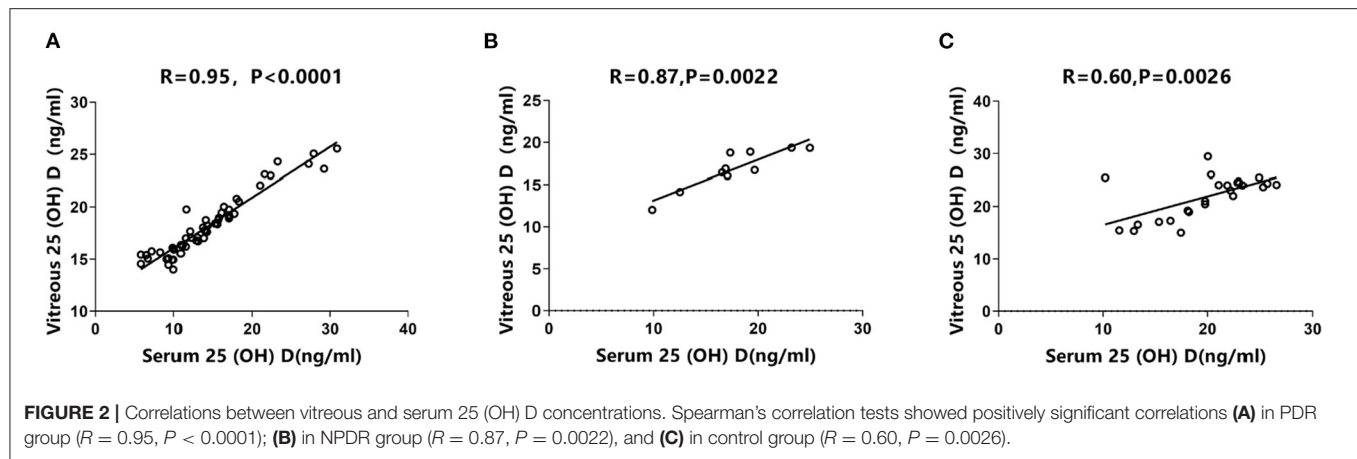
In this study, the patients were randomly assigned to control, NPDR, and PDR groups. **Table 1** summarizes the basic systemic and ocular characteristics. Among the three groups, no significant difference was observed in gender, body mass index (BMI), or blood pressure. While the mean age of patients in PDR group was  $51.07 \pm 11.50$ , this was significantly lower than that in control ( $61.68 \pm 10.63$ ,  $P < 0.01$ ) and NPDR ( $65.50 \pm 9.30$ ,  $P < 0.01$ ) groups. In addition, the PDR group had a higher HbA1c level than NPDR group. Regarding the ocular characteristics, vitreous hemorrhage, tractional retinal detachment (TRD), previous laser treatment, epiretinal fibrosis, and silicon oil filling were recorded in NPDR and PDR groups after operations.

### Quantitative Analysis of NLRP3 Inflammasome Pathway, 25 (OH) D Concentration, and VEGF

We evaluated the expression of NLRP3 inflammasome pathway, including NLRP3, caspase-1, and IL-1 $\beta$  in vitreous, as well as the concentration of 25 (OH) D both in vitreous and serum among the three groups (**Table 1**). We found that PDR group had significantly higher NLRP3 expression than the control group. Moreover, PDR eyes had a much higher expression of NLRP3 than NPDR eyes (**Figure 1A**). Meanwhile, 25 (OH) D concentrations were significantly lower in the PDR group than in the control group, both in serum and vitreous fluid (**Figures 1B,C**). Finally, the expression of IL-1 $\beta$ , caspase-1, and VEGF followed the same pattern as NLRP3 (**Figures 1D–F**).

### Correlation Analysis of Vitreous 25 (OH) D Concentrations and Serum 25 (OH) D Concentrations as Well as Their Predictive Value for DR

Using Spearman's correlation test, the three groups exhibited a significant positive correlation between vitreous and serum 25



(OH) D concentrations. Specifically, the PDR group had the highest correlation ( $R = 0.95$ ,  $P < 0.0001$ , **Figure 2A**), which was slightly higher than NPDR group ( $R = 0.87$ ,  $P = 0.0022$ , **Figure 2B**). Conversely, the control group exhibited a relatively weak positive correlation between vitreous and serum 25 (OH) D concentrations ( $R = 0.60$ ,  $P = 0.0026$ , **Figure 2C**). According to ROC-curve analyses, both serum and vitreous 25 (OH) D showed discriminatory ability in predicting DR (NPDR and PDR) and PDR. In DR prediction, they obtained the same area under curve (AUC) of 0.77 (**Figure 3A**). In particular, serum 25 (OH) D has a better predictive value (AUC: 0.77) than serum 25 (OH) D (AUC: 0.66) in PDR prediction (**Figure 3B**).

## Correlation Analysis of Vitreous NLRP3 Pathway Levels and 25 (OH) D Concentrations

The correlations between vitreous NLRP3 levels and 25 (OH) D concentrations varied significantly among the three groups. The control group exhibited no significant correlation between vitreous NLRP3 levels and serum/vitreous 25 (OH) D concentrations ( $R = 0.06$ ,  $P = 0.77$ ;  $R = 0.152$ ,  $P = 0.47$ , **Figures 4A,B**). However, the PDR group exhibited a negative association between vitreous NLRP3 levels and both serum and vitreous 25 (OH) D concentrations ( $R = 0.71$ ,  $P < 0.0001$ ;  $R = 0.77$ ,  $P < 0.0001$ , **Figures 4C,D**). The same

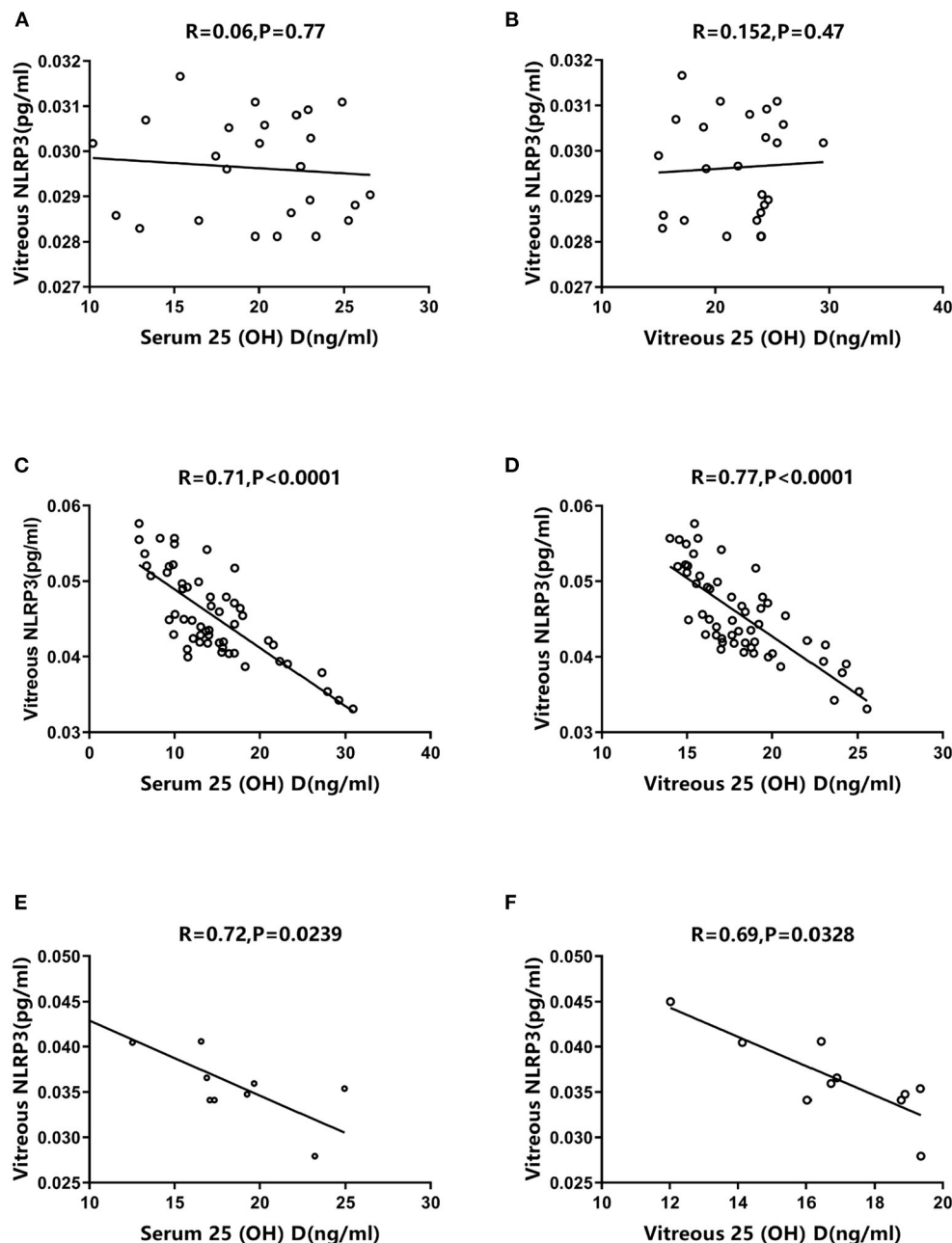


**FIGURE 4 |** Correlations between vitreous NLRP3 levels and serum/vitreous 25 (OH) D concentrations. Spearman's correlation tests exhibited no significant correlations **(A)** between vitreous NLRP3 level and serum 25 (OH) D concentration in control group ( $R = 0.06, P = 0.77$ ), and **(B)** between vitreous NLRP3 level and vitreous 25 (OH) D concentration in control group ( $R = 0.152, P = 0.47$ ). Spearman's correlation tests presented negatively significant correlations **(C)** between vitreous NLRP3 level and serum 25 (OH) D concentration in PDR group ( $R = 0.71, P < 0.0001$ ), **(D)** between vitreous NLRP3 level and vitreous 25 (OH) D concentration in PDR group ( $R = 0.77, P < 0.0001$ ), **(E)** between vitreous NLRP3 level and serum 25 (OH) D concentration in NPDR group ( $R = 0.72, P = 0.0239$ ) and **(F)** between vitreous NLRP3 level and vitreous 25 (OH) D concentration in NPDR group ( $R = 0.69, P = 0.0328$ ).

negative correlations were also observed in NPDR group ( $R = 0.72, P = 0.0239$ ;  $R = 0.69, P = 0.0328$ , **Figures 4E,F**). Moreover, in PDR group, we tested the correlation between 25 (OH) D concentrations and the downstream effects

of NLRP3 such as IL-1 $\beta$  and caspase-1 levels. Again, the negative correlation trends were observed between the downstream of NLRP3 pathway and 25 (OH) D concentrations (**Figure 5**).

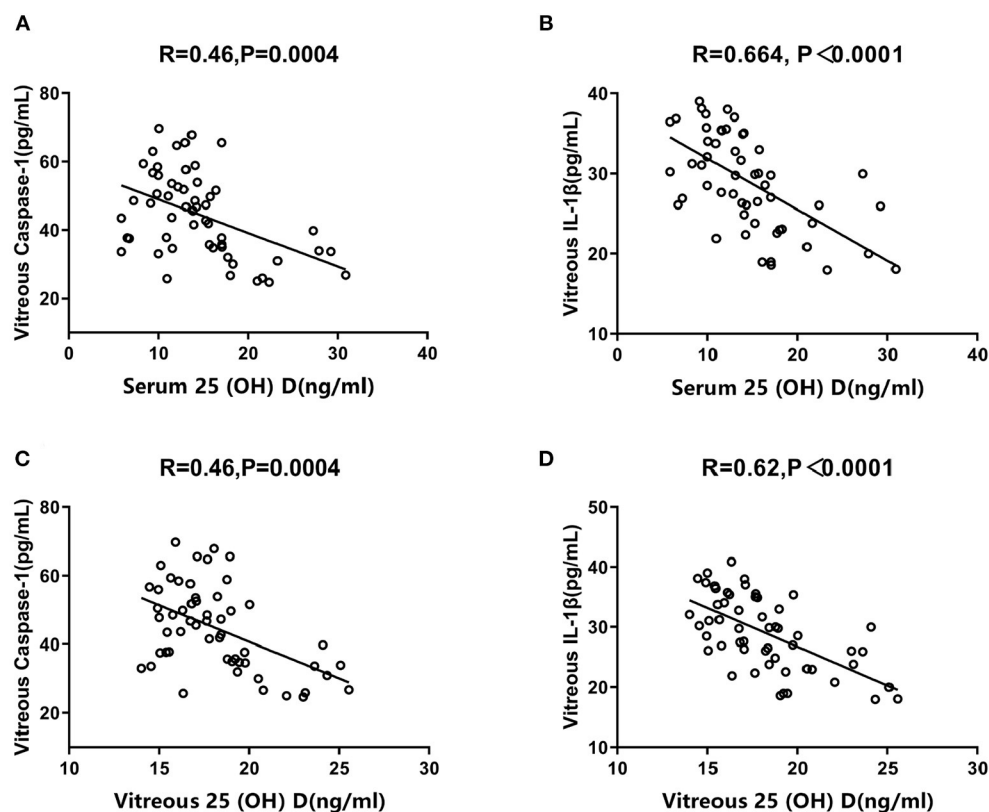


**FIGURE 5 |** Correlations between vitreous Caspase-1/IL-1 $\beta$  levels and serum/vitreous 25 (OH) D concentrations in PDR group. Spearman's correlation tests presented negatively significant correlations **(A)** between vitreous Caspase-1 level and serum 25 (OH) D concentration ( $R = 0.46$ ,  $P = 0.0004$ ), **(B)** between vitreous IL-1 $\beta$  level and serum 25 (OH) D concentration ( $R = 0.664$ ,  $P < 0.0001$ ), **(C)** between vitreous Caspase-1 level and vitreous 25 (OH) D concentration ( $R = 0.46$ ,  $P = 0.0004$ ) and **(D)** between vitreous IL-1 $\beta$  level and vitreous 25 (OH) D concentration ( $R = 0.62$ ,  $P < 0.0001$ ).

**TABLE 2 |** Level of inflammatory factor and vitreous 25 (OH) D in PDR patients with or without tractional retinal detachment.

	TRD ( $n = 21$ )	Non-TRD ( $n = 34$ )	$P$ -value
NLRP3 (ng/mL)	$0.05 \pm 0.01$	$0.04 \pm 0.00$	$<0.0001$
VVD (ng/mL)	$16.14 \pm 1.44$	$19.49 \pm 2.85$	$<0.0001$
Caspase-1 (pg/mL)	$49.26 \pm 9.45$	$41.60 \pm 13.09$	0.0182
IL-1 $\beta$ (pg/mL)	$32.48 \pm 4.33$	$26.89 \pm 6.21$	0.0007
VEGF (pg/mL)	$387.60 \pm 71.55$	$327.60 \pm 78.90$	0.0011

Data are presented as mean  $\pm$  SD.  $P < 0.05$  is considered statistically significant.

TRD, tractional retinal detachment; VVD, vitreous 25 (OH) D; IL-1 $\beta$ , interleukin-1 $\beta$ ; VEGF, vascular endothelial growth factor.

## Subgroup Analysis of PDR Group

Based on various ocular characteristics observed during operations, we further performed subgroup analyses from two perspectives in PDR group. First, based on TRD presence, we divided the results into two parts and compared the levels of NLRP3 inflammasome pathway, 25 (OH) D, and VEGF in vitreous fluid (Table 2). We found that TRD eyes ( $n = 21$ ) had significantly higher levels of NLRP3 ( $P < 0.0001$ ), caspase-1 ( $P = 0.0182$ ), IL-1 $\beta$  ( $P = 0.0007$ ), and VEGF ( $P = 0.0011$ ) and

lower concentrations of 25 (OH) D ( $P < 0.0001$ ). Second, we classified patients into three groups depending on their past laser treatment status, including no laser treatment group, incomplete pan-retinal photocoagulation group, and pan-retinal photocoagulation (PRP) group. PRP is defined following our previously published study (22). Then, the factors compared in the first perspective were compared in the second perspective. All above proteins were considerably decreased in the PRP group compared with the no laser treatment group, while 25 (OH) D concentrations did not differ significantly across the three groups (Table 3).

## DISCUSSION

Vitamin D, a steroid hormone, is critical for calcium and bone homeostasis. Extraskelatal effects have also been documented (23), including regulating cardiovascular homeostasis, tuning immunity systems, and modulating inflammation (24, 25). Furthermore, several clinical research studies have indicated the link between DR characterized by persistent low-grade inflammation and vitamin D deficiency (15, 26). This study confirmed that PDR patients had significantly lower vitreous or serum 25 (OH) D concentrations and higher vitreous levels

**TABLE 3 |** Level of inflammatory factor and vitreous 25 (OH) D in PDR patients according to pan-retinal laser photocoagulation state.

	Non-PRP (n = 27)	IRP (n = 9)	PRP (n = 19)	P-value		
				<i>p</i> <sup>a</sup>	<i>p</i> <sup>b</sup>	<i>p</i> <sup>c</sup>
NLRP3 (ng/mL)	0.05 ± 0.01	0.04 ± 0.01	0.04 ± 0.00	0.0752	0.0017	>0.99
VVD (ng/mL)	17.67 ± 2.88	18.62 ± 3.76	18.78 ± 2.50	>0.99	0.3051	>0.99
Caspase-1 (pg/mL)	49.68 ± 10.71	45.77 ± 9.46	36.60 ± 11.96	>0.99	0.0006	0.1141
IL-1β (pg/mL)	31.56 ± 5.65	30.56 ± 5.37	24.70 ± 4.96	>0.99	0.0003	0.0673
VEGF (pg/mL)	394.40 ± 80.45	341.80 ± 41.37	292.30 ± 55.52	0.4580	<0.0001	0.0971

<sup>a</sup>*P*, Non-PRP vs. IRP; <sup>b</sup>*P*, Non-PRP vs. PRP; <sup>c</sup>*P*, IRP vs. PRP.

Data are shown as mean ± SD. *P* < 0.05 was considered statistically significant.

PRP, pan retinal photocoagulation; IRP, incomplete retinal laser photocoagulation; VVD, vitreous 25 (OH) D; IL-1β, interleukin-1β; VEGF, vascular endothelial growth factor.

of NLRP3 inflammasome than those without DM. Meanwhile, we observed a significant positive correlation between vitreous and serum 25 (OH) D concentrations in the three groups and a negative correlation between vitreous NLRP3 levels and serum/vitreous vitamin D concentrations in NPDR and PDR groups. To the best of our knowledge, this is the first report to evaluate vitamin D concentrations in human vitreous fluid. Our current findings imply that vitamin D deficiency may be a possible mechanism to activate NLRP3 inflammasome pathway during PDR pathogenesis.

The tendency of vitamin D observed in the present study was consistent with other studies on DM or diabetic complications (27–29). The majority of those studies have concluded that the link between vitamin D and DM as well as its complications is mainly because vitamin D deficiency contributes to their key pathological processes through multiple mechanisms such as enhancement of insulin resistance and β-cell death (30). In other words, vitamin D deficiency is a factor in DM development and its complications. Vitamin D deficiency and insufficiency is a global health problem. About 30% of children and 60% of adults worldwide are vitamin D deficient and insufficient, respectively (31). In this study, even the serum vitamin D concentrations of the control patients (19.83 ± 4.51) were defined as vitamin D deficiency (32). The main cause of vitamin D deficiency is inadequate dietary intake and lack of exposure to sunlight, which is the main source of vitamin D synthesis for most children and adults (33). As PDR patients with the highest BMI of the three groups, T2DM-related obesity may lead to vitamin D dilution in body fat and exacerbate vitamin D deficiency (34). Besides, vitamin D deficiency is also an issue affecting people of all ages, especially the elderly. Individuals older than 51 years have less sun exposure and a weaker capacity of the skin to produce vitamin D (32). However, in this study, most participants were older than 51 years, indicating that age was not the primary factor for the difference in vitamin D concentrations between PDR and control groups. Most PDR patients hospitalized for surgery were in the working population, whereas IHM patients in the control group tended to be older when they underwent surgery. It is well-known that the vitreous becomes more liquefied with age (35). During surgery, we found that vitreous liquefaction occurred in most participants, resulting in a more uniform distribution of factors tested in the vitreous fluid.

Other studies have also focused on vitamin D's impact on inflammation, which has been demonstrated to reduce the numbers of activated macrophages and chronic inflammatory response in retina (36). On the other hand, vitamin D deficiency might cause increased production of proinflammatory cytokines in PDR patients (37). However, combining our present and previous studies has enabled us to thoroughly discuss the underlying mechanisms of vitamin D's role in DR. *In vivo*, we demonstrated that vitamin D3 could maintain normal retinal structure and retinal vascular function and suppress apoptosis of retinal cells in diabetic rats. While, *in vitro*, we provided evidence that vitamin D3 decreased ROS and further suppressed ROS/TXNIP/NLRP3 inflammasome pathway in high-glucose-induced retinal microvascular endothelial cells (7). As a result, our prior findings partially explained the differences in NLRP3 levels and 25 (OH) D concentrations among the three groups in the current study, while the correlation between vitreous NLRP3 levels and serum/vitreous 25 (OH) D concentrations also provides further evidence for previous animal and cellular research.

Despite the above-mentioned principal conclusions, several valuable analyses were conducted and yielded intriguing findings. First, we performed additional correlation analysis of vitreous and serum 25 (OH) D concentrations in the three groups and obtained positive correlation results in each case. Interestingly, the correlation degree appears to be linked to DR severity, with the highest correlation observed in PDR group (*R* = 0.95). There is a dearth of evidence reporting the correlation between vitamin D levels in different body fluids. Lin et al. reported that following 8 weeks of vitamin D supplementation, the elevated vitamin D levels in the tear fluid and aqueous humor were parallel with increased plasma concentrations in rabbits, but this was not found in the vitreous fluid (38). We believe that the dominant reason for this discrepancy is that blood-retinal barrier (BRB) was destroyed in PDR patients, facilitating vitamin D shift due to higher vascular permeability (39). Simultaneously, ROC-curve analyses revealed that serum 25(OH) D performed well in predicting DR, especially PDR. Thus, serum 25(OH) D concentration could be an accessible potential diagnostic marker of PDR. Second, a subgroup analysis was performed in PDR group based on two dimensions: whether the patient presented with TRD and whether the patient received preoperative laser



photocoagulation treatment. We found that PDR eyes with TRD had significantly lower concentrations of vitreous 25 (OH) D and higher levels of NLRP3 inflammasome pathway as well as VEGF (Table 2). Angiogenesis and fibrous tissue proliferation are critical in diabetic TRD pathophysiology (40, 41). Undoubtedly, VEGF is the most crucial factor in this process. In addition, activating NLRP3 inflammasome pathway is required for fibrosis development (42). Notably, vitamin D<sub>3</sub> can concurrently suppress NLRP3 inflammasome pathway while decreasing VEGF level, as demonstrated by our results from diabetic animals (7), which could also account for our present findings. Preoperative PRP may be considered as an effective DR treatment, particularly if the eye never received any laser or if the previous laser appears inadequate. As a result, it prevents TRD by inhibiting neovascularization and stabilizes PDR eyes with TRD. The main mechanism underlying this effect is to produce oxygen benefit in the treated area of retina, thereby alleviating the elevated VEGF levels in diabetic retina (22, 43). Whereas, vitreous 25 (OH) D concentrations did not appear to be influenced by PRP's completion, with no significant difference among the three groups (Table 3). We speculate that instantaneous thermal effect generated by laser targeting neuroretina and retinal pigment epithelium (RPE) will have little influence on the vitreous during laser irradiation (44). There is a possibility that vitamin D supplementation could play a greater role in conjunction with PRP treatment.

Several limitations remain in the current study. To better reflect the actual pathological changes in the retinal microenvironment, we evaluated 25 (OH) D concentrations and NLRP3 inflammasome pathway levels, mainly in the vitreous. Although we excluded eyes with recent vitreous hemorrhage (<1 month), the slower degrading blood components may still pose a potential contamination risk to the vitreous sample. Unlike our earlier research, which employed the activated metabolite, 1,25-dihydroxy vitamin D<sub>3</sub> as a target, the present study utilized the best marker of vitamin D status, 25 (OH) D, to measure vitamin D concentrations in human tissues (45), benefiting from its longer half-life and better stability (46).

In conclusion, our current study confirmed NLRP3 inflammasome pathway activation and serum/vitreous vitamin D deficiency in PDR patients. In particular, we found a significant positive correlation between vitamin D and the inflammatory factor NLRP3. By combining our prior findings in diabetic rats and high glucose-induced human retinal microvascular endothelial cells, we partly demonstrated that decreased

NLRP3 inflammasome pathway levels caused by vitamin D have protective effects on DR, particularly PDR pathogenesis. Additionally, the link between vitreous and serum vitamin D concentrations and ROC-curve analyses may offer a potentially accessible diagnostic marker of PDR. Moreover, subgroup analyses highlighted the clinical value of vitamin D during PDR treatment. All above results demonstrate the critical importance of vitamin D supplementation in preventing DR onset and/or progression.

## DATA AVAILABILITY STATEMENT

The raw data supporting the conclusions of this article will be made available by the authors, without undue reservation.

## ETHICS STATEMENT

The studies involving human participants were reviewed and approved by the Ethics Committee of the First Affiliated Hospital of University of Science and Technology of China. Written informed consent for participation was not required for this study in accordance with the national legislation and the institutional requirements.

## AUTHOR CONTRIBUTIONS

LL and CL: design of the study. GZ, LC, QL, and MW: acquisition, analysis, and interpretation of data. LL and GZ: drafting of the manuscript. LL and MW: statistical analysis. LL, QL, and MW: obtaining the fund. CL: supervising the process. All authors revision and approval of the manuscript.

## FUNDING

This study was supported by grants from the Fundamental Research Funds for the Central Universities (grant no. WK9110000099), the Natural Science Foundation of Jiangsu Province (grant no. BK20200211), and the Young Talent Program of Gusu Health Project (grant no. GSW2020014).

## SUPPLEMENTARY MATERIAL

The Supplementary Material for this article can be found online at: <https://www.frontiersin.org/articles/10.3389/fmed.2021.736316/full#supplementary-material>

## REFERENCES

1. Song P, Yu J, Chan KY, Theodoratou E, Rudan I. Prevalence, risk factors and burden of diabetic retinopathy in China: a systematic review and meta-analysis. *J Glob Health*. (2018) 8:010803. doi: 10.7189/jogh.08.010803
2. Yau JW, Rogers SL, Kawasaki R, Lamoureux EL, Kowalski JW, Bek T, et al. Global prevalence and major risk factors of diabetic retinopathy. *Diabetes Care*. (2012) 35:556–64. doi: 10.2337/dc11-1909
3. Williams R, Colagiuri S, Chan J, Gregg E, Ke C, Lim L-L, et al. *IDF Atlas 9th Edition* (2019).
4. El-Asrar AM. Role of inflammation in the pathogenesis of diabetic retinopathy. *Middle East Afr J Ophthalmol*. (2012) 19:70–4. doi: 10.4103/0974-9233.92118
5. Brownlee M. The pathobiology of diabetic complications: a unifying mechanism. *Diabetes*. (2005) 54:1615–25. doi: 10.2337/diabetes.54.6.1615
6. Chaurasia SS, Lim RR, Parikh BH, Wey YS, Tun BB, Wong TY, et al. The NLRP3 inflammasome may contribute to pathologic neovascularization in the advanced stages of diabetic retinopathy. *Sci Rep*. (2018) 8:2847. doi: 10.1038/s41598-018-21198-z

7. Lu L, Lu Q, Chen W, Li J, Li C, Zheng Z. Vitamin D3 protects against diabetic retinopathy by inhibiting high-glucose-induced activation of the ROS/TXNIP/NLRP3 inflammasome pathway. *J Diabetes Res.* (2018) 2018:8193523. doi: 10.1155/2018/8193523
8. Chen W, Zhao M, Zhao S, Lu Q, Ni L, Zou C, et al. Activation of the TXNIP/NLRP3 inflammasome pathway contributes to inflammation in diabetic retinopathy: a novel inhibitory effect of minocycline. *Inflamm Res.* (2017) 66:157–66. doi: 10.1007/s00011-016-1002-6
9. Zhang X, Xu A, Lv J, Zhang Q. Development of small molecule inhibitors targeting NLRP3 inflammasome pathway for inflammatory diseases. *Eur J Med Chem.* (2019) 2019:111822. doi: 10.1016/j.ejmech.2019.111822
10. Chen H, Zhang X, Liao N, Mi L, Peng Y, Liu B, et al. Enhanced expression of NLRP3 inflammasome-related inflammation in diabetic retinopathy. *Invest Ophthalmol Vis Sci.* (2018) 59:978–85. doi: 10.1167/iovs.17-22816
11. Leavy O. Inflammasome: turning on and off NLRP3. *Nat Rev Immunol.* (2013) 13:1. doi: 10.1038/nri3366
12. Loukovaara S, Piippo N, Kinnunen K, Hytti M, Kaarniranta K, Kauppinen A. NLRP3 inflammasome activation is associated with proliferative diabetic retinopathy. *Acta Ophthalmol.* (2017) 95:803–8. doi: 10.1111/aos.13427
13. Lin LM, Peng F, Liu YP, Chai DJ, Ning RB, Xu CS, et al. Coadministration of VDR and RXR agonists synergistically alleviates atherosclerosis through inhibition of oxidative stress: an *in vivo* and *in vitro* study. *Atherosclerosis.* (2016) 251:273–81. doi: 10.1016/j.atherosclerosis.2016.06.005
14. Chagas CE, Borges MC, Martini LA, Rogero MM. Focus on vitamin D, inflammation and type 2 diabetes. *Nutrients.* (2012) 4:52–67. doi: 10.3390/nu4010052
15. Aksoy H, Akçay F, Kurtul N, Baykal O, Avci B. Serum 1, 25 dihydroxy vitamin D (1, 25 (OH) 2 D 3), 25 hydroxy vitamin D (25 (OH) D) and parathormone levels in diabetic retinopathy. *Clin Biochem.* (2000) 33:47–51. doi: 10.1016/S0009-9120(99)00085-5
16. Kaur H, Donaghue KC, Chan AK, Benitez-Aguirre P, Hing S, Lloyd M, et al. Vitamin D deficiency is associated with retinopathy in children and adolescents with type 1 diabetes. *Diabetes Care.* (2011) 34:1400–2. doi: 10.2337/dc11-0103
17. PA. P, PF. V, Q. S, IA. W, DA. B. Vitamin D and retinopathy in adults with diabetes mellitus. *Arch Ophthalmol.* (2012) 130:756–60. doi: 10.1001/archophthalmol.2011.2749
18. N S, T Y, H K, N K, A K, F S, et al. Vitamin D deficiency is significantly associated with retinopathy in young Japanese type 1 diabetic patients. *Diabetes Res Clin Pract.* (2014) 106:e41–e3. doi: 10.1016/j.diabres.2014.08.005
19. Flaxel CJ, Adelman RA, Bailey ST, Fawzi A, Lim JJ, Vemulakonda GA, et al. Diabetic retinopathy preferred practice pattern(R). *Ophthalmology.* (2020) 127:P66–145. doi: 10.1016/j.ophtha.2019.09.025
20. Lu Q, Lu L, Chen W, Lu P. Expression of angiopoietin-like protein 8 correlates with VEGF in patients with proliferative diabetic retinopathy. *Graefes Arch Clin Exp Ophthalmol.* (2017) 255:1515–23. doi: 10.1007/s00417-017-3676-z
21. Kocak FE, Bahadır Ozturk, Ozben Ozden Isiklar, Ozlem Genc, Ali Unlu, Altuntas I. A comparison between two different automated total 25-hydroxyvitamin D immunoassay methods using liquid chromatography-tandem mass spectrometry. *Biochem Med.* (2015) 25:430–8. doi: 10.11613/BM.2015.044
22. Chen W, Lu Q, Lu L, Guan H. Increased levels of alphaB-crystallin in vitreous fluid of patients with proliferative diabetic retinopathy and correlation with vascular endothelial growth factor. *Clin Exp Ophthalmol.* (2017) 45:379–84. doi: 10.1111/ceo.12891
23. Bouillon R, Marcocci C, Carmeliet G, Bikle D, White JH, Dawson-Hughes B, et al. Skeletal and extraskeletal actions of vitamin D: current evidence and outstanding questions. *Endocr Rev.* (2019) 40:1109–51. doi: 10.1210/er.2018-00126
24. Ni W, Watts SW, Ng M, Chen S, Glenn DJ, Gardner DG. Elimination of vitamin D receptor in vascular endothelial cells alters vascular function. *Hypertension.* (2014) 64:1290–8. doi: 10.1161/HYPERTENSIONAHA.114.03971
25. Chun RF, Liu PT, Modlin RL, Adams JS, Hewison M. Impact of vitamin D on immune function: lessons learned from genome-wide analysis. *Front Physiol.* (2014) 5:151. doi: 10.3389/fphys.2014.00151
26. Afarid M, Ghattavi N, Johari M. Serum levels of vitamin D in diabetic patients with and without retinopathy. *J Ophthalmol Vis Res.* (2020) 15:172–7. doi: 10.18502/jovr.v15i2.6734
27. Deng X, Cheng J, Shen M. Vitamin D improves diabetic nephropathy in rats by inhibiting renin and relieving oxidative stress. *J Endocrinol Invest.* (2016) 39:657–66. doi: 10.1007/s40618-015-0414-4
28. Alcobierre N, Valls J, Rubinat E, Cao G, Esquerda A, Traveset A, et al. Vitamin D deficiency is associated with the presence and severity of diabetic retinopathy in type 2 diabetes mellitus. (2015) 2015:374178. doi: 10.1155/2015/374178
29. Al Dossari KK, Ahmad G, Aljowair A, Alqahtani N, Shibrayn MB, Alshathri M, et al. Association of vitamin d with glycemic control in Saudi patients with type 2 diabetes: a retrospective chart review study in an emerging university hospital. *J Clin Lab Anal.* (2020) 34:e23048. doi: 10.1002/jcla.23048
30. Chiu KC, Chu A, Go VL, Saad MF. Hypovitaminosis D is associated with insulin resistance and beta cell dysfunction. *Am J Clin Nutr.* (2004) 79:820–5. doi: 10.1093/ajcn/79.5.820
31. Daly RM, Gagnon C, Lu ZX, Magliano DJ, Dunstan DW, Sikaris KA, et al. Prevalence of vitamin D deficiency and its determinants in Australian adults aged 25 years and older: a national, population-based study. *Clin Endocrinol.* (2012) 77:26–35. doi: 10.1111/j.1365-2265.2011.04320.x
32. Holick MF, Binkley NC, Bischoff-Ferrari HA, Gordon CM, Hanley DA, Heaney RP, et al. Evaluation, treatment, and prevention of vitamin D deficiency: an Endocrine Society clinical practice guideline. *J Clin Endocrinol Metab.* (2011) 96:1911–30. doi: 10.1210/jc.2011-0385
33. Holick MF. The vitamin D deficiency pandemic: approaches for diagnosis, treatment and prevention. *Rev Endocr Metab Disord.* (2017) 18:153–65. doi: 10.1007/s11554-017-9424-1
34. Wortsman J, Matsuoka LY, Chen TC, Lu Z, Holick MF. Decreased bioavailability of vitamin D in obesity. *Am J Clin Nutr.* (2000) 72:690–3. doi: 10.1093/ajcn/72.3.690
35. Yamashita K, Sakakura S, Ofuji Y, Sato M, Nagamoto T, Kubono H, et al. Micro-incision vitrectomy surgery for primary rhegmatogenous retinal detachments with posterior vitreous detachments in elderly patients: preoperative characteristics and surgical outcomes. *PLoS ONE.* (2021) 16:e0244614. doi: 10.1371/journal.pone.0244614
36. Lee V, Rekhi E, Hoh Kam J, Jeffery G. Vitamin D rejuvenates aging eyes by reducing inflammation, clearing amyloid beta and improving visual function. *Neurobiol Aging.* (2012) 33:2382–9. doi: 10.1016/j.neurobiolaging.2011.12.002
37. Yi X, Sun J, Li L, Wei Q, Qian Y, Chen X, et al. 1,25-Dihydroxyvitamin D3 deficiency is involved in the pathogenesis of diabetic retinopathy in the uygur population of China. *IUBMB Life.* (2016) 68:445–51. doi: 10.1002/iub.1501
38. Lin Y, Ubels JL, Schotanus MP, Yin Z, Pintea V, Hammock BD, et al. Enhancement of vitamin D metabolites in the eye following vitamin D3 supplementation and UV-B irradiation. *Curr Eye Res.* (2012) 37:871–8. doi: 10.3109/02713683.2012.688235
39. El-Remessy AB, Al-Shabraway M, Khalifa Y, Tsai NT, Caldwell RB, Liou GI. Neuroprotective and blood-retinal barrier-preserving effects of cannabidiol in experimental diabetes. *Am J Pathol.* (2006) 168:235–44. doi: 10.2353/ajpath.2006.050500
40. Iyer SSR, Regan KA, Burnham JM, Chen CJ. Surgical management of diabetic tractional retinal detachments. *Survey Ophthalmol.* (2019) 64:780–809. doi: 10.1016/j.survophthal.2019.04.008
41. Antonetti DA, Klein R, Gardner TW. Diabetic retinopathy. *N Engl J Med.* (2012) 366:1227–39. Epub 2012/03/30. doi: 10.1056/NEJMr1005073
42. Robert S, Gicquel T, Victoni T, Valenca S, Barreto E, Bailly-Maitre B, et al. Involvement of matrix metalloproteinases (MMPs) and inflammasome pathway in molecular mechanisms of fibrosis. *Biosci Rep.* (2016) 36:e00360. doi: 10.1042/BSR20160107
43. Yu DY, Cringle SJ, Su E, Yu PK, Humayun MS, Dorin G. Laser-induced changes in intraretinal oxygen distribution in pigmented rabbits. *Invest Ophthalmol Vis Sci.* (2005) 46:988–99. doi: 10.1167/iovs.04-0767
44. Koinzer S, Hesse C, Caliebe A, Saeger M, Baade A, Schlott K, et al. Photocoagulation in rabbits: optical coherence tomographic lesion classification, wound healing reaction, and retinal temperatures. *Lasers Surg Med.* (2013) 45:427–36. doi: 10.1002/lsm.22163

45. Sempos CT, Heijboer AC, Bikle DD, Bollerslev J, Bouillon R, Brannon PM, et al. Vitamin D assays and the definition of hypovitaminosis D: results from the First International Conference on Controversies in Vitamin D. *Br J Clin Pharmacol.* (2018) 84:2194–207. doi: 10.1111/bcp.13652
46. Hayashi H, Okamatsu M, Ogasawara H, Tsugawa N, Isoda N, Matsuno K, et al. Oral supplementation of the vitamin D metabolite 25(OH)D3 against influenza virus infection in mice. *Nutrients.* (2020) 12:2000. doi: 10.3390/nu12072000

**Conflict of Interest:** The authors declare that the research was conducted in the absence of any commercial or financial relationships that could be construed as a potential conflict of interest.

**Publisher's Note:** All claims expressed in this article are solely those of the authors and do not necessarily represent those of their affiliated organizations, or those of the publisher, the editors and the reviewers. Any product that may be evaluated in this article, or claim that may be made by its manufacturer, is not guaranteed or endorsed by the publisher.

Copyright © 2021 Lu, Zou, Chen, Lu, Wu and Li. This is an open-access article distributed under the terms of the Creative Commons Attribution License (CC BY). The use, distribution or reproduction in other forums is permitted, provided the original author(s) and the copyright owner(s) are credited and that the original publication in this journal is cited, in accordance with accepted academic practice. No use, distribution or reproduction is permitted which does not comply with these terms.



# Long-Term Retinal Neurovascular and Choroidal Changes After Panretinal Photocoagulation in Diabetic Retinopathy

Tian Huang<sup>1†</sup>, Xiaoli Li<sup>1,2†</sup>, Jie Xie<sup>1</sup>, Liang Zhang<sup>1</sup>, Guanrong Zhang<sup>3</sup>, Aiping Zhang<sup>1</sup>, Xiangting Chen<sup>4</sup>, Ying Cui<sup>1\*</sup> and Qianli Meng<sup>1\*</sup>

<sup>1</sup> Department of Ophthalmology, Guangdong Provincial People's Hospital, Guangdong Eye Institute, The Second School of Clinical Medicine, Southern Medical University, Guangdong Academy of Medical Sciences, Guangzhou, China, <sup>2</sup> State Key Laboratory of Ophthalmology, Zhongshan Ophthalmic Center, Sun Yat-sen University, Guangzhou, China, <sup>3</sup> Information and Statistical Center, Guangdong Provincial People's Hospital, Guangdong Academy of Medical Sciences, Guangzhou, China, <sup>4</sup> Department of Ophthalmology, Guangzhou First People's Hospital, Guangzhou, China

## OPEN ACCESS

### Edited by:

Shaochong Zhang,  
Sun Yat-sen University, China

### Reviewed by:

Zhengxuan Jiang,  
Anhui Medical University, China  
Wei Chi,  
Sun Yat-sen University, China

### \*Correspondence:

Ying Cui  
cuiying-sysu@163.com  
Qianli Meng  
mengqly@163.com

<sup>†</sup>These authors have contributed  
equally to this work and share first  
authorship

### Specialty section:

This article was submitted to  
Ophthalmology,  
a section of the journal  
Frontiers in Medicine

**Received:** 03 August 2021

**Accepted:** 16 September 2021

**Published:** 18 October 2021

### Citation:

Huang T, Li X, Xie J, Zhang L,  
Zhang G, Zhang A, Chen X, Cui Y and  
Meng Q (2021) Long-Term Retinal  
Neurovascular and Choroidal  
Changes After Panretinal  
Photocoagulation in Diabetic  
Retinopathy. *Front. Med.* 8:752538.  
doi: 10.3389/fmed.2021.752538

**Purpose:** To evaluate the long-term retinal microvascular, neural, and choroidal changes in the patients with severe nonproliferative diabetic retinopathy (NPDR) and proliferative diabetic retinopathy (PDR) following panretinal photocoagulation (PRP).

**Methods:** Forty-five eyes of 28 patients with treatment-naïve severe NPDR and PDR were included and followed for 12 months after PRP. Microvascular and neural changes in the macular and peripapillary areas were assessed by using optical coherence tomography angiography. Subfoveal choroidal thickness (SFCT) was measured by using optical coherence tomography. A Linear mixed-effects model was used to highlight the differences for the variables after adjusting for sex, age, and axial length.

**Results:** Compared to baseline, there were no statistical differences in the best corrected visual acuity (BCVA), macular and peripapillary vessel density (VD), and SFCT following PRP. Macular thickness significantly increased at 1 and 3–6 months after PRP ( $p < 0.05$ ), while the peripapillary retinal nerve fiber layer (RNFL) and ganglion cell complex (GCC) thickness significantly increased at 1 month postoperatively ( $p < 0.01$ ). Global loss volume and focal loss volume significantly decreased at the same time point ( $p < 0.05$ ).

**Conclusion:** The unchanged BCVA, VD, the thickness of RNFL and GCC, and SFCT during the 12-month follow-up period suggest that PRP may prevent the retinal neurovascular and choroidal damage.

**Keywords:** choroid, diabetic retinopathy, microvasculature, neural retina, optical coherence tomography angiography, panretinal photocoagulation

## INTRODUCTION

Diabetic retinopathy (DR) is one of the most common microvascular complications of diabetes and is the leading cause of visual impairment among the working-age population across the globe (1). Changes in the retinal microvascular and neural structure due to diabetes are considered fundamental to the pathophysiology and progression of DR. Reduction of the choroidal thickness (CT) (2, 3) and choroidal perfusion (4, 5) has also been reported in DR. Panretinal



photocoagulation (PRP) is demonstrated to prevent the impairment of visual function due to the proliferative diabetic retinopathy (PDR) and diabetic macular edema (DME) in the landmark clinical trials such as the Diabetic Retinopathy Study (DRS) (6, 7) and the Early Treatment Diabetic Retinopathy Study (ETDRS) (8). The physiological mechanism of PRP is generally considered to involve the physical light energy destroying the photoreceptors and decreasing oxygen consumption, which improves oxygen flux to reach the inner retina, relieves inner retinal hypoxia, and raises the oxygen tension, resulting in reducing or stopping the production of the growth factors and neovascularization (9, 10).

Since fundus fluorescein angiography (FFA) is a gold standard for the diagnosis and grading of DR, the neural and choroidal changes cannot be evaluated by FFA with two-dimensional images. Emerging as a noninvasive and depth-resolved imaging technique without dye injection, optical coherence tomography angiography (OCTA) allows for fast visualization of the macular microvasculature, differentiation of various retinal vascular layers, and quantification of vessel density or thickness of macular area, retinal nerve fiber layer (RNFL), and ganglion cell complex (GCC). Accumulating evidence supports OCTA as a potential tool for the evaluation of the severity of DR and efficacy of the therapies for DR (11, 12). A previous study quantified a set of the neurovascular parameters of OCTA related to the severity of DR, which might have potential clinical applications for DR staging (11). Previous longitudinal studies have shown that the microangiopathy and neurodegeneration appear in parallel and are highly progressive even in the early stage of DR (13), but few studies explored these features following PRP. To the best of our knowledge, the comprehensive retinal vascular and neural changes in the macular and peripapillary area and subfoveal choroidal thickness (SFCT) changes after PRP have not been reported.

In this study, we present a prospective, longitudinal, and observational study to investigate the retinal microvascular, neural, and choroidal changes up to 1 year after PRP in severe non-PDR (NPDR) and PDR by using multimodal imaging.

## MATERIALS AND METHODS

This study was conducted at the Department of Ophthalmology of Guangdong Provincial People's Hospital between October 2018 and June 2020. All the procedures adhered to the tenets of the Declaration of Helsinki and were approved by the research ethics committee of Guangdong Provincial People's Hospital. All the participants provided written informed consent.

### Patients

Patients with type 2 diabetic diagnosed with severe NPDR or PDR who were the candidates for PRP treatment were enrolled. The DR assessment and grading were based on the FFA and color fundus photography (CFP) by using the proposed international Diabetic Retinopathy Severity Scale (14). The exclusion criteria, as shown in **Figure 1**, included the history of ophthalmic intervention, the coexistence of the other ocular diseases affecting the assessment, clinically significant macular

edema (CSME) (central subfield macular thickness  $\geq 300 \mu\text{m}$ ) (15), axial length (AL)  $< 20.0 \text{ mm}$  or  $> 27.0 \text{ mm}$ , and the low-quality OCTA images.

## Ophthalmic and Systemic Examinations

A comprehensive ophthalmic examination was performed in all the participants at baseline and at 1, 3–6, and 12 months after PRP including best corrected visual acuity (BCVA), intraocular pressure, slit-lamp examination, dilated funduscopy, 45° CFP (TRC-NW8 fundus camera, TOPCON, Tokyo, Japan), OCT (HRA-OCT, Heidelberg Engineering, Germany), and OCTA (Optovue, Fremont, California, USA). FFA (Spectralis HRA, Heidelberg Engineering, Jena, Germany) was performed at baseline and 3–6 and 12 months after PRP. AL was obtained by using ocular biometry (LS900 Haag-Streit Diagnostics, Köniz, Switzerland) at baseline to correct the retinal magnification of each OCTA image.

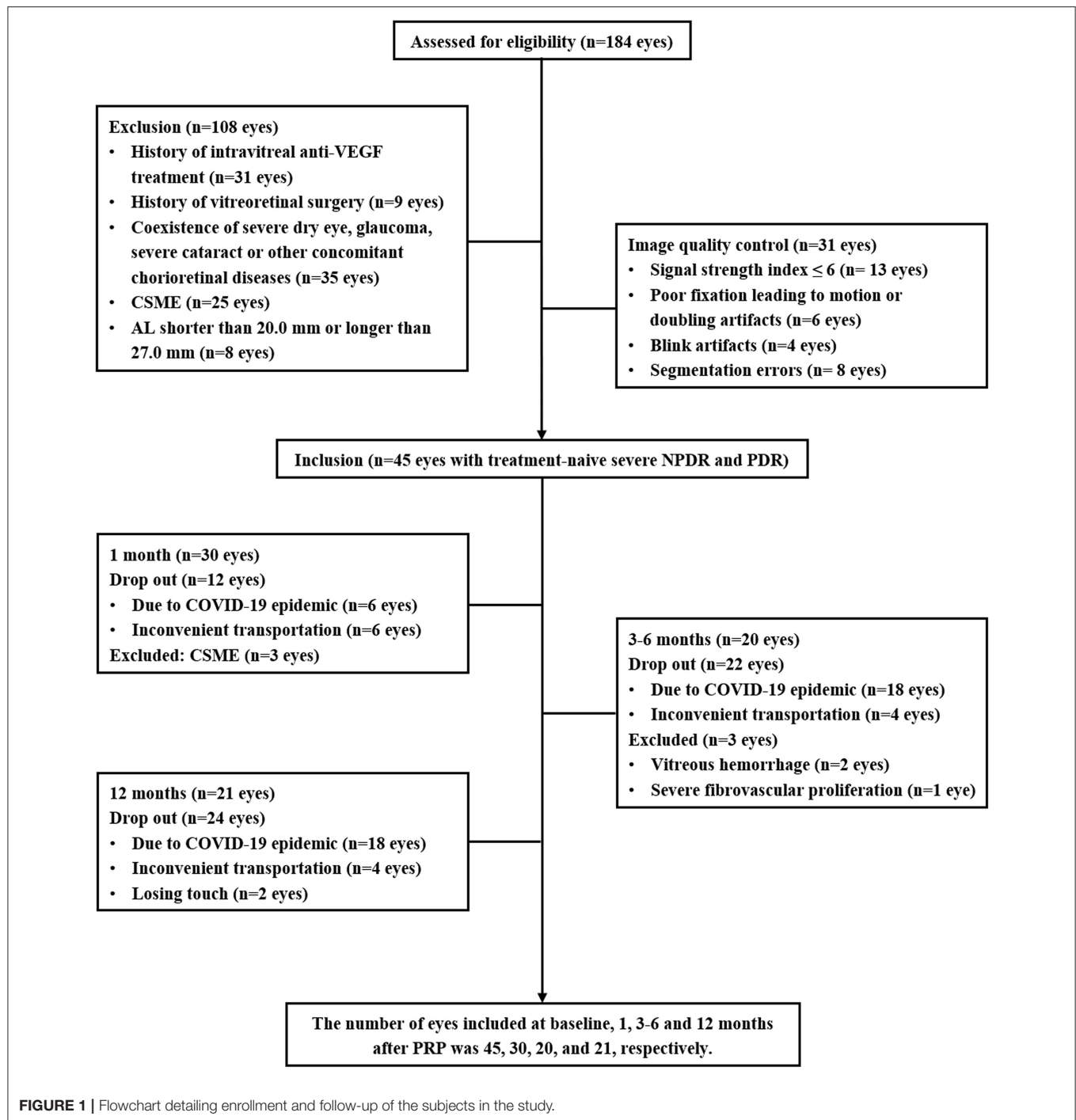
Demographic and systemic parameters including the age, sex, duration of diabetes, blood pressure, body mass index (BMI), waist-hip ratio (WHR), glycated hemoglobin (HbA1c), creatinine, and creatinine clearance rate (Ccr) within 1 week before initiating PRP were recorded.

## Optical Coherence Tomography Angiography and OCT Image Process

The OCTA images were obtained by using the split-spectrum amplitude-decorrelation angiography algorithm incorporated with the RTVue XR Avanti device with AngioVue 2.0 (Optovue Inc., Fremont, California, USA) (16). In this study, the OCTA image acquisition and parameter analysis are described in detail (11). In brief, HD Angio Retina 6.0 mm scan centered on the fovea was used to assess the retinal vessel density (VD), macular thickness, and foveal avascular zone (FAZ). Macular VD and thickness were distinctly evaluated in both the superficial capillary plexus (SCP) and deep capillary plexus (DCP) within the ETDRS  $6 \times 6$  whole grid. The FAZ parameters, including the FAZ area, FAZ perimeter, acircularity index (AI), and FD-300, were evaluated by using the nonflow area tool to provide the automated FAZ segmentation. HD Angio Disk 4.5 mm scan centered on the optic disk was used to quantify the inside of disk and peripapillary VD and the RNFL thickness in the radial peripapillary capillary segment (refer to figure, **Supplementary Figure 1**, which shows the angio retina and disk measurement zones). The GCC scan focused on the ganglion cells was used to automatically calculate the GCC thickness, global loss volume (GLV), and focal loss volume (FLV). SFCT was assessed by using OCT with the enhanced depth-imaging (OCT-EDI) technique.

Optical coherence tomography angiography and OCT images were independently evaluated by the two masked ophthalmologists (XL and YC) at different time points and in different orders. A third trained grader (QM) adjudicated all the cases of discrepancy. All the images were evaluated on the instrument display screen in a standardized and dimmed environment. Manual segmentation was performed to correct the automated segmentation errors when needed.





## Panretinal Photocoagulation

All the participants received the first PRP session within 3 days of the baseline evaluation by using a frequency doubled scan laser relying on a 532 nm (green) light according to the recommendations of the ETDRS (6). PRP was performed in the three or four sessions with an interval of 1 week between the sessions. The retinal spot size of 200  $\mu\text{m}$  and

laser duration of 0.2 s were employed. The effective power of the laser was determined by the yellowish-white coagulative spots. The average number of the shots was 1,373 burns (range: 868–1,982). Treatment was deemed adequate when no further neovascularization or hemorrhage was detected during follow-up visits at 1, 3–6, and 12 months after the final laser treatment session.

**TABLE 1** | Demographic and systemic characteristics of the participants.

Characteristics	Mean $\pm$ SD/Median (interquartile range)		P-value
	Baseline	12 months after PRP	
Patients (eyes)	28 (45)	13 (21)	
Sex, male (%)	14 (50%)	8 (62%)	
Duration of diabetes (years)	11.79 $\pm$ 8.23	–	
Age (years)	57.46 $\pm$ 8.67	58.54 $\pm$ 8.78	0.772
BMI (kg/m <sup>2</sup> )	23.09 $\pm$ 2.50	23.04 $\pm$ 2.52	0.943
SBP (mmHg)	139.61 $\pm$ 19.63	139.21 $\pm$ 19.19	0.940
DBP (mmHg)	79.71 $\pm$ 13.40	80.57 $\pm$ 13.18	0.810
HbA1c (%)	8.26 $\pm$ 2.07	8.07 $\pm$ 1.92	0.724
Creatinine ( $\mu$ mol/L)	92.45 (70.16–123.37)	94.25 (71.36–128.54)	0.781
Ccr (ml/min)	61.66 $\pm$ 23.78	60.69 $\pm$ 24.82	0.776
AL (mm)	22.85 $\pm$ 0.63	22.90 $\pm$ 0.64	0.455

*p*-values are calculated by using a *t*-test.

SBP, systolic blood pressure; DBP, diastolic blood pressure; BMI, body mass index; HbA1c, glycated hemoglobin; Ccr, creatinine clearance rate; AL, axial length.

## Statistical Analysis

The statistical analyses were performed by using SPSS version 25.0 software (SPSS Inc., Chicago, Illinois, USA). Graphs were plotted by using GraphPad Prism 8 (GraphPad Software, San Diego, California, USA). Quantitative variables were tested with Shapiro–Wilk to determine the normality and presented as mean  $\pm$  SD, median (interquartile range), or 95% CI. For statistical analysis, visual acuity was converted to the logarithm of the minimum angle of resolution (LogMAR). Descriptive statistics were used to characterize the demographics of the study population. A linear mixed-effects model was used to highlight the differences for the continuous OCTA and OCT parametric variables, adjusting for sex, age, and AL. All the statistical tests were two-sided and a *p* < 0.05 was considered statistically significant.

## RESULTS

In this prospective study, a total of 45 eyes with treatment-naïve severe NPDR and PDR from 28 patients with type 2 diabetes were enrolled. An overview of the demographic and clinical characteristics at baseline and 12 months after PRP is presented in **Table 1**. To avoid the effects of antivascular endothelial growth factor (VEGF) intravitreal injection (IVI) and vitrectomy on the retinal neurovascular and choroidal parameters measured by OCTA and OCT, the patients who received IVI for CSME or vitrectomy for the vitreous hemorrhage and severe fibrovascular proliferation during the follow-up were excluded. Some participants were lost to follow-up due to the novel coronavirus disease 2019 (COVID-19). Thus, the number of eyes included in 1, 3–6, and 12 months after PRP was 30, 20, and 21, respectively (**Figure 1**).

There were no significant differences in age, BMI, blood pressure, HbA1c, and renal function at baseline and at 12 months

after PRP. The BCVA was LogMAR 0.20 (95% CI 0.10–0.29) at baseline adjusting for the age, sex, and AL and showed an improved trend after PRP, although no statistical difference was observed (**Table 2**).

## Longitudinal Changes of the Retinal Vessel Density, Thickness, and FAZ in the Macular Area After PRP

There were no statistical differences in the macular VD including SCP and DCP and FAZ between the baseline and after PRP (**Table 2**), while macular thickness including whole parafoveal areas and perifoveal areas was significantly increased at 1 and 3–6 months (whole macular thickness: *p* = 0.007, *p* = 0.016, respectively; parafoveal thickness: *p* = 0.022, *p* = 0.002, respectively; and perifoveal areas: *p* = 0.023, *p* = 0.034), but then declined at 12 months after PRP. However, increased foveal thickness persisted up to 12 months postoperatively (*p* < 0.001, *p* = 0.019, *p* = 0.007, respectively) (**Figures 2A–D**, **Supplementary Table 1**).

## Longitudinal Changes of the Peripapillary VD and RNFL Thickness After PRP

None of the statistical changes were observed in the whole peripapillary VD and eight peripapillary segments (**Table 2**). Compared to baseline, RNFL thickness in the whole peripapillary area and seven peripapillary segments except for the temporal inferior segment significantly increased at 1 month after PRP (whole peripapillary RNFL thickness, superior nasal peripapillary RNFL thickness, nasal superior peripapillary RNFL thickness, nasal inferior peripapillary RNFL thickness, inferior nasal peripapillary RNFL thickness, inferior temporal peripapillary RNFL thickness, temporal superior peripapillary RNFL thickness, superior temporal peripapillary RNFL thickness: *p* < 0.001, *p* = 0.023, *p* = 0.018, *p* = 0.001, *p* = 0.013, *p* = 0.013, *p* = 0.031, *p* = 0.003, respectively), while temporal inferior RNFL thickness was unchanged during 12 months. However, the nasal inferior RNFL thickness was significantly increased at 1 and 12 months (1 month: *p* = 0.001, 12 months: *p* = 0.025) (**Figures 2E–M**, **Supplementary Table 1**).

## Longitudinal Changes of the GCC Thickness, GLV, and FLV After PRP

**Figures 2N–P** shows the GCC thickness, GLV, and FLV that were stable at 12-month follow-up. However, compared to baseline, GCC thickness significantly increased (*p* = 0.005) and GLV and FLV significantly decreased at 1 month postoperatively (*p* = 0.003, *p* = 0.013, respectively) (**Supplemental Table 1**).

## Longitudinal Changes of SFCT After PRP

**Table 2** shows the mean SFCT that was 252.43  $\mu$ m (95% CI 220.92–283.95) at baseline. No statistical differences of SFCT were observed during the follow-up visit after PRP, although an increasing trend was shown.

**TABLE 2 |** Longitudinal changes of the best corrected visual acuity (BCVA), subfoveal choroidal thickness (SFCT), macular vessel density, and foveal avascular zone (FAZ) after panretinal photocoagulation [mean (95% CI)].

Variables	Baseline (n = 45)	1 month (n = 30)	3-6 months (n = 20)	12 months (n = 21)	P-value
BCVA (LogMAR)	0.20 (0.10–0.29)	0.14 (0.05–0.23)	0.15 (0.07–0.23)	0.14 (0.06–0.23)	0.355
SFCT ( $\mu\text{m}$ )	252.43 (220.92–283.95)	259.98 (227.48–292.47)	261.79 (229.11–294.47)	263.73 (230.08–297.39)	0.507
Macular SCP VD (%)					
Whole VD	46.27 (43.88–48.66)	46.45 (44.17–48.73)	45.67 (43.34–48.00)	46.06 (43.66–48.46)	0.593
Foveal VD	17.26 (12.84–21.69)	20.66 (16.01–25.31)	17.52 (13.30–21.74)	18.5 (14.07–22.93)	0.094
Parafoveal VD	45.80 (42.74–48.87)	45.99 (43.13–48.86)	45.03 (42.14–47.92)	44.79 (41.82–47.77)	0.391
Perifoveal VD	47.21 (44.73–49.70)	47.59 (45.21–49.97)	46.79 (44.3–49.28)	46.94 (44.44–49.44)	0.579
Macular DCP VD (%)					
Whole VD	43.05 (40.79–45.31)	42.91 (40.84–44.97)	42.38 (40.01–44.76)	43.65 (41.21–46.09)	0.703
Foveal VD	27.52 (23.28–31.75)	28.17 (23.9–32.43)	27.86 (23.77–31.95)	27.51 (23.11–31.91)	0.942
Parafoveal VD	47.43 (45.27–49.59)	46.89 (44.77–49.01)	46.28 (43.93–48.62)	47.88 (45.56–50.2)	0.443
Perifoveal VD	43.93 (41.50–46.37)	44.10 (41.82–46.38)	43.52 (41.03–46.01)	44.72 (42.08–47.37)	0.746
FAZ (6.0 mm scan)					
FAZ ( $\text{mm}^2$ )	0.38 (0.30–0.46)	0.32 (0.23–0.41)	0.34 (0.25–0.44)	0.36 (0.26–0.46)	0.412
Perimeter (mm)	2.49 (2.21–2.77)	2.26 (1.94–2.57)	2.33 (1.99–2.76)	2.41 (2.06–2.76)	0.396
AI	1.16 (1.13–1.20)	1.15 (1.11–1.19)	1.13 (1.09–1.17)	1.16 (1.11–1.20)	0.376
FD-300	47.17 (44.85–49.49)	48.41 (45.84–50.98)	45.22 (42.52–47.92)	45.78 (43.02–48.54)	0.108
Peripapillary VD (%)					
Peripapillary	49.02 (47.32–50.72)	48.12 (46.28–49.97)	48.67 (46.78–50.55)	47.52 (45.59–49.45)	0.146
Superior Nasal	45.90 (43.76–48.04)	44.93 (42.48–47.37)	46.81 (44.32–49.30)	45.09 (42.52–47.67)	0.444
Nasal Superior	43.60 (41.26–45.95)	42.67 (40.15–45.2)	43.76 (41.19–46.32)	42.04 (39.42–44.66)	0.235
Nasal Inferior	43.90 (42.05–45.76)	43.98 (41.84–46.11)	43.17 (40.97–45.37)	43.18 (40.9–45.46)	0.848
Inferior Nasal	48.48 (45.69–51.26)	47.62 (44.63–50.6)	47.72 (44.69–50.74)	46.24 (43.16–49.33)	0.174
Inferior Temporal	55.37 (52.79–57.95)	53.76 (50.92–56.59)	54.51 (51.61–57.40)	54.47 (51.50–57.45)	0.415
Temporal Inferior	51.92 (50.06–53.78)	51.35 (49.21–53.50)	53.16 (50.95–55.38)	51.13 (48.83–53.42)	0.359
Temporal Superior	54.25 (52.01–56.5)	53.79 (51.14–56.45)	53.86 (51.10–56.63)	54.87 (51.99–57.75)	0.896
Superior Temporal	51.92 (49.06–54.78)	51.50 (48.23–54.77)	52.09 (48.72–55.45)	51.96 (48.48–55.44)	0.986

p-values are calculated by using a linear mixed-effects model before and after panretinal photocoagulation adjusting for age, sex, and axial length.

LogMAR, the logarithm of the minimum angle of resolution; SCP, superficial capillary plexus; VD, vessel density; DCP, deep capillary plexus; AI = acircularity index.

## Longitudinal Morphological Changes of Vascular Abnormality by Using the Multimodal Images

We observed the changes in the morphology of the neovascularization of the disk (NVD), from large and dense to small and loose, in eight eyes out of 12 eyes (67%) during the follow-up visit after PRP by using OCTA. Correspondingly, reduced fluorescein leakage of the NVD was observed on FFA (**Figure 3**). Furthermore, regression of neovascularization after PRP was documented in 18 eyes (18/22 eyes, 82%; **Figure 4**) and among them, the complete regression was in two eyes and partial regression was in 16 eyes post-PRP. No significant longitudinal changes of parameters, including BCVA, retinal VD and thickness, FAZ, peripapillary VD and RNFL thickness, GCC thickness, FLV and GLV, and SFCT, were observed in the total 18 PDR eyes with regression of neovascularization after PRP during the follow-up period (**Supplementary Table 2**). In addition, the new blood vessels, similar to the intraretinal microvascular abnormalities (IRMAs), were observed in the macular nonperfusion area of the severe NPDR eyes (**Figure 5**)

and the changes of vascular morphology in the macular arch were also observed during the follow-up period.

## DISCUSSION

This study was a prospective longitudinal study to investigate the long-term comprehensive changes of the retinal microvasculature, neural retina, and choroid following PRP. In this study, results showed no significant microvascular (macular and peripapillary VD); neural (whole macular thickness, peripapillary RNFL thickness, and GCC thickness); and the SFCT changes at 12 months after PRP, despite the increase of whole macular thickness, peripapillary RNFL, and GCC thickness at the early post-PRP phase. The regression of neovascularization and the unchanged BCVA in this study confirmed that PRP effectively alleviated retinal ischemia and protected the neural retina. These findings suggest that PRP may prevent diabetic microvascular, neural, and choroidal damage at 12 months in the treatment-naïve patients with severe NPDR and PDR without DME.

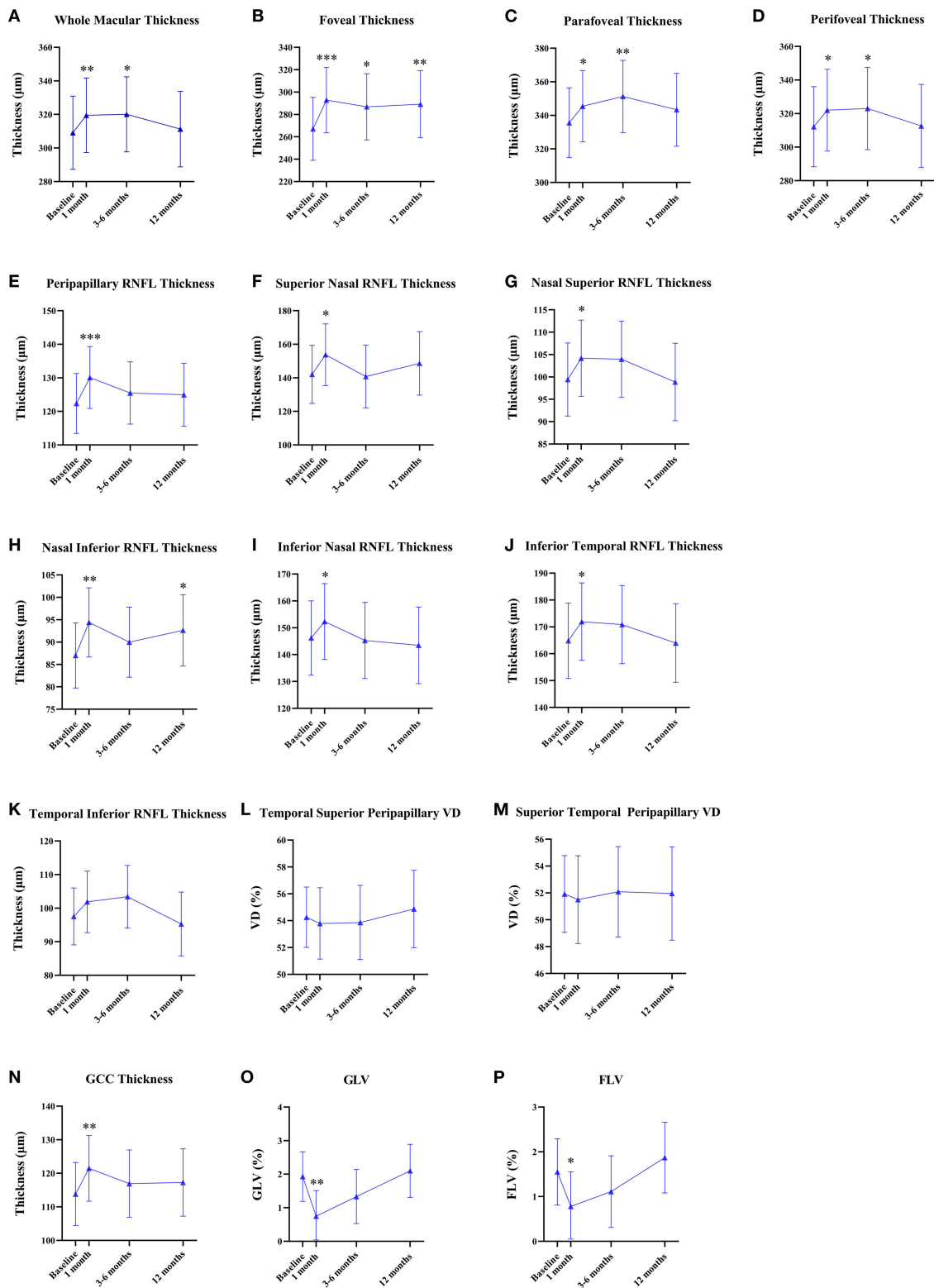


**FIGURE 2 |** Quantitative analyses of the longitudinal microvascular and neural changes in the macular and peripapillary areas during 12 months after panretinal photocoagulation (PRP). **(A–D)** Longitudinal changes of macular thickness [mean (95% CI),  $\mu\text{m}$ ] after PRP. **(E–M)** Longitudinal changes of peripapillary retinal nerve fiber layer (RNFL) thickness [mean (95% CI),  $\mu\text{m}$ ] after PRP. **(N–P)** Longitudinal changes of the ganglion cell complex (GCC) thickness [mean (95% CI),  $\mu\text{m}$ ]; global loss volume (GLV) [mean (95% CI), %]; and focal loss volume (FLV) [mean (95% CI), %] after PRP. \* $p < 0.05$ , \*\* $p < 0.01$ , \*\*\* $p < 0.001$ .



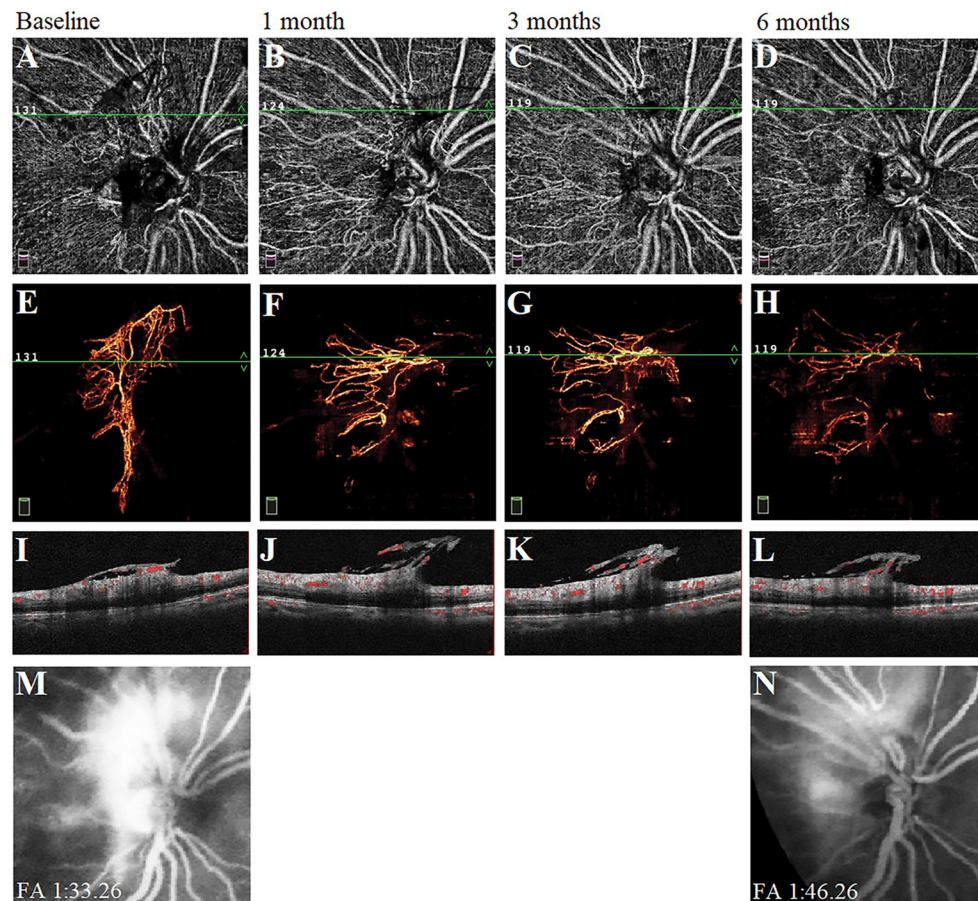


**FIGURE 3** | A typical proliferative diabetic retinopathy case showed the neovascularization of the disk (NVD) changed from large, dense, and strong fluorescein leakage to small, loose, and weak fluorescein leakage at 6 months after panretinal photocoagulation (PRP). **(A–D)** Retina en-face slab images of NVD were observed by optical coherence tomography angiography (OCTA). **(E–H)** Vitreous en-face slab images of OCTA. **(I–L)** B-scan image of OCTA. **(M,N)** Images of fluorescein angiography at baseline and 6 months.

There were no statistical differences in macular VD after PRP, although the decreased trend was observed at the 3–6 months follow-up, which was similar to the results reported in other literature (17–19). Microvascular abnormalities and subsequent capillary occlusion have been demonstrated to aggravate the decrease of the VD and enlargement of the FAZ with the progression of DR (11). However, Fawzi et al. found an overall increase in the flow metrics of all the macular capillary layers following PRP by the mathematical model, although no significant difference for the vascular density parameters was shown (17). Therefore, the unchanged macular VD and FAZ area during the 12 months following PRP in this study may indicate stabilization of the macular microcirculation and control of ischemia.

Although several studies showed a significant reduction in the macular choroidal thickness after PRP (20–22), results showed no significant change during the 12-month follow-up. This discrepancy might be due to the differences in the profiles of the patient. This study included the severe NPDR or PDR patients without DME, while the previous reports included the eyes with

DME or with IVI. On one hand, the subfoveal choroid is thicker in the eyes with DME compared to those without the eyes with DME (22), which leads to a higher baseline level. On the other hand, the downregulation of VEGF due to the IVI may induce a decrease in choroidal blood flow and thickness (23), which perhaps affect the assessment of the macular choroidal thickness after PRP. Taken together, our results showing the long-term stability of VD in the macula, peripapillary area, and subfoveal choroid indicate an overall redistribution of the capillary blood flow to the posterior pole following PRP.

Although the VD in the posterior pole remained unchanged, macular retinal thickness significantly increased after PRP, especially at the fovea 1–6 months postoperatively. This finding may be explained by the retinal inflammation and edema caused by PRP in the early postoperative phase (24). However, we found that macular thickness was significantly decreased in the eyes receiving IVI plus PRP (**Supplementary Table 3**). This group included 10 eyes with CSME (central subfield macular thickness  $\geq 300 \mu\text{m}$ ) in seven patients with severe NPDR and PDR. All of the participants received one-time IVI before initial PRP within



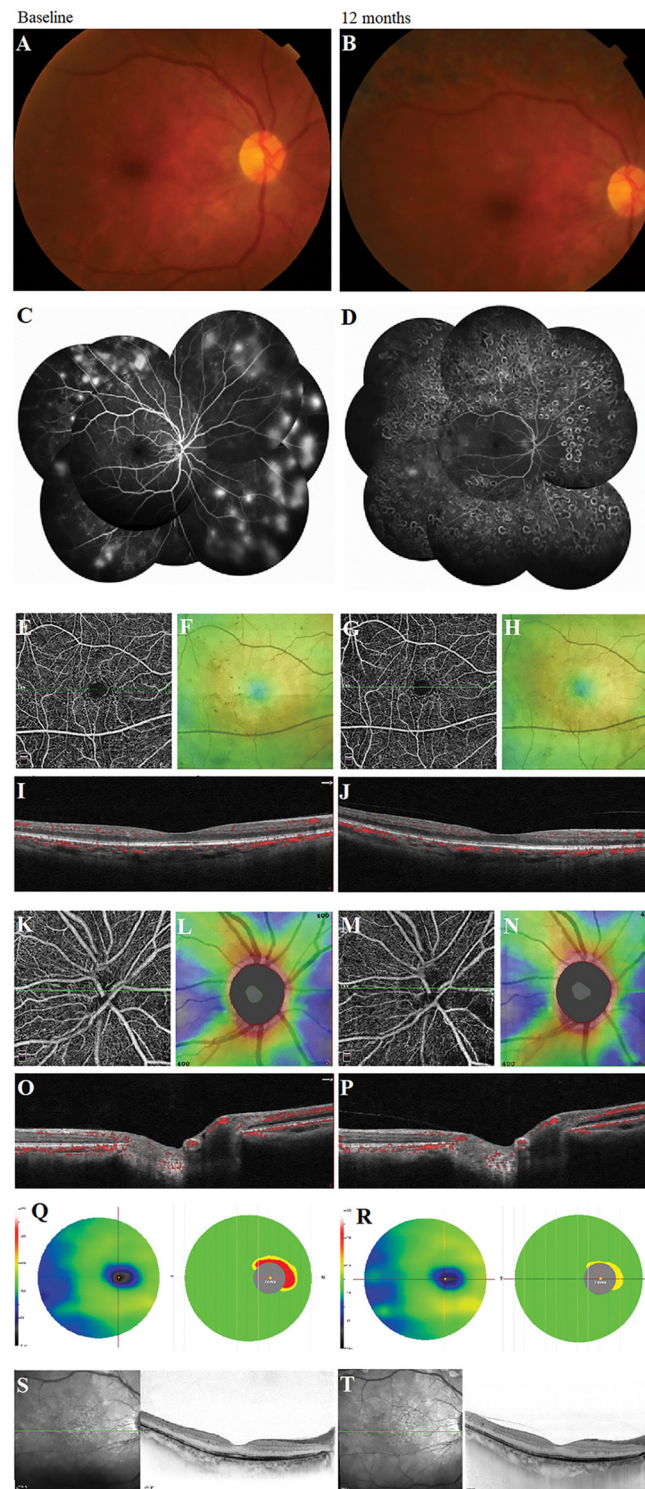


**FIGURE 4 |** A typical proliferative diabetic retinopathy case showed the retinal neovascularization regression with the unchanged vessel density, the thickness of retinal nerve fiber layer and ganglion cell complex, and subfoveal choroidal thickness at 12 months after panretinal photocoagulation (PRP) in the multimodal images. **(A,B)** Images of color fundus photography. **(C,D)** Images of fundus fluorescein angiography. **(E,G)** Retina en-face slab images in HD Angio Retina 6.0 mm scan by optical coherence tomography angiography (OCTA). **(F,H)** Full retinal thickness images in HD Angio Retina 6.0 mm scan of OCTA. **(I,J)** B-scan images in HD Angio Retina 6.0 mm scan of OCTA. **(K,M)** Retina en-face slab images in HD Angio Disk 4.5 mm scan by OCTA. **(L,N)** Retinal nerve fiber layer thickness images of OCTA. **(O,P)** B-scan images in HD Angio Retina 6.0 mm scan of OCTA. **(Q,R)** Ganglion cell complex scan images of OCTA. **(S,T)** Images of the OCT with the enhanced depth-imaging (OCT-EDI) technique.

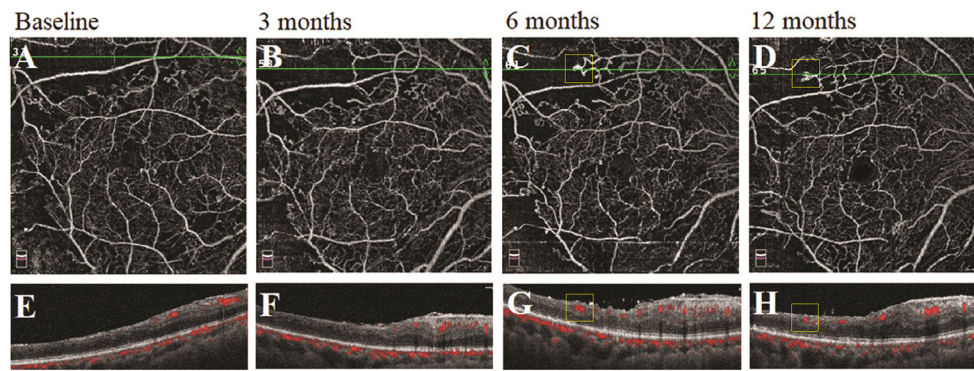


**FIGURE 5 |** A typical severe nonproliferative diabetic retinopathy (NPDR) case showed the morphological changes of the similar intraretinal microvascular abnormalities (IRMAs) in the nonperfusion area following panretinal photocoagulation (PRP). **(A–D)** Retina en-face slab images of optical coherence tomography angiography (OCTA). **(E–H)** B-scan images of OCTA.

7 days. Reinjection was performed if obvious CSME reoccurred during the 12-month follow-up. These findings supported by the other studies (25, 26) suggest that treatment with adjunctive IVI before or after PRP could reduce macular edema and stabilizes the blood-retinal barrier. Of course, it is necessary to perform a further study in a larger sample to confirm this finding.

The changes in the RNFL and GCC thickness showed similar trends that were significantly increased at 1 month following PRP, while the GLV and FLV were significantly decreased during the early post-PRP period. Over the long-term follow-up, they gradually returned to the baseline level. Many of the previous studies using OCT obtained similar results (27, 28). They considered that the retinal inflammation and edema caused by PRP at the early postoperative phase could damage the retinal neural cell and tissue and later recovery might be attributed to the absorption and healing of the edema and the laser-induced photoreceptors and ganglion cell damage. However, other studies showed PRP to decrease the thickness of the peripapillary RNFL and GCC (29) suggesting that the presence of diabetes itself could cause neurodegenerative changes in the retina and subsequent degeneration of RNFL by retinal cell loss in the late PRP phase. To the best of our knowledge, there are no relevant studies observing the changes of the RNFL and GCC after PRP using OCTA.

This study comprehensively evaluated the retinal microvascular, neural, and choroidal changes after PRP in the treatment-naïve patients with severe NPDR and PDR during a long-term follow-up period. To achieve the standard differences among the visits, all the OCTA and OCT metrics were adjusted for age, sex, and AL. This study had some limitations. First, the limited field view provided by OCTA only showed the macular area without the laser spots and could not completely evaluate the whole retina. Thus, wide-field OCTA will improve the accuracy of evaluation in the future. Second, the patients were excluded due to the changes in treatment (such as IVI and PPV), which resulted in the absence of observation in some of the patients with DME or with aggravation. Third, the dropout of the subjects during the follow-up period, partially due to the COVID-19, might make the resulting

bias. In addition, since PRP is generally recommended for the treatment of the severe stages of DR (severe NPDR and PDR), it is difficult to longitudinally observe the changing features of these parameters in the untreated patients with severe DR, which is the main cause for the lack of a control group in this study.

In conclusion, the unchanged BCVA, VD, the thickness of RNFL and GCC, and SFCT during the 12-month follow-up period suggest that PRP may prevent the retinal microvascular, neural, and choroidal damages in the eyes with the severe NPDR and PDR without DME. Inclusion of the other metrics of visual function such as contrast sensitivity and visual field testing will help to better understand the mechanism of PRP.

## DATA AVAILABILITY STATEMENT

The original contributions presented in the study are included in the article/**Supplementary Material**, further inquiries can be directed to the corresponding authors.

## ETHICS STATEMENT

The studies involving human participants were reviewed and approved by Ethics Committee of Guangdong Provincial People's Hospital. The patients/participants provided their written informed consent to participate in this study.

## AUTHOR CONTRIBUTIONS

TH and XL collected data, performed analyses, and wrote the manuscript. JX collected data and revised the manuscript. LZ provided patients' information and supervised the process. GZ interpreted data. AZ and XC collected data. YC and QM interpreted data, revised the manuscript, gained the fund, and supervised the process. All authors contributed to the article and approved the submitted version.

## FUNDING

This study was supported by the Guangdong Basic and Applied Basic Research Foundation (2019A1515010697, 2021A1515010921); the Guangzhou Science and Technology Program Project (202002030400); the National Natural Science Foundation, Beijing, China (82000897), and the Bethune-Lumitin Research Funding for the Young and Middle-aged Ophthalmologists (BJ-LM2019004J). The funding

organizations had no role in the design or conduct of this research.

## SUPPLEMENTARY MATERIAL

The Supplementary Material for this article can be found online at: <https://www.frontiersin.org/articles/10.3389/fmed.2021.752538/full#supplementary-material>

## REFERENCES

- Lee R., Wong TY., Sabanayagam C. Epidemiology of diabetic retinopathy, diabetic macular edema and related vision loss. *Eye Vis (Lond)*. (2015) 2:17. doi: 10.1186/s40662-015-0026-2
- Wang W, Liu S, Qiu Z, He M, Wang L, Li Y, et al. Choroidal thickness in diabetes and diabetic retinopathy: a swept source OCT study. *Invest Ophthalmol Vis Sci*. (2020) 61:29. doi: 10.1167/iovs.61.4.29
- Lains I, Talcott KE, Santos AR, Marques JH, Gil P, Gil J, et al. Choroidal thickness in diabetic retinopathy assessed with swept-source optical coherence tomography. *Retina*. (2018) 38:173–82. doi: 10.1097/iae.0000000000001516
- Conti FF, Qin VL, Rodrigues EB, Sharma S, Rachitskaya AV, Ehlers JP, et al. Choriocapillaris and retinal vascular plexus density of diabetic eyes using split-spectrum amplitude decorrelation spectral-domain optical coherence tomography angiography. *Br J Ophthalmol*. (2019) 103:452–6. doi: 10.1136/bjophthalmol-2018-311903
- Ro-Mase T, Ishiko S, Omae T, Ishibazawa A, Shimouchi A, Yoshida A. Association between alterations of the choriocapillaris microcirculation and visual function and cone photoreceptors in patients with diabetes. *Invest Ophthalmol Vis Sci*. (2020) 61:1. doi: 10.1167/iovs.61.6.1
- Photocoagulation treatment of proliferative diabetic retinopathy. Clinical application of Diabetic Retinopathy Study (DRS) findings, DRS Report Number 8. The Diabetic Retinopathy Study Research Group. *Ophthalmology*. (1981) 88:583–600. doi: 10.1016/S0161-6420(81)34978-1
- Ferris FL, Podgor MJ, Davis MD. Macular edema in Diabetic Retinopathy Study patients. Diabetic retinopathy study report number 12. *Ophthalmology*. (1987) 94:754–60. doi: 10.1016/s0161-6420(87)33526-2
- Treatment techniques and clinical guidelines for photocoagulation of diabetic macular edema. Early treatment diabetic retinopathy study report number 2. Early Treatment diabetic retinopathy study research group. *Ophthalmology*. (1987) 94:761–74. doi: 10.1016/s0161-6420(87)33527-4
- Stefánsson E. The therapeutic effects of retinal laser treatment and vitrectomy. A theory based on oxygen and vascular physiology. *Acta Ophthalmol Scand*. (2001) 79:435–40. doi: 10.1034/j.1600-0420.2001.790502.x
- Hessemer V, Schmidt KG. Influence of panretinal photocoagulation on the ocular pulse curve. *Am J Ophthalmol*. (1997) 123:748–52. doi: 10.1016/s0002-9394(14)71121-3
- Li X, Xie J, Zhang L, Cui Y, Zhang G, Chen X, et al. Identifying microvascular and neural parameters related to the severity of diabetic retinopathy using optical coherence tomography angiography. *Invest Ophthalmol Vis Sci*. (2020) 61:39. doi: 10.1167/iovs.61.5.39
- Shimouchi A, Ishibazawa A, Ishiko S, Omae T, Ro-Mase T, Yanagi Y, et al. A proposed classification of intraretinal microvascular abnormalities in diabetic retinopathy following panretinal photocoagulation. *Invest Ophthalmol Vis Sci*. (2020) 61:34. doi: 10.1167/iovs.61.3.34
- Aschauer J, Pollreis A, Karst S, Hülsmann M, Hajdu D, Datlinger F, et al. Longitudinal analysis of microvascular perfusion and neurodegenerative changes in early type 2 diabetic retinal disease. *Br J Ophthalmol*. (2020). doi: 10.1136/bjophthalmol-2020-317322
- Wilkinson CP, Ferris FL, Klein RE, Lee PP, Agardh CD, Davis M, et al. Proposed international clinical diabetic retinopathy and diabetic macular edema disease severity scales. *Ophthalmology*. (2003) 110:1677–82. doi: 10.1016/S0161-6420(03)00475-5
- Musat O, Cernat C, Labib M, Gheorghe A, Toma O, Zamfir M, et al. Diabetic macular edema. *Romanian journal of ophthalmology*. (2015) 59:133–6.
- Jia Y, Tan O, Tokayer J, Potsaid B, Wang Y, Liu JJ, et al. Split-spectrum amplitude-decorrelation angiography with optical coherence tomography. *Opt Express*. (2012) 20:4710–25. doi: 10.1364/oe.20.004710
- Fawzi AA, Fayed AE, Linsenmeier RA, Gao J, Yu F. Improved macular capillary flow on optical coherence tomography angiography after panretinal photocoagulation for proliferative diabetic retinopathy. *Am J Ophthalmol*. (2019) 206:217–27. doi: 10.1016/j.ajo.2019.04.032
- Faghihi H, Riazi-Esfahani H, Khodabande A, Khalili Pour E, Mirshahi A, Ghassemi F, et al. Effect of panretinal photocoagulation on macular vasculature using optical coherence tomography angiography. *Eur J Ophthalmol*. (2020) 31:1877–84. doi: 10.1177/1120672120952642
- Lorusso M, Milano V, Nikolopoulou E, Ferrari LM, Cicinelli MV, Querques G, et al. Panretinal photocoagulation does not change macular perfusion in eyes with proliferative diabetic retinopathy. *Ophthalmic Surg Lasers Imaging Retina*. (2019) 50:174–8. doi: 10.3928/23258160-20190301-07
- Mirshahi A, Ghassemi F, Fadakar K, Mirshahi R, Bazvand F, Riazi-Esfahani H. Effects of panretinal photocoagulation on retinal vasculature and foveal avascular zone in diabetic retinopathy using optical coherence tomography angiography: A pilot study. *J Curr Ophthalmol*. (2019) 31:287–91. doi: 10.1016/j.joco.2019.06.001
- Kang HM, Lee NE, Choi JH, Koh HJ, Lee SC. Significant reduction of both peripapillary and subfoveal choroidal thickness after panretinal photocoagulation in patients with type 2 diabetes. *Retina*. (2018) 38:1905–12. doi: 10.1097/iae.0000000000001804
- Kim JT., Lee DH., Joe SG., Kim JG., Yoon YH. Changes in choroidal thickness in relation to the severity of retinopathy and macular edema in type 2 diabetic patients. *Invest Ophthalmol Vis Sci*. (2013) 54:3378–84. doi: 10.1167/iovs.12-11503
- Bressler NM, Beck RW, Ferris FL. Panretinal photocoagulation for proliferative diabetic retinopathy. *N Engl J Med medicine*. (2011) 365:1520–6. doi: 10.1056/NEJMc0908432
- Nonaka A, Kiryu J, Tsujikawa A, Yamashiro K, Nishijima K, Kamizuru H, et al. Inflammatory response after scatter laser photocoagulation in nonphotocoagulated retina. *Invest Ophthalmol Vis Sci*. (2002) 43:1204–9.
- Figueira J, Fletcher E, Massin P, Silva R, Bandello F, Midena E, et al. Ranibizumab plus panretinal photocoagulation versus panretinal photocoagulation alone for high-risk proliferative diabetic retinopathy (PROTEUS Study). *Ophthalmology*. (2018) 125:691–700. doi: 10.1016/j.optha.2017.12.008
- Roohipour R, Sharifian E, Moghimi S, Fard MA, Ghassemi F, Zarei M, et al. The effect of panretinal photocoagulation (PRP) versus intravitreal bevacizumab (IVB) plus PRP on peripapillary retinal nerve fiber layer (RNFL) thickness analyzed by optical coherence tomography in patients with proliferative diabetic retinopathy. *J Ophthalmic Vis Res*. (2019) 14:157–63. doi: 10.4103/jovr.jovr\_160\_17
- Filek R, Hooper P, Sheidow T, Gonder J, Varma DK, Heckler L, et al. Structural and functional changes to the retina and optic nerve following panretinal photocoagulation over a 2-year time period. *Eye (Lond)*. (2017) 31:1237–44. doi: 10.1038/eye.2017.66
- Demirok G, Kocamaz ME, Topalak Y, Altay Y, Tabakci B, Sengün A. Changes in the macular ganglion cell complex thickness and central macular thickness

- after argon laser panretinal photocoagulation. *Semin Ophthalmol.* (2017) 32:759–63. doi: 10.1080/08820538.2016.1177098
29. Kim J., Woo S. J., Ahn J., Park K. H., Chung H., Park K. H. Long-term temporal changes of peripapillary retinal nerve fiber layer thickness before and after panretinal photocoagulation in severe diabetic retinopathy. *Retina.* (2012) 32:2052–60. doi: 10.1097/IAE.0b013e3182562000

**Conflict of Interest:** The authors declare that the research was conducted in the absence of any commercial or financial relationships that could be construed as a potential conflict of interest.

The handling editor and the reviewer WC declared a shared affiliation with one of the authors XL at time of review.

**Publisher's Note:** All claims expressed in this article are solely those of the authors and do not necessarily represent those of their affiliated organizations, or those of the publisher, the editors and the reviewers. Any product that may be evaluated in this article, or claim that may be made by its manufacturer, is not guaranteed or endorsed by the publisher.

Copyright © 2021 Huang, Li, Xie, Zhang, Zhang, Zhang, Chen, Cui and Meng. This is an open-access article distributed under the terms of the Creative Commons Attribution License (CC BY). The use, distribution or reproduction in other forums is permitted, provided the original author(s) and the copyright owner(s) are credited and that the original publication in this journal is cited, in accordance with accepted academic practice. No use, distribution or reproduction is permitted which does not comply with these terms.





## OPEN ACCESS

## Edited by:

Haijiang Lin,  
Massachusetts Eye & Ear Infirmary,  
Harvard Medical School,  
United States

## Reviewed by:

Wenqi Su,  
Tianjin Medical University General  
Hospital, China  
Shuo Sun,  
Tianjin Medical University Eye  
Hospital, China

## \*Correspondence:

Shao-Peng Wang  
904268100@qq.com

## †ORCID:

Hui Lu  
[orcid.org/0000-0002-4379-2525](https://orcid.org/0000-0002-4379-2525)  
Tao Yue  
[orcid.org/0000-0003-4185-9180](https://orcid.org/0000-0003-4185-9180)  
Na Liu  
[orcid.org/0000-0002-6521-7070](https://orcid.org/0000-0002-6521-7070)  
Gai-Xia Zhai  
[orcid.org/0000-0002-9882-7780](https://orcid.org/0000-0002-9882-7780)  
Zuo-Fen Wang  
[orcid.org/0000-0002-6670-4890](https://orcid.org/0000-0002-6670-4890)  
Dong-Ming Mi  
[orcid.org/0000-0002-4560-7215](https://orcid.org/0000-0002-4560-7215)  
Jing Zhang  
[orcid.org/0000-0003-2036-2634](https://orcid.org/0000-0003-2036-2634)  
Shao-Peng Wang  
[orcid.org/0000-0003-0043-2463](https://orcid.org/0000-0003-0043-2463)

## Specialty section:

This article was submitted to  
Ophthalmology,  
a section of the journal  
Frontiers in Medicine

Received: 05 June 2021

Accepted: 24 September 2021

Published: 21 October 2021

## Citation:

Lu H, Yue T, Liu N, Wang Z-F,  
Zhai G-X, Mi D-M, Zhang J and  
Wang S-P (2021) Efficacy of  
Conbercept in the Treatment of  
Choroidal Neovascularization  
Secondary to Pathologic Myopia.  
Front. Med. 8:720804.  
doi: 10.3389/fmed.2021.720804

# Efficacy of Conbercept in the Treatment of Choroidal Neovascularization Secondary to Pathologic Myopia

Hui Lu<sup>1†</sup>, Tao Yue<sup>2†</sup>, Na Liu<sup>1†</sup>, Zuo-Fen Wang<sup>1†</sup>, Gai-Xia Zhai<sup>1†</sup>, Dong-Ming Mi<sup>1†</sup>,  
Jing Zhang<sup>3†</sup> and Shao-Peng Wang<sup>1\*†</sup>

<sup>1</sup> Department of Ophthalmology, Zibo Central Hospital, Zibo, China, <sup>2</sup> Department of Gerontology, Zibo Central Hospital, Zibo, China, <sup>3</sup> Jinan No.8 Retired Cadres Rest and Recuperation Home of Shandong Provincial Military Region, Jinan, China

**Purpose:** To observe the clinical efficacy of conbercept in the treatment of choroidal neovascularization (CNV) secondary to pathologic myopia.

**Methods:** We used retrospective analysis of the clinical data of 20 patients (24 eyes) with pathologic myopia choroidal neovascularization (PM-CNV). All patients were treated with intravitreal injection of conbercept 0.5 mg (0.05 ml), a vascular endothelial growth factor (VEGF) receptor fusion protein, and all patients completed at least 6 months of follow-up. Fundus, best corrected visual acuity (BCVA), fundus fluorescein angiography (FFA), optical coherence tomography (OCT), multifocal electroretinogram (mfERG) were assessed before and after treatment. Primary outcome was the functional change in amplitude by mfERG and secondary outcome was the structural change in central macular thickness (CRT) by OCT. The CNV area, leakage of CNV lesions, ocular and systemic adverse events were observed before and after treatment.

**Results:** The BCVA were  $64.33 \pm 10.83$  letters,  $65.42 \pm 11.24$  letters,  $67.67 \pm 7.07$  letters after treatment 1, 3, 6 month, respectively, which showed improvement compared with the baseline ( $P < 0.05$ ). The CRT decreased significantly from  $308.50 \pm 45.48 \mu\text{m}$  to  $219.63 \pm 30.27 \mu\text{m}$ ,  $221.33 \pm 40.65 \mu\text{m}$ ,  $220.96 \pm 33.09 \mu\text{m}$  after treatment 1, 3, 6 month, respectively ( $P < 0.05$ ). The P1 response of mfERG amplitude improved from  $40.71 \pm 9.69 \text{ nv/deg}^2$  to  $50.67 \pm 9.48 \text{ nv/deg}^2$ ,  $54.92 \pm 8.45 \text{ nv/deg}^2$ ,  $55.67 \pm 6.74 \text{ nv/deg}^2$  after treatment 1, 3, 6 month, respectively ( $P < 0.05$ ). After 6 months of treatment, the leakage of CNV lesions disappeared in 20 (83.3%) eyes, and the leakage area of CNV lesions was significantly reduced in 4 (16.7%) eyes.

**Conclusion:** The intravitreal injection of conbercept significantly reduced CRT and the CNV area, inhibited the leakage of CNV, improved the BCVA, increased the response of mfERG amplitude, and restored the retinal function. The intravitreal injection of conbercept can change the morphology and function of the macular in PM-CNV, which is safe and effective for the treatment of PM-CNV.

**Keywords:** conbercept, vascular endothelial growth factor, choroidal neovascularization, pathologic myopia, efficacy, VEGF receptor fusion protein



## BACKGROUND

Pathological myopia (PM) is an important cause of low vision and blindness, especially in Asian populations (1). PM was originally described as high myopia accompanied by characteristic degenerative changes in the sclera, choroid, and retinal pigment epithelium (RPE) with compromised visual function (2). Although there is no universally accepted definition of PM, it is frequently defined as globe elongation and a refractive error of at least 26 diopters (3) and/or axial length of  $>26.5$  mm (4) associated with degenerative changes in the retina (5, 6). The typical pathological features include arc spots, posterior staphyloma, lacquer cracks, Fuchs spots, choroidal atrophy, choroidal neovascularization (CNV), etc., of which the major cause of visual impairment is macular CNV (7). The pathogenesis of PM-CNV is still unclear. The possible mechanisms are choroidal and retinal microcirculation disorders, Bruch membrane rupture, hypoxic and ischemic macular areas, stimulation of the secretion of vascular endothelial growth factor (VEGF) and promotion of CNV breakage through the Bruch membrane into the subretinal space (8). The treatment of PM-CNV includes surgical treatment, drug treatment, laser photocoagulation, etc. (9).

The factors that stimulate pathologic neovascularization are not very clear, but VEGF is considered to be one of the main elements in angiogenesis, and several reports have provided evidence that VEGF-a plays an important role in promoting CNV in PM (10–15). Moreover, studies have shown increased VEGF concentrations in the aqueous humor of patients with CNV secondary to PM compared to controls (16).

Before 2011, the most widely used pharmaceutical agents were monoclonal antibodies that block VEGF-A, which include ranibizumab (Lucentis; Genentech, Inc., South San Francisco, CA, USA) that has been approved by the Food and Drug Administration, and bevacizumab (Avastin; Genentech Inc.) (17–19). Aflibercept (Eylea; Regeneron, Inc., Tarrytown, NJ, USA) was approved as a VEGF receptor fusion protein in 2011 in the USA, and it works as a multitarget VEGF family blocker and binds to isoforms of VEGF-A and VEGF-B as well as placenta growth factor (PlGF) (20). Conbercept (Langmu; Kanghong, Inc., Sichuan, China) is a different VEGF receptor (VEGFR) fusion protein that blocks all isoforms of VEGF-A, VEGF-B, VEGFC, and PlGF, and it has a long half-life in the vitreous body (21). Studies on conbercept have shown that it is an efficient drug for the treatment of neovascular age-related macular degeneration (AMD) (22).

In this study, we observed the clinical efficacy of conbercept for the treatment of PM-CNV to provide guidance for the clinical application of conbercept in PM-CNV.

## METHODS

A retrospective analysis of the clinical data from 20 patients (24 eyes) with PM-CNV diagnosed in Department of Ophthalmology, Zibo Central Hospital, from September 2016 to June 2018 was performed. The diagnosis of PM-CNV was confirmed by choroidal neovascular leakage on fluorescein

fundus angiography (FFA) and intraretinal or subretinal fluid as determined by optical coherence tomography (OCT). The inclusion criteria were eyes with refractive diopter  $\geq 6.0$  D or axial length  $\geq 26.0$  mm, PM-CNV without any treatment, CNV leakage seen with FFA, and a minimum follow-up period of 6 months after the first intravitreal conbercept injections. This study excluded patients with the following criteria: (1) history of ocular trauma; (2) age-related macular degeneration, uveitis, vasculitis, retinal breaks, etc.; (3) history of intraocular injection of drugs and previous photodynamic therapy of PM-CNV; (4) syphilis, tuberculosis and other systemic diseases; (5) refractive interstitial opacity could not be smoothly examined other retinal diseases; (6) patients refused to sign informed consent; and (7) pregnant women. This study was conducted in line with the Helsinki Declaration and was approved by the Ethics Committee of the Zibo Central Hospital, and all patients signed informed consent before surgery.

The intraocular injections were carried out under operating theater conditions. Following topical application of proparacaine, the eyelids, lashes, and conjunctiva were cleaned with 5% povidone iodine. After placement of a speculum to keep the eyelids open, conbercept (0.05 ml/0.5 mg; Chengdu Kang Hong Biotechnology Co., Ltd.) was injected at a distance of 4 mm from the superior temporal quadrant. After the injection, the patient was given a topical antibiotic in the quinolone group to use 4 times each day for a period of 7 days.

The decision to administer further injections was made on an as-needed basis. Each visit incorporated a biomicroscopic examination of the anterior segment, the best-corrected visual acuity (BCVA) was measured using the ETDRS scale, intraocular pressure (IOP) measured using non-contact tonometer (TX-20, Canon, Japan), a fundus examination, and a central retinal thickness (CRT) measurement using OCT (Optovue, Inc., Fremont, CA, USA). The mean central retinal thickness (CRT) was defined as the sum of the thickness of the neurosensory retina and the height of the subretinal fluid. FFA (Spectralis, Heidelberg, Germany) was performed before and 6 months after the intravitreal conbercept injections. The size of CNV was measured in the early-phase FA images using VK-2 5.5.5.0 in the fundus camera (KOWA non-myd 7; Kowa, Japan). Multifocal electroretinogram (mfERG) were examined before and after treatment in 1, 3, 6 month after treatment.

**TABLE 1 |** Patients basic characteristics ( $\bar{x} \pm s$   $n = 24$ ).

Characteristics		Patients, $N = 20$ (eyes, $N = 24$ )
Gender (eye)	Male	11
	female	13
Age (year)		$40.30 \pm 14.27$
Axis (mm)		$28.28 \pm 1.53$
Course of disease (day)		$8.20 \pm 5.06$
Diopter (D)		$-(10.58 \pm 2.49)$
Type (eye)	Subfoveal	12
	Parafovea	12

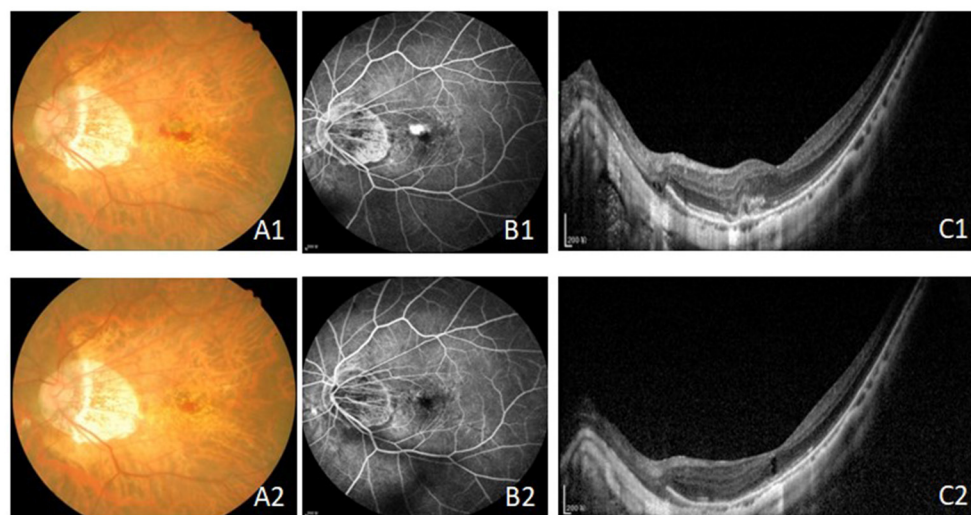


**FIGURE 1 |** The fundus, FFA and OCT results before (A1–C1) and after treatment (A2–C2) with intravitreal injection of conbercept in 6 month. The leakage of CNV were inhibited and the CRT and the CNV area were reduced. Bars = 200  $\mu$ m. FFA, fundus fluorescein angiography; OCT, optical coherence tomography; CRT, central retinal thickness; CNV, choroidal neovascularization.

**TABLE 2 |** BCVA, CRT, Amp-P1 before and after treatment ( $\bar{x} \pm s$   $n = 24$ ).

Time	BCVA (letters)	CRT ( $\mu$ m)	Amp-P1 (nv/deg <sup>2</sup> )	CNV area (mm <sup>2</sup> )
Before treatment	49.96 $\pm$ 9.65	308.50 $\pm$ 45.48	40.71 $\pm$ 9.69	0.35 $\pm$ 0.13
1 month	64.33 $\pm$ 10.83*	219.63 $\pm$ 30.27*	50.67 $\pm$ 9.48*	–
3 month	65.42 $\pm$ 11.24*	221.33 $\pm$ 40.65*	54.92 $\pm$ 8.45*	–
6 month	67.67 $\pm$ 7.07*	220.96 $\pm$ 33.09*	55.67 $\pm$ 6.74*	0.20 $\pm$ 0.10*

\* $P < 0.05$  compared with the data before treatment.

MfERG stimulation was performed with the Visual Evoked Response Imaging System (Retiscan, Wiesbaden/Brandenburg, Germany) equipped with a CRT stimulator. Responses were recorded monocularly using Jet electrode, which was positioned on the inferior cornea along the lid margin and temporally fixed. The pupil of the eye was dilated ( $\geq 8$  mm) with tropicamide (0.5%, Santen, Japan). Gold-cup reference and surface electrodes were applied on the temple and forehead, respectively. The measurement of mfERG was done as reported (23). Waveform Analysis For each waveform, the amplitude of the first positive peak (P1) of the first-order kernel were determined. P1 amplitude was measured from the trough of the first negative wave to the peak of the positive wave while the implicit time was measured from stimulus onset to the first prominent response peak. MfERG data were grouped into five concentric rings, with ring 1 representing the foveal response.

The following criteria were considered when making a decision about reinjection: persistence or recurrence of subretinal fluid or cystic structures via OCT; an increase in the most recent OCT measurement of CRT of 50  $\mu$ m or more, incipient CNV, incipient hemorrhage, and a loss of 5 or more letters when compared with the last recorded BCVA.

SPSS version 17.0 was used for statistical analysis. The values are presented as the mean  $\pm$  SD. The Student's *t*-test or the Mann–Whitney U test was used to determine the significance of the differences in the BCVA, CRT, CNV area and P1 amplitude in ring 1 of mfERG value recorded. A *P*-value  $< 0.05$  considered statistically significant.

## RESULTS

The study included 9 males (11 eyes) and 11 females (13 eyes); the age ranged from 21 to 65 years, with an average value of  $40.30 \pm 14.27$  years; the refractive diopter ranged from  $-6.5$  to  $-15.5$  D, with an average value of  $-10.58 \pm 2.49$  D; the average axial length was  $28.28 \pm 1.53$  mm; and there were 12 eyes with the subfoveal type and 12 eyes with the parafoveal type (Table 1).

All 24 eyes had reduced or stable size of CNV at the last visit (Figure 1). In terms of the mean CNV size, patients with intravitreal conbercept showed a significant reduction of mean CNV size reduction from  $0.35 \pm 0.13$  mm<sup>2</sup> at baseline to  $0.20 \pm 0.10$  mm<sup>2</sup> at month 6 ( $p < 0.05$ ) (Table 2; Figure 2). An absence of CNV angiographic leakage was observed by FFA in in 20

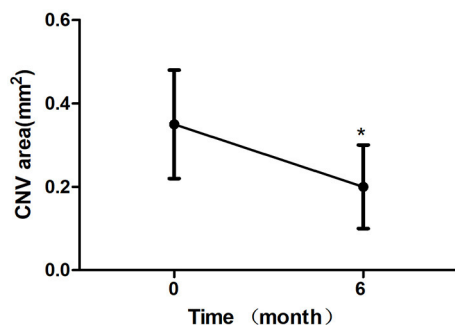


**FIGURE 2 |** Mean change in choroidal neovascularization (CNV) area over 6 months. The significant reduction of CNV area were observed at 6 month compared with baseline values (\* $P < 0.05$ ). Error bar represents standard deviation.

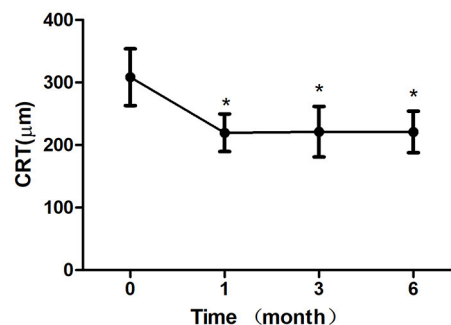


**FIGURE 4 |** Mean change in central retinal thickness (CRT) over 6 months. The significant improvements in CRT were observed at each follow-up visit compared with baseline values (\* $P < 0.05$ ). Error bar represents standard deviation.

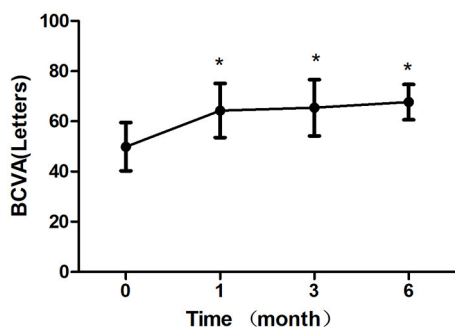


**FIGURE 3 |** Mean change in best-corrected visual acuity (BCVA) over 6 months. The significant improvements in vision were observed at each followup visit compared with baseline values (\* $P < 0.05$ ). Error bar represents standard deviation.

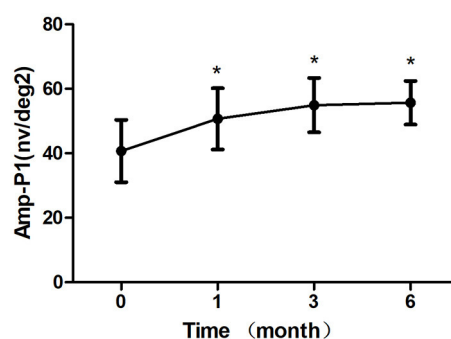


**FIGURE 5 |** Mean change in amplitude response density in ring 1 of mfERG amplitude (Amp-P1) over 6 months. The significant improvements in Amp-P1 were observed at each follow-up visit compared with baseline values (\* $P < 0.05$ ). Error bar represents standard deviation.

eyes (83.3%), while slight leakage persisted in 4 eyes (16.7%) at month 6.

After 1 month of treatment, 2 eyes (8.33%) demonstrated an increase in the BCVA to  $<5$  letters, 2 eyes (8.33%) increased to 5–10 letters, 16 eyes (66.7%) increased to 10–20 letters, and 4 eyes (16.7%) increased to  $\geq 20$  letters. The BCVA were  $64.33 \pm 10.83$  letters,  $65.42 \pm 11.24$  letters,  $67.67 \pm 7.07$  letters after treatment 1, 3, 6 month, respectively, which showed improvement compared with the baseline ( $P < 0.05$ ; baseline vs. 1, 3, 6 months) (Table 2; Figure 3). The CRT decreased significantly from  $308.50 \pm 45.48 \mu\text{m}$  to  $219.63 \pm 30.27 \mu\text{m}$ ,  $221.33 \pm 40.65 \mu\text{m}$ ,  $220.96 \pm 33.09 \mu\text{m}$  after treatment 1, 3, 6 month, respectively ( $P < 0.05$ ; baseline vs. 1, 3, 6 months) (Table 2; Figure 4). The P1 response of mfERG amplitude improved from  $40.71 \pm 9.69 \text{ nv/deg}^2$  to  $50.67 \pm 9.48 \text{ nv/deg}^2$ ,  $54.92 \pm 8.45 \text{ nv/deg}^2$ ,  $55.67 \pm 6.74 \text{ nv/deg}^2$  after treatment 1, 3, 6 month, respectively ( $P < 0.05$ ; baseline vs. 1, 3, 6 months) (Table 2; Figure 5).

During the follow-up period of 6 months, 17 eyes received 1 intravitreal injection of conbercept, 5 eyes received 2 injections, and 2 eyes received 3 injections.

Subconjunctival hemorrhage occurred in 3 eyes and was absorbed spontaneously 7 days later. The intraocular pressure in

2 eyes increased temporarily and then decreased to normal levels without any treatment. Corneal epithelial injury occurred in 1 eye and was repaired 3 days later. None of the 24 eyes showed obvious ocular or systemic adverse events, such as endophthalmitis, glaucoma, cataract progression, or embolism.

## DISCUSSION

The main treatment for PM-CNV is considered to be photodynamic therapy (8), but the efficacy is poor. Research has reported that (16) the VEGF concentration in the eyes of PM-CNV patients significantly increases, suggesting that the pathogenesis of CNV may be related to VEGF. Conbercept, as a recombinant fusion protein, can inhibit the binding of VEGF to its receptor, thus inhibiting the formation of CNV. Conbercept has many characteristics, such as having many targets, a strong affinity and a long intraocular action time (24). Lu Hang et al. (25) retrospectively observed the clinical data of 62 wet AMD eyes treated with intravitreal injection of conbercept. At the last follow-up, the visual acuity of ETDRS increased to 26.20 letters on average compared with the baseline value. The CRT was

significantly thinner than the baseline value, and the difference was statistically significant. In view of the significant efficacy of conbercept in wet AMD patients, this drug may also have a certain effect on PM-CNV.

Some studies (26) have already evaluated the clinical efficacy of conbercept in the treatment of PM-CNV according to the BCVA, CRT and lesion leakage. OCT reflects the regression of macular edema, and FFA reflects the leakage of CNV lesions. How to predict the clinical efficacy of anti-VEGF drugs in the treatment of PM-CNV is difficult. Studies have shown that the anti-VEGF drug response is related to the corrected visual acuity, individual gene type, and size and type of CNV lesions secondary to wet AMD (27).

OCT and FFA can only observe retinal morphology but cannot quantify retinal function. mfERG is currently an effective method for assessing posterior retinal function (28) and has great value for microscopic macular degeneration before morphological changes occur. The P1 response of mfERG amplitude (Amp-P1) values before and after treatment in this study could be sensitive and intuitive for demonstrating that conbercept could improve retinal function of the macular area in PM-CNV. This study innovatively combined the BCVA, CRT and Amp-P1 data to observe the changes in the morphology and function of the macular area in PM-CNV via treatment with conbercept in order to evaluate the efficacy and monitor the changes in the disease (29).

This study was a retrospective analysis of clinical data from 20 patients (24 eyes) with PM-CNV. The results showed that after 1 month of intravitreal conbercept injection, 2 eyes (8.33%) demonstrated an increase in the BCVA to <5 letters, 2 eyes (8.33%) increased to 5–10 letters, 16 eyes (66.7%) increased to 10–20 letters, and 4 eyes (16.7%) increased to  $\geq 20$  letters; additionally, there were no significant differences in the BCVA, CRT or Amp-P1 between 1, 3, and 6 months ( $P > 0.05$ ). CNV size and CRT decreased significantly until the end of the follow-up period. This indicates that conbercept is effectively combined with a high concentration of VEGF to improve the BCVA. There were significant differences in the BCVA, CRT and Amp-P1 at each time point after treatment compared with the baseline values ( $P < 0.05$ ). A study showed that (30) the ocular axis of pathologic myopia was  $>30$  mm, and the incidence of fundus lesions was significantly increased. At the same time, we found that 2 eyes with a BCVA increase  $<5$  letters after 1 month of treatment had an axis of  $>30$  mm. In this study, the intraocular pressure increased temporarily in 2 eyes, probably due to the increase in the vitreous cavity content.

A phase III clinical trial of conbercept showed that most patients with retinal disease had a significant increase in visual acuity after 1 month of intravitreal injections and 3 consecutive injections (29, 31). In this study, during the follow-up period of 6 months, 17 eyes received 1 intravitreal injection of conbercept, 5 eyes received 2 injections, and 2 eyes received 3 injections, indicating that the 1+PRN treatment strategies may improve

prognosis for most PM-CNV patients and may reduce the economic burden of patients. Advantages of conbercept over other anti-VEGF drugs in PM-CNV need to be observed in the future. A study (32) reported that anti-VEGF drugs increased the risk of cardiovascular and cerebrovascular diseases, but no systemic adverse events were found in this study.

This study found that after conbercept treatment, subretinal fluid and/or intraretinal fluid were significantly absorbed, macular edema was significantly reduced, and corrected visual acuity was significantly improved. We also sensitively and intuitively found that the value of Amp-P1 was significantly improved, so conbercept improved the retinal function of the macular area in PM-CNV. In addition, after 6 months of treatment, the leakage of CNV lesions disappeared in 20 (83.3%) eyes, and the leakage area of CNV lesions was significantly reduced in 4 (16.7%) eyes.

Intravitreal injection of conbercept can reduce the CNV area, macular CRT, inhibit CNV leakage, improve the BCVA, increase the response density of the macular central retina, and restore retinal function in PM-CNV patients. Conbercept can change macular morphology and function in PM-CNV patients, and it is safe and effective for the treatment of PM-CNV. Due to the limited sample size and short observation duration, the long-term efficacy may need long-term observation of large samples.

## DATA AVAILABILITY STATEMENT

The raw data supporting the conclusions of this article will be made available by the authors, without undue reservation.

## ETHICS STATEMENT

The studies involving human participants were reviewed and approved by the Ethics Committee of the Zibo Central Hospital. The patients/participants provided their written informed consent to participate in this study.

## AUTHOR CONTRIBUTIONS

HL and TY wrote the manuscript. NL and D-MM were the patient's operators. G-XZ, Z-FW, and JZ reviewed the literature and contributed to manuscript drafting. S-PW was responsible for the revision of the manuscript for important intellectual content and contributed to diagnosis. All authors issued final approval for the version to be submitted.

## FUNDING

This work was supported by the Medical and health development plan of Shandong Province, No.2011QW036 and No.2017WS162; and Key Research and Development Plan of Zibo City, Nos. 2019gy010046 and 2019ZC010166.



## REFERENCES

- Wong TY, Ferreira A, Hughes R, Carter G, Mitchell P. Epidemiology and disease burden of pathologic myopia and myopic choroidal neovascularization: an evidence-based systematic review. *Am J Ophthalmol.* (2014) 127:9–25.e12. doi: 10.1016/j.ajo.2013.08.010
- Duke-Elder S, Abrams D. Pathological refractive errors. In: Duke-Elder S, editors. *Systems of Ophthalmology*. Volume 5. St Louis, MO: CV Mosby (1970). P. 297–374.
- Fredrick DR. Myopia. *BMJ.* (2002) 324:1195–9. doi: 10.1136/bmj.324.7347.1195
- Miller DG, Singerman LJ. Natural history of choroidal neovascularisation in high myopia. *Curr Opin Ophthalmol.* (2001) 12:222–4. doi: 10.1097/00055735-200106000-00014
- Tokoro T. On the definition of pathologic myopia in group studies. *Acta Ophthalmol Suppl.* (1988) 185:107–8. doi: 10.1111/j.1755-3768.1988.tb02681.x
- Morgan IG, Ohno-Matsui K, Saw SM. Myopia. *Lancet.* (2012) 379:1739–48. doi: 10.1016/S0140-6736(12)60272-4
- Ohno-Matsui K, Yoshida T, Futagami S, Yasuzumi K, Shimada N, Kojima A, et al. Patchy atrophy and lacquer cracks predispose to the development of choroidal neovascularization in pathologic myopia. *Br J Ophthalmol.* (2003) 87:570–3. doi: 10.1136/bjo.87.5.570
- Blinder KJ, Blumenkranz MS, Bressler NM, Bressler SB, Donato G, Lewis H, et al. Verteporfin therapy of subfoveal choroidal neovascularization in pathologic myopia: 2-year results of a randomized clinical trial—VIP report no. 3. *Ophthalmology.* (2003) 110:667–73. doi: 10.1016/S0161-6420(02)01998-X
- Soubrane G. Choroidal neovascularization in pathologic myopia: recent developments in diagnosis and treatment. *Surv Ophthalmol.* (2008) 53:121–38. doi: 10.1016/j.survophthal.2007.12.004
- Nguyen QD, Shah S, Tatlipinar S, Do DV, Anden EV, Campochiaro PA. Bevacizumab suppresses choroidal neovascularization caused by pathological myopia. *Br J Ophthalmol.* (2005) 89:1368–70. doi: 10.1136/bjo.2005.066431
- Yamamoto I, Rogers AH, Reichel E, Yates PA, Duker JS. Intravitreal bevacizumab (Avastin) as treatment for subfoveal choroidal neovascularisation secondary to pathological myopia. *Br J Ophthalmol.* (2007) 91:157–60. doi: 10.1136/bjo.2006.096776
- Sakaguchi H, Ikuno Y, Gomi F, Kamei M, Sawa M, Tsujikawa M, et al. Intravitreal injection of bevacizumab for choroidal neovascularisation associated with pathological myopia. *Br J Ophthalmol.* (2007) 91:161–5. doi: 10.1136/bjo.2006.099887
- Laud K, Spaide RF, Freund KB, Slakter J, Klancnik JM. Treatment of choroidal neovascularization in pathologic myopia with intravitreal bevacizumab. *Retina.* (2006) 26:960–3. doi: 10.1097/01.iae.0000240121.28034.c3
- Tewari A, Dhalla MS, Apte RS. Intravitreal bevacizumab for treatment of choroidal neovascularization in pathologic myopia. *Retina.* (2006) 26:1093–4. doi: 10.1097/01.iae.0000254896.78766.74
- Hernández-Rojas ML, Quiroz-Mercado H, Dalma-Weiszhausz J, Fromow-Guerra J, Amaya-Espinosa A, Solís-Vivanco A, et al. Short-term effects of intravitreal bevacizumab for subfoveal choroidal neovascularization in pathologic myopia. *Retina.* (2007) 27:707–12. doi: 10.1097/GIM.0b013e3180a03276
- Tong JP, Chan WM, Liu DT, Lai TY, Choy KW, Pang CP, et al. Aqueous humor levels of vascular endothelial growth factor and pigment epithelium-derived factor in polypoidal choroidal vasculopathy and choroidal neovascularization. *Am J Ophthalmol.* (2006) 141:456–62. doi: 10.1016/j.ajo.2005.10.012
- Brown DM, Kaiser PK, Michels M, Soubrane G, Heier JS, Kim RY, et al. Ranibizumab versus verteporfin for neovascular age-related macular degeneration. *N Engl J Med.* (2006) 355:1432–44. doi: 10.1056/NEJMoa062655
- Heier JS, Brown DM, Chong V, Korobelnik JF, Kaiser PK, Nguyen QD, et al. Intravitreal aflibercept (VEGF trap-eye) in wet age-related macular degeneration. *Ophthalmology.* (2012) 119:2537–48. doi: 10.1016/j.ophtha.2012.09.006
- Martin DF, Maguire MG, Fine SL, Ying GS, Jaffe GJ, Grunwald JE, et al. Ranibizumab and bevacizumab for treatment of neovascular age-related macular degeneration: two-year results. *Clin Colorectal Cancer.* (2013) 12:73–85. doi: 10.1016/j.ophtha.2020.01.029
- Mitchell EP. Targeted therapy for metastatic colorectal cancer: role of a?ibercept. *Clin Colorectal Cancer.* (2013) 12:73–85. doi: 10.1016/j.clcc.2012.08.001
- Lu X, Sun X. Profile of conbercept in the treatment of neovascular age-related macular degeneration. *Drug Des Dev Ther.* (2015) 9:2311–20. doi: 10.2147/DDDT.S67536
- Cui J, Sun D, Lu H, Dai R, Xing L, Dong H, et al. Comparison of effectiveness and safety between conbercept and ranibizumab for treatment of neovascular age-related macular degeneration. A retrospective case-controlled non-inferiority multiple center study. *Eye.* (2018) 32:391–9. doi: 10.1038/eye.2017.187
- Song AP, Yu T, Wang JR, Liu W, Sun Y, Ma SX. Multifocal electroretinogram in non-pathological myopic subjects: correlation with optical coherence tomography. *Int J Ophthalmol.* (2016) 9:286–29. doi: 10.18240/ijo.2016.02.21
- Wu Z, Zhou P, Li X, Wang H, Luo D, Qiao H, et al. Structural characterization of a recombinant fusion protein by instrumental analysis and molecular modeling. *PLoS One.* (2013) 8:e57642. doi: 10.1371/journal.pone.0057642
- Lu H, Cui J, Dong H, Luo B, Xiu W, Li H. Clinical efficacy of conbercept in the treatment of wet age-related macular degeneration. *Chin J Ophthalmol.* (2015) 51:818–21. doi: 10.3760/cma.j.issn.0412-4081.2015.11.005
- Yang D, Guo D. Therapeutic effect of intravitreal injection of conbercept on the treatment of pathological myopic choroidal neovascularization. *J Prac Med Tech.* (2018) 25:77–9.
- Phasukkijwatana N, Tan ACS, Chen X, Freund KB, Sarraf D. Optical coherence tomography angiography of type 3 neovascularisation in age-related macular degeneration after antiangiogenic therapy. *Br J Ophthalmol.* (2017) 101:597–602. doi: 10.1136/bjophthalmol-2016-308815
- Farecki ML, Gutfleisch M, Faatz H, Rothaus K, Heimes B, Spital G, et al. Characteristics of type 1 and 2 CNV in exudative AMD in OCT-Angiography. *Graefes Arch Clin Exp Ophthalmol.* (2017) 255:913–21. doi: 10.1007/s00417-017-3588-y
- Lei B, Xu X, Song Y. *Conbercept for Treatment of Wet Age-Related Macular Degeneration (AMD) [D]*. Switzerland: ISOPT Symposium Secretariat, Paragon Group, (2014).
- Guan G, Zhan Y, Yu Y, Wang Y, Peng Y, Liu Y, et al. Correlation of axial length, diopter, age and fundus damage in children and adolescents with high myopia. *Chin J Prac Ophthalmol.* (2000) 18:409–11. doi: 10.3760/cma.j.issn.1006-4443.2000.07.009
- Li X, Xu G, Wang Y, Xu X, Liu X, Tang S, et al. Safety and efficacy of conbercept in neovascular age-related macular degeneration: results from a 12-month randomized phase 2 study: AURORA study. *Ophthalmology.* (2014) 121:1740–7. doi: 10.1016/j.ophtha.2014.03.026
- Schmidt-Erfurth U, Chong V, Loewenstein A, Larsen M, Souied E, Schlingemann R, et al. Guidelines for the management of neovascular age-related macular degeneration by the European Society of Retina Specialists (EURETINA). *Br J Ophthalmol.* (2014) 98:1144–67. doi: 10.1136/bjophthalmol-2014-305702

**Conflict of Interest:** The authors declare that the research was conducted in the absence of any commercial or financial relationships that could be construed as a potential conflict of interest.

**Publisher's Note:** All claims expressed in this article are solely those of the authors and do not necessarily represent those of their affiliated organizations, or those of the publisher, the editors and the reviewers. Any product that may be evaluated in this article, or claim that may be made by its manufacturer, is not guaranteed or endorsed by the publisher.

Copyright © 2021 Lu, Yue, Liu, Wang, Zhai, Mi, Zhang and Wang. This is an open-access article distributed under the terms of the Creative Commons Attribution License (CC BY). The use, distribution or reproduction in other forums is permitted, provided the original author(s) and the copyright owner(s) are credited and that the original publication in this journal is cited, in accordance with accepted academic practice. No use, distribution or reproduction is permitted which does not comply with these terms.





# Effects of the Pars Plana Vitrectomy on the Chronic Total Rhegmatogenous Retinal Detachment in the Young Adults

Jinguo Yu<sup>1</sup>, Xingxing Hu<sup>1,2</sup>, Jiangkai Zhang<sup>1</sup>, Han Han<sup>1,2</sup>, Bo Huang<sup>3</sup>, Rodrigo Brant<sup>4</sup>, Cheng Zhang<sup>5</sup> and Hua Yan<sup>1,2\*</sup>

<sup>1</sup> Department of Ophthalmology, Tianjin Medical University General Hospital, Tianjin, China, <sup>2</sup> Laboratory of Molecular Ophthalmology, Tianjin Medical University, Tianjin, China, <sup>3</sup> Department of Ophthalmology, University of Mississippi Medical Center, Jackson, MS, United States, <sup>4</sup> Department of Ophthalmology and Visual Sciences, Federal University of São Paulo, São Paulo, Brazil, <sup>5</sup> Department of Ophthalmology and Visual Sciences, Montefiore Medical Center, Albert Einstein College of Medicine, Bronx, NY, United States

## OPEN ACCESS

### Edited by:

Haijiang Lin,  
Massachusetts Eye & Ear Infirmary  
and Harvard Medical School,  
United States

### Reviewed by:

Dong Ho Park,  
Kyungpook National University  
Hospital, South Korea  
Saad Al-Kadhi,  
University of Massachusetts Medical  
School, United States

### \*Correspondence:

Hua Yan  
zyyyanhua@tmu.edu.cn

### Specialty section:

This article was submitted to  
Ophthalmology,  
a section of the journal  
Frontiers in Medicine

**Received:** 08 August 2021

**Accepted:** 20 September 2021

**Published:** 22 October 2021

### Citation:

Yu J, Hu X, Zhang J, Han H, Huang B,  
Brant R, Zhang C and Yan H (2021)  
Effects of the Pars Plana Vitrectomy  
on the Chronic Total Rhegmatogenous  
Retinal Detachment in the Young  
Adults. *Front. Med.* 8:755389.  
doi: 10.3389/fmed.2021.755389

**Objective:** To observe the characteristics and evaluate the efficacy and safety of the chronic total rhegmatogenous retinal detachment (RRD) treatment by the 23-gauge pars plana vitrectomy (PPV) in young adults and to analyze the related factors.

**Methods:** A retrospective chart review was performed for the young adults who underwent the 23-gauge PPV for the chronic total RRD at the Tianjin Medical University General Hospital from 2011 to 2018. A total of 54 eyes of 48 patients were included in this study. The preoperative vision ranged from 2.00 to 1.00. The mean duration of RRD was  $9 \pm 0.6$  months with a range from 4 to 18 months. The proliferative vitreoretinopathy (PVR) grade D1 and grade D2 was diagnosed in 48 eyes and 6 eyes, respectively. About 37 eyes were filled with C3F8 and 17 eyes were filled with silicone oil tamponade. The follow-up ranged from 9 to 78 months with a mean of  $23 \pm 2.2$  months.

**Results:** The postoperative visual acuity increased in all the eyes at the final observation. The retinal attachment was achieved in 49 eyes (90.7%) in the primary PPV. Five eyes (9.3%) with the failed retinal attachment finally achieved the attachment after the second procedure. The postoperative complications mainly included temporary intraocular pressure (IOP) elevation, hyphema, and retinal redetachment.

**Conclusion:** Chronic total RRD can be treated via the 23-gauge PPV with a great anatomical and visual prognosis in the young adult. The successful treatment of the chronic total RRD in young adults is mainly associated with the complete dissection of the severe vitreoretinopathy, especially for the epiretinal membrane at the retinal breaks and degenerations and the subretinal proliferation during surgery.

**Keywords:** rhegmatogenous retinal detachment, 23-gauge pars plana vitrectomy, proliferative vitreoretinopathy, young adults, surgery

## INTRODUCTION

Rhegmatogenous retinal detachment (RRD), which often causes difficult recovery of the retinal function due to the delayed retinal reattachment by a surgical procedure, is one of the most common reasons for severely decreased vision in young adults. RRD has multiple etiologies in young adults (1). The characteristics and outcomes of the pediatric RRD have been reported in numerous studies (2–6). It has been reported that the incidence of RRD in the young adults is different from RRD in the adults; it is  $\sim 0.38$ – $0.69$  per 100,000 individuals in the children and  $7.98$ – $12.4$  per 100,000 individuals in the adults (2, 7).

Chronic total RRD is one of the most refractory retinal detachments with poor outcomes in young adults. Two approaches, a scleral buckling procedure and pars plana vitrectomy (PPV), are typically used to treat RRD in young adults. The selection of surgical procedures according to the vitreoretinopathy is important for the final outcomes in the chronic total RRD in the young adults. The purpose of choosing an optimal approach to treating the chronic total RRD in young adults is to provide the patients with an individualized management conceptual design according to the etiology and severity of the proliferative vitreoretinopathy (PVR).

The scleral buckling procedure has been an effective surgical approach for RRD for more than 60 years (8). However, this procedure is only compatible with simple RRD. PPV has been adopted in treating RRD with PVR grade C or worse with the successful results in many instances in adults. Since PPV is effective for RRD, this study strictly choose the surgery for the chronic total RRD in young adults because of the difficulty in completely removing the cortical vitreous, higher postoperative intraocular cellular activity, unpredictable tamponade such as silicone oil or gas intraoperatively, and difficulty in maintaining the head position.

In this retrospective study, the anatomical characteristics of the chronic total RRD in the young adults were reported and emphasized the experiences in surgical expertise with the management of the epiretinal membrane around the retinal breaks and retinal degenerations and the subretinal proliferation in treating the chronic total RRD by the 23-gauge PPV.

## METHODS

### Patients

This study was approved by the Medical Ethics Committee of the Tianjin Medical University General Hospital and complies with the Declaration of Helsinki including current revisions and with the Good Clinical Practice guidelines. The procedures followed were in accordance with the institutional guidelines and all the subjects provided their written informed consent for the treatment according to the Declaration of Helsinki. All the subjects were recruited from the ophthalmology department of the Tianjin Medical University General Hospital.

In this study, the age of the young adults ranged from 12 to 35 years old. About 54 eyes of 48 consecutive young adult patients who had the chronic total RRD underwent the 23-gauge PPV combined with tamponades of C3F8 or silicone oil at the Tianjin Medical University General Hospital from 2011

to 2018. About 34 patients were male and 14 patients were female. The age ranged from 12 to 33 years with a mean of  $23 \pm 2$  years. The mean refraction of myopia was  $-6.50 \pm -1.25$  diopters with a range from  $-2.75$  to  $-10$  diopters. The lens was transparent in all the patients. The mean duration of RRD was  $9 \pm 0.6$  months with a range from 4 to 18 months. The preoperative vision ranged from 2.00 to 1.00 and the mean preoperative intraocular pressure (IOP) was  $14.12 \pm 2.22$  mm Hg. The follow-up ranged from 9 to 78 months with an average of  $23 \pm 2.2$  months (shown in **Table 1**). Eyes with a prior history of congenital or developmental structural ocular abnormalities, ocular trauma, previous ophthalmologic surgery, retinal laser photocoagulation, ocular tumors, corneal opacity, and preceding uveitis were excluded.

### Preoperative Examinations

Complete preoperative evaluations including symptoms, best corrected visual acuity (BCVA) [logarithm of the minimum angle of resolution (LogMAR)], IOP, duration of retinal detachment, ocular and systemic disease history, and funduscopy were obtained. The extension of retinal detachment, number and location of the retinal break(s), and grade of PVR were evaluated by using the indirect ophthalmoscopy and the Goldmann three-mirror contact lens. Additional B-scan examinations were adopted in all the patients to exclude the other retinal and choroidal diseases.

### Surgical Procedures

All the surgeries were performed by the same surgeon, Dr. Yan, with the 23-gauge PPV by using a three-port technique. The eye received 2% lidocaine retrobulbar anesthesia and was then prepared for a standard three-port 23-gauge PPV. The 23-gauge infusion cannula was placed 3.5 mm behind the limbus at the inferotemporal quadrant; then, the 23-gauge sclerotomies for the optic fibers and vitrectomy (Stellaris® PC, Bausch & Lomb, USA) were created. A non-contact wide-angle viewing system (Resight 700, Carl Zeiss Meditec AG, Jena, Germany) was activated and the fundus could be viewed thoroughly and clearly by the illumination of the light probe. A full examination of the fundus was performed to locate all the retinal breaks and to detect the additional areas of the vitreoretinopathy intraoperatively.

During PPV, the posterior hyaloid separation was induced and completely excised by the suction and cutting by using a vitreous cutter over the optic nerve head in the eyes without the posterior vitreous detachment. Then, triamcinolone (TA) was injected into the vitreous cavity for staining the residual proliferative vitreous and epiretinal membrane that was difficult to discriminate. In each case, the meticulous shaving of the vitreous base and epiretinal membrane at the retinal breaks and degeneration area was performed under a wide-angle viewing system with the assisted sclera depression. Retinectomy was conducted and the subretinal membrane was removed appropriately in the cases with the local severe retinal stiffness and shrinkage. The intraocular laser photocoagulation was applied around the margins of the retinal breaks and degenerations in all the patients without any additional cryotherapy after the air-fluid exchange. About 37 eyes were filled with C3F8 and 17 eyes were filled with silicone oil tamponade. The routine postoperative examinations

**TABLE 1** | Characteristics of the young adult patients with chronic total RRD.

Characteristics	Value
Patients	48
Male	34
Female	14
Eyes	54
Age (years), Mean $\pm$ SD (range)	23 $\pm$ 2 (12–33)
Myopia (diopters), Mean $\pm$ SD (range)	−6.50 $\pm$ −1.25 (−2.75 to −10.00)
Duration of RRD (months), Mean $\pm$ SD (range)	9 $\pm$ 0.6 (4–18)
<b>PVR classification (eyes, %)</b>	
Grade D1	48 (88.9)
Grade D2	6 (11.1)
<b>Number of retinal breaks, n (%)</b>	
One	16 (29.6)
Two	11 (20.4)
Three	15 (27.8)
Four	6 (11.1)
Six	4 (7.4)
Seven	2 (3.7)
<b>Site of retinal breaks, n (%)</b>	
Superior site	16 (29.6)
Inferior site	28 (51.9)
Both sites	10 (18.5)
<b>Numbers of patients with symptom of visual field defects</b>	
preop.	49
postop.	0
<b>BCVA (range)</b>	
preop.	2.00–1.00
postop.	1.30–0.10
<b>IOP (mmHg), Mean <math>\pm</math> SD</b>	
preop.	14.12 $\pm$ 2.22
postop.	13.75 $\pm$ 3.13
Retinal attachment after single surgery, n (%)	49 (90.7%)
<b>Postoperative complications, n (%)</b>	
Temporary IOP elevation	5 (9.3)
Hyphema	1 (1.9)
Retinal redetachment	5 (9.3)
Follow-up (months), Mean $\pm$ SD	23 $\pm$ 2.2 (9–78)

RRD, rhegmatogenous retinal detachment; PVR, proliferative vitreoretinopathy; BCVA, best corrected visual acuity; IOP, intraocular pressure.

were performed 1, 2, 3, and 7 days; 2, 3, and 12 weeks; and 1 year after the surgery. The postoperative evaluations included BCVA, IOP, retinal anatomy, and complications. The paired Student's *t*-test was used to analyze the changes in the pre- and postoperative IOP.

## RESULTS

### Best Corrected Visual Acuity

The postoperative BCVA ranged from 1.30 to 0.10 (LogMAR). The BCVA increased in all eyes (100%) at the final follow-up. The

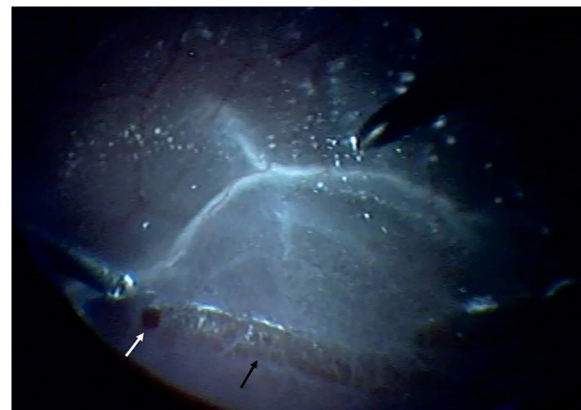


**FIGURE 1** | Retinal break (white arrow) and degeneration (black arrow) were observed in the inferior site intraoperatively.

symptoms of the visual field defects disappeared in all the eyes (shown in **Table 1**).

## Retinal Anatomy

### Retinal Breaks

There was only one retinal break in 16 eyes (29.6%), two retinal breaks in 11 eyes (20.4%), three retinal breaks in 15 eyes (27.8%), four retinal breaks in 6 eyes (11.1%), six retinal breaks in 4 eyes (7.4%), and seven retinal breaks in 2 eyes (3.7%). The retinal breaks were found in the superior site in 16 eyes (29.6%), in the inferior site in 28 eyes (51.9%) (shown in **Figure 1**), and in both the superior and inferior sites in 10 eyes (18.5%) (shown in **Table 1**).

### Proliferative Vitreoretinopathy

The criteria of the PVR classification were obtained from the Retina Society Terminology Committee. PVR grade D1 was diagnosed in 48 eyes (88.9%) and PVR grade D2 was diagnosed in 6 eyes (11.1%) (shown in **Table 1**).

### Retinal Attachment

Overall, retinal attachment with a single surgery was achieved in 49 eyes (90.7%) among all the operated eyes (shown in **Figure 2**). Only five eyes (9.3%) received a second vitrectomy procedure for the recurrent retinal detachment repair and the retina finally attached (100%). The retinal reattachment rate was 100% at the final follow-up.

### Intraocular Pressure

The postoperative IOP was 13.75  $\pm$  3.13 mm Hg and there was no significant difference between the postoperative and preoperative IOP at the final follow-up ( $p > 0.05$ ).

## Postoperative Complications

The postoperative complications mainly included the temporary IOP elevation in five eyes (9.3%), hyphema in one eye (1.9%), and retinal redetachment in five eyes (9.3%) after the primary PPV. No epiretinal membrane formation occurred after PPV at the final observation.

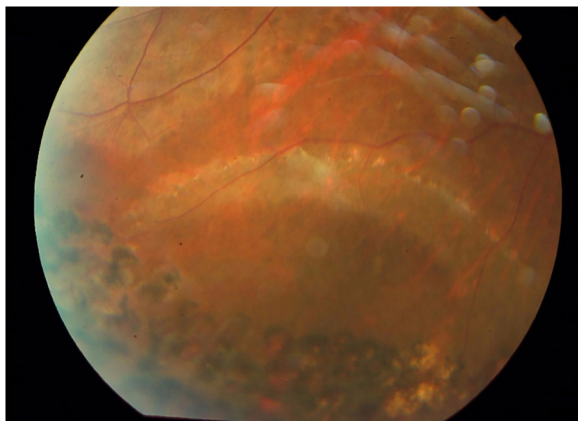


**FIGURE 2 |** Retinal break closure and retinal attachment were present with the laser scar formation at the final follow-up.

## DISCUSSION

According to the previous studies, the main reasons for RRD in children are trauma, myopia, previous ophthalmic surgeries, and congenital or developmental anomalies (2, 9–13). However, the idiopathic or unknown causes of retinal detachment are still a common phenomenon in young adults. The retinal breaks are present in 5–10% of the general public; however, very few lead to RRD. PVR is always significant when RRD is diagnosed in young adults. In this study, grade D PVR was present in all the young adult RRD patients, possibly because of their delayed diagnosis. Akabane (14) reported a PVR incidence in the children was 29.8–37.5%, while in adults, it was 5–10%. Therefore, the early precision examination, diagnosis, and treatment are important in young adults who have the symptoms of blurred vision or vision loss and potential RRD.

The symptoms and retinal structures of the chronic total RRD in young adults have their own special characteristics. Young adults with RRD may not have any complaints of the decreased vision or loss of vision at the beginning and a few patients detect the decreased vision incidentally when covering the fellow eye due to the chronic and mild retinal detachment. In this study, the most common presenting symptom was a gradual vision decrease or loss of vision in 88% of the eyes and the retinal detachments had a longer history ranging from 4 to 18 months. Sultan (15) reported that the most common presenting symptom was a gradual vision decrease or loss of vision in 45.7% of the eyes and the incidental findings in the routine examinations or follow-up in 23% of the eyes. Gonzales (13) reported that 46% of the patients had to present symptoms related to retinal detachment. There is no obvious ocular history in most of the RRD in young adults; therefore, complete and careful examinations of the vitreous and retina should be performed by the different methods preoperatively.

Since all the retinal breaks were small and/or various in the patients, this study detected all the retinal breaks by the indirect ophthalmoscopy and the Goldmann three-mirror contact lens preoperatively. In this study, total retinal detachment was found

in all the eyes and the main reasons might be the small retinal holes and chronic nature. Sultan (15) reported that the vast majority of the cases had retinal breaks or holes identified in 86.75% of the eyes intraoperatively, while no retinal breaks or holes were identified in 7.22% of the eyes. In this study, it is found that all the retinal breaks, including the atrophic holes in the lattice, were the round holes with RRD and without any horseshoe tears. There was only one retinal hole in 29.6% of the eyes, two retinal holes in 20.4% of the eyes, and multiple holes in 50% of the eyes. The retinal breaks were found in the superior site in 29.6% of the eyes, in the inferior site in 51.9% of the eyes, and in both the superior and inferior sites in 18.5% of the eyes. Sultan (15) reported multiple holes in 22.3% of the eyes with RRD in the children. In this study, there was no macular hole, giant retinal tear, or retinal dialysis. Sultan (15) reported that 20.8% of the eyes with RRD had retinal dialysis and giant tears were found in 22.9% of the eyes. Yokoyama (3) reported retinal dialysis in 27% of RRD in the children. From the previous study, it is known that after an RRD in one eye, the risk of RRD is ~10% in the fellow eye. Therefore, the fellow eye should be examined carefully and treated early.

The surgical repair methods in the young adults RRD generally include the buckling procedure and PPV. The selection of surgical repair for the young adults RRD depends on the etiology and features of retinal detachment such as the severity of PVR, site, size, and the number of the retinal breaks. The scleral buckling procedure was the commonly used method for the treatment of RRD in young adults before PPV was widely used (16). However, the scleral buckling or band as the primary procedure was not commonly used in the total RRD after the PPV era. In this study, all the RRDs had a chronic nature and PVR was severe at grade D. Total RRD in the young adults with PVR grade D cannot be treated successfully with the scleral buckling procedure. Therefore, the only vitrectomy is the optimal method for treating the chronic total RRD with PVR grade D in young adults by completely eliminating PVR, peeling the epiretinal membrane, and even performing retinectomy for the removal of the subretinal membrane. Some surgeons reported that the vitrectomy with or without a buckling procedure was adopted in the primary surgical procedure for RRD in the children and achieved better results (14, 15, 17–19).

Treatment of the chronic total RRD with the 23-gauge PPV in the young adults has superiority with more safety, quick recovery, and less damage compared to the 20-gauge PPV due to a small sutureless self-sealing incision. The technique of treating the chronic total RRD in young adults is different from the fresh RRD for its own peculiarity of vitreoretinopathy, especially at the retinal holes and degenerations. Performing complete removal of the cortical vitreous on the detached retina is often difficult, as there is less frequent posterior vitreous detachment and stronger vitreoretinal adhesion in the young adult patients with RRD. The most important procedure of treating the chronic total RRD in young adults during vitrectomy is to address the vitreous adherent to the retinal holes and degenerations. Usually, the vitreous is ropier in young adults, especially at the vitreous base and peripheral retinal area (10, 20). In addition, the posterior vitreous adherent to the epiretinal



proliferative membrane becomes tighter at the retinal holes and degeneration, which is more difficult to excise completely during the vitrectomy. In this study, five eyes with the failed retinal attachment at the primary PPV had the retinal detachment at the inferior site and the epiretinal membrane and vitreous traction were not completely removed. Therefore, in cases with the retinal detachment at the inferior site, the local proliferative vitreous and epiretinal membrane should be excised completely because they can cause recurrent retinal detachment, which is easily induced by the traction of the residual vitreous and epiretinal membrane. Else, the successful retinal attachment will not be obtained even with C3F8 or silicone oil tamponade. Conversely, the scleral buckling procedure may have a better success rate in the retinal attachment because it does not disturb the intraocular tissue compared with vitrectomy. TA is always used for staining the proliferative vitreous and epiretinal membrane during the vitrectomy (21), but with TA, difficulty in discriminating the proliferative vitreous and epiretinal membrane can be easily resolved, providing the clear observation and thorough excision that promote the final successful rate by closing the retinal hole with the laser photocoagulation during surgery. Both the cryopexy and laserpexy can be used for closing the retinal holes and as the prophylactic treatment for retinal degenerations. Generally, the vitreous and retina have a proliferative trend after the cryotherapy for the retinal hole closure and retinal degeneration compared with after laser photocoagulation (22, 23) and this effect is more significant in young adults than in adults. Therefore, laser photocoagulation was adopted to manage the retinal holes and degenerations in all of our patients who did not experience any related postoperative proliferations. Retinectomy is a better option to preserve the retinal attachment in cases with local severe retinal stiffness and shrinkage induced by fibrosis. Adequate retinectomy should be performed and the subretinal membranes should be removed appropriately if needed. Complete subretinal fluid drainage during the vitrectomy seems to be unnecessary for all the RRD surgical procedures in cases with a retinal hole in the peripheral area.

The final visual outcome after the treatment of the chronic total RRD in the young adults is associated with retinal attachment, especially for the macular attachment and function. Since the retinal hole closure and retinal attachment are achieved, the final vision improvement is still limited in some of the cases due to the long-term retinal and macular detachment. In this study, the postoperative vision ranged from 1.30 to 0.10 with increased vision in 100% of the eyes at the final follow-up. The symptoms of the visual field defects disappeared in all the eyes. Since 100% of the eyes achieved the vision improvement after the successful retinal attachment, the vision remained inadequate postoperatively due to the chronic nature of total RRD, initial poor vision, greater extent of RRD such as total RRD, and the presence of preoperative PVR grade D. This analysis of poor postoperative vision is almost the same compared to the previous reports (3, 4, 13, 16, 24).

In this study, only five eyes (9.3%) had postoperative temporary IOP elevation. This temporary elevation is probably caused by the intrinsic characteristics of RRD and/or surgical

procedures. In patients with RRD, the aqueous humor circulation has a passageway in addition to the routine anterior chamber passageway in which the aqueous humor outflows and is absorbed through the choroid and sclera due to the retinal detachment that induces decreased IOP. However, the passageway of the aqueous humor outflowing through the choroid and sclera is significantly decreased or stopped due to the closure of the retinal holes and retinal attachment after vitrectomy and the aqueous humor mainly outflows through the anterior chamber intensively. Therefore, IOP elevation may occur in some of the successful retinal attachment cases. Alternatively, an early postoperative IOP increase may be caused by the severe inflammation and ciliary body stimulation during the vitrectomy and the possible mechanisms include ciliary body edema and inflammatory trabecular meshwork obstruction. Other reasons for the postoperative IOP elevation may be intraocular gas expansion, a pupillary block from gas or fibrin, erythroclastic glaucoma, and silicon oil-related glaucoma (25–28).

The risk factors of hyphema after the RRD surgeries include high myopia, aspirin treatment, cryotherapy impacts, trans-scleral drainage, scleral buckling, PPV, surgery duration, IOP, and systemic hypertension (29). In this study, only one eye (1.9%) had hyphema postoperatively and it was absorbed spontaneously within 7 days. The anterior chamber bleeding might come from the sclerotomies rather than from the episcleral vessels. In this study, the occurrence of hyphema did not affect the final anatomical success rate which was the same as compared to the previous studies (15, 30). The single-operation anatomical success rate was 90.7% in the primary PPV and 100% after the second PPV. Sultan (15) reported that the single-operation anatomical success rate was 74.2% in the primary PPV group and 77% in the second PPV group.

In summary, since, the 23-gauge PPV is an effective and safe approach by completely removing the epiretinal proliferation around the retinal breaks and retinal degenerations and the subretinal proliferation under a non-contact wide-angle viewing system in treating the chronic total RRD of the young adults, the vitreoretinal surgery should be prudently employed in treating the fresh RRD because it is more complex compared to the scleral buckling procedures. The details of symptoms and characteristics of the chronic total RRD in young adults should be emphasized.

## DATA AVAILABILITY STATEMENT

The raw data supporting the conclusions of this article will be made available by the authors, without undue reservation.

## ETHICS STATEMENT

The studies involving human participants were reviewed and approved by Tianjin Medical University General Hospital Medical Ethics Committee. Written informed consent to participate in this study was provided by the participants' legal guardian/next of kin.

## AUTHOR CONTRIBUTIONS

HY and JY: research design and manuscript preparation. JY and XH: data acquisition, research design, and data analysis and manuscript preparation. JZ and HH: data acquisition and data analysis and manuscript preparation. BH, RB, and CZ: research design and manuscript preparation. All authors contributed to the article and approved the submitted version.

## REFERENCES

- Go SL, Hoyng CB, Klaver CC. Genetic risk of rhegmatogenous retinal detachment: a familial aggregation study. *Arch Ophthalmol*. (2005) 123:1237–41. doi: 10.1001/archophth.123.9.1237
- Fivgas GD, Capone Jr A. Pediatric rhegmatogenous retinal detachment. *Retina*. (2001) 21:101–6. doi: 10.1097/00006982-200104000-00001
- Yokoyama T, Kato T, Minamoto A, Sugihara A, Imada M, Kuwabara R, et al. Characteristics and surgical outcomes of paediatric retinal detachment. *Eye*. (2004) 18:889–92. doi: 10.1038/sj.eye.6701341
- Weinberg DV, Lyon AT, Greenwald MJ, Mets MB. Rhegmatogenous retinal detachments in children. *Ophthalmology*. (2003) 110:1708–13. doi: 10.1016/S0161-6420(03)00569-4
- Nagpal M, Nagpal K, Rishi P, Nagpal PN. Juvenile rhegmatogenous retinal detachment. *Indian J Ophthalmol*. (2004) 52:297–302.
- Chang PY, Yang CM, Yang CH, Huang JS, Ho TC, Lin CP, et al. Clinical characteristics and surgical outcomes of pediatric rhegmatogenous retinal detachment in Taiwan. *Am J Ophthalmol*. (2005) 139:1067–72. doi: 10.1016/j.ajo.2005.01.027
- Chen SN, Lian IeB, Wei YJ. Epidemiology and clinical characteristics of rhegmatogenous retinal detachment in Taiwan. *Br J Ophthalmol*. (2016) 100:1216–20. doi: 10.1136/bjophthalmol-2015-307481
- Schepens CL. Scleral buckling procedures. *Trans Am Acad Ophthalmol Otolaryngol*. (1958) 62:206–18.
- Rosner M, Treister G, Belkin M. Epidemiology of retinal detachment in childhood and adolescence. *J Pediatr Ophthalmol Strabismus*. (1987) 24:42–4. doi: 10.3928/0191-3913-19870101-09
- Chen SN, Jiunn-Feng H, Te-Cheng Y. Pediatric rhegmatogenous retinal detachment in Taiwan. *Retina*. (2006) 26:410–4. doi: 10.1097/01.iae.0000238546.51756.cd
- Sadeh AD, Dotan G, Bracha R, Lazar M, Loewenstein A. Characteristics and outcomes of paediatric rhegmatogenous retinal detachment treated by segmental scleral buckling plus an encircling element. *Eye*. (2001) 15:31–3. doi: 10.1038/eye.2001.8
- Lee RW, Mayer EJ, Markham RH. The etiology of pediatric rhegmatogenous retinal detachment: 15 years experience. *Eye*. (2008) 22:636–40. doi: 10.1038/sj.eye.6702724
- Gonzales CR, Singh S, Yu F, Kreiger AE, Gupta A, Schwartz SD. Pediatric rhegmatogenous retinal detachment: clinical features and surgical outcomes. *Retina*. (2008) 28:847–52. doi: 10.1097/IAE.0b013e3181679f79
- Akabane N, Yamamoto S, Tsukahara I, Ishida M, Mitamura Y, Yamamoto T, et al. Surgical outcomes in juvenile retinal detachment. *Jpn J Ophthalmol*. (2001) 45:409–11. doi: 10.1016/S0021-5155(01)00361-6
- Sultan AZ, Saba AR, Essam AH, Eman AK, Ahmed MA. Rhegmatogenous retinal detachment in children 16 years of age or younger. *Clin Ophthalmol*. (2013) 7:1001–14. doi: 10.2147/OPHTH.S40056
- Winslow RL, Tasman W. Juvenile rhegmatogenous retinal detachment. *Ophthalmology*. (1978) 85:607–18. doi: 10.1016/S0161-6420(78)35641-4
- Oono Y, Uehara K, Haruta M, Yamakawa R. Characteristics and surgical outcomes of pediatric rhegmatogenous retinal detachment. *Clin Ophthalmol*. (2012) 6:939–43. doi: 10.2147/OPHTH.S31765
- Wadhwa N, Venkatesh P, Sampangi R, Garg S. Rhegmatogenous retinal detachments in children in India: clinical characteristics, risk factors, and surgical outcomes. *J AAPOS*. (2008) 12:551–4. doi: 10.1016/j.jaapos.2008.05.002
- Scott IU, Flynn HW Jr, Azen SP, Lai MY, Schwartz S, Trese MT. Silicone oil in the repair of pediatric complex retinal detachments:

## FUNDING

This is supported by the National Natural Science Foundation of China (Grant Number 82020108007, 81830026), the Beijing-Tianjin-Hebei Special Project (Grant Number 19JCZDJC64300(Z), 20JCZXJC00180), and the Tianjin Natural Science Foundation (Grant Number 19JCQNJC11300).

- a prospective, observational, multicenter study. *Ophthalmology*. (1999) 106:1399–408. doi: 10.1016/S0161-6420(99)00731-9
- Yan H, Wang NL, Yao K. *Text Book of Ophthalmology*. 6th ed. Beijing: Qinghua University Press (2016).
- Couch SM, Bakri SJ. Use of triamcinolone during vitrectomy surgery to visualize membranes and vitreous. *Clin Ophthalmol*. (2008) 2:891–6. doi: 10.2147/OPHTH.S3434
- Lira RP, Takasaka I, Arieta CE, Nascimento MA, Caldato R, Panetta H. Cryotherapy vs laser photocoagulation in scleral buckle surgery: a randomized clinical trial. *Arch Ophthalmol*. (2010) 128:1519–22. doi: 10.1001/archophth.2010.271
- Bonnet M, Fleury J, Guenoun S, Yaniali A, Dumas C, Hajjar C. Cryopexy in primary rhegmatogenous retinal detachment: a risk factor for postoperative proliferative vitreoretinopathy? *Graefes Arch Clin Exp Ophthalmol*. (1996) 234:739–43. doi: 10.1007/BF00189354
- Wang NK, Tsai CH, Chen YP, Yeung L, Wu WC, Chen TL, et al. Pediatric rhegmatogenous retinal detachment in East Asians. *Ophthalmology*. (2005) 112:1890–5. doi: 10.1016/j.ophtha.2005.06.019
- Zborowski-Gutman L, Treister G, Naveh N, Chen V, Blumenthal M. Acute glaucoma following vitrectomy and silicone oil injection. *Br J Ophthalmol*. (1987) 71:90–906. doi: 10.1136/bjo.71.12.903
- Desai UR, Alhalel AA, Schiffman RM, Campen TJ, Sundar G, Muhich A. Intraocular pressure elevation after simple pars plana vitrectomy. *Ophthalmology*. (1997) 104:781–6. doi: 10.1016/S0161-6420(97)30233-4
- Budenz DL, Taba KE, Feuer WJ, Eliezer R, Cousins S, Henderer J, et al. Surgical management of secondary glaucoma after pars plana vitrectomy and silicone oil injection for complex retinal detachment. *Ophthalmology*. (2001) 108:1628–32. doi: 10.1016/S0161-6420(01)00658-3
- Mangouritsas G, Mourtoukos S, Portaliou DM, Georgopoulos VI, Dimopoulou A, Feretis E. Glaucoma associated with the management of rhegmatogenous retinal detachment. *Clin Ophthalmol*. (2013) 7:727–34. doi: 10.2147/OPHTH.S42792
- Brillat E, Rouberol F, Palombi K, Quesada JL, Bernheim D, Albaladejo P, et al. A case-control study to assess aspirin as a risk factor of bleeding in rhegmatogenous retinal detachment surgery. *Graefes Arch Clin Exp Ophthalmol*. (2015) 253:1899–905. doi: 10.1007/s00417-014-2900-3
- Kung YH, Wu TT. Risk factors of hyphema following surgeries for primary rhegmatogenous retinal detachment. *Ophthalmologica*. (2016) 236:159–65. doi: 10.1159/000452254

**Conflict of Interest:** The authors declare that the research was conducted in the absence of any commercial or financial relationships that could be construed as a potential conflict of interest.

**Publisher's Note:** All claims expressed in this article are solely those of the authors and do not necessarily represent those of their affiliated organizations, or those of the publisher, the editors and the reviewers. Any product that may be evaluated in this article, or claim that may be made by its manufacturer, is not guaranteed or endorsed by the publisher.

Copyright © 2021 Yu, Hu, Zhang, Han, Huang, Brant, Zhang and Yan. This is an open-access article distributed under the terms of the Creative Commons Attribution License (CC BY). The use, distribution or reproduction in other forums is permitted, provided the original author(s) and the copyright owner(s) are credited and that the original publication in this journal is cited, in accordance with accepted academic practice. No use, distribution or reproduction is permitted which does not comply with these terms.



# Clinical Characteristics of Pediatric Coats' Disease With Retinal Cyst Using Wide-Angle Fluorescein Angiography

Jing-Hua Liu, Guangda Deng, Jing Ma, Liang Li, Yuxin Fang, Songfeng Li\* and Hai Lu\*

Beijing Tongren Hospital, Capital Medical University, Beijing, China

## OPEN ACCESS

### Edited by:

Haijiang Lin,  
Harvard Medical School,  
United States

### Reviewed by:

Menglu Yang,  
Schepens Eye Research Institute,  
United States  
Yuguang He,  
University of Texas Southwestern  
Medical Center, United States  
Wei-Chi Wu,  
Linkou Chang Gung Memorial  
Hospital, Taiwan

### \*Correspondence:

Songfeng Li  
lsf\_03979@163.com  
Hai Lu  
trdr\_luhai2017@163.com

### Specialty section:

This article was submitted to  
Ophthalmology,  
a section of the journal  
Frontiers in Medicine

Received: 14 May 2021

Accepted: 23 September 2021

Published: 27 October 2021

### Citation:

Liu J-H, Deng G, Ma J, Li L, Fang Y,  
Li S and Lu H (2021) Clinical  
Characteristics of Pediatric Coats'  
Disease With Retinal Cyst Using  
Wide-Angle Fluorescein Angiography.  
Front. Med. 8:709522.  
doi: 10.3389/fmed.2021.709522

**Purpose:** To assess the demographic and treatment features of pediatric patients of Coats' disease with retinal cyst using wide-angle FA.

**Design:** A retrospective, hospital based, cross-sectional study.

**Participants:** Pediatric patients of Coats' disease underwent wide-angle FA.

**Methods:** A retrospective review of pediatric patients of Coats' disease who underwent wide-angle FA at a single center from January 2015 to July 2020. Demographic and treatment features were compared between patients with or without retinal cyst.

**Main Outcome Measures:** Demographic and treatment outcomes.

**Results:** There were 123 pediatric Coats' patients in our study, and 18.70% (23/123) of the patients developed complications with retinal cyst, 73.9% (17/23) of the retinal cysts were located in the inferior-temporal quadrant and 82.6% (19/23) of the retinal cysts were located in the peripheral retina anterior to the vortex veins. Compared with patients without retinal cyst, patients with retinal cyst had more clock-hours of telangiectasia on FA (7.32 vs. 5.41,  $p = 0.031$ ), and may need more total treatments (7.47 vs. 3.53,  $p = 0.023$ ) including laser photocoagulation (4.08 vs. 2.31,  $p = 0.019$ ) or intravitreal anti-VEGF (3.13 vs. 2.23,  $p = 0.039$ ), and also required a longer time for telangiectasia resolution (22.33 vs. 18.53 months,  $p = 0.043$ ).

**Conclusion:** Pediatric patients with Coats' disease complicated by retinal cyst presented with more clock-hours of telangiectasia on FA and needed more total treatments and longer time for telangiectasia resolution.

**Keywords:** pediatric, Coats' disease, retinal cyst, wide-angle fluorescein angiography, clinical characteristics

## INTRODUCTION

Coats' disease is a congenital, idiopathic retinal telangiectasia characterized by intraretinal and/or subretinal exudation leading to progressive exudative retinal detachment without retinal or vitreous traction (1, 2). It remains a great challenge of diagnosis and treatment because of its varied clinical presentation, and the majority of the cases present with advanced stages ending with poor visual acuity prognosis in spite of aggressive treatment (3, 4).

Retinal cyst is defined as a fluid-filled space derived from or in the retina (5), and may be related to focal anoxia or degeneration caused by long-standing retinal detachment such as Coats' disease (6). There are a few reports about Coats' disease complicated with retinal cyst, but these have either been single cases or have given few details of its clinical and treatment features (7, 8).

We hereby retrospectively reviewed a case series of pediatric Coats' disease and gave a descriptive analysis of pediatric Coats' disease complicated with retinal cyst, using RetCam III imaging combined with wide-angle fluorescence angiography (FA).

## METHODS

The medical and imaging records of 123 children ( $\leq 18$  years) with Coats' disease who underwent treatment with the surveillance of RetCam III imaging combined with wide-angle FA in Beijing Tongren Hospital from January 2015 to July 2020 were retrospectively reviewed. This study has been approved by the Hospital Board and was performed in accordance with the Declaration of Helsinki and we have obtained informed consent from guardians of all the patients. To be included in the study, the patients had to show idiopathic retinal telangiectasia defined as irregular, dilated small, or medium vessels manifested on wide-angle FA, and/or retinal lipid exudation. Patients with uncertain diagnosis and without complete records were excluded.

Coats' disease was staged based on a previously published classification system (9): Stage 1 (only retinal telangiectasia); Stage 2a (telangiectasia and extrafoveal exudation); Stage 2b (telangiectasia and foveal exudation); Stage 3a (subtotal exudative retinal detachment); Stage 3b (total exudative retinal detachment); Stage 4 (total exudative retinal detachment and secondary glaucoma); Stage 5 (phthisis bulbi).

Fundus examination under anesthesia including indirect ophthalmoscopy, color photography and FA with Retcam III was arranged for both eyes of all the patients, each patient was given an intravenous bolus of 20% sodium fluorescein (0.1 ml/kg) before performing FA. Color Doppler ultrasonography and OCT were used to document the presence and extent of retinal detachment and retinal cyst in some cases.

Ablative therapies such as 532-nm laser, cryotherapy, or both were administrated to the areas of retinal non-perfusion and telangiectatic vessels according to FA findings. Cryotherapy was used only when there was confluent extensive exudation of the telangiectatic vascular areas. Intravitreal injection of Ranibizumab (Lucentis; Genentech Inc., South San Francisco, CA, USA) was used for patients with exudative retinal detachment (stage 3 or over). Vitreoretinal surgery, which included any combination of subretinal fluid drainage, pars plana vitrectomy were arranged for some cases.

The patients were monitored between 4 and 12 weeks after treatment, and further treatment was undertaken if there was a lack of telangiectatic vascular resolution or an increase of exudation at follow-up appointment. Demographic data including age at presentation, sex, laterality, clinical features such

**TABLE 1 |** Demographics of Coats' disease with or without retinal cyst.

Variable	Patients with retinal cyst	Patients without retinal cyst	p-value
No. of patients (eyes)	23 (23)	100 (100)	
Age at presentation (years)			0.057
Mean $\pm$ SD	6.35 $\pm$ 3.28	5.41 $\pm$ 2.12	
Range	2–15	3–15	
Follow-up (months)			0.731
Mean $\pm$ SD	29.61 $\pm$ 11.30	32.02 $\pm$ 15.07	
Range	9–60	6–65	
Sex, no. (%)			0.933
Male	21 (91.30%)	92 (92.0%)	
Female	2 (8.70%)	8 (8.0%)	
Eye laterality, no. (%)			0.789
Right eye	11 (47.83%)	46 (46.0%)	
Left eye	12 (52.17%)	54 (54.0%)	

as pre- and postoperative visual acuity, Coats' disease stages, macular involvement (macular involvement was defined in this study as retinal detachment or yellow hard exudate involving the macular fovea and with a diameter more than one optic disc), retinal cyst and its location, clock hours of FA telangiectasia, treatment modalities, and anatomical prognosis were reviewed and compared between the two groups with or without retinal cysts. Snellen visual acuities were recorded and converted to logarithm of the minimum angle of resolution (log MAR) units for statistical evaluation.

Statistical analysis was performed using SPSS software (version 17.0, SPSS Inc., Chicago, IL, USA). Kolmogorov-Smirnov test was used to analyze the normal distribution of continuous variables, and Mann-Whitney U test was used to compare continuous variables if the data did not follow a normal distribution, Student sample *t*-test was used to compare continuous variables if the data followed a normal distribution between groups with or without retinal cyst; Fisher exact test was used to compare categorical variables between groups and *p*-value of 0.05 or less was considered statistically significant.

## RESULTS

Demographic features of the study participants: 123 children with Coats' disease (123 eyes) were identified in this study, with at least 6 months follow-up. Overall average age at presentation was 5.59 years ( $5.59 \pm 2.40$ ) and the predominant sex was male (113/123, 91.87%). Retinal cyst was complicated in 23 patients (23 eyes, 23/123, 18.70%), and a comparison of demographic features between patients with and without retinal cyst were listed in **Table 1**. Statistical analysis revealed no significant difference in presenting age, sex, affected eye (**Table 1**), preoperative visual acuity, Coats' disease stages and macular involvement between the two groups, but FA showed more clock hours of telangiectasia in the group of patients with retinal cyst compared with cases



**TABLE 2 |** Baseline ocular characteristics of Coats' disease with or without retinal cyst.

Variable	Patients with retinal cyst	Patients without retinal cyst	p-value
No. of patients (eyes)	23 (23)	100 (100)	
Best-corrected visual acuity (log MAR) no. (%)			0.062
≤ 0.7	2 (8.70%)	4 (4.0%)	
1.70–0.7	3 (13.04%)	21 (21.0%)	
≥ 1.70	15 (65.22%)	58 (58.0%)	
Uncooperative	3 (13.04%)	17 (17%)	
Coats' disease stage, no. (%)			0.157
1	0 (0)	0 (0)	
2a	3 (13.04%)	17 (17.0%)	
2b	3 (13.04%)	33 (33.0%)	
3a	16 (69.57%)	44 (44.0%)	
3b	1 (4.35%)	5 (5.0%)	
4	0	1 (1.0%)	
5	0	0	
Macular involvement			0.238
Yes	19 (82.6%)	81 (81.0%)	
No	4 (17.4%)	19 (19.0%)	
Combined stages of Coats', no. (%)			0.023*
Stages 1 to 2B	6 (26.09%)	50 (50%)	
Stages 3A to 5	17 (73.91%)	50 (50%)	
Fluorescein angiography telangiectasia clock hours			0.031*
Mean ± SD	7.32 ± 2.73	5.41 ± 3.02	
Range	4–12	1–12	

without retinal cyst (7.32 vs. 5.41,  $p = 0.031$ ), and there was a trend for eyes in patients with retinal cyst to demonstrate more advanced stages of disease (stage 3A to 5) than those in patients without retinal cyst (73.91 vs. 50.0%,  $p = 0.023$ ) (Table 2).

Retinal cysts complicated in those cases with Coats' disease manifested as round, clear-demarcated, protuberant cystic pathologies located in posterior or peripheral retina. Retinal cysts were mostly located in the inferior-temporal quadrant (17/23, 73.91%) and the superior-temple quadrant (5/23, 21.72%), only 1 eye with retinal cyst located in the superior-nasal quadrant, and no eye with retinal cyst located in the inferior-nasal quadrant was seen in our case series; 82.60% (19/23) of the retinal cysts located in the peripheral retina (anterior to the vortex veins), and 17.39% (4/23) of the retinal cysts located in the posterior retina (posterior to the vortex veins).

In addition to common clinical features on FA of Coats' disease such as widespread retinovascular telangiectasia, microaneurysms as well as capillary non-perfusion, retinal cyst on FA revealed round, well-demarcated, bullous pathologies with cystic cavity, with capillary non-perfusion areas in the anterior layer of the cyst and late-phase punctate hyperfluorescence of the posterior layer, also telangiectatic and aneurysmal vessels and

multiple areas of peripheral capillary non-perfusion at or around the edge of the cyst (Figure 1).

Color Doppler Image (CDI) showed intraocular cystic mass connected with the hyperechoic area of ocular wall (Figure 2), with localized vascular signal on the anterior layer (Figure 2C). OCT showed retinal cyst as separation of the inner and the outer layer of the retina (Figure 3).

Treatment features of patients in our study are listed in Table 3 and a comparison of treatment features between the two groups revealed that the group of patients with retinal cyst had greater total number of treatments (7.47 vs. 3.53,  $p = 0.023$ ); and more use of laser photocoagulation (4.08 vs. 2.31,  $p = 0.019$ ), and intravitreal anti-VEGF (3.13 vs. 2.23,  $p = 0.039$ ).

Other treatment modalities such as cryotherapy, pars plana vitrectomy and subretinal fluid drainage were also used for these patients, but without statistically significant differences between the two groups ( $p = 0.072$ ): 11 eyes of the 123 eyes (11/123, 8.9%) underwent cryotherapy, of which 3 eyes presented with retinal cyst and the other 8 eyes without retinal cyst; 8 eyes of the 123 eyes (8/123, 6.5%) underwent pars plana vitrectomy, of which 2 eyes presented with retinal cyst and the other 6 eyes without retinal cyst; 8 eyes of the 123 eyes (8/123, 6.5%) underwent subretinal fluid drainage, of which 3 eyes presented with retinal cyst and the other 5 eyes without retinal cyst.

Figures 4, 5 showed fundus photographs of pre-and postoperative fundus photographs of patients with retinal cysts, indicating different degrees of retinal cyst resolution after combined treatment modalities.

Postoperative last-visit visual acuity and percentages of resolution of leaking telangiectasia were also compared and without statistically significant differences between the two groups, but patients with retinal cysts needed longer times for the resolution of leaking telangiectasia (22.33 vs. 18.53 months,  $p = 0.043$ ) (Table 4).

## DISCUSSION

Coats' disease represents a broad clinical spectrum of retinal vasculopathy and presents numerous challenges in the management across the disease spectrum (10, 11). Retinal cyst is usually complicated in long-standing rhegmatogenous or exudative retinal detachment such as Coats' disease, which causes focal retinal anoxia or focal retinal cell liquefaction and degeneration.

With the advent of wide-field portable RetCam III imaging, intraoperative FA can be obtained and thus facilitates full identification of abnormal retinovascular areas, where treatment such as laser or cryotherapy could be administrated under general anesthesia for pediatric patients (12–15). The purpose of the study was to investigate the clinical and treatment features of Coats' disease with retinal cyst compared with that without retinal cyst in pediatric patients underwent RetCam III wide-angle FA guided treatment.

We reviewed our clinical experience with Coats' disease in pediatric patients and found that several factors have not changed compared with previous studies (16–19), such as

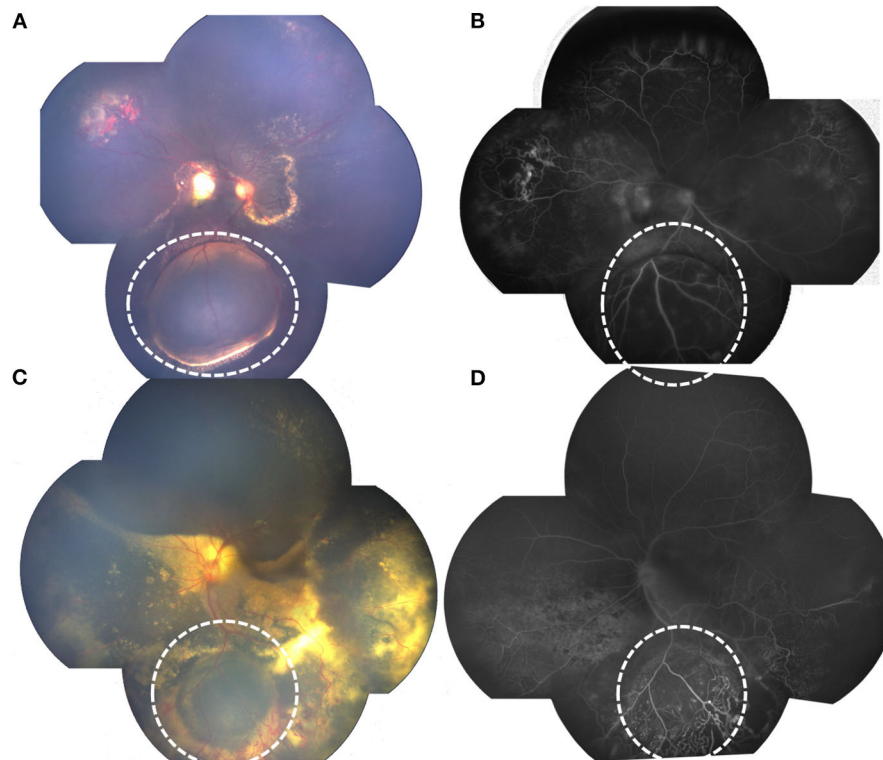


**FIGURE 1 |** RetCam fundus and FA photographs showing Coats' disease with retinal cysts: **(A)** bullous retinal cyst in the inferior quadrant, surrounded with yellow hard exudation (white dotted circle); **(B)** FA of **(A)** showing well-demarcated, protuberant pathology, with anterior layer capillary non-perfusion and late-phase punctate hyperfluorescence of the posterior layer, telangiectasia located at the edge of the cyst (white dotted circle). **(C)** retinal cyst (white dotted circle), surrounded with massive telangiectasia; **(D)** FA of **(C)** showing protuberant cyst, with anterior layer capillary non-perfusion and telangiectasia.

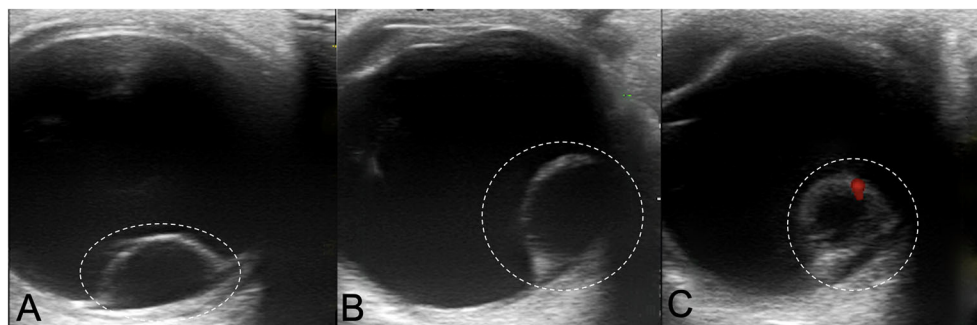


**FIGURE 2 |** Color Doppler Image showing Coats' disease with retinal cysts: **(A,B)** intraocular cystic mass connected with the hyperechoic area of ocular wall (white dotted circle); **(C)** localized vascular signal on the anterior layer (red signal).

median age at presentation, predominant sex as male (113/123, 91.8%), predominant Coats' disease stage as stage 3a (48.78 vs. 42%). Our study also showed that patients with retinal cyst had more clock hours of telangiectasia on FA compared with patients without retinal cyst, indicating that patients with retinal cyst may have had longer and much more severe exudative retinal detachment that induced longer time of retinal anoxia or degeneration, which is the pathophysiological basis of retinal cyst formation.

We reviewed the literature and found only Vineet Mutha described the location of retinal cyst in a 5-year-old boy with Coats' disease staged as 3A, and the complicated retinal cyst located in the superonasal quadrant of the fundus (7). In our study, retinal cysts were mostly located in the inferior-temporal quadrant and the superior-temporal quadrant, and 82.6% (19/23) of the retinal cysts located in the peripheral retina. We also found in our study that severe combined stages of Coats' disease (3A-5) had larger proportions of retinal cysts formation.

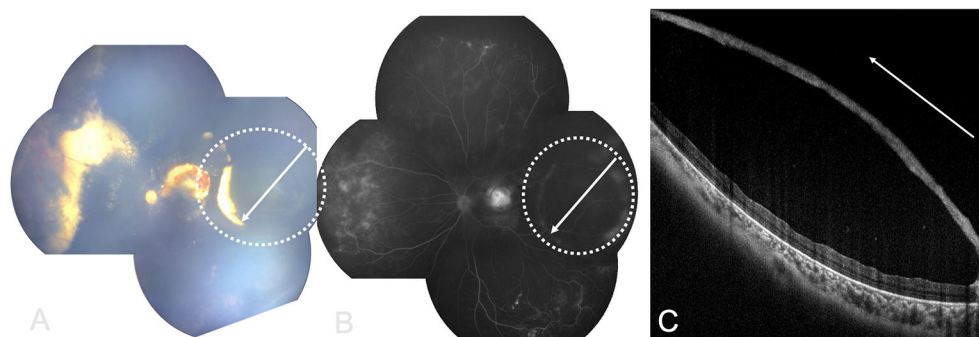


**FIGURE 3 |** RetCam fundus, FA and OCT images showing Coats' disease with retinal cysts: **(A)** retinal cyst (white dotted circle), white arrow showing OCT scan direction; **(B)** FA of **(A)**, white arrow showing OCT scan direction; **(C)** OCT image showing retinal cyst with separation of the inner and outer layers of retina (white arrow showing OCT scan direction).

**TABLE 3 |** Treatment features of Coats' disease with or without retinal cyst.

Treatment features	Patients with retinal cyst	Patients without retinal cyst	<i>p</i> -value
No. of patients (eyes)	23 (23)	100 (100)	
Number of total treatments per patient			0.023*
Mean $\pm$ SD	7.47 $\pm$ 3.01	3.53 $\pm$ 2.31	
Range	(4–12)	(1–12)	
Argon laser photocoagulation			0.019*
Number of treatments per patient			
Mean $\pm$ SD	4.08 $\pm$ 1.35	2.31 $\pm$ 0.99	
Range	(2–6)	(1–5)	
Anti-VEGF			0.039*
Number of treatments per patient			
Mean $\pm$ SD	3.13 $\pm$ 1.03	2.23 $\pm$ 1.57	
Range	(2–5)	(0–4)	

\*Statistically significant.

( $p = 0.023$ ). It is not difficult to interpret those results because subretinal fluid accumulated in the inferior quadrant because of gravity, or around the telangiectasia area, which is always located in the peripheral fundus, especially in cases with much severe stages, so long-time exudative retinal detachment may be located in the inferior and peripheral retina in cases with severe Coats' stages, thus forming the pathological basis of retinal cyst formation.

In addition to FA documentation of telangiectasia, light bulb aneurysm, peripheral non-perfusion, and cystoid macular edema, which are frequently seen in Coats' patients (20–22), patients with retinal cysts also demonstrated with well-demarcated, bullous cystic pathologies with the hypo-fluorescence anterior layer “flapping” in the vitreous cavity, late-phase hyper-fluorescence or capillary fluorescence leakage of the posterior layer of the cyst could also be seen, which is different from FA appearance of retinal detachment. Another differential diagnosis of FA appearance of Coats' disease with retinal cysts is retinoschisis,

which is always bilaterally involved and without telangiectasia or light bulb aneurysm.

Ultrasonography has long been known to be an essential tool for diagnosis of ocular cysticercosis, and Coats' disease with retinal cyst could manifest as a cystic mass on ultrasonography mimicking a cysticercus cyst with scolex (10). Color Doppler image showed intraocular cystic masses with its hyperechogenic wall connected with the echo of ocular wall, also red vascular signals on the anterior layer, which can be differentiate from cysticercus scolex.

But a smaller retinal cyst (<2 diameters of optic disc) which was buried in extensive retinal detachment, was difficult to distinguish by FA or Ultrasonography.

Exudative retinal detachment complication in Coats' disease is difficult to differentiate from retinal cyst on a fundus photograph, but OCT may give an excellent differentiation as **Figure 3** showed: retinal cyst manifested as separation of the inner and the outer layer of the neuroretina, while retinal detachment was the separation of neuroretina and the retinal epithelium.

Treatment of Coats' disease should be directed toward obliterating the telangiectasia by laser photocoagulation or cryotherapy (23–25), more advanced cases complicated by severe exudative retinal detachment may require combined therapies such as intravitreal anti-VEGF, or subretinal fluid drainage to facilitate resolution of the exudate or subretinal fluid (26, 27). For cases complicated with vitreoretinal traction or opacities, pars plana vitrectomy may be needed (28).

The average total number of treatments of all the patients in our study is 4.42, which is comparable with the latest studies in the 2010's (8, 15, 19). Our results also revealed that patients with retinal cyst had a greater total number of treatments, and more use of laser photocoagulation and intravitreal anti-VEGF, probably because of the increased number of hours of telangiectasia on FA of patients with retinal cyst which needs more treatments including laser photocoagulation and intravitreal anti-VEGF for the complete resolution of Coats' pathologies, furthermore, vascular telangiectasia may locate around the anterior edge of retinal cyst just as **Figure 1** shows, and the protuberant cyst may make it much more difficult

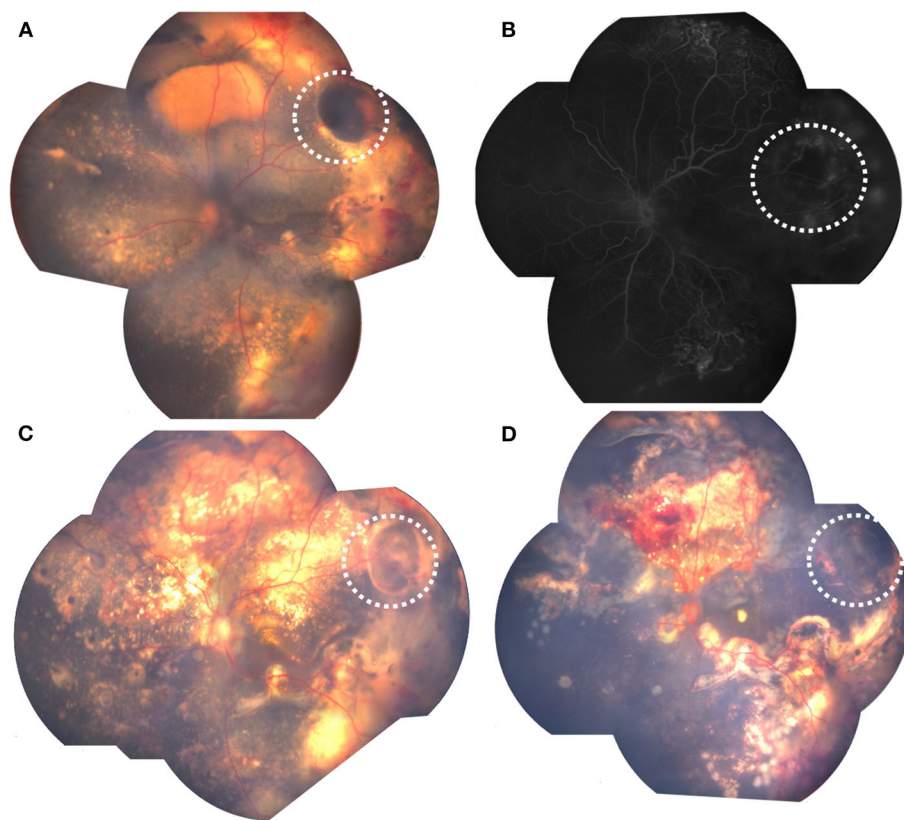


**FIGURE 4 |** Pre- and postoperative fundus photographs of Coats' with retinal cyst.: **(A)** preoperative retinal cyst (white dotted circle), surrounded with exudative retinal detachment; **(B)** FA showing protuberant cyst (white dotted circle); **(C)** decreased retinal cyst (white dotted circle), with retinal attachment after 2 laser photocoagulation combined with intravitreal anti-VEGF; **(D)** retinal cyst resolution (white dotted circle), with retinal attachment after 2 additional laser photocoagulation.

for the thorough laser photocoagulation of the telangiectasia area through binocular indirect ophthalmoscope. Comparisons of other treatments such as cryotherapy, pars plana vitrectomy or subretinal fluid drainage between the two groups in our study revealed no statistical differences, probably because a small number of patients underwent those treatments in our study, and future research with many more patients will be needed.

The presence of thick foveal exudation (stage 2B and above) usually portends a worse visual prognosis both preoperatively and postoperatively, our study showed that 70.27% (78/111) of the patients had postoperative visual acuity worse than log MAR 1.70, which was comparable to previous studies (29, 30), and statistical differences about postoperative visual acuity were not found between the two groups with or without retinal cyst, because most of the patients in our study presented with late Coats' disease stages accompanied by retinal detachment or thick foveal exudation involving the macula with no statistical differences in the macular involvement percentages ( $p = 0.238$ ) between the two groups, hence the poor visual acuity prognosis.

Shields et al. reported that improvement of stabilization of the disease was achieved in almost 76% of their patients from an anatomic standpoint, and 85.37% (105/123) of the

patients in our study had leaking telangiectasia resolution at last visit, with no statistical differences between the two groups ( $p = 0.750$ ). However, our results showed that patients with retinal cysts needed longer time for resolution of leaking telangiectasia (22.33 vs. 18.53 months,  $p = 0.043$ ), which may be explained by the fact that patients with retinal cysts had much more clock-hours of telangiectasia and needed longer time for total resolution of leaking telangiectasia.

This retrospective study has many limitations including its relatively short time of follow-up and the potential bias that patients in our study were mostly referred from other hospitals and had very severe pathologies with lower ages at presentation, so the retinal cyst percentage of 18.70% may not be suitable for all the Coats' patients. But it has its advantages of being the largest series of studies investigating the clinical characteristics of pediatric Coats' patients with retinal cyst. However, with the long life span of these patients, further studies with longer-term follow up and more paralleled cases is necessary to explore the visual and anatomical prognosis of these patients.

In summary, we have reviewed our experience with Coats' disease complicated with retinal cysts, and our results showed



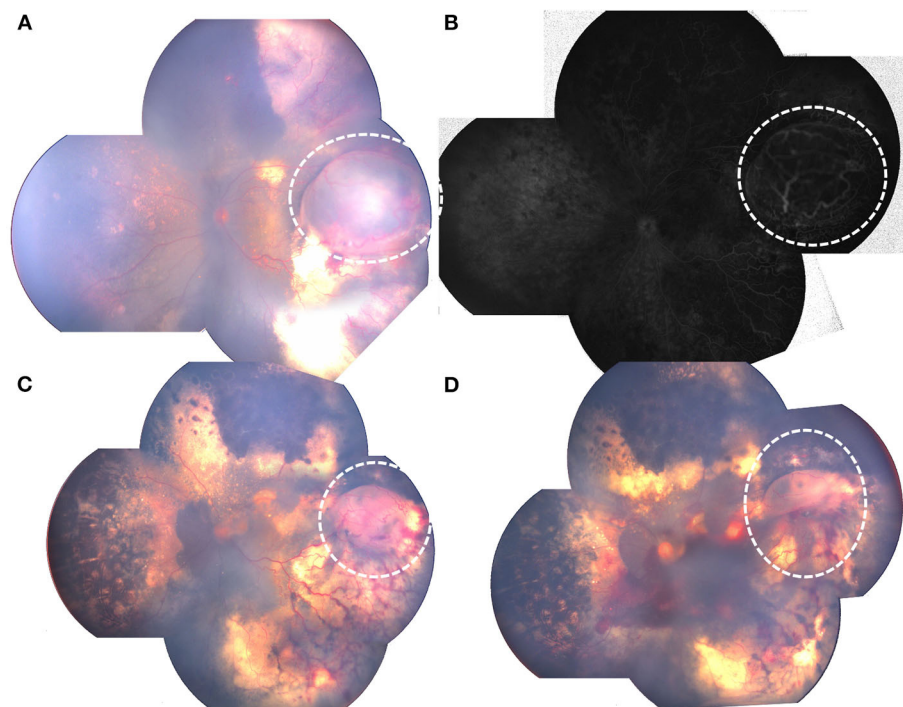


**FIGURE 5 |** Pre- and postoperative fundus photograph of Coats' with retinal cyst.: **(A)** preoperative retinal cyst (white dotted circle); **(B)** FA showing protuberant cyst (white dotted circle); **(C)** decreased retinal cyst (white dotted circle) after 3 laser photocoagulation combined with intravitreal anti-VEGF; **(D)** partial retinal cyst resolution (white dotted circle), with minimal vitreous hemorrhage after 3 additional laser photocoagulation combined with 2 intravitreal anti-VEGF.

**TABLE 4 |** Outcomes of Coats' disease with or without retinal cyst.

Outcomes	Patients with retinal cyst	Patients without retinal cyst	p-value
No. of patients (eyes)	23 (23)	100 (100)	
Best corrected visual acuity (log MAR) no. (%)			0.639
≤ 0.7	2 (2/23, 8.70%)	4 (4/100, 4.00%)	
1.70–0.7	4 (4/23, 17.39%)	23 (23/100, 23.00%)	
≥ 1.70	16 (16/23, 69.57%)	62 (62/100, 62.00%)	
Uncooperative	1 (1/23, 4.35%)	11 (11/100, 11.00%)	
Leaking telangiectasia resolution no. (%)			0.750
Resolved	18 (18/23, 78.26%)	87 (87/100, 87.00%)	
Not resolved	5 (5/23, 21.74%)	13 (13/100, 13.00%)	
Time to resolution (months)			0.043*
Mean ± SD	22.33 ± 7.98	18.53 ± 5.47	
Range	(15–33)	(9–29)	

that 18.70% (23/123) of the Coats' patients may present with complications of retinal cyst, and retinal cysts were mostly located in the inferior-temporal quadrant and in the

peripheral retina; patients with retinal cyst had more clock-hours of telangiectasia on FA, and may need more treatments including laser photocoagulation or intravitreal anti-VEGF, also longer time for telangiectasia resolution. Our results should assist the ophthalmologist in predicting treatment difficulties or poorer prognoses for Coats' patients with retinal cyst.

## SYNOPSIS

123 children with Coats' who underwent wide-angle FA were retrospectively reviewed and results showed 18.70% (23/123) of the patients developed complications with retinal cyst and patients with retinal cyst presented with more clock-hours of telangiectasia on FA and needed more total treatments and longer time for telangiectasia resolution.

## DATA AVAILABILITY STATEMENT

The raw data supporting the conclusions of this article will be made available by the authors, without undue reservation.

## ETHICS STATEMENT

The studies involving human participants were reviewed and approved by the Ethics Committee of Beijing Tongren

Hospital. Written informed consent to participate in this study was provided by the participants' legal guardian/next of kin.

## AUTHOR CONTRIBUTIONS

HL and SL: conceptualization and methodology. J-HL: data collection and writing original draft preparation. JM, LL, and

GD: patient reviewing. YF: image preparation and editing. All authors contributed to the article and approved the submitted version.

## FUNDING

This study was supported by Beijing Tongren Hospital, Capital Medical University (TRZDYXZY201703).

## REFERENCES

- Shields JA, Shields CL. Differentiation of coats' disease and retinoblastoma. *J Pediatr Ophthalmol Strabismus*. (2001) 38:262–6. doi: 10.3928/0191-3913-20010901-05
- Shields JA, Shields CL, Honavar SG, Demirci H. Clinical variations and complications of Coats disease in 150 cases: the 2000 Sanford Gifford Memorial Lecture. *Am J Ophthalmol*. (2001) 131:561–71. doi: 10.1016/S0002-9394(00)00883-7
- Morris B, Foot B, Mulvihill A. A population-based study of Coats disease in the United Kingdom I: epidemiology and clinical features at diagnosis. *Eye*. (2010) 24:1797–801. doi: 10.1038/eye.2010.126
- Shields JA, Shields CL. Review: coats disease: the 2001 LuEsther T. Mertz lecture. *Retina*. (2002) 22:80–91. doi: 10.1097/00006982-200202000-00014
- Keith CG. Retinal cysts and retinoschisis. *Br J Ophthalmol*. (1966) 50:617–28. doi: 10.1136/bjo.50.11.617
- Marcus DF, Aaberg TM. Intraretinal macrocysts in retinal detachment. *Arch Ophthalmol*. (1979) 97:1273–5. doi: 10.1001/archophth.1979.01020020015003
- Mutha V, Agrawal S, Chandra P, Kumar A. Coats disease with exudative retinal detachment simulating cysticercus cyst: misleading ultrasonography! *BMJ Case Rep*. (2018) 2018:bcr2017222975. doi: 10.1136/bcr-2017-222975
- Shields CL, Udyaver S, Dalvin LA, Lim LS, Atalay HT, Khoo CT, et al. Coats disease in 351 eyes: Analysis of features and outcomes over 45 years (by decade) at a single center. *Indian J Ophthalmol*. (2019) 67:772–83. doi: 10.4103/ijo.IJO\_449\_19
- Shields JA, Shields CL, Honavar SG, Demirci H, Cater J. Classification and management of Coats disease: the 2000 Proctor Lecture. *Am J Ophthalmol*. (2001) 131:572–83. doi: 10.1016/S0002-9394(01)00896-0
- Gomez Morales A. Coats' disease. Natural history and results of treatment. *Am J Ophthalmol*. (1965) 60:855–65. doi: 10.1016/0002-9394(65)92006-4
- Kiratli H, Eldem B. Management of moderate to advanced Coats' disease. *Ophthalmologica*. (1998) 212:19–22. doi: 10.1159/000027253
- Kim JW, Ngai LK, Sada S, Murakami Y, Lee DK, Murphree AL. Retcam fluorescein angiography findings in eyes with advanced retinoblastoma. *Br J Ophthalmol*. (2014) 98:1666–71. doi: 10.1136/bjophthalmol-2014-305180
- Temkar S, Azad SV, Chawla R, Damodaran S, Garg G, Regani H, et al. Ultra-widefield fundus fluorescein angiography in pediatric retinal vascular diseases. *Indian J Ophthalmol*. (2019) 67:788–94. doi: 10.4103/ijo.IJO\_1688\_18
- Koozekanani DD, Connor TB, Wirostko WJ. RetCam II fluorescein angiography to guide treatment and diagnosis of coats disease. *Ophthalmic Surg Lasers Imaging*. (2010) 9:1–3. doi: 10.3928/15428877-20100215-86
- Suzani M, Moore AT. Intraoperative fluorescein angiography-guided treatment in children with early Coats' disease. *Ophthalmology*. (2015) 122:1195–202. doi: 10.1016/j.ophtha.2015.02.002
- Al-Qahtani AA, Almasaud JM, Ghazi NG. Clinical characteristics and treatment outcomes of coats disease in a Saudi Arabian population. *Retina*. (2015) 35:2091–9. doi: 10.1097/IAE.0000000000000594
- Daruich AL, Moulin AP, Tran HV, Matet A, Munier FL. Subfoveal nodule in coats' disease: toward an updated classification predicting visual prognosis. *Retina*. (2017) 37:1591–8. doi: 10.1097/IAE.0000000000001399
- Daruich A, Matet A, Munier FL. Younger age at presentation in children with Coats disease is associated with more advanced stage and worse visual prognosis: A Retrospective Study. *Retina*. (2018) 38:2239–46. doi: 10.1097/IAE.0000000000001866
- Ong SS, Buckley EG, McCuen BW, Jaffe GJ, Postel EA, Mahmoud TH, et al. Comparison of visual outcomes in Coats' disease: A 20-year experience. *Ophthalmology*. (2017) 124:1368–76. doi: 10.1016/j.ophtha.2017.03.051
- Singh SR, Jayakumar K, Jain S, Arora A, Yangzes S, Katoch D, et al. Diagnosis and treatment of bilateral Coats disease in a 5-year-old girl. *J AAPOS*. (2019) 23:243–45. doi: 10.1016/j.jaapos.2019.04.002
- Ong SS, Cummings TJ, Vajzovic L, Mruthyunjaya P, Toth CA. Comparison of optical coherence tomography with fundus photographs, fluorescein angiography, and histopathologic analysis in assessing coats disease. *JAMA Ophthalmol*. (2019) 137:176–83. doi: 10.1001/jamaophthalmol.2018.5654
- Jeng-Miller KW, Soomro T, Scott NL, Rao P, Marlow E, Chang EY, et al. Longitudinal examination of fellow-eye vascular anomalies in coats' disease with widefield fluorescein angiography: a multicenter study. *Ophthalmic Surg Lasers Imaging Retina*. (2019) 50:221–7. doi: 10.3928/23258160-20190401-04
- Scheffler AC, Berrocal AM, Murray TG. Advanced Coats' disease. Management with repetitive aggressive laser ablation therapy. *Retina*. (2008) 28(Suppl. 3):S38–41. doi: 10.1097/IAE.0b013e318163cd7c
- Tarkkanen A, Laatikainen L. Coat's disease: clinical, angiographic, histopathological findings and clinical management. *Br J Ophthalmol*. (1983) 67:766–76. doi: 10.1136/bjo.67.11.766
- Ridley ME, Shields JA, Brown GC, Tasman W. Coats' disease. Evaluation of management. *Ophthalmology*. (1982) 89:1381–7. doi: 10.1016/S0161-6420(82)34634-5
- Ramasubramanian A, Shields CL. Bevacizumab for Coats' disease with exudative retinal detachment and risk of vitreoretinal traction. *Br J Ophthalmol*. (2012) 96:356–9. doi: 10.1136/bjophthalmol-2011-300141
- Fiorentzis M, Stavridis E, Seitz B, Viestenz A. Anti-VEGF als Adjuvans bei Morbus Coats [Adjuvant anti-VEGF therapy in Coats' disease]. *Ophthalmologie*. (2015) 112:451–4. doi: 10.1007/s00347-014-3122-0
- Karacorlu M, Hocaoglu M, Sayman Muslubas I, Arf S. Long-term anatomical and functional outcomes following vitrectomy for advanced coats disease. *Retina*. (2017) 37:1757–64. doi: 10.1097/IAE.0000000000001415
- Li S, Deng G, Liu J, Ma Y, Lu H. The effects of a treatment combination of anti-VEGF injections, laser coagulation and cryotherapy on patients with type 3 Coats' disease. *BMC Ophthalmol*. (2017) 17:76. doi: 10.1186/s12886-017-0469-4
- Shields CL, Udyaver S, Dalvin LA, Lim LS, Atalay HT, Khoo C, et al. Visual acuity outcomes in Coats disease by classification stage in 160 patients. *Br J Ophthalmol*. (2020) 104:422–31. doi: 10.1136/bjophthalmol-2019-314363

**Conflict of Interest:** The authors declare that the research was conducted in the absence of any commercial or financial relationships that could be construed as a potential conflict of interest.

**Publisher's Note:** All claims expressed in this article are solely those of the authors and do not necessarily represent those of their affiliated organizations, or those of the publisher, the editors and the reviewers. Any product that may be evaluated in this article, or claim that may be made by its manufacturer, is not guaranteed or endorsed by the publisher.

Copyright © 2021 Liu, Deng, Ma, Li, Fang, Li and Lu. This is an open-access article distributed under the terms of the Creative Commons Attribution License (CC BY). The use, distribution or reproduction in other forums is permitted, provided the original author(s) and the copyright owner(s) are credited and that the original publication in this journal is cited, in accordance with accepted academic practice. No use, distribution or reproduction is permitted which does not comply with these terms.



# Ellipsoid Zone and External Limiting Membrane-Related Parameters on Spectral Domain-Optical Coherence Tomography and Their Relationships With Visual Prognosis After Successful Macular Hole Surgery

## OPEN ACCESS

### Edited by:

Haijiang Lin,  
Massachusetts Eye & Ear Infirmary  
and Harvard Medical School,  
United States

### Reviewed by:

Wen-Bin Wei,  
Capital Medical University, China  
Zhao Mingwei,  
Peking University People's  
Hospital, China

### \*Correspondence:

Changguan Wang  
docwcg@126.com  
Xuemin Li  
lxm66@sina.com

<sup>†</sup> These authors have contributed  
equally to this work and share first  
authorship

### Specialty section:

This article was submitted to  
Ophthalmology,  
a section of the journal  
Frontiers in Medicine

**Received:** 19 September 2021

**Accepted:** 20 October 2021

**Published:** 10 November 2021

### Citation:

Yang J, Xia H, Liu Y, Wang X, Yuan H,  
Hou Q, Ge Y, Ding Y, Wang Y, Wang C  
and Li X (2021) Ellipsoid Zone and  
External Limiting Membrane-Related  
Parameters on Spectral  
Domain-Optical Coherence  
Tomography and Their Relationships  
With Visual Prognosis After Successful  
Macular Hole Surgery.  
Front. Med. 8:779602.  
doi: 10.3389/fmed.2021.779602

Jiarui Yang<sup>1†</sup>, Huaqin Xia<sup>1†</sup>, Yushi Liu<sup>1†</sup>, Xinglin Wang<sup>1</sup>, Hao Yuan<sup>1</sup>, Qingyi Hou<sup>1</sup>,  
Yimeng Ge<sup>1</sup>, Yi Ding<sup>1</sup>, Yuexin Wang<sup>1</sup>, Changguan Wang<sup>1,2\*</sup> and Xuemin Li<sup>1,2\*</sup>

<sup>1</sup> Department of Ophthalmology, Peking University Third Hospital, Beijing, China, <sup>2</sup> Beijing Key Laboratory of Restoration of Damaged Ocular Nerve, Beijing, China

**Purpose:** To compare structural diameters of the ellipsoid zone (EZ) and external limiting membrane (ELM) bands on spectral domain-optical coherence tomography (SD-OCT) images between vision-improved (group A) and vision-unimproved (group B) patients, and investigate the connection between these parameters and visual prognosis.

**Materials and Methods:** Forty-five eyes of 43 patients with idiopathic full-thickness macular hole closed after vitrectomy were retrospectively reviewed. Best-corrected visual acuity (BCVA) and SD-OCT were conducted preoperatively and at 1 week, 1 month and 6 months postoperatively. Structural and functional parameters were then measured using ImageJ software.

**Results:** Among structural and functional parameters, the relative reflectivity of EZ and the ratio of continuous ELM and EZ in group A were significantly higher than in group B from the 1-month postoperative visit. At the 6-month follow-up, the diameter of EZ disruption in group A was significantly smaller than in group B, and the relative reflectivity of ELM/EZ was significantly higher than group B. At 6-months, BCVA was statistically significantly correlated with baseline BCVA, basal diameter (BD), macular hole index (MHI), and diameter of ELM/EZ disruption. Change in BCVA from baseline was found to be significantly correlated with axial length and diameter hole index (DHI).

**Conclusions:** Postoperative BCVA outcome was significantly correlated with integrity, thickness and reflectivity of the EZ band. Patients with smaller diameter of EZ disruption and higher reflectivity of EZ band tended to have better visual outcomes. Given that the EZ band reflects the recovery of mitochondria in photoreceptors, it is a promising parameter for their functional evaluation.

**Keywords:** idiopathic macular hole, optical coherence tomography (OCT), ellipsoid zone (EZ), external limiting membrane, visual prognosis

## INTRODUCTION

Idiopathic macular hole (MH), first described by Johnson and Gass in 1988 (1), is a full-thickness anatomical defect of the neural retina at the fovea that can lead to central vision loss. The standard treatment for MH is pars plana vitrectomy with internal limiting membrane (ILM) peeling and intravitreal gas tamponade, for which anatomic success rates of 85–100% have been reported (2–4). However, a sealed MH does not guarantee improvement in visual acuity despite the high surgical success rate, and studies have been conducted to identify the factors affecting the post-operative vision outcome of MH.

Optical coherence tomography (OCT) is a widely used non-invasive medical imaging technique that provides *in vivo* retinal images and is considered the current gold standard for MH diagnosis, staging, and monitoring (5–7). Recent developments in OCT have furthered the understanding of the healing process after MH closure and may provide insight into maximizing surgical success and predicting visual outcomes. Several OCT measurements including MH width, height, and volume, along with ellipsoid zone (EZ) alterations and external limiting membrane (ELM) features have been associated with successful MH closure and visual acuity improvement (8–13). However, limited data exist on the comprehensive evaluation of these OCT features after successful surgical repair, and it is not clear whether one single parameter or time point on OCT correlates best with visual outcome.

This study aimed to evaluate anatomical outcomes of MH surgery and their associations with visual function. We assessed OCT measurements of the EZ and ELM, including the newly developed EZ-related angle parameters of MH, in subjects with successfully closed idiopathic MH and identified factors affecting postoperative visual acuity outcomes.

## MATERIALS AND METHODS

### Patients

This was a retrospective study approved by the Institutional Review Board of Peking University Third Hospital and conducted in accordance with the tenets of the Declaration of Helsinki. Subjects who met the following criteria were included in this study: diagnosed with stage 2, 3, or 4 MH between January 2018 and July 2020 with follow-up surgery; postoperative follow-up duration longer than 6 months and at least 3 visits; best-corrected visual acuity (BCVA) and spectral-domain OCT (SD-OCT) measured at each postoperative visit. We excluded patients with other retinal diseases such as age-related macular degeneration, diabetic retinopathy, retinal detachment, and epiretinal membrane, as well as patients whose MH was not successfully closed via primary surgery. Patients with newly developed cataract postoperatively were also excluded. Demographic information was obtained from medical records, and axial length was measured using IOL Master Biometry (Carl Zeiss Meditec, Jena, Germany).

All patients underwent 25-gauge pars plana vitrectomy, 0.25% indocyanine green was used to facilitate ILM peeling, and sterilized air tamponade was applied. All patients were instructed

to maintain a prone position for at least 3 days. In cases with cataract, phacoemulsification was performed before vitrectomy. Slit lamp examinations were performed at every postoperative visit, and no obvious turbidity was found in the phakic eye. All patients provided written informed consent prior to surgery.

Patients were classified into two groups based on BCVA at the 6-month postoperative visit. Group A consisted of patients whose BCVA improved two lines or more on a standard logarithmic visual acuity chart, and those who improved less than 2 lines were included in group B. BCVA then was converted to logMAR units for statistical analysis, and  $\Delta$ BCVA was defined as preoperative BCVA minus 6-month postoperative BCVA.

### OCT

OCT images were captured using SD-OCT in Autorescan mode (Spectralis; Heidelberg Engineering, Heidelberg, Germany) before the surgery and at 1 week, 1 month, and 6 months after surgery. Due to the delay in air absorption, qualified images were obtained in only 32 eyes (22 in group A and 10 in group B) at the 1-week postoperative visit. Minimum linear diameter (MLD) (14), basal diameter (BD) (14), height (H) of MH (15), diameter of ELM disruption, diameter of EZ disruption (16), maximum distance between EZ and retinal pigment epithelium (RPE), macular ILM-RPE distance, ELM reflectivity, EZ reflectivity, and RPE reflectivity were measured using ImageJ software (1.47v, Wayne Rasband, National Institutes of Health, Bethesda, MD, USA, <http://imagej.nih.gov/ij>) on the horizontal orientation of the OCT image. MLD was defined as the minimal extent of the hole (14). BD was defined as the diameter of the hole at the level of the RPE (14). H was defined as the vertical distance from the midpoint of the nerve fiber layer on both edges to the RPE (15). Diameter of ELM disruption was defined as the distance between the two edges at the ELM, as was the diameter of EZ (16). Other indexes were calculated using the above parameters: diameter hole index (DHI)=MLD/BD, MH index (MHI)=H/BD, and traction hole index (THI) = H/MLD (17). The absolute reflectivity of ELM, EZ and RPE were obtained using the “plot profile” function of ImageJ (18). This function drew the reflectivity graph from a straight line through the center of the fovea. As the outermost highly reflective band was thought to represent the RPE, we regarded the highest value as the reflectivity of the RPE, the high reflectivity value adjacent to the RPE band was assumed to represent the EZ band, and high reflectivity value adjacent to the EZ band was assumed to represent the ELM band. If the EZ or ELM band was disrupted at the fovea, the reflectivity at the corresponding position was recorded. Relative reflectivity was calculated according to the following formula: Relative reflectivity (arbitrary unit) = (reflectivity of EZ or ELM)/(reflectivity of RPE)×100 (18).

Additionally, we developed new EZ-related structural parameters including EZ-MH angle, EZ-edge angle, EZ-nerve fiber layer (EZ-NFL) angle, EZ-ganglion cell layer (EZ-GCL) angle, EZ-internal nuclear layer (EZ-INL) angle, EZ-outer plexiform layer (EZ-OPL) angle, and EZ-outer nuclear layer (EZ-ONL) angle. The EZ-MH angle referred to the angle whose vertex was located at the center of the hole, and the endpoints of both sides were located at the anterior border of the EZ band edge.



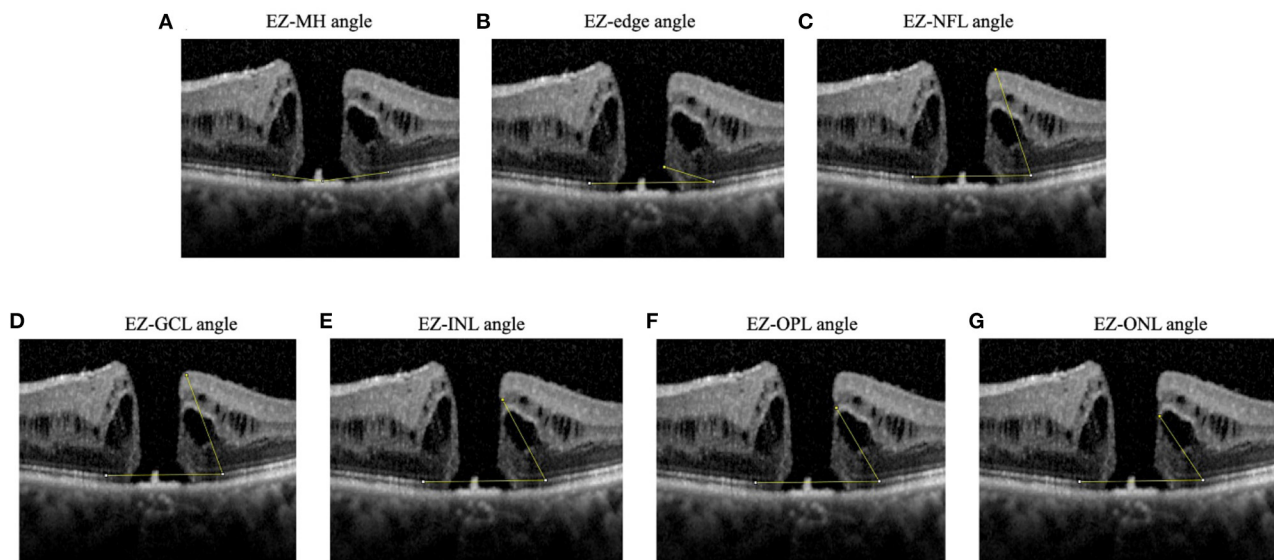


**FIGURE 1 |** Diagrams showing angles measured. **(A)** EZ-MH angle: the angle whose vertex located at the center of the hole and the endpoints of both sides were located at the anterior border of the EZ band edge, **(B)** EZ-edge angle: the angle between a line connecting the upper edge of the EZ band and a line through the most protruding point of either edge of the MH, **(C)** EZ-NFL angle, **(D)** EZ-GCL angle, **(E)** EZ-INL angle, **(F)** EZ-OPL angle, **(G)** EZ-ONL angle. The EZ-NFL, EZ-GCL, EZ-INL, EZ-OPL, and EZ-ONL angles were each between a line connecting the two upper edges of the EZ band, and a line through the upper edge of the respective band. If measurements were different between left and right hole edge, the smaller angle was recorded. EZ, ellipsoid zone; GCL, ganglion cell layer; INL, inner nuclear layer; NFL, nerve fiber layer; ONL, outer nuclear layer; OPL, outer plexiform layer.

The EZ-edge angle was between a line connecting the upper edge of the EZ band and a line through the most protruding point of either edge of the MH. The EZ-NFL, EZ-GCL, EZ-INL, EZ-OPL, and EZ-ONL angles were each between a line connecting the two upper edges of the EZ band, and a line through the upper edge of the respective band. We then take the average angle of two sides for analysis (**Figure 1**). All measurements were performed twice by the same clinician and the average of the two measurements were used for analysis.

## Statistical Analysis

All statistical analyses were performed using IBM SPSS for Mac version 26.0 (IBM Corp., Armonk, NY, USA). The repeatability was excellent for the measurement of structural parameters (intraclass correlation coefficient > 0.90 for all parameters). Parameters between the two groups before surgery and 1 week, 1 month, 6 months after surgery were compared using independent-sample *t*-tests if they showed homogeneity of variance on Levene's test, otherwise non-parametric analyses were used. Repeated-measures analysis of variance was used to compare BCVA, diameter of EZ/ELM disruption, and ELM/EZ relative reflectivity over time. Chi-square tests were used to compare whether the rate of closed ELM/EZ band in group A was higher than that in group B at the 1- and 6-month follow-up visits. Spearman's correlation analysis was used to test the correlation between each preoperative parameter and baseline BCVA,  $\Delta$ BCVA, and BCVA at 6 months.  $P < 0.05$  was considered statistically significant.

## RESULTS

### Demographics and Baseline Data

Initially, 46 eyes were included in this study, of which 1 eye with MH recrudescence at the 6-month postoperative visit was excluded. Therefore, 45 eyes (19 OD, 26 OS) of 43 patients (12 male, 31 female) with a mean ( $\pm$  standard deviation) age of  $64.33 \pm 7.60$  years were included in this study. Sixteen eyes were classified as stage 2 MH, nine eyes as stage 3, and twenty eyes as stage 4. The mean BCVA was  $0.98 \pm 0.33$  logMAR; the mean axial length was  $23.83 \pm 1.36$  mm; and the mean MLD, BD, and H were  $578.46 \pm 339.65$   $\mu$ m,  $1319.17 \pm 575.10$   $\mu$ m, and  $439.87 \pm 105.53$   $\mu$ m, respectively. The mean preoperative diameters of ELM and EZ disruption were  $2049.94 \pm 700.77$   $\mu$ m and  $2379.87 \pm 799.06$   $\mu$ m, respectively (**Table 1**).

On a standard logarithmic visual acuity chart, BCVA improved two lines or more in 30 eyes (group A) and less than 2 lines in 15 eyes (group B). Demographic parameters such as age, axial length, and proportion of patients at each MH stage showed no significant differences between groups ( $P = 0.902$ ,  $P = 0.729$ ). Baseline BCVA was also similar in the two groups ( $P = 0.096$ ). From the structural perspective, BD was significantly smaller in group A than group B ( $P = 0.031$ ). Distance parameters MLD ( $P = 0.276$ ), H ( $P = 0.277$ ), diameter of ELM and EZ disruption ( $P = 0.149$  and  $0.710$ , respectively), maximum distance between EZ and RPE ( $P = 0.444$ ), and fovea ILM-RPE distance ( $P = 0.621$ ) showed no significant difference between groups. Indexes calculated based on the above parameters were also similar between groups (DHI,  $P = 0.886$ ; THI,  $P = 0.148$ ; FC,  $P = 0.886$ ). All angle parameters were comparable in both groups (EZ-MH

**TABLE 1** | Demographic data<sup>a</sup>.

Item	Value
Number of eyes	45
Sex, M/F	12/31
Eye, OD/OS	19/26
Age, years	64.33 ± 7.60
Axial length, mm	23.83 ± 1.36
MH stage, n (%)	
2	16 (35.6%)
3	9 (20.0%)
4	20 (44.4%)
BCVA, Log MAR	0.98 ± 0.33
MLD, $\mu$ m	578.46 ± 339.65
BD, $\mu$ m	1319.17 ± 575.10
H, $\mu$ m	439.87 ± 105.53
Preoperative diameter of ELM disruption, $\mu$ m	2049.94 ± 700.77
Preoperative diameter of EZ disruption, $\mu$ m	2379.87 ± 799.06

<sup>a</sup>All values are mean ± standard deviation unless otherwise indicated. BCVA, best-corrected visual acuity; BD, basal diameter; H, height; ELM, external limiting membrane; EZ, ellipsoid zone; MLD, minimal linear diameter.

angle,  $P = 0.866$ ; EZ-end angle,  $P = 0.084$ ; EZ-NFL angle,  $P = 0.485$ ; EZ-GCL angle,  $P = 0.337$ ; EZ-INL angle,  $P = 0.146$ ; EZ-OPL angle,  $P = 0.177$ ; EZ-ONL angle,  $P = 0.219$ ) (Table 2).

## Functional and Anatomic Rehabilitation

BCVA changes over time were significantly different between groups ( $P < 0.001$ ). BCVA in both groups first declined at 1 week compared with baseline, then improved at 1 and 6 months postoperatively. BCVA in group A improved from  $0.93 \pm 0.32$  at baseline to  $0.45 \pm 0.24$  at 6 months and in group B from  $1.10 \pm 0.34$  to  $1.00 \pm 0.20$ , and BCVA differed between groups at 1 and 6 months postoperatively ( $P = 0.001$  and  $P < 0.001$  respectively) (Figure 2A).

The ELM and EZ disruption diameters reduced at each postoperative visit in both groups. Although the change over time, analyzed by repeated-measures analysis of variance, showed no significant difference between groups A and B ( $P = 0.961$  and  $P = 0.706$  respectively), Group A had less EZ disruption at 6 months postoperatively ( $P = 0.045$ ) (Figures 2B,C).

Reflectivity is reportedly an essential parameter when evaluating the recovery of ELM and EZ bands (18). Both the absolute (Supplementary Figure 1) and relative reflectivity of ELM and EZ bands (Figures 2D,E) increased over time in both groups, and both the absolute and relative reflectivity of the EZ band in group A was higher than that in group B at 1 month ( $P = 0.024$ ,  $P = 0.015$ ) and 6 months ( $P < 0.001$ ,  $P < 0.001$ ) postoperatively, and for the ELM band at 6 months ( $P = 0.012$ ,  $P = 0.015$ ).

Foveal ILM-RPE thickness showed no significant difference at any time between the two groups (Supplementary Table 1), while group A showed greater ELM and EZ thickness compared with group B at the 1-month ( $P = 0.009$ ,  $P = 0.001$ ) and 6-month ( $P = 0.001$ ,  $P < 0.001$ ) postoperative visits (Figures 2F,G).

**TABLE 2** | Preoperative parameter comparisons between groups A and B<sup>a</sup>.

	Group A	Group B	P value
Number	30	15	
Age, years	64.43 ± 7.99	64.13 ± 7.01	0.902
MH stage			
2	11	5	
3	5	4	0.729
4	14	6	
Axial length, mm	23.56 ± 1.23	24.38 ± 1.49	0.100
BCVA, Log MAR	0.93 ± 0.32	1.10 ± 0.34	0.096
MLD, $\mu$ m	535.02 ± 335.16	659.13 ± 345.35	0.276
BD, $\mu$ m	1181.49 ± 486.79	1584.69 ± 654.54	0.031*
H, $\mu$ m	424.68 ± 85.28	469.17 ± 135.34	0.277
Diameter of ELM disruption, $\mu$ m	1934.69 ± 712.57	2280.45 ± 641.05	0.149
Diameter of EZ disruption, $\mu$ m	2345.52 ± 870.04	2448.56 ± 661.24	0.710
Maximum distance between EZ and RPE, $\mu$ m	26.20 ± 8.60	28.89 ± 12.77	0.444
Fovea ILM-RPE distance, $\mu$ m	51.51 ± 13.81	49.00 ± 16.07	0.621
DHI	0.43 ± 0.18	0.42 ± 0.18	0.886
MHI	0.42 ± 0.20	0.33 ± 0.13	0.148
THI	1.09 ± 0.71	0.91 ± 0.49	0.413
Angle			
EZ-MH	168.63 ± 4.59	168.35 ± 5.30	0.866
EZ-end	38.51 ± 9.57	44.61 ± 11.45	0.084
EZ-NFL	68.34 ± 12.67	71.31 ± 12.75	0.485
EZ-GCL	65.43 ± 12.23	69.30 ± 11.63	0.337
EZ-INL	58.38 ± 13.83	64.49 ± 9.71	0.146
EZ-OPL	54.15 ± 14.07	60.04 ± 10.73	0.177
EZ-ONL	50.40 ± 14.47	55.95 ± 11.43	0.219

<sup>a</sup>All values are mean ± standard deviation unless otherwise indicated. BCVA, best-corrected visual acuity; BD, basal diameter; ELM, external limiting membrane; EZ, ellipsoid zone; GCL, ganglion cell layer; H, height; ILM, internal limiting membrane; INL, inner nuclear layer; MLD, minimal linear diameter; NFL, nerve fiber layer; ONL, outer nuclear layer; OPL, outer plexiform layer; RPE, retinal pigment epithelium. \* $P < 0.05$ .

Our results indicate that the thicknesses and reflectivity of EZ and ELM might better predict visual rehabilitation than integrity indicators.

## Factors Associated With Visual Rehabilitation

Due to unabsorbed intraocular gas in 13 eyes at the 1-week postoperative visit, a total of 32 OCT images were captured at this time point. In group A, ELM was restored in one (4.5%) eye at the 1-week postoperative visit, 12 (40%) eyes at 1 month, and 23 (76.7%) eyes at 6 months postoperatively. No eyes with continuous EZ bands were found in group A at 1-week; this band was intact in 9 (30%) eyes and 19 (63.3%) eyes at 1 and 6 months, respectively. In Group B, none of the eyes showed an intact ELM band at the 1-week postoperative visit, and the band was restored in 1 (6.7%) eye and 5 (33.3%) eyes at 1- and 6-months respectively. The EZ band was intact only in one (6.7%) eye at the 6-month postoperative visit (Table 3). At the 1-month visit,

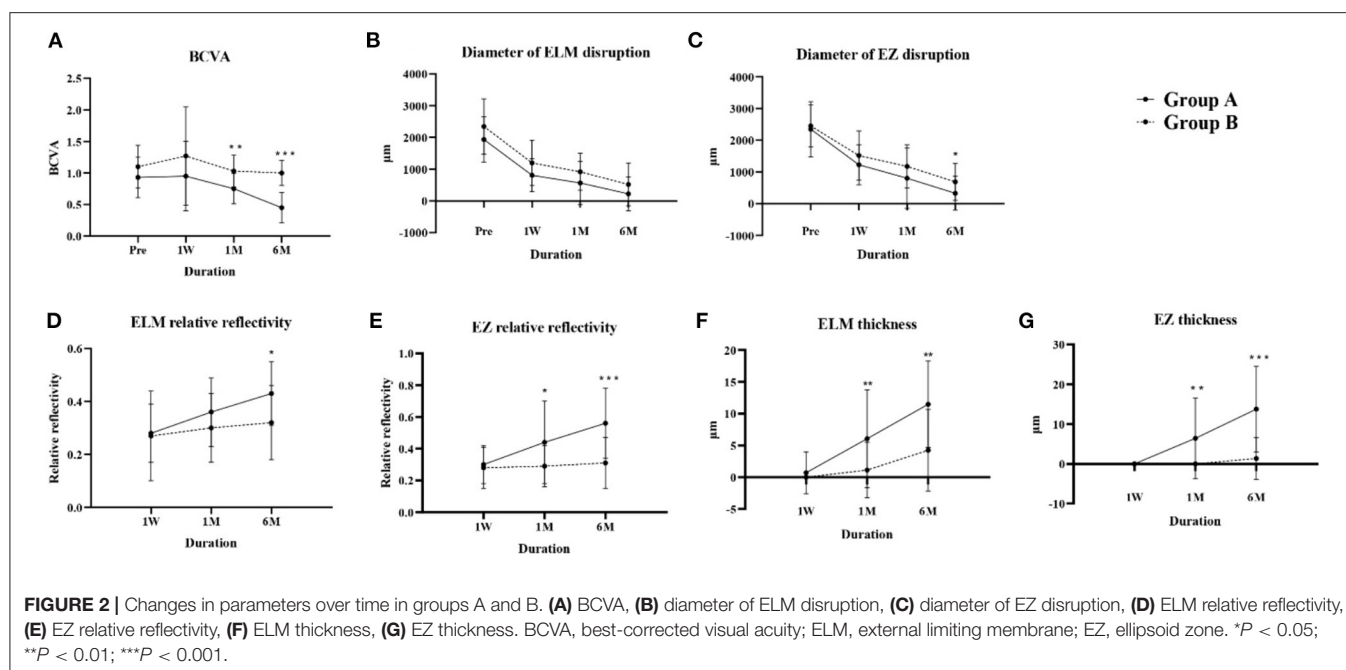


**TABLE 3 |** Cases of ELM/EZ restored in groups A and B over time.

		Group A (intact/disrupted)	Group B (intact/disrupted)	P value
ELM	Postoperative 1 Week	1/21	0/10	1.000
	Postoperative 1 Month	12/18	1/14	0.034*
	Postoperative 6 Months	23/7	5/10	0.008*
EZ	Postoperative 1 Week	0/22	0/10	-
	Postoperative 1 Month	9/21	0/15	0.020*
	Postoperative 6 Months	19/11	1/14	<0.001*

ELM, external limiting membrane; EZ, ellipsoid zone. \* $P < 0.05$ .

the ratio of intact ELM and EZ were both significantly higher than in group B ( $P = 0.034$  and  $P = 0.020$ , respectively) and remained significantly higher at 6 months ( $P = 0.008$  and  $P < 0.001$ , respectively).

In further exploration of the predictive value of baseline parameters for visual rehabilitation, correlation analysis showed a significant correlation between baseline BCVA and preoperative diameter of ELM disruption ( $r = 0.350$ ,  $P = 0.029$ ), MLD ( $r = 0.334$ ,  $P = 0.035$ ), DHI ( $r = 0.366$ ,  $P = 0.019$ ), MHI ( $r = -0.376$ ,  $P = 0.015$ ), and THI ( $r = -0.393$ ,  $P = 0.012$ ). BCVA at 6 months was significantly correlated with baseline BCVA ( $r = 0.615$ ,  $P < 0.001$ ), BD ( $r = 0.398$ ,  $P = 0.010$ ), MHI ( $r = -0.392$ ,  $P = 0.011$ ), preoperative diameter of ELM ( $r = 0.461$ ,  $P = 0.003$ ), and EZ disruption ( $r = 0.395$ ,  $P = 0.013$ ).  $\Delta$ BCVA was significantly correlated with axial length ( $r = -0.424$ ,  $P = 0.013$ ) and DHI ( $r = 0.435$ ,  $P = 0.004$ ) (Table 4). Our results showed that BCVA outcome was strongly correlated with baseline BCVA and that no EZ-related parameter was predictive of BCVA improvement.

## DISCUSSION

The role of EZ and ELM bands in the recovery of BCVA following MH repair has attracted much attention in recent years. Here we divided MH patients into two groups based on whether their BCVA improved at the 6-month postoperative visit and analyzed the pre- and postoperative parameters including the EZ and ELM bands to explore whether they could predict BCVA outcome. To our knowledge, this is the first study to explore differences of structural and functional parameters of EZ band between BCVA-improved patients and BCVA-unimproved patients. Our results showed that EZ and ELM recovery are strongly related to visual rehabilitation, suggesting that the EZ and ELM bands played important roles in visual recovery. Baseline BCVA correlated most strongly with BCVA outcome, and  $\Delta$ BCVA correlated only with DHI and axial length.

Currently, pars plana vitrectomy with ILM peeling is the standard treatment for MH, but successful MH closure does not suggest the recovery of BCVA, and some studies have found BCVA recovery to be closely related to EZ band status (13, 19). In the present study, the parameters used to evaluate the EZ band included integrity, thickness, angle and reflectivity. For integrity of EZ band, Ooka et al. reported that EZ disruption at 1, 3, and 6-months postoperatively were closely correlated with BCVA (20). de Sistiernes et al. showed that less EZ disruption indicated better BCVA outcome (21). Our study found that the ratio of closed EZ band in Group A was significantly higher than in Group B at 1- and 6-months postoperative visits, showing a positive correlation between EZ band recovery and BCVA, which is consistent with previous studies. In terms of thickness, Lee et al. found that BCVA was affected by inner retinal layer thickness, which was in turn significantly associated with EZ recovery (22). A study by Sevgi et al. showed that EZ-RPE thickness at 1-month follow-up in MH patients was significantly correlated with BCVA at

**TABLE 4 |** Spearman's correlation analysis between preoperative factors and baseline BCVA, 6-month postoperative BCVA and  $\Delta$ BCVA.

Item		Baseline BCVA	6M BCVA	$\Delta$ BCVA
Age	r	-0.228	-0.048	-0.143
	P	0.132	0.753	0.347
Baseline BCVA, Log MAR	r	-	0.615	0.250
	P	-	< 0.001*	0.097
Axial length	r	-0.227	0.098	-0.424
	P	0.197	0.580	0.013*
Preoperative diameter of ELM disruption	r	0.350	0.461	-0.198
	P	0.029*	0.003*	0.227
Preoperative diameter of EZ disruption	r	0.211	0.395	-0.246
	P	0.197	0.013*	0.132
Macular ILM-RPE distance	r	-0.068	-0.028	-0.063
	P	0.691	0.871	0.709
MLD	r	0.334	0.273	0.048
	P	0.035*	0.298	0.768
BD	r	0.273	0.398	-0.200
	P	0.084	0.010*	0.209
H	r	-0.111	0.078	-0.207
	P	0.489	0.629	0.194
DHI	r	0.366	-0.007	0.435
	P	0.019*	0.965	0.004*
MHI	r	-0.376	-0.392	0.105
	P	0.015*	0.011*	0.515
THI	r	-0.393	-0.205	-0.182
	P	0.012*	0.204	0.262

BCVA, best-corrected visual acuity; 6M BCVA, 6-month best corrected visual acuity; BD, basal diameter; ELM, external limiting membrane; EZ, ellipsoid zone; H, height; ILM, internal limiting membrane; MLD minimal linear diameter; RPE, retinal pigment epithelium.  $\Delta$ BCVA was defined as preoperative BCVA minus 6-month postoperative BCVA. \* $P < 0.05$ .

12 months postoperatively (23). We found that ELM and EZ in group A were significantly thicker than in group B at the 1- and 6-month postoperative visits, suggesting that recovery of ELM and EZ band thicknesses also indicate better BCVA outcome. As for angle, we initially hypothesized that the EZ-related angle reflected MH structural aspects and may be one of the predictive factors for BCVA recovery. However, although parameters including a range of EZ angles were larger in group B than in group A, the difference was not statistically significant. Chhablani et al. found no significant correlation between MH angle and final visual acuity (24), which correlated with our results. However, in some patients with high myopia, posterior scleral staphyloma may affect the measurement of these angles mentioned above. Of the 45 eyes involved in this study, only one eye had posterior scleral staphyloma, thus we did not separate this patient for analysis. In future research, it is necessary to explore the influence of the posterior pole scleral morphology on angle measurement. In terms of reflectivity, Tuan et al. found that the absolute and relative reflectivity of the EZ band gradually increased after MH

surgery and were significantly correlated with improvement in BCVA (18). To exclude the influence of the image itself, we used RPE reflectivity as a reference to obtain the relative reflectivity for analysis. Relative reflectivity of EZ band in group A was higher than in group B from 1 month postoperatively, and the ELM showed a similar difference at the 6-month visit. These results suggest that relative reflectivity is related to BCVA and could be a promising parameter to describe the EZ function.

The ELM is the outermost hyperreflective band on SD-OCT and is thought to be composed of Müller cell terminal processes and microvilli (25). From a pathological perspective, it was hypothesized that Müller cells provide primary structural support for the fovea, acting like a plug to bind together photoreceptor cells (26). Müller cell dysfunction would increase susceptibility to MH formation, so Müller cell recovery is thought to be essential for retinal structure repair and later for visual rehabilitation. From a clinical perspective, Padron-Perez et al. demonstrated that ELM recovery after treatment was positively correlated with visual acuity recovery (27). Consistent with this, our results showed that the ELM closure rate was higher in group A than group B at 1 and 6 months postoperatively.

The EZ band is adjacent and anterior to ELM, the second outer hyperreflective band on SD-OCT, and its anatomical correlation remains contentious (28). It was previously believed to represent the junction between the inner and outer segments (IS/OS junction) of the photoreceptors (29). Recent research suggests that it is anatomically related to (and named for) the ellipsoid portion of the photoreceptor inner segment, a cellular compartment containing numerous mitochondria (28). Since mitochondria are the most light-scattering organelles, this explanation for a hyper reflective band seems reasonable (30). As a result, the recovery of the EZ band after MH surgery is thought to represent the enrichment of mitochondria generating cellular energy in the photoreceptors (25), and therefore EZ recovery may indicate improved photoreceptor function. In our study, the relative reflectivity of EZ in group A was significantly higher than that of group B from the 1-month visit and after and was connected to BCVA improvement. Therefore, we speculate that reflectivity may be a promising indicator of mitochondria recovery, which then extending to the recovery of photoreceptor function. More studies are needed to confirm correlation between EZ reflectivity and functional recovery of photoreceptors, and the measurement of reflectivity needs to be standardized.

The ELM and EZ bands are closely connected. Bottoni et al. reported that the ELM was the first structure to recover after MH closure (9). Lee and colleagues demonstrated that ELM and EZ recovery occurred 1.5 and 6.1 months after full-thickness MH, respectively, and all subjects with intact EZ showed intact ELM, indicating that ELM may be a prerequisite for EZ recovery (22). In our study, the rate of EZ recovery was lower than that of the ELM, and patients with an intact EZ also had an intact ELM, supporting the hypothesis that their recoveries are closely connected. We speculate that Müller cell recovery may be helpful to enhance mitochondria numbers in photoreceptors. However, we only recorded structural changes in the first 6 months after surgery, and it is possible that once ELM integrity is restored, EZ recovery might be observed over long-term follow-up.



Although EZ recovery was found connected with visual rehabilitation in our study, no preoperative EZ-related parameter was significantly different between the two groups, and BD appeared to be more valuable for visual prognosis. A study by Sevgi et al. showed that baseline MH width and volume were negatively correlated with postoperative BCVA (23). Our research revealed that mean MLD, mean BD, and mean diameter of ELM and EZ disruption in group A were smaller than those in group B, but only BD was statistically significant. Spearman's correlation analysis showed that 6-month BCVA was mainly determined by the baseline BCVA, BD, MHI, and diameter of ELM/EZ disruption, among which baseline BCVA showed the strongest significance, indicating that patients with better baseline BCVA tend to have better BCVA outcomes.  $\Delta$ BCVA was significantly correlated with axial length and DHI at baseline. Lee et al. found that long axial length may impair EZ recovery, resulting in poorer functional visual outcomes (22), which is consistent with our finding of a negative correlation between axial length and  $\Delta$ BCVA. As no single EZ-related preoperative parameter differed significantly between groups A and B, a larger sample size and measurement of other OCT parameters related to the EZ band are needed in future research investigating the close relationship between the EZ band and photoreceptor function. The effects of different treatment strategies on the EZ band also need to be clarified.

Our study had several limitations. First, the number of eyes included was not large, and the 6-month follow-up time was relatively short. Second, our data were collected in clinical practice, so there was a lack of uniform protocols to ensure consistency for patients at different clinical visits. Third, we only evaluated BCVA to assess visual function, and adding more parameters such as visual field tests would make the results more comprehensive. Last, we only measured the horizontal direction of OCT image, and future study should focus on all directions of OCT images to comprehensively analyze the structural parameters.

In conclusion, this study demonstrated significant correlations between EZ band integrity, thickness, and reflectivity

and postoperative BCVA outcome. Patients with smaller diameter of EZ disruption and higher EZ band reflectivity tend to have better BCVA. Moreover, given that the EZ band reflects mitochondria recovery in photoreceptors, related parameters could be useful for evaluation of photoreceptor function after MH treatment.

## DATA AVAILABILITY STATEMENT

The raw data supporting the conclusions of this article will be made available by the authors, without undue reservation.

## ETHICS STATEMENT

The studies involving human participants were reviewed and approved by Institutional Review Board of Peking University Third Hospital. Written informed consent for participation was not required for this study in accordance with the national legislation and the institutional requirements.

## AUTHOR CONTRIBUTIONS

XL and CW supervised the project. JY, HX, and YL developed the original idea and wrote the manuscript. HX and YL conducted the statistical analysis. XW, HY, QH, YG, YD, and YW collected the data. All authors contributed to the article and approved the submitted version.

## FUNDING

This study was supported by Natural Science Foundation of Beijing, China (Grant Number: 7202229).

## SUPPLEMENTARY MATERIAL

The Supplementary Material for this article can be found online at: <https://www.frontiersin.org/articles/10.3389/fmed.2021.779602/full#supplementary-material>

## REFERENCES

- Johnson R. Idiopathic macular holes: observations, stage of formation, and implications for surgical intervention. *Ophthalmology*. (1988) 95:917–24. doi: 10.1016/S0161-6420(88)33075-7
- Krishnan R, Tossounis C, Yang YF. 20-gauge and 23-gauge phacovitrectomy for idiopathic macular holes: comparison of complications and long-term outcomes. *Eye*. (2013) 27:72–7. doi: 10.1038/eye.2012.227
- Passemar M, Yakoubi Y, Muselier A, Hubert I, Guillaubey A, Bron AM, et al. Long-term outcome of idiopathic macular hole surgery. *Am J Ophthalmol*. (2010) 149:120–6. doi: 10.1016/j.ajo.2009.08.003
- Ch'ng SW, Patton N, Ahmed M, Ivanova T, Baumann C, Charles S, et al. The manchester large macular hole study: is it time to reclassify large macular holes? *Am J Ophthalmol*. (2018) 195:36–42. doi: 10.1016/j.ajo.2018.07.027
- Xu D, Yuan A, Kaiser PK, Srivastava SK, Singh RP, Sears JE, et al. A novel segmentation algorithm for volumetric analysis of macular hole boundaries identified with optical coherence tomography. *Invest Ophthalmol Vis Sci*. (2013) 54:163–9. doi: 10.1167/iovs.12-10246
- Huang D, Swanson EA, Lin CP, Schuman JS, Stinson WG, Chang W, et al. Optical coherence tomography. *Science*. (1991) 254:1178–81. doi: 10.1126/science.1957169
- Hee MR, Puliafito CA, Wong C, Duker JS, Reichel E, Schuman JS, et al. Optical coherence tomography of macular holes. *Ophthalmology*. (1995) 102:748–56. doi: 10.1016/S0161-6420(95)30959-1
- Wakely L, Rahman R, Stephenson J, A. a comparison of several methods of macular hole measurement using optical coherence tomography, and their value in predicting anatomical and visual outcomes. *Br J Ophthalmol*. (2012) 96:1003–7. doi: 10.1136/bjophthalmol-2011-301287
- Bottoni F, Angelis SD, Luc Ca Relli S, Cigada M, Staurenghi G. The dynamic healing process of idiopathic macular holes after surgical repair: a spectral-domain optical coherence tomography study. *Invest Ophthalmol Vis Sci*. (2011) 52:4439–46. doi: 10.1167/iovs.10-6732
- Wakabayashi T, Fujiwara M, Sakaguchi H, Kusaka S, Oshima Y. Foveal microstructure and visual acuity in surgically closed macular holes: spectral-domain optical coherence tomographic analysis. *Ophthalmology*. (2010) 117:1815–24. doi: 10.1016/j.ophtha.2010.01.017

11. Goldberg RA, Waheed NK, Duker JS. Optical coherence tomography in the preoperative and postoperative management of macular hole and epiretinal membrane. *Br J Ophthalmol*. (2014) 98:ii20–3. doi: 10.1136/bjophthalmol-2013-304447
12. Ehlers JP, Uchida A, Srivastava SK, Hu M. Predictive model for macular hole closure speed: insights from intraoperative optical coherence tomography. *Transl Vis Sci Technol*. (2019) 8:18. doi: 10.1167/tvst.8.1.18
13. Sano M, Shimoda Y, Hashimoto H, Kishi S. Restored photoreceptor outer segment and visual recovery after macular hole closure. *Am J Ophthalmol*. (2009) 147:313–8. doi: 10.1016/j.ajo.2008.08.002
14. Ullrich S, Haritoglou C, Gass C, Schaumberger M, Ulbig MW, Kampik A. Macular hole size as a prognostic factor in macular hole surgery. *Br J Ophthalmol*. (2002) 86:390–3. doi: 10.1136/bjo.86.4.390
15. Yu Y, Liang X, Wang Z, Wang J, Liu W. Clinical and morphological comparisons of idiopathic macular holes between stage 3 and stage 4. *Graefes Arch Clin Exp Ophthalmol*. (2018) 256:2327–33. doi: 10.1007/s00417-018-4158-7
16. Hasebe H, Matsuoka N, Terashima H, Sasaki R, Ueda E, Fukuchi T. Restoration of the ellipsoid zone and visual prognosis at 1 year after surgical macular hole closure. *J Ophthalmol*. (2016) 2016:1769794. doi: 10.1155/2016/1769794
17. Alkabes M, Padilla L. Assessment of OCT measurements as prognostic factors in myopic macular hole surgery without foveoschisis. *Graefes Arch Clin Exp Ophthalmol*. (2013) 251:2521–7. doi: 10.1007/s00417-013-2347-y
18. Tuan BY, Karaba L, Yenihayat F, Suba S, Zkan B. Correlation of visual recovery and increased ellipsoid zone reflectivity after successful macular hole surgery. *Turk Oftalmoloji Gazetesi*. (2020) 50:283–7. doi: 10.4274/tjo.galenos.2020.21456
19. Baba T, Yamamoto S, Arai M, Arai E, Sugawara T, Mitamura Y, et al. Correlation of visual recovery and presence of photoreceptor inner/outer segment junction in optical coherence images after successful macular hole repair. *Retina*. (2008) 28:453–8. doi: 10.1097/IAE.0b013e3181571398
20. Ooka E, Mitamura Y, Baba T, Kitahashi M, Oshitari T, Yamamoto S. Foveal microstructure on spectral-domain optical coherence tomographic images and visual function after macular hole surgery. *Am J Ophthalmol*. (2011) 152:283–90. doi: 10.1016/j.ajo.2011.02.001
21. de Sistiernes L, Hu J, Rubin DL, Leng T. Visual prognosis of eyes recovering from macular hole surgery through automated quantitative analysis of spectral-domain optical coherence tomography (SD-OCT) scans. *Invest Ophthalmol Vis Sci*. (2015) 56:4631–43. doi: 10.1167/iovs.14-16344
22. Lee MW, Kim TY, Song YY, Baek SK, Lee YH. Changes in each retinal layer and ellipsoid zone recovery after full-thickness macular hole surgery. *Sci Rep*. (2021) 11:11351. doi: 10.1038/s41598-021-90955-4
23. Sevgi DD, Yee PS, Srivastava SK, Le TK, Abraham JR, Reese J, et al. Longitudinal ellipsoid zone dynamics following macular hole repair in the discover study: structure-function assessment. *Retina*. (2020) 41:915–20. doi: 10.1097/IAE.0000000000002983
24. Chhablani J, Khodani M, Hussein A, Bondalapati S, Rao HB, Narayanan R, et al. Role of macular hole angle in macular hole closure. *Br J Ophthalmol*. (2015) 99:1634–8. doi: 10.1136/bjophthalmol-2015-307014
25. Cuenca N, Ortuño-Lizarán I, Sánchez-Sáez X, Kutsyr O, Albertos-Arranz H, Fernández-Sánchez L, et al. Interpretation of OCT and OCTA images from a histological approach: clinical and experimental implications. *Prog Retin Eye Res*. (2020) 77:100828. doi: 10.1016/j.preteyeres.2019.100828
26. Gass JDM. Müller cell cone, an overlooked part of the anatomy of the fovea centralis: hypotheses concerning its role in the pathogenesis of macular hole and foveomacular retinoschisis. *Arch Ophthalmol*. (1999) 117:821–3. doi: 10.1001/archophth.117.6.821
27. Padrón-Pérez N, Català-Mora J, Díaz J, Arias L, Prat J, Caminal JM. Swept-source and optical coherence tomography angiography in patients with X-linked retinoschisis. *Eye*. (2018) 32:707–15. doi: 10.1038/eye.2017.281
28. Staurengi G, Sadda S, Chakravarthy U, Spaide RF. Proposed lexicon for anatomic landmarks in normal posterior segment spectral-domain optical coherence tomography: the IN•OCT consensus. *Ophthalmology*. (2014) 121:1572–8. doi: 10.1016/j.ophtha.2014.02.023
29. Fernández EJ, Hermann B, Povazay B, Unterhuber A, Sattmann H, Hofer B, et al. Ultrahigh resolution optical coherence tomography and pancorrection for cellular imaging of the living human retina. *Opt Express*. (2008) 16:11083–94. doi: 10.1364/OE.16.011083
30. Wilson JD, Cottrell WJ, Foster TH. Index-of-refraction-dependent subcellular light scattering observed with organelle-specific dyes. *J Biomed Opt*. (2007) 12:014010. doi: 10.1117/1.2437765

**Conflict of Interest:** The authors declare that the research was conducted in the absence of any commercial or financial relationships that could be construed as a potential conflict of interest.

**Publisher's Note:** All claims expressed in this article are solely those of the authors and do not necessarily represent those of their affiliated organizations, or those of the publisher, the editors and the reviewers. Any product that may be evaluated in this article, or claim that may be made by its manufacturer, is not guaranteed or endorsed by the publisher.

Copyright © 2021 Yang, Xia, Liu, Wang, Yuan, Hou, Ge, Ding, Wang, Wang and Li. This is an open-access article distributed under the terms of the Creative Commons Attribution License (CC BY). The use, distribution or reproduction in other forums is permitted, provided the original author(s) and the copyright owner(s) are credited and that the original publication in this journal is cited, in accordance with accepted academic practice. No use, distribution or reproduction is permitted which does not comply with these terms.



# Factors for Visual Acuity Improvement After Anti-VEGF Treatment of Wet Age-Related Macular Degeneration in China: 12 Months Follow up

Yan Lu<sup>1</sup>, Wenzhi Huang<sup>2</sup>, Yuehong Zhang<sup>2</sup>, Xiongfei Huang<sup>2</sup>, Xu Zhang<sup>2</sup>, Haizhi Ma<sup>1</sup>, Guoliang Ren<sup>2</sup>, Feng Shi<sup>2</sup>, Lihui Kuang<sup>2</sup>, Shigang Yan<sup>1</sup>, Shuke Luo<sup>1</sup>, Junyan Zhang<sup>3</sup>, Jingfang He<sup>4</sup>, Weizhong Yang<sup>2</sup>, Zongyin Gao<sup>2</sup> and Yunxia Leng<sup>2\*</sup>

## OPEN ACCESS

### Edited by:

Shaochong Zhang,  
Sun Yat-sen University, China

### Reviewed by:

Jiaying Zhang,  
Guizhou Provincial People's  
Hospital, China  
Hua Zhong,  
Kunming Medical University, China  
Mingkai Lin,  
Sun Yat-sen University, China  
Yangfan Yang,  
Sun Yat-sen University, China

### \*Correspondence:

Yunxia Leng  
eylengyx@scut.edu.cn

### Specialty section:

This article was submitted to  
Ophthalmology,  
a section of the journal  
Frontiers in Medicine

Received: 02 July 2021

Accepted: 05 October 2021

Published: 11 November 2021

### Citation:

Lu Y, Huang W, Zhang Y, Huang X,  
Zhang X, Ma H, Ren G, Shi F,  
Kuang L, Yan S, Luo S, Zhang J, He J,  
Yang W, Gao Z and Leng Y (2021)  
Factors for Visual Acuity Improvement  
After Anti-VEGF Treatment of Wet  
Age-Related Macular Degeneration in  
China: 12 Months Follow up.  
Front. Med. 8:735318.  
doi: 10.3389/fmed.2021.735318

<sup>1</sup> Department of Ophthalmology, Foshan Second People's Hospital, Foshan, China, <sup>2</sup> Department of Ophthalmology, Guangzhou First People's Hospital, South China University of Technology, Guangzhou, China, <sup>3</sup> Bothwin Clinical Study Consultant, Redmond, WA, United States, <sup>4</sup> Bothwin Clinical Study Consultant, Shanghai, China

**Purpose:** To evaluate the treatment solutions and effectiveness of intravitreal ranibizumab (RBZ) or conbercept in patients with wet age-related macular degeneration (wAMD) in a real-life setting in China.

**Methods:** The medical records of 368 patients with wAMD who started RBZ or conbercept treatment between 1 May 2014 and 30 April 2018 were evaluated. All patients were defined on fundus angiography at baseline to determine the subtype of AMD (PCV or CNV). We report visual acuity (VA) and central retinal thickness (CRT) measurements at baseline and 12 months.

**Results:** The average number of anti-VEGF injections was  $2.1 \pm 1.2$ . The BCVA improvement of these two groups was similar with a difference of 1.00 letter (95% CI:  $-1.4 \sim 3.4$ ,  $p = 0.8505$ ). At the end of the study, a BCVA increase of at least 5 letters was determined to be a satisfactory efficacy endpoint. Several factors were related to the possible improvement in the satisfactory efficacy endpoint, including female sex (OR 2.07, 95% CI 1.22~3.51), number of injections (OR 1.40, 95% CI 1.12~1.75) and VA change at the first month (OR 13.75, 95% CI 7.41~25.51). Additionally, some factors were related to the possible reduction in the satisfactory efficacy endpoint, including diabetes (OR 0.27, 95% CI 0.10~0.73) and disease history (OR 0.75, 95% CI 0.57~0.98).

**Conclusion:** Our study demonstrates that anti-VEGF drugs can effectively improve BCVA and reduce CRT in AMD patients. Sex, number of injections, VA change at the first month, diabetes and disease history are the most important factors affecting visual acuity.

**Keywords:** age-related macular degeneration, ranibizumab, conbercept, polypoidal choroidal vasculopathy (PCV), choroidal neovascularization (CNV)

## INTRODUCTION

Age-related macular degeneration (AMD) is a chronic degenerative disease that occurs in the macular area of the retina. The number of moderate-to-severe visual impairments caused by AMD is more than 8 million globally, and it is one of the main causes of irreversible visual impairment in people over 55 years old in developed countries (1, 2). The prevalence of AMD is increasing in China due to the accelerated aging of the population (3–5). The early stages of AMD are hidden, and progression is slow. If the lesion progresses to the macular area, the patient's vision will be severely reduced. This will acutely affect the patient's quality of life (6). The main pathological change in exudative AMD is the formation of choroidal neovascularization (CNV) in the macular region (1, 3, 7). Many studies have shown that overexpression of vascular endothelial growth factor (VEGF) plays a decisive role in its pathogenesis (8–11).

The last decade has seen the introduction of intravitreal anti-VEGF agents, which have revolutionized the treatment of wAMD, offering patients previously unachievable improvements in vision. Bevacizumab (avasim) was approved for use in the treatment of AMD in 2005 (12, 13), RBZ (lucentis) was approved in 2006 (14, 15), and conbercept was approved in 2013 (16, 17). RBZ (Lucentis) is a humanized monoclonal antibody fragment (18, 19). Conbercept, also known as KH902 (Chengdu Kanghong Biotech Co., Ltd, Sichuan, China), is a recombinant fusion protein designed as a decoy receptor and is composed of the VEGF-binding domains of VEGFR-1 and VEGFR-2 with the Fc portion of human IgG1 (16, 17).

Recently, a large number of real-world studies in developed countries in Europe and the Americas have shown that anti-VEGF requires regular and continuous administration for AMD to achieve better vision improvement (20). AMD treatment guidelines in many countries recommend 3 injections plus the Pro Re Nata (3+PRN) regimen to achieve better results.

However, the 3+PRN treatment regimen deviates significantly from real-world clinical use data, and the economic status of patients in China largely determines the number of injections. The deviation of treatment plans also led to a large difference in the efficacy of anti-VEGF treatments for AMD reported in China and other countries (21, 22).

Therefore, we designed this retrospective study to assess the usage and efficacy of intravitreal anti-VEGF (including RBZ and conbercept) in patients with untreated wAMD in real-world practice conditions in China.

## METHODS

### Ethical Approval

The medical ethics committee of Second Affiliated Hospital of South China University of Technology and Foshan Second People's Hospital approved this study. The accession number was K-2018-123-02.

## Research Subjects

Patients diagnosed with wAMD who were treated in the Department of Ophthalmology at Second Affiliated Hospital of South China University of Technology or Foshan Second People's Hospital from 1 May 2014 to 30 April 2018 were recruited. These patients were diagnosed with wAMD by ophthalmologists according to fundus fluorescein angiography (FFA), indocyanine green angiography (ICGA) and optical coherence tomography (OCT) examination, including polypoidal choroidal vasculopathy (PCV) and CNV.

**Study Design:** All patients were continuously followed up at the Second Affiliated Hospital of South China University of Technology and at Foshan Second People's Hospital. They were treated at least once with intravitreal injections of anti-VEGF (RBZ or conbercept). During the follow-up process, it is recommended that patients visit the doctor every 4–8 weeks for at least 1 year. Patients were required to undergo best-corrected visual acuity (BCVA) assessment, slit-lamp examination, indirect ophthalmoscopy, fundus photography, and optical coherence tomography (OCT) each time. The standards and recommendations for retreatment also depend on the results of these examinations.

## The Inclusion Criteria

- Diagnosis of wAMD with completed follow up data.
- Age above 18 years.
- At least one treatment with anti-VEGF intraocular injection.
- Follow-up for at least 1 year after the first injection.

## The Exclusion Criteria

- Major ocular surgical procedures 3 months before the first injection.
- Myopia > -6.00 D.
- Ocular axial length > 26 mm.
- Concurrent retinal vascular disorders in the studied eyes.
- All patients who underwent ocular surgery performed during the follow-up period, including cataract, glaucoma, vitreoretinal, macular laser grid photocoagulation, or YAG (neodymium-doped yttrium aluminum garnet) capsulotomy.

## Examinations

For all patients, the examinations included the BCVA based on the Snellen chart. The Snellen fraction was converted into an approximate Early Treatment Diabetic Retinopathy Study (ETDRS) equivalent letter score (23). Before anti-VEGF intravitreal injection, all patients had to be diagnosed with CNV or PCV by the results of FFA or ICGA (Heidelberg, Germany). A Cirrus HD-OCT 5000 (Zeiss, Germany) was used for OCT. The central retinal thickness (CRT) was measured before the first anti-VEGF injection and after the initial injection at 1, 2, 3, 6, and 12 months.

## Treatment Regimens

Before the initial anti-VEGF injection, patients were advised to take the continuous regimen of 3+PRN. Additional reinjections were given if any of the following changes were observed by the evaluating physician: (1) visual acuity loss of at least five letters



and (2) an increase in OCT central retinal thickness of at least 100  $\mu\text{m}$ . However, additional injections and treatment regimens were dependent on many factors, such as the patient's visual acuity improvement and economic status.

## Data Collection

The following data were collected retrospectively: the number of injections, intraocular pressure, BCVA, CRT, subtype of AMD, lesion diameter, duration, hypertension, diabetes, and demographic data. Each patient had baseline characteristics and data from the 12 months of follow-up. BCVA was recorded using the Snellen visual acuity chart, and the Snellen readings were converted into ETDRS letters for statistical analysis, according to Amoaku et al. (24).

## Statistical Analysis

Stata SE 13 (serial number 401306302851) was used for the statistical analysis. Continuous variables with normal distributions are presented as means and standard deviations. Continuous variables with abnormal distributions are continuous variables which were, respectively, presented as medians and interquartile ranges (IQRs). Baseline normal and abnormal quantitative data were respectively analyzed using student *T*-test and Wilcoxon rank-sum test. Categorical variables at baseline were analyzed using the chi-square test. For the outcomes analysis, multivariate logistic regression analysis was performed to identify the associations between dependent and independent variables. The results are expressed as adjusted odds ratios (ORs) with 95% confidence intervals (95% CIs). Significance was accepted as two-sided test with an alpha level of 0.05. Restricted cubic spline(RCS) analyses were performed by using EmpowerStats software (www.empowerstats.com, X&Y solutions, Inc. Boston MA).

Two-sided 95% confidence intervals was used to calculate sample size together with 95% power. Assuming 40% of patients with diabetics can improve their BCVA to 5 letters while OR was 4 for those without diabetics based on our clinical experiences. Since there were more patients without diabetes than those with, we used a 10:1 ratio to put their data into this study.

## RESULTS

### Patient Characteristics

According to our inclusion criteria, 368 untreated wAMD (PCV/CNV) patients (368 eyes) were included. Among them, 223 were males, and 145 were females. All patients received intravitreal injections of RBZ or Conbercept at least once from May 2014 to November 2018. Each of these patients was followed up for at least 12 months. The mean age was  $68.9 \pm 9.5$  years. A total of 781 anti-VEGF injections were used (605 RBZ and 176 conbercept). **Table 1** shows the baseline characteristics and clinical data of all patients. The average number of intraocular anti-VEGF injections was  $2.1 \pm 1.2$  (showed in **Table 2**).

### BCVA Changes Compared With Baseline Values (ETDRS Letters)

In this study, BCVA was  $31.3 \pm 13.3$  letters at baseline with a median of 25. **Table 2** shows that the mean changes in the BCVA letters at the 1st, 2nd, 3rd, 6th, and 12th months after the initial anti-VEGF injection were  $5.09 \pm 10.09$ ,  $6.33 \pm 10.16$ ,  $8.77 \pm 11.5$ ,  $9.18 \pm 11.41$ , and  $8.23 \pm 10.80$ , respectively (**Table 3**, **Figures 1A,B**).

### CRT Changes Compare With Baseline Values ( $\mu\text{m}$ )

CRT was  $440.6 \pm 228.6 \mu\text{m}$  at baseline with a median of 372. **Table 2** also shows that the mean changes in CRT at the 1st, 2nd, 3rd, 6th, and 12th months after the initial anti-VEGF injection were  $-93.9 \pm 148.1$ ,  $-142.8 \pm 187.1$ ,  $-151.8 \pm 200.9$ ,  $-163.6 \pm 203.0$ , and  $-154.18 \pm 236.3$ , respectively (**Table 4**, **Figures 1C,D**).

### Comparative Analysis of the RBZ Group With Conbercept Group

Two anti-VEGF drugs, RBZ and conbercept, were used in this analysis. Two hundred eighty patients were treated with RBZ, while the other 88 patients were treated with conbercept. There were no differences between these two groups at baseline in terms of epidemiological data and disease characteristics (**Table 1**). However, the average injection numbers of the two drugs were different (**Table 2**). The average number of injections for RBZ was  $2.2 \pm 1.2$  and that for Conbercept was  $1.8 \pm 1.2$  ( $p = 0.001$ ). The difference between the two groups was 0.41 (SE 0.15, 95% CI 0.12~0.70).

Analysis of the BCVA improvement with the two treatment regimens (**Table 3**) showed that in the first month after the initial injection, the RBZ group increased by  $5.3 \pm 10.5$  (median 1) letters, while the conbercept group increased by  $4.3 \pm 8.7$  (median 1.5) letters. The BCVA improvement of these two groups was similar with a difference of 1.00 letter (95% CI:  $-1.4 \sim 3.4$ ,  $p = 0.8505$ ). At the 12th month after the initial injection, the RBZ group increased by  $8.7 \pm 11.0$  (median 5) letters, and the conbercept group increased by  $6.9 \pm 10.0$  (median 4) letters. The BCVA improvement of these two groups was similar with a difference of 1.8 (95% CI  $-0.8 \sim 4.4$ ,  $p = 0.1561$ ). A comparative analysis of CRT changes showed that during the first month after the initial injection, the CRT change in the RBZ group was  $-99.7 \pm 150.7$  (median  $-61$ ) mm and that in the conbercept group was  $-75.8 \pm 138.9$  (median  $-56.5$ ) mm. The CRT change value of the RBZ group at the 12th month after the initial injection was  $-164.7 \pm 215.4$  (median  $-116$ ) mm, while it was  $-120.8 \pm 292.0$  (median  $-102$ ) mm in the conbercept group. There was no significant difference between the two groups; the difference was  $43.9 \mu\text{m}$  (95% CI:  $-12.7 \sim 100.6$ ).

### Comparative Analysis of PCV and CNV

This study included two subtypes of wAMD. One hundred thirty-five (36.68%) of all patients were diagnosed with PCV, and the other 233 (63.32%) were diagnosed with CNV. There was no

**TABLE 1 |** Baseline characteristics of all patients.

	ALL	CNV	PCV	P	Conbercept	RBZ	P
Patients (eyes)	368	233	135		88	280	
<b>Age (years)</b>							
mean $\pm$ SD	68.9 $\pm$ 9.5	69.5 $\pm$ 9.9	67.8 $\pm$ 8.9	0.098*	68.6 $\pm$ 8.9	69.0 $\pm$ 9.7	0.725*
median (IQR)	69 (61.5~76)	69 (62~77)	67 (61~75)		69 (62~75.5)	69 (61~76.5)	
min~max	40~95	40~95	48~90		50~90	40~95	
Female sex n (%)	145 (39.4%)	93 (39.9%)	52 (38.5%)	0.792 <sup>#</sup>	31 (35.2%)	114 (40.7%)	0.358 <sup>#</sup>
CNV/PCV	233/135	—	—		46/42	187/93	0.014 <sup>#</sup>
Diabetes n (%)	33 (9.0%)	25 (10.7%)	8 (5.9%)	0.120 <sup>#</sup>	8 (9.1%)	25 (8.9%)	0.963 <sup>#</sup>
Hypertension n (%)	119 (32.3%)	74 (31.8%)	45 (33.3%)	0.756 <sup>#</sup>	26 (30.0%)	93 (33.2%)	0.521 <sup>#</sup>
Smoking n (%)	11 (3.0%)	4 (1.7%)	7 (5.2%)	0.060 <sup>#</sup>	2 (2.3%)	9 (3.2%)	0.651 <sup>#</sup>
<b>Disease history (month)</b>							
mean $\pm$ SD	10.2 $\pm$ 18.5	9.8 $\pm$ 17.9	11.0 $\pm$ 19.6	0.849 <sup>^</sup>	10.2 $\pm$ 19.7	10.2 $\pm$ 18.2	0.702 <sup>^</sup>
median (IQR)	3 (1~12)	3 (1~11)	3 (1~12)		3 (1~11.5)	3 (1~12)	
min~max	0.1~123	0.1~123	0.1~120		0.1~120	0.1~123	
<b>Diameter of lesion (<math>\mu</math>m)</b>							
mean $\pm$ SD	2495.5 $\pm$ 1559.5	2389.9 $\pm$ 1529.9	2677.8 $\pm$ 1598.6	0.067 <sup>^</sup>	2378.3 $\pm$ 1447.2	2532.3 $\pm$ 1593.8	0.452 <sup>^</sup>
median (IQR)	2,204 (1429.5~3266.5)	2,109 (1,428~3,043)	2,423 (1,434~3,712)		2,067 (1,417~3120.5)	2,264 (1434.5~3,338)	
min~max	92~12,700	107~12,700	92~7,597		92~6,549	107~12,700	
<b>BCVA (ETDRS letters)</b>							
mean $\pm$ SD	31.3 $\pm$ 13.3	31.6 $\pm$ 13.7	30.8 $\pm$ 12.7	0.905 <sup>^</sup>	31.6 $\pm$ 13.4	31.2 $\pm$ 13.3	0.906 <sup>^</sup>
median (IQR)	25 (23~40)	25 (22~40)	25 (23~40)		25 (22.5~40)	25 (23~40)	
min~max	20~75	20~75	20~75		20~70	20~75	
<b>CRT (mm)</b>							
mean $\pm$ SD	440.6 $\pm$ 228.6	420.7 $\pm$ 214.4	475.1 $\pm$ 248.4	0.008 <sup>^</sup>	448.6 $\pm$ 236.5	438.1 $\pm$ 226.5	0.869 <sup>^</sup>
median (IQR)	372 (277~541)	353 (269~522)	416 (321~590)		372 (275~566)	372.5 (285.5~535)	
min~max	100~1,632	100~1,221	123~1,632		143~1,238	100~1,632	
PDT n (%)	46 (12.5%)	13 (5.6%)	33 (24.4%)	<0.0001 <sup>#</sup>	5 (5.7%)	41 (14.6%)	0.027 <sup>#</sup>

\*Student t-test; <sup>^</sup>Mann-Whitney U-test; <sup>#</sup>chi-square.**TABLE 2 |** Number of injections of all patients.

	ALL	CNV	PCV	P	Conbercept	RBZ	P
<b>Number of injection</b>							
mean $\pm$ SD	2.1 $\pm$ 1.2	2.2 $\pm$ 1.2	2.0 $\pm$ 1.2	0.052 <sup>^</sup>	1.8 $\pm$ 1.2	2.2 $\pm$ 1.2	0.001 <sup>^</sup>
median (IQR)	2 (1~3)	2 (1~3)	2 (1~3)		1 (1~2)	2 (1~3)	
min~max	1~8	1~8	1~8		1~7	1~8	
anti-VEGF injections Conbercept/RBZ	176/605	95/419	64/203	0.071 <sup>#</sup>	—	—	—
Patient number in treatment group Conbercept/RBZ	88/280	46/187	42/93	0.014 <sup>#</sup>	—	—	—
PDT n (%)	46 (12.5%)	13 (5.6%)	33 (24.4%)	<0.0001 <sup>#</sup>	5 (5.7%)	41 (14.6%)	0.027 <sup>#</sup>

<sup>^</sup>Mann-Whitney U-test; <sup>#</sup>chi-square.

significant difference in epidemiological data between the two groups. The average injection number of patients with PCV was  $2.0 \pm 1.2$ , and the average injection number for those with CNV was  $2.2 \pm 1.2$ , as shown in **Table 2**.

A comparative analysis of the BCVA improvement of the two subtype groups at the 1st month after the initial injection showed that the BCVA increased by  $4.6 \pm 9.7$  (median 2) letters among PCV patients and  $5.4 \pm 10.3$  (median 1) letters among CNV patients. The BCVA increased by  $7.30 \pm 10.41$  (median 4) letters

at the 12th month for these PCV patients and  $8.8 \pm 11.0$  (median 5) letters for the CNV patients (**Table 3**).

There was no significant difference between the two groups. At the 1st month after the initial injection, CRT changes were  $-107.3 \pm 169.5$  (median  $-79$ )  $\mu$ m for PCV patients and  $-86.2 \pm 134.0$  (median  $-53$ )  $\mu$ m for CNV patients. At the 12th month, CRT changes were  $-179.7 \pm 249.2$  ( $-138$ )  $\mu$ m for PCV patients and  $-139.4 \pm 227.8$  (median  $-96$ )  $\mu$ m for CNV patients. There was no significant difference between the two groups (**Table 3**).

**TABLE 3 |** Mean BCVA changes compared with baseline (ETDRS letters).

	ALL	CNV	PCV	P	Conbercept	RBZ	P
<b>Baseline</b>							
mean $\pm$ SD	31.3 $\pm$ 13.3	31.6 $\pm$ 13.7	30.8 $\pm$ 12.7	0.905 <sup>^</sup>	31.6 $\pm$ 13.4	31.2 $\pm$ 13.3	0.906 <sup>^</sup>
median (IQR)	25 (23~40)	25 (22~40)	25 (23~40)		25 (22.5~40)	25 (23~40)	
min~max	20~75	20~75	20~75		20~70	20~75	
<b>M1 change</b>							
mean $\pm$ SD	5.1 $\pm$ 10.1	5.4 $\pm$ 10.3	4.6 $\pm$ 9.7	0.840 <sup>^</sup>	4.3 $\pm$ 8.7	5.3 $\pm$ 10.5	0.851 <sup>^</sup>
median (IQR)	1 (0~9.5)	1 (0~10)	2 (0~8)		1.5 (0~7.5)	1 (0~11)	
min~max	-35~51	-35~50	-27~51		-23~30	-35~51	
<b>M2 change</b>							
mean $\pm$ SD	6.3 $\pm$ 10.2	6.6 $\pm$ 10.8	5.9 $\pm$ 8.9	0.544 <sup>^</sup>	5.7 $\pm$ 9.3	6.5 $\pm$ 10.4	0.853 <sup>^</sup>
median (IQR)	3 (0~13)	3 (0~13)	2 (0~13)		3 (0~8.75)	3 (0~13)	
min~max	-35~53	-35~53	-17~37		-23~37	-35~53	
<b>M3 change</b>							
mean $\pm$ SD	8.7 $\pm$ 11.5	9.3 $\pm$ 11.5	7.9 $\pm$ 11.6	0.123 <sup>^</sup>	7.5 $\pm$ 11.2	9.2 $\pm$ 11.6	0.177 <sup>^</sup>
median (IQR)	5 (0~15)	7 (2~15)	4 (0~15)		4 (0~15)	6 (1~16)	
min~max	-27~52	-27~52	-20~52		-23~52	-27~52	
<b>M6 change</b>							
mean $\pm$ SD	9.2 $\pm$ 11.4	9.9 $\pm$ 11.7	8.0 $\pm$ 10.8	0.113 <sup>^</sup>	8.4 $\pm$ 11.0	9.4 $\pm$ 11.5	0.537 <sup>^</sup>
median (IQR)	5.75 (1~15)	7 (2~15)	4 (0~15)		4 (0~15)	6 (1~15)	
min~max	-27~52	-27~52	-18~37		-23~33	-27~52	
<b>M12 change</b>							
mean $\pm$ SD	8.2 $\pm$ 10.8	8.8 $\pm$ 11.0	7.3 $\pm$ 10.4	0.131 <sup>^</sup>	6.9 $\pm$ 10.0	8.7 $\pm$ 11.0	0.156 <sup>^</sup>
median (IQR)	5 (0~15)	5 (1~15)	4 (0~15)		4 (0~14)	5 (0~15)	
min~max	-27~50	-27~50	-19~37		-23~32	-27~50	

<sup>^</sup>Mann-Whitney U-test.

## Univariate and Multivariate Analyses

BCVA improvement of more than 5 letters on the ETDRS chart was considered to be a satisfactory efficacy endpoint. The univariate and multivariate analyses are shown below in **Table 5**.

Several factors were related to the increased probability of reaching this satisfactory efficacy endpoint, including female sex (OR 2.07, 95% CI 1.22~3.51), number of injections (OR 1.40, 95% CI 1.12~1.75) and VA change at the first month (OR 13.75, 95% CI 7.41~25.51). Additionally, some factors were related to reducing the probability of reaching a satisfactory efficacy endpoint, including diabetes (OR 0.27, 95% CI 0.10~0.73) and AMD disease history (OR 0.75, 95% CI 0.57~0.98).

RCS analyses generated a curve showing that those patients whose VA was not decreased at the 1st month had a higher probability of gaining more than 5 letters at month 12 ( $p < 0.001$  **Figure 2**).

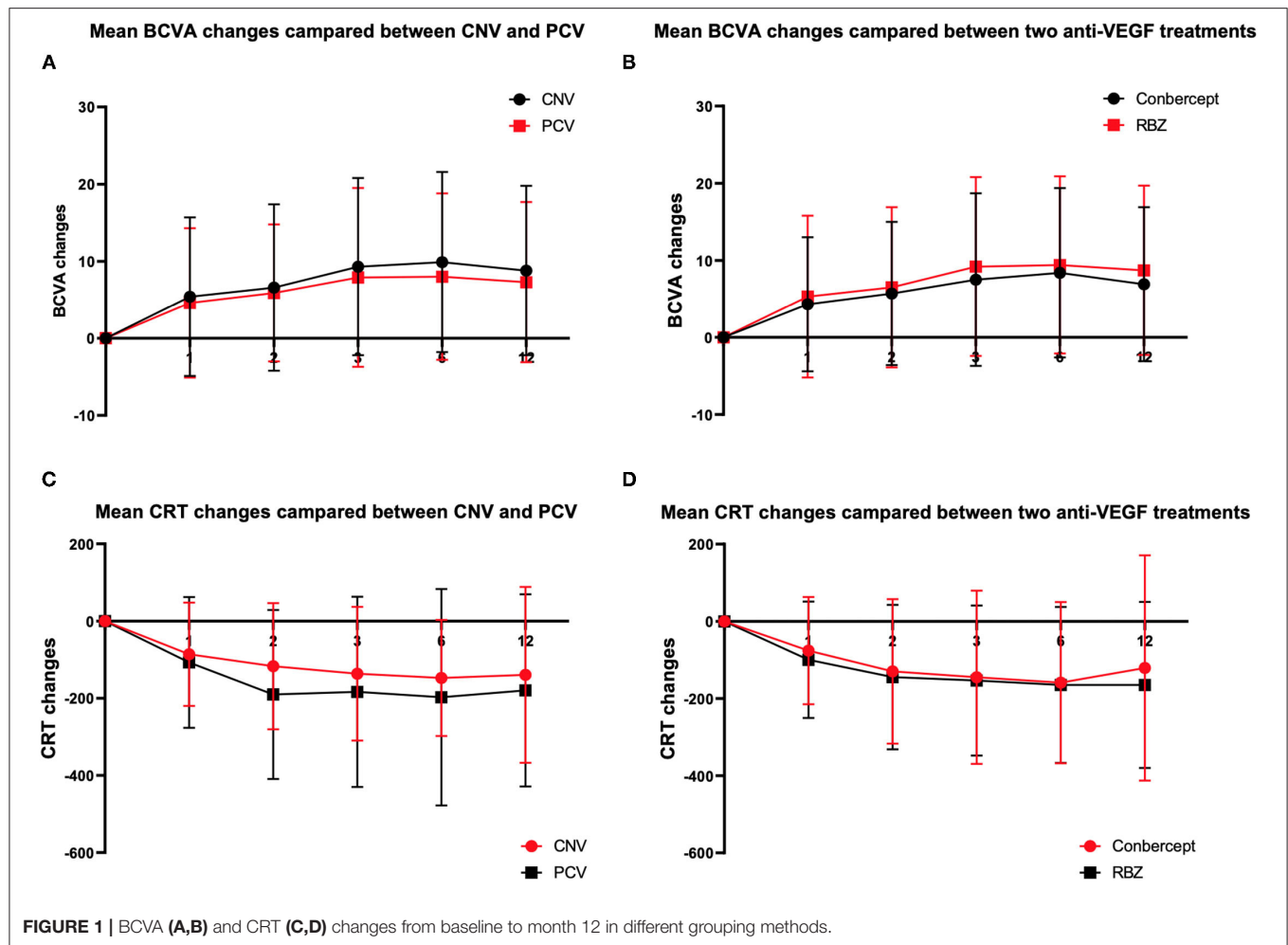
## DISCUSSION

This was a real-life study of anti-VEGF therapy for wAMD between 2014 and 2018 in Guangdong Province, China, which reported changes in the BCVA and CRT of patients from initial baseline to the 12th month. Our results confirmed that BCVA and anatomical benefits could be maintained for at least 12

months after intravitreal injection of anti-VEGF. This outcome is consistent with the results of most previous anti-VEGF studies in the treatment of wAMD (25–28).

Many previous studies have shown more effectiveness of anti-VEGF in the treatment of wAMD if patients accepted the 3 + PRN or 5 + 3 + 2 in the 3-year treatment regimen (29–31). However, in China, these two anti-VEGF drugs were not approved by health insurance for use in patients with wAMD until May 2019. Prior to this date, the large cost of high-priced drugs greatly affected the patient's treatment compliance and compromised data integrity (32, 33). Therefore, the anti-VEGF treatment regimen and its efficacy in wAMD patients in China before 2019 were different from the data reported worldwide. For example, in our study, the mean number of intravitreal injections of anti-VEGF was only 2.1, and only 37.5% of patients completed the treatment regimen of 3+PRN, which was far lower than the mean number of injections reported in European countries (34–37).

The first-year result of the LUMINOUS study with 3,379 patients globally showed that the mean number of intravitreal injections was 5.0, and VA increased by 3.1 letters on average (38). In China (92 patients), the average number of intravitreal injections was 2.9, and VA increased by 1.1 letters on average. In Canada (376 patients), the average number of intravitreal



injections was 7.0, with VA increasing by an average of 2.5 letters. In Germany (128 patients), the average number of intravitreal injections was 5.2, with VA increasing by an average of 2.3 letters. In South Korea (52 patients), the average number of intravitreal injections was 5.2, and VA increased by an average of 9.8 letters. The average number of injections and the increase in VA letters at 1 year in our study results were different from the multinational data in the LUMINOUS study.

Conbercept is an anti-VEGF drug produced in China that is permitted for the treatment of wAMD. However, the efficacy of conbercept in wAMD still lacks data support compared with other anti-VEGF drugs (39–42). In this study, we compared RBZ and conbercept, two kinds of anti-VEGF drugs. The results showed that the mean number of injections for RBZ was slightly higher than that for conbercept and that the BCVA improvement of RBZ was better than that of conbercept. However, there were no significant differences between the two groups. This indicates that RBZ and conbercept have similar efficacy in wAMD. The reason for the difference may be that more injections lead to better visual benefits. Our result was similar to the results of a randomized controlled study between

RBZ and aflibercept. Many real-world studies did not show any significant difference in VA improvement between RBZ and aflibercept (43–47).

PCV and CNV are two subtypes of wAMD. They have many common clinical characteristics and risk factors, but there are also many different epidemiological characteristics, indicating that they have different pathophysiological processes (48–50). These differences have led to a certain difference in the therapeutic effect between intravitreal injection of anti-VEGF drugs on PCV and CNV (51, 52). In epidemiology, compared to CNV secondary to AMD in Western populations, polypoidal PCV appears to be the main subtype of exudative AMD in Asian populations (53).

Our study included 135 PCV and 233 CNV cases. Our analysis found that the average number of injections for PCV was lower than that for CNV. However, the changes in BCVA and CRT in CNV were better than those in PCV. This finding is consistent with previous reports in the relevant literature (54).

At the end of the treatment in the 12th month, BCVA improved more than 5 letters on the ETDRS chart and was considered satisfactory efficacy. Univariate and multivariate



**TABLE 4 |** Mean CRT changes compared with baseline ( $\mu\text{m}$ ).

	ALL	CNV	PCV	P	Conbercept	RBZ	P
<b>Baseline</b>							
mean $\pm$ SD	440.6 $\pm$ 228.6	420.7 $\pm$ 214.4	475.1 $\pm$ 248.4	0.008 <sup>^</sup>	448.6 $\pm$ 236.5	438.1 $\pm$ 226.5	0.869 <sup>^</sup>
median (IQR)	372 (277~541)	353 (269~522)	416 (321~590)		372 (275~566)	372.5 (285.5~535)	
min~max	100~1,632	100~1,221	123~1,632		143~1,238	100~1,632	
<b>M1 change</b>							
mean $\pm$ SD	-93.9 $\pm$ 148.1	-86.2 $\pm$ 134.0	-107.3 $\pm$ 169.5	0.071 <sup>^</sup>	-75.8 $\pm$ 138.9	-99.7 $\pm$ 150.7	0.316 <sup>^</sup>
median (IQR)	-61 (-143.5~-16)	-53 (-116~-16)	-79 (-161~-16)		-56.5 (-117~-4)	-61 (-147~-19.5)	
min~max	-835~365	-835~262	-800~365		-562~344	-835~365	
<b>M2 change</b>							
mean $\pm$ SD	-141.8 $\pm$ 187.1	-116.9 $\pm$ 163.5	-190.2 $\pm$ 219.11	0.002 <sup>^</sup>	-129.8 $\pm$ 187.2	-144.4 $\pm$ 187.5	0.535 <sup>^</sup>
median (IQR)	-82 (-210~-27)	-64 (-176~-21)	-125 (-259~-53)		-81 (-154~-6)	-82 (-211~-27)	
min~max	-977~151	-962~151	-977~111		-893~90	-977~151	
<b>M3 change</b>							
mean $\pm$ SD	-151.8 $\pm$ 200.9	-136.5 $\pm$ 173.4	-183.4 $\pm$ 246.5	0.142 <sup>^</sup>	-145.1 $\pm$ 224.8	-153.6 $\pm$ 194.6	0.238 <sup>^</sup>
median (IQR)	-89 (-218~-45)	-81 (-191~-44)	-126 (-266~-51)		-70.5 (-232~-4)	-96 (-209~-51)	
min~max	-1,344~387	-807~387	-1,344~191		-908~134	-1,344~387	
<b>M6 change</b>							
mean $\pm$ SD	-163.6 $\pm$ 203.1	-147.3 $\pm$ 150.7	-197.4 $\pm$ 280.7	0.162 <sup>^</sup>	-158.8 $\pm$ 208.7	-164.7 $\pm$ 202.3	0.463 <sup>^</sup>
median (IQR)	-106.5 (-215~-51)	-100 (-203~-47)	-140 (-243~-55)		-95 (-197~-21)	-111 (-224~-54)	
min~max	-1,392~385	-700~108	-1,392~385		-717~212	-1,392~385	
<b>M12 change</b>							
mean $\pm$ SD	-154.2 $\pm$ 236.3	-139.4 $\pm$ 227.8	-179.7 $\pm$ 249.2	0.078 <sup>^</sup>	-120.8 $\pm$ 292.0	-164.7 $\pm$ 215.4	0.218 <sup>^</sup>
median (IQR)	-110.5 (-228.5~-48.5)	-96 (-213~-48)	-138 (-238~-49)		-102 (-199.5~-29)	-116 (-238.5~-49)	
min~max	-1,392~2,013	-988~2,013	-1,392~398		-908~2,013	-1,392~512	

<sup>^</sup>Mann-Whitney U-test.**TABLE 5 |** Univariate and multivariate analyses.

	Univariate			Multivariate		
	OR	95% CI	p	OR	95% CI	p
Sex, F vs. M	1.44	0.95~2.20	0.087	2.07	1.22~3.51	0.007
Age (above 65 years)	0.76	0.50~1.17	0.213	0.80	0.47~1.36	0.402
Smoking	1.49	0.45~4.99	0.514	1.94	0.44~8.45	0.379
Hypertension	1.26	0.81~1.96	0.298	1.53	0.86~2.72	0.150
Diabetics	0.50	0.23~1.09	0.083	0.27	0.10~0.73	0.010
PCV/CNV	0.77	0.50~1.18	0.230	0.82	0.47~1.44	0.495
AMD disease history (more than 12 months; 3~12 months; 1~3 months; 1 and below)	0.77	0.64~0.94	0.011	0.75	0.57~0.98	0.033
PDT	1.04	0.56~1.93	0.905	0.79	0.35~1.79	0.577
Anti-VEGF-RBZ/Conbercept	1.69	1.03~2.77	0.039	1.48	0.79~2.73	0.222
Number of injections	1.13	0.96~1.34	0.150	1.40	1.12~1.75	0.003
Diameter of lesion above 500	0.14	0.03~0.64	0.011	0.24	0.04~1.34	0.105
Baseline OCT	1.00	1.00~1.00	0.005	1.00	1.00~1.00	0.208
VA change at the 1st month above 5 letters.	10.92	6.33~18.86	<0.001	13.75	7.41~25.51	<0.001

Adjusted by sex, age, smoking status, hypertension, diabetics, PCV/CNV, AMD disease history, PDT usage, kind of anti-VEGF, diameter of lesion, baseline OCT, and whether VA changing at the 1st month above 5 letters.

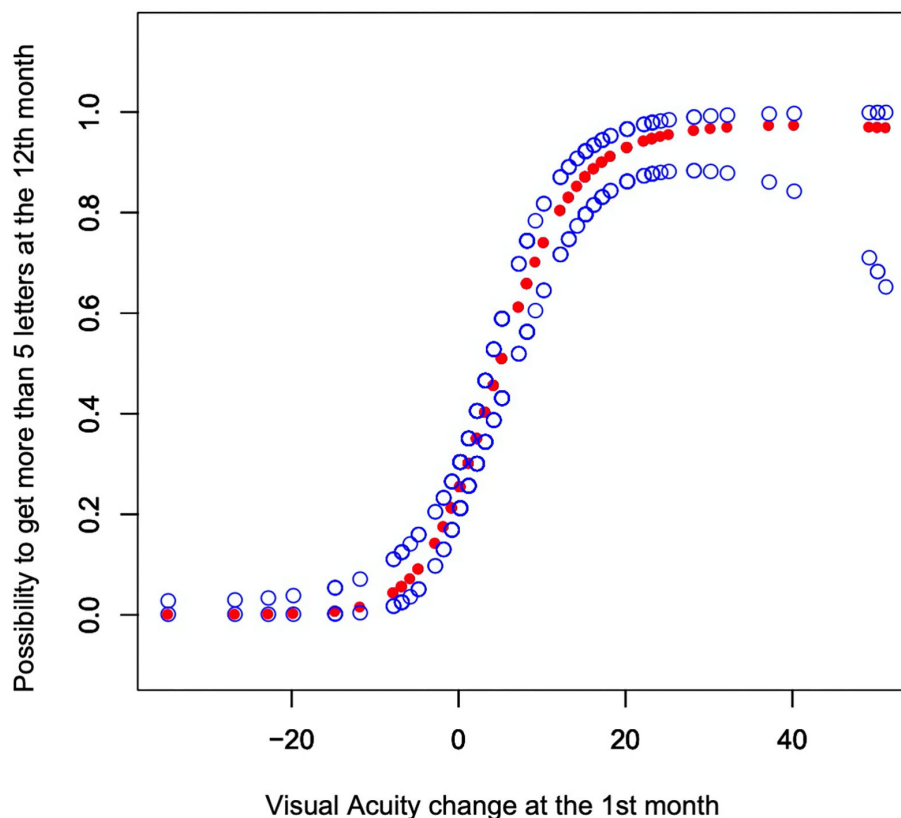


**FIGURE 2 |** The y-axis shows the possibility to get more than 5 letters at the 12th month with the 95% CI. The model was adjusted by sex, age, smoking status, hypertension, diabetes, PCV or CNV, history of wet AMD, PDT (photodynamic therapy), treatment groups, number of injections, diameter of lesions, and baseline OCT.

analyses showed that females were more likely to experience good treatment effects than males. Moreover, increasing the number of injections has better vision benefits. This result is consistent with a number of studies (33, 38, 55).

Because this was a retrospective study, there were some limitations. First, we found that treatment was more effective in women than men. This may be related to the fact that Chinese women are more likely to follow the doctor's advice on matters such as less alcohol consumption and less tobacco usage, but we did not collect data on the frequency or amount of alcohol consumed. Although our results showed that tobacco had no significant effect on the efficacy of wAMD, the interaction between alcohol and tobacco was not included. Additionally, conbercept has been used only since the beginning of 2016, causing the sample size for conbercept to be smaller than that for RBZ. Therefore, the efficacy comparison between RBZ and conbercept still needs to be confirmed by further studies, especially RCTs.

Overall, this study is about the actual application of anti-VEGF in the treatment of wAMD among Chinese patients from 2014 to 2018. The Chinese medical insurance system did not reimburse such wAMD patients due to the cost of anti-VEGF treatment during that period. The anti-VEGF treatment of AMD patients was largely limited by their financial status. Therefore, the average number of injections for AMD in this

study was much lower than that in developed countries. However, since 2019, anti-VEGF treatment for AMD has entered the era of comprehensive medical insurance payment in China. AMD patients in China can be more active in the selection of anti-VEGF treatment, which may produce better treatment results.

## DATA AVAILABILITY STATEMENT

The original contributions presented in the study are included in the article/**Supplementary Material**, further inquiries can be directed to the corresponding author/s.

## ETHICS STATEMENT

The studies involving human participants were reviewed and approved by the Medical Ethics Committee of the Second Affiliated Hospital of South China University of Technology and Foshan Second People's Hospital. Written informed consent to participate in this study was provided by the participants' legal guardian/next of kin.

## AUTHOR CONTRIBUTIONS

YLe and YLu contributed to the design, performed the experiments, and discussed the results. JZ and JH

analyzed the data and prepared the tables and figures for the manuscript. FS, HM, and GR performed the medical record data collection. WH, LK, WY, XH, SY, and ZG followed up with the patients. All authors reviewed the manuscript.

## FUNDING

This research was supported by the Natural Science Foundation of Guangdong Province (No. 2018A030313761).

## REFERENCES

- Randolph SA. Age-related macular degeneration. *Workplace Health Saf.* (2014) 62:352. doi: 10.3928/21650799-20140708-06
- Prokofyeva E, Zrenner E. Epidemiology of major eye diseases leading to blindness in Europe: a literature review. *Ophthalmic Res.* (2012) 47:171–88. doi: 10.1159/000329603
- Cheung LK, Eaton A. Age-related macular degeneration. *Pharmacotherapy.* (2013) 33:838–55. doi: 10.1002/phar.1264
- Li X, Luo H, Zuo C, Zhang Z, Zhang J, Zhang M. Conbercept in patients with treatment-naïve neovascular age-related macular degeneration in real-life setting in China. *Retina.* (2019) 39:1353–60. doi: 10.1097/IAE.0000000000002152
- Song P, Du Y, Chan KY, Theodoratou E, Rudan I. The national and subnational prevalence and burden of age-related macular degeneration in China. *J Glob Health.* (2017) 7:020703. doi: 10.7189/jogh.07.020703
- van Lookeren Campagne M, LeCouter J, Yaspan BL, Ye W. Mechanisms of age-related macular degeneration and therapeutic opportunities. *J Pathol.* (2014) 232:151–64. doi: 10.1002/path.4266
- Shen YS, Cheng CK. Using optical coherence tomography angiography in assessment of the anti-vascular endothelial growth factor effect for pathological vascular tissue in age-related macular degeneration and polypoidal choroidal vasculopathy. *Eur J Ophthalmol.* (2020) 31:1267–80. doi: 10.1177/1120672120913012
- Ding K, Eaton L, Bowley D, Rieser M, Chang Q, Harris MC, et al. Generation and characterization of ABBV642, a dual variable domain immunoglobulin molecule (DVD-Ig) that potently neutralizes VEGF and PDGF-BB and is designed for the treatment of exudative age-related macular degeneration. *MAbs.* (2017) 9:269–84. doi: 10.1080/19420862.2016.1268305
- Gao Y, Yu T, Zhang Y, Dang G. Anti-VEGF monotherapy versus photodynamic therapy and Anti-VEGF combination treatment for neovascular age-related macular degeneration: a meta-analysis. *Invest Ophthalmol Vis Sci.* (2018) 59:4307–17. doi: 10.1167/iov.17-23747
- Fursova AZ, Chubar NV, Tarasov MS, Vasilyeva MA, Gusarevich OG. [Anti-VEGF therapy for age-related macular degeneration]. *Vestn Oftalmol.* (2018) 134:59–67. doi: 10.17116/oftalma201813406159
- Kamenskih TG. [A differentiated approach to analysis of retinal fluid and assessment of its effect on anti-VEGF therapy of neovascular age-related macular degeneration]. *Vestn Oftalmol.* (2019) 135:134–40. doi: 10.17116/oftalma2019135061134
- Rosenfeld PJ, Moshfeghi AA, Puliafito CA. Optical coherence tomography findings after an intravitreal injection of bevacizumab (avastin) for neovascular age-related macular degeneration. *Ophthalmic Surg Lasers Imaging.* (2005) 36:331–5. doi: 10.3928/1542-8877-20050701-14
- Michels S, Rosenfeld PJ, Puliafito CA, Marcus EN, Venkatraman AS. Systemic bevacizumab (Avastin) therapy for neovascular age-related macular degeneration twelve-week results of an uncontrolled open-label clinical study. *Ophthalmology.* (2005) 112:1035–47. doi: 10.1016/j.ophtha.2005.02.007
- Pieramici DJ, Avery RL. Ranibizumab: treatment in patients with neovascular age-related macular degeneration. *Expert Opin Biol Ther.* (2006) 6:1237–45. doi: 10.1517/14712598.6.11.1237
- Carvounis PE, Kopel AC, Benz MS. Retinal pigment epithelium tears following ranibizumab for exudative age-related macular degeneration. *Am J Ophthalmol.* (2007) 143:504–5. doi: 10.1016/j.ajo.2006.11.028
- Wang Q, Li T, Wu Z, Wu Q, Ke X, Luo D, et al. Novel VEGF decoy receptor fusion protein conbercept targeting multiple VEGF isoforms provide remarkable anti-angiogenesis effect in vivo. *PLoS One.* (2013) 8:e70544. doi: 10.1371/journal.pone.0070544
- Nguyen TT, Guymer R. Conbercept (KH-902) for the treatment of neovascular age-related macular degeneration. *Expert Rev Clin Pharmacol.* (2015) 8:541–8. doi: 10.1586/17512433.2015.1075879
- Ferrara N, Damico L, Shams N, Lowman H, Kim R. Development of ranibizumab, an anti-vascular endothelial growth factor antigen binding fragment, as therapy for neovascular age-related macular degeneration. *Retina.* (2006) 26:859–70. doi: 10.1097/01.iae.0000242842.14624.e7
- Rosenfeld PJ, Brown DM, Heier JS, Boyer DS, Kaiser PK, Chung CY, et al. Ranibizumab for neovascular age-related macular degeneration. *N Engl J Med.* (2006) 355:1419–31. doi: 10.1056/NEJMoa054481
- Rayess N, Houston SK III, Gupta OP, Ho AC, Regillo CD. Treatment outcomes after 3 years in neovascular age-related macular degeneration using a treat-and-extend regimen. *Am J Ophthalmol.* (2015) 159:3–8 e1. doi: 10.1016/j.ajo.2014.09.011
- Wu B, Li J, Lin H, Wu H. Different strategies for the treatment of age-related macular degeneration in china: an economic evaluation. *J Ophthalmol.* (2016) 2016:7689862. doi: 10.1155/2016/7689862
- Zhang Y, Hu S, Chang J. Burden of wet age-related macular degeneration in China. *Value Health.* (2014) 17:A782. doi: 10.1016/j.jval.2014.08.381
- Kaiser PK. Prospective evaluation of visual acuity assessment: a comparison of snellen versus ETDRS charts in clinical practice (An AOS Thesis). *Trans Am Ophthalmol Soc.* (2009) 107:311–24.
- Amoaku WM, Chakravarthy U, Gale R, Gavin M, Ghanchi F, Gibson J, et al. Defining response to anti-VEGF therapies in neovascular AMD. *Eye.* (2015) 29:721–31. doi: 10.1038/eye.2015.48
- Minnella AM, Federici M, Falsini B, Barbano L, Gambini G, Lanza A, et al. Choroidal thickness changes after intravitreal ranibizumab for exudative age-related macular degeneration. *BioDrugs.* (2016) 30:353–9. doi: 10.1007/s40259-016-0179-0
- Johnston RL, Lee AY, Buckle M, Antcliff R, Bailey C, McKibbin M, et al. UK Age-Related Macular Degeneration Electronic Medical Record System (AMD EMR) users group report IV: incidence of blindness and sight impairment in ranibizumab-treated patients. *Ophthalmology.* (2016) 123:2386–92. doi: 10.1016/j.ophtha.2016.07.037
- Madhusudhana KC, Lee AY, Keane PA, Chakravarthy U, Johnston RL, Egan CA, et al. UK neovascular age-related macular degeneration database. report 6: time to retreatment after a pause in therapy. outcomes from 92 976 intravitreal ranibizumab injections. *Br J Ophthalmol.* (2016) 100:1617–22. doi: 10.1136/bjophthalmol-2015-308077
- Liu K, Song Y, Xu G, Ye J, Wu Z, Liu X, et al. Conbercept for treatment of neovascular age-related macular degeneration: results of the randomized Phase 3 PHOENIX study. *Am J Ophthalmol.* (2019) 197:156–67. doi: 10.1016/j.ajo.2018.08.026
- Menon G, Chandran M, Sivaprasad S, Chavan R, Narendran N, Yang Y. Is it necessary to use three mandatory loading doses when commencing therapy for neovascular age-related macular degeneration using bevacizumab? (BeMOc Trial). *Eye.* (2013) 27:959–63. doi: 10.1038/eye.2013.93
- Wang F, Yuan Y, Wang L, Ye X, Zhao J, Shen M, et al. One-year outcomes of 1 dose versus 3 loading doses followed by pro re nata regimen using

## ACKNOWLEDGMENTS

We would like to thank Bozheng Zhang (Bothwin Clinical Study Consultant, WA, USA) for English editing.

## SUPPLEMENTARY MATERIAL

The Supplementary Material for this article can be found online at: <https://www.frontiersin.org/articles/10.3389/fmed.2021.735318/full#supplementary-material>

- ranibizumab for neovascular age-related macular degeneration: the ARTIS trial. *J Ophthalmol.* (2019) 2019:7530458. doi: 10.1155/2019/7530458
31. Sugiyama A, Sakurada Y, Honda S, Miki A, Matsumiya W, Yoneyama S, et al. Retreatment of exudative age-related macular degeneration after loading 3-monthly intravitreal ranibizumab. *Ophthalmologica.* (2018) 239:52–59. doi: 10.1159/000480439
  32. Gao L, Liu J, Zhang P, Ma J, Wang H. Clinical outcomes of 1 + PRN and 3 + Q3M regimens of intravitreal conbercept injection for exudative age-related macular degeneration. *Sci Rep.* (2020) 10:8010. doi: 10.1038/s41598-020-65000-5
  33. Gao L, Tao Y, Liu M, Li L, Zhang P, Wang H, et al. Different conbercept injection strategies for the treatment of exudative age-related macular degeneration: a retrospective cohort study. *Medicine.* (2020) 99:e19007. doi: 10.1097/MD.00000000000019007
  34. Investigators IS, Chakravarthy U, Harding SP, Rogers CA, Downes SM, Lotery AJ, et al. Ranibizumab versus bevacizumab to treat neovascular age-related macular degeneration: one-year findings from the IVAN randomized trial. *Ophthalmology.* (2012) 119:1399–411. doi: 10.1016/j.ophtha.2012.04.015
  35. Busbee BG, Ho AC, Brown DM, Heier JS, Suner JJ, Li Z, et al. Twelve-month efficacy and safety of 0.5 mg or 2.0 mg ranibizumab in patients with subfoveal neovascular age-related macular degeneration. *Ophthalmology.* (2013) 120:1046–56. doi: 10.1016/j.ophtha.2012.10.014
  36. Chavan R, Panneerselvam S, Adhana P, Narendran N, Yang Y. Bilateral visual outcomes and service utilization of patients treated for 3 years with ranibizumab for neovascular age-related macular degeneration. *Clin Ophthalmol.* (2014) 8:717–23. doi: 10.2147/OPTH.S60763
  37. Muether PS, Hoerster R, Hermann MM, Kirchhof B, Fauser S. Long-term effects of ranibizumab treatment delay in neovascular age-related macular degeneration. *Graefes Arch Clin Exp Ophthalmol.* (2013) 251:453–8. doi: 10.1007/s00417-012-2038-0
  38. Holz FG, Figueroa MS, Bandello F, Yang Y, Ohji M, Dai H, et al. Ranibizumab treatment in treatment-naïve neovascular age-related macular degeneration: results from luminous, a global real-world study. *Retina.* (2019) 40:1673–85. doi: 10.1097/IAE.00000000000002670
  39. Wang L, Zhang C, Hua R. Clinical effectiveness of ranibizumab and conbercept for neovascular age-related macular degeneration: a meta-analysis. *Drug Des Devel Ther.* (2018) 12:3625–33. doi: 10.2147/DDDT.S176021
  40. Cui J, Sun D, Lu H, Dai R, Xing L, Dong H, et al. Comparison of effectiveness and safety between conbercept and ranibizumab for treatment of neovascular age-related macular degeneration: a retrospective case-controlled non-inferiority multiple center study. *Eye.* (2018) 32:391–9. doi: 10.1038/eye.2017.187
  41. Jin E, Bai Y, Luo L, Huang L, Zhu X, Ding X, et al. Serum levels of vascular endothelial growth factor before and after intravitreal injection of ranibizumab or conbercept for neovascular age-related macular degeneration. *Retina.* (2017) 37:971–7. doi: 10.1097/IAE.0000000000001274
  42. Zhang J, Liang Y, Xie J, Li D, Hu Q, Li X, et al. Conbercept for patients with age-related macular degeneration: a systematic review. *BMC Ophthalmol.* (2018) 18:142. doi: 10.1186/s12886-018-0807-1
  43. Hirakata T, Fujinami K, Watanabe K, Sasaki M, Noda T, Akiyama K. One-year outcome of intravitreal aflibercept injection for age-related macular degeneration resistant to ranibizumab: rapid morphologic recovery and subsequent visual improvement. *Clin Ophthalmol.* (2016) 10:969–77. doi: 10.2147/OPTH.S101596
  44. Garweg JG, Gerhardt C, Kodjikian L, Pfister IB. Real-life experience with aflibercept and ranibizumab in the treatment of newly diagnosed neovascular age-related macular degeneration over 24 months. *J Ocul Pharmacol Ther.* (2017) 33:567–72. doi: 10.1089/jop.2017.0031
  45. Kiss S, Malangone-Monaco E, Wilson K, Varker H, Stetsovsky D, Smith D, et al. Real-world injection frequency and cost of ranibizumab and aflibercept for the treatment of neovascular age-related macular degeneration and diabetic macular edema. *J Manag Care Spec Pharm.* (2020) 26:253–66. doi: 10.18553/jmcp.2020.19245
  46. Gillies MC, Nguyen V, Daien V, Arnold JJ, Morlet N, Barthelmes D. Twelve-month outcomes of ranibizumab vs. aflibercept for neovascular age-related macular degeneration: data from an observational study. *Ophthalmology.* (2016) 123:2545–53. doi: 10.1016/j.ophtha.2016.08.016
  47. Kim JH, Lee DW, Chang YS, Kim JW, Kim CG. Twelve-month outcomes of treatment using ranibizumab or aflibercept for neovascular age-related macular degeneration: a comparative study. *Graefes Arch Clin Exp Ophthalmol.* (2016) 254:2101–9. doi: 10.1007/s00417-016-3353-7
  48. Huang L, Li Y, Guo S, Sun Y, Zhang C, Bai Y, et al. Different hereditary contribution of the CFH gene between polypoidal choroidal vasculopathy and age-related macular degeneration in Chinese Han people. *Invest Ophthalmol Vis Sci.* (2014) 55:2534–8. doi: 10.1167/iovs.13-13437
  49. Baek J, Lee JH, Jung BJ, Kook L, Lee WK. Morphologic features of large choroidal vessel layer: age-related macular degeneration, polypoidal choroidal vasculopathy, and central serous chorioretinopathy. *Graefes Arch Clin Exp Ophthalmol.* (2018) 256:2309–17. doi: 10.1007/s00417-018-4143-1
  50. Chen XL, Hu QR, Bai YJ, Deng Y, Wang HW, Liu S, et al. A comparison of risk factors for age-related macular degeneration and polypoidal choroidal vasculopathy in Chinese patients. *Graefes Arch Clin Exp Ophthalmol.* (2018) 256:1449–57. doi: 10.1007/s00417-018-4020-y
  51. Takahashi Y, Koizumi H, Hasegawa T, Izumi T, Maruko I, Sonoda S, et al. Comparison of subfoveal choroidal structures in typical neovascular age-related macular degeneration and polypoidal choroidal vasculopathy. *Jpn J Ophthalmol.* (2018) 62:576–83. doi: 10.1007/s10384-018-0615-4
  52. Fenner BJ, Ting DSW, Tan ACS, Teo K, Chan CM, Mathur R, et al. Real-world treatment outcomes of age-related macular degeneration and polypoidal choroidal vasculopathy in Asians. *Ophthalmol Retina.* (2020) 4:403–14. doi: 10.1016/j.oret.2019.10.019
  53. Wong CW, Yanagi Y, Lee WK, Ogura Y, Yeo I, Wong TY, et al. Age-related macular degeneration and polypoidal choroidal vasculopathy in Asians. *Prog Retin Eye Res.* (2016) 53:107–39. doi: 10.1016/j.preteyeres.2016.04.002
  54. Cheung CM, Li X, Mathur R, Lee SY, Chan CM, Yeo I, et al. A prospective study of treatment patterns and 1-year outcome of Asian age-related macular degeneration and polypoidal choroidal vasculopathy. *PLoS One.* (2014) 9:e101057. doi: 10.1371/journal.pone.0101057
  55. Gupta ADSP, LUMINOUS: Detailed Statistical Methodology for Interim and Final Analyses. Novartis Internal Document; Observational Study Protocol RFB002A2406: RAP Module 3, release date 31 July 2014 (2014).

**Conflict of Interest:** The authors declare that the research was conducted in the absence of any commercial or financial relationships that could be construed as a potential conflict of interest.

**Publisher's Note:** All claims expressed in this article are solely those of the authors and do not necessarily represent those of their affiliated organizations, or those of the publisher, the editors and the reviewers. Any product that may be evaluated in this article, or claim that may be made by its manufacturer, is not guaranteed or endorsed by the publisher.

Copyright © 2021 Lu, Huang, Zhang, Huang, Zhang, Ma, Ren, Shi, Kuang, Yan, Luo, Zhang, He, Yang, Gao and Leng. This is an open-access article distributed under the terms of the Creative Commons Attribution License (CC BY). The use, distribution or reproduction in other forums is permitted, provided the original author(s) and the copyright owner(s) are credited and that the original publication in this journal is cited, in accordance with accepted academic practice. No use, distribution or reproduction is permitted which does not comply with these terms.





# Dysregulated Serum Lipid Metabolism Promotes the Occurrence and Development of Diabetic Retinopathy Associated With Upregulated Circulating Levels of VEGF-A, VEGF-D, and PIGF

Xinyuan Zhang<sup>1\*</sup>, Bingjie Qiu<sup>1†</sup>, Qiyun Wang<sup>1†</sup>, Sobha Sivaprasad<sup>2</sup>, Yanhong Wang<sup>3</sup>, Lin Zhao<sup>1†</sup>, Rui Xie<sup>1†</sup>, Lei Li<sup>1†</sup> and Wenting Kang<sup>1†</sup>

## OPEN ACCESS

### Edited by:

Shaochong Zhang,  
Sun Yat-sen University, China

### Reviewed by:

Kelvin Yi Chong Teo,  
Singapore National Eye  
Center, Singapore  
Yi-Ting Hsieh,  
National Taiwan University  
Hospital, Taiwan

### \*Correspondence:

Xinyuan Zhang  
mmzy2010@163.com

<sup>†</sup>Beijing Retinal and Choroidal  
Vascular Diseases Study Group

<sup>‡</sup>These authors have contributed  
equally to this work

### Specialty section:

This article was submitted to  
Ophthalmology,  
a section of the journal  
Frontiers in Medicine

Received: 18 September 2021

Accepted: 05 October 2021

Published: 22 November 2021

### Citation:

Zhang X, Qiu B, Wang Q,  
Sivaprasad S, Wang Y, Zhao L, Xie R,  
Li L and Kang W (2021) Dysregulated  
Serum Lipid Metabolism Promotes the  
Occurrence and Development of  
Diabetic Retinopathy Associated With  
Upregulated Circulating Levels of  
VEGF-A, VEGF-D, and PIGF.  
Front. Med. 8:779413.  
doi: 10.3389/fmed.2021.779413

<sup>1</sup> Beijing Tongren Eye Center, Beijing Institute of Ophthalmology, Tongren Hospital, Capital Medical University, Beijing, China,  
<sup>2</sup> National Institute for Health Research (NIHR) Moorfield's Biomedical Research Center, Moorfield's Eye Hospital, London,  
United Kingdom, <sup>3</sup> Department of Epidemiology and Biostatistics, School of Basic Medicine, Peking Union Medical College,  
Institute of Basic Medical Sciences, Chinese Academy of Medical Sciences, Beijing, China

**Purpose:** This study aims to explore the correlations of arteriosclerosis-associated plasma indices with various severity levels of diabetic retinopathy (DR) and to test the hypothesis that elevated circulating level of known angiogenic cytokines induced by hyperglycemia is associated with dyslipidemia on DR.

**Methods:** This cross-sectional study consists of 131 patients with type 2 diabetes. The patients were categorized based on their DR status into those with no DR (diabetes mellitus, DM), non-proliferative diabetic retinopathy (NPDR), and proliferative diabetic retinopathy (PDR) groups. The biochemical profile including fasting glucose, glycated hemoglobin (HbA1c), lipid profile were estimated, plasma angiogenic cytokines (vascular endothelial growth factor, VEGF-A, -C, -D) and placental growth factor (PIGF) were analyzed by protein microarrays. The atherogenic plasma index (API) was defined as low-density lipoprotein cholesterol/high-density lipoprotein cholesterol (LDL-C/HDL-C); atherogenic index (AI) was calculated as (TC-(HDL-C))/HDL-C and atherogenic index of plasma (AIP) was defined as log (TG/HDL-C).

**Results:** No significant differences were detected in the duration of hypertension, age, and gender between the three groups. Serum TC and LDL-C, AI, and API in the NPDR group and PDR group were significantly higher than those in the DM group. The circulating level of PIGF, VEGF-A, and VEGF-C were significantly correlated with the severity of DR. VEGF-D is a risk factor independent of API ( $Z = -2.61$ ,  $P = 0.009$ ) and AI ( $Z = -2.40$ ,  $P = 0.016$ ). Multivariate logistic regression showed that AI and API are strong risk factors for the occurrence and severity of DR. Associated with AI and API, VEGF-D and PIGF contribute to DR: VEGF-D [AI:  $P = 0.038$ , odd ratio (OR) = 1.38; VEGF-D:  $P = 0.002$ , OR = 1.00. API:  $P = 0.027$ , OR = 1.56, VEGF-D:  $P = 0.002$ , OR = 1.00] and PIGF [AI:  $P = 0.021$ , OR = 1.43; VEGF-D:  $P = 0.004$ , OR = 1.50. API:  $P = 0.011$ , OR = 1.66; VEGF-D:  $P = 0.005$ , OR = 1.49].

**Conclusions:** Total cholesterol (TC) and LDL-C are risk factors for presence of any DR. Atherogenic index and API are novel and better predictive indicators for the occurrence and severity of DR in comparison with the traditional lipid profiles. Abnormal lipid metabolism are associated with the upregulation of circulating cytokines that are linked to the severity of DR.

**Keywords:** dyslipidemia, diabetes mellitus, diabetic retinopathy, lipid profile, serum cytokines, arteriosclerosis-associated plasma parameters

## INTRODUCTION

Diabetic retinopathy (DR) is the most common ocular microvascular complication of diabetes mellitus (DM). Vision threatening diabetic retinopathy (VTDR) is a leading cause of blindness in the working-age (20–65 years) in both developed and developing countries (1). Duration of diabetes is an established non-modifiable risk factor for DR (1, 2). Hyperglycemia is the strongest modifiable risk factor but people with optimal glycemic control also develop DR. The fenofibrate intervention and event lowering in diabetes (FIELD) and the action to control cardiovascular risk in diabetes (ACCORD) studies demonstrated that abnormal lipid metabolism is associated with the onset and progression of DR but the underlying mechanisms are yet to be elucidated (3, 4).

Anti-vascular endothelial growth factor (VEGF) therapy has revolutionized the management of DR and diabetic macular edema (DME). Ranibizumab and bevacizumab are VEGF-A inhibitors while aflibercept blocks VEGF-A and placental growth factor (PlGF). Although these anti-VEGF agents are superior to macular laser and a considerable proportion of patients improve visual acuity, the results of Diabetic Retinopathy Collaboration Network (DRCR.net) Protocol I and T studies show that persistent macular edema was seen in approximately 51–73% at 12 weeks and 32–66% after 24 weeks of regular anti-VEGF injections (5–8).

The role of dyslipidemia in DR risk is now receiving increasing attention. However, unlike the well-established direct correlations between serum lipid dysregulated with macrovascular complication (9, 10), the correlation of traditional serum lipid parameters with DR is controversial (11, 12). In recent years, a large number of clinical and laboratory studies have confirmed that arteriosclerosis-associated plasma parameters, including atherogenic plasma index (API), low-density lipoprotein cholesterol/high-density lipoprotein cholesterol (LDL-C/HDL-C), atherogenic index (AI), total cholesterol (TC)-HDL-C/HDL-C, and atherogenic index of

plasma (AIP), log (triglycerides(TG)/HDL-C) are critical indicators of cardiovascular and microvascular diseases (13, 14). These lipid ratios reflect two or three traditional lipid parameters, respectively, and could be better indicators to mirror the metabolic and clinical interactions between lipid fractions. Atherogenic plasma index is an independent risk factor for the occurrence of DM, and AIP has a predictive effect on the occurrence of macrovascular and microvascular diseases in the early stage of DM, but it is not known whether these indices are associated with the presence of DR (15, 16).

In the present study, we aimed to explore the association of arteriosclerosis-associated plasma indices with increasing severity of DR. We further investigated the correlations between these atherogenic indices and circulating levels of VEGF-A, VEGF-C, VEGF-D, and PlGF in patients with DM with and without DR to elucidate disease mechanisms that can be translated to novel therapeutic targets for DR.

## SUBJECTS AND METHODS

### Participants

This prospective study followed the principles of the Declaration of Helsinki and was approved by the Ethics Committee of Beijing Tongren Hospital, Capital Medical University. All subjects signed an informed consent form before participation.

A total of 131 patients with type 2 DM, including 77 males and 54 females, aged 27–76 years old were recruited from the outpatient clinic of Beijing Tongren Hospital from April 2016 to September 2020. The participants were assigned to the DM group if they had no DR [32 patients, aged 37–75 years, median (IQR): 56 (48–65) years], non-proliferative diabetic retinopathy (NPDR) [56 patients, aged 29–76 years, 56 (51–61)] years, and proliferative diabetic retinopathy (PDR) [43 patients, aged 27–74 years, 55 (49–60) years].

### Inclusion and Exclusion Criteria

Participants with type 2 DM were included in the study. Type 2 DM was defined according to the 2020 American Diabetes Association (ADA) guidelines of DM (5) and 2017 A Position Statement of DR (6). Those with the ability to provide informed consent were included in the study. Exclusion criteria included people with type 2 DM with macular edema secondary to other retinal vascular diseases; co-existent other retinal diseases such as age-related macular degeneration, uveitis, and inherited retinal diseases; recent history of posterior segment or cataract surgery; ocular media opacity; and unable to tolerate examinations due to

**Abbreviations:** ADA, American Diabetes Association; ACCORD study, action to control cardiovascular risk in diabetes study; AI, atherogenic index; AIP, atherogenic index of plasma; API, atherogenic plasma index; BCVA, best corrected visual acuity; DM, diabetes mellitus; DME, diabetic macular edema; DR, diabetic retinopathy; FIELD study, fenofibrate intervention and event lowering in diabetes study; HDL, high density lipoprotein; IQR, interquartile range; LDL, low density lipoprotein; NPDR, non-proliferative diabetic retinopathy; NCEP, national cholesterol education program; PDR, proliferative diabetic retinopathy; PlGF, placental growth factor; TC, total cholesterol; TG, triglycerides; VEGF, vascular endothelial growth factor; VTDR, vision threatening diabetic retinopathy.

severe system diseases. Patients with history of lipid disorders or on lipid-lowering therapy were also excluded.

## Eye Examination

### Routine Eye Examination

The participants underwent assessment of best-corrected visual acuity (BCVA), non-contact intraocular pressure (TX20 Automatic Non-contact Tonometer, Canon Co., Ltd., Tokyo, Japan), slit-lamp microscopic examination (SL-IE Slit Lamp Microscope, Topcon Co., Ltd., Tokyo, Japan), and fundus examination with mydriasis. Fundus photography (CR-1 non-mydriatic Fundus Camera, Canon Co., Ltd.) was done to capture at least two-field centered on optic disc and macula of both eyes. Ophthalmologists ascertained the DR status of the participants based on the International DR severity scale (6). Swept-source optical coherent tomography was applied (DRI OCT1 Atlantis scanner, Topcon Co., Ltd., Tokyo, Japan or Plex Elite 9000, Carl Zeiss Meditec, Inc., Oberkochen, German) for all the enrolled subjects. B-scan images were obtained by a  $9 \times 9$  mm scanning range mode. The DR status of the worse eye was recorded as an individual's DR grade. The participants were categorized into "PDR" group if they had retinal and/or optic disc neovascularization in at least one eye. Those with any other DR grade were categorized as NPDR group and participants with no DR in both eyes were assigned to the "DM" group.

Other data was also collected included age, gender, and duration of diabetes.

Blood biochemistry profile: Fasting biochemical examination was performed to detect the blood lipid profile of the participants. These include TC and LDL-C TGs, glycated hemoglobin (HbA1c), fasting blood glucose ect.

## Definition of Dyslipidemia

The definition was followed to the national cholesterol education program (NCEP) adult treatment panel-III (ATP-III) report in 2001 and the guidelines for the prevention and treatment of dyslipidemia in Chinese adults 2016. Dyslipidemia was defined as high cholesterol (TC) group ( $TC > 5.17$  mmol/L), high TG group ( $TG > 1.70$  mmol/L), or high low-density lipoprotein cholesterol (low-density lipoprotein cholesterol, LDL-C) group ( $LDL-C > 3.37$  mmol/L).

## Determination of the Cutoff Value of AIP, API, and AI by Receiver Operating Characteristic Curve

Arteriosclerosis indices including API ( $LDL-C/HDL-C$ ), AI [ $(TC-HDL-C)/HDL-C$ ], and AIP [ $\log(TG/HDL-C)$ ] were calculated. Atherogenic plasma index, AI, and AIP with high sensitivity and specificity were selected as the cutoff values on receiver operating characteristic (ROC) curve. Patients with  $API > 2.24$  (AUC: 0.746; sensitivity = 0.708, specificity = 0.517),  $AI > 2.91$  (AUC, 0.723; sensitivity = 0.629; specificity = 0.724) or  $AIP > 0.01$  (AUC 0.564; sensitivity = 0.607, specificity = 0.552) were assigned to high API, high AI, and high AIP groups, respectively.

## Determination of the Plasma Level of Cytokines

The Luminex technology (Luminex 200™ liquid chip detector, Millipore, Boston, Massachusetts, USA) was applied to detect the plasma level of cytokines, VEGF-A, VEGF-C, VEGF-D, and PlGF according to the manufacturer's instructions.

## Sample Size Calculation

Sample size was determined by using the Cochran's sample size formula and also reference the previous studies (12). Sample size was calculated at 95% confidence level with a margin of error of  $\pm 5\%$ . To detect the difference (0.83) between means of expression level of angio-cytokines with a significance level of ( $\alpha$ ) 0.05. The minimum sample size was calculated to be 25 in each group. However, since there is variability in the circulating level of angio-cytokines/serum lipid profiles and highly variable parameters, the sample size was increased to above 30 in the present study.

## Statistical Analysis

Statistical analysis was performed using SPSS software (SPSS, Inc., 23.0, Chicago, IL, USA). Normality was assessed by Kolmogorov-Smirnov test and Shapiro-Wilk test. Variance homogeneity was tested by the Levene's test. Age of participant, duration of diabetes, fasting blood glucose, glycosylated hemoglobin, hypertension, TG, TC, and LDL-C were described by means  $\pm$  standard deviation (mean  $\pm$  SD) or median (interquartile range). The comparisons among groups were analyzed by one-way analysis of variance (ANOVA) or the Kruskal-Wallis test. The circulating levels of cytokines VEGF-A, VEGF-C, VEGF-D, and PlGF were reported as mean  $\pm$  SD or median (interquartile range), comparisons between groups [DM, NPDR, and PDR groups, or DM and DR groups (combined NPDR with PDR as DR group)] was analyzed by independent sample *t*-test or Mann-Whitney U-test according to the data distribution (If the data were not normally distributed or variance homogeneity was not met). Bonferroni corrections was applied for comparison between the three groups. The effects of age, gender, the duration of diabetes, AI, API, AIP as well as their relationships with VEGF-A, VEGF-C, VEGF-D, and PlGF on DR patients were analyzed by multiple logistic regression analysis.  $P < 0.05$  indicated statistical significance.

## RESULTS

### Baseline Demographic and Clinical Characteristics

No statistically significant differences in age or gender were detected between the DM (with no DR), NPDR and PDR groups ( $P_{age} = 0.692$ ;  $P_{gender} = 0.756$ ). The average duration of DM was shorter in the DM group compared to that in the NPDR and the PDR group ( $12.59 \pm 5.79$  vs.  $9.14 \pm 6.76$  years,  $P_{NPDRvs.DM} = 0.013$ ;  $12.86 \pm 6.76$  vs.  $9.14 \pm 6.76$  years,  $P_{PDRvs.DM} = 0.021$ ). There was no statistical significance of fasting blood glucose in the DM, NPDR, and PDR groups ( $P = 0.151$ ). The difference between the NPDR and the DM groups [ $6.80$  (6.18–7.83) vs.  $7.75$  (7.03–8.98) years,  $P = 0.018$ ], PDR and the

**TABLE 1** | Baseline demographic, clinical characteristics, biochemical parameters, and the circulating angiogenic cytokines of the enrolled subjects.

Group	DM	NPDR	PDR	H/F/ $\chi^2$	P-value
Number	32	56	43	—	—
Age (years)	55.5 (48.25–65.00)	56 (50.50–61.00)	55 (49.00–60.00)	0.74 <sup>a</sup>	0.692
Female sex (%) (M/F)	43.75	37.5	44.17	0.56 <sup>b</sup>	0.756
Duration of DM (years)	9.14 ± 6.76	12.59 ± 5.79	12.86 ± 6.76	3.82 <sup>c</sup>	0.025*
Duration of HBP (years)	3.00 (0–10.00)	0.00 (0–5.00)	2.75 (0–10.00)	4.27 <sup>a</sup>	0.118
Fasting blood glucose (mmol/L)	7.46 (5.81–8.72)	8.25 (6.38–9.67)	8.46 (6.42–11.20)	3.78 <sup>a</sup>	0.151
HbA1c (%)	6.8 (6.18–7.83)	7.75 (7.03–8.98)	7.8 (6.68–9.10)	5.21 <sup>a</sup>	0.074
Triacylglycerol (mmol/L)	1.32 (1.01–2.60)	1.2 (0.82–1.81)	1.4 (0.92–2.49)	2.33 <sup>a</sup>	0.312
Cholesterol (mmol/L)	4.30 (3.91–5.03)	4.59 (3.74–5.68)	4.99 (4.32–5.89)	6.84 <sup>a</sup>	0.033*
LDL-C (mmol/L)	2.50 (2.05–3.09)	2.80 (2.03–3.60)	3.06 (2.58–3.92)	9.03 <sup>a</sup>	0.011*
HDL-C (mmol/L)	1.17 (1.00–1.40)	1.16 (0.98–1.48)	1.13 (0.98–1.43)	1.15 <sup>a</sup>	0.562
API	2.19 ± 0.71	2.42 ± 0.91	2.82 ± 0.95	5.05 <sup>a</sup>	0.008*
AI	2.75 ± 0.97	2.92 ± 1.17	3.44 ± 1.20	4.07 <sup>b</sup>	0.019*
AIP	0.08 ± 0.39	0.004 ± 0.31	0.11 ± 0.30	1.41 <sup>b</sup>	0.247
VEGF-A (pg/ml)	15.47 (11.40–25.92)	27.64 (20.62–35.32)	24.85 (18.59–33.54)	17.15 <sup>a</sup>	<0.001*
VEGF-C (pg/ml)	52.61 (13.41–150.07)	87.76 (55.69–142.05)	99.82 (53.81–198.35)	4.87 <sup>a</sup>	0.088
VEGF-D (pg/ml)	129.31 (47.14–218.77)	248.54 (150.45–428.89)	274.2 (172.90–401.96)	19.70 <sup>a</sup>	<0.001*
PIGF (pg/ml)	1.41 (0.58–2.44)	2.69 (1.89–3.31)	2.41 (1.65–3.87)	16.38 <sup>a</sup>	<0.001*

DM, diabetes mellitus; NPDR, non-proliferative diabetic retinopathy; PDR, proliferative diabetic retinopathy; HbA1c, hemoglobin; LDL-C, low density lipoprotein cholesterol; HDL-C, high density lipoprotein cholesterol; VEGF, vascular endothelial growth; PIGF, placental growth factor; API/AI/AIP, atherogenic index of plasma; API, atherogenic plasma index, defined as LDL-C/HDL-C; AI, atherogenic index, was calculated as TC-(LDL-C)/HDL-C; AIP, atherogenic index of plasma, defined as log triglycerides TG/HDL-C; PIGF, placental growth factor; VEGF, vascular endothelial growth factor.

\*Statistically significant:  $P \leq 0.05$ . According to the type of data and the data distribution, one-way ANOVA analysis (a), Post-hoc LSD correction. b Kruskal–Wallis (a) were applied.

DM groups [6.80 (6.18–7.83) vs. 7.80 (6.68–9.10) years,  $P = 0.017$ ] of the glycosylated hemoglobin levels were statistically significant. No significant difference was detected in the duration of hypertension among the three groups ( $\chi^2 = 4.27$ ,  $P = 0.118$ ) (Table 1).

## Correlations Between Lipid Profile and DR Severity

The level of TC in the three groups differed significantly [4.30 (3.91–5.03) vs. 4.59 (3.74–5.68) vs. 4.99 (4.32–5.89) mmol/L,  $P = 0.033$ ], with the level of TC in the PDR group being higher than that in the DM group [4.99 (4.32–5.89) vs. 4.30 (3.91–5.03) mmol/L,  $P = 0.006$ ]. In addition, LDL-C also showed statistical differences [2.50 (2.05–3.09) vs. 2.80 (2.03–3.60) vs. 3.06 (2.58–3.92) mmol/L,  $P = 0.011$ ], with the level in the PDR group being higher than that in the DM group [3.06 (2.58–3.92) vs. 2.80 (2.03–3.60) mmol/L,  $P = 0.002$ ]. No statistically significant difference was detected in the three groups with respect to TG and HDL ( $P_{TG} = 0.312$ ;  $P_{HDL-C} = 0.562$ ) (Table 1).

## Associations Between Atherogenic Indices and DR

The API in the three DR groups showed a statistically significant difference ( $2.19 \pm 0.71$  vs.  $2.42 \pm 0.91$  vs.  $2.82 \pm 0.95$ ,  $P = 0.008$ ), with the value of the PDR group higher than that of the DM group ( $P = 0.003$ ). The difference of AI in the three groups also differed significantly ( $2.75 \pm 0.97$  vs.  $2.92 \pm 1.17$  vs.  $3.44 \pm 1.20$ ,  $P = 0.019$ ), with the value in the PDR group significantly higher than that in the NPDR and DM group ( $P_{PDRvs.NPDR} = 0.024$ ,

$P_{PDRvs.DM} = 0.010$ ). There was no difference of the AIP-value between the three groups ( $P = 0.247$ ) (Table 1).

## Correlations Between the Circulating Level of Angiogenic Cytokines and DR Severity

The plasma level of VEGF-A differed significantly [15.47 (11.40–25.92) vs. 27.64 (20.62–35.32) vs. 24.85 (18.59–33.54) pg/ml,  $P < 0.001$ ], with the level of VEGF-A in NPDR and PDR groups significantly higher than that in the DM group ( $P_{NPDRvs.DM} = 0.002$ ,  $P_{PDRvs.DM} = 0.001$ ). There was also a significant difference in VEGF-D between the three groups ( $P < 0.001$ ), with higher level in NPDR and PDR groups than that in DM group ( $P_{NPDRvs.DM} < 0.001$ ,  $P_{PDRvs.DM} < 0.001$ ). The level of PIGF in the three groups differed significantly [1.41 (0.58–2.44) vs. 2.69 (1.89–3.31) vs. 2.41 (1.65–3.87) pg/ml,  $P < 0.001$ ], with the level of PIGF in the NPDR and PDR groups significantly higher than that in the DM group [2.69 (1.89–3.31) vs. 1.41 (0.58–2.44) pg/ml,  $P_{NPDRvs.DM} = 0.012$ , 2.41 (1.65–3.87) vs. 1.41 (0.58–2.44) pg/ml,  $P_{PDRvs.DM} < 0.001$ ]. No statistical significance was detected in the three groups with the circulating level of VEGF-C ( $P = 0.088$ ) (Table 1).

## Associations Between Atherogenic Indices and the Circulating Level of Angiogenic Cytokines

There was a significant difference in the plasma level of VEGF-D between the normal and abnormal API group [154.10 (71.78–274.36) vs. 255.58 (147.91–400.44) pg/ml,  $P = 0.009$ ]. Similarly, differed expression level of VEGF-D was found between the



**TABLE 2 |** Comparison of the circulating level of VEGF-A, VEGF-C, VEGF-D, and PlGF in patients with abnormal and normal arteriosclerosis-associated plasma indices (API, AI, AIP).

Cytokines	VEGF-A (pg/ml)	VEGF-C (pg/ml)	VEGF-D (pg/ml)	PlGF (pg/ml)
<b>API</b>				
Normal API group	22.45 (14.59–32.91)	80.58 (36.06–127.49)	154.1 (71.78–274.36)	2.13 ± 1.32
Abnormal API group	24.85 (18.24–34.29)	90.86 (53.81–182.03)	255.58 (147.91–400.44)	2.54 ± 1.28
<i>t/z</i>	–1.25 <sup>c</sup>	–1.54 <sup>c</sup>	–2.61 <sup>c</sup>	–1.63 <sup>b</sup>
<i>P-value</i>	0.211	0.124	0.009*	0.106
<b>AI</b>				
Normal AI group	22.77 (15.35–31.86)	80.58 (37.28–127.49)	179.77 (72.09–280.18)	2.16 ± 1.26
Abnormal AI group	26.8 (18.24–35.72)	101.57 (53.81–187.19)	255.59 (147.91–400.45)	2.59 ± 1.32
<i>t/z</i>	–1.70 <sup>c</sup>	–1.85 <sup>c</sup>	–2.40 <sup>c</sup>	–1.76 <sup>b</sup>
<i>P-value</i>	0.09	0.064	0.016*	0.081
<b>AIP</b>				
Normal AIP group	23.08 (17.63–32.30)	82.65 (38.17–145.62)	192.47 (83.52–286.23)	2.25 ± 1.28
Abnormal AIP group	24.85 (17.63–34.53)	99.82 (51.41–175.89)	252.01 (137.00–389.96)	2.50 ± 1.33
<i>t/z</i>	–0.94 <sup>c</sup>	–1.15 <sup>c</sup>	–1.60 <sup>c</sup>	–1.01 <sup>b</sup>
<i>P-value</i>	0.346	0.249	0.111	0.316

\*Statistically significant:  $P \leq 0.05$ . According to the type of data and the data distribution, <sup>a</sup> Kruskal-Wallis test, <sup>b</sup> independent-sample *t*-test, and <sup>c</sup> Mann-Whitney *U*-test were applied. VEGF, vascular endothelial growth; PlGF, placental growth factor; DM, diabetes mellitus; NPDR, non-proliferative diabetic retinopathy; PDR, proliferative diabetic retinopathy; API, atherogenic plasma index (LDL-C/HDL-C); AI, atherogenic index: (TC-(LDL-C))/HDL-C; AIP, atherogenic index of plasma: log (TG/HDL-C).

normal AI and abnormal group [179.77 (72.09–280.18) vs. 255.59 (147.91–400.45) pg/ml,  $P = 0.016$ ]. There is no significant difference in the expression level of VEGF-A, VEGF-C, and PlGF in between the normal API, AI, and AIP groups. No significant difference was found in the expression level of VEGF-D between the normal AIP and abnormal AIP groups (Table 2).

### Associations Between VEGF-A, -B, -C, -D, PGF in All Patients With Abnormal and Normal TC, TG, LDL-C, and HDL-C

The level of VEGF-A, VEGF-C, VEGF-D, PlGF is significantly higher in the abnormal TC group in comparison with the normal TC group ( $P_{VEGF-A} = 0.008$ ;  $P_{VEGF-C} = 0.001$ ,  $P_{VEGF-D} = 0.035$ ;  $P_{PlGF} = 0.004$ ). Similarly, in the abnormal LDL-C group, the level of VEGF-A, VEGF-C, VEGF-D, and PlGF is significantly higher than that in the normal LDL-C group ( $P_{VEGF-A} = 0.032$ ;  $P_{VEGF-C} = 0.006$ ;  $P_{VEGF-D} = 0.018$ ,  $P_{PlGF} = 0.006$ ). No statistical difference was found between the circulating level of VEGF-A, -C, -D, and PlGF in the abnormal TG, HDL-C groups, compared with that in the normal TG and HDL-C groups, respectively, indicating the circulating level of the angiogenic cytokines is correlated with the abnormal serum level of TC and LDL-C (Table 3).

### Multiple Ordinal Logistic Regression Models Show the Correlations of AI, AIP, API, and Circulating Levels of VEGF-A, VEGF-C, VEGF-D, PlGF in Normal, DM, or DR Groups

Table 4 shows the correlations of the plasma level of VEGF-A, VEGF-C, VEGF-D, and PlGF with atherogenic indices on

the occurrence and severity of DR using multiple ordinal logistic regression models. When DM, NPDR, and PDR were considered as independent variables, after controlling the duration of diabetes and hypertension, the serum level of hemoglobins and fasting glucose, AI and API are strong risk factors for the occurrence and severity of DR. Atherogenic index is associated with VEGF-D [AI:  $P = 0.038$ , OR = 1.38 (1.02–1.86); VEGF-D:  $P = 0.002$ , OR = 1.00 (1.00–1.01)] and PlGF [AI:  $P = 0.021$ , OR = 1.43 (1.06–1.92); PlGF:  $P = 0.004$ , OR = 1.50 (1.14–1.98)] contributed to DR (Table 4A). Atherogenic plasma index is associated with VEGF-D (Table 4B): [API:  $P = 0.027$ , OR = 1.56 (1.05–2.30); VEGF-D:  $P = 0.002$ , OR = 1.00 (1.00–1.01)] and PlGF [API:  $P = 0.011$ , OR = 1.66 (1.12–2.47); PlGF:  $P = 0.005$ , OR = 1.49 (1.13–1.96)] (Table 4B). The correlations between AIP and VEGF-C, VEGF-D, VEGF-A, PlGF were summarized in Table 4C.

### The Arteriosclerosis-Associated Plasma Indices AI and API Are More Reliable DR Predictors Than the Traditional Lipid Parameters LDL-C, TC TG, and HDL-C

The above analysis has proved that API and AI strongly associated with DR severity. A greater area under the ROC (AUC) means a more useful test of the statistical model. The AUC of AI (AUC:0.72; 95% CI: 0.62–0.82) and API (AUC: 0.75; 95% CI: 0.65–0.84) is much higher than TC (AUC:0.68; 95% CI: 0.58–0.78), TG (AUC: 0.54; 95% CI 0.41–0.67) LDL-C (AUC:0.72; 95% CI: 0.62–0.82), HDL-C (AUC:0.57, 95% CI: 0.45–0.69), indicating that both API and AI have higher capacity to differential DR.

**TABLE 3 |** Comparison of the circulating level of VEGF-A, VEGF-C, VEGF-D, and PlGF in all patients with abnormal and normal TC, LDL, TG, and HDL.

	VEGF-A (pg/ml)	VEGF-C (pg/ml)	VEGF-D (pg/ml)	PlGF (pg/ml)
<b>TC:</b>				
Normal TC group	22.45 (17.09–32.30)	77.16 (43.40–125.32)	201.47 (122.13–335.91)	2.14 (0.99–3.10)
Abnormal TC group	27.64 (19.86–37.45)	122.65 (61.12–219.99)	266.55 (142.79–427.94)	2.84 (1.78–3.66)
<i>z</i>	–2.66 <sup>b</sup>	–3.31 <sup>b</sup>	–2.11 <sup>b</sup>	–2.87 <sup>b</sup>
<i>P-value</i>	0.008*	0.001*	0.035*	0.004*
<b>LDL-C:</b>				
Normal LDL-C group	22.77 (17.41–32.30)	78.50 (42.61–128.59)	196.32 (102.48–335.91)	2.14 (1.00–3.13)
Abnormal LDL-C group	27.64 (19.33–37.06)	118.52 (55.69–212.44)	266.55 (178.27–433.74)	2.84 (1.69–3.66)
<i>z</i>	–2.14 <sup>b</sup>	–2.77 <sup>b</sup>	–2.36 <sup>b</sup>	–2.74 <sup>b</sup>
<i>P-value</i>	0.032*	0.006*	0.018*	0.006*
<b>TG:</b>				
Normal TG group	24.85 (18.59–34.20)	82.65 (46.90–140.71)	245.08 (128.21–395.90)	2.47 (1.34–3.28)
Abnormal TG group	24.49 (16.68–32.01)	115.51 (48.03–207.07)	209.77 (121.46–361.79)	1.85 (1.31–3.51)
<i>z</i>	–0.84 <sup>b</sup>	–1.48 <sup>b</sup>	–0.51 <sup>b</sup>	–0.74 <sup>b</sup>
<i>P-value</i>	0.400	0.140	0.610	0.458
<b>HDL-C:</b>				
Normal HDL-C group	24.85 (17.76–33.56)	99.82 (47.23–186.00)	227.54 (110.30–405.02)	2.41 ± 1.34
Abnormal HDL-C group	24.86 (18.06–33.30)	81.95 (46.60–117.01)	233.87 (136.74–363.15)	2.33 ± 1.17
<i>t/z</i>	–0.29 <sup>b</sup>	–0.99 <sup>b</sup>	–0.10 <sup>b</sup>	–0.37 <sup>a</sup>
<i>P-value</i>	0.772	0.321	0.921	0.712

VEGF, vascular endothelial growth; PlGF, placental growth factor; TC, cholesterol; TG, triglycerides; LDL-C, low-density lipoprotein cholesterol; HDL-C, high density lipoprotein cholesterol.

\*Statistically significant:  $P \leq 0.05$ . According to the type of data and the data distribution, <sup>a</sup> independent-sample *t*-test, and <sup>b</sup> Mann-Whitney *U*-test were applied.

## DISCUSSION

In this study, we found that serum TC, LDL-C, AI, and API in the NPDR and PDR groups were significantly higher than those in the DM group. The circulating level of PlGF, VEGF-A, and C were significantly correlated with the severity of DR. Multivariate logistic regression showed that diabetes duration, AI and API are strong risk factors for DR. Furthermore, AI and API have synergic effects with VEGF-D and PlGF with various severity levels of DR, indicating AI and API are novel predictors of DR. This study, for the first time, clarified and elucidated the pathological mechanism of dyslipidemia in the pathogenesis of DR.

It has been reported that the prevalence of DR is 35% globally by a meta-analysis (17). The duration of DM is a key risk factor for DR. In addition, systemic factors such as hyperglycemia, hypertension and hyperlipidemia contribute and accelerate the progression and deterioration of DR. Several studies have indicated that a high level of TC and LDL-C promotes the occurrence and progression of retinopathy and coronary heart disease in DM (18–20). The exact mechanism(s) underlying hyperlipidemia-mediated DR has not yet been elucidated. The current study provided the first evidence that abnormal lipid metabolism promotes the occurrence and development of DR by upregulating the expression of VEGF-A, VEGF-C, VEGF-D, and PlGF in the circulating of patients with DR.

## Abnormal Lipid Metabolism Is Closely Correlated to the Occurrence and Progression of DR

The Wisconsin Epidemiologic Study of DR first identified that a long-term increase in the serum level of TC might be a risk factor for hard exudates in DR in 1991 (21), FIELD and ACCORD study further confirmed that lipid-lowering therapy with fenofibrate significantly reduce the progression of DR and the need for laser treatment (3, 22), indicating that intensive lipid control is correlated with improved clinical prognosis. Statins are the most effective drug to reduce TC and LDL-C. However, the role of statins is more profound in cardiovascular disease than DR (3, 22–24).

Our study found that the levels of TC and LDL-C in the NPDR and PDR groups were significantly higher than those in the DM group, which are consistent with the results of previous studies on type 1 DM (25). In addition, the serum levels of TC and LDL-C in PDR patients were significantly increased compared to those patients with NPDR and DM, suggesting that the increased levels of TC and LDL-C in serum accelerate the progression of DR.

## AI and API Are Independent Risk Factors for DR

In this study, the lipid metabolism indices were used to explore the relationship between dysregulated lipid metabolism and the expression level of circulating cytokines and DR severity. In routine clinical practice, LDL-C is calculated (by the Friedewald

**TABLE 4 |** Multiple ordinal logistic regression models showing that AI and API contributed to the occurrence and severity of DR associated with elevated circulating level of VEGF-D and PIGF.

		Variable	Estimate	StdErr	P-value	OR
(A)						
	Model 1	AI	0.39	0.15	0.010*	1.48 (1.10–1.99)
		VEGF-A	0.02	0.01	0.098	1.02 (1.00–1.04)
	Model 2	AI	0.35	0.16	0.027*	1.41 (1.04–1.92)
		VEGF-C	0.00	0.00	0.093	1.00 (1.00–1.01)
	Model 3	AI	0.32	0.15	0.038*	1.38 (1.02–1.86)
		VEGF-D	0.00	0.00	0.002*	1.00 (1.00–1.01)
	Model 4	AI	0.35	0.15	0.021*	1.43 (1.06–1.92)
		PIGF	0.41	0.14	0.004*	1.50 (1.14–1.98)
(B)						
	Model 1	API	0.56	0.20	0.004*	1.74 (1.19–2.59)
		VEGF-A	0.02	0.01	0.093	1.02 (1.00–1.04)
	Model 2	API	0.50	0.20	0.013*	1.65 (1.11–2.45)
		VEGF-C	0.00	0.00	0.105	1.00 (1.00–1.01)
	Model 3	API	0.44	0.20	0.027*	1.56 (1.05–2.30)
		VEGF-D	0.00	0.00	0.002*	1.00 (1.00–1.01)
	Model 4	API	0.50	0.20	0.011*	1.66 (1.12–2.45)
		PIGF	0.40	0.14	0.005*	1.49 (1.13–1.96)
(C)						
	Model 1	AIP	0.39	0.50	0.444	1.47 (0.55–3.95)
		VEGF-A	0.02	0.01	0.084	1.02 (1.00–1.04)
	Model 2	AIP	0.14	0.52	0.783	1.15 (0.42–3.20)
		VEGF-C	0.00	0.00	0.037	1.00 (1.00–1.01)
	Model 3	AIP	0.34	0.51	0.507	1.40 (0.52–3.82)
		VEGF-D	0.00	0.00	0.001*	1.00 (1.00–1.01)
	Model 4	AIP	0.27	0.51	0.593	1.31 (0.49–3.55)
		PIGF	0.44	0.14	0.002*	1.55 (1.18–2.04)

API, atherogenic plasma index (LDL-C/HDL-C); AI, atherogenic index (TC-(LDL-C))/HDL-C; DM, diabetes mellitus; NPDR, non-proliferative diabetic retinopathy; PDR, proliferative diabetic retinopathy; PIGF, placental growth factor; VEGF-D, vascular endothelial growth factor D; HBP, hypertension; HbA1c, hemoglobin A1c. When DM, NPDR, and PDR were considered as the independent variable, after controlling the age, sex, duration of diabetes and hypertension, fast glucose, and hemoglobin, the multiple ordinal regression models show that AI and API contributed to the occurrence and severity of DR associated with elevated plasma level of VEGF-D and PIGF. \* $P \leq 0.05$  is considered statistical significance.

formula) than measured directly. Several studies have found that the estimation of LDL-C has significant limitations, especially in individuals with hypertriglyceridemia with DM (it may contain abnormal composition of the TG-rich lipoproteins which is not considered in the Friedewald formula) (14, 26–28).

Non-HDL-C represents the cholesterol components carried by atherogenic lipoproteins such as LDL, very low density lipoprotein, and intermediate density lipoprotein and has been recommended as the primary lipid-lowering target by the 2019 American College of Cardiology (ACC) and American Heart Association (AHA) guidelines on the management of blood cholesterol (29).

It has been confirmed by studies in cardiovascular diseases that AI and API reflect two or three traditional parameters, which are simple and economic and can be used as biomarkers. Atherogenic index and API have several key advantages than the traditional lipid parameters: they have explicit pathophysiologic link to the development of atherosclerosis, robust from a laboratory measurement standpoint etc. (14) API, AI, and

AIP have been applied for assessing plasma lipid homeostasis and are also implicated in the pathogenesis of macrovascular complications, especially in the early stage of the disease when the unaltered concentration of various lipids is increased (30). Atherogenic plasma index is a sensitive predictor of asymptomatic type 2 DM patients with coronary atherosclerosis and the incidence of microvascular complications and peripheral neuropathy in DM patients increased significantly with the increased AIP (15, 31). Since this is the first study to apply the indices in eye study, we used the ROC curve, the objective method to obtain the cut off value, and also referred to the value of the lipid metabolism in cardiovascular and atherosclerosis studies [API: 0.16–2.24 (32), AI: 3.21–3.37 (33), AIP: 0.6–0.21 (34, 35)].

In this study, we found that the AUC of AI (TC-(HDL-C)/HDL-C) (a) and API (LDL-C/HDL-C) is significantly higher than TC, TG, LDL-C, and HDL-C, indicating these simpler combined parameters have higher diagnostic capacity than the traditional parameters for DR. Furthermore, logistic regression

analysis showed that AI and API are independent risk factors for DR, and provide evidence for a link between lipid metabolism and DR.

## **Dysregulated Circulating Lipid Metabolism Promotes the Occurrence and Development of DR by Upregulating VEGF-A, VEGF-C, VEGF-D, and PlGF**

VEGF-A is not only the most important vascular leakage inducer but also a key angiogenesis factor and a target of anti-VEGF therapy in ocular conditions (36, 37). However, macular oedema does not resolve completely in a number of patients with DR suggesting that there are other influencers in the pathogenesis of DR. Our study shows that other family members of VEGF are also raised in DR, indicating the need for novel molecular targets. Both VEGF-C and VEGF-D are secreted glycoproteins that exhibit structural homology but have differential receptor binding (Flk-1 and Flt-3, respectively) and regulatory mechanism is a vital mediator to angiogenesis in ischemic heart disease in type 2 DM (38). These cytokines have been demonstrated as independent predictors for suspected coronary artery disease and are associated with all-cause mortality (39). In a previous study, VEGF-A-FLK-1 signaling has been shown as a primary mediator of endothelial cell mitogenesis, survival, and microvascular permeability (40). Together with VEGF-A, VEGF-C, and VEGF-D promote blood vessel development (angiogenesis) by binding and activating VEGF-R-2 and VEGF-R-3. VEGF-C is also a potent inducer of vascular permeability and angiogenesis in AMD. The ongoing phase III trial is investigating a soluble form of VEGF-R-3, which comprises the extracellular domains 1–3 of human VEGF-R3. In addition, the Fc fragment of human IgG1 suppresses the binding of VEGF-C and -D to VEGF-R 2 and 3, respectively (ClinicalTrials.gov Identifier: NCT02543229). The positive outcome from the phase II trial has shown that the combined intravitreal administration of OPT-302 and ranibizumab is better than ranibizumab alone for the patient's vision prognosis. Furthermore, PlGF is deemed to play a crucial role in both experimental animal models and retinal vascularization (41, 42). A high expression level of PlGF has also been detected in vitreous and PDR membrane in patients with PDR (43–46).

In the present study, based on a significant body of evidence in preclinical and clinical studies that support the pathological function of VEGF-A, -C, -D, and PlGF, a protein chip-Luminex technology was applied to quantitatively detect the circulating expression levels in patients with abnormal lipid metabolism group and normal group, respectively. We found that the circulating level of VEGF-D significantly contributed to the occurrence and severity of DR associated with AI and API, confirmed the previous finding that VEGF-D is also an important regulator of genes related to lipid metabolism and inflammation (47–50). Our results also provide evidence for the first time that besides diabetes duration, AI, API, VEGF-D, and PlGF are strong risk factors for the occurrence and progression of DR. Atherogenic index and API have synergic effects with

VEGF-D and PlGF. Placental growth factor may release VEGF-A by binding to VEGF-R-1 to activate VEGF-R-2, thereby indirectly stimulating angiogenesis, or combined with VEGF-R-1 to promote the proliferation of endothelial cells and angiogenesis (44). Animal experiments also have shown that PlGF promotes the infiltration of macrophages in early atherosclerotic lesions in apolipoprotein E deficiency (Apo E<sup>-/-</sup>) mice and rabbits with high TC. In this study, by logistic regression analysis, after controlling the age, sex, duration of diabetes and VEGF-A, -C, -D, the serum level of TC and LDL was found to concomitant with higher level expression of PlGF in either DM or DR group, HDL was found to be negatively with PlGF expression. Thus, it could be speculated that high non-HDL-C promotes the development of DR by upregulating the expression of PlGF.

Presently, the specific regulatory mechanism of abnormal lipid metabolism involved in the progression of DR is yet to be clarified. Nevertheless, the present study has some limitations. Due to the small sample size, confounding factors could not be eliminated in the analysis process, and various measurement methods and correction factors might also affect the results of this study. Well-matched and large-scale prospective clinical trials and cohort studies are warranted to validate the conclusions in the study.

In summary, the ratios of LDL-C/HDL-C and TC-LDL-C/HDL-C are useful and simple indicators of DR. The present study further found that dysregulation of lipid metabolism promotes the development of DR and are associated with upregulation of circulating VEGF-A, VEGF-C, VEGF-D, and PlGF. The current results may partly explain why the response to anti-VEGF varies between individuals. Strengthening the management of blood lipids in patients with DM may help to reduce the levels of VEGF and PlGF and resultant oedema. Therefore, patients with DM should focus on the management of blood lipids in addition to their glycemic status. Further understanding the correlation between the arteriosclerosis-associated plasma indices and circulating levels of angiogenic cytokines can be translated to novel therapeutic targets for DR.

## **DATA AVAILABILITY STATEMENT**

The original contributions presented in the study are included in the article/supplementary materials, further inquiries can be directed to the corresponding author.

## **ETHICS STATEMENT**

The studies involving human participants were reviewed and approved by Beijing Tongren Hospital. The patients/participants provided their written informed consent to participate in this study.

## **AUTHOR CONTRIBUTIONS**

XZ contributed to conception and design of the study, perform the statistical analysis, revise and draft the manuscript. BQ and QW organized the database, performed the experiments,



performed the statistical analysis and drafted the manuscript. SS provided comments and revised the manuscript. LZ, RX, and WK helped to enroll patients and were involved in the experiments. YW and LL performed the statistical analysis. All authors contributed to manuscript revision, read, and approved the submitted version.

## REFERENCES

- Cheung N, Mitchell P, Wong TY. Diabetic retinopathy. *Lancet*. (2010) 376:124–36. doi: 10.1016/S0140-6736(09)62124-3
- Sayin N, Kara N, Pekel G. Ocular complications of diabetes mellitus. *World J Diabetes*. (2015) 6:92–108. doi: 10.4239/wjd.v6.i1.92
- Keech AC, Mitchell P, Summanen PA, O'Day J, Davis TME, Moffitt MS, et al. Effect of fenofibrate on the need for laser treatment for diabetic retinopathy (FIELD study): a randomised controlled trial. *Lancet*. (2007) 370:1687–97. doi: 10.1016/S0140-6736(07)61607-9
- Chew EY, Ambrosius WT. Update of the ACCORD eye study. *N Engl J Med*. (2011) 364:188–9. doi: 10.1056/NEJMc1011499
- Diabetic Retinopathy Clinical Research Network, Wells JA, Glassman AR, Ayala AR, Jampol LM, Aiello LP, Antoszyk AN, et al. Aflibercept, bevacizumab, or ranibizumab for diabetic macular edema. *N Engl J Med*. (2015) 372:1193–203. doi: 10.1056/NEJMoa1414264
- Diabetic Retinopathy Clinical Research Network, Bressler SB, Ayala AR, Bressler NM, Melia M, Qin H, Ferris FL, et al. Persistent macular thickening after ranibizumab treatment for diabetic macular edema with vision impairment. *JAMA Ophthalmol*. (2016) 134:278–85. doi: 10.1001/jamaophthalmol.2015.5346
- Diabetic Retinopathy Clinical Research Network, Bressler NM, Beaulieu WT, Glassman AR, Blinder KJ, Bressler SB, Jampol LM, et al. Persistent macular thickening following intravitreal aflibercept, bevacizumab, or ranibizumab for central-involved diabetic macular edema with vision impairment: a secondary analysis of a randomized clinical trial. *JAMA Ophthalmol*. (2018) 136:257–69. doi: 10.1001/jamaophthalmol.2017.6565
- Diabetic Retinopathy Clinical Research Network, Elman MJ, Aiello LP, Beck RW, Bressler NM, Bressler SB, Edwards AR, et al. Randomized trial evaluating ranibizumab plus prompt or deferred laser or triamcinolone plus prompt laser for diabetic macular edema. *Ophthalmology*. (2010) 117:1064–77.e35. doi: 10.1016/j.ophtha.2010.02.031
- Benarous R, Sasongko MB, Qureshi S, Fenwick E, Dirani M, Wong TY, et al. Differential association of serum lipids with diabetic retinopathy and diabetic macular edema. *Invest Ophthalmol Vis Sci*. (2011) 52:7464–9. doi: 10.1167/iovs.11-7598
- ACCORD Eye Study Group, Chew EY, Ambrosius WT, Davis MD, Danis RP, Gangaputra S, Greven CM, et al. Effects of medical therapies on retinopathy progression in type 2 diabetes. *N Engl J Med*. (2010) 367:2458. doi: 10.1056/NEJMoa1001288
- Miljanovic B, Glynn RJ, Nathan DM, Manson JE, Schaumberg DA, A. prospective study of serum lipids and risk of diabetic macular edema in type 1 diabetes. *Diabetes*. (2004) 53:2883–92. doi: 10.2337/diabetes.53.11.2883
- Klein BEK, Myers CE, Howard KP, Klein R. Serum lipids and proliferative diabetic retinopathy and macular edema in persons with long-term type 1 diabetes mellitus: the Wisconsin Epidemiologic Study of Diabetic Retinopathy. *JAMA Ophthalmol*. (2015) 133:503–10. doi: 10.1001/jamaophthalmol.2014.5108
- Dobiášová M, Frohlich J. The plasma parameter log (TG/HDL-C) as an atherogenic index: correlation with lipoprotein particle size and esterification rate in apoB-lipoprotein-depleted plasma (FER(HDL)). *Clin Biochem*. (2001) 37:583–8. doi: 10.1016/S0009-9120(01)00263-6
- National Lipid Association Taskforce on Non-HDL Cholesterol. Blaha MJ, Blumenthal RS, Brinton EA, Jacobson TA. The importance of non-HDL cholesterol reporting in lipid management. *J Clin Lipidol*. (2008) 2:267–73. doi: 10.1016/j.jacl.2008.06.013
- Hermans MP, Ahn SA, Rousseau MF. The atherogenic dyslipidemia ratio [log(TG)/HDL-C] is associated with residual vascular risk, beta-cell function loss and microangiopathy in type 2 diabetes females. *Lipids Health Dis*. (2012) 11:132. doi: 10.1186/1476-511X-11-132
- Wei L, Wei M, Chen L, Liang S, Gao F, Cheng X, et al. Low-density lipoprotein cholesterol: high-density lipoprotein cholesterol ratio is associated with incident diabetes in Chinese adults: a retrospective cohort study. *Diabetes Invest*. (2021) 12:91–8. doi: 10.1111/jdi.13316
- Yau JWY, Rogers SL, Kawasaki R, Lamoureux EL, Kowalski JW, Bek T, et al. Global prevalence and major risk factors of diabetic retinopathy. *Diabetes Care*. (2012) 35:556–64. doi: 10.2337/dc11-1909
- Srinivasan S, Raman R, Kulothungan V, Swaminathan G, Sharma T. Influence of serum lipids on the incidence and progression of diabetic retinopathy and macular oedema: Sankara Nethralaya Diabetic Retinopathy Epidemiology And Molecular genetics Study-II. *Clin Exp Ophthalmol*. (2017) 45:894–900. doi: 10.1111/ceo.12990
- Itoh H, Ueshima K, Komuro I. Intensive treat-to-target statin therapy in high-risk Japanese patients with hypercholesterolemia and diabetic retinopathy: report of a randomized study. *Diabetes Care*. (2018) 41:1275–84. doi: 10.2337/dci18-0028
- Zhou Y, Wang C, Shi K, Yin X. Relationship between dyslipidemia and diabetic retinopathy: a systematic review and meta-analysis. *Medicine (Baltimore)*. (2018) 97:e12283. doi: 10.1097/MD.00000000000012283
- Klein BE, Moss SE, Klein R, Surawicz TS. The wisconsin epidemiologic study of diabetic retinopathy XIII. Relationship of serum cholesterol to retinopathy and hard exudate. *Ophthalmology*. (1991) 98:1261–5. doi: 10.1016/S0161-6420(91)32145-6
- Action to Control Cardiovascular Risk in Diabetes Eye Study Research Group. Chew EY, Davis MD, Danis RP, Lovato JE, Perdue LH, Greven C, et al. The effects of medical management on the progression of diabetic retinopathy in persons with type 2 diabetes: the Action to Control Cardiovascular Risk in Diabetes (ACCORD) Eye Study. *Ophthalmology*. (2014) 121:2443–51. doi: 10.1016/j.ophtha.2014.07.019
- Nielsen SF, Nordestgaard BG. Statin use before diabetes diagnosis and risk of microvascular disease: a nationwide nested matched study. *Lancet Diabetes Endocrinol*. (2014) 2:894–900. doi: 10.1016/S2213-8587(14)70173-1
- Kang EY-C, Chen T-H, Garg SJ, Sun C-C, Kang J-H, Wu W-C, et al. Association of statin therapy with prevention of vision-threatening diabetic retinopathy. *JAMA Ophthalmol*. (2019) 137:363–71. doi: 10.1001/jamaophthalmol.2018.6399
- Wong TY, Cheung N, Tay WT, Wang JJ, Aung T, Saw SM, et al. Prevalence and risk factors for diabetic retinopathy: the Singapore Malay Eye Study. *Ophthalmology*. (2008) 115:1869–75. doi: 10.1016/j.ophtha.2008.05.014
- Expert Panel on Detection, Evaluation, and Treatment of High Blood Cholesterol in Adults. Executive Summary of the third report of the national cholesterol education program (NCEP) expert panel on detection, evaluation, and treatment of high blood cholesterol in adults (adult treatment panel III). *JAMA*. (2001) 285:2486–97. doi: 10.1001/jama.285.19.2486
- Tremblay AJ, Morrisette H, Gagné J-M, Bergeron J, Gagné C, Couture P. Validation of the Friedewald formula for the determination of low-density lipoprotein cholesterol compared with beta-quantification in a large population. *Clin Biochem*. (2004) 37:785–90. doi: 10.1016/j.clinbiochem.2004.03.008
- Friedewald WT, Levy RI, Fredrickson DS. Estimation of the concentration of low-density lipoprotein cholesterol in plasma, without use of the preparative ultracentrifuge. *Clin Chem*. (1972) 18:499–502. doi: 10.1093/clinchem/18.6.499

## FUNDING

This work was supported by the National Natural Science Foundation of China (Grants 81570850, 81170859, and 82070988) and the Ministry of Science and Technology Foundation of China (Grant 2016YFC1305604).

29. Pwf W, Polonsky TS, Miedema MD, Khera A, Kosinski AS, Kuvini JT. Correction to: Systematic Review for the 2018 AHA/ACC/AACVPR/AAPA/ABC/ACPM/ADA/AGS/APhA/ASPC/NLA/PCNA guideline on the management of blood cholesterol: a report of the American College of Cardiology/American Heart Association Task Force on Clinical Practice Guidelines. *Circulation*. (2019) 139:e1144–61. doi: 10.1161/CIR.0000000000000700
30. Brizzi P, Tonolo G, Carusillo F, Malaguarnera M, Maioli M, Musumeci S. Plasma lipid composition and LDL oxidation. *Clin Chem Lab Med*. (2003) 41:56–60. doi: 10.1515/CCLM.2003.010
31. Fujihara K, Suzuki H, Sato A, Kodama S, Heianza Y, Saito K, et al. Carotid artery plaque and LDL-to-HDL cholesterol ratio predict atherosclerotic status in coronary arteries in asymptomatic patients with type 2 diabetes mellitus. *Atheroscler Thromb*. (2013) 20:452–64. doi: 10.5551/jat.14977
32. Zhu XW, Deng FY, Lei SF. Meta-analysis of atherogenic index of plasma and other lipid parameters in relation to risk of type 2 diabetes mellitus. *Prim Care Diabetes*. (2015) 9:60–7. doi: 10.1016/j.pcd.2014.03.007
33. Wasana KGP, Attanayake AP, Weeraratna TP, Jayatilaka KAPW. Efficacy and safety of a herbal drug of *Coccinia grandis* (Linn.) Voigt in patients with type 2 diabetes mellitus: a double blind randomized placebo controlled clinical trial. *Phytomedicine*. (2021) 81:153431. doi: 10.1016/j.phymed.2020.153431
34. Cho SK, Kim JW, Huh JH, Lee KJ. Atherogenic index of plasma is a potential biomarker for severe acute pancreatitis: a prospective observational study. *J Clin Med*. (2020) 9:2982. doi: 10.3390/jcm9092982
35. Wang Q, Zheng D, Liu J, Fang L, Li Q. Atherogenic index of plasma is a novel predictor of non-alcoholic fatty liver disease in obese participants: a cross-sectional study. *Lipids Health Dis*. (2018) 17:284. doi: 10.1186/s12944-018-0932-0
36. Ferrara N. Role of vascular endothelial growth factor in physiologic and pathologic angiogenesis: therapeutic implications. *Semin Oncol*. (2002) 29:10–4. doi: 10.1053/sonc.2002.37264
37. Sharma T. Evolving role of anti-VEGF for diabetic macular oedema: from clinical trials to real life. *Eye (Lond)*. (2020) 34:415–7. doi: 10.1038/s41433-019-0590-0
38. Klimontov VV, Tyan NV, Orlov NB, Shevchenko AV, Prokofiev VF, Myakina NE, et al. Association of serum levels and gene polymorphism of vascular endothelium growth factor with ischemic heart disease in type 2 diabetic patients. *Kardiologiia*. (2017) 57:17–22.
39. Wada H, Suzuki M, Matsuda M, Ajiro Y, Shinozaki T, Sakagami S, et al. Distinct characteristics of VEGF-D and VEGF-C to predict mortality in patients with suspected or known coronary artery disease. *Amer Heart Assoc*. (2020) 9:e015761. doi: 10.1161/JAHA.119.015761
40. American Diabetes Association. Standards of Medical Care in Diabetes-2017. *Diabetes Care*. (2017) 40:S4–5. doi: 10.2337/dc17-S003
41. Carmeliet P, Moons L, Luttun A, Vincenti V, Compernelle V, Mol MD, et al. Synergism between vascular endothelial growth factor and placental growth factor contributes to angiogenesis and plasma extravasation in pathological conditions. *Nat Med*. (2001) 7:575–83. doi: 10.1038/87904
42. Huang H, He J, Johnson DK, Wei Y, Liu Y, Wang S, et al. Deletion of placental growth factor prevents diabetic retinopathy and is associated with Akt activation and HIF1 $\alpha$ -VEGF pathway inhibition. *Diabetes*. (2015) 64:200–12. doi: 10.2337/db14-0016
43. Kahtani EA, Xu Z, Rashaed SA, Wu L, Mahale A, Tian J, et al. Vitreous levels of placental growth factor correlate with activity of proliferative diabetic retinopathy and are not influenced by bevacizumab treatment. *Eye (Lond)*. (2017) 31:529–36. doi: 10.1038/eye.2016.246
44. Nguyen QD, Falco SD, Behar-Cohen F, Lam W-C, Li X, Reichhart N, et al. Placental growth factor and its potential role in diabetic retinopathy and other ocular neovascular diseases. *Acta Ophthalmol*. (2018) 96:e1–9. doi: 10.1111/aos.13325
45. Khaliq A, Foreman D, Ahmed A, Weich H, Gregor Z, McLeod D, et al. Increased expression of placenta growth factor in proliferative diabetic retinopathy. *Lab Invest*. (1998) 78:109–16.
46. Miyamoto N, Kozak, YD, Jeanny, JC, Glotin, A, Mascarelli, F, Massin, P, et al. Placental growth factor-1 and epithelial haemato-retinal barrier breakdown: potential implication in the pathogenesis of diabetic retinopathy. *Diabetologia*. (2007) 50:461–70. doi: 10.1007/s00125-006-0539-2
47. Tirronen A, Vuorio T, Kettunen S, Hokkanen K, Ramms B, Niskanen H, et al. Deletion of lymphangiogenic and angiogenic growth factor VEGF-D leads to severe hyperlipidemia and delayed clearance of chylomicron remnants. *Arterioscler Thromb Vasc Biol*. (2018) 38:2327–37. doi: 10.1161/ATVBAHA.118.311549
48. Chakraborty A, Barajas S, Lammoglia GM, Reyna AJ, Morley TS, Johnson JA, et al. Vascular endothelial growth factor-D (VEGF-D) overexpression and lymphatic expansion in murine adipose tissue improves metabolism in obesity. *Am J Pathol*. (2019) 189:924–39. doi: 10.1016/j.ajpath.2018.12.008
49. Alitalo AK, Proulx ST, Karaman S, Aebischer D, Martino S, Jost M, et al. VEGF-C and VEGF-D blockade inhibits inflammatory skin carcinogenesis. *Cancer Res*. (2013) 73:4212–21. doi: 10.1158/0008-5472.CAN-12-4539
50. Karaman S, Hollmén M, Robciuc MR, Alitalo A, Nurmi H, Morf B, et al. Blockade of VEGF-C and VEGF-D modulates adipose tissue inflammation and improves metabolic parameters under high-fat diet. *Mol Metab*. (2015) 4:93–105. doi: 10.1016/j.molmet.2014.11.006

**Conflict of Interest:** The authors declare that the research was conducted in the absence of any commercial or financial relationships that could be construed as a potential conflict of interest.

**Publisher's Note:** All claims expressed in this article are solely those of the authors and do not necessarily represent those of their affiliated organizations, or those of the publisher, the editors and the reviewers. Any product that may be evaluated in this article, or claim that may be made by its manufacturer, is not guaranteed or endorsed by the publisher.

Copyright © 2021 Zhang, Qiu, Wang, Sivaprasad, Wang, Zhao, Xie, Li and Kang. This is an open-access article distributed under the terms of the Creative Commons Attribution License (CC BY). The use, distribution or reproduction in other forums is permitted, provided the original author(s) and the copyright owner(s) are credited and that the original publication in this journal is cited, in accordance with accepted academic practice. No use, distribution or reproduction is permitted which does not comply with these terms.



# Choroidal Neovascularization in Pediatric Patients: Analysis of Etiologic Factors, Clinical Characteristics and Treatment Outcomes

Ting Zhang<sup>1,2†</sup>, You Wang<sup>1,2†</sup>, Wenjia Yan<sup>1,2</sup>, Yafen Liu<sup>1,2</sup>, Jinglin Lu<sup>1,2</sup>, Limei Sun<sup>1,2</sup>, Songshan Li<sup>1,2</sup>, Li Huang<sup>1,2</sup>, Zhaotian Zhang<sup>1,2</sup> and Xiaoyan Ding<sup>1,2\*</sup>

<sup>1</sup> State Key Laboratory of Ophthalmology, Zhongshan Ophthalmic Center, Sun Yat-Sen University, Guangzhou, China,

<sup>2</sup> Guangdong Provincial Key Laboratory of Ophthalmology and Visual Science, Guangdong Provincial Clinical Research Center for Ocular Diseases, Guangzhou, China

## OPEN ACCESS

### Edited by:

Haijiang Lin,  
Harvard Medical School,  
United States

### Reviewed by:

Changzheng Chen,  
Renmin Hospital of Wuhan  
University, China  
Sumit Randhir Singh,  
University of California, San Diego,  
United States

### \*Correspondence:

Xiaoyan Ding  
dingxiaoyan@gzoc.com

<sup>†</sup>These authors have contributed  
equally to this work

### Specialty section:

This article was submitted to  
Ophthalmology,  
a section of the journal  
Frontiers in Medicine

Received: 03 July 2021

Accepted: 27 October 2021

Published: 29 November 2021

### Citation:

Zhang T, Wang Y, Yan W, Liu Y, Lu J,  
Sun L, Li S, Huang L, Zhang Z and  
Ding X (2021) Choroidal  
Neovascularization in Pediatric  
Patients: Analysis of Etiologic Factors,  
Clinical Characteristics and Treatment  
Outcomes. *Front. Med.* 8:735805.  
doi: 10.3389/fmed.2021.735805

**Background and Objectives:** Choroidal neovascularization (CNV) is a common pathologic lesion that occurs in various chorioretinopathy, but very limited published data have reported in pediatric patients. This study aimed to investigate the etiologic factors, clinical features, and treatment outcomes of choroidal neovascularization (CNV) in children.

**Methods:** In this study, 33 eyes in 30 patients aged 18 years or younger with CNV were included. Comprehensive ophthalmic examination was performed in all the patients. The demographic profiles, laterality, visual acuity, optical coherence tomographic findings, fundus fluorescein angiographic findings, and the underlying pathology were analyzed. The types, locations, treatment outcomes, and recurrences of CNV were noted.

**Results:** The average age was  $11.2 \pm 4.6$  (range, 1–18) years. Most CNVs affecting children were classic and type 2. The most common etiologic factors of CNV in pediatric patients were congenital/developing abnormalities (9/30, 30.0%) and inflammatory retinochoroidopathy (9/30, 30.0%), followed by idiopathic CNV (8/30, 26.7%). Subtype analysis showed that the etiologic factor was inflammatory retinochoroidopathy in children 12 years or older, whereas congenital/developing abnormalities were present in children younger than 12 years. Eyes with active CNVs required a mean of  $1.40 \pm 0.58$  injections. No recurrence was observed during follow-up.

**Conclusions:** The etiologic factors of CNV in young Chinese patients were diverse, with congenital/developing abnormalities, inflammatory retinochoroidopathy and idiopathic CNV being the 3 most common ones. Eyes with active CNVs had good responses to antivascular endothelial growth factor treatment with low recurrence.

**Keywords:** pediatric choroidal neovascularization, etiologic factor, congenital/developing abnormality, inflammatory retinochoroidopathy, anti-vascular endothelial growth factor

## INTRODUCTION

Choroidal neovascularization (CNV) is a common pathologic lesion that occurs in various chorioretinopathy. The most common cause of CNV is age-related macular degeneration, followed by pathologic myopia (1). However, in children and adolescents, the reasons related with CNV are diverse and the lesion have a severe impact on visual acuity and quality of life over patients' lifetime (2–4). Although the incidence of CNV is quite rare in children and adolescents, its impact in view of the number of blind years lived is tremendous (5).

In the pediatric population, CNV has been reported to be collected with myopia, infection, inflammation, congenital anomalies, retinal dystrophies, and may also be idiopathic (2). The management of CNV in the pediatric patient setting is challenging, and a number of options, such as observation, photodynamic therapy, laser photocoagulation and anti-vascular endothelial growth factor (anti-VEGF) treatment has been reported, variable visual outcomes has been observed (6–9). However, because of the lack of complaints and symptoms, early diagnosis and regular monitoring of CNV is difficult in young children.

So far, very limited published data have reported the etiologic factors, clinical characteristics, natural history, and treatment outcomes of CNV in pediatric patients, and the observed subjects were mostly Western (10). Hence, we performed this study to investigate the etiologic factors, clinical characteristics, and treatment outcomes of CNV in Chinese pediatric patients.

## MATERIALS AND METHODS

This was a consecutive case series of patients aged 18 years or younger with CNV who were referred to Zhongshan Ophthalmic Center in Guangzhou, China, from January 2014 to September 2020. The study protocol was approved by the Institutional Review Board at Zhongshan Ophthalmic Center, Sun Yat-sen University, and was in accordance with the tenets of the Declaration of Helsinki. Informed consent was obtained from the parents of all the patients.

Complete ophthalmic examination was performed in children with CNV and their family members, including the visual acuity test, intraocular pressure test, slit-lamp biomicroscopy, optical coherence tomography (OCT), optical coherence tomography angiography (OCTA), fundus autofluorescence (FAF), fundus fluorescein angiography (FFA) and indocyanine green angiography (ICGA). The diagnosis of CNV was made on the basis of fundus findings, OCTA and FFA. Clinical data were collected, including age at presentation, gender, laterality, refractive errors, axial length, family history, and ocular findings in their family members.

With FFA and OCT, CNV lesions were classified as type 1 [within the sub-retinal pigment epithelium (RPE) space, typically corresponding to angiographically occult CNV], type 2 (within the subretinal space, typically corresponding to angiographically classic CNV), and type 3 (intraretinal retinal angiomatous proliferation) (11). CNVs were identified as active in case of any

of the following findings: clinical evidence of exudate, presence of fluid or hemorrhage, leakage on FFA, and presence of sub- or intraretinal fluid on OCT. With or without treatment, the lesion was considered regressed if there was no hemorrhage clinically, no dye leakage on FFA, and no sub- or intraretinal fluid on OCT. CNV was considered stable if lesion characteristics and visual acuity (if available) remained unchanged for at least 6 months. We defined recurrence as the reappearance or worsening of lesion activity after complete regression or stabilization. The types of lesions, frequency of treatment, duration of follow-up, and recurrence rate of CNV were recorded. According to FFA and OCT, if CNV included the central fovea, the location of CNV was classified as subfoveal; if the margin of CNV was within 200  $\mu$ m from the central fovea, it was classified as juxtafoveal (12). Peripapillary CNV (ppCNV) is defined as CNV located within 1 disc diameter of the margin of the optic nervehead (13).

The etiology of CNV was documented as follows. Simple high myopia was defined as a refractive error of  $-6$  diopters (D) or worse, whereas pathologic myopia was defined as an refractive error of  $-6$  D or worse, along with fundus changes such as diffuse/patchy chorioretinal atrophy, macular atrophy, lacquer cracks, or posterior staphyloma (14). Multifocal choroiditis was observed as chorioretinal lesions extending to the periphery and was associated with peripheral inflammation or panuveitis (15). The diagnosis of Best vitelliform macular dystrophy was confirmed by typical macular lesions and genetic testing. Other etiologies of CNV—such as optic disc hamartoma, ocular toxoplasmosis, optic disc drusen, and morning glory syndrome (MGS)—were defined on the basis of the presence of specific clinical and angiographic findings. If a case of CNV could not be attributed to any etiology, it was defined as idiopathic.

Statistical analyses were performed using SPSS Statistics for Windows (v23; IBM Corp, Armonk, NY, USA). Continuous variables were presented as mean (SD) after assessing for normality by inspecting histograms and were compared using the unpaired *t*-test. The chi-squared or Fisher exact test was used for categorical data. Statistical significance was defined as a *P*-value  $< 0.05$ .

## RESULTS

### Characteristics of CNV in Children

A total of 30 pediatric patients (33 eyes) with a mean age of onset  $11.2 \pm 4.6$  (range, 1–18) years were included in this study. The youngest patient was 1.8 years old. The number of males and females was 17 (56.7%) and 13 (43.3%), causing a male-to-female ratio of 1.3:1.0. The mean age of onset in males and females was  $12.5 \pm 3.9$  and  $10.1 \pm 4.9$  years, respectively, with no statistical differences ( $P = 0.39$ ). Among the participants, 29 were Hans and 1 was Russian. The average duration of follow-up was  $29.0 \pm 13.8$  months, ranging from 6 to 60 months. None of the patients had any systemic diseases. Unilateral presentation was the most common, which was found in 27/30 (90.0%) children. Bilateral CNVs were noted in 3/30 (10.0%) children. Best corrected visual acuity (BCVA) was present in 87.9% (29/33) eyes, and the mean BCVA was  $0.95 \pm 0.63$  logMAR.



**TABLE 1 |** Demographic profile and ocular associations.

Features	Numbers
Subjects ( <i>n</i> )	30 (33 eyes)
<b>Presenting visual acuity</b>	
<b>Age (years)</b>	
Mean	11.2 ± 4.6
Male	12.5 ± 3.9
Female	10.1 ± 4.9
Median	11
Range	1–18
<b>Gender</b>	
Male	17 (56.7%)
Female	13 (43.3%)
<b>Laterality</b>	
Unilateral	27 (90.0%)
Bilateral	3 (10.0%)
<b>Ocular associations</b>	
Congenital/developing abnormalities	9 (30.0%, 10 eyes)
Best vitelliform macular dystrophy	3 (10.0%, 4 eyes)
Retinitis pigmentosa	2 (6.7%, 2 eyes)
Optic disc drusen	1 (3.3%, 1 eye)
Morning glory disc anomaly	1 (3.3%, 1 eye)
Optic disc hamartoma	2 (6.7%, 2 eyes)
Inflammatory retinochoroidopathy	9 (30.0%, 10 eyes)
Ocular toxoplasma retinochoroiditis	5 (16.7%, 6 eyes)
Ocular toxocariasis retinochoroiditis	1 (3.3%, 1 eye)
Multifocal choroiditis	3 (10.0%, 3 eyes)
Idiopathic	8 (26.7%, 8 eyes)
High myopia	4 (13.3%, 5 eyes)

Among the 33 affected eyes with CNV, the majority (32/33, 97.0%) were with type 2 CNV, only 1/33 (3.0%) eye was with type 1, and no eye with type 3; 84.8% (28/33) CNVs were active and 15.2% (5/33) inactive; 84.8% (28/33) CNVs were located subfoveally, and 15.2% (5/33) CNVs were located in the peripapillary area (Table 2). All 5 eyes with ppCNV had congenital pathology: optic disc drusen (1 eye), morning glory syndrome (1 eye), congenital optic disc hamartoma (2 eyes), and retinitis pigmentosa (1 eye), and 80.0% (4/5) ppCNVs were active. The demographic profiles, characteristics of all affected eyes, and etiologic factors are presented in Tables 1, 2.

## Analysis of Etiologic Factors Associated With CNV in Children

A wide range of etiologic factors associated with CNV were identified in this study. Diverse congenital retinal or optic disc anomalies were seen in 10 eyes in 9 children, including Best vitelliform macular dystrophy (4 eyes in 3 children) (Figure 1), retinitis pigmentosa (2 eyes in 2 children), optic disc drusen (1 eye in 1 child) (Figure 2), morning glory disc anomaly (1 eye in 1 child), and optic disc hamartoma (2 eyes in 2 children). Inflammatory retinochoroidopathy was observed in 10 eyes in 9 children, including toxoplasma chorioretinitis (6 eyes in 5

**TABLE 2 |** Characteristics of CNVM.

Feature	<i>n</i> (%)
<b>Location (<i>n</i> = 33)</b>	
Subfoveal	28 (84.8)
Peripapillary	5 (15.2)
<b>Activity at presentation (<i>n</i> = 33)</b>	
Active	28 (84.8)
Inactive	5 (15.2)
<b>Pattern of leakage in active CNVMs where FFA was available (<i>n</i> = 28)</b>	
Classic	27 (96.4)
Occult	1 (3.6)
<b>Types of CNVMs where OCT was available (<i>n</i> = 33)</b>	
Type 1	1 (3.0)
Type 2	32 (97.0)

children) (Figure 3), multifocal choroiditis (3 eyes in 3 children), and ocular toxocariasis (1 eye in 1 child). Simple high myopia was identified in 4 eyes in 3 children, and 1 eye with pathologic myopia with fundus changes was found (Figure 4). In addition, idiopathic CNV was defined in 8 eyes in 8 children. Overall, within these associated factors, congenital retinal or optic disc anomalies (9/30, 30.0%) and inflammatory retinochoroidopathy (9/30, 30.0%) are the most common etiologic factors, followed by idiopathic CNV (8/30, 26.7%). Details of all affected eyes are presented in Table 1.

Subgroup analysis based on the age of onset showed the most common etiologic factor of CNV in patients 12 years or older was inflammatory chorioretinopathy (5/13, 38.5%), followed by high myopia (4/13, 30.7%), idiopathic CNV (3/13, 23.1%), and congenital/developmental anomalies (1/12, 7.7%). However, congenital/developmental anomalies were the major etiologic factor in patients younger than 12 years (8/17, 47.1%), followed by idiopathic CNV (5/17, 29.4%) and inflammatory chorioretinopathy (4/17, 23.5%). A statistically significant difference was found in etiology between patients 12 years or older and those younger than 12 years ( $\chi = 9.3$ ,  $P = 0.02$ ) (Table 3).

Among these 30 children, three cases presented with bilateral CNVs, including Best disease (1), high myopia (1), and toxoplasma (1). The patient with Best disease has active stage III lesion in both eyes at the time of diagnosis. The bilateral CNVs in high myopia were active. However, the bilateral CNVs secondary to toxoplasma were inactive and this child was left to observe without any treatment.

## Anti-VEGF Treatment and Outcomes of CNV in Pediatric Patients

According to the reported studies and our previous experience with myopic CNV in adults, where the majority belonged to type 2 CNV, one anti-VEGF injection followed by a pro re nata (1 + PRN) regimen was found to be quite effective (16). Thus, the 1 + PRN treatment modality was used in 25 eyes in 23 children with active CNV lesions in this study. The eye with active CNV

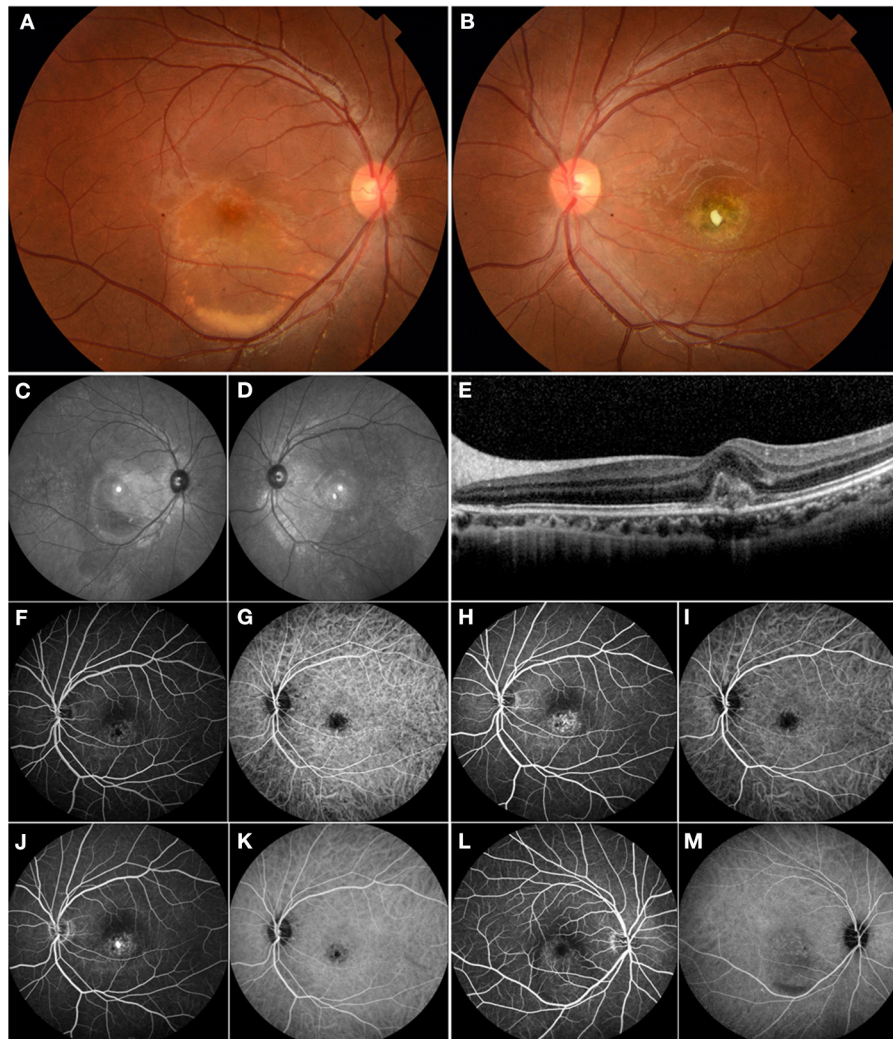


**FIGURE 1 |** Multimodal imaging of a 17-year-old male who presented with choroidal neovascularization (CNV) related to Best vitelliform macular dystrophy. His family history was unremarkable. His BCVA was 0.1 logMAR in the right eye and 1.1 logMAR in the left eye. **(A)** Fundus examination of the right eye revealed a color photo: a vitelliform lesion in the submacular area indicating Best disease. **(B)** The left eye showed a yellow-white fibrotic membrane—an area of atrophy and pigmentation. **(C,D)** The red-free images showed macular hyperautofluorescence in both eyes. **(E)** OCT revealed the typical subfoveal hyperreflective at the level of the RPE. **(F,H,J)** FFA demonstrated mild hyperfluorescence in the macular area and frank hyperfluorescence in the late phase consistent with subfoveal CNV in the left eye. **(G,I,K)** ICGA showed hypofluorescence in the macular area consistent with the lesion. **(L)** FFA demonstrated mild hyperfluorescence in the macular area secondary to a vitelliform lesion in the right eye. **(M)** ICGA showed mild hypofluorescence secondary to a vitelliform lesion in the right eye. The patient underwent intravitreal ranibizumab treatment for his left eye. However, he did not notice any significant visual improvement.

due to toxocariasis uveitis was treated with pars plana vitrectomy combined with oral anti-inflammatory glucocorticoid. Two eyes in 2 children did not receive treatment because of rejection from their guardians. Five eyes with inactive CNVs were left to observe, including 2 eyes in 1 patient with toxoplasma. Standard dose of anti-VEGF (aflibercept 2 mg and ranibizumab 0.5 mg) was used in this study.

The outcome of anti-VEGF treatment for CNVs in 25 eyes (23 children) is summarized in **Table 4**. BCVA was available in 23/25 eyes. The average baseline BCVA before anti-VEGF treatment was  $0.96 \pm 0.49$  logMAR; it increased to  $0.85 \pm 0.44$  logMAR 3 months after the treatment and stabilized at  $0.85 \pm$

$0.42$  logMAR at final follow-up. No significant difference was noted in comparing BCVA pre- and post-treatment ( $P > 0.05$ ). A slight improvement in BCVA was seen in 12 (12/23, 52.1%) eyes at follow-up, including 6 (6/6, 100%), 1 (1/7, 14.3%), 1 (1/5, 20%) and 4 (4/5, 80%) eyes with idiopathic CNV, congenital retina and optic disc anomalies, high myopia and inflammatory retinchoroidopathy, respectively. No significant changes were observed in 11 (11/23, 47.9%) eyes at follow-up, including 0 (0/6, 0%), 6 (6/7, 85.7%), 4 (4/5, 80%), and 1 (1/5, 20%) eyes with idiopathic CNV, congenital retina and optic disc anomalies, high myopia and inflammatory retinchoroidopathy, respectively. The average frequency of initial anti-VEGF treatment was  $1.40 \pm$

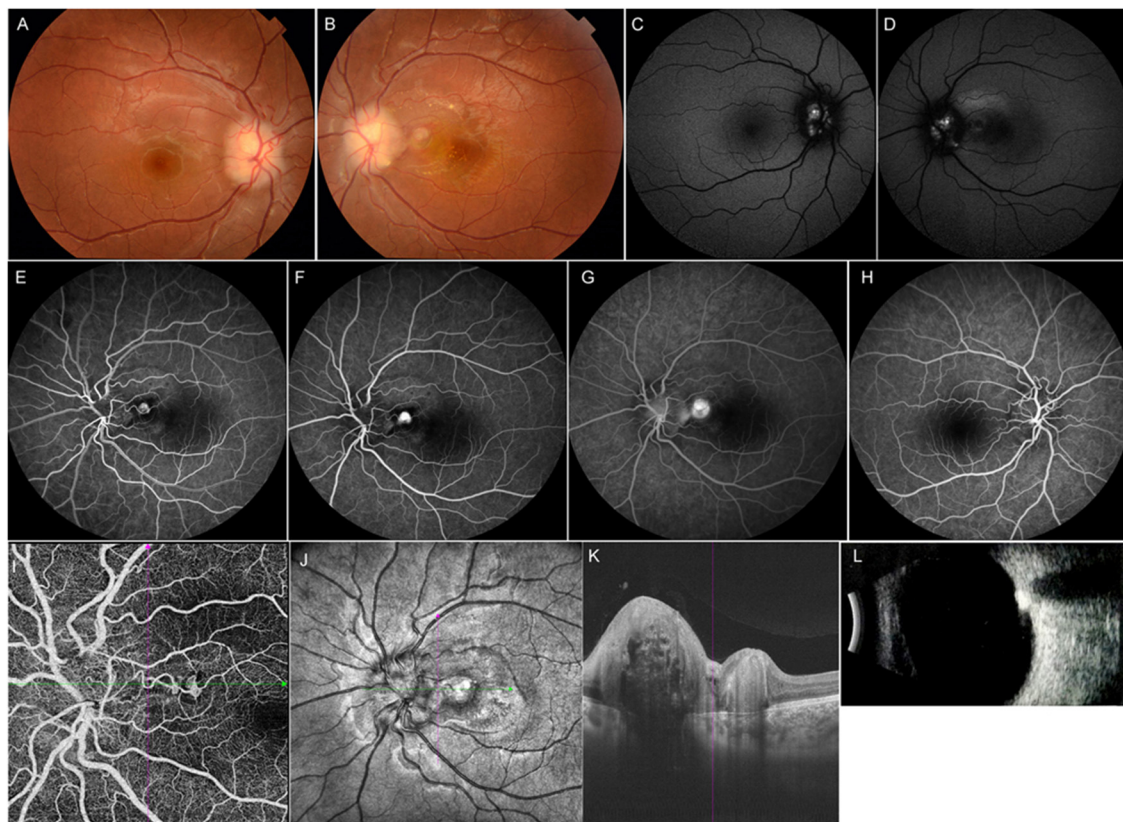


**FIGURE 2 |** Multimodal imaging of an 11-year-old female with optic disc drusen. Her BCVA was 0.8 logMAR in the left eye and 0.1 logMAR in the right eye. Her ocular and systemic history was unremarkable. **(A,B)** Fundus photograph showed elevated optic discs with blurred margins in both eyes. **(C,D)** Mild hyperautofluorescence was observed around the disc bilaterally. **(E–G)** FFA showed a lesion located in the peripapillary area with hyperfluorescence in the early phase and leakage in the late phase in the left eye. **(H)** FFA image of the right eye. **(I,J)** OCT angiography clearly showed CNV located in the peripapillary area. **(K)** OCT image of the left eye revealed subretinal hyperreflectivity. **(L)** Ultrasound B-scan showed a strong signal in front of the optic disc. The girl underwent intravitreal ranibizumab treatment, and her BCVA improved to 0.1 logMAR at final follow-up.

0.58 injections. Among the eyes that received 1+ PRN intravitreal anti-VEGF treatment as the loading dose, CNVs in 16/25 (64.0%) eyes in 14 children were stabilized with 1 injection only, whereas 8/25 (32.0%) eyes received a second injection during the loading stage at treatment initiation, and 1 eye received a third injection. No recurrence occurred during the study period. CNVs in 25/25 (100.0%) eyes were stabilized at final follow-up. There were no significant ocular or systemic complications in these children.

## DISCUSSION

CNV is quite a rare, but sight-threatening disease affecting children and adolescents. The first and only available population-based incidence of CNV was reported recently by Moosajee et al. from the United Kingdom in those aged 16 years or younger, with an annual incidence of 0.21 per 100 000 (2). To date, there are no other detailed data on the prevalence of CNV in the pediatric population, and most knowledge of this topic comes from case series or single case reports. Because of the low incidence, only a few series of CNVs in children have been reported. To the best

of our knowledge, this is the first study to report the etiologic factors, clinical characteristics, and treatment outcomes of CNV in a series of Chinese pediatric population younger than 18 years.

## Etiologic Factors and Clinical Characteristics

In this study including 33 eyes of 30 pediatric patients with CNV, at least 1 contributing etiology could be identified in 25/33 (75.8%) eyes of the patients. A study by Tapas et al. demonstrated that retinal dystrophies had the leading ocular correlation with CNV in pediatric patients younger than 18 years (10). In our series, identifiable ocular association could not be found in only 8/30 (26.7%) patients, whereas congenital/developing anomalies and inflammatory retinochoroidopathy were noted to be the major etiologic factors of CNV in children. Among them, Best vitelliform macular dystrophy was the most common reason, which is in line with the study of Tapas et al. (10). Furthermore, one of the strengths of our study is the findings concerning the distribution of etiology. Subgroup analysis based on the age of the patients at the onset of CNV showed that the most



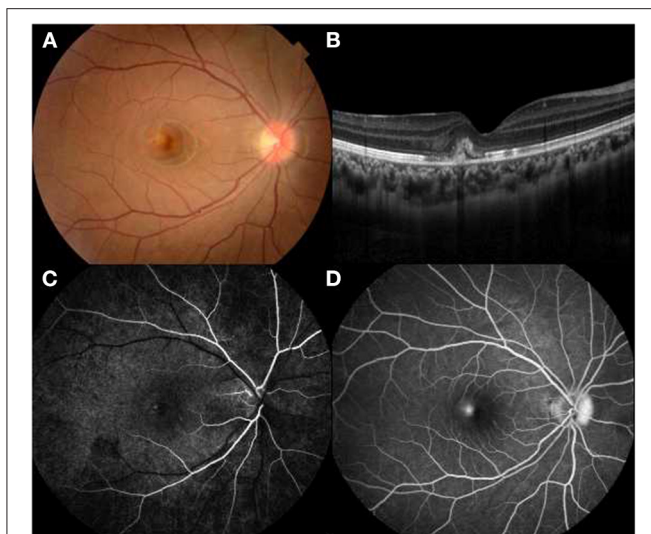


**FIGURE 3 |** Multimodal imaging of a 14-year-old female with idiopathic choroidal neovascularization. Her BCVA was 0.9 logMAR in the right eye and 0.1 logMAR in the left eye. **(A)** A parafoveal yellowish lesion was noted on funduscopy. **(B)** OCT showed a hyperreflective area located in subretinal space with surrounding serous retinal detachment. **(C,D)** Hyperfluorescence in the early phase and leakage in the late phase FFA revealed an active lesion parafoveally.

common etiology of CNV in patients younger than 12 years was congenital/developmental anomalies (8/17, 47.1%), whereas inflammatory retinochoroidopathy was the major etiologic factor in patients older than 12 years (5/11, 38.5%).

Moreover, in previous studies on CNV in the pediatric population, high myopia had a low incidence, especially in studies conducted in the West (5). However, our data showed that high myopia (4/11, 30.7%) plays an important role in Chinese patients 12 years or older with CNV, which was probably because myopia is more prevalent in Eastern Asians (17). Interestingly, in adults, subretinal CNV generally develops in an eye with diffuse or patchy macular atrophy and lacquer cracks, which was identified as pathologic myopia. CNVs are usually present at the edges of lacquer cracks, atrophy plaque, or steep staphylomatous area (18, 19), whereas in pediatric patients in our study, they were observed in 1 pathologic myopic eye with lacquer cracks and 3 highly myopic eyes without evident myopic fundus changes at the posterior pole, which was identified as simple high myopia. All CNVs due to simple high myopia were seen in teenagers, ranging from 14 to 18. The underlying pathogenesis is still elusive. We suggest that the contribution of dramatic elongation of the globe during adolescence is considered, which may produce biomechanical stretching of the retina, RPE, and choroid with a straightening and thinning of retinal vessels with reduction of retinal vascular flow and a diminished density of the retinal capillary network and choriocapillaris (20).

Because of the rarity of ppCNV in the pediatric population, the natural history, prognosis, and treatment strategy are not clear so far. In the current series, all 5 ppCNVs occurred in patients younger than 12 years who had a preexisting

ocular pathology, including optic nervehead drusen, optic disc hamartoma, morning glory disc anomaly, and retinitis pigmentosa. In our series, 4/5 (80%) ppCNVs were active. The natural course of untreated ppCNVs has been reported to be variable by ranging from spontaneous involution to fulminant enlargement toward the fovea, which is vision threatening (21). Thus, in our series, all the active lesions, although some of them were not affecting the vision, were treated with anti-VEGF therapy. CNVs responded well with an average of 1.25 injections. Non-active CNVs associated with MGS were left to observe and kept stable within the 36 months of follow-up.

## Treatments and Outcomes

Children with CNVs seem to respond well to anti-VEGF treatment. Kozak et al. analyzed the data of 45 eyes in 39 children with intravitreal bevacizumab or ranibizumab for CNV over a mean follow-up period of 12.8 months. 2.2 injections per eye was required for treatment. An improvement in BCVA of 3 lines was seen in 22 (49.0%) eyes, and only 1 eye had worsened vision after treatment (7). In our study, it was found that an average of  $1.40 \pm 0.58$  anti-VEGF injections were needed for the regression or stabilization of CNV membrane (CNVM), which is significantly lower than what is commonly seen with CNVM in adults, even less than that reported in a study by Kozak et al. (7, 16). Injections on a 1+PRN basis demonstrated similar results as monthly injections. The need for retreatments is definitely much less than that for adults in prior reports (16). In our series, it was usually between 1 and 3 in only 36% of children. However, the number of patients in this study was too small to draw any clear conclusions regarding which options performs better for post-treatment recurrence. However, visual improvement is poor in CNVs in the pediatric population after the stabilization, or even regression, of CNV lesions. In our series, 12/23 (52.1%) patients showed a slight improvement, whereas 11/23 (47.9%) did not show any significant improvement in visual acuity during follow-up. Similarly, 90% of the patients in a case series of Goshorn et al. with initial visual acuity of  $<1.0$  logMAR remained unchanged (22). The improvement in BCVA was seen in 6 (6/6, 100%) eyes with idiopathic CNV and 4 (4/5, 80%) eyes with inflammatory retinochoroidopathy, respectively. The results showed better treatment effects in idiopathic CNV and inflammatory retinochoroidopathy.

CNV in children has a more favorable prognosis than in adults with AMD, even if left for observation. In our cohort, 2 eyes with active CNV in 2 patients were left to observe because of rejection from their guardians, including 1 eye with retinitis pigmentosa and 1 with ocular toxoplasma retinochoroiditis. Both eyes had a spontaneous regression of CNV, although visual acuity did not show any improvement. Five eyes with inactive CNV in 4 patients still remained inactive, and no improvement in BCVA was observed during follow-up. Goshorn et al. reported spontaneous regression of CNV in 11/19 (58.0%) untreated eyes in children and 9 patients obtained visual acuity better than or equal to 20/50 (22). Rishi et al. reported spontaneous involution of CNV in 15/17 untreated eyes and suggested the less need for treatment was related to the better health of RPE pump in children (3). RPE play an important role by mixing with fibrocytes, collagen,



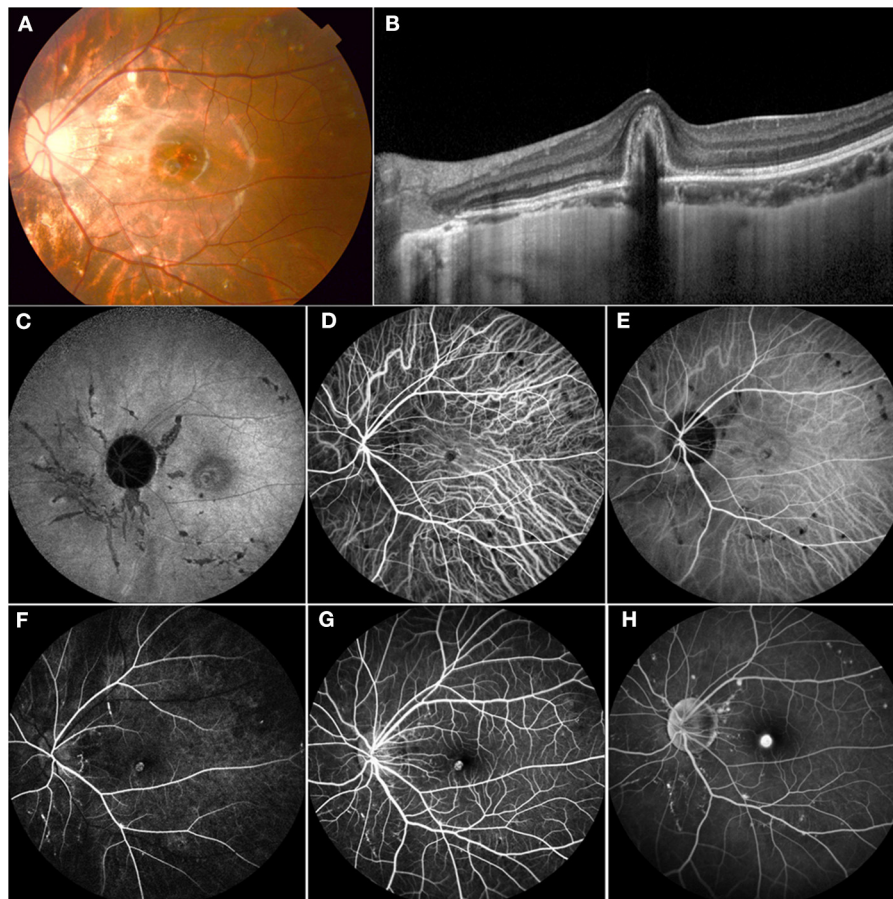


**FIGURE 4 |** Multimodal imaging of an 11-year-old female who presented with decreasing vision in her left eye. Her BCVA was 0.3 logMAR with a refraction of  $-6.00 - 1.50 \times 5$  in the left eye and 0.9 logMAR with a refraction of  $-5.5 - 1.25 \times 177$  in the right eye. **(A)** Color fundus demonstrated mottled fundus, lacquer cracks, and myopia conus. **(B)** OCT showed a subretinal high-refractive material with fuzzy margins and the absence of the inner segment/outer segment junction. **(C)** FAF showed hypofluorescence secondary to mechanical linear breaks in the elastic layer of the Bruch membrane. **(D,E)** ICGA showed an abnormal vascular network and hypofluorescence corresponding to the areas of LC. **(F-H)** FFA demonstrated hyperfluorescence in the early phase and leakage in the late phase of CNV and a hyperfluorescence linear area consistent with LC. This patient received 1 intravitreal injection of ranibizumab, and the vision was stable at 0.3 at follow-up.

vascular endothelium and lymphocytes to form the CNV. In the late stage of CNV, the RPE proliferated to enclose CNV and caused its regression (23). Observation of CNVs in children might be a reasonable option; but, so far, it is difficult to assess which CNV would regress or progress. Moreover, Rishi et al. noted that visual outcome in eyes with treated CNV was better than in those with spontaneously regressed CNV (3). Thus, according to the effectiveness and favorable prognosis with limited anti-VEGF treatment, we suggest timely treatment is considered for CNV in the pediatric population.

There are several limitations of this study that need to be considered. First, as CNV is rare in the pediatric population, the number of included patients was limited. Second, because of the young age of the patients in this case series, some details—such as visual acuity, refractive status, clinical presentation, and OCT findings—were lacking. Third, referral biases might be existed as our hospital is a tertiary referral institute for pediatric retinal diseases. Fourth, the non-compliance of OCTA in young cases

limited the consequent analysis of the microstructure modeling of CNV. Therefore, a prospective multicenter clinical study with more detailed objective information may be warranted. However, this study—with a relatively large sample size—was the first to reveal that the etiologic factors of CNV in the Chinese pediatric population varied significantly from those in adults.

In conclusion, we analyzed the etiologic factors, clinical features, and treatment outcomes of CNV in the pediatric population. Most of the CNVs were found to be classic on FFA and type 2 on OCT and had a subfoveal location. In our study, according to age, congenital/developmental abnormalities were the major etiologic factor in patients younger than 12 years, whereas inflammatory retinopathy was the most common reason in those older than 12 years. The high prevalence of inflammatory CNV in pediatric and young teenage patients catches the attention of ophthalmologists. Intravitreal anti-VEGF treatment on a PRN basis after the first injection was demonstrated to be effective. With a long follow-up,

**TABLE 3 |** Distribution of etiology by age range for patients with choroidal neovascular membrane.

Etiologic factors	N (%)	Subgroup analysis	
		0–11 years, N	12–18 years, N
Congenital retina and optic disc anomalies	9 (30.0%)	8 (47.1%)	1 (7.7%)
Best vitelliform macular dystrophy	3	2	1
Retinitis pigmentosa	2	2	0
Optic disc drusen	1	1	0
Morning glory disc anomaly	1	1	0
Optic disc hamartoma	2	2	0
Inflammatory retinochoroidopathy	9 (30.0%)	4 (23.5%)	5 (38.5%)
Ocular toxoplasma retinochoroiditis	5	3	2
Ocular toxocariasis retinochoroiditis	1	1	0
Multifocal choroiditis	3	0	3
Idiopathic	8 (26.7%)	5 (29.4%)	3 (23.1%)
High myopia	4 (13.3%)	0	4 (30.7%)
Total	30	17	13

**TABLE 4 |** Treatment profile.

Treatment types (n = 25)	N/ $\bar{x} \pm s$
Ranibizumab	17
Conbercept	5
Aflibercept	3
<b>Average frequency</b>	1.40 $\pm$ 0.58
1 injection	16
2 injections	8
3 injections	1
<b>BCVA (23 eyes, logMAR)</b>	
Baseline	0.96 $\pm$ 0.49
Post-treatment	0.85 $\pm$ 0.443
Final visit	0.85 $\pm$ 0.42
<b>Outcome of BCVA (n = 23)</b>	
Improvement	12
Stability	11

it has been shown that children with CNVs respond well to anti-VEGF treatment. In summary, CNV in the pediatric population in our study differed from that in the adult population according to etiology, angiographic characteristics, and treatment response.

## DATA AVAILABILITY STATEMENT

The raw data supporting the conclusions of this article will be made available by the authors, without undue reservation.

## ETHICS STATEMENT

The studies involving human participants were reviewed and approved by the Institutional Review Board at Zhongshan

Ophthalmic Center, Sun Yat-sen University. Written informed consent to participate in this study was provided by the participants' legal guardian/next of kin.

## AUTHOR CONTRIBUTIONS

TZ, YW, and XD conceptualized and designed the study, drafted the initial manuscript, and reviewed and revised the manuscript. WY, YL, JL, and LS designed the data collection instruments, collected data, and carried out the initial analyses. SL, LH, and ZZ conceptualized and designed the study, coordinated and supervised data collection, and critically reviewed the manuscript for important intellectual content. All authors approved the final manuscript as submitted and agree to be accountable for all aspects of the work.

## FUNDING

This study is supported in part by grants from the Fundamental Research Funds of State Key Laboratory of Ophthalmology, research funds of Sun Yat-sen University (15ykjxc22d; Guangzhou, Guangdong, China), Science and Technology Program Guangzhou, China (201803010031; Guangzhou, Guangdong, China), the National Natural Science Foundation of China (no. 81900896), Science and Technology Program Guangzhou, China (202102010430010067; Guangzhou, Guangdong, China). The sponsors and funding organizations had no role in the design or conduct of this research.

## ACKNOWLEDGMENTS

The authors would like to thank Miss Xiao-ling Luo, Bi-lin Yu and Li-ming Cao from Zhongshan ophthalmology Center for collection of data.

## REFERENCES

- Ho CPS, Lai TYY. Pharmacotherapy for choroidal neovascularization due to uncommon causes. *Curr Pharm Des.* (2018) 24:4882–95. doi: 10.2174/1381612825666190206105943
- Moosajee M, Abbouda A, Foot B, Bunce C, Moore AT, Acheson J, et al. Active surveillance of choroidal neovascularisation in children: incidence, aetiology and management findings from a national study in the UK. *Br J Ophthalmol.* (2018) 102:438–43. doi: 10.1136/bjophthalmol-2017-310445
- Rishi P, Gupta A, Rishi E, Shah BJ. Choroidal neovascularization in 36 eyes of children and adolescents. *Eye.* (2013) 27:1158–68. doi: 10.1038/eye.2013.155
- Miller DG, Singerman LJ. Vision loss in younger patients: a review of choroidal neovascularization. *Optom Vis Sci.* (2006) 83:316–25. doi: 10.1097/01.opx.0000216019.88256.eb
- Barth T, Zeman F, Helbig H, Oberacher-Velten I. Etiology and treatment of choroidal neovascularization in pediatric patients. *Eur J Ophthalmol.* (2016) 26:388–93. doi: 10.5301/ejo.5000820
- Bloom SM. Subfoveal neovascular lesions in age-related macular degeneration. *Arch Ophthalmol.* (1993) 111:900–1. doi: 10.1001/archoph.1993.01090070018004
- Kozak I, Mansour A, Diaz RI, Calzada JJ, Pichi F, Cruz-Villegas V, et al. Outcomes of treatment of pediatric choroidal neovascularization with intravitreal antiangiogenic agents: the results of the KKESH International Collaborative Retina Study Group. *Retina.* (2014) 34:2044–52. doi: 10.1097/IAE.0000000000000200
- Kohly RP, Muni RH, Kertes PJ, Lam WC. Management of pediatric choroidal neovascular membranes with intravitreal anti-VEGF agents: a retrospective consecutive case series. *Can J Ophthalmol.* (2011) 46:46–50. doi: 10.3129/i10-123
- Viola F, Villani E, Mapelli C, Staurenghi G, Ratiglia R. Bilateral juvenile choroidal neovascularization associated with Best's vitelliform dystrophy: observation versus photodynamic therapy. *J Pediatr Ophthalmol Strabismus.* (2010) 47:121–2. doi: 10.3928/01913913-20100308-14
- Padhi TR, Anderson BJ, Abbey AM, Yonekawa Y, Stem M, Alam D, et al. Choroidal neovascular membrane in paediatric patients: clinical characteristics and outcomes. *Br J Ophthalmol.* (2018) 102:1232–7. doi: 10.1136/bjophthalmol-2017-310497
- Gass JD. Biomicroscopic and histopathologic considerations regarding the feasibility of surgical excision of subfoveal neovascular membranes. *Trans Am Ophthalmol Soc.* (1994) 92:91–111; discussion –6.
- Varano M, Iacono P, Giorno P, Chiaravalloti A, Parravano M. Photodynamic therapy in subfoveal and juxtafoveal myopic choroidal neovascularization: a 10-year retrospective analysis. *Ophthalmologica.* (2014) 231:204–10. doi: 10.1159/000357504
- Lopez PF, Green WR. Peripapillary subretinal neovascularization. A review. *Retina.* (1992) 12:147–71. doi: 10.1097/00006982-199212020-00012
- Ohno-Matsui K, Kawasaki R, Jonas JB, Cheung CM, Saw SM, Verhoeven VJ, et al. International photographic classification and grading system for myopic maculopathy. *Am J Ophthalmol.* (2015) 159:877–83.e7. doi: 10.1016/j.ajo.2015.01.022
- Joondeph BC, Tessler HH. Multifocal choroiditis. *Int Ophthalmol Clin.* (1990) 30:286–90. doi: 10.1097/00004397-199030040-00015
- Xiao H, Zhao X, Li S, Sun L, Xin W, Wang Z, et al. Risk factors for subretinal fibrosis after anti-VEGF treatment of myopic choroidal neovascularisation. *Br J Ophthalmol.* (2021) 105:103–8. doi: 10.1136/bjophthalmol-2019-315763
- Xu C, Pan C, Zhao C, Bi M, Ma Q, Cheng J, et al. Prevalence and risk factors for myopia in older adult east Chinese population. *BMC Ophthalmol.* (2017) 17:191. doi: 10.1186/s12886-017-0574-4
- Ohno-Matsui K, Yoshida T, Futagami S, Yasuzumi K, Shimada N, Kojima A, et al. Patchy atrophy and lacquer cracks predispose to the development of choroidal neovascularisation in pathological myopia. *Br J Ophthalmol.* (2003) 87:570–3. doi: 10.1136/bjo.87.5.570
- Spaide RF. Choroidal neovascularization. *Retina.* (2017) 37:609–10. doi: 10.1097/IAE.0000000000001575
- Sayanagi K, Ikuno Y, Uematsu S, Nishida K. Features of the choriocapillaris in myopic maculopathy identified by optical coherence tomography angiography. *Br J Ophthalmol.* (2017) 101:1524–9. doi: 10.1136/bjophthalmol-2016-309628
- Jutley G, Jutley G, Tah V, Menon G. Treating peripapillary choroidal neovascular membranes: a review of the evidence. *Eye.* (2011) 25:675–81. doi: 10.1038/eye.2011.24
- Goshorn EB, Hoover DL, Eller AW, Friberg TR, Jarrett WH, Sorr EM. Subretinal neovascularization in children and adolescents. *J Pediatr Ophthalmol Strabismus.* (1995) 32:178–82. doi: 10.3928/0191-3913-19950501-11
- Lutty G, Grunwald J, Majji AB, Uyama M, Yoneya S. Changes in choriocapillaris and retinal pigment epithelium in age-related macular degeneration. *Mol Vis.* (1999) 5:35.

**Conflict of Interest:** The authors declare that the research was conducted in the absence of any commercial or financial relationships that could be construed as a potential conflict of interest.

**Publisher's Note:** All claims expressed in this article are solely those of the authors and do not necessarily represent those of their affiliated organizations, or those of the publisher, the editors and the reviewers. Any product that may be evaluated in this article, or claim that may be made by its manufacturer, is not guaranteed or endorsed by the publisher.

Copyright © 2021 Zhang, Wang, Yan, Liu, Lu, Sun, Li, Huang, Zhang and Ding. This is an open-access article distributed under the terms of the Creative Commons Attribution License (CC BY). The use, distribution or reproduction in other forums is permitted, provided the original author(s) and the copyright owner(s) are credited and that the original publication in this journal is cited, in accordance with accepted academic practice. No use, distribution or reproduction is permitted which does not comply with these terms.



# Retinal Nerve Fibre Layer Thickness Change Following Femtosecond Laser-Assisted *in situ* Keratomileusis

Yang Jiang<sup>1,2</sup>, Zhonghai Wang<sup>1,2\*</sup>, Ying Li<sup>1,2\*</sup>, Yong Li<sup>3\*</sup> and Thomas Chengxuan Lu<sup>4</sup>

<sup>1</sup> Department of Ophthalmology, Peking Union Medical College Hospital, Chinese Academy of Medical Sciences, Beijing, China, <sup>2</sup> Key Laboratory of Ocular Fundus Diseases, Chinese Academy of Medical Sciences, Peking Union Medical College, Beijing, China, <sup>3</sup> Department of Ophthalmology, Xi'an Fourth Hospital, Xi'an, China, <sup>4</sup> School of Medicine, University of New South Wales, Kensington, NSW, Australia

## OPEN ACCESS

### Edited by:

Haijiang Lin,  
Harvard Medical School,  
United States

### Reviewed by:

Lijun Zhang,  
Dalian Medical University, China  
Ke Ma,  
Sichuan University, China

### \*Correspondence:

Zhonghai Wang  
wzhpunch@sina.com  
Ying Li  
liyingpunch@126.com  
Yong Li  
344813995@qq.com

### Specialty section:

This article was submitted to  
Ophthalmology,  
a section of the journal  
Frontiers in Medicine

Received: 17 September 2021

Accepted: 19 October 2021

Published: 29 November 2021

### Citation:

Jiang Y, Wang Z, Li Y, Li Y and Lu TC  
(2021) Retinal Nerve Fibre Layer  
Thickness Change Following  
Femtosecond Laser-Assisted *in situ*  
Keratomileusis. *Front. Med.* 8:778666.  
doi: 10.3389/fmed.2021.778666

**Purpose:** To evaluate the effect of femtosecond laser-assisted *in situ* keratomileusis (FS-LASIK) on retinal fovea thickness, volume, and retinal nerve fibre layer (RNFL) thickness.

**Methods:** Thirty-seven eyes (37 patients) undergoing FS-LASIK were included in this prospective study. Optical coherence tomography (OCT) was performed 1 day before, 1 h and 1 day after FS-LASIK surgery.

**Result:** Eighteen male and nineteen females were enrolled. Mean patient age was  $22.94 \pm 4.22$  years. One hour postoperatively, macula fovea thicknesses, macula fovea volume, macula parafovea thickness, macula parafovea volume, macula perifovea thickness, macula perifovea volume, temporal RNFL thickness, and superior RNFL thickness measures showed significant decrease ( $t = 6.171, 6.032, \text{ and } 9.837, 9.700, 2.532, 4.393, 4.926, 2.265; p = 0.000, 0.000, 0.000, 0.000, 0.016, 0.000, 0.000, \text{ and } 0.011$ ). Day 1 post-operation, macula fovea thicknesses, macula fovea volume, macula parafovea thickness, macula parafovea volume, and inferior RNFL thickness measures showed significant change compared to preoperative measures ( $t = 3.620, 3.220, 2.901, 2.910, 3.632; p = 0.001, 0.003, 0.006, 0.006, \text{ and } 0.001$ ).

**Conclusion:** Our data suggest there are alterations in retinal foveal and RNFL measurements by OCT 1 h and 1 day after FS-LASIK surgery.

**Keywords:** femtosecond laser-assisted *in situ* keratomileusis, macular thickness, retinal nerve fibre layer thickness, optical coherence tomography, myopia

## INTRODUCTION

Laser-assisted *in situ* keratomileusis is a popular corneal refractive technique utilised to enhance visual acuity. Both traditional microkeratome and modern femtosecond laser laser-assisted *in situ* keratomileusis (FS-LASIK) involve the dissection of a superficial lamellar flap by suction to reveal the corneal stroma for remodelling. FS-LASIK creates a predictable homogeneously thick stromal flap, which is elevated by a suction ring. It leads to better refractive results in comparison to standard microkeratomers most likely due to more predictable and planar corneal flaps (1).



During the LASIK procedure, the intraocular pressure (IOP) is abruptly increased. Dramatic IOP change has been theorised to vitreous traction, thereby causing postoperative optic nerve and vitreoretinal complications. As such, glaucoma is also a contraindication (2, 3). It is evident from the literature that LASIK with mechanical microkeratome is not detrimental to retinal nerve fibre layers of healthy individuals (4, 5). The evidence surrounding FS-LASIK and foveal and retinal thickness is conflicting and sparse. Some studies have demonstrated changes within the retina, following FS-LASIKS (6), whilst others have not (7), and there is uncertainty in the clinical significance of such change (8).

The objective of this study was to determine whether FS-LASIK induces changes in retinal foveal and RNFL measurements with optical coherence tomography (OCT) immediately post-procedure.

## MATERIALS AND METHODS

All patients underwent corneal pachymetry and topography preoperatively. Patients with contraindication to LASIKs were excluded. Contraindications include ocular disease, ocular surface disorder, glaucoma, corneal thickness < 500 microns, and/or irregular corneal topography. The patients were also excluded from the study if their preoperative best-corrected visual acuity was < 20/40 or if they had prior laser or intraocular surgery. Our prospective study recruited patients undergoing FS-LASIK by one surgeon (WZH).

All patients on examination had an intraocular pressure (IOP) < 21 mmHg and normal optic disk. A normal optic disk was defined by a vertical cup-to-disk asymmetry <0.2, cup/disk ratio <0.6, and an intact neuro-retinal rim without peripapillary haemorrhages, notches, localised pallor, or nerve fibre layer defect.

All patients underwent FS-LASIK treatment using the VISX™ (Abbott Medical Optics Inc., Santa Clara, CA, USA) under topical anaesthesia. A corneal flap, 110-micron thick, was created by IFS IntraLase™ 150 HZ (Abbott Medical Optics Inc., Santa Ana, CA, USA). Suction during the creation of a flap lasted ~45 s. Retinal fovea thickness, volume, and retinal nerve fibre layer (RNFL) thickness were measured preoperatively, and postoperatively at 1 h and 1 day, following FS-LASIK surgery. OCT (Optovue Inc., Fremont, CA, USA) performed 360° circular scans with a diameter of 3.45 mm centred on the optic disk.

Only the right eyes of the participants were included to be observed.

## Statistical Analysis

Volume and thickness of the inner retina (macula fovea, parafovea, and perifovea), and the thickness of the RNFL (superior, inferior, nasal, and temporal) were recorded pre- and postoperatively. The mean and standard deviation were calculated for both pre- and postoperative measurements. A paired *t*-test was utilised to determine any statistical difference between pre- and postoperative measurements. A *p*-value < 0.05 was considered statistically significant.

**TABLE 1 |** Mean macular fovea thickness and volume before and after femtosecond laser laser-assisted *in situ* keratomileusis (FS-LASIK) surgery.

	Fovea thickness (μm)	Fovea volume (mm <sup>2</sup> )	Parafovea thickness (μm)	Parafovea volume (mm <sup>2</sup> )	Perifovea thickness (μm)	Perifovea volume (mm <sup>2</sup> )
<b>Mean macular fovea thickness and volume (n = 37) (Mean ± SD)</b>						
Before LASIK	67.18 ± 10.25	0.527 ± 0.081	124.29 ± 7.61	0.780 ± 0.047	98.83 ± 2.57	2.128 ± 0.199
1 h post-op	57.81 ± 10.5	0.454 ± 0.082	100.43 ± 15.98	0.634 ± 0.098	91.81 ± 1.48	1.941 ± 0.183
<i>t</i> -value	6.171	6.032	9.837	9.700	2.532	4.393
<i>P</i> -value	0.000*	0.000*	0.000*	0.000*	0.016*	0.000*
1 day post-op	62.24 ± 10.64	0.495 ± 0.088	120.18 ± 8.33	0.755 ± 0.052	100.75 ± 4.41	2.107 ± 0.187
<i>t</i> -value	3.620	3.220	2.901	2.910	0.694	0.525
<i>P</i> -value	0.001*	0.003*	0.006*	0.006*	0.492	0.603

**TABLE 2 |** Mean retinal nerve fibre layer thickness before and after FS-LASIK surgery.

	Temporal	Superior	Nasal	Inferior
<b>Mean retinal nerve fibre layer (n = 37) (μm) (Mean ± SD)</b>				
Before LASIK	98.08 ± 10.14	129.24 ± 12.79	58.00 ± 9.08	124.29 ± 13.56
1 h post-op	86.86 ± 13.56	123.97 ± 17.16	58.67 ± 11.52	122.05 ± 17.42
<i>t</i> -value	4.926	2.265	0.443	0.997
<i>P</i> -value	0.000*	0.011*	0.66	0.325
1 day post-op	99.59 ± 12.4	126.78 ± 14.69	59.51 ± 9.98	129.24 ± 14.17
<i>t</i> -value	0.905	1.166	1.727	3.632
<i>P</i> -value	0.372	0.251	0.093	0.001*

## RESULT

Eighteen males and nineteen females ( $n = 37$ ) were enrolled in this study. Mean patient age was  $22.94 \pm 4.22$  years. The thickness and volume of the macula declined significantly 1 h post operation (Table 1). By Day 1, post operation, five out of the six measures of the macula showed decreases compared to the preoperative values, but only four (fovea thickness and volume, parafovea thickness, and volume) of these were statistically significant (Table 1). All showed increases compared to immediate postoperatively.

The mean RNFL decreased 1 h postoperatively in the temporal and superior RNFL (Table 2). At 1 day post-operation, the RNFL was only significantly increased in the inferior portion compared to the preoperative measures. All measurements of macula and RNFL thickness and volume increased between 1 h postoperatively and 1 day postoperatively.

## DISCUSSION

Our study showed significant differences in preoperative and postoperative FS-LASIKs measurements of the macula and RNFL thickness as determined by OCT. Eight of ten measurements 1 h after FS-LASIKs were significantly different, whilst only five of ten measurements 1 day after FS-LASIKs were significantly different compared to preoperative measurements of the macula and RNFL. All measurements showed improvement between 1 and 1 day postoperatively. We hypothesise that our results are due to alterations in corneal architecture, thereby inducing artefactual OCT measurements.

There is conflicting evidence regarding measurements of macular edema and RNFL measurements by OCT in FS-LASIKs. Some studies have demonstrated changes within the macula and RNFL post FS-LASIKs (6, 8) and have attributed these effects to macular edema associated with IOP elevation during procedure. Elevation of IOP during LASIKs can be significant. In a previous study, intraoperative microkeratome LASIKs lead to IOP values of  $> 150$  mmHg (9). Whilst FS-LASIKs leads to reduced IOP values during the suction, they lead to a greater period of maintenance of high IOP pressure, and there is uncertainty in comparative effect of FS-LASIKs on retinal measurements (10).

A range of microkeratome LASIK studies has demonstrated no detrimental effects on RNFL and macular thickness (3–5) and suggested that changes demonstrated *via* OCT are secondary to

corneal aberrations, leading to artefactual measurements of the retina and fovea since there was no possibility that substantive decrease and the following increase of retina thickness can happen. The most likely cause of this phenomenon would be the reflectivity change, following the refractive procedure. Furthermore, larger studies with longer follow-up times have demonstrated that LASIKs is rarely associated with vitreoretinal pathology (11, 12).

Optical coherence tomography evaluates the reflectivity of posterior segment structures. Utilising these data, the RNFL thickness can consequently be calculated. FS-LASIK produces corneal spherical aberrations (13) and alters the refractive properties of the cornea. Consequently, this can interfere with OCT measurements, reducing reliability within the immediate postoperative period. These changes in refraction can be compensated for such as in scanning laser polarimetry (SLP) (14, 15). We should be aware of this measurement changes following the refractive procedure, since the myopia patients are the well-known potential high-risk group of glaucoma and retina disease in which OCT is one of the most important diagnostic tools.

## CONCLUSION

In our study, FS-LASIKs induced alterations in the inner retina and RNFL measurements by OCT. This is unlikely to be actual structural changes but is associated with changes in refractive properties of the cornea.

## DATA AVAILABILITY STATEMENT

The raw data supporting the conclusions of this article will be made available by the authors, without undue reservation.

## AUTHOR CONTRIBUTIONS

All authors listed have made a substantial, direct, and intellectual contribution to the work and approved it for publication.

## FUNDING

This work was supported by The Non-profit Central Research Institute Fund of Chinese Academy of Medical Sciences (2018PT32029).

## REFERENCES

- Gil-Cazorla R, Teus MA, de Benito-Llopis L, Mikropoulos DG. Femtosecond laser vs. mechanical microkeratome for hyperopic laser *in situ* keratomileusis. *Am J Ophthalmol.* (2011) 152:16–21.e2. doi: 10.1016/j.ajo.2011.01.009
- Lee AG, Kohner T, Ebner R, Bennett JL, Miller NR, Carlow TJ, et al. Optic neuropathy associated with laser *in situ* keratomileusis. *J Cataract Refract Surg.* (2000) 26:1581–4. doi: 10.1016/S0886-3350(00)00688-X
- Whitson JT, McCulley JP, Cavanagh HD, Song J, Bowman RW, Hertzog L. Effect of laser *in situ* keratomileusis on optic nerve head topography and retinal nerve fiber layer thickness. *J Cataract Refract Surg.* (2003) 29:2302–5. doi: 10.1016/S0886-3350(03)00466-8
- Dementyev DD, Kourenkov VV, Rodin AS, Fadeykina TL, Diaz Martines TE. Retinal nerve fiber layer changes after LASIK evaluated with optical coherence tomography. *J Refract Surg.* (2005) 21:S623–7. doi: 10.3928/1081-597X-20050902-13
- Aristeidou AP, Labiris G, Paschalis EI, Foudoulakis NC, Koukoulas SC, Kozobolis VP. Evaluation of the retinal nerve fiber layer measurements, after photorefractive keratectomy and laser *in situ* keratomileusis, using scanning laser polarimetry (GDx VCC). Graefe's archive for clinical and experimental ophthalmology = Albrecht von Graefes Archiv

- fur klinische und experimentelle. *Ophthalmologie*. (2010) 248:731–6. doi: 10.1007/s00417-009-1273-5
6. Zhang J, Zhou YH. Effect of suction on macular thickness and retinal nerve fiber layer thickness during LASIK used femtosecond laser and Moria M2 microkeratome. *Int J Ophthalmol*. (2015) 8:777–83. doi: 10.3980/j.issn.2222-3959.2015.04.24
  7. Zhang J, Zhou Y, Zheng Y, Liu Q, Zhai C, Wang Y. Effect of suction on macular and retinal nerve fiber layer thickness during femtosecond lenticule extraction and femtosecond laser-assisted laser *in situ* keratomileusis. *J Cataract Refract Surg*. (2014) 40:1994–2001. doi: 10.1016/j.jcrs.2014.03.027
  8. Zhao PF, Zhou YH, Zhang J, Wei WB. Analysis of macular and retinal nerve fiber layer thickness in children with refractory amblyopia after femtosecond laser-assisted laser *in situ* keratomileusis: a retrospective study. *Chinese Med J*. (2017) 130:2234–40. doi: 10.4103/0366-6999.213959
  9. Bradley JC, McCartney DL, Craenen GA. Continuous intraocular pressure recordings during lamellar microkeratotomy of enucleated human eyes. *J Cataract Refract Surg*. (2007) 33:869–72. doi: 10.1016/j.jcrs.2007.02.017
  10. Katsanos A, Arranz-Marquez E, Canones R, Lauzirika G, Rodriguez-Perez I, Teus MA. Retinal nerve fiber layer thickness after laser-assisted subepithelial keratomileusis and femtosecond LASIK: a prospective observational cohort study. *Clin Ophthalmol*. (2018) 12:1213–8. doi: 10.2147/OPHTH.S168033
  11. Arevalo JF, Ramirez E, Suarez E, Morales-Stopello J, Cortez R, Ramirez G, et al. Incidence of vitreoretinal pathologic conditions within 24 months after laser *in situ* keratomileusis. *Ophthalmology*. (2000) 107:258–62. doi: 10.1016/S0161-6420(99)00078-0
  12. Ruiz-Moreno JM, Alio JL. Incidence of retinal disease following refractive surgery in 9,239 eyes. *J Refract Surg*. (2003) 19:534–47. doi: 10.3928/1081-597X-20030901-08
  13. Zhang H, Wang Y, Li H. Corneal spherical aberration and corneal asphericity after small incision lenticule extraction and femtosecond laser-assisted LASIK. *J Ophthalmol*. (2017) 2017:4921090. doi: 10.1155/2017/4921090
  14. Choplin NT, Schallhorn SC, Sinai M, Tanzer D, Tidwell JL, Zhou Q. Retinal nerve fiber layer measurements do not change after LASIK for high myopia as measured by scanning laser polarimetry with custom compensation. *Ophthalmology*. (2005) 112:92–7. doi: 10.1016/j.ophtha.2004.07.027
  15. Halkiadakis I, Anglionto L, Ferensowicz M, Triebwasser RW, van Westenbrugge JA, Gimbel HV. Assessment of nerve fiber layer thickness before and after laser *in situ* keratomileusis using scanning laser polarimetry with variable corneal compensation. *J Cataract Refract Surg*. (2005) 31:1035–41. doi: 10.1016/j.jcrs.2004.12.045

**Conflict of Interest:** The authors declare that the research was conducted in the absence of any commercial or financial relationships that could be construed as a potential conflict of interest.

**Publisher's Note:** All claims expressed in this article are solely those of the authors and do not necessarily represent those of their affiliated organizations, or those of the publisher, the editors and the reviewers. Any product that may be evaluated in this article, or claim that may be made by its manufacturer, is not guaranteed or endorsed by the publisher.

Copyright © 2021 Jiang, Wang, Li, Li and Lu. This is an open-access article distributed under the terms of the Creative Commons Attribution License (CC BY). The use, distribution or reproduction in other forums is permitted, provided the original author(s) and the copyright owner(s) are credited and that the original publication in this journal is cited, in accordance with accepted academic practice. No use, distribution or reproduction is permitted which does not comply with these terms.



# Evaluation of Choroidal Thickness Using Optical Coherent Tomography: A Review

Rui Xie<sup>1,2</sup>, Bingjie Qiu<sup>1,2</sup>, Jay Chhablani<sup>3</sup> and Xinyuan Zhang<sup>1,2\*</sup>

<sup>1</sup> Beijing Institute of Ophthalmology, Beijing Tongren Eye Center, Tongren Hospital, Capital Medical University, Beijing, China, <sup>2</sup> Beijing Retinal and Choroidal Vascular Diseases Study Group, Beijing, China, <sup>3</sup> The University of Pittsburgh Medical Center Eye Center, University of Pittsburgh, Pittsburgh, PA, United States

## OPEN ACCESS

### Edited by:

Hetian Lei,  
Shenzhen Eye Hospital, China

### Reviewed by:

Yifei Zhang,  
Hospital Conde S. Januário, Macao  
SAR, China  
Ramesh Venkatesh,  
Narayana Nethralaya, India

### \*Correspondence:

Xinyuan Zhang  
mmzy2010@163.com

### Specialty section:

This article was submitted to  
Ophthalmology,  
a section of the journal  
Frontiers in Medicine

**Received:** 26 September 2021

**Accepted:** 18 October 2021

**Published:** 03 December 2021

### Citation:

Xie R, Qiu B, Chhablani J and Zhang X  
(2021) Evaluation of Choroidal  
Thickness Using Optical Coherent  
Tomography: A Review.  
Front. Med. 8:783519.  
doi: 10.3389/fmed.2021.783519

The choroid is the main source of blood and nourishment supply to the eye. The dysfunction of the choroid has been implicated in various retinal and choroidal diseases. The identification and in-depth understanding of pachychoroid spectrum disorders are based on the tremendous progress of optical coherence tomography (OCT) technology in recent years, although visibility of choroid is challenging in the era of the time or spectral domain OCT. The recent rapid revolution of OCTs, such as the enhanced depth imaging OCT and the swept-source OCT, has greatly contributed to the significant improvement in the analysis of the morphology and physiology of the choroid precisely, especially to the choroid–scleral boundary and vasculature. The present review highlights the recently available evidence on the measurement methodology and the clinical significance of choroidal thickness in retinal or choroidal disorders.

**Keywords:** choroidal thickness, optical coherence tomography, swept-source optical coherence tomography, methodology, morphological investigation

## INTRODUCTION

The choroid is mainly composed of blood vessels and is the posterior portion of the uveal tract with rich and slow blood flow. As the main source of blood supply to the retinal epithelium, the outer retina, and the optic nerve, the choroid plays a significant role in maintaining the normal metabolism of the retinal pigment epithelium (RPE) and photoreceptors (1). The dysfunction of the choroid has been implicated in various retinal and choroidal diseases. Additionally, choroidal thickness (ChT) is a sensitive biomarker in the prediction, diagnosis, intervention, and follow-up of various acute or chronic retinal and choroidal diseases, including polypoidal choroidal vasculopathy (PCV), central serous chorioretinopathy (CSCR), and idiopathic macular hole (IMH) (2–4).

Optical coherence tomography (OCT) is a non-invasive fundus imaging modality, which plays a vital role in revealing the pathogenesis and development of retinal–choroidal diseases. Compared to other imaging modalities, OCT has greatly improved clinical diagnosis and research since its inception in the 1990s. Furthermore, the wide use of OCT-angiography boosts the OCT field from structural imaging to vascular imaging and provides an opportunity for the quantitative analysis of both ocular structure and vasculature, especially the choroid thickness. Compared to the traditional methods such as ultrasound and indocyanine green angiography (ICGA), the advantage of OCT is non-invasive and repeatable with a higher resolution (5, 6).

Choroidal thickness measuring *in vivo* has been reported in various diseases using different available methods/devices including ultrasound and OCT since 1979 (7, 8). To date, ChT has



become a vital predictive imaging biomarker for both retinal and choroidal disorders. In-depth understanding of pathogenesis of these disorders drives us to understand the standard method to measure ChT.

Presently, there is no unified international protocol for ChT measurement by OCT, the most popular methods being manual and automatic segmentation. In this review, we have highlighted the recently available evidence on the measurement methodology of ChT, and the significance of ChT in various retinal or choroidal disorders.

## ANATOMICAL CHARACTERISTICS OF THE CHOROID

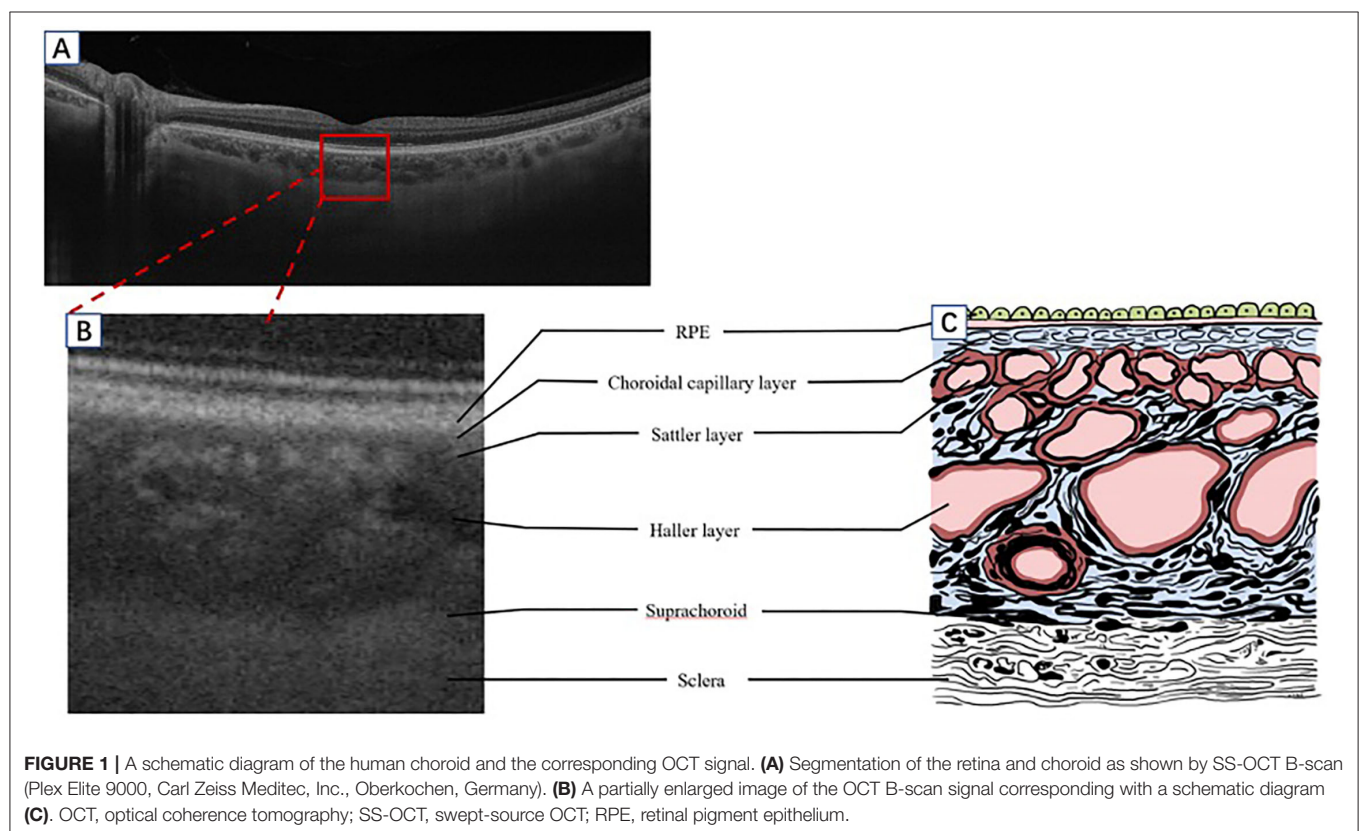
The choroid is located between the retina and the sclera. Anatomically, from inside toward outside, it has been described as five layers: Bruch's membrane (BrM), the choroidal capillary (CC), the Sattler, the Haller layers, and the suprachoroid cavity. Approximately 90% of the ocular blood perfusion is supplied by the choroid, 70% of which is from the CC layer. The CC layer has high blood flow, high vascular density, and abundant interstices that play a significant role in the metabolism of photoreceptor cells and the RPE (9). The choroidal blood vasculature is distributed in a leaflet shape and arranged into layers. As the choroidal blood vessel is the only source of nourishment supply for the fovea, the sub-macular choroid is the thickest part. The large vessel calibers of the Haller layer run parallel with its branch in a fan shape, forming a

network of lobular capillaries, which communicate with each other and supply blood in different regions. The function of these anastomoses is to shunt blood to balance the circulation pressure of the lobules, and it is the basis for maintaining the function of the retina (9–11). In addition to the blood supply, choroid tissue has various functions, including temperature regulation and the absorption of light to form a dark chamber (12) (Figure 1).

## PRINCIPLE OF CHOROID IMAGING BY OCT

As a non-invasive fundus imaging technology, OCT works by dividing the monochromatic light into two beams through the coupler: the reference arm and the measuring arm, which penetrates the intraocular refractive stroma to the surface of the retina. The two beams are reflected by a mirror, and the fundus tissue could be assessed, respectively. After being combined with the coupler from the interference, the beams were detected by the photodetector based on the heterogeneity and different depths of the tissue. The two or three-dimensional structure images of the biological tissue can be obtained by collecting the varied reflected interference signal (13).

Time domain (TD)-OCT realizes axial scanning (A scan) by reference to the rapid changes in the optical delay lines generated by the mechanical motion of the reference arm, but the scanning depth is limited, and the speed is slow (14, 15). The reference arm of the spectral domain (SD)-OCT is fixed,



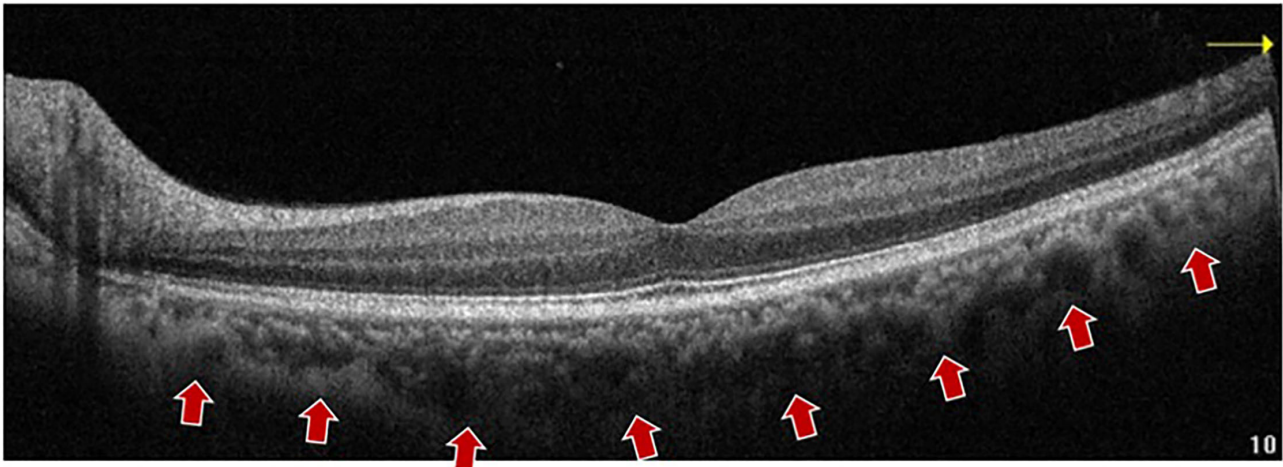


**FIGURE 2 |** A representative EDI-OCT B-scan imaging of a 57 years old subject. The choroid boundary is detected vaguely. An EDI-OCT (Optovue, Inc., California, United States) B-scan image shows the choroid–sclera boundary (arrows) with a central wavelength of 850 nm, which made the zero-delay line to the choroid by moving the device closer to the eye, thus improving image resolution and facilitating the identification of the choroid–scleral interface. EDI OCT, enhanced depth imaging OCT; SD-OCT, spectral domain OCT.

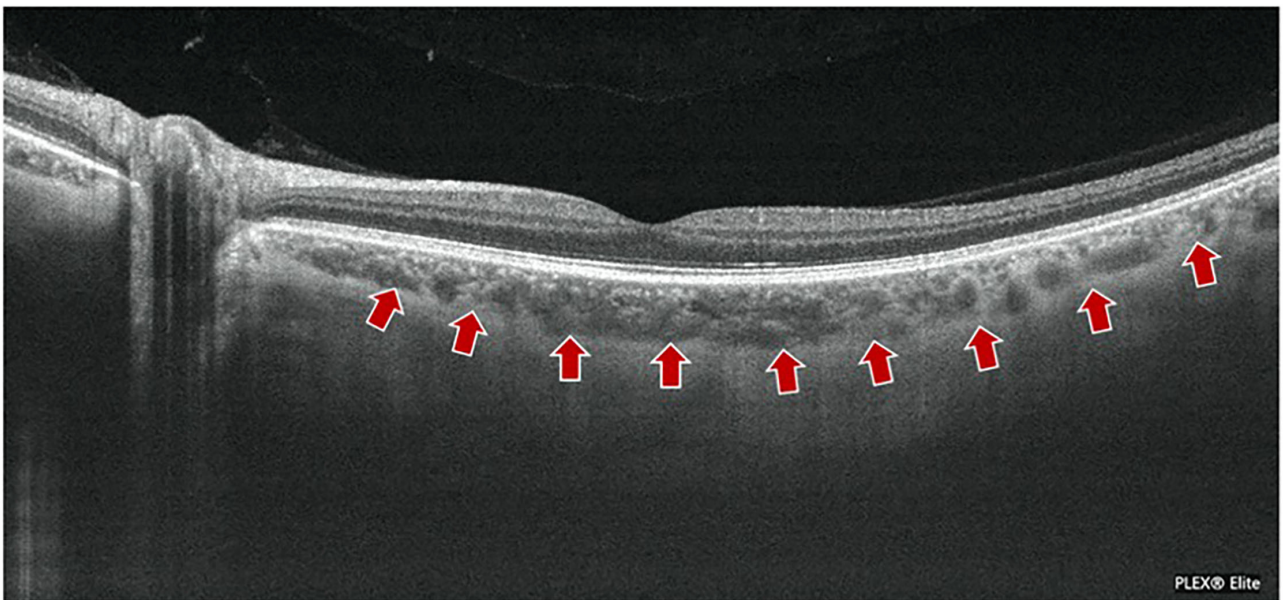


**FIGURE 3 |** A representative imaging of SS-OCT in normal subject. The boundary of choroid–scleral (arrows) and choroidal vasculature in a 49 year-old man are clearly shown using an SS-OCT (Plex Elite 9000, Carl Zeiss Meditec, Inc., Oberkochen, Germany). SS-OCT could reach up to 6 mm depth, 200,000 A scans per second (Plex Elite 9000) with 200,000 A scans per second, and 6.3  $\mu\text{m}$  of axial resolution.

the interference signal data is recorded through the spectrometer receiver and assessed by Fourier (inverse) transform to obtain the axial depth information, thus greatly improving the speed and depth of the OCT (16). Nevertheless, due to the attenuation and scattering of light by the RPE, TD-OCT, and SD-OCT cannot delineate the choroid details and choroidal scleral interface, rendering it challenging to achieve a high-resolution tomography

of the choroid. In addition, Spaide et al. developed an enhanced depth imaging (EDI)-OCT in 2008, which can measure ChT for the first time by moving the zero delay line toward the choroid to present the choroid details of the structure (17). With the development of laser technology, swept-source (SS)-OCT emerged, which improved the imaging speed, depth, software algorithm, and eye-movement tracking technology. This

increases the tissue resolution and image signal-to-noise ratio and contributed to an in-depth understanding of choroidal diseases (18–20).

However, compared to ICGA, OCT can only detect the lesion in a static state. Various blood flows are graded to interpret the active blood flow lesions in the dynamic state and quantitate the blood signal, which would be the trend in the future.

## EDI-OCT and the Choroid

Conventional SD-OCT uses a high-resolution spectrophotometer to separate the wavelengths due to the zero-delay line at the posterior vitreous boundary level and the light scattering of the RPE layer, making the obtained tomographic images unable to identify the choroid–scleral interface clearly. EDI-OCT proposed by Spaide for the first time in 2008 (17), with a central wavelength of 850 nm, made the zero-delay line to the choroid by moving the device closer to the eye, thus improving image resolution and facilitating the identification of the choroid–scleral interface. In addition, the image averaging technique could increase the signal-to-noise ratio and reduce speckle for enhanced choroid visualization (21, 22) (Figure 2).

## SS-OCT and the Choroid

Compared to SD-OCT, SS-OCT uses a light source with a longer wavelength and a double-balanced light detector. The central wavelength is 1,050 nm/1,060 nm, with strong penetration, and hence is less affected by the light scattering of RPE, lens turbidities, and less signal attenuation, giving a better visualization of the deep layer (23–25). SS-OCT could reach up to 6 mm of depth, 200,000 A scans per second (Plex Elite 9000, Carl Zeiss Meditec, Inc., Oberkochen, Germany), and 6.3  $\mu\text{m}$  of axial resolution (26). After technical innovation of SS-OCT in microelectronics mechanical systems, tunable filter technology, and vertical-current surface-emitting laser, an intensive scanning mode and greater scanning area are realized. Beyond that, the eye movement artifact could be reduced to improve the quality of imaging and make faster imaging inspection with higher efficiency and a wide scanning range (27–29) (Figure 3).

## METHODS FOR MEASURING ChT

### Histopathological and Ultrasound

The ChT measured by histopathology is objective but thinner than the true value with respect to the choroid, which is a highly vascularized tissue and ChT varying with its blood perfusion. Moreover, histological fixation can lead to the deformation and shrinkage of the choroid, and the correlation between the measured value and the true value cannot be quantified accurately (30, 31). ICGA is a traditional method for assessing the morphology of choroidal vessels but could not provide anatomical tomography images.

The resolution of ultrasound is lower than that of OCT for choroidal tomography. Ultrasound at 20 MHz achieves posterior imaging, which is mainly used in the case of refractive media opacity and can evaluate the deeper structure (32).

## Optical Coherence Tomography

Presently, there is no international unified reference standard for OCT measurement of ChT. The mainstream methods are mainly divided into manual single-point or multi-point measurement and automatic segmentation methods (Table 1).

### Manual Method

Manual methods have been described as single-point and multi-point methods. Theoretically, subfoveal choroidal thickness (SFCT) is the thickest part of the choroid, but single-point measurement cannot reflect the overall information of the choroid (47). The multi-point methods were further categorized into horizontal and vertical techniques. The horizontal multi-point method was utilized to measure the SFCT, the nasal and temporal sides of the fovea. The multipoint can be three points, seven points, and nine points. The three points are located at 750  $\mu\text{m}$  and 1,000  $\mu\text{m}$  to the fovea temporally and nasally, the seven points and nine points are located at 500  $\mu\text{m}$  intervals in the horizontal section (6, 35, 36, 39, 40). Some other multi-point methods simultaneously measure the ChT horizontally and vertically. Five or nine points are placed at the SFCT and its superior, inferior, nasal, and temporal sides. The five points are located at the 1,500  $\mu\text{m}$  or 3,000  $\mu\text{m}$  to the fovea superiorly, inferiorly, temporally and nasally. The nine-points are located at the 1,000  $\mu\text{m}$ , 3,000  $\mu\text{m}$  or with the 1,500  $\mu\text{m}$  interval to the fovea superiorly, inferiorly, temporally and nasally (37, 38, 41, 42). Although manual measurement has good repeatability (48), it is difficult to avoid errors. The multipoint and multi-quadrant measurement reflects the average ChT, the distribution, and trend of ChT in cohort population and reduces the single-point error (Figure 4).

### Automatic Segmentation Method

The choroid is segmented scanned by EDI-OCT (Heidelberg Spectralis, Heidelberg Engineering, Heidelberg, Germany) and SS-OCT (Triton DRI OCT, Topcon, Tokyo, Japan) through the Early Treatment Diabetic Retinopathy Study (ETDRS) grid using the Heidelberg Engineering software and the TOPCON Advanced Boundary Segmentation-TABS software (49, 50). Each image is constituted by the average of 32 overlapping continuous scans, covering an area of 12 mm  $\times$  9 mm with 12 radial scans, providing a three-dimensional ChT mapping by measuring ChT at any point in the macula (51). The reference line is adjusted from the retinal boundary (the internal limiting membrane—RPE) to the choroid boundary (the RPE–choroid–scleral junction), and then an ETDRS map is generated automatically, which can be corrected manually. The ETDRS grid is composed of three concentric circles: the diameter of the fovea, parafovea, and perifovea are 1, 3, and 6 mm, respectively. The average ChT in the central circular and the eight sectors of the nasal inner macula, superior inner macula, temporal inner macula, inferior inner macula, nasal outer macula, superior outer macula, temporal outer macula, and inferior outer macula areas can be calculated, respectively (44–46, 52, 53) (Figure 5).



**TABLE 1 |** Methods for measuring choroidal thickness.

Methods for measuring choroidal thickness		References	Description of measurement, location, and method
Manual measurement	Subfoveal choroidal thickness (SFCT)	(33)	From the Bruch's membrane to the sclerochoroidal interface at fovea.
		(34)	At the fovea with enhanced depth imaging OCT, 9-mm horizontal and vertical scans through the foveal center.
	Three-point method	(6)	From the outer edge of the hyper-reflective RPE to the sclerochoroidal interface at the fovea, 750 $\mu\text{m}$ temporal to the fovea, and 750 $\mu\text{m}$ nasal to the fovea.
		(35)	From the outer edge of the hyper-reflective RPE to the sclerochoroidal interface at the fovea and at 1,000 $\mu\text{m}$ nasal and temporal to the fovea.
		(36)	
		(37)	The vertical distance from the Bruch's membrane to the sclerochoroidal interface at fovea and 1,500 $\mu\text{m}$ nasally, 1,500 $\mu\text{m}$ superiorly, 1,500 $\mu\text{m}$ temporally, and 1,500 $\mu\text{m}$ inferiorly apart from the foveal center.
	Five-point method	(38)	At the fovea and 3,000 $\mu\text{m}$ nasal, temporal, superior, and inferior to the fovea in the horizontal and vertical sections.
		(39)	At the fovea and 500 $\mu\text{m}$ , 1,000 $\mu\text{m}$ and 1,500 $\mu\text{m}$ nasal and temporal to the fovea.
	Seven-point method	(40)	The vertical distance from the Bruch membrane to the sclerochoroidal interface at fovea, and nasal respective temporal at 500 $\mu\text{m}$ , 1,000 $\mu\text{m}$ , 1,500 $\mu\text{m}$ and 2,000 $\mu\text{m}$ distance from the fovea.
		(41)	At the fovea and 1,000 $\mu\text{m}$ and 3,000 $\mu\text{m}$ to the fovea superiorly, inferiorly, temporally, and nasally.
	Nine-point method	(42)	At the fovea and 1,500 $\mu\text{m}$ and 3,000 $\mu\text{m}$ from the center of the fovea in areas of superior, temporal, inferior, and nasal quadrants.
		(43)	The fovea and 1,000 $\mu\text{m}$ intervals from the fovea to a distance of 3,000 $\mu\text{m}$ in the nasal, temporal, superior, and inferior directions. The average of 14 choroidal thickness readings was recorded as the macular choroidal thickness.
		(44)	
Automatic measurement	Macular choroidal thickness	(3)	The choroidal thickness was automatically measured with choroidal thickness map using the Early Treatment Diabetic Retinopathy Study grid (EDTRS). It's divided into 9 sectors in the grid.
		(45)	The diameters for central foveal circle, parafoveal circle, and perifoveal circle were 1, 3, and 6 mm, respectively.
		(46)	

## CHOROIDAL THICKNESS AND ITS INFLUENCING FACTORS

The majority of the studies measured the ChT as the height from the BrM to the choroid–scleral interface (33, 37, 40, 54, 55); however, some studies have defined it as the height from the lower boundary of the hyperreflective RPE to the choroid–scleral interface (34, 38, 42, 43, 56). Margolis and Spaide (57) pointed out that subfoveal CT (SFCT) is the thickest part in the average age of 50.4-years among the 54 normal eyes in a retrospective study, and the average SFCT was  $287 \pm 76$  microns by using Spectralis OCT (Spectralis, Heidelberg Engineering Co, Germany). Subsequently, ChT is rather thin from subfoveal to peripheral retina, temporal thicker than nasal, upward than downward, and peri-optic papilla is the thinnest, which is associated with choroidal vein distribution (58). Interestingly, the results of the study by Ikuno and Ruiz-Moreno are similar (59, 60).

As one of the objective biomarkers for the evaluation of choroid, ChT is dependent on the physiological and pathological factors of the body, and varies with age, refractive, axial length, or diurnal variation (17, 61, 62). A large number of studies have confirmed that age and axial length are the primary factors influencing ChT, and both are negatively correlated with ChT

(63–65). Spaide et al. pointed out that ChT decreases 15  $\mu\text{m}$  per 10 years (17). In a longitudinal study based on 3,233 Chinese individuals, SFCT was reported to be  $254 \pm 107 \mu\text{m}$  (Spectralis, Heidelberg Engineering Co) with an average age of 65 years (55). Lee et al. reported that SFCT was [median (IQR): 370] 312–406  $\mu\text{m}$  (Spectralis, Heidelberg Engineering Co.) in 741 young adults aged 19–30 years (66).

In addition, the normal ChT differs among different measuring instruments. Bhayana (63) reported that the ChT measured by SS-OCT (DRI-OCT Triton Plus, Topcon, Tokyo, Japan) was slightly higher than that of SD-OCT (Spectralis, Heidelberg Engineering Co.), which was consistent with the results of Matsuo and Copete. This could be attributed to the ability of SS-OCT to identify the choroid–scleral interface precisely (67–69).

Moreover, it is yet to be elucidated whether cardiovascular risk factors have an impact on the choroid as it is a vascular tissue. In a case–control study, Schuster et al. (40) demonstrated that SFCT was associated with the left ventricular end-diastolic blood pressure, systolic blood pressure, epidermal growth factor receptor, and dyslipidemia. By logistic analysis, it was suggested that this correlation is associated with age. Thus, additional qualitative and quantitative studies are warranted to provide more clinical evidence of ChT.



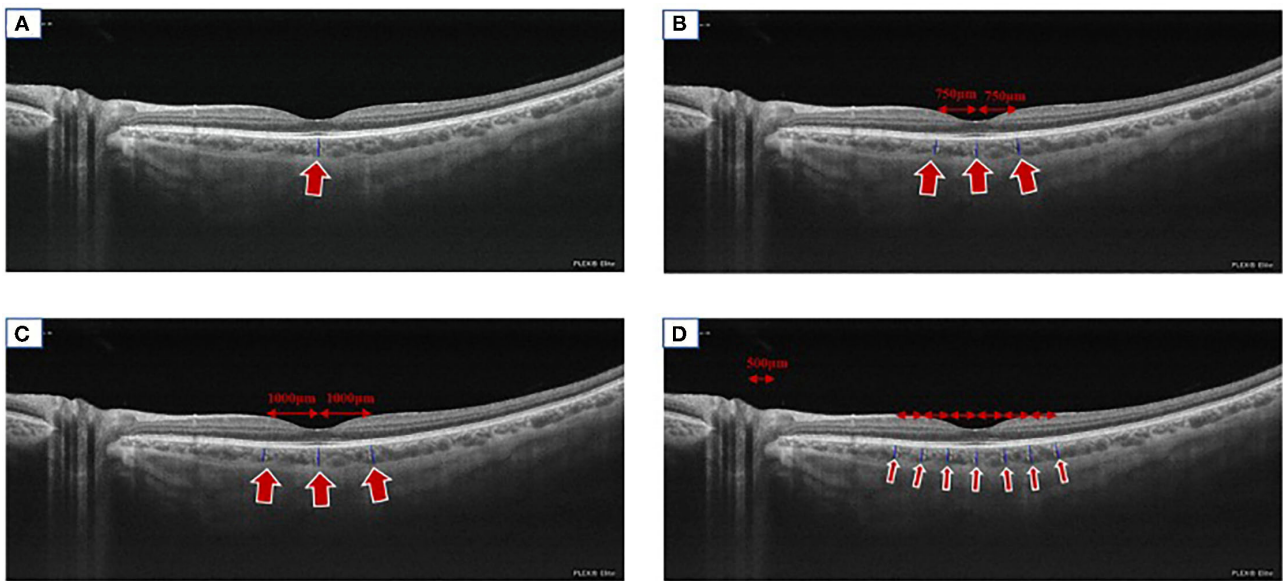


**FIGURE 4 |** Manual measuring methods. A representation of imaging showing the routinely used manual measuring methods. **(A)** We took SS-OCT (Plex Elite 9000, Carl Zeiss Meditec, Inc., Oberkochen, Germany) as an example to display the single-point method (arrow). **(B)** The three-point method (the fovea, at 750 nasally to the fovea and temporal to the fovea, arrows). **(C)** The three-point method (the fovea, 1,000  $\mu\text{m}$  nasally to the fovea and temporally to the fovea, arrows). **(D)** The seven-point method (the fovea, 500, 1,000, and 1,500  $\mu\text{m}$  nasally and temporally to the fovea respectively, arrows).

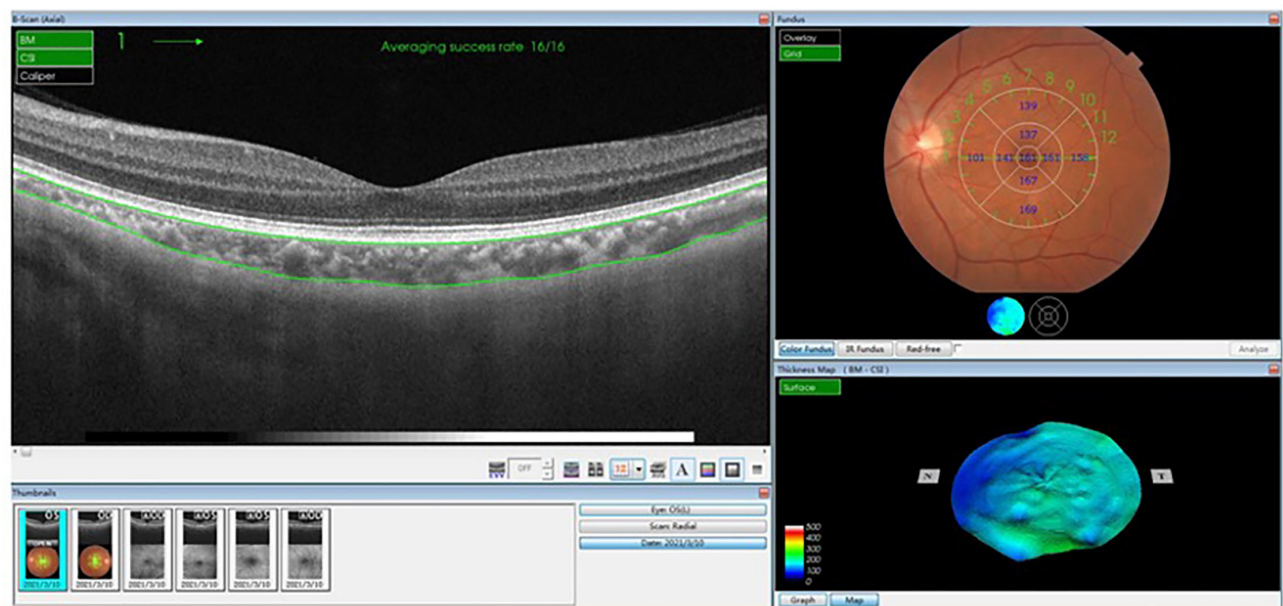


**FIGURE 5 |** The ETDRS automatic segmentation method using TOPCON advanced boundary segmentation-TABS software. An ETDRS map is generated automatically, which can be corrected manually. The ETDRS grid is composed of three concentric circles: the diameter of the fovea, parafovea, and perifovea are 1, 3, and 6 mm, respectively. The average choroidal thickness in the central circular and the eight sectors of superior, inferior, nasal, and temporal areas can be calculated, respectively. ETDRS, Early Treatment Diabetic Retinopathy Study.

## CLINICAL SIGNIFICANCE OF ChT

The choroid provides oxygen and nutrition to the outer five layers of the retina and plays a vital role in the metabolism of RPE

and photoreceptors. Therefore, its pathological state is closely related to several diseases, especially pachychoroid spectrum diseases (PCDs), age-related macular degeneration (AMD), and choroidal atrophy associated with pathological myopia.

Choroidal vasodilation and/or hyper-perfusion and elevated hydrostatic pressure lead to increased choroidal permeability and focal choroidal exudation with ChT thickening (70). While hypoperfusion and ChT thinning lead to metabolic disorders of RPE and photoreceptor, the growth factors secreted by RPE are insufficient to maintain the physiological needs of the choroidal vessels in reverse, which form a vicious circle and accelerate the progress of the disease (71). Therefore, ChT can be used as a quantitative index to evaluate and reveal the pathophysiology of choroidal diseases.

## Diseases With Increased ChT

### Pachychoroid Spectrum Diseases

Pachychoroid spectrum disease is a new entity in recent years, which is characterized by the thickening of choroidal layers and dysfunction of choroidal vasculature. PCD usually exhibits chronic continuous thickening and abnormal expansion of the vasculature in the Haller layer and compression of the Sattler and CC layers. The dysfunction of the RPE–BrM–CC complex, intralobular congestion, and stasis may produce an ischemic microenvironment, promote vascular endothelial growth factor (VEGF) expression, leading to secondary choroidal neovascularization (72). Presently, PCD comprises seven major diseases: CSCR, pachychoroid pigment epitheliopathy, pachychoroid neovasculopathy, PCV/aneurysmal type 1 neovascularization, peripapillary pachychoroid disease, and focal choroidal excavation (73).

Polypoidal choroidal vasculopathy is a choroidal vascular disease characterized by polypoidal lesions with diffuse or local dilation of choroidal vascular endings and an abnormal branch vascular network. In a cross-sectional study, Jordan-Yu et al. investigated 100 treatment-naïve PCV eyes, and they found that total lesion areas and polypoidal lesion areas tend to be larger in eyes with increasing SFCT (74), indicating that the pathological features of choroidal background might be the predictive factors influencing the phenotype or progression of PCV. Furthermore, choroidal thickening is a major risk factor in the pathogenesis of PCV, which is a strong evidence differentiated from wet AMD.

Central serous chorioretinopathy is characterized by serous detachment of the neurosensory retina secondary to one or more focal lesions of the RPE. In a prospective study, 34 patients with CSCR in 44 eyes were assessed by SS-OCT. The average ChT in the choroidal leakage area in fluorescein fundus angiography was significantly greater than that in the non-leakage area, and the average ChT in the high permeability region in ICGA was significantly larger than that in the non-pathological area, indicating that increase of hydrostatic pressure in the local choroidal region contributes to CSCR (3). Furthermore, ChT plays a major role in the follow-up of CSCR, which predicts the recurrence or progression of CSCR (75, 76). Half-dose or half-fluence photodynamic therapy reduces SFCT, but patients with a thicker choroid are more likely to have recurrence CSCR (77, 78).

### Peripheral Exudative Hemorrhagic Chorioretinopathy

Peripheral exudative hemorrhagic chorioretinopathy (PEHCR), also known as eccentric degeneration, extramacular disciform degeneration, and peripheral AMD, is characterized by

peripheral subretinal or sub-RPE hemorrhages and/or exudation or peripheral neovascularization in elderly patients. PEHCR primarily affects the neurosensory retina or RPE and the lesions are mostly located at the temporal side of the retina (79). PEHCR and PCV share some mutual clinical and pathophysiological features such as serous or hemorrhagic pigment epithelium detachment, lipid exudation, and abnormal choroid branching vascular network visible on ICGA or OCTA, suggesting that PEHCR may be a peripheral subtype of PCV (80). Yorihiisa et al. (81) documented that PEHCR has choroidal vascular alterations resembling PCV in the affected area on ICGA in a 74-year-old patient. In a retrospective, observational, comparative case series, the choroid was significantly thicker in temporal periphery in PEHCR eyes than that in control eyes ( $272.70 \pm 80.20 \mu\text{m}$  vs.  $166.60 \pm 40.10 \mu\text{m}$ ,  $p = 0.0002$ ), the mean large choroidal vessel thickness is significantly thicker in PEHCR eyes in comparison with the control eyes ( $202.40 \pm 50.80 \mu\text{m}$  vs.  $160.60 \pm 40.50 \mu\text{m}$ ,  $p = 0.0235$ ), suggesting the favor inclusion of PEHCR in the pachychoroid disease spectrum (82). Larger cohort studies are warranted to further understand the pathophysiology of PEHCR and to investigate whether PEHCR is a new entity of PCD.

### Vogt–Koyanagi–Harada Disease

Vogt–Koyanagi–Harada (VKH) is autoimmune granulomatous inflammatory disorder, involving bilateral eyes. Studies have shown that the ChT increased in the acute stage of VKH while it decreased in the recovery period (83, 84). Nakayama (85) demonstrated that the subclinical manifestations were  $>100 \mu\text{m}$  ChT with recurrent VKH before ocular inflammation; therefore, ChT could be used as an indicator for the acute deterioration of inflammation. In patients with chronic VKH (average course of disease 106.3 months), Jap et al. (86) found that the mean SFCT ( $272.38 \pm 118.72 \mu\text{m}$ ) in the active period verified by ICGA was significantly higher than that in the quiet period ( $187.31 \pm 109.90 \mu\text{m}$ ) ( $P = 0.002$ ), SFCT could be used to monitor the activity of chronic VKH. However, continuously thinning ChT was observed in patients with long-term chronic VKH (36).

## Diseases With Decreased ChT

### Age-Related Macular Degeneration

Wet AMD is characterized by the formation of the macular neovascularization (MNV), dry form is characterized by atrophy of RPE and photoreceptors. Moderate-sized drusen ( $>63 \mu\text{m}$  in diameter) and RPE changes were the early stage of pathologic changes, proceeding with geographic atrophy and MNV in the late stage. Clinical studies have shown that ChT in patients with advanced AMD was thinner than that of normal controls, while it did not differ from that of normal individuals with early AMD (87–89). Decreased ChT reflects the degree of choroidal atrophy, suggesting that the development of AMD is related to the involvement and loss of microvessels, which is an indicator in the differential of PCV (37).

The occurrence and development of MNV are accompanied by choroidal thickening in the corresponding local regions, and thus, regular measurement of ChT is valuable in predicting MNV formation (90). Furthermore, SFCT could be used as an

independent predictor of prognosis of wet AMD, the thicker the choroid is, the more anti-VEGF intervention is needed (91).

### Pathological Myopia

Several studies have confirmed that the decrease in ChT is related to the degree of refraction. SFCT becomes thinner with the increase in diopter and the lengthening of the ocular axis, accompanied by the thinning of the sclera (92–94). It has been reported that SFCT decreased by 15  $\mu\text{m}$  for every 1 D increase in the myopia diopter, and 32  $\mu\text{m}$  for every 1 mm increase in the axial length in the range of myopia diopter above  $-1.00$  D (55). Ho et al. (56) reported that the average SFCT ( $118 \pm 68 \mu\text{m}$ ) was negatively correlated with diopter in a cross-sectional study of 56 myopic patients (average diopter  $-8.7$  D); for every 1 D increase, SFCT decreased by 6.205  $\mu\text{m}$ ; and for every 10  $\mu\text{m}$  increase in SFCT, visual acuity improved by 0.02 LogMAR visual acuity. Choroidal thinning is correlated with the pathogenesis of myopic fundus lesions. A 2-year prospective study revealed that SFCT is an independent predictor of the progression of myopic macular disease (95). With the increase in diopter and axial length, ChT becomes thinner, proceeded with decreased retinal blood supply leading to secondary pathological changes such as lacquer cracks and MNV-related maculopathy.

### Idiopathic Macular Hole

Idiopathic macular hole is characterized by retinal neuroepithelial tissue defect in the fovea, which is the most common type of macular hole. IMHs are more common in females than in males and usually manifest in 55 years or older adults. In a cross-sectional study of 50 patients with IMH, Zeng et al. (41) revealed that the SFCT of IMH ( $206.82 \pm 67.09 \mu\text{m}$ ) was significantly thinner than that of the controls ( $248.88 \pm 63.10 \mu\text{m}$ ) ( $P = 0.002$ ), and the SFCT of contralateral eyes ( $228.34 \pm 80.71 \mu\text{m}$ ) was thinner than that of controls, albeit not significantly. The results of the studies by Zhang and Reibaldi were consistent, suggesting that choroidal perfusion may play a vital role in the pathogenesis of IMH. The contralateral eye with thinner ChT was also prone to IMH, such that routine follow-up is necessary (4, 96). However, Sogawa pointed out that SFCT did not have a significant correlation with total choroidal blood flow and subfoveal choroidal blood flow (97). In conclusion, except for the traction mechanism proposed by Gass (98), the significant thinning of ChT may be related to the ischemic degeneration of the outer retina, which might be crucial for the occurrence and development of IMH.

### Other Systemic Diseases

Craig et al. found that decreased ChT in chronic kidney disease correlated with lower estimated glomerular filtration rate and

severe proteinuria, concomitated with the increased expression level of IL-6, C-reactive protein, and endothelin-1 (99). It was also found that endothelial dysfunction markers (endothelin-1, von Willebrand factor) were negatively correlated with ChT in cirrhosis patients (100), indicating that the morphological changes of the choroid are mediated by inflammatory diseases. Further well-designed randomized clinical trials are warranted to investigate whether ChT can be used as an auxiliary biomarker for systemic disorders. In addition, the thinner choroid in patients with Alzheimer's disease was found, which may be associated with vascular wall deposition of amyloid beta-protein (101). Similarly, whether ChT could be used as an early biomarker of Alzheimer's disease to predict disease progression is yet to be confirmed.

## CONCLUSION

Currently, EDI SD-OCT and SS-OCT could be used clinically due to its non-invasive, high-resolution, cross-sectional imaging characteristics of the choroid and measuring the ChT with good repeatability (6, 102). To date, there is no unified standard for ChT measurement that is carried out manually or via automatic segmentation method according to the ETDRS grid. Thus, methods for ChT measurement need to be standardized to objectively reflect the choroidal structure and reveal its clinical significance in the occurrence and development of the diseases. The establishment of ChT normal value needs large-scale, multicenter research to explore the pathogenesis of the fundus diseases and provide a new horizon on the management. In addition, whether ChT could quantitatively reflect the choroidal blood flow needs further study. The eye could be regarded as a monitoring window of systemic diseases and an auxiliary biomarker of the eye or systemic diseases, which plays a vital role in the diagnosis, management, and follow-up of diseases.

## AUTHOR CONTRIBUTIONS

XZ contributed to the conception and revised the manuscript. RX drafted the manuscript. BQ helped to draft the manuscript. JC provided comments and revised the manuscript. All authors contributed to the manuscript revision, read, and approved the submitted version.

## FUNDING

This work was supported by the National Natural Science Foundation of China [Grant Nos: 81570850, 81170859, and 82070988] and the Ministry of Science and Technology Foundation of China [Grant No: 2016YFC1305604].

## REFERENCES

1. Linsenmeier R, Padnick-Silver L. Metabolic dependence of photoreceptors on the choroid in the normal and detached retina. *Invest. Ophthalmol. Visual Sci.* (2000) 41:10:3117–23.
2. Lee K, Park J, Park Y, Park Y. Analysis of choroidal thickness and vascularity in patients with unilateral polypoidal choroidal vasculopathy. *Graefes Arch Clin Exp Ophthalmol.* (2020) 2586:1157–64. doi: 10.1007/s00417-020-04620-z
3. Jirattanasopa P, Ooto S, Tsujikawa A, Yamashiro K, Hangai M, Hirata M, et al. Assessment of macular choroidal thickness by optical coherence tomography and angiographic changes in central serous chorioretinopathy. *Ophthalmology.* (2012) 119:1666–78. doi: 10.1016/j.ophtha.2012.02.021



4. Zhang P, Zhou M, Wu Y, Lu B, Li T, Zhao J, et al. Choroidal thickness in unilateral idiopathic macular hole: a cross-sectional study and meta-analysis. *Retina*. (2017) 37:160–9. doi: 10.1097/IAE.0000000000001118
5. Borrelli E, Sarraf D, Freund K, Sadda S. OCT angiography and evaluation of the choroid and choroidal vascular disorders. *Progr Retinal Eye Res*. (2018) 67:30–55. doi: 10.1016/j.preteyeres.2018.07.002
6. Branchini L, Regatieri C, Flores-Moreno I, Baumann B, Fujimoto J, Duker J. Reproducibility of choroidal thickness measurements across three spectral domain optical coherence tomography systems. *Ophthalmology*. (2012) 119:119–23. doi: 10.1016/j.ophtha.2011.07.002
7. Coleman D, Luzzi F. *In vivo* choroidal thickness measurement. *Am J Ophthalmol*. (1979) 88:369–75. doi: 10.1016/0002-9394(79)90635-4
8. Hillenkamp J, Hussain A, Jackson T, Cunningham J, Marshall J. The influence of path length and matrix components on ageing characteristics of transport between the choroid and the outer retina. *Invest Ophthalmol Visual Sci*. (2004) 45:1493–8. doi: 10.1167/iov.03-0765
9. Bill A, Sperber G, Ujii K. Physiology of the choroidal vascular bed. *Int Ophthalmol*. (1983) 62:101–7. doi: 10.1007/BF00127638
10. Yoneya S, Tso M. Angioarchitecture of the human choroid. *Arch Ophthalmol*. (1987) 105:681–7. doi: 10.1001/archophth.1987.01060050099046
11. Olver, J. Functional anatomy of the choroidal circulation: methyl methacrylate casting of human choroid. *Eye*. (1990) :262–72. doi: 10.1038/eye.1990.38
12. Nickla D, Wallman J. The multifunctional choroid. *Progr Retinal Eye Res*. (2010) 29:144–68. doi: 10.1016/j.preteyeres.2009.12.002
13. Aumann S, Donner S, Fischer J, Müller F. Optical Coherence Tomography (OCT): principle and technical realization. In: Bille JF, editor. *High Resolution Imaging in Microscopy and Ophthalmology: New Frontiers in Biomedical Optics*. Cham: Springer Copyright 2019 (2019). p. 59–85. doi: 10.1007/978-3-030-16638-0\_3
14. Fercher A, Mengedoh K, Werner W. Eye-length measurement by interferometry with partially coherent light. *Opt Lett*. (1988) 13:186–8. doi: 10.1364/OL.13.000186
15. Forte R, Cennamo G, Finelli M, de Crecchio G. Comparison of time domain Stratus OCT and spectral domain SLO/OCT for assessment of macular thickness and volume. *Eye*. (2009) 23:11:2071–8. doi: 10.1038/eye.2008.363
16. Schmitt JM. Optical coherence tomography (OCT): a review. *IEEE J Selected Top Quant Electron*. (2002) 54:1205–15. doi: 10.1109/2944.796348
17. Spaide R, Koizumi H, Pozzoni M, Pozzoni M. Enhanced depth imaging spectral-domain optical coherence tomography. *Am J Ophthalmol*. (2008) 146:496–500. doi: 10.1016/j.ajo.2008.05.032
18. Sainter AW, King TA, Dickinson MR. Effect of target biological tissue and choice of light source on penetration depth and resolution in optical coherence tomography. *J Biomed Opt*. (2004) 9:193–9. doi: 10.1117/1.1628243
19. Marschall S, Pedersen C, Andersen PE. Investigation of the impact of water absorption on retinal OCT imaging in the 1060 nm range. *Biomed Opt Express*. (2012) 3:7:1620. doi: 10.1364/BOE.3.001620
20. Itakura H, Kishi S, Li D, Akiyama H. En face imaging of posterior precortical vitreous pockets using swept-source optical coherence tomography. *Invest Ophthalmol Vis*. (2015) 56:2898–2900. doi: 10.1167/iov.15-16451
21. Spaide R, Ledesma-Gil G. Novel method for image averaging of optical coherence tomography angiography images. *Retina*. (2020) 40:11:2099–105. doi: 10.1097/IAE.0000000000002877
22. Mrejen S, Spaide R. Optical coherence tomography: imaging of the choroid and beyond. *Survey Ophthalmol*. (2013) 58:387–429. doi: 10.1016/j.survophthal.2012.12.001
23. Mansouri K, Medeiros F, Marchase N, Tatham A, Auerbach D, Weinreb R. Assessment of choroidal thickness and volume during the water drinking test by swept-source optical coherence tomography. *Ophthalmology*. (2013) 120:12:2508–16. doi: 10.1016/j.ophtha.2013.07.040
24. Ferrara D, Mohler KJ, Waheed N, Adhi M, Liu JJ, Grulkowski I, et al. En Face enhanced-depth swept-source optical coherence tomography features of chronic central serous chorioretinopathy. *Ophthalmology*. (2014) 121:3:719–26. doi: 10.1016/j.ophtha.2013.10.014
25. Motaghiannezhad R, Schwartz D, Fraser S. *In vivo* human choroidal vascular pattern visualization using high-speed swept-source optical coherence tomography at 1060 nm. *Invest Ophthalmol Vis Sci*. (2012) 53:4:2337–48. doi: 10.1167/iov.11-7823
26. Blatter C, Klein T, Grajciar B, Schmoll T, Wieser W, Andre R, et al. Ultrahigh-speed non-invasive widefield angiography. *J Biomed Opt*. (2012) 17:070505. doi: 10.1117/1.JBO.17.7.070505
27. Choi WJ, Waheed NK, Moulton EM, Adhi M, Fujimoto JG. Ultrahigh speed swept source optical coherence tomography angiography of retinal and choriocapillaris alterations in diabetic patients with and without retinopathy. *Retina*. (2016) 37:11. doi: 10.1097/IAE.0000000000001250
28. Moulton EM, Waheed NK, Novais EA, Choi WJ, Lee BK, Ploner SB, et al. Swept-source optical coherence tomography angiography reveals choriocapillaris alterations in eyes with nascent geographic atrophy and drusen-associated geographic atrophy. *Retina*. (2016) 36:S2–11. doi: 10.1097/IAE.0000000000001287
29. Yokoi T, Toriyama N, Yamane T, Nakayama Y, Nishina S, Azuma N. Development of a premacular vitreous pocket. *JAMA Ophthalmol*. (2013) 131:8:1095–6. doi: 10.1001/jamaophthalmol.2013.240
30. Anger E, Unterhuber A, Hermann B, Sattmann H, Schubert C, Morgan J, et al. Ultrahigh resolution optical coherence tomography of the monkey fovea. Identification of retinal sublayers by correlation with semithin histology sections. *Exp Eye Res*. (2004) 78:6:1117–25. doi: 10.1016/j.exer.2004.01.011
31. Manjunath V, Taha M, Fujimoto J, Duker J. Choroidal thickness in normal eyes measured using Cirrus HD optical coherence tomography. *Am J Ophthalmol*. (2010) 150:3:325–9.e1. doi: 10.1016/j.ajo.2010.04.018
32. Coleman D, Silverman R, Chabi A, Rondeau M, Shung K, Cannata J, et al. High-resolution ultrasonic imaging of the posterior segment. *Ophthalmology*. (2004) 111:7:1344–51. doi: 10.1016/j.ophtha.2003.10.029
33. Bo Q, Yan Q, Shen M, Song M, Sun M, Yu Y, et al. appearance of polypoidal lesions in patients with polypoidal choroidal vasculopathy using swept-source optical coherence tomographic angiography. *JAMA Ophthalmol*. (2019) 137:6:642–50. doi: 10.1001/jamaophthalmol.2019.0449
34. Koizumi H, Kano M, Yamamoto A, Saito M, Maruko I, Sekiryu T, et al. subfoveal choroidal thickness during aflibercept therapy for neovascular age-related macular degeneration: twelve-month results. *Ophthalmology*. (2016) 123:3:617–24. doi: 10.1016/j.ophtha.2015.10.039
35. Eymard P, Gerardy M, Bouys L, Mehanna C, Bertherat J, Behar-Cohen F, et al. Choroidal imaging in patients with Cushing syndrome. *Acta Ophthalmol*. (2020) 99:5:533–7. doi: 10.1111/aos.14664
36. da Silva F, Sakata V, Nakashima A, Hirata C, Olivalves E, Takahashi W, et al. Enhanced depth imaging optical coherence tomography in long-standing Vogt-Koyanagi-Harada disease. *Br J Ophthalmol*. (2013) 97:1:70–4. doi: 10.1136/bjophthalmol-2012-302089
37. Chung S, Kang S, Lee J, Kim Y. Choroidal thickness in polypoidal choroidal vasculopathy and exudative age-related macular degeneration. *Ophthalmology*. (2011) 118:5:840–5. doi: 10.1016/j.ophtha.2010.09.012
38. Fang Y, Du R, Nagaoka N, Yokoi T, Shinohara K, Xu X, et al. OCT-based diagnostic criteria for different stages of myopic maculopathy. *Ophthalmology*. (2019) 126:7:1018–32. doi: 10.1016/j.ophtha.2019.01.012
39. Govetto A, Sarraf D, Figueroa M, Pierro L, Ippolito M, Risser G, et al. Choroidal thickness in non-neovascular versus neovascular age-related macular degeneration: a fellow eye comparative study. *Br J Ophthalmol*. (2017) 101:6:764–9. doi: 10.1136/bjophthalmol-2016-309281
40. Schuster A, Leuschner A, Feretos C, Blumenstein P, Troebs S, Schwuchow S, et al. Choroidal thickness is associated with cardiovascular risk factors and cardiac health: the Gutenberg Health Study. *Clin Res Cardiol*. (2020) 109:2:172–82. doi: 10.1007/s00392-019-01498-8
41. Zeng J, Li J, Liu R, Chen X, Pan J, Tang S, et al. Choroidal thickness in both eyes of patients with unilateral idiopathic macular hole. *Ophthalmology*. (2012) 119:11:2328–33. doi: 10.1016/j.ophtha.2012.06.008
42. Moschos M, Nitoda E, Laios K, Ladas D, Chatziralli I. The impact of chronic tobacco smoking on retinal and choroidal thickness in greek population. *Oxidat Med Cell Longevity*. (2016) 2016:2905789. doi: 10.1155/2016/2905789
43. Wu W, Shih C, Wang N, Lien R, Chen Y, Chao A, et al. Choroidal thickness in patients with a history of retinopathy of prematurity. *JAMA Ophthalmol*. (2013) 131:11:1451–8. doi: 10.1001/jamaophthalmol.2013.5052
44. Yuan N, Li J, Tang S, Li F, Lee C, Ng M, et al. Association of secondhand smoking exposure with choroidal thinning in children aged 6 to 8 years: the



- Hong Kong children eye study. *JAMA Ophthalmol.* (2019) 13712:1406–14. doi: 10.1001/jamaophthalmol.2019.4178
45. Suh M, Zangwill L, Manalastas P, Belgith A, Yarmohammadi A, Medeiros F, et al. Deep retinal layer microvasculature dropout detected by the optical coherence tomography angiography in glaucoma. *Ophthalmology.* (2016) 12312:2509–18. doi: 10.1016/j.ophtha.2016.09.002
  46. Shin J, Shin Y, Lee B. Choroidal thickness and volume mapping by a six radial scan protocol on spectral-domain optical coherence tomography. *Ophthalmology.* (2012) 1195:1017–23. doi: 10.1016/j.ophtha.2011.10.029
  47. Lim H, Kim K, Won Y, Lee W, Lee M, Kim J. A comparison of choroidal thicknesses between pachychoroid and normochoroid eyes acquired from wide-field swept-source OCT. *Acta Ophthalmol.* (2020) 99:e117–23. doi: 10.1111/aos.14522
  48. Rahman W, Chen F, Yeoh J, Patel P, Tufail A, Da Cruz L. Repeatability of manual subfoveal choroidal thickness measurements in healthy subjects using the technique of enhanced depth imaging optical coherence tomography. *Invest Ophthalmol Vis Sci.* (2011) 525:2267–71. doi: 10.1167/iovs.10-6024
  49. Wiacek M, Machalińska A. Evaluation of choroidal parameters in eyes at the first onset of acute anterior uveitis. *BMC Ophthalmol.* (2019) 191:63. doi: 10.1186/s12886-019-1072-7
  50. Nagasawa T, Mitamura Y, Katome T, Shinomiya K, Naito T, Nagasato D, et al. Macular choroidal thickness and volume in healthy pediatric individuals measured by swept-source optical coherence tomography. *Invest Ophthalmol Vis Sci.* (2013) 5410:7068–74. doi: 10.1167/iovs.13-12350
  51. Esmaelpour M, Povazay B, Hermann B, Hofer B, Kojic V, Kapoor K, et al. Three-dimensional 1060-nm OCT: choroidal thickness maps in normal subjects and improved posterior segment visualization in cataract patients. *Invest Ophthalmol Vis Sci.* (2010) 5110:5260–6. doi: 10.1167/iovs.10-5196
  52. Fang D, Li Q, Yan K, Xu S, Jiang J, Che X, et al. Retinal and choroidal thickness in relation to c-reactive protein on swept-source optical coherence tomography. *J Immunol Res.* (2021) 2021:6628224. doi: 10.1155/2021/6628224
  53. Agawa T, Miura M, Ikuno Y, Makita S, Fabritius T, Iwasaki T, et al. Choroidal thickness measurement in healthy Japanese subjects by three-dimensional high-penetration optical coherence tomography. *Graefes Arch Clin Exp Ophthalmol.* (2011) 24910:1485–92. doi: 10.1007/s00417-011-1708-7
  54. Xu J, Xu L, Du K, Shao L, Chen C, Zhou J, et al. Subfoveal choroidal thickness in diabetes and diabetic retinopathy. *Ophthalmology.* (2013) 12010:2023–8. doi: 10.1016/j.ophtha.2013.03.009
  55. Wei W, Xu L, Jonas J, Shao L, Du K, Wang S, et al. Subfoveal choroidal thickness: the Beijing Eye Study. *Ophthalmology.* (2013) 1201:175–80. doi: 10.1016/j.ophtha.2012.07.048
  56. Ho M, Liu D, Chan V, Lam D. Choroidal thickness measurement in myopic eyes by enhanced depth optical coherence tomography. *Ophthalmology.* (2013) 1209:1909–14. doi: 10.1016/j.ophtha.2013.02.005
  57. Margolis R, Spaide R. A pilot study of enhanced depth imaging optical coherence tomography of the choroid in normal eyes. *Am J Ophthalmol.* (2009) 1475:811–5. doi: 10.1016/j.ajo.2008.12.008
  58. Touhami S, Philippakis E, Mrejen S, Couturier A, Casteran C, Levent P, et al. Topographic variations of choroidal thickness in healthy eyes on swept-source optical coherence tomography. *Invest Ophthalmol Vis Sci.* (2020) 613:38. doi: 10.1167/iovs.61.3.38
  59. Ikuno Y, Kawaguchi K, Nouchi T, Yasuno Y. Choroidal thickness in healthy Japanese subjects. *Invest Ophthalmol Vis.* (2010) 514:2173. doi: 10.1167/iovs.09-4383
  60. Ruiz-Moreno JM, Flores-Moreno I, Lugo F, Ruiz-Medrano J, Montero JA, Akiba M. Macular choroidal thickness in normal pediatric population measured by swept-source optical coherence tomography. *Invest Ophthalmol Vis Sci.* (2012) 54:353–9. doi: 10.1167/iovs.12-10863
  61. Tan C, Ouyang Y, Ruiz H, Sadda S. Diurnal variation of choroidal thickness in normal, healthy subjects measured by spectral domain optical coherence tomography. *Invest Ophthalmol Vis Sci.* (2012) 531:261–6. doi: 10.1167/iovs.11-8782
  62. Ding X, Li J, Zeng J, Ma W, Liu R, Li T, et al. Choroidal thickness in healthy Chinese subjects. *Invest Ophthalmol Vis Sci.* (2011) 5213:9555–60. doi: 10.1167/iovs.11-8076
  63. Bhayana A, Kumar V, Tayade A, Chandra M, Chandra P, Kumar A. Choroidal thickness in normal Indian eyes using swept-source optical coherence tomography. *Indian J Ophthalmol.* (2019) 67:252–5. doi: 10.4103/ijo.IJO\_668\_18
  64. Wakatsuki Y, Shinojima A, Kawamura A, Yuzawa M. Correlation of aging and segmental choroidal thickness measurement using swept source optical coherence tomography in healthy eyes. *PLoS ONE.* (2015) 1012:e0144156. doi: 10.1371/journal.pone.0144156
  65. Hirata M, Tsujikawa A, Matsumoto A, Hangai M, Ooto S, Yamashiro K, et al. Macular choroidal thickness and volume in normal subjects measured by swept-source optical coherence tomography. *Invest Ophthalmol Vis Sci.* (2011) 528:4971–8. doi: 10.1167/iovs.11-7729
  66. Lee S, Lingham G, Alonso-Caneiro D, Chen F, Yazar S, Hewitt A, et al. Choroidal thickness in young adults and its association with visual acuity. *Am J Ophthalmol.* (2020) 214:40–51. doi: 10.1016/j.ajo.2020.02.012
  67. Matsuo Y, Sakamoto T, Yamashita T, Tomita M, Shirasawa M, Terasaki H. Comparisons of choroidal thickness of normal eyes obtained by two different spectral-domain OCT instruments and one swept-source OCT instrument. *Invest Ophthalmol Vis Sci.* (2013) 5412:7630–6. doi: 10.1167/iovs.13-13135
  68. Adhi M, Liu J, Qavi A, Grulkowski I, Lu C, Mohler K, et al. Choroidal analysis in healthy eyes using swept-source optical coherence tomography compared to spectral domain optical coherence tomography. *Am J Ophthalmol.* (2014) 1576:1272–81.e1. doi: 10.1016/j.ajo.2014.02.034
  69. Copete S, Flores-Moreno I, Montero J, Duker J, Ruiz-Moreno J. Direct comparison of spectral-domain and swept-source OCT in the measurement of choroidal thickness in normal eyes. *Br J Ophthalmol.* (2014) 983:334–8. doi: 10.1136/bjophthalmol-2013-303904
  70. Castro-Navarro V, Behar-Cohen F, Chang W, Jousseaume A, Lai T, Navarro R, et al. Pachychoroid: current concepts on clinical features and pathogenesis. *Graefes Arch Clin Exp Ophthalmol.* (2020) 2596:1385–400. doi: 10.1007/s00417-020-04940-0
  71. Chirco K, Sohn E, Stone E, Tucker B, Mullins R. Structural and molecular changes in the aging choroid: implications for age-related macular degeneration. *Eye.* (2017) 311:10–25. doi: 10.1038/eye.2016.216
  72. Prunte C, Flammer J. Choroidal capillary and venous congestion in central serous chorioretinopathy. *Am J Ophthalmol.* (1996) 1211:26–34. doi: 10.1016/S0002-9394(14)70531-8
  73. Borooah S, Sim P, Phatak S, Moraes G, Wu C, Cheung C, et al. Pachychoroid spectrum disease. *Acta Ophthalmol.* (2020) 99:e806–22. doi: 10.1111/aos.14683
  74. Jordan-Yu J, Teo K, Chakravarthy U, Gan A, Tan A, Cheong K, et al. Polypoidal choroidal vasculopathy features vary according to subfoveal choroidal thickness. *Retina.* (2021) 415:1084–93. doi: 10.1097/IAE.0000000000002966
  75. Maruko I, Iida T, Sugano Y, Ojima A, Ogasawara M, Spaide R. Subfoveal choroidal thickness after treatment of central serous chorioretinopathy. *Ophthalmology.* (2010) 1179:1792–9. doi: 10.1016/j.ophtha.2010.01.023
  76. Alovici C, Piccolino F, Nassisi M, Eandi CM. Choroidal structure after half-dose photodynamic therapy in chronic central serous chorioretinopathy. *J Clin Med.* (2020) 9:2734. doi: 10.3390/jcm9092734
  77. Kim Y, Ryoo N, Woo S, Park K. Choroidal thickness changes after photodynamic therapy and recurrence of chronic central serous chorioretinopathy. *Am J Ophthalmol.* (2015) 1601:72–84.e71. doi: 10.1016/j.ajo.2015.04.011
  78. Kim D, Joe S, Yang H, Lee J, Kim J, Yoon Y. Subfoveal choroidal thickness changes in treated idiopathic central serous chorioretinopathy and their association with recurrence. *Retina.* (2015) 359:1867–74. doi: 10.1097/IAE.0000000000000557
  79. Annesley WH Jr. Peripheral exudative hemorrhagic chorioretinopathy. *Trans Am Ophthalmol Soc.* (1980) 78:321–64
  80. Mantel I, Schalenbourg A, Zografos L. Peripheral exudative hemorrhagic chorioretinopathy: polypoidal choroidal vasculopathy and hemodynamic modifications. *Am J Ophthalmol.* (2012) 1535:910–22.e2. doi: 10.1016/j.ajo.2011.10.017
  81. Kitagawa Y, Shimada H, Kawamura A, Tanaka K, Mori R, Onoe H, et al. A case of bilateral pachychoroid disease: polypoidal choroidal vasculopathy in one eye and peripheral exudative hemorrhagic

- chorioretinopathy in contralateral eye. *BMC Ophthalmol.* (2021) 21:320. doi: 10.1186/s12886-021-02067-2
82. Shroff D, Sharma M, Chhablani J, Gupta P, Gupta C, Shroff C. Peripheral exudative hemorrhagic chorioretinopathy—a new addition to the spectrum of pachychoroid disease? *Retina.* (2021) 417:1518–25. doi: 10.1097/IAE.0000000000003063
  83. Takahashi H, Takase H, Ishizuka A, Miyana M, Kawaguchi T, Ohno-Matsui K, et al. Choroidal thickness in convalescent vogt-koyanagi-harada disease. *Retina.* (2014) 344:775–80. doi: 10.1097/IAE.0b013e3182a6b3f6
  84. Fong A, Li K, Wong D. Choroidal evaluation using enhanced depth imaging spectral-domain optical coherence tomography in Vogt-Koyanagi-Harada disease. *Retina.* (2011) 313:502–9. doi: 10.1097/IAE.0b013e3182083beb
  85. Nakayama M, Keino H, Okada A, Watanabe T, Taki W, Inoue M, et al. Enhanced depth imaging optical coherence tomography of the choroid in Vogt-Koyanagi-Harada disease. *Retina.* (2012) 3210:2061–9. doi: 10.1097/IAE.0b013e318256205a
  86. Jap A, Chee S. The role of enhanced depth imaging optical coherence tomography in chronic Vogt-Koyanagi-Harada disease. *Br J Ophthalmol.* (2017) 1012:186–9. doi: 10.1136/bjophthalmol-2015-308091
  87. Jonas J, Forster T, Steinmetz P, Schlichtenbrede F, Harder B. Choroidal thickness in age-related macular degeneration. *Retina.* (2014) 346:1149–55. doi: 10.1097/IAE.0000000000000035
  88. Yiu G, Chiu S, Petrou P, Stinnett S, Sarin N, Farsiu S, et al. Relationship of central choroidal thickness with age-related macular degeneration status. *Am J Ophthalmol.* (2015) 1594:617–26. doi: 10.1016/j.ajo.2014.12.010
  89. Sigler E, Randolph J. Comparison of macular choroidal thickness among patients older than age 65 with early atrophic age-related macular degeneration and normals. *Invest Ophthalmol Vis Sci.* (2013) 549:6307–13. doi: 10.1167/iov.13-12653
  90. Park J, Kang M, Kim B, Chung K, Sim H, Lee S, et al. Topographic changes in choroidal thickness in age-related macular degeneration during the development of active choroidal neovascularization. *Retina.* (2020) 412:409–22. doi: 10.1097/IAE.0000000000000285
  91. Kumar J, Wai K, Ehlers J, Singh R, Rachitskaya A. Subfoveal choroidal thickness as a prognostic factor in exudative age-related macular degeneration. *Br J Ophthalmol.* (2019) 1037:918–21. doi: 10.1136/bjophthalmol-2018-312625
  92. Xie J, Chen Q, Yu J, Zhou H, He J, Wang W, et al. Morphologic features of myopic choroidal neovascularization in pathologic myopia on swept-source optical coherence tomography. *Front Med.* (2020) 7:615902. doi: 10.3389/fmed.2020.615902
  93. Wu Q, Chen Q, Lin B, Huang S, Wang Y, Zhang L, et al. Relationships among retinal/choroidal thickness, retinal microvascular network and visual field in high myopia. *Acta Ophthalmol.* (2020) 98:e709–14. doi: 10.1111/aos.14372
  94. Fledelius H, Jacobsen N, Li X, Goldschmidt E. Choroidal thickness at age 66 years in the Danish high myopia study cohort 1948 compared with follow-up data on visual acuity over 40 years: a clinical update adding spectral domain optical coherence tomography. *Acta Ophthalmol.* (2018) 961:46–50. doi: 10.1111/aos.13659
  95. Li Z, Wang W, Liu R, Wang D, Zhang J, Xiao O, et al. Choroidal thickness predicts progression of myopic maculopathy in high myopes: a 2-year longitudinal study. *Br J Ophthalmol.* (2020) 1–7. doi: 10.1136/bjophthalmol-2020-316866
  96. Reibaldi M, Boscia F, Avitabile T, Uva M, Russo V, Zagari M, et al. Enhanced depth imaging optical coherence tomography of the choroid in idiopathic macular hole: a cross-sectional prospective study. *Am J Ophthalmol.* (2011) 1511:112–7.e2. doi: 10.1016/j.ajo.2010.07.004
  97. Sogawa K, Nagaoka T, Takahashi A, Tanano I, Tani T, Ishibazawa A, et al. Relationship between choroidal thickness and choroidal circulation in healthy young subjects. *Am J Ophthalmol.* (2012) 1536:1129–32.e1. doi: 10.1016/j.ajo.2011.11.005
  98. Gass J. Reappraisal of biomicroscopic classification of stages of development of a macular hole. *Am J Ophthalmol.* (1995) 1196:752–9. doi: 10.1016/S0002-9394(14)72781-3
  99. Balmforth C, van Bragt J, Ruijs T, Cameron J, Kimmitt R, Moorhouse R, et al. Chorioretinal thinning in chronic kidney disease links to inflammation and endothelial dysfunction. *JCI Insight.* (2016) 1:e89173. doi: 10.1172/jci.insight.89173
  100. Gifford F, Moroni F, Farrah T, Hetherington K, MacGillivray T, Hayes P, et al. The Eye as a non-invasive window to the microcirculation in liver cirrhosis: a prospective pilot study. *J Clin Med.* (2020) 910:3332. doi: 10.3390/jcm9103332
  101. Salobrar-García E, Méndez-Hernández C, Hoz R, Ramírez A, López-Cuenca I, Fernández-Albarral J, et al. Ocular vascular changes in mild alzheimer's disease patients: foveal avascular zone, choroidal thickness, and ONH hemoglobin analysis. *J Personalized Med.* (2020) 104:231. doi: 10.3390/jpm10040231
  102. Mansouri K, Medeiros F, Tatham A, Marchase N, Weinreb R. Evaluation of retinal and choroidal thickness by swept-source optical coherence tomography: repeatability and assessment of artifacts. *Am J Ophthalmol.* (2014) 1575:1022–32. doi: 10.1016/j.ajo.2014.02.008

**Conflict of Interest:** The authors declare that the research was conducted in the absence of any commercial or financial relationships that could be construed as a potential conflict of interest.

**Publisher's Note:** All claims expressed in this article are solely those of the authors and do not necessarily represent those of their affiliated organizations, or those of the publisher, the editors and the reviewers. Any product that may be evaluated in this article, or claim that may be made by its manufacturer, is not guaranteed or endorsed by the publisher.

Copyright © 2021 Xie, Qiu, Chhablani and Zhang. This is an open-access article distributed under the terms of the Creative Commons Attribution License (CC BY). The use, distribution or reproduction in other forums is permitted, provided the original author(s) and the copyright owner(s) are credited and that the original publication in this journal is cited, in accordance with accepted academic practice. No use, distribution or reproduction is permitted which does not comply with these terms.



# Sustained Release of Gas6 via mPEG-PLGA Nanoparticles Enhances the Therapeutic Effects of MERTK Gene Therapy in RCS Rats

Shen Wu<sup>1,2†</sup>, Yingyan Mao<sup>1,3†</sup>, Qian Liu<sup>1,2</sup>, Xuejing Yan<sup>1,2</sup>, Jingxue Zhang<sup>1,2,3\*</sup> and Ningli Wang<sup>1,2,3\*</sup>

<sup>1</sup> Beijing Institute of Ophthalmology, Beijing Tongren Eye Center, Beijing Tongren Hospital, Capital Medical University, Beijing Ophthalmology & Visual Sciences Key Laboratory, Beijing, China, <sup>2</sup> Collaborative Innovation Center for Brain Disorders, Beijing Institute of Brain Disorders, Capital Medical University, Beijing, China, <sup>3</sup> Beijing Advanced Innovation Center for Big Data-Based Precision Medicine, Beijing Tongren Hospital, Beihang University, Capital Medical University, Beijing, China

## OPEN ACCESS

### Edited by:

Shaochong Zhang,  
Sun Yat-sen University, China

### Reviewed by:

Songtao Yuan,  
Nanjing Medical University, China  
Shipeng Wen,  
Beijing University of Chemical  
Technology, China

### \*Correspondence:

Ningli Wang  
wningli@vip.163.com  
Jingxue Zhang  
jingxuezh@ccmu.edu.cn

<sup>†</sup>These authors have contributed  
equally to this work

### Specialty section:

This article was submitted to  
Ophthalmology,  
a section of the journal  
Frontiers in Medicine

**Received:** 13 October 2021

**Accepted:** 24 November 2021

**Published:** 14 December 2021

### Citation:

Wu S, Mao Y, Liu Q, Yan X, Zhang J  
and Wang N (2021) Sustained  
Release of Gas6 via mPEG-PLGA  
Nanoparticles Enhances the  
Therapeutic Effects of MERTK Gene  
Therapy in RCS Rats.  
Front. Med. 8:794299.  
doi: 10.3389/fmed.2021.794299

Previous researches utilizing MER proto-oncogene tyrosine kinase (MERTK) gene therapy in Royal College of Surgeons (RCS) rats evidenced its effectiveness in treating MERTK-associated retinitis pigmentosa (RP). Specific ligands for receptor tyrosine kinases, such as growth arrest-specific 6 (Gas6), may enhance retinal phagocytosis via the MERTK receptor, and consequently, enhance the therapeutic effects of gene therapy. In order to overcome the short life effect of the injected Gas6 protein, we constructed a Gas6 loaded methoxy-poly (ethylene glycol)-poly (lactic-co-glycolic acid) (mPEG-PLGA) nanoparticles (Gas6 NPs) system which allowed for localized and sustained Gas6 protein release, and therefore, a prolonged biological effect. Our data demonstrated that Gas6 protein release from Gas6 NPs preserved the bioactivity and promoted retinal pigment epithelium (RPE) phagocytosis *in vitro*. *In vivo* studies showed that RCS rats in the hMERTK/Gas6 NPs group exhibiting the highest electroretinogram responses and more complete retinal structure than that in other groups, further demonstrating that the co-administration of AAV2-BEST1-hMERTK and Gas6 NPs could protect photoreceptors from degeneration. These findings strongly suggest that Gas6 NPs are a promising method to enable the sustained release of Gas6 protein and could therefore enhance the therapeutic effects of gene therapy for MERTK-associated RP.

**Keywords:** retinitis pigmentosa, Gas6 nanoparticles, sustained release, phagocytosis, gene therapy

## INTRODUCTION

Retinitis pigmentosa (RP), a group of progressive, hereditary diseases that causes irreversible vision loss, is responsible for blindness in more than 2 million people worldwide (1, 2). Mutations in more than 70 genes have been associated with RP (1). One of the mutation genes is the MER proto-oncogene tyrosine kinase (MERTK), which encodes a transmembrane receptor tyrosine kinase, have been identified to cause RP in patients (3). Two large-scale molecular surveys of retinal

dystrophies revealed ~3% of RP cases are attributable to MERTK mutations (4, 5). Such mutations result in defective phagocytosis, which causes the retinal pigment epithelium (RPE) failing to shed photoreceptor outer segments (6).

Numerous studies have reported on the effectiveness of gene replacement therapy for MERTK-associated RP (7, 8). For example, by transplanting an RPE-specific AAV vector, AAV-VMD2-hMerTK, into subretinal space or vitreous cavity could provide long-term photoreceptor rescue in the RCS rats (MERTK-associated retinal dystrophy model) (9, 10). However, although pre-clinical animal models and initial clinical trials suggested a beneficial effect, double-blinded clinical trials with large cohorts of patients failed to show efficacy (11). These disappointing results were attributed, at least partially, long-term MerTK mutations can lead to destruction of retina microenvironment (12). Clearly, it is important to explore more effective therapies to rescue retinal function and morphology in individuals with MERTK-associated RP, especially after the initiation of retinal degeneration.

Specific ligands for receptor tyrosine kinases, such as growth arrest-specific 6 (Gas6), may enhance retinal phagocytosis *via* the MERTK receptor (13). Modulating local environmental factors by Gas6 to provide conditions that are more conducive for functional rescue and repair may maximize the therapeutic effect for RP due to phagocytic dysfunction. However, using Gas6 protein as a drug has many disadvantages, such as short half-life and chemical instability *in vivo*, and may necessitate frequent intraocular injections to maintain long-term effects. This can lead to many complications, such as inflammation, bleeding, and patient compliance issues, which will greatly limit its widespread practical application. To overcome these drawbacks, sustained-release formulations that deliver the protein continuously, thus maintaining the concentration within the therapeutic window for an extended period, have been explored (14). Encapsulating proteins into injectable microspheres or nanoparticles comprised of biodegradable polymers ensures that it maintains its properties and activities (15, 16). Polymers derived from D,L-lactic and glycolic acids, like poly(lactide-co-glycolide) (PLGA), are widely employed with the latter aim in mind (17, 18). PLGA has been approved for use in drug and protein delivery systems by the United States Food and Drug Administration (U.S. FDA) due to its controlled and sustained-release properties, low toxicity, and biocompatibility with tissue and cells.

In this study, Gas6 protein was encapsulated into methoxy-poly (ethylene glycol)-poly (lactic-co-glycolic acid) (mPEG-PLGA) nanoparticles (Gas6 NPs) using the double emulsion technique (Figure 1A). We investigated the bioactivity of Gas6 protein released from Gas6 NPs *in vitro*. To assess whether Gas6 NPs enhance the therapeutic effects of gene therapy for MERTK-associated RP *in vivo*, we co-transplanted AAV2-BEST1-hMERTK and Gas6 NPs (hMERTK/Gas6 NPs) into RCS rats to demonstrate its therapeutic potential in terms of visual function (Figure 1B). In addition, we examined whether the AAV2-BEST1-hMERTK/Gas6 NPs system is effective in rescuing photoreceptors from degeneration in RCS rats.

## RESULTS

### Characterization and *in vitro* Protein Release of Gas6 NPs

Gas6 NPs were prepared using the double emulsion (w/o/w) technique as illustrated in Figure 1A. The encapsulation of Gas6 into mPEG-PLGA nanoparticles was confirmed by FTIR spectroscopy (Figure 2A). In the FTIR spectrum of Gas6, the peaks at 1,633 and 3,339  $\text{cm}^{-1}$  are attributed to N-H deformation and C=O stretching vibrations, respectively. Compared to the FTIR spectrum of pure mPEG-PLGA nanoparticles (blank NPs), the peaks at 1,633 and 3,339  $\text{cm}^{-1}$  corresponding to the signal of Gas6 appeared in the FTIR spectrum of Gas6 NPs, confirming the presence of Gas6 in Gas6 NPs.

The encapsulation percentage of the resultant Gas6 NPs was 75%. A TEM image of the resultant Gas6 NPs is presented in Figure 2B. It is observed that Gas6 NPs have a well-defined spherical morphology and high uniformity. The average hydrodynamic diameter of Gas6 NPs determined by DLS was 175.3 nm (Figure 2C). DLS data also evidenced low polydispersity and asymmetric size distributions. As observed by DLS, the size of Gas6 NPs in room temperature water can be maintained at ~180 nm for at least 7 days (Figure 2D). Combining the results of FTIR spectroscopy, TEM observations, and DLS characterizations, it can be concluded that Gas6 was successfully encapsulated into Gas6 NPs.

Gas6 protein release kinetics were determined by the Human Gas6 Elisa Kit (19). Based on the standard curve established in advance, the cumulative amount of Gas6 released at each time point was calculated. The Gas6 release profile exhibited a gradual sustained release pattern throughout the experimental period (Figure 2E) and indicated that Gas6 can be continuously released for more than 2 weeks.

### *In vitro* Biocompatibility and Bioactivity of Gas6 NPs

In order to be clinically applicable, a material must have excellent biocompatibility. We therefore investigated the effect of Gas6 NPs on the growth and proliferation of hRPE cells to determine its biocompatibility. As depicted in Figure 3A, the hRPE cells co-cultured with Gas6 NPs exhibited similar cell morphology and proliferation as the control group. Moreover, *in vitro* biocompatibility of Gas6 NPs was assessed using CCK8 (Figure 3B). The results demonstrated that the absorbance of CCK8 in the group treated with Gas6 NPs was almost the same as that of the control group before 4 d, but was slightly lower than that of the control group from 5 d to 7 d. We then calculated the relative proliferation rate, which represents cell viability. As indicated in Figure 3C, the cell viability of Gas6 NPs decreases from day 1 to 6 and stabilizes on day 7. The cell viability is  $87.61 \pm 1.23\%$  on day 7 in the group treated with Gas6 NPs. According to the evaluation criterion in the International Standard ISO10993, the cytotoxicity of Gas6 NPs can be given a ranking of 1 and qualified. This result demonstrated that the Gas6 NPs system has good biocompatibility.

Thereafter, we examined the effects of Gas6 and Gas6 NPs on the phagocytic function of hRPE cells by phagocytosis



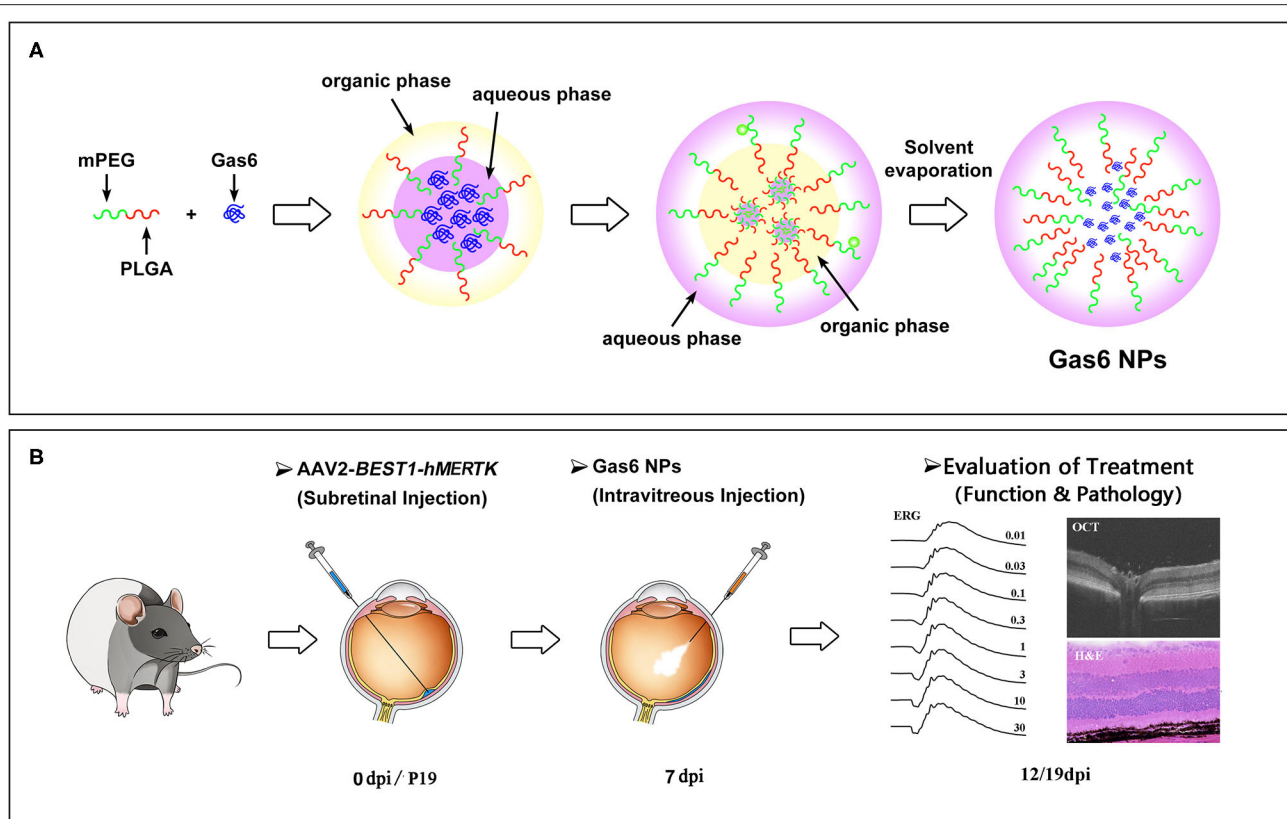


**FIGURE 1 |** Schematic illustration of (A) the preparation of Gas6 NPs and (B) Evaluation of the protect effects by co-administration of AAV2-BEST1-hMERTK and Gas6 NPs in RCS rats. dpi: days post injection.

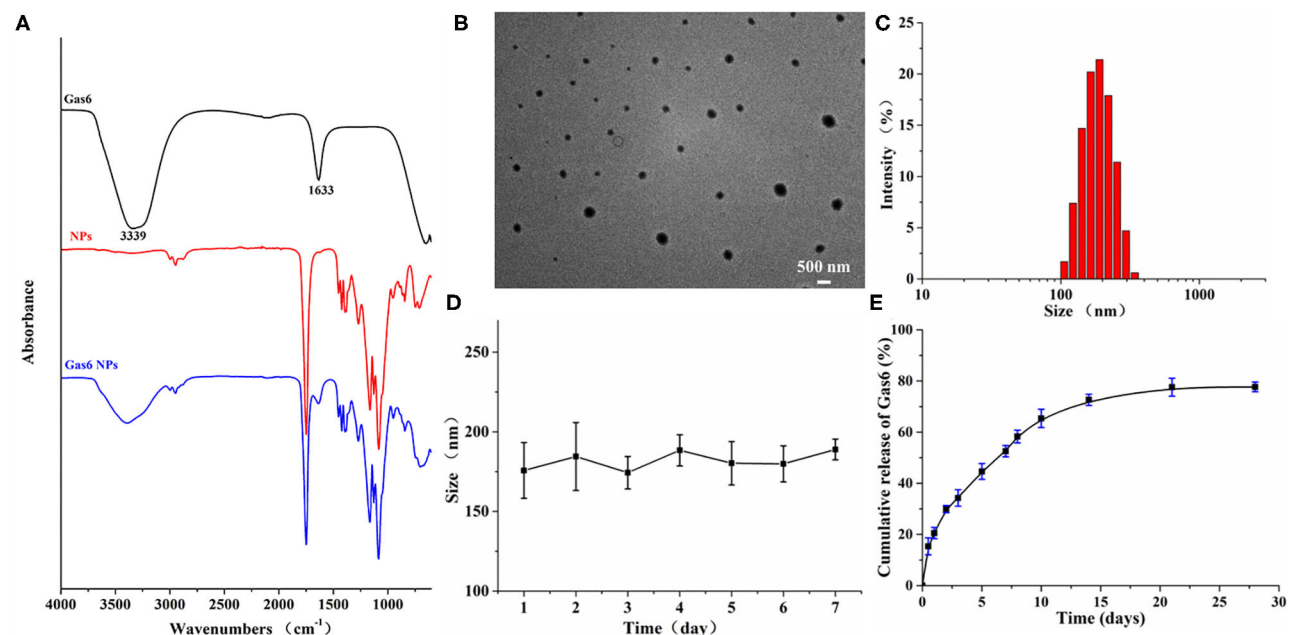


**FIGURE 2 |** Characterization of Gas6 NPs. (A) FTIR spectra of Gas6, NPs, and Gas6 NPs. (B) TEM image of Gas6 NPs. Scale bar=200 nm. (C) DLS characterization of Gas6 NPs. (D) Stability of Gas6 NPs sizes during 7 days characterized by DLS ( $n = 3$ ). (E) Cumulative Gas6 release of Gas6 NPs ( $n = 3$ ) at 37°C.

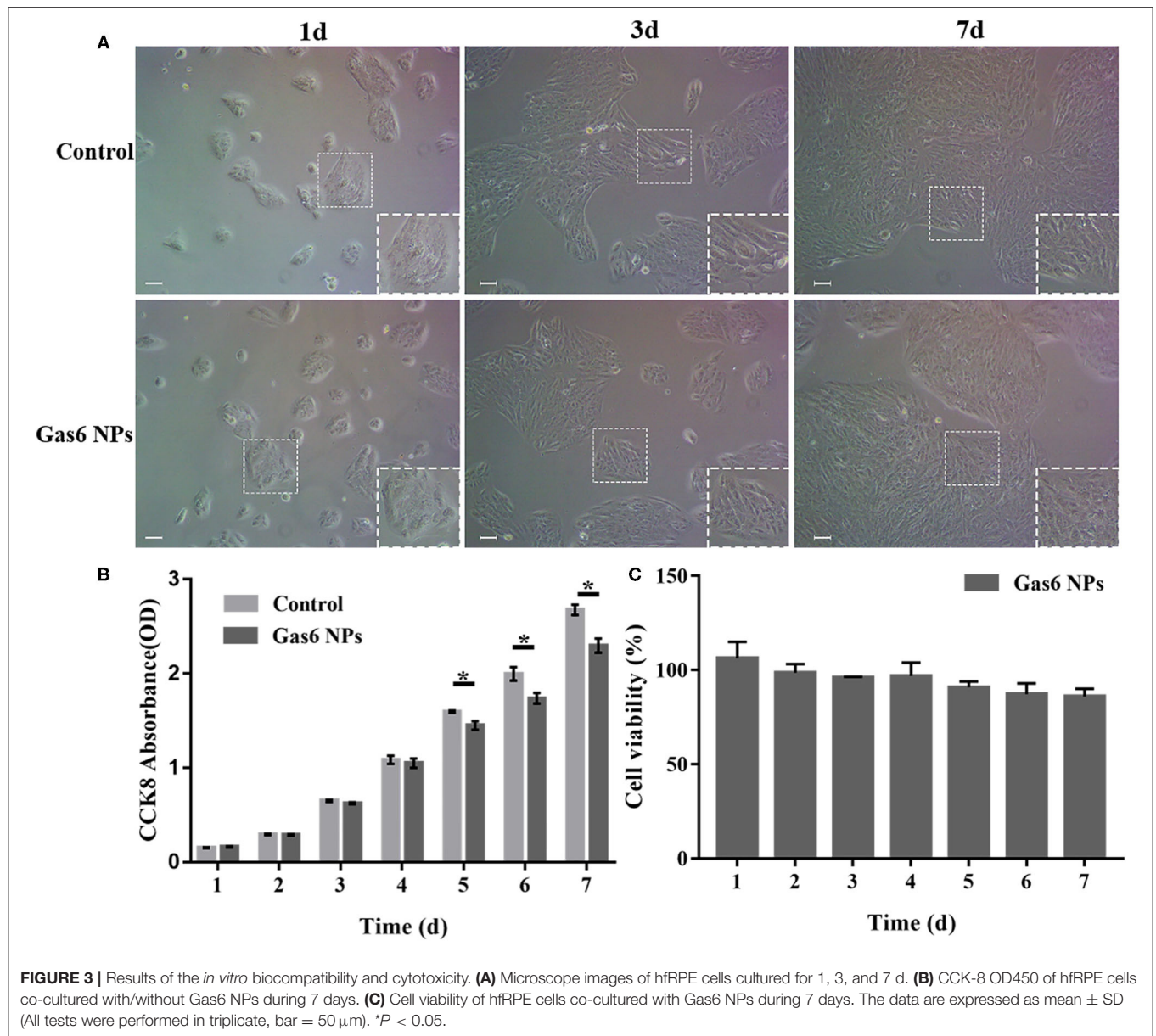
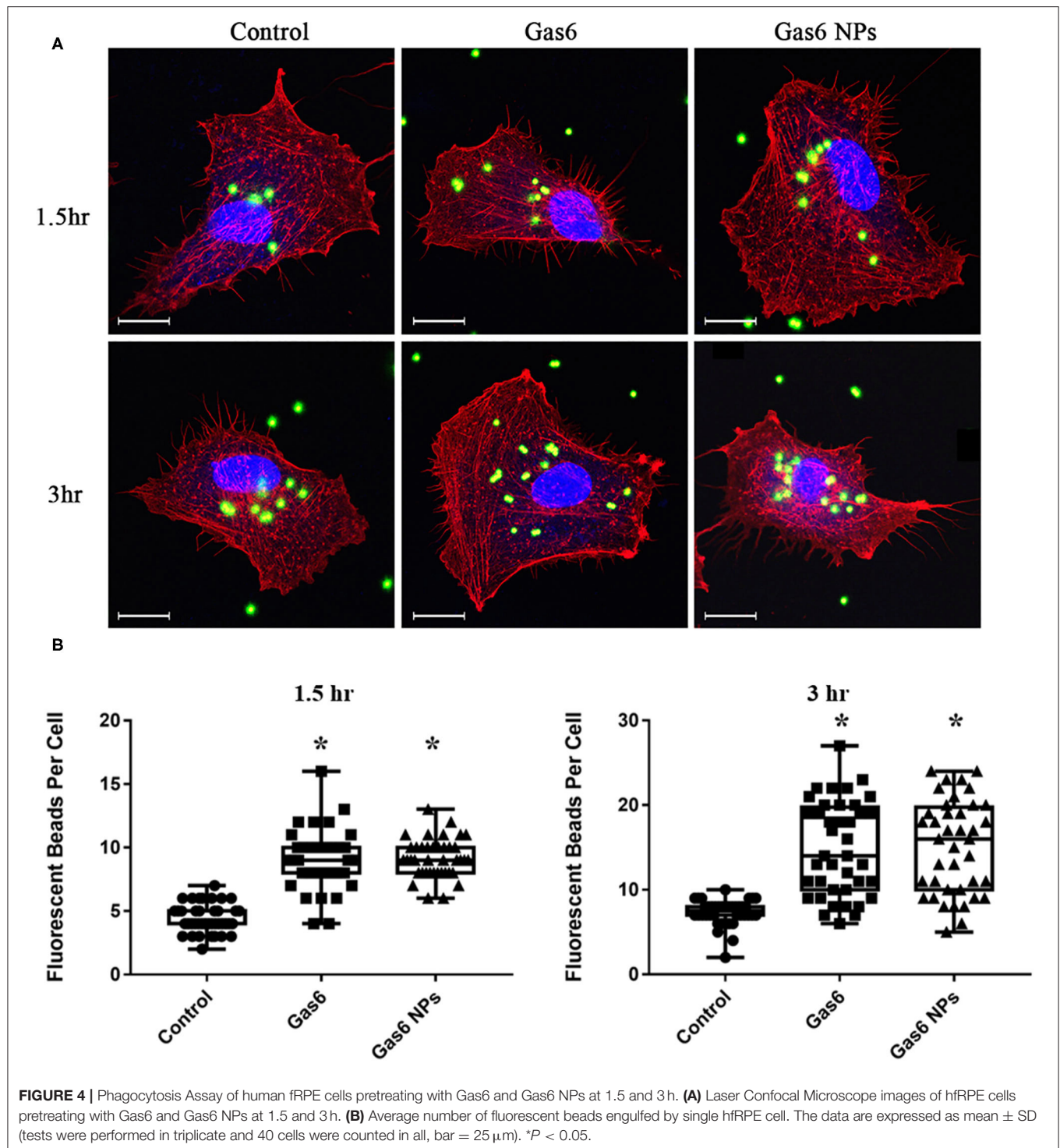


**FIGURE 3 |** Results of the *in vitro* biocompatibility and cytotoxicity. **(A)** Microscope images of hRPE cells cultured for 1, 3, and 7 d. **(B)** CCK-8 OD450 of hRPE cells co-cultured with/without Gas6 NPs during 7 days. **(C)** Cell viability of hRPE cells co-cultured with Gas6 NPs during 7 days. The data are expressed as mean  $\pm$  SD (All tests were performed in triplicate, bar = 50  $\mu$ m). \* $P < 0.05$ .

assay. When pretreating with Gas6 protein and Gas6 NPs, the location of the fluorescent beads engulfed by hRPE cells was observed by laser confocal microscope (**Figure 4A**). The number of fluorescent beads engulfed by hRPE cells in both Gas6 and Gas6/NPs groups were significantly higher than that of the control group at 1.5 h ( $8.95 \pm 2.30$  and  $9.15 \pm 1.51$ , respectively, compared to  $4.43 \pm 1.13$  engulfed beads/cell) and 3 h ( $14.88 \pm 5.54$  and  $15.08 \pm 5.51$ , respectively, compared to  $7.33 \pm 1.47$  engulfed beads/cell) (**Figure 4B**).

The Gas6 protein is the ligand of the MERTK receptor and can enhance phagocytosis by RPE cells *via* the MERTK-FakY861-Rac1 signaling pathway (13). Therefore, we detected key proteins involved in Gas6-induced phagocytosis by western

blotting (**Figure 5A**). The fold changes of pFAKY861, GTP-Rac1, and pAKT473 in hRPE cells pretreated with Gas6 ( $4.911 \pm 3.262$ ,  $2.744 \pm 1.181$ , and  $7.061 \pm 3.547$ ) and Gas6 NPs ( $5.591 \pm 2.412$ ,  $2.784 \pm 1.159$ , and  $9.680 \pm 6.285$ ) were higher than that of the control group 1.5 h after the beads were added (**Figure 5B**). When the incubation time was extended to 3 h, the expression of active proteins remained higher than that of the control group and fold changes were computed as  $2.300 \pm 0.985$  (pFAK861),  $1.939 \pm 0.232$  (GTP-Rac1), and  $2.352 \pm 0.513$  (pAKT473) pretreated with Gas6 and  $2.667 \pm 1.250$  (pFAK861),  $1.957 \pm 0.348$  (GTP-Rac1), and  $2.266 \pm 0.845$  (pAKT473) pretreated with Gas6 NPs (**Figure 5B**). Collectively, these results suggest that Gas6 NPs provide a safe and effective mean for delivery of Gas6 *in vitro*.



### **In vivo Rescue of MERTK-Associated Retinal Degeneration by Gas6 NPs**

RCS rats with inherited retinal degeneration caused by a deletion in the *MERTK* gene were used to evaluate the protective effect of the combination strategy. Firstly, we demonstrated that the hMERTK protein could be sexpressed in the RPE cell layer of

RCS rats (Figure 6) following the subretinal injection of AAV2-BEST1-hMERTK.

Additionally, in order to assess whether Gas6 NPs enhanced the therapeutic effects of gene therapy in RCS rats, we recorded and analyzed the ERG response and OCT results of the rats at 12 days post injection (12 dpi, 5 days after Gas6 and Gas6

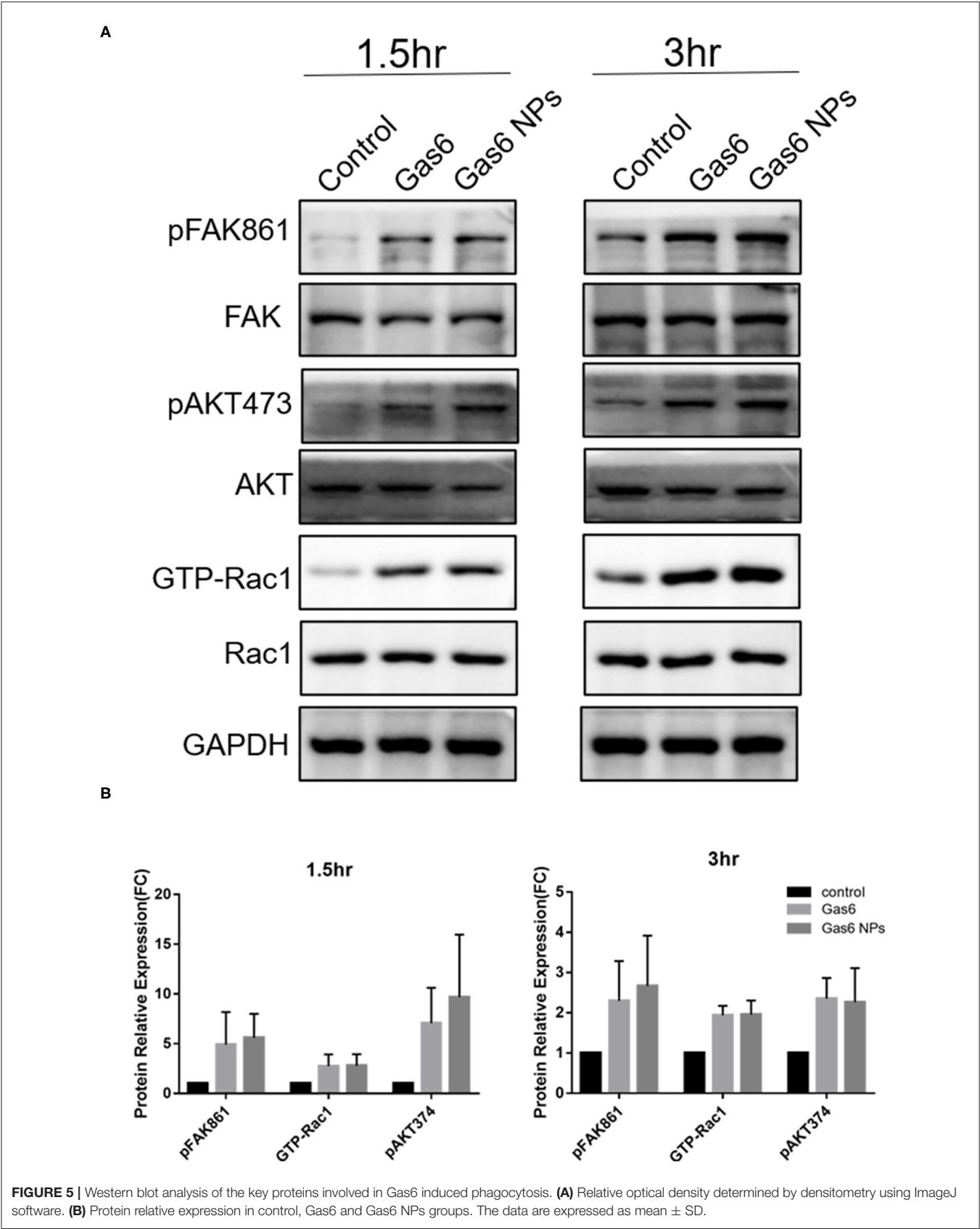
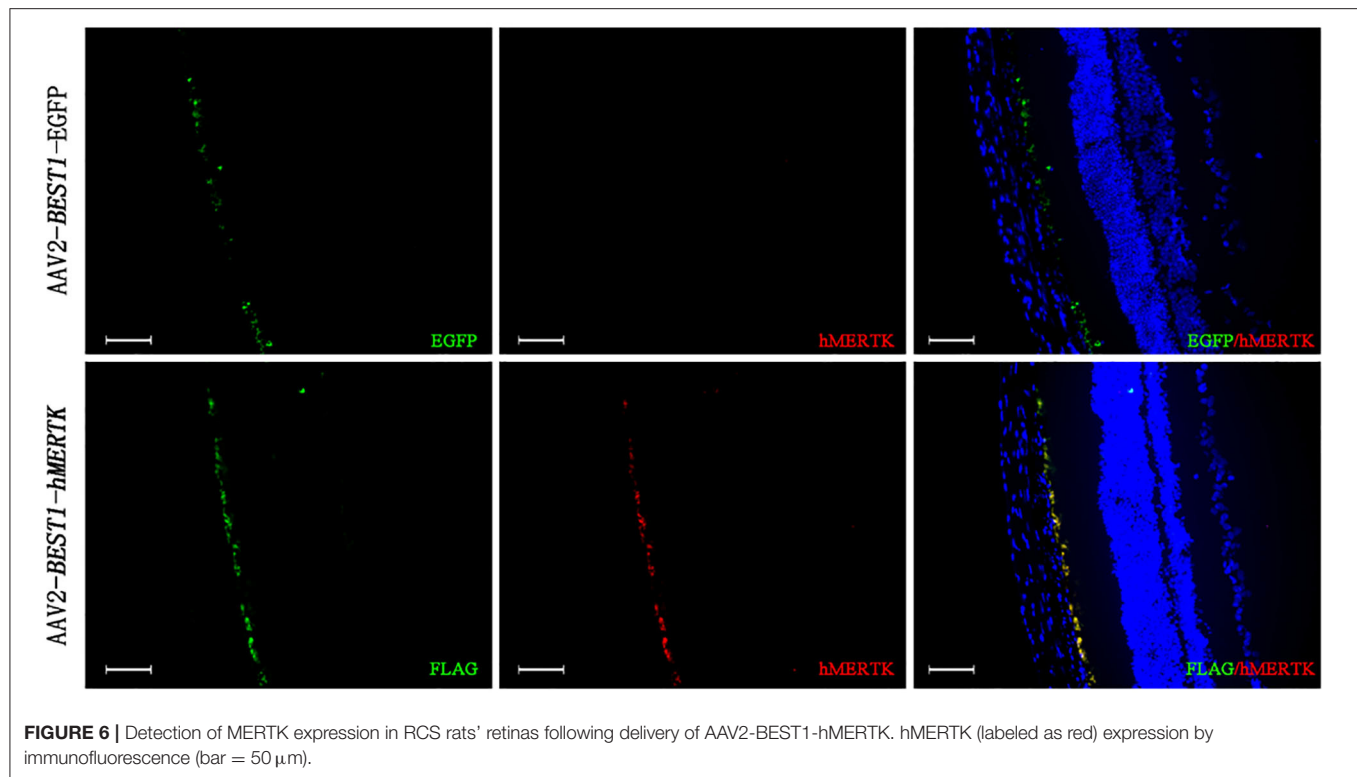


**FIGURE 5 |** Western blot analysis of the key proteins involved in Gas6 induced phagocytosis. **(A)** Relative optical density determined by densitometry using ImageJ software. **(B)** Protein relative expression in control, Gas6 and Gas6 NPs groups. The data are expressed as mean  $\pm$  SD.





NPs intervention) and 19 dpi (12 days after Gas6 and Gas6 NPs intervention). The RCS rats in all groups demonstrated typical ERG responses with a and b-waves (**Figure 7** and **Supplementary Figure 1**). At 12 dpi, the hMERTK/Gas6 NPs group exhibited significantly higher b-wave ( $295.533 \pm 61.598 \mu\text{V}$ ) in dark-adapted ERG responses at  $0.01 \text{ cd.s/m}^2$  than other groups. The b-wave amplitudes of the hMERTK group ( $199.022 \pm 28.187 \mu\text{V}$ ) and hMERTK/Gas6 group ( $214.114 \pm 50.677 \mu\text{V}$ ) were also higher than that of the control group ( $146.179 \pm 29.720 \mu\text{V}$ ) at  $0.01 \text{ cd.s/m}^2$ ; there is no significant difference between the hMERTK group and hMERTK/Gas6 group (**Figure 7A**). To evaluate the sustained protective effect of the combined treatment, we also recorded ERGs at 19 dpi. As illustrated in **Figure 7B**, the dark-adapted ERG responses in the hMERTK, hMERTK/Gas6 and hMERTK/Gas6 NPs groups were all significantly higher than that of the control group at low light intensity ( $0.01 \text{ cd.s/m}^2$ ). Moreover, the hMERTK/Gas6 NPs group had the largest b-wave amplitude among the 3 treatment groups, similar to that recorded at 12 dpi. There was no significant difference between the hMERTK and hMERTK/Gas6 groups at 19 dpi too.

We further evaluated the architecture in the retina of the RCS rats *via* OCT. Representative OCT images of the retina were taken horizontally across the optic nerve head (ONH), and the imaging location was marked on the fundus image with a black line (**Figure 8A**). Then we quantitatively measure the thickness of the outer nuclear layer (ONL) at 100, 200, 400- $\mu\text{m}$  of temporal retina and 100, 200, 400, 600- $\mu\text{m}$  of nasal retina from the ONH (**Figure 8B**). We can clearly note that the ONL thickness

curve of the nasal side was clearly separated (**Figure 8B**). The average ONL thickness of the nasal retina was calculated and shown in **Figure 8C**. After co-administration of AAV2-BEST1-hMERTK and Gas6 NPs, the thickness of nasal ONL was  $54.70 \pm 7.53 \mu\text{m}$  and  $31.09 \pm 5.27 \mu\text{m}$  respectively at 12 dpi and 19 dpi. The thickness of the ONL was significantly higher than that of the Control group ( $39.00 \pm 7.50 \mu\text{m}$  and  $19.54 \pm 2.73 \mu\text{m}$ ), hMERTK group ( $48.45 \pm 6.98 \mu\text{m}$  and  $24.51 \pm 2.52 \mu\text{m}$ ), and hMERTK/Gas6 group ( $49.35 \pm 5.78 \mu\text{m}$  and  $25.77 \pm 4.95 \mu\text{m}$ ).

The rats were finally sacrificed and the eyeballs were taken out. The H&E staining images of retina were shown in **Figure 9A**. The results evidenced that the ONL nuclear layers in control group ( $3 \pm 0.71$ ) was significantly less than that of the hMERTK group ( $6.11 \pm 1.23$ ), hMERTK/Gas6 group ( $6.56 \pm 1.24$ ), and hMERTK/Gas6 NPs group ( $10.89 \pm 1.36$ ) (**Figure 9B**). A statistically significant difference was observed between the hMERTK/Gas6 NP group and the other 2 treatment groups. However, there was no significant difference between the hMERTK and hMERTK/Gas6 group. And the result of the ONL thickness is consistent with the result of ONL nuclear layers (**Supplementary Figure 2**). Altogether, these results suggest that the combined treatment of AAV2-BEST1-hMERTK and Gas6 NPs had a greater protective effect on photoreceptors.

## DISCUSSION

In this study, we prepared Gas6 protein-loaded mPEG-PLGA nanoparticles (Gas6 NPs), which allowed for localized and sustained Gas6 protein release to overcome the short half-life of

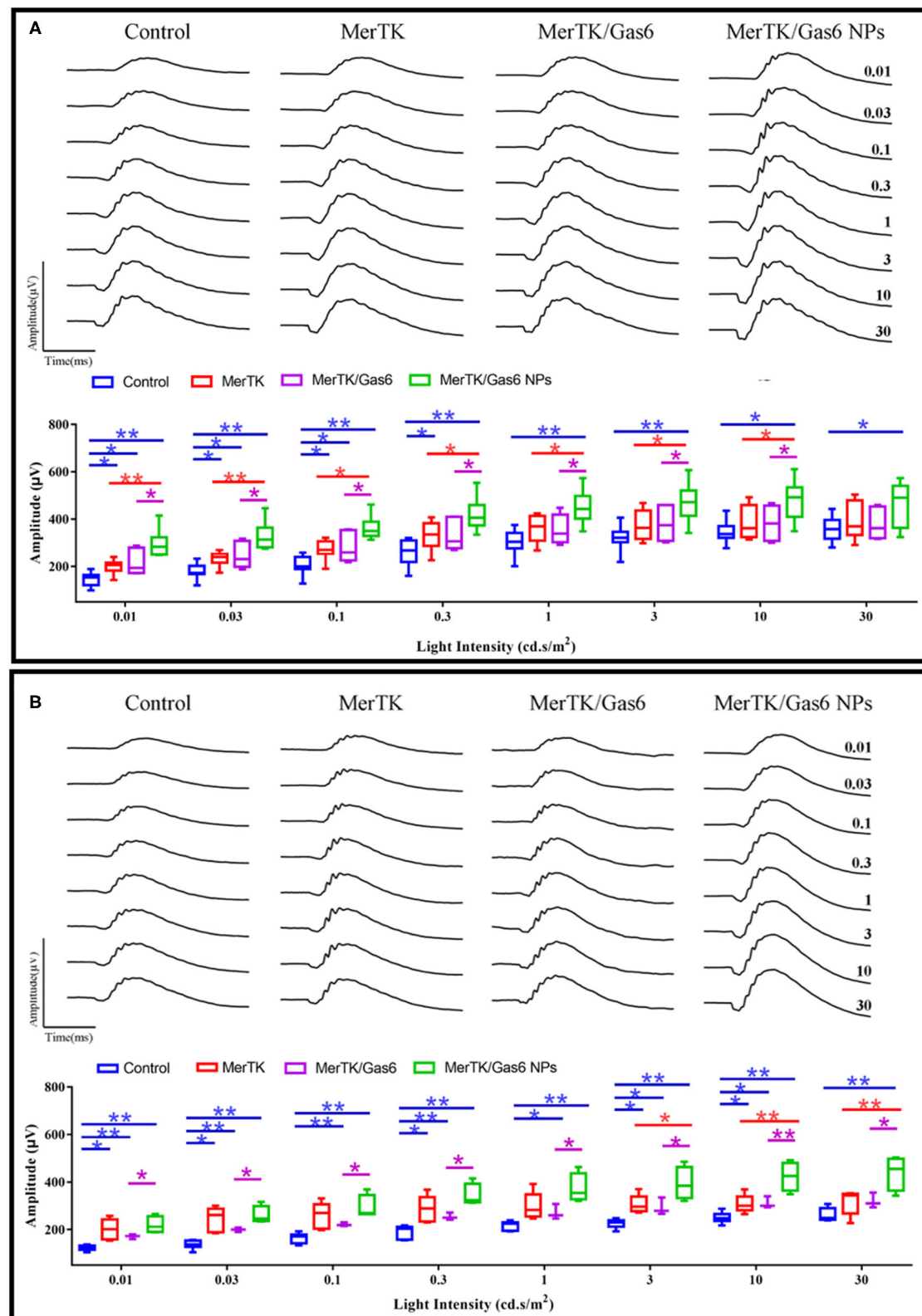


**FIGURE 7 |** B-wave of dark-adapted (scotopic) ERG data of the representative RCS rats at 12 dpi and 19 dpi. **(A)** Scotopic ERG response (12 dpi) at a series of intensity from 0.01 to 30 cd\*s/m<sup>2</sup>. Control: *n* = 7; MerTK: *n* = 9; MerTK/Gas6: *n* = 7; MerTK/Gas6 NPs: *n* = 6. **(B)** Scotopic ERG response (19 dpi) at a series of intensity from 0.01 to 30 cd\*s/m<sup>2</sup>. Control: *n* = 6; MerTK: *n* = 5; MerTK/Gas6: *n* = 3; MerTK/Gas6 NPs: *n* = 4. \**P* < 0.05, \*\**P* < 0.005.

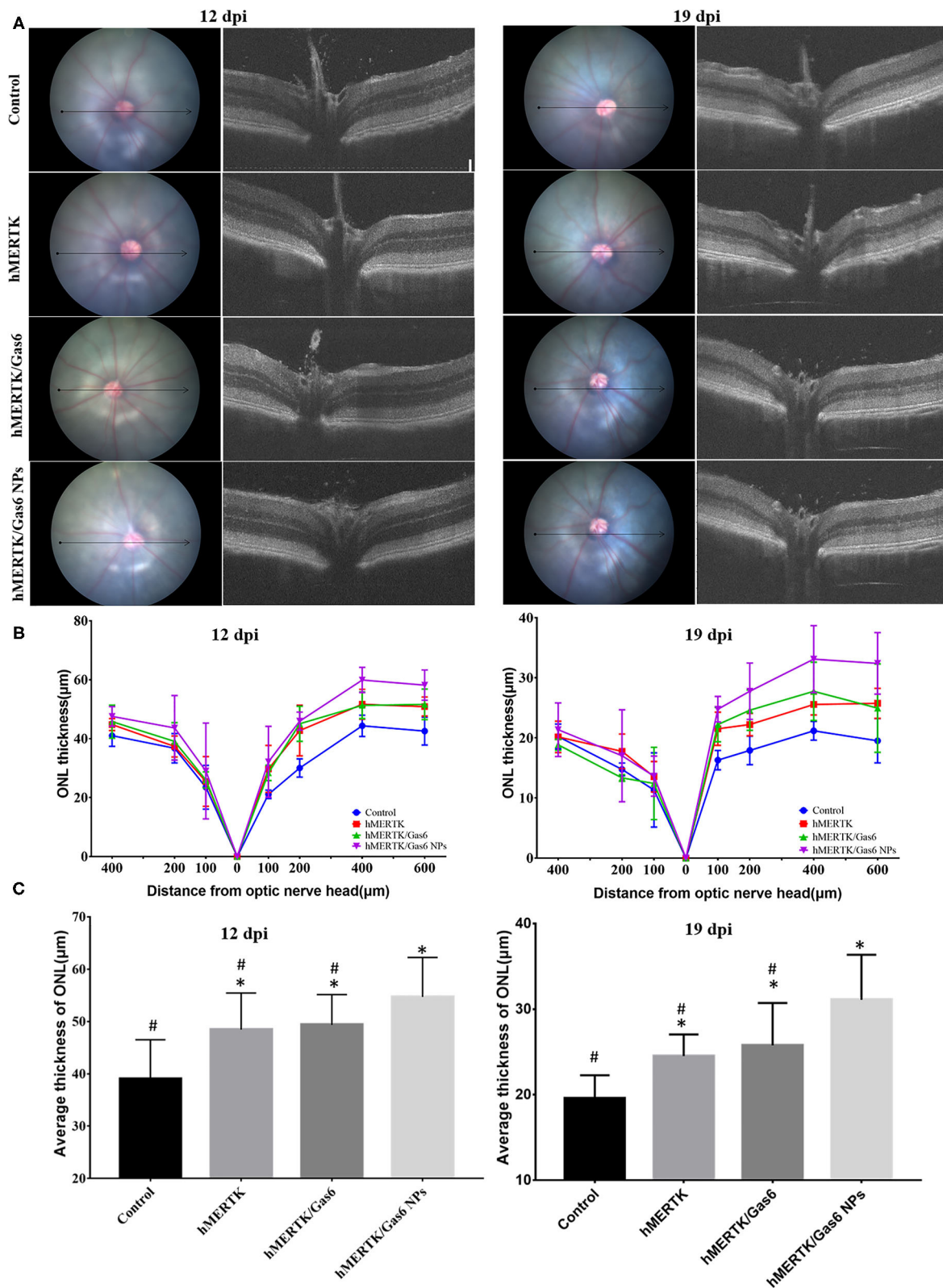
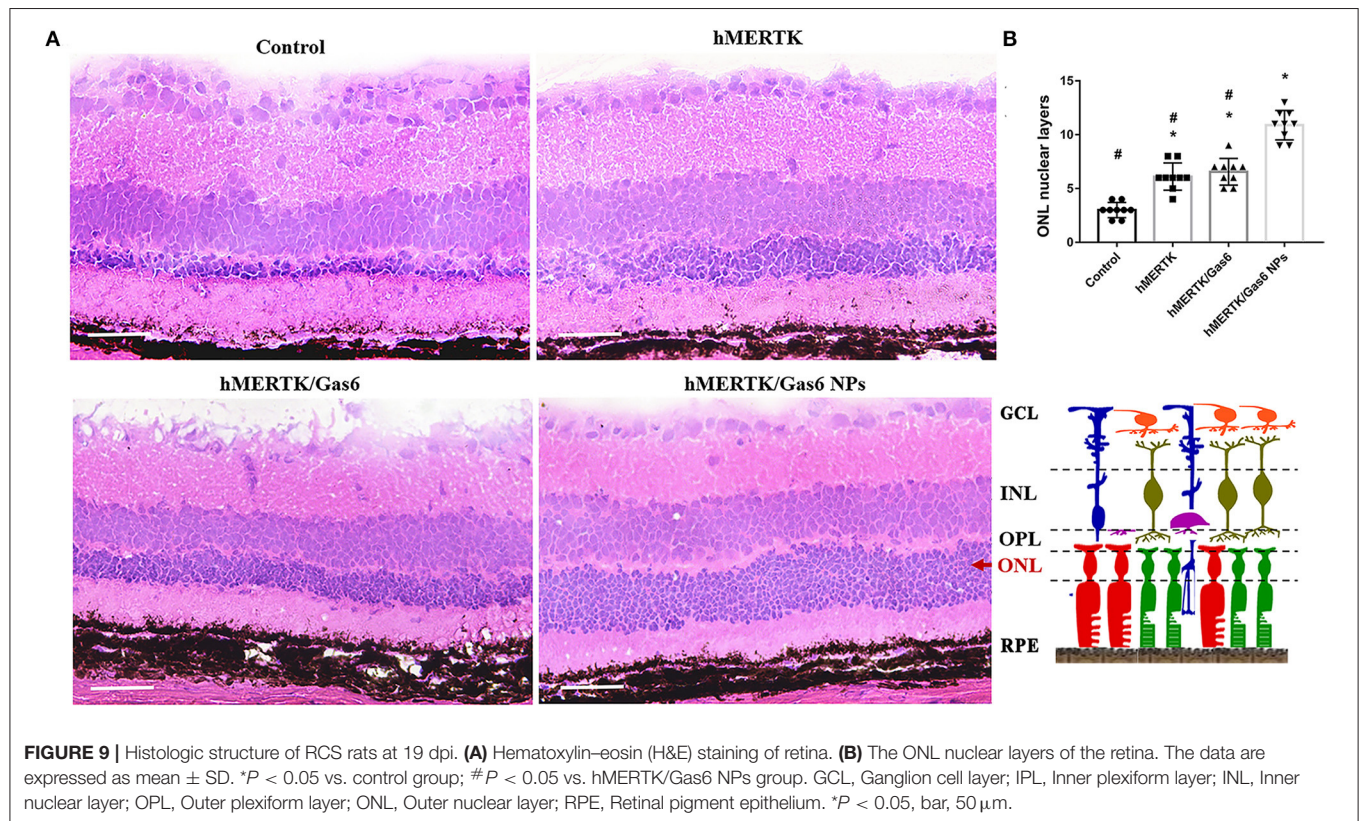


**FIGURE 8 |** Architecture in the retina of the representative RCS rats at 12 dpi and 19 dpi. **(A)** Representative retinal cross section B-scan OCT image (the location was indicated with a black line in ocular fundus) at 12 dpi and 19 dpi; **(B)** Quantitative measurements of retinal thickness in different locations at 12 dpi and 19 dpi; **(C)** Average thickness of temporal retina at 200, 400, and 600 microns at 12 dpi and 19 dpi. \* $P < 0.05$  vs. control group; # $P < 0.05$  vs. hMERTK/Gas6 NPs group. (Continued)



**FIGURE 8** | Sample size at 12 dpi: Control:  $n = 6$ ; MerTK:  $n = 5$ ; MerTK/Gas6:  $n = 5$ ; MerTK/Gas6 NPs:  $n = 6$ . Sample size at 19 dpi: Control:  $n = 3$ ; MerTK:  $n = 4$ ; MerTK/Gas6:  $n = 3$ ; MerTK/Gas6 NPs:  $n = 4$ .



the Gas6 protein *in vivo*. We identified that Gas6 NPs preserved Gas6 protein bioactivity and promoted RPE phagocytosis *in vitro*. Additionally, we assessed whether Gas6 NPs enhanced the therapeutic effects of gene therapy in RCS rat model of MERTK-associated retinal dystrophy. Our results demonstrate that the co-administration of AAV2-BEST1-hMERTK and Gas6 NPs could protect photoreceptors from degeneration in RCS rats. Consequently, the ERG response was remarkably ameliorated and more structure of retina was preserved in the hMERTK/Gas6 NPs group. These findings strongly suggest that Gas6 NPs are a promising method for the sustained release of Gas6 protein and could enhance the therapeutic effect of gene therapy for MERTK-associated RP.

MERTK gene replacement therapy is considered as a promising treatment for MERTK-associated RP and demonstrated therapeutic efficacy (20–23). Recent studies have indicated that the use of Gas6 enhances retinal phagocytosis *via* the MERTK receptor either alone or in combination with other specific ligands for receptor tyrosine kinases, which may enhance the therapeutics effects of gene therapy (13). Whereas, Gas6 as a recombinant protein has many disadvantages such as short *in vivo* half-lives and chemical instability, may necessitate frequent administration over time to maintain long term effect. Therefore, we encapsulated Gas6 into mPEG-PLGA

nanoparticles (Gas6 NPs) and conducted a series of evaluations to determine the safety and function of Gas6 NPs *in vitro*. Our results demonstrated that both Gas6 protein and Gas6 NPs induced phagocytosis in hRPE cells, which is consistent with previous reports (13). Moreover, our results confirm the bioactivity of the released Gas6 protein, which provides a solid foundation for the application of Gas6 NPs in enhancing the therapeutic effect of gene therapy.

To confirm the effect of Gas6 NPs *in vivo*, we designed the co-administration strategy of Gas6 NPs with MERTK gene and subsequently evaluated its therapeutic effects in RCS rats. Our results evidenced that the hMERTK/Gas6 group had a similar ERG response to that of the hMERTK group, while the hMERTK/Gas6 NPs group attained the highest amplitude based on ERG response. This suggested the sustained release of Gas6 protein within the therapeutic window for an extended period was essential for enhancing visual function. The mPEG-PLGA formulation would offer numerous advantages, including the protection of Gas6 from degradation or elimination and the ability to deliver Gas6 locally to the retina, it is likely to enhance the therapeutic effect of gene therapy. Moreover, the dark-adapted ERG response of the control, hMERTK, and hMERTK/Gas6 groups was significantly weakened at certain light intensities at 19 dpi compared to 12 dpi, whereas no



such difference was observed in the hMERTK/Gas6 NPs group. It is possible that the sustained release of the Gas6 protein induced a prolonged effect within the retinal environment, and consequently enhanced RPE phagocytosis *via* the MERTK receptor for an extended period.

To our knowledge, it is the first time we proposed the concept of sustained release of Gas6 protein within the therapeutic window for enhancing the effects of gene therapy for MERTK-associated RP. Here, the mPEG-PLGA was used to encapsulate Gas6 protein, which has good biocompatible and its degradation depends on molecular weight, conformation, and copolymer composition (24). The Gas6 protein release kinetics obtained in this study demonstrate that mPEG-PLGA nanoparticles are a suitable protein delivery system and, more specifically, an effective sustained-release system. While, nearly 70% of Gas6 had been released from Gas6 NPs by day 12, after which its release slowed down. In the clinical setting, we need the release of Gas6 to be sustained for a longer duration in order to reduce the frequency of administration and increase patient compliance and comfort. This requires us to optimize this sustained-release system in future research to finally achieve an extended-release system.

Our findings strongly suggest that Gas6 NPs could enhance RPE phagocytosis *in vitro* and be used for enhancing the effects of gene therapy for MERTK-associated RP *in vivo*. We propose that the promotion of RPE phagocytosis *via* the sustained released of Gas6 may enhance the therapeutic efficiency of gene therapy in RCS rats. The potential mechanisms underlying the manner in which the Gas6 protein enhances the therapeutic efficiency of MERTK gene therapy is unknown and should be addressed by further studies. However, it has been reported that Gas6 is a multi-functional circulating protein with multiple roles related to inflammation and immune system (25), and retinitis pigmentosa is usually accompanied by inflammation. Of note, once it is identified that Gas6 enhances the therapeutic effect of MERTK gene therapy by up-regulating phagocytosis and improving the retinal microenvironment, early administration of retinal microenvironment *via* Gas6 sustained release system could be applicable to other subtypes of retinal degenerative diseases.

In summary, we designed the hMERTK/Gas6 NPs co-administration system and evaluated its therapeutic effects on RP treatment. We developed injectable Gas6 NPs with mPEG-PLGA *via* the double emulsion technique. The Gas6 NPs facilitated the development of a localized Gas6 delivery system with improved retention time. *In vitro* studies demonstrated that the Gas6 NPs remarkably increased the phagocytic function of hRPE cells. Meanwhile, *in vivo* studies evidenced that the co-administration of Gas6 NPs with MERTK gene replacement therapy remarkably ameliorated the functional recovery of the ERG response and preserved more retinal structure.

## MATERIALS AND METHODS

### Preparation of Gas6 NPs

mPEG-PLGA (mPEG5000-PLGA 75/25 [70000]) was purchased from Shanghai Zhong-Liang Oil and Fat Chemical Co.,

Ltd. (Shanghai, China). Moreover, polyvinyl alcohol (PVA), pluronic F68, esteramide (EA), and dichloromethane (DCM), all having a purity of at least 99%, were purchased from Sigma Chemical Corp. (St. Louis, Missouri, United States). mPEG-PLGA nanoparticles loaded with Gas6 were prepared using the double emulsion (w/o/w) technique. Briefly, 10 mg mPEG-PLGA was dissolved in 0.5 mL EA, after which 0.1 mL Gas6 solution (3 g/dL) was added. This mixture was transferred to a centrifuge tube and emulsified by sonication for 3 min at 80 W. Thereafter, the resultant emulsion was slowly added to 0.7 mL 2% (m/v) PVA and 0.3 mL 2% (m/v) pluronic F68, which was then stirred vigorously for 10 min. The mixture was subsequently emulsified *via* sonication for 5 min at 250 W. Both emulsification steps were performed in an ice bath. After the solvent was evaporated by applying vacuum, the Gas6 NPs were collected by centrifugation at 10,000 rcf. for 10 min and then washed twice using distilled water.

### Characterization of Gas6 NPs

Fourier transform infrared (FTIR) spectra were recorded using an FTIR spectrometer (Spectrum One, PerkinElmer). The average size of Gas6 NPs was determined by dynamic light scattering (DLS) using a ZetaSizer Nano ZS (Malvern Instruments Ltd., Malvern, Worcestershire, United Kingdom). Samples were appropriately diluted with distilled water, and subsequently measured at 633 nm at 25°C and a constant angle of 90°. Stability experiments were regularly performed for the duration of 1 week by measuring the size of Gas6 NPs in phosphate-buffered saline (PBS) solution at room temperature. The concentration of Gas6 NPs used in the stability experiments was the same as that in the *in vivo* study. Furthermore, the morphology of Gas6 NPs was confirmed using a transmission electron microscope (TEM; JEM-200CX, JEOL Ltd., Tokyo, Japan).

### Determination of the Encapsulation Efficiency

The encapsulation efficiency percentage (EE%) of Gas6 NPs was calculated as follows:

$$EE\% = \frac{Gas6_{total} - Gas6_{free}}{Gas6_{total}} * 100\%$$

where Gas6<sub>total</sub> is the total amount of Gas6 in the nanoparticle and suspension, while Gas6<sub>free</sub> is the amount of free Gas6 in the suspension. Enzyme-linked immune absorbent assay (ELISA) was applied to detect Gas6<sub>free</sub> in the suspension.

### *In vitro* Gas6 Release

Gas6 protein release kinetics were determined by the Human Gas6 ELISA Kit (Sigma-Aldrich Corp., St. Louis, Missouri, USA). Briefly, Gas6 NPs were immersed in PBS at 4°C with gentle shaking. At determined intervals, the suspension was centrifuged and the supernatant was replaced and collected. The Gas6 concentration in the supernatant was determined by the Human Gas6 Elisa Kit. The *in vitro* release reactions were carried out in triplicate for each sample.

## Cell Culture and Animals

Human fetal RPE (hFRPE) cells were kindly provided by Professor Guoping Fan (University of California, Los Angeles, California, US) (26). These cells were cultured in DMEM/F12(1:1) medium supplemented with 15% fetal bovine serum (FBS) (SH3007003HI; Thermo Fisher Scientific) at 37°C in a humidified incubator with a 5% CO<sub>2</sub>/95% air atmosphere. The medium was replaced every 2 days.

RCS rats were also kindly provided by Professor Guoping Fan and kept in Capital Medical University, Beijing, China. The animals were kept in temperature-controlled rooms with a 12-h light/dark cycle and were provided with standard food and water *ad libitum*. The study was approved and monitored by the Institutional Animal Care and Use Committee of the Capital Medical University (IACUC; AEEI-2018-198), and conformed to the National Institute of Health Guide for the Care and Use of Laboratory Animals as well as the Association for Research in Vision and Ophthalmology (ARVO) Statement for the Use of Animals in Ophthalmic and Vision Research.

## Cell Viability Assay

The hFRPE cells ( $0.5 \times 10^4$  cells/well) were allowed to adhere overnight after plated in 96-well plates before being incubated for 7 days. Cells were then treated with Gas6 NPs dispersion (final concentration of Gas6 was 500 ng/mL) and incubated for an additional 7 days. Cell viability was tested daily. Briefly, the culture medium was replaced by 200  $\mu$ L 10% CCK8 reagent (CA1210; Solarbio, Beijing, China) and incubated for 2 h at 37°C. The optical density (OD) value was measured at 450 nm using an ELISA reader (BioTek, Winooski, Vermont, USA) according to the manufacturer's instructions. The relative proliferation rate was calculated as follows:  $RPR = (OD_{TEST}/OD_{Control}) \times 100\%$

## Phagocytosis Assay

The hFRPE cells were plated at a density of  $5 \times 10^4$  cells/well into poly-L-lysine coated 24-well plates and allowed to adhere overnight. Cells were then pretreated with Gas6 NPs dispersion (final concentration of Gas6 was 500 ng/mL) or recombinant Gas6 protein (final concentration 500 ng/mL) for 1 h. Thereafter, 5  $\mu$ L of 1  $\mu$ m fluorescein isothiocyanate (FITC)-labeled carboxylate-modified microspheres (1933365; 1:10 dilution; Invitrogen, USA) was added, and initially incubated for 1.5 h and 3 h at 37°C with a 5% CO<sub>2</sub> atmosphere. The medium was then removed and cells were washed 6 times to remove excess beads. Cells were subsequently labeled with 4',6-diamidino-2-phenylindole (DAPI) and tetramethylrhodamine (TRITC) phalloidin (CA1610; Solarbio, Beijing, China). Four images were taken of each well using a Leica SP5 microscope. Additionally, the amounts of beads per cell was counted in 40 cells per condition.

## Western Blotting Analysis

The hFRPE cells were plated at a density of  $5 \times 10^5$  cells/well into poly-L-lysine coated 6-well plates and allowed to adhere overnight. Cells were then pretreated with Gas6 NPs dispersion (final concentration of Gas6 was 500 ng/mL) or recombinant Gas6 protein (final concentration 500 ng/mL)

for 1 h. Thereafter, 15  $\mu$ L of 1  $\mu$ m fluorescein isothiocyanate (FITC)-labeled carboxylate-modified microspheres (1933365; 1:10 dilution; Invitrogen, USA) was added, and incubated for 1.5 h and 3 h at 37°C with a 5% CO<sub>2</sub> atmosphere. Thereafter, proteins were extracted from cells and their total concentration was measured using a BCA Protein Assay Kit (CWBIO) according to the manufacturer's instructions. Equal quantities (40  $\mu$ g) of proteins per gel lane were separated on 10% polyacrylamide gels by sodium dodecyl sulfate–polyacrylamide gel electrophoresis (SDS-PAGE) and then transferred to polyvinylidene fluoride membranes using an electroblotting apparatus (Bio-Rad). Membranes were blocked using a solution containing 5% non-fat milk and TBS-Tween20 and then incubated separately at 4°C overnight with the following primary antibodies: GAPDH (sc-25778; 1:1000; SantaCruz Biotechnology), active GTP-Rac1 (26903; 1:200; Neweast Biosciences), Rac1 (ab155938; 1:600; Abcam), p-FAK861 (44-626G; 1:800; Invitrogen), FAK (AHO0502; 1:200; Invitrogen), p-AKT473 (4060s; 1:500; CST), and AKT (9272; 1:500; CST). Membranes were then incubated with horseradish-peroxidase (HRP)-conjugated secondary antibody (goat anti-mouse/rabbit IgG antibody; G21240/G21234; 1:1000; Invitrogen) for 1 h at room temperature. Membranes were then washed 3 times (10 min per wash) with 0.1% TBS-Tween20 after each antibody application. Thereafter, immuno-labeled proteins were detected using the ECL Plus Detection System (Invitrogen) according to the manufacturer's instructions. The band was analyzed using Image-Pro Plus (IPP) software.

## Animal Experiments

The pAAV2-BEST1-hMERTK vector was prepared by Vigene Biosciences Inc. Briefly, the human MERTK gene and BEST1 promoter were amplified from a Human Retina Marathon-Ready cDNA Library (Clontech) and cloned into the pUC19 vector. The sequence of the construct was verified by Sanger sequencing. Thereafter, the expression cassette, containing the BEST1 promoter, hMERTK cDNA, and 3xFLAG tag, was excised by restriction enzymes and cloned into the pAAV plasmid. The pAAV2-BEST1-MERTK plasmid was then transfected into HEK293 cells and the virus was harvested. The final concentration of AAV2-BEST1-hMERTK was  $3.37 \times 10^{13}$  vg/mL. The map of pAAV2-BEST1-hMERTK and pAAV2-BEST1-EGFP were showed in **Supplementary Figure 3**. The sequence of BEST1 promoter was list in **Supplementary Table 1**.

Subretinal injections of the AAV2-BEST1-hMERTK virus were administered to RCS rats at P19 (0 dpi). RCS rats were divided into 4 different groups based on the administered treatment, namely Control group (AAV2-BEST1-EGFP), hMERTK group (AAV2-BEST1-hMERTK), hMERTK/Gas6 group (AAV2-BEST1-hMERTK & Gas6 protein), and hMERTK/Gas6 NPs group (AAV2-BEST1-hMERTK & Gas6 NPs). Rats were anesthetized using an intraperitoneal injection containing 30 mg/kg pentobarbital sodium and 5 mg xylazine hydrochloride. Pupils were dilated using 0.2 mg/mL tropicamide phenylephrine (Santen Pharmaceutical Co., Ltd., Shiga Plant, Shiga, Japan) and topically anesthetized with 0.5% proparacaine (Santen Pharmaceutical Co., Ltd.). A 31-gauge insulin syringe

was used to carefully puncture the temporal corneoscleral limbus. Thereafter, a 33-gauge blunt needle (Hamilton) was used to administer the subretinal injection. The blunt needle tip was inserted through the sclerotic puncture and aimed at the contralateral subretinal space. Subsequently, 1  $\mu$ L of AAV2-*BEST1*-EGFP (control group) or AAV2-*BEST1*-hMERTK virus (hMERTK, hMERTK/Gas6, and hMERTK/Gas6 NPs groups) was injected into the subretinal space of the RCS rats' right eye. Tobramycin and dexamethasone eye ointment (ALCON) were applied once daily for 3 days after injection.

At 7 dpi, 2  $\mu$ L PBS (control and hMERTK groups), 2  $\mu$ L Gas6 protein (hMERTK/Gas6 group; 0.5  $\mu$ g/ $\mu$ L), or 2  $\mu$ L Gas6 NPs (hMERTK/Gas6 NPs group; 0.5  $\mu$ g Gas6/ $\mu$ L) was administered *via* intravitreal injection. The ERG and OCT were recorded at 12 dpi and 19 dpi. Animals exhibiting retinal bleeding and cataracts were excluded.

## Electroretinographic Analysis

The Espion Visual Electrophysiology System (Diagnosys, USA) was used to record the electroretinogram. After at least 12 h of dark adaptation, animals were anesthetized and their pupils were dilated using 0.2 mg/mL tropicamide phenylephrine. Animals were placed on a regulated heating pad throughout the experiment. Electroretinograms (ERGs) were recorded by means of a golden ring that made contact with the corneal surface through a layer of 0.2% carbomer. Additionally, needle electrodes were inserted into the cheeks and tails of animals and served as the reference and ground leads, respectively. Scotopic testing at eight-intensity stimulus-response series (0.01 cd.s/m<sup>2</sup> to 30 cd.s/m<sup>2</sup>) were presented; the resulting b-wave amplitudes were measured from the trough of the a-wave to the crest of the b-wave.

## Optical Coherence Tomography

OCT was performed using a Micron III (Phoenix Research Labs, Pleasanton, CA). Animals were anesthetized and their pupils were dilated using 0.2 mg/mL tropicamide phenylephrine. The corneal surface was protected using a 1.5% hydroxyethylcellulose solution. The rat ocular fundus was monitored using the fundus camera of the Micron. Representative OCT images of the retina were taken horizontally across the optic nerve head (ONH), and the imaging location was marked on the image with a black line. Thirty images were averaged to eliminate projection artifacts. The acquired OCT images were quantitatively analyzed using the InSight software (Phoenix Research Labs). The thickness of the outer nuclear layer (ONL) was measured at 100, 200, 400- $\mu$ m of temporal retina and 100, 200, 400, 600- $\mu$ m of nasal retina from the ONH. The average value of the ONL in nasal retina at 200, 400, and 600 microns was used represent the average thickness of ONL.

## Tissue Immunofluorescence Staining

Samples were cut into 10  $\mu$ m sections using a cryostat (Leica Microsystems, Wetzlar, Germany). Thereafter, sections were rinsed 3 times with PBS for 5 min at room temperature, and then blocked with 5% bovine serum albumin (BSA) for 30 min at room temperature. Sections were subsequently transferred to a

moist chamber containing rabbit recombinant monoclonal anti-hMERTK antibody (ab52968; 1:200; Abcam) at 4°C overnight. Thereafter, sections were rinsed 3 times with PBS and incubated with Alexa Fluor 594 anti-rabbit secondary antibody (R37119; 1:1000; Invitrogen) in the dark for 1 h at room temperature. Cell nuclei were then stained with DAPI and fluorescent signals were visualized using a Zeiss fluorescence microscope (Observer Z1).

## Histological Analysis

To quantify the layers and the thickness of outer nuclear layer (ONL) after combined treatment, hematoxylin and eosin (H&E) staining was performed. Rats were anesthetized using 400 mg/kg chloral hydrate, after which their eyes were enucleated, fixed in 4% paraformaldehyde for 4 h, washed 3 times with PBS, and embedded in paraffin. Eight-micron-thick paraffin sections were used for H&E staining. Stained slices were visualized by a Leica microscope. The ONL layers was counted in a double-blind manner. The thickness of the ONL was measured using Image-Pro Plus (IPP) software. There are 3 animals in each group, and the layers and thickness of ONL of each animal were measured in 3 different slices.

## Statistical Analysis

All data were presented as the mean  $\pm$  standard deviation (SD). Independent Samples *T*-test analysis was used to compare the CCK8 absorbance between the control group and Gas6 NPs group. One-way analysis of variance (ANOVA) and Fisher's least significant difference (LSD) test were used to determine whether significant differences exist between the ERG amplitudes of the different treatment groups. Two-way analysis of variance and Fisher's least significant difference (LSD) test were used to determine whether significant differences exist among the OCT results. The independent Samples *T*-test analysis was used to compare the differences between the cell viability of each group. Statistical analyses were performed by SPSS 20.0 (SPSS Inc., Chicago, Illinois, USA). *P* < 0.05 indicated statistical significance.

## DATA AVAILABILITY STATEMENT

The original contributions presented in the study are included in the article/**Supplementary Material**, further inquiries can be directed to the corresponding authors.

## ETHICS STATEMENT

The animal study was reviewed and approved by Institutional Animal Care and Use Committee of the Capital Medical University (IACUC; AEEI-2018-198).

## AUTHOR CONTRIBUTIONS

SW and YM conducted the experiments, analysis the data, and wrote the paper. JZ and NW designed the experiments and revised the paper. QL and XY provided the materials. All authors contributed to manuscript revision, read, and approved the submitted version.



## FUNDING

This work was supported by National Key R&D Program of China (2017YFA0104100 and 2016YFC0905201), Beijing Municipal Institute of Public Medical Research Development and Reform Pilot Project (2018-2), Beijing Hospitals Authority Youth Program (QML20180208), and Beijing Institute of Ophthalmology Key Program (2019003). These funders had no role in study design, data collection and analysis, decision to publish, or preparation of the manuscript.

## REFERENCES

- Dias MF, Joo K, Kemp JA, Fialho SL, Jessica A, Woo SJ, et al. Molecular genetics and emerging therapies for retinitis pigmentosa: basic research and clinical perspectives. *Prog Rtein Eye Res.* (2018) 63:107–31. doi: 10.1016/j.preteyeres.2017.10.004
- Sahel J, Bonnel S, Mrejen S, Paques M. Retinitis pigmentosa and other dystrophies. *Dev Ophthalmol.* (2010) 47:160–7. doi: 10.1159/000320079
- Charbel Issa P, Bolz HJ, Ebermann I, Domeier E, Holz FG, Scholl HPN. Characterisation of severe rod-cone dystrophy in a consanguineous family with a splice site mutation in the MERTK gene. *Br J Ophthalmol.* (2009) 93:920–5. doi: 10.1136/bjo.2008.147397
- Abu-Safieh L, Alrashed M, Anazi S, Alkuraya H, Khan AO, Al-Owain M, et al. Autozygome-guided exome sequencing in retinal dystrophy patients reveals pathogenetic mutations and novel candidate disease genes. *Genome Res.* (2013) 23:236–47. doi: 10.1101/gr.144105.112
- Patel N, Aldahmesh MA, Alkuraya H, Anazi S, Alsharif H, Khan AO, et al. Expanding the clinical, allelic, and locus heterogeneity of retinal dystrophies. *Genet. Med.* (2016) 18:554–62. doi: 10.1038/gim.2015.127
- Bok D, Hall MO. The role of the pigment epithelium in the etiology of inherited retinal dystrophy in the rat. *J Cell Biol.* (1971) 49:664–82. doi: 10.1083/jcb.49.3.664
- Zhang JX, Wang NL, Lu QJ. Development of gene and stem cell therapy for ocular neurodegeneration. *Int J Ophthalmol.* (2015) 3:622–30. doi: 10.3980/j.issn.2222-3959.2015.03.33
- Boye SE, Boye SL, Lewin AS, Hauswirth WW. A comprehensive review of retinal gene therapy. *Mol Ther.* (2013) 21:509–19. doi: 10.1038/mt.2012.280
- Conlon TJ, Deng WT, Erger K, Cossette T, Pang JJ, Ryals R, et al. Preclinical potency and safety studies of an AAV<sub>2</sub>-mediated gene therapy vector for the treatment of MERTK associated retinitis pigmentosa. *Hum Gene Ther Clin Dev.* (2013) 24:23–8. doi: 10.1089/humc.2013.037
- Ghazi NG, Abboud EB, Nowilaty SR, Alkuraya H, Alhommedi A, Cai H, et al. Treatment of retinitis pigmentosa due to MERTK mutations by ocular subretinal injection of adeno-associated virus gene vector: results of a phase I trial. *Hum Genet.* (2016) 135:327–43. doi: 10.1007/s00439-016-1637-y
- Law AL, Parinot C, Chatagnon J, Gravez B, Sahel J-A, Bhattacharya SS, et al. Cleavage of Mer Tyrosine Kinase (MERTK) from the cell surface contributes to the regulation of retinal phagocytosis. *J Biol Chem.* (2015) 290:4941–52. doi: 10.1074/jbc.M114.628297
- Pelaez D. Stem Cells for microenvironmental modulation and retinal regeneration. *Curr Tissue Eng.* (2016) 5:52–9. doi: 10.2174/2211542004666150713191117
- Albert R, Kristóf E, Zahuczky G, Tóth M, Veréb Z, Oláh B, et al. Triamcinolone regulated apopto-phagocytic gene expression patterns in the clearance of dying retinal pigment epithelial cells. A key role of MERTK in the enhanced phagocytosis. *BBA Gen Subjects.* (2015) 1850:435–46. doi: 10.1016/j.bbagen.2014.10.026
- Putney SD, Burke PA. Improving protein therapeutics with sustained-release formulations. *Nat. Biotechnol.* (1998) 16:153–7. doi: 10.1038/nbt0298-153
- Rauck BM, Novosot TL, Oudega M, Wang Y. Biocompatibility of a coacervate-based controlled release system for protein delivery to the injured spinal cord. *Acta Biomater.* (2015) 11:204–11. doi: 10.1016/j.actbio.2014.09.037
- Li Z, Qu T, Ding C, Ma C, Sun H, Li S, et al. Injectable gelatin derivative hydrogels with sustained vascular endothelial growth factor release for induced angiogenesis. *Acta Biomater.* (2015) 13:88–100. doi: 10.1016/j.actbio.2014.11.002
- Zhang Z, Tongchusak S, Mizukami Y, Kang YJ, Ioji T, Touma M, et al. Induction of anti-tumor cytotoxic T cell responses through PLGA-nanoparticle mediated antigen delivery. *Biomaterials.* (2011) 32:3666–78. doi: 10.1016/j.biomaterials.2011.01.067
- Wu C, Baldursdottir S, Yang M, Mu H. Lipid and PLGA hybrid microparticles as carriers for protein delivery. *J Drug Deliv Sci Technol.* (2018) 43:65–72. doi: 10.1016/j.jddst.2017.09.006
- Kurowska-Stolarska M, Alivernini S, Garcia Melchor E, Elmesmari A, Tolusso B, Tange C, et al. MicroRNA-34a dependent regulation of AXL controls the activation of dendritic cells in inflammatory arthritis. *Nat Commun.* (2017) 8:1–13. doi: 10.1038/ncomms15877
- Koch S, Sothilingam V, Garrido MG, Tanimoto N, Becirovic E, Koch F, et al. Gene therapy restores vision and delays degeneration in the CNGB1<sup>1/1</sup> mouse model of retinitis pigmentosa. *Hum Mol Genet.* (2012) 21:4486–96. doi: 10.1093/hmg/dds290
- LaVail MM, Yasumura D, Matthes MT, Yang H, Hauswirth WW, Deng WT, et al. Gene therapy for MERTK-associated retinal degenerations. *Adv Exp Med Biol.* (2016) 854:487–93. doi: 10.1007/978-3-319-17121-0\_65
- Wert KJ, Davis RJ, Sancho-Pelluz J, Nishina PM, Tsang SH. Gene therapy provides long-term visual function in a pre-clinical model of retinitis pigmentosa. *Hum Mol Genet.* (2013) 22:558–67. doi: 10.1093/hmg/ddt466
- Deng WT, Dinculescu A, Li Q, Boye SL, Li J, Gorbatyuk MS, et al. Tyrosine-mutant AAV8 delivery of human MERTK provides long-term retinal preservation in RCS rats. *Invest Ophthalmol Vis Sci.* (2012) 53:1895–904. doi: 10.1167/iovs.11-8831
- Csaba N, Sánchez A, Alonso MJ. PLGA: Poloxamer and PLGA: Poloxamine blend nanostructures as carriers for nasal gene delivery. *J Control Release.* (2006) 113:164–72. doi: 10.1016/j.jconrel.2006.03.017
- Lemke G. Biology of the TAM receptors. *Cold Spring Harb Perspect Biol.* (2013) 5:a009076. doi: 10.1101/cshperspect.a009076
- Liao JL, Yu J, Huang K, Hu J, Diemer T, Ma Z, et al. Molecular signature of primary retinal pigment epithelium and stem-cell-derived RPE cells. *Hum Mol Genet.* (2010) 19:4229–38. doi: 10.1093/hmg/ddq341

**Conflict of Interest:** The authors declare that the research was conducted in the absence of any commercial or financial relationships that could be construed as a potential conflict of interest.

**Publisher's Note:** All claims expressed in this article are solely those of the authors and do not necessarily represent those of their affiliated organizations, or those of the publisher, the editors and the reviewers. Any product that may be evaluated in this article, or claim that may be made by its manufacturer, is not guaranteed or endorsed by the publisher.

Copyright © 2021 Wu, Mao, Liu, Yan, Zhang and Wang. This is an open-access article distributed under the terms of the Creative Commons Attribution License (CC BY). The use, distribution or reproduction in other forums is permitted, provided the original author(s) and the copyright owner(s) are credited and that the original publication in this journal is cited, in accordance with accepted academic practice. No use, distribution or reproduction is permitted which does not comply with these terms.





# Comparison of Intraocular Cytokine Levels of Choroidal Neovascularization Secondary to Different Retinopathies

Chenyi Liu<sup>1</sup>, Shian Zhang<sup>1,2</sup>, Xinyi Deng<sup>1,2</sup>, Yijing Chen<sup>1,2</sup>, Lijun Shen<sup>1,2</sup>, Liang Hu<sup>1,2\*</sup> and Jianbo Mao<sup>1,2\*</sup>

<sup>1</sup> School of Optometry and Ophthalmology, Wenzhou Medical University, Wenzhou, China, <sup>2</sup> Eye Hospital of Wenzhou Medical University, Wenzhou, China

## OPEN ACCESS

### Edited by:

Shaochong Zhang,  
Sun Yat-sen University, China

### Reviewed by:

Pablo De Gracia,  
Midwestern University, United States

Dequan Li,  
Baylor College of Medicine,  
United States

### \*Correspondence:

Liang Hu  
liang\_hu@live.cn  
Jianbo Mao  
rocket222@sina.com

### Specialty section:

This article was submitted to  
Ophthalmology,  
a section of the journal  
Frontiers in Medicine

**Received:** 25 September 2021

**Accepted:** 01 December 2021

**Published:** 21 December 2021

### Citation:

Liu C, Zhang S, Deng X, Chen Y,  
Shen L, Hu L and Mao J (2021)  
Comparison of Intraocular Cytokine  
Levels of Choroidal Neovascularization  
Secondary to Different Retinopathies.  
Front. Med. 8:783178.  
doi: 10.3389/fmed.2021.783178

**Purpose:** To investigate and compare the aqueous concentrations of vascular endothelial growth factor (VEGF) and other inflammatory cytokines in various choroidal neovascularization (CNV) diseases and types.

**Methods:** This observational study included 127 naive eyes with CNV and 43 control eyes with cataracts. Aqueous humor (AH) samples were obtained prior to intravitreal anti-VEGF injection or cataract surgery. Multiple inflammatory cytokines, including VEGF, interleukin (IL) 6, IL-8, IL-10, interferon-inducible protein 10 (IP-10), and monocyte chemotactic protein 1 (MCP-1) levels, were measured using a multiplex bead assay. The angiogenesis index was defined as the ratio of IP-10 to MCP-1. In addition, the relationship among AH cytokine levels, central macular thickness (CMT), and CNV size on optical coherence tomography angiography (OCTA) was evaluated.

**Results:** Except in the myopic CNV group ( $P = 0.452$ ), the AH concentration of VEGF was significantly higher in all other CNV groups than in the control group ( $P < 0.05$  for all comparisons). IL-8, IL-10, IP-10, and MCP-1 levels ( $P < 0.05$  for all groups) were significantly higher in all CNV diseases except those with neovascular central serous chorioretinopathy. The angiogenesis index was significantly higher in all CNV diseases ( $P < 0.05$  for all comparisons). The VEGF level may be associated with the size of the CNV on OCTA ( $p = 0.043$ ).

**Conclusions:** The level of intraocular inflammatory cytokines varied among different CNV diseases and CNV types. Therefore, the angiogenesis index may be a more sensitive indicator of angiogenesis.

**Keywords:** choroidal neovascularization, age-related macular degeneration (AMD), polypoidal choroidal vasculopathy (PCV), high myopic, central serous chorioretinopathy (CSC), cytokine, vascular endothelial growth factor

## INTRODUCTION

Choroidal neovascularization (CNV) is the formation of new blood vessels in the choroid. It often occurs in the macular area, causing macular hemorrhage and serous exudation under the retina, which can result in blindness. CNV is a characteristic finding in many fundus diseases, such as age-related macular degeneration (AMD), pathologic myopia, polypoidal choroidal vasculopathy (PCV), and central serous chorioretinopathy (CSC) (1, 2).

Although the pathogenesis of CNV remains poorly understood, it is believed to involve a variety of cell growth factors, and the angiogenesis is controlled by a dynamic equilibrium between proangiogenic and anti-angiogenic cytokines (2). Vascular endothelial growth factor (VEGF) is considered the most critical regulator in ocular angiogenesis (3). Currently, intravitreal anti-VEGF injections are recommended as the first-line treatment in patients with neovascular age-related macular degeneration (nAMD). However, anti-inflammatory therapy has also achieved curative efficacy in patients with neovascularization (4–6). It is still unclear whether the neovascularization in various CNV diseases results from the elevation in the VEGF concentration or the presence of the inflammatory response, and the application of anti-inflammatory treatment remains controversial (7–10).

CNVs are classified into Type 1 and Type 2 CNVs depending on the anatomic localization of the neovascularization. Further research is warranted to discover the aqueous concentration of cytokines in these two neovascularization types and investigate the potential mechanisms linked to their inflammatory response. In addition, CNV size was found to be associated with functional prognosis, suggesting that it could predict the response to anti-VEGF therapy (11). However, it is unknown whether the reason is related to VEGF or inflammatory cytokines.

Secondary CNV was reported in 5% of chronic CSC cases in which the concentration of VEGF did not increase (12, 13). Previous studies have not investigated the change in VEGF levels or the difference in cytokine profiling between neovascular CSC (nCSC) and other CNV diseases.

This study investigated and compared the aqueous concentrations of VEGF and other inflammatory cytokines in different CNV diseases and CNV types. Additionally, it preliminarily explored the association between VEGF levels and the size of CNV on optical coherence tomography angiography (OCTA) images.

## METHODS

This observational study was conducted between May 2019 and July 2021 and included 127 eyes of patients treated for active CNV in nAMD, PCV, myopic choroidal neovascularization (mCNV), and nCSC. This study was approved by the Wenzhou Medical University Affiliated Eye Hospital Ethics Committee, and the procedures followed the tenets of the Declaration of Helsinki (IRB number #121-K-107-01). All patients provided written informed consent for inclusion in the study.

The inclusion criteria were (1) age over 18 years, (2) no previous history of intraocular surgery or intravitreal injections, (3) CNV in the active stage diagnosed by fluorescein angiography and indocyanine green angiography, and (4) a spherical equivalent of the eyes with mCNV  $\leq -6.00$  D and an axial length of  $>26$  mm in patients with high myopia. The exclusion criteria were (1) any other retinopathy such as diabetic retinopathy, retinal vascular occlusion or retinal detachment (2) glaucoma and/or iris neovascularization; (3) uveitis; and (4) any previous treatment for CNV, including laser treatment within the past 6 months. The control group consisted of 43 eyes that underwent cataract surgery and had no other ocular or immune-mediated diseases.

All patients received a comprehensive ophthalmological examination before their anti-VEGF injection or cataract surgery, including slit lamp biomicroscopy and dilated fundus examination. The axial length was measured using the IOL-Master 700 (Carl Zeiss Meditec, Jena, Germany). The OCTA images were obtained using a spectral domain optical coherence tomography (SD-OCT) device (RTVue XR Avanti, Optovue, Inc., Fremont, CA, USA) with a split-spectrum amplitude-decorrelation angiography algorithm. The size of CNV was marked with the manual selection tools and calculated using the built-in software. The image quality for analysis was no lower than 7 out of 10. All measurements were performed by two independent and masked readers. Disagreements over readings were resolved by open adjudication between readers. The CNV size was classified as small ( $<0.5$  mm<sup>2</sup>), medium ( $\geq 0.5$  mm<sup>2</sup> and  $<2.0$  mm<sup>2</sup>), and large ( $\geq 2.0$  mm<sup>2</sup>).

CNVs were categorized into two groups, Type 1 and Type 2, depending on their anatomical location. Type 1 CNV was characterized by any abnormal vasculature localized between Bruch's membrane and the retinal pigment epithelium on SD-OCT, and Type 2 CNV was characterized by any abnormal vasculature localized above the retinal pigment epithelium and beneath the photoreceptor outer segments on SD-OCT. Central macular thickness (CMT) was defined as the average retinal thickness within the 1 mm-diameter central field of the Early Treatment Diabetic Retinopathy Study.

Aqueous humor (AH) samples were collected before cataract surgery or intravitreal anti-VEGF injections. Approximately 0.05 mL of AH was withdrawn using a 30 gauge insulin syringe via limbal paracentesis. Each AH sample was immediately transferred into a sterile plastic tube and kept at  $-84^{\circ}\text{C}$  until the assay. The levels of VEGF, interleukin (IL) 6, IL-8, IL-10, interferon-inducible protein 10 (IP-10), and monocyte chemoattractant protein 1 (MCP-1) were measured in undiluted AH samples using a Luminex 200 (BIO-RAD, Hercules, CA, USA). Each cytokine concentration (pg/mL) was calculated using the standard curve provided by the kit. All steps were performed at room temperature and in dark illumination to protect the samples from light-induced degradation. The angiogenesis index was defined as the ratio of IP-10 to MCP-1.

All statistical analyses were performed using SPSS for Windows (version 26.0, SPSS Inc., Chicago, IL, USA). Continuous variables are expressed as means  $\pm$  standard deviation. The normality of the cytokine data distribution

**TABLE 1** | Differences in cytokine concentrations (pg/mL) between CNV groups and controls.

	Control (n = 43)	nAMD (n = 47)	PCV (n = 37)	mCNV (n = 30)	nCSC (n = 13)
Age	70.9 ± 7.3	71.3 ± 10.8	65.6 ± 11.6	57.6 ± 16.0	51.3 ± 9.2
Sex (M/F)	14/29	12/35	13/24	9/21	7/6
VEGF	29.78 ± 11.76	41.65 ± 19.06	40.31 ± 21.29	32.02 ± 14.49	36.99 ± 10.86
		0.004	0.007	0.452	0.044
IL-6	6.99 ± 7.89	6.50 ± 12.89	6.65 ± 10.42	12.23 ± 16.20	2.13 ± 0.91
		0.246	0.44	0.052	0.021
IL-8	9.37 ± 5.90	14.48 ± 19.69	34.95 ± 58.96	19.10 ± 13.08	4.87 ± 1.40
		0.262	0.018	<0.001	0.007
IL-10	0.68 ± 0.23	1.02 ± 0.46	1.37 ± 1.60	0.93 ± 0.18	0.69 ± 0.09
		<0.001	<0.001	<0.001	0.299
IP-10	178.87 ± 105.13	380.62 ± 266.52	709.68 ± 659.11	580.84 ± 513.65	225.07 ± 128.10
		<0.001	<0.001	<0.001	0.165
MCP-1	452.93 ± 193.11	494.82 ± 403.46	701.84 ± 549.77	752.72 ± 478.40	319.68 ± 71.62
		0.881	0.013	<0.001	0
Angiogenesis Index	0.42 ± 0.27	0.82 ± 0.47	1.08 ± 0.56	0.76 ± 0.39	0.70 ± 0.37
		<0.001	<0.001	<0.001	0.003

nAMD, neovascular age-related macular degeneration; PCV, polypoidal choroidal vasculopathy; mCNV, myopic choroidal neovascularization; nCSC, neovascular central serous chorioretinopathy; VEGF, vascular endothelial growth factor; IL-6, interleukin 6; IL-8, interleukin 8; IL-10, interleukin 10; IP-10, interferon-inducible protein 10; MCP-1, monocyte chemotactic protein 1. *P*-values calculated by Spearman rank correlation analysis. *P*-values calculated by Mann-Whitney U-test.

was assessed using the Shapiro–Wilk test. For data that were not normally distributed, comparisons between groups were performed by non-parametric analysis of variance with either the Mann–Whitney U test or the Kruskal–Wallis test. For the Kruskal–Wallis test, significant values were adjusted using the Bonferroni correction for multiple tests of continuous variables.  $P < 0.05$  was considered statistically significant.

## RESULTS

In this observational study, 127 patients with CNV (nAMD = 47, PCV = 37, mCNV = 30, and nCSC = 13) and 43 control patients with cataracts were enrolled. The demographic features are summarized in **Table 1**.

### VEGF Levels Were Higher in Most CNV Diseases

The AH concentrations of cytokines in all groups are presented in **Table 1**. The VEGF levels in the CNV groups (except the mCNV group,  $P = 0.452$ ) were significantly higher than that in the control group ( $P < 0.05$  for all comparisons, **Table 1**). In the AMD group, the levels of IL-10 and IP-10 were higher than those in the control group ( $P < 0.001$  for both comparisons). In PCV and mCNV groups, the levels of IL-8, IL-10, IP-10, and MCP-1 were significantly higher than that in the control group ( $P < 0.05$  for all comparisons). In addition, the angiogenesis indices in all CNV groups were significantly higher than that in the control group ( $P < 0.05$  for all comparisons). No correlation was observed between cytokine levels and CMT ( $P > 0.05$  for all comparisons, **Table 2**).

**TABLE 2** | Correlation between cytokines concentrations (pg/mL) and CMT at baseline.

	VEGF	IL-6	IL-8	IL-10	IP-10	MCP-1
nAMD	−0.196	−0.116	0.078	0.152	0.143	0.074
	0.238	0.488	0.64	0.364	0.39	0.658
PCV	0.161	−0.019	−0.129	0.007	0.007	0.04
	0.357	0.915	0.462	0.97	0.967	0.821
mCNV	0.065	0.349	−0.076	0.01	−0.206	−0.087
	0.757	0.087	0.717	0.963	0.324	0.68
nCSC	0.133	−0.35	−0.427	0.018	−0.25	−0.65
	0.732	0.356	0.252	0.963	0.516	0.058

CMT, central macular thickness; nAMD, neovascular age-related macular degeneration; PCV, polypoidal choroidal vasculopathy; mCNV, myopic choroidal neovascularization; nCSC, neovascular central serous chorioretinopathy; VEGF, vascular endothelial growth factor; IL-6, interleukin 6; IL-8, interleukin 8; IL-10, interleukin 10; IP-10, interferon-inducible protein 10; MCP-1, monocyte chemotactic protein 1. *P*-values calculated by Spearman rank correlation analysis.

### Intraocular Inflammatory Cytokine Levels in PCV Were Quite Different From Those in AMD

In the AMD Type 2 group, the levels of VEGF and IL-10 were significantly higher than those in the AMD Type 1 group ( $P < 0.05$  for both comparisons). In the PCV group, the levels of IL-8, IL-10, and MCP-1 were higher than those in the AMD Type 1 group, but the levels of VEGF were lower than those in the AMD Type 2 group ( $P < 0.05$  for all comparisons). Moreover, the level of IP-10 in the PCV group was significantly higher than that in

**TABLE 3** | Differences in cytokine concentrations (pg/mL) among PCV groups and nAMD Type1/Type 2 groups.

	nAMD Type 1 (n = 27)	nAMD Type 2 (n = 20)	PCV (n = 37)	Type 1 vs. Type 2	Type 1 vs. PCV	Type 2 vs. PCV
VEGF	36.50 ± 18.12	48.60 ± 18.49	40.31 ± 21.29	0.024	0.348	0.037
IL-6	7.63 ± 16.43	4.98 ± 5.39	6.65 ± 10.42	0.966	0.833	0.841
IL-8	10.55 ± 7.76	19.79 ± 28.36	34.95 ± 58.96	0.156	0.039	0.488
IL-10	0.88 ± 0.30	1.20 ± 0.56	1.37 ± 1.60	0.019	0.028	0.718
IP-10	346.99 ± 245.80	426.02 ± 292.43	709.68 ± 659.11	0.159	<0.001	0.026
MCP-1	506.60 ± 483.30	478.90 ± 272.01	701.84 ± 549.77	0.445	0.007	0.091
Angiogenesis Index	0.75 ± 0.41	0.92 ± 0.54	1.08 ± 0.56	0.2	0.005	0.192

nAMD, neovascular age-related macular degeneration; PCV, polypoidal choroidal vasculopathy; VEGF, vascular endothelial growth factor; IL-6, interleukin 6; IL-8, interleukin 8; IL-10, interleukin 10; IP-10, interferon-inducible protein 10; MCP-1, monocyte chemotactic protein 1. *P*-values calculated by Mann-Whitney U-test.

**TABLE 4** | Differences in cytokine concentrations (pg/mL) of CNV diseases in the same Type 1 or Type 2 CNV.

	Type 1			Type 2		
	nAMD (N = 27)	nCSC (N = 13)	<i>P</i> -value	nAMD (N = 20)	mCNV (N = 27)	<i>P</i> -value
VEGF	36.50 ± 18.12	36.99 ± 10.86	0.475 <sup>b</sup>	48.60 ± 18.49	31.65 ± 12.85	0.001 <sup>a</sup>
IL-6	7.63 ± 16.43	2.13 ± 0.91	0.151 <sup>b</sup>	4.98 ± 5.39	12.63 ± 16.87	0.009 <sup>b</sup>
IL-8	10.55 ± 7.76	4.87 ± 1.40	0.006 <sup>b</sup>	19.79 ± 28.36	19.35 ± 13.79	0.102 <sup>b</sup>
IL-10	0.88 ± 0.30	0.69 ± 0.09	0.005 <sup>a</sup>	1.20 ± 0.56	0.93 ± 0.19	0.031 <sup>b</sup>
IP-10	346.99 ± 245.80	319.68 ± 71.622	0.120 <sup>b</sup>	426.02 ± 292.43	589.25 ± 539.16	0.451 <sup>b</sup>
MCP-1	506.60 ± 483.30	319.68 ± 71.62	0.019 <sup>b</sup>	478.90 ± 272.01	763.92 ± 500.56	0.001 <sup>b</sup>

nAMD, neovascular age-related macular degeneration; mCNV, myopic choroidal neovascularization; nCSC, neovascular central serous chorioretinopathy; VEGF, vascular endothelial growth factor; IL-6, interleukin 6; IL-8, interleukin 8; IL-10, interleukin 10; IP-10, interferon-inducible protein 10; MCP-1, monocyte chemotactic protein 1. <sup>a</sup>Independent samples *t*-test; <sup>b</sup>Mann-Whitney U-test.

the AMD Type 1 and AMD Type 2 groups ( $P < 0.05$  for both comparisons, **Table 3**).

## The Same Types of CNV Secondary to Different Causes Were Not Completely Similar in Cytokine Levels

Type 1 CNV was observed in 40 eyes (27 eyes with AMD and 13 eyes with CSC). The levels of IL-8, IL-10, and MCP-1 in eyes with AMD Type 1 were higher than those in eyes with CSC ( $P < 0.05$  for all comparisons, **Table 4**). Type 2 CNV was observed in 47 eyes (20 eyes with AMD and 27 eyes with mCNV). The levels of IL-6 and MCP-1 in eyes with AMD Type 2 were lower than those in eyes with mCNV, but the level of VEGF was higher ( $P < 0.05$  for all comparisons, **Table 3**).

## The Association Between Cytokines and Size of CNV

A significant difference was observed among the three CNV size groups ( $p = 0.043$ , **Table 5**, **Figure 1**). The VEGF level increased with the size of CNV.

## DISCUSSION

The present study yielded six main findings. First, VEGF levels increased significantly in all CNV diseases except for mCNV. Second, some inflammatory cytokine levels increased

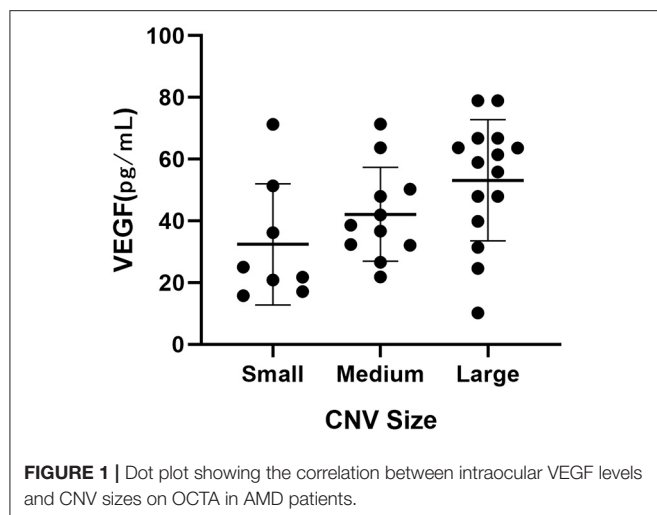
**TABLE 5** | Differences in cytokine concentrations (pg/mL) in groups of different vessel size (mm<sup>2</sup>).

	Small <0.5 (n = 8)	Medium ≥0.5 and <2 (n = 11)	Large ≥2 (n = 15)	<i>P</i> -value
VEGF	32.43 ± 19.62	42.14 ± 15.20	53.14 ± 19.63	0.043 <sup>a</sup>
IL-6	7.38 ± 8.56	2.69 ± 1.61	11.07 ± 21.47	0.522 <sup>b</sup>
IL-8	10.54 ± 8.13	17.41 ± 17.24	17.41 ± 17.24	0.297 <sup>b</sup>
IL-10	0.80 ± 0.38	0.89 ± 0.35	1.15 ± 0.48	0.057 <sup>b</sup>
IP-10	306.06 ± 241.69	349.963 ± 257.06	403.57 ± 313.35	0.657 <sup>b</sup>
MCP-1	421.11 ± 187.37	414.68 ± 105.51	413.75 ± 158.99	0.665 <sup>b</sup>

VEGF, vascular endothelial growth factor; IL-6, interleukin 6; IL-8, interleukin 8; IL-10, interleukin 10; IP-10, interferon-inducible protein 10; MCP-1, monocyte chemotactic protein 1. *P*-values calculated by Spearman rank correlation analysis. <sup>a</sup>One-way ANOVA test; <sup>b</sup>Kruskal-Wallis test.

significantly in all CNV diseases except for nCSC. Third, the angiogenesis index increased significantly in all CNV diseases, and it may be a more sensitive indicator of the presence of CNV than inflammatory cytokine levels. Fourth, intraocular inflammatory cytokine levels in PCV were quite different from those in AMD. Fifth, the same types of CNV secondary to different causes were not completely similar in cytokine levels. Sixth, VEGF levels may have a positive relationship with CNV size on OCTA.





Our results were consistent with previous studies showing that the ocular concentration of VEGF was elevated in all CNV groups except for mCNV compared with the control group (14, 15). The most plausible explanation for the normal level of VEGF in mCNV is the dilution effect in the anterior chamber and vitreous cavity due to the extended axial length (16).

Choroidal vessel hyperpermeability and congestion were suggested to be the cause of CSC (17), which is a disease in the pachychoroid spectrum. Secondary CNV in CSC is also called pachychoroid neovasculopathy (18), which may also be affected by the dysregulation and hyperpermeability of the choroidal vessels (19). To our knowledge, although previous studies have shown that the VEGF level in CSC eyes without neovascularization was similar to those in normal human eyes (20, 21), no research has investigated the VEGF level in the AH of patients with nCSC. In addition, differences in VEGF levels have been found between acute and chronic CSC eyes, and the VEGF level was positively correlated with typical choroidal abnormalities (12, 22). Our results demonstrated that in the nCSC group, only the level of VEGF increased; other pro-inflammatory cytokines remained unchanged, which supports the current view that the mechanism of neovascularization in pachychoroid disease differs greatly from that in AMD (23). The results also provide a theoretical basis for the treatment outcome reported by another study in which all patients with nCSC exhibited reduced pigment epithelial detachment thickness after 6 months of intravitreal anti-VEGF injection treatment (18). In the nAMD group, the levels of the inflammatory cytokines IL-10 and IP-10 both increased. This could explain why anti-VEGF treatment was equally effective in both diseases but eyes with pachychoroid neovasculopathy required fewer injections for maintenance (24).

In our study, the IP-10 level was elevated in all CNV groups except the nCSC group. IP-10 was capable of inhibiting both retinal and choroidal neovascularization as an inflammation-related chemokine (25). However, the molecular mechanism remains unknown. A previous *in vitro* study suggested that

IP-10 inhibits VEGF-mediated m-calpain activation, thereby disrupting any newly formed vessels via chemokine receptor 3 (CXCR3) signaling (26). Fujimura et al. (27) found that CXCR3-mediated angiostasis was independent of the VEGF signaling pathway. The ocular balance between angiogenic and angiostatic factors determines blood vessel formation, which is essential for the progression of neovascularization (28). In line with our results, Liu et al. found that the level of IP-10 was elevated in the AH of AMD patients (20). We speculated that the increase in IP-10 level in naive eyes was a compensatory response to excessively elevated VEGF, but the angiostatic chemokine level was not always high enough to prevent neovascular outgrowth.

MCP-1, as a member of the CC chemokine family, was shown to mediate neovascularization (29). The angiogenesis induced by MCP-1 was as potent as that induced by VEGF *in vivo* angiogenesis assays (28). A positive regulatory feedback loop exists between VEGF and MCP-1 expression by the ocular tissues in mediating angiogenesis (28). VEGF mediates MCP-1-induced angiogenesis, whereas MCP-1 induces VEGF expression via the upregulation of hypoxia-inducible factor 1 alpha gene expression (30, 31). This is a potential mechanism of resistance in anti-VEGF therapy because the anti-VEGF agent only focuses on a single pathogenic mechanism and the high baseline level of MCP-1 could reinduce VEGF expression. For such patients, combined anti-inflammatory therapy or new target agents may be necessary. In addition, we speculate that the co-expression and interrelationship between MCP-1 and IP-10 may have biological effects of angiogenesis regulation, similar to the interrelationship between VEGF and IP-10. We propose the ratio of IP-10 to MCP-1 as a new indicator called the angiogenesis index, which was elevated in all CNV groups in this study. Notably, even if the IP-10 and MCP-1 levels were both elevated in the PCV and mCNV groups, with VEGF at a normal level in mCNV, the angiogenesis index in these groups was still higher than that in the control group. Thus, it may be a more sensitive indicator of the imbalance between the facilitation and inhibition of neovascularization.

It remains controversial whether PCV is an AMD subtype. Recently, a growing consensus is that PCV lies within the pachychoroid disease spectrum, characterized by its hyperpermeable and dilated choroidal vessels. PCV is also a variant of Type 1 (sub-retinal pigment epithelium) neovascularization (19). Tong et al. found that the VEGF levels in PCV eyes were lower than those in exudative AMD eyes (32), but other previous studies observed no significant differences in cytokine levels between patients with AMD and PCV (14, 33, 34). These discrepancies in outcomes may be due to the lack of distinction between Type 1 and Type 2 CNVs. Our study compared PCV with AMD Type 1 CNV and the AMD Type 2 CNV and observed a significant difference in VEGF and IL-10 between the AMD Type 1 and Type 2 CNV groups. The VEGF level in PCV was similar to that in AMD Type 1 CNV, and both were lower than that in AMD Type 2 CNV. In the PCV group, the angiogenesis index and levels of inflammatory cytokines (i.e., IL-8, IL-10, IP-10, and MCP-1) were increased compared with the AMD Type 1 CNV group. This suggests that inflammation plays a role in PCV, which is different from the pathogenic mechanism in AMD.

The variation in the AH concentration of VEGF we found in different types of CNV may explain why different types of CNV showed different responses to anti-VEGF treatment (35). This variation may depend on whether the neovascularization has penetrated the retinal pigment epithelium; the penetration of such a crucial intraocular biological barrier can affect the AH concentration of VEGF and anti-VEGF agents (36).

The same type of CNV, secondary to different causes, is not completely similar in cytokines. In the mCNV Type 2 group, the VEGF level was lower, but the inflammatory cytokines (i.e., IL-6, IL-10, and MCP-1) levels were higher than that in the AMD Type 2 groups, which supported a possible connection between highly myopic eyes and low-grade or subclinical inflammation (37). The IL-6 level increased with the elongation of the eye globe, indicating a connection between inflammation and eye globe elongation (37). Zhao et al. (38) demonstrated that the upregulation of MCP-1 in fibroblasts raised the scleral macrophage density and matrix metalloproteinase 2 levels, which then contributed to axial length elongation and myopia development. However, whether these changes in inflammatory cytokines are a result or a cause of this disease is unclear. Further investigation is required to determine whether anti-inflammatory treatment is effective in patients who are not sensitive to anti-VEGF treatment.

We also observed an association of the intraocular VEGF levels with CNV sizes on OCTA in AMD patients. To our knowledge, no similar results have previously been reported. This is a preliminary result obtained from patients with high-quality images. Further studies are required to validate this finding.

One limitation of this study is the relatively small number of cases. In addition, the location of CNV varied, and the focal changes of cytokines in the intraocular microenvironment may not be well-reflected when they are solely based on AH samples. Finally, only six cytokines were examined in this study, and

other cytokines may contribute more strongly to the formation of CNV.

In conclusion, we confirmed the differences in intraocular inflammatory cytokine levels in eyes with different CNV diseases and types. The angiogenesis index may be a more sensitive indicator of angiogenesis than inflammatory cytokine levels. The positive relationship between VEGF and CNV size requires further validation in future studies.

## DATA AVAILABILITY STATEMENT

The original contributions presented in the study are included in the article/supplementary materials, further inquiries can be directed to the corresponding authors.

## ETHICS STATEMENT

The studies involving human participants were reviewed and approved by Wenzhou Medical University Affiliated Eye Hospital Ethics Committee. The patients/participants provided their written informed consent to participate in this study.

## AUTHOR CONTRIBUTIONS

CL, JM, LH, and LS designed the study. CL, SZ, XD, and YC performed the study. XD and YC performed data collection. CL and SZ performed data analysis and interpretation. CL and LS performed manuscript review and revision. All authors read and approved the final manuscript.

## FUNDING

This work was supported by the Key Project jointly constructed by Zhejiang Province and Ministry (WKJ-ZJ-2037) and Medical and Health Platform Project of Zhejiang Province (2021KY810).

## REFERENCES

- Jian L, Panpan Y, Wen X. Current choroidal neovascularization treatment. *Ophthalmologica*. (2013) 230:55–61. doi: 10.1159/000351660
- Jia J, Qiu D, Lu C, Wang W, Li N, Han Y, et al. Transcriptome analysis of choroid and retina from tree shrew with choroidal neovascularization reveals key signaling moieties. *Front Genet*. (2021) 12:654955. doi: 10.3389/fgene.2021.654955
- Cabral T, Mello LGM, Lima LH, Polido J, Regatieri CV, Belfort R, et al. Retinal and choroidal angiogenesis: a review of new targets. *Int J Retina Vitreous*. (2017) 3:31. doi: 10.1186/s40942-017-0084-9
- Zhang K, Chen Y, Sun X, Zhong Q, Lin L, Gao Y, et al. Periocular triamcinolone acetonide injection for treating polypoidal choroidal vasculopathy concurrent with hemorrhagic retinal detachment. *Medicine*. (2018) 97:e12464. doi: 10.1097/MD.00000000000012464
- Kaya C, Zandi S, Pfister IB, Gerhardt C, Garweg JG. Adding a corticosteroid or switching to another anti-VEGF in insufficiently responsive wet age-related macular degeneration. *Clin Ophthalmol*. (2019) 13:2403–9. doi: 10.2147/OPTH.S224456
- Altun A, Kanar HS, Aki SF, Arsan A, Hacisalihoglu A. Effectiveness and safety of coadministration of intravitreal dexamethasone implant and silicone oil endotamponade for proliferative diabetic retinopathy with tractional diabetic macular edema. *J Ocul Pharmacol Ther*. (2021) 37:131–7. doi: 10.1089/jop.2020.0079
- Giancipoli E, Pinna A, Boscia F, Zasa G, Sotgiu G, Dore S, et al. Intravitreal dexamethasone in patients with wet age-related macular degeneration resistant to anti-VEGF: a prospective pilot study. *J Ophthalmol*. (2018) 2018:5612342. doi: 10.1155/2018/5612342
- Todorich B, Thanos A, Yonekawa Y, Mane G, Hasbrook M, Thomas BJ, et al. Simultaneous dexamethasone intravitreal implant and anti-VEGF therapy for neovascular age-related macular degeneration resistant to anti-VEGF monotherapy. *J Vitreoretin Dis*. (2017) 1:65–74. doi: 10.1177/2474126416683299
- Calvo P, Ferreras A, Al Adel F, Wang Y, Brent MH. Dexamethasone intravitreal implant as adjunct therapy for patients with wet age-related macular degeneration with incomplete response to ranibizumab. *Br J Ophthalmol*. (2015) 99:723–6. doi: 10.1136/bjophthalmol-2014-305684
- Chaudhary V, Barbosa J, Lam WC, Mak M, Mavrikakis E, Mohaghegh PS. Ozurdex in age-related macular degeneration as adjunct to ranibizumab (the OARA study). *Can J Ophthalmol*. (2016) 51:302–5. doi: 10.1016/j.jcjo.2016.04.020
- Ashraf M, Souka A, Adelman RA. Age-related macular degeneration: using morphological predictors to modify current treatment protocols. *Acta Ophthalmol*. (2018) 96:120–33. doi: 10.1111/aos.13565

12. Karska-Basta I, Pocij-Marciak W, Chrzaszcz M, Kubicka-Trzaska A, Romanowska-Dixon B, Sanak M. Altered plasma cytokine levels in acute and chronic central serous chorioretinopathy. *Acta Ophthalmol.* (2021) 99:e222–e31. doi: 10.1111/aos.14547
13. Jung SH, Kim KA, Sohn SW, Yang SJ. Cytokine levels of the aqueous humor in central serous chorioretinopathy. *Clin Exp Optom.* (2014) 97:264–9. doi: 10.1111/cxo.12125
14. Zhou H, Zhao X, Yuan M, Chen Y. Comparison of cytokine levels in the aqueous humor of polypoidal choroidal vasculopathy and neovascular age-related macular degeneration patients. *BMC Ophthalmol.* (2020) 20:15. doi: 10.1186/s12886-019-1278-8
15. Wakabayashi T, Ikuno Y, Oshima Y, Hamasaki T, Nishida K. Aqueous concentrations of vascular endothelial growth factor in eyes with high myopia with and without choroidal neovascularization. *J Ophthalmol.* (2013) 2013:257381. doi: 10.1155/2013/257381
16. Costagliola C, Semeraro F, dell'Omo R, Romano MR, Russo A, Aceto F, et al. Effect of intravitreal ranibizumab injections on aqueous humor concentrations of vascular endothelial growth factor and pigment epithelium-derived factor in patients with myopic choroidal neovascularization. *Br J Ophthalmol.* (2015) 99:1004–8. doi: 10.1136/bjophthalmol-2014-306465
17. Romdhane K, Zola M, Matet A, Daruich A, Elalouf M, Behar-Cohen F, et al. Predictors of treatment response to intravitreal anti-vascular endothelial growth factor (anti-VEGF) therapy for choroidal neovascularisation secondary to chronic central serous chorioretinopathy. *Br J Ophthalmol.* (2020) 104:910–6. doi: 10.1136/bjophthalmol-2019-314625
18. Schworm B, Luft N, Keidel LE, Hagenau F, Kern C, Herold T, et al. Response of neovascular central serous chorioretinopathy to an extended upload of anti-VEGF agents. *Graefes Arch Clin Exp Ophthalmol.* (2020) 258:1013–21. doi: 10.1007/s00417-020-04623-w
19. Cheung CMG, Lee WK, Koizumi H, Dansingani K, Lai TYY, Freund KB. Pachychoroid disease. *Eye.* (2019) 33(1):14–33. 20. doi: 10.1038/s41433-018-0158-4
20. Liu F, Ding X, Yang Y, Li J, Tang M, Yuan M, et al. Aqueous humor cytokine profiling in patients with wet AMD. *Mol Vis.* (2016) 22:352–61. Available online at: <http://www.molvis.org/molvis/v22/352>
21. Shin MC, Lim JW. Concentration of cytokines in the aqueous humor of patients with central serous chorioretinopathy. *Retina.* (2011) 31:1937–43. doi: 10.1097/IAE.0b013e31820a6a17
22. Terao N, Koizumi H, Kojima K, Yamagishi T, Nagata K, Kitazawa K, et al. Association of upregulated angiogenic cytokines with choroidal abnormalities in chronic central serous chorioretinopathy. *Invest Ophthalmol Vis Sci.* (2018) 59:5924–31. doi: 10.1167/iovs.18-25517
23. Sacconi R, Tomasso L, Corbelli E, Carnevali A, Querques L, Casati S, et al. Early response to the treatment of choroidal neovascularization complicating central serous chorioretinopathy: a OCT-angiography study. *Eye.* (2019) 33:1809–17. doi: 10.1038/s41433-019-0511-2
24. Cho HJ, Jung SH, Cho S, Han JO, Park S, Kim JW. Intravitreal anti-vascular endothelial growth factor treatment for pachychoroid neovascularopathy. *J Ocul Pharmacol Ther.* (2019) 35:174–81. doi: 10.1089/jop.2018.0107
25. Bucher F, Aguilar E, Marra KV, Rapp J, Arnold J, Diaz-Aguilar S, et al. CNTF prevents development of outer retinal neovascularization through upregulation of CXCL10. *Invest Ophthalmol Vis Sci.* (2020) 61:20. doi: 10.1167/iovs.61.10.20
26. Bodnar RJ, Yates CC, Wells A. IP-10 blocks vascular endothelial growth factor-induced endothelial cell motility and tube formation via inhibition of calpain. *Circ Res.* (2006) 98:617–25. doi: 10.1161/01.RES.0000209968.66606.10
27. Fujimura S, Takahashi H, Yuda K, Ueta T, Iriyama A, Inoue T, et al. Angiostatic effect of CXCR3 expressed on choroidal neovascularization. *Invest Ophthalmol Vis Sci.* (2012) 53:1999–2006. doi: 10.1167/iovs.11-8232
28. Nawaz MI, Van Raemdonck K, Mohammad G, Kangave D, Van Damme J, Abu El-Asrar AM, et al. Autocrine CCL2, CXCL4, CXCL9 and CXCL10 signal in retinal endothelial cells and are enhanced in diabetic retinopathy. *Exp Eye Res.* (2013) 109:67–76. doi: 10.1016/j.exer.2013.01.008
29. Keeley EC, Mehrad B, Strieter RM. Chemokines as mediators of tumor angiogenesis and neovascularization. *Exp Cell Res.* (2011) 317:685–90. doi: 10.1016/j.yexcr.2010.10.020
30. Hong KH, Ryu J, Han KH. Monocyte chemoattractant protein-1-induced angiogenesis is mediated by vascular endothelial growth factor-A. *Blood.* (2005) 105:1405–7. doi: 10.1182/blood-2004-08-3178
31. Yamada M, Kim S, Egashira K, Takeya M, Ikeda T, Mimura O, et al. Molecular mechanism and role of endothelial monocyte chemoattractant protein-1 induction by vascular endothelial growth factor. *Arterioscler Thromb Vasc Biol.* (2003) 23:1996–2001. doi: 10.1161/01.ATV.0000096208.80992.63
32. Tong JP, Chan WM, Liu DT, Lai TY, Choy KW, Pang CP, et al. Aqueous humor levels of vascular endothelial growth factor and pigment epithelium-derived factor in polypoidal choroidal vasculopathy and choroidal neovascularization. *Am J Ophthalmol.* (2006) 141:456–62. doi: 10.1016/j.ajo.2005.10.012
33. Sakurada Y, Nakamura Y, Yoneyama S, Mabuchi F, Gotoh T, Tateno Y, et al. Aqueous humor cytokine levels in patients with polypoidal choroidal vasculopathy and neovascular age-related macular degeneration. *Ophthalmic Res.* (2015) 53:2–7. doi: 10.1159/000365487
34. Agrawal R, Balne PK, Wei X, Bijin VA, Lee B, Ghosh A, et al. Cytokine profiling in patients with exudative age-related macular degeneration and polypoidal choroidal vasculopathy. *Invest Ophthalmol Vis Sci.* (2019) 60:376–82. doi: 10.1167/iovs.18-24387
35. Kim JM, Cho HJ, Kim Y, Jung SH, Lee DW, Kim JW. Responses of types 1 and 2 neovascularization in age-related macular degeneration to anti-vascular endothelial growth factor treatment: optical coherence tomography angiography analysis. *Semin Ophthalmol.* (2019) 34:168–76. doi: 10.1080/08820538.2019.1620791
36. Terasaki H, Sakamoto T, Shirasawa M, Yoshihara N, Otsuka H, Sonoda S, et al. Penetration of bevacizumab and ranibizumab through retinal pigment epithelial layer *in vitro*. *Retina.* (2015) 35:1007–15. doi: 10.1097/IAE.0000000000000428
37. Yuan J, Wu S, Wang Y, Pan S, Wang P, Cheng L. Inflammatory cytokines in highly myopic eyes. *Sci Rep.* (2019) 9:3517. doi: 10.1038/s41598-019-39652-x
38. Zhao F, Wu H, Reinach PS, Wu Y, Zhai Y, Lei Y, et al. Up-Regulation of matrix metalloproteinase-2 by scleral monocyte-derived macrophages contributes to myopia development. *Am J Pathol.* (2020) 190:1888–908. doi: 10.1016/j.ajpath.2020.06.002

**Conflict of Interest:** The authors declare that the research was conducted in the absence of any commercial or financial relationships that could be construed as a potential conflict of interest.

**Publisher's Note:** All claims expressed in this article are solely those of the authors and do not necessarily represent those of their affiliated organizations, or those of the publisher, the editors and the reviewers. Any product that may be evaluated in this article, or claim that may be made by its manufacturer, is not guaranteed or endorsed by the publisher.

Copyright © 2021 Liu, Zhang, Deng, Chen, Shen, Hu and Mao. This is an open-access article distributed under the terms of the Creative Commons Attribution License (CC BY). The use, distribution or reproduction in other forums is permitted, provided the original author(s) and the copyright owner(s) are credited and that the original publication in this journal is cited, in accordance with accepted academic practice. No use, distribution or reproduction is permitted which does not comply with these terms.



# Peroxisome Proliferator-Activated Receptor $\alpha$ Activation Protects Retinal Ganglion Cells in Ischemia-Reperfusion Retinas

Fei Yao<sup>1,2,3†</sup>, Xuan Zhang<sup>1,2,3†</sup>, Xueyan Yao<sup>1,2,3</sup>, Xiaohua Ren<sup>3,4</sup>, Xiaobo Xia<sup>3,4</sup>, Jian Jiang<sup>1,2,3\*</sup> and Lexi Ding<sup>1,2,3\*</sup>

<sup>1</sup> Eye Center of Xiangya Hospital, Central South University, Changsha, China, <sup>2</sup> Hunan Key Laboratory of Ophthalmology, Changsha, China, <sup>3</sup> National Clinical Research Center for Geriatric Disorders, Xiangya Hospital, Changsha, China, <sup>4</sup> Department of Human Resource, Xiangya Hospital, Central South University, Changsha, China

## OPEN ACCESS

### Edited by:

Hetian Lei,  
Shenzhen Eye Hospital, China

### Reviewed by:

Xiaoyan Dai,  
Guangzhou Medical University, China  
Serenella Anzilotti,  
Institute of Research and Medical  
Care (IRCCS) SDN, Italy

### \*Correspondence:

Jian Jiang  
jiangjianxy@126.com  
Lexi Ding  
lexiding@csu.edu.cn

<sup>†</sup>These authors have contributed  
equally to this work and share first  
authorship

### Specialty section:

This article was submitted to  
Ophthalmology,  
a section of the journal  
Frontiers in Medicine

Received: 03 October 2021

Accepted: 24 November 2021

Published: 23 December 2021

### Citation:

Yao F, Zhang X, Yao X, Ren X, Xia X,  
Jiang J and Ding L (2021) Peroxisome  
Proliferator-Activated Receptor  $\alpha$   
Activation Protects Retinal Ganglion  
Cells in Ischemia-Reperfusion Retinas.  
Front. Med. 8:788663.  
doi: 10.3389/fmed.2021.788663

**Background and Objective:** Retinal ischemia-reperfusion (IR) leads to massive loss of retinal ganglion cells (RGC) and characterizes several blind-causing ophthalmic diseases. However, the mechanism related to retinal IR is controversial, and a drug that could prevent the RGC loss caused by IR is still lacking. This study aimed to investigate the role of endogenous retinal peroxisome proliferator-activated receptor (PPAR) $\alpha$  and the therapeutic effect of its agonist, fenofibric acid (FA), in IR-related retinopathy.

**Materials and Methods:** Fenofibric acid treatment was applied to the Sprague–Dawley rats with IR and retinal cell line 28 cells with oxygen-glucose deprivation (OGD) (an *in vitro* model of IR). Western blotting, real-time PCR, and immunofluorescence were used to examine the expression levels of PPAR $\alpha$ , glial fibrillary acidic protein (GFAP), and cyclooxygenase-2 (COX2). Hematoxylin and eosin (HE) staining, propidium iodide (PI) staining, retrograde tracing, and flash visual-evoked potential (FVEP) were applied to assess RGC injury and visual function.

**Results:** Retinal IR down-regulated PPAR $\alpha$  expression *in vitro* and *in vivo*. Peroxisome proliferator-activated receptor  $\alpha$  activation by FA promoted survival of RGCs, mitigated thinning of the ganglion cell complex, and decreased the latency of positive waves of FVEPs after IR injury. Further, FA treatment enhanced the expression of endogenous PPAR $\alpha$  and suppressed the expression of GFAP and COX2 significantly.

**Conclusion:** Peroxisome proliferator-activated receptor  $\alpha$  activation by FA is protective against RGC loss in retinal IR condition, which may occur by restoring PPAR $\alpha$  expression, inhibiting activation of glial cells, and suppressing retinal inflammation. All these findings indicate the translational potential of FA in treating IR-related retinopathy.

**Keywords:** peroxisome proliferator-activated receptor  $\alpha$ , fenofibric acid, ischemia-reperfusion, neuroprotection, retinal ganglion cell, retinal diseases

## INTRODUCTION

Retinal ganglion cells (RGCs) are the only retinal neurons that directly project their axons to the central nervous system and perform visual function (1). Many retinal diseases such as acute angle-closure glaucoma, retinal vascular occlusions, and anterior ischemic optic neuropathy can directly or indirectly lead to the irreversible death of RGCs and severely threaten eyesight (2–4).



The common pathologic feature among these diseases is retinal ischemia/reperfusion (IR). However, the precise pathways and molecular mechanism related to retinal IR are not well-understood and are controversial. A therapeutic drug to prevent RGC death caused by IR is lacking (5). Accordingly, understanding the pathological mechanism of retinal IR and developing effective therapy are imperative.

Peroxisome proliferator-activated receptor (PPAR) $\alpha$  is a ligand-activated transcription factor and member of the nuclear receptor superfamily. It plays an important part in regulation of lipid metabolism and has anti-inflammatory and antioxidant effects under several pathologic conditions (6–9). In the retina, PPAR $\alpha$  is expressed in multiple cell types, including the retinal pigment epithelium (RPE), outer nuclear layer (ONL), inner nuclear layer (INL), and ganglion cell layer (GCL) (10), which is essential for lipid metabolism and neuronal survival in the retina (11).

Previous studies have demonstrated that PPAR $\alpha$  expression is down-regulated in the retinas of patients suffering from diabetes mellitus (DM), as well as in the retinas of rodents with diabetic retinopathy or oxygen-induced proliferative retinopathy (10, 12). Knockout of PPAR $\alpha$  expression aggravates retinal microvascular damage (12), overexpression of PPAR $\alpha$  reduces retinal vascular leakage and retinal inflammation caused by diabetes (10), and alleviates retinal neovascularization in diabetic retinopathy (13). Moreover, Fenofibrate (a specific agonist of PPAR $\alpha$ ) can alleviate retinal damage by reducing apoptosis of capillary pericytes *via* amelioration of retinal inflammation and oxidative stress (14–16). Qiu et al. showed that PPAR $\alpha$  activation by fenofibrate displayed therapeutic effects on age-related macular degeneration induced by lasers in rodents (17).

Taken together, these studies suggest that PPAR $\alpha$  is a potential therapeutic target for ophthalmic diseases. However, the relationship between PPAR $\alpha$  and ophthalmic diseases characterized by retinal IR is unclear. This study investigated whether PPAR $\alpha$  is involved in IR-induced retinal injury (by increasing the intraocular pressure to 110 mmHg for 1 h *via* a saline-perfusion system). We also identified whether PPAR $\alpha$  activation has protective effects on RGCs in this condition and explored the underlying mechanism of action.

## MATERIALS AND METHODS

### Ethical Approval of the Study Protocol

Experiments were undertaken in accordance with the Guide for the Care and Use of Laboratory Animals (National Institutes of Health, No. 80-23, Bethesda, MD, USA). The study protocol was approved by the Animal Research Committee of the Xiangya School of Medicine (Changsha City, China).

### Animals

Female Sprague–Dawley rats (200–250 g; 8 weeks; Slaccas, Changsha, China) were housed in an environment with free access to food and water under a 12-h light–dark cycle. In all procedures, rats were anesthetized with a solution of 2% sodium pentobarbital (80 mg/kg, i.p.; Sanshu, Beijing, China) and xylazine (10 mg/kg, i.p.; Huamu, Beijing, China). Oxybuprocaine

hydrochloride (Santen Pharmaceuticals, Tokyo, Japan) was used to anesthetize corneas and tropicamide phenylephrine (Santen Pharmaceuticals) was used to dilate pupils.

### Model of Retinal IR

Retinal IR injury was induced by increasing the pressure in the anterior chamber *via* the saline-perfusion system described by Tong et al. (18). Briefly, anesthetized animals with anesthetized corneas and dilated pupils were fixed on a heat-preservation countertop, and their underjaws were raised to prevent death from aspiration of saline. Then, 31-G needles were inserted into the anterior chamber and the intraocular pressure was increased gradually to 110 mmHg for 1 h (**Figure 1A**). Eyes that underwent needle puncture only but not perfusion were regarded as Sham operation (SO) eyes. During and after the procedure, antibiotic eye ointment was used to keep the eyes moist and uninfected. Only rats without saline-leaking or lens injury were included in our study (a total of two rats were excluded because of lens injury and one rat was discarded because of saline-leaking).

### Cell Culture and Oxygen-Glucose Deprivation Model

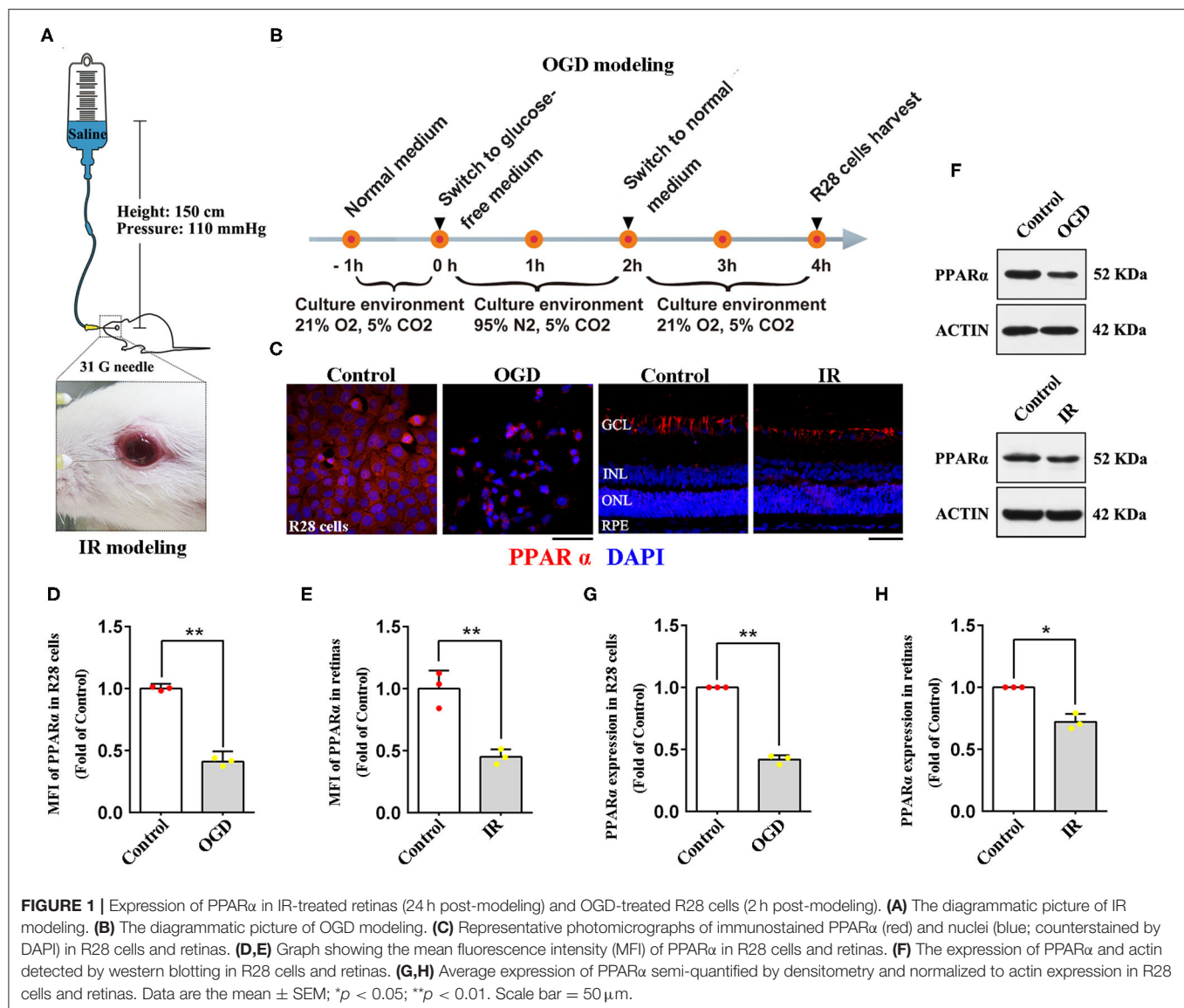
Retinal cell line 28 (R28) is an adherent retinal precursor cell line derived from neonatal Sprague–Dawley rat retina, which was immortalized by the 12S E1A gene and commonly used to study the function and neuroprotection of RGCs *in vitro* (19). In this study, R28 cells were offered by the Department of Anatomy and Neurobiology (Central South University, Changsha, China). Cells were cultured in low glucose DMEM (11885084; Gibco, Carlsbad, USA) with 10% fetal calf serum (0500; ScienCell, San Diego, USA), 1% L-glutamine (G3126; Sigma, St. Louis, USA), 1% non-essential amino acids (M7145; Sigma, St. Louis, USA), and 1% penicillin-streptomycin (60162ES76; Yeasen, Shanghai, China). To establish the Oxygen-Glucose Deprivation (OGD) model, an *in vitro* model of retinal IR, R28 cells were incubated in a glucose-free DMEM (11966025; Gibco, Carlsbad, USA) with an anoxic environment (95% N<sub>2</sub>, 5% CO<sub>2</sub>) for 2 h, then the cells were cultured in normal medium and reoxygenated (21% O<sub>2</sub>, 5% CO<sub>2</sub>) for 2 h before being examined (**Figure 1B**).

### PPAR $\alpha$ Activation

Fenofibric acid (FA) is a specific agonist of PPAR $\alpha$ . *In vivo*, FA (S4527; Selleck Chemicals, Houston, TX, USA) was dissolved in dimethyl sulfoxide (DMSO; Solarbio, Beijing, China) at 10 mg/ml. One hour before IR modeling, animals were injected (i.p.) with FA at 1 ml/kg bodyweight. Treatment was administered once a day (excluding the modeling day) until rats were sacrificed 24 or 72 h after modeling. *In vitro*, 25  $\mu$ M FA was added to the cell culture medium 1 h before OGD modeling and maintained until the cells were examined.

### Retina Immunofluorescence and Staining

Anesthetized rats were perfused transcardially with pre-cooled phosphate-buffered saline. Intact eyes were enucleated and fixed in FAS eyeball fixative solution (G1109; Servicebio, Beijing, China) for 24 h at room temperature. After fixation, eyeballs were dehydrated in ethanol and embedded in paraffin.



Sections (3  $\mu$ m) were made around the optic nerve for further immunofluorescence staining and hematoxylin and eosin (HE) staining. Dewaxed and antigen-retrieved paraffin retinal slices were applied to immunofluorescence, as described in our previous study (20). Three antibodies (all from Abcam, Cambridge, UK) were used: anti-PPAR $\alpha$  (ab215270; 1:100), anti-glial fibrillary acidic protein (GFAP; ab33922; 1:300), and anti-cyclooxygenase 2 (COX2; ab62331; 1:100). Retina HE staining was performed by the Hematoxylin-Eosin/HE Staining Kit (G1120; Servicebio, Wuhan, China) according to the manufacturer's instructions.

### Cell Immunofluorescence and Staining

Retinal cell line 28 cells were fixed in 4% paraformaldehyde for 15 min (G1101; Servicebio, Beijing, China) at room temperature before immunofluorescence staining. The specific procedures and antibodies applied were the same as those used for retinal

slices. Besides, propidium iodide (PI; P4170; Sigma, St. Louis, USA) staining and Hoechst staining (A3472; APExBIO, Houston, USA) were applied to detect the survival rate of R28 cells according to the manufacturer's instructions.

### Western Blotting

Freshly isolated retinal tissues were homogenized and lysed in RIPA buffer (P0013; Beyotime, Beijing, China). The protein concentration was quantified by a Bicinchoninic Acid kit (Pierce, Rockford, IL, USA). Western blotting was done as described in our previous study (20) with the following antibodies: anti-PPAR $\alpha$  (ab215270; Abcam; 1:1,000), anti-GFAP (ab33922; Abcam; 1:1,000), anti-COX2 (ab62331; Abcam; 1:1,000), and anti- $\beta$ -actin (GB12001; Servicebio; 1:3,000). The expression levels of PPAR $\alpha$ , GFAP and COX2 were quantified by Image-Pro Plus 6.0 (Media Cybernetics, Rockville, MD, USA) and normalized by the densitometry of  $\beta$ -actin.

## Real-Time PCR

Total RNA was isolated from fresh retinal tissues with RNAiso buffer (GB3013; Servicebio, Wuhan, China). Peroxisome proliferator-activated receptor  $\alpha$  mRNA was reverse transcribed to cDNA with the Servicebio® RT First Strand cDNA Synthesis Kit (G3330; Servicebio), according to the manufacturer's instructions. Peroxisome proliferator-activated receptor  $\alpha$  mRNA expression was quantified using 2 $\times$ SYBR Green qPCR Master Mix (G3322; Servicebio). Peroxisome proliferator-activated receptor  $\alpha$  mRNA levels were normalized to GAPDH mRNA levels. The following specific primers were synthesized by Servicebio: rat PPAR $\alpha$  primers, forward 5'-CATCGAGTGTCTGAATATGTGG-3' and reverse 5'-GCAGTACTGGCATTGTTC-3'; rat GAPDH primers, forward 5'-GGAAGCTTGTCATCAATGGAAATC-3' and reverse 5'-TGATGACCCTTTTGGCTCCC-3'.

## Retrograde Tracing of RGCs

One week before IR modeling, 4% fluorogold (FG; Fluorochrome, Denver, CO, USA) solution was injected into the bilateral superior colliculi of rats (6 mm posterior to the bregma, 1.8 mm lateral to the cranial midline, and 4 mm deep to the cranial surface) to retrograde label RGCs, as described in our previous study (21).

## Counting FG-Labeled RGCs

Flattened retinas were examined by a fluorescence microscope (DM5000 B; Leica, Wetzlar, Germany). Twelve images per retina were taken at 0.85, 2.26, and 3.68 mm (approximately 1/6, 1/2, and 5/6 retinal radius) from the optic disk in superonasal, inferonasal, superotemporal, and inferotemporal quadrants. A double-blind method and Image-Pro Plus 6.0 were used to count the labeled RGCs in each photomicrograph.

## Thickness of the Ganglion Cell Complex (GCC)

The GCC consists of a retinal nerve-fiber layer, GCL and inner plexiform layer, and corresponds to the anatomic distribution of RGCs in the retina (22). To better represent the change in GCC thickness, 12 points of GCC thickness per retinal slice stained by HE were measured by Image-Pro Plus 6.0 according to the following parameters: perpendicular to the surface of the RPE layer as well as  $\pm 800$ ,  $\pm 1,600$ ,  $\pm 2,400$ ,  $\pm 3,200$ ,  $\pm 4,000$ , and  $\pm 4,800$   $\mu$ m away from the center of the optic nerve (Figure 3F).

## Flash Visual-Evoked Potentials

Flash Visual-Evoked Potentials (FVEPs) were obtained using a multifocal electroretinography recorder (GT-2008V-VI; Gotec, Chongqing, China) for functional evaluation of retinas 24 or 72 h after modeling. The stimuli intensity was set to 10.0 cd $\cdot$ s/m<sup>2</sup>, the flash frequency was 1 Hz, and the number of flashes was 64. After light adaptation for 15 min, anesthetized animals were fixed on a special holder with one silver-plate electrode inserted under the skin of the occipital bone (anode), anterior bregma (cathode), and ear (ground electrode), respectively. Then, the FVEP of right and left eyes was recorded in order by a Ganzfeld electrodiagnostic system (Gotec, Chongqing, China). The latency

of the first positive wave (P1) and second positive wave (P2) of FVEP was analyzed.

## Statistical Analysis

SPSS 22.0 (IBM, Armonk, NY, USA) was utilized for statistical analyses. Data are the mean  $\pm$  SEM. The Student's *t*-test and one-way analysis of variance followed by Tukey's *post-hoc* test were used for comparisons between two groups and more than two groups. Statistical significance was set at  $p < 0.05$ .

## RESULTS

### Retinal IR Down-Regulated PPAR $\alpha$ Expression *in vitro* and *in vivo*

To verify whether PPAR $\alpha$  is involved in the pathological process of retinal IR, we delineated PPAR $\alpha$  expression in R28 cells and retinas after OGD/IR modeling by immunofluorescence analyses and western blotting. Oxygen-glucose deprivation-treated R28 cells showed significant cytoplasmic declination of PPAR $\alpha$  expression compared with that in the control group (Figures 1C,D,E,G). In retinas, immunostained PPAR $\alpha$  was detected in the GCL, INL, ONL, and the RPE, but most PPAR $\alpha$  was expressed in the GCL (Figure 1C). Twenty-four hours after IR modeling, retinal immunolabeling level of PPAR $\alpha$  was down-regulated, and this change was manifested mainly in the GCL (Figures 1C,E,F,H). Taken together, these data suggested that retinal IR procedure induced down-regulation of PPAR $\alpha$  expression both *in vitro* and *in vivo*; PPAR $\alpha$  was likely to participate in the pathological mechanism of retinal IR.

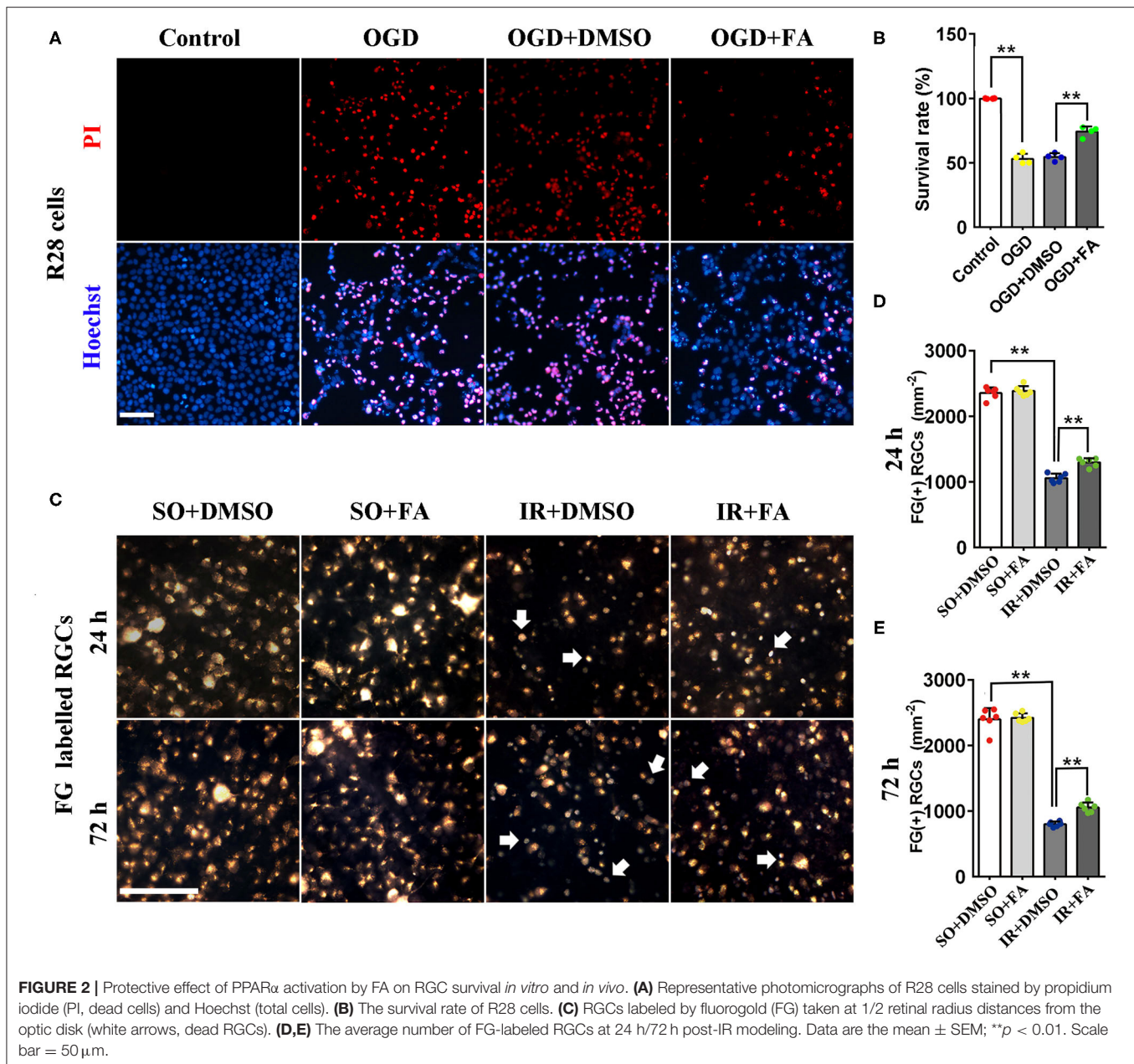
### Protective Effect of PPAR $\alpha$ Activation on RGC Survival

To clarify the role of PPAR $\alpha$  in retinal IR, we used FA to activate PPAR $\alpha$  and evaluated the effect of PPAR $\alpha$  activation on R28 cells and RGC survival after OGD/IR modeling. As shown in Figures 2A,B, OGD modeling led to nearly half of R28 cells death 2 h after modeling, and FA treatment ameliorated OGD-induced cell death significantly ( $p = 0.0001$ ,  $n = 4$  per group). *In vivo*, surviving RGCs labeled by FG had a granular appearance with clear borders and golden color, whereas dead RGCs had a smaller volume and lighter color (white arrows, Figure 2C). Photomicrographs identified that dead RGCs appeared only in IR groups. The number of surviving RGCs was decreased markedly in IR rats in comparison with SO rats 24 and 72 h after modeling ( $p = 0.0001$  for both,  $n = 6$  per group). Moreover, FA treatment was able to increase the number of surviving RGCs ( $p = 0.0001$  at 24 h and  $p = 0.002$  at 72 h,  $n = 6$  per group) (Figures 2D,E; Supplementary Table 1). These results suggested that PPAR $\alpha$  activation by FA had a protective effect on IR-induced RGC loss.

### PPAR $\alpha$ Activation Mitigated Thinning of the GCC

To further determine the protective effect of PPAR $\alpha$  activation on retinal IR, HE staining was used to measure GCC thickness. At 72 h post-modeling, GCC thickness was decreased significantly in IR rats when compared with SO rats ( $p = 0.0001$ ,  $n = 7$  in the IR group and  $n = 5$  in the SO group). Fenofibric acid treatment efficaciously attenuated GCC thinning ( $p = 0.014$ ,





$n = 7$  per group), and all of these changes occurred in the whole retina. However, 24 h after modeling, no obvious difference was found between groups ( $n = 5$  per group) (Figure 3; Supplementary Table 1). In summary, FA alleviated the GCC damage induced by IR at 72 h, suggesting that PPAR $\alpha$  activation by FA had a protective effect on IR-induced retinal injury.

### Protective Effect of PPAR $\alpha$ Activation on Visual Function

Moreover, we investigated the protective effect of PPAR $\alpha$  activation on visual function. Flash visual-evoked potentials were

applied to assess the effect of FA on retinal electrophysiologic activity. The latency of P1 waves and P2 waves was increased by IR at 24 and 72 h after modeling ( $p = 0.0001$  for all,  $n = 6$  per group), indicating that retinal IR severely affected the conduction function of vision. Furthermore, FA treatment decreased the latency of the P1 wave at 24 h ( $p = 0.021$ ,  $n = 6$  per group) and P2 wave at 24 or 72 h after modeling in IR rats ( $p = 0.001$  for 24 h and  $p = 0.008$  for 72 h,  $n = 6$  per group) (Figure 4; Supplementary Table 1), suggesting that PPAR $\alpha$  activation by FA ameliorated IR-induced retinal dysfunction.



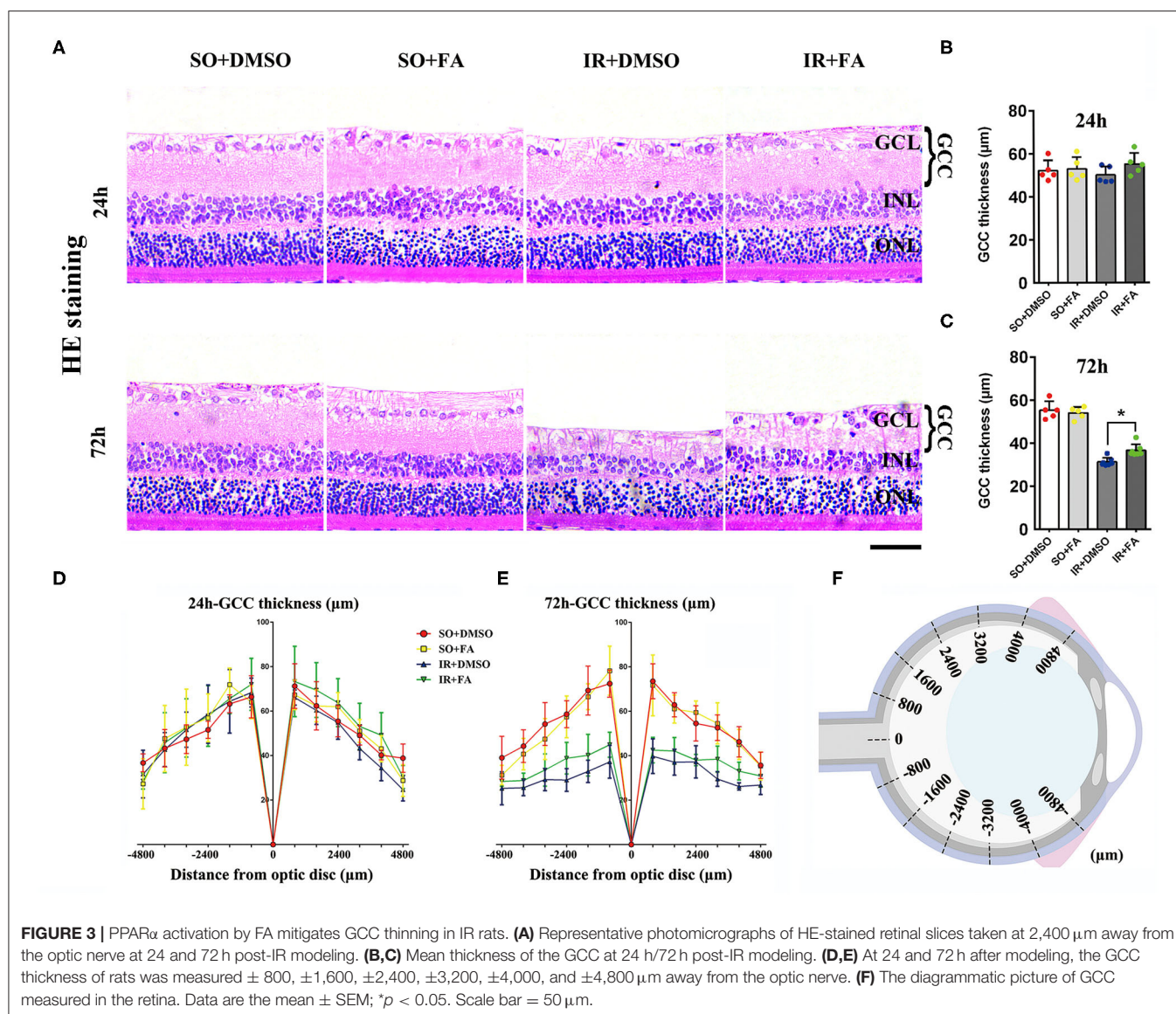


**FIGURE 3 |** PPAR $\alpha$  activation by FA mitigates GCC thinning in IR rats. **(A)** Representative photomicrographs of HE-stained retinal slices taken at 2,400  $\mu$ m away from the optic nerve at 24 and 72 h post-IR modeling. **(B,C)** Mean thickness of the GCC at 24 h/72 h post-IR modeling. **(D,E)** At 24 and 72 h after modeling, the GCC thickness of rats was measured  $\pm$  800,  $\pm$  1,600,  $\pm$  2,400,  $\pm$  3,200,  $\pm$  4,000, and  $\pm$  4,800  $\mu$ m away from the optic nerve. **(F)** The diagrammatic picture of GCC measured in the retina. Data are the mean  $\pm$  SEM; \* $p$  < 0.05. Scale bar = 50  $\mu$ m.

## FA Increased PPAR $\alpha$ Expression *in vitro* and *in vivo*

We have demonstrated that retinal IR down-regulated PPAR $\alpha$  expression *in vitro* and *in vivo*, and PPAR $\alpha$  activation by FA alleviated IR-induced injury and protected visual function. However, the effect of FA on endogenous PPAR $\alpha$  expression remains unclear. The immunofluorescence results showed that FA treatment increased PPAR $\alpha$  expression in R28 cells and retinas after OGD/IR modeling (Figure 5A; Supplementary Figures 1A,B). Western blotting and Real-time PCR showed that retinal PPAR $\alpha$  and mRNA levels were decreased at 24 h post-modeling, while FA treatment effectively reversed these changes ( $p$  = 0.035 for Western blotting and  $p$  = 0.0001 for PCR,  $n$  = 3 per group) (Figures 5B–D). These results suggested that FA as an agonist of PPAR $\alpha$  could increase the transcription and translation level of PPAR $\alpha$ .

## Activation of PPAR $\alpha$ Repressed GFAP and COX2 Expression

We wished to determine the underlying mechanism of PPAR $\alpha$  activation on RGCs in IR rats. Over-activation of glial cells is one of the crucial pathogenic factors after retinal stress injury, up-regulation of GFAP [a marker of glial cells (23)] is regarded as a sensitive non-specific response of glial cells activation (24). In this study, the expression of GFAP was measured in retinas 24 h after IR modeling. Retinal GFAP was expressed mainly in the GCL, and such expression was up-regulated in the GCL of IR rats. However, FA treatment suppressed an up-regulation of GFAP in the GCL (Figure 6A; Supplementary Figure 1C). Consistent with the results of immunofluorescence analyses, western blotting showed that GFAP expression in retinas was also increased after IR modeling ( $p$  = 0.0001,  $n$  = 3 per group), FA decreased retinal GFAP level ( $p$  = 0.0001,  $n$  =

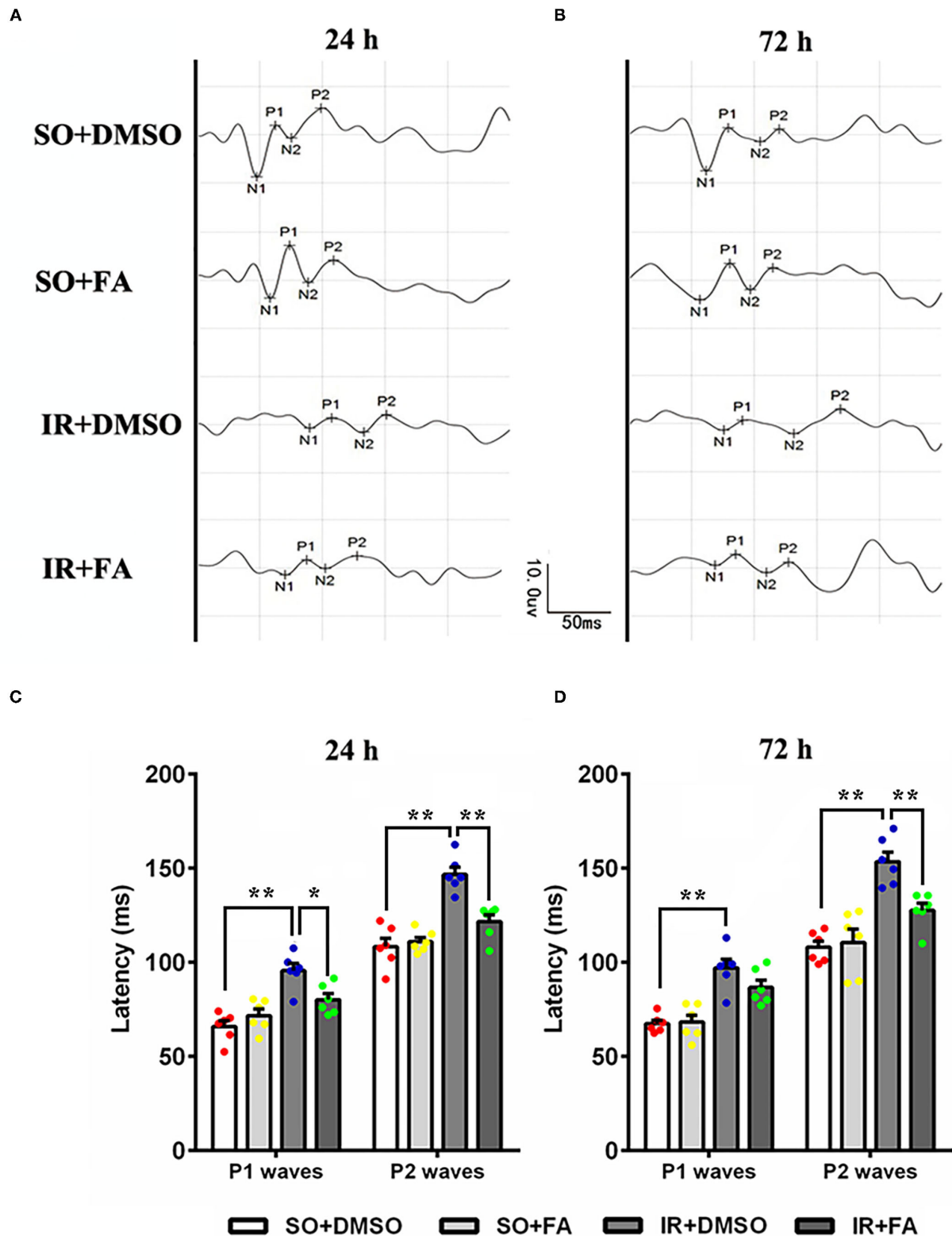
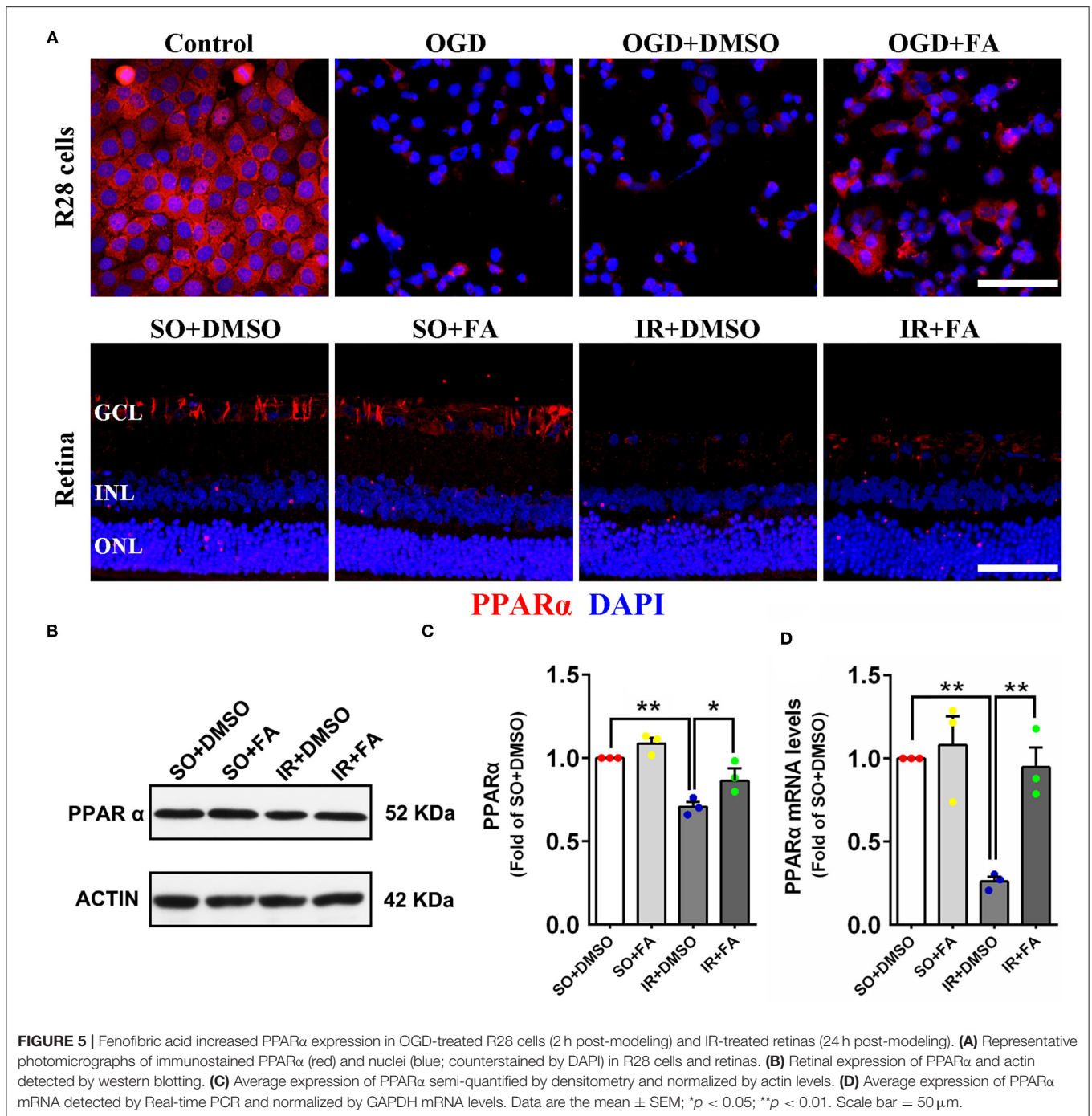


**FIGURE 4 |** Protective effect of PPAR $\alpha$  activation by FA on FVEPs in IR rats. **(A)** Representative images of FVEPs at 24 h post-IR modeling. **(B)** Representative images of FVEPs at 72 h post-IR modeling. **(C)** The latency of the first positive wave (P1 wave) and second positive wave (P2 wave) of FVEPs in rats at 24 h post-IR modeling. **(D)** The latency of the P1 wave and P2 wave of FVEPs in rats at 72 h post-IR modeling. Data are the mean  $\pm$  SEM; \* $p$  < 0.05; \*\* $p$  < 0.01. Scale bar = 10.0  $\mu$ V and 50 ms.



3 per group) and that there was no difference between rats treated by FA and those treated by DMSO in the SO group (Figures 6C,D).

Cyclooxygenase-2 is an important pro-inflammatory molecule (25). To further elucidate the therapeutic mechanism of FA on IR rats, we measured retinal level of COX2 24 h after IR modeling. Immunostained COX2 was detected in the all layers of the retina. Ischemia-reperfusion modeling increased COX2 level in the GCL and inner plexiform layers significantly.

In contrast, FA treatment decreased COX2 level (Figure 6B; Supplementary Figure 1D). Western blotting showed that IR-induced retinopathy up-regulated COX2 level in the retina ( $p = 0.001$ ,  $n = 3$  per group), but this level was down-regulated by FA ( $p = 0.0001$ ,  $n = 3$  per group). Moreover, there was no distinction between rats treated by FA and those treated by DMSO (Figures 6C,E).

In summary, these results indicated that FA decreased GFAP and COX2 expression in the retina significantly, suggesting that



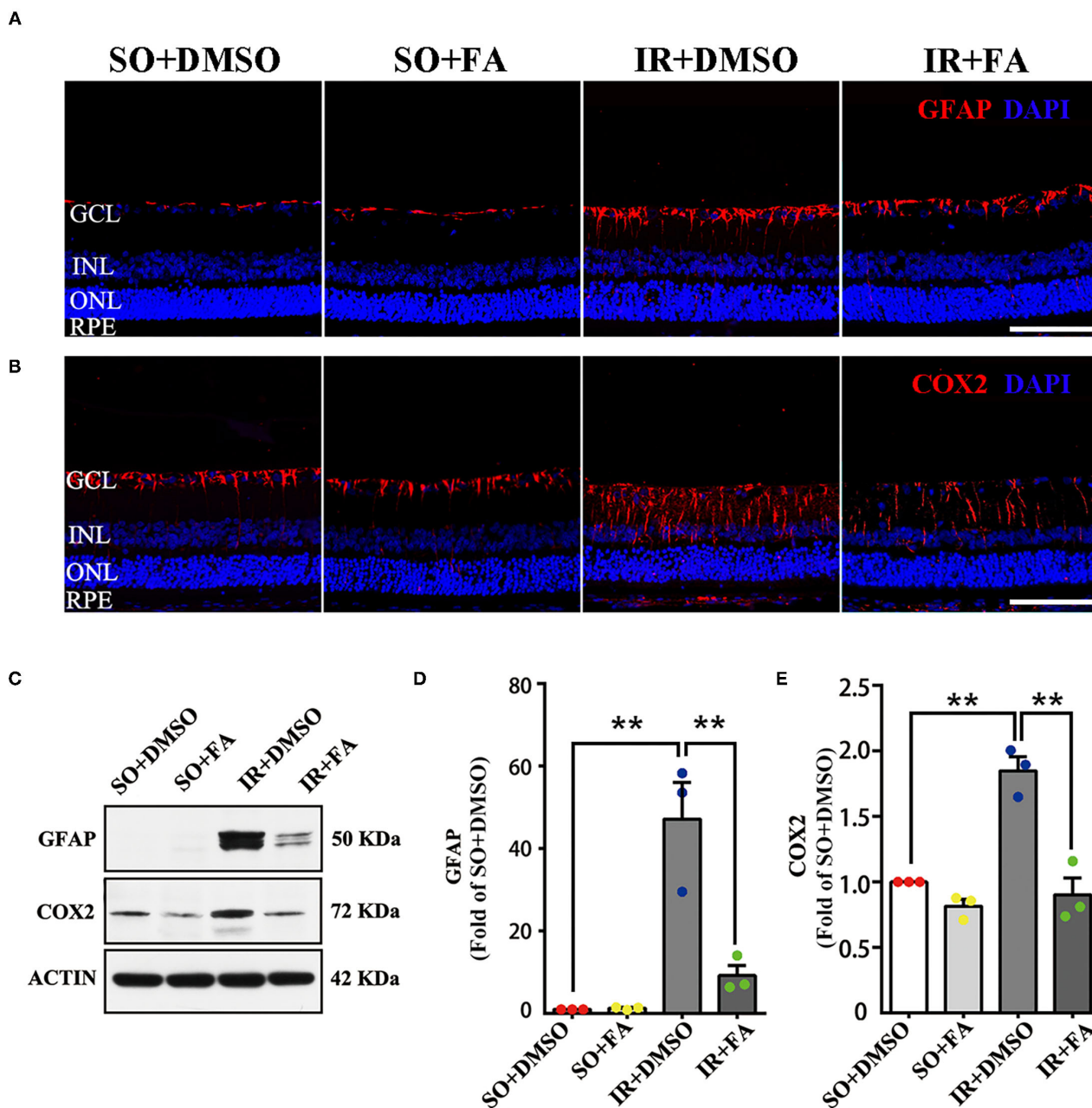


**FIGURE 6 |** Activation of PPAR $\alpha$  by FA repressed GFAP and COX2 expression in the retinas of IR rats. **(A,B)** Representative photomicrographs of immunostained GFAP/COX2 (red) and nuclei (blue; counterstained by DAPI) in retinal sections at 24 h post-modeling. **(C)** Retinal expression of GFAP, COX2, and actin detected by western blotting. **(D,E)** Average expression of GFAP/COX2 semi-quantified by densitometry and normalized by actin levels in retinas. Data are the mean  $\pm$  SEM; \*\* $p < 0.01$ . Scale bar = 50  $\mu$ m.

PPAR $\alpha$  activation mediated the repression of glial cells activation and suppression of retinal inflammation.

## DISCUSSION

Peroxisome proliferator-activated receptor  $\alpha$  is an important lipid-regulating transcription factor. It has been reported

that PPAR $\alpha$  plays an important part in ophthalmic diseases (14–17). However, the PPAR $\alpha$  function in retinal IR is remained unknown. In this study, we first measured PPAR $\alpha$  expression in retinal IR condition, and provided evidence that PPAR $\alpha$  activation by FA (a PPAR $\alpha$  agonist) ameliorated IR-induced RGC injury *in vitro* and *in vivo*. Our results suggested that this beneficial effect was through



inhibition of activation of retinal glial cells and suppression of retinal inflammation.

Studies have shown that PPAR $\alpha$  is expressed in the retina, kidney, intestine, heart and brain (10, 26–28). Peroxisome proliferator-activated receptor  $\alpha$  expression in the retina under chronic ischemic and hypoxic conditions has been studied (10, 12), but PPAR $\alpha$  expression under acute ischemia and hypoxia has not. Therefore, we first measured PPAR $\alpha$  expression in the retinas of IR rats. Consistent with down-regulation of PPAR $\alpha$  expression in chronic ischemic retinopathy [e.g., DM-induced retinopathy (10), oxygen-induced proliferative retinopathy (15)] and in other non-retinal organs injured by IR [e.g., heart (29), kidney (30), and intestine (31)], PPAR $\alpha$  expression in the IR retina was decreased 24 h after modeling, indicating that PPAR $\alpha$  was involved in the retinal pathological process of IR injury. However, unlike the reduction of PPAR $\alpha$  expression in the whole retina caused by DM (10), the decrease in IR-induced PPAR $\alpha$  expression was manifested mainly in the GCL. One hypothesis is that IR modeling mainly hindered the blood supply of the inner retina by blocking the central retinal artery and central retinal vein (32). In this case, the GCL was more susceptible to ischemia and hypoxia. This hypothesis could be correct because the thickness of the retinal ONL was not affected by IR (**Supplementary Figure 2**).

To verify the effect of PPAR $\alpha$  in IR-induced retinopathy, we used a specific PPAR $\alpha$  agonist, FA, to activate PPAR $\alpha$  and ascertain if PPAR $\alpha$  plays an important part in this pathologic process. First, we used FG to retrograde-label surviving RGCs in the retina. Retinal ganglion cell loss is a crucial feature of acute angle-closure glaucoma, retinal vascular occlusions, and anterior ischemic optic neuropathy. We found that IR modeling led to a significant loss of RGCs 24 and 72 h after modeling, which is consistent with the pathologic process of the diseases mentioned above. Peroxisome proliferator-activated receptor  $\alpha$  activation by FA reduced the RGC loss caused by IR efficaciously, indicating that PPAR $\alpha$  had a protective role in this process. Second, we measured retinal GCC thickness [a widely used indicator for detection of RGC loss in clinical diagnoses (33, 34)] after FA treatment to further demonstrate the protective effect of PPAR $\alpha$  on RGCs. Our results showed that GCC was thinner than the normal group at 72 h post-modeling, and FA treatment alleviated this structural change in the IR retina. However, a change in GCC thickness 24 h after modeling was not found, indicating that the change in GCC thickness occurred later than RGC death. Third, we detected RGC function. Use of FVEPs is a sensitive method that reflects the function of visual pathways (35). Studies have demonstrated that RGC damage would directly affect the visual conduction function, resulting in extension of the latency of each peak of FVEPs (36, 37). In our study, IR-induced RGC injury also increased the latency of the P1 wave and P2 wave of FVEPs, but FA treatment reduced the prolongation of latency. In summary, PPAR $\alpha$  activation by FA alleviated IR-induced damage to the structure and function of RGCs, actions that are consistent with its protective effects in diabetic retinopathy or oxygen-induced proliferative retinopathy (14–17). In addition, our results are also consistent with the studies reported by Bulhak et al. (38) and Ravingerova et al. (39), they both demonstrate that PPAR $\alpha$  activation protects myocardium from IR injury. All these results

suggest that PPAR $\alpha$  activation had a protective role in the retina, and PPAR $\alpha$  itself could be a potential target for treatment of IR-induced retinopathy.

Fenofibrate is a synthetic ligand of PPAR $\alpha$  and has been used as a hypolipidemic drug for >30 years (40). Fenofibrate is safe and inexpensive, and use of fenofibrate for treating retinal diseases was inspired by two large clinical studies (FIELD and ACCORD) in which researchers reported its robust therapeutic effects on retinopathy in patients with type-2 DM (41, 42). Fenofibric acid is the active metabolite of fenofibrate (43) and retains the function and advantage of fenofibrate while avoiding some off-target effects caused by direct application of fenofibrate [e.g., inhibition of cytochrome-P450 expression or suppression of voltage-dependent K<sup>+</sup> channels (44, 45)]. All of these advantages might be conducive to convert FA to a drug for clinical treatment. As for the potential time window for FA treatment of ophthalmic clinical disease (such as acute angle-closure glaucoma, retinal vascular occlusions, and anterior ischemic optic neuropathy), we cannot predict the occurrence of these diseases and administer FA in advance as in this study, so we consider that FA should be administered as soon as these diseases are diagnosed.

We investigated the underlying mechanism of the neuroprotective effect of PPAR $\alpha$  activation. Some *in vitro* studies have shown that fenofibrate and FA have a stimulatory effect on elevation of PPAR $\alpha$  levels in osteogenic precursor cells (46) and palmitate treated retinal precursor cells (47). Our results demonstrated that FA also increased the expression of PPAR $\alpha$  in a retinal IR model, indicating that FA exerts its neuroprotective effect partially relies on up-regulation of PPAR $\alpha$ . Glial cells are crucial for maintaining the blood–retinal barrier and RGC survival (24, 48, 49). It has been reported that glial cells may lose their physiologic functions and be activated in disease or injury, and that over-activation of glial cells is related to retinal neurodegeneration (24). Moran et al. demonstrated that PPAR $\alpha$  activation can attenuate over-activation of glial cells in an oxygen-induced retinopathy model (15). Hence, we conjectured that PPAR $\alpha$  exerted its protective role in an IR model through this mechanism. We found that expression of GFAP (a marker of glial cells) was increased markedly in the GCL after IR modeling, and that FA treatment reduced GFAP expression significantly. Besides, we measured expression of COX2 (an important proinflammatory mediator produced by activated glial cells) because increased COX2 expression can aggravate local inflammation and promote RGC death (50). After IR modeling, COX2 expression increased significantly, and FA treatment attenuated this increase markedly. These data are in accordance with the work of Zhang et al., who also found that activated glial cells could produce COX2 rapidly in injured optic nerves (51). All these results suggested that the therapeutic effect of PPAR $\alpha$  activation was due (at least in part) to inhibition of activation of glial cells and reduction of inflammation in the retina. Importantly, the changes in expression of GFAP and COX2 manifested mainly in the inner layer of the retina (especially in the GCL), which provides further evidence that activation of glial cells and inflammation had direct roles in RGC injury.

## CONCLUSION

In this study, we demonstrated, for the first time, that PPAR $\alpha$  is involved in the pathologic process of retinal IR. Peroxisome proliferator-activated receptor  $\alpha$  activation by FA ameliorates IR-induced RGC injury and protects visual function, inhibits activation of glial cells and suppresses retinal inflammation. Taken together, these findings suggest that PPAR $\alpha$  could be a new target for the treatment of retinal IR-related ophthalmic diseases.

## DATA AVAILABILITY STATEMENT

The original contributions presented in the study are included in the article/**Supplementary Materials**, further inquiries can be directed to the corresponding author/s.

## ETHICS STATEMENT

The animal study was reviewed and approved by Animal Research Committee of the Xiangya School of Medicine.

## AUTHOR CONTRIBUTIONS

FY wrote the first draft of the paper. XZ, XX, and LD edited the paper. FY, JJ, and LD designed research. FY,

XZ, and XY performed research. FY and XR analyzed data. All authors contributed to the article and approved the submitted version.

## FUNDING

This work was supported by the National Natural Science Foundation of China (81500720 and 82070966 to LD) and the Science and Technology Innovation Program of Hunan Province (2021RC3026 to LD).

## ACKNOWLEDGMENTS

We thank Prof. Ma Jianxing (Health Sciences Center, Oklahoma University, Oklahoma, USA) for helpful comments on the manuscript, Yangzhou Zhang, Jingning Long, Rong Rong, Mengling You, and Zhaolin Gao for technical assistance.

## SUPPLEMENTARY MATERIAL

The Supplementary Material for this article can be found online at: <https://www.frontiersin.org/articles/10.3389/fmed.2021.788663/full#supplementary-material>

## REFERENCES

- Sanes JR, Masland RH. The types of retinal ganglion cells: current status and implications for neuronal classification. *Annu Rev Neurosci.* (2015) 38:221–46. doi: 10.1146/annurev-neuro-071714-034120
- Flores-Sanchez BC, Tatham AJ. Acute angle closure glaucoma. *Br J Hosp Med (Lond).* (2019) 80:C174–9. doi: 10.12968/hmed.2019.80.12.C174
- Scott IU, Campochiaro PA, Newman NJ, Bioussé V. Retinal vascular occlusions. *Lancet.* (2020) 396:1927–40. doi: 10.1016/S0140-6736(20)31559-2
- Akbari M, Abdi P, Fard MA, Afzali M, Ameri A, Yazdani-Abyaneh A, et al. Retinal Ganglion cell loss precedes retinal nerve fiber thinning in nonarteritic anterior ischemic optic neuropathy. *J Neuroophthalmol.* (2016) 36:141–6. doi: 10.1097/WNO.0000000000000345
- Boia R, Ruzafa N, Aires ID, Pereiro X, Ambrosio AF, Vecino E, et al. Neuroprotective Strategies for retinal Ganglion cell degeneration: current status and challenges ahead. *Int J Mol Sci.* (2020) 21:2262. doi: 10.3390/ijms21072262
- Bordet R, Ouk T, Petraut O, Gele P, Gautier S, Laprais M, et al. PPAR: a new pharmacological target for neuroprotection in stroke and neurodegenerative diseases. *Biochem Soc Trans.* (2006) 34(Pt 6):1341–6. doi: 10.1042/BST0341341
- Chen XR, Besson VC, Palmier B, Garcia Y, Plotkine M, Marchand-Leroux C. Neurological recovery-promoting, anti-inflammatory, and anti-oxidative effects afforded by fenofibrate, a PPAR alpha agonist, in traumatic brain injury. *J Neurotrauma.* (2007) 24:1119–31. doi: 10.1089/neu.2006.0216
- Araki M, Nakagawa Y, Oishi A, Han SI, Wang Y, Kumagai K, et al. The peroxisome proliferator-activated receptor alpha (PPARalpha) agonist pemafibrate protects against diet-induced obesity in mice. *Int J Mol Sci.* (2018) 19:2148. doi: 10.3390/ijms19072148
- Wojtowicz S, Strosznajder AK, Jezyna M, Strosznajder JB. The novel role of PPAR alpha in the brain: promising target in therapy of Alzheimer's disease and other neurodegenerative disorders. *Neurochem Res.* (2020) 45:972–88. doi: 10.1007/s11064-020-02993-5
- Hu Y, Chen Y, Ding L, He X, Takahashi Y, Gao Y, et al. Pathogenic role of diabetes-induced PPAR-alpha down-regulation in microvascular dysfunction. *Proc Natl Acad Sci U S A.* (2013) 110:15401–6. doi: 10.1073/pnas.1307211110
- Pearsall EA, Cheng R, Zhou K, Takahashi Y, Matlock HG, Vadvalkar SS, et al. PPARalpha is essential for retinal lipid metabolism and neuronal survival. *BMC Biol.* (2017) 15:113. doi: 10.1186/s12915-017-0451-x
- Chen Q, Qiu F, Zhou K, Matlock HG, Takahashi Y, Rajala RVS, et al. Pathogenic role of microRNA-21 in diabetic retinopathy through downregulation of PPARalpha. *Diabetes.* (2017) 66:1671–82. doi: 10.2337/db16-1246
- Wang Y, Lin W, Ju J. MicroRNA-409-5p promotes retinal neovascularization in diabetic retinopathy. *Cell Cycle.* (2020) 19:1314–25. doi: 10.1080/15384101.2020.1749484
- Ding L, Cheng R, Hu Y, Takahashi Y, Jenkins AJ, Keech AC, et al. Peroxisome proliferator-activated receptor alpha protects capillary pericytes in the retina. *Am J Pathol.* (2014) 184:2709–20. doi: 10.1016/j.ajpath.2014.06.021
- Moran E, Ding L, Wang Z, Cheng R, Chen Q, Moore R, et al. Protective and antioxidant effects of PPARalpha in the ischemic retina. *Invest Ophthalmol Vis Sci.* (2014) 55:4568–76. doi: 10.1167/iovs.13-13127
- Feng X, Gao X, Wang S, Huang M, Sun Z, Dong H, et al. PPAR-alpha Agonist fenofibrate prevented diabetic nephropathy by inhibiting M1 macrophages via improving endothelial cell function in db/db mice. *Front Med (Lausanne).* (2021) 8:652558. doi: 10.3389/fmed.2021.652558
- Qiu F, Matlock G, Chen Q, Zhou K, Du Y, Wang X, et al. Therapeutic effects of PPARalpha agonist on ocular neovascularization in models recapitulating neovascular age-related macular degeneration. *Invest Ophthalmol Vis Sci.* (2017) 58:5065–75. doi: 10.1167/iovs.17-22091
- Tong JB, Chen D, Zeng LP, Mo XY, Wang H, Huang J, et al. Differential changes of local blood supply in rat retinae are involved in the selective loss of retinal ganglion cells following the acute high intraocular pressure. *Curr Eye Res.* (2010) 35:425–34. doi: 10.3109/02713680903514675
- Rong R, Xia X, Peng H, Li H, You M, Liang Z, et al. Cdk5-mediated Drp1 phosphorylation drives mitochondrial defects and neuronal apoptosis in radiation-induced optic neuropathy. *Cell Death Dis.* (2020) 11:720. doi: 10.1038/s41419-020-02922-y
- Xiong Y, Ji H, You Z, Yao F, Zhou R, Song W, et al. Otx2 enhances transdifferentiation of Muller cells-derived retinal stem cells into photoreceptor-like cells. *J Cell Mol Med.* (2019) 23:943–53. doi: 10.1111/jcmm.13995

21. Yao F, Zhang E, Gao Z, Ji H, Marmouri M, Xia X. Did you choose appropriate tracer for retrograde tracing of retinal ganglion cells? The differences between cholera toxin subunit B and fluorogold. *PLoS ONE*. (2018) 13:e0205133. doi: 10.1371/journal.pone.0205133
22. Bloch E, Yonova-Doing E, Jones-Odeh E, Williams KM, Kozareva D, Hammond CJ. Genetic and environmental factors associated with the Ganglion cell complex in a healthy aging British cohort. *JAMA Ophthalmol*. (2017) 135:31–8. doi: 10.1001/jamaophthalmol.2016.4486
23. Yang Z, Wang KK. Glial fibrillary acidic protein: from intermediate filament assembly and gliosis to neurobiomarker. *Trends Neurosci*. (2015) 38:364–74. doi: 10.1016/j.tins.2015.04.003
24. Bringmann A, Pannicke T, Biedermann B, Francke M, Iandiev I, Grosche J, et al. Role of retinal glial cells in neurotransmitter uptake and metabolism. *Neurochem Int*. (2009) 54:143–60. doi: 10.1016/j.neuint.2008.10.014
25. Chan PC, Hsiao FC, Chang HM, Wabitsch M, Hsieh PS. Importance of adipocyte cyclooxygenase-2 and prostaglandin E2-prostaglandin E receptor 3 signaling in the development of obesity-induced adipose tissue inflammation and insulin resistance. *FASEB J*. (2016) 30:2282–97. doi: 10.1096/fj.201500127
26. Chinetti G, Fruchart JC, Staels B. Peroxisome proliferator-activated receptors (PPARs): nuclear receptors at the crossroads between lipid metabolism and inflammation. *Inflamm Res*. (2000) 49:497–505. doi: 10.1007/s000110050622
27. Wayman NS, Hattori Y, McDonald MC, Mota-Filipe H, Cuzzocrea S, Pisano B, et al. Ligands of the peroxisome proliferator-activated receptors (PPAR- $\gamma$  and PPAR- $\alpha$ ) reduce myocardial infarct size. *FASEB J*. (2002) 16:1027–40. doi: 10.1096/fj.01-0793com
28. Chandra S, Jana M, Pahan K. Aspirin induces lysosomal biogenesis and attenuates amyloid plaque pathology in a mouse model of Alzheimer's disease via PPARAspirin induces lysosomal biogenesis and attenuates amyloid plaque pathology in a mouse model of Alzheimer's disease via PPAR $\alpha$ . *J Neurosci*. (2018) 38:6682–99. doi: 10.1523/JNEUROSCI.0054-18.2018
29. Yuan J, Mo H, Luo J, Zhao S, Liang S, Jiang Y, et al. PPAR $\alpha$  activation alleviates damage to the cytoskeleton during acute myocardial ischemia/reperfusion in rats. *Mol Med Rep*. (2018) 17:7218–26. doi: 10.3892/mmr.2018.8771
30. Sivarajah A, Chatterjee PK, Hattori Y, Brown PA, Stewart KN, Todorovic Z, et al. Agonists of peroxisome-proliferator activated receptor- $\alpha$  (clofibrate and WY14643) reduce renal ischemia/reperfusion injury in the rat. *Med Sci Monit*. (2002) 8:BR532–9. doi: 10.1017/S155770X11000337
31. Li LX, Yin LH, Gao M, Xu LN, Qi Y, Peng JY. MiR-23a-5p exacerbates intestinal ischemia-reperfusion injury by promoting oxidative stress via targeting PPAR  $\alpha$ . *Biochem Pharmacol*. (2020) 180:114194. doi: 10.1016/j.bcp.2020.114194
32. Osborne NN, Casson RJ, Wood JP, Chidlow G, Graham M, Melena J. Retinal ischemia: mechanisms of damage and potential therapeutic strategies. *Prog Retin Eye Res*. (2004) 23:91–147. doi: 10.1016/j.preteyeres.2003.12.001
33. Dascalescu D, Corbu C, Coviltir V, Schmitzer S, Constantin M, Burcel M, et al. The ganglion cell complex as a useful tool in glaucoma assessment. *Rom J Ophthalmol*. (2018) 62:300–3. doi: 10.22336/rjo.2018.46
34. Asanad S, Tian JJ, Frousiakis S, Jiang JP, Kogachi K, Felix CM, et al. Optical coherence tomography of the retinal Ganglion cell complex in leber's hereditary optic neuropathy and dominant optic atrophy. *Curr Eye Res*. (2019) 44:638–44. doi: 10.1080/02713683.2019.1567792
35. Young B, Eggenberger E, Kaufman D. Current electrophysiology in ophthalmology: a review. *Curr Opin Ophthalmol*. (2012) 23:497–505. doi: 10.1097/ICU.0b013e328359045e
36. Huo Y, Yin XL, Ji SX, Zou H, Lang M, Zheng Z, et al. Amino-Nogo inhibits optic nerve regeneration and functional recovery via the integrin  $\alpha$ 5 $\beta$ 1 signaling pathway in rats. *Cell Physiol Biochem*. (2015) 35:616–26. doi: 10.1159/000369723
37. Liu L, Sun Q, Wang R, Chen Z, Wu J, Xia F, et al. Methane attenuates retinal ischemia/reperfusion injury via anti-oxidative and anti-apoptotic pathways. *Brain Res*. (2016) 1646:327–33. doi: 10.1016/j.brainres.2016.05.037
38. Bulhak AA, Jung C, Ostenson CG, Lundberg JO, Sjoquist PO, Pernow J. PPAR- $\alpha$  activation protects the type 2 diabetic myocardium against ischemia-reperfusion injury: involvement of the PI3-Kinase/Akt and NO pathway. *Am J Physiol Heart Circ Physiol*. (2009) 296:H719–27. doi: 10.1152/ajpheart.00394.2008
39. Ravingerova T, Carnicka S, Nemcekova M, Ledvenyiova V, Adameova A, Kelly T, et al. PPAR- $\alpha$  activation as a preconditioning-like intervention in rats *in vivo* confers myocardial protection against acute ischaemia-reperfusion injury: involvement of PI3K-Akt. *Can J Physiol Pharmacol*. (2012) 90:1135–44. doi: 10.1139/y2012-052
40. Canzler H, Bojanovski D. Lowering effect of fenofibrate (procetofene) on lipoproteins in different types of hyperlipoproteinemias. *Artery*. (1980) 8:171–8.
41. Keech AC, Mitchell P, Summanen PA, O'Day J, Davis TM, Moffitt MS, et al. Effect of fenofibrate on the need for laser treatment for diabetic retinopathy (FIELD study): a randomised controlled trial. *Lancet*. (2007) 370:1687–97. doi: 10.1016/S0140-6736(07)61607-9
42. Group AS, Group AES, Chew EY, Ambrosius WT, Davis MD, Danis RP, et al. Effects of medical therapies on retinopathy progression in type 2 diabetes. *N Engl J Med*. (2010) 363:233–44. doi: 10.1056/NEJMoa1001288
43. Vlase L, Popa A, Muntean D, Leucuta SE. Pharmacokinetics and comparative bioavailability of two fenofibrate capsule formulations in healthy volunteers. *Arzneimittelforschung*. (2010) 60:560–3. doi: 10.1055/s-0031-1296325
44. Li H, Shin SE, Seo MS, An JR, Jung WK, Ha KS, et al. The PPAR $\alpha$  activator fenofibrate inhibits voltage-dependent K(+) channels in rabbit coronary arterial smooth muscle cells. *Eur J Pharmacol*. (2017) 812:155–62. doi: 10.1016/j.ejphar.2017.07.027
45. Gong Y, Shao Z, Fu Z, Edin ML, Sun Y, Liegl RG, et al. Fenofibrate inhibits cytochrome P450 epoxygenase 2C activity to suppress pathological ocular angiogenesis. *EBioMedicine*. (2016) 13:201–11. doi: 10.1016/j.ebiom.2016.09.025
46. Kim YH, Jang WG, Oh SH, Kim JW, Lee MN, Song JH, et al. Fenofibrate induces PPAR $\alpha$  and BMP2 expression to stimulate osteoblast differentiation. *Biochem Biophys Res Commun*. (2019) 520:459–65. doi: 10.1016/j.bbrc.2019.10.048
47. Deng G, Moran EP, Cheng R, Matlock G, Zhou K, Moran D, et al. Therapeutic Effects of a novel agonist of peroxisome proliferator-activated receptor  $\alpha$  for the treatment of diabetic retinopathy. *Invest Ophthalmol Vis Sci*. (2017) 58:5030–42. doi: 10.1167/iov.16-21402
48. Kaur C, Foulds WS, Ling EA. Blood-retinal barrier in hypoxic ischaemic conditions: basic concepts, clinical features and management. *Prog Retin Eye Res*. (2008) 27:622–47. doi: 10.1016/j.preteyeres.2008.09.003
49. Biesecker KR, Srien AI, Shimoda AM, Agarwal A, Bergles DE, Kofuji P, et al. Glial cell calcium signaling mediates capillary regulation of blood flow in the retina. *J Neurosci*. (2016) 36:9435–45. doi: 10.1523/JNEUROSCI.1782-16.2016
50. Luo H, Zhuang J, Hu P, Ye W, Chen S, Pang Y, et al. Resveratrol delays retinal ganglion cell loss and attenuates gliosis-related inflammation from ischemia-reperfusion injury. *Invest Ophthalmol Vis Sci*. (2018) 59:3879–88. doi: 10.1167/iov.18-23806
51. Zhang X, Neufeld AH. Signal transduction pathways for epidermal growth factor stimulated cyclooxygenase-2 induction in astrocytes. *Exp Eye Res*. (2007) 85:280–8. doi: 10.1016/j.exer.2007.05.002

**Conflict of Interest:** The authors declare that the research was conducted in the absence of any commercial or financial relationships that could be construed as a potential conflict of interest.

**Publisher's Note:** All claims expressed in this article are solely those of the authors and do not necessarily represent those of their affiliated organizations, or those of the publisher, the editors and the reviewers. Any product that may be evaluated in this article, or claim that may be made by its manufacturer, is not guaranteed or endorsed by the publisher.

Copyright © 2021 Yao, Zhang, Yao, Ren, Xia, Jiang and Ding. This is an open-access article distributed under the terms of the Creative Commons Attribution License (CC BY). The use, distribution or reproduction in other forums is permitted, provided the original author(s) and the copyright owner(s) are credited and that the original publication in this journal is cited, in accordance with accepted academic practice. No use, distribution or reproduction is permitted which does not comply with these terms.



# Axl Is Essential for *in-vitro* Angiogenesis Induced by Vitreous From Patients With Proliferative Diabetic Retinopathy

Wenyi Wu<sup>1,2</sup>, Huizuo Xu<sup>1,2</sup>, Zhishang Meng<sup>3</sup>, Jianxi Zhu<sup>4</sup>, Siqi Xiong<sup>1,2\*</sup>, Xiaobo Xia<sup>1,2\*</sup> and Hetian Lei<sup>5\*</sup>

<sup>1</sup> Department of Ophthalmology, National Clinical Research Center for Geriatric Disorders, Xiangya Hospital of Central South University, Changsha, China, <sup>2</sup> Department of Ophthalmology, Hunan Key Laboratory of Ophthalmology, Changsha, China, <sup>3</sup> Department of Ophthalmology, The Second Xiangya Hospital of Central South University, Changsha, China, <sup>4</sup> Department of Orthopedics, Xiangya Hospital of Central South University, Changsha, China, <sup>5</sup> Department of Ophthalmology, Shenzhen Eye Institute, Shenzhen Eye Hospital, Jinan University, Shenzhen, China

## OPEN ACCESS

### Edited by:

Haijiang Lin,  
University of Massachusetts,  
United States

### Reviewed by:

Junhui Shen,  
Zhejiang University, China  
Jiaxu Hong,  
Fudan University, China

### \*Correspondence:

Siqi Xiong  
petersage1221@126.com  
Xiaobo Xia  
xbxia21@163.com  
Hetian Lei  
leihetian18@hotmail.com

### Specialty section:

This article was submitted to  
Ophthalmology,  
a section of the journal  
Frontiers in Medicine

**Received:** 30 September 2021

**Accepted:** 08 November 2021

**Published:** 23 December 2021

### Citation:

Wu W, Xu H, Meng Z, Zhu J, Xiong S, Xia X and Lei H (2021) Axl Is Essential for *in-vitro* Angiogenesis Induced by Vitreous From Patients With Proliferative Diabetic Retinopathy. *Front. Med.* 8:787150. doi: 10.3389/fmed.2021.787150

Proliferative diabetic retinopathy (PDR), characterized mainly with abnormal epiretinal angiogenesis forming fibrovascular membranes (FVMs), threatens vision of people with diabetes; FVMs consist of extracellular matrix and a variety of cell types including vascular endothelial cells. Axl, one of receptor tyrosine kinases, can be activated indirectly by vascular endothelial growth factor-A (VEGF-A) *via* an intracellular route for promoting angiogenesis. In this study, we revealed that growth arrest-specific protein 6 (Gas6), a specific ligand of Axl, was elevated in vitreous from patients with PDR and that Axl was activated in FVMs from patients with PDR. In addition, we demonstrated that in cultured human retinal microvascular endothelial cells (HRECs), Axl inhibition *via* suppression of Axl expression with Clustered Regularly Interspaced Short Palindromic Repeats/CRISPR-associated protein 9 or through inactivation with its specific inhibitor R428 blocked PDR vitreous-induced Akt activation and proliferation of HRECs. Furthermore, PDR vitreous-heightened migration and tube formation of HRECs were also blunted by restraining Axl. These results indicate that in the pathogenesis of PDR, Axl can be activated by Gas6 binding directly and by VEGF-A *via* an intracellular route indirectly, suggesting that Axl plays a pivotal role in the development of PDR and that Axl inhibition shows a bright promise for PDR therapy.

**Keywords:** PDR vitreous, GAS6, Axl, CRISPR/Cas9, R428, HRECs

## INTRODUCTION

Diabetic retinopathy (DR) is one of diabetic complications that affects eyes and proliferative DR (PDR) is the serious stage of DR. It is caused by damage to retinal microvascular endothelial cells, leading to vision-threatening exudation and hemorrhage. Retinal angiogenesis is a key pathological cause for PDR (1), and current PDR therapy mainly focuses on laser and antivascular endothelial growth factor (VEGF) drugs. However, photocoagulation has limited efficacy and acts as a devastating method; some patients poorly respond to current anti-VEGF therapy, but factors contributing to the limited response remain large. Further studies to identify and understand the molecular alterations that frequently occur in DR are vital to develop additional effective treatment options.



Vascular endothelial growth factor-A (VEGF-A) stimulates survival, proliferation, and migration of vascular endothelial cells (ECs) and promotes vascular permeability, which is critical for vascular development and angiogenesis. Due to its essential role in angiogenesis, VEGF-A signaling pathway has received great attention for angiogenesis therapeutics in the past decade. However, other growth factors also engage similar downstream signaling pathways including the phosphatidylinositol 3-kinase/protein kinase B pathway to promote angiogenesis.

Axl, whose name came from the Greek word “anexelekto” meaning uncontrolled, is a member of the family of receptor tyrosine kinase (RTK). Its activation is stimulated by binding to its specific ligand growth arrest-specific protein 6 (GAS6) (2). In addition, Axl is also activated indirectly by VEGF-A via an intracellular pathway of reactive oxygen species (ROS)/Src family kinases (SFKs) (3). Furthermore, Axl has been found to confer resistance to anti-insulin-like growth factor 1 receptor (4); Fibroblast growth factor receptor 1-induced Akt activation is associated with Axl activity (5). Notably, Axl null mice respond poorly to VEGF-A-induced vascular permeability and angiogenesis (3). We previously showed that the normal bovine vitreous promotes endothelial cell proliferation and migration via Axl activation (6); however, whether Axl was activated in epiretinal fibrovascular membranes from patients with PDR remained elusive and the Axl role in human retinal vascular endothelial cells (HRECs) stimulated by PDR also needs to be clarified; for these answers, it will improve our understanding of the underlining mechanisms of pathogenesis of PDR and advance the development of additional effective treatment strategies for PDR.

## RESULTS

### Axl Is Activated in Fibrovascular Membranes From Patients With PDR

Inhibition of Axl with a pharmacological inhibitor suppressed retinal angiogenesis in a mouse model of oxygen-induced retinopathy (6). To study if this finding was related to a clinical significance, we investigated if Gas6 was enriched in vitreous from patients with PDR by ELISA. In this assay, vitreous from the macular hole was used as a control. As shown in **Figure 1A**, in PDR vitreous, Gas6 was elevated compared with that in the control vitreous. Next, we evaluated if Axl was activated in fibrovascular membranes from patients with PDR by immunohistochemistry. The results (**Figures 1B–E**) showed that Axl was indeed activated in the PDR membranes, suggesting that Gas6 in the PDR vitreous is one of the possible agents inducing Axl activation in the PDR membranes.

### Proliferative Diabetic Retinopathy Vitreous Heightens Activation of Axl and Akt and Cellular Events Related to Angiogenesis

We next assessed if Axl activation could be induced by PDR vitreous in cultured HRECs. As expected, activation of Axl and Akt was heightened in HRECs after stimulation by PDR vitreous whose effect on induction was better than normal

vitreous (**Figure 2A**). These signaling events might transform to angiogenesis-related cellular responses such as proliferation, migration, and tube formation (7–10).

Data from proliferation assays with HRECs showed that there was a significant increase in both the total cell number and Ki-67 (a nuclear protein that is associated with proliferation) positive cell number when these cells were treated with PDR vitreous (**Figures 2B,C**), indicating that PDR vitreous enhances cell proliferation.

Subsequently, we employed a wound healing assay to assess the migratory ability of HRECs induced by PDR vitreous. The results (**Figures 2D,E**) showed that PDR vitreous promoted HRECs migration, which is an important feature in angiogenesis.

Subsequently, we evaluated the effect of PDR vitreous on angiogenesis in an *in-vitro* model of a tube formation assay (6). As shown in **Figures 2F,G**, PDR vitreous heightened the ability of HRECs in forming tubes, suggesting that the signaling pathway of Gas6/Axl might play an important role in these PDR vitreous-enhanced cellular events intrinsic to angiogenesis.

### Suppression of Axl Impedes PDR Vitreous-Induced Cell Proliferation, Migration, and Tube Formation

To investigate the role of Axl in PDR vitreous-induced angiogenesis *in vitro*, expression of Axl was depleted in HRECs by using a CRISPR/Cas9 approach. As shown in **Figure 3A**, western blot analysis demonstrated that Axl depletion resulted from SpCas9 editing of genomic DNA under the single guide RNA-1 (sgRNA-1) guidance. In addition, we found that depletion of Axl attenuated PDR vitreous-induced cell proliferation (**Figure 3B**) and decreased the migratory capability of HRECs (**Figures 3C,D**). Furthermore, Axl removal resulted in a reduction in PDR vitreous-induced tube formation of the HRECs (**Figures 3E,F**). These results demonstrate that Axl plays a central part in PDR vitreous-stimulated activation of Akt and angiogenesis-related cellular responses of HRECs.

### Inhibition of Axl Prevents PDR Vitreous-Induced Akt Activation and Cellular Responses Related to Angiogenesis

We next sought to find if pharmacological inhibition of Axl could block PDR vitreous-induced Akt activation, so that a potential pharmacological inhibitor could be used for treating retinal pathological angiogenesis. R428, a small molecule inhibitor specific for Axl, inhibited Axl at 4  $\mu$ M without showing obvious toxicity to HRECs. Therefore, we treated HRECs with PDR vitreous along with R428 and found that 4  $\mu$ M R428 completely blocked PDR vitreous-induced Akt activation (**Figure 4A**). As expected, R428 at this concentration also inhibited vitreous-stimulated proliferation, migration, and tube formation of HRECs (**Figures 4B–G**), suggesting that Axl is a potential mediator of retinal angiogenesis.

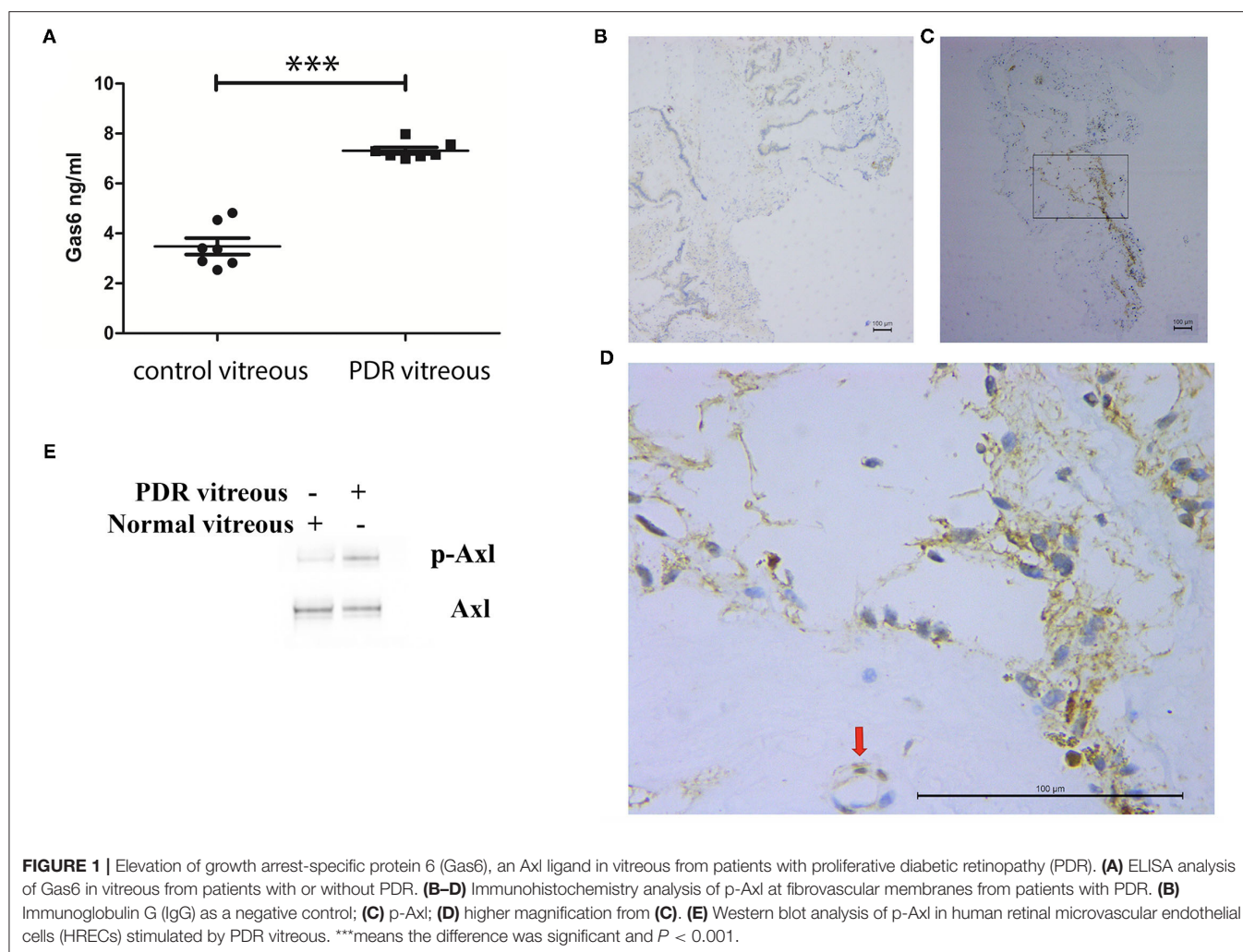


**FIGURE 1 |** Elevation of growth arrest-specific protein 6 (Gas6), an Axl ligand in vitreous from patients with proliferative diabetic retinopathy (PDR). **(A)** ELISA analysis of Gas6 in vitreous from patients with or without PDR. **(B–D)** Immunohistochemistry analysis of p-Axl at fibrovascular membranes from patients with PDR. **(B)** Immunoglobulin G (IgG) as a negative control; **(C)** p-Axl; **(D)** higher magnification from **(C)**. **(E)** Western blot analysis of p-Axl in human retinal microvascular endothelial cells (HRECs) stimulated by PDR vitreous. \*\*\*means the difference was significant and  $P < 0.001$ .

## DISCUSSION

In this study, we report that Axl, one of receptor tyrosine kinases, is essential for vitreous-induced angiogenesis with a patient *in vitro*. In the vitreous from patients with PDR, levels of VEGF-A are elevated (11). It has been reported that Axl is essential for VEGF-A-dependent activation of the PI3K/Akt signaling, which plays a central role in angiogenesis (3). In addition, Gas6, a traditional ligand of Axl, is also present in such vitreous. Thus, we proposed that there are at least two routes for activating Axl by the PDR vitreous. One is that Axl is directly activated by its ligand Gas6 binding to trigger the signaling pathway of Axl/PI3K/Akt; the other is that Axl is indirectly activated by VEGF-A *via* Vascular endothelial growth factor receptor-2/ROS/SFKs (3) (**Figure 5**). However, the pathway for Axl plays a predominant role that needs further investigation.

We have previously reported that normal bovine vitreous is also able to activate Axl for engaging activation and angiogenesis of Akt (6). In this study, the vitreous from patients with PDR shows a similar effect to normal bovine

vitreous on *in-vitro* angiogenesis; however, PDR vitreous is obviously more relevant to pathophysiological conditions and, thus, these novel findings may provide a significant clue to develop novel approaches to prevent or cure diabetes-related retinal angiogenesis.

We have found that R428, a specific small molecule inhibitor of Axl, inhibits either normal bovine vitreous or PDR vitreous-activated Akt and angiogenesis *in vitro* and *in vivo*. Small molecules have some disadvantages in clinical settings including short half-life, non-specific, etc. Therefore, based on the essential role of Axl in pathological retinal angiogenesis, we may develop novel approaches such as genome-editing Axl for its inactivation in retinal vascular ECs to prevent retinal angiogenesis.

Currently, intravitreal injection of anti-VEGF agents including aflibercept and ranibizumab is mainstream for treating patients with diabetes-related eye diseases; however, there are still numerous such patients who do not respond to the anti-VEGF treatment or develop resistance to the anti-VEGF therapy. In such cases, an anti-Axl therapy may shed a light on those anti-VEGF-resistant patients.

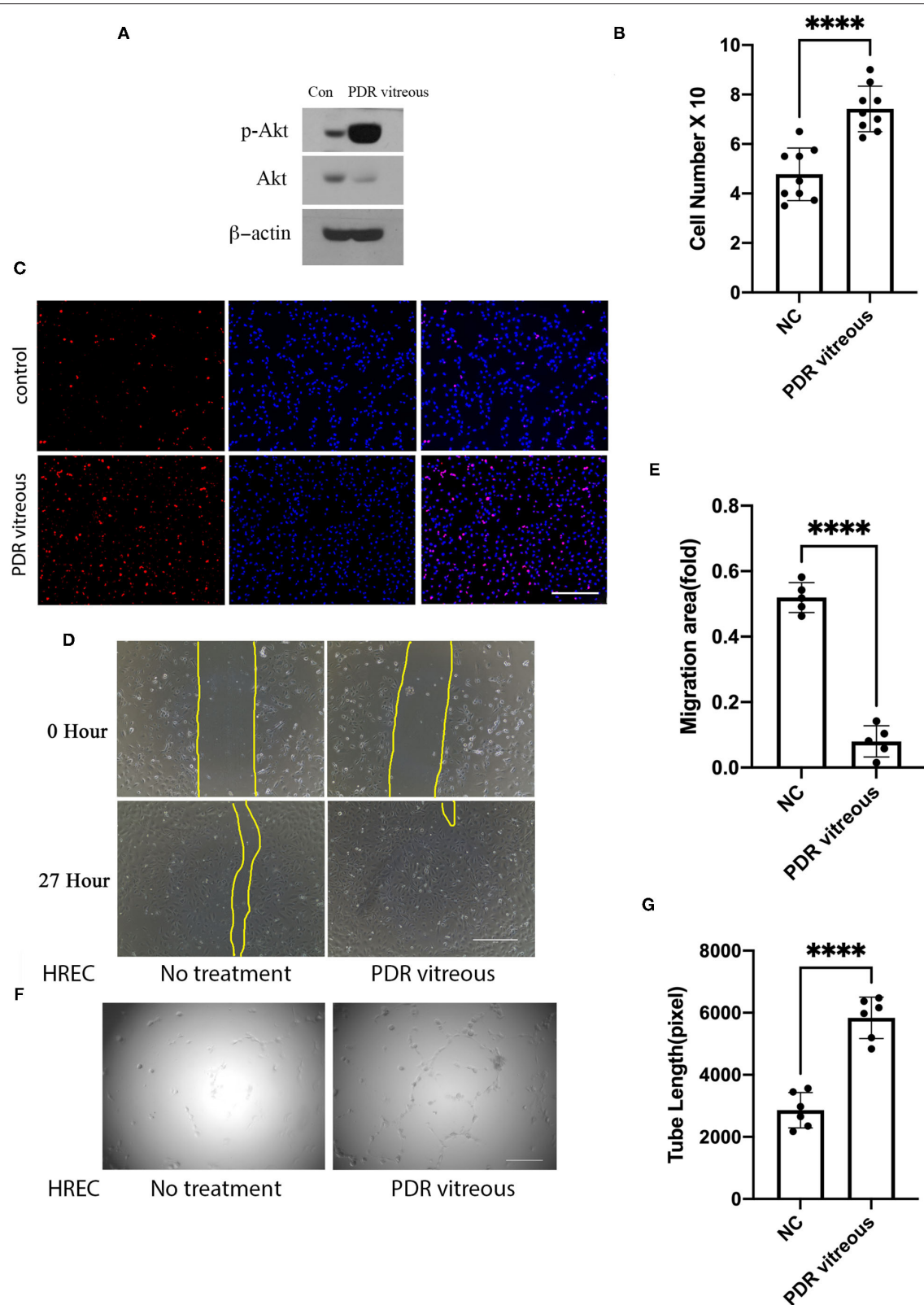


**FIGURE 2 |** PDR vitreous enhanced proliferation, migration, and tube formation of vascular endothelial cells. **(A)** Western blot analysis of p-Akt in HRECs induced by PDR vitreous. This is representative of three independent experiments. **(B,C)** Proliferation of HRECs induced by PDR vitreous was assessed using two methods. **(B)** Total cell number counting; **(C)** Ki67 staining of proliferative cells. Scale bar: 1,000  $\mu$ m. **(D,E)** A wound healing assay to measure the migration of HRECs stimulated by (Continued)



**FIGURE 2 |** PDR vitreous. **(D)** Representative photos, scale bar: 400  $\mu$ m; **(E)** Bar graphs show five independent experiments. **(F,G)** A matrigel assay to assess the tube formation of HRECs induced by PDR vitreous. **(F)** Representative photos of five independent experiments, Scale bar: 400  $\mu$ m; **(G)** Bar graphs of tube lengths in five representative photos of three independent experiments. \*\*\*\* means the difference was significant and  $p < 0.0001$ .

## METHODS AND REAGENTS

### Sample and Major Reagents

The Internal Review Committee of Xiangya Hospital approved this study. Research protocols adhered to the Association for Research in Vision and Ophthalmology Statement on Human Subjects and the tenets of the Declaration of Helsinki. All the participants gave a written informed consent prior to surgery and inclusion in this study. Surgical samples were collected at the Department of Xiangya Hospital. Most of the antibodies and reagents in this study were listed in our previous study (6).

### Cell Culture

Human retinal microvascular endothelial cells (Cell Systems, Kirkland, Washington, USA) were grown in an endothelial growth medium (EGM)-2 (Lonza, Walkersville, Maryland, USA) supplemented with a kit of growth factors (Lonza, Walkersville, Maryland, USA). Human embryonic kidney (HEK) 293T cells were cultured in high-glucose (4.5 g/l) Dulbecco's Modified Eagle Medium supplemented with 10% Foetal Bovine Serum. All the cells were cultured at 37°C in a humidified 5% CO<sub>2</sub> atmosphere (12).

### Deoxyribonucleic Acid Constructs

The transfer vector of lentivirus was constructed by replacing different sgRNA in *BsmBI*-digested lentiCRISPR v2 vector as previously described (6). The three protospacer sequences from Axl loci (NC\_000004.12) were 5'-AAGGTTCCCTTCACTA TCAGG-3' (A1), 5'-GGGAATATCACAGGTGCCCG-3' (A2), and 5'-CTTCTACCGGGAACTGACT-3' (A3) and the control sgRNA sequence targeting *LacZ* from *Escherichia coli* was (5'-TGCGAATACGCCACGCGATGGG-3') (13). All the clones were confirmed by DNA sequencing using a primer 5'-GGACTATCATATGCTTACCG-3' from the sequence of U6 promoter that drives expression of sgRNAs. Both the synthesis of primers and oligos and sequencing of PCR products and clones were performed at Sangon Biotech (Shanghai, China). All the plasmids used were purchased from Addgene (Cambridge, Massachusetts, USA).

### Production of Lentivirus

The procedure for lentivirus production was described in detail in our previous publication (14). Lentiviruses were produced by triple transfection of HEK 293T cells with pLentiCRISPRv2, the lentiviral packaging plasmid which encodes HIV-1 Gag, Pol, Tat and Rev proteins, and pVSV-G [catalog number 52,961, 12,260, and 8,454 from Addgene (Cambridge, Massachusetts, USA), respectively] using lipofectamine 3000. After harvest, viruses were concentrated by centrifuging in a JA17 rotor (Beckman Coulter, Brea, California) at 25,000 g for 90 min at 4°C. The concentrated virus was resuspended in 300  $\mu$ l of sterile TNE

(50 mM Tris, pH 7.8, 130 mM sodium chloride, and 1 mM Ethylenediaminetetraacetic acid) with gentle rotation overnight at 4°C. Next, these dissolved retroviruses were tittered for infecting HRECs in combination with 8  $\mu$ g/ml polybrene (Sigma-Aldrich Corporation, St Louis, Mosby, USA) or kept at -80°C (12, 15, 16). The infected cells were selected in media with puromycin (Sigma-Aldrich Corporation, St Louis, Mosby, USA) (0.5  $\mu$ g/ml) and the resultant cells were examined by Western blot analysis (12, 15, 16).

### Western Blot

Human retinal microvascular endothelial cells were seeded in a 24-well plate at 70% confluence and then starved for 6–8 h in media deprived from serum and growth factors. Subsequently, the starved cells were pretreated with PDR vitreous (200  $\mu$ l/ml) for 30 min and the control group was pretreated with boiled PDR vitreous. In certain experiments, cells were treated with different inhibitors for 30 min. All the cells were lysed in Radioimmunoprecipitation assay in the presence of a protease inhibitor (MedChemExpress Shanghai, China). The protein-transferred membranes were blocked by 5% fat-free milk dissolved in Tris Buffered Saline/0.05% Tween-20 for 30 min and incubated with first antibodies (1:1,000) overnight at 4°C. After thoroughly washing, the membranes were incubated with horse radish peroxidase-conjugated secondary antibodies (1:5,000) and visualized using LumiBest enhanced chemiluminescence.  $\beta$ -actin and total Akt were served for normalization across the samples. Experiments were repeated at least three times and blot signal intensity was determined by densitometry using the National Institutes of Health ImageJ software (12).

### Cell Proliferation Assay

Human retinal microvascular endothelial cells were seeded at a density of  $2 \times 10^4$  cells/well in 24-well plates and counted in a cell number counter after 48 h of continuous treatment with endothelial cell growth media-2 or PDR vitreous (1:3 dilution in EGM-2). At least three independent experiments were performed as described previously (6). In addition, immunofluorescent staining for Ki67 (rabbit anti-Ki67; Proteintech, Rosemont, IL, USA) for marking proliferating cells was performed as previously described (17).

### Scratch-Wound Migration Assay

Migration was assessed with a scratch-wound assay (18). Once cells reached 80% confluence in 24-well plates, they were starved for 4 h. After the cell monolayer was scraped with a sterile pipette tip (200  $\mu$ l), the cells were washed twice to remove detached cells. One scratch was generated per well and imaged on an Leica imaging system every 6 h for 48 h. Images were analyzed by measuring the number of pixels



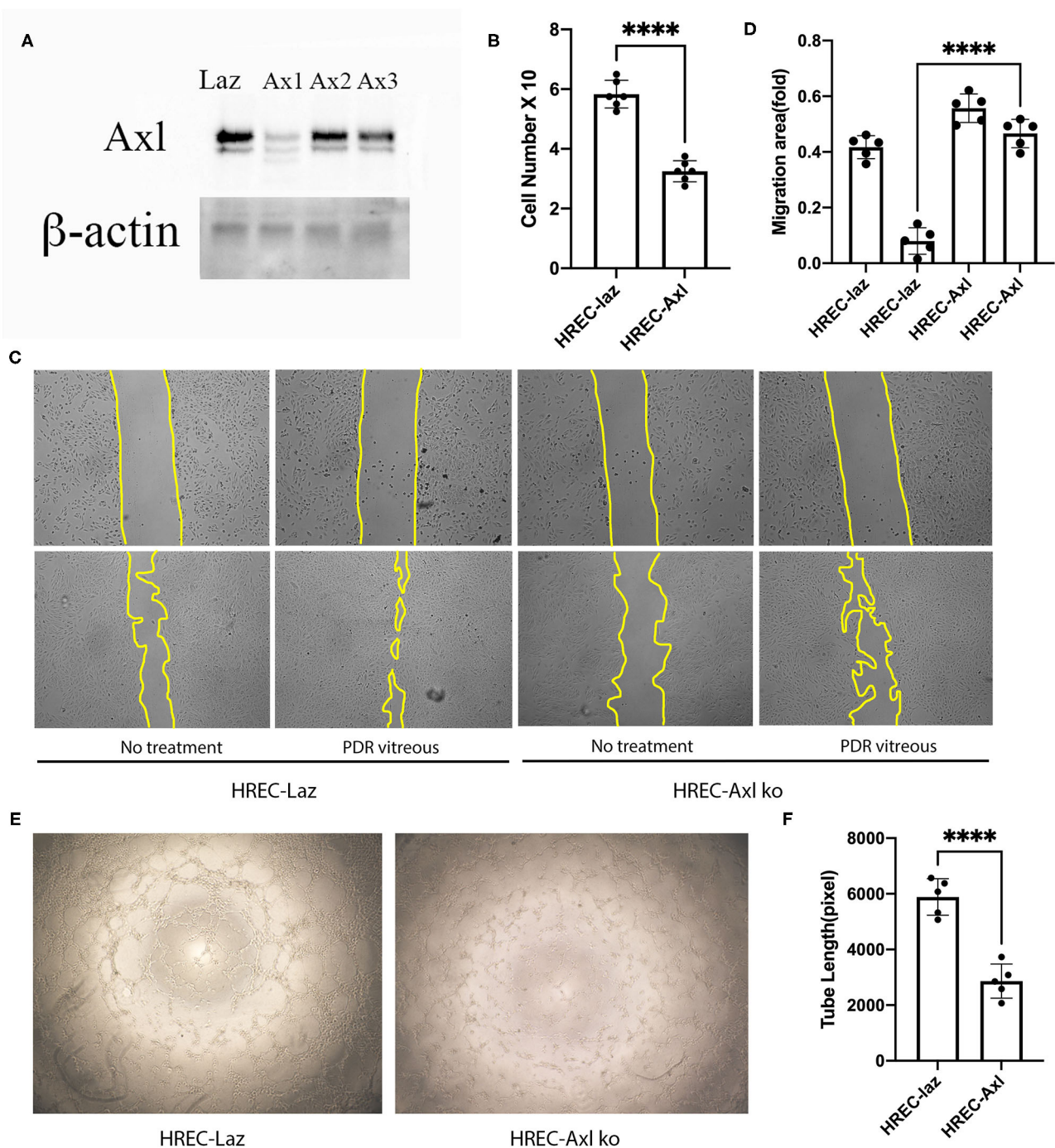


**FIGURE 3 |** Suppression of Axl suppressed PDR vitreous-induced proliferation, migration, and tube formation. **(A)** Western blot analysis of lysates from HRECs expressing CRISPR/Cas9 targeting *lacZ* or *Axl* using indicated antibodies. This is representative of three independent experiments. **(B)** Proliferation of HRECs expressing CRISPR/Cas9 targeting *lacZ* or *Axl* was induced by PDR vitreous and cell number was counted in a hemocytometer under a light microscope. **(C,D)** Migration of HRECs expressing CRISPR/Cas9 targeting *lacZ* or *Axl* was induced by PDR vitreous in a wound assay. **(D)** Representative photos of the wound areas, scale bar: 400  $\mu$ m; bar graphs of wound areas in five representative photos from three independent experiments. **(E,F)** A matrigel assay was used to evaluate tube formation of HRECs expressing CRISPR/Cas9 targeting *lacZ* or *Axl* induced by PDR vitreous. **(F)** Representative photos, scale bar: 1,000  $\mu$ m; Bar graphs of tube lengths in five representative photos of three independent experiments. \*\*\*\* means the difference was significant and  $p < 0.0001$ .

in the wound area using Adobe Photoshop (Adobe Systems, San Jose, California, USA) and analyzed using the ImageJ software (3).

### Tube Formation Assay

This assay was performed as previously described (19). A total of 15,000 HRECs were placed onto wells

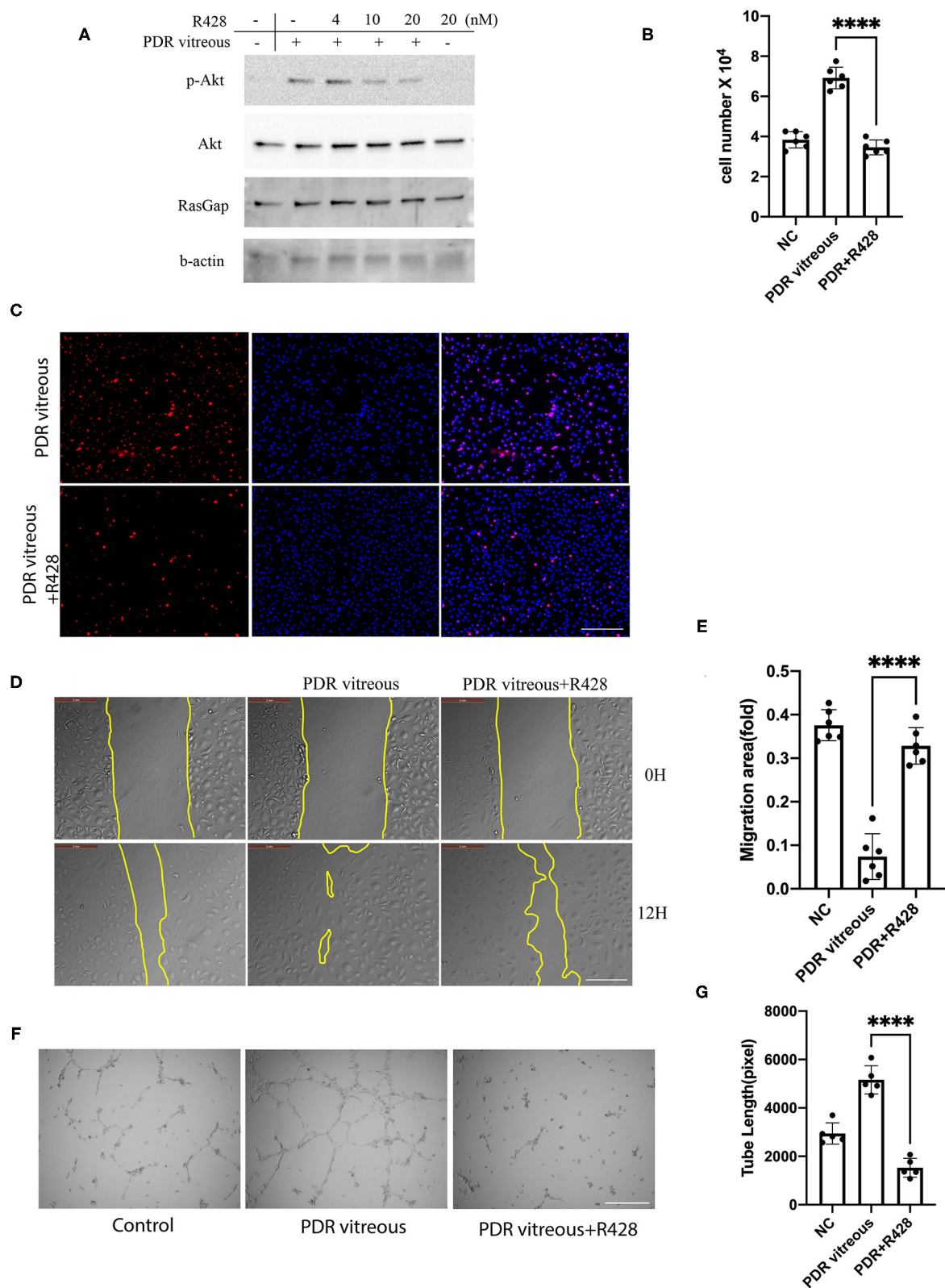


**FIGURE 4 |** Pharmacological inhibition of Axl blunted PDR vitreous-induced Akt activation, proliferation, migration, and tube formation. **(A)** Western blot analysis of p-Akt in HRECs treated with PDR vitreous and a serial of R428 (an Axl-specific inhibitor) concentrations using indicated antibodies. This is representative of three independent experiments. **(B,C)** Proliferation of HRECs induced with PDR vitreous supplemented with R428 (4  $\mu$ M) was evaluated by counting cell number **(B)** and *(Continued)*

**FIGURE 4 |** Ki67 staining, scale bar: 1,000  $\mu\text{m}$  (C). Bar graphs in (B) show the mean  $\pm$  SD from five independent experiments. (D,E) A wound healing assay of migration of HRECs induced by PDR vitreous supplemented with R428 (4  $\mu\text{M}$ ). (D) Representative of the photographed wound, scale bar: 400  $\mu\text{m}$ ; (E) Bar graphs show the mean  $\pm$  SD from five representative figures. (F,G) A matrigel assay of HRECs induced by PDR vitreous supplemented with R428 (4  $\mu\text{M}$ ). (F) Representative photos, scale bar: 400  $\mu\text{m}$ ; (G) Bar graphs of tube lengths in five representative photos of three independent experiments. \*\*\*\* means the difference was significant and  $p < 0.0001$ .

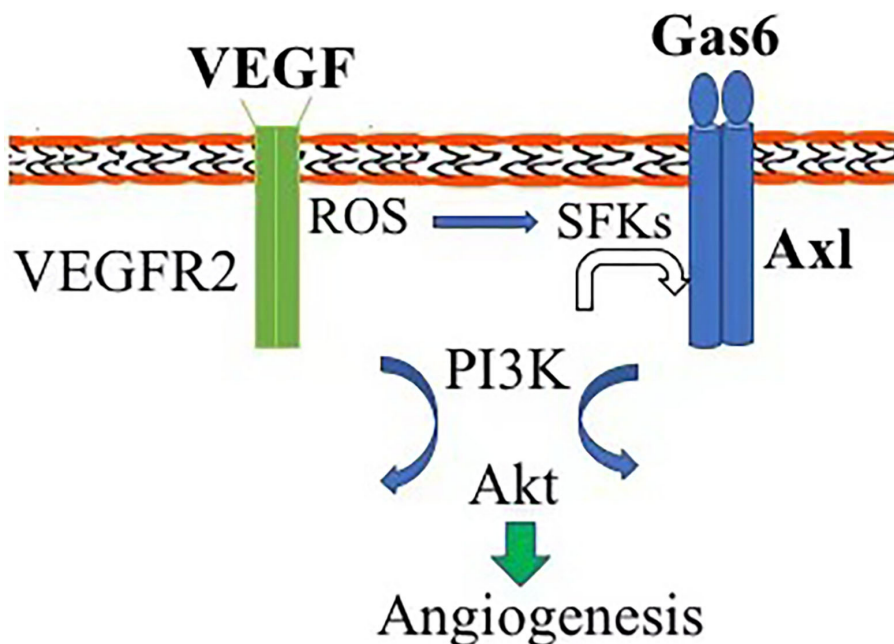


**FIGURE 5 |** Diagram of Axl contribution to angiogenesis. Axl can be activated by Gas6 direct binding and vascular endothelial growth factor (VEGF) indirectly via reactive oxygen species (ROS)/Src-family protein tyrosine kinases, triggering the signaling pathway of PI3K/Akt and initiating pathological angiogenesis.

precoated with basement membrane extract (R&D Systems, Minneapolis, MN, US), which was from the storage at  $-80^{\circ}\text{C}$  and thawed overnight at ice. Cells were imaged 4–6 h after cell plating and tube formation was quantified for the total length using the Angiogenesis Analyzer plugin for the ImageJ software (National Institutes of Health) (20).

### Statistical Analysis

Results are presented as mean  $\pm$  SD. The Student's *t*-test was performed for comparisons between two groups and the one-way ANOVA (Kruskal–Wallis test) was used for comparisons among the multiple groups.  $p < 0.05$  was considered as statistically significant.

### DATA AVAILABILITY STATEMENT

The original contributions presented in the study are included in the article/Supplementary Material, further inquiries can be directed to the corresponding author/s.

### ETHICS STATEMENT

The studies involving human participants were reviewed and approved by Xiangya Hospital, Central South University. The

patients/participants provided their written informed consent to participate in this study.

### AUTHOR CONTRIBUTIONS

WW performed the study and wrote the manuscript. HX provided patient-derived vitreous and PDR membrane. ZM and JZ contributed to the quantification of the experiment data. SX, XX, and HL analyzed the data and revised the manuscript. All authors contributed to the article and approved the submitted version.

### FUNDING

This study was supported by the grant National Natural Science Foundation of China (grant nos. 81900893 to WW, 81974137 to SX, 81974134 to XX, 82070989 to HL, and 82002373 to JZ), the Science and Technology Plan Project of Hunan Province (grant no. 2019RS2011) to WW, the Youth Science Foundation of Xiangya Hospital (grant no. 2019Q19 to JZ), and the Natural Science Foundation of Hunan Province (grant nos. 2021JJ41030 to WW, 2020JJ5958 to JZ, and 2019JJ40507 to SX).



## ACKNOWLEDGMENTS

We thank the Department of Central Laboratory (Xiangya Hospital) and the Laboratory of Medical Genetics (Central South University) for supporting this study.

## REFERENCES

- Gariano RF, Gardner TW. Retinal angiogenesis in development and disease. *Nature*. (2005) 438:960–6. doi: 10.1038/nature04482
- Zhu C, Wei Y, Wei X. Axl receptor tyrosine kinase as a promising anti-cancer approach: functions, molecular mechanisms and clinical applications. *Mol Cancer*. (2019) 18:153. doi: 10.1186/s12943-019-1090-3
- Ruan GX, Kazlauskas A. Axl is essential for VEGF-A-dependent activation of PI3K/Akt. *EMBO J*. (2012) 31:1692–703. doi: 10.1038/emboj.2012.21
- Lee HJ, Pham PC, Pei H, Lim B, Hyun SY, Baek B, et al. Development of the phenylpyrazolo[3,4-d]pyrimidine-based, insulin-like growth factor receptor/Src/AXL-targeting small molecule kinase inhibitor. *Theranostics*. (2021) 11:1918–36. doi: 10.7150/thno.48865
- Humtsoe JO, Kim HS, Leonard B, Ling S, Keam B, Marchionni L, et al. Newly identified members of FGFR1 splice variants engage in cross-talk with AXL/AKT axis in salivary adenoid cystic carcinoma. *Cancer Res*. (2021) 81:1001–13. doi: 10.1158/0008-5472.CAN-20-1780
- Wu W, Xia X, Tang L, Yao F, Xu H, Lei H, et al. Normal vitreous promotes angiogenesis via activation of Axl. *Faseb J*. (2021) 35:e21152. doi: 10.1096/fj.201903105R
- Franke TF, Kaplan DR, Cantley LC, Toker A. Direct regulation of the Akt proto-oncogene product by phosphatidylinositol-3,4-bisphosphate. *Science*. (1997) 275:665–8. doi: 10.1126/science.275.5300.665
- Sarbassov DD, Guertin DA, Ali SM, Sabatini DM. Phosphorylation and regulation of Akt/PKB by the rictor-mTOR complex. *Science*. (2005) 307:1098–101. doi: 10.1126/science.1106148
- Chen J, Somanath PR, Razorenova O, Chen WS, Hay N, Bornstein P, et al. Akt1 regulates pathological angiogenesis, vascular maturation and permeability *in vivo*. *Nat Med*. (2005) 11:1188–96. doi: 10.1038/nm1307
- Wu W, Duan Y, Ma G, Zhou G, Park-Windhol C, D'Amore PA, et al. AAV-CRISPR/Cas9-mediated depletion of VEGFR2 blocks angiogenesis *in vitro*. *Invest Ophthalmol Vis Sci*. (2017) 58:6082–90. doi: 10.1167/iovs.17-21902
- Aiello LP, Avery RL, Arrigg PG, Keyt BA, Jampel HD, Shah ST, et al. Vascular endothelial growth factor in ocular fluid of patients with diabetic retinopathy and other retinal disorders. *N Engl J Med*. (1994) 331:1480–7. doi: 10.1056/NEJM199412013312203
- Lei H, Qian CX, Lei J, Haddock LJ, Mukai S, Kazlauskas A, et al. RasGAP promotes autophagy and thereby suppresses platelet-derived growth factor receptor-mediated signaling events, cellular responses, and pathology. *Mol Cell Biol*. (2015) 35:1673–85. doi: 10.1128/MCB.01248-14
- Swiech L, Heidenreich M, Banerjee A, Habib N, Li Y, Trombetta J, et al. *In vivo* interrogation of gene function in the mammalian brain using CRISPR-Cas9. *Nat Biotechnol*. (2015) 33:102–6. doi: 10.1038/nbt.3055
- Yang Y, Wu W, Liu T, Dong L, Lei H. A robust method for protein depletion based on gene editing. *Methods*. (2021) 194:3–11. doi: 10.1016/j.jymeth.2021.03.001
- Lei H, Kazlauskas A. Growth factors outside of the PDGF family employ ROS/SFKs to activate PDGF receptor alpha and thereby promote proliferation and survival of cells. *J Biol Chem*. (2009) 284:6329–36. doi: 10.1074/jbc.M808426200
- Lei H, Velez G, Cui J, Samad A, Maberley D, Matsubara J, et al. N-acetylcysteine suppresses retinal detachment in an experimental model of proliferative vitreoretinopathy. *Am J Pathol*. (2010) 177:132–40. doi: 10.2353/ajpath.2010.090604
- Hitchcock CL. Ki-67 staining as a means to simplify analysis of tumor cell proliferation. *Am J Clin Pathol*. (1991) 96:444–6. doi: 10.1093/ajcp/96.4.444
- Liang CC, Park AY, Guan JL. *In vitro* scratch assay: a convenient and inexpensive method for analysis of cell migration *in vitro*. *Nat Protoc*. (2007) 2:329–33. doi: 10.1038/nprot.2007.30
- Lam JD, Oh DJ, Wong LL, Amarnani D, Park-Windhol C, Sanchez AV, et al. Identification of RUNX1 as a mediator of aberrant retinal angiogenesis. *Diabetes*. (2017) 66:1950–6. doi: 10.2337/db16-1035
- Arnautova I, Kleinman HK. *In vitro* angiogenesis: endothelial cell tube formation on gelled basement membrane extract. *Nat Protoc*. (2010) 5:628–35. doi: 10.1038/nprot.2010.6

**Conflict of Interest:** The authors declare that the research was conducted in the absence of any commercial or financial relationships that could be construed as a potential conflict of interest.

**Publisher's Note:** All claims expressed in this article are solely those of the authors and do not necessarily represent those of their affiliated organizations, or those of the publisher, the editors and the reviewers. Any product that may be evaluated in this article, or claim that may be made by its manufacturer, is not guaranteed or endorsed by the publisher.

Copyright © 2021 Wu, Xu, Meng, Zhu, Xiong, Xia and Lei. This is an open-access article distributed under the terms of the Creative Commons Attribution License (CC BY). The use, distribution or reproduction in other forums is permitted, provided the original author(s) and the copyright owner(s) are credited and that the original publication in this journal is cited, in accordance with accepted academic practice. No use, distribution or reproduction is permitted which does not comply with these terms.

## SUPPLEMENTARY MATERIAL

The Supplementary Material for this article can be found online at: <https://www.frontiersin.org/articles/10.3389/fmed.2021.787150/full#supplementary-material>





## OPEN ACCESS

**Approved by:**  
Frontiers Editorial Office,  
Frontiers Media SA, Switzerland

**\*Correspondence:**  
Frontiers Production Office  
production.office@frontiersin.org

**Specialty section:**  
This article was submitted to  
Ophthalmology,  
a section of the journal  
Frontiers in Medicine

**Received:** 18 January 2022

**Accepted:** 18 January 2022

**Published:** 07 February 2022

**Citation:**  
Frontiers Production Office (2022)  
Erratum: Axl Is Essential for *in-vitro*  
Angiogenesis Induced by Vitreous  
From Patients With Proliferative  
Diabetic Retinopathy.  
*Front. Med.* 9:857417.  
doi: 10.3389/fmed.2022.857417

# Erratum: Axl Is Essential for *in-vitro* Angiogenesis Induced by Vitreous From Patients With Proliferative Diabetic Retinopathy

**Frontiers Production Office\***

Frontiers Media SA, Lausanne, Switzerland

**Keywords:** PDR vitreous, GAS6, Axl, CRISPR/Cas9, R428, HRECs

## An Erratum on

**Axl Is Essential for *in-vitro* Angiogenesis Induced by Vitreous From Patients With Proliferative Diabetic Retinopathy**

by Wu, W., Xu, H., Meng, Z., Zhu, J., Xiong, S., Xia, X., and Lei, H. (2021). *Front. Med.* 8:787150.  
doi: 10.3389/fmed.2021.787150

Due to a production error, there was an error in affiliations 1 and 4. Instead of “The Second Xiangya Hospital of Central South University,” it should be “Xiangya Hospital of Central South University.” The publisher apologizes for this mistake. The original version of this article has been updated.

Copyright © 2022 Frontiers Production Office. This is an open-access article distributed under the terms of the Creative Commons Attribution License (CC BY). The use, distribution or reproduction in other forums is permitted, provided the original author(s) and the copyright owner(s) are credited and that the original publication in this journal is cited, in accordance with accepted academic practice. No use, distribution or reproduction is permitted which does not comply with these terms.



# Serum Sodium Concentration and Increased Risk for Primary Epiretinal Membrane

Can Can Xue<sup>1,2†</sup>, Jing Cui<sup>3†</sup>, Xiao Bo Zhu<sup>4</sup>, Jie Xu<sup>2</sup>, Chun Zhang<sup>1\*</sup>, Dong Ning Chen<sup>3\*</sup>,  
Ya Xing Wang<sup>2\*</sup> and Jost B. Jonas<sup>2,5,6,7</sup>

<sup>1</sup> Department of Ophthalmology, Peking University Third Hospital, Beijing, China, <sup>2</sup> Beijing Ophthalmology and Visual Sciences Key Laboratory, Beijing Institute of Ophthalmology, Beijing Tongren Hospital, Capital Medical University, Beijing, China, <sup>3</sup> Department of Physical Examination, Beijing Tongren Hospital, Capital Medical University, Beijing, China, <sup>4</sup> Department of Ophthalmology, Dongfang Hospital, Beijing University of Chinese Medicine, Beijing, China, <sup>5</sup> Medical Faculty Mannheim, Department of Ophthalmology, Heidelberg University, Mannheim, Germany, <sup>6</sup> Institute of Clinical and Scientific Ophthalmology and Acupuncture Jonas & Panda, Heidelberg, Germany, <sup>7</sup> Institute of Molecular and Clinical Ophthalmology, Basel, Switzerland

## OPEN ACCESS

### Edited by:

Shaochong Zhang,  
Sun Yat-sen University, China

### Reviewed by:

Yi-Ting Hsieh,  
National Taiwan University  
Hospital, Taiwan  
Alessandro Meduri,  
University of Messina, Italy

### \*Correspondence:

Ya Xing Wang  
yaxingw@gmail.com  
Dong Ning Chen  
tr13501082964@163.com  
Chun Zhang  
zhangc1@yahoo.com

<sup>†</sup>These authors have contributed  
equally to this work and share first  
authorship

### Specialty section:

This article was submitted to  
Ophthalmology,  
a section of the journal  
Frontiers in Medicine

**Received:** 03 September 2021

**Accepted:** 02 December 2021

**Published:** 24 December 2021

### Citation:

Xue CC, Cui J, Zhu XB, Xu J,  
Zhang C, Chen DN, Wang YX and  
Jonas JB (2021) Serum Sodium  
Concentration and Increased Risk for  
Primary Epiretinal Membrane.  
Front. Med. 8:770362.  
doi: 10.3389/fmed.2021.770362

**Aims:** To examine the prevalence of primary epiretinal membranes (ERMs) and associated systemic factors.

**Methods:** The cross-sectional, community-based Tongren Health Care Study enrolled participants who received regular health examinations in the Beijing Tongren Hospital from 2017 to 2019. Using fundus photographs, retinal specialists assessed the presence of ERMs and their systemic associations.

**Results:** Primary ERMs were detected in 841/22820 individuals, with a prevalence of 3.7% [95% confidence intervals (CI): 3.4–3.9%] in the total study population (mean age: 44.5 ± 13.8 years) and 6.5% (95% CI: 6.1–7.0%) in individuals aged 40+ years. In multivariable analysis, a higher ERMs prevalence was associated with older age [odds ratio (OR): 1.10;  $P < 0.001$ ], higher serum cholesterol concentration (OR: 1.14;  $P = 0.003$ ) and higher serum sodium concentration (SSC) (OR: 1.12;  $P < 0.001$ ). In women, a higher SSC, even within the normal range, was associated with an increased risk of ERMs (OR: 1.19;  $P < 0.001$ ). Female participants with an SSC of 144–145 mmol/L as compared with those with an SSC of 135–137 mmol/L had a 5-fold increased odds of having ERMs (All women: OR: 5.33;  $P < 0.001$ ; Women aged 40+ years: OR: 4.63;  $P < 0.001$ ).

**Conclusion:** Besides older age and higher serum cholesterol concentration, a higher SSC, even if within the normal range, was independently associated with a higher ERM prevalence in women.

**Keywords:** epiretinal membrane, associated factors, serum sodium, prevalence, epidemiology

## INTRODUCTION

Epiretinal membranes (ERMs) are a common cause of visual impairment in the elderly population (1–5), with the pooled prevalence from population-based studies to be 9.7% (6). While intraocular causes including retinal diseases, previous intraocular surgeries, hyperopia, or myopia were reported to be associated with secondary ERMs, to mention a few (1, 3, 5, 7, 8), idiopathic ERMs

present in eyes without evident abnormality, and their causes remain to be elusive (9). Systemic factors associated with the presence of ERMs were older age, female sex, ethnic background, hyperlipidemia, smoking, diabetes mellitus, and a lower serum concentration of uric acid (1, 3, 4, 7, 10, 11), however, none of the above-mentioned factors were consistently reported besides the increasing age.

Most ERMs remain relatively stable and treatment is not required, while vitrectomy surgery is indicated for ERMs patients associated with symptoms that severely affect their activities of daily living, including decreased visual acuity, metamorphopsia, double vision, or difficulty using their eyes together (2, 12). Of particular note is that even a very successful vitrectomy does not always ensure a desirable visual outcome (2). Our knowledge on the pathophysiology of ERM has been improved greatly by histopathological studies and advanced image technologies, however, there're no preventive measures since the exact pathological mechanisms of ERMs remain unknown.

The current community-based large-scale study was conducted in 20,000+ participants with comprehensive general medical examinations, with the aim to explore systemic factors associated with the primary ERMs.

## METHODS

The cross-sectional, community-based Tongren Health Care Study included individuals who attended regular health care check-up examinations in the Beijing Tongren Hospital from July 2017 to December 2019. The study population has been described in detail recently (13). The eligibility criterion for inclusion into the current study was an age of 18+ years. The study was conducted in adherence to the Declaration of Helsinki and approved by the Medical Ethics Committee of Beijing Tongren Hospital.

The examinations included an interview in which general demographic data and information about the medical history and other health-related events were obtained. The physical examinations included the assessment of anthropometric parameters such as body height and weight and circumferences of the waist and hip, measurement of blood pressure and electrocardiography, and biochemical examinations of samples of blood. Arterial hypertension was defined as a systolic blood pressure of 140 mmHg or more, a diastolic blood pressure of 90 mmHg or more, or a physician's-based diagnosis of hypertension or use of antihypertensive medication. Diabetes mellitus was defined based on the history of a previously diagnosed diabetes or receiving a glucose-lowering therapy and/or fasting blood glucose concentration of  $\geq 7.0$  mmol/L. The estimated glomerular filtration rate (eGFR) was calculated based on the serum creatinine concentration and using the Chronic Kidney Disease Epidemiology Collaboration equation (14).

The ophthalmological examinations, performed by experienced ophthalmologists, consisted of the measurement of best-corrected visual acuity, non-contact tonometry, slit

lamp-based biomorphometry of the anterior and posterior segment of the eye, and 45° non-mydratic fundus photography (Topcon TRG-NW7SE, Topcon, Tokyo, Japan; or Cannon, CR6-45NM, Canon, Tokyo, Japan). Based on the assessment of the fundus photographs, an ERM was classified into either a less severe subtype termed as cellophane macular reflex (CMR) or a more severe form termed as preretinal macular fibrosis (PMF) (3, 15). Eyes with the coexistence of CMR and PMF were classified as having PMF. A secondary ERM was defined as being associated with intraocular diseases including diabetic retinopathy, late-stage age-related macular degeneration, other retinopathy, and previous intraocular surgery including cataract surgery or vitreous retinal surgery (3). All ERMs without any associated intraocular disorder were classified as primary ERMs.

The data were analyzed using the statistical software SPSS 26.0 (SPSS Inc., Chicago, IL, USA) and the Statistical Package for the R (version 1.4.1103). Continuous variables were presented as mean  $\pm$  standard deviation and categorical variables as the number of cases/percentages. In the univariable analysis, a binary logistic regression analysis was performed to assess associations between the ERM prevalence and other systemic parameters, without and with adjustment for age, the odds ratios (ORs) and their 95% confidence intervals (CI) were calculated. The multivariable analysis was then performed with the ERM prevalence as the dependent variable, and all those parameters with  $P$ -values  $\leq 0.10$  in the age-adjusted analysis as the independent variables, in all participants, in men and in women, respectively. The collinearity was considered when a variance inflation factor (VIF) of more than 5 was observed. After detecting the association between serum sodium concentration (SSC) and ERM, we re-assessed our findings by excluding individuals with hyponatremia (SSC  $> 145$  mmol/L) and hypernatremia (SSC  $< 135$  mmol/L) to eliminate their confounding effects. We compared the SSCs among different age groups in the whole participants, in men and women respectively, using one-way analysis of variance (ANOVA) and adjusted by Bonferroni when a significant difference was detected. We stratified the SSC into four groups (135.0–137.0, 138.0–140.0, 141.0–143.0, and 144.0–145.0 mmol/L) and assessed its association with the ERM prevalence. A three-dimensional surface plot was created to visualize the associations among age, SSC, and the presence of ERM for women aged 40+ years, as most epidemiologic studies included individuals aged 40+ years old. A two-tailed  $P$ -value of  $< 0.05$  was considered statistically significant.

## RESULTS

Out of 22,945 individuals (12,574 men, 54.8%) who were examined during the study period, 125 (0.54%) participants were excluded due to unreadable fundus photographs. The study eventually included 22,820 participants (12,514 women, 54.8%) with a mean age of  $44.5 \pm 13.8$  years (range: 18–97 years). The mean uncorrected visual acuity, best-corrected visual acuity, and intraocular pressure were  $0.40 \pm 0.40$  logarithm of the minimal angle of resolution (logMAR),  $0.04 \pm 0.10$  logMAR, and  $14.3 \pm 3.0$  mmHg, respectively.

**Abbreviations:** ERM, epiretinal membrane; SSC, serum sodium concentration; CMR, cellophane macular reflex; PMF, pre-macular fibrosis.

## Prevalence of Epiretinal Membranes

ERMs were found in 988 participants ( $4.3 \pm 0.1\%$ ; 95% CI: 4.1–4.6%), among whom 147 subjects ( $0.6 \pm 0.1\%$ ; 95% CI: 0.5–0.7%) with diabetic retinopathy (19/12.9%), retinal vascular diseases (7/4.8%), late-stage age-related macular degeneration (6/4.1%), other types of retinopathies (20/13.6%), history or signs of vitreous or retinal surgery (7/4.7%), and previous cataract surgery (88/59.9%) were classified as secondary ERMs and were excluded.

Primary ERMs (described as “ERMs” in the following paragraphs) were detected in 841 [345 (41.0%) men] out of the 22,820 individuals, with a prevalence of  $3.7 \pm 0.1\%$  (95% CI: 3.4–3.9%). Unilateral ERMs and bilateral ERMs were found in 618 participants (73.5%) and 223 subjects (26.5%), respectively. For individuals aged 40+ years, the prevalence of ERMs was  $6.5 \pm 0.2\%$  (95% CI: 6.1–7.0%),  $5.8 \pm 0.3\%$  (95% CI: 5.2–6.4%), and  $7.2 \pm 0.3\%$  (95% CI: 6.6–7.9%) for all individuals, for men, and for women, respectively (Table 1).

**TABLE 1** | Prevalence of primary epiretinal membranes (ERMs) in all, in men and in women.

Age group (years)	All		Men		Women	
	<i>n</i>	%	<i>n</i>	%	<i>n</i>	%
<40	17/10,196	0.2 (0.1, 0.3)	7/4,453	0.2 (0.05, 0.3)	10/5,743	0.2 (0.1, 0.3)
40–49	40/4,805	0.8 (0.6, 1.1)	17/2,242	0.8 (0.4, 1.1)	23/2,563	0.9 (0.5, 1.3)
50–59	221/4,118	5.4 (4.7, 6.1)	85/1,933	4.4 (3.6, 5.4)	136/2,185	6.2 (5.2, 7.5)
60–69	436/2,736	15.9 (14.7, 17.7)	170/1,239	13.7 (11.9, 16.3)	266/1,497	17.8 (16.0, 20.5)
70+	127/965	13.2 (11.3, 16.0)	66/439	15.0 (11.8, 21.5)	61/526	11.6 (9.1, 15.5)
Total	841/22,820	3.7 (3.4, 3.9)	345/10,306	3.3 (3.0, 3.7)	496/12,514	4.0 (3.6, 4.3)

The prevalence of primary ERMs is shown as the number of patients / all study participants and mean (95% confidence interval).

**TABLE 2** | Factors associated with primary epiretinal membranes (ERMs) by univariable logistic analysis and age-adjusted logistic analysis.

	No-ERMs	Primary ERMs	Univariable analysis		Age-adjusted analysis	
	<i>N</i> = 21,832	<i>N</i> = 841	<i>P</i> -value	OR (95%CI)	<i>P</i> -value	OR (95%CI)
Age (year)	43.6 ± 13.3	62.4 ± 8.7	<0.001	1.10 (1.09, 1.11)		
Women ( <i>n</i> /%)	11,940/54.7	496/59.0	0.014	1.19 (1.04, 1.37)	0.002	1.26 (1.09, 1.46)
Body mass index (kg/m <sup>2</sup> )	23.9 ± 3.7	24.3 ± 3.1	0.001	1.03 (1.01, 1.05)	0.552	0.99 (0.97, 1.02)
Waist-hip circumference ratio	0.85 ± 0.11	0.88 ± 0.07	<0.001	16.12 (6.28, 41.35)	0.037	0.31 (0.10, 0.93)
Heart rate	74.8 ± 10.0	74.2 ± 10.0	0.098	0.99 (0.99, 1.001)	0.363	0.99 (0.99, 1.00)
Systolic blood pressure (mmHg)	126.8 ± 17.9	137.4 ± 19.8	<0.001	1.03 (1.025, 1.03)	0.088	0.99 (0.99, 1.00)
Diastolic blood pressure (mmHg)	76.6 ± 11.1	79.0 ± 10.8	<0.001	1.02 (1.01, 1.02)	0.564	1.002 (0.99, 1.01)
Sodium (mmol/L)	139.6 ± 2.1	140.4 ± 1.9	<0.001	1.24 (1.19, 1.29)	<0.001	1.12 (1.07, 1.16)
Potassium (mmol/L)	4.18 ± 0.30	4.21 ± 0.31	0.001	1.50 (1.19, 1.91)	0.243	0.87 (0.68, 1.10)
Calcium (mmol/L)	2.34 ± 0.09	2.33 ± 0.09	0.009	0.34 (0.15, 0.76)	0.951	1.03 (0.44, 2.38)
Phosphate (mmol/L)	1.13 ± 0.15	1.12 ± 0.15	0.030	0.59 (0.36, 0.95)	0.174	1.42 (0.86, 2.34)
Blood urea nitrogen (mmol/L)	4.73 ± 1.27	5.16 ± 1.29	<0.001	1.23 (1.18, 1.29)	0.011	0.93 (0.88, 0.98)
Uric acid (μmol/L)	328.6 ± 87.0	324.4 ± 81.0	0.164	0.99 (0.99, 1.00)	0.004	0.99 (0.99, 0.99)
Estimated glomerular filtration rate (ml/min/1.73 m <sup>2</sup> )	102.8 ± 14.8	88.4 ± 13.0	<0.001	0.95 (0.94, 0.95)	0.047	1.005 (1.001, 1.01)
Blood glucose (mmol/L)	5.34 ± 1.26	5.70 ± 1.29	<0.001	1.15 (1.11, 1.19)	0.042	0.94 (0.89, 0.99)
High sensitive C-reactive peptide (mg/L)	1.44 ± 3.14	1.77 ± 4.83	0.006	1.02 (1.006, 1.04)	0.662	0.99 (0.97, 1.02)
Lipoprotein a (mg/L)	19.6 ± 22.1	23.5 ± 24.4	<0.001	1.007 (1.004, 1.01)	0.057	1.00 (1.00, 1.01)
Triglyceride (mmol/L)	1.36 ± 1.20	1.50 ± 1.12	0.001	1.07 (1.03, 1.12)	0.479	1.02 (0.96, 1.09)
Total cholesterol (mmol/L)	4.89 ± 0.94	5.15 ± 0.97	<0.001	1.29 (1.21, 1.38)	<0.001	1.14 (1.07, 1.23)
Low density lipoprotein (mmol/L)	2.89 ± 0.78	3.08 ± 0.83	0.000	1.31 (1.21, 1.42)	0.001	1.16 (1.07, 1.26)
High density lipoprotein (mmol/L)	1.45 ± 0.40	1.48 ± 0.41	0.112	1.15 (0.97, 1.36)	0.070	1.18 (0.99, 1.40)
Arterial hypertension ( <i>n</i> /%)	1,117/5.2	121/14.5	<0.001	3.11 (2.54, 3.81)	0.189	0.86 (0.69, 1.08)
Diabetes mellitus ( <i>n</i> /%)	1,858/8.5	142/16.9	<0.001	2.19 (1.82, 2.64)	0.033	0.81 (0.66, 0.98)

Data are presented as mean ± standard deviation for continuous variables, and as the number of cases/percentages for categorical variables, respectively.

OR, odds ratio; CI, confidence interval.

All variables in the univariable analysis were further adjusted by age.

Two-tailed values of *P* < 0.05 were considered statistically significant.



**TABLE 3 |** Risk factors associated with primary epiretinal membranes by multivariable analysis.

	All		Men		Women	
	P-value	OR (95% CI)	P-value	OR (95% CI)	P-value	OR (95% CI)
Age (year)	<0.001	1.10 (1.10, 1.11)	<0.001	1.11 (1.10, 1.13)	<0.001	1.11 (1.09, 1.13)
Women (%)	0.341	1.10 (0.91, 1.33)	/	/	/	/
Waist-hip circumference ratio	0.737	0.86 (0.34, 2.14)	0.559	0.51 (0.05, 5.01)	0.638	1.67 (0.20, 14.16)
Systolic blood pressure (mmHg)	0.498	0.998 (0.993, 1.003)	0.530	1.002 (0.99, 1.01)	0.221	0.99 (0.99, 1.003)
Sodium (mmol/L)	<0.001	1.12 (1.07, 1.17)	0.369	1.04 (0.96, 1.12)	<0.001	1.18 (1.10, 1.27)
Blood urea nitrogen (mmol/L)	0.076	0.94 (0.88, 1.01)	0.684	0.98 (0.88, 1.08)	0.596	0.97 (0.88, 1.08)
Urine acid ( $\mu$ mol/L)	0.644	1.00 (0.998, 1.001)	0.227	1.001 (0.99, 1.003)	0.156	0.99 (0.99, 1.001)
Blood glucose (mmol/L)	0.256	0.96 (0.89, 1.03)	0.119	0.90 (0.79, 1.03)	0.644	1.03 (0.90, 1.19)
Lipoprotein a (mg/L)	0.880	1.00 (0.997, 1.004)	0.505	1.002 (0.99, 1.01)	0.788	0.99 (0.99, 1.004)
Total cholesterol (mmol/L)	0.003	1.14 (1.05, 1.24)	0.328	1.07 (0.93, 1.24)	0.031	1.15 (1.01, 1.30)
High density lipoprotein (mmol/L)	0.122	1.19 (0.96, 1.48)	0.590	0.89 (0.59, 1.36)	0.293	1.19 (0.86, 1.65)
Estimated glomerular filtration rate (ml/min/1.73m <sup>2</sup> )	0.050	1.01 (1.00, 1.02)	0.106	1.01 (0.99, 1.03)	0.721	1.002 (0.99, 1.02)
Diabetes mellitus (%)	0.977	1.01 (0.73, 1.40)	0.157	1.38 (0.88, 2.14)	0.159	0.70 (0.43, 1.15)

OR, odds ratio; CI, confidence interval; Low-density lipoprotein was not included as it shares the co-linearity with the total cholesterol (variance inflation factors > 5). Two-tailed values of  $P < 0.05$  were considered statistically significant.

## Serum Sodium Concentration as a Risk Factor for Epiretinal Membranes

In the univariable analysis, a higher ERM prevalence was associated with older age, female sex, higher prevalence of hypertension and diabetes, higher body mass index, waist-hip circumference ratio, systolic and diastolic blood pressure, SSC, higher serum concentrations of potassium, blood urea nitrogen, glucose, high sensitive C-reactive protein, lipoprotein a, triglycerides, total cholesterol, and low-density lipoprotein, and lower serum concentrations of calcium, phosphate and lower eGFR (all  $P \leq 0.05$ ) (Table 2). In the multivariable analysis, a higher ERM prevalence remained to be significantly associated with older age (OR: 1.10;  $P < 0.001$ ), higher SSC (OR: 1.12;  $P < 0.001$ ), higher total cholesterol (OR: 1.14;  $P = 0.003$ ), and borderline with eGFR (OR: 1.01;  $P = 0.05$ ) for all participants. A higher ERM prevalence was consistently associated with increasing age, in men and women, respectively, whereas its association with higher SSC and higher total cholesterol only remained statistically significant in women but not men (Table 3).

The mean SSC was  $139.6 \pm 2.1$  mmol/L (range: 120–150 mmol/L) measured in 21,054 participants, with 30 (0.1%) individuals with hypernatremia and 250 (1.2%) participants with hyponatremia. In individuals with normal SSC (135–145

mmol/L), a positive correlation between higher SSC and older age was found in women ( $r = 0.33$ ,  $P < 0.001$ , Pearson correlation analysis) but not in men ( $P = 0.35$ ). In women, SSC increased continuously from the age of 50 years to the age of 70 years (one-way ANOVA,  $P < 0.05$ ), after which it dropped slightly. The SSC did not differ significantly among the age groups in men (one-way ANOVA,  $P = 0.18$ ) (Table 4; Figure 1).

The association between SSC and ERM was modified by sex in the univariable analysis ( $P$  for interaction  $<0.001$ ). In multivariable analysis, the association between SSC and ERMs remained statistically significant in the whole study population and in women (both  $P < 0.001$ ), but not in men (both  $P > 0.05$ ) (Tables 3, 5). In women, the ERM prevalence significantly increased from 0.9% in the subgroup with SSC of 135–137 mmol/L, to 3.0% (SSC: 138–140 mmol/L), 7.1% (SSC: 141–143 mmol/L) and to 11.0% (SSC: 144–145 mmol/L) (linear-by-linear association chi-square test,  $X^2 = 160.04$ ,  $P < 0.001$ ). Female participants with an SSC of 144–145 mmol/L as compared with women with an SSC of 135–137 mmol/L had a 5.3-fold increased risk of ERMs (OR: 5.33;  $P < 0.001$ ) in the multivariable analysis (Figure 2; Table 6).

If only participants aged 40+ years were included, the SSC was again significantly ( $P < 0.001$ ) higher in women with primary ERMs ( $140.6 \pm 1.8$  mmol/L) as compared with women without ERMs ( $139.7 \pm 2.0$  mmol/L). Women with SSC of 144 mmol/L

**TABLE 4 |** Serum sodium concentration in the study population, stratified by age and sex (with serum sodium concentration within the normal range).

Age group (years)	All		Men		Women		P-value (men vs. women)
	n	Sodium (mmol/L)	n	Sodium (mmol/L)	n	Sodium (mmol/L)	
<40	9,949	139.4 ± 1.8	4,055	140.1 ± 1.7	5,394	138.8 ± 1.7	<0.001
40–49	4,268	139.4 ± 1.9	1,943	140.1 ± 1.8	2,325	138.8 ± 1.7	<0.001
50–59	3,666	140.2 ± 1.9*†	1,671	140.1 ± 1.9	1,995	140.3 ± 1.9*†	0.032
60–69	2,479	140.4 ± 1.9*†‡	1,133	140.1 ± 1.9	1,346	140.6 ± 1.8*†‡	<0.001
70+	912	140.1 ± 2.0*†#	423	139.9 ± 2.0	489	140.2 ± 2.0*†#	0.089
Total	20,774	139.7 ± 1.9	9,225	140.1 ± 1.8	11,549	139.3 ± 1.9	<0.001

The concentrations of serum sodium are displayed as mean ± standard deviation.

Serum sodium concentrations between the men and women were compared by independent t-test.

Serum sodium concentrations among different age groups were compared by one-way analysis of variance, and post hoc tests adjusted by Bonferroni were performed when a significant difference was detected.

Two-tailed values of  $P < 0.05$  were considered statistically significant.

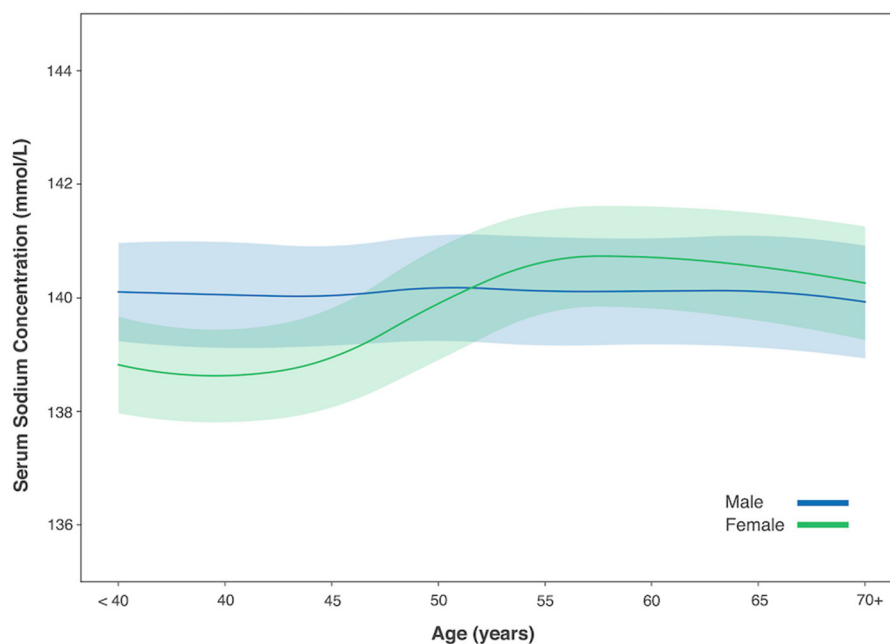
\*Compared with participants <40 years old,  $P < 0.05$ .

†Compared with participant age 40–49,  $P < 0.05$ .

‡Compare with participants aged 50–59,  $P < 0.05$ .

#Compared with participants aged 60–69,  $P < 0.05$ .

Note there was a decrease in sodium level in people aging 70+ years.

**FIGURE 1 |** Serum sodium concentration with age in male and female gender. Figure was shown with mean value (solid line) and 1/2 standard deviation (shadow).

to 145 mmol/L as compared to women with an SSC of 135–137 mmol/L had 4.6-folds increased risk of ERM (OR: 4.63; 95% CI: 2.10–10.21;  $P < 0.001$ ) (Figure 3).

In a next step, all female patients with ERM were compared with 1:1 age-matched female controls, for a sensitivity analysis. A significant higher SSC was found in ERM patients ( $n = 436$ , age:  $62.0 \pm 8.4$  years, SSC:  $140.6 \pm 1.8$  mmol/L) in comparing with age-matched controls ( $n = 436$ , age:  $62.0 \pm 8.5$  years, SSC:  $137.5 \pm 1.3$  mmol/L)

after multivariable analysis (OR: 6.39; 95% CI: 4.61–8.88;  $P < 0.001$ ).

When comparing the subtypes of ERM, female participants with PMFs as compared to those with CMR also show a slightly but significantly higher SSC ( $140.8 \pm 1.8$  vs.  $140.3 \pm 2.0$  mmol/L;  $P = 0.01$ ).

Inter-observer agreement was assessed by examining the photographs of 100 participants by both examiners (CCX, XBZ), with a kappa value of 0.851 ( $P < 0.001$ ).

**TABLE 5 |** Serum sodium concentration in study participants with vs. without primary epiretinal membranes (ERMs) (with serum sodium concentration within the normal range).

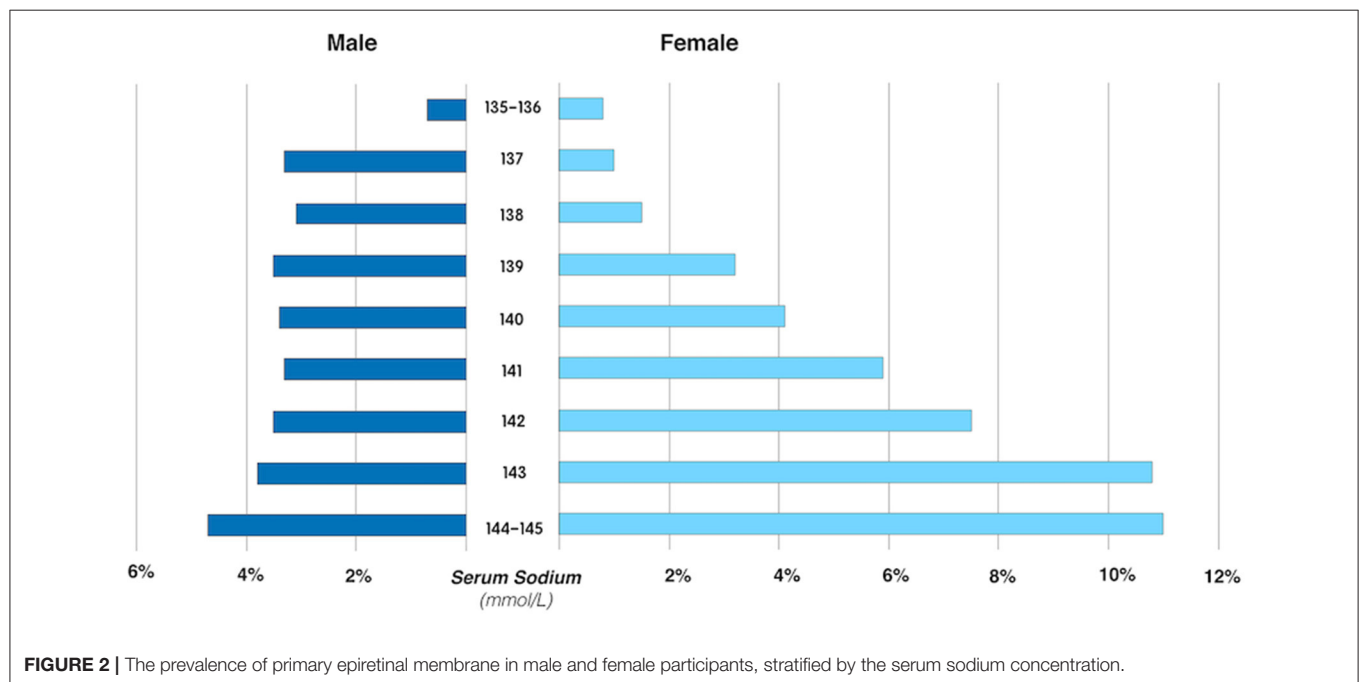
	All	Primary ERMs	No ERMs	Crude analysis		Age-adjusted analysis		Multivariable analysis*	
				P-value	OR (95%CI)	P-value	OR (95%CI)	P-value	OR (95%CI)
Men	140.1 ± 1.8 (9,105)	140.3 ± 1.8 (306)	140.1 ± 1.8 (8,799)	0.07	1.06 (0.99, 1.13)	0.026	1.08 (1.01, 1.15)	0.364	1.04 (0.96, 1.13)
Women	139.3 ± 1.9 (11,422)	140.6 ± 1.8 (436)	139.3 ± 1.9 (10,986)	<0.001	1.41 (1.34, 1.49)	<0.001	1.15 (1.09, 1.21)	<0.001	1.19 (1.11, 1.28)
All	139.7 ± 1.9 (20,527)	140.5 ± 1.8 (742)	139.6 ± 1.9 (19,785)	<0.001	1.25 (1.21, 1.30)	<0.001	1.12 (1.07, 1.16)	<0.001	1.12 (1.07, 1.18)

\*Adjusted by age, waist-hip circumference ratio, blood urea nitrogen, urine acid, estimated glomerular filtration rate, glucose, lipoprotein a, total cholesterol and high-density lipoprotein as continuous variables, and the presence of diabetes mellitus and sex (except in sex-specific analysis) as binary variables.

OR, odds ratio; CI, confidence interval.

The concentrations of serum sodium are presented as mean ± standard deviation (number of individuals).

Two-tailed values of  $P < 0.05$  were considered statistically significant.

**FIGURE 2 |** The prevalence of primary epiretinal membrane in male and female participants, stratified by the serum sodium concentration.

## DISCUSSION

The prevalence of primary ERMs in our study population was 3.7% and increased with older age. Factors associated with a higher ERM prevalence were, besides older age, a higher serum concentration of total cholesterol and a higher SSC. If the study population was stratified by sex, the correlation between a higher SSC, even within the normal range, with a higher ERM prevalence, was valid for women but not for men. Women with an SSC of 144–145 mmol/L as compared with those with an SSC of 135–137 mmol/L had a 5.3-fold increased odds of having an ERM for the whole age group, and 4.6-fold increased odds of having an ERM for those aged 40+ years.

The prevalence of primary ERMs as found in our study population was higher than the ERM frequency observed in other

Asian populations (4, 5, 7, 16), but was very comparable to the pooled data of a recent meta-analysis (6).

Increasing age is a well-established risk factor for ERM development, as consistently reported by previous population-based studies and ours (1, 5, 17–19). One may discuss that vitreoretinal interface changes caused by a posterior vitreous detachment may be causally associated with the age-related increase of the ERM prevalence.

The association between female gender and higher ERM prevalence was inconsistently reported. While in a recent meta-analysis pooled 13 studies with 49,696 participants, female individuals tended to have a higher ERM prevalence than men with an OR of 1.34 (6), many investigations as well as ours did not find a sex-specific difference in the ERM prevalence (5, 7, 20, 21). The discrepancies in the association between sex

**TABLE 6 |** Association between the prevalence of primary epiretinal membranes (ERMs) and the serum sodium concentration by multivariable analysis, stratified by sex.

Sodium Level (mmol/L)	Total (n = 20,661)			Women (n = 11,494)			Men (n = 9,167)		
	N	ERMs (%)	OR (95% CI)*	n	ERM (%)	OR (95% CI)*	n	ERM (%)	OR (95% CI)*
135–137	2,678	1.3 ± 0.2	Reference	1,957	0.9 ± 0.2	Reference	721	2.4 ± 0.6	Reference
138–140	11,101	3.1 ± 0.2	2.29 (1.52, 3.46)	6,495	3.0 ± 0.2	2.76 (1.51, 5.01)	4,606	3.3 ± 0.3	1.69 (0.92, 3.09)
141–143	6,439	5.0 ± 0.3	2.478 (1.64, 3.75)	2,833	7.1 ± 0.5	3.45 (1.85, 6.44)	3,606	3.4 ± 0.3	1.52 (0.80, 2.89)
144–145	443	7.7 ± 1.5	3.44 (1.99, 5.95)	209	11.0 ± 2.2	5.33 (2.41, 11.79)	234	4.7 ± 1.7	1.75 (0.70, 4.39)
P-value			<0.001			<0.001			0.363

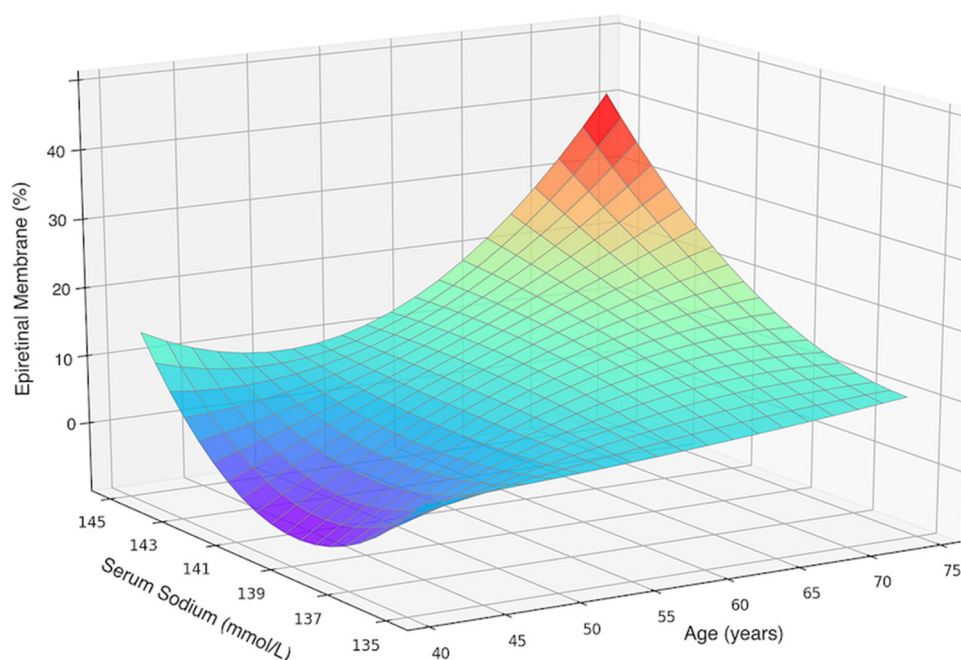
\*Adjusted by age, waist-hip circumference ratio, blood urea nitrogen, urine acid, estimated glomerular filtration rate, glucose, lipoprotein a, total cholesterol and high-density lipoprotein as continuous variables, the presence of diabetes mellitus and sex (except in sex-specific analysis) as binary variables.

OR, odds ratio; CI, confidence interval.

The prevalence rate of primary ERMs displayed as mean ± standard error.

Two-tailed values of  $P < 0.05$  were considered statistically significant.

A significantly linear association between higher SCC and the ERMs prevalence was detected in women (linear-by-linear association chi-square test,  $\chi^2 = 160.04$ ,  $P < 0.001$ ), but not in men ( $\chi^2 = 2.238$ ,  $P = 0.137$ ).

**FIGURE 3 |** Three-dimensional surface plot visualizing the functional associations between the presence of primary epiretinal membrane and two dependent variables including age and serum sodium concentration in female participants aged 40 and over. An increase in epiretinal membrane prevalence with an increased sodium level was not dependent on age.

and ERM may be due to variations of the ethnicities, study designs, and techniques to detect ERM.

The new finding in our study was the relationship between a higher SSC and a higher primary ERM prevalence, including or excluding participants with an abnormal SSC. In a case series study, sodium was detected in 10 out 20 ERM samples and tended to be more frequent in the thicker ERM (22), which is consistent with the significantly higher SSC in PMF patients than CMR patients in our study. In a study involving 27 participants with

a macular hole or ERM, the sodium concentration in the vitreous was significantly higher than that in the fasting serum samples obtained perioperatively ( $146.7 \pm 3.3$  vs.  $139.7 \pm 3.4$  mmol/L;  $P < 0.0001$ ) (23).

Our findings combined with these studies suggest that sodium may be a factor involved in the pathogenesis of ERM, perhaps by modulating the glial activity and cell migration (22–25), whereas the exact mechanism remains to be explored. A cross-sectional study from Korea observed no difference in sodium



intake between participants with and without ERM (16). One may take into account, however, that their data of the sodium intake were self-reported and not equivalent to the SSC.

Sodium ( $\text{Na}^+$ ) is a major electrolyte in the serum and extracellular fluids. Both higher and lower SSC, even within the normal range (135–145 mmol/L), are associated with primary cardiovascular events (26). A higher SSC is related to elevated serum lipid concentrations and elevated blood pressure, and extracellular sodium directly affects lipid metabolism by increasing the lipid accumulation in cultured adipocytes (27). Thus, the association between higher cholesterol and ERM prevalence observed in our study and previous similar findings (4, 8, 10, 18) may also help to explain the relationship between a higher SSC and higher ERM prevalence.

A positive correlation between SSC and age was found in women but not in men. The SSC in women was lower than that in men up to the age of 50 years, while beyond 50 years the association even reversed. This tendency has also been previously observed (28, 29). Besides, the female gender was also found to be an independent risk factor for hyponatremia (30–32). Possible explanations for these sex-specific differences may be the impact of female sex hormones in regulating serum sodium, sex differences in regulation of arginine vasopressin, renal sodium secretion, and absorption (28, 29, 33, 34). Interestingly, menopause among Chinese women occurs at approximately the age of 50 years, consisting with the age when the difference in SSC between women and men started to reverse.

Notably, though the age-related variations in SSC might have functioned as confounding factors, the significant association between SSC and ERM prevalence remained after age and multivariable adjustment, in all female participants and in those age 40+ years. It was also shown in a three-dimensional surface plot in which the ERM prevalence increases with the SSC, after stratification by age (**Figure 3**). Our findings may help to explain the higher ERM prevalence in women than men detected by other groups.

The strengths of our study include its large sample size, and the relatively large number of systemic parameters included in the statistical analysis. These parameters included the blood pressure, glucose, lipids and kidney function, and presence of hypertension and diabetes, which may be potential confounding factors for any association with SSC. Our study has several limitations. First, a selection bias may exist since our results were not derived from a population-based sample. However, most of our participants were employees or retirees from fixed organizations and were consecutively enrolled without considering their health conditions or other factors. Second, the lack of optical coherence tomography might have led to

an underestimation of the ERM prevalence. However, fundus photography, as also adopted by other groups (1, 3, 4), has the advantage of a wider angle of imaging so that the identification of ERMs at the temporal vascular arcades became easier. In addition, the primary ERM prevalence in our study was comparable to that reported in a recent meta-analysis (6). Third, the medication and dietary information were not available for the current study, thus we are not sure about the causes of high SSC in individuals with ERM. Whether a low-salt diet would prevent the development or progression of ERM might be of interest to explore in the future. Fourth, our study is a cross-sectional investigation that could assess only factors associated with the prevalence of ERM but not risk factors for the incidence of ERM.

In conclusion, besides older age and higher total cholesterol, a higher serum sodium level may be an independent factor associated with the presence of ERM.

## DATA AVAILABILITY STATEMENT

The raw data supporting the conclusions of this article will be made available on reasonable request from the corresponding authors.

## ETHICS STATEMENT

The Institutional Review Board of Beijing Tongren Hospital approved the study design and waived the informed consent, under the measures for ethical reviews of biomedical research involving humans initiated by the Chinese government and consistent with the FDA guidance.

## AUTHOR CONTRIBUTIONS

YW and JJ: design of the study and critical review of manuscript. CX, JC, XZ, and JX: conduct of the study and collection and management of the data. CX, JC, CZ, DC, and YW: analysis and interpretation of data. CX, JC, and YW: preparation of manuscript. All authors provided important feedback on the methods and results and approved the final version of the manuscript.

## FUNDING

The work was funded by the Research Development Fund of Beijing Municipal Health Commission (2019–4). The funder of this study had no role in study design, data collection, data analysis, data interpretation, or writing of the manuscript.

## REFERENCES

- Cheung N, Tan SP, Lee SY, Cheung GCM, Tan G, Kumar N, et al. Prevalence and risk factors for epiretinal membrane: the Singapore Epidemiology of Eye Disease study. *Br J Ophthalmol*. (2017) 101:371–6. doi: 10.1136/bjophthalmol-2016-308563
- Flaxel CJ, Adelman RA, Bailey ST, Fawzi A, Lim JJ, Vemulakonda GA, et al. Idiopathic epiretinal membrane and vitreomacular traction preferred practice pattern (R). *Ophthalmology*. (2020) 127:P145–83. doi: 10.1016/j.optha.2019.09.022
- Mitchell P, Smith W, Chey T, Wang JJ, Chang A. Prevalence and associations of epiretinal membranes. The Blue Mountains Eye Study. *Aust Ophthalmol*. (1997) 104:1033–40. doi: 10.1016/S0161-6420(97)30190-0

4. Miyazaki M, Nakamura H, Kubo M, Kiyohara Y, Iida M, Ishibashi T, et al. Prevalence and risk factors for epiretinal membranes in a Japanese population: the Hisayama study. *Graefes Arch Clin Exp Ophthalmol*. (2003) 241:642–6. doi: 10.1007/s00417-003-0723-8
5. You Q, Xu L, Jonas JB. Prevalence and associations of epiretinal membranes in adult Chinese: the Beijing eye study. *Eye*. (2008) 22:874–9. doi: 10.1038/sj.eye.6702786
6. Xiao W, Chen X, Yan W, Zhu Z, He M. Prevalence and risk factors of epiretinal membranes: a systematic review and meta-analysis of population-based studies. *BMJ Open*. (2017) 7:e014644. doi: 10.1136/bmjopen-2016-014644
7. Duan XR, Liang YB, Friedman DS, Sun LP, Wei WB, Wang JJ, et al. Prevalence and associations of epiretinal membranes in a rural Chinese adult population: the Handan Eye Study. *Invest Ophthalmol Vis Sci*. (2009) 50:2018–23. doi: 10.1167/iovs.08-2624
8. Koh V, Cheung CY, Wong WL, Cheung CM, Wang JJ, Mitchell P, et al. Prevalence and risk factors of epiretinal membrane in Asian Indians. *Invest Ophthalmol Vis Sci*. (2012) 53:1018–22. doi: 10.1167/iovs.11-8557
9. Bu SC, Kuijter R, Li XR, Hooymans JM, Los LI. Idiopathic epiretinal membrane. *Retina*. (2014) 34:2317–35. doi: 10.1097/IAE.0000000000000349
10. Ye H, Zhang Q, Liu X, Cai X, Yu W, Yu S, et al. Prevalence and associations of epiretinal membrane in an elderly urban Chinese population in China: the Jiangning Eye Study. *Br J Ophthalmol*. (2015) 99:1594–7. doi: 10.1136/bjophthalmol-2015-307050
11. Zhu XB, Yang MC, Wang YX, Qian W, Yan YN, Yang JY, et al. Prevalence and risk factors of epiretinal membranes in a Chinese population: The Kailuan Eye Study. *Invest Ophthalmol Vis Sci*. (2020) 61:37. doi: 10.1167/iovs.61.11.37
12. Forlini M, Date P, D'Eliseo D, Rossini P, Bratu A, Volinia A, et al. Limited vitrectomy versus complete vitrectomy for epiretinal membranes: a comparative multicenter trial. *J Ophthalmol*. (2020) 2020:6871207. doi: 10.1155/2020/6871207
13. Xue CC, Cui J, Gao LQ, Zhang C, Dou HL, Chen DN, et al. Peripheral monocyte count and age-related macular degeneration. The Tongren Health Care Study. *Am J Ophthalmol*. (2021) 227:143–53. doi: 10.1016/j.ajo.2021.03.010
14. Levey AS, Stevens LA, Schmid CH, Zhang YL, Castro AF III, Feldman HI, et al. A new equation to estimate glomerular filtration rate. *Ann Intern Med*. (2009) 150:604–12. doi: 10.7326/0003-4819-150-9-200905050-00006
15. Klein R, Klein BE, Wang Q, Moss SE. The epidemiology of epiretinal membranes. *Trans Am Ophthalmol Soc*. (1994) 92:403–25; discussion 425–430.
16. Kim JM, Lee H, Shin JP, Ahn J, Yoo JM, Song SJ, et al. Epiretinal membrane: prevalence and risk factors from the Korea National Health and Nutrition Examination Survey, 2008 through 2012. *Korean J Ophthalmol*. (2017) 31:514–23. doi: 10.3341/kjo.2016.0098
17. Aung KZ, Makeyeva G, Adams MK, Chong EW, Busija L, Giles GG, et al. The prevalence and risk factors of epiretinal membranes: the Melbourne Collaborative Cohort Study. *Retina*. (2013) 33:1026–34. doi: 10.1097/IAE.0b013e3182733f25
18. Bae JH, Song SJ, Lee MY. Five-year incidence and risk factors for idiopathic epiretinal membranes. *Retina*. (2019) 39:753–60. doi: 10.1097/IAE.0000000000002024
19. Yang Y, Yan YN, Wang YX, Xu J, Ren J, Xu L, et al. Ten-year cumulative incidence of epiretinal membranes assessed on fundus photographs. The Beijing Eye Study 2001/2011. *PLoS ONE*. (2018) 13:e0195768. doi: 10.1371/journal.pone.0195768
20. Kawasaki R, Wang JJ, Sato H, Mitchell P, Kato T, Kawata S, et al. Prevalence and associations of epiretinal membranes in an adult Japanese population: the Funagata study. *Eye*. (2009) 23:1045–51. doi: 10.1038/eye.2008.238
21. Ng CH, Cheung N, Wang JJ, Islam AF, Kawasaki R, Meuer SM, et al. Prevalence and risk factors for epiretinal membranes in a multi-ethnic United States population. *Ophthalmology*. (2011) 118:694–9. doi: 10.1016/j.ophtha.2010.08.009
22. Romano MR, Cennamo G, Montorio D, Del Prete S, Ferrara M, Cennamo G. Correlation between various trace elements and ultramicroscopic structure of epiretinal macular membranes and glial cells. *PLoS ONE*. (2018) 13:e0204497. doi: 10.1371/journal.pone.0204497
23. Kokavec J, Min SH, Tan MH, Gilhotra JS, Newland HS, Durkin SR, et al. Biochemical analysis of the living human vitreous. *Clin Exp Ophthalmol*. (2016) 44:597–609. doi: 10.1111/ceo.12732
24. Rose CR, Chatton JY. Astrocyte sodium signaling and neuro-metabolic coupling in the brain. *Neuroscience*. (2016) 323:121–34. doi: 10.1016/j.neuroscience.2015.03.002
25. Rose CR, Verkhratsky A. Principles of sodium homeostasis and sodium signalling in astroglia. *Glia*. (2016) 64:1611–27. doi: 10.1002/glia.22964
26. Cole NI, Suckling RJ, Swift PA, He FJ, MacGregor GA, Hinton W, et al. The association between serum sodium concentration, hypertension and primary cardiovascular events: a retrospective cohort study. *J Hum Hypertens*. (2019) 33:69–77. doi: 10.1038/s41371-018-0115-5
27. Gao S, Cui X, Wang X, Burg MB, Dmitrieva NI. Cross-sectional positive association of serum lipids and blood pressure with serum sodium within the normal reference range of 135–145 mmol/L. *Arterioscler Thromb Vasc Biol*. (2017) 37:598–606. doi: 10.1161/ATVBAHA.116.308413
28. Goldstein P, Leshem M. Dietary sodium added salt, and serum sodium associations with growth and depression in the US general population. *Appetite*. (2014) 79:83–90. doi: 10.1016/j.appet.2014.04.008
29. Lu ZH, Zhu XX, Tang ZQ, Gang GQ, Du J, Wang XL, et al. Female sex hormones are associated with the reduction of serum sodium and hypertension complications in patients with aldosterone-producing adenoma. *Endocr J*. (2013) 60:1261–8. doi: 10.1507/endocrj.EJ13-0123
30. Berghuis B, van der Palen J, de Haan GJ, Lindhout D, Koeleman BPC, Sander JW, et al. Carbamazepine- and oxcarbazepine-induced hyponatremia in people with epilepsy. *Epilepsia*. (2017) 58:1227–33. doi: 10.1111/epi.13777
31. Druschky K, Bleich S, Grohmann R, Engel RR, Kleimann A, Stubner S, et al. Use and safety of antiepileptic drugs in psychiatric inpatients-data from the AMSP study. *Eur Arch Psychiatry Clin Neurosci*. (2018) 268:191–208. doi: 10.1007/s00406-017-0827-5
32. Filippone EJ, Ruzieh M, Foy A. Thiazide-associated hyponatremia: clinical manifestations and pathophysiology. *Am J Kidney Dis*. (2020) 75:256–64. doi: 10.1053/j.ajkd.2019.07.011
33. Stachenfeld NS, Keefe DL. Estrogen effects on osmotic regulation of AVP and fluid balance. *Am J Physiol Endocrinol Metab*. (2002) 283:E711–21. doi: 10.1152/ajpendo.00192.2002
34. Stachenfeld NS, Taylor HS. Sex hormone effects on body fluid and sodium regulation in women with and without exercise-associated hyponatremia. *J Appl Physiol*. (2009) 107:864–72. doi: 10.1152/japophysiol.91211.2008

**Conflict of Interest:** The authors declare that the research was conducted in the absence of any commercial or financial relationships that could be construed as a potential conflict of interest.

**Publisher's Note:** All claims expressed in this article are solely those of the authors and do not necessarily represent those of their affiliated organizations, or those of the publisher, the editors and the reviewers. Any product that may be evaluated in this article, or claim that may be made by its manufacturer, is not guaranteed or endorsed by the publisher.

Copyright © 2021 Xue, Cui, Zhu, Xu, Zhang, Chen, Wang and Jonas. This is an open-access article distributed under the terms of the Creative Commons Attribution License (CC BY). The use, distribution or reproduction in other forums is permitted, provided the original author(s) and the copyright owner(s) are credited and that the original publication in this journal is cited, in accordance with accepted academic practice. No use, distribution or reproduction is permitted which does not comply with these terms.



# Targeting Pyroptotic Cell Death Pathways in Retinal Disease

Mary Zhao\*, Siqi Li and Joanne A. Matsubara

Department of Ophthalmology and Visual Sciences, Eye Care Centre, Faculty of Medicine, University of British Columbia, Vancouver, BC, Canada

Pyroptosis is a gasdermin-mediated, pro-inflammatory form of cell death distinct from apoptosis. In recent years, increasing attention has shifted toward pyroptosis as more studies demonstrate its involvement in diverse inflammatory disease states, including retinal diseases. This review discusses how currently known pyroptotic cell death pathways have been implicated in models of age-related macular degeneration, diabetic retinopathy, and glaucoma. We also identify potential future therapeutic strategies for these retinopathies that target drivers of pyroptotic cell death. Presently, the drivers of pyroptosis that have been studied the most in retinal cells are the nucleotide-binding and oligomerization domain-like receptor family pyrin domain-containing 3 (NLRP3) inflammasome, caspase-1, and gasdermin D (GSDMD). Targeting these proteins may help us develop new drug therapies, or supplement existing therapies, in the treatment of retinal diseases. As novel mechanisms of pyroptosis come to light, including those involving other inflammatory caspases and members of the gasdermin protein family, more targets for pyroptosis-mediated therapies in retinal disease can be explored.

**Keywords:** pyroptosis, cell death, NLRP3, caspase-1, GSDMD, age-related macular degeneration, diabetic retinopathy, glaucoma

## OPEN ACCESS

### Edited by:

Hetian Lei,  
Shenzhen Eye Hospital, China

### Reviewed by:

Youssef Achoui,  
University of Arkansas for Medical  
Sciences, United States  
Juan Pablo de Rivero Vaccari,  
University of Miami, United States

### \*Correspondence:

Mary Zhao  
zhaomary@student.ubc.ca

### Specialty section:

This article was submitted to  
Ophthalmology,  
a section of the journal  
Frontiers in Medicine

**Received:** 26 October 2021

**Accepted:** 29 November 2021

**Published:** 03 January 2022

### Citation:

Zhao M, Li S and Matsubara JA  
(2022) Targeting Pyroptotic Cell Death  
Pathways in Retinal Disease.  
Front. Med. 8:802063.  
doi: 10.3389/fmed.2021.802063

## INTRODUCTION

Cell death has long been a subject of interest in the study of retinal pathology. The role of programmed cell death (PCD) in retinal diseases is a particularly exciting avenue of research as the regulated nature of these cell death pathways implies that they can potentially be interrupted or manipulated by pharmacological interventions. Traditionally, apoptosis was equated to PCD because it was the most well-studied and well-characterized form of PCD. Research from the 1990's suggested that apoptosis was the main mechanism of regulated cell loss in retinal degeneration and this remained a popular view for most of the 21<sup>st</sup> century (1–3). The Nomenclature Committee on Cell Death now recognizes that there are other types of regulated cell death besides apoptosis—including necroptosis, ferroptosis, and pyroptosis (4). Necroptosis involves the activation of the pseudokinase mixed-lineage kinase domain-like protein (MLKL), receptor-interacting protein kinase 1 (RIPK1), and receptor-interacting protein kinase 3 (RIPK3) (5). Ferroptosis, as the name suggests, is iron-dependent and is driven by severe lipid peroxidation that results from loss of activity of the lipid repair enzyme glutathione peroxidase 4 (GPX4) (6). Finally, pyroptosis is characterized by membrane pore formation and rapid plasma membrane rupture caused by the binding of the N-terminal of gasdermin proteins to the inner leaflet of the plasma membrane (7–9). As the mechanisms of these cell death pathways have become clearer, more research has emerged supporting their involvement in retinal disease. A recent review summarized the role of necroptosis and

ferroptosis in blinding eye disease (10); however, no such a review exists for pyroptosis. Here, we discuss the current understanding of pyroptosis, the research implicating pyroptotic cell death pathways in retinal diseases, and how this knowledge can be applied to identifying novel therapeutic approaches to retinopathies. Specifically, we will focus on the role of pyroptosis in the pathogenesis and potential treatment of three of the most prevalent retinal diseases—age-related macular degeneration, diabetic retinopathy, and glaucoma.

## OVERVIEW OF PYROPTOSIS

The term “pyroptosis” was first coined in 2001 by Cookson and Brennan from the Greek roots “pyro,” relating to fire or fever, and “ptosis” meaning falling, to describe pro-inflammatory PCD (11). This distinguished pyroptosis from apoptosis, which is non-inflammatory PCD. Initially, caspase-1 was believed to be the effector of pyroptosis after *Salmonella*-infected macrophages were found to undergo a caspase-1-dependent form of cell death that was associated with pore formation and was distinguishable from apoptosis (11–13). Later, this role shifted to gasdermin D (GSDMD) when it was discovered that the cleaved, N-terminal of GSDMD (GSDMD-N) could bind to and form pores in the cell membrane, leading to pyroptotic cell death (14). Interestingly, pore-forming activity is not exclusive to GSDMD-N; in fact, most gasdermins have an N-terminal pore-forming domain and have the ability to induce pyroptosis (7). This has led to our current understanding of pyroptosis as gasdermin-mediated cell death.

The gasdermin protein family includes gasdermin A/B/C/D/E (GSDMA/B/C/D/E) and DFNB59 (Pejvakin, PJVK) in humans. Gasdermin proteins share 45% sequence homology, and all members (except for Pejvakin) contain C-terminal and N-terminal domains (7, 15). The C-terminal domain is a repressor domain that, when linked to the N-terminal domain, auto-inhibits the N-terminal's cytotoxic activity (16, 17). Inflammatory caspases or granzymes can cleave inactive, full-length gasdermin and liberate its N-terminal domain (14, 18–20). When freed, the N-terminal can then bind to phosphoinositides or cardiolipin on the inner leaflet of the plasma membrane and form membrane pores characteristic of pyroptotic cell death. Pyroptosis is also associated with the release of pro-inflammatory cytokines IL-18 and IL-1 $\beta$ , through these approximately 18 nm-wide membrane pores (21). This adds an additional pathological stressor to cells that is not present with apoptotic cell death and is what earns pyroptosis its designation as a pro-inflammatory form of cell death (7, 8, 13, 15). It was previously thought that extracellular fluid also enters plasma membrane pores during pyroptosis, passively causing plasma membrane rupture (PMR) through oncotic cell swelling. However, PMR is actually an active event mediated by the cell-surface protein Ninjurin 1 (NINJ1) and has been proposed to occur after pyroptotic cell death and IL-18/IL-1 $\beta$  release (22).

Multiple different mechanisms can lead to gasdermin cleavage in pyroptosis. The two most well-studied mechanisms are the canonical and non-canonical inflammasome pathways. The canonical inflammasome pathway, leading to canonical

pyroptosis, is mediated by caspase-1. Inflammasomes are multimeric protein complexes, composed of a central sensor protein, an adaptor protein ASC (apoptosis-associated speck-like protein containing a caspase activation and recruitment domain), and pro-caspase-1. The most well-studied sensor proteins known to assemble canonical inflammasomes are NLRP1, NLRP3, NLRC4, AIM2, and pyrin (23, 24). Other proteins such as human NLRP2 and murine NLRP6 have also been implicated in inflammasome signaling (25, 26). These proteins respond to pathogen-associated and danger-associated molecular patterns (PAMPs and DAMPs), which causes “activation” (i.e., assembly) of the inflammasome. Pro-caspase-1 within the activated inflammasome undergoes autocatalytic cleavage into mature caspase-1, and mature caspase-1 can then cleave GSDMD to cause pyroptosis (14, 23, 27). Mature caspase-1 also has the ability to convert pro-IL-18 and pro-IL-1 $\beta$  into their mature forms that are released from membrane pores during pyroptosis (8, 12, 13). Intriguingly, inflammasomes can also be activated and release inflammatory cytokines without necessarily causing cell death through an unknown mechanism that may involve the Toll-IL-1R protein SARM (sterile alpha and HEAT armadillo motif-containing protein) (9, 28). The non-canonical pyroptosis pathway does not depend on caspase-1; rather, it is triggered by the direct binding of procaspase-4/5 in humans, or -11 in mice, to intracellular lipopolysaccharide (LPS). Like caspase-1, activated caspase-4/5/11 can then go on to cleave GSDMD to execute pyroptosis. However, these caspases cannot directly process pro-IL-18 and pro-IL-1 $\beta$  into their mature forms (15, 18, 29, 30).

Up until recently, the canonical and non-canonical inflammasome pathways leading to GSDMD activation were the only known pyroptotic pathways. However, in 2017, both *in vitro* and *in vivo* studies showed that pyroptosis could be induced by GSDME expression and cleavage of GSDME into GSDME-N by caspase-3 (31, 32). Furthermore, in 2018, it was found that GSDMD could also be cleaved by caspase-8 in mouse macrophages (33, 34). These findings were especially interesting because caspases 3 and 8 were previously associated with apoptosis and were not thought to be able to interact with gasdermins. Overall, these studies improve our understanding of pyroptosis as we now know that activation of other caspases besides caspases 1/4/5/11 and other gasdermins besides GSDMD can also cause pyroptotic cell death.

## ROLE OF PYROPTOSIS IN RETINAL DISEASE

Major findings from studies investigating pyroptosis in age-related macular degeneration, diabetic retinopathy, and glaucoma are summarized in **Tables 1–3**, respectively.

### Pyroptosis and Age-Related Macular Degeneration

Age-related macular degeneration (AMD) is the most common cause of irreversible vision loss among the elderly in the developed world, and is projected to affect 288 million people globally by 2040 (58). AMD is a neurodegenerative



**TABLE 1** | Studies investigating pyroptosis in AMD.

Study	Model/Cell type studied	Technique	Findings	Relevance of findings to pyroptosis
Tarallo et al. (35)	Human RPE cells transfected with pAlu	MTS cell viability assay	The cytoprotective agent glycine (pyroptosis inhibitor) did not rescue <i>Alu</i> RNA-induced RPE degeneration	<i>Alu</i> RNA accumulation (a feature of GA) may not induce RPE degeneration via pyroptosis
Kerur et al. (36)	Human RPE cells transfected with pAlu, subretinal injection of pAlu in mice	Immunohistochemistry	<i>Gsdmd</i> <sup>-/-</sup> mice were resistant to <i>Alu</i> RNA-induced RPE degeneration; however, there was no observed cleavage of GSDMD into its N-terminal-pore-forming p30 fragment in pAlu-transfected human primary RPE cells or WT mice subretinally injected with <i>Alu</i> RNA	GSDMD is required for <i>Alu</i> RNA-induced RPE degeneration, but plays a non-pyroptotic role
Tseng et al. (37)	Lysosomal destabilization in ARPE-19 cells using Leu-Leu-OMe treatment	LDH release, caspase-1 inhibition with 10 $\mu$ M Z-YVAD-FMK	Lysosomal destabilization induced LDH release from ARPE-19 cells, mediated by caspase-1	ARPE-19 cells undergo pyroptosis in response to lysosomal destabilization
Gao et al. (38)	A $\beta$ intravitreal injections in Long-Evans rats	Western blotting	RPE-choroid protein lysates of rats receiving A $\beta$ injections showed significantly greater cleavage of pro-GSDMD into GSDMD-N compared to controls	A $\beta$ upregulates GSDMD-N, a driver of pyroptosis, in RPE cells
Sun et al. (39)	A $\beta$ -treated ARPE-19 cells	Flow cytometry for positive PI and caspase-1 staining	A $\beta$ significantly increased the proportion of ARPE-19 cells staining positive for both PI and caspase-1	A $\beta$ induces pyroptosis in ARPE-19 cells
Yang et al. (40)	A $\beta$ -treated ARPE-19 cells	Immunofluorescence, scanning electron microscopy	A $\beta$ triggered increased levels of GSDMD-N, as well as swelling, bubbling, and cell membrane rupture in ARPE-19 cells	A $\beta$ causes upregulation of a pyroptosis effector and morphological characteristics of pyroptosis in ARPE-19 cells
Liao et al. (41)	atRAL-treated ARPE-19 cells	Western blotting	Lysates of ARPE-19 cells treated with 15 $\mu$ M atRAL showed increased levels of cleaved GSDME at 6 and 12 h but GSDMD remained full-length	atRAL-treated ARPE-19 cells may undergo GSDME-mediated, rather than GSDMD-mediated, pyroptosis

RPE, retinal pigment epithelium; pAlu, plasmid coding for *Alu* RNA; GA, geographic atrophy; WT, wild-type; ARPE-19, human adult retinal pigment; LDH, lactate dehydrogenase; A $\beta$ , amyloid beta; PI, propidium iodide; GSDMD/E, gasdermin D/E; GSDMD-N, N-terminal of gasdermin D; atRAL, all-trans retinal.

disease; accumulation of drusen deposits results in progressive degeneration of photoreceptors and retinal pigment epithelium (RPE), primarily in the macula. Clinically, AMD can present as a spectrum of disease phenotypes, with the severity of the disease depending on drusen size. Earlier stages of AMD are defined by the presence of medium-sized drusen deposits and do not present with vision loss. As drusen grow in size and number, atrophy of photoreceptors, RPE, and choriocapillaris and scotoma development can occur. These features are characteristic of a late stage of AMD called geographic atrophy (GA or “dry AMD”). Large drusen also increase the risk of developing neovascular AMD, in which new, abnormal vessels form and invade the outer retina, subretinal space, or subRPE space. Exudative or “wet AMD” occurs when these new vessels rupture and leak exudates, causing fluid accumulation/hemorrhage and severe central vision loss if left untreated (59, 60).

In 2011, Kaneko and colleagues discovered that reduction of the RNase DICER1 led to accumulation of *Alu* RNA, non-coding RNA transcripts expressed by the *Alu* retrotransposon, in RPE from human donor eyes with GA. *Alu* RNA accumulation, in turn, resulted in RPE degeneration in both humans and mice (61). A year later, the same group found that *Alu* RNA did not induce RPE degeneration in *Nlrp3*<sup>-/-</sup> or *Casp1*<sup>-/-</sup>

mice. This suggested that the canonical NLRP3/caspase-1-dependent pyroptotic pathway may be involved in RPE degeneration in AMD. However, glycine, a cytoprotective agent that attenuates pyroptosis, did not rescue *Alu* RNA-induced RPE degeneration in the same study. The authors concluded that while NLRP3 and caspase-1 are critical for *Alu* RNA-induced RPE degeneration, *Alu* RNA does not induce RPE degeneration via pyroptosis (35). *Gsdmd*<sup>-/-</sup> mice, like *Nlrp3*<sup>-/-</sup> and *Casp1*<sup>-/-</sup> mice, were shown to be resistant to *Alu* RNA-induced RPE degeneration in a study by Kerur et al. (36), but there was no observed cleavage of GSDMD into its N-terminal pore-forming domain. Furthermore, reconstituting *Gsdmd*<sup>-/-</sup> mice with a GSDMD mutant unable to undergo cleavage (pGSDMD-D276A) restored susceptibility to *Alu* RNA-induced RPE degeneration. Full-length GSDMD cannot induce pyroptosis; thus, it must exert its effects on *Alu* RNA-induced RPE toxicity through another mechanism. Administration of mature IL-18 to *Gsdmd*<sup>-/-</sup> mice restored *Alu* RNA-induced RPE degeneration and led to the appearance of annexin V positive, propidium iodide (PI) negative staining RPE cells. This suggested that GSDMD plays a role in *Alu* RNA-induced cytotoxicity via IL-18-dependent apoptosis, rather than pyroptosis, in RPE (36). While the above studies do not support that RPE cells undergo pyroptotic cell death in response

to *Alu* RNA, they do identify NLRP3, caspase-1, and full-length GSDMD as potential therapeutic targets for AMD, particularly for GA.

Lysosomal destabilization, which can result from drusen accumulation and trigger inflammasome activation, has also been studied for its potential to cause pyroptosis in AMD. Lysosomal destabilization with Leu-Leu-OMe treatment induced IL-1 $\beta$  and LDH release from ARPE-19 cells, mediated by caspase-1. These findings indicate that lysosomal destabilization leads to a caspase-1-dependent, pro-inflammatory, and lytic form of cell death in RPE, characteristic of pyroptosis (37). Caspase-1 inhibition may also therefore be a worthwhile therapeutic strategy for AMD treatment.

Additional support for RPE pyroptosis in AMD comes from research on amyloid beta (A $\beta$ ), a component of drusen. After the NLRP3 inflammasome was activated by repeated intravitreal injections of A $\beta$  into the eyes of Long-Evans rats, RPE-choroid protein lysates from A $\beta$ -injected animals showed significantly increased levels of GSDMD-N and decreased levels of full-length GSDMD (38). This supported that GSDMD-mediated pyroptosis can be activated in RPE cells and that NLRP3 and GSDMD-N are possible targets for AMD therapy. In another study using A $\beta$ -induced ARPE-19 cells as a model for AMD, Baicalin was found to alleviate A $\beta$ -induced pyroptosis detected by flow cytometry for positive PI and caspase-1 labeling (39). The protective action of Baicalin was mediated by upregulating miRNA-223, which had been previously found to reduce the expression of NLRP3 (62). Baicalin's anti-pyroptotic effects were reversed by miRNA-223 knockdown, whereas adding MCC950 (an NLRP3 inhibitor) once again reduced pyroptosis (39). Lycium Barbarum Polysaccharides (LBP), present in Goji berries, also rescued A $\beta$ -induced reduction of RPE cell viability at low (3.5 mg/L) and high (14 mg/L) doses via attenuation of pyroptosis. A $\beta$  triggered increased levels of GSDMD-N and caused morphological changes in RPE characteristic of pyroptosis, both of which were reversed by LBP treatment (40). As such, inhibiting pyroptosis using Baicalin or LBP may potentially be therapeutic for AMD.

There is also evidence that GSDME-mediated, rather than GSDMD-mediated, pyroptosis occurs in RPE in the all-trans retinal (atRAL) model of AMD. atRAL is generated during the visual (retinoid) cycle and can accumulate in visual cycle anomalies, causing RPE atrophy in AMD. Cleavage of GSDME was detected at 6 and 12 h in lysates of atRAL-treated ARPE-19 cells but GSDMD remained intact, suggesting that atRAL triggers pyroptosis in ARPE-19 cells by activating the caspase-3/GSDME pathway of pyroptosis (41). Research on GSDME-mediated pyroptosis in retinal cells is sparse and further study is required to see if this pathway can be targeted for the treatment of AMD.

## Pyroptosis and Diabetic Retinopathy

Diabetic retinopathy (DR) is a leading cause of preventable vision loss in working-age adults and can be broadly classified into two clinical stages: non-proliferative diabetic retinopathy (NPDR) and proliferative diabetic retinopathy (PDR) (63). Early in NPDR, retinal pericytes that support retinal capillaries are lost, causing capillary occlusion and increased vascular permeability.

On fundoscopy, intra-retinal hemorrhages, microaneurysms, and exudates called "cotton wool spots" may be observed in NPDR. NPDR can eventually lead to PDR, in which vascular endothelial growth factor (VEGF) promotes neovascularization in the retina. These newly formed vessels have leaky tight junctions that can result in vitreous hemorrhage or tractional retinal detachment (TRD), and cause vision loss. Another cause of vision loss in DR is diabetic macular edema (DME), where the macula becomes thickened due to breakdown of the blood-retina barrier (BRB) (64). DR is primarily considered a microvascular disease and breakdown of the BRB is key to this disease state. Maintenance of the BRB depends on the functioning of an interdependent network of cells—including endothelial cells that make up the inner BRB, supportive Müller cells and pericytes, and RPE cells which form the outer BRB (65).

A previous review discussed modes of retinal cell death in DR (66). Only Müller cell loss in diabetes was outlined to show characteristics of pyroptosis while other retinal cells including endothelial cells and pericytes were thought to primarily undergo apoptosis or necrosis. More recent studies have found signs of possible pyroptotic cell death in many types of retinal cells in DR models including endothelial cells, pericytes, Müller cells, and RPE. Endothelial cells line the retinal microvasculature and comprise the highly selective inner BRB (65). NLRP3/caspase-1 activation and IL-1 $\beta$  release have been recorded in retinal endothelial cells (RECs) in various *in vivo* and *in vitro* models of DR (42, 43, 67). Pyroptotic cell death and caspase-1 activity were markedly increased in human retinal microvascular endothelial cells (HRMECs) incubated in 30 mM high glucose compared to controls (44). Pyroptosis was identified in this study using PI/caspase-1 fluorochrome inhibitor (FLICA) staining and flow cytometry. This suggests that canonical pyroptosis may take place in RECs and targeting NLRP3 and caspase-1 may be a treatment strategy to prevent their loss in DR. Retinal pericytes provide structural support to retinal vessel walls and regulate the expression of tight junctions in adjacent endothelial cells (65). A study published in 2020 showed that silencing GSDMD inhibits IL-1 $\beta$  and IL-18 release, decreases pore formation, and decreases lysis of human retinal pericytes exposed to 30 mM high glucose (45). Another study using advanced glycation endproducts modified bovine serum albumin (AGE-BSA) to simulate the DR environment found increased expression of active caspase-1 and GSDMD-N as well as increased secretion of IL-1 $\beta$ , IL-18, and lactate dehydrogenase (LDH) in human retinal pericytes (HRPCs) alongside decreased HRPC viability (46). Thus, pyroptotic pericyte loss may occur in DR and blocking caspase-1 and GSDMD can potentially preserve pericyte viability. Müller cells are the principal glial cells of the retina and, because of their innate role in mediating neuroinflammation, have long been speculated to participate in pyroptosis (66). Protein levels of NLRP3, ASC, cleaved caspase-1 and cleaved IL-1 $\beta$  were increased by 30 mM high glucose in mouse primary retinal Müller cells. Furthermore, NLRP3 antagonism with the inhibitor drug MCC950 downregulated high glucose-induced upregulation of pro-angiogenic factors including VEGF (47). This implicated activation of the NLRP3 inflammasome pathway in Müller cells in DR and provided support that NLRP3

**TABLE 2 |** Studies investigating pyroptosis in DR.

Study	Model/Cell type studied	Technique	Findings	Relevance of findings to pyroptosis
Jiang et al. (42)	Primary human RECs incubated in 25 mM high glucose	Western blotting	Increased protein levels of NLRP3, cleaved caspase-1, and IL-1 $\beta$ in high glucose vs. normal glucose group	The NLRP3/caspase-1-mediated pyroptotic pathway may be activated in HRMECs in response to high glucose
Chen et al. (43)	HRMECs incubated in 30 mM high glucose	Western blotting	Increased protein levels of NLRP3, cleaved caspase-1, and IL-1 $\beta$ in high glucose vs. normal glucose group	The NLRP3/caspase-1-mediated pathway may be activated in RECs in response to high glucose
Gu et al. (44)	HRMECs incubated in 30 mM high glucose	PI and caspase-1 FLICA staining, flow cytometry	Pyroptosis and caspase-1 activity were markedly increased in high-glucose-treated HRMECs vs. the control group	High glucose promotes pyroptotic cell death in HRMECs
Gan et al. (45)	HRPs incubated in 30 mM high glucose	Pore formation: PI uptake Cell lysis: LDH release Cytokine release: ELISA	High glucose-treated HRPs experienced greater pore-formation, cell lysis, and release of IL-1 $\beta$ and IL-18 compared to controls $\rightarrow$ these effects were reversed with NLRP3, caspase-1, or GSDMD inhibition	High glucose can induce the loss of HRPs via GSDMD-mediated pyroptosis
Yu et al. (46)	HRPs incubated in 200 $\mu$ g/ml AGE-BSA	Protein expression: Western blotting Cytokine release: ELISA LDH activity: LDH assay kit Cell viability: cell counting kits	AGE-BSA increased expression of active caspase-1 and GSDMD-N and promoted secretion of IL-1 $\beta$ , IL-18, and LDH in HRPs, alongside decreasing HRP viability	HRPs undergo GSDMD-mediated pyroptosis when treated with AGE-BSA
Du et al. (47)	Mouse primary retinal Müller cells incubated in 30 mM high glucose	Western blotting	Increased levels of NLRP3, cleaved caspase-1, and IL-1 $\beta$ in high glucose-treated mouse retinal Müller cells	The NLRP3/caspase-1-mediated pyroptotic pathway may be activated in Müller cells cultured under high glucose conditions
Xi et al. (48)	ARPE-19 cells incubated in 50 mM high glucose	Western blotting	High glucose upregulated protein expression of caspase-1, GSDMD, NLRP3, IL-1 $\beta$ , and IL-18 in ARPE-19 cells	High glucose may promote GSDMD-mediated pyroptosis in ARPE-19 cells
Zha et al. (49)	ARPE-19 cells incubated in 50 mM high glucose	Western blotting	High glucose upregulated protein expression of caspase-1, GSDMD, NLRP3, IL-1 $\beta$ , and IL-18 in ARPE-19 cells	High glucose may promote GSDMD-mediated pyroptosis in ARPE-19 cells

HRMECs, human retinal microvascular endothelial cells; RECs, retinal endothelial cells; PI, propidium iodide; FLICA, fluorochrome-labeled inhibitors of caspases; HRPs, human retinal pericytes; LDH, lactate dehydrogenase; ELISA, enzyme-linked immunosorbent assay; AGE-BSA, advanced glycation end-product modified bovine serum albumin; ARPE-19, human adult retinal pigment epithelial cell line-19; NLRP3, nucleotide-binding and oligomerization domain (NOD)-like receptor family pyrin domain-containing 3; IL-1 $\beta$ , interleukin-1 $\beta$ ; IL-18, interleukin-18; GSDMD, gasdermin D; GSDMD-N, N-terminal of gasdermin D.

specifically plays a role in late-stage neovascularization. Finally, while the RPE (part of the outer BRB) is not traditionally viewed to play a central role in the pathophysiology of DR, ARPE-19 cells have recently been found to undergo pyroptotic cell death under stimulation with 50mM glucose, which increased expression of pyroptosis-associated proteins NLRP3, caspase-1, and GSDMD (48, 49). Overall, the NLRP3/caspase-1/GSDMD canonical pyroptotic pathway appears to play a role in the loss of endothelial cells, pericytes, Müller cells, and RPE in cell culture, and in animal and human models for DR. However, few studies have directly demonstrated that the effector of pyroptosis, GSDMD-N, is activated in DR. Future studies aimed at GSDMD-N are needed to evaluate its potential to be a target for DR therapy.

## Pyroptosis and Glaucoma

Glaucoma is a group of ocular diseases characterized by the progressive loss of retinal ganglion cells (RGCs), the neurons that communicate visual information from the retina to the

brain (68). It is another leading cause of irreversible blindness worldwide and is projected to affect 112 million individuals aged 40–80 by 2040 (69). Various risk factors for glaucoma have been identified—the most notable being elevated intraocular pressure (IOP) and age—but the exact molecular mechanisms that link these risk factors to RGC loss are still under investigation. Past research has demonstrated that RGCs die by apoptosis (70). However, recent studies have implicated inflammasomes, caspase-1, and GSDMD in acute and chronic models of glaucoma, suggesting that apoptosis is not the only form of cell death involved in glaucomatous RGC loss.

In a mouse model for acute elevated IOP-induced glaucoma, NLRP1, NLRP3, ASC, and caspase-1 levels were rapidly upregulated in the retina after ischemic injury. Knockdown of the gene encoding toll-like receptor 4 (TLR4) using *TLR4*<sup>-/-</sup> mice reduced inflammasome production and RGC death after ischemic injury (50). TLR4 deficiency therefore seems to protect against RGC death through the inactivation of canonical inflammasomes and may be a potential treatment strategy for

**TABLE 3 |** Studies investigating pyroptosis in glaucoma.

Study	Model/Cell type studied	Technique	Findings	Relevance of findings to pyroptosis
Chi et al. (50)	Mouse model of acute IOP-induced glaucoma	PCR, western blotting	TLR4 deficiency protected against inflammasome activation and RGC death after acute IOP elevation via caspase-1 and caspase-8-dependent pathways	Pyroptosis-associated inflammatory pathways take place and cause RGC death after acute IOP elevation
Chi et al. (51)	Mouse model of acute IOP-induced glaucoma	PCR, western blotting	Inhibition of HMGB1, like TLR4 deficiency, protected against inflammasome activation and RGC death after acute IOP elevation via caspase-1 and caspase-8-dependent pathways	Pyroptosis-associated inflammatory pathways take place and cause RGC death after acute IOP elevation
Qi et al. (52)	RIR injury rat model	TUNEL staining, western blotting	Inhibition of TLR4 increased RGC survival by decreasing apoptosis	TLR4-mediated pathway may lead to RGC apoptosis rather than pyroptosis after RIR injury
Pronin et al. (53)	Acute OHT mouse model	Western blotting, immunohistochemistry	Within a few hours of inducing acute OHT in mouse eyes, retinal levels of GSDMD, caspase-1, and NLRP3 were significantly increased	Markers of GSDMD-mediated pyroptosis are upregulated in the retina after exposure to acute OHT
Chen et al. (54)	RIR injury mouse model	HE staining, retrograde FG-labeled imaging, immunofluorescence, western blotting	Genetic deletion of <i>GSDMD</i> significantly increased retinal thickness and decreased RGC death after RIR injury	Absence of an effector of pyroptosis protects against RGC death after RIR injury
Dong et al. (55)	Chronic OHT rat model	Western blotting	Protein levels of mature caspase-1 were elevated in rat retinas after chronic OHT	Caspase-1 processing, which can lead to pyroptosis, is increased in rat retinas with chronic OHT
Zhang et al. (56)	Chronic OHT mouse model	Western blotting	Protein levels of NLRP3 and cleaved caspase-1 were elevated during the chronic OHT process	Components of the canonical pyroptotic pathway are activated in a chronic OHT mouse model
Wan et al. (57)	RIR injury mouse model	Western blotting	RIR injury increased GSDMD-N expression in Iba-1+ microglia	An effector of pyroptosis is upregulated in microglia after RIR injury

IOP, intra-ocular pressure; RGC, retinal ganglion cell; PCR, polymerase chain reaction; RIR, retinal ischemia/reperfusion; TUNEL, terminal deoxynucleotidyl transferase dUTP nick end labeling; OHT, ocular hypertension; HE, hematoxylin and eosin; FG, fluoro-gold; NLRP3, nucleotide-binding and oligomerization domain (NOD)-like receptor family pyrin domain-containing 3; IL-1 $\beta$ , interleukin-1 $\beta$ ; IL-18, interleukin-18; GSDMD, gasdermin D; GSDMD-N, N-terminal of gasdermin D; TLR4, toll-like receptor 4; HMGB1, high-mobility group box 1.

acute glaucoma. Chi et al. (50) also showed that caspase-8 is the link between TLR4 and NLRP1/NLRP3 activation. As discussed previously, caspase-8 is traditionally thought of as an initiator of apoptosis but has also been found to play non-apoptotic roles (71). In support of this idea, this study demonstrated that inhibition of caspase-8 significantly reduced levels of NLRP1, NLRP3, ASC, caspase-1, and IL-1 $\beta$ , and also attenuated IOP-induced RGC death. Interestingly, inhibition of caspase-8 completely suppressed production of IL-1 $\beta$  while inhibition of caspase-1 only partially suppressed production of IL-1 $\beta$ . Therefore, therapeutic strategies targeting caspase-8 may be more effective at preventing inflammation in acute glaucoma than those targeting caspase-1. A year later, the same authors found that high-mobility group box 1 (HMGB1), an endogenous ligand of TLR4, is also involved in the above pathway. Inhibition of HMGB1 suppressed the production of NLRP3, ASC, activated caspase-1, activated caspase-8, and IL-1 $\beta$ , and also decreased RGC death after acute IOP elevation similarly to TLR4 (51). Thus, blocking HMGB1 is another way to target TLR4-induced inflammasome pathways in the treatment of acute glaucoma. A study using a retinal ischemia/reperfusion (RIR) injury rat model provided further support for TLR4-induced activation of NLRP3

and also found that inhibition of TLR4 decreased loss of RGCs. However, the type of cell death studied and detected to occur in these RGCs was apoptosis rather than pyroptosis (52). Aside from acute ischemic injury, inflammasomes are also involved in RGC loss from optic nerve crush injury. Following partial optic nerve crush (pONC) in mice, NLRP3 was upregulated at the site of injury and then propagated to the optic nerve head (ONH) and the entire retina within 1 day. Furthermore, *NLRP3*<sup>-/-</sup> mice experienced delayed RGC somal loss for 1 week and similarly delayed/decreased axon loss (72). These findings are in congruence with those from previous studies and support that NLRP3 is important for inflammation and RGC death in models of acute glaucoma, making it a worthwhile target for therapy.

The above studies implicated drivers of canonical pyroptosis in glaucomatous RGC death, but they did not study the effector of canonical pyroptosis, GSDMD. Pronin et al. (53) found that within a few hours of inducing acute ocular hypertension (OHT) in mouse eyes, retinal levels of GSDMD, in addition to activated caspase-1 and NLRP3, were significantly increased. RGCs were also shown to be the first cell type in the ganglion cell layer (GCL) to significantly express cleaved GSDMD after acute OHT injury (53). Taken together, these findings suggest that after acute



elevation of IOP, inflammasomes are activated in the retina and caspase-1 cleaves GSDMD to potentially trigger pyroptosis in RGCs. In a mouse RIR injury model, intravitreal injection of a *Casp1* inhibitor (Z-YVAD-fmk) markedly reduced cleavage of IL-1 $\beta$  and GSDMD, and restored RGC numbers during RIR injury. Furthermore, genetic deletion of *GSDMD* significantly increased retinal thickness and decreased RGC death after RIR injury (54). Therefore, both caspase-1 inhibition and knockdown of *GSDMD* expression are possible strategies to therapeutically attenuate RGC death in acute glaucoma. This study also reconciled the previously discovered role of caspase-8 in elevated IOP-induced RGC death with findings from other disease states that caspase-8 can cleave GSDMD, by showing that *Casp8* silencing in mice significantly lowered levels of cleaved GSDMD protein after RIR injury (refer to **Supplementary Figure 1** for a summary of proposed caspase-8-mediated apoptotic and pyroptotic pathways in acute glaucoma) (33, 34, 54).

The bulk of the research on pyroptosis in glaucoma has been done on acute models, as outlined above. Few studies have looked at the role of pyroptosis in chronic glaucoma. In human donor eyes of chronic glaucoma patients, various inflammasome components, including NLRP3 and caspase-1, were found to be upregulated along with significant cleaved caspase-1 expression in the retina. These early findings suggested that caspase-1 is activated by inflammasome assembly in chronic glaucomatous human retinas (73). NLRP3 and cleaved caspase-1 protein levels were also elevated in the retina of rodent models of chronic OHT (55, 56). These studies implicated P2X7 as the upstream activator of NLRP3. P2X7 receptors are nonselective cation channel receptors that contribute to inflammation in the central nervous system and are activated by ATP (74). Activation of the P2X7 receptor with an agonist (BzATP) increased expression of *NLRP3*, *Casp-1*, and *ASC* in rat retinal microglia. Inhibition of the above pathway using the P2X7 inhibitor A438079 or the NLRP3 inhibitor MCC950 decreased microglial activation and protected against RGC death (56). Thus, inhibiting the P2X7-NLRP3 pathway may be a therapeutic strategy for reducing microglial activation and subsequent RGC death in chronic glaucoma. Research on inflammatory signaling in glaucoma pathogenesis has also identified other ion channels located at the surface of RGCs, such as Transient Receptor Potential Vanilloid isoform 4 (TRPV4) and Pannexin-1 (Panx1), that act as potential sensors and effectors of mechanical strain, ischemia, and inflammatory responses. These signaling pathways are also associated with RGC axonal injury and cell death and can be further explored for potential interactions with inflammasome pathways in chronic glaucoma (75).

NLRP3 and caspase-1 were shown to be increased in the retina in the chronic glaucoma models above. However, whether these pyroptosis inducers and the pyroptosis effector GSDMD are expressed in neurons and RGCs specifically is still debated. There is evidence from other disease states that neurons express NLRP3. Functional inflammasomes and caspase-1 activity were present in cultured human CNS neurons and NLRP3 expression was detected in mesencephalic neurons in a Parkinson's disease model (76–78). However, in glaucomatous human donor eyes, cleaved caspase-1 was more prominent in

non-ganglion cells (Brn-3-negative glial cells) (73). This favored that RGCs may undergo cell death through a glial-cell mediated inflammatory pathway. Pronin et al. (53), discussed above, demonstrated the upregulation of NLRP3 inflammasome in RGCs and astrocytes in acute OHT. Zhang et al. (56) from above also supported a glial cell-mediated inflammatory pathway by showing increased expression of inflammasome components in rat retinal microglia rather than RGCs. Our recent research using chronic glaucoma mouse model DBA/2J demonstrated an age-dependent upregulation of NLRP3 in RGCs and a concomitant increase in intraocular pressure (79). RIR injury in mice increased GSDMD-N expression in Iba-1+ microglia, suggesting that microglia undergo pyroptosis in response to RIR injury. On the other hand, RGCs in this study were found to undergo apoptosis (57). All in all, these controversies suggest that inflammation in the glaucomatous eye consists of multiple levels of responses that, at present, we do not fully understand. Neuronal cells including RGCs, possibly perturbed by age-related and/or IOP-induced inflammatory stress, activate glial cells by releasing DAMPs and PAMPs, which could further result in the release of pro-inflammatory cytokines and contribute to neurotoxicity and loss of RGCs. Alternatively, sensors on RGCs may respond to ischemia and inflammatory stress and lead to the remodeling of axons and cell death (50, 80). More research is needed, particularly in chronic models of glaucoma, to determine how pyroptosis fits into this inflammatory picture and whether pyroptotic drivers are appropriate therapeutic targets for glaucoma.

## IMPACT OF TARGETING PYROPTOTIC CELL DEATH PATHWAYS ON EXISTING THERAPEUTIC STRATEGIES FOR RETINAL DISEASES

Potential novel therapeutic targets for AMD, DR, and glaucoma have been highlighted throughout this review and are summarized in **Table 4**. In brief, majority of the suggested strategies target the canonical, NLRP3/caspase-1/GSDMD-mediated pyroptotic cell death pathway. A few studies also supported targeting caspase-3/GSDME and caspase-8/GSDMD pathways in AMD and glaucoma. Aside from the possibility of using these targets to develop new drugs for retinal diseases, targeting pyroptotic cell death pathways can also have an impact on existing therapies for retinal diseases, namely anti-VEGF. Anti-VEGF therapy is the mainstay of treatment for ocular angiogenic disease processes including AMD and DR (81). Studies have shown that NLRP3 inflammasome-mediated pathways can also affect angiogenesis in AMD and DR, and this evidence will be reviewed below. Targeting these pathways may be an alternative strategy to anti-VEGF treatment or enhance the therapeutic effect of existing anti-VEGF treatments.

We know that inflammasome activation and release of inflammatory cytokines are associated with pyroptotic cell death; thus, we may expect that inhibiting these factors would have a protective effect in retinal disease. On the contrary, *Nlrp3*<sup>-/-</sup> and *IL-18*<sup>-/-</sup> mice showed significantly

**TABLE 4 |** Potential pyroptotic targets for AMD, DR, and glaucoma therapy.

Disease	Potential pyroptotic targets for therapy					
	NLRP3	Caspase-1	Caspase-3	Caspase-8	GSDMD, GSDMD-N	GSDME, GSDME-N
AMD	✓	✓	✓		✓	✓
DR	✓	✓			✓	
Acute glaucoma	✓	✓		✓	✓	
Chronic glaucoma	✓	✓				

✓ represents that the pyroptosis-related protein has been demonstrated to play a role in the retinal disease on the left and may therefore be a potential novel therapeutic target for that disease. AMD, age-related macular degeneration; DR, diabetic retinopathy; NLRP3, nucleotide-binding and oligomerization domain (NOD)-like receptor family pyrin domain-containing 3; GSDMD/E-N, gasdermin-D/E; GSDMD-N, N-terminal of gasdermin D/E.

more choroidal neovascularization (CNV) development and subretinal hemorrhage compared to wild-type (WT) mice in a laser-induced model of wet AMD. Furthermore, intravitreal injections of IL-18-neutralizing antibodies after laser-induced CNV resulted in significantly increased CNV development in WT mice, suggesting that IL-18 may protect against CNV through the downregulation of VEGF. Indeed, treatment with IL-18 significantly decreased the amount of VEGF secreted by human ARPE-19 cells as well as mouse brain microvascular endothelial cells (82). Therefore, NLRP3 could be used as a protective agent against AMD and delivering IL-18 to the eye may have a therapeutic effect on CNV progression by decreasing VEGF. The latter was also supported by another study that found that deficiency of IL-18 significantly increased the number of CNV lesions in VEGF-A<sup>hyper</sup> mice (83). In 2014, Doyle et al. (84) further demonstrated that IL-18 injection would be safe to use in human eyes. They did not find any measurable cell death, changes in cell morphology, or compromise of plasma membrane integrity even when hyper-physiological doses of recombinant human IL-18 were applied to human ARPE-19 cells and native human RPE cells from three donors. Interestingly, Doyle et al. (84) also showed that IL-18 could enhance the CNV-attenuating effects of anti-VEGF therapy when applied in tandem as an intravitreal injection or systemically via a single subcutaneous dose. CNV volume was most significantly reduced when intravitreal injection of DMS1529 (mouse anti-VEGF) was combined with either intravitreal or subcutaneous administration of GSK (mouse IL-18) in C57BL/6J mice after laser-induced CNV. Systemic IL-18 therapy was also effective at reducing CNV volume alone—subcutaneous administration of GSK at a dose of 0.1 or 1.0 mg/kg 1 day before, and on each day after, laser-induced CNV both significantly attenuated CNV and CNV-induced permeability with no observable adverse effects (84). This shows the potential of using intravitreal or subcutaneous IL-18 separately or as an adjunct to existing anti-VEGF therapies to treat wet AMD pathology.

While the above research is promising, it has been met with some controversy. Tarallo et al. (35) found the opposite effect of IL-18 where IL-18 neutralization protected against RPE death in a mouse model for GA and IL-18 levels were significantly greater in human eyes with GA than in healthy

controls. This implies that IL-18 is cytotoxic and may signify that IL-18 plays different roles in wet vs. dry AMD. IL-18 levels were also found to be significantly elevated in the serum of AMD patients compared to healthy controls, suggesting that higher systemic levels of IL-18 are associated with AMD diagnosis (85). This opposes the above suggestion that systemic injection of IL-18 can be therapeutic for AMD. Furthermore, while the studies by Doyle and colleagues suggested that NLRP3 could be used as a protective agent in AMD, other studies have found that NLRP3 activation/consequent increase in active IL-1 $\beta$  is pro-angiogenic and promotes VEGF-induced AMD pathologies (83). Nucleoside reverse transcriptase inhibitors (NRTIs) such as stavudine (d4T) also reduced CNV volume in a laser-induced mouse model of CNV via blockade of a P2X7-induced pathway of inflammasome activation (86). In DR, studies have proposed that the pro-inflammatory events associated with NLRP3 activity cause breakdown of the BRB and subsequent neovascular response leading to PDR (87). Inhibition of caspase-1 with minocycline prevented acellular capillary development in STZ-induced diabetic and galactosemia mouse models (88). Elevated protein expression of NLRP3, caspase-1, and inflammatory cytokines was found in the proliferative membranes of human donor eyes with PDR compared to healthy controls (89). Similar results were seen in vitreous fluid samples of DR patients, especially in PDR eyes with TRD and active neovessel formation (90, 91). Finally, NLRP3 inhibition with MCC950 downregulated high glucose-induced upregulation of pro-angiogenic factors including VEGF (47). In sum, NLRP3-mediated inflammatory pathways are involved in angiogenic disease processes in AMD and DR, but further research is required to resolve the debate over whether its role is deleterious or beneficial.

## DISCUSSION

In this review, we have outlined the role of pyroptosis as a gasdermin-mediated inflammatory form of PCD in three common retinal diseases—age-related macular degeneration, diabetic retinopathy, and glaucoma. In AMD, GSDMD-mediated pyroptosis appears to occur in RPE when triggered by lysosomal destabilization or A $\beta$  while GSDME-mediated pyroptosis occurs in the aRAL model of AMD. The research on pyroptosis in

DR is in more preliminary stages, with most of its evidence for pyroptosis being limited to inflammasome activation rather than gasdermin activation in endothelial cells, pericytes, Müller cells, and RPE. Finally, there is support for gasdermin involvement in RGC loss in acute glaucoma, but evidence in chronic glaucoma models remains in its infancy. All in all, as our understanding of pyroptosis has grown and evolved, there is more support for its involvement in retinal disease. However, there are still many limitations in our understanding of pyroptosis in retinal disease that must be addressed.

Firstly, the involvement of pyroptosis in retinal disease does not exclude the occurrence of other forms of PCD such as apoptosis, ferroptosis, and necroptosis. There is substantial evidence for the involvement of these other PCD pathways in retinal disease as well (10, 66, 92). Further research is needed to uncover how different forms of PCD interact with each other in the retina and what factors ultimately determine the type of PCD an individual retinal cell will succumb to in pathological states. This information is vital in the development of therapies targeting PCD. If we target a form of PCD that is not the primary mode of cell death naturally occurring in AMD, DR, or glaucoma, then such treatments for these diseases may be ineffective. Or, if blocking one form of PCD such as apoptosis causes another, more inflammatory cell death mechanism to occur, we could potentially do more harm. A limited number of studies have provided some insight into how different types of PCD may be linked. Jiang et al. (93) showed that the caspase-3/GSDME pathway can result in either apoptosis or pyroptosis, depending on the expression level of GSDME. GSDME may therefore be the link between PCD pathways we have been looking for and provide an explanation for why we have been able to identify both apoptotic and pyroptotic mechanisms in retinal disease. On the other hand, Kayagaki et al. (22) identified that NINJ1 plays a potent role in causing plasma membrane rupture and DAMP-release not only following pyroptosis, but also during apoptosis and necrosis. Therefore, targeting NINJ1 could be a downstream therapeutic strategy that suppresses propagation of the cell death-associated inflammatory response regardless of its upstream mechanism (pyroptotic or otherwise).

We also need to be wary of the limitations in how we interpret the existing literature on pyroptosis in retinal disease. Because the essential role of gasdermin in pyroptosis was only recently established in 2015, earlier research on pyroptosis in retinal disease could only aim to identify inflammasome and caspase-1 activation in these diseases. We now know that activated inflammasomes can cause caspase-1 to cleave and release inflammatory cytokines without resulting in cell death (9, 28). Thus, we cannot assume that inflammasome activity, presence of mature caspase-1, and release of inflammatory cytokines in retinal cells necessarily means that pyroptosis is occurring in those cells. In addition, with the discovery that caspases 3 and 8 can activate GSDME and GSDMD (respectively) to mediate pyroptosis, we must also re-evaluate previous results suggesting that activation of these caspases in retinal cells represented

apoptotic cell death. This also supports that there is significant overlap and a complex interplay between pyroptotic and apoptotic cell death that we do not currently understand. Many questions related to this require further study. For one, under what conditions do caspases 3 and 8 favor cleaving gasdermin over their usual apoptotic substrates? Furthermore, what other cell types and pathologies besides those already identified demonstrate caspase-3/8-mediated pyroptosis as opposed to the more well-known mechanisms of pyroptosis? GSDME-mediated pyroptosis is increasingly being demonstrated to play a role in cancer (94), but its involvement in neurodegenerative diseases including retinal diseases is still largely unexplored. There is also the question of if GSDMA/B/C-mediated pyroptosis has a role to play in retinal diseases. The gold standard for demonstrating the occurrence of pyroptosis should be the identification of cleaved N-terminal of gasdermin proteins in well-established models of retinal disease. More studies like this would provide a better foundation for us to determine if gasdermin-mediated therapy is a viable strategy for the treatment of retinal pathologies. Gasdermin-mediated therapies are currently being studied in tumor treatment (9), and potential translation of these therapies to retinal diseases is another area for future research.

## AUTHOR CONTRIBUTIONS

MZ sourced and analyzed the referenced literature, conceived the structure of the manuscript, and wrote the manuscript. SL was a significant contributor in reviewing the drafts of the manuscript, adding to section “Pyroptosis and Glaucoma” of the manuscript, and creating supplementary figures. JM was a significant contributor in refining the topic of the review, conceiving the structure of the manuscript, reviewing the drafts of the manuscript, creating supplementary figures, and providing funding for the study. All authors have read and approved the final manuscript.

## FUNDING

Authors acknowledge funding from Canadian Institutes of Health Research, Natural Science and Engineering Research Council, and National Institutes of Health Research.

## ACKNOWLEDGMENTS

Authors wish to acknowledge Faculty of Medicine (UBC), Jing Cui, Eleanor To, Jeanne Xi, Gideon Obasanmi and Manjosh Uppal.

## SUPPLEMENTARY MATERIAL

The Supplementary Material for this article can be found online at: <https://www.frontiersin.org/articles/10.3389/fmed.2021.802063/full#supplementary-material>

## REFERENCES

- Remé CE, Grimm C, Hafezi F, Wenzel A, Williams TP. Apoptosis in the retina: the silent death of vision. *News Physiol Sci.* (2000) 15:120–5. doi: 10.1152/physiologyonline.2000.15.3.120
- Remé CE, Grimm C, Hafezi F, Marti A, Wenzel A. Apoptotic cell death in retinal degenerations. *Prog Retin Eye Res.* (1998) 17:443–64. doi: 10.1016/S1350-9462(98)00009-3
- Portera-Cailliau C, Sung CH, Nathans J, Adler R. Apoptotic photoreceptor cell death in mouse models of retinitis pigmentosa. *Proc Natl Acad Sci U S A.* (1994) 91:974–8. doi: 10.1073/pnas.91.3.974
- Galluzzi L, Vitale I, Aaronson SA, Abrams JM, Adam D, Agostinis P, et al. Molecular mechanisms of cell death: recommendations of the nomenclature committee on cell death 2018. *Cell Death Differ.* (2018) 25:486–541. doi: 10.1038/s41418-018-0102-y
- Pasparakis M, Vandenabeele P. Necroptosis and its role in inflammation. *Nature.* (2015) 517:311–20. doi: 10.1038/nature14191
- Yang WS, Stockwell BR. Ferroptosis: death by lipid peroxidation. *Trends Cell Biol.* (2016) 26:165–76. doi: 10.1016/j.tcb.2015.10.014
- Ding J, Wang K, Liu W, She Y, Sun Q, Shi J, et al. Pore-forming activity and structural autoinhibition of the gasdermin family. *Nature.* (2016) 535:111–6. doi: 10.1038/nature18590
- Liu X, Zhang Z, Ruan J, Pan Y, Magupalli VG, Wu H, et al. Inflammasome-activated gasdermin D causes pyroptosis by forming membrane pores. *Nature.* (2016) 535:153–8. doi: 10.1038/nature18629
- Yu P, Zhang X, Liu N, Tang L, Peng C, Chen X. Pyroptosis: mechanisms and diseases. *Signal Transduct Target Ther.* (2021) 6:1. doi: 10.1038/s41392-021-00507-5
- Peng JJ, Song WT, Yao F, Zhang X, Peng J, Luo XJ, et al. Involvement of regulated necrosis in blinding diseases: focus on necroptosis and ferroptosis. *Exp Eye Res.* (2020) 191:107922. doi: 10.1016/j.exer.2020.107922
- Brennan MA, Cookson BT. Salmonella induces macrophage death by caspase-1-dependent necrosis. *Mol Microbiol.* (2000) 38:31–40. doi: 10.1046/j.1365-2958.2000.02103.x
- Bergsbaken T, Fink SL, Cookson BT. Pyroptosis: host cell death and inflammation. *Nat Rev Microbiol.* (2009) 7:99–109. doi: 10.1038/nrmicro2070
- Fink SL, Cookson BT. Caspase-1-dependent pore formation during pyroptosis leads to osmotic lysis of infected host macrophages. *J Immunol.* (2006) 202:1913–26. doi: 10.1111/j.1462-5822.2006.00751.x
- Shi J, Zhao Y, Wang K, Shi X, Wang Y, Huang H, et al. Cleavage of GSDMD by inflammatory caspases determines pyroptotic cell death. *Nature.* (2015) 526:660–5. doi: 10.1038/nature15514
- Shi J, Gao W, Shao F. Pyroptosis: gasdermin-mediated programmed necrotic cell death. *Trends Biochem Sci.* (2017) 42:245–54. doi: 10.1016/j.tibs.2016.10.004
- Liu Z, Wang C, Yang J, Zhou B, Yang R, Ramachandran R, et al. Crystal structures of the full-length murine and human gasdermin d reveal mechanisms of autoinhibition, lipid binding, and oligomerization. *Immunity.* (2019) 51:43–9. doi: 10.1016/j.immuni.2019.04.017
- Kuang S, Zheng J, Yang H, Li S, Duan S, Shen Y, et al. Structure insight of GSDMD reveals the basis of GSDMD autoinhibition in cell pyroptosis. *Proc Natl Acad Sci U S A.* (2017) 114:10642–7. doi: 10.1073/pnas.1708194114
- Kayagaki N, Stowe IB, Lee BL, O'Rourke K, Anderson K, Warming S, et al. Caspase-11 cleaves gasdermin D for non-canonical inflammasome signalling. *Nature.* (2015) 526:666–71. doi: 10.1038/nature15541
- Zhou Z, He H, Wang K, Shi X, Wang Y, Su Y, et al. Granzyme A from cytotoxic lymphocytes cleaves GSDMB to trigger pyroptosis in target cells. *Science.* (2020) 368:eaaz7548. doi: 10.1126/science.aaz7548
- Zhang Z, Zhang Y, Xia S, Kong Q, Li S, Liu X, et al. Gasdermin E suppresses tumour growth by activating anti-tumour immunity. *Nature.* (2020) 579:415–20. doi: 10.1038/s41586-020-2071-9
- Ruan J, Xia S, Liu X, Lieberman J, Wu H. Cryo-EM structure of the gasdermin A3 membrane pore. *Nature.* (2018) 557:62–7. doi: 10.1038/s41586-018-0058-6
- Kayagaki N, Kornfeld OS, Lee BL, Stowe IB, O'Rourke K, Li Q, et al. NIN1 mediates plasma membrane rupture during lytic cell death. *Nature.* (2021) 591:131–6. doi: 10.1038/s41586-021-03218-7
- Place DE, Kanneganti TD. Recent advances in inflammasome biology. *Curr Opin Immunol.* (2018) 50:32–8. doi: 10.1016/j.coi.2017.10.011
- Broz P, Dixit VM. Inflammasomes: mechanism of assembly, regulation and signalling. *Nat Rev Immunol.* (2016) 16:407–20. doi: 10.1038/nri.2016.58
- Minkiewicz J, de Rivero Vaccari JP, Keane RW. Human astrocytes express a novel NLRP2 inflammasome. *Glia.* (2013) 61:1113–21. doi: 10.1002/glia.22499
- Levy M, Thaïs CA, Zeevi D, Dohnalová L, Zilberman-Schapira G, Mahdi JA, et al. Microbiota-modulated metabolites shape the intestinal microenvironment by regulating NLRP6 inflammasome signaling. *Cell.* (2015) 163:1428–43. doi: 10.1016/j.cell.2015.10.048
- Yerramothu P, Vijay AK, Willcox MDP. Inflammasomes, the eye and anti-inflammasome therapy. *Eye.* (2018) 32:491–505. doi: 10.1038/eye.2017.241
- Carty M, Kearney J, Shanahan KA, Hams E, Sugisawa R, Connolly D, et al. Cell survival and cytokine release after inflammasome activation is regulated by the Toll-IL-1R protein SARM. *Immunity.* (2019) 50:1412–24. doi: 10.1016/j.immuni.2019.04.005
- Aglietti RA, Estevez A, Gupta A, Ramirez MG, Liu PS, Kayagaki N, et al. GsdmD p30 elicited by caspase-11 during pyroptosis forms pores in membranes. *Proc Natl Acad Sci U S A.* (2016) 113:7858–63. doi: 10.1073/pnas.1607769113
- Shi J, Zhao Y, Wang Y, Gao W, Ding J, Li P, et al. Inflammatory caspases are innate immune receptors for intracellular LPS. *Nature.* (2014) 514:187–92. doi: 10.1038/nature13683
- Wang Y, Gao W, Shi X, Ding J, Liu W, He H, et al. Chemotherapy drugs induce pyroptosis through caspase-3 cleavage of a gasdermin. *Nature.* (2017) 547:99–103. doi: 10.1038/nature22393
- Rogers C, Fernandes-Alnemri T, Mayes L, Alnemri D, Cingolani G, Alnemri ES. Cleavage of DFNA5 by caspase-3 during apoptosis mediates progression to secondary necrotic/pyroptotic cell death. *Nat Commun.* (2017) 8:1–14. doi: 10.1038/ncomms14128
- Sarhan J, Liu BC, Muendlein HI, Li P, Nilson R, Tang AY, et al. Caspase-8 induces cleavage of gasdermin D to elicit pyroptosis during Yersinia infection. *Proc Natl Acad Sci U S A.* (2018) 115:E10888–97. doi: 10.1073/pnas.1809548115
- Orning P, Weng D, Starheim K, Ratner D, Best Z, Lee B, et al. Pathogen blockade of TAK1 triggers caspase-8-dependent cleavage of gasdermin D and cell death. *Science.* (2018) 362:1064–9. doi: 10.1126/science.aau2818
- Tarallo V, Hirano Y, Gelfand BD, Dridi S, Kerur N, Kim Y, et al. DICER1 loss and Alu RNA induce age-related macular degeneration via the NLRP3 inflammasome and MyD88. *Cell.* (2012) 149:847–59. doi: 10.1016/j.cell.2012.03.036
- Kerur N, Fukuda S, Banerjee D, Kim Y, Fu D, Apicella I, et al. cGAS drives noncanonical-inflammasome activation in age-related macular degeneration. *Nat Med.* (2018) 24:50–61. doi: 10.1038/nm.4450
- Tseng WA, Thein T, Kinnunen K, Lashkari K, Gregory MS, D'Amore PA, et al. NLRP3 inflammasome activation in retinal pigment epithelial cells by lysosomal destabilization: implications for age-related macular degeneration. *Invest Ophthalmol Vis Sci.* (2013) 54:110–20. doi: 10.1167/iovs.12-10655
- Gao J, Cui JZ, To E, Cao S, Matsubara JA. Evidence for the activation of pyroptotic and apoptotic pathways in RPE cells associated with NLRP3 inflammasome in the rodent eye. *J Neuroinflammation.* (2018) 15:13–5. doi: 10.1186/s12974-018-1062-3
- Sun HJ, Jin XM, Xu J, Xiao Q. Baicalin alleviates age-related macular degeneration via miR-223/NLRP3-regulated pyroptosis. *Pharmacology.* (2020) 105:28–38. doi: 10.1159/000502614
- Yang M, So KF, Lo ACY, Lam WC. The effect of lycium barbarum polysaccharides on pyroptosis-associated amyloid  $\beta$ (1–40) oligomers-induced adult retinal pigment epithelium 19 cell damage. *Int J Mol Sci.* (2020) 21:4658. doi: 10.3390/ijms21134658
- Liao Y, Zhang H, He D, Wang Y, Cai B, Chen J, et al. Retinal pigment epithelium cell death is associated with NLRP3 inflammasome activation by all-trans retinal. *Invest Ophthalmol Vis Sci.* (2019) 60:3034–45. doi: 10.1167/iovs.18-26360
- Jiang Y, Liu L, Curtiss E, Steinle JJ. Epac1 blocks NLRP3 inflammasome to reduce IL-1 $\beta$  in retinal endothelial cells and mouse retinal vasculature. *Mediators Inflamm.* (2017) 2017:2860956. doi: 10.1155/2017/2860956
- Chen W, Zhao M, Zhao S, Lu Q, Ni L, Zou C, et al. Activation of the TXNIP/NLRP3 inflammasome pathway contributes to inflammation in diabetic retinopathy: a novel inhibitory effect of minocycline. *Inflamm Res Off J Eur Histamine Res Soc.* (2017) 66:157–66. doi: 10.1007/s00011-016-1002-6



44. Gu C, Draga D, Zhou C, Su T, Zou C, Gu Q, et al. miR-590-3p Inhibits pyroptosis in diabetic retinopathy by targeting NLRP1 and inactivating the NOX4 signaling pathway. *Invest Ophthalmol Vis Sci.* (2019) 60:4215–23. doi: 10.1167/iov.19-27825
45. Gan J, Huang M, Lan G, Liu L, Xu F. High glucose induces the loss of retinal pericytes partly via NLRP3-caspase-1-GSDMD-mediated pyroptosis. *Biomed Res Int.* (2020) 2020:1–12. doi: 10.1155/2020/4510628
46. Yu X, Ma X, Lin W, Xu Q, Zhou H, Kuang HY. Long noncoding RNA MIAT regulates primary human retinal pericyte pyroptosis by modulating miR-342-3p targeting of CASP1 in diabetic retinopathy. *Exp Eye Res.* (2020). doi: 10.1016/j.exer.2020.108300
47. Du J, Wang Y, Tu Y, Guo Y, Sun X, Xu X, et al. A prodrug of epigallocatechin-3-gallate alleviates high glucose-induced pro-angiogenic factor production by inhibiting the ROS/TXNIP/NLRP3 inflammasome axis in retinal Müller cells. *Exp Eye Res.* (2020) 196:108065. doi: 10.1016/j.exer.2020.108065
48. Xi X, Yang Y, Ma J, Chen Q, Zeng Y, Li J, et al. MiR-130a alleviated high-glucose induced retinal pigment epithelium (RPE) death by modulating TNF- $\alpha$ /SOD1/ROS cascade mediated pyroptosis. *Biomed Pharmacother.* (2020) 125:109924. doi: 10.1016/j.biopha.2020.109924
49. Zha X, Xi X, Fan X, Ma M, Zhang Y, Yang Y. Overexpression of METTL3 attenuates high-glucose induced RPE cell pyroptosis by regulating miR-25-3p/PTEN/Akt signaling cascade through DGCR8. *Aging.* (2020) 12:8137–50. doi: 10.18632/aging.103130
50. Chi W, Li F, Chen H, Wang Y, Zhu Y, Yang X, et al. Caspase-8 promotes NLRP1/NLRP3 inflammasome activation and IL-1 $\beta$  production in acute glaucoma. *Proc Natl Acad Sci U S A.* (2014) 111:11181–6. doi: 10.1073/pnas.1402819111
51. Chi W, Chen H, Li F, Zhu Y, Yin W, Zhuo Y. HMGB1 promotes the activation of NLRP3 and caspase-8 inflammasomes via NF- $\kappa$ B pathway in acute glaucoma. *J Neuroinflammation.* (2015) 12:1–12. doi: 10.1186/s12974-015-0360-2
52. Qi Y, Zhao M, Bai Y, Huang L, Yu W, Bian Z, et al. Retinal ischemia/reperfusion injury is mediated by tolllike receptor 4 activation of NLRP3 inflammasomes. *Investig Ophthalmol Vis Sci.* (2014) 55:5466–75. doi: 10.1167/iov.14-14380
53. Pronin A, Pham D, An W, Dvorianchikova G, Reshetnikova G, Qiao J, et al. Inflammasome activation induces pyroptosis in the retina exposed to ocular hypertension injury. *Front Mol Neurosci.* (2019) 12:36. doi: 10.3389/fnmol.2019.00036
54. Chen H, Deng Y, Gan X, Li Y, Huang W, Lu L, et al. NLRP12 collaborates with NLRP3 and NLRC4 to promote pyroptosis inducing ganglion cell death of acute glaucoma. *Mol Neurodegener.* (2020) 15:1–16. doi: 10.1186/s13024-020-00372-w
55. Dong L, Hu Y, Zhou L, Cheng X. P2X7 receptor antagonist protects retinal ganglion cells by inhibiting microglial activation in a rat chronic ocular hypertension model. *Mol Med Rep.* (2018) 17:2289–96. doi: 10.3892/mmr.2017.8137
56. Zhang Y, Xu Y, Sun Q, Xue S, Guan H, Ji M. Activation of P2X7R-NLRP3 pathway in retinal microglia contribute to retinal ganglion cells death in chronic ocular hypertension (COH). *Exp Eye Res.* (2019) 188:107771. doi: 10.1016/j.exer.2019.107771
57. Wan P, Su W, Zhang Y, Li Z, Deng C, Li J, et al. LncRNA H19 initiates microglial pyroptosis and neuronal death in retinal ischemia/reperfusion injury. *Cell Death Differ.* (2020) 27:176–91. doi: 10.1038/s41418-019-0351-4
58. Wong WL, Su X, Li X, Cheung CMG, Klein R, Cheng CY, et al. Global prevalence of age-related macular degeneration and disease burden projection for 2020 and 2040: a systematic review and meta-analysis. *Lancet Glob Heal.* (2014) 2:e106–16. doi: 10.1016/S2214-109X(13)70145-1
59. Mitchell P, Liew G, Gopinath B, Wong TY. Age-related macular degeneration. *Lancet.* (2018) 392:1147–59. doi: 10.1016/S0140-6736(18)31550-2
60. Fleckenstein M, Keenan TDL, Guymer RH, Chakravarthy U, Schmitz-Valckenberg S, Klaver CC, et al. Age-related macular degeneration. *Nat Rev Dis Prim.* (2021) 7:1. doi: 10.1038/s41572-021-00265-2
61. Kaneko H, Dridi S, Tarallo V, Gelfand BD, Fowler BJ, Cho WG, et al. DICER1 deficit induces alu RNA toxicity in age-related macular degeneration. *Nature.* (2011) 471:325–32. doi: 10.1038/nature09830
62. Hu Z, Lv X, Chen L, Gu X, Qian H, Fransisca S, et al. Protective effects of microRNA-22-3p against retinal pigment epithelial inflammatory damage by targeting NLRP3 inflammasome. *J Cell Physiol.* (2019) 234:18849–57. doi: 10.1002/jcp.28523
63. Cheung N, Mitchell P, Wong TY. Diabetic retinopathy. *Lancet.* (2010) 376:124–36. doi: 10.1016/S0140-6736(09)62124-3
64. Wang W, Lo ACY. Diabetic retinopathy: pathophysiology and treatments. *Int J Mol Sci.* (2018) 19:6. doi: 10.3390/ijms19061816
65. Lechner J, O'Leary OE, Stitt AW. The pathology associated with diabetic retinopathy. *Vision Res.* (2017) 139:7–14. doi: 10.1016/j.visres.2017.04.003
66. Feenstra DJ, Yego EC, Mohr S. Modes of retinal cell death in diabetic retinopathy. *J Clin Exp Ophthalmol.* (2013) 04:1–16. doi: 10.4172/2155-9570.1000298
67. Jiang Y, Steinle JJ. Epac1 inhibits PKR to reduce NLRP3 inflammasome proteins in retinal endothelial cells. *J Inflamm Res.* (2019) 12:153–9. doi: 10.2147/JIR.S210441
68. Weinreb RN, Aung T, Medeiros FA. The pathophysiology and treatment of glaucoma: a review. *JAMA.* (2014) 311:1901–11. doi: 10.1001/jama.2014.3192
69. Tham YC, Li X, Wong TY, Quigley HA, Aung T, Cheng C-Y. Global prevalence of glaucoma and projections of glaucoma burden through 2040: a systematic review and meta-analysis. *Ophthalmology.* (2014) 121:2081–90. doi: 10.1016/j.ophtha.2014.05.013
70. Almasieh M, Wilson AM, Morquette B, Cueva Vargas JL, Di Polo A. The molecular basis of retinal ganglion cell death in glaucoma. *Prog Retin Eye Res.* (2012) 31:152–81. doi: 10.1016/j.preteyeres.2011.11.002
71. Nagata S, Tanaka M. Programmed cell death and the immune system. *Nat Rev Immunol.* (2017) 17:333–40. doi: 10.1038/nri.2016.153
72. Puyang Z, Feng L, Chen H, Liang P, Troy JB, Liu X. Retinal ganglion cell loss is delayed following optic nerve crush in NLRP3 knockout mice. *Sci Rep.* (2016) 6:6–13. doi: 10.1038/srep20998
73. Yang X, Luo C, Cai J, Powell DW, Yu D, Kuehn MH, et al. Neurodegenerative and inflammatory pathway components linked to TNF- $\alpha$ /TNFR1 signaling in the glaucomatous human retina. *Invest Ophthalmol Vis Sci.* (2011) 52:8442–54. doi: 10.1167/iov.11-8152
74. Stokes L, Spencer SJ, Jenkins TA. Understanding the role of P2X7 in affective disorders—are glial cells the major players? *Front Cell Neurosci.* (2015) 9:1–6. doi: 10.3389/fncel.2015.00258
75. Križaj D, Ryskamp DA, Tian N, Tezel G, Mitchell CH, Slepak VZ, et al. From Mechanosensitivity to inflammatory responses: new players in the pathology of glaucoma. *Curr Eye Res.* (2014) 39:105–19. doi: 10.3109/02713683.2013.836541
76. Kaushal V, Dye R, Pakavathkumar P, Foveau B, Flores J, Hyman B, et al. Neuronal NLRP1 inflammasome activation of Caspase-1 coordinately regulates inflammatory interleukin-1-beta production and axonal degeneration-associated Caspase-6 activation. *Cell Death Differ.* (2015) 22:1676–86. doi: 10.1038/cdd.2015.16
77. von Herrmann KM, Salas LA, Martinez EM, Young AL, Howard JM, Feldman MS, et al. NLRP3 expression in mesencephalic neurons and characterization of a rare NLRP3 polymorphism associated with decreased risk of Parkinson's disease. *npj Park Dis.* (2018) 4:1. doi: 10.1038/s41531-018-0061-5
78. Cheng X, Xu S, Zhang C, Qin K, Yan J, Shao X. The BRCC3 regulated by Cdk5 promotes the activation of neuronal NLRP3 inflammasome in Parkinson's disease models. *Biochem Biophys Res Commun.* (2020) 522:647–54. doi: 10.1016/j.bbrc.2019.11.141
79. Li S, Gao J, Cui JZ, Matsubara JA. NLRP3 inflammasome contributes to retinal ganglion cell (RGC) death during glaucoma pathogenesis in DBA/2J mouse model. *Invest Ophthalmol Vis Sci.* (2019) 60:3790–3790. doi: 10.14288/1.0394326
80. Lu W, Albalawi F, Beckel JM, Lim JC, Laties AM, Mitchell CH. The P2X7 receptor links mechanical strain to cytokine IL-6 up-regulation and release in neurons and astrocytes. *J Neurochem.* (2017) 141:436–48. doi: 10.1111/jnc.13998
81. Tah V, Orlans HO, Hyer J, Casswell E, Din N, Sri Shanmuganathan V, et al. Anti-VEGF therapy and the retina: an update. *J Ophthalmol.* (2015) 2015:627674. doi: 10.1155/2015/627674
82. Doyle SL, Campbell M, Ozaki E, Salomon RG, Mori A, Kenna PF, et al. NLRP3 has a protective role in age-related macular degeneration through

- the induction of IL-18 by drusen components. *Nat Med.* (2012) 18:791–8. doi: 10.1038/nm.2717
83. Marneros AG. NLRP3 inflammasome blockade inhibits VEGF-A-induced age-related macular degeneration. *Cell Rep.* (2013) 4:945–58. doi: 10.1016/j.celrep.2013.08.002
  84. Doyle SL, Ozaki E, Brennan K, Humphries MM, Mulfaul K, Keaney J, et al. IL-18 attenuates experimental choroidal neovascularization as a potential therapy for wet age-related macular degeneration. *Sci Transl Med.* (2014) 6:230ra44. doi: 10.1126/scitranslmed.3007616
  85. Weaver C, Cyr B, de Rivero Vaccari JC, de Rivero Vaccari JP. Inflammasome proteins as inflammatory biomarkers of age-related macular degeneration. *Transl Vis Sci Technol.* (2020) 9:1–9. doi: 10.1167/tvst.9.13.27
  86. Fowler BJ, Gelfand BD, Kim Y, Kerur N, Tarallo V, Hirano Y, et al. Nucleoside reverse transcriptase inhibitors possess intrinsic anti-inflammatory activity. *Science.* (2014) 346:1000–3. doi: 10.1126/science.1261754
  87. Chaurasia SS, Lim RR, Parikh BH, Wey YS, Tun BB, Wong TY, et al. The NLRP3 inflammasome may contribute to pathologic neovascularization in the advanced stages of diabetic retinopathy. *Sci Rep.* (2018) 8:2847–z. doi: 10.1038/s41598-018-21198-z
  88. Vincent JA, Mohr S. Inhibition of caspase-1/interleukin-1 $\beta$  signaling prevents degeneration of retinal capillaries in diabetes and galactosemia. *Diabetes.* (2007) 56:224–30. doi: 10.2337/db06-0427
  89. Zhang Y, Lv X, Hu Z, Ye X, Zheng X, Ding Y, et al. Protection of Mcc950 against high-glucose-induced human retinal endothelial cell dysfunction. *Cell Death Dis.* (2017) 8:e2941. doi: 10.1038/cddis.2017.308
  90. Loukovaara S, Piippo N, Kinnunen K, Hytti M, Kaarniranta K, Kauppinen A. NLRP3 inflammasome activation is associated with proliferative diabetic retinopathy. *Acta Ophthalmol.* (2017) 95:803–8. doi: 10.1111/aos.13427
  91. Chen H, Zhang X, Liao N, Mi L, Peng Y, Liu B, et al. Enhanced expression of NLRP3 inflammasome-related inflammation in diabetic retinopathy. *Invest Ophthalmol Vis Sci.* (2018) 59:978–85. doi: 10.1167/iovs.17-22816
  92. Telegina DV, Kozhevnikova OS, Kolosova NG. Molecular mechanisms of cell death in retina during development of age-related macular degeneration. *Adv Gerontol.* (2017) 7:17–24. doi: 10.1134/S2079057017010155
  93. Jiang M, Qi L, Li L, Li Y. The caspase-3/GSDME signal pathway as a switch between apoptosis and pyroptosis in cancer. *Cell Death Discov.* (2020) 6:1. doi: 10.1038/s41420-020-00349-0
  94. Wang M, Jiang S, Zhang Y, Li P, Wang K. The multifaceted roles of pyroptotic cell death pathways in cancer. *Cancers.* (2019) 11:1313. doi: 10.3390/cancers11091313

**Conflict of Interest:** The authors declare that the research was conducted in the absence of any commercial or financial relationships that could be construed as a potential conflict of interest.

**Publisher's Note:** All claims expressed in this article are solely those of the authors and do not necessarily represent those of their affiliated organizations, or those of the publisher, the editors and the reviewers. Any product that may be evaluated in this article, or claim that may be made by its manufacturer, is not guaranteed or endorsed by the publisher.

Copyright © 2022 Zhao, Li and Matsubara. This is an open-access article distributed under the terms of the Creative Commons Attribution License (CC BY). The use, distribution or reproduction in other forums is permitted, provided the original author(s) and the copyright owner(s) are credited and that the original publication in this journal is cited, in accordance with accepted academic practice. No use, distribution or reproduction is permitted which does not comply with these terms.



# Choroidal Morphologic and Vascular Features in Patients With Myopic Choroidal Neovascularization and Different Levels of Myopia Based on Image Binarization of Optical Coherence Tomography

Xinglin Wang<sup>1†</sup>, Jiarui Yang<sup>1†</sup>, Yushi Liu<sup>1†</sup>, Luling Yang<sup>1†</sup>, Huaqin Xia<sup>1</sup>, Xiaotong Ren<sup>1</sup>, Qingyi Hou<sup>1</sup>, Yimeng Ge<sup>1</sup>, Changguan Wang<sup>1,2\*</sup> and Xuemin Li<sup>1,2\*</sup>

## OPEN ACCESS

### Edited by:

Haijiang Lin,  
Harvard Medical School,  
United States

### Reviewed by:

Yi Zhen,  
Capital Medical University, China  
Yong Tao,  
Capital Medical University, China

### \*Correspondence:

Changguan Wang  
docwcg@126.com  
Xuemin Li  
lxm166@sina.com

<sup>†</sup>These authors have contributed  
equally to this work and share first  
authorship

### Specialty section:

This article was submitted to  
Ophthalmology,  
a section of the journal  
Frontiers in Medicine

Received: 07 October 2021

Accepted: 29 November 2021

Published: 04 January 2022

### Citation:

Wang X, Yang J, Liu Y, Yang L, Xia H,  
Ren X, Hou Q, Ge Y, Wang C and Li X  
(2022) Choroidal Morphologic and  
Vascular Features in Patients With  
Myopic Choroidal Neovascularization  
and Different Levels of Myopia Based  
on Image Binarization of Optical  
Coherence Tomography.  
Front. Med. 8:791012.  
doi: 10.3389/fmed.2021.791012

<sup>1</sup> Department of Ophthalmology, Peking University Third Hospital, Beijing, China, <sup>2</sup> Beijing Key Laboratory of Restoration of Damaged Ocular Nerve, Beijing, China

**Purpose:** To characterize the choroidal morphologic and vascular features in different levels of myopes and patients with myopic choroidal neovascularization (mCNV).

**Methods:** A total of 148 subjects were enrolled in this cross-sectional study, including 78 low-to-moderate myopes (LMM), 53 high myopes (HM), and 17 high myopic patients with mCNV. Ocular biometrics were measured using an optical low-coherence reflectometry device. Retinal and choroidal imaging was performed using enhanced depth imaging (EDI) spectral domain optical coherence tomography (OCT). Retinal parameters including retinal thickness and retinal volume were obtained from a built-in software. Binarization technique was adopted to investigate choroidal parameters including choroidal thickness (CT), vascular area, stromal area, and choroidal vascularity index (CVI). Choroidal parameters were measured at five locations to cover as much area of choroid as possible, and their patterns of distribution were further analyzed.

**Results:** Patients with mCNV had an atrophic retina of comparable thickness to HM ( $273.65 \pm 17.28$  vs.  $276.49 \pm 13.29 \mu\text{m}$ ,  $p = 0.47$ ), but the choroid was thinner than that of HM ( $153.94 \pm 15.12$  vs.  $236.09 \pm 38.51 \mu\text{m}$ ,  $p < 0.001$ ). Subfoveal CVI was greatest in the mCNV eyes ( $0.651 \pm 0.009$ ), followed by HM ( $0.645 \pm 0.012$ ) and LMM eyes ( $0.636 \pm 0.012$ ). Similar to CT, CVI was also found significantly different among these three groups at all five locations ( $p$  for trend  $< 0.001$  for all locations). Axial length (AL) was negatively correlated with retinal volume ( $r = -0.236$ ,  $p = 0.009$ ), which is the only significant finding in associations between ocular factors and retinal parameters. Strong, negative correlations were identified between AL and subfoveal choroidal thickness (SFCT,  $r = -0.820$ ,  $p < 0.001$ ). However, AL was positively correlated with subfoveal CVI ( $r = 0.668$ ,  $p < 0.001$ ). CVI was greater in myopic eyes with thinner choroid ( $r = -0.578$ ,  $p < 0.001$ ). BCVA exhibited no significant association with CVI ( $r = 0.139$ ,  $p = 0.092$ ), but was negatively correlated with SFCT ( $r = -0.386$ ,  $p < 0.001$ ) and positively correlated with AL ( $r = 0.351$ ,  $p < 0.001$ ).

**Conclusion:** Choroid in patients with mCNV was thinner yet more vascularized than that in HM and LMM subjects. CVI increased with a longer AL which was associated with a smaller SFCT, choroidal vascular area (VA), and total choroidal area (TCA). Better BCVA was achieved in subjects with thicker SFCT and shorter AL.

**Keywords:** choroidal structure, high myopia, myopic choroidal neovascularization (mCNV), choroidal vascularity index (CVI), optical coherence tomography

## INTRODUCTION

Myopia is one of the most common ocular disease globally, with a prevalence of 10–30% in the adult population and 80–90% in young adults in East and Southeast Asia (1). Pathological myopia is one of the leading causes of visual impairment in the world, in which excessive axial elongation of the globe causes biomechanical stretching and thinning of choroid and retinal pigmented epithelium (RPE) layers (2–4), leading to increased risk of chorioretinal complications such as myopic choroidal neovascularization (mCNV), posterior staphyloma, lacquer cracks, and myopic foveoschisis, among which mCNV is considered to be sight-threatening with poor prognosis without treatment (5–10).

Recent development of enhanced depth imaging (EDI) optical coherence tomography (OCT) has enabled non-invasive, quantitative assessment of the choroid in myopia (11–13). A number of studies have found that with the progression of myopia, choroidal-related factors measured by OCT including choroidal thickness (CT) and choroidal vascular index (CVI) change significantly, indicating that the choroidal morphologic and vascular alterations may accompany the development of myopia (14–17). Reduction in choroidal circulation flow has been shown to occur in high myopia, which may be important in the pathogenesis of mCNV, and a reduction in CT in pathological myopic eyes with mCNV has been demonstrated using OCT imaging (18). Yet, to the best of our knowledge, these studies mostly focused on the choroidal capillary plexus density as shown in OCTA (19–21), or only identified total choroidal vascular density (including choroidal capillary plexus, Haller's and Sattler's layer of choroid) in subfoveal areas (16, 22). There is a lack of investigation on the variations of full-layer choroidal structure in different subretinal areas, and the role of choroidal vessel distributions in the pathogenesis of mCNV remains unclear.

The aim of our study was to compare the morphologic and vascular features of the choroid in patients with mCNV with those of different levels of myopia. Additionally, choroid was divided into five sectors to observe the CT and CVI variation in different regions and to characterize patterns of distribution of choroidal blood flow and their potential connections to the pathogenesis and clinical development of mCNV.

## METHODS

### Study Population

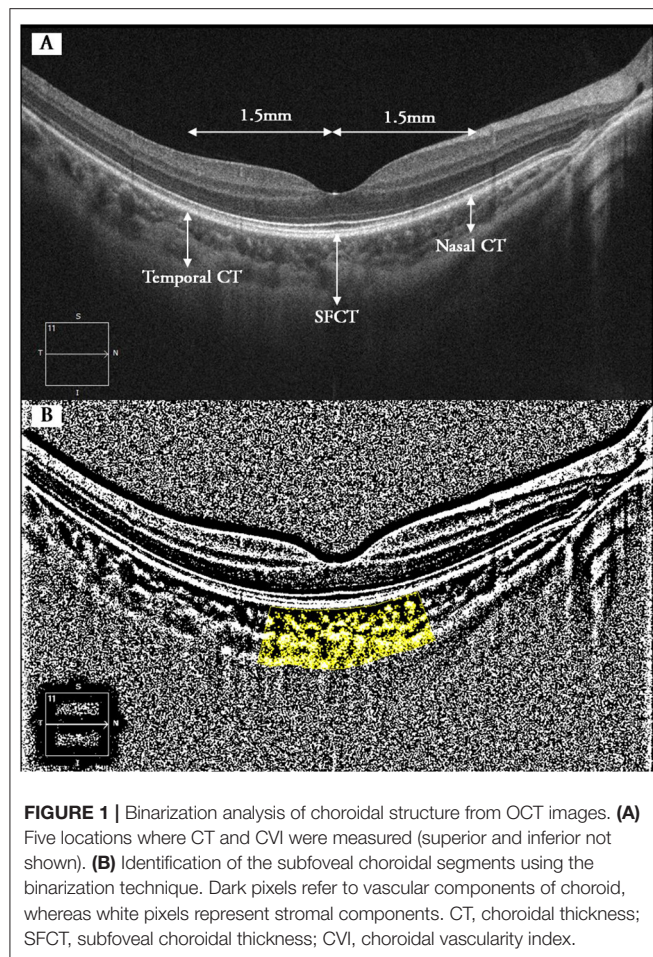
This cross-sectional study was conducted in accordance with the tenets of the Declaration of Helsinki and was approved

by the Ethical Committee of Peking University Third Hospital. Informed consent was obtained before enrollment. Myopic subjects without any previous significant ocular trauma or surgery and/or any clinically significant ocular comorbidity other than mCNV were enrolled and were further categorized into three groups based on their spherical equivalent (SE) and the presence of mCNV: (1) low-to-moderate myopes (LMM): low-to-moderate myopia [SE,  $-5.75$  to  $-1.00$  diopter (D)], and with-the-rule astigmatism no  $> -1.50$ D; (2) high myopes (HM): high myopia [SE,  $-6.00$  diopter or worse (D)], and with-the-rule astigmatism no  $> -1.50$ D, and (3) mCNV group. The inclusion criteria of mCNV group were as follows: (1) newly developed active CNV confirmed with fundus fluorescein angiography (FFA), and (2) bilateral pathological myopia, defined as SE of  $< -6$  diopters (D) in phakic patients (unless previously undergone refractive surgery) or axial length (AL) more than 26.5 mm, with typical degenerative changes in pathological myopia (19). Patients in mCNV group with Fuch's hemorrhage or CNV secondary to other causes other than pathological myopia, and subjects in the LMM/HM group with best corrected visual acuity (BCVA) higher than 0 [LogMAR], were excluded. We did not rule out subjects with the presence of peripapillary atrophy, lacquer crack, posterior staphyloma, or chorioretinal atrophy, as such changes are commonly seen in HM.

### Ophthalmic Examination and Measurements

All subjects underwent a standardized ophthalmologic examination including measurement of refractive error/SE, BCVA, intraocular pressure (IOP), and AL. Refractive error was screened with autorefraction (Canon Autorefractor RK-F1; Canon Inc. Ltd., Tochigiken, Japan) and confirmed with manifest refraction in which the BCVA was measured monocularly using a logarithm of the minimum angle of resolution (LogMAR) chart (Lighthouse International, New York, NY, USA) at a distance of 4 meters. Biometry measurements (i.e., AL, anterior chamber depth [ACD], and keratometry readings) were obtained from the non-contact Zeiss IOLMaster (V3.01; Carl Zeiss Meditec AG, Jena, Germany). Non-contact tonometry (Auto Non-Contact Tonometer, NT-3000; Nidek, Gamagori, Japan) was used for measuring IOP, and Goldmann applanation tonometry (Haag-Streit, Bern, Switzerland) was performed by study ophthalmologists if IOP was found to be 21 mmHg or more. Slit-lamp examination and dilated fundus examination were carried out in all subjects. Fundus photography was performed using retinal camera (Canon CR-DGI with a 10-DSLR back, Tokyo, Japan). FFA was performed in HM with susceptible





subretinal hyperreflective material overlying the RPE on OCT to confirm the presence of mCNV (TRC-50X/IMAGENet 2000; Topcon, Tokyo, Japan).

## OCT Imaging—Retinal and Choroidal Parameters

The retina and choroidal architectural parameters were determined using cirrus HD-OCT in EDI mode (Carl Zeiss Meditec Inc., Dublin, CA, USA). Choroid was imaged with EDI modality after pupil dilation. EDI is a method that improves resolution of choroidal detail by automatically setting the choroid closer to the zero-delay line and thus theoretically provides better visualization of the choroid scleral interface (CSI) than in standard retinal SD-OCT images (22). A 21-line 6-mm raster (0.3 mm between the lines, using the automatic averaging and eye-tracking features of the proprietary device) and a 512 × 128 macular cube scan (128 lines consisting of 512 A-scans and a central horizontal HD B-scan) centered onto the fovea of both eyes of each subject were obtained. Three horizontal lines passing through the center of the fovea and 1.5 mm superior and inferior to the fovea were selected for analysis.

Data of the retinal parameters including central thickness, volume cube, and average thickness were collected directly from

**TABLE 1 |** Baseline characteristics of study subjects.

	LMM ( <i>n</i> = 78)	HM ( <i>n</i> = 53)	mCNV ( <i>n</i> = 17)	<i>p</i> -value
Age, years	26.58 (0.56)	28.13 (1.63)	43.06 (1.91)	<0.001
Male/Female	41/37	29/24	10/7	0.89
Axial length, mm	24.95 (1.05)	26.42 (0.95)	28.08 (1.11)	<0.001
Spherical equivalent, D	−4.26 (1.35)	−7.62 (1.18)	−9.37 (1.79)	<0.001
BCVA, LogMAR	−0.27 (0.06)	−0.02(0.04)	0.10 (0.11)	<0.001
Intraocular pressure, mmHg	15.84 (3.02)	16.77 (5.33)	16.29 (3.02)	0.36

Data presented are means (standard deviations).

LMM, low-to-moderate myopia; HM, high myopia; mCNV, myopic choroidal neovascularization; BCVA, best-corrected visual acuity.

the built-in 512 × 128 macular cube scan report. CT was measured as the distance between the Bruch membrane (located at the lower edge of the RPE) and the CSI, using the built-in calipers tool at five locations (subfoveal, 1.5 mm temporal, nasal, superior, and inferior to the fovea).

Choroidal vascularity index was calculated manually by exporting all selected images with a 1:1 pixel ratio into ImageJ 1.7.0 software (National Institutes of Health, Bethesda, MD, USA) in which further measurement was taken. Briefly, the polygon tool was used to select the region of interest (choroid) in different areas with a length of 1.5 mm and centered at the same spots where retinal and CT were metered (Figure 1). After converting the image into eight bit, Niblack's auto-local threshold was applied to binarize the image and demarcate the choroidal vascular and stromal area (VA and SA, respectively). The total choroidal area (TCA), VA, and SA were measured and calculated as suggested previously (23). CVI was defined as the ratio of TCA divided by VA.

Binocular images were collected but only right eyes were chosen for subsequent analysis. In addition, we evaluated the intraobserver reliability of choroidal measurements at all five locations in three groups. All measurements were taken again by the same experienced clinician who was masked to subject characteristics and clinical diagnosis after an interval of 3 days. The average of the two measurements were recorded and used for further analysis.

## Statistical Analysis

Statistical analysis was performed using SPSS version 20.0 (SPSS, Inc, Chicago, IL), and *p* < 0.05 was considered to be statistically significant. All values were represented as mean ± SD or mean (SD), unless otherwise stated. The intrasession repeatability of the CT and CVI was measured by the absolute agreement model of the intraclass correlation coefficient (ICC) (24). The normality of the data was tested using the Kolmogorov–Smirnov test. One-way ANOVA test and chi-squared test were used to make comparisons among three or more groups for descriptive and categorical data, respectively, followed by Bonferroni post-test. Repeated-measures ANOVA with Bonferroni post-test was used to compare CT and CVI at various locations within each group. Independent samples

**TABLE 2 |** Intraobserver reliability of choroidal parameters in LMM, HM, and mCNV groups at different locations.

Locations of measurement	LMM (n = 78)		HM (n = 53)		mCNV (n = 17)	
	ICC (95%CI)	Mean difference* (SD)	ICC (95%CI)	Mean difference* (SD)	ICC (95%CI)	Mean difference* (SD)
<b>CT (<math>\mu\text{m}</math>)</b>						
Subfoveal	0.98 (0.96–0.99)	9.42 (12.88)	0.96 (0.93–0.98)	8.27 (10.75)	0.95 (0.90–0.99)	10.32 (14.96)
Nasal, 1.5 mm	0.96 (0.93–0.98)	–9.85 (14.07)	0.96 (0.93–0.98)	9.11 (11.71)	0.95 (0.91–0.99)	–8.90 (13.77)
Temporal, 1.5 mm	0.97 (0.95–0.99)	8.31 (10.43)	0.97 (0.95–0.99)	10.32 (13.94)	0.96 (0.93–0.98)	10.41 (16.10)
Superior, 1.5 mm	0.96 (0.93–0.99)	9.28 (7.15)	0.96 (0.93–0.98)	–7.14 (8.41)	0.96 (0.93–0.98)	9.45 (6.15)
Inferior, 1.5 mm	0.96 (0.93–0.98)	10.17 (12.51)	0.96 (0.93–0.98)	8.58 (11.85)	0.98 (0.97–0.99)	10.27 (16.33)
<b>CVI</b>						
Subfoveal	0.96 (0.92–0.99)	0.018 (0.021)	0.97 (0.95–0.99)	0.014 (0.012)	0.96 (0.93–0.98)	0.019 (0.024)
Nasal, 1.5 mm	0.95 (0.90–0.99)	0.026 (0.015)	0.95 (0.90–0.99)	0.017 (0.025)	0.97 (0.96–0.99)	0.023 (0.016)
Temporal, 1.5 mm	0.95 (0.90–0.98)	–0.007 (0.013)	0.96 (0.93–0.98)	0.011 (0.010)	0.95 (0.91–0.99)	0.016 (0.017)
Superior, 1.5 mm	0.96 (0.93–0.98)	0.020 (0.041)	0.97 (0.96–0.99)	–0.009 (0.021)	0.95 (0.90–0.98)	0.018 (0.022)
Inferior, 1.5 mm	0.97 (0.95–0.99)	0.014 (0.012)	0.96 (0.92–0.99)	0.011 (0.012)	0.96 (0.93–0.98)	–0.015 (0.014)

ICC, intraclass correlation coefficient; CI, confidence interval; SD, standard deviation. LMM, low-to-moderate myopia; HM, high myopia; mCNV, myopic choroidal neovascularization; CT, choroidal thickness; CVI, choroidal vascularity index.

\*Mean difference was determined from the 1st measurement minus 2nd measurement.

*t*-tests were used for comparing the differences between two groups. Generalized linear model was used to assess the mean CT and CVI across different locations in eyes with varying degree of myopia, and conditions such as posterior staphyloma and chorioretinal atrophy were included to adjust for potential residual confounding. Pearson's correlation analysis was used to analyze the associations between OCT parameters and ocular factors.

## RESULTS

### Patient Characteristics and Intraobserver Reliability

One hundred and sixty subjects were enrolled initially, including 80 LMMs, 60 HMs, and 20 mCNVs. We excluded 12 subjects because their choroidal images were not of optimal quality to perform accurate measurements of their choroidal traits, leaving 148 subjects with complete data for analysis. The demographics and ocular characteristics of the study population are shown in **Table 1**. Of all the subjects enrolled, only three participants in the mCNV group suffered from mild nuclear cataract of NO2NC2 according to LOCS III grading system. Among the HM and mCNV groups, 84.29% (59/70) had peripapillary atrophy, 27.14% (19/70) had posterior staphyloma, 12.86% (9/70) had chorioretinal atrophy, and 2.86% (2/70) had lacquer cracks. In terms of reliability of CT and CVI measurements, the intraobserver reliability for LMM, HM, and mCNV groups was excellent for all locations of choroidal parameters (**Table 2**).

### Difference in OCT Parameters Among Three Groups

**Table 3** presents retinal and choroidal morphological and vascular characteristics of eyes with different myopic conditions in each group. Significant difference was found in volume cube ( $p = 0.003$ ) and retinal average thickness ( $p = 0.009$ ) among these three groups whereas all groups had comparable retinal

central thickness ( $p = 0.23$ , **Table 3** and **Figure 2A**). However, HM eyes and mCNV eyes showed similar retinal characteristics in terms of retinal volume ( $9.96 \pm 0.49$  vs.  $9.82 \pm 0.43$ ,  $p = 0.62$ ), retinal average thickness ( $276.49 \pm 13.29$  vs.  $273.65 \pm 17.28$ ,  $p = 0.53$ ), and retinal central thickness ( $246.29 \pm 20.68$  vs.  $243.94 \pm 21.27$ ,  $p = 0.15$ ). LMM eyes had thicker retinal average thickness and larger retinal volume than the other two groups of eyes (**Table 3** and **Figures 2B,C**). Choroidal parameters, including TCA, choroidal vascular area (VA), choroidal stromal area (SA), and CT, decreased when subjects had a higher stage and worse condition of myopia (**Table 3** and **Figures 2D–G**). Subfoveal CVI was greatest in the mCNV eyes ( $0.651 \pm 0.009$ ), followed by HM ( $0.645 \pm 0.012$ ) and LMM eyes ( $0.636 \pm 0.012$ ), as shown in **Table 3** and **Figure 2H**.

### Choroidal Structure Changes at Different Locations

Choroidal thickness varied significantly across these three groups at all the locations ( $p$  for trend  $< 0.001$  for all locations, **Table 4**). Eyes with mCNV had the significantly thinnest choroid at all locations, followed by HM and LMM eyes. In mCNV and HM eyes, choroid was found to be thinnest at the nasal location, followed by the inferior, subfoveal, superior, and temporal locations ( $p < 0.001$ ). In comparison, the choroid in LMM eyes was thinnest at the nasal location, followed by the inferior, temporal, subfoveal, and superior locations ( $p < 0.001$ ). Similar to the CT, CVI was also found significantly different among these three groups at all five locations ( $p$  for trend  $< 0.001$  for all locations, **Table 4**). However, the variation in CVI at all locations in each group was insignificant.

### Correlations Between Ocular Factors and OCT Parameters in All Myopes

Ocular factors including AL, SE (as all subjects were myopic, the absolute value of SE was applied), IOP, and BCVA were analyzed for their correlations with OCT parameters mentioned

**TABLE 3 |** Retinal and choroidal morphological and vascular characteristics on OCT in LMM, HM, and mCNV eyes.

	LMM (n = 78)	HM (n = 53)	mCNV (n = 17)	p-value <sup>#</sup>
<b>Retinal parameters on OCT</b>				
Central thickness, $\mu\text{m}$	251.40 (17.16)	246.29 (20.68)	243.94 (21.27)	0.23
Volume cube, $\text{mm}^3$	10.17 (0.37)	9.96 (0.49)	9.82 (0.43)	0.003
Average thickness, $\mu\text{m}$	282.63 (10.35)	276.49 (13.29)	273.65 (17.28)	0.009
<b>Choroidal parameters on OCT</b>				
Total choroidal area, $\text{mm}^2$	2.58 (0.70)	1.82 (0.61)	1.00 (0.25)	<0.001
Vascular area, $\text{mm}^2$	1.63 (0.42)	1.17 (0.38)	0.65 (0.16)	<0.001
Stromal area, $\text{mm}^2$	0.95 (0.28)	0.65 (0.24)	0.35 (0.09)	<0.001
Choroidal thickness, $\mu\text{m}$	295.14 (41.52)	236.09 (38.51)	153.94 (15.12)	<0.001
CVI	0.636 (0.012)	0.645 (0.012)	0.651 (0.009)	<0.001

Data presented are means (standard deviations).

LMM, low to moderate myopia; HM, high myopia; mCNV, myopic choroidal neovascularization; OCT, optical coherence tomography; CVI, choroidal vascularity index.

<sup>#</sup>Based on one-way ANOVA.

earlier, including retinal central thickness, retinal volume, retinal average thickness, SFCT, TCA, choroidal VA, choroidal SA, and CVI at subfoveal location (**Figures 3A–D**). IOP was not correlated with any of these OCT parameters (data not shown). AL was negatively correlated with retinal volume ( $r = -0.236$ ,  $p = 0.009$ ), which is the only significant finding in associations between ocular factors and retinal parameters. Strong, negative correlations were identified between AL and SFCT (**Figure 3C**,  $r = -0.820$ ,  $p < 0.001$ ), TCA ( $r = -0.857$ ,  $p < 0.001$ ), VA ( $r = -0.860$ ,  $p < 0.001$ ), and SA ( $r = -0.849$ ,  $p < 0.001$ ). However, AL was positively correlated with subfoveal CVI (**Figure 3B**,  $r = 0.668$ ,  $p < 0.001$ ). CVI was greater in myopic eyes with thinner choroid (**Figure 3D**,  $r = -0.578$ ,  $p < 0.001$ ). These results indicate that the increasing intraocular compression against fundus in eyes with long AL contributes to a thinner yet more vascularized choroid with less vascular and stromal choroidal area. BCVA was not correlated with CVI ( $r = 0.139$ ,  $p = 0.092$ ), but was negatively correlated with SFCT ( $r = -0.386$ ,  $p < 0.001$ ) and positively correlated with AL ( $r = 0.351$ ,  $p < 0.001$ ).

## DISCUSSION

Myopia is not only a very common abnormal refractive condition, but also a potential sight-threatening ophthalmic disease when staged into its severe form (pathologic myopia). To our knowledge, our study here is the first comprehensive research on morphology and vasculature of the retina and choroid in different levels of myopes and pathological myopic eyes with mCNV. We discovered that both HM and mCNV eyes presented a thinner retina with a thinner yet more vascularized choroid than LMM. Although the morphology of retina was comparable

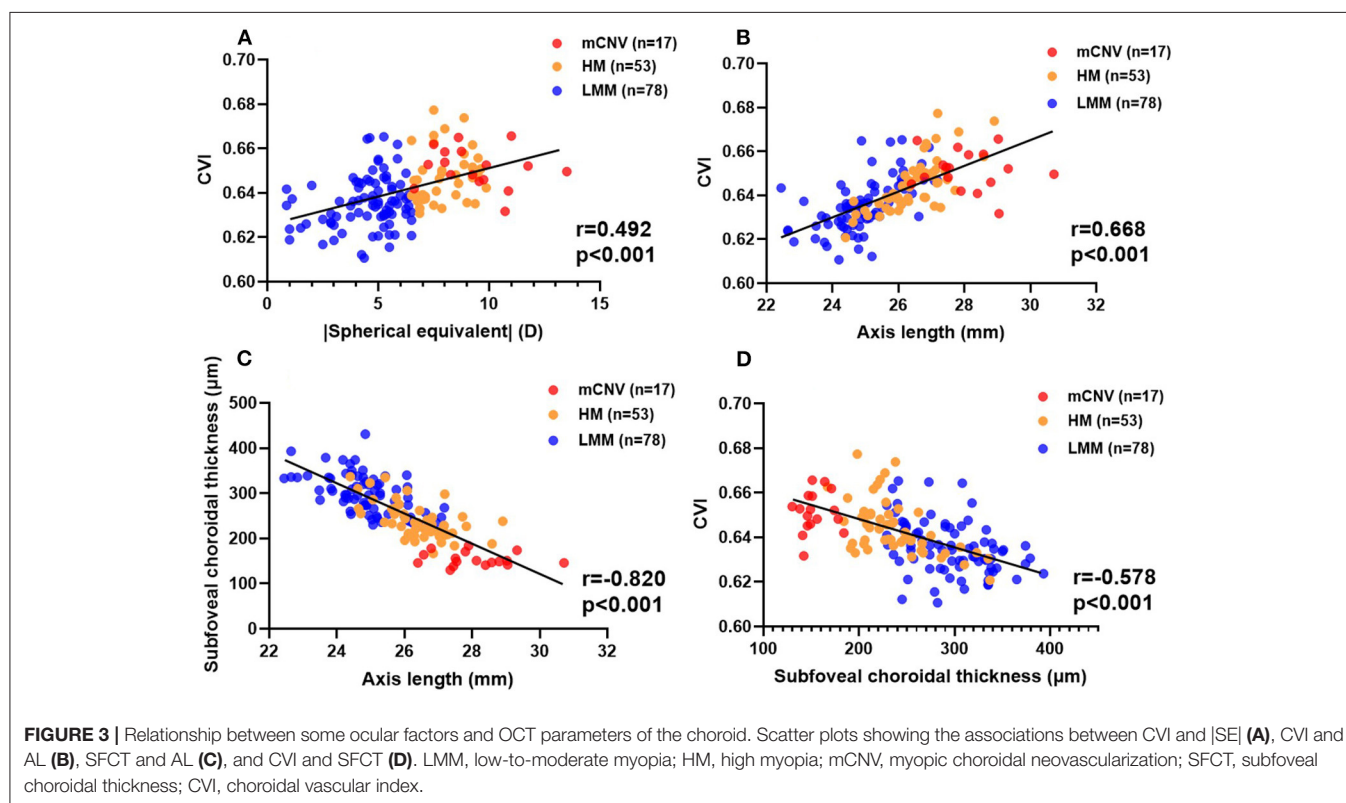
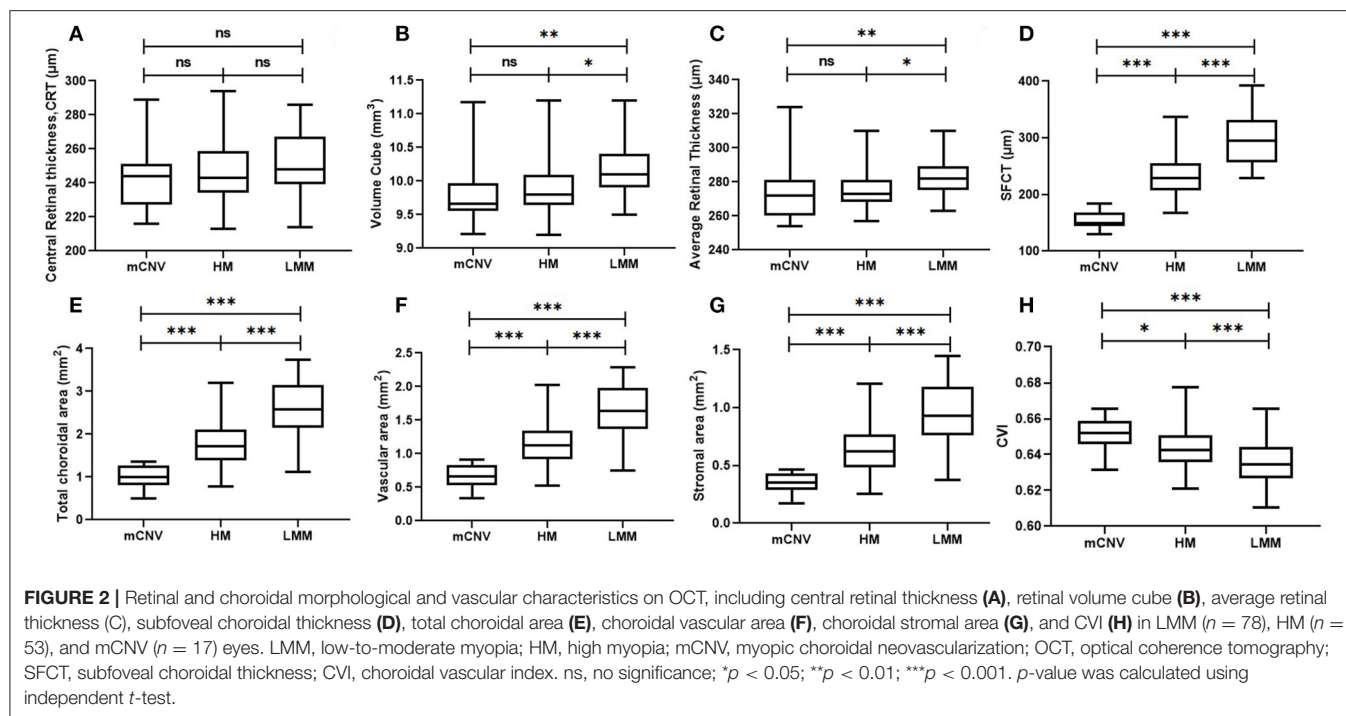
between HM and mCNV eyes, mCNV eyes showed significant increase in CVI and reduction in both choroidal vascular and stromal area, which indicates the atrophy of choroidal components may lead to the pathologic state of myopia.

We adopted the binarization technique to manually measure the CT and differentiate the luminal (vascular) and stromal components of the choroid in OCT images. On the other hand, all retinal-related parameters were automatically acquired by the commercial OCT built-in software. To balance the comprehensiveness of our assessment of the choroid and labor workload, we selected and covered five different spots or areas on OCT images. The great intraobserver reliability at different locations among all subjects laid a solid foundation for our subsequent analysis.

In this study, mCNV and HM eyes were both high myopic ( $SE \leq -6.0\text{D}$ ), but mCNV group had a higher AL than HM group ( $28.08 \pm 1.11$  vs.  $26.42 \pm 0.95$  mm,  $p < 0.001$ ), suggesting that the continuous growth of AL may lead to pathologic state of high myopia (1). Subjects with high myopia or mCNV possessed a thinner retina with less volume and average thickness than that of LMM subjects. This is in accordance with previous studies regarding the alterations of retinal thickness and volume in different levels of myopia (11, 25, 26). However, all retinal parameters on OCT did not differ between HM and mCNV eyes. This implies that atrophy of retina, which is a pathological condition in HM, may have limited association with the onset of mCNV and is not a recommended parameter to distinguish mCNV and HM eyes. Previous studies have yielded that myopic eyes had thinner choroid than emmetropic eyes (16), but choroidal morphology and vascular characteristics were left undiscovered in mCNV eyes. In our study, we found that compared with LMM and HM eyes, CT, TCA, choroidal VA, and choroidal SA at all locations decreased the most in mCNV eyes. The consistent change in choroidal parameters as degree of myopia deepens suggests that the progressive choroidal thinning should be of greater concern to early detect and predict the onset of mCNV in HM. Patients with mCNV had the highest CVI among three groups whereas both the numerator (choroidal VA) and denominator (TCA) of CVI decreased in mCNV eyes. These findings reveal that mCNV eyes suffered from a higher level of choroidal atrophy than HM eyes, with relatively greater reduction in the stromal component compared with vascular components, which was further supported by the strong correlation between CVI and AL. However, effects of choroidal atrophy on the pathogenesis of pathologic myopia and mCNV remain to be elucidated.

Anatomic studies demonstrate that choroid plays a crucial role in supporting photoreceptor function; such atrophy may have significant deleterious impact on outer retina and RPE health. Previous studies have put forth the theory that alterations in the choroidal blood perfusion may lead to degenerative changes in pathological myopia and high myopia (2). Narrowing and loss of large choroidal vessels, and occlusion of choriocapillaris, have been suggested to be important in the pathogenesis of chorioretinal atrophy in pathological myopia (25). Dramatic reductions in CT and choroidal circulation have been observed in highly myopic eyes (27). Ischemia and





vascular changes have also been proposed to be important factors in the pathogenesis of lacquer cracks and mCNV (26). Our discoveries may add important implications in the pathogenesis and possibly treatment response and may help to

better understand choroidal involvement in high myopic and mCNV eyes.

Choroid was thickest superiorly and thinnest nasally in LMM eyes, which agrees with the previous studies (22, 28) and can be



**TABLE 4 |** Distribution of CT and CVI at five different locations across the LMM, HM, and mCNV groups.

Locations of measurement	LMM ( <i>n</i> = 78)	HM ( <i>n</i> = 53)	mCNV ( <i>n</i> = 17)	Changes in choroidal parameters across 3 myopic groups	
				Beta	p for trend <sup>†</sup>
Choroidal thickness, μm					
Subfoveal	295.14 (41.52)	234.55 (37.12)	153.94 (15.12)	−70.68	<0.001
Nasal, 1.5 mm	248.86 (39.27)	188.14 (44.20)	106.32 (16.17)	−71.27	<0.001
Temporal, 1.5 mm	294.26 (46.34)	251.07 (30.56)	169.54 (21.05)	−62.37	<0.001
Superior, 1.5 mm	303.21 (35.74)	236.09 (38.51)	161.43 (19.91)	−70.88	<0.001
Inferior, 1.5 mm	292.44 (31.45)	229.06 (42.20)	142.28 (17.97)	−75.07	<0.001
	<i>p</i> < 0.001 <sup>#</sup>	<i>p</i> < 0.001 <sup>#</sup>	<i>p</i> < 0.001 <sup>#</sup>		
CVI					
Subfoveal	0.6355 (0.1208)	0.6446 (0.0120)	0.6513 (0.0090)	0.0079	<0.001
Nasal, 1.5 mm	0.6353 (0.0306)	0.6440 (0.0148)	0.6500 (0.0109)	0.0074	<0.001
Temporal, 1.5 mm	0.6356 (0.0148)	0.6415 (0.0281)	0.6425 (0.0148)	0.0035	0.0072
Superior, 1.5 mm	0.6354 (0.0279)	0.6441 (0.0193)	0.6512 (0.0184)	0.0079	<0.001
Inferior, 1.5 mm	0.6355 (0.0923)	0.6443 (0.0378)	0.6488 (0.0469)	0.0067	<0.001
	<i>p</i> = 0.806 <sup>#</sup>	<i>p</i> = 0.344 <sup>#</sup>	<i>p</i> = 0.409 <sup>#</sup>		

Data presented are mean (standard deviations), adjusted for the presence of posterior staphyloma and chorioretinal atrophy.

<sup>†</sup> Generalized linear model, adjusted for the presence of posterior staphyloma and chorioretinal atrophy.

<sup>#</sup> Repeated-measures ANOVA, comparing the distribution of CT across subfoveal, nasal (1.5 mm), temporal (1.5 mm), superior (1.5 mm), and inferior (1.5 mm) locations.

explained by two possible reasons that the choroidal watershed and the fetal choroidal fissure closes inferiorly at 7 weeks (29). In HMM and mCNV eyes, the thickest and thinnest choroid was at temporal and nasal locations. It is likely that the presence of posterior staphyloma, of which the most common types involve the macula and optic nerve regions (10, 30), may contribute to the thinning of the nasal choroid and the temporal shift in thickest point in high myopic eyes (31). The variation in CVI at all locations in each group was insignificant, indicating that the atrophy of vascular and stromal components covered entire choroid with comparable extent.

In addition to our finding that thinning choroid is a structural feature of high myopia, our results reveal that the extent of choroidal thinning and vascularization is significantly correlated with the magnitude of refractive error and prolongation of AL. Interestingly, CVI was greater in myopic eyes with thinner choroid which can be probably interpreted as a choroidal structural compensation mechanism to provide more oxygen and nourishment against the reduction in total blood flow caused by atrophy of choroid.

In contrast to Gupta's study (22) that demonstrated no correlation between choroidal parameters and visual acuity, we found a significant association between SFCT and BCVA. The discrepancy may be due to differences in study participants since we enrolled all levels of myopes (especially patients with mCNV with thinner choroid whose vision has already been compromised), whereas Gupta's study only covered HM and emmetropes. Interestingly, no such correlation was found between CVI and BCVA. Based on these findings, we speculated that a thin choroid, even though more vascularized, delivers

decreased amounts of oxygen and nutrients to the retina, thus potentially affecting signal generation from the photoreceptors or cause loss of the overlying photoreceptors as a consequence.

There are several limitations of our study that needs to be addressed. First, our study has a relatively small sample size with <20 patients with mCNV and 40 HM recruited. Second, the cause–effect relationship cannot be ascertained owing to the cross-sectional nature of our study. Further endeavors validating the alteration of choroidal morphology and blood perfusion during progress of pathological myopia are needed. Third, The difference in AL and age between mCNV and HM groups cannot be ignored since older age and longer AL have been proven to be associated with thinner choroid (31). Here in our study, age was not associated with variation in CVI ( $r = 0.089$ ,  $p = 0.237$ ) and showed no correlation with SFCT in the multiple linear regression analysis ( $\beta = -0.023$ , 95% CI:  $-1.039-0.667$ ,  $p = 0.667$ ). However, to evaluate and compare the choroidal characteristics in HM and pathologic myopes more accurately and convincingly, upcoming studies should attempt to enroll AL- and age-matched subjects with high myopia and mCNV, respectively.

In conclusion, this study characterized choroidal structural and vascular features and patterns of distribution of choroidal blood flow in patients with mCNV, whose choroid was thinner yet more vascularized than that in HM and LMM subjects. CVI increased with a longer AL, which was associated with smaller SFCT, VA, and TCA. Better BCVA was achieved in subjects with thicker SFCT and shorter AL. The technique used to evaluate the choroids of mCNV should be applied in future investigations of mechanisms and interventions of pathological myopia

## DATA AVAILABILITY STATEMENT

The raw data supporting the conclusions of this article will be made available by the authors, without undue reservation.

## ETHICS STATEMENT

The studies involving human participants were reviewed and approved by Institutional Review Board of Peking University Third Hospital. The patients/participants provided their written informed consent to participate in this study.

## REFERENCES

- Baird PN, Saw SM, Lanca C, Guggenheim JA, Smith Iii EL, Zhou X, et al. Myopia. *Nat Rev Dis Primers*. (2020) 6:99. doi: 10.1038/s41572-020-00231-4
- Gao R, Ma J, Zhang Z, Shang Q, Duan J. Spectral domain-optical coherence tomography retinal biomarkers in choroidal neovascularization of multifocal choroiditis, myopic choroidal neovascularization, and idiopathic choroidal neovascularization. *Ann Med*. (2021) 53:1270–8. doi: 10.1080/07853890.2021.1961015
- Yang TJ, Yao MD, Sun YN, Li XM, Jiang Q, Yan B. Suppression of choroidal neovascularization by silencing of long non-coding RNA IPW. *Aging*. (2021) 13:10584–602. doi: 10.18632/aging.202822
- Leveziel N, Marillet S, Dufour Q, Lichtwitz O, Bentaieb Y, Pelen F, et al. Prevalence of macular complications related to myopia - results of a multicenter evaluation of myopic patients in eye clinics in France. *Acta Ophthalmol*. (2020) 98:e245–e51. doi: 10.1111/aos.14246
- Wong TY, Ferreira A, Hughes R, Carter G, Mitchell P. Epidemiology and disease burden of pathologic myopia and myopic choroidal neovascularization: an evidence-based systematic review. *Am J Ophthalmol*. (2014) 157:9–25.e12. doi: 10.1016/j.ajo.2013.08.010
- Wong TY, Ohno-Matsui K, Leveziel N, Holz FG, Lai TY, Yu HG, et al. Myopic choroidal neovascularisation: current concepts and update on clinical management. *Br J Ophthalmol*. (2015) 99:289–96. doi: 10.1136/bjophthalmol-2014-305131
- Chakraborty R, Read SA, Collins MJ. Monocular myopic defocus and daily changes in axial length and choroidal thickness of human eyes. *Exp Eye Res*. (2012) 103:47–54. doi: 10.1016/j.exer.2012.08.002
- Chiang STH, Phillips JR, Backhouse S. Effect of retinal image defocus on the thickness of the human choroid. *Ophthalmic Physiol Opt*. (2015) 35:405–13. doi: 10.1111/opo.12218
- Cheung CMG, Loh BK, Li X, Mathur R, Wong E, Lee SY, et al. Choroidal thickness and risk characteristics of eyes with myopic choroidal neovascularization. *Acta Ophthalmol*. (2013) 91:e580–e1. doi: 10.1111/aos.12117
- Hsiang HW, Ohno-Matsui K, Shimada N, Hayashi K, Moriyama M, Yoshida T, et al. Clinical characteristics of posterior staphyloma in eyes with pathologic myopia. *Am J Ophthalmol*. (2008) 146:102–10. doi: 10.1016/j.ajo.2008.03.010
- Ang M, Wong CW, Hoang QV, Cheung GCM, Lee SY, Chia A, et al. Imaging in myopia: potential biomarkers, current challenges and future developments. *Br J Ophthalmol*. (2019) 103:855–62. doi: 10.1136/bjophthalmol-2018-312866
- Singh SR, Vupparaboina KK, Goud A, Dansingani KK, Chhablani J. Choroidal imaging biomarkers. *Surv Ophthalmol*. (2019) 64:312–33. doi: 10.1016/j.survophthal.2018.11.002
- Iovino C, Pellegrini M, Bernabei F, Borrelli E, Sacconi R, Govetto A, et al. Choroidal vascularity index: an in-depth analysis of this novel optical coherence tomography parameter. *J Clin Med*. (2020) 9:595. doi: 10.3390/jcm9020595
- Alshareef RA, Khuthaila MK, Goud A, Vupparaboina KK, Jana S, Chhablani J. Subfoveal choroidal vascularity in myopia: evidence from spectral-domain optical coherence tomography. *Ophthalmic Surg Lasers Imaging Retina*. (2017) 48:202–7. doi: 10.3928/23258160-20170301-02
- Ng WY, Ting DSW, Agrawal R, Khandelwal N, Htoon HM, Lee SY, et al. Choroidal structural changes in myopic choroidal neovascularization after treatment with antivascular endothelial growth factor over 1 year. *Invest Ophthalmol Vis Sci*. (2016) 57:4933–9. doi: 10.1167/iovs.16-20191
- Gupta P, Thakku SG, Saw SM, Tan M, Lim E, Tan M, et al. Characterization of choroidal morphologic and vascular features in young men with high myopia using spectral-domain optical coherence tomography. *Am J Ophthalmol*. (2017) 177:27–33. doi: 10.1016/j.ajo.2017.02.001
- Wu H, Zhang G, Shen M, Xu R, Wang P, Guan Z, et al. Assessment of choroidal vascularity and choriocapillaris blood perfusion in anisomyopic adults by SS-OCT/OCTA. *Invest Ophthalmol Vis Sci*. (2021) 62:8. doi: 10.1167/iovs.62.1.8
- Liu Y, Wang L, Xu Y, Pang Z, Mu G. The influence of the choroid on the onset and development of myopia: from perspectives of choroidal thickness and blood flow. *Acta Ophthalmol*. (2021). doi: 10.1111/aos.14773
- Tan ACS, Tan GS, Denniston AK, Keane PA, Ang M, Milea D, et al. An overview of the clinical applications of optical coherence tomography angiography. *Eye*. (2018) 32:262–86. doi: 10.1038/eye.2017.181
- Miyata M, Ooto S, Hata M, Yamashiro K, Tamura H, Akagi-Kurashige Y, et al. Detection of myopic choroidal neovascularization using optical coherence tomography angiography. *Am J Ophthalmol*. (2016) 165:108–14. doi: 10.1016/j.ajo.2016.03.009
- Li S, Sun L, Zhao X, Huang S, Luo X, Zhang A, et al. Assessing the activity of myopic choroidal neovascularization: comparison between optical coherence tomography angiography and dye angiography. *Retina*. (2020) 40:1757–64. doi: 10.1097/IAE.0000000000002650
- Gupta P, Saw SM, Cheung CY, Girard MJA, Mari JM, Bhargava M, et al. Choroidal thickness and high myopia: a case-control study of young Chinese men in Singapore. *Acta Ophthalmol*. (2015) 93:e585–92. doi: 10.1111/aos.12631
- Sonoda S, Sakamoto T, Yamashita T, Shirasawa M, Uchino E, Terasaki H, et al. Choroidal structure in normal eyes and after photodynamic therapy determined by binarization of optical coherence tomographic images. *Invest Ophthalmol Vis Sci*. (2014) 55:3893–9. doi: 10.1167/iovs.14-14447
- Fleiss JL, Cohen J. The equivalence of weighted kappa and the intraclass correlation coefficient as measures of reliability. *Educ Psychol Meas*. (1973) 33:613–9. doi: 10.1177/001316447303300309
- Flores-Moreno I, Ruiz-Medrano J, Duker JS, Ruiz-Moreno JM. The relationship between retinal and choroidal thickness and visual acuity in highly myopic eyes. *Br J Ophthalmol*. (2014) 98:143–4. doi: 10.1136/bjophthalmol-2013-304358
- Wu Q, Chen Q, Lin B, Huang S, Wang Y, Zhang L, et al. Relationships among retinal/choroidal thickness, retinal microvascular network and visual field in high myopia. *Acta Ophthalmol*. (2020) 98:e709–e14. doi: 10.1111/aos.14372
- Yang YS, Koh JW. Choroidal Blood Flow Change in Eyes with High Myopia. *Korean J Ophthalmol*. (2015) 29:309–14. doi: 10.3341/kjo.2015.29.5.309
- Margolis R, Spaide RF. A pilot study of enhanced depth imaging optical coherence tomography of the choroid in normal eyes. *Am J Ophthalmol*. (2009) 147:811–5. doi: 10.1016/j.ajo.2008.12.008

## AUTHOR CONTRIBUTIONS

XL and CW: supervised the project. XW and JY: developed the original idea and wrote the manuscript. XW, YL, and LY: conducted the statistical analysis. XW, HX, XR, QH, and YG: collected the data. All authors contributed to the article and approved the submitted version.

## FUNDING

This study was supported by Natural Science Foundation of Beijing, China (grant number 7202229).

29. Sadler TW. *Langman's Medical Embryology, 11e (International Edition)*. Baltimore, MD: Lippincott Williams & Wilkins (2009).
30. Ikuno Y, Tano Y. Retinal and choroidal biometry in highly myopic eyes with spectral-domain optical coherence tomography. *Invest Ophthalmol Vis Sci.* (2009) 50:3876–80. doi: 10.1167/iovs.08-3325
31. Goldenberg D, Moisseiev E, Goldstein M, Loewenstein A, Barak A. Enhanced depth imaging optical coherence tomography: choroidal thickness and correlations with age, refractive error, and axial length. *Ophthalmic Surg Lasers Imaging.* (2012) 43:296–301. doi: 10.3928/15428877-20120426-02

**Conflict of Interest:** The authors declare that the research was conducted in the absence of any commercial or financial relationships that could be construed as a potential conflict of interest.

**Publisher's Note:** All claims expressed in this article are solely those of the authors and do not necessarily represent those of their affiliated organizations, or those of the publisher, the editors and the reviewers. Any product that may be evaluated in this article, or claim that may be made by its manufacturer, is not guaranteed or endorsed by the publisher.

Copyright © 2022 Wang, Yang, Liu, Yang, Xia, Ren, Hou, Ge, Wang and Li. This is an open-access article distributed under the terms of the Creative Commons Attribution License (CC BY). The use, distribution or reproduction in other forums is permitted, provided the original author(s) and the copyright owner(s) are credited and that the original publication in this journal is cited, in accordance with accepted academic practice. No use, distribution or reproduction is permitted which does not comply with these terms.



# The Role of Internal Limiting Membrane as a Biomarker in the Evolution of Myopic Traction Maculopathy

Dong Fang<sup>1†</sup>, Jindi Su<sup>2†</sup>, Lu Chen<sup>1</sup> and Shaochong Zhang<sup>1\*</sup>

<sup>1</sup> Shenzhen Eye Hospital, Jinan University, Shenzhen Key Laboratory of Ophthalmology, Shenzhen, China, <sup>2</sup> Affiliated Shenzhen Maternity and Child Healthcare Hospital, Southern Medical University, Shenzhen, China

## OPEN ACCESS

### Edited by:

Enrico Borrelli,  
University of California, Los Angeles,  
United States

### Reviewed by:

Zongming Song,  
Henan Provincial Third People's  
Hospital, China  
Zhao Mingwei,  
Peking University People's  
Hospital, China

### \*Correspondence:

Shaochong Zhang  
shaochongzhang@outlook.com

<sup>†</sup>These authors have contributed  
equally to this work and share first  
authorship

### Specialty section:

This article was submitted to  
Ophthalmology,  
a section of the journal  
Frontiers in Medicine

Received: 26 October 2021

Accepted: 30 November 2021

Published: 07 January 2022

### Citation:

Fang D, Su J, Chen L and Zhang S  
(2022) The Role of Internal Limiting  
Membrane as a Biomarker in the  
Evolution of Myopic Traction  
Maculopathy. *Front. Med.* 8:802626.  
doi: 10.3389/fmed.2021.802626

**Purpose:** To describe the longitudinal structural changes of myopic traction maculopathy (MTM) based on optical coherence tomography (OCT) and to detect biomarkers in the evolution of MTM.

**Methods:** A retrospective study was conducted on patients with MTM as defined by OCT. A minimum follow-up of 6 months was necessary for study inclusion. The effects of comprehensive OCT-based structure on the evolution of MTM, the progression rates, and resolution rates of MTM were evaluated.

**Results:** A total of 120 eyes (120 patients) were included with an average follow-up of 15.4 months. During the follow-up, MTM progressed in 32 eyes (26.67%). The most common pattern of progression observed was the increased extent of retinoschisis in 12 eyes. The multivariate analysis showed that the presence of MTM progression had a significant correlation with internal limiting membrane (ILM) detachment and retinoschisis involved the entire macula at baseline. Five eyes (4.17%) experienced MTM resolution, of which 2 eyes developed disruptions of detached ILM, two eyes developed disruptions of epiretinal membrane, and one eye developed partial posterior vitreous detachment. Eyes with foveal detachment showed the highest progression rate (41.67%) and highest resolution rate (16.67%) compared to the eyes with other foveal complications.

**Conclusion:** ILM detachment is a risk factor for MTM progression and MTM resolution can occur after ILM disruption. These suggest that ILM may play an important role as a biomarker in the evolution of MTM.

**Keywords:** internal limiting membrane, optical coherence tomography, evolution, biomarker, myopic traction maculopathy (MTM)

## INTRODUCTION

Myopia is a major global public health problem. Approximately, one in six of population of the world is myopic (1). It is expected that nearly half of population of the world may be myopic by 2050, with as much as 10% highly myopic (2). Complications related to high myopia are now a major cause of visual impairment and blindness worldwide, especially in east Asia (3). Among them, myopic traction maculopathy (MTM) is one of the main causes for the progressive vision impairment in patients with high myopia, affecting as many as one-third of eyes with posterior staphyloma (4, 5).



Myopic traction maculopathy was proposed by Panozzo et al. (6) in 2004. It is an umbrella term that encompasses a wide spectrum of pathologic features generated by the traction in the pathologic myopic environment. In addition to the typical myopic tractional changes of myopic retinoschisis, generalized MTM also includes vitreoretinal interface abnormalities and foveal complications generated by traction. The detailed pathogenesis of MTM has not been clarified. However, tractional forces from vitreoretinal interfaces such as vitreomacular traction (VMT), epiretinal membrane (ERM), internal limiting membrane (ILM), or a combination of these are thought to be important factors (7, 8). To study the natural course of MTM, several study groups have conducted follow-up studies on MTM (9, 10). However, long-term follow-up studies on large samples are scarce and the long-term outcome and the biomarkers in MTM evolution remain unclear.

Myopic traction maculopathy covers a range of conditions whose prognoses vary significantly. Previous studies have verified that its prognosis is related to the retinoschisis grading (11). However, optical coherence tomography (OCT)-based structural changes including vitreoretinal interface abnormalities and various types of foveal complications are closely associated with the outcome of MTM. These structural changes were rarely considered in previous studies, thereby leading to an incomplete understanding of the natural history and prognosis of the disease.

In this study, the longitudinal changes of MTM in a large sample of highly myopic Chinese individuals were evaluated. Further, OCT-based structural changes, including the grading of retinoschisis, vitreoretinal interface abnormalities, and foveal complications, were comprehensively analyzed to identify the biomarkers in MTM evolution.

## METHODS

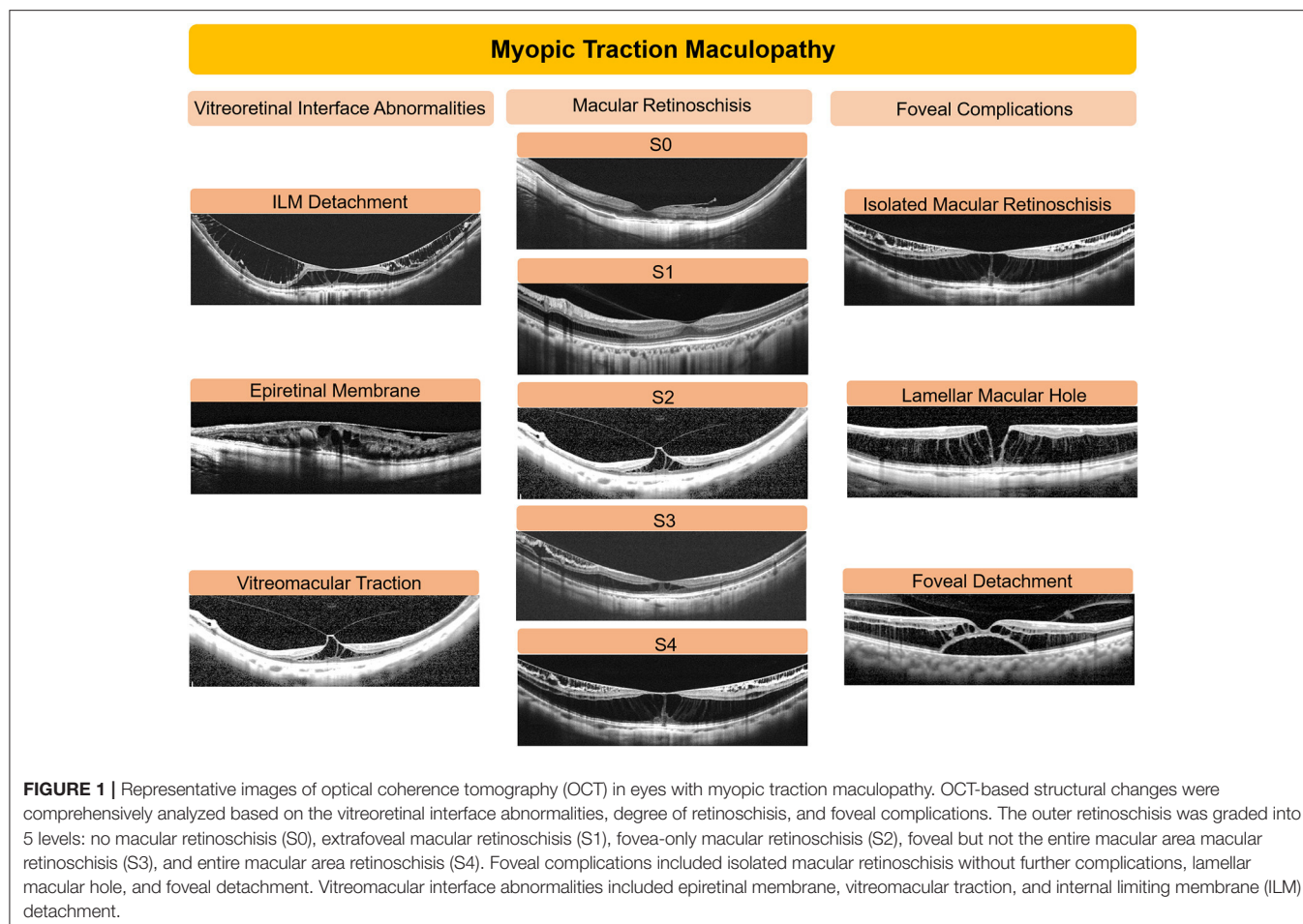
This study was approved by the Institutional Review Board of Shenzhen Eye Hospital (Shenzhen China) and was conducted in accordance with the World Medical Association Declaration of Helsinki. The medical records of consecutive patients with high myopia at the Shenzhen Eye Hospital between September 2017 and October 2020 were reviewed. Inclusion criteria were: (1) highly myopic eyes, defined by refractive error [expressed as spherical equivalent (SE)]  $< -6$  D or by an axial length  $\geq 26.5$  mm; (2) undergone spectral-domain OCT examinations including vertical, horizontal, and radial scans through the fovea; (3) OCT features corresponding to the diagnosis standards of MTM proposed by Panozzo et al. (6); and (4) a minimum follow-up period of 6 months, unless there was either resolution or progression. Exclusion criteria were: (1) eyes with previous vitreoretinal surgery; (2) eyes with any associated or concomitant retinopathy that could confound the retinal interpretation of OCT images; (3) eyes with macular chorioretinal atrophy or myopic choroidal neovascularization; and (4) OCT images with poor quality, which was defined as insufficient visualization of the retinal pigment epithelium (RPE) line in the macular area. Only one eye of each participant was used for analysis. When both eyes

of the same individuals were included, the eye with worse best corrected visual acuity (BCVA) was considered for the analysis.

All the patients underwent a comprehensive ophthalmological examination including BCVA, refractometry using autorefractor (KR-8800, Topcon, Tokyo, Japan), fundus photographs (Visucam, Carl Zeiss Meditec, Jena, Germany, UK), and spectral-domain OCT. The axial length of each participant was measured using IOLMaster (Carl Zeiss Meditec, Jena, Germany, UK). OCT imaging was performed with either OCT (Optovue Incorporation, Fremont, California, USA) or Spectralis OCT (Heidelberg Engineering, Heidelberg, Germany, UK). Vertical and horizontal scans, passing through the center of the fovea and radial scans, covering all the macular complications, were performed for each patient in OCT examination. Patients underwent a series of OCT scans spanning in a period of more than 6 months, unless there was either resolution or progression during the follow-up period. All the OCT images were read by an experienced OCT grader (SZ) masked to all the clinical data at the time of grading.

Changes of OCT-based structure were evaluated in three aspects including retinoschisis grading, foveal complications, and vitreomacular interface abnormalities. Representative images are shown in **Figure 1**. The outer retinoschisis was graded according to the location and the size as suggested by Parolini et al. (11): no macular retinoschisis (S0), extrafoveal macular retinoschisis (S1), fovea-only macular retinoschisis (S2), foveal but not the entire macular area macular retinoschisis (S3), and entire macular area macular retinoschisis (S4). Foveal complications including lamellar macular hole (MH), foveal detachment, and full-thickness MH were recorded. Vitreomacular interface abnormalities including ERM, VMT, and ILM detachment were also analyzed. MTM was defined as progressed in the event of: (1) for the macular retinoschisis, an increase of more than 100  $\mu$ m in height or an enlargement of the macular retinoschisis toward the area that did not have a retinoschisis (11); (2) development of any foveal complications including lamellar MH, foveal detachment, and full-thickness MH; and (3) for foveal complications, an increase of more than 100  $\mu$ m in height or an enlargement toward the area that did not have the lesion at baseline. A resolution of MTM was defined in the event of: (1) a decrease in the height or extent of the macular retinoschisis without any sign of progression and (2) a decrease in the height or extent of foveal complications without any sign of progression. Alternatively, an eye without progression or resolution was defined as stable. The rate of progression and resolution in MTM and the prognostic factors for progression were analyzed.

The BCVA was presented as the logarithm of the minimum angle of resolution (logMAR). Continuous variables between groups were compared using the one-way ANOVA test or the Mann-Whitney *U*-test and the Kruskal-Wallis test. Multiple comparisons between different groups were adjusted by the Bonferroni test. Categorical data were compared using the Pearson's chi-squared test or the Fisher's exact test. The multivariate binary regression analysis was performed with the presence of MTM progression as the dependent variable and age, axial length, the categories of retinoschisis, the presence of foveal complications, the presence of ILM detachment, and tractional



lesions as independent variables.  $p < 0.05$  was considered as statistically significant. All the data were analyzed using the SPSS 19.0 statistical software (SPSS Incorporation, Chicago, Illinois, USA).

## RESULTS

### Clinical Characteristics of Eyes With MTM at Presentation

A total of 120 eyes of 120 consecutive patients with a diagnosis of MTM were studied. The subjects comprised 73 women and 47 men with a mean age of  $52.78 \pm 9.91$  years ranging from 21.0 to 76.0 years. The mean baseline BCVA was  $0.42 \pm 0.40$  with a range of 0 to 1.85. The mean refractive error was  $-14.27 \pm 5.75$  D ranging from  $-5.5$  to  $-29.0$  D. The mean axial length was  $30.18 \pm 2.43$  mm with a range of 24.85–35.93 mm.

The baseline characteristics of MTM in each group are shown in **Table 1**. Among the 120 eyes with MTM, 31 eyes (25.83%), 30 eyes (25.00%), 12 eyes (10.00%), 22 eyes (18.33%), and 25 eyes (20.83%) had grades of S0, S1, S2, S3, and S4, respectively. The 31 eyes with S0 included 22 eyes with an isolated ERM, 4 eyes with an isolated VMT, 2 eyes with an ERM and coexisting

VMT, and 3 eyes with subfoveal retinal thickness  $> 200$  mm, but without evidence of a macular retinoschisis. Among the 12 eyes with S2, 9 eyes were accompanied by lamellar MH and one eye was accompanied by foveal detachment. Among the 22 eyes with S3, 8 eyes had coexisting lamellar MH and 3 eyes exhibited foveal detachment. In 25 eyes with S4, 8 eyes presented foveal detachment and 10 eyes displayed lamellar MH, 2 of which showed both the complications. The differences were not significant in age ( $p = 0.05$ , ANOVA test) and in axial length ( $p = 0.06$ , ANOVA test) at baseline between the eyes with different categories of retinoschisis (S0–S4). There were significant differences in BCVA among the eyes with different categories of retinoschisis ( $p < 0.001$ , Kruskal–Wallis test). Patients with S3 and S4 as compared with individuals with S0 and S1 had a significantly worse BCVA at baseline ( $p = 0.006$ ,  $p < 0.001$ ,  $p = 0.03$ ,  $p < 0.001$ ).

In terms of foveal complications, eyes were divided into 3 groups including isolated retinoschisis, lamellar MH, and foveal detachment (**Table 2**). None of the eyes with full-thickness MH was enrolled for their short duration of follow-up. A total of 83 eyes showed isolated retinoschisis, 27 eyes presented retinoschisis and coexisting lamellar MH, and 12 eyes displayed retinoschisis accompanied with foveal detachment (2 eyes had

**TABLE 1** | Baseline characteristics of patients with different categories of retinoschisis.

Characteristics	S0 (31 eyes)	S1 (30 eyes)	S2 (12 eyes)	S3 (22 eyes)	S4 (25 eyes)
<b>Age (y)</b>					
Mean $\pm$ SD	54.35 $\pm$ 8.13	50.10 $\pm$ 11.13	57.58 $\pm$ 6.33	49.45 $\pm$ 6.46	54.64 $\pm$ 12.72
Range	41–76	26–70	47–71	37–66	21–74
<b>BCVA (logMAR)</b>					
Mean $\pm$ SD	0.21 $\pm$ 0.17	0.25 $\pm$ 0.20	0.44 $\pm$ 0.29	0.54 $\pm$ 0.51	0.78 $\pm$ 0.44
Range	0.00–0.70	0.00–0.70	0.10–1.00	0.00–1.85	0.05–1.85
<b>Axial length (mm)</b>					
Mean $\pm$ SD	29.41 $\pm$ 2.61	31.08 $\pm$ 2.33	31.09 $\pm$ 2.20	29.98 $\pm$ 2.12	29.82 $\pm$ 2.35
Range	24.85–35.93	25.42–35.47	27.69–34.32	27.03–32.86	26.66–33.48
Progressed (eyes)	2 (6.45%)	5 (16.67%)	3 (25.00%)	8 (36.36%)	14 (56.00%)
Pathology enlargement*	0	4	3	4	9
Enlargement of retinoschisis	0	4	2	3	3
Enlargement of LMH	0	0	1	0	2
Enlargement of foveal RD	0	0	0	1	4
Newly onset pathology	3	2	0	4	5
Development of retinoschisis	2	0	0	0	0
Development of LMH	1	2	0	1	1
Development of foveal RD	0	0	0	2	4
Development of FTMH	0	0	0	1	0
Duration of progression	15.5	19.4	15	12.13	11.46
Improved (eyes)	0 (0%)	1 (3.33%)	0 (0%)	3 (13.64%)	1 (4.00%)
Stable (eyes)	29 (93.55%)	24 (80.00%)	9 (75.00%)	11 (50.00%)	10 (40.00%)

BCVA, best corrected visual acuity; logMAR, logarithm of the minimum angle of resolution; RD, retinal detachment; LMH, lamellar macular hole; FTMH, full-thickness MH.

\*Increased height or extent of the pathology.

both the lamellar MH and foveal detachment). Similarly, the differences were not significant in age ( $p = 0.71$ , ANOVA test) and in axial length ( $p = 0.10$ , ANOVA test) at the initial visit between the eyes with different foveal complications. There were significant differences in BCVA among the 3 groups ( $p < 0.001$ , Kruskal–Wallis test). Patients with foveal detachment presented a significantly worse BCVA at baseline as compared with individuals with lamellar MH and isolated retinoschisis ( $p < 0.001$ ,  $p < 0.001$ ).

Vitreomacular interface abnormalities including ILM detachment, ERM, and VMT were evaluated. An ILM detachment was present in 32 eyes (26.67%) and all of them showed concomitant outer retinoschisis. Tractional lesions including ERM and VMT were present in 88 eyes, of which 59 eyes showed isolated ERM, 22 eyes showed isolated VMT, and the remaining 7 eyes showed both the lesions.

## Characteristics in MTM Progression in High Myopia

The mean length of follow-up was  $15.4 \pm 12.2$  months (range, 6–61 months). Among the 120 eyes included, 32 eyes (26.67%) showed MTM progression. Overall, the progression rate increased with the increasing severity of retinoschisis (S0–S4,  $p < 0.001$ , Fisher's exact test). A summary of the progression of MTM is given in **Figure 2A**, **Table 1**. A significantly higher progression rate was found in eyes with S4 as compared with eyes with S0 and S1 ( $p < 0.001$ ;  $p = 0.003$ ).

A total of 14 newly onset lesions developed in 13 eyes in the OCT findings during the follow-up period, including one eye changed from S0 to extrafoveal retinoschisis (S1), one eye changed from S0 to extrafoveal retinoschisis (S1) with coexisting lamellar MH, 4 eyes developed lamellar MH, 6 eyes developed foveal detachment, and one eye developed full-thickness MH. In addition, a total of 20 lesion changes were identified in 20 eyes with progressive MTM. The most common pattern of progression observed was increasing height or extent of macular retinoschisis in 12 eyes, accounting for 60% of the total number of lesions changes and 37.5% of MTM progressions, followed by the enlargement of foveal detachment in 5 eyes (15.63%).

On the other hand, eyes with different foveal complications exhibited different progression rates (**Figure 2B**, **Table 2**). Eyes with foveal detachment showed the highest progression rate (41.67%), followed by the eyes with lamellar MH (33.33%) and the eyes with isolated retinoschisis (22.89%). Notably, among the 12 eyes with foveal detachment, 5 eyes experienced progression in a short average duration of 2.9 months (range, 39 days to 7 months). Representative cases of foveal detachment progression are shown in **Figure 3**. Among them, the eye with the most rapid progression showed an elevation of foveal detachment and a break of outer retina in only 39 days (**Figure 3**, Patient 1).

In 32 eyes with ILM detachment, progressions of MTM were observed in 13 eyes (40.63%), whereas a lower progression rate (21 eyes, 23.86%) was detected in the eyes without ILM detachment. The eyes with tractional lesions displayed a similar

**TABLE 2 |** Baseline characteristics of patients with different foveal complications.

Characteristics	Retinoschisis (83 eyes)	LMH (27 eyes)	Foveal RD (12 eyes)
<b>Age (y)</b>			
Mean $\pm$ SD	52.43 $\pm$ 9.54	53.07 $\pm$ 11.48	54.92 $\pm$ 8.22
Range	26–76	21–72	39–70
<b>BCVA (logMAR)</b>			
Mean $\pm$ SD	0.30 $\pm$ 0.29	0.64 $\pm$ 0.39	0.91 $\pm$ 0.53
Range	0.00–1.85	0.10–1.30	0.22–1.85
<b>Axial length (mm)</b>			
Mean $\pm$ SD	29.88 $\pm$ 2.52	30.83 $\pm$ 2.25	31.11 $\pm$ 1.61
Range	24.85–35.93	26.69–34.32	28.85–33.48
Progressed (eyes)	19 (22.89%)	9 (33.33%)	5 (41.67%)
Pathology enlargement*			
Enlargement of retinoschisis	9	7	5
Enlargement of LMH	9	3	0
Enlargement of LMH	0	3	0
Enlargement of foveal RD	0	1	5
Newly onset pathology	12	2	0
Development of retinoschisis	2	0	0
Development of LMH	5	0	0
Development of foveal RD	4	2	0
Development of FTMH	1	0	0
Duration of progression	16.1 $\pm$ 3.9	12.3 $\pm$ 4.1	2.9 $\pm$ 2.3
Improved (eyes)	3 (3.61%)	0 (0%)	2 (16.67%)
Stable (eyes)	61 (73.49%)	18 (66.67%)	5 (41.67%)

BCVA, best corrected visual acuity; logMAR, logarithm of the minimum angle of resolution; RD, retinal detachment; LMH, lamellar macular hole; FTMH, full-thickness MH.

\*Increased height or extent of the pathology.

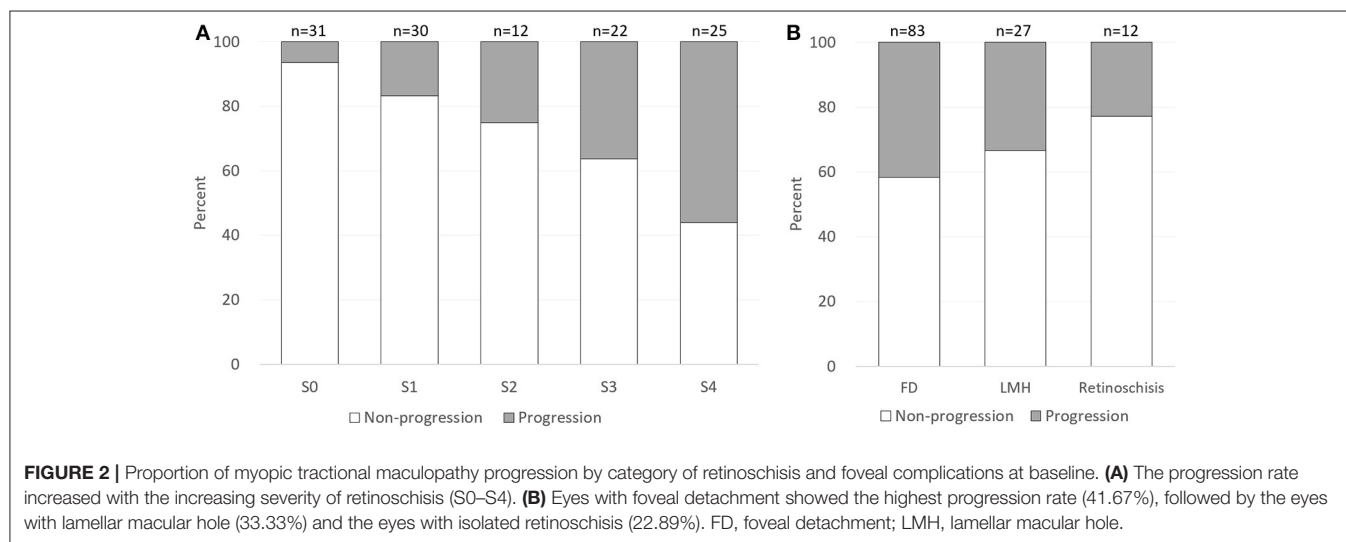


**FIGURE 2 |** Proportion of myopic tractional maculopathy progression by category of retinoschisis and foveal complications at baseline. **(A)** The progression rate increased with the increasing severity of retinoschisis (S0–S4). **(B)** Eyes with foveal detachment showed the highest progression rate (41.67%), followed by the eyes with lamellar macular hole (33.33%) and the eyes with isolated retinoschisis (22.89%). FD, foveal detachment; LMH, lamellar macular hole.

rate of progression compared to the eyes without tractional lesions (29.55 vs. 25%).

## Visual Outcome and Risk Factors for MTM Progression

Mean BCVA of the whole cohort at the end of follow-up was  $0.50 \pm 0.47$ , which was comparable to that at baseline ( $0.42 \pm$

$0.40$ ) ( $p = 0.49$ , Mann–Whitney  $U$ -test). For the patients whose MTM had progressed, the BCVA at the final examination ( $0.81 \pm 0.47$ ) was significantly worse than that at the initial examination ( $0.58 \pm 0.45$ ) ( $P = 0.04$ , Mann–Whitney  $U$ -test). The BCVA at the initial and final examinations was not statistically different in either the group with stable MTM or the group with resolved MTM ( $p = 0.76$ ,  $p = 0.78$ , Mann–Whitney  $U$ -test). The multivariate binary analysis adjusted for age and axial length was



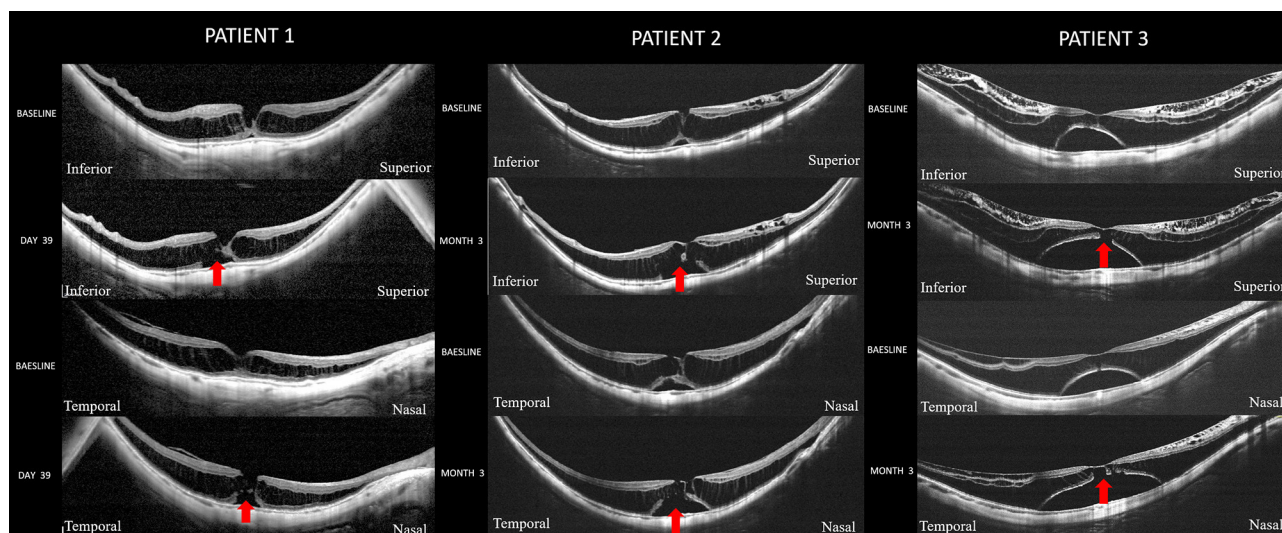


**FIGURE 3 |** Cases with foveal detachment experienced rapid progression. **Patient 1** is a woman (55-year-old) with a spherical equivalent refractive error of  $-23.0$  D and an axial length of 32.4 mm. Optical coherence tomography (OCT) scan across the fovea at the initial visit showed a retinoschisis spanning the entire macula with a lamellar MH. A slight foveal elevation can be seen. Thirty-nine days later, the extent of foveal detachment has increased and disruption of the outer retina (red arrow) has developed. The best corrected visual acuity (BCVA) declined from the logarithm of the minimum angle of resolution (logMAR) 0.70 to logMAR 1.0. **Patient 2** is a woman (61-year-old) with an axial length of 31.74 mm. At baseline, she had S4 retinoschisis involving the entire macula and a shallow foveal detachment. At the third month of the follow-up, the extent of foveal detachment increased with a disruption of the outer retina (red arrow) developed. The BCVA declined from logMAR 1.00 to logMAR 1.3. **Patient 3** is a woman (50-year-old) with an axial length of 30.21 mm. OCT scan at baseline showed an outer retinoschisis spanning the entire macula with commitment inner retinoschisis and internal limiting membrane detachment. A foveal detachment was observed. 3 months later, the foveal detachment has further enlarged and disruption of the outer retina (red arrow) was noted. The BCVA declined from logMAR 1.00 to logMAR 1.3.

done to reveal the risk factors for MTM progression. The results showed that MTM progression had significant correlation with the presence of ILM detachment ( $p = 0.02$ ; odds ratio, 3.68; 95% CI, 1.25–10.84, multivariate binary regression analysis) and eyes with S4 category of MTM at baseline ( $p = 0.004$ ; odds ratio, 3.85; 95% CI, 1.54–9.62, multivariate binary regression analysis).

### Characteristics in MTM Resolution in High Myopia

Among the 120 eyes with MTM, resolution of MTM occurred in 5 patients (4.17%) with a mean duration of 19.8 months (range, 6–46 months). The mean age was  $54.60 \pm 3.91$  years ranging from 49 to 70 years. The average SE was  $-16.10 \pm 2.12$  D ranging from  $-23.50$  to  $-11.50$  D and the average axial length was  $30.63 \pm 1.12$  mm with a range from 27.05 to 32.86 mm. The OCT changes in these eyes included a decrease in the height of the macular retinoschisis in 2 eyes, a complete resolution of the macular retinoschisis in 2 eyes, and a complete resolution of foveal detachment in one eye. Two eyes were accompanied with ILM detachment and experienced spontaneous disruption of the detached ILM during the follow-up period, two eyes were accompanied with ERM and experienced spontaneous disruption of ERM during the follow-up period, and the remaining one eye developed partial posterior vitreous detachment (PVD) during the follow-up period. Representative cases are shown in **Figure 4**. For retinoschisis grading, resolutions were found in none of the S0 eyes, 3.33% of the S1 eyes, none of the S2 eyes, 13.64% of the S3 eyes, and 4.00% of the S4 eyes. The differences in the

improvement rate among the 5 groups were not significant ( $p = 0.15$ , Fisher's exact test). In terms of foveal complications, eyes with foveal detachment showed the highest resolution rate, whereas eyes with isolated retinoschisis and lamellar MH showed a lower resolution rate (16.67, 3.61, and 0%;  $p = 0.1$ ).

The changes of OCT features in patients with different prognosis during the follow-up period are shown in **Table 3**. The eyes with MTM resolution during the follow-up period experienced spontaneous ILM disruption at a significantly higher rate than the other two groups ( $p = 0.001$ , Fisher's exact probability test). Similarly, a significantly higher incidence of spontaneous ERM disruption was observed in the eyes with MTM resolution compared with the other two groups ( $p = 0.03$ , Fisher's exact probability test). There was no significant difference in the rate of PVD development among the groups that showed improvement, no change, or progression during the course. One eye experienced MTM progression, despite complete PVD development during the follow-up period.

### DISCUSSION

By comprehensively evaluating the state of the vitreous, retina, and fovea on OCT, we found that ILM detachment and retinoschisis involving the entire macula at baseline were predictors for MTM progression. On the other hand, a higher proportion of spontaneous ILM disruption were found in the eyes with MTM resolution. These suggest that ILM may play

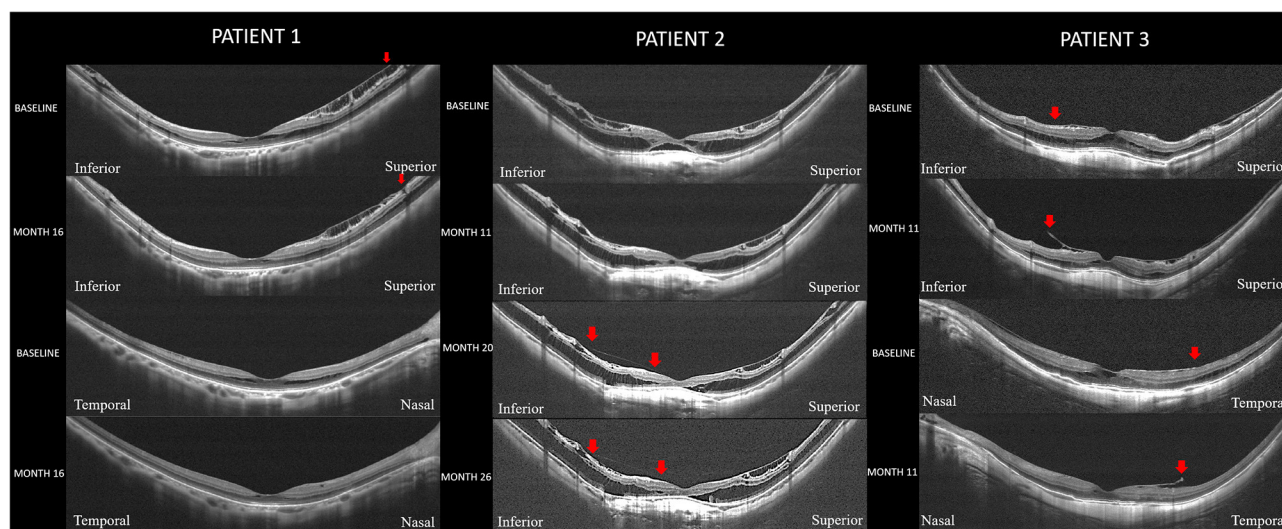


**FIGURE 4 |** Representative cases with spontaneous resolution of myopic traction maculopathy. **Patient 1:** Resolution of a macular retinoschisis in an eye with a disruption of the internal limiting membrane (ILM). Right eye with an axial length of 27.05 mm in a woman (50-year-old). Optical coherence tomography (OCT) scan in both the vertical and horizontal section at baseline showed a shallow foveal retinoschisis with ILM detachment. Sixteen months later, a disruption of the detached ILM superior to the fovea is observed (red arrow) and the foveal retinoschisis is disappeared. **Patient 2:** Resolution of a foveal detachment in an eye with a partial posterior vitreous detachment (PVD). Right eye with an axial length of 32.86 mm in a man (53-year-old). OCT scan in vertical section at baseline showed a shallow foveal detachment with retinoschisis spanning the entire macula. No signs of PVD were noted. Eleven months later, the foveal detachment has almost resolved and both the inner and outer retinoschisis has resolved. Twenty months after the initial visit, the foveal detachment has completely resolved. A residual vitreoretinal adhesion (between two red arrows) left after partial PVD can be seen. Twenty-six months of follow-up, the retinoschisis and vitreoretinal adhesion (between two red arrows) are stable. **Patient 3:** Resolution of a macular retinoschisis in an eye with a disruption of the epiretinal membrane (ERM). Left eye with an axial length of 31.46 mm in a man (51-year-old). OCT scan in both the vertical and horizontal sections at baseline showed a shallow retinoschisis with tractional ERM. Eleven months later, disruptions are noted in the ERM (red arrow) nasal and inferior to the fovea. The foveal retinoschisis has disappeared and the extrafoveal retinoschisis has been resolved.

**TABLE 3 |** Changes of OCT features in patients with different prognosis.

OCT Changes during the Follow-up Period	Prognosis			P-value
	Progressed (32 eyes)	Stable (83 eyes)	Improved (5 eyes)	
Spontaneous disruption of ILM	0 (0%)	0 (0%)	2 (40.00%)	<b>0.001*</b>
ILM detachment	2 (6.25%)	0 (0%)	0 (0%)	>0.05
Spontaneous disruption of ERM	1 (3.13%)	4 (4.82%)	2 (40.00%)	<b>0.03*</b>
Posterior vitreous detachment	1 (3.13%)	1 (1.20%)	1 (20.00%)	>0.05
Vitreomacular traction	1 (3.13%)	0 (0%)	0 (0%)	>0.05

OCT, optical coherence tomography; LMH, lamellar macular hole; ILM, internal limiting membrane; ERM, epiretinal membrane.

\*Fisher's exact tests.

Statistically significant p-values were reported in bold.

a crucial role as a biomarker in the evolution of MTM. In addition, patients with foveal detachment at baseline were found to have a higher possibility of progression at a rapid speed, and a higher possibility of resolution as well, indicating that this was an unstable stage and required close follow-up. To the best of our knowledge, we first demonstrate the significance of ILM in the evolution of MTM. We believe that this study will contribute to a better understanding of the pathogenesis of MTM and provide references for predicting prognosis and surgical decision-making of MTM.

To date, there are few studies that have documented the progression of MTM using longitudinal data and the reported

progression rate was quite different, ranging from 11.6 to 69.0% (9–11). Gaucher et al. (9) conducted a long-term follow-up of 50 eyes of 38 patients with myopic retinoschisis, among whom 14 eyes (28%) experienced progression in terms of visual acuity at the end of the follow-up. Shimada et al. (10) followed 207 eyes with MTM and found that the progression rate was only 11.6% during the follow-up. In this study, retinoschisis was divided into five grades (S0–S4) according to the location and extent of retinoschisis. Among the patients, 42.5% of them were not fovea involved (milder retinoschisis) and only 13.5% of them were entirely macula involved. Parolini et al. (11) studied the evolution of MTM in 72 eyes and found that the retinal pattern

evolved from inner/outer maculoschisis to predominantly outer maculoschisis, then maculoschisis-macular detachment, and finally macular detachment. In this study, we followed 120 patients with MTM and found that the progression rate was 26.67%, which was different from previous studies. The reason may be related to the sample size and the composition of cases. The prognosis of MTM was affected by various factors. Among them, the vitreoretinal interface factors, which represented inner ocular force, are one of the most important independent factors. However, the pattern of vitreoretinal interface, including VMT, ERM and ILM detachment, was less evaluated in previous studies.

In this study, we comprehensively evaluated the pattern of the vitreoretinal interface, retina, and fovea on OCT and found that ILM detachment was one of the predictors for MTM progression. The ILM acts as a basal membrane for retinal Müller cells. Its major components are collagen types IV, VI, and VIII, associated with glycoproteins. Proper ILM stiffness is vital for the mechanical balance and stability between the vitreoretinal interface, while rigid ILM may play an important role in vitreoretinal abnormalities such as MTM. Our previous studies found that in eyes with MTM, the ILM presented abnormal ultrastructure including long irregular indentations and increased cell debris, which might result from Müller cell reactive gliosis responding to mechanical stress during the elongation of axial length in pathologic myopia (12). In the meantime, we found that removal of ILM during pars plana vitrectomy is beneficial to the recovery of postoperative anatomy and visual function for patients with MTM (13). These suggested that ILM is vital in the pathogenesis of MTM. In this study, we found that ILM detachment is a risk factor for MTM progression; meanwhile, MTM resolution can occur after spontaneous ILM disruption. These findings further verified that pathological ILM is not only involved in the occurrence of MTM, but also a risk factor for MTM development. We proposed that pathological ILMs with increased stiffness generate a centripetal traction in retina, contributing to the retinal splitting in pathologic myopia. In contrary, released traction resulting from spontaneous disruption of ILM that could lead to MTM resolution. Thus, monitoring the state of the ILM might help us to better predict the prognosis and make surgical decision for MTM.

Foveal detachment is a severe complication of pathologic myopia, which is often accompanied by serious visual impairment and poor prognoses (14). Huang et al. (15) found that preoperative foveal detachment is one of the risk factors for MH retinal detachment after vitrectomy in MTM. This study found that patients with foveal detachment were more likely to experience progression at a rapid speed (5/12, 41.67%). Similarly, Shimada et al. (10) studied 10 cases of foveal detachment and found a progression rate of 100% during a mean follow-up duration of 31.7 months. Interestingly, we found that this group of patients was more likely to experience resolution (16.67%) as well. No significant difference was detected in age and in axial length between the eyes with and without foveal detachment. This was consistent to Lai et al. (16), who reported eight cases of foveal detachment experienced spontaneous resolution during the follow-up. These revealed that foveal detachment is an unstable intermediate stage in the development of MTM. In a

mechanical view, in eyes with foveal detachment, the outer retina exhibited a steep, curved shape with an undulated surface. We proposed that the sharp changes of curvature in the outer retina at the detached region may contribute to the lower structural stability of foveal detachment. Thus, this group of patients needs intensive follow-up and timely intervention.

Resolution of MTM is a relatively rare phenomenon. Previous studies were mostly based on case reports and only one study (11) reported the incidence of spontaneous resolution of MTM in a large sample. The reported resolution rate of 3.9% was similar with the rate of 4.2% obtained in this study. In 2003, the resolution of MTM without surgical intervention was first reported by Polito et al. (17). They reported a spontaneous resolution after PVD in a patient with foveoschisis and foveal detachment. Subsequently, spontaneous resolution in cases with foveoschisis, foveal detachment, and even MH retinal detachment was reported (16, 18). At present, it is believed that multiple factors result in the resolution of MTM including the release of anterior traction and the morphological changes of posterior sclera (18). The 5 cases with resolution observed in this study all experienced the release of anterior traction such as the disruption of the anterior ERM, the disruption of the detached ILM, and partial PVD. However, little is known when a spontaneous resolution will develop and further exploration with larger sample size is needed.

This study has several limitations. Given the retrospective design of this study, durations of follow-up were variable. Further prospective investigations with larger sample size would be demanded.

In summary, this study found that during a mean follow-up period of 15.4 months, the rate of progression and resolution in MTM were 26.67 and 4.17%, respectively. The ILM detachment is a risk factor for the MTM progression, whereas the MTM resolution can occur after the spontaneous disruption of ILM, indicating that ILM might be one of the biomarkers of the evolution of MTM. Patients with foveal detachment are unstable and require close follow-up and timely intervention. By comprehensively analyzing the OCT-based structural alterations, namely, the retinoschisis grading, the foveal complications and vitreoretinal interface abnormalities, and investigating the risk factors for MTM progression, we believe that this study will contribute to a better understanding of the pathogenesis of MTM and provide references for predicting prognosis and surgical decision-making of MTM.

## DATA AVAILABILITY STATEMENT

The original contributions presented in the study are included in the article/supplementary material, further inquiries can be directed to the corresponding author/s.

## ETHICS STATEMENT

The studies involving human participants were reviewed and approved by the Institutional Review Board of



Shenzhen Eye Hospital (Shenzhen, China). Written informed consent for participation was not required for this study in accordance with the national legislation and the institutional requirements.

## AUTHOR CONTRIBUTIONS

DF contributed to the study design and wrote the manuscript. JS contributed to the clinical data collection, data analyses, and manuscript polishing. LC contributed to manuscript preparation and clinical data collection. SZ contributed to the conception of

the study, study design, and manuscript polishing. All authors have read and approved the final version of the manuscript.

## FUNDING

This study was supported by grants from the Sanming Project of Medicine in Shenzhen (SZSM202011015), the Natural Science Foundation of Guangdong Province (2021A1515011090), and the National Natural Science Foundation of China (81900877). These funding organizations had no role in the design or conduct of this study.

## REFERENCES

- Morgan IG, French AN, Ashby RS, Guo X, Ding X, He M, et al. The epidemics of myopia: aetiology and prevention. *Prog Retinal Eye Res.* (2018) 62:134–49. doi: 10.1016/j.preteyeres.2017.09.004
- Holden BA, Fricke TR, Wilson DA, Jong M, Naidoo KS, Sankaridurg P, et al. Global prevalence of myopia and high myopia and temporal trends from 2000 through 2050. *Ophthalmology.* (2016) 123:1036–42. doi: 10.1016/j.ophtha.2016.01.006
- Cedrone C, Nucci C, Scuderi G, Ricci F, Cerulli A, Culasso F. Prevalence of blindness and low vision in an Italian population: a comparison with other European studies. *Eye.* (2006) 20:661–7. doi: 10.1038/sj.eye.6701934
- Baba T, Ohno-Matsui K, Futagami S, Yoshida T, Yasuzumi K, Kojima A, et al. Prevalence and characteristics of foveal retinal detachment without macular hole in high myopia. *Am J Ophthalmol.* (2003) 135:338–42. doi: 10.1016/S0002-9394(02)01937-2
- Benhamou N, Massin P, Haouchine B, Erginay A, Gaudric A. Macular retinoschisis in highly myopic eyes. *Am J Ophthalmol.* (2002) 133:794–800. doi: 10.1016/S0002-9394(02)01394-6
- Panozzo G, Mercanti A. Optical coherence tomography findings in myopic traction maculopathy. *Arch Ophthalmol.* (2004) 122:1455–60. doi: 10.1001/archophth.122.10.1455
- Vanderbeek BL, Johnson MW. The diversity of traction mechanisms in myopic traction maculopathy. *Am J Ophthalmol.* (2012) 153:93–102. doi: 10.1016/j.ajo.2011.06.016
- Ikuno Y, Comi F, Tano Y. Potent retinal arteriolar traction as a possible cause of myopic foveoschisis. *Am J Ophthalmol.* (2005) 139:462–7. doi: 10.1016/j.ajo.2004.09.078
- Gaucher D, Haouchine B, Tadayoni R, Massin P, Erginay A, Benhamou N, et al. Long-term follow-up of high myopic foveoschisis: natural course and surgical outcome. *Am J Ophthalmol.* (2007) 143:455–62. doi: 10.1016/j.ajo.2006.10.053
- Shimada N, Tanaka Y, Tokoro T, Ohno-Matsui K. Natural course of myopic traction maculopathy and factors associated with progression or resolution. *Am J Ophthalmol.* (2013) 156:948–57. doi: 10.1016/j.ajo.2013.06.031
- Parolini B, Palmieri M, Finzi A, Besozzi G, Lucente A, Nava U, et al. The new myopic traction maculopathy staging system. *Eur J Ophthalmol.* (2021) 31:1299–312. doi: 10.1177/1120672120930590
- Chen L, Wei Y, Zhou X, Zhang Z, Chi W, Gong L, et al. Morphologic, biomechanical, and compositional features of the internal limiting membrane in pathologic myopic foveoschisis. *Invest Ophthalmol Visual Sci.* (2018) 59:5569–78. doi: 10.1167/iiov.18-24676
- Zhang Z, Wei Y, Jiang X, Zhang S. Pars plana vitrectomy and wide internal limiting membrane peeling with perfluoropropane tamponade for highly myopic foveoschisis-associated macular hole. *Retina.* (2017) 37:274–82. doi: 10.1097/IAE.0000000000001146
- Fujimoto M, Hangai M, Suda K, Yoshimura N. Features associated with foveal retinal detachment in myopic macular retinoschisis. *Am J Ophthalmol.* (2010) 150:863–70. doi: 10.1016/j.ajo.2010.06.023
- Huang Y, Huang W, Ng DSC, Duan A. Risk factors for development of macular hole retinal detachment after pars plana vitrectomy for pathologic myopic foveoschisis. *Retina J Retinal Vitreous Dis.* (2017) 37:1049–54. doi: 10.1097/IAE.0000000000001322
- Lai TT, Ho TC, Yang CM. Spontaneous resolution of foveal detachment in traction maculopathy in high myopia unrelated to posterior vitreous detachment. *BMC Ophthalmol.* (2016) 16:18. doi: 10.1186/s12886-016-0195-3
- Polito A, Lanzetta P, Del Borrello M, Bandello F. Spontaneous resolution of a shallow detachment of the macula in a highly myopic eye. *Am J Ophthalmol.* (2003) 135:546–7. doi: 10.1016/S0002-9394(02)02080-9
- Polascik BW, Zhang W, Grewal DS, Fekrat S. Spontaneous improvement of myopic macular retinoschisis: case report and review of literature. *Canad J Ophthalmol.* (2017) 52:E11–3. doi: 10.1016/j.cjco.2016.06.008

**Conflict of Interest:** The authors declare that the research was conducted in the absence of any commercial or financial relationships that could be construed as a potential conflict of interest.

**Publisher's Note:** All claims expressed in this article are solely those of the authors and do not necessarily represent those of their affiliated organizations, or those of the publisher, the editors and the reviewers. Any product that may be evaluated in this article, or claim that may be made by its manufacturer, is not guaranteed or endorsed by the publisher.

Copyright © 2022 Fang, Su, Chen and Zhang. This is an open-access article distributed under the terms of the Creative Commons Attribution License (CC BY). The use, distribution or reproduction in other forums is permitted, provided the original author(s) and the copyright owner(s) are credited and that the original publication in this journal is cited, in accordance with accepted academic practice. No use, distribution or reproduction is permitted which does not comply with these terms.





# Novel Findings of Retinal and Choroidal Features Utilizing Optical Coherence Tomography Angiography Analysis in Patients With Autoimmune Posterior Uveitis

Junhui Shen, Jinfeng Kong, Si Chen, Xin Liu, Yan Teng, Hailan Wu, Lijuan Wang, Manman Wu, Zhaoan Su and Lei Feng\*

## OPEN ACCESS

### Edited by:

Hetian Lei,  
Shenzhen Eye Hospital, China

### Reviewed by:

Xiaofeng Xie,  
Eye Institute of Shandong University of  
Traditional Chinese Medicine, China

Jing Li,  
Shanghai Jiaotong University, China  
He Jianfeng,  
Shanghai Jiao Tong University, China

### \*Correspondence:

Lei Feng  
leifeng@zju.edu.cn

### Specialty section:

This article was submitted to  
Ophthalmology,  
a section of the journal  
Frontiers in Medicine

**Received:** 24 October 2021

**Accepted:** 08 December 2021

**Published:** 11 January 2022

### Citation:

Shen J, Kong J, Chen S, Liu X,  
Teng Y, Wu H, Wang L, Wu M, Su Z  
and Feng L (2022) Novel Findings of  
Retinal and Choroidal Features  
Utilizing Optical Coherence  
Tomography Angiography Analysis in  
Patients With Autoimmune Posterior  
Uveitis. *Front. Med.* 8:801036.  
doi: 10.3389/fmed.2021.801036

Eye Center, Second Affiliated Hospital, School of Medicine, Zhejiang University, Hangzhou, China

**Purpose:** To analyze the quantitative parameters acquired by optical coherence tomography angiography (OCTA) in patients with autoimmune posterior uveitis.

**Methods:** OCTA images of 65 eyes affected with uveitis and 65 normal control (NC) eyes were obtained. The central macular thickness (CMT), retinal thicknesses, foveal avascular zone (FAZ) area, foveal density 300  $\mu$ m (FD300), and vascular density (VD) were compared among acute uveitic eyes, chronic uveitic eyes, and NC eyes. VDs were evaluated in the choriocapillaris, outer retina, optic disk, whole and parafovea superficial capillary plexus (SCP), and whole and parafovea deep capillary plexus (DCP). Correlation analysis was used to analyze the relationship between LogMAR best-corrected visual acuity (BCVA) and quantitative parameters from OCTA.

**Results:** Compared with NC eyes, the CMT and retinal thicknesses were increased significantly in eyes with uveitis ( $p < 0.05$ , respectively). No significant difference was observed in the FAZ area. FD300, VDs in the optic disk, SCP, and DCP both in whole image and parafovea, choriocapillaris were significantly decreased in uveitis eyes ( $p < 0.05$ , respectively) compared with NC eyes, only the acute group had decreased VD of the outer retina and choriocapillaris compared with the NC group ( $p < 0.05$ ). Moreover, quantitative parameters of OCTA showed a significant correlation with LogMAR BCVA in the patients with uveitis. Whole VD DCP was the best predictive factor for BCVA in the patients with uveitis.

**Conclusion:** Quantitative measurement by OCTA is a promising strategy for objective assessment of autoimmune posterior uveitis.

**Keywords:** optical coherence tomography angiography, quantitative measurements, uveitis, vessel density, inflammation

## INTRODUCTION

Optical coherence tomography angiography is a new non-invasive fundus imaging technique that can be used to acquire information about retinal and choroidal blood flow with high resolution *in vivo* (1). The high resolution enables the display of the signals of the retinal capillary network and choroidal capillary network in different layers. OCTA has unique advantages in the detection of retinal or choroidal vascular changes, the measurement of foveal avascular zone (FAZ), the quantification of vascular density (VD) in the inner retina, outer retinal circulation, or choriocapillaris. The technique has already been applied in the study of glaucoma (2) and various kinds of retinopathy, such as central serous choroidopathy (3), choroidal neovascularization (4), polypoid choroidal vasculopathy (PCV) (5), and diabetic retinopathy (6).

When the uvea is in an inflammatory state, the blood flow of the short posterior ciliary artery and the choroid are decreased, and the morphology and the function of retinal blood vessels are also compromised. To date, alterations of the retinal vessels in anterior, posterior, and panuveitis have been studied. OCTA has also proved to be an effective diagnostic tool in birdshot chorioretinopathy (7), multifocal choroiditis (8, 9), punctate inner choroidopathy (PIC) (10), acute macular neuroretinopathy (11), multiple evanescent white dot syndrome (12), acute posterior multifocal placoid pigment epitheliopathy (APMPPE) (13), and serpiginous-like choroiditis (14). Several researchers have revealed that OCTA can provide quantitative analysis for uveitis. Koca et al. found that retinal VD decreased and the perifoveal microvascular network changed in ocular-involved Behçet's (15). Liang et al. found that deep capillary plexus (DCP) VD was significantly lower in patients with Vogt-Koyanagi-Harada disease (VKH) than in normal controls (NCs), and that DCP VD was associated with a visual outcome (1). So far, published studies on the quantitative analysis of OCTA in uveitis are very limited, especially in patients with posterior segment-involved autoimmune uveitis. There is a lack of investigation about the vascular beds below the retinal pigmented epithelium (RPE) complex, quantitative analysis of the outer retina, or choriocapillaris abnormalities.

In this study, retinal and choroidal microvasculature changes in patients with uveitis, and healthy controls were studied. We aimed to summarize OCTA features from uveitis at different stages to explore the potential clinical values of quantitative OCTA results and to assess the values of OCTA measurement in the diagnosis, follow-up, and prognosis of patients with autoimmune posterior uveitis.

## MATERIALS AND METHODS

### Study Participants

The present study employed a retrospective approach. Patients diagnosed with autoimmune posterior uveitis and NCs who were at the Second Affiliated Hospital of Zhejiang University School of Medicine between May 2020 and September 2020 were enrolled. The consent procedure and study protocol followed the tenets of the Declaration of Helsinki and were approved by

the Institutional Review Board of the Second Affiliated Hospital of Zhejiang University School of Medicine. Written informed consent was obtained from the patients.

### Inclusion Criteria

All autoimmune posterior uveitis cases were diagnosed based on the American Uveitis Society's revised international criteria through clinical examination techniques such as slit-lamp evaluations of the anterior segment, color fundus, OCTA, fluorescein angiography, and indocyanine green angiography if needed. Laboratory examinations, including white blood cell counts, serologic examinations for syphilis, and tuberculin tests, were assessed to determine the underlying cause of uveitis. Patients with posterior uveitis were grouped into two stages according to the classic Moorthy criteria: (1) acute uveitic stage: disease course within 3 months or (2) chronic stage: disease course exceeding 3 months. In cases of bilateral uveitis, only one eye was chosen randomly in the analysis.

During the same period, age-matched healthy volunteers without a history of ocular inflammation, injury, surgery, or other remarkable ocular diseases were recruited. Only one eye was chosen randomly in the analysis.

Medical records of the patients and NCs were reviewed retrospectively, including sex, age, uveitis diagnosis, OCTA images, and best-corrected visual acuity (BCVA).

### Exclusion Criteria

We excluded patients with infectious posterior uveitis. Eyes with retinal or choroidal vascular disease not associated with uveitis (e.g., diabetic retinopathy, retinal vascular occlusion, and age-related macular degeneration), masquerade syndrome, glaucoma, and high myopia were excluded. The subjects who were unable to fixate or who had significant media opacities were excluded. OCTA images with poor quality, such as projection artifacts from vessels located above the plane of the image or an overly dark image filled with extremely thick outer choroidal vessels, were excluded.

### OCTA Image Analysis

All patients and NCs were imaged with the AngioVue Imaging System (RTVue XR Avanti; Optovue, Inc., Fremont, CA) (16) by the same experienced examiner. OCTA image analysis covering the 4.5 mm × 4.5 mm area centered on the papilla and the 6 mm × 6 mm area centered on the fovea was performed. The qualities of the images were graded automatically by the AngioAnalytics software (Optovue, Inc.) from Q1 (lowest quality) to Q10 (highest quality), and only images with qualities of Q7 or higher were included in the analysis. A CUSTOM function in the AngioVue software (version 2018.1.0.43; Optovue, Inc.) was used to measure retinal nerve fiber layer (RNFL), CMT, retinal thickness, FAZ area, FD300, and VDs in the optic disk, superficial capillary plexus (SCP), DCP, outer retina, and choriocapillaris.

According to the manufacturer's instructions, central macular thickness (CMT) was defined as the vertical distance from the inner limiting membrane (ILM) to the Bruch's membrane (BRM) at the central fovea of macula. RNFL thickness was defined as the vertical distance from the ILM to the nerve fiber

layer (NFL) of the peripapillary region. Measurement of the thickness of the retina is according to the early treatment diabetic retinopathy study (ETDRS) grid. The ETDRS grid comprised of three concentric rings: 1 mm center, 1–3 mm (parafovea), and an outer ring of 3–6-mm diameters (perifovea). The FAZ is the retinal capillary free area located in the central fovea. The FAZ area was measured automatically using AngioVue software using a slab from the ILM offset to the outer plexiform layer (OPL) offset. Foveal density 300  $\mu\text{m}$  (FD300) was defined as the blood flow density in a 300- $\mu\text{m}$  width of a double loop around the FAZ. The radial peripapillary capillary plexus was from ILM to NFL. Optic disk vessel density (VD) defined by the percentage of area occupied by OCTA detected vasculature, including inside the disk area and the peripapillary region. SCP was defined as from ILM to 10  $\mu\text{m}$  above internal plexiform layer (IPL), DCP was defined as from 10  $\mu\text{m}$  above IPL to 10  $\mu\text{m}$  below OPL, outer retina was defined as from 10  $\mu\text{m}$  below OPL to 10  $\mu\text{m}$  above BRM, and choriocapillaris was defined as from 10  $\mu\text{m}$  above BRM to 30  $\mu\text{m}$  below BRM (Figure 1). Parafovea was defined as the area outside of a 1 mm  $\times$  1 mm circle centered on the fovea in SCP and DCP. Optic disk vessel density (VD) defined by the percentage of the area occupied by OCTA detected vasculature, including inside the disk area and the peripapillary region (Figure 1).

## Statistical Analysis

IBM SPSS Statistics (Armonk, NY, IBM Corp.) for Windows version 22.0 was used for statistical analysis. GraphPad Prism® (GraphPad Software Inc., La Jolla, CA) version 6.01 was used to plot graphs. Chi square test was used to compare the categorical variables. Shapiro Wilk's W-test was used to test the normality of the numerical variables. For comparison between the two groups, the unpaired *t*-test and the Mann–Whitney U-test were used. One-way ANOVA followed by Dunnett's *post hoc* test was used to compare the different test groups with the control as indicated. Multiple kinds of testing were corrected using the Bonferroni method. The correlation between various parameters and LogMAR BCVA was evaluated using Pearson's correlation analysis. Continuous data are shown as the mean  $\pm$  standard deviation (SD). Statistical significance was set at  $p < 0.05$ .

## RESULTS

### Study Population Characteristics

Sixty-five patients with autoimmune posterior uveitis (31 females and 34 males; 65 eyes) with a mean age of  $40.86 \pm 15.96$  years and 65 age-matched NCs (31 females and 34 males; 65 eyes) with a mean age of  $45.32 \pm 12.11$  years were included in the study. There was no statistically significant difference between the patients with uveitis and NCs in terms of age and sex ( $p = 0.118$  and  $p = 0.992$ , respectively). The demographic and clinical characteristics of study groups are summarized in Table 1. In the uveitis group, there were 40 cases of idiopathic panuveitis ( $n = 40$ ; 61.5%), 15 cases of Vogt-Koyanagi-Harada disease ( $n = 15$ ; 23.1%), and 10 cases of Behçet's ( $n = 10$ ; 15.4%).

The mean logMAR BCVA between the patients with uveitis ( $0.24 \pm 0.15$ ) and NCs ( $0.01 \pm 0.17$ ) was different ( $p < 0.001$ ).

OCTA images with quality indices of Q7 or above were included. In total, 65 OCTA images of the affected eyes and 65 images of NCs were analyzed. Among them, 32 patients and 32 eyes (32 images), as well as 33 patients and 33 eyes (33 images), were classified into the acute and chronic eye groups.

## Comparison of Fundus Fluorescein Angiography and OCTA Technique in Assessment of Uveitis

Fundus Fluorescein Angiography is a very sensitive imaging method for detecting retinal vascular inflammation, because even slight inflammation of the retinal vascular wall may cause vascular leakage. FFA leakage is a very useful feature for assessing potential uveitis activity. OCTA cannot detect leakage, but it can describe changes in the blood vessel density of the different layers of retina such as superficial or deep capillary plexus, and optic disk. These results indicate that OCTA may be used to quantitatively measure the degree of intraocular inflammation (Figure 2).

## Comparison of OCTA Data in Uveitis Eyes and Normal Control Eyes

The comparisons of RNFL, CMT, retinal thickness, FAZ, FD, and VDs in the optic disk, SCP, DCP, outer retina, and choriocapillaris between uveitis eyes and NCs are summarized in Table 2. As compared to normal eyes, RNFL, CMT, retinal thickness (1–3)  $\mu\text{m}$ , retinal thickness (3–6)  $\mu\text{m}$ , and retinal thickness (0–6)  $\mu\text{m}$  were increased in uveitis eyes (all  $p < 0.05$ ). The FAZ area had no significant change between uveitis and NC ( $p = 0.07$ ). FD-300 Area Density and FD-300 Length Density were decreased in uveitis eyes (all  $p < 0.001$ ). VD in the optic disk was  $53.08 \pm 5.49$  and  $56.28 \pm 2.51$  in uveitis eyes and normal eyes, respectively. SCP was  $46.11 \pm 4.98$  and  $49.01 \pm 3.83$  in the whole image and  $46.82 \pm 5.29$  and  $50.79 \pm 5.29$  in parafovea in uveitis eyes and normal eyes, respectively. DCP was  $45.63 \pm 5.25$  and  $48.36 \pm 6.53$  in the whole image and  $51.76 \pm 5.71$  and  $54.19 \pm 4.65$  in parafovea in uveitis eyes and normal eyes, respectively. Outer retina was  $14.72 \pm 3.75$  and  $14.59 \pm 3.15$  in uveitis eyes and normal eyes, respectively. Choriocapillaris was  $23.69 \pm 1.59$  and  $24.22 \pm 1.16$  in the uveitis eyes and normal eyes, respectively. As compared to normal eyes, VDs in the optic disk, SCP, and DCP both in whole image and parafovea, choriocapillaris were significantly decreased in uveitis eyes ( $p < 0.001$ ,  $p < 0.001$ ,  $p < 0.001$ ,  $p = 0.009$ ,  $p = 0.009$ , and  $p = 0.031$ , respectively). Differences in VDs in the outer retina between uveitis eyes and normal eyes were not significant ( $p = 0.826$ ).

## Analyses of Correlations Between the BCVA and Quantitative Parameters From OCTA

BCVA was recorded in the logarithm of the minimum angle of resolution (logMAR) units. Correlation analyses between LogMAR BCVA and the quantitative parameters from OCTA are shown in Table 3. In uveitis eyes, LogMAR BCVA was statistically significant and correlated with VDs of whole and parafovea SCP, and whole and parafovea DCP, outer retina.



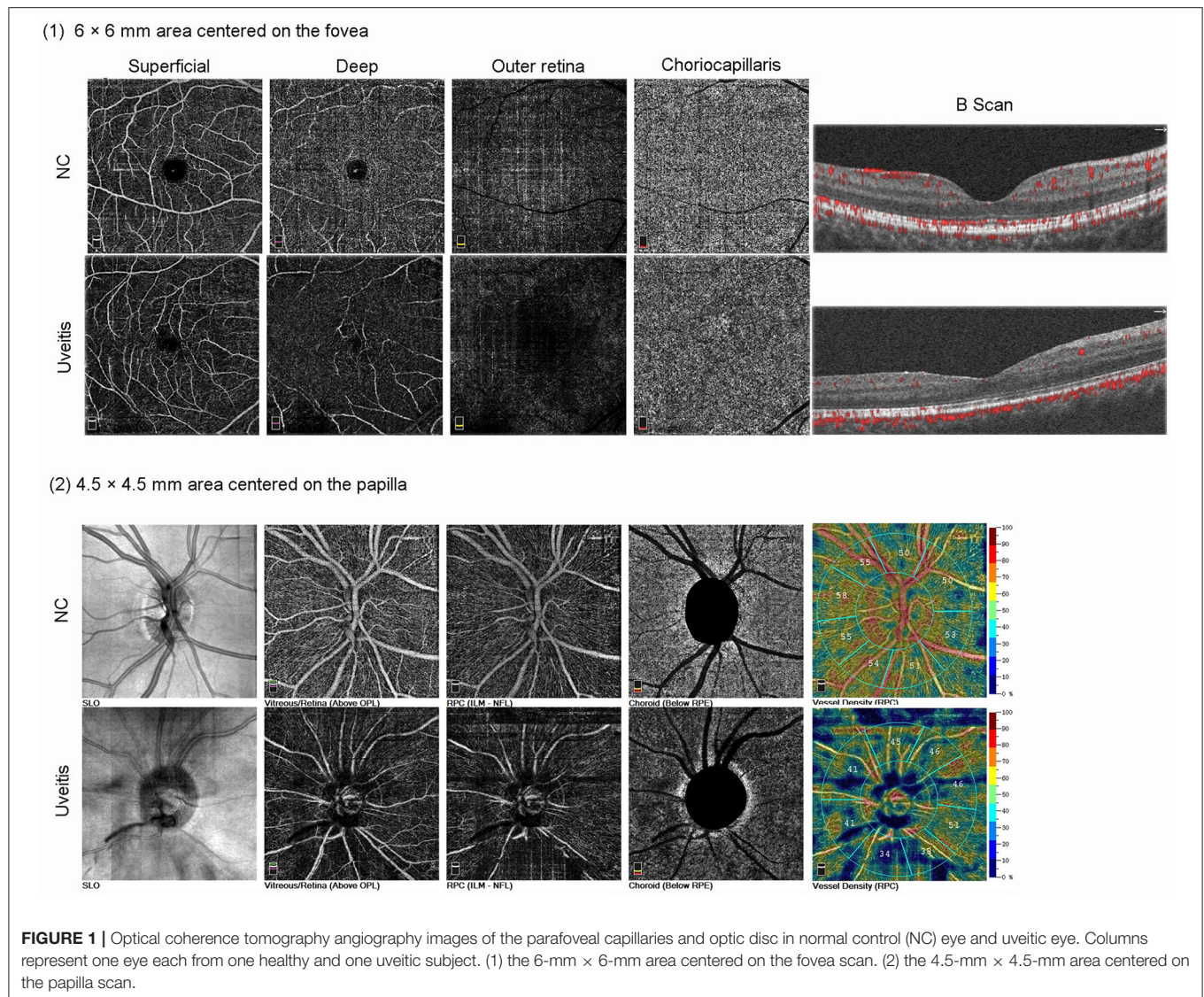


**FIGURE 1 |** Optical coherence tomography angiography images of the parafoveal capillaries and optic disc in normal control (NC) eye and uveitic eye. Columns represent one eye each from one healthy and one uveitic subject. (1) the 6-mm × 6-mm area centered on the fovea scan. (2) the 4.5-mm × 4.5-mm area centered on the papilla scan.

**TABLE 1 |** Statistical comparison of demographic characteristics of study participants.

	Normal control (NC)	Autoimmune posterior uveitis	Acute uveitis	Chronic uveitis	<i>p</i> -value
Number of eye/individuals	65/65	65/65	32/32	33/33	
Age (years)	40.86 ± 15.96	45.32 ± 12.11	42.75 ± 19.22	39.03 ± 12.02	0.118
Sex, female/male	31/34	31/34	15/17	16/17	0.992
BCVA(logMAR)	0.24 ± 0.15	0.01 ± 0.17	/	/	< 0.001

However, the RNFL, CMT, retinal thickness (0–6)  $\mu\text{m}$ , FAZ area, FD300, and VDs of optic disc, choriocapillaris were not correlated with visual acuity (all  $p > 0.05$ ). In normal eyes, none of them were correlated with LogMAR BCVA (all  $p > 0.05$ ).

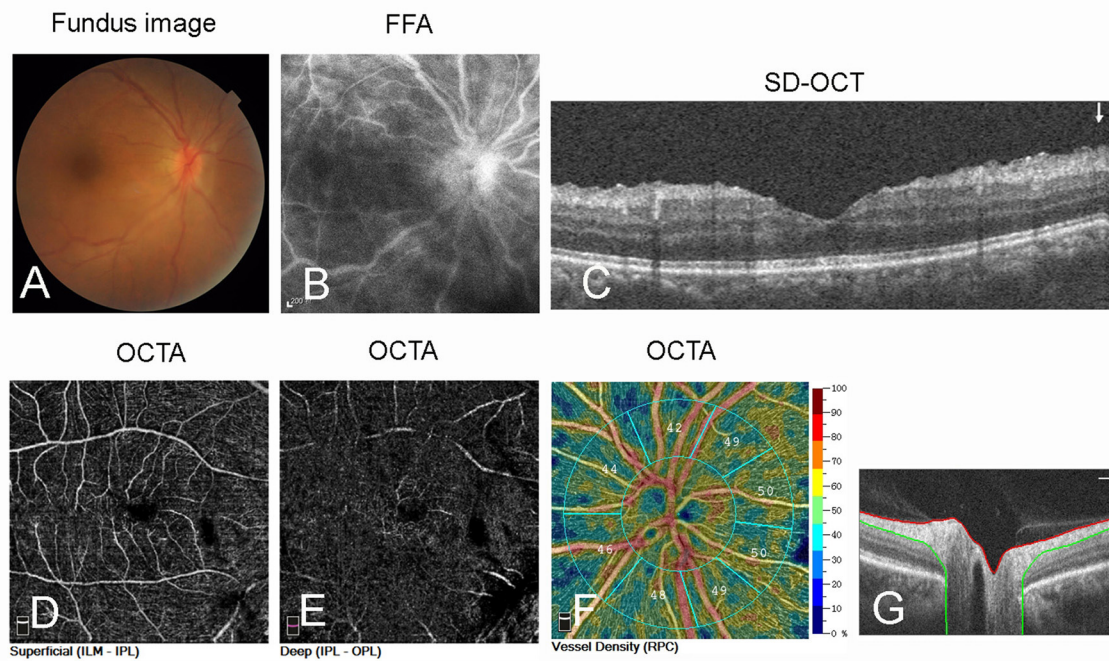
### Subgroup Analysis of Patients With Uveitis

Uveitis eyes were next divided into an acute group and chronic group. Table 4 shows that, compared with NC eyes, both the

acute and the chronic groups had significantly increased RNFL, CMT, retinal thickness (1–3)  $\mu\text{m}$ , retinal thickness (3–6)  $\mu\text{m}$ , and retinal thickness (0–6)  $\mu\text{m}$ . FD-300 Area Density ( $p < 0.001$  and  $p < 0.001$ , respectively) and FD-300 Length Density ( $p < 0.001$  and  $p = 0.017$ , respectively) were decreased in the acute group and the chronic group. Whole SCP VD ( $p < 0.001$  and  $p = 0.047$ , respectively), parafovea SCP VD (both  $p < 0.001$ ), DCP VD ( $p = 0.017$  and  $p = 0.042$ , respectively), and parafovea DCP VD ( $p = 0.030$  and  $p = 0.020$ ) were statistically significantly decreased



## (1) Uveitis



## (2) NC

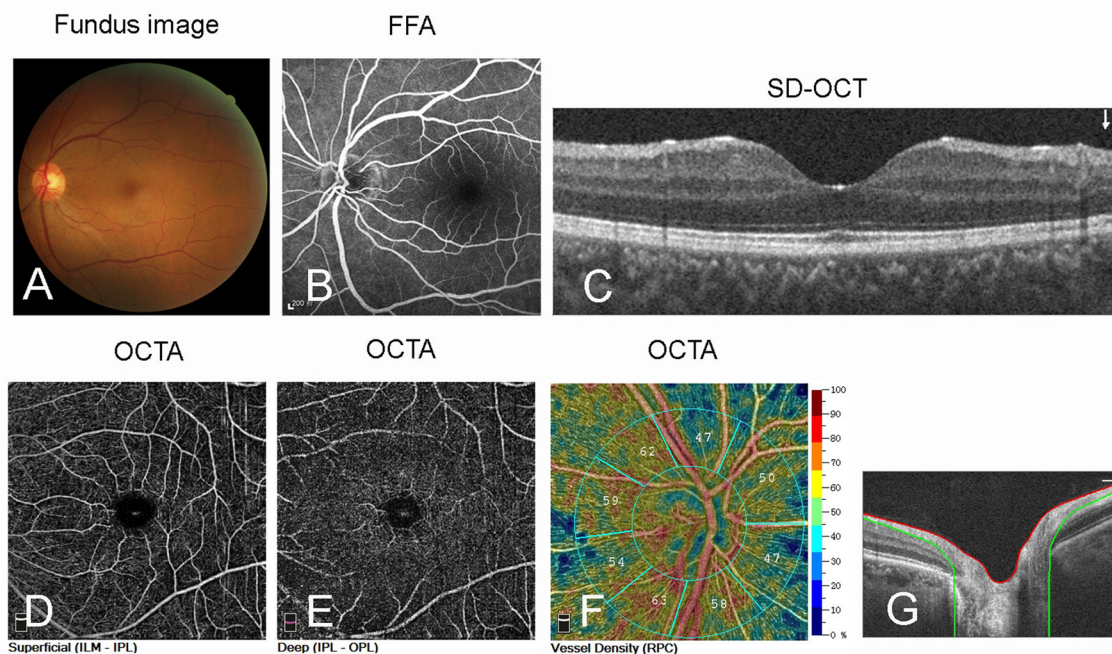


**FIGURE 2 |** (1) Fundus images of a patient with autoimmune posterior uveitis using different techniques. **(A)** Fundus photography shows optic disk hyperemia and edema, and the absence of foveal reflex. **(B)** Fundus fluorescein angiography (FFA) shows optic disk staining, capillary dilation, and leakage. **(C)** Optical coherent tomography (OCT) shows the thickening of retinal neuroepithelial layer in the macular area. **(D–F)** Optical coherence tomography angiography (OCTA) scan shows decrease of VDs in the superficial capillary plexus (SCP) and deep capillary plexus (DCP) of retina and optic disk. **(G)** The OCTA optic disc scan shows thickening optic disc. (2) Fundus images of a normal control (NC) eye.

**TABLE 2 |** The RNFL, CMT, retinal thickness, FAZ, FD-300, and VDs in the optic disk, SCP, DCP, outer retina, and choriocapillaris in uveitis eyes and normal eyes.

	Uveitis eye	Normal eye	p-value
RNFL ( $\mu\text{m}$ )	120.80 $\pm$ 24.07	101.20 $\pm$ 10.01	<0.001
CMT ( $\mu\text{m}$ )	264.60 $\pm$ 56.16	240.90 $\pm$ 20.58	<0.001
Retinal thickness (1–3) $\mu\text{m}$	338.30 $\pm$ 25.32	323.0 $\pm$ 10.31	0.001
Retinal thickness (3–6) $\mu\text{m}$	308.00 $\pm$ 27.28	281.70 $\pm$ 11.52	<0.001
Retinal thickness (0–6) $\mu\text{m}$	313.70 $\pm$ 28.27	290.10 $\pm$ 10.38	<0.001
FAZ ( $\text{mm}^2$ )	0.31 $\pm$ 0.09	0.33 $\pm$ 0.13	0.248
FD-300 area density	47.62 $\pm$ 7.50	54.02 $\pm$ 5.61	<0.001
FD-300 length density	9.92 $\pm$ 2.71	11.55 $\pm$ 2.25	<0.001
Optic disk VD	53.08 $\pm$ 5.49	56.28 $\pm$ 2.51	<0.001
Whole VD SCP (%)	46.11 $\pm$ 4.98	49.01 $\pm$ 3.83	<0.001
Parafovea VD SCP (%)	46.82 $\pm$ 5.29	50.79 $\pm$ 5.29	<0.001
Whole VD DCP (%)	45.63 $\pm$ 5.25	48.36 $\pm$ 6.53	0.009
Parafovea VD DCP (%)	51.76 $\pm$ 5.71	54.19 $\pm$ 4.65	0.009
VD outer retina (%)	14.72 $\pm$ 3.75	14.59 $\pm$ 3.15	0.826
VD Choriocapillaris (%)	23.69 $\pm$ 1.59	24.22 $\pm$ 1.16	0.031

The data were presented as mean  $\pm$  SD. SD, standard deviation; CMT, central macular thickness; FAZ, foveal avascular zone; VD, vascular density; FD300, Foveal density 300  $\mu\text{m}$ ; SCP, superficial capillary plexus; DCP, deep capillary plexus.

between the acute group vs. the NC group or the chronic group vs. the NC group.

However, only the acute group had decreased VDs of the outer retina ( $p = 0.037$ ) and choriocapillaris ( $p < 0.001$ ) compared with the NC group. In contrast, no significant differences were observed in the FAZ area in the acute group and the chronic group when compared with NC ( $p > 0.05$ ).

As compared to the chronic group, the acute group had a significantly decreased VDs of whole and parafovea SCP (both  $p = 0.006$ ), outer retina ( $p = 0.002$ ), and choriocapillaris ( $p = 0.046$ ).

## DISCUSSION

Uveitis is a general term for inflammation of iris, ciliary body, choroid, and retina tissue. This disease is a common ophthalmic disease that can cause some serious complications and sequelae, and it is one of the main causes of blindness worldwide (17–19). Based on the effect of intraocular inflammation on the pathological changes of blood vessels, fundus angiography tools, including fundus fluorescein angiography and indocyanine green angiography (ICGA), are important in evaluating uveitis. However, angiography is invasive, with certain safety risks, and some patients are allergic to the contrast media. In addition, it cannot be used for quantitative assessment. Seeking for a new, objective, and quantitative method to estimate retinal and choroidal microvascular changes is necessary for medical development.

OCTA is able to evaluate inflammatory eye diseases as vascular changes in the iris, choroid, and retina play an important role in the pathophysiology of ocular inflammation (20). OCTA has been used for the visualization and characterization of perifoveal

**TABLE 3 |** Correlation between BCVA and quantitative analysis in OCTA.

		r	p-value
Uveitis eye	RNFL ( $\mu\text{m}$ )	0.009	0.944
	CMT ( $\mu\text{m}$ )	−0.015	0.903
	Retinal thickness (0–6) $\mu\text{m}$	0.186	0.139
	FAZ ( $\text{mm}^2$ )	0.033	0.797
	FD-300 area density (%)	−0.099	0.431
	FD-300 length density (%)	−0.012	0.921
	Optic disk VD (%)	−0.068	0.585
	Whole VD SCP (%)	−0.375	<0.001
	Parafovea VD SCP (%)	−0.306	<0.001
	Whole VD DCP (%)	−0.437	<0.001
	Parafovea VD DCP (%)	−0.34	0.005
	VD outer retina (%)	0.472	<0.001
	VD choriocapillaris (%)	−0.079	0.527
Normal eye	RNFL ( $\mu\text{m}$ )	−0.119	0.341
	CMT ( $\mu\text{m}$ )	−0.088	0.482
	Retinal thickness (0–6) $\mu\text{m}$	−0.079	0.531
	FAZ ( $\text{mm}^2$ )	0.025	0.844
	FD-300 area density (%)	−0.001	0.996
	FD-300 length density (%)	−0.041	0.748
	Optic disk VD (%)	−0.045	0.718
	Whole VD SCP (%)	−0.123	0.331
	Parafovea VD SCP (%)	−0.099	0.432
	Whole VD DCP (%)	−0.201	0.109
	Parafovea VD DCP (%)	−0.201	0.095
	VD outer retina (%)	0.014	0.913
	VD Choriocapillaris (%)	0.071	0.572

BCVA, best-corrected visual acuity; OCTA, optical coherence tomography angiography; CMT, central macular thickness; FAZ, foveal avascular zone; FD300, Foveal density 300  $\mu\text{m}$ ; VD, vascular density; SCP, superficial capillary plexus; DCP, deep capillary plexus.

microvascular changes in several kinds of uveitis. Recently, it has also provided quantitative analysis for retinal vascular flow abnormalities, which help demonstrate microvascular changes accompanied with uveitis (1, 21, 22). OCTA analysis has the advantage of: (1) detecting early microvascular changes, which might be beneficial for early diagnosis; (2) quantitatively evaluate the disease status before and after treatment. Similar to Spectral domain optical coherence tomography, OCTA can also measure retinal thickness in different layers, such as RNFL, CMT, and retinal thickness (0–6)  $\mu\text{m}$ . Although several previous studies using OCTA have identified vascular flow abnormalities in patients with uveitis, the vascular beds below the RPE complex have not been thoroughly investigated, and quantitative analysis of optic disk, outer retina, and choriocapillaris vascular abnormalities in posterior uveitis is limited. In addition, fewer studies explore the correlation between BCVA and vascular flow in patients with uveitis. In the present study, we aimed to measure vascular flow in different layers, including optic disk, whole SCP, parafovea SCP, whole DCP, parafovea DCP, outer retina, and choriocapillaris.

Our research revealed that patients with posterior uveitis had a significant reduction of VDs in the whole and parafovea SCP

**TABLE 4 |** The comparisons of RNFL, CMT, retinal thickness, FAZ, FD-300, and VDs in the optic disk, SCP, DCP, outer retina, and choriocapillaris among acute and chronic uveitis eyes and normal eyes.

	Acute uveitis	Chronic uveitis	Normal	p-value	p: Acute-Chronic	p: Acute-Normal	p: Chronic-Normal
RNFL ( $\mu\text{m}$ )	123.70 $\pm$ 21.86	117.10 $\pm$ 25.69	102.02 $\pm$ 10.01	<0.001	0.273	<0.001	<0.001
CMT ( $\mu\text{m}$ )	281.90 $\pm$ 64.94	254.10 $\pm$ 37.08	240.90 $\pm$ 20.58	<0.001	0.039	0.026	<0.001
Retinal thickness (1–3) $\mu\text{m}$	338.40 $\pm$ 34.04	338.20 $\pm$ 37.14	323.00 $\pm$ 10.31	0.004	0.062	0.002	0.001
Retinal thickness (3–6) $\mu\text{m}$	310.80 $\pm$ 32.62	306.50 $\pm$ 22.03	281.70 $\pm$ 11.52	<0.001	0.537	<0.001	<0.001
Retinal thickness (0–6) $\mu\text{m}$	322.60 $\pm$ 29.61	304.50 $\pm$ 23.94	290.10 $\pm$ 10.38	<0.001	0.009	<0.001	<0.001
FAZ ( $\text{mm}^2$ )	0.27 $\pm$ 0.07	0.33 $\pm$ 0.09	0.33 $\pm$ 0.13	0.060	0.823	0.070	0.150
FD-300 area density	47.25 $\pm$ 5.80	47.14 $\pm$ 8.62	54.02 $\pm$ 5.61	<0.001	0.953	<0.001	<0.001
FD-300 Length Density	9.58 $\pm$ 2.44	10.24 $\pm$ 2.95	11.55 $\pm$ 2.26	<0.001	0.332	<0.001	0.017
Optic disk VD	53.00 $\pm$ 5.82	53.16 $\pm$ 5.24	56.28 $\pm$ 2.52	0.001	0.908	0.001	0.001
Whole VD SCP (%)	44.15 $\pm$ 5.45	47.43 $\pm$ 3.82	49.01 $\pm$ 3.83	<0.001	0.006	<0.001	0.047
Parafovea VD SCP (%)	46.51 $\pm$ 6.06	47.13 $\pm$ 4.49	50.79 $\pm$ 5.29	<0.001	0.006	<0.001	0.001
Whole VD DCP (%)	45.21 $\pm$ 4.69	46.04 $\pm$ 5.77	48.36 $\pm$ 6.53	0.031	0.529	0.017	0.042
Parafovea VD DCP (%)	52.05 $\pm$ 4.15	51.42 $\pm$ 6.91	54.19 $\pm$ 4.65	0.026	0.655	0.030	0.020
VD outer retina (%)	16.10 $\pm$ 3.62	13.39 $\pm$ 3.41	14.59 $\pm$ 3.15	0.005	0.002	0.037	0.086
VD Choriocapillaris (%)	23.31 $\pm$ 1.39	24.10 $\pm$ 1.72	24.22 $\pm$ 1.16	0.009	0.046	<0.001	0.675

The data were presented as mean  $\pm$  SD. SD, standard deviation; CMT, central macular thickness; FAZ, foveal avascular zone; VD, vascular density; FD300, Foveal density 300  $\mu\text{m}$ ; SCP, superficial capillary plexus; DCP, deep capillary plexus.

and the whole and parafovea DCP compared to healthy controls ( $p < 0.05$ ). Consistent with previous findings, the patients with Behçet's disease and VKH, both VDs, were reported to present decreased SCP and DCP compared to healthy controls (1, 15). A reduction of VDs in the SCP and DCP detected by OCTA in birdshot chorioretinopathy has also been reported (23). It was also found in children with anterior uveitis that the VDs in the SCP and DCP were significantly reduced when compared with NCs, suggesting anterior segment inflammation in pediatric uveitis is associated with reduced retinal vascular density (22). In this study, we not only analyzed the blood flow density of SCP and DCP in a more detailed way but also added some new parameters, such as VDs of the optic disk, outer retina, and choriocapillaris, as well as FD300. FD300 is the foveal blood flow density within a width of 300  $\mu\text{m}$  around the FAZ area. We found that VDs in the optic disk, FD300, and choriocapillaris had significantly decreased when compared with NC, while VD in the outer retina had no significant change. We found whole SCP VD, parafovea SCP VD, DCP VD, and parafovea DCP VD were statistically significantly decreased between the acute group vs. the NC group or the chronic group vs. the NC group. In addition, VDs of the optic disk, FD300, were significantly decreased both in the acute group and the chronic group when compared with the NC group, respectively. However, only the acute group had decreased VDs of the outer retina ( $p = 0.037$ ) and choriocapillaris ( $p < 0.001$ ) compared with the NC group. It is possible because the patients in the acute phase had more severe inflammation than in the chronic phase (1). All this evidence indicates that blood flow impairment might be a result of inflammation.

We should carefully interpret the above findings. Intraocular inflammation, regardless of localization, can induce macular edema. This is thought to be the result of a breakdown of the

inner and outer blood–retinal barrier and due to inflammatory structural changes, leading to disturbed ocular blood flow (24). Since retinal edema could produce masking artifacts that lead to artificially reduced flow signals from the retina, it is not possible to attribute causality of these vascular changes to either macular edema or uveitis alone solely based on this cross-sectional study, since a longitudinal analysis following patients before, during, and after the development of retinal edema was not performed using OCTA in our study. Future studies should take macular edema into account for the analysis.

The FAZ is largely responsible for visual acuity and central vision. Its size reflects the health of retinal microcirculation (25). Therefore, the measurement of FAZ plays an important role in the diagnosis and management of retinal vascular diseases (6, 26). Interestingly, in our study, the patients with uveitis showed no significant difference from NC in the mean area of FAZ ( $p = 0.248$ ). Waizel et al. reported that eyes suffering from non-infectious posterior uveitis presented significantly larger deep FAZ when compared to healthy controls (26). On the contrary, in multiple evanescent white dot syndrome (MEWDS) eyes and birdshot chorioretinopathy, significantly enlarged FAZ was found (7, 12). It has also been reported that the FAZ area was not different between patients with Behçet's and the control group (15). Therefore, the clinical application of FAZ to indicate pathological changes is controversial. In addition, the area of FAZ in healthy people is highly variable due to individual differences, partly because of the impact of the ocular axis and other factors (27–29). Instead, we found that FD300 decreased significantly. One explanation for this finding is that FD300 is more accurate in reflecting the ischemic degree of fovea, that is, a more sensitive marker than FAZ. FD300 may be a more valuable marker than the FAZ area for detecting pathology in patients with autoimmune posterior uveitis.



Uveitis sometimes causes irreversible vision loss; we analyzed the relationship between LogMAR BCVA and all the quantitative results from OCTA. We found that logMAR BCVA was negatively correlated with VDs in the whole and parafovea SCP, whole and parafovea DCP, and outer retina, while there were no correlations between logMAR BCVA and RNFL, CMT, retinal thickness, FAZ, FD30, and VD in the optic disk, choriocapillaris in patients with uveitis. In addition, whole DCP was the best predictive factor for BCVA in the patients with uveitis. One possible explanation is that DCP is closer to the choroid. The location of the watershed makes it more susceptible to inflammation (7). Similar findings were also found in VKH, in which DCP VD was significantly correlated with visual acuity (1). OCTA is a promising indicator for uveitis prognosis and treatment guidance.

On the other hand, structural measurements of all retinal layers could be provided by OCTA. In the present study, RNFL, CMT, and retinal thickness were found to be significantly thicker in patients with uveitis than in healthy controls. A thicker RNFL in patients with uveitis had been reported. Similar to our study, Yilmaz et al. found RNFL was significantly thicker in patients with uveitis; patients with acute uveitis had a thicker RNFL than the NCs and the patients with quiescent uveitis (30). The difference in CMT and retinal thickness was found to be statistically significant in patients with uveitis and healthy controls. Ataş et al. found out that macular thickness was thinner in patients with Behçet's disease than in the healthy control group (31). However, previous studies were assessed by optical coherence tomography but not by OCTA.

Our study had some limitations: for example, the overall sample size was modest. Even so, statistically significant differences were found between uveitis and NC. In addition, there is no more detailed subgroup analysis according to the etiology of uveitis. Considering all of the above, we believe that further studies should be carried out to evaluate the microvasculature by OCTA in a variety of autoimmune posterior uveitis with different etiology, such as Behçet's disease, and VKH.

In conclusion, this was a clinical OCTA-based investigation of the microvascular changes associated with autoimmune posterior uveitis and posterior uveitis. Our results demonstrated a novel finding that VDs of optic disk, retinal, and choroidal decreased, and that perifoveal microvascular network changed in patients with uveitis. Quantitative measurement by OCTA demonstrates good ability for detecting pathological changes and is a potential tool to assist the diagnosis and inflammation evaluation in patients with autoimmune posterior uveitis.

## DATA AVAILABILITY STATEMENT

The raw data supporting the conclusions of this article will be made available by the authors, without undue reservation.

## ETHICS STATEMENT

The study was approved by the Ethics Committee of the Second Affiliated Hospital, School of Medicine, Zhejiang University. The patients/participants provided their written informed consent to participate in this study. Written informed consent was obtained from the individual(s) for the publication of any potentially identifiable images or data included in this article.

## AUTHOR CONTRIBUTIONS

JS: conception, design, image interpretation, and manuscript preparation. JK and SC: manuscript preparation and data collection. XL, YT, HW, LW, and MW: patient treatment and data collection. ZS and LF: conception and design. All authors have read and approved the final manuscript.

## FUNDING

This study was supported in part by the National Natural Science Foundation of China (Nos. 81870648, 82070949, and 82000886) and Natural Science Foundation of Zhejiang Province (No. LQ20H120011).

## REFERENCES

- Liang A, Zhao C, Jia S, Gao F, Han X, Pei M, et al. Retinal microcirculation defects on OCTA correlate with active inflammation and vision in Vogt-Koyanagi-Harada disease. *Ocul Immunol Inflamm.* (2020) 1–7. doi: 10.1080/09273948.2020.1751212
- Li Z, Xu Z, Liu Q, Chen X, Li L. Comparisons of retinal vessel density and glaucomatous parameters in optical coherence tomography angiography. *PLoS ONE.* (2020) 15:e0234816. doi: 10.1371/journal.pone.0234816
- Sulzbacher F, Schütze C, Burgmüller M, Vécsei-Marlovits P, Weingessel B. Clinical evaluation of neovascular and non-neovascular chronic central serous chorioretinopathy (CSC) diagnosed by swept source optical coherence tomography angiography (SS OCTA). *Graefes Arch Clin Exp Ophthalmol.* (2019) 257:1581–90. doi: 10.1007/s00417-019-04297-z
- Colantuono D, Souied E, Borrelli E, Capuano V, Amoroso F, Sacconi R, et al. Quantitative deep vascular complex analysis of different AMD stages on optical coherence tomography angiography. *Eur J Ophthalmol.* (2020) 31:2474–80. doi: 10.1177/1120672120968758
- Luo M, Zhao X, Zhao N, Yuan M, Yang J, Dai R, et al. Comparison of choriocapillary flow density between fellow eyes of polypoidal choroidal vasculopathy and neovascular age-related macular degeneration. *BMC Ophthalmol.* (2020) 20:162. doi: 10.1186/s12886-020-01386-0
- Barraso M, Alé-Chilet A, Hernández T, Oliva C, Vinagre I, Ortega E, et al. Optical coherence tomography angiography in type 1 diabetes mellitus. report 1: diabetic retinopathy. *Transl Vis Sci Technol.* (2020) 9:34. doi: 10.1167/tvst.9.10.34
- Pichi F, Sarraf D, Arepalli S, Lowder C, Cunningham E, Neri P, et al. The application of optical coherence tomography angiography in uveitis and inflammatory eye diseases. *Prog Retin Eye Res.* (2017) 59:178–201. doi: 10.1016/j.preteyeres.2017.04.005
- Cerquaglia A, Lupidi M, Fiore T, Iaccheri B, Perri PC, Agini C. Deep inside multifocal choroiditis: an optical coherence tomography angiography approach. *Int Ophthalmol.* (2017) 37:1047–51. doi: 10.1007/s10792-016-0300-x
- Zahid S, Chen K, Jung J, Balaratnasingam C, Ghadiali Q, Sorenson J, et al. Optical coherence tomography angiography of Chorioretinal



- lesions due to idiopathic multifocal choroiditis. *Retina*. (2017) 37:1451–63. doi: 10.1097/IAE.0000000000001381
10. Levison A, Baynes K, Lowder C, Kaiser PSrivastava S. Choroidal neovascularisation on optical coherence tomography angiography in punctate inner choroidopathy and multifocal choroiditis. *Br J Ophthalmol*. (2017) 101:616–22. doi: 10.1136/bjophthalmol-2016-308806
  11. Thanos A, Faia L, Yonekawa Y, Randhawa S. Optical coherence tomographic angiography in acute macular neuroretinopathy. *JAMA Ophthalmol*. (2016) 134:1310–4. doi: 10.1001/jamaophthalmol.2016.3513
  12. Pichi F, Srivastava S, Chexal S, Lembo A, Lima L, Neri P, et al. En face optical coherence tomography and optical coherence tomography angiography of multiple evanescent white dot syndrome: new insights into pathogenesis. *Retina*. (2016) 36 Suppl 1:S178–88. doi: 10.1097/IAE.0000000000001255
  13. Klufas M, Phasukkijwatana N, Iafe N, Prasad P, Agarwal A, Gupta V, et al. Optical coherence tomography angiography reveals choriocapillaris flow reduction in placoid chorioretinitis. *Ophthalmol Retina*. (2017) 1:77–91. doi: 10.1016/j.oret.2016.08.008
  14. Mandadi S, Agarwal A, Aggarwal K, Moharana B, Singh R, Sharma A, et al. Novel findings on optical coherence tomography angiography in patients with tubercular serpiginous-like choroiditis. *Retina*. (2017) 37:1647–59. doi: 10.1097/IAE.0000000000001412
  15. Koca S, Onan D, Kalayci D, Alli N. Comparison of optical coherence tomography angiography findings in patients with Behçet's disease and healthy controls. *Ocul Immunol Inflamm*. (2020) 28:806–13. doi: 10.1080/09273948.2019.1635167
  16. Wang Y, Hu Z, Zhu T, Su Z, Fang X, Lin J, et al. Optical coherence tomography angiography-based quantitative assessment of morphologic changes in active myopic choroidal neovascularization during anti-vascular endothelial growth factor therapy. *Front Med*. (2021) 8:657772. doi: 10.3389/fmed.2021.657772
  17. Tsirouki T, Dastiridou A, Symeonidis C, Tounakaki O, Brazitikou I, Kalogeropoulos C, et al. A focus on the epidemiology of uveitis. *Ocul Immunol Inflamm*. (2018) 26:2–16. doi: 10.1080/09273948.2016.1196713
  18. Scoles D, Bracha P, Aleman TS, Bhatt N, Cunningham ET. Diagnostic and therapeutic challenges. *Retina*. (2021) 41:1999–2003. doi: 10.1097/IAE.0000000000003042
  19. Lu M, Wang X, Lei L, Deng Y, Yang T, Dai Y, et al. Quantitative analysis of anterior chamber inflammation using the novel CASIA2 optical coherence tomography. *Am J Ophthalmol*. (2020) 216:59–68. doi: 10.1016/j.ajo.2020.03.032
  20. Pichi F, Sarraf D, Morara M, Mazumdar S, Neri PGupta V. Pearls and pitfalls of optical coherence tomography angiography in the multimodal evaluation of uveitis. *J Ophthalmic Inflamm Infect*. (2017) 7:20. doi: 10.1186/s12348-017-0138-z
  21. Lommatzsch C, Bauermann P, Heimes-Bussmann B, Nolte CHeinz C. Optical coherence tomography angiography in uveitic glaucoma—a pilot study. *Ocul Immunol Inflamm*. (2020) 1–7. doi: 10.1080/09273948.2020.1745246
  22. Qu Y, Zhao C, Pei M, Liang A, Gao F, Zhang M. Anterior segment inflammation in pediatric uveitis is associated with reduced retinal vascular density as quantified by optical coherence tomography angiography. *Ocul Immunol Inflamm*. (2020) 1–5. doi: 10.1080/09273948.2020.1803923
  23. Roberts P, Nesper P, Goldstein D, Fawzi A. Retinal capillary density in patients with birdshot chorioretinopathy. *Retina*. (2018) 38:387–94. doi: 10.1097/IAE.0000000000001543
  24. Karampelas M, Sim DA, Chu C, Carreno E, Keane PA, Zarranz-Ventura J, et al. Quantitative analysis of peripheral vasculitis, ischemia, and vascular leakage in uveitis using ultra-widefield fluorescein angiography. *Am J Ophthalmol*. (2015) 159:1161–8.e1. doi: 10.1016/j.ajo.2015.02.009
  25. Drinkwater J, Chen F, Brooks A, Davis B, Turner A, Davis T, et al. Carotid disease and retinal optical coherence tomography angiography parameters in type 2 diabetes: the fremantle diabetes study phase II. *Diabetes Care*. (2020) 43:3034–41. doi: 10.2337/dc20-0370
  26. Waizel M, Todorova M, Terrada C, LeHoang P, Massamba N, Bodaghi B. Superficial and deep retinal foveal avascular zone OCTA findings of non-infectious anterior and posterior uveitis. *Graefes Arch Clin Exp Ophthalmol*. (2018) 256:1977–84. doi: 10.1007/s00417-018-4057-y
  27. Mammo Z, Balaratnasingam C, Yu P, Xu J, Heisler M, Mackenzie P, et al. Quantitative non-invasive angiography of the fovea centralis using speckle variance optical coherence tomography. *Invest Ophthalmol Vis Sci*. (2015) 56:5074–86. doi: 10.1167/iovs.15-16773
  28. Tan C, Lim L, Chow V, Chay I, Tan S, Cheong K, et al. Optical coherence tomography angiography evaluation of the parafoveal vasculature and its relationship with ocular factors. *Invest Ophthalmol Vis Sci*. (2016) 57: OCT224–34. doi: 10.1167/iovs.15-18869
  29. Popovic Z, Knutsson P, Thaug J, Owner-Petersen M, Sjöstrand J. Noninvasive imaging of human foveal capillary network using dual-conjugate adaptive optics. *Invest Ophthalmol Vis Sci*. (2011) 52:2649–55. doi: 10.1167/iovs.10-6054
  30. Yilmaz H, Koşlu M, Çakır B, Küçükcilioglu M, Durukan A, Bayer A, et al. Uveitis as a confounding factor in retinal nerve fiber layer analysis using optical coherence tomography. *Ocul Immunol Inflamm*. (2020) 1–6. doi: 10.1080/09273948.2020.1811353
  31. Ataş M, Yuvaci I, Demircan S, Güler E, Altunel O, Pangal E, et al. Evaluation of the macular, peripapillary nerve fiber layer and choroid thickness changes in Behçet's disease with spectral-domain OCT. *J Ophthalmol*. (2014) 2014:865394. doi: 10.1155/2014/865394

**Conflict of Interest:** The authors declare that the research was conducted in the absence of any commercial or financial relationships that could be construed as a potential conflict of interest.

**Publisher's Note:** All claims expressed in this article are solely those of the authors and do not necessarily represent those of their affiliated organizations, or those of the publisher, the editors and the reviewers. Any product that may be evaluated in this article, or claim that may be made by its manufacturer, is not guaranteed or endorsed by the publisher.

Copyright © 2022 Shen, Kong, Chen, Liu, Teng, Wu, Wang, Wu, Su and Feng. This is an open-access article distributed under the terms of the Creative Commons Attribution License (CC BY). The use, distribution or reproduction in other forums is permitted, provided the original author(s) and the copyright owner(s) are credited and that the original publication in this journal is cited, in accordance with accepted academic practice. No use, distribution or reproduction is permitted which does not comply with these terms.



# Adalimumab in Vogt-Koyanagi-Harada Disease Refractory to Conventional Therapy

Shizhao Yang<sup>1†</sup>, Tianyu Tao<sup>1†</sup>, Zhaohao Huang<sup>1</sup>, Xiuxing Liu<sup>1</sup>, He Li<sup>1</sup>, Lihui Xie<sup>1</sup>, Feng Wen<sup>1,2</sup>, Wei Chi<sup>1,2</sup> and Wenru Su<sup>1,2\*</sup>

<sup>1</sup> State Key Laboratory of Ophthalmology, Zhongshan Ophthalmic Center, Sun Yat-sen University, Guangzhou, China,

<sup>2</sup> Guangdong Provincial Clinical Research Center for Ocular Diseases, Guangzhou, China

## OPEN ACCESS

### Edited by:

Hetian Lei,  
Shenzhen Eye Hospital, China

### Reviewed by:

ShiYing Li,  
Xiamen University, China  
Meixia Zhang,  
Sichuan University, China

### \*Correspondence:

Wenru Su  
suwr3@mail.sysu.edu.cn

<sup>†</sup>These authors have contributed  
equally to this work

### Specialty section:

This article was submitted to  
Ophthalmology,  
a section of the journal  
Frontiers in Medicine

Received: 21 October 2021

Accepted: 20 December 2021

Published: 12 January 2022

### Citation:

Yang S, Tao T, Huang Z, Liu X, Li H,  
Xie L, Wen F, Chi W and Su W (2022)  
Adalimumab in Vogt-Koyanagi-Harada  
Disease Refractory to Conventional  
Therapy. *Front. Med.* 8:799427.  
doi: 10.3389/fmed.2021.799427

**Background:** No study explores the effectiveness of adalimumab in sight-threatening Vogt-Koyanagi-Harada (VKH) patients in China.

**Objective:** To evaluate the short-term effectiveness and safety of adalimumab (ADA) in patients with sight-threatening Vogt-Koyanagi-Harada (VKH) disease refractory to conventional therapy.

**Methods:** Medical records of VKH patients who had been treated with systemic glucocorticoids and immunosuppressants but whose condition was poorly controlled were collected and analyzed. Primary outcomes comprised of best-corrected visual acuity (BCVA), intraocular inflammation, relapses, and glucocorticoid-sparing effects. Other outcomes included central macular thickness (CMT), intraocular manifestations and adverse events (AEs).

**Results:** Nine refractory VKH patients with a median age of 30 (16, 43) years old were enrolled in this study and received treatment for a median of 10 (7, 11) months. Mean BCVA improved from LogMar 0.63 ± 0.50 (20/72 or 0.36 ± 0.26 in Snellen chart) at baseline to LogMar 0.50 ± 0.37 (20/82 or 0.41 ± 0.28 in Snellen chart) at final visit ( $P = 0.090$ ). The anterior chamber cell grade decreased from 2 (1.75, 3)+ at baseline to 0.5 (0, 1.25)+ cell at final visit ( $P < 0.001$ ). The vitritis grade decreased from 1 (1, 1) + cell at baseline to 0 (0, 1)+ cell at final visit ( $P < 0.001$ ). Patients suffered a median of 1 (0, 2) relapse during treatment. CMT remained stable from 238.50 ± 144.94 μm at baseline to 219.28 ± 77.20 μm at final visit ( $P = 0.553$ ). The mean prednisone dosage decreased from 21.91 ± 18.39 mg/d to 2.73 ± 4.10 mg/d ( $P = 0.005$ ). No severe AEs were found during treatment.

**Conclusions:** The outcomes indicated that ADA was an effective and safe option for VKH patients refractory to conventional therapy by controlling inflammation, preserving visual function and reducing the daily glucocorticoid dose.

**Keywords:** adalimumab, TNF- $\alpha$  inhibitor, Vogt-Koyanagi-Harada (VKH), refractory, treatment

## INTRODUCTION

Vogt-Koyanagi-Harada (VKH) disease is an autoimmune disorder characterized by severe bilateral granulomatous panuveitis, frequently in association with various systemic manifestations including pleocytosis in the cerebrospinal fluid, tinnitus, alopecia, poliosis, and vitiligo (1–4). Although the prevalence of the disease varies among races worldwide, it has been reported that pigmented races, for instance Asians, Latin Americans, and Middle Easterners, are the primary targets.

Both ocular inflammation and complications, including complicated cataract, secondary glaucoma, choroidal neovascularization and subretinal fibrosis, can result in severe vision loss in VKH patients. The present mainstay principle of treatment in VKH relies largely on early control of intraocular inflammation with systemic high-dose glucocorticoids and immunosuppressive agents. However, the prognosis of VKH remains pessimistic, and prolonged high-dose glucocorticoid administration produces a well-known series of steroid-related side effects.

Although the pathology of VKH remains uncertain, studies have revealed that tumor necrosis factor- $\alpha$  (TNF- $\alpha$ ) plays a significant role in non-infectious uveitis, including VKH, by inducing the expression of chemokines, adhesion molecules and cytokines associated with ocular inflammation (5–8). Therefore, counteracting TNF- $\alpha$  with TNF- $\alpha$  inhibitors is a reliable strategy in the treatment of non-infectious uveitis.

A fully humanized TNF- $\alpha$  inhibitor, adalimumab (ADA, Humira, AbbVie, North Chicago, Illinois), has achieved promising efficacy in several rheumatic diseases. In 2016, the US FDA granted the indication of ADA in the treatment of non-infectious uveitis. However, only a few case reports have introduced the clinical outcomes of ADA in patients with sight-threatening refractory VKH (9–14). The aim of this study was to evaluate the short-term efficacy and safety of ADA in patients with sight-threatening refractory VKH disease.

## PATIENTS AND METHODS

We initiated this study in VKH patients who had been systemically treated with glucocorticoids and immunosuppressive agents but whose condition was poorly controlled. All patients had been treated for no <3 months. The medical records of VKH patients who were refractory to conventional therapy were collected and analyzed. This study was granted by the Zhongshan Ophthalmic Center Ethics Committee and the registration number was ChiCTR2000030236. The patients or their guardians were thoroughly informed of the potential hazards, and written informed consent was obtained before initiation of treatment.

Inclusion criteria: (1) had been diagnosed of VKH disease according to the Revised Diagnostic Criteria for VKH disease and the Development and Evaluation of Diagnostic Criteria for VKH disease, and met the profiles of fluorescein angiography (FFA), Indocyanine green angiography (ICGA), and optic coherent tomography (OCT) of VKH (15–17); (2) ocular inflammation was uncontrolled, with continuous degradation of visual acuity

in the past 3 months or suffered at least two relapses, which could not be alleviated by increasing dose of systemic medical glucocorticoids and at least one immunosuppressive agent; (3) ocular inflammatory activity was present (anterior chamber cell grade or/and vitritis grade  $\geq 1+$  cells, optic nerve injury, vasculitis, retinitis or choroiditis); (4) patients had negative T-SPOT test results, or, in the event of a positive test, they had no signs of active tuberculosis and received precautionary anti-tuberculosis treatment.

Patients were excluded if: (1) presence of active systemic infections; (2) coexisting of contraindications to ADA, such as malignant diseases or tuberculosis.

## Treatment

ADA treatment was started with an induction dose of 80 mg subcutaneously, followed by 40 mg 1 week later and 40 mg every other week thereafter. Withdrawal of ADA or extension of the injection interval was based on stability of inflammation remission, patients' wishes and other situations (such as inadequate response, intolerance, side effects or treatment costs). Glucocorticoids (given orally or intravenously) and immunosuppressants, such as methotrexate (MTX), cyclosporine A (CsA) or mycophenolate mofetil (MMF), were prescribed depending on the previous medication and baseline severity of disease, and the doses of glucocorticoids and immunosuppressants were adjusted according to changes in diseases (with MTX  $\leq 15$  mg per week, CsA  $\leq 2$  mg/d, MMF  $\leq 0.5$  g/d at baseline). Children received roughly the same level with adult in dosage per weight unit. Local treatments, such as intraocular anti-vascular endothelial growth factor treatment, glucocorticoid droplets, dexamethasone implants, and anti-glaucoma treatment, were provided according to the conditions.

## Patient Monitoring

The patient evaluations comprised a comprehensive physical examination, a thorough ophthalmic examination and laboratory blood tests (including routine bloodwork, liver and renal function tests, urinalysis, blood chemistry, the T-spot test, and other infectious disease tests). The primary outcomes included best corrected visual acuity (BCVA), intraocular inflammation, relapse and glucocorticoid sparing effects. Other outcomes included retinal morphology, intraocular manifestations and adverse events. All parameters were recorded at baseline and at every visit. All surgical information was recorded, especially for procedures that could improve visual function, such as cataract extraction.

## Best Corrected Visual Acuity

BCVA was evaluated by Snellen chart and converted to LogMar format. In patients with exceptionally poor visual function of "counting fingers/hand motion/light perception," BCVA was converted to a quantified visual acuity value for statistical convenience (18).

**TABLE 1** | Demographics and concomitant treatments of 11 refractory VKH patients.

Patient no.	Age/ gender/ laterality	Category	History (months)	Treatment period (months)	ADA ongoing at final visit/ADA injections <sup>a</sup>	Systemic treatment	Concomitant IS at final visit	Local therapy
1 (ZQ)	49/M/OU	C	26	11	−/16	Pred/MTX/CsA	MTX	DEX ivr (OS)
2 (CQM)	41/F/OU	IC	4	10	−/12	Pred/MTX/CsA	Pred/MTX/CsA	
3 (CZJ)	45/M/OU	P	114	7	−/14	Pred/MTX/CsA	Pred/MTX/CsA	
4 (HJZ)	21/F/OU	C	8	10	−/16	Pred/MMF	MMF	
5 (HWZ)	43/M/OU	P	9	12	+/22	MTX	MTX/CsA	
6 (HZM)	16/F/OU	IC	50	7	+/15	Pred/MTX/CsA	CsA/MMF	
7 (TYL)	15/F/OU	C	5	9	+/16	Pred/MTX/CsA	Pred/MTX/CsA	DEX sc (OU)
8 (XHX)	6/F/OU	P	5	12	+/22	Pred/MTX/CsA	MTX/MMF	
9 (WXP)	34/F/OU	C	3	7	+/12	MMF	MMF	
8 (YLP)	30/M/OU	IC	4	10	+/21	Pred/MTX/CsA	Pred/MTX/CsA	TA (OU)
9 (ZQY)	21/F/OU	P	10	11	+/25	Pred/MTX/MMF	MTX	

Category: C, complete VKH; IC, incomplete VKH; P, probable VKH; <sup>a</sup>Whether ADA treatment was ongoing at the final visit (+, yes; −, no). ADA, adalimumab; IS, immunosuppressants; OU, oculus uterque (both eyes); OS, oculus sinister (left eye); CsA, cyclosporin A; MTX, methotrexate; MMF, mycophenolate mofetil; TA, triamcinolone acetonide periocular injection; DEX ivr, Ozurdex intravitreal implant; DEX sc, subconjunctival injection of dexamethasone.

### Intraocular Inflammation

The recommendation of the Standardization of Uveitis Nomenclature (SUN) Group in 1990 was used to assess anterior chamber inflammation, and the Nussenblatt scale was used to assess the vitritis grade (19, 20). The SUN Group grading scheme for anterior chamber inflammation is based on the number of anterior chamber cells in 1mm by 1mm slit beam field, and the anterior chamber inflammation is divided into five grades (0, 0.5+, 1+, 2+, 3+, 4+). In the Nussenblatt scale, clarity of optic disc, retinal vessels and nerve fiber layer is used to assess the vitritis into four grades (1+ to 4+).

### Relapse

A relapse was defined as the emergence or exacerbation of anterior chamber cells, vitritis, mutton-fat keratic precipitates or iris nodules.

### Central Macular Thickness

CMT was defined as the average retinal thickness within a 1-mm-diameter region in the macular fovea by Cirrus HD-OCT (Carl Zeiss, CA, USA).

### Intraocular Manifestations

These manifestations included new onset of complicated cataracts, serous retinal detachment (SRD), sunset glow fundus, Dalen-Fuchs nodules, iris nodules, mutton-fat KPs, iris neovascularization, pigmentation scatter, iris nodules (including Koeppe nodules and Busacca nodules), iris synechiae and any other associated complications.

### Glucocorticoid-Sparing Effect

The glucocorticoid-sparing effect was defined as the reduction of glucocorticoid use at the final visit.

### Adverse Events

Patients were instructed to report any AEs during the treatment so that their regimen could be evaluated and adjusted. AEs were defined as activation of infections, allergic reactions and any other immunogenicity-related events. The severity of AEs was assessed under the guidance of European Medicines Agency. <[https://www.ema.europa.eu/en/documents/other/eudravigilance-inclusion/exclusion-criteria-important-medical-events-list\\_en.pdf](https://www.ema.europa.eu/en/documents/other/eudravigilance-inclusion/exclusion-criteria-important-medical-events-list_en.pdf)>. This guidance includes the potential severe AEs which resulted in death, life-threatening situations, demanded or prolonged hospitalization, persisting or significant disability or birth defects.

### Statistical Analysis

For continuous parameters, the mean (SD) or median (interquartile range, or IQR) was used to describe the data. For categorical parameters, numbers or percentages were used. Student's *t*-test was used to compare the BCVA and CMT before and after the treatment. The Wilcoxon test was used to compare pretreatment and posttreatment intraocular inflammation. SPSS ver.25.0 software was used for statistical analysis. *P*-value <0.05 was considered as statistically significant.

## RESULTS

Between April 2020 and May 2021, four males and seven females (a total of 11 patients/22 eyes) were enrolled. The median age at presentation was 30 (16, 43), including one of the participants was a pediatric patient aged 6 years. All patients were biologics-naïve and were at the typical chronic recurrent stage of the VKH course according to the revised diagnostic criteria (RDC) for VKH (16), defined by the presence of sunset glow fundus (except in patient no. 6 and no. 7, who had complete iris synechiae and a completely opaque lens such that the fundus could not



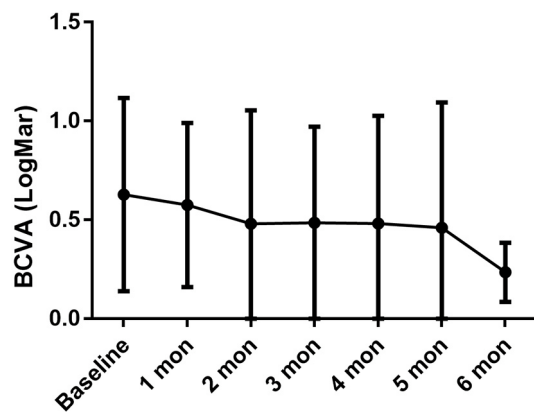


**FIGURE 1 |** BCVA persistently increased during the treatment period, with baseline LogMar BCVA  $0.63 \pm 0.49$ ,  $0.58 \pm 0.41$  in 1-month ( $P = 0.033$  compared with baseline),  $0.48 \pm 0.57$  in 2-month ( $P = 0.057$ ),  $0.49 \pm 0.49$  in 3-month ( $P = 0.029$ ),  $0.48 \pm 0.54$  in 4-month ( $P = 0.017$ ),  $0.46 \pm 0.63$  in 5-month ( $P = 0.192$ ),  $0.24 \pm 0.15$  in 6-month ( $P = 0.027$ ).

be distinguished); all of the patients had suffered relapse attacks before the ADA treatment, and most of them had iris nodules or mutton-fat keratic precipitates (KPs). Four patients had complete VKH, three patients had incomplete VKH, and four had probable VKH (Table 1). The median history of disease before ADA initiation was 8 (4, 26) months.

Patients received a median of 10 (7, 11) months of treatment. Apart from ADA, the systemic immunosuppressants that the patients were using as of the baseline visit and the final visit are listed in Table 1. For local treatments, all patients initially received Pred Forte droplets four times/day; the frequency was reduced over time, and the formula was eventually replaced with weaker glucocorticoid droplets. In addition, patient no. 1 received a dexamethasone-delivery implant (Ozurdex, Allergan, California) once in the left eye at baseline due to cystoid macular edema; patient no. 7 received a dexamethasone subconjunctival injection at baseline for severe anterior chamber inflammation; and patient no. 10 received a periocular injection of triamcinolone acetonide once at baseline due to vitritis. Three eyes of two patients (right eye in patient no. 1 and both eyes in no. 7) received cataract surgery during the treatment period, and patient no. 1 received an Ozurdex intravitreal implant in left eye at baseline.

Due to the pandemic quarantine protocol, some patients missed a few monthly visits and temporally discontinued treatment. As of the final visit, seven patients continued their original ADA regimens and the ADA injection interval was successfully extended to 3 weeks in three patients (no. 7, no. 8, and no. 9); two patients (no. 2 and no. 3) successfully withdrew ADA for stability of ocular inflammation and high cost of ADA; while two patients discontinued ADA due to onychomycosis (no. 1) and lack of response (no. 4).

After ~10 months of treatment, the mean BCVA improved from LogMar  $0.63 \pm 0.50$  (20/72 or  $0.36 \pm 0.26$  in Snellen chart) at baseline to LogMar  $0.50 \pm 0.37$  (20/82 or  $0.41 \pm 0.28$  in Snellen

chart) at final visit ( $P = 0.090$ ). The monthly changes in BCVA are presented in Figure 1. Patients had a median of 1 (0, 2) relapse during treatment. At baseline, almost all patients had an anterior chamber cell grade of at least 1 (except for patient no. 2, who had a grade of 0.5+ cells in both eyes), and the median grade was 2 (1.75, 3) + cells. After ~10 months of treatment, the anterior chamber cell grade was reduced to 0.5 (0, 1.25) + cell ( $P < 0.001$ ). The vitritis grade was reduced from 1 (1, 1) + cell at baseline to 0 (0, 1) + cell at the final visit ( $P < 0.001$ ). Macular thickness remained stable from  $238.50 \pm 144.94 \mu\text{m}$  at baseline to  $219.28 \pm 77.20 \mu\text{m}$  at the final visit ( $P = 0.553$ ). The ocular parameters are presented in Table 2. Patients no. 7 and no. 11 had temporary slightly increased intraocular pressure over 21 mmHg, which decreased to normal without medical intervention. Other ocular manifestations that occurred during the treatment and final visit are listed in Table 3.

Regarding the glucocorticoid-sparing effect, the mean prednisone dosage was reduced from  $21.91 \pm 18.39 \text{ mg/d}$  to  $2.73 \pm 4.10 \text{ mg/d}$  ( $P = 0.005$ ). The monthly variations in oral prednisone dosages are illustrated in Figure 2.

No severe AEs were reported that needed clinical intervention or warranted the discontinuation of ADA treatment. However, mild AEs were found in the following patients, which may or may not be related to ADA treatment: patient no. 1 had onychomycosis; patient no. 4 had a mild urinary infection and delayed ADA for 1 month while receiving antibiotic treatment; patient no. 5 and no. 6 reported an injection-site reaction, which was alleviated by a cold compress; and patient no. 8 had a rash on her back and developed a fever of  $37.7^\circ\text{C}$ , both of which disappeared within days; patient no. 10 had occasional fever after long-time work; patient no. 11 had insomnia and occasional premature ventricular contractions which required no medical intervention. A typical case was presented in Figure 3.

## DISCUSSION

VKH accounts for 15.9% of all panuveitis in China and is one of the most common clinical entities in uveitis (21). Previous studies have indicated that treatment of VKH depends largely on early control of intraocular inflammation, and patients treated properly might have an optimistic prognosis for visual function. Unfortunately, many VKH patients do not receive proper treatment, instead receiving delayed or inadequate therapy (suboptimal medication, premature tapering of medication or absence of immunosuppressants), and the disease inevitably progresses to the chronic recurrent stage, in which granulomatous ocular inflammation recurs and most ocular complications emerge, including complicated cataract, secondary glaucoma, choroidal neovascularization, subretinal fibrosis and others (17, 22–24). It has been indicated that ~21% of VKH patients become legally blind (25).

The conventional mainstay of treatment in VKH is combination therapy with systemic glucocorticoids and immunosuppressive agents, including cyclosporine, azathioprine and methotrexate. However, patients with chronic, recurrent, refractory VKH exhibit some resistance and intolerance to

**TABLE 2 |** Ocular parameters of 11 refractory VKH patients.

Patient no.	Eye	BCVA at baseline	BCVA at final visit	Relapse	Anterior inflammation at baseline	Anterior inflammation at final visit	Vitritis at baseline	Vitritis at final visit	CMT at baseline ( $\mu\text{m}$ )	CMT at final visit ( $\mu\text{m}$ )
1 (ZQ)	OD	0.025	0.025	1	1	2	1	0	500	500
	OS	0.25	0.4	1	2	0.5	1	0	724	170
2 (CQM)	OD	0.1	0.2	1	0.5	0	1	1	123	120
	OS	0.1	0.25	1	0.5	0.5	1	0	127	140
3 (CZJ)	OD	0.32	0.32	0	4	0.5	3	0	200	200
	OS	0.25	0.25	0	4	0.5	3	0	200	200
4 (HJZ)	OD	0.4	0.2	1	4	1	1	1	185	205
	OS	0.5	0.2	1	4	1	1	1	185	240
5 (HWZ)	OD	0.63	0.4	2	3	3	1	1	220	220
	OS	0.8	0.25	2	3	3	1	1	220	220
6 (HZM) <sup>a</sup>	OD	0.1	0.2	0	3	0	-	0	-	-
	OS	0.075	0.1	0	3	0	-	0	-	-
7 (TYL) <sup>a</sup>	OD	0.025	0.16	3	2	2	-	0	-	260
	OS	0.025	0.25	3	2	2	-	0	-	260
8 (XHX)	OD	0.5	0.63	2	2	1	2	0	220	220
	OS	0.4	0.63	2	2	1	2	1	220	220
9 (WXP)	OD	0.8	1.0	0	1	0	1	0	240	235
	OS	0.63	0.8	0	1	0	1	0	235	230
10 (YLP)	OD	0.63	0.8	2	2	0	1	0	180	205
	OS	0.63	0.8	2	2	0	1	1	180	210
11 (ZQY)	OD	0.4	0.8	1	3	0	1	0	160	178
	OS	0.4	0.8	1	3	0.5	1	0	174	234

OD, oculus dexter (right eye); OS, oculus sinister (left eye); BCVA, best corrected visual acuity; CMT, central macular thickness. <sup>a</sup>Patient no. 6 and no. 7 had complete iris synechiae and a completely opaque lens at baseline, and fundus or OCT examination could not be distinguished. After cataract surgery, fundus and OCT examination in patient no. 7 were feasible.

**TABLE 3 |** Ocular manifestations during the treatment period.

Patient no.	Baseline ocular manifestations	New ocular during the treatment	New ocular at final visit
1 (OD)	Cataract, macular CNV scar	-	IOL
1 (OS)	IOL, CME, KN	-	-
2 (OD)	Pigmentation, subretinal fibrosis, secondary CSC	KN, BN	-
2 (OS)	Pigmentation, subretinal fibrosis, secondary CSC	KN, BN	-
3 (OD)	KN, BN, IOL	-	-
3 (OS)	KN, BN, IOL	-	-
4 (OD)	KN, BN	-	IOP elevation
4 (OS)	KN, BN	-	IOP elevation
5 (OD)	KN, BN	KN, BN	KN, cataract
5 (OS)	KN, BN	KN, BN	KN, cataract
6 (OD)	Iris synechiae, cataract	IOP elevation	-
6 (OS)	Iris synechiae, cataract	IOP elevation	-
7 (OD)	Mutton-fat KPs, BN, Iris synechiae, Sugiura's sign, INV, cataract	KN, BN	IOL
7 (OS)	Mutton-fat KPs, BN, Iris synechiae, Sugiura's sign, INV, cataract	KN, BN, IOP elevation	IOL
8 (OD)	Iris synechiae, cataract	IOP elevation	-
8 (OS)	Iris synechiae, cataract	IOP elevation	-
9 (OD)	-	-	-
9 (OS)	-	-	-
10 (OD)	Cataract, KN, retinal pigmentation	KN, IOP elevation	-
10 (OS)	Cataract, KN, retinal pigmentation	KN, IOP elevation	-
11 (OD)	KN, BN,	IOP elevation	IOP elevation
11 (OS)	KN, BN	IOP elevation	-

OD, oculus dexter (right eye); OS, oculus sinister (left eye); CNV, choroidal neovascularization; IOL, intraocular lens; KN, Koeppe nodules; BN, Busacca nodules; CSC, central serous chorioretinopathy; CME, cystoid macular edema; KPs, keratic precipitates; INV, iris neovascularization; IOP, intraocular pressure.

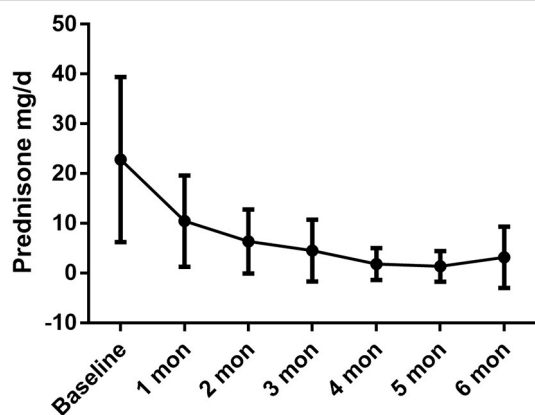


**FIGURE 2 |** The daily oral prednisone dose was dramatically reduced during the treatment period, with baseline dose of  $22.82 \pm 16.61$  mg/d,  $10.45 \pm 9.16$  mg/d in 1-month ( $P = 0.001$  compared with baseline),  $6.36 \pm 6.43$  mg/d in 2-month ( $P = 0.001$ ),  $4.55 \pm 6.20$  mg/d in 3-month ( $P = 0.001$ ),  $1.82 \pm 3.21$  mg/d in 4-month ( $P < 0.001$ ),  $1.36 \pm 3.08$  mg/d in 5-month ( $P < 0.001$ ),  $3.00 \pm 6.40$  mg/d in 6 month ( $P = 0.002$ ).

conventional therapy (26, 27). In this scenario, remedial treatments are required.

Although the exact etiology remains unknown, TNF- $\alpha$  is regarded as a critical cytokine in the development of uveitis,

including VKH. TNF- $\alpha$  inhibitors, which can bind to and deactivate TNF- $\alpha$ , indicate the pathogenesis of uveitis. ADA was the first anti-TNF- $\alpha$  antibody indicated for non-infectious uveitis by the FDA, the European Medicines Agency and the National Medical Products Administration (NMPA) of China. However, there are relatively few focused on the efficacy of ADA in VKH patients. Diaz-Liapis et al. conducted a prospective study on 131 patients with non-infectious uveitis, and ADA was well-tolerated and showed an overall good anti-inflammatory efficacy. However, in that study, very few of the patients had VKH, and the condition of these VKH patients was not described in detail (28). Kwon et al., Su et al. and Jeroudi et al. reported that ADA effectively treated refractory VKH, preserving the patients' BCVA, deactivating ocular inflammation and reducing the daily prednisone dose. However, these studies were case reports with only 1 or 2 patients, and they focused mainly on pediatric patients (9–13). Hitherto, the largest series of VKH patients treated with ADA was a retrospective case series of 14 patients reported by Couto et al. (29). Those investigators concluded that ADA was effective and safe for the treatment of VKH. However, in their study, the degree of vitritis before and after the treatment was unknown, and no ocular manifestations were mentioned. In this study, we explored the efficacy of ADA treatment in refractory VKH patients, and the results indicated that ADA seemed to be a favorable option for these patients. During the treatment period, the ocular inflammation, including anterior chamber inflammation and vitritis, was well controlled in most patients.

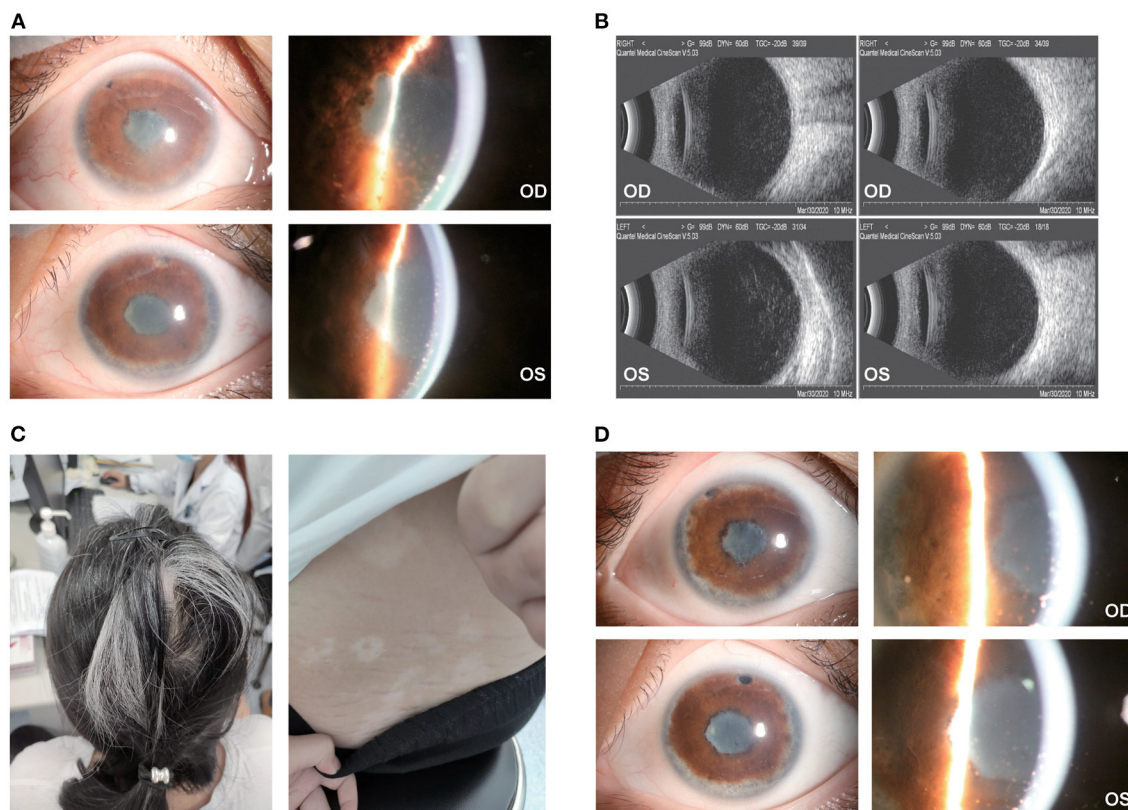


**FIGURE 3 |** Ocular and extraocular manifestation of patient no. 7. **(A)** The patient had dense and fresh mutton-fat KPs with severe anterior chamber inflammation in the right eye (top) and left eye (bottom); **(B)** dense light spots in the vitreous cavity could be found in both eyes; **(C)** the patient had severe hair loss, white hair and vitiligo along with Tinnitus and headache; **(D)** a month after ADA treatment, the KPs atrophied, and the anterior chamber inflammation relieved in both eyes.

The relapse frequency of ocular inflammation was relatively small during the treatment. And a substantial cut of the dosage of daily prednisone was achieved without severe side effect.

To our knowledge, this study is the first study on VKH patients treated with ADA in China. In this pilot case series, all patients had received systemic glucocorticoids plus immunosuppressants for over 3 months, but their condition was poorly controlled. We evaluated the short-term efficacy of ADA in refractory VKH patients. ADA seemed to effectively control inflammation and preserve visual function. More importantly, ADA was helpful in reducing the daily glucocorticoid dose without causing additional side effects. Despite local glucocorticoids were applied (including periocular injection of triamcinolone acetonide and Ozurdex intravitreal implant), the pharmacokinetics profile of TA decided that TA did not provide long-term anti-inflammation effect as their half-life periods are merely days or even few hours. However, DEX could provided a relatively long period anti-inflammation effect only for about 3 months (the implant dissolved at 3-month visit). But we only applied Ozurdex implant in the patients with severe ocular inflammation as a reinforcement, and only one patient (1 eye) received Ozurdex implant. Compared

with the overall data, we can prudently presume that local therapy had little impact on the treatment of this cohort of patients.

As for the safety profile, no patient in this cohort suffered from severe AEs, which made ADA seemed to be a safe product in management of VKH disease. The most common adverse events in these patients were mild infections (ranging from respiratory system infection, integumentary system and urinary system infection) and mild injection reaction. However, it's necessary to point out that due to the relatively small sample size, the long-term and larger-size observation is still demanded to evaluate the safety of ADA, as some researchers had indicated that ADA might be associated with more severe AEs compared with placebo, including cancers, active or latent tuberculosis, demyelinating disorder and others (30).

However, this study had some unavoidable limitations. First, since this was only a pilot study, the scale of patients was relatively small and it would be worthwhile to carry out additional research exploring long-term efficacy, long-term tolerance and safety. Second, the present study focused mainly on the efficacy of ADA in refractory VKH. ADA is generally considered a second-line treatment in VKH patients. It remains unknown



whether ADA could achieve better efficacy in treatment-naïve patients, especially compared to conventional therapy with glucocorticoids and immunosuppressants.

## CONCLUSION

The outcomes indicated that ADA was an effective and safe option for patients with VKH refractory to conventional therapy; this drug effectively controlled inflammation, preserved visual function and reduced the daily glucocorticoid dose.

## DATA AVAILABILITY STATEMENT

The raw data supporting the conclusions of this article will be made available by the authors, without undue reservation.

## ETHICS STATEMENT

The studies involving human participants were reviewed and approved by Zhongshan Ophthalmic Center Ethics Committee.

## REFERENCES

- Read RW, Rechoudouni A, Butani N, Johnston R, LaBree LD, Smith RE, et al. Complications and prognostic factors in Vogt-Koyanagi-Harada disease. *Am J Ophthalmol.* (2001) 131:599–606. doi: 10.1016/S0002-9394(01)00937-0
- Forster DJ, Cano MR, Green RL, Rao NA. Echographic features of the Vogt-Koyanagi-Harada syndrome. *Arch Ophthalmol.* (1990) 108:1421–6. doi: 10.1001/archophth.1990.01070120069031
- Moorthy RS, Inomata H, Rao NA. Vogt-Koyanagi-Harada syndrome. *Surv Ophthalmol.* (1995) 39:265–92. doi: 10.1016/S0039-6257(05)80105-5
- Fang W, Yang P. Vogt-koyanagi-harada syndrome. *Curr Eye Res.* (2008) 33:517–23. doi: 10.1080/02713680802233968
- Ramanan AV, Dick AD, Jones AP, McKay A, Williamson PR, Compeyrot-Lacassagne S, et al. Adalimumab plus methotrexate for uveitis in juvenile idiopathic arthritis. *N Engl J Med.* (2017) 376:1637–46. doi: 10.1056/NEJMoa1614160
- Nguyen QD, Merrill PT, Jaffe GJ, Dick AD, Kurup SK, Sheppard J, et al. Adalimumab for prevention of uveitic flare in patients with inactive non-infectious uveitis controlled by corticosteroids (VISUAL II): a multicentre, double-masked, randomised, placebo-controlled phase 3 trial. *Lancet.* (2016) 388:1183–92. doi: 10.1016/S0140-6736(16)31339-3
- Atienza-Mateo B, Martín-Varillas JL, Calvo-Río V, Demetrio-Pablo R, Beltrán E, Sánchez-Bursón J, et al. Comparative study of infliximab versus adalimumab in refractory uveitis due to Behçet's disease: national multicenter study of 177 cases. *Arthritis Rheumatol.* (2019) 71:2081–9. doi: 10.1002/art.41026
- Xu J, Qin Y, Chang R, Tan H, Wang Q, Su G, et al. Aqueous cytokine levels in four common uveitis entities. *Int Immunopharmacol.* (2020) 78:106021. doi: 10.1016/j.intimp.2019.106021
- Díaz Llopis M, Amselem L, Romero FJ, García-Delpech S, Hernández ML. [Adalimumab therapy for Vogt-Koyanagi-Harada syndrome]. *Arch Soc Esp Oftalmol.* (2007) 82:131–2. doi: 10.4321/S0365-66912007000300003
- Jeroudi A, Angeles-Han ST, Yeh S. Efficacy of adalimumab for pediatric Vogt-Koyanagi-Harada syndrome. *Ophthalmic Surg Lasers Imaging Retina.* (2014) 45:332–4. doi: 10.3928/23258160-20140709-09
- Su E, Oza VS, Latkany P. A case of recalcitrant pediatric Vogt-Koyanagi-Harada disease successfully controlled with adalimumab. *J Formos Med Assoc.* (2019) 118:945–50. doi: 10.1016/j.jfma.2018.12.014
- Takayama K, Obata H, Takeuchi M. Efficacy of adalimumab for chronic vogt-koyanagi-harada disease refractory to conventional corticosteroids and immunosuppressive therapy and complicated by central serous chorioretinopathy. *Ocul Immunol Inflamm.* (2020) 28:509–12. doi: 10.1080/09273948.2019.1603312
- Street D, Sivaguru A, Sreekantam S, Mollan SP. Vogt-Koyanagi-Harada disease. *Pract Neurol.* (2019) 19:364–7. doi: 10.1136/practneurol-2018-002152
- Kwon HY, Woo SJ. A case of recurrent vogt-koyanagi-harada disease successfully treated with adalimumab in young female adult patient. *Korean J Ophthalmol.* (2020) 34:92–3. doi: 10.3341/kjo.2019.0052
- Yang P, Zhong Y, Du L, Chi W, Chen L, Zhang R, et al. Development and evaluation of diagnostic criteria for vogt-koyanagi-harada disease. *JAMA Ophthalmol.* (2018) 136:1025–31. doi: 10.1001/jamaophthalmol.2018.2664
- Read RW, Holland GN, Rao NA, Tabbara KF, Ohno S, Arellanes-Garcia L, et al. Revised diagnostic criteria for Vogt-Koyanagi-Harada disease: report of an international committee on nomenclature. *Am J Ophthalmol.* (2001) 131:647–52. doi: 10.1016/S0002-9394(01)00925-4
- Du L, Kijlstra A, Yang P. Vogt-Koyanagi-Harada disease: novel insights into pathophysiology, diagnosis and treatment. *Prog Retin Eye Res.* (2016) 52:84–111. doi: 10.1016/j.preteyeres.2016.02.002
- Schulze-Bonsel K, Feltgen N, Burau H, Hansen L, Bach M. Visual acuities “hand motion” and “counting fingers” can be quantified with the freiburg visual acuity test. *Invest Ophthalmol Vis Sci.* (2006) 47:1236–40. doi: 10.1167/iops.05-0981
- Jabs DA, Nussenblatt RB, Rosenbaum JT. Standardization of Uveitis Nomenclature (SUN) Working Group. Standardization of uveitis nomenclature for reporting clinical data Results of the First International Workshop. *Am J Ophthalmol.* (2005) 140:509–16. doi: 10.1016/j.ajo.2005.03.057
- Nussenblatt RB, Palestine AG, Chan CC, Roberge F. Standardization of vitreal inflammatory activity in intermediate and posterior uveitis. *Ophthalmology.* (1985) 92:467–71. doi: 10.1016/S0161-6420(85)34001-0
- Yang P, Zhang Z, Zhou H, Li B, Huang X, Gao Y, et al. Clinical patterns and characteristics of uveitis in a tertiary center for uveitis in China. *Curr Eye Res.* (2005) 30:943–8. doi: 10.1080/02713680500263606
- Yang P, Sun M. Band-shaped keratopathy in Chinese patients with Vogt-Koyanagi-Harada syndrome. *Cornea.* (2011) 30:1336–40. doi: 10.1097/ICO.0b013e31820f774c
- Yang P, Wang C, Su G, Pan S, Qin Y, Zhang J, et al. Prevalence, risk factors and management of ocular hypertension or glaucoma in patients with Vogt-Koyanagi-Harada disease. *Br J Ophthalmol.* (2021) 105:1678–82. doi: 10.1136/bjophthalmol-2020-316323

The patients/participants provided their written informed consent to participate in this study. Written informed consent was obtained from the individual(s), and minor(s)' legal guardian/next of kin, for the publication of any potentially identifiable images or data included in this article.

## AUTHOR CONTRIBUTIONS

WS: conceptualization, writing–review and editing, and supervision. SY, TT, and WS: methodology. SY, TT, ZH, XL, HL, LX, WC, and FW: formal analysis and investigation. SY: writing–original draft preparation. All authors contributed to the article and approved the submitted version.

## FUNDING

This work was supported by the National Key Research and Development Program of China (2017YFA0105804) and the Local Innovative and Research Teams Project of Guangdong Pearl River Talents Program (2017BT01S138).

24. Yang P, Liu X, Zhou H, Guo W, Zhou C, Kijlstra A. Vogt-Koyanagi-Harada disease presenting as acute angle closure glaucoma at onset. *Clin Exp Ophthalmol*. (2011) 39:639–47. doi: 10.1111/j.1442-9071.2011.02523.x
25. Reiff A. Clinical presentation, management, and long-term outcome of pars planitis, panuveitis, and vogt-koyanagi-harada disease in children and adolescents. *Arthritis Care Res (Hoboken)*. (2020) 72:1589–96. doi: 10.1002/acr.24056
26. Fukutomi A, Mashimo H, Yoshioka M, Haruta M, Minami T, Shimojo H, et al. Steroid resistant vogt-koyanagi-harada disease treated effectively with cyclosporine. *Nihon Ganka Gakkai Zasshi*. (2017) 121:480–6.
27. Futagami Y, Sugita S, Fujimaki T, Yokoyama T, Morio T, Mochizuki M. Bilateral anterior granulomatous keratouveitis with sunset glow fundus in a patient with autoimmune polyglandular syndrome. *Ocul Immunol Inflamm*. (2009) 17:88–90. doi: 10.1080/09273940802596518
28. Díaz-Llopis M, Salom D, García-de-Vicuña C, Cordero-Coma M, Ortega G, Ortego N, et al. Treatment of refractory uveitis with adalimumab: a prospective multicenter study of 131 patients. *Ophthalmology*. (2012) 119:1575–81. doi: 10.1016/j.ophtha.2012.02.018
29. Couto C, Schlaen A, Frick M, Khoury M, Lopez M, Hurtado E, et al. Adalimumab treatment in patients with vogt-koyanagi-harada disease. *Ocul Immunol Inflamm*. (2018) 26:485–9. doi: 10.1080/09273948.2016.1236969
30. Jaffe GJ, Dick AD, Brézín AP, Nguyen QD, Thorne JE, Kestelyn P, et al. Adalimumab in patients with active noninfectious uveitis. *N Engl J Med*. (2016) 375:932–43. doi: 10.1056/NEJMoa1509852

**Conflict of Interest:** The authors declare that the research was conducted in the absence of any commercial or financial relationships that could be construed as a potential conflict of interest.

**Publisher's Note:** All claims expressed in this article are solely those of the authors and do not necessarily represent those of their affiliated organizations, or those of the publisher, the editors and the reviewers. Any product that may be evaluated in this article, or claim that may be made by its manufacturer, is not guaranteed or endorsed by the publisher.

Copyright © 2022 Yang, Tao, Huang, Liu, Li, Xie, Wen, Chi and Su. This is an open-access article distributed under the terms of the Creative Commons Attribution License (CC BY). The use, distribution or reproduction in other forums is permitted, provided the original author(s) and the copyright owner(s) are credited and that the original publication in this journal is cited, in accordance with accepted academic practice. No use, distribution or reproduction is permitted which does not comply with these terms.



# Case Report: Associated Ocular Adverse Reactions With Inactivated COVID-19 Vaccine in China

Kunpeng Pang<sup>†</sup>, Lijie Pan<sup>†</sup>, Hui Guo and Xinyi Wu<sup>\*</sup>

Department of Ophthalmology, Qilu Hospital of Shandong University, Jinan, China

## OPEN ACCESS

### Edited by:

Haijiang Lin,  
University of Massachusetts,  
United States

### Reviewed by:

Wei Chi,  
Sun Yat-sen University, China  
Li Cai,  
Shenzhen University General  
Hospital, China

### \*Correspondence:

Xinyi Wu  
xywu8868@163.com

<sup>†</sup>These authors have contributed  
equally to this work and share first  
authorship

### Specialty section:

This article was submitted to  
Ophthalmology,  
a section of the journal  
Frontiers in Medicine

**Received:** 27 November 2021

**Accepted:** 17 December 2021

**Published:** 17 January 2022

### Citation:

Pang K, Pan L, Guo H and Wu X  
(2022) Case Report: Associated  
Ocular Adverse Reactions With  
Inactivated COVID-19 Vaccine in  
China. *Front. Med.* 8:823346.  
doi: 10.3389/fmed.2021.823346

The vaccine is still the best clinical measure for effective prevention and control of coronavirus disease 2019 (COVID-19). The vaccine-associated ocular adverse reactions should be noted in detail among the medical community. We reported twelve eyes of 9 patients presented at the Department of Ophthalmology, Qilu Hospital of Shandong University from March to August 2021 with ocular complaints following COVID-19 vaccination. The main inclusion criterion was the development of ocular symptoms within 14 days after receiving a dose of an inactivated COVID-19 vaccine. The mean (SD) age was  $44.7 \pm 16.5$  years (range, 19–78 years), among which seven (77.8%) cases were women. The mean time of ocular adverse events was 7.1 days (range, 1–14 days) after receiving the inactivated COVID-19 vaccine. One patient was diagnosed with choroiditis, 1 with uveitis, 4 with keratitis, 1 with scleritis, 1 with acute retinal necrosis, and 1 with iridocyclitis. Although the causal relationship between vaccines and ocular adverse events cannot be established from this case series report, physicians should pay attention to the ocular adverse reactions following the COVID-19 vaccine administration.

**Keywords:** ocular adverse event, vaccine, COVID-19, uveitis, keratitis

## INTRODUCTION

Coronavirus diseases 2019 (COVID-19) is caused by a coronavirus named severe acute respiratory syndrome coronavirus two (SARS-CoV-2). According to the data from WHO, as of November 2021, the COVID-19 pandemic has caused more than 250 million infections and more than 5 million deaths all over the world (1). The vaccine is still the best clinical measure for effective prevention and control of COVID-19 (2). In general, vaccines trigger a protective immune system response against a specified infectious organism through a variety of methods of antigen exposure (3). There are five categories of vaccines including subunits, live-attenuated, inactivated, toxoid, and genetic sequencing vaccines (consisting of DNA or messenger RNA based on genetic sequencing information from the pathogen) (3, 4). So far, more than 292 candidates' vaccines have been being developed for COVID-19 (5).

In China, three types of COVID-19 vaccines have been approved by the Chinese Center for Disease Control and Prevention (CCDC) including inactivated vaccines (Sinopharm, Sinovac, etc.), recombinant vaccine (CHO cells), and adenovirus vector vaccine (Adenovirus Type 5 vector). As of November 2021, more than 2 billion doses of inactivated COVID-19 vaccines have been inoculated in China. We hereby presented a case series of ocular adverse events presenting at Qilu Hospital of Shandong University from March to August 2021, soon after receiving an inactivated COVID-19 vaccine. Color fundus photography was obtained with photography (Carl Zeiss, Germany VISUCAM 224)

camera. Optical coherence tomography (OCT) was obtained with a spectral-domain machine (Carl Zeiss, Germany Cirrus HD-OCT 5000). Intraocular pressure was obtained by Topcon, Japan CT-80. Intraocular fluid testing was performed in Beijing GiantMed Diagnostics. Slit-lamp images were taken by Topcon, Japan SL-D7 with optional Digital Photo Attachments. Sex, age, medical history, and clinical data were self-reported and collected.

In this study, twelve eyes of 9 patients presenting with ocular complaints following COVID-19 vaccination were included in this study. The mean (SD) age was  $44.7 \pm 16.5$  years (range, 19–78 years), among which 7 (77.8%) cases were women. The mean time of ocular adverse events was 7.1 days (range, 1–14 days) after receiving the inactivated COVID-19 vaccine. Patients were diagnosed with choroiditis (case 1), uveitis (case 2), keratitis (case 3, 4, 5, 7), scleritis (case 6), acute retinal necrosis (case 8) and iridocyclitis (case 9). The detail of these cases is summarized in Table 1.

## SELECTED CASES DESCRIPTION

### Case 2

Patient 2 had an ocular history of optic disc vasculitis in her both eyes 1 month after she received the flu shot in November 2020 and was resolved after receiving a tapering dose of oral prednisone. She denied having other medical histories. In March 2021, she presented to our clinic with blurred vision in both eyes 5 days after the administration of the second dose of inactivated COVID-19 vaccine. The best-corrected visual acuity (BCVA) was 20/25 in both eyes. Fine dust-like keratic precipitates (KP) and flare in the anterior chamber were noticed in both eyes. Two small iris nodules were seen at the pupillary margin in her left eye. Pigment deposits were dispersed on the surface of the lens. The edge of both eyes' optic discs was unclear. The patient received the topical application of prednisolone acetate and oral prednisone 5 mg per day. In May 2021, the patient complained about vision loss and visual distortions in her both eyes. The dilated fundus examination (OD/OS) reveals signs of "sunset glow" (Figure 1A). The foveal neurosensory detachment in the right eye was noticed by OCT (Figure 1B). In addition to the topical application of prednisolone acetate, the patient received a systemic tapering dose of glucocorticoids and cyclosporin. At 2-month follow-up, the BCVA in both eyes was back to 20/20. Most of the retinal neurosensory layer in foveola returned back to the retinal pigment epithelium in the right eye (Figure 1C).

### Case 4

Patient 4 complained about eye redness and blurred vision in her left eye 7 days after receiving the second dose of inactivated COVID-19 vaccine in May 2021. She denied the medical history. In August 2021, she presented to our clinic with seriously blurred vision in her left eye. The BCVA was 20/20 in her right eye and 20/200 in her left eye. The intraocular pressure (IOP) was 16 mmHg in the right eye and 15 mmHg in the left eye. Slit-lamp examination revealed a dendritic ulcer with terminal bulbs in the central cornea and it becomes readily apparent with fluorescein staining (Supplementary Figure 1A). Ganciclovir gel

and cyclosporine eyedrop was used for 4 weeks. The cornea ulcer healed with a light nebula left and the BCVA of her left eye returned to 20/100 (Supplementary Figure 1B).

### Case 5

Patient 5 presented to our clinic in June 2021 with foreign body sensation, lacrimation, and redness in her red-eye, accompanied by groups of fluid-filled blisters on her right forehead 1 day after receiving the first dose of vaccine (Figure 2A). The BCVA at the presentation was 20/20 in her right eye and 20/25 in her left eye. The intraocular pressure was 17 and 16 mmHg, respectively. The patient had edema in her right eyelid, conjunctival congestion, shallow corneal ulcer close to the limbus, and positive fluorescein staining in her right eye. No cells and flare were noticed in the right eye anterior chamber. After being given an intravenous injection of ganciclovir and plus with topical application of ganciclovir gel and cyclosporine eyedrop for 2 months, the facial blisters and corneal ulcer in her right eye healed (Figure 2B, Supplementary Figure 2).

### Case 6

Patient 6 had a 10-year medical history of hypertension. Before presenting to our clinic in August 2021, he had accepted a cataract surgery in his right eye for 2 months. Three days after receiving the first dose of COVID-19 inactivated vaccine in July 2021, he complained the redness, lacrimation, and visual loss in his right eye, and was diagnosed as having scleritis in a local clinic. He was given the treatment of the eyedrops of tobramycin and dexamethasone for 1 month in his right eye, and the symptoms were getting worse. In August, he was referred to our clinic. The BCVA at the presentation was 20/50 OD and 20/67 OS. The intraocular pressure was 19 and 20 mmHg, respectively. The slit lamp examinations revealed serious conjunctival congestion and a 3 mm × 3 mm nodule on the temporal sclera of his right eye. The cornea was clear, and no cells or flares were observed in the anterior chamber (Figure 3).

## DISCUSSION

Since the role of vaccination is to prevent diseases, the vaccine has been widely administered to a large group of healthy individuals. The safety and side effects raise concerns among the human community. Local reactions (swelling, erythema, and pain around the site of injection) at injection sites and mild systemic reactions (transient fever, tiredness, headache, or chills) are common, but serious side effects are uncommon. According to the data from CCDC (From December 2020 to April 2021), the adverse events of COVID-19 vaccines were reported at 11.86 per 100,000 persons in China (6). Regarding this, 82.96% of the total events were general reactions including fever, swollen and callosity at injection sites, and 17.04% were uncommon adverse reactions such as allergic skin rash, angioedema, and acute severe allergic reaction.

Here, we reported 9 cases of ocular adverse events after receiving inactivated COVID-19 vaccines, although the causal relationship cannot be established in this study. Cases 1, 2, and 9 (5 of 6 eyes) were different types of uveitis and were reported at



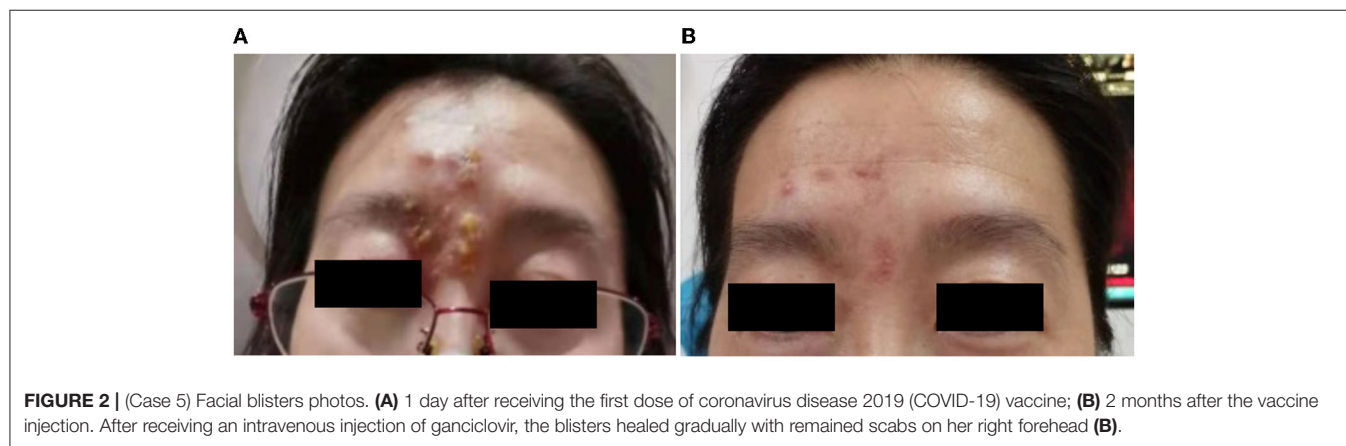
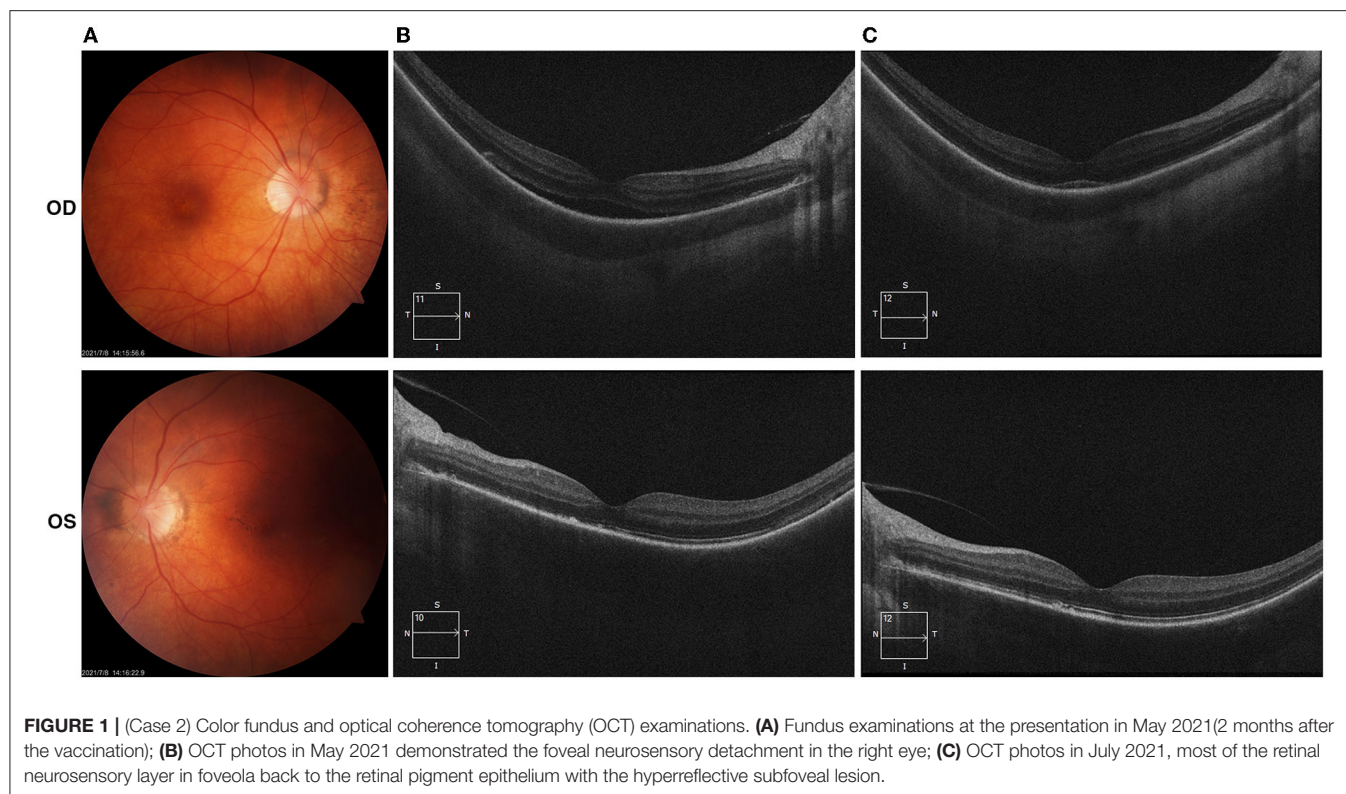
**TABLE 1** | Demographic characteristics of people receiving coronavirus disease 2019 (COVID-19) vaccines and the plans for treatment of these ocular adverse events.

#	Gender	Age (years)	Ocular history	Medical history	Diagnosis	Vaccine type	Days after vaccination	Doses	Treatment
1	Female	50	N/A	N/A	Choroiditis (OU)	Inactivated	5	1	One-time periocular triamcinolone acetonide injection; Oral prednisone
2	Female	34	Optic disc vasculitis (OU)	N/A	Uveitis (OU)	Inactivated	5	2	Topical application of prednisolone acetate; Oral prednisone
3	Female	43	N/A	N/A	Keratoconjunctivitis (OD)	Inactivated	7	2	Topical application of ganciclovir ophthalmic gel, tobramycin and dexamethasone
4	Female	55	N/A	N/A	Keratitis (OS)	Inactivated	7	2	Topical application of ganciclovir ophthalmic gel and ciclosporin
5	Female	45	N/A	N/A	Keratitis (OD)	Inactivated	1	1	Topical application of ganciclovir ophthalmic gel and ciclosporin; Intravenous injection of ganciclovir
6	Male	78	Cataract surgery (right eye) for 2 months	10 years history of hypertension	Scleritis (OD)	Inactivated	3	1	Topical application of ganciclovir ophthalmic gel, ciclosporin, tobramycin and dexamethasone; Oral aciclovir tablets
7	Male	19	N/A	N/A	Keratitis (OU)	Inactivated	14	2	Topical application of ganciclovir ophthalmic gel and ciclosporin; Intravenous injection of ganciclovir
8	Female	46	N/A	N/A	Acute Retinal Necrosis (OD)	Inactivated	8	N/A	Intravenous and intravitreal injection of ganciclovir; Oral prednisone
9	Female	32	Recurrent iritis (both eyes) for 6 years	N/A	Iridocyclitis (OS)	Inactivated	14	3	Topical application of prednisolone acetate, tobramycin and dexamethasone

a mean of 8 days after vaccination. After being given the topical application and oral steroids, all their clinical manifestations disappeared and BCVA was back to a normal level. Cases of uveitis in association with vaccine administration have been reported with nearly all vaccines (7). Benage et al. reported a total of 289 cases of vaccine-associated uveitis between 1984 and 2014, and the median time from vaccination to uveitis onset was 16 days (7), among which 199 cases occurred in women vs. 77 in men. Our reports were consistent with their findings that all three cases were women. The literature of COVID-19 vaccines-related uveitis was rare. Renisi et al. reported a case of anterior uveitis 14 days after the second dose of BNT162b2 COVID (8). The precise pathogenesis frequently remains unclear. Different mechanisms have been hypothesized including the direct infection by the attenuated but still, active virus strain and inflammation induced by one or more adjuvants (such as aluminum salts), routinely used in inactivated or subunit/conjugate vaccines (9). Adjuvants are used to enhance the immunogenicity response and result in a reduced frequency and amount of vaccination required to obtain adequate preventive immunity (10). Adaptive and the innate arms of the immune system are both influenced by adjuvants via various mechanisms including the activation of

Toll-like receptors, NOD-like receptors, etc., and lead to their downstream cytokines generation. Moreover, the activation of antigen presented cells transfers the antigen to B-cell and T-cell leading to the heightened adaptive immune response to antigen (11–13). The autoinflammation and autoimmune conditions induced by adjuvants, known as Shoenfeld syndrome, often occur in patients with a personal or history of autoimmune disease (9, 14). However, the presented patients denied medical history or family history of autoimmune disease. The enhancement of immune response might play an important role in these uveitis cases.

In addition to uveitis, keratitis was reported in 4 of 9 cases (age range between 19 and 55 years) at a mean of 14 days (range between 1 and 43 days) after the administration of the vaccine. Although we did not do the PCR for virus test to confirm the type of keratitis, all cases were resolved with topical application of ganciclovir ophthalmic gel and ciclosporin or systemic ganciclovir. Keratitis in association with vaccines appeared to be uncommon. Furthermore, three cases of herpes simplex virus (HSV) keratitis were reactivated after COVID-19 vaccination (2 of 3 were associated with BNT162b2 mRNA vaccination, the third one was AstraZeneca) (15, 16). A



review reported 24 cases of keratitis in association with herpes zoster or varicella vaccination (17). Two possible mechanisms involved in the pathogenesis included molecular mimicry and autoinflammation triggering the host response and promoting the HSV replication (16). Hence, the treating physician should be mindful of such associations between vaccination and keratitis.

The vaccine-associated scleritis was uncommon. Pichi et al. (18) reported a case of episcleritis and 2 cases of anterior scleritis which were noted soon after the administration of inactivated COVID-19 vaccines. Consistent with the report, the presented case of scleritis was noted 3 days after receiving the first dose of the vaccine. The symptoms of the case were mild and responsive

to glucocorticoids. Noteworthy, there were two reports of scleritis (one case of episcleritis and two cases of anterior scleritis) after the outbreak of coronavirus in 2019 (19, 20).

A case of varicella-zoster virus (VZV) related acute retinal necrosis (ARN) was reported previously following one dose of the COVID-19 vaccine (21). Case 8 was presented to our clinic 8 days after the vaccination. PCR from the aqueous humor sample was positive for both HSV and VZV. Of note, 4 cases of ARN (3 cases were HSV related, 1 case was VZV related) have been reported after the infection of SARS-CoV-2 (22–24). The unconceivable risk of aberrant immune reactions leading to the reactivation of HSV or VZV needs to be kept in mind after the COVID-19 vaccination.

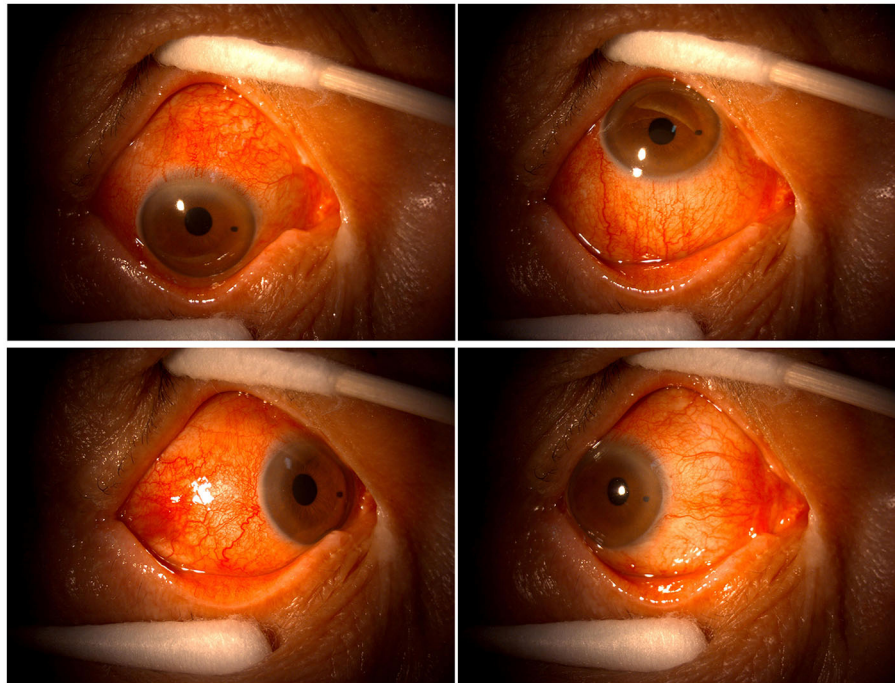


**FIGURE 3** | (Case 6) Slit-lamp examination photos at the presentation.

## CONCLUSION

Although we reported 9 cases of COVID-19 vaccine-related ocular adverse events, the causal relationship cannot be established in this study design. Due to the serious complications of coronavirus diseases 2019, vaccination is still the most effective way to combat the SARS-CoV-2 at present. The benefits of immunization against the virus far outweigh the risks. However, physicians should keep an eye on the ocular adverse reactions following the COVID-19 administration.

## DATA AVAILABILITY STATEMENT

The original contributions presented in the study are included in the article/**Supplementary Material**, further inquiries can be directed to the corresponding author/s.

## ETHICS STATEMENT

The studies involving human participants were reviewed and approved by Medical Ethics Committee of Qilu Hospital of Shandong University. The patients/participants provided their written informed consent to participate in this study. Written informed consent was obtained from the individual(s) for the publication of any potentially identifiable images or data included in this article.

## AUTHOR CONTRIBUTIONS

KP, LP, HG, and XW were all the treating physicians of the patient. KP and LP recollected all the medical history of the

patient and wrote the core of this article. HG and XW helped in the reviewing and editing of the article. All authors contributed to the article and approved the submitted version.

## FUNDING

This study was funded by National Natural Science Foundation of China (81770893).

## ACKNOWLEDGMENTS

We thank the patients and their families, and all the clinical technicians' support for this study.

## SUPPLEMENTARY MATERIAL

The Supplementary Material for this article can be found online at: <https://www.frontiersin.org/articles/10.3389/fmed.2021.823346/full#supplementary-material>

**Supplementary Figure 1** | (Case 4) Slit-lamp images after receiving the second dose of COVID-19 inactivated vaccine. **(A)** photos taken in August 2021; **(B)** photos taken in September 2021.

**Supplementary Figure 2** | (Case 5) Slit-lamp examinations of the cornea. **(A)** 2 months after receiving the first dose of COVID-19 vaccine; **(B)** 2.5 months after the vaccine injection. Unfortunately, we missed the first day's slit lamp photos of the cornea. The corneal ulcer healed with slight nebula **(B)** after receiving intravenous injection of ganciclovir and plus with topical application of ganciclovir gel and cyclosporine eyedrops.



## REFERENCES

- World Health Organization. *WHO Coronavirus (COVID-19) Overview* (2021). Available at: <https://covid19.who.int/> (accessed November 15, 2021).
- Chakraborty R, Parvez S. COVID-19: An overview of the current pharmacological interventions, vaccines, and clinical trials. *Biochem Pharmacol.* (2020) 180:114184. doi: 10.1016/j.bcp.2020.114184
- Cheng JY, Margo CE. Ocular adverse events following vaccination: overview and update. *Surv Ophthalmol.* (2021) 16:S0039-6257(21)00099-0. doi: 10.1016/j.survophthal.2021.04.001
- van Riel D, de Wit E. Next-generation vaccine platforms for COVID-19. *Nat Mater.* (2020) 19:810–2. doi: 10.1038/s41563-020-0746-0
- Alsharri AS, Hudu SA, Imran M, Asdaq SMB, Ali AM, Rabbani SI. Innovations and development of Covid-19 vaccines: a patent review. *J Infect Public Health.* (2021) S1876-0341(21)00342–7. doi: 10.1016/j.jiph.2021.10.021
- Chinese Center for Disease Control and Prevention. *A Report: The Adverse Events After Receiving COVID-19 Vaccines in China (April 30th, 2021)*. (2021). Available at: [https://www.chinacdc.cn/jkzt/ymyz/ymyzjz\\_6758/202105/t20210528\\_230911.html](https://www.chinacdc.cn/jkzt/ymyz/ymyzjz_6758/202105/t20210528_230911.html) (accessed November 15, 2021).
- Benage M, Fraunfelder FW. Vaccine-Associated Uveitis. *Mo Med.* (2016) 113:48–52.
- Renisi G, Lombardi A, Stanzione M, Invernizzi A, Bandera A, Gori A. Anterior uveitis onset after bnt162b2 vaccination: is this just a coincidence? *Int J Infect Dis.* (2021) 110:95–7. doi: 10.1016/j.ijid.2021.07.035
- Cunningham ET, Moorthy RS, Fraunfelder FW, Zierhut M. Vaccine-associated uveitis. *Ocul Immunol Inflamm.* (2019) 27:517–20. doi: 10.1080/09273948.2019.1626188
- McElrath MJ. Selection of potent immunological adjuvants for vaccine construction. *Semin Cancer Biol.* (1995) 6:375–85. doi: 10.1016/1044-579X(95)90007-1
- Coffman RL, Sher A, Seder RA. Vaccine adjuvants: putting innate immunity to work. *Immunity.* (2010) 33:492–503. doi: 10.1016/j.immuni.2010.10.002
- Watad A, Sharif K, Shoenfeld Y. The ASIA syndrome: basic concepts. *Mediterr J Rheumatol.* (2017) 28:64–9. doi: 10.31138/mjr.28.2.64
- Israeli E, Agmon-Levin N, Blank M, Shoenfeld Y. Adjuvants and autoimmunity. *Lupus.* (2009) 18:1217–25. doi: 10.1177/0961203309345724
- Watad A, Quaresma M, Brown S, Cohen Tervaert JW, Rodríguez-Pint I, Cervera R, et al. Autoimmune/inflammatory syndrome induced by adjuvants (Shoenfeld's syndrome)—an update. *Lupus.* (2017) 26:675–81. doi: 10.1177/0961203316686406
- Alkhalifah MI, Alsobki HE, Alwael HM, Fawaz AM Al, Al-Mezaine HS. Herpes simplex virus keratitis reactivation after SARS-CoV-2 BNT162b2 mRNA vaccination: a report of two cases. *Ocul Immunol Inflamm.* (2021) 12:1–3. doi: 10.1080/09273948.2021.1986548
- Richardson-May J, Rothwell A, Rashid M. Reactivation of herpes simplex keratitis following vaccination for COVID-19. *BMJ Case Rep.* (2021) 14:1–3. doi: 10.1136/bcr-2021-245792
- Grillo AP, Fraunfelder FW. Keratitis in association with herpes zoster and varicella vaccines. *Drugs of Today.* (2017) 53:393–7. doi: 10.1358/dot.2017.53.7.2667582
- Pichi F, Aljneibi S, Neri P, Hay S, Dackiw C, Ghazi NG. Association of ocular adverse events with inactivated COVID-19 vaccination in patients in Abu Dhabi. *JAMA Ophthalmol.* (2021) 139:1131–5. doi: 10.1001/jamaophthalmol.2021.3477
- Méndez Mangana C, Barraquer Kargacin A, Barraquer RI. Episcleritis as an ocular manifestation in a patient with COVID-19. *Acta Ophthalmol.* (2020) 98:e1056–7. doi: 10.1111/aos.14484
- Feizi S, Meshksar A, Naderi A, Esfandiari H. Anterior scleritis manifesting after coronavirus disease 2019: a report of two cases. *Cornea.* (2021) 40:1204–6. doi: 10.1097/ICO.0000000000002795
- Mishra SB, Mahendradas P, Kawali A, Sanjay S, Shetty R. Reactivation of varicella zoster infection presenting as acute retinal necrosis post COVID 19 vaccination in an Asian Indian male. *Eur J Ophthalmol.* (2021) 18:11206721211046484. doi: 10.1177/11206721211046485
- Gonzalez MP, Rios R, Pappaterra M, Hernandez M, Toledo A, Santos C, et al. Reactivation of acute retinal necrosis following SARS-CoV-2 infection. *Case Rep Ophthalmol Med.* (2021) 2021:1–4. doi: 10.1155/2021/7336488
- Soni A, Narayanan R, Tyagi M, Belenje A, Basu S. Acute retinal necrosis as a presenting ophthalmic manifestation in COVID 19 recovered patients. *Ocul Immunol Inflamm.* (2021) 29:722–5. doi: 10.1080/09273948.2021.1938135
- Gupta A, Dixit B, Stamoulas K, Akshikar R. Atypical bilateral acute retinal necrosis in a coronavirus disease 2019 positive immunosuppressed patient. *Eur J Ophthalmol.* (2020) 22:1120672120974941. doi: 10.1177/1120672120974941

**Conflict of Interest:** The authors declare that the research was conducted in the absence of any commercial or financial relationships that could be construed as a potential conflict of interest.

**Publisher's Note:** All claims expressed in this article are solely those of the authors and do not necessarily represent those of their affiliated organizations, or those of the publisher, the editors and the reviewers. Any product that may be evaluated in this article, or claim that may be made by its manufacturer, is not guaranteed or endorsed by the publisher.

Copyright © 2022 Pang, Pan, Guo and Wu. This is an open-access article distributed under the terms of the Creative Commons Attribution License (CC BY). The use, distribution or reproduction in other forums is permitted, provided the original author(s) and the copyright owner(s) are credited and that the original publication in this journal is cited, in accordance with accepted academic practice. No use, distribution or reproduction is permitted which does not comply with these terms.





## OPEN ACCESS

## EDITED BY

Maddalena De Bernardo,  
University of Salerno, Italy

## REVIEWED BY

Veena Rao Raji,  
Rush University, United States

## \*CORRESPONDENCE

Yusuke Kameda  
y09025618059@leaf.ocn.ne.jp

## SPECIALTY SECTION

This article was submitted to  
Ophthalmology,  
a section of the journal  
Frontiers in Medicine

RECEIVED 12 July 2022

ACCEPTED 07 September 2022

PUBLISHED 21 September 2022

## CITATION

Kameda Y, Kaneko Y, Sugai M,  
Ishinabe K and Fukuoka N (2022)  
Commentary: Case report: Associated  
ocular adverse reactions with  
inactivated COVID-19 vaccine in  
China. *Front. Med.* 9:991862.  
doi: 10.3389/fmed.2022.991862

## COPYRIGHT

© 2022 Kameda, Kaneko, Sugai,  
Ishinabe and Fukuoka. This is an  
open-access article distributed under  
the terms of the [Creative Commons  
Attribution License \(CC BY\)](#). The use,  
distribution or reproduction in other  
forums is permitted, provided the  
original author(s) and the copyright  
owner(s) are credited and that the  
original publication in this journal is  
cited, in accordance with accepted  
academic practice. No use, distribution  
or reproduction is permitted which  
does not comply with these terms.

# Commentary: Case report: Associated ocular adverse reactions with inactivated COVID-19 vaccine in China

Yusuke Kameda<sup>1\*</sup>, Yutaka Kaneko<sup>2</sup>, Megumi Sugai<sup>1</sup>,  
Karin Ishinabe<sup>1</sup> and Nichika Fukuoka<sup>1</sup>

<sup>1</sup>Yotsuya-sanchome Ekimae Eye Clinic, Tokyo, Japan, <sup>2</sup>Department of Ophthalmology and Visual  
Sciences, Faculty of Medicine, Yamagata University, Yamagata, Japan

## KEYWORDS

COVID-19 vaccination, herpes keratitis, herpes simplex virus (HSV), varicella zoster  
virus (VZV), PCR, COVID-19

## A Commentary on

### Case report: Associated ocular adverse reactions with inactivated COVID-19 vaccine in China

by Pang, K., Pan, L., Guo, H., Wu, X. (2022). *Front. Med. (Lausanne)*. 8:823346.  
doi: 10.3389/fmed.2021.823346

## Introduction

We read the article by Pang et al. with considerable interest, a case series study that provided interesting novel insights into ocular adverse events that occurred after administering the coronavirus disease 2019 (COVID-19) vaccine (1). Although we congratulate the authors for a valuable case presentation, we had some doubts regarding the four cases of keratitis. Therefore, through many years of our experience regarding herpetic eye disease, we would like to provide critical comments for each case.

## Case 3

There were no images or descriptions of the findings in the case presentation. Even if the article type explained the selected case, the authors should add the characteristic appearances and outcomes in the table, such as the study by Bolletta et al. (2). While insufficient disclosure of information about case 3 made it difficult for the readers to imagine the causative factors of keratitis, we assumed that the underlying pathogenesis in this case was herpes virus because the patient was treated with ganciclovir ophthalmic gel. The diagnosis of recurrent or typical herpes keratitis can be made based only on clinical findings; however, no history of this disease and evidence suggesting a typical case were noted in case 3 (3, 4). Therefore, the polymerase chain reaction test is ideal for accurate diagnosis of atypical or complicated cases (3, 5, 6).

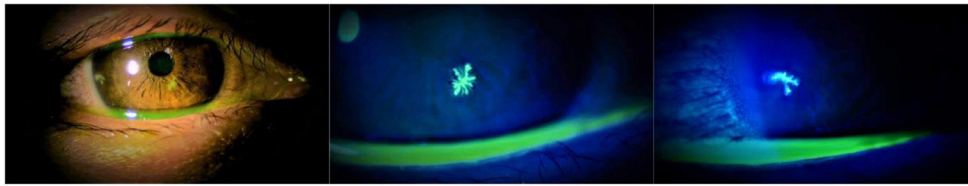


FIGURE 1

Slit-lamp examination of the right eye of the patient showing a herpes keratitis that occurred on the day after the third dose of BNT162b2 (Pfizer). Photos were taken 2 days after the vaccination.

## Case 4

The authors observed a dendritic ulcer with terminal bulbs in the central cornea on slit-lamp examination of Supplementary Figure 1A in Pang et al.'s article. However, we could not confirm this finding due to low-resolution images. Moreover, about 3 months before the first examination, the patient had received COVID-19 vaccination; a relatively long interval between the first presentation and vaccination indicated that the likelihood of other causative factors was higher. Thus, it was very difficult to determine whether the development of keratitis in case 4 was affected by COVID-19 vaccination.

## Case 5

The authors diagnosed case 5 as keratitis, although they observed a red eye in the patient. This finding suggested that keratoconjunctivitis, as in case 2, was preferable to the aforementioned diagnosis. As shown in Figure 2 of Pang et al.'s article, the cutaneous reaction seemed to be a typical varicella zoster virus reactivation. Although reactivation following COVID-19 vaccination was well-documented even at the study period, the authors never addressed the relationship; therefore, this should be discussed with more references (7–9). Moreover, similar to case 4, we felt that the images in Supplementary Figure 2 of Pang et al.'s article showed the slit-lamp examination of case 5 was too low in resolution and long between the onset and the photographing date to draw a positive conclusion.

## Case 7

Like case 3, despite no images or description of findings, the authors speculated that the causative factor of keratitis was herpes virus due to the administration of ganciclovir ophthalmic gel. The onset time was 14 days after vaccination, which could be affected by other influences because of a longer duration

than herpes keratitis cases following COVID-19 vaccination, as documented in previous reports (2, 4, 5, 10). Incidentally, at our institution, widespread COVID-19 vaccinations afforded some opportunities to examine the occurrence of herpes keratitis in patients who had recently received the vaccination; the onset time in all the patients was within a few days of vaccination.

## Conclusion

In the COVID-19 pandemic era, accumulated case series and isolated case reports have suggested that herpes keratitis could occur after COVID-19 vaccination (2, 4–6, 10). We also presented images of herpes keratitis that occurred on the day after COVID-19 vaccination (Figure 1). The picture quality seemed sufficient to explain the two dendritic ulcers with terminal bulbs. In contrast, it is difficult to determine whether the relationship between herpes keratitis that occurred immediately after inoculation and the vaccine was causative or coincidental because this disease is a common illness. Moreover, even if case series and isolated case reports with detailed descriptions of findings and images that can convince readers are accumulated, these study types are generally regarded as “low level” evidence (11). Therefore, future study with high evidence level will be required to determine whether the COVID-19 vaccination was associated with the incidence of herpes keratitis.

## Author contributions

YKam researched the study by Pang et al., wrote the manuscript, and contributed to the critical comments. YKan, MS, KI, and NF helped in the reviewing and editing of the manuscript. As the corresponding author and guarantor of this manuscript, YKam takes full responsibility for the work as a whole. All authors have read and agree to the published

version of the manuscript and approved the final version of the manuscript.

## Conflict of interest

The authors declare that the research was conducted in the absence of any commercial or financial relationships that could be construed as a potential conflict of interest.

## References

1. Pang K, Pan L, Guo H, Wu X. Case report: associated ocular adverse reactions with inactivated COVID-19 vaccine in China. *Front Med.* (2022) 8:823346. doi: 10.3389/fmed.2021.823346
2. Bolletta E, Iannetta D, Mastrofilippo V, Simone LD, Gozzi F, Croci S, et al. Uveitis and other ocular complications following COVID-19 vaccination. *J Clin Med.* (2021) 10:5960. doi: 10.3390/jcm10245960
3. Todokoro D, Hosogai M, Nakano S, Akiyama H. Effective diagnosis by real-time PCR of herpes simplex diffuse endotheliitis that is similar in appearance to fungal keratitis: case series. *J Ophthalmic Inflamm Infect.* (2021) 11:20. doi: 10.1186/s12348-021-00250-6
4. Richardson-May J, Rothwell A, Rashid M. Reactivation of herpes simplex keratitis following vaccination for COVID-19. *BMJ Case Rep.* (2021) 14:e245792. doi: 10.1136/bcr-2021-245792
5. Li S, Jia X, Fei Yu F, Wang Q, Zhang T, Yuan J. Herpetic keratitis preceded by COVID-19 vaccination. *Vaccines.* (2021) 9:1394. doi: 10.3390/vaccines9121394
6. Alkhalifah MI, Alsobki HE, Alwael HM, Fawaz A, Al-Mezaine HS. Herpes simplex virus keratitis reactivation after SARS-CoV-2 BNT162b2 mRNA vaccination: a report of two cases. *Ocul Immunol Inflamm.* (2021) 29:1238–40. doi: 10.1080/09273948.2021.1986548
7. Català A, Muñoz-Santos C, Galván-Casas C, Roncero Riesco M, Revilla Nebreda D, Solà-Truyols A, et al. Cutaneous reactions after SARS-CoV-2 vaccination: a cross-sectional Spanish nationwide study of 405 cases. *Br J Dermatol.* (2022) 186:142–52. doi: 10.1111/bjd.20639
8. Rodríguez-Jiménez P, Chicharro P, Cabrera LM, Seguí M, Morales-Caballero Á, Llamas-Velasco M, et al. Varicella-zoster virus reactivation after SARS-CoV-2 BNT162b2 mRNA vaccination: report of 5 cases. *JAAD Case Rep.* (2021) 12:58–9. doi: 10.1016/j.jidcr.2021.04.014
9. Psychogiou M, Samarkos M, Mikos N, Hatzakis A. Reactivation of varicella zoster virus after vaccination for SARS-CoV-2. *Vaccines.* (2021) 9:572. doi: 10.3390/vaccines9060572
10. Alkwicki H, Alenazi M, Alanazi W, Alruwaili S. Herpetic keratitis and corneal endothelitis following COVID-19 vaccination: a case series. *Cureus.* (2022) 14:e20967. doi: 10.7759/cureus.20967
11. Oxford centre for evidence-based medicine. *Levels of Evidence.* Available online at: <http://www.cebm.net/index.aspx?o=1025> (accessed September 1, 2022).

## Publisher's note

All claims expressed in this article are solely those of the authors and do not necessarily represent those of their affiliated organizations, or those of the publisher, the editors and the reviewers. Any product that may be evaluated in this article, or claim that may be made by its manufacturer, is not guaranteed or endorsed by the publisher.



# Study of the Biological Developmental Characteristics of the Eye in Children After Laser Surgery for the Treatment of Retinopathy of Prematurity

Xianlu Zeng<sup>1</sup>, Miaohong Chen<sup>1</sup>, Lei Zheng<sup>1</sup>, Ruyin Tian<sup>1</sup>, Yi Chen<sup>1</sup>, Honghui He<sup>1</sup>, Jian Zeng<sup>1</sup>, Jicang He<sup>2\*</sup> and Guoming Zhang<sup>1\*</sup>

<sup>1</sup> Shenzhen Key Laboratory of Ophthalmology, Shenzhen Eye Hospital, Affiliated Shenzhen Eye Hospital of Jinan University, Shenzhen University School of Medicine, Shenzhen, China, <sup>2</sup> New England College of Optometry, Boston, MA, United States

## OPEN ACCESS

### Edited by:

Haijiang Lin,  
Massachusetts Eye and Ear Infirmary  
and Harvard Medical School,  
United States

### Reviewed by:

Zhao Mingwei,  
Peking University People's  
Hospital, China  
Yu Xu,  
Shanghai Jiao Tong University, China

### \*Correspondence:

Guoming Zhang  
13823509060@163.com  
Jicang He  
jihe07@gmail.com

### Specialty section:

This article was submitted to  
Ophthalmology,  
a section of the journal  
Frontiers in Medicine

**Received:** 26 September 2021

**Accepted:** 20 December 2021

**Published:** 25 January 2022

### Citation:

Zeng X, Chen M, Zheng L, Tian R, Chen Y, He H, Zeng J, He J and Zhang G (2022) Study of the Biological Developmental Characteristics of the Eye in Children After Laser Surgery for the Treatment of Retinopathy of Prematurity. *Front. Med.* 8:783552. doi: 10.3389/fmed.2021.783552

**Objective:** To observe the differences in ocular biology between premature infants who had undergone retinal laser photocoagulation (LP) for retinopathy of prematurity (ROP) and full-term infants and to investigate the relationships between these differences and the development of the refractive state.

**Methods:** This retrospective, cross-sectional study included 25 children (50 eyes) who had undergone laser treatment for aggressive posterior retinopathy of prematurity (AP-ROP), ROP in zone I requiring treatment, or ROP in zone II requiring treatment in the posterior pole (laser group) and 29 full-term infants (58 eyes) who had not (control group). Basic information, spherical equivalent (SE), and best corrected visual acuity (BCVA) were collected from the two groups. Their mean ages were  $7.32 \pm 2.85$  and  $7.34 \pm 2.57$  years, respectively ( $t = -0.047$ ,  $P = 0.96$ ). Ocular biology data were measured using an IOL Master 700 instrument (Carl Zeiss Meditec AG) and the data were processed using MATLAB (R2016a, Mathworks Inc.). The data markers included central corneal thickness (CCT), anterior and posterior surface corneal curvature radius (CCR), anterior chamber depth (ACD), lens thickness (LT), lens anterior surface curvature radius, lens posterior surface curvature radius, and eye axis length (AL). Optometric data were collected simultaneously and all BCVA values were converted to the logarithm of the minimum angle of resolution (LogMAR) for analysis. The data were statistically analyzed using SPSS software (V.23.0). Independent sample *t*-tests were used for the assessment of ocular biology and refractive indices in both groups of children and Pearson correlation coefficients were used to evaluate the correlations between age, gestational age at birth and ocular biology structural parameters.  $P < 0.05$  was considered statistically significant.

**Results:** Comparisons of ocular biomarkers, refractive status, and BCVA between children in the laser and control groups showed relationships among ocular biomarkers, including the corneal-related parameters of CCT ( $0.54 \pm 0.04$  mm and  $0.56 \pm 0.03$  mm,  $t = -2.116$ ,  $P < 0.05$ ), anterior surface CCR ( $7.53 \pm 0.33$  mm and  $7.84 \pm 0.30$  mm,  $t = -5.063$ ,  $P < 0.05$ ), posterior surface CCR ( $6.75 \pm 0.34$  mm and  $7.03 \pm 0.24$  mm,  $t = -4.864$ ,  $P < 0.05$ ); as well as those related to anterior chamber



depth (ACD) were  $3.24 \pm 0.26$  mm and  $3.64 \pm 0.26$  mm, respectively ( $t = -8.065$ ,  $P < 0.05$ ), lens-related parameters (LT) were  $3.80 \pm 0.19$  mm and  $3.45 \pm 0.16$  mm, respectively ( $t = 10.514$ ,  $P < 0.05$ ); anterior lens surface curvature radius were  $10.02 \pm 0.93$  mm and  $10.52 \pm 0.85$  mm, respectively ( $t = -2.962$ ,  $P < 0.05$ ); posterior lens surface curvature radius were  $5.55 \pm 0.51$  mm and  $5.80 \pm 0.36$  mm, respectively ( $t = -2.917$ ,  $P < 0.05$ ), and ocular axis (AL) were  $22.60 \pm 1.42$  mm and  $23.45 \pm 1.23$  mm, respectively ( $t = -3.332$ ,  $P < 0.05$ ). Moreover, comparison of refractive status and BCVA between two groups of children showed an SE of  $-1.23 \pm 3.38$  D and  $-0.07 \pm 2.00$  D ( $t = -2.206$ ,  $P < 0.05$ ) and LogMAR (BCVA) of  $0.12 \pm 0.13$  and  $0.05 \pm 0.11$  ( $t = 3.070$ ,  $P < 0.05$ ). Analysis of the correlations between age and ocular biomarkers and refractive status of children in the laser and control groups showed correlations between age and ocular biomarkers in the two groups, in which age in the laser group was positively correlated with AL ( $r = 0.625$ ,  $P < 0.05$ ) but not with other biomarkers ( $P > 0.05$ ). Age in the control group was negatively correlated with CCT, ACD, and AL ( $r = 0.303$ ,  $0.468$ ,  $0.703$ ,  $P < 0.05$ ), as well as with LT ( $r = -0.555$ ,  $P < 0.05$ ), with no correlation with other biomarkers ( $P > 0.05$ ). Analysis of the correlation between age and refractive status of children in both groups showed that the age of children in both laser and control groups was negatively correlated with SE ( $r = -0.528$ ,  $-0.655$ ,  $P < 0.05$ ) and LogMAR (BCVA) ( $r = -0.538$ ,  $-0.542$ ,  $P < 0.05$ ). Analysis of the correlations between refractive status and ocular biomarkers in children in the laser and control groups showed that the refractive status in children in the laser group was negatively correlated with AL ( $r = -0.773$ ,  $P < 0.05$ ) but not with other biomarkers in this group ( $P > 0.05$ ). The refractive status of children in the control group was negatively correlated with ACD and AL ( $r = -0.469$ ,  $-0.734$ ,  $P < 0.05$ ), positively correlated with LT ( $r = 0.364$ ,  $P < 0.05$ ), and was not correlated with other biomarkers in this group ( $P > 0.05$ ). Analysis of the correlations of gestational age at birth with ocular biomarkers and refractive status in children in the laser group showed a positive correlation between gestational age at birth and AL ( $r = 0.435$ ,  $P < 0.05$ ) but no other correlations with the other biomarkers ( $P > 0.05$ ). Moreover, gestational age at birth was negatively correlated with SE ( $r = -0.334$ ,  $P < 0.05$ ) and LogMAR (BCVA) ( $r = -0.307$ ,  $P < 0.05$ ) in children in the laser group.

**Conclusions:** Compared to full-term infants, the development of CCT, ACD, LT, and AL was relatively delayed after ROP laser surgery, resulting in thin central corneal thickness, steep corneas, shallow anterior chambers, thicker lenses, “rounder” lens morphology, increased refractive power, and short eye axes, leading to the development of myopia. The changes in refractive status were mainly influenced by increased lens thickness. The results of this study showed that the lower the gestational age at birth, the greater the effects on emmetropization in children after ROP, and the more likely the development of myopia.

**Keywords:** retinopathy of prematurity, laser photocoagulation, ocular biology, refractive error, central corneal thickness, lens thickness

## INTRODUCTION

Retinopathy of prematurity (ROP) is the leading cause of childhood blindness worldwide. In recent years, with the development of neonatal intensive care techniques, the survival rate of preterm and low birth weight infants has been increasing annually, while the incidence of ROP has also increased significantly (1, 2). Retinal LP is currently the gold standard for the treatment of early ROP (3).

Previous studies showed extensive choroidal scarring with retinal atrophy and glial cell proliferation, retinal pigment epithelium loss, choroidal atrophy, and impaired vascularization in the peripheral retina after ROP laser treatment. These histological changes in the fundus may alter and affect the retinal signals required for eye development and/or the scleral reception and response to these signals, delaying or interfering with normal scleral development, resulting in the abnormal development of the anterior segment structures (4). It can be seen that the corneal parameters, anterior chamber depth, and lens thickness in the anterior segment of children after ROP laser also undergo corresponding changes, which are important markers of refractive error (5, 6).

Previous studies have also observed a significant positive correlation between gestational age at birth and anterior chamber depth, lens thickness, and eye axis. Thus, birth gestational age has a large impact on the development of the biological structures of the anterior segment as well as the development of the refractive state. However, the main factors affecting refractive error in children after ROP laser surgery have not been clarified (7, 8).

Therefore, in this study intends to compare the differences in indicators such as the anterior segment, eye axis length and refractive status in children after ROP laser surgery and full-term infants to understand the impact of laser surgery on children's long-term vision, so as to better guide clinical work.

## APPROACH

### Study Subjects

This retrospective, cross-sectional study included data from a total of 25 children (male: 17; female: 8) aged 3–11 years (mean age  $7.32 \pm 2.85$  years) diagnosed with AP-ROP, requiring treatment in zone I or zone II of the posterior pole, who had completed ROP laser treatment and had complete follow-up data between May 2019 and February 2021 at Shenzhen Eye Hospital. A total of 29 full-term children (male: 16; female: 13), aged 3–11 years (mean age  $7.34 \pm 2.57$  years) were also age-matched in the outpatient clinic (Table 1). The study followed the guidelines of the Declaration of Helsinki, was approved by the hospital ethics committee, and obtained informed parental consent before performing the study. The inclusion criteria were as follows: (1) Children in the laser group who were initially diagnosed

with AP-ROP, ROP in zone I requiring treatment, or ROP in zone II of the posterior pole requiring treatment; (2) Children with ROP who received only laser treatment; (3) Children able to undergo continuous follow-up until the lesion had resolved; (4) Children (or their guardians) who agreed to participate and who cooperated with relevant tests and for whom reliable test data were available; (5) Children in whom the same patterns of data collection were used in follow-up visits and for whom the data were complete. The exclusion criteria were as follows: (1) Children with eye diseases other than ROP; (2) Children having received treatment other than laser treatment; (3) Children with a family history of high myopia; (4) Children unable to cooperate in completing tests or in whom poor cooperation had affected the data quality.

## METHODS

### ROP Screening Methods

All screened children were administered compound tropicamide eye drops for mydriasis every 5 min for a total of 5 times until the pupil diameter reached 6 mm. Both eyes were then administered one dose of proparacaine hydrochloride eye drops for surface anesthesia before the examination. Wide-angle retinal images were captured using a third-generation wide-angle digital retinal imaging system for children (RetCam 3, Clarity, USA) according to the Chinese ROP screening guidelines (9). Ten images of different orientations (optic disc-centered, macula-centered, temporal, temporal-distal peripheral, superior, superior distal peripheral, nasal, nasal distal peripheral, inferior, and inferior distal peripheral) were taken to ensure that each image had the optimal focal length and appropriate brightness to obtain a clear and complete picture of the fundus tissue structures. All fundus images were reviewed by two retinal specialists for consensus. Binocular indirect ophthalmoscopy with scleral parietal pressure was performed as needed. According to the Early Treatment of Retinopathy of Prematurity (ETROP) criteria, the ROP severity was staged according to the international classification criteria for ROP. Examinations were repeated at specific intervals until the retinal vascularization reached zone III or until the ROP had completely subsided after treatment (10).

### Retinal Laser Photocoagulation

Within 72 h after diagnosis, basal anesthesia was performed using 0.5% procaine (Alcaine, Alcon Laboratories Inc., USA). LP was performed using an 810 nm diode laser (IRIS Medical Oculight SL 810 nm infrared laser; Iris Medical Inc., USA) in conjunction with a 20 D lens. The laser spot was distributed over the entire avascular retina. The laser parameters were as follows: energy: 200–350 mW and a repetitive mode with a 0.2 s exposure interval. The laser treatments were all performed by the same experienced ophthalmologist. Postoperative corticosteroids, antibiotic eye drops, and cycloplegic agents were used for 7 days to reduce postoperative reactions and prevent infection. The first follow-up visit was scheduled on day 7 after treatment and then every 2 weeks or monthly until the ROP had completely subsided, but not necessarily up to the temporal serrated edge (11, 12).

**TABLE 1** | Statistical comparisons of baseline information between the laser and control groups.

Baseline information	Laser group	Control group	$\chi^2/t$	<i>P</i>
Gestational age at birth (W)	28.16 $\pm$ 2.15	–	–	–
Birth weight (g)	1,230 $\pm$ 585.56	–	–	–
Number of eyes/person	50/25	58/29	–	–
Sex (m/f)	17/8	16/13	0.930	0.34*
Age (years)	7.32 $\pm$ 2.85	7.34 $\pm$ 2.57	–0.047	0.96

\* $\chi^2$  test; Age was an independent sample *t*-test.

## IOL Master700 Test Method

All subjects were scanned using the same IOL Master 700 ocular biometry device, with a light source wavelength of 1,035–1,077 nm, a scanning depth of 44 mm, a scanning width of 6 mm, a resolution of 22  $\mu$ m, and a scanning speed of 2,000 scan/s. The children were fully communicated with the examiner before the examination and natural blinking was permitted during the examination to avoid factors such as fixation differences and tear film rupture that could affect the results. The measurements were carried out by the same experienced technician (13). Three examinations were performed in each eye to assess the repeatability and reliability of the measured. Images of poor quality and with deviations in the visual axis position were removed; thus, only examination results with the best quality were selected for storage in the device. The following parameters were collected and measured by the IOL Master 700 device: central corneal thickness (CCT), anterior surface corneal curvature radius (CCR), anterior chamber depth (ACD), lens thickness (LT), and eye axis length (AL).

## Optometry and BCVA Examinations

All children in the group were given compound tropicamide drops for mydriasis every 5 min for 4 times until the pupil diameter reached 6 mm, refractive error was measured using a Topcon KR 800 optometer, and retinoscopy was performed 0.5 h later using a band light detector. BCVA was performed using a standard Snellen visual acuity chart, decimal visual acuity was recorded, the optometric data of the two groups of children were separately recorded and finally converted them into logarithmic (LogMAR) visual acuity at the minimum angle of resolution for statistical analysis.

## Image Data Pre-processing

The image data from the IOL Master 700 device were visualized in MATLAB by statistical parametric mapping 12 (SPM12; University College London). The images were extracted from the anterior segment corneal and lens images during segmentation, each segmentation line in the software was converged with the anterior and posterior surfaces of the cornea and lens to match exactly, and the data were saved. The posterior surface CCR, anterior surface curvature radius of the lens, and posterior surface curvature radius of the lens were then extracted (14).

## Statistical Methods

The statistical analysis was performed using SPSS software (V.23.0). Independent-sample *t*-tests were used for measurement data, chi-square tests were used for count data, and Pearson correlation coefficients were used to evaluate the correlations between parameters.  $P < 0.05$  was considered statistically significant.

## RESULTS

### Ocular Biomarkers and Refractive Status

There were statistically significant differences in all observation markers between the two groups ( $P < 0.05$ ) (Table 2).

**TABLE 2 |** Comparisons of ocular biology factors and refractive status in the laser and control groups.

Observation markers	Laser group	Control group	<i>t</i>	<i>P</i>
CCT (mm)	0.54 $\pm$ 0.04	0.56 $\pm$ 0.03	−2.116	0.04*
Anterior surface CCR (mm)	7.53 $\pm$ 0.33	7.84 $\pm$ 0.30	−5.063	0.000*
Posterior surface CCR (mm)	6.75 $\pm$ 0.34	7.03 $\pm$ 0.24	−4.864	0.000*
ACD (mm)	3.24 $\pm$ 0.26	3.64 $\pm$ 0.26	−8.065	0.000*
LT (mm)	3.80 $\pm$ 0.19	3.45 $\pm$ 0.16	10.514	0.000*
Curvature radius of the anterior surface of the lens (mm)	10.02 $\pm$ 0.93	10.52 $\pm$ 0.85	−2.962	0.004*
Curvature radius of the posterior surface of the lens (mm)	5.55 $\pm$ 0.51	5.80 $\pm$ 0.36	−2.917	0.004*
AL (mm)	22.60 $\pm$ 1.42	23.45 $\pm$ 1.23	−3.332	0.001*
SE(D)	−1.23 $\pm$ 3.38	−0.07 $\pm$ 2.00	−2.206	0.03*
LogMAR (BCVA)	0.12 $\pm$ 0.13	0.05 $\pm$ 0.11	3.070	0.003*

Two-sample *t*-tests were performed for all markers; \* $P < 0.05$ .

CCT, central corneal thickness; CCR, anterior surface corneal curvature radius; ACD, anterior chamber depth; LT, lens thickness; AL, eye axis length; SE, spherical equivalent; BCVA, best-corrected visual acuity; LogMAR, logarithm of the minimal angle of resolution.

Children who had undergone ROP laser surgery had a thinner central cornea ( $t = -2.116$ ,  $P = 0.04$ ), a steeper cornea ( $t = -5.063$ ,  $P = 0.000$ ;  $t = -4.864$ ,  $P = 0.000$ ), a shallower anterior chamber ( $t = -8.065$ ,  $P = 0.000$ ), and a thicker lens ( $t = 10.514$ ,  $P = 0.000$ ) compared to those in full-term infants. Moreover, the lens was “round” ( $t = -2.962$ ,  $P = 0.004$ ;  $t = -2.917$ ,  $P = 0.004$ ), the eye axis was short ( $t = -3.332$ ,  $P = 0.001$ ), and the visual acuity was poor ( $t = 3.070$ ,  $P = 0.003$ ) (Table 2).

## Correlations of Age With Ocular Biology and Refractive Status

In the laser group, age was positively correlated with AL ( $r = 0.625$ ,  $P = 0.000$ ); negatively correlated with SE ( $r = -0.528$ ,  $P = 0.000$ ) and LogMAR (BCVA) ( $r = -0.538$ ,  $P = 0.000$ ); and not correlated with other markers in this group ( $P > 0.05$ ) (Table 3).

In the control group, age was positively correlated with CCT, ACD, and AL ( $r = 0.303$ ,  $P = 0.02$ ;  $r = 0.468$ ,  $P = 0.000$ ; and  $r = 0.703$ ,  $P = 0.000$ ); negatively correlated with LT ( $r = -0.555$ ,  $P = 0.000$ ) SE ( $r = -0.655$ ,  $P = 0.000$ ), and LogMAR (BCVA) ( $r = -0.542$ ,  $P = 0.000$ ); and not correlated with other markers in this group ( $P > 0.05$ ) (Table 3).

CCT, ACD, and LT changed significantly with age in both groups of children ( $P < 0.05$ ) (Table 3).

## Correlation Between Ocular Biology and Refractive State

In the laser group, refractive status was negatively correlated with AL ( $r = -0.773$ ,  $P = 0.000$ ) but not with other markers ( $P > 0.05$ ) (Table 4).

**TABLE 3 |** Correlations of age with eye biology and refractive status in the laser and control groups.

Observation markers	Age of the laser group	Age of the control group
CCT (mm)	$r = 0.256, P = 0.07$	$r = 0.303, P = 0.02^*$
Anterior surface CCR (mm)	$r = -0.079, P = 0.59$	$r = 0.079, P = 0.56$
Posterior surface CCR (mm)	$r = -0.109, P = 0.45$	$r = -0.068, P = 0.61$
ACD (mm)	$r = 0.261, P = 0.07$	$r = 0.468, P = 0.000^*$
LT (mm)	$r = -0.231, P = 0.11$	$r = -0.555, P = 0.000^*$
Curvature radius of the anterior surface of the lens (mm)	$r = 0.234, P = 0.10$	$r = 0.063, P = 0.64$
Curvature radius of the posterior surface of the lens (mm)	$r = 0.232, P = 0.11$	$r = 0.149, P = 0.27$
AL (mm)	$r = 0.625, P = 0.000^*$	$r = 0.703, P = 0.000^*$
SE (D)	$r = -0.528, P = 0.000^*$	$r = -0.655, P = 0.000^*$
LogMAR (BCVA)	$r = -0.538, P = 0.000^*$	$r = -0.542, P = 0.000^*$

Pearson correlation analysis was performed for all markers;  $^*P < 0.05$ .

CCT, central corneal thickness; CCR, anterior surface corneal curvature radius; ACD, anterior chamber depth; LT, lens thickness; AL, eye axis length; SE, spherical equivalent; BCVA, best-corrected visual acuity; LogMAR, logarithm of the minimal angle of resolution.

**TABLE 4 |** Correlations between refractive status and eye biology in the laser and control groups.

Observation markers	SE (laser group)	SE (control group)
CCT (mm)	$r = -0.231, P = 0.11$	$r = -0.087, P = 0.52$
Anterior surface CCR (mm)	$r = 0.051, P = 0.73$	$r = 0.138, P = 0.30$
Posterior surface CCR (mm)	$r = 0.053, P = 0.72$	$r = 0.244, P = 0.07$
ACD (mm)	$r = 0.101, P = 0.49$	$r = -0.469, P = 0.000^*$
LT (mm)	$r = -0.139, P = 0.34$	$r = 0.364, P = 0.01^*$
Curvature radius of the anterior surface of the lens (mm)	$r = 0.167, P = 0.25$	$r = -0.123, P = 0.36$
Curvature radius of the posterior surface of the lens (mm)	$r = -0.034, P = 0.82$	$r = 0.073, P = 0.59$
AL (mm)	$r = -0.773, P = 0.000^*$	$r = -0.734, P = 0.000^*$

Pearson correlation analysis was performed for all markers;  $^*P < 0.05$ .

CCT, central corneal thickness; CCR, anterior surface corneal curvature radius; ACD, anterior chamber depth; LT, lens thickness; AL, eye axis length.

In the control group, refractive status was negatively correlated with ACD and AL ( $r = -0.469, P = 0.000; r = -0.734, P = 0.000$ ), positively correlated with LT ( $r = 0.364, P = 0.01$ ), and not correlated with other indices in this group ( $P > 0.05$ ) (Table 4).

In full-term infants, the refractive state of the eye tended to undergo emmetropization, AL growth was accompanied by anterior chamber deepening and lens thinning ( $P < 0.05$ ). In the laser group, the ocular biomarkers were not significantly altered ( $P < 0.05$ ). Hence, the change in refractive state in children after ROP laser surgery was mainly related to the non-significant changes in ACD and LT (Table 4).

**TABLE 5 |** Correlations of gestational age at birth with eye biology and refractive status in the laser group.

Observation markers	Gestational age at birth
CCT (mm)	$r = 0.263, P = 0.07$
Anterior surface CCR (mm)	$r = 0.032, P = 0.83$
Posterior surface CCR (mm)	$r = -0.072, P = 0.62$
ACD (mm)	$r = 0.161, P = 0.26$
LT (mm)	$r = -0.168, P = 0.24$
Curvature radius of the anterior surface of the lens (mm)	$r = 0.086, P = 0.55$
Curvature radius of the posterior surface of the lens (mm)	$r = 0.279, P = 0.05$
AL (mm)	$r = 0.435, P = 0.002^*$
SE (D)	$r = -0.334, P = 0.02^*$
LogMAR (BCVA)	$r = -0.307, P = 0.03^*$

Pearson correlation analysis was performed for all markers;  $^*P < 0.05$ .

CCT, central corneal thickness; CCR, anterior surface corneal curvature radius; ACD, anterior chamber depth; LT, lens thickness; AL, eye axis length; SE, spherical equivalent; BCVA, best-corrected visual acuity; LogMAR, logarithm of the minimal angle of resolution.

## Correlations of Gestational Age at Birth With Ocular Biology and Refractive Status in the Laser Group

In the laser group, gestational age at birth was positively correlated with AL ( $t = 0.435, P = 0.002$ ), negatively correlated with SE ( $t = -0.334, P = 0.02$ ) and LogMAR (BCVA) ( $t = -0.307, P = 0.03$ ), and not correlated with other markers ( $P > 0.05$ ) (Table 5).

## DISCUSSION

ROP remains the leading cause of visual impairment in children globally. This condition can be prevented with early screening and interventions to avoid visual impairment and ocular atrophy (15). With improved neonatal intensive care techniques, more preterm infants with younger gestational age and lower weight are surviving, resulting in a high prevalence of ROP in many developing countries (16, 17). LP is based on the principle of ablating the avascular zone of the peripheral retina to reduce VEGF overproduction and, thus, induce regression of neovascularization. This procedure is currently the gold standard for the treatment of ROP (18, 19).

## Eye Development Patterns in Normal Children

In full-term infants, most of the growth and development of the eye occurs in the first year of life; thus, the period before 1 year of age is critical one the development of the anterior segment of the eye, emmetropization, and visual development. During the development of the human eye, different components of the optics system develop to prevent refractive errors, a functional tendency known as “emmetropization.” The key to emmetropization is a negative correlation between the length of the eye axis and the refractive powers of both the lens and



cornea. As the eye axis grows, the refractive state of the cornea and lens changes, with the anterior chamber deepening while corneal curvature and lens thickness begin to decrease and the cornea gradually flattens (20).

Previous studies investigating the refractive status of adolescents have shown that there are no significant differences in the examination results or final refraction value after pupil recovery between pupil dilation with compound tropicamide drops and with atropine ophthalmic ointment (21). In the past, ophthalmic examination after pupil dilation with atropine ophthalmic ointment for definite diagnosis has mainly been advocated to avoid the occurrence of inadequate relaxation effects due to excessive accommodation. However, the use of atropine ophthalmic ointment leads to the maintenance of pupil dilation for a relatively long time, and side effects such as redness and dryness of the skin or mucosa can occur (22). In addition, the children included in the present study were mostly examined over the weekend and had to attend school on the following Monday. Therefore, tropicamide was administered as it is a short-acting ciliary muscle-paralyzing agent with a more rapid onset and shorter duration of action than atropine ophthalmic ointment, which enabled the restoration of normal vision within the day of examination and avoided affecting the school activities of the children on the following day. Studies have shown that there are no significant differences in the results of ophthalmic examination between the use of atropine and tropicamide, indicating that tropicamide eye drops can serve as a substitute in situations where the use of atropine ophthalmic ointment is not appropriate. Therefore, all children included in this study were provided compound tropicamide drops for pupil dilation prior to the examinations.

## Comparisons of Ocular Biomarkers and Refractive Status Between the Two Groups

We observed a thinner central corneal thickness, steeper corneal morphology, shallower anterior chamber, thicker lens, “round” lens morphology, shorter eye axis, and poorer refractive status in children in the laser group compared to those in full-term infants (Table 2). The causes of these changes in the anterior segment structure and refractive status include changes in retinal tissue anatomy after ROP laser surgery affecting signals from the retina and/or the sclera’s reception and response to these signals required for eye development; delayed or affected normal development of the sclera, resulting in “abnormal” anterior segment structure development; and effects on emmetropization of the eye, leading to abnormalities in the development of the anterior segment tissue (10, 11, 23). Laser-treated eyes show a thinner and steeper cornea, which is contrary to the developmental trend of progressively flatter corneal morphology during emmetropization. LP affects the emmetropization process of the postoperative eye by hindering the corneal flattening process. The corneas of children after ROP laser surgery are also steeper than those of full-term infants; these children also show increased refractive error and a higher risk of myopia. Fielder et al. (24) reported that preterm infants had a “thermal defect” of 1.0 to 2.0°C that was never compensated for postnatally compared to

full-term infants. Moreover, reduced relative ocular temperature after birth decreases the likelihood of ocular growth in preterm infants, leading to reduced flattening of the corneal geometry during emmetropization, resulting in a steeper corneal shape in myopia. This hypothesis is supported by animal studies in which changes in the “thermal gradient” of the ocular surface were a contributing factor to myopia (25). Thus, steep corneal morphology is related to both prematurity itself and laser treatment, with a combination of contributing factors. Steeper corneas enhance the traction on the central cornea, resulting in a thinner central corneal thickness compared to those in full-term infants.

Wu et al. (26) reported disrupted tissue in the avascular zone of the peripheral retina and blocked local growth signal from the peripheral retina after laser treatment, resulting in altered ciliary or lens development with a thickened lens. We also observed changes in anterior chamber depth and lens, with a thickened lens and a shallow anterior chamber. We speculate that, due to the increased lens thickness, the anterior surface of the lens moved forward, causing the anterior chamber to become shallow, a finding consistent with those of previous related studies (5).

After ROP laser treatment, eye axis development is shorter than that in full-term infants due to extensive peripheral retinal destruction and glial cell proliferation, which alter eye growth and development and affect emmetropization; thus, the process of eye axis growth is hindered (4).

In normal eye development, the refractive state tends to be emmetropic at 9 years of age. The results of our study indicated that ROP laser treatment affected the normal development of the anterior segment structures in children, resulting in steeper corneal morphology, a “rounded” lens, increased refractive power, and a higher incidence of myopia in postoperative children.

## Correlation of Age With Ocular Biomarkers and Refractive Status Between the Two Groups

We observed that the changes in central corneal thickness, anterior chamber depth, and lens thickness in children in the laser group did not change significantly with age compared to full-term infants (Table 3), indicating damage to the tissue of the avascular zone of the retina in the peripheral part of children after ROP laser surgery and blocking of the local growth signal from the peripheral part of the retina, which affected the normal cornea and lens development. These abnormalities in the development of the anterior segment of the eye lead to changes in the refractive power postoperatively, resulting in poorer visual acuity.

We observed a positive correlation between age and eye axis and a negative correlation with refractive status in both the laser and control groups in the present study (Table 3), indicating that the eye axis gradually increases with age and that the BCVA improved gradually in both groups of children, consistent with the natural patterns of eye axis and visual acuity development during postnatal emmetropization. Comparisons of the differences in eye axis and BCVA between the two groups showed shorter eye axis and poorer BCVA after ROP laser

treatment compared to those in full-term infants. We could not compare the differences in these factors between these two groups of children as they developed over a longer time. Thus, additional studies with larger sample sizes and longer follow-up periods are needed to verify our findings.

## Correlations Between Ocular Biomarkers and Refractive Status in the Two Groups

In this study, the refractive status of full-term infants was negatively correlated with AL and ACD and positively correlated with LT, while the refractive status of children after ROP laser treatment was negatively correlated with AL and not with other biomarkers (Table 4). During emmetropization, the eye axis grows gradually. Following ROP laser treatment in children, ACD and LT are not as significantly developed compared to those in full-term children, which leads to changes in refractive status in children after ROP laser treatment. Fieß et al. (27) observed little correlation between steep corneal morphology and refractive error. Presumably, alterations in lens development play a more important role in changes in refractive development. Garcia-Valenzuela and Kaufman (28) also concluded that children were more prone to refractive error after ROP laser surgery and that changes in refractive status were mainly influenced by changes in the lens. The change in anterior chamber depth is greatly influenced by lens thickness and morphology, which has a greater impact on the refractive status. The results of the present study confirm that the development of the lens in children after ROP laser is blocked, the lens is thicker, and the refractive capacity of the lens is enhanced, which make these children more susceptible to myopia.

## Correlation of Gestational Age at Birth With Ocular Biomarkers and Refractive Status in Children in the Laser Group

The results of the present study analyzing the correlation between gestational age at birth and biological development of the eye in children in the laser group showed that gestational age was positively correlated with the eye axis and negatively correlated with LogMAR (BCVA), while there were no correlations with other markers (Table 5). Thus, the younger the gestational age at birth, the slower the development of the eye axis in preterm children, the shorter the eye axis, and the poorer visual acuity development compared to those in full-term infants. Ozdemir et al. (8) reported a lower gestational age at birth was associated with poorer visual acuity development in preterm children. Their analysis of gestational age at birth, and ocular biological parameters showed that gestational age at birth was positively correlated with anterior chamber depth, lens thickness, and ocular axis length, with a higher correlation with the eye axis length. These previous findings are not entirely consistent with those of the present study. One possible reason for discordance may be the short follow-up period of the children in this study. Therefore, additional studies with a larger population are required to verify these findings.

## Study Limitations

This retrospective study included no pre-term infants without ROP or children with ROP degenerative. Hence, we cannot rule out whether the change in ocular biology and refractive status was entirely due to prematurity itself or to laser photocoagulation. Further confirmation is needed by increasing the subgroup types and sample sizes in the follow-up cases. The severity of the condition on ROP treatment and laser spots that were not completely identical may have resulted in some bias in data analysis. The follow-up periods for both groups of children were short and only one set of cross-sectional phase comparison data was observed. In future studies, the follow-up time will be increased, and the longitudinal follow-up study will be increased.

## CONCLUSION

### Children Were More Prone to Myopia After ROP Laser Surgery

Compared to full-term infants, pre-mature children who underwent ROP laser surgery showed delayed development of the biological structure of the eye, a steeper cornea, a shallow anterior chamber, a thicker lens, and a shorter eye axis, leading to a greater risk of myopia in postoperatively.

### Myopia Occurred in Children After ROP Laser Surgery Mainly Due to Increased Lens Thickness, for Which Gestational Age at Birth Is Also an Important Cause

The results of this study showed that the occurrence of myopia in children after ROP laser surgery was mainly caused by lens increased thickness. The lower the birth gestational age of the child who underwent post-ROP laser surgery, the more the emmetropization of the eye was affected and the more likely it was to lead to the development of myopia.

## DATA AVAILABILITY STATEMENT

The raw data supporting the conclusions of this article will be made available by the authors, without undue reservation.

## ETHICS STATEMENT

The studies involving human participants were reviewed and approved by Medical Ethics Committee of Shenzhen Eye Hospital. Written informed consent to participate in this study was provided by the participants' legal guardian/next of kin.

## AUTHOR CONTRIBUTIONS

XZ, RT, YC, HH, and GZ: performing the screening and diagnosis of ROP. XZ, HH, and MC: collection and assembly of data. XZ, LZ, JZ, JH, and GZ: data analysis and interpretation. All authors contributed to the study conception and design, manuscript writing, and final approval of manuscript.

## FUNDING

This work was supported by the Construction Fund of Medical Key Disciplines of Shenzhen (No. SZXK038), Guangdong

Provincial Key High-level Clinical Specialty (Supporting Construction Funds of Shenzhen) (No. SZGSP014), Shenzhen-Hong Kong Joint Funded Projects (Category A), and the Project of Discipline Layout (Item No: JCYJ20170817112542555).

## REFERENCES

- Fieß A, Kölb-Keerl R, Schuster AK, Knuf M, Kirchhof B, Muether PS, et al. Prevalence and associated factors of strabismus in former preterm and full-term infants between 4 and 10 years of age. *BMC Ophthalmol.* (2017) 17:1228. doi: 10.1186/s12886-017-0605-1
- Wongwai P, Suwannaraj S, Asawaphureekorn S. Diagnostic accuracy of a digital fundus photographic system for detection of retinopathy of prematurity requiring treatment (ROP-RT). *PloS ONE.* (2018) 13:e0201544. doi: 10.1371/journal.pone.0201544
- Good WV. Final results of the Early Treatment for Retinopathy of Prematurity (ETROP) randomized trial. *Trans Am Ophthalmol Soc.* (2004) 102:233–48; discussion 48–50.
- Wang J, Ren X, Shen L, Yanni SE, Leffler JN, Birch EE. Development of refractive error in individual children with regressed retinopathy of prematurity. *Investig Ophthalmol Vis Sci.* (2013) 54:6018–24. doi: 10.1167/iov.13-11765
- McLoone EM, O'Keefe M, McLoone SF, Lanigan BM. Long-term refractive and biometric outcomes following diode laser therapy for retinopathy of prematurity. *J AAPOS.* (2006) 10:454–9. doi: 10.1016/j.jaapos.2006.05.005
- Yang CS, Wang AG, Shih YF, Hsu WM. Long-term biometric optic components of diode laser-treated threshold retinopathy of prematurity at 9 years of age. *Acta Ophthalmol.* (2013) 91:e276–82. doi: 10.1111/aos.12053
- Venincasa VD, Bugg V, Dvorak J, Ding K, Bhatti F, Siatkowski RM. Temporal profile of retinopathy of prematurity in extremely premature compared to premature infants. *J Pediatr Ophthalmol Strabismus.* (2019) 56:116–23. doi: 10.3928/01913913-20190205-01
- Ozdemir O, Tunay ZO, Acar DE, Erol MK, Sener E, Acar U. The relationship of birth weight, gestational age, and postmenstrual age with ocular biometry parameters in premature infants. *Arquivos Brasil Oftalmol.* (2015) 78:146–9. doi: 10.5935/0004-2749.20150038
- Ophthalmology Group of Chinese Medical Association Ophthalmology Branch. Screening guidelines for retinopathy of prematurity in China 2014. *Chin J Ophthalmol.* (2014) 50:933–5. doi: 10.3760/cma.j.issn.0412-4081.2014.12.017
- Fierion WM. Screening examination of premature infants for retinopathy of prematurity. *Pediatrics.* (2018) 142:e20183061. doi: 10.1542/peds.2018-3061
- Zhang M, Xu G, Wang X, Ni Y, Huang X. Rate and treatment of retinopathy of prematurity in extremely low birth weight infants with gestational age  $\leq 28$  weeks in eastern China. *Risk Manage Healthc Policy.* (2020) 13:2867–73. doi: 10.2147/RMHP.S282102
- Lyu J, Zhang Q, Chen C, Xu Y, Ji X, Zhao P. Ranibizumab injection and laser photocoagulation to treat type 1 retinopathy of prematurity after 40 weeks post menstrual age: a retrospective case series study. *BMC Ophthalmol.* (2019) 19:60. doi: 10.1186/s12886-019-1067-4
- Song JS, Yoon DY, Hyon JY, Jeon HS. Comparison of ocular biometry and refractive outcomes using IOL master 500, IOL master 700, lenstar LS900. *Korean J Ophthalmol.* (2020) 34:126–32. doi: 10.3341/kjo.2019.0102
- Chen YS, Chen HL, Lu CH, Lee CY, Chou KH, Chen MH, et al. The corticolimbic structural covariance network as an early predictive biosignature for cognitive impairment in Parkinson's disease. *Sci Rep.* (2021) 11:862. doi: 10.1038/s41598-020-79403-x
- Brown AC, Nwanyanwu K. *Retinopathy of Prematurity*. Treasure Island, FL: StatPearls. (2021).
- Cayabyab R, Ramanathan R. Retinopathy of prematurity: therapeutic strategies based on pathophysiology. *Neonatology.* (2016) 109:369–76. doi: 10.1159/000444901
- Kong L, Fry M, Al-Samarraie M, Gilbert C, Steinkuller PG. An update on progress and the changing epidemiology of causes of childhood blindness worldwide. *J AAPOS.* (2012) 16:501–7. doi: 10.1016/j.jaapos.2012.09.004
- Martínez-Castellanos MA, González HLA, Romo-Aguas JC, Gonzalez-Gonzalez LA. A proposal of an algorithm for the diagnosis and treatment of recurrence or treatment failure of retinopathy of prematurity after anti-VEGF therapy based on a large case series. *Graefes Arch Clin Exp Ophthalmol.* (2020) 258:767–72. doi: 10.1007/s00417-020-04605-y
- Wang F, Hao LX. Efficacy and safety of laser therapy for the treatment of retinopathy of prematurity: a protocol for systematic review of randomized controlled trials. *Medicine.* (2020) 50:e23282. doi: 10.1097/MD.00000000000023282
- Gordon RA, Donzis PB. Refractive development of the human eye. *Arch Ophthalmol.* (1985) 103:785–9. doi: 10.1001/archophth.1985.01050060045020
- Kremer LJ, Reith DM, Medlicott N, Broadbent R. Systematic review of mydriatics used for screening of retinopathy in premature infants. *BMJ Paediatr Open.* (2019) 3:e000448. doi: 10.1136/bmjpo-2019-000448
- Whelan NC, Castillo-Alcala F, Lizarraga I. Efficacy of tropicamide, homatropine, cyclopentolate, atropine and hyoscine as mydriatics in Angora goats. *N Z Vet J.* (2011) 59:328–31. doi: 10.1080/00480169.2011.609476
- Multicenter trial of cryotherapy for retinopathy of prematurity. Preliminary results. Cryotherapy for retinopathy of prematurity cooperative group. *Arch Ophthalmol.* (1988) 106:471–9. doi: 10.1001/archophth.1988.01060130517027
- Fielder AR, Levene MI, Russell-Eggitt IM, Weale RA. Temperature—a factor in ocular development?. *Dev Med Child Neurol.* (1986) 28:279–84. doi: 10.1111/j.1469-8749.1986.tb03873.x
- Hodos W, Revzin AM, Kuenzel WJ. Thermal gradients in the chick eye: a contributing factor in experimental myopia. *Investig Ophthalmol Vis Sci.* (1987) 28:1859–66.
- Wu LH, Yang YH, Lin CH, Lin YJ, Cheng CL. Hypotension associated with intravitreal bevacizumab therapy for retinopathy of prematurity. *Pediatrics.* (2016) 137:e20152005. doi: 10.1542/peds.2015-2005
- Fieß A, Nickels S, Schulz A, Münzel T, Wild PS, Beutel ME, et al. The relationship of ocular geometry with refractive error in normal and low birth weight adults. *J Optometry.* (2021) 14:50–7. doi: 10.1016/j.optom.2020.08.004
- Garcia-Valenzuela E, Kaufman LM. High myopia associated with retinopathy of prematurity is primarily lenticular. *J AAPOS.* (2005) 9:121–8. doi: 10.1016/j.jaapos.2004.12.018

**Conflict of Interest:** The authors declare that the research was conducted in the absence of any commercial or financial relationships that could be construed as a potential conflict of interest.

**Publisher's Note:** All claims expressed in this article are solely those of the authors and do not necessarily represent those of their affiliated organizations, or those of the publisher, the editors and the reviewers. Any product that may be evaluated in this article, or claim that may be made by its manufacturer, is not guaranteed or endorsed by the publisher.

Copyright © 2022 Zeng, Chen, Zheng, Tian, Chen, He, Zeng, He and Zhang. This is an open-access article distributed under the terms of the Creative Commons Attribution License (CC BY). The use, distribution or reproduction in other forums is permitted, provided the original author(s) and the copyright owner(s) are credited and that the original publication in this journal is cited, in accordance with accepted academic practice. No use, distribution or reproduction is permitted which does not comply with these terms.



# Treat-and-Extend vs. Pro Re Nata Regimen of Ranibizumab for Diabetic Macular Edema—A Two-Year Matched Comparative Study

Tso-Ting Lai<sup>1,2</sup>, Ta-Ching Chen<sup>1</sup>, Chang-Hao Yang<sup>1,3</sup>, Chung-May Yang<sup>1,3</sup>, Tzzy-Chang Ho<sup>1</sup> and Yi-Ting Hsieh<sup>1\*</sup>

<sup>1</sup> Department of Ophthalmology, National Taiwan University Hospital, Taipei, Taiwan, <sup>2</sup> College of Medicine, Graduate Institute of Clinical Medicine, National Taiwan University, Taipei, Taiwan, <sup>3</sup> College of Medicine, National Taiwan University, Taipei, Taiwan

**Purpose:** To compare 2-year treatment outcomes of ranibizumab using treat-and-extend (T&E) or pro re nata (PRN) regimens for diabetic macular edema (DME) in clinical settings.

**Methods:** We retrospectively enrolled 34 patients (34 eyes) with DME treated with ranibizumab using the T&E regimen, and 34 patients (34 eyes) treated with ranibizumab using the PRN regimen and matched to cases in the treat-and-extend group by baseline best-corrected visual acuity (BCVA) and central foveal thickness (CFT). BCVA and CFT changes, number of injections and recurrence of macular edema over 2 years were compared between the groups.

**Results:** The average BCVA gain in the T&E and PRN groups was 16.2 and 7.6 ETDRS letters at 2 years ( $p = 0.011$ ), respectively. The mean CFT reduction was  $145.5 \pm 127.3$  and  $97.3 \pm 152.5 \mu\text{m}$  in the T&E and PRN groups at 2 years ( $p = 0.035$ ), respectively. The T&E group had a higher proportion of patients with BCVA gain  $\geq 15$  letters at months 18 ( $p = 0.015$ ) and 24 ( $p = 0.029$ ) than the PRN group. During the 2-year treatment periods, the T&E group received more injections than the PRN group ( $11.0 \pm 3.2$  vs.  $6.2 \pm 2.0$ ;  $p < 0.001$ ), while the PRN group had more recurrence of macular edema than the T&E group (71 vs. 41%;  $p = 0.015$ ).

**Conclusions:** After 2-year ranibizumab treatment for DME, better visual and anatomical improvement and less recurrence of macular edema were achieved in the T&E group, with more injections administered.

**Keywords:** diabetic macular edema, ranibizumab, anti-VEGF (vascular endothelial growth factor), pro re nata (PRN), treat-and-extend (T&E)

## INTRODUCTION

Currently, the first-line treatment for diabetic macular edema (DME), a condition that leads to severe visual impairment in 28–29% of patients with diabetes mellitus (1), is anti-vascular endothelial growth factor (VEGF) therapy (2). The superior effectiveness over laser photocoagulation in improving visual acuity and reducing edema in DME has been demonstrated

## OPEN ACCESS

### Edited by:

Shaochong Zhang,  
Sun Yat-sen University, China

### Reviewed by:

Miho Nozaki,  
Nagoya City University, Japan  
Mengju Tsai,  
Tao Yuan General Hospital, Ministry of  
Health and Welfare, Taiwan  
Vivek Dave,  
LV Prasad Eye Institute, India

### \*Correspondence:

Yi-Ting Hsieh  
ythtyh@gmail.com

### Specialty section:

This article was submitted to  
Ophthalmology,  
a section of the journal  
Frontiers in Medicine

**Received:** 22 September 2021

**Accepted:** 06 December 2021

**Published:** 25 January 2022

### Citation:

Lai T-T, Chen T-C, Yang C-H,  
Yang C-M, Ho T-C and Hsieh Y-T  
(2022) Treat-and-Extend vs. Pro Re  
Nata Regimen of Ranibizumab for  
Diabetic Macular Edema—A Two-Year  
Matched Comparative Study.  
Front. Med. 8:781421.  
doi: 10.3389/fmed.2021.781421



in several clinical trials (3–7). With various treatment protocols applied in different studies, patients were able to gain 6.1–10.3 Early Treatment Diabetic Retinopathy Study (ETDRS) letters of vision in 1 year. Furthermore, visual benefits could be maintained after 4–5 years with continuous anti-VEGF injections (8, 9). However, the favorable outcomes from these clinical trials did not always translate into similar results in clinical practice settings. Globally, real-world clinical practice studies have reported poorer visual improvements along with the use of fewer injections than reported in clinical trials (10–14). The need for frequent follow-up visits and repeated injections, along with other factors, leads to poor compliance in patients with DME and is responsible for the inferior outcomes in real-world studies (14).

Different treatment protocols for anti-VEGF therapy have been developed in recent years to optimize the treatment effects and cost effectiveness. A fixed dosing regimen, either monthly or bimonthly treatment after a loading phase, was proven to be effective in phase III registrational trials, such as RISE, RIDE (7), VIVID and VISTA (15), but was difficult to follow in real-world clinical practice. An “as needed” or *pro re nata* (PRN) approach was developed to decrease the number of injections while maintaining a fixed follow-up schedule to closely monitor treatment responses. Clinical trials using the PRN regimen reduced the mean injections to 7–10 in the first year with monthly monitoring (3, 5, 6, 16). A treat-and-extend (T&E) regimen, different from other protocols, involved gradual increase in duration between each follow-up visit once the patient achieved a preset “stable” condition along with an injection administered at every visit (17). The RETAIN study (18) first reported the use of the T&E protocol for patients with DME and found a similar visual improvement as that with the PRN regimen, while reducing 46% of clinic visits. The TREX-DME study (19) further demonstrated similar visual and anatomical improvements in both T&E and monthly dosing groups in their 2-year results, with significantly reduced injections using their T&E algorithm. The sustainable efficiency of the T&E regimen and its ability to reduce treatment burden shown in clinical trials may further benefit patients in real-world conditions. However, there is limited evidence regarding the use of the T&E protocol in DME in clinical settings.

Herein, we compared the 2-year real-world visual and anatomical outcomes of patients with DME treated with either the T&E or PRN regimen to better understand their efficacy in clinical practice setting.

## METHODS

### Study Population and Setting

In this matched comparative study, we retrospectively reviewed all patients who received their first anti-VEGF injection for DME at the National Taiwan University Hospital between November 2014 and November 2016. Patients who received intravitreal injection (IVI) of 0.5 mg ranibizumab (Lucentis®, Genentech, San Francisco, CA/Norvartis, Basel, Switzerland) following a T&E regimen and who were followed up for at least 2 years were included in the study (T&E) group. The same number of patients who received ranibizumab injection using a PRN protocol during

the same period and were matched to the cases in the T&E group by baseline best-corrected visual acuity (BCVA) (difference  $\leq 1$  line) and baseline central foveal thickness (CFT) (difference  $\leq 10\%$ ) on optical coherence tomography (OCT), were randomly selected and included in the control (PRN) group. The other inclusion criteria were as follows: baseline Snellen BCVA between 20/400 and 20/40, baseline CFT above 300  $\mu\text{m}$ , and evidence of DME on fluorescence angiography (FA) without other causes of macular edema. Patients who had received anti-VEGF therapy at another hospital or for other etiologies within 6 months prior to the first injection at our hospital were excluded. Patients who underwent intraocular surgery other than IVI (such as cataract surgery or vitrectomy) during the study period and those who used different anti-VEGF agents during the follow-up period were also excluded. This study adhered to the tenets of the Declaration of Helsinki. The National Taiwan University Hospital Research Ethics Committee approved the study (No.: 201811023RIFD), and waiver of informed consent was obtained due to its retrospective nature.

### Treatment Protocols

All patients received 3-monthly loading injections of ranibizumab. After the loading phase, patients in the T&E group could extend their follow-up and treatment visits if they had no disease activity on OCT images and the BCVA was either improved or stable compared to that at the last visit. The follow-up interval was extended by 4 weeks each time, starting from 4 weeks at baseline. The longest allowed follow-up interval was 24 weeks. An injection was administered at each visit after the BCVA was measured and the OCT image was acquired. The follow-up interval was shortened by 4 weeks if OCT revealed new disease activity, with a minimum of 4 weeks between each visit.

In the PRN group, the patients received monthly injections after the loading phase until the OCT image showed no disease activity and the BCVA was either improved or stable compared to that at the last visit. The patients then received regular follow-up, usually every 1–3 months, as determined by the treating physician and the patient, and received no further injection unless recurrence of disease activity was noted on OCT during follow-up.

Disease activity on OCT was defined as fluid accumulation (either intraretinal or subretinal) with a CFT  $> 300 \mu\text{m}$ . For patients with persistent disease activity after the loading treatment, the physicians might add supplementary treatments, including macular laser or subtenon injection of triamcinolone acetonide. For patients with decreased but persistent disease activity after 5 monthly injections of ranibizumab, we extended the treatment interval (in the T&E group) or discontinued the treatment (in the PRN group). Details of the treatment protocols are shown in **Supplementary Table 1**.

### Clinical Data Collection

Baseline demographic data, including age, sex, serum HbA1c, and previous treatments such as focal/grid laser, steroid injections, panretinal photocoagulation, and anti-VEGF injection, were recorded. The BCVA was converted to the logarithm of the minimum angle of resolution (logMAR)

score for calculation, and the change in BCVA was converted to a number of ETDRS letters. All patients underwent FA examination at baseline, and the images were reviewed independently by two retinal specialists (TTL and YTH) for the presence of proliferative diabetic retinopathy. All OCT images at baseline were reviewed by the two investigators for the presence of epiretinal membrane (ERM), intraretinal cyst (IRC), subretinal fluid (SRF), hyperreflective foci (HF), ellipsoid zone (EZ) disruption, and disorganization of the retinal inner layers (DRIL). The CFT was measured using the central 1-mm thickness built-in thickness map program of RTVue OCT (Optovue, Inc., Fremont, CA). The numbers of injections and clinic visits for each patient in the first and second years were recorded. The number of recurrences of DME, defined as disease activity on OCT leading to shortening of the treatment interval in the T&E group or restart of IVI in the PRN group, was also documented.

## Statistical Analysis

The BCVA and CFT at preset time points (at baseline and at 3, 6, 12, 18, and 24 months after the first injection) were evaluated, with the last observation carried forward method used for any missing data because of the individualized follow-up schedule. For comparison between the T&E and PRN groups, we used paired *t*-tests for all continuous variables and Fisher's exact tests for all categorical variables. The proportions of patients with BCVA gain  $\geq 15$  letters or with visual loss  $\geq 5$  letters at each time point were compared between the two groups. The comparison of BCVA and CFT between baseline and different follow-up time points for individual patients was performed using paired *t*-tests. Factors associated with the final BCVA improvement were analyzed using linear regression. Baseline BCVA, baseline OCT biomarkers (CFT, IRC, SRF, HF, DRIL, and EZ disruption), treatment protocol, total number of injections, and recurrence of macular edema were included in the univariate analysis with adjustment for age and baseline BCVA and CFT. Factors that were significantly associated with final BCVA improvement in the univariate analysis were then included in the multivariate linear regression using the stepwise approach. Data were analyzed using SPSS software (SPSS 22.0; SPSS Inc., Chicago, IL, USA). Statistical significance was set at  $p < 0.05$ .

## RESULTS

### Baseline Characteristics

Thirty-four eyes of 34 patients with DME who received ranibizumab injection using a T&E protocol were included in the study group, and 34 eyes of 34 patients treated under a PRN protocol were included in the control group. The baseline demographics and OCT findings of the two groups are summarized in **Table 1**. The two groups were matched for the baseline BCVA and CFT, and there were no differences in age, sex, previous treatments, or severity of diabetic retinopathy between the two groups. As for OCT biomarkers, the proportions of patients with ERM, IRC, SRF, HF, and EZ disruption at baseline were similar in both groups, except that more patients in the PRN group had DRIL at baseline.

**TABLE 1 |** Baseline characteristics and optical coherence tomographic findings of patients with diabetic macular edema who underwent anti-vascular endothelial growth factor therapy using pro re nata or treat-and-extend protocol.

	PRN 34 eyes	T&E 34 eyes	P-value
Age (years, mean $\pm$ SD)	62.3 $\pm$ 7.3	60.6 $\pm$ 8.8	0.377
Sex (M:F)	21:13	17:17	0.329
HbA1c (mean $\pm$ SD)	7.54 $\pm$ 1.10	7.42 $\pm$ 1.18	0.677
Pseudophakic (No./%)	5 (14.7)	8 (23.5)	0.355
PDR (No./%)	14 (41.2)	17 (50.0)	0.465
PRP (No./%)	12 (35.3)	11 (32.4)	0.798
Previous anti-VEGF (No./%)	7 (20.6)	6 (17.6)	0.758
Previous non-anti-VEGF treatment (No./%)	3 (8.8)	5 (14.7)	0.709
Preoperative BCVA (logMAR, mean $\pm$ SD)	0.710 $\pm$ 0.310	0.723 $\pm$ 0.333	0.487
<b>Baseline OCT features</b>			
CFT ( $\mu$ m, mean $\pm$ SD)	446.2 $\pm$ 126.7	438.2 $\pm$ 119.2	0.629
ERM (No./%)	9 (26.5)	5 (14.7)	0.369
IRC (No./%)	33 (91.1)	31 (91.2)	0.614
SRF (No./%)	12 (35.3)	9 (26.5)	0.431
DRIL (No./%)	24 (70.6)	10 (29.4)	0.001
HF (No./%)	31 (91.2)	30 (88.2)	1.000
EZ disruption (No./%)	20 (58.8)	15 (44.1)	0.225

BCVA, best-corrected visual acuity; CFT, central foveal thickness; DRIL, disorganization of retinal inner layers; ERM, epiretinal membrane; EZ, ellipsoid zone; HF, hyperreflective foci; IRC, intraretinal cyst; logMAR, logarithm of the minimum angle of resolution; OCT, optical coherence tomography; PDR, proliferative diabetic retinopathy; PRN, pro re nata; PRP, panretinal photocoagulation; SD, standard deviation; SRF, subretinal fluid; T&E, treat-and-extend; VEGF, vascular endothelial growth factor.

**TABLE 2 |** Treatment outcomes of patients with diabetic macular edema who underwent anti-vascular endothelial growth factor therapy using ranibizumab with pro re nata or treat-and-extend protocol.

	PRN 34 eyes	T&E 34 eyes	P-value
<b>OPD visits (mean <math>\pm</math> SD)</b>			
Year 1	6.9 $\pm$ 2.0	7.4 $\pm$ 1.7	0.270
Year 2	5.8 $\pm$ 1.6	5.5 $\pm$ 1.8	0.560
Total	12.7 $\pm$ 2.6	12.9 $\pm$ 3.1	0.782
<b>Injection numbers (mean <math>\pm</math> SD)</b>			
Year 1	4.9 $\pm$ 1.5	7.6 $\pm$ 1.8	<0.001
Year 2	1.3 $\pm$ 1.2	3.5 $\pm$ 1.9	<0.001
Total	6.2 $\pm$ 2.0	11.0 $\pm$ 3.2	<0.001
Recurrence of macular edema (No./%)	24 (70.6)	14 (41.2)	0.015
VH (No./%)	5 (14.7)	3 (8.8)	0.709
BCVA at 12 months (logMAR, mean $\pm$ SD)	0.615 $\pm$ 0.386	0.437 $\pm$ 0.247	0.005
BCVA at 24 months (logMAR, mean $\pm$ SD)	0.559 $\pm$ 0.417	0.398 $\pm$ 0.294	0.021
CFT at 12 months ( $\mu$ m, mean $\pm$ SD)	321.8 $\pm$ 151.8	289.1 $\pm$ 65.1	0.287
CFT at 24 months ( $\mu$ m, mean $\pm$ SD)	348.9 $\pm$ 141.1	293.2 $\pm$ 62.7	0.019

BCVA, best corrected visual acuity; CFT, central foveal thickness; logMAR, logarithm of the minimum angle of resolution; OPD, outpatient clinic; PRN, pro re nata; SD, standard deviation; T&E, treat-and-extend; VH, vitreous hemorrhage.

## Visual Outcomes

In both groups, the BCVA improved significantly at months 3, 6, 12, 18, and 24 compared to that at the baseline, except for a borderline significance at month 12 in the PRN group ( $p < 0.001$  at every time point in the T&E group;  $p < 0.001$ ,  $p = 0.012$ ,  $0.084$ ,  $0.036$ , and  $0.006$  in the PRN group at 3, 6, 12, 18, and 24 months, respectively). The average BCVA was significantly better in the T&E group at month 12 ( $0.437 \pm 0.247$  [95% CI, 0.351–0.524]) and month 24 ( $0.398 \pm 0.294$  [95% CI, 0.296–0.501]) than in the PRN group (month 12:  $0.615 \pm 0.386$  [95% CI, 0.481–0.750],  $p = 0.005$ ; month 24:  $0.559 \pm 0.417$  [95% CI, 0.414–0.704],  $p = 0.021$ ; **Table 2**). The mean changes in BCVA at different time points are shown in **Figure 1A**. The average BCVA gains were 7.0, 10.8, 14.3, 14.4, and 16.2 ETDRS letters in the T&E group at months 3, 6, 12, 18, and 24, respectively, which showed a continuous increase from month 3 to month 24. On the other hand, the

BCVA gains remained constant from month 3 to month 24 in the PRN group (6.9, 6.9, 4.8, 6.6, and 7.6 letters at months 3, 6, 12, 18, and 24, respectively), and were significantly lower than those in the T&E group at 12, 18, and 24 months ( $p = 0.003$ ,  $0.013$ , and  $0.011$ , respectively).

**Figure 2** shows the proportions of patients with VA gain  $\geq 15$  letters and those with VA loss  $\geq 5$  letters. The T&E group had a higher proportion of patients with VA gain  $\geq 15$  letters at months 18 ( $p = 0.015$ ) and 24 ( $p = 0.029$ ) than the PRN group. On the other hand, a lower proportion of patients in the T&E group had VA loss  $\geq 5$  letters at month 6 than those in the PRN group ( $p = 0.025$ ).

## Anatomical Outcomes

The CFTs at months 12 and 24 in both groups are shown in **Table 2**. The CFT was significantly lower in the T&E group than

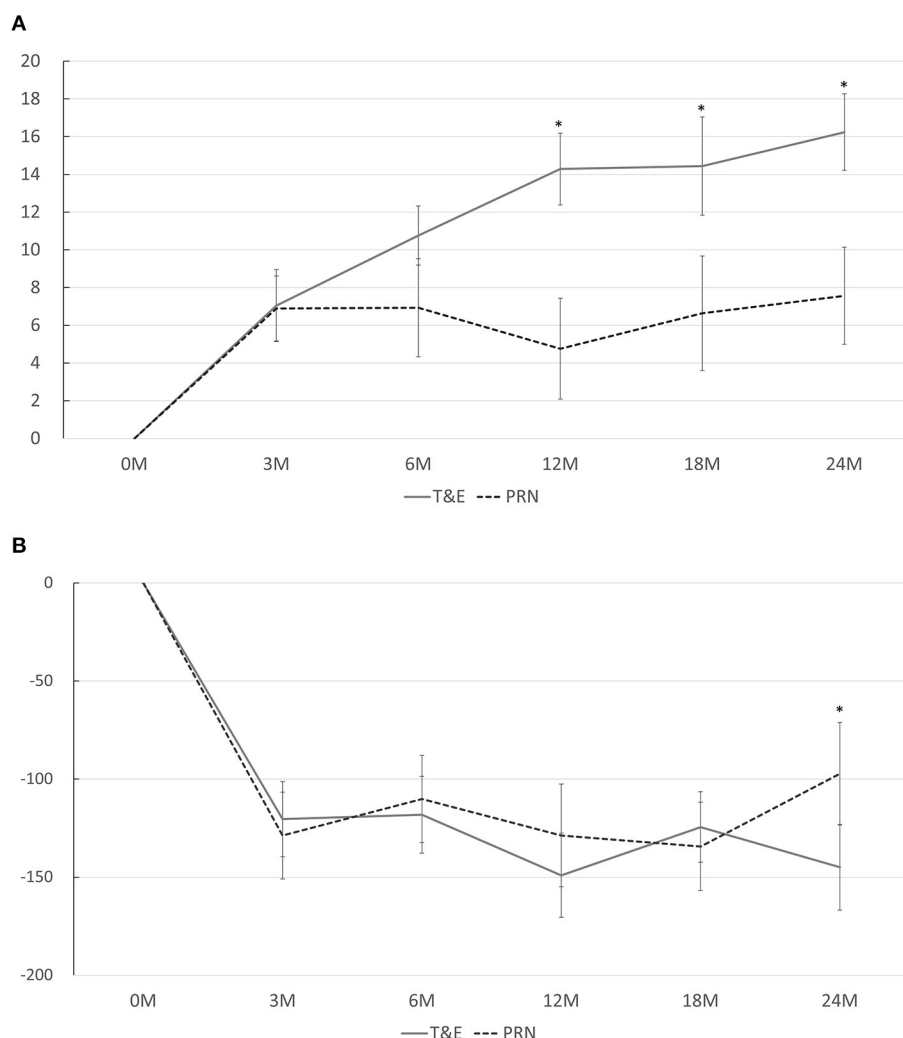


**FIGURE 1 | (A)** Mean changes in the best-corrected visual acuity from baseline at different time points. A significant difference between the T&E and PRN groups is found at 12, 18, and 24 months. **(B)** Mean changes in the central foveal thickness from baseline at different time points. A significant difference between the T&E and PRN groups is found at 24 months. T&E, treat-and-extend; PRN, pro re nata. \* $p < 0.05$ .

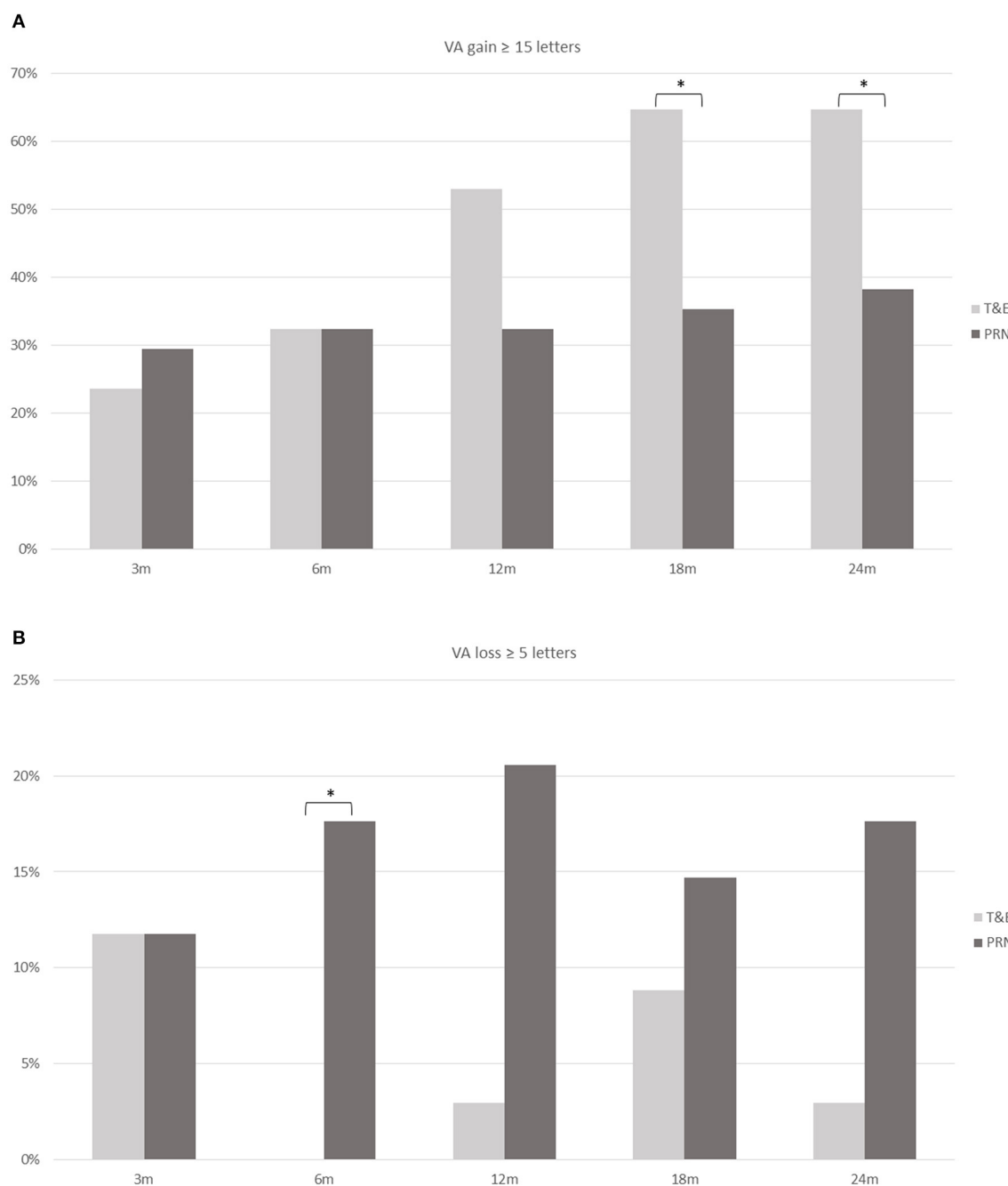


**FIGURE 2 |** The proportion of patients who achieved a gain of  $\geq 15$  ETDRS letters (**A**) and those who had a loss of  $\geq 5$  letters (**B**) at different time points in the T&E and PRN groups. A significant difference (asterisk) is found at 18 and 24 months in those who gained  $\geq 15$  letters and at 6 months in those who had a loss of  $\geq 5$  letters. ETDRS, Early Treatment Diabetic Retinopathy Study; T&E, treat-and-extend; PRN, pro re nata; VA, visual acuity. \* $p < 0.05$ .

in the PRN group at month 24 ( $p = 0.019$ ) but not at month 12 ( $p = 0.287$ ). While the CFT in each group significantly reduced at every time point compared to that at the baseline, no difference was found between the CFT reductions in both groups at each time point except for month 24 ( $p = 0.035$ ; **Figure 1B**). Six patients (17.6%) in the T&E group and 7 patients (20.6%) in the PRN groups had decreased but persistent disease activity after

five consecutive monthly injections ( $p = 0.758$ ). During the study period, 14 (41%) patients in the T&E group and 24 (71%) in the PRN group experienced at least one episode of recurrence of macular edema ( $p = 0.015$ ). Furthermore, three (9%) patients in the T&E group and five (15%) in the PRN group experienced at least one episode of vitreous hemorrhage during the 2-year follow-up period ( $p = 0.709$ ).



## Injections and Follow-Up Frequency

The number of clinic visits and injections are summarized in **Table 2**. In the T&E group, the average number of injections was  $7.6 \pm 1.8$  (95% CI, 6.9–8.2) in the first year and  $3.5 \pm 1.9$  (95% CI, 2.8–4.2) in the second year, whereas patients in the PRN group received significantly less injections in the first ( $4.9 \pm 1.5$  [95% CI, 4.4–5.4],  $p < 0.001$ ) and second year ( $1.3 \pm 1.2$  [95% CI, 0.9–1.7],  $p < 0.001$ ). Meanwhile, both groups had similar number of clinic visits in the first (T&E vs. PRN:  $7.4 \pm 1.7$  [95% CI, 6.8–8.0] vs.  $6.9 \pm 2.0$  [95% CI, 6.2–7.6],  $p = 0.236$ ) and second year ( $5.5 \pm 1.8$  [95% CI, 4.9–6.2] vs.  $5.8 \pm 1.6$  [95% CI, 5.3–6.3],  $p = 0.503$ ). In the T&E group, the last injection interval was 12 weeks or longer in 21 (62%) patients, and 9 (26%) patients received injections at a 16-week interval or longer. During the 2-year study period, macular laser was performed in 4 and 3 patients in the T&E and PRN groups, respectively ( $p = 1.00$ ); steroid was given in 10 and 4 patients in the T&E and PRN groups ( $p = 0.132$ ), respectively.

## Factors Associated With Better Visual Improvement

In the univariate regression analysis, three factors, including worse baseline BCVA, T&E regimen, and absence of DRIL on baseline OCT, were associated with better BCVA gain at the final visit. Neither the total number of injections nor other baseline OCT biomarkers were associated with the final BCVA improvement. In the multivariate regression analysis, baseline BCVA and the treatment regimen were still significantly associated with the final BCVA improvement ( $p = 0.029$  and  $0.009$ , respectively) but not with the presence of DRIL (**Table 3**).

**TABLE 3 |** Predicting factors for best corrected visual acuity improvement at Month 24 in patients with diabetic macular edema treated with pro re nata or treat-and-extend protocol.

Factors	Univariate regression*		Multivariate regression	
	Coefficient	P-value	Coefficient	P-value
Age	0.003	0.445		
Baseline BCVA	−0.299	0.010	−0.224	0.029
Baseline CFT on OCT	0.001	0.073		
IRC on OCT	0.016	0.910		
SRF on OCT	−0.017	0.822		
HF on OCT	−0.087	0.431		
DRIL on OCT	0.135	0.048	0.188	0.136
EZ disruption on OCT	0.083	0.281		
T&E (reference) vs. PRN	0.162	0.013	0.173	0.009
Total injection numbers	−0.019	0.059		
Recurrence of edema	0.103	0.143		

\*Adjustment for age, baseline BCVA, and baseline CFT.

BCVA, best-corrected visual acuity; CFT, central foveal thickness; DRIL, disorganization of retinal inner layers; EZ, ellipsoid zone; HF, hyperreflective foci; IRC, intraretinal cyst; OCT, optical coherence tomography; PRN, pro re nata; SRF, subretinal fluid; T&E, treat-and-extend.

## DISCUSSION

We conducted a retrospective matched comparative study to compare the real-world treatment outcomes of patients with DME who underwent IVI ranibizumab therapy following two different regimens: T&E and PRN protocols. While both regimens resulted in significantly improved visual acuity at 2 years, the T&E group had significantly more visual acuity gain and anatomical improvement at 2 years than the PRN group despite similar visual acuity and CFT at baseline. The proportion of patients with VA gain  $\geq 15$  letters at 24 months from the baseline was also higher in the T&E group than in the PRN group.

The treatment regimen for anti-VEGF therapy has evolved in recent years. In the treatment of neovascular age-related macular degeneration (nAMD), earlier trials used a fixed dosing regimen and reported favorable results (20). Subsequently, the PRN regimen, which used monthly evaluation and as needed treatment to reduce the number of injections, demonstrated non-inferior visual improvement at 1 year along with significantly fewer injections (21). Recently, clinical trials that incorporated the T&E regimen and a flexible visiting interval with injection at every visit after disease stabilization, demonstrated comparable visual outcomes between the T&E protocol and fixed monthly injections (22, 23). The non-inferior outcomes achieved by the T&E regimen and reduced number of visits and injections have led to increased popularity of the T&E approach. Results from a meta-analysis demonstrated that the T&E regimen resulted in better real-world visual outcomes compared to the PRN regimen in treating nAMD (24, 25). The success of the T&E regimen in reducing the number of injections (compared to monthly treatment) and visits (compared to PRN) as well as maintaining favorable visual outcomes has led to the application of the T&E protocol in treating DME.

The T&E regimen was first evaluated for its efficacy in treating DME in the RETAIN study, which showed comparable visual improvements in the T&E and PRN groups with a median of 12 injections in the T&E group and 10 injections in the PRN group in 24 months (18). The TREX-DME study compared the T&E and monthly injection regimens, and reported similar visual and anatomical outcomes in the two groups, while significantly fewer injections were needed in the T&E group (19). A small single-center, randomized study by Eichenbaum et al. also reported similar visual improvement after 2 years of ranibizumab injection following either monthly or T&E regimen for patients with DME (26). Despite the success of using the T&E protocol with ranibizumab in treating patients with DME in these clinical trials, there is limited evidence regarding the efficacy of T&E regimen in treating these patients under real-life conditions. A study by Ebnetter et al. compared the 1-year visual outcomes of patients with DME treated using a BCVA-guided PRN regimen or an OCT-guided T&E regimen and reported similar visual gain (8.3 vs. 9.3%, respectively) at 12 months (27). A non-comparative study reported the 2-year visual outcomes of T&E protocol in patients with DME using ranibizumab, in which an average of 4.7 letters was achieved after a mean of 9.7 injections in the first year and 7.9 injections in the second year (28). In

another study, a mean BCVA gain of 6.3 letters was noted at 1 year after 10 ranibizumab injections (29). In our study, greater visual improvement was observed in the T&E group than in the PRN group. The patients in the PRN group in our study received less frequent monitoring and injections compared to those in the clinical trial, which is frequently observed in real-life situations (10, 14, 30, 31). This might have led to inferior results in our patients. On the other hand, patients in the T&E group of our study had a similar number of visits yet received more injections during the study period, which resulted in better visual improvements. Beside more anti-VEGF injections, patients in the T&E group also received more subtenon steroid injection although the difference was not statistically significant. This might indicate that patients in the T&E group were treated more aggressively for DME, thus having better visual gain. In addition, visual gain in the T&E group was greater in our study than that in other real-world studies, despite fewer injections in the first and second years. The inferior baseline visual acuity might be responsible for this difference. Based on our results, we suggest the use of the T&E regimen for treating patients with DME in clinical practice.

The maximum allowed treatment intervals were usually set at 3 months in the previous studies using the T&E regimen (18, 19, 26, 28, 32–34), and 25–75% of the enrolled patients had their treatment intervals extended to 12 weeks (19, 28, 32–34). The results of our study were in line with those of previous reports, with more than half of our patients in the T&E group receiving injections every 3 months or longer at the final visit. In Protocol I study, the median number of injections was 2–3 in the second year, indicating that a significant proportion of patients might not need frequent treatment in the second year (9). Therefore, we allowed a maximum 24-week interval between the treatments. Under such a protocol, the treatment interval could be further lengthened to 16 weeks or longer in 25% of our cohort. Another study by Hirano et al. reported that 66.7% of their patients could have the treatment interval extended to 16 weeks (the maximum allowed interval) under their T&E protocol using aflibercept (35). In their study, after a mean of 11.4 injections, the average BCVA improved from 60.5 to 66.6 letters at 2 years. The inferior initial visual acuity noted in our study might indicate a more severe disease at baseline, and therefore, our patients required more frequent injections than those reported by Hirano et al. in their study. Our study results and the evidence from previous reports suggest that the maximum allowed treatment interval for patients with DME could be set at 16 weeks or longer in some patients when the T&E regimen was applied.

In the present study, the presence of DRIL at baseline was associated with less visual improvement at 2 years. Patients with diabetic retinopathy, either with or without DME, have been reported to have worse baseline visual acuity if DRIL was present on baseline OCT (36, 37). A previous study showed that DRIL was linked to vascular ischemia with poor vessel density in the inner retina (38), and patients with DME with low vessel density in the inner retina also had poorer visual improvement after resolution of macular edema (39). Furthermore, some studies reported that patients with resolved DRIL after treatment had better visual improvements (36, 40). A recent study by Zur et al.

showed that patients without baseline DRIL showed better visual improvement after treatment with dexamethasone implants (41). Our study further supports the predictive value of baseline DRIL as a biomarker for poor visual improvement in patients with DME, not only in those treated with steroid implants, but also in those treated with anti-VEGF therapy.

In our study, patients in the PRN group had a lower number of injections but a higher proportion of macular edema recurrence, yet these two factors were not significantly correlated with final visual improvement in the regression analysis. Regarding the injection number, since patients with rapid response to anti-VEGF therapy in both groups may have received less injections due to improved vision and absence of disease activity, the total injection number could be affected by the aggressiveness of treatment and individual susceptibility to anti-VEGF therapy. Therefore, the total number of injection may not correlate with final visual outcome when evaluated at the individual patient level (i.e., in regression analysis). However, when the correlation was evaluated among 2 groups of patients (i.e., PRN vs. T&E), the injection number might represent the aggressiveness of treatment. As for recurrence of macular edema, it is shown that the average CFT increased at month 6 in the PRN group, while the vision deteriorated at month 12. This means that recurrence of macular edema may precede the visual deterioration, although resolution of recurrent macular edema could be achieved after further treatment with visual regain. Theoretically, frequent recurrence of macular edema may result in poor long-term visual outcomes, but this might not be significantly detected during the 2-year follow-up period. Further studies with longer follow-up periods are needed to confirm our hypothesis.

There are several limitations to our study, including the small sample size and the retrospective study design. Another concern was that the decision to apply the T&E or PRN regimen in each patient was not randomized. Although the groups of patients were matched for baseline BCVA and CFT, there is a possibility of undetected bias between the groups of patients. Additionally, the follow-up intervals in the PRN group not only were individualized and determined by the treatment response of individual patients, but might also be affected by socioeconomic factors such as the availability of frequent clinic visits. However, it was difficult to determine the exact number of visits that patients skipped their injection according to their own will due to the retrospective nature of this study. In addition, since the patients were treated under real-life condition, some patients might have received the PRN injection a few days later than the clinic visit due to the unavailability of the patients or the treating physicians. However, this just reflects the disadvantage of the PRN regimen in the clinical settings. Another limitation of the present study was that we only included patients that have completed 2 years of follow-ups, and we were not able to evaluate the difference of compliance between the T&E and PRN groups. However, our results reflect the true conditions that physicians might encounter in their daily practice in a real-life setting; hence, it will serve as an important reference for the real-world treatment outcomes of patients with DME.

In conclusion, this study demonstrated the superior treatment response of the T&E regimen of ranibizumab in treating DME

with better visual and anatomical outcomes compared to the PRN regimen in a real-world setting. The 2-year results of our study confirmed the usefulness of the T&E regimen and decreased the need for both injections and clinic visits in the second year.

## DATA AVAILABILITY STATEMENT

The raw data supporting the conclusions of this article will be made available by the authors, without undue reservation.

## ETHICS STATEMENT

The studies involving human participants were reviewed and approved by the National Taiwan University Hospital Research Ethics Committee (No.: 201811023RIFD). Written informed consent for participation was not required for this study in accordance with the national legislation and the institutional requirements.

## REFERENCES

- Klein R, Klein BE, Moss SE, Davis MD, DeMets DL. The Wisconsin epidemiologic study of diabetic retinopathy. IV. diabetic macular edema. *Ophthalmology*. (1984) 91:1464–74. doi: 10.1016/S0161-6420(84)34102-1
- Schmidt-Erfurth U, Garcia-Arumi J, Bandello F, Berg K, Chakravarthy U, Gerendas BS, et al. Guidelines for the management of diabetic macular edema by the European Society of Retina Specialists (EURETINA). *Ophthalmologica*. (2017) 237:185–222. doi: 10.1159/000458539
- Massin P, Bandello F, Garweg JG, Hansen LL, Harding SP, Larsen M, et al. Safety and efficacy of ranibizumab in diabetic macular edema (RESOLVE Study): a 12-month, randomized, controlled, double-masked, multicenter phase II study. *Diabetes Care*. (2010) 33:2399–405. doi: 10.2337/dc10-0493
- Nguyen QD, Shah SM, Khwaja AA, Channa R, Hatef E, Do DV, et al. Two-year outcomes of the ranibizumab for edema of the macula in diabetes (READ-2) study. *Ophthalmology*. (2010) 117:2146–51. doi: 10.1016/j.ophtha.2010.08.016
- Mitchell P, Bandello F, Schmidt-Erfurth U, Lang GE, Massin P, Schlingemann RO, et al. The RESTORE study: ranibizumab monotherapy or combined with laser versus laser monotherapy for diabetic macular edema. *Ophthalmology*. (2011) 118:615–25. doi: 10.1016/j.ophtha.2011.01.031
- Diabetic Retinopathy Clinical Research N, Elman MJ, Aiello LP, Beck RW, Bressler NM, Bressler SB, et al. Randomized trial evaluating ranibizumab plus prompt or deferred laser or triamcinolone plus prompt laser for diabetic macular edema. *Ophthalmology*. (2010) 117:1064–77 e35. doi: 10.1016/j.ophtha.2010.02.031
- Nguyen QD, Brown DM, Marcus DM, Boyer DS, Patel S, Feiner L, et al. Ranibizumab for diabetic macular edema: results from 2 phase III randomized trials: RISE and RIDE. *Ophthalmology*. (2012) 119:789–801. doi: 10.1016/j.ophtha.2011.12.039
- Boyer DS, Nguyen QD, Brown DM, Basu K, Ehrlich JS, Ride, et al. Outcomes with as-needed ranibizumab after initial monthly therapy: long-term outcomes of the phase III RIDE and RISE trials. *Ophthalmology*. (2015) 122:2504–13 e1. doi: 10.1016/j.ophtha.2015.08.006
- Elman MJ, Ayala A, Bressler NM, Browning D, Flaxel CJ, Glassman AR, et al. Intravitreal Ranibizumab for diabetic macular edema with prompt versus deferred laser treatment: 5-year randomized trial results. *Ophthalmology*. (2015) 122:375–81. doi: 10.1016/j.ophtha.2014.08.047
- Lai TT, Yang CM, Yang CH, Ho TC, Hsieh YT. Treatment outcomes and predicting factors for diabetic macular edema treated with ranibizumab - one-year real-life results in Taiwan. *J Formos Med Assoc*. (2019) 118:194–202. doi: 10.1016/j.jfma.2018.03.009

## AUTHOR CONTRIBUTIONS

Y-TH contributed to conception and design of the study. T-TL and Y-TH organized the database. T-TL performed the statistical analysis and wrote the first draft of the manuscript. T-CC, C-HY, C-MY, T-CH, and Y-TH wrote sections of the manuscript. All authors contributed to manuscript revision, read, and approved the submitted version.

## FUNDING

Novartis Taiwan sponsored this study. The funding agreement ensured the authors' independence in designing the study, interpreting the data, writing, and publishing the report.

## SUPPLEMENTARY MATERIAL

The Supplementary Material for this article can be found online at: <https://www.frontiersin.org/articles/10.3389/fmed.2021.781421/full#supplementary-material>

- Bertelmann T, Feltgen N, Scheffler M, Hufenbach U, Wiedon A, Wilhelm H, et al. Vision-related quality of life in patients receiving intravitreal ranibizumab injections in routine clinical practice: baseline data from the German OCEAN study. *Health Qual Life Outcomes*. (2016) 14:132. doi: 10.1186/s12955-016-0536-1
- Granstrom T, Forsman H, Lindholm Olinder A, Gkretsis D, Eriksson JW, Granstam E, et al. Patient-reported outcomes and visual acuity after 12months of anti-VEGF-treatment for sight-threatening diabetic macular edema in a real world setting. *Diabetes Res Clin Pract*. (2016) 121:157–65. doi: 10.1016/j.diabres.2016.09.015
- Sato S, Shinoda H, Nagai N, Suzuki M, Uchida A, Kurihara T, et al. Predictive factors of better outcomes by monotherapy of an antivascular endothelial growth factor drug, ranibizumab, for diabetic macular edema in clinical practice. *Medicine*. (2017) 96:e6459. doi: 10.1097/MD.00000000000006459
- Holekamp NM, Campbell J, Almony A, Ingraham H, Marks S, Chandwani H, et al. Vision outcomes following anti-vascular endothelial growth factor treatment of diabetic macular edema in clinical practice. *Am J Ophthalmol*. (2018) 191:83–91. doi: 10.1016/j.ajo.2018.04.010
- Korobelnik JF, Do DV, Schmidt-Erfurth U, Boyer DS, Holz FG, Heier JS, et al. Intravitreal aflibercept for diabetic macular edema. *Ophthalmology*. (2014) 121:2247–54. doi: 10.1016/j.ophtha.2014.05.006
- Diabetic Retinopathy Clinical Research N, Wells JA, Glassman AR, Ayala AR, Jampol LM, Aiello LP, et al. Aflibercept, bevacizumab, or ranibizumab for diabetic macular edema. *N Engl J Med*. (2015) 372:1193–203. doi: 10.1056/NEJMoa1414264
- Freund KB, Korobelnik JF, Devenyi R, Framme C, Galic J, Herbert E, et al. Treat-and-extend regimens with anti-vegf agents in retinal diseases: a literature review and consensus recommendations. *Retina*. (2015) 35:1489–506. doi: 10.1097/IAE.0000000000000627
- Prunte C, Fajnkuchen F, Mahmood S, Ricci F, Hatz K, Studnicka J, et al. Ranibizumab 0.5 mg treat-and-extend regimen for diabetic macular oedema: the RETAIN study. *Br J Ophthalmol*. (2016) 100:787–95. doi: 10.1136/bjophthalmol-2015-307249
- Payne JE, Wykoff CC, Clark WL, Bruce BB, Boyer DS, Brown DM, et al. Randomized trial of treat and extend ranibizumab with and without navigated laser versus monthly dosing for diabetic macular edema: TREX-DME 2-year outcomes. *Am J Ophthalmol*. (2019) 202:91–9. doi: 10.1016/j.ajo.2019.02.005
- Rosenfeld PJ, Brown DM, Heier JS, Boyer DS, Kaiser PK, Chung CY, et al. Ranibizumab for neovascular age-related macular degeneration. *N Engl J Med*. (2006) 355:1419–31. doi: 10.1056/NEJMoa054481

21. Group CR, Martin DF, Maguire MG, Ying GS, Grunwald JE, Fine SL, et al. Ranibizumab and bevacizumab for neovascular age-related macular degeneration. *N Engl J Med.* (2011) 364:1897–908. doi: 10.1056/NEJMoa1102673
22. Wykoff CC, Ou WC, Brown DM, Croft DE, Wang R, Payne JF, et al. Randomized trial of treat-and-extend versus monthly dosing for neovascular age-related macular degeneration: 2-year results of the TREX-AMD study. *Ophthalmol Retina.* (2017) 1:314–21. doi: 10.1016/j.oret.2016.12.004
23. Silva R, Berta A, Larsen M, Macfadden W, Feller C, Mones J, et al. Treat-and-extend versus monthly regimen in neovascular age-related macular degeneration: results with ranibizumab from the TREND study. *Ophthalmology.* (2018) 125:57–65. doi: 10.1016/j.ophtha.2017.07.014
24. Mehta H, Tufail A, Daien V, Lee AY, Nguyen V, Ozturk M, et al. Real-world outcomes in patients with neovascular age-related macular degeneration treated with intravitreal vascular endothelial growth factor inhibitors. *Prog Retin Eye Res.* (2018) 65:127–46. doi: 10.1016/j.preteyeres.2017.12.002
25. Okada M, Kandasamy R, Chong EW, McGuinness M, Guymer RH. The treat-and-extend injection regimen versus alternate dosing strategies in age-related macular degeneration: a systematic review and meta-analysis. *Am J Ophthalmol.* (2018) 192:184–97. doi: 10.1016/j.ajo.2018.05.026
26. Eichenbaum DA, Duerr E, Patel HR, Pollack SM. Monthly versus treat-and-extend ranibizumab for diabetic macular edema: a prospective, randomized trial. *Ophthalmic Surg Lasers Imaging Retina.* (2018) 49:e191–7. doi: 10.3928/23258160-20181101-17
27. Ebnetter A, Waldmeier D, Zysset-Burri DC, Wolf S, Zinkernagel MS. Comparison of two individualized treatment regimens with ranibizumab for diabetic macular edema. *Graefes Arch Clin Exp Ophthalmol.* (2017) 255:549–55. doi: 10.1007/s00417-016-3502-z
28. Giannakaki-Zimmermann H, Behrndt A, Hoffmann L, Guichard MM, Tuerksever C, Prunte C, et al. Predictors for 2-year functional and morphological outcomes of a treat and extend regimen with ranibizumab in patients with diabetic macular edema. *Ophthalmic Res.* (2021) 64:465–75. doi: 10.1159/000514721
29. Schwarzer P, Ebnetter A, Munk M, Wolf S, Zinkernagel MS. One-year results of using a treat-and-extend regimen without a loading phase with anti-VEGF Agents in patients with treatment-naïve diabetic macular edema. *Ophthalmologica.* (2019) 241:220–5. doi: 10.1159/000495623
30. Best AL, Fajnkuchen F, Nghiem-Buffet S, Grenet T, Quentel G, Delahaye-Mazza C, et al. Treatment efficacy and compliance in patients with diabetic macular edema treated with ranibizumab in a real-life setting. *J Ophthalmol.* (2018) 2018:4610129. doi: 10.1155/2018/4610129
31. Ehlken C, Helms M, Bohringer D, Agostini HT, Stahl A. Association of treatment adherence with real-life VA outcomes in AMD, DME, and BRVO patients. *Clin Ophthalmol.* (2018) 12:13–20. doi: 10.2147/OPHTH.S151611
32. Curry BA, Sanfilippo PG, Chan S, Hewitt AW, Verma N. Clinical outcomes of a treat and extend regimen with intravitreal aflibercept injections in patients with diabetic macular edema: experience in clinical practice. *Ophthalmol Ther.* (2020) 9:87–101. doi: 10.1007/s40123-019-00224-x
33. Kim YC, Shin JP, Pak KY, Kim HW, Sagong M, Lee SJ, et al. Two-year outcomes of the treat-and-extend regimen using aflibercept for treating diabetic macular oedema. *Sci Rep.* (2020) 10:22030. doi: 10.1038/s41598-020-78954-3
34. Pak KY, Shin JP, Kim HW, Sagong M, Kim YC, Lee SJ, et al. One-year results of treatment of diabetic macular edema with aflibercept using the treat-and-extend dosing regimen: the VIBIM study. *Ophthalmologica.* (2020) 243:255–62. doi: 10.1159/000504753
35. Hirano T, Toriyama Y, Takamura Y, Sugimoto M, Nagaoka T, Sugiyama Y, et al. Outcomes of a 2-year treat-and-extend regimen with aflibercept for diabetic macular edema. *Sci Rep.* (2021) 11:4488. doi: 10.1038/s41598-021-83811-y
36. Sun JK, Lin MM, Lammer J, Prager S, Sarangi R, Silva PS, et al. Disorganization of the retinal inner layers as a predictor of visual acuity in eyes with center-involved diabetic macular edema. *JAMA Ophthalmol.* (2014) 132:1309–16. doi: 10.1001/jamaophthalmol.2014.2350
37. Joltikov KA, Sesi CA, de Castro VM, Davila JR, Anand R, Khan SM, et al. Disorganization of Retinal Inner Layers (DRIL) and neuroretinal dysfunction in early diabetic retinopathy. *Invest Ophthalmol Vis Sci.* (2018) 59:5481–86. doi: 10.1167/iiov.18-24955
38. Cennamo G, Montorio D, Fossataro F, Fossataro C, Tranfa F. Evaluation of vessel density in disorganization of retinal inner layers after resolved diabetic macular edema using optical coherence tomography angiography. *PLoS One.* (2021) 16:e0244789. doi: 10.1371/journal.pone.0244789
39. Hsieh YT, Alam MN, Le D, Hsiao CC, Yang CH, Chao DL, et al. OCT angiography biomarkers for predicting visual outcomes after ranibizumab treatment for diabetic macular edema. *Ophthalmol Retina.* (2019) 3:826–834. doi: 10.1016/j.oret.2019.04.027
40. Radwan SH, Soliman AZ, Tokarev J, Zhang L, van Kuijk FJ, Koozekanani DD. Association of disorganization of retinal inner layers with vision after resolution of center-involved diabetic macular edema. *JAMA Ophthalmol.* (2015) 133:820–5. doi: 10.1001/jamaophthalmol.2015.0972
41. Zur D, Iglicki M, Sala-Puigdollers A, Chhablani J, Lupidi M, Fraser-Bell S, et al. Disorganization of retinal inner layers as a biomarker in patients with diabetic macular oedema treated with dexamethasone implant. *Acta Ophthalmol.* (2020) 98:e217–23. doi: 10.1111/aos.14230

**Conflict of Interest:** T-TL, T-CC, C-HY, C-MY, T-CH, and Y-TH received honoraria for speeches from Novartis Taiwan.

**Publisher's Note:** All claims expressed in this article are solely those of the authors and do not necessarily represent those of their affiliated organizations, or those of the publisher, the editors and the reviewers. Any product that may be evaluated in this article, or claim that may be made by its manufacturer, is not guaranteed or endorsed by the publisher.

Copyright © 2022 Lai, Chen, Yang, Yang, Ho and Hsieh. This is an open-access article distributed under the terms of the Creative Commons Attribution License (CC BY). The use, distribution or reproduction in other forums is permitted, provided the original author(s) and the copyright owner(s) are credited and that the original publication in this journal is cited, in accordance with accepted academic practice. No use, distribution or reproduction is permitted which does not comply with these terms.





# A Comparison of Face-Down Positioning and Adjustable Positioning After Pars Plana Vitrectomy for Macular Hole Retinal Detachment in High Myopia

Yan Gao<sup>1,2</sup>, Ting Ruan<sup>1,2</sup>, Nan Chen<sup>1,2</sup>, Bin Yu<sup>1,2</sup>, Xiaoli Xing<sup>1,2</sup>, Qing Du<sup>1,2</sup>, Yan Qi<sup>1,2</sup> and Jun Li<sup>1,2\*</sup>

<sup>1</sup> Qingdao Eye Hospital of Shandong First Medical University, Qingdao, China, <sup>2</sup> State Key Laboratory Cultivation Base, Shandong Provincial Key Laboratory of Ophthalmology, Shandong Eye Institute, Shandong First Medical University & Shandong Academy of Medical Sciences, Qingdao, China

## OPEN ACCESS

### Edited by:

Hajiang Lin,  
Harvard Medical School,  
United States

### Reviewed by:

Mario Damiano Toro,  
Medical University of Lublin, Poland  
Navneet Mehrotra,  
Retina Foundation and Retina  
Care, India

### \*Correspondence:

Jun Li  
doctor\_jl@126.com  
orcid.org/0000-0001-9121-6162

### Specialty section:

This article was submitted to  
Ophthalmology,  
a section of the journal  
Frontiers in Medicine

**Received:** 21 September 2021

**Accepted:** 17 January 2022

**Published:** 16 February 2022

### Citation:

Gao Y, Ruan T, Chen N, Yu B, Xing X,  
Du Q, Qi Y and Li J (2022) A  
Comparison of Face-Down  
Positioning and Adjustable Positioning  
After Pars Plana Vitrectomy for  
Macular Hole Retinal Detachment in  
High Myopia. *Front. Med.* 9:780475.  
doi: 10.3389/fmed.2022.780475

**Purpose:** To compare the anatomical and functional outcomes of macular hole retinal detachment (MHRD) in high myopia after pars plana vitrectomy (PPV) with face-down positioning and adjustable positioning.

**Methods:** Fifty-three eyes from 53 patients with MHRD were analyzed in this study. All patients received PPV with silicon oil for tamponade and then subdivided into 2 groups: 28 were included in a face-down positioning group and 25 were included in the adjustable positioning group. Patients were followed up for at least 6 months. The main outcome was the rate of anatomical macular hole (MH) closure and retinal reattachment. Secondary outcome measures were the best-corrected visual acuity and postoperative complications.

**Results:** There was no significant difference in the rate of MH closure (53.6 vs. 72.0%,  $p = 0.167$ ) and retinal reattachment (100 vs. 96%,  $p = 0.472$ ) between the face-down group and adjustable group. Compared with the mean preoperative best-corrected visual acuity (BCVA), the mean postoperative BCVA at the 6-month follow-up improved significantly in both groups ( $p = 0$ , both). But there was no significant difference in the mean postoperative BCVA ( $p = 0.102$ ) and mean BCVA improvement ( $p = 0.554$ ) at 6 months after surgery between the two groups. There was no significant difference in the high intraocular pressure (IOP) after surgery between the two groups (53.6 vs. 44%,  $p = 0.487$ ). There were no other complications that occurred during the follow-up.

**Conclusion:** Adjustable positioning after PPV with silicon oil tamponade for MHRD repair is effective and safe. Face-down positioning does not seem to be necessary for all patients with MHRD.

**Keywords:** adjustable positioning, face-down positioning, high myopia, macular hole, retinal detachment

## INTRODUCTION

Macular hole retinal detachment (MHRD) is a serious vision impairment complication associated with high myopia. The pathogenesis of MHRD is not completely clear; however, it is believed that the tangential macular traction by the vitreoretinal interface, remnants of the cortical vitreous, inflexible internal limiting membrane (ILM), and the retinal vasculature is one of the factors (1, 2). In addition, the weakened retinal adherence to the posterior pole caused by choroidal and retinal pigment epithelium (RPE) atrophy is also one of the factors (3). Since it was first described by Gonvers and Machemer, pars plana vitrectomy (PPV) procedures have been used in the surgical treatment of MHRD with high myopia (4). Vitrectomy combined posterior vitreous cortex removal, epiretinal membrane removal, and ILM removal, with gas or silicone oil tamponade to become the standard treatment for MHRD with a higher retinal reattachment rate (5). Since Michalewska et al. first presented the inverted ILM flap technique (6), modified techniques, such as temporal ILM flap or inverted ILM insertion, have been introduced to potentially improve the surgical outcomes in MH and MHRD (7–20), or to enhance the success rate in eyes with persistent full-thickness macular hole undergoing secondary PPV (21).

More than 90% of vitreoretinal surgeons worldwide recommend some period of face-down positioning after macular hole (MH) repair surgery (22). However, it is a tough challenge for most patients to keep a strict face-down positioning after operation for a long time. Elderly patients or patients with systemic diseases have serious difficulties persisting in the face-down positioning. Furthermore, some rare postoperative complications, like ulnar nerve palsies, pulmonary embolism, thrombophlebitis, and decubitus, would develop after a long period of face-down position (23, 24). Multiple groups have reported the efficacy of postoperative positioning without the maintenance of a face-down positioning after vitrectomy for MH (22, 25–30) and retinal detachment (RD) (31–35). However, MHRD is excluded from their observation. The purpose of the current study was to evaluate the 6-month outcomes of adjustable positioning compared to face-down positioning after PPV for MHRD in high myopia.

## MATERIALS AND METHODS

This retrospective study analyzed a consecutive series of 53 eyes (53 patients) with MHRD in high myopia who underwent primary PPV between January 2018 and December 2019 at Qingdao Eye Hospital. The study followed the tenets of the Declaration of Helsinki and was approved by the Institutional Review Board of Qingdao Eye Hospital of Shandong First Medical University.

The inclusion criteria were as follows: (1) eyes with an axial length (AL)  $\geq 26$  mm; (2) the diagnosis of MHRD confirmed by optical coherence tomography (OCT) before surgery, and RD extending by more than 1 disk diameter around the full-thickness MH; and (3) the follow-up time is more than 6 months. Those eyes

with previous vitreoretinal surgery, ocular trauma, and presence of peripheral retinal breaks before surgery, diabetic retinopathy, and other proliferative vitreoretinopathy were excluded.

The following general information was obtained for analysis: sex, age, systemic diseases, and bilaterality. All the patients accepted the preoperative and postoperative examinations that included best-corrected visual acuity (BCVA), intraocular pressure (IOP), slit-lamp examination, AL, B-ultrasound, fundus photography, and OCT. The decimal BCVA was converted to the logarithm of the minimum angle of resolution (logMAR) units for statistical analyses. The AL was measured using a Master 500 (Carl Zeiss, Germany). The area of the RD was determined by the images from a panoramic scanning laser ophthalmoscope (SLO) (Optos, Scotland), which was used to classify patients into those whose RD was within or beyond the vascular arcade. The presence of an MH, MH closure, and retina reattachment were evaluated in the OCT images (Optovue, USA).

## Surgical Technique

Pars plana vitrectomy (PPV) procedures were performed using a standard 25-gauge 3-port system (Constellation, Alcon, USA). Core vitrectomy was performed by intravitreal injection of triamcinolone acetonide to visualize the vitreous gel and the posterior hyaloid. Peripheral vitreous base vitrectomy was performed under scleral depression. After being stained with indocyanine green (ICG) for 30 s, the ILM was peeled over the entire macular area and inserted into the MH to fill the hole. Fluid–gas exchange with drainage of subretinal fluid through the MH was performed. Finally, silicone oil was filled in all patients.

Patients were subdivided into two groups according to the postoperative positioning based on the recommendation of the surgeon. Face-down, as a routine treatment, meant keeping a face-down positioning for at least 12 h per day for at least 1 month after the surgery. Patients were encouraged to stay face-down during sleeping hours, as long as possible. In the adjustable group, patients were in a non-recumbent positioning during the daytime and fall asleep in the lateral positioning at night.

The primary endpoint was the MH closure and anatomical reattachment rate at 6 months after surgery. Secondary endpoints included BCVA change, change of IOP, and frequency of reported complications.

## Statistical Analysis

Data were analyzed using the chi-square test and the Fisher exact test for categorical variables, and the *t*-test and the Mann–Whitney U test for numerical and ordinal variables. A *P*-value of 0.05 was considered statistically significant.

## RESULTS

A total of 53 eyes of 53 patients (28 eyes in the face-down group and 25 eyes in the adjustable group) were analyzed. They

**TABLE 1** | The baseline parameters, status, and surgical procedure of patients.

	Total	Face-down group	Adjustable group	P value
No. of eyes/patients	53	28	25	
Age (year) (mean $\pm$ SD; range)	62.4 $\pm$ 8.0 (40–81)	63.7 $\pm$ 5.8 (52–75)	61.0 $\pm$ 9.9 (40–81)	0.237
<b>Gender, no. (%)</b>				
Men	4 (7.5)	1 (3.6)	3 (12.0)	0.523
Woman	49 (92.5)	27 (96.4)	22 (88.0)	
Systemic disease, no. (yes/no)	30/23	18/10	12/13	0.232
<b>Eyes, no. (%)</b>				
Right	37 (69.8)	22 (78.6)	15 (60.0)	0.142
Left	16 (30.2)	6 (21.4)	10 (40.0)	
Axial length (mm) (mean $\pm$ SD; range)	29.98 $\pm$ 2.01 (26.54–35.82)	29.99 $\pm$ 1.76 (27.50–33.30)	29.96 $\pm$ 2.28 (26.54–35.82)	0.970
<b>Preoperative BCVA</b>				
LogMAR (mean $\pm$ SD; range)	2.25 $\pm$ 0.76 (0.7–4.0)	2.27 $\pm$ 0.71 (1.3–3.0)	2.22 $\pm$ 0.84 (0.7–4.0)	0.692
Preoperative IOP (mmHg) (mean $\pm$ SD; range)	12.7 $\pm$ 3.1 (6–19)	12.1 $\pm$ 2.7 (7–17)	13.4 $\pm$ 3.4 (6–19)	0.137
<b>Lens status, no. (%)</b>				
Phakia	45 (84.9)	26 (92.9)	19 (76.0)	0.147
Pseudophakia	6 (11.3)	1 (3.6)	5 (20.0)	
Aphakia	2 (3.8)	1 (3.6)	1 (4.0)	
Beyond vascular arcade, no. (%)	35 (66)	18 (64.3)	17 (68.0)	0.776
Combined choroidal detachment, no. (%)	6 (11.3)	3 (10.7)	3 (12.0)	1.000
Combined macular membrane, no. (%)	14 (26.4)	9 (32.1)	5 (20.0)	0.317
Combined lattice degeneration, no. (%)	24 (45.3)	13 (46.4)	11 (44.0)	0.859
<b>Lens surgery, no. (%)</b>				
No	31 (58.5)	16 (57.1)	15 (60.0)	0.179
Phaco	20 (37.7)	12 (42.9)	8 (32.0)	
Phaco+IOL implantation	2 (3.8)	0 (0.0)	2 (8.0)	
Silicone oil volume (ml) (mean $\pm$ SD; range)	6.7 $\pm$ 1.2 (4.3–9.5)	6.7 $\pm$ 1.2 (4.5–9.5)	6.7 $\pm$ 1.4 (4.3–9.0)	0.944

BCVA, best corrected visual acuity; ILM, internal limiting membranes; IOL, intraocular lens; IOP, intraocular pressure; LogMAR, logarithm of the minimum angle of resolution.

were 49 women and 4 men with a mean ( $\pm$ SD) age of 62.4  $\pm$  8 years (range 40–81 years). There are more female patients (96.4% in the face-down group vs. 88% in the adjustable group,  $p = 0.523$ ) and more right eyes (78.6 vs. 60%,  $p = 0.142$ ) in both groups. The mean preoperative axial length was 29.98  $\pm$  2.01 mm with a range of 26.54 to 35.82 mm. No significant differences in baseline parameters were found between the two groups ( $p > 0.05$ ), including age, gender, systemic diseases (including hypertension, diabetes, coronary heart disease, and asthma), bilaterality, axial length, preoperative BCVA, and IOP. There were also no significant differences in the status related to retinal detachment between the two groups ( $p > 0.05$ ), including whether it is an extent of RD beyond vascular arcade (64.3 vs. 68%,  $p = 0.776$ ), combined with choroidal detachment (10.7 vs. 12%,  $p = 1$ ), combined with macular membrane (32.1 vs. 20%,  $p = 0.317$ ), and combined with lattice degeneration (46.4 vs. 44.0%,  $p = 0.859$ ). There was no significant difference in the number of lens surgery and silicone oil volume between the groups ( $p > 0.05$ ). The baseline parameters, status, and surgical procedure of the patients for the two groups are listed in **Table 1**.

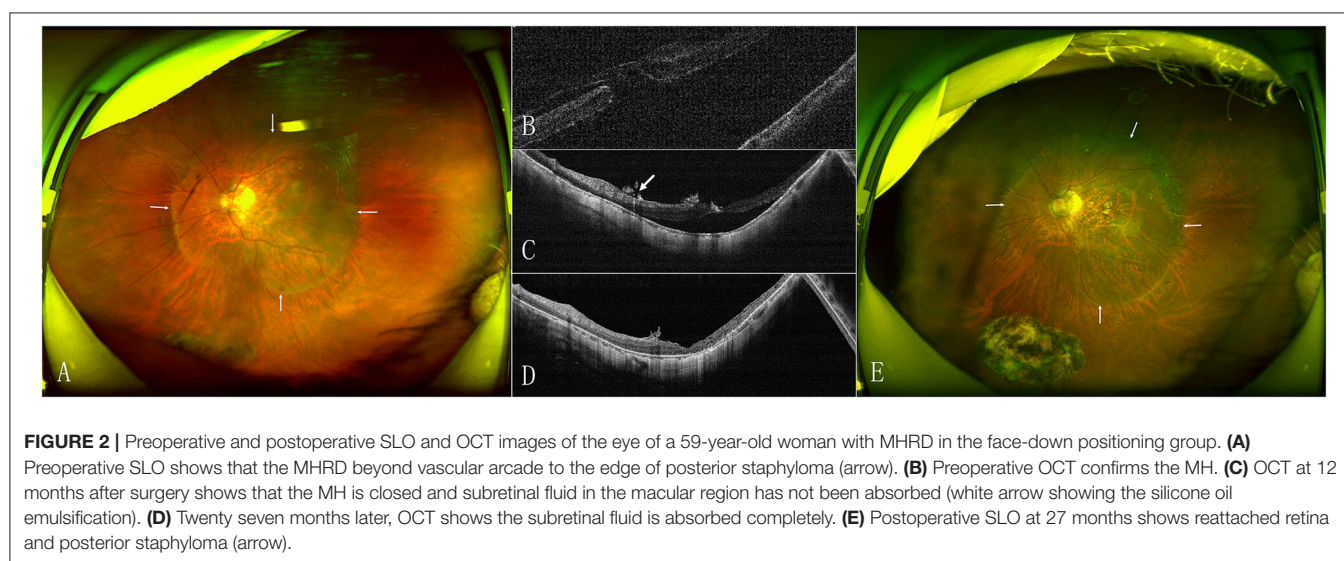
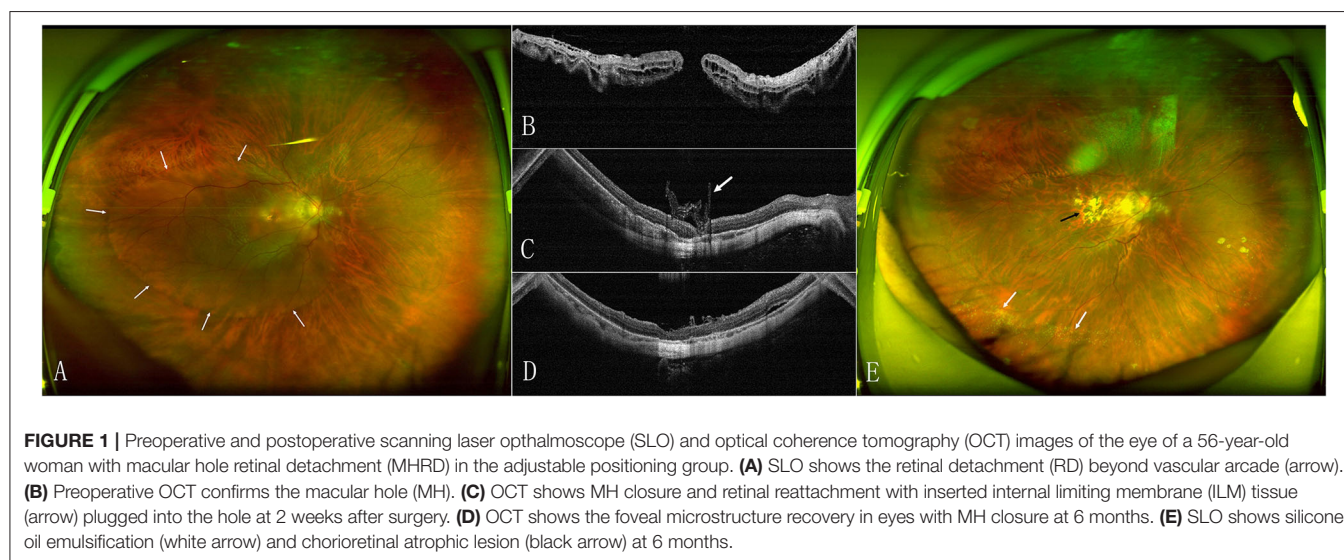
We collected the 6-month visual and anatomic outcomes for all the patients (as shown in **Table 2**). There was no significant difference in the mean postoperative BCVA at 6 months after surgery between the two groups ( $p = 0.102$ ). Compared with the mean preoperative BCVA, the mean postoperative BCVA at the 6-month follow-up improved significantly in both groups ( $p = 0$  in both groups), but no significant difference in mean BCVA improvement was found between the two groups ( $p = 0.554$ ).

The MH closed after the initial surgery in 15 (53.6%) eyes in the face-down group and 18 (72%) eyes in the adjustable group (**Figure 1**). The retinal reattached after initial surgery in 28 (100%) eyes in the face-down group (**Figure 2**) and 24 (96%) eyes in the adjustable group. There was no significant difference in the rate of MH closure ( $p = 0.167$ ) and retinal reattachment ( $p = 0.472$ ) between the two groups. Only one patient in the adjustable group did not achieve an MH closure and retinal reattachment. During the follow-up, she was unwilling to undergo another surgery, but the extent of retinal detachment gradually narrowed, and the MH was still not closed until 21 months after surgery (**Figure 3**). There were 15 eyes (53.6%)

**TABLE 2 |** Visual and anatomic results at 6 months after surgery.

	Face-down group	Adjustable group	P value
No. of eyes/patients	28	25	
Postoperative BCVA at 6 months			
LogMAR (mean $\pm$ SD; range)	1.3 $\pm$ 0.4 (0.5–2.0)	1.1 $\pm$ 0.4 (0.4–2.2)	0.102
Compared with preoperative ( <i>P</i> value)	<i>P</i> = 0.000	<i>P</i> = 0.000	
BCVA improvement (mean $\pm$ SD)	–1.0 $\pm$ 0.7	–1.1 $\pm$ 0.7	0.554
MH closure after initial surgery, no. (%)	15 (53.6)	18 (72.0)	0.167
Retinal reattachment after initial surgery, no. (%)	28 (100.0)	24 (96.0)	0.472
Postoperative high IOP, no. (%)	15 (53.6)	11 (44.0)	0.487

BCVA, best corrected visual acuity; IOP, intraocular pressure; LogMAR, logarithm of the minimum angle of resolution; MH, macular hole.



and 11 eyes (44%) with high IOP after surgery in the two groups ( $p = 0.487$ ). All eyes with high IOP were controlled within the normal range after the treatment with anti-glaucoma

drugs, and no surgical intervention was performed. There were no retinal detachment and other complications occurred during the follow-up.



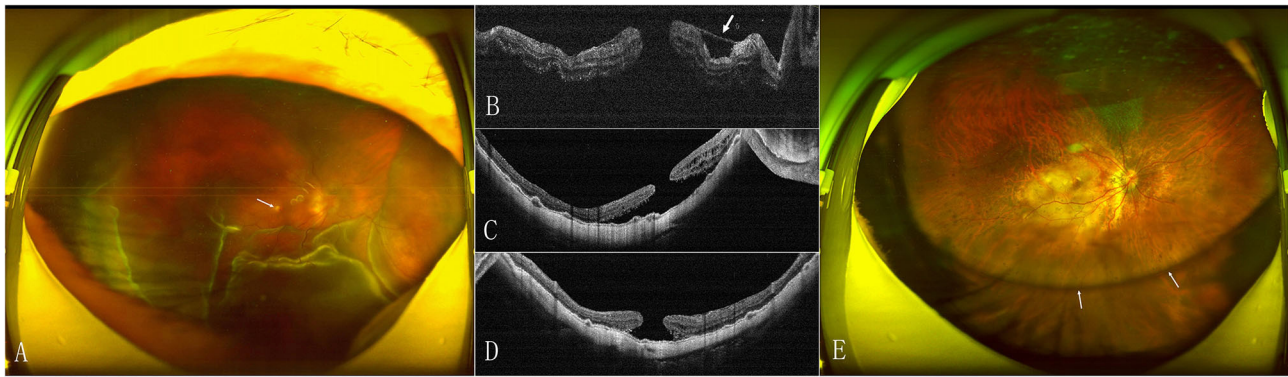


**FIGURE 3 |** Preoperative and postoperative SLO and OCT images of the eye of a 66-year-old woman with MHRD in the adjustable positioning group. **(A)** Preoperative SLO shows the RD with MH (arrow) beyond vascular arcade. **(B)** OCT confirms the MHRD with an epiretinal membrane (arrow). **(C)** OCT at 6 months after surgery shows that the MH still open and the extent of RD is narrowed. **(D)** Twenty one months later, OCT shows the MH is not closed and the retina around the MH is not reattached. **(E)** Postoperative SLO at 21 months shows that the silicon oil has not been removed yet (arrow).

## DISCUSSION

A face-down positioning is a routine requirement for patients after vitrectomy and gas/silicone oil tamponade for RD. But face-down positioning is an important source of discomfort and complications for patients (23, 24), which gradually attracted the attention of the doctor. Chen et al. (32) designed a controlled study to address the issue of positioning after PPV and gas tamponade surgery for rhegmatogenous retinal detachment (RRD). There was no significant difference in the anatomical success rates, BCVA, and the rates of complications between the face-down group and the adjustable positioning group. Martínez-Castillo et al. (31, 33) reported that PPV alone with complete drainage of sub-retinal fluid achieves a high reattachment rate in the management of primary pseudophakic RRD due to inferior retinal breaks. Their patients did not perform a prone position or any other type of positioning during the postoperative period. In the study of Casswell et al. (34), findings suggest that face-down positioning was associated with a reduction in the rate and amplitude of postoperative retinal displacement after macular-involving RD repair and with a reduction in binocular diplopia. Despite this, no association was found with visual acuity or postoperative distortion. However, none of these studies accepted RRD caused by MH in eyes with high degree myopia ( $-6$  diopter or above).

Pars plana vitrectomy (PPV) with ILM peeling and gas tamponade is an important surgical method for the MH. It has been reported that face-down positioning, following an MH surgery, provides no functional or anatomical benefit (36). Some scholars think that a postoperative non-supine positioning is adequate for all the patients with MH after surgery (25–27). Therefore, randomized controlled trials have been conducted to evaluate whether face-down positioning is necessary for recovery from MH surgery (37, 38). The meta-analysis provides sufficient evidence that a non-face-down postoperative positioning is not inferior to a face-down positioning when the MH is smaller than  $400\ \mu\text{m}$ . Although a face-down postoperative positioning

is highly recommended in MHs larger than  $400\ \mu\text{m}$ , the ideal visual improvement rate was not influenced by postoperative positioning (37). Zhu et al. (39) used a novel surgical protocol using vitrectomy, ILM peeling, and autologous blood clot covering the MH at the end of the MH surgery, which eliminated the gas tamponade and thus, the need for postoperative face-down positioning. Complete MH closure was achieved in all 18 eyes at the end of the follow-up period, and among them were five large MHs (minimum diameter  $> 400\ \mu\text{m}$ ).

Among myopic patients with MH, the incidence of RD increased as myopia worsened (1.1% RD in myopia under  $-3\ \text{D}$ , 67.7% RD in myopia between  $-8$ , and  $-3.25\ \text{D}$ , and 97.6% RD in myopia over  $-8.25\ \text{D}$ ) (1). AL elongation and posterior staphyloma contribute to the disparity in the length of the retina and the RPE-choroid-sclera complex, leading to the progression of retinal detachment (1, 2). The articles on MHRD surgery published in the past 5 years are mostly from East Asia (7–20) (as shown in Table 3). A total of 404 eyes in 403 patients were observed, including 331 women (82.1%) and 72 men (17.9%), and the majority of female patients were similar to the population data (40, 41). If vitrectomy and ILM peeling have become the standard treatment for MHRD with a retinal reattachment rate of 91.5%, then the inverted ILM flap groups can achieve 97.3% (42). Otherwise, the inverted ILM insertion technique seems to improve the anatomical results in terms of MH closure rate with there being a tendency for better postoperative visual acuity in the inverted ILM insertion group (43). In these studies, none of them gave up the face-down positioning, and after filling with gas or silicone oil, the patients were asked to keep a prone positioning for 1–2 weeks and avoid supine positioning afterward.

Previous studies have reported that the healing of MHs begins within 24 h after the surgery, and the bridge configuration occurs around 3 days thereafter (44). The MHs were basically healed within 3 days after surgery, and those that were not healed within 3 days were still open during the 3-month follow-up (45). Seno et al. (46) observed and scored the compliance of the face-down positioning four times per day for 3 days post-surgery

**TABLE 3 |** Published studies about macular hole retinal detachment (MHRD) in the last 5 years.

References	Country/ Region	Groups	No. of eyes	Female/Male	Age	AL	RD within/ beyond the arcade	PPV procedure	ILM dyeing	Tamponade agent	Postoperative positioning	Initial MH closure	Initial retinal reattachment
Gu et al. (19)	China	Inverted ILM flap	22	20/2	61.5 ± 8.6	28.28 ± 2.01	/	23G/25G	ICG	C3F8/SO	Maintain a facedown position for 1 week.	20 (90.9%)	22 (100%)
Zhu et al. (20)	China	ILM peeling	20	19/1	63.6 ± 8.2	28.34 ± 1.78	6/20	23G	ICG	Air/SO	A prone position for ≥ 8 h per day for 1 week	8 (40%)	19 (95%)
		Inverted ILM insertion	26	21/5	63 ± 5	27.82 ± 2.20						19 (73%)	26 (100%)
		Inverted ILM flap	23	16/7	60 ± 8	28.92 ± 2.86						20 (87%)	21 (91%)
Kim et al. (18)	Korea	Inverted ILM flap	3	21/1	61.8 ± 10.1	28.96 ± 1.57	/	20G/23G /25G	ICG/BBG	SF6/C3F8/SO	Stay in a strict face-down position for 1 to 7 days after surgery	2 (66.7%)	3 (100%)
		ILM peeling	19									11 (57.9%)	19 (100%)
Ho et al. (15)	Taiwan, China	Inverted ILM flap	18	14/3	60.2 ± 8.2	29.25 ± 2.10	4/14	23G/25G	ICG	C3F8	Keep a prone position for 1 week and avoid a supine position afterwards	18 (100%)	17 (94%)
Chen et al. (14)	Taiwan, China	Inverted ILM flap	13	8/5	65.5 ± 7.7	29.75 ± 2.21	10/3	23G/25G	ICG	SF6/C3F8	Keep in a facedown position over night and no supine for 1 week	13 (100%)	13 (100%)
		ILM peeling	14	9/5	62.4 ± 8.6	29.45 ± 1.58	12/2	23G/25G	ICG	SF6/C3F8		6 (42.9%)	14 (100%)
Wakabayashi et al. (17)	Japan	Inverted ILM insertion	13	11/2	67.8 ± 9.9	29.4 ± 0.9	5/8	20G/23G /25G	TA/ICG /BBG	SF6/C3F8/S	/	12 (92%)	12 (92%)
		ILM peeling	36	34/2	69.2 ± 9.1	29.6 ± 1.7	7/29	20G/23G /25G	TA/ICG /BBG	SF6/C3F8/SO		14 (39%)	31 (86%)
Takahashi et al. (16)	Japan	Inverted ILM flap	16	14/2	68.4 ± 7.8	29.1 ± 1.9	8/8	23G/25G /27G	BBG	SF6/C3F8/SO	Maintain a facedown position for mean 12 days	12 (75%)	13 (81%)
		ILM peeling	16	15/1	69.1 ± 8.5	29.6 ± 1.1	9/7	23G/25G /27G	BBG	SF6/C3F8/SO		4 (25%)	15 (93%)
Xu et al. (13)	China	Inverted ILM flap	18	15/3	60.17±9.04	27.37±0.91	10/8	23G	BBG	C3F8	Maintain a facedown position for 3 to 4 weeks	16 (89%)	18 (100%)
		ILM peeling	17	13/4	59.47±8.53	27.71±0.81	12/5	23G	BBG	C3F8		8 (47%)	17 (100%)
Kinoshita et al. (11)	Japan	Inverted ILM flap	5	3/2	64.4 ± 4.5	31.76 ± 2.38	/	25G	BBG	SF6/C3F8	Maintain a facedown position for 10 to 14 days.	5 (100%)	5 (100%).

(Continued)

**TABLE 3 |** Continued

References	Country/ Region	Groups	No. of eyes	Female/Male	Age	AL	RD within/ beyond the arcade	PPV procedure	ILM dyeing	Tamponade agent	Postoperative positioning	Initial MH closure	Initial retinal reattachment
Sasaki et al. (12)	Japan	Inverted ILM flap	6	5/1	75.0 ± 6.4	30.47 ± 2.57	1/5	25G	BBG	SF6/C3F8	Maintain a facedown position postoperatively for at least 5 days	6 (100%)	6 (100%)
		ILM peeling	9	7/2	66.0 ± 12.5	30.10 ± 1.95	3/6	25G	BBG	SF6/C3F8		5 (55.5%)	5 (55.5%)
Baba et al. (10)	Japan	Inverted ILM flap	10	5/5	74	28.95	6/4	25G	BBG	C3F8	Maintain a prone position for approxi- mately 5 days after surgery	8 (80%)	10 (100%)
		ILM peeling	11	8/3	68	30.30	7/4	25G	BBG	C3F8		4 (36%)	10 (91%)
Chen et al. (8)	Taiwan, China	Inverted ILM insertion	20	16/4	62.06 ± 8.90	28.40 ± 1.94	11/9	23G	ICG	C3F8	Keep in a facedown position over night and no supine for 1 week	20 (100%)	20 (100%)
Matsumura et al. (9)	Japan	ILM peeling	20	14/6	60.53 ± 8.78	29.35 ± 1.88	10/10	23G	ICG	C3F8		7 (35%)	20 (100%)
		Inverted ILM flap	10	8/2	67.7 ± 9.7	28.4 ± 2.2		25G	BBG	SF6/C3F8/SO	Maintain a prone position postoperatively for at least 1 week	9 (90%)	9 (90%)
		ILM peeling	12	11/1	75.3 ± 8.7	30.4 ± 1.6		25G	BBG	SF6/C3F8/SO		4 (33.3%)	6 (50.0%)
Lai et al. (7)	Taiwan, China	Inverted ILM insertion	27	24/3	59.1 ± 10.6	29.37 ± 1.92	9/18	23G	ICG	C3F8	Remain in a prone position for 1 day and to avoid the supine position afterward	26 (96%)	26 (96%)

AL, axial length; BBG, brilliant blue G; C3F8, perfluoropropane; ICG, indocyanine green; ILM, internal limiting membranes; MH, macular hole; PPV, pars plana vitrectomy; RD, retinal detachment; SF6, sulfur hexafluoride; SO, silicon oil; TA, triamcinolone acetonide.

for patients who had undergone a primary vitrectomy and gas tamponade for MH or RRD. In fact, the compliance with the face-down positioning was considerably varied among patients, and some patients failed nearly or more than half the time, with considerable variation among patients and better adherence by the female patients, but without associations to the outcomes. When the eye is filled with gas or silicone oil after surgery, the tamponade agent can keep contact with the retina, exert the effect of surface tensions, and close the hole or break except in the lowest position of the vitreous cavity. The macular hole is located at the posterior pole of the eyeball and is not at the lowest position in the eye except during supine positioning. Silicone oil can close the macular hole in the non-facedown positioning. Based on these, it is enough for patients to avoid supine positioning.

To the best of our knowledge, this is the first study to address the issue of positioning after PPV and silicone oil tamponade surgery for MHRD. There was no significant difference in the MH closure, retinal reattachment, and postoperative BCVA between the face-down group and adjustable group in our study. In addition, better postoperative BCVA was gained in both the groups. The rate of MH closure and retinal reattachment was similar to previous reports (42). No complications occurred after the operation.

There are several limitations in our study that should be addressed. First, the study was non-randomized and lacked a randomized model for the positioning choice. Second, the follow-up period was probably short to observe the full recovery of foveal micro-structures. Third, all the eyes were tamponade by silicon oil because we lack the supply of C3F8.

In conclusion, the results of this study suggest that adjustable positioning after PPV with silicon oil tamponade for MHRD repair is effective and safe, and choosing an adjustable positioning over a face-down positioning approach does not reduce the possibility of MH closure, retinal reattachment, and improvement of visual acuity or significantly increase the risk of complications. Face-down positioning does not seem to be necessary for all patients with MHRD. A larger and prospective

randomized controlled trial study is recommended to determine the long-term outcomes of adjustable positioning after PPV surgery for MHRD.

## DATA AVAILABILITY STATEMENT

The raw data supporting the conclusions of this article will be made available by the authors, without undue reservation.

## ETHICS STATEMENT

The studies involving human participants were reviewed and approved by Institutional Review Board of Qingdao Eye Hospital of Shandong First Medical University. The patients/participants provided their written informed consent to participate in this study.

## AUTHOR CONTRIBUTIONS

Material preparation, data collection, and analysis were performed by YG and TR. The first draft of the manuscript was written by JL. All authors contributed to the conception and design of the study, provided comments on the manuscript, and read and approved the final manuscript.

## FUNDING

The funding was provided by the Qingdao Science and Technology Demonstration and Guidance Project (20-3-4-45-nsh) and the Academic Promotion Plan of Shandong First Medical University & Shandong Academy of Medical Sciences (2019ZL001).

## ACKNOWLEDGMENTS

We thank Zhen Guo and Xiuqing Shi for their help in statistical analysis.

## REFERENCES

- Morita H, Ideta H, Ito K, Yonemoto J, Sasaki K, Tanaka S. Causative factors of retinal detachment in macular holes. *Retina*. (1991) 11:281–4. doi: 10.1097/00006982-199111030-00002
- Akiba J, Konno S, Yoshida A. Retinal detachment associated with a macular hole in severely myopic eyes. *Am J Ophthalmol*. (1999) 128:654–5. doi: 10.1016/S0002-9394(99)00240-8
- Grossniklaus HE, Green WR. Pathologic findings in pathologic myopia. *Retina*. (1992) 12:127–33. doi: 10.1097/00006982-199212020-00009
- Gonvers M, Machemer R. A new approach to treating retinal detachment with macular hole. *Am J Ophthalmol*. (1982) 94:468–72. doi: 10.1016/0002-9394(82)90240-9
- Su J, Liu X, Zheng L, Cui H. Vitrectomy with internal limiting membrane peeling vs. no peeling for Macular Hole-induced Retinal Detachment (MHRD): a meta-analysis. *BMC Ophthalmol*. (2015) 15:62. doi: 10.1186/s12886-015-0048-5
- Michalewska Z, Michalewski J, Adelman RA, Nawrocki J. Inverted internal limiting membrane flap technique for large macular holes. *Ophthalmology*. (2010) 117:2018–25. doi: 10.1016/j.ophtha.2010.02.011
- Lai CC, Chen YP, Wang NK, Chuang LH, Liu L, Chen KJ, et al. Vitrectomy with internal limiting membrane repositioning and autologous blood for macular hole retinal detachment in highly myopic eyes. *Ophthalmology*. (2015) 122:1889–98. doi: 10.1016/j.ophtha.2015.05.040
- Chen SN, Yang CM. Inverted internal limiting membrane insertion for macular hole-associated retinal detachment in high myopia. *Am J Ophthalmol*. (2016) 162:99–106.e1. doi: 10.1016/j.ajo.2015.11.013
- Matsumura T, Takamura Y, Tomomatsu T, Arimura S, Gozawa M, Kobori A, et al. Comparison of the inverted internal limiting membrane flap technique and the internal limiting membrane peeling for macular hole with retinal detachment. *PLoS ONE*. (2016) 11:e0165068. doi: 10.1371/journal.pone.0165068
- Baba R, Wakabayashi Y, Umazume K, Ishikawa T, Yagi H, Muramatsu D, et al. Efficacy of the inverted internal limiting membrane flap technique with vitrectomy for retinal detachment associated with myopic macular holes. *Retina*. (2017) 37:466–71. doi: 10.1097/IAE.0000000000001211
- Kinoshita T, Onoda Y, Maeno T. Long-term surgical outcomes of the inverted internal limiting membrane flap technique in highly myopic macular hole retinal detachment. *Graefes Arch Clin Exp Ophthalmol*. (2017) 255:1101–6. doi: 10.1007/s00417-017-3614-0



12. Sasaki H, Shiono A, Kogo J, Yomoda R, Munemasa Y, Syoda M, et al. Inverted internal limiting membrane flap technique as a useful procedure for macular hole-associated retinal detachment in highly myopic eyes. *Eye*. (2017) 31:545–50. doi: 10.1038/eye.2016.263
13. Xu CZ, Wu JH, He JW, Feng C. [Observation of single-layered inverted internal limiting membrane flap technique for macular hole with retinal detachment in high myopia]. *Zhonghua Yan Ke Za Zhi*. (2017) 53:338–43. doi: 10.3760/cma.j.issn.0412-4081.2017.05.005
14. Chen SN, Hsieh YT, Yang CM. Multiple free internal limiting membrane flap insertion in the treatment of macular hole-associated retinal detachment in high myopia. *Ophthalmologica*. (2018) 240:143–9. doi: 10.1159/000487337
15. Ho TC, Ho A, Chen MS. Vitrectomy with a modified temporal inverted limiting membrane flap to reconstruct the foveolar architecture for macular hole retinal detachment in highly myopic eyes. *Acta Ophthalmol*. (2018) 96:e46–e53. doi: 10.1111/aos.13514
16. Takahashi H, Inoue M, Koto T, Itoh Y, Hirota K, Hirakata A. Inverted Internal limiting membrane flap technique for treatment of macular hole retinal detachment in highly myopic eyes. *Retina*. (2018) 38:2317–26. doi: 10.1097/IAE.0000000000001898
17. Wakabayashi T, Ikuno Y, Shiraki N, Matsumura N, Sakaguchi H, Nishida K. Inverted internal limiting membrane insertion versus standard internal limiting membrane peeling for macular hole retinal detachment in high myopia: one-year study. *Graefes Arch Clin Exp Ophthalmol*. (2018) 256:1387–93. doi: 10.1007/s00417-018-4046-1
18. Kim HY, Lee JJ, Kwon HJ, Park SW, Lee JE. Long-term outcomes of macular hole retinal detachment in highly myopic eyes after surgical reattachment. *Korean J Ophthalmol*. (2019) 33:539–46. doi: 10.3341/kjo.2019.0045
19. Gu X, Hu Z, Qian H, Francisca S, Mugisha A, Wang J, et al. Perfluorocarbon liquid-assisted inverted internal limiting membrane flap technique versus internal limiting membrane peeling for highly myopic macular hole retinal detachment. *Retina*. (2020) 41:317–23. doi: 10.1155/2020/2374650
20. Zhu K, Lei B, Wong W, Zhang J, Guo Y, Chen H, et al. Comparison of the internal limiting membrane insertion technique and the inverted internal limiting membrane flap technique with vitrectomy to treat macular hole-associated retinal detachment. *Retina*. (2020) 41:37–44. doi: 10.1097/IAE.0000000000002804
21. Wrzesińska D, Nowomiejska K, Nowakowska D, Toro MD, Bonfiglio V, Reibaldi M, et al. Secondary vitrectomy with internal limiting membrane plug due to persistent full-thickness macular hole OCT-Angiography and microperimetry features: case series. *J Ophthalmol*. (2020) 2020:2650873. doi: 10.1155/2020/2650873
22. Elborgy ES, Starr MR, Kotowski JG, Chehade J, Iezzi R. No face-down positioning surgery for the repair of chronic idiopathic macular holes. *Retina*. (2018) 40:282–9. doi: 10.1097/IAE.0000000000002396
23. Salam A, Harrington P, Raj A, Babar A. Bilateral Ulnar nerve palsies: an unusual complication of posturing after macular hole surgery. *Eye*. (2004) 18:95–7. doi: 10.1038/sj.eye.6700515
24. Starr MR, Iezzi R. Mesenteric venous thrombosis after face-down positioning for retina detachment surgery. *Ophthalmol Retina*. (2018) 2:1174–5. doi: 10.1016/j.oret.2018.06.002
25. Nadal J, Delas B, Piñero A. Vitrectomy without face-down posturing for idiopathic macular holes. *Retina*. (2012) 32:918–21. doi: 10.1097/IAE.0b013e318229b20e
26. Iezzi R, Kapoor KG. No face-down positioning and broad internal limiting membrane peeling in the surgical repair of idiopathic macular holes. *Ophthalmology*. (2013) 120:1998–2003. doi: 10.1016/j.ophtha.2013.06.001
27. Alberti M, la Cour M. Face-down positioning versus non-supine positioning in macular hole surgery. *Br J Ophthalmol*. (2015) 99:236–9. doi: 10.1136/bjophthalmol-2014-305569
28. Ruparelia S, Tuli R, Park J, Shoham-Hazon N, Berco E. Inverted internal limiting membrane flap technique without post-operative face-down positioning for macular hole repair. *Retina*. (2021). doi: 10.1097/IAE.0000000000003350
29. Veith M, Vránová J, Němčanský J, Studnička J, Penčák M, Stranák Z, et al. Surgical treatment of idiopathic macular hole using different types of tamponades and different postoperative positioning regimens. *J Ophthalmol*. (2020) 2020:8858317. doi: 10.1155/2020/8858317
30. Pasu S, Bell L, Zenasni Z, Lanz D, Simmonds IA, Thompson A, et al. Facedown positioning following surgery for large full-thickness macular hole: a multicenter randomized clinical trial. *JAMA Ophthalmol*. (2020) 138:725–30. doi: 10.1001/jamaophthalmol.2020.0987
31. Martínez-Castillo V, Boixadera A, Verdugo A, García-Arumí J. Pars plana vitrectomy alone for the management of inferior breaks in pseudophakic retinal detachment without facedown position. *Ophthalmology*. (2005) 112:1222–6. doi: 10.1016/j.ophtha.2004.12.046
32. Chen X, Yan Y, Hong L, Zhu L. A comparison of strict face-down positioning with adjustable positioning after pars plana vitrectomy and gas tamponade for rhegmatogenous retinal detachment. *Retina*. (2015) 35:892–8. doi: 10.1097/IAE.0000000000000413
33. Martínez-Castillo VJ, García-Arumí J, Boixadera A. Pars plana vitrectomy alone for the management of pseudophakic rhegmatogenous retinal detachment with only inferior breaks. *Ophthalmology*. (2016) 123:1563–9. doi: 10.1016/j.ophtha.2016.03.032
34. Casswell EJ, Yorston D, Lee E, Heeren TFC, Harris N, Zvobgo TM, et al. Effect of face-down positioning vs support-the-break positioning after macula-involving retinal detachment repair: the PostRD randomized clinical trial. *JAMA Ophthalmol*. (2020) 138:634–42. doi: 10.1001/jamaophthalmol.2020.0997
35. Lin Z, Sun JT, Wu RH, Moonasar N, Zhou YH. The safety and efficacy of adjustable postoperative position after pars plana vitrectomy for rhegmatogenous retinal detachment. *J Ophthalmol*. (2017) 2017:5760173. doi: 10.1155/2017/5760173
36. Tranos PG, Peter NM, Nath R, Singh M, Dimitrakos S, Charteris D, et al. Macular hole surgery without prone positioning. *Eye*. (2007) 21:802–6. doi: 10.1038/sj.eye.6702339
37. Xia S, Zhao XY, Wang EQ, Chen YX. Comparison of face-down posturing with nonsupine posturing after macular hole surgery: a meta-analysis. *BMC Ophthalmol*. (2019) 19:34. doi: 10.1186/s12886-019-1047-8
38. Ye T, Yu JG, Liao L, Liu L, Xia T, Yang LL. Macular hole surgery recovery with and without face-down posturing: a meta-analysis of randomized controlled trials. *BMC Ophthalmol*. (2019) 19:265. doi: 10.1186/s12886-019-1272-1
39. Zhu D, Ma B, Zhang J, Huang R, Liu Y, Jing X, et al. Autologous blood clot covering instead of gas tamponade for macular holes. *Retina*. (2019) 40:1751–6. doi: 10.1097/IAE.00000000000002651
40. Cheng CY, Hsu WM, Liu JH, Tsai SY, Chou P. Refractive errors in an elderly Chinese population in Taiwan: the Shihpai Eye Study. *Invest Ophthalmol Vis Sci*. (2003) 44:4630–8. doi: 10.1167/iops.03-0169
41. Xu L, Li J, Cui T, Hu A, Fan G, Zhang R, et al. Refractive error in urban and rural adult Chinese in Beijing. *Ophthalmology*. (2005) 112:1676–83. doi: 10.1016/j.ophtha.2005.05.015
42. Xu Q, Luan J. Vitrectomy with inverted internal limiting membrane flap versus internal limiting membrane peeling for macular hole retinal detachment in high myopia: a systematic review of literature and meta-analysis. *Eye*. (2019) 33:1626–34. doi: 10.1038/s41433-019-0458-3
43. Lai CC. ILM peeling in macular hole retinal detachment: insert or not. *Graefes Arch Clin Exp Ophthalmol*. (2018) 256:1385–6. doi: 10.1007/s00417-018-4049-y
44. Kikushima W, Imai A, Toriyama Y, Hirano T, Murata T, Ishibashi T. Dynamics of macular hole closure in gas-filled eyes within 24 h of surgery observed with swept source optical coherence tomography. *Ophthalmic Res*. (2015) 53:48–54. doi: 10.1159/000368437
45. Zhang Y, Chen X, Hong L, Yan Y, Zeng M, Huang Z, et al. Facedown positioning after vitrectomy will not facilitate macular hole closure based on swept-source optical coherence tomography imaging in gas-filled eyes: a prospective, randomized comparative interventional study. *Retina*. (2019) 39:2353–9. doi: 10.1097/IAE.00000000000002325
46. Seno Y, Shimada Y, Mizuguchi T, Tanikawa A, Horiguchi M. Compliance with the face-down positioning after vitrectomy and gas tamponade for rhegmatogenous retinal detachments.

*Retina.* (2015) 35:1436–40. doi: 10.1097/IAE.0000000000000479

**Conflict of Interest:** The authors declare that the research was conducted in the absence of any commercial or financial relationships that could be construed as a potential conflict of interest.

**Publisher's Note:** All claims expressed in this article are solely those of the authors and do not necessarily represent those of their affiliated organizations, or those of the publisher, the editors and the reviewers. Any product that may be evaluated in

this article, or claim that may be made by its manufacturer, is not guaranteed or endorsed by the publisher.

*Copyright © 2022 Gao, Ruan, Chen, Yu, Xing, Du, Qi and Li. This is an open-access article distributed under the terms of the Creative Commons Attribution License (CC BY). The use, distribution or reproduction in other forums is permitted, provided the original author(s) and the copyright owner(s) are credited and that the original publication in this journal is cited, in accordance with accepted academic practice. No use, distribution or reproduction is permitted which does not comply with these terms.*



# Screening of Common Retinal Diseases Using Six-Category Models Based on EfficientNet

Shaojun Zhu<sup>1,2†</sup>, Bing Lu<sup>1†</sup>, Chenghu Wang<sup>3</sup>, Maonian Wu<sup>1,2</sup>, Bo Zheng<sup>1,2</sup>, Qin Jiang<sup>3\*</sup>, Ruili Wei<sup>4\*</sup>, Qixin Cao<sup>5</sup> and Weihua Yang<sup>3\*</sup>

## OPEN ACCESS

### Edited by:

Shaochong Zhang,  
Shenzhen Eye Hospital, China

### Reviewed by:

Carl-Magnus Svensson,  
Leibniz Institute for Natural Product  
Research and Infection  
Biology, Germany  
Yalin Zheng,  
University of Liverpool,  
United Kingdom  
João Almeida,  
Federal University of Maranhão, Brazil

### \*Correspondence:

Qin Jiang  
jqin710@vip.sina.com  
Ruili Wei  
rui.liwei@126.com  
Weihua Yang  
benben0606@139.com

<sup>†</sup>These authors have contributed  
equally to this work and share first  
authorship

### Specialty section:

This article was submitted to  
Ophthalmology,  
a section of the journal  
Frontiers in Medicine

**Received:** 03 November 2021

**Accepted:** 12 January 2022

**Published:** 23 February 2022

### Citation:

Zhu S, Lu B, Wang C, Wu M,  
Zheng B, Jiang Q, Wei R, Cao Q and  
Yang W (2022) Screening of Common  
Retinal Diseases Using Six-Category  
Models Based on EfficientNet.  
Front. Med. 9:808402.  
doi: 10.3389/fmed.2022.808402

<sup>1</sup> School of Information Engineering, Huzhou University, Huzhou, China, <sup>2</sup> Zhejiang Province Key Laboratory of Smart Management and Application of Modern Agricultural Resources, Huzhou University, Huzhou, China, <sup>3</sup> The Affiliated Eye Hospital of Nanjing Medical University, Nanjing, China, <sup>4</sup> Department of Ophthalmology, Shanghai Changzheng Hospital, Huangpu, China, <sup>5</sup> Huzhou Traditional Chinese Medicine Hospital Affiliated to Zhejiang University of Traditional Chinese Medicine, Huzhou, China

**Purpose:** A six-category model of common retinal diseases is proposed to help primary medical institutions in the preliminary screening of the five common retinal diseases.

**Methods:** A total of 2,400 fundus images of normal and five common retinal diseases were provided by a cooperative hospital. Two six-category deep learning models of common retinal diseases based on the EfficientNet-B4 and ResNet50 models were trained. The results from the six-category models in this study and the results from a five-category model in our previous study based on ResNet50 were compared. A total of 1,315 fundus images were used to test the models, the clinical diagnosis results and the diagnosis results of the two six-category models were compared. The main evaluation indicators were sensitivity, specificity, F1-score, area under the curve (AUC), 95% confidence interval, kappa and accuracy, and the receiver operator characteristic curves of the two six-category models were compared in the study.

**Results:** The diagnostic accuracy rate of EfficientNet-B4 model was 95.59%, the kappa value was 94.61%, and there was high diagnostic consistency. The AUC of the normal diagnosis and the five retinal diseases were all above 0.95. The sensitivity, specificity, and F1-score for the diagnosis of normal fundus images were 100, 99.9, and 99.83%, respectively. The specificity and F1-score for RVO diagnosis were 95.68, 98.61, and 93.09%, respectively. The sensitivity, specificity, and F1-score for high myopia diagnosis were 96.1, 99.6, and 97.37%, respectively. The sensitivity, specificity, and F1-score for glaucoma diagnosis were 97.62, 99.07, and 94.62%, respectively. The sensitivity, specificity, and F1-score for DR diagnosis were 90.76, 99.16, and 93.3%, respectively. The sensitivity, specificity, and F1-score for MD diagnosis were 92.27, 98.5, and 91.51%, respectively.

**Conclusion:** The EfficientNet-B4 model was used to design a six-category model of common retinal diseases. It can be used to diagnose the normal fundus and five common retinal diseases based on fundus images. It can help primary doctors in the screening for

common retinal diseases, and give suitable suggestions and recommendations. Timely referral can improve the efficiency of diagnosis of eye diseases in rural areas and avoid delaying treatment.

**Keywords:** fundus, retinal diseases, computer simulation, vision screening, optical imaging

## INTRODUCTION

Common retinal diseases include retinal vein occlusion (RVO), high myopia, glaucoma, diabetic retinopathy (DR), and macular degeneration (MD) (1–5). DR and MD are high-incidence fundus diseases in China. According to statistics, patients with fundus diseases account for 54.7% of all blindness patients in China. There are more than three million people suffering from fundus diseases and more than two-thirds of patients with fundus diseases face blindness every year. Ophthalmologists use a non-mydratic fundus color camera to obtain images of the fundus in these five common retinal diseases. A diagnosis is made by reading and interpreting the fundus images (6). At present, China's rural areas have inefficient transportation systems, poor medical conditions, and few professional ophthalmologists. Hence, patients with ophthalmopathy often only go to hospitals in the city to seek for treatment when the disease has already progressed; this may lead to delays in getting the best available treatment and may cause serious consequences for the patient.

A six-category model consisting of the normal retina and five common retinal diseases was designed to help patients with ophthalmopathy. This may be useful in rural areas for the preliminary diagnosis, accurate classification, and timely referral of retinal diseases.

In recent years, feature extraction methods using traditional machine learning have become a common method for diagnosing ophthalmologic diseases. The pertinent features of the ophthalmologic diseases were manually selected then identified through machine learning (7–13). Deep learning used convolutional neural networks to automatically extract image features; it obtained satisfactory results in the field of ophthalmology (14–23). Many researchers have used deep learning to diagnose retinal diseases using fundus images.

Nagasato et al. (24) compared the ability of machine learning technology and deep learning technology in the detection of branch RVO through the ultra-wide field-of-view fundus images; they found that deep learning technology had higher sensitivity and specificity. Li et al. (20) used convolutional neural networks to design a system based on macular images obtained through optical coherence tomography to identify the visual conditions of patients with high myopia; the said system had high area under the curve (AUC), sensitivity, and specificity. Ahn et al. (25) trained a new neural network model using fundus photos that can detect early and late glaucoma, with a high AUC. The Google team of Gulshan et al. (26) trained a deep learning model to diagnose DR through fundus images, and automatically graded DR; they obtained satisfactory results and carried out clinical trials upon patient follow-up. Yim et al. (21) combined a three-dimensional optical coherence tomography image and the corresponding automatic tissue map to design an artificial

intelligence model to predict the progress of the other eye's conversion to exudative age-related macular degeneration of a patient with one eye diagnosed to have the said ophthalmologic disease. There were also a few studies that focused on the simultaneous screening of multiple diseases. Zheng et al. (15) used 2,000 fundus images to design a five-category model of common retinal diseases based on ResNet50; the model was able to diagnose common retinal diseases, except for macular degeneration (MD). Cen et al. (27) used deep neural networks to identify 39 retinal diseases and conditions that needed to be referred to higher facilities of care; although satisfactory results were achieved, the amount of data required for training was too large.

Our team in a previous study used the ResNet50 to create a five-category model that consisted of the normal fundus and four common fundus diseases (RVO, high myopia, glaucoma, and DR) (15), with an AUC above 0.92 and a kappa value of 89.33%. The retinal diseases in the previous study did not include MD because of its complicated features and different subtypes. However, since MD is a common retinal disease, our team included it in the new classification model used in this study.

This study designed a six-category model for common retinal diseases based on the EfficientNet model. It was used to detect the normal fundus and five common retinal diseases using fundus images. The model can help patients with ophthalmopathy in rural areas in their initial diagnosis of common retinal diseases for their prompt referral.

## MATERIALS AND METHODS

### Data Source

The images used in this study were obtained from the Intelligent Ophthalmology Database of the Ophthalmology Hospital of Nanjing Medical University. These images were obtained by various types of non-mydratic fundus cameras. This study used the EfficientNet model to train a six-category model for common fundus diseases. A total of 2,400 fundus images were used as training data; there were 400 fundus images for each retinal disease and 400 images of normal fundus. A total of 1,315 fundus images were used as test data. The research had no restrictions on the sex and age of the patients who had their fundus images taken. The relevant personal information of the patients were removed before the fundus images were delivered to the researchers. Therefore, this research did not determine the demographic information of the patients who had their fundus images taken.

The fundus images provided by the cooperative hospital were of high quality. The actual diagnoses of the images were given at the same time and were regarded as the diagnoses from the expert ophthalmologist. Two other experienced



ophthalmologists independently diagnosed the fundus images. If the two ophthalmologists had the same diagnosis, then it was regarded as the final diagnosis. However, if the two ophthalmologists had different diagnoses, then the expert ophthalmologist would assess the fundus image and gave the final diagnosis. The fundus images only had one disease and did not contain multiple retinal diseases. A fundus image could only be assessed as normal or diagnosed with one of the five common retinal diseases (RVO, high myopia, glaucoma, DR, and MD). The normal fundus image and the fundus images of the five common retinal diseases are shown in the first column of **Figure 1**.

## Model Training

The EfficientNet-B4 model (28) was used to classify the normal fundus and the five common retinal diseases using the fundus images. The EfficientNet model was proposed by Google. EfficientNet-B0 provided the backbone; its depth, width, and resolution were jointly adjusted to obtain the other models. Finally, eight models with different parameters, from EfficientNet-B0 to EfficientNet-B7, were created. EfficientNet-B4 is mainly composed of one stem, seven blocks, and one final layer. The seven blocks mainly included modules 1, 2, and 3. All modules were mainly composed of the convolutional layer, pooling layer, and activation layer. The model structure and learning curves of EfficientNet-B4 is shown in **Figures 2, 3**, respectively.

The classic classification model of deep learning also included other models like VGG16 (28) and ResNet50 (29), among others. Their basic network structure mainly included convolutional layers, pooling layers, and fully connected layers. Our team previously used ResNet50 to train a five-category intelligent auxiliary diagnosis model for common retinal diseases (normal fundus and four common retinal diseases, excluding MD in that study) (15). Hence, in this study, the ResNet50 model was used to classify the normal fundus and the five common retinal diseases. The results of the ResNet50 model were compared with the results of the EfficientNet-B4 model.

The six-category model of common retinal diseases only changed the output layer category; there were no changes on the original network structure of the EfficientNet-B4 model during training. The initial parameters of the six-category model obtained after training were transferred to the ImageNet Large Scale Visual Recognition Challenge (30) to improve the initial performance of the model. Then, 2,400 fundus images were used to train the model iteratively to obtain the best weighted parameters. Finally, the six-category model of common retinal diseases was obtained.

## Statistical Analysis

SPSS version 22.0 statistical software was used for statistical analysis. The receiver operating characteristic curve was used to analyze the diagnostic performance of the model, and kappa value was used to test the consistency of the diagnosis between the expert and the model. A kappa value of 0.61–0.80 indicated significant consistency, and >0.80 indicated high consistency. The sensitivity, specificity, F1-score, 95% confidence interval,

AUC and other indicators of the six-category model of the normal fundus and the five common retinal diseases were calculated. The classification effect of the AUC values were interpreted as follows: >0.85, high; 0.7–0.85, average; and 0.5–0.7, poor.

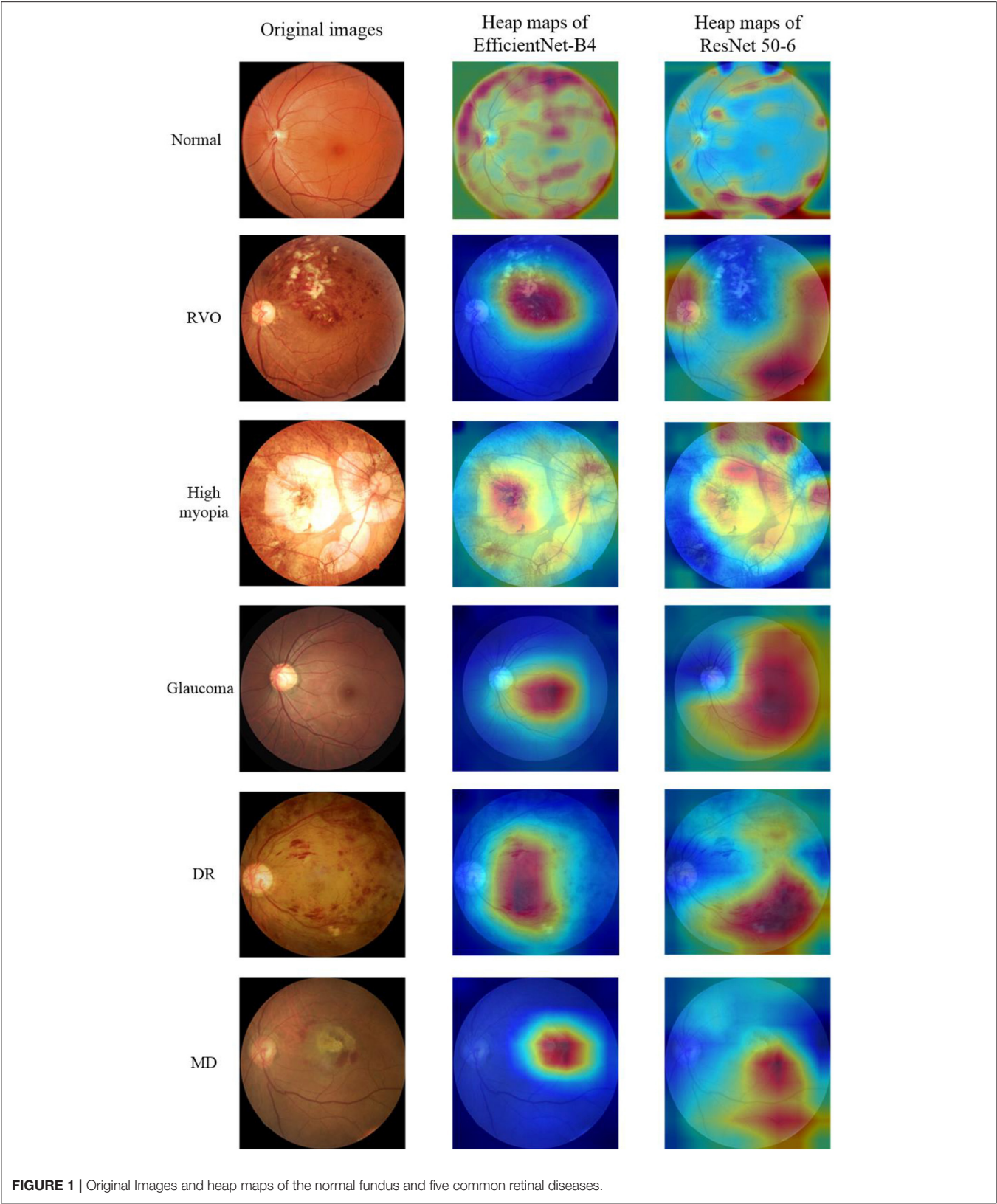
## RESULTS

There were 1,315 fundus images used to test the six-category models of the common retinal diseases. The expert ophthalmologist diagnosed 300 fundus images as normal, 162 fundus images as RVO, 308 fundus images as high myopia, 126 fundus images as glaucoma, 238 fundus images as DR, and 181 fundus images as MD. The EfficientNet-B4 six-category model diagnosed 301 fundus images as normal, 171 fundus images as RVO, 300 fundus images as high myopia, 134 fundus images as glaucoma, 225 fundus images as DR, and 167 fundus images as MD. The ResNet50 six-category model diagnosed 301 fundus images as normal, 168 fundus images as RVO, 265 fundus images as high myopia, 161 fundus images as glaucoma, 221 fundus images as DR, and 199 fundus images as MD. The results of the EfficientNet-B4 model and the ResNet50 model are shown in **Tables 1, 2**, respectively.

Compared with the expert diagnosis group, the EfficientNet-B4 six-category model had 95% sensitivity for the diagnoses of RVO, high myopia, and glaucoma, while 90% sensitivity was found for the diagnoses of DR and MD. The specificity for diagnosing the five retinal diseases was approximately 99%. All the AUCs were above 95%, and the kappa value was 94.61%; this implies a high consistency of the model. The ResNet50 six-category model (ResNet 50-6) had >80% sensitivity for the diagnoses of RVO, high myopia, glaucoma, and DR. However, the sensitivity of the model for diagnosing MD was only at 67.96%. There was >93% specificity for diagnosing the five retinal diseases. All the AUCs were above 80%, and the kappa value was 81.31%; thus, there was high consistency of the model. The ResNet50 five-category model (15) (ResNet50-5) was made by our team; it is a five-category intelligent auxiliary diagnosis model of common retinal diseases. All the indicators for diagnosing the normal fundus images of the three models can reach 99%. The evaluation index results of the three models are shown in **Table 3**.

The EfficientNet-B4 and ResNet50-6 models are six-category models, while the ResNet50-5 model is a five-category model for common retinal diseases. The EfficientNet-B4 model was found to be superior to the ResNet50-6 and ResNet50-5 models in terms of sensitivity and specificity in the diagnoses of RVO, high myopia, glaucoma, and DR. The ResNet50-5 model could diagnose more accurately RVO, high myopia, glaucoma, and DR than the ResNet50-6 model. **Figure 3** shows the accuracy and loss curves of Efficient-B4. **Figure 4** shows the comparison of ROC curves between the EfficientNet-B4 model and the ResNet50-6 model for the assessment of the images of the normal fundus and of the five common retinal diseases.

This study used Grad-CAM (31) to make heat maps for the EfficientNet-B4 and ResNet 50-6 models, as shown in the second and third columns of **Figure 1**, respectively. It can be seen from



the figure that the focus area marked by the heat map of the EfficientNet-B4 model is more accurate, while the accuracy of the focus area marked by the ResNet 50-6 model is slightly worse. In this study, when the same algorithm is used to obtain the

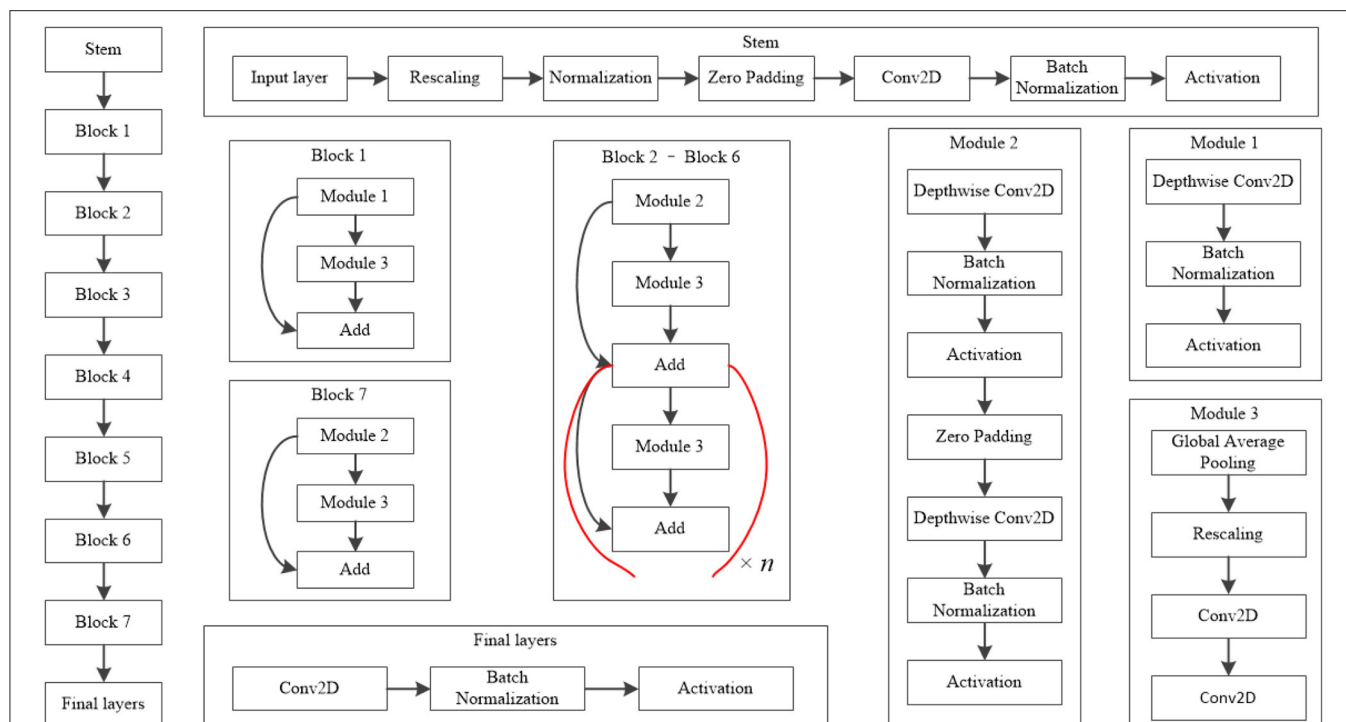


**FIGURE 2 |** Model structure of EfficientNet-B4. The values of  $n$  in this figure of Block 2–Block 6 is 2, 2, 4, 4, and 6, respectively.

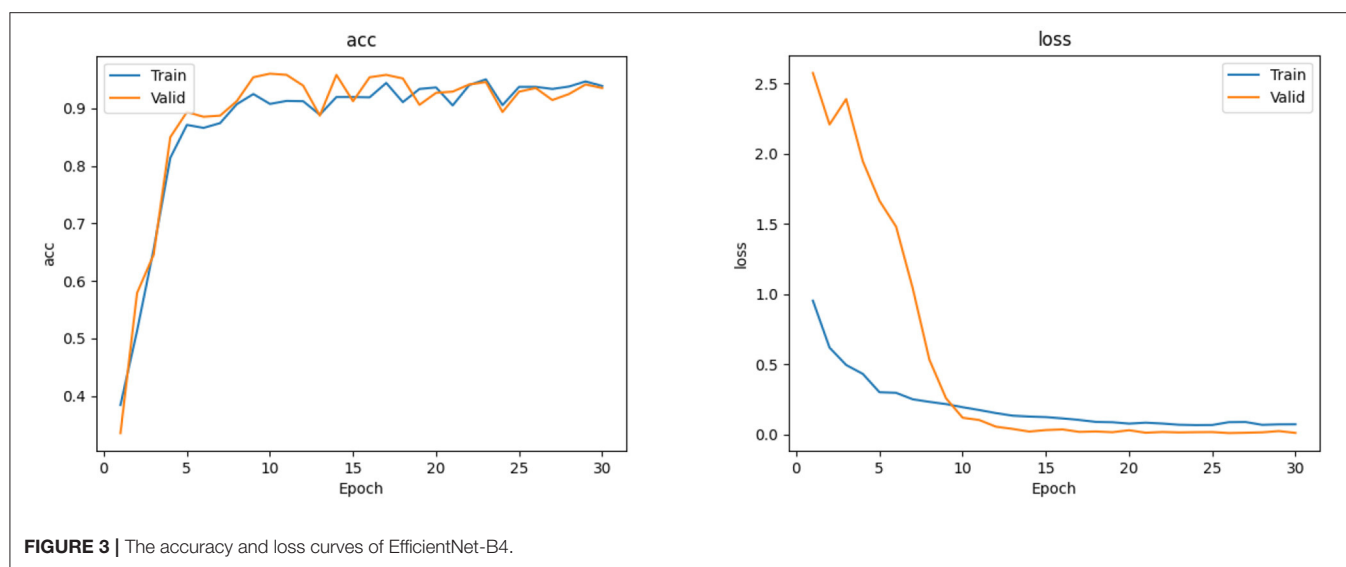


**FIGURE 3 |** The accuracy and loss curves of EfficientNet-B4.

heat map, the better the evaluation index of the model, the more accurate the heat map area obtained.

## DISCUSSION

In 1998, LeCun et al. (32) proposed the LeNet-5 model that used convolutional neural networks to recognize handwritten digits. Their study laid the foundation for the basic convolutional neural network (CNN) architecture of convolution, pooling,

and fully connected layers. After the year 2012, deep learning had developed rapidly. The AlexNet (33) model, VGG model, GoogleNet (34) model, and ResNet model had obtained the best results for the image classification or object detection using the ImageNet Large Scale Visual Recognition Challenge. In 2019, Google researchers proposed the EfficientNet model. First, the MnasNet (35) method was used to design EfficientNet-B0 that served as the basebone of EfficientNet-B1 to B7. The network depth, width, and resolution were refined in the succeeding

**TABLE 1** | Diagnostic results of the EfficientNet-B4 model.

Clinical	EfficientNet-B4 Model						
	Normal	RVO	High myopia	Glaucoma	DR	MD	Total
Normal	300	0	0	0	0	0	300
RVO	0	155	0	1	4	2	162
High myopia	0	1	296	7	2	2	308
Glaucoma	0	0	1	123	0	2	126
DR	1	9	1	0	216	11	238
MD	0	6	2	3	3	167	181
Total	301	171	300	134	225	184	1,315

RVO, retinal vein occlusion; DR, diabetic retinopathy; MD, macular degeneration.

**TABLE 2** | Diagnostic results of the ResNet50 model.

Clinical	ResNet50 Model						
	Normal	RVO	High myopia	Glaucoma	DR	MD	Total
Normal	299	0	0	0	0	1	300
RVO	0	133	1	3	15	10	162
High myopia	0	2	259	18	1	28	308
Glaucoma	0	1	0	108	3	14	126
DR	0	15	0	9	191	23	238
MD	2	17	5	23	11	123	181
Total	301	168	265	161	221	199	1,315

RVO, retinal vein occlusion; DR, diabetic retinopathy; MD, macular degeneration.

**TABLE 3** | Evaluation of the index results of the three models.

Model	Evaluation indicators	Normal	RVO	High myopia	Glaucoma	DR	MD
EfficientNet-B4	Sensitivity	100%	95.68%	96.10%	97.62%	90.76%	92.27%
	Specificity	99.90%	98.61%	99.60%	99.07%	99.16%	98.50%
	F1-score	99.83%	93.09%	97.37%	94.62%	93.30%	91.51%
	AUC	1	0.971	0.979	0.983	0.950	0.954
	95% CI	0.998–1	0.953–0.990	0.966–0.991	0.968–0.999	0.928–0.971	0.931–0.977
	Kappa				94.61%		
	Accuracy				95.59%		
ResNet50-6	Sensitivity	99.67%	82.10%	84.09%	85.71%	80.25%	67.96%
	Specificity	99.80%	96.96%	99.40%	95.54%	97.21%	93.30%
	F1-score	99.50%	80.61%	90.40%	75.26%	83.22%	64.74%
	AUC	0.997	0.895	0.917	0.906	0.887	0.806
	95% CI	0.993–1	0.860–0.931	0.893–0.942	0.870–0.943	0.857–0.918	0.765–0.848
	Kappa				81.31%		
	Accuracy				84.64%		
ResNet50-5 (15)	Sensitivity	99.33%	87.65%	87.34%	95.24%	88.24%	—
	Specificity	100.00%	96.50%	99.52%	96.43%	97.66%	—
	F1-score	99.67%	84.02%	92.60%	85.11%	89.55%	—
	AUC	0.996	0.921	0.934	0.958	0.929	—
	95% CI	0.991–1	0.890–0.951	0.912–0.956	0.936–0.981	0.905–0.954	—
	Kappa				89.33%		
	Accuracy				90.59%		

AUC, area under the curve; CI, confidence interval; RVO, retinal vein occlusion; DR, diabetic retinopathy; MD, macular degeneration.



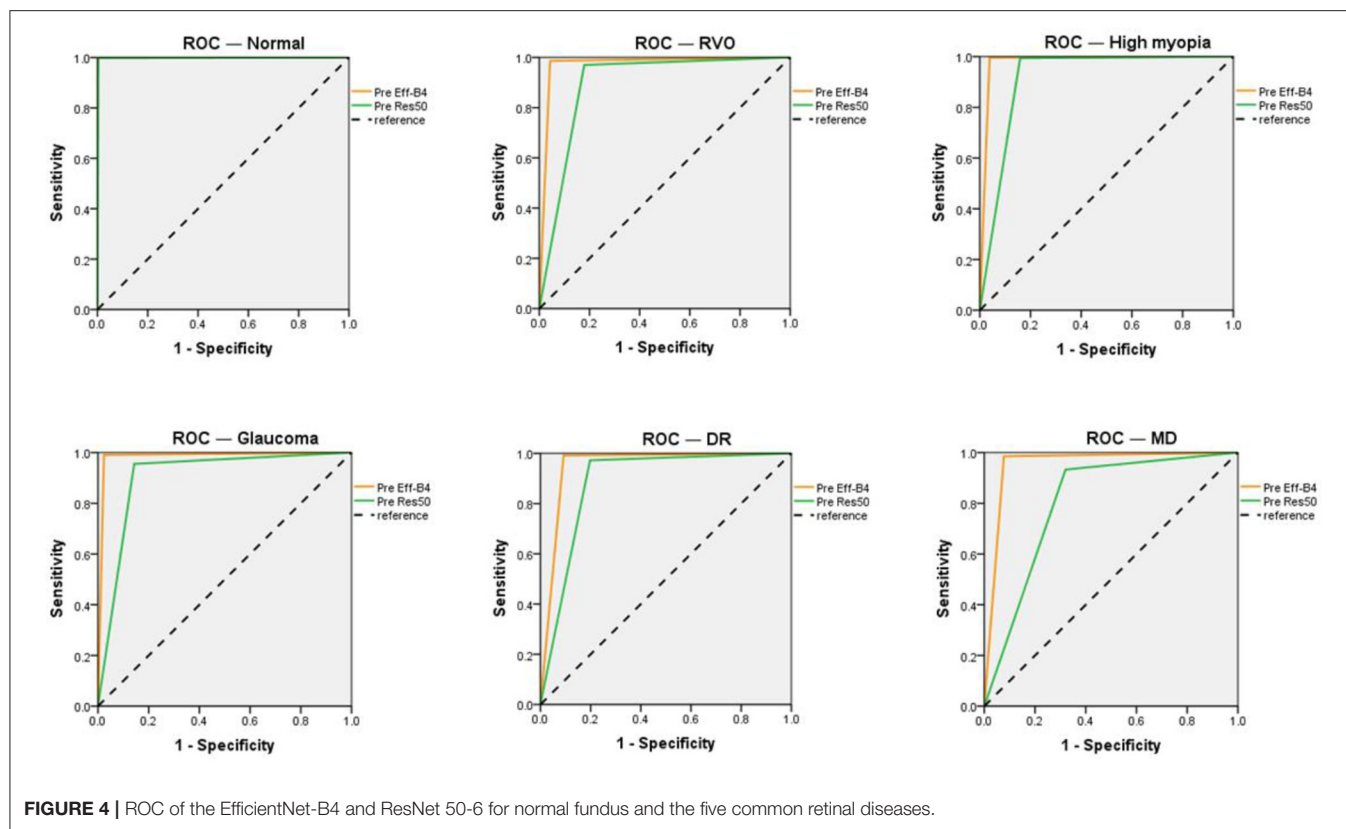


**FIGURE 4 |** ROC of the EfficientNet-B4 and ResNet 50-6 for normal fundus and the five common retinal diseases.

versions. In this study, the EfficientNet model was selected to classify the normal and the five common retinal diseases based on the fundus images. Compared with other models, EfficientNet showed a better ability to extract the internal features, hence the classification and diagnoses were improved.

Tables 1, 2 shows that the EfficientNet-B4 model had a better diagnostic ability as compared with the ResNet50-6 model. The main reason could be explained by the complexity of the fundus images; there were inconsistent focus areas and varying characteristics of the different retinal diseases. The ResNet 50 model had 50 layers, while the EfficientNet-B4 model had deeper layers. Thus, the deep features of the fundus image could be extracted through operations, such as convolution. These deep features could help increase the accuracy of the model's assessment of the fundus image's diagnosis. However, the models used in this study had poor diagnostic results for MD. It was misdiagnosed as other diseases in large numbers because of its complicated manifestation in fundus images. The models had a difficulty in determining MD from other types of macular lesions, hence leading to misdiagnosis.

Our team had proposed a five-category model for normal fundus images and the four common retinal diseases based on the ResNet50 model. MD was not included in the four common retinal diseases in that study. Moreover, the results of the related retinal diseases were compared with the results of the five-category model. The results of the ResNet50-5 model in Table 3

are based on the five-category model. The addition of new categories will increase the difficulty of the model's identification of the target. The accuracy of the classification of the results by the model would decrease. This would apply to the features of other retinal diseases that may contain the features of MD that would make the diagnosis of MD more difficult. Consequently, this increases the probability of misdiagnosing MD as other types of retinal disease.

Some researchers had also done research on multi-class fundus diseases. Karthikeyan et al. (36) used deep learning to detect 12 major retinal complications, and the verification accuracy was 92.99%. Wang et al. (37) used the EfficientNet model to do multi-label classification research and the accuracy was 92%. The accuracy of the EfficientNet-B4 model in this study is 95.59%, but the images only had single labels, which was normal and five common fundus diseases. Other fundus diseases were usually classified into five fundus diseases, and then they would be diagnosed again by a doctor.

Tables 1–3, show that the two six-category models could diagnose normal fundus images. It is rare for normal fundus images to be diagnosed with retinal disease. There was one or two images with retinal disease that were diagnosed as normal images for the two models; the misdiagnosis mainly occurred in the fundus images of DR and MD. In the typical process of making a diagnosis, the doctor would need to confirm the results after the preliminary diagnosis using the

classification model. The DR and MD lesions were relatively apparent, and even non-ophthalmologists could make good judgments after basic training. Therefore, the missed diagnosis of these two retinal diseases will be greatly reduced after the doctor's confirmation.

The six-category model for common fundus diseases based on EfficientNet-B4 had high sensitivity and specificity for diagnosing normal fundus and five common retinal diseases. Therefore, it may be suitable for the primary diagnosis of common retinal diseases at the primary hospital. It may help increase diagnostic accuracy in primary care and support early detection, diagnosis, treatment, and referral. However, the model also had some shortcomings. For example, the sensitivity of diagnosing DR and MD was lower than in the other retinal diseases. The model could be further improved by increasing the number of training images to attain a better diagnostic performance.

## DATA AVAILABILITY STATEMENT

The raw data supporting the conclusions of this article will be available from the corresponding author on reasonable request.

## REFERENCES

- Hogarty DT, Mackey DA, Hewitt AW. Current state and future prospects of artificial intelligence in ophthalmology: a review. *Clin Experiment Ophthalmol.* (2019) 47:128–39. doi: 10.1111/ceo.13381
- Yang WH, Zheng B, Wu MN, Zhu SJ, Fei FQ, Weng M, et al. An evaluation system of fundus photograph-based intelligent diagnostic technology for diabetic retinopathy and applicability for research. *Diabetes Ther.* (2019) 10:1811–22. doi: 10.1007/s13300-019-0652-0
- Armstrong GW, Lorch AC. A (eye): a review of current applications of artificial intelligence and machine learning in ophthalmology. *Int Ophthalmol Clin.* (2020) 60:57–71. doi: 10.1097/IIO.0000000000000298
- Nagasato D, Tabuchi H, Masumoto H, Enno H, Ishitobi N, Kameoka M, et al. Automated detection of a nonperfusion area caused by retinal vein occlusion in optical coherence tomography angiography images using deep learning. *PLoS ONE.* (2019) 14:1–14. doi: 10.1371/journal.pone.0223965
- Tan TE, Anees A, Chen C, Li SH, Xu XX, Li ZX, et al. Retinal photograph-based deep learning algorithms for myopia and a blockchain platform to facilitate artificial intelligence medical research: a retrospective multicohort study. *Lancet Digit Health.* (2021) 3:e317–29. doi: 10.1016/S2589-7500(21)00055-8
- Walter T, Massin P, Erginay A, Ordonez R, Jeulin C, Klein JC. Automatic detection of microaneurysms in color fundus images. *Med Image Anal.* (2007) 11:555–66. doi: 10.1016/j.media.2007.05.001
- Hosoda Y, Miyake M, Yamashiro K, Ooto S, Takahashi A, Oishi A, et al. Deep phenotype unsupervised machine learning revealed the significance of pachychoroid features in etiology and visual prognosis of age-related macular degeneration. *Sci Rep.* (2020) 10:1–13. doi: 10.1038/s41598-020-75451-5
- Xu J, Yang W, Wan C, Shen J. Weakly supervised detection of central serous chorioretinopathy based on local binary patterns and discrete wavelet transform. *Comput Biol Med.* (2020) 127:104056. doi: 10.1016/j.compbiomed.2020.104056
- Chowdhury A R, Banerjee S. Detection of abnormalities of retina due to diabetic retinopathy and age related macular degeneration using SVM. *Sci J Circuits Syst Signal Process.* (2016) 5:1–7. doi: 10.11648/j.cssp.20160501.11
- Rajan A, Ramesh G P. Automated early detection of glaucoma in wavelet domain using optical coherence tomography images. *Biosci Biotechnol Res Asia.* (2015) 12:2821–8. doi: 10.13005/bbra/1966

## AUTHOR CONTRIBUTIONS

SZ and BZ wrote the manuscript. CW, MW, and WY reviewed the manuscript. BL and QJ trained the model. RW and QC collected and labeled the data. All authors issued final approval for the version to be submitted.

## FUNDING

This research supported by the National Natural Science Foundation of China (No. 61906066), Natural Science Foundation of Zhejiang Province (No. LQ18F020002), Science and Technology Planning Project of Huzhou Municipality (No. 2016YZ02), and Nanjing Enterprise Expert Team Project. The Medical Science and Technology Development Project Fund of Nanjing (Grant No. YKK21262); Teaching Reform Research Project of Zhejiang Province (jg20190446).

## ACKNOWLEDGMENTS

We would like to thank Editage ([www.editage.cn](http://www.editage.cn)) for English language editing.

- Zhang H, Chen Z, Chi Z, Fu H. Hierarchical local binary pattern for branch retinal vein occlusion recognition with fluorescein angiography images. *Electron Lett.* (2014) 50:1902–4. doi: 10.1049/el.2014.2854
- Liu J, Wong D W K, Lim J H, Tan N M, Zhang Z, Li H, et al. Detection of pathological myopia by PAMELA with texture-based features through an SVM approach. *J Healthc Eng.* (2010) 1:1–11. doi: 10.1260/2040-2295.1.1.1
- Bizios D, Heijl A, Hougaard J L, Bengtsson B. Machine learning classifiers for glaucoma diagnosis based on classification of retinal nerve fibre layer thickness parameters measured by Stratus OCT. *Acta Ophthalmol.* (2010) 88:44–52. doi: 10.1111/j.1755-3768.2009.01784.x
- Fu H, Li F, Sun X, Cao X, Liao J, Orlando J I, et al. AGE challenge: angle closure glaucoma evaluation in anterior segment optical coherence tomography. *Med Image Anal.* (2020) 66:101798. doi: 10.1016/j.media.2020.101798
- Zheng B, Jiang Q, Lu B, He K, Wu M N, Hao X L, et al. Five-Category intelligent auxiliary diagnosis model of common fundus diseases based on fundus images. *Transl Vis Sci Technol.* (2021) 10:1–10. doi: 10.1167/tvst.10.7.20
- Xu J, Wan C, Yang W, Zheng B, Yan Z, Shen J. A novel multi-modal fundus image fusion method for guiding the laser surgery of central serous chorioretinopathy. *Math Biosci Eng.* (2021) 18:4797–816. doi: 10.3934/mbe.2021244
- Zheng B, Liu Y, He K, Wu M, Jin L, Jiang Q, et al. Research on an intelligent lightweight-assisted pterygium diagnosis model based on anterior segment images. *Dis Markers.* (2021) 2021:1–8. doi: 10.1155/2021/7651462
- Zhang H, Niu K, Xiong Y, Yang W, He Z, Song H. Automatic cataract grading methods based on deep learning. *Comput Methods Programs Biomed.* (2019) 182:104978. doi: 10.1016/j.cmpb.2019.07.006
- Tang Z, Zhang X, Yang G, Zhang G, Gong Y, Zhao K, et al. Automated segmentation of retinal nonperfusion area in fluorescein angiography in retinal vein occlusion using convolutional neural networks. *Med Phys.* (2021) 48:648–58. doi: 10.1002/mp.14640
- Li Y, Feng W, Zhao X, Liu B, Zhang Y, Chi W, et al. Development and validation of a deep learning system to screen vision-threatening conditions in high myopia using optical coherence tomography images. *Br J Ophthalmol.* (2020) 0:1–7. doi: 10.1136/bjophthalmol-2020-317825
- Yim J, Chopra R, Spitz T, Winkens J, Obika A, Kelly C, et al. Predicting conversion to wet age-related macular degeneration using deep learning. *Nat Med.* (2020) 26:892–9. doi: 10.1038/s41591-020-0867-7

22. Yan Q, Weeks D E, Xin H, Swaroop A, Chew E Y, Huang H, et al. Deep-learning-based prediction of late age-related macular degeneration progression. *Nat Mach Intell.* (2020) 2:141–50. doi: 10.1038/s42256-020-0154-9
23. Orlando J I, Fu H, Breda J B, Keer K, Bathula D R, Rinto A D, et al. Refuge challenge: A unified framework for evaluating automated methods for glaucoma assessment from fundus photographs. *Med Image Anal.* (2020) 59:101570. doi: 10.1016/j.media.2019.101570
24. Nagasato D, Tabuchi H, Ohsugi H, Masumoto H, Enno H, Ishitobi N, et al. Deep-learning classifier with ultrawide-field fundus ophthalmoscopy for detecting branch retinal vein occlusion. *Int J Ophthalmol.* (2019) 12:94–99. doi: 10.18240/ijo.2019.01.15
25. Ahn J M, Kim S, Ahn K S, Cho S H, Lee K B, Kim US. A deep learning model for the detection of both advanced and early glaucoma using fundus photography. *PloS ONE.* (2018) 13:1–8. doi: 10.1371/journal.pone.0207982
26. Gulshan V, Peng L, Coram M, Stumpe M C, Wu D, Narayanaswamy A, et al. Development and validation of a deep learning algorithm for detection of diabetic retinopathy in retinal fundus photographs. *JAMA.* (2016) 316:2402–10. doi: 10.1001/jama.2016.17216
27. Cen L P, Ji J, Lin J W, Ju S T, Lin H J, Li T P, et al. Automatic detection of 39 fundus diseases and conditions in retinal photographs using deep neural networks. *Nat Commun.* (2021) 12:1–13. doi: 10.1038/s41467-021-25138-w
28. Tan M, Le Q. Efficientnet: rethinking model scaling for convolutional neural networks. In: *International Conference on Machine Learning*. Los Angeles, CA: PMLR (2019). p. 6105–14.
29. Simonyan K, Zisserman A, Simonyan K, Zisserman A. Very deep convolutional networks for large-scale image recognition. arXiv preprint arXiv:1409.1556 (2014). Available online at: <https://arxiv.org/abs/1409.1556>. pdf
30. Deng J, Dong W, Socher R, Li L-J, Li K, Li F-F. Imagenet: a large-scale hierarchical image database. In: *IEEE conference on computer vision and pattern recognition*. Miami, FL. (2009). p.248–55. doi: 10.1109/CVPR.2009.5206848
31. Selvaraju RR, Cogswell M, Das A, Vedantam R, Parikh D, Batra D. Grad-cam: visual explanations from deep networks via gradient-based localization. In: *Proceedings of the IEEE international conference on computer vision*. Venice. (2017). p. 618–26.
32. LeCun Y, Bottou L, Bengio Y, Haffner P. Gradient-based learning applied to document recognition. *Proceedings of the IEEE.* (1998) 86:2278–324. doi: 10.1109/5.726791
33. Krizhevsky A, Sutskever I, Hinton GE. Imagenet classification with deep convolutional neural networks. *Adv Neural Inf Process Syst.* (2012) 25:1097–105. doi: 10.1145/3065386
34. Szegedy C, Liu W, Jia Y, Sermanet P, Reed S, Anguelov D, et al. Going deeper with convolutions. In: *Proceedings of the IEEE conference on computer vision and pattern recognition*. Boston, MA. (2015). p. 1–9.
35. Tan M, Chen B, Pang R, Vasudevan V, Sandler M, Howard A, et al. Mnasnet: Platform-aware neural architecture search for mobile. In: *Proceedings of the IEEE/CVF Conference on Computer Vision and Pattern Recognition*. Long Beach, CA. (2019). p. 2820–8.
36. Karthikeyan S, Kumar PS, Madhusudan RJ, Sundaramoorthy SK, Namboori PKK. Detection of multi-class retinal diseases using artificial intelligence: an expeditious learning using deep CNN with minimal data. *Biomed Pharmacol J.* (2019) 12:1577–86. doi: 10.13005/bpj/1788
37. Wang J, Yang L, Huo Z, He W, Luo J. Multi-label classification of fundus images with EfficientNet. *IEEE Access.* (2020) 8:212499–508. doi: 10.1109/ACCESS.2020.3040275

**Conflict of Interest:** The authors declare that the research was conducted in the absence of any commercial or financial relationships that could be construed as a potential conflict of interest.

**Publisher's Note:** All claims expressed in this article are solely those of the authors and do not necessarily represent those of their affiliated organizations, or those of the publisher, the editors and the reviewers. Any product that may be evaluated in this article, or claim that may be made by its manufacturer, is not guaranteed or endorsed by the publisher.

Copyright © 2022 Zhu, Lu, Wang, Wu, Zheng, Jiang, Wei, Cao and Yang. This is an open-access article distributed under the terms of the Creative Commons Attribution License (CC BY). The use, distribution or reproduction in other forums is permitted, provided the original author(s) and the copyright owner(s) are credited and that the original publication in this journal is cited, in accordance with accepted academic practice. No use, distribution or reproduction is permitted which does not comply with these terms.



# Predicting Optical Coherence Tomography-Derived High Myopia Grades From Fundus Photographs Using Deep Learning

## OPEN ACCESS

### Edited by:

Hetian Lei,  
Shenzhen Eye Hospital, China

### Reviewed by:

Weiq Chen,  
Shantou University and the Chinese  
University of Hong Kong, China  
Lu Chen,  
Shenzhen Eye Hospital, China

### \*Correspondence:

Yingfeng Zheng  
yingfeng.zheng@qq.com  
Lin Lu  
lulin888@126.com

<sup>†</sup>These authors have contributed  
equally to this work and share first  
authorship

### Specialty section:

This article was submitted to  
Ophthalmology,  
a section of the journal  
Frontiers in Medicine

**Received:** 24 December 2021

**Accepted:** 09 February 2022

**Published:** 03 March 2022

### Citation:

Wu Z, Cai W, Xie H, Chen S, Wang Y,  
Lei B, Zheng Y and Lu L (2022)  
Predicting Optical Coherence  
Tomography-Derived High Myopia  
Grades From Fundus Photographs  
Using Deep Learning.  
Front. Med. 9:842680.  
doi: 10.3389/fmed.2022.842680

Zhenquan Wu<sup>1†</sup>, Wenjia Cai<sup>1†</sup>, Hai Xie<sup>2†</sup>, Shida Chen<sup>1</sup>, Yanbing Wang<sup>1</sup>, Baiying Lei<sup>2</sup>,  
Yingfeng Zheng<sup>1\*</sup> and Lin Lu<sup>1\*</sup>

<sup>1</sup> State Key Laboratory of Ophthalmology, Zhongshan Ophthalmic Center, Sun Yat-sen University, Guangzhou, China, <sup>2</sup> Health Science Center, School of Biomedical Engineering, Shenzhen University, Shenzhen, China

**Purpose:** To develop an artificial intelligence (AI) system that can predict optical coherence tomography (OCT)-derived high myopia grades based on fundus photographs.

**Methods:** In this retrospective study, 1,853 qualified fundus photographs obtained from the Zhongshan Ophthalmic Center (ZOC) were selected to develop an AI system. Three retinal specialists assessed corresponding OCT images to label the fundus photographs. We developed a novel deep learning model to detect and predict myopic maculopathy according to the atrophy (A), traction (T), and neovascularisation (N) classification and grading system. Furthermore, we compared the performance of our model with that of ophthalmologists.

**Results:** When evaluated on the test set, the deep learning model showed an area under the receiver operating characteristic curve (AUC) of 0.969 for category A, 0.895 for category T, and 0.936 for category N. The average accuracy of each category was 92.38% (A), 85.34% (T), and 94.21% (N). Moreover, the performance of our AI system was superior to that of attending ophthalmologists and comparable to that of retinal specialists.

**Conclusion:** Our AI system achieved performance comparable to that of retinal specialists in predicting vision-threatening conditions in high myopia via simple fundus photographs instead of fundus and OCT images. The application of this system can save the cost of patients' follow-up, and is more suitable for applications in less developed areas that only have fundus photography.

**Keywords:** artificial intelligence, high myopia, fundus photographs, optical coherence tomography, deep learning



## INTRODUCTION

Myopia has been recognized as an important public health problem worldwide (1). The global number of myopic subjects will increase to 5 billion by 2050, and about 20% of them will suffer from high myopia (2). The high prevalence of myopia and high myopia leads to an increase in pathological myopia (PM), especially in East Asian countries (3). Patients with PM usually suffer from myopic maculopathy, which is one of the most common causes of irreversible blinding vision loss (4). Visually impaired people tend to have lower capacity for work and higher rate of depression, imposing a significant burden on individuals and society (5). Formulating an applicable strategy for risk stratification is conducive to surveillance and early treatment, (6, 7) but the diagnosis and assessment of myopic maculopathy in the clinic are relatively complex (8).

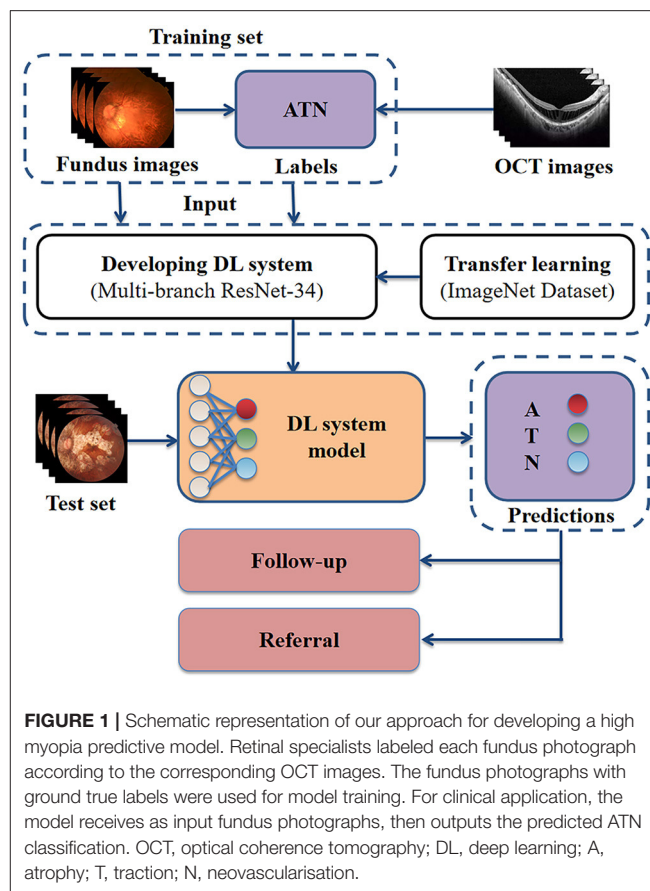
The atrophy, traction, and neovascularisation (ATN) classification and grading system proposed by Jorge Ruiz-Medrano is currently a common clinical diagnostic criterion, allowing a simple and systematic grading of myopic maculopathy that is both understandable and widely applicable (3). It contains three categories: atrophy (A), traction (T), and neovascularisation (N). Clinically, the diagnosis of category A can depend on fundus photographs, but the diagnosis of categories T and N is difficult based on fundus photographs only, and optical coherence tomography (OCT) images are also required. However, it is difficult to widely adopt OCT examinations as a routine screening method because of the high cost and the lack of equipment in primary hospitals or communities. Therefore, rapid screening and timely referral for PM is handicapped because the T and N conditions cannot be reliably detected by humans using fundus photographs alone. Ophthalmologists with sufficient experience in diagnosing and treating high myopia are also scarce in primary hospitals.

A potential solution is development of artificial intelligence (AI) technology, which has been applied to identify various ophthalmic diseases (9–16). Previous studies reported that AI systems can predict diseases from fundus photographs, such as cardiovascular risk factors and refractive error (17, 18). A recent study successfully predicted OCT-derived center-involved diabetic macular oedema (ci-DME) from fundus photographs using deep learning (19). It suggested that the AI system can discover the underlying association between the disease and the details of fundus photographs. As for high myopia, previous studies only focused on automated lesion identification based on fundus or OCT images (20, 21). Further exploration is required to allow making predictions in high myopia via two-dimensional images (fundus photographs) without three-dimensional images (OCT images).

This study aimed to develop an AI system that can predict OCT-derived ATN classification using monoscopic fundus photographs.

## MATERIALS AND METHODS

This study was approved by the Ethics Committee of Zhongshan Ophthalmic Center (ZOC, Guangzhou, China)



(ID: 2021KYPJ175) and the requirement of informed consent was waived in this retrospective study. And this study was performed in accordance with the principles of the Declaration of Helsinki; all private information that could identify individuals was excluded.

## Patients and Images

Patients with high myopia presenting to the retinal clinic at ZOC between January 2014 and February 2021 were reviewed and analyzed. High myopia was defined as refractive error (RE)  $\leq -6.0$  D or axial length (AL)  $\geq 26.0$  mm. None of the patients had previously undergone surgery. Patients with coexisting or previous ocular disorders, such as diabetic retinopathy, retinal vascular abnormalities, uveitis, and age-related macular degeneration, were excluded.

Fundus photographs were collected using a Topcon fundus camera (TRC-50; Topcon, Tokyo, Japan), and one single macula-centered 50° color fundus photograph was obtained for each eye. All fundus photographs were downloaded using the standard tiff or jpeg compression formats. The corresponding spectral domain OCT images (Heidelberg Engineering, Heidelberg, Germany) were collected. The OCT images with horizontal and vertical slices through the fovea were downloaded in a standard image format according to the manufacturer's software instructions,

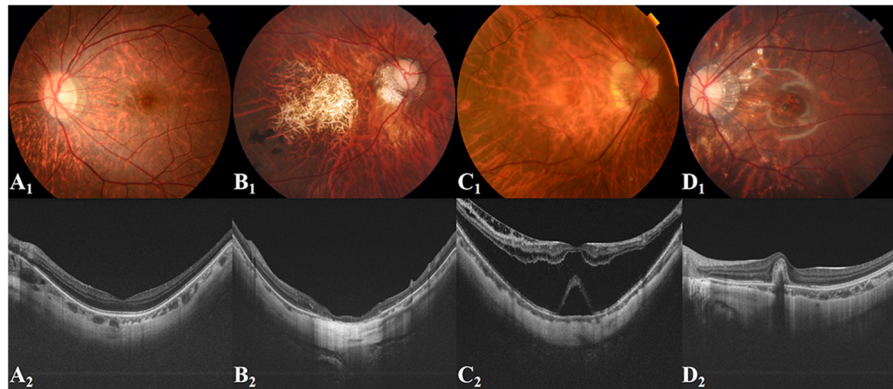


**FIGURE 2 |** Representative fundus images and related OCT images. (**A<sub>1</sub>,A<sub>2</sub>**) Tessellated fundus; (**B<sub>1</sub>,B<sub>2</sub>**) Macular atrophy; (**C<sub>1</sub>,C<sub>2</sub>**) Retinal detachment; (**D<sub>1</sub>,D<sub>2</sub>**) PMCNV. OCT, optical coherence tomography; PMCNV, pathological myopic choroidal neovascularisation.

and the scan length was 6 mm. These slices can detect most vision-threatening conditions associated to high myopia. For some patients, the same eye was examined multiple times to monitor disease progression. If the interval between the two examinations exceeded 1 month and the multiple examinations showed that the disease is progressing, the images of the multiple examinations will be included as separate data in this study. There were no exclusion criteria based on age, sex, or race.

## Image Labeling Process Based on the ATN System

Three Chinese board-certified retinal specialists with over 10 years of experience were invited to label each fundus photograph according to the corresponding OCT images of each eye (**Figure 1**). Initial quality control was conducted for all fundus photographs. Images in which the optic disc and macula could not be identified clearly were considered poor quality and removed from the database. Duplicated images and those with incorrect magnification were also excluded. Qualified fundus photographs were used to train the AI system, whereas OCT images were used only to aid labeling. The labeling standard was consistent with the ATN system of Ruiz-Medrano et al. (3). All fundus photographs were graded separately for the A, T, and N categories and placed into the dataset accordingly. Each image was examined, discussed, and labeled until all three retinal specialists agreed on the final diagnosis. When dissent could not be resolved, another retinal specialist with over 20 years of experience was invited to the group discussion to make the final decision. Representative fundus photographs and relative OCT images are shown in **Figure 2**.

## Development of a Deep Learning Model

We used binary classification to simplify the ATN system, which can screen out patients who need close follow-up or

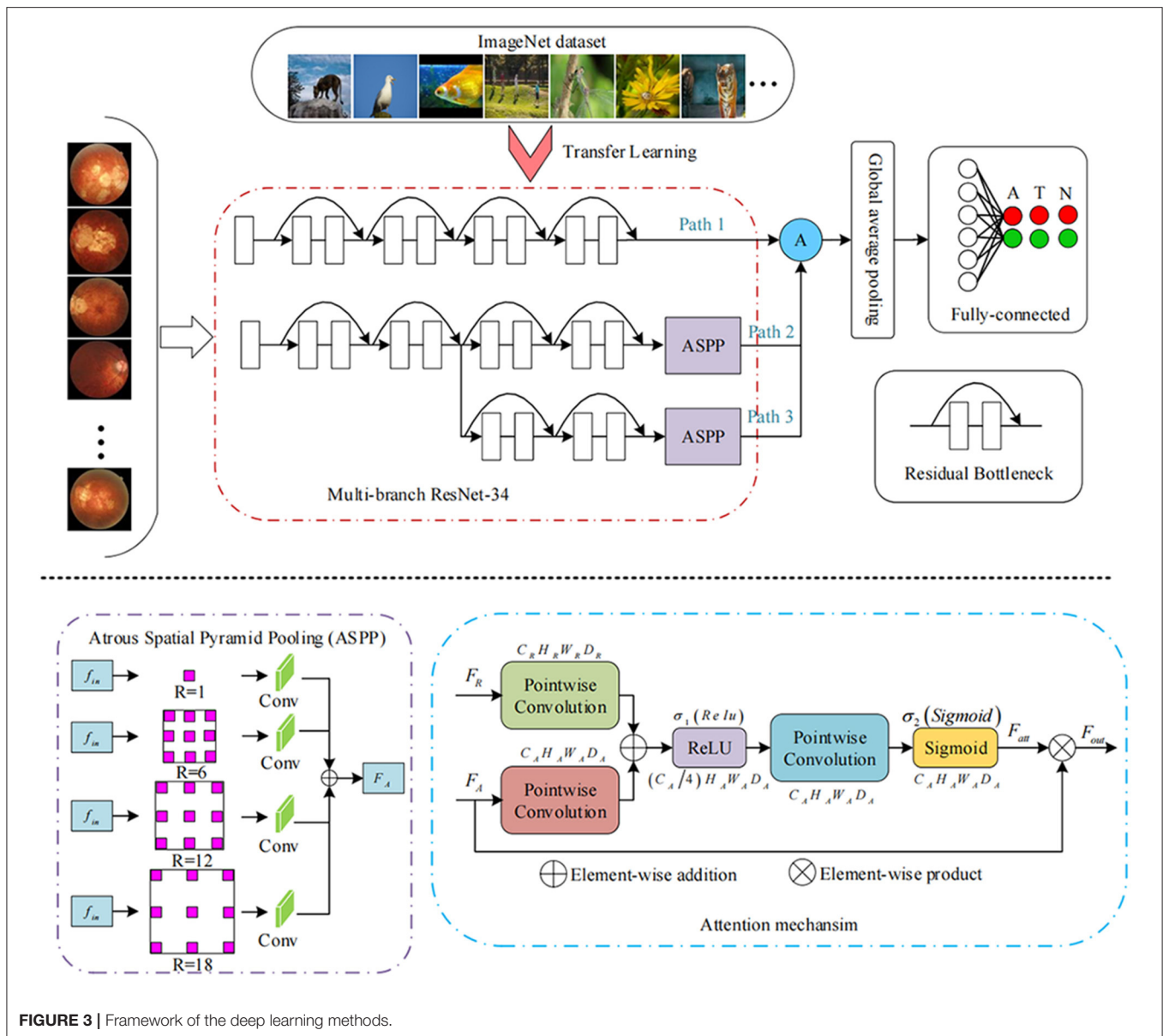
**TABLE 1 |** Final classification standard.

Atrophic component (A)	Tractional component (T)	Neovascular component (N)
A0: No myopic retinal lesions, or tessellated fundus only	T0: No macular traction, or foveoschisis only	N0: No PMCNV
A1: Retinal atrophy	T1: MH or retinal detachment	N1: PMCNV

PMCNV, Pathological myopic choroidal neovascularisation; MH, Macular hole.

treatment. Specifically, retinal atrophy (A1), macular hole or retinal detachment (T1), and pathological myopic choroidal neovascularisation (PMCNV) (N1) were detected or predicted (**Table 1**). In addition, we attempted to use multi-classification to divide category A into three grades, including normal fundus (no myopic retinal lesions), tessellated fundus, and retinal atrophy. The purpose of this task was to further distinguish the presence of high myopia in fundus photographs without retinal atrophy.

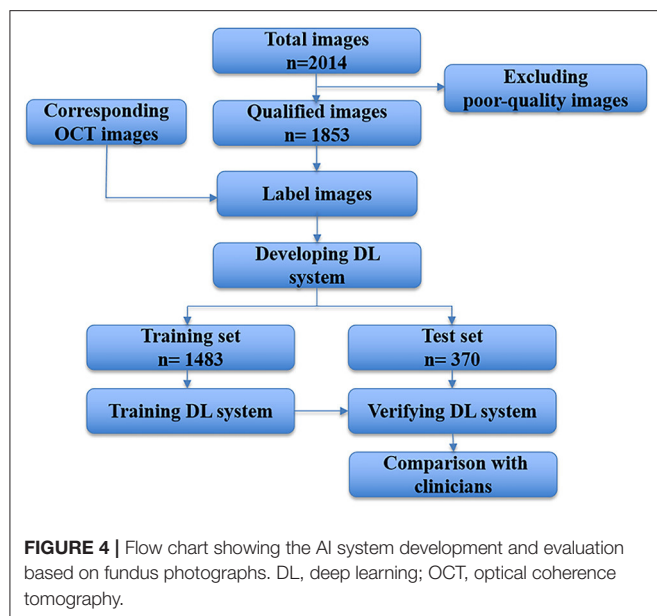
The devised framework used the residual network ResNet-34 model as the backbone to build a multi-branch ResNet-34 structure, which is utilized to extract rich high-level feature information (22, 23). We used the pre-trained parameters on the ImageNet dataset to train the designed multi-branch ResNet-34 model in transfer learning mode. The atrous spatial pyramid pooling (ASPP) module was employed to extract contextual feature information by expanding the receptive field, with the atrous rate set to 1, 6, 12, and 18. To force the network to focus on the feature extraction of the key areas, the attention module was used to refine the extracted feature by the multi-branch network so that discriminative features could be obtained. Subsequently, we used the global average pooling operation to process the extracted features. Following the pooling layer, a fully connected layer was used to map the extracted features to the



category space. Finally, the entire network was trained and tested to output the predicted results using the softmax layer (22). The entire framework of the proposed deep learning model is shown in **Figure 3**. We used the Pytorch library as the framework to build the network. One NVIDIA TITAN XP GPU was employed to accelerate training and testing. The batch size was set to 16, and the maximum epoch of training was 60. The input images were resized to  $512 \times 512$  pixels. The initial learning rate was set to 0.0001, which was multiplied by 0.1 every 20 epochs. Afterward, the data were randomly classified into training set and testing set in the ratio of 0.8:0.2 in each category. The flow chart in **Figure 4** shows the development and evaluation of the AI system based on fundus photographs.

## Quantification and Statistical Analysis

We used accuracy, precision, sensitivity, specificity, and F1 score to evaluate the performance and stability of the classification model. Accuracy was measured by dividing the number of correct predictions by the total number of samples. Precision was measured by dividing the number of true positives by the total number of true positives and false positives. Sensitivity was determined by dividing the number of true positives by the total number of true positives and false negatives. Specificity, was determined by dividing the number of true negatives by the total number of true negatives and false positives. The F1 score was calculated as twice the product of precision and sensitivity divided by their sum and measures the balance of the positive

**TABLE 2 |** Demographic characteristics of subjects.

Parameters	High myopia	Normal
Number of gradable images	1,653	200
Number of subjects	704	116
Gender (male/female)	310/394	51/65
Age (years)	52.62 ± 14.03	56.37 ± 9.23
BCVA (LogMAR)	0.57 ± 0.53	0.11 ± 0.10
AL (mm)	29.54 ± 2.44	23.09 ± 0.91
SE (D)	-11.90 ± 7.20	0.03 ± 0.99

Data are presented as mean ± standard deviation.

BCVA, best corrected visual acuity; AL, Axial length; SE, spherical equivalent.

and negative samples at the same time. For further evaluation, two retinal specialists and two attending ophthalmologists were invited to classify the images to compare with the AI system. The area under the receiver operating characteristic (ROC) curve (AUC) was calculated to assess the total performance of AI models and clinicians.

## RESULTS

### Imaging Datasets and Clinical Characteristics of Patients

A total of 2,014 fundus photographs were collected, including 1,814 high myopia fundus photographs (704 subjects) and 200 normal fundus photographs (116 subjects). After quality control, 161 poor quality images were excluded. Finally, 1,853 fundus photographs were selected to develop and evaluate our AI system. We split the data assigning 1,483 images to the training dataset and 370 to the test dataset. The demographic characteristics of included subjects are shown in **Table 2**.

## Performance of the AI System

The AUCs of the proposed method were 0.969, 0.895, and 0.936 for categories A, T, and N, respectively, and the accuracies were 92.38, 85.34, and 94.21%, respectively (**Figure 5A**; **Table 3**). Compared with other methods, the proposed method achieved the highest AUC values and accuracies for all categories. Further indicators including precision, sensitivity, specificity, and F1-score are shown in **Table 3**. We also produced t-distributed stochastic neighbor embedding (t-SNE) visualizations for the different methods using the last extracted features (**Figure 5B**). Red and green points represent negative and positive results, respectively. Points of the same color were clustered, while those of different color were separated, indicating the good classification ability of the model. We can observe that the proposed method could separate the categories more easily than other methods.

In addition, we trained the model to perform a multi-classification task for category A. Compared with the binary classification model, this multiclass model can distinguish tessellated fundus independently, which is more conducive to the identification of early lesions. The accuracies of the four methods (ResNet-34, MB, MB-ASPP, and Proposed method) were 89.05, 90.71, 90.95, and 91.67%, respectively. **Figure 6A** shows the AUCs of the different methods for the classification of category A with three sub-grades. The AUCs of the proposed method were 1.000, 0.956, and 0.966 in normal fundus, tessellated fundus, and retinal atrophy, respectively. The results indicate that proposed method had the best performance. **Figure 6B** shows the t-SNE visualizations with respect to the different methods. The proposed method could separate the categories more easily than other methods.

## Comparison of the Performance of the AI System With That of Clinicians

We compared the classification performance of the AI system with that of ophthalmologists, including two retinal specialists and two attending ophthalmologists. To illustrate the superiority of the proposed method, we plotted the ROC curves and marked the operating points of the four ophthalmologists as well (**Figure 5A**). The average accuracies of the two attending ophthalmologists were 84.46, 75.14, and 84.59% for categories A, T, and N, respectively; while those of the two retinal specialists were 90.00, 82.03, and 91.49%, respectively. When compared with clinicians, the proposed method performed better than attending ophthalmologists and comparably to retinal specialists.

## DISCUSSION

Previous studies have shown that AI technology can use fundus photographs to predict cardiovascular risk, refractive errors, and ci-DME, significantly outperforming specialists (17–19). Varadarajan et al. reported that their AI system, applied fundus photographs to predict the presence of ci-DME, achieved 85% sensitivity and 80% specificity. Compared with the AI system, retinal specialists have similar sensitivities (82–85%), but only half the specificity (19). In the current study, we used fundus



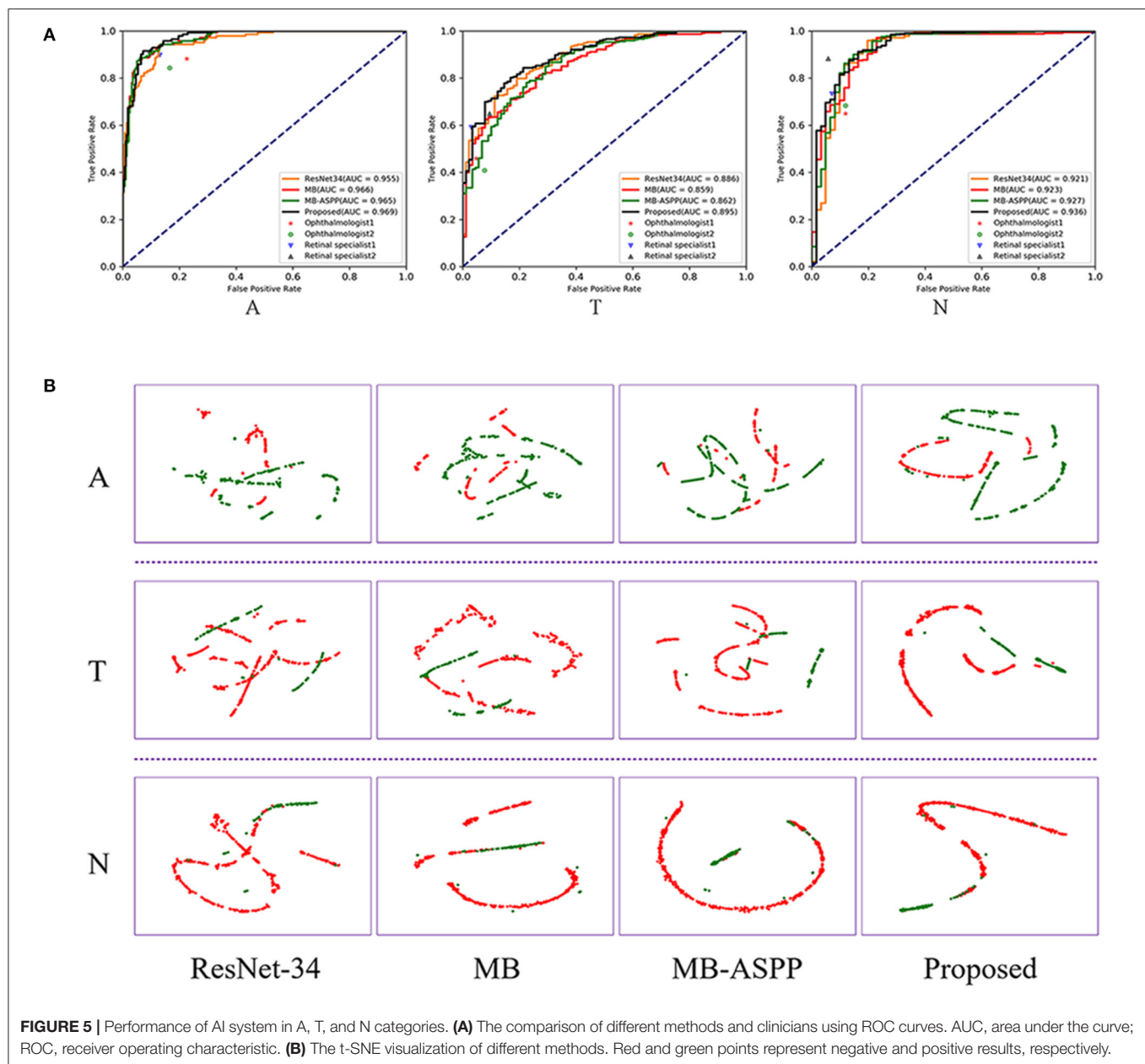


**FIGURE 5 |** Performance of AI system in A, T, and N categories. **(A)** The comparison of different methods and clinicians using ROC curves. AUC, area under the curve; ROC, receiver operating characteristic. **(B)** The t-SNE visualization of different methods. Red and green points represent negative and positive results, respectively.

photography to predict the presence of treatment-requiring conditions (macular hole, retinal detachment, and PMCNV), and also achieved high accuracy in categories T (85.34%) and N (94.21%). The performance was greater than that of attending ophthalmologists and comparable to that of retinal specialists. Our system can pick up more occult lesions which might be overlooked by ophthalmologists based on fundus photographs alone. The application of this model in less developed areas is expected to solve the problem of inadequate equipment and doctors in primary hospitals or communities.

In previous researches, Li et al. (24) developed an AI model with 5505 OCT images to identify vision-threatening

conditions (retinoschisis, macular hole, retinal detachment, and PMCNV) in patients with high myopia and achieved reliable sensitivities and specificities. The OCT images can clearly reveal retinal traction and neovascularisation because of the cross-sectional information, but the cost is relatively high, and there is no such equipment in many primary hospitals or communities. Therefore, it is not suitable for long-term follow-up of myopia patients in less developed areas. In this study, the AI system we developed to predict ATN classification of high myopia via fundus photographs without OCT images is comparable in performance to retinal specialists. This work demonstrates the potential of AI technology to enable

**TABLE 3 |** Comparison of different methods in the testing dataset (%).

	Method	Accuracy	Precision	Sensitivity	Specificity	F1-score
A	ResNet-34	90.71	89.36	90.03	87.94	89.68
	MB	91.43	90.19	90.74	88.65	90.46
	MB-ASPP	92.14	91.25	91.10	87.94	91.18
	Proposed	<b>92.38</b>	<b>91.07</b>	<b>92.16</b>	<b>91.48</b>	<b>91.57</b>
T	ResNet-34	83.51	81.24	68.52	96.24	71.66
	MB	82.72	76.46	71.92	94.18	73.67
	MB-ASPP	84.55	80.67	72.72	94.88	75.40
	Proposed	<b>85.34</b>	<b>83.58</b>	<b>72.45</b>	<b>96.58</b>	<b>75.78</b>
N	ResNet-34	92.63	88.29	83.02	96.87	85.34
	MB	93.68	89.51	86.29	97.18	87.79
	MB-ASPP	93.95	90.83	85.79	97.81	88.05
	Proposed	<b>94.21</b>	<b>91.69</b>	<b>85.94</b>	<b>98.12</b>	<b>88.48</b>

ResNet-34, original ResNet-34 model; MB, Multi-branch ResNet-34 model; MB-ASPP, Multi-branch ResNet-34 & ASPP model; Proposed, Multi-branch ResNet-34 & ASPP & Attention model. The bold values represent the results of our proposed method.

diagnostics on inexpensive equipment, replacing previously expensive equipment.

Automatic diagnosis of retinal detachment and/or PMCNV by fundus photographs has been reported in some studies (25, 26). Hemelings et al. developed an algorithm for PM detection using 400 fundus photographs, and the F1 score for retinal detachment was 0.71 (25). However, it is a challenge to identify minimal changes in early stage of myopic maculopathy using only fundus photographs for both ophthalmologists and AI system. In the current study, retinal specialists labeled the fundus photographs by referring to the results of the corresponding OCT images. Some minimal lesions, which were latent on fundus photographs but present obviously on corresponding OCT images, were also included in the training dataset. Therefore, our system can pick up more details (all kinds of macular hole, retinal detachment, and PMCNV) than ophthalmologists. The connection between lesion features and results might have been built during the training process, allowing the achievement of higher predictive ability.

Some researchers have performed automatic identification and segmentation of myopic lesions based on fundus photographs, and achieved promising performance (25–28). Tan et al. developed an algorithm which achieved high diagnostic performance, with an AUC of 0.913 for high myopia and 0.969 for myopic maculopathy (26). Baid et al. developed another algorithm for PM detection and achieved an AUC of 0.99 (28). However, these studies only made a preliminary diagnosis of PM or focused on identifying one or two categories of myopic maculopathy. Our AI system can simultaneously predict atrophy, traction, and neovascularisation. Using our AI system, patients with macular hole and/or RD will be accurately predicted and referred to retinal specialists for timely surgery. PMCNV will also be predicted, and the patient referred for further examination to formulate a plan for anti-vascular endothelial growth factor treatment. Regular follow-up is advised to monitor disease progression in patients with tessellated fundus or retinal atrophy

alone. Therefore, primary hospitals can achieve risk stratification and promptly detect and refer patients requiring treatment, which helps patients receive treatment in time to restore vision.

Due to the large population of patients with myopia, it is challenging for ophthalmologists to conduct large-scale screenings (5, 29). If all patients with myopia were to be referred to advanced hospitals for diagnosis or follow-up, they could overwhelm the medical system. Therefore, there is an urgent need to establish an effective community-based myopia-screening system. The non-expert-dependent AI system we developed has important clinical value, as it can reduce the large influx of patients to advanced hospitals and reduce individual and social costs. It can also be convenient for patients who require long-term follow-up. In addition, the application of this AI system in primary hospitals and healthcare institutions during the COVID-19 pandemic will reduce the concentration in large hospitals, and thus the risk of infection.

This study had some limitations. First, the ATN classification in this study has been simplified. However, the system can accurately identify patients who need referral and can save the cost of patient follow-up. Second, all images in our study were collected from the same hospital. Images from multiple centers could be obtained as external data to further improve and assess our AI system. In addition, this AI system can detect PMCNV, but it is difficult to estimate the activity of the lesion. This problem could be solved by collecting more images from the long-term follow-up of patients with PMCNV to compare the different features over time.

In conclusion, the AI system we developed can predict ATN classification of high myopia using the cheaper and more widely available fundus photographs, with performance comparable to that of retinal specialists. Its clinical applications would provide a comprehensive diagnosis to triage and referral and reduce the individual and social costs. Such promising performance recommends its extensive application as a large-scale screening tool in primary medical institutions.

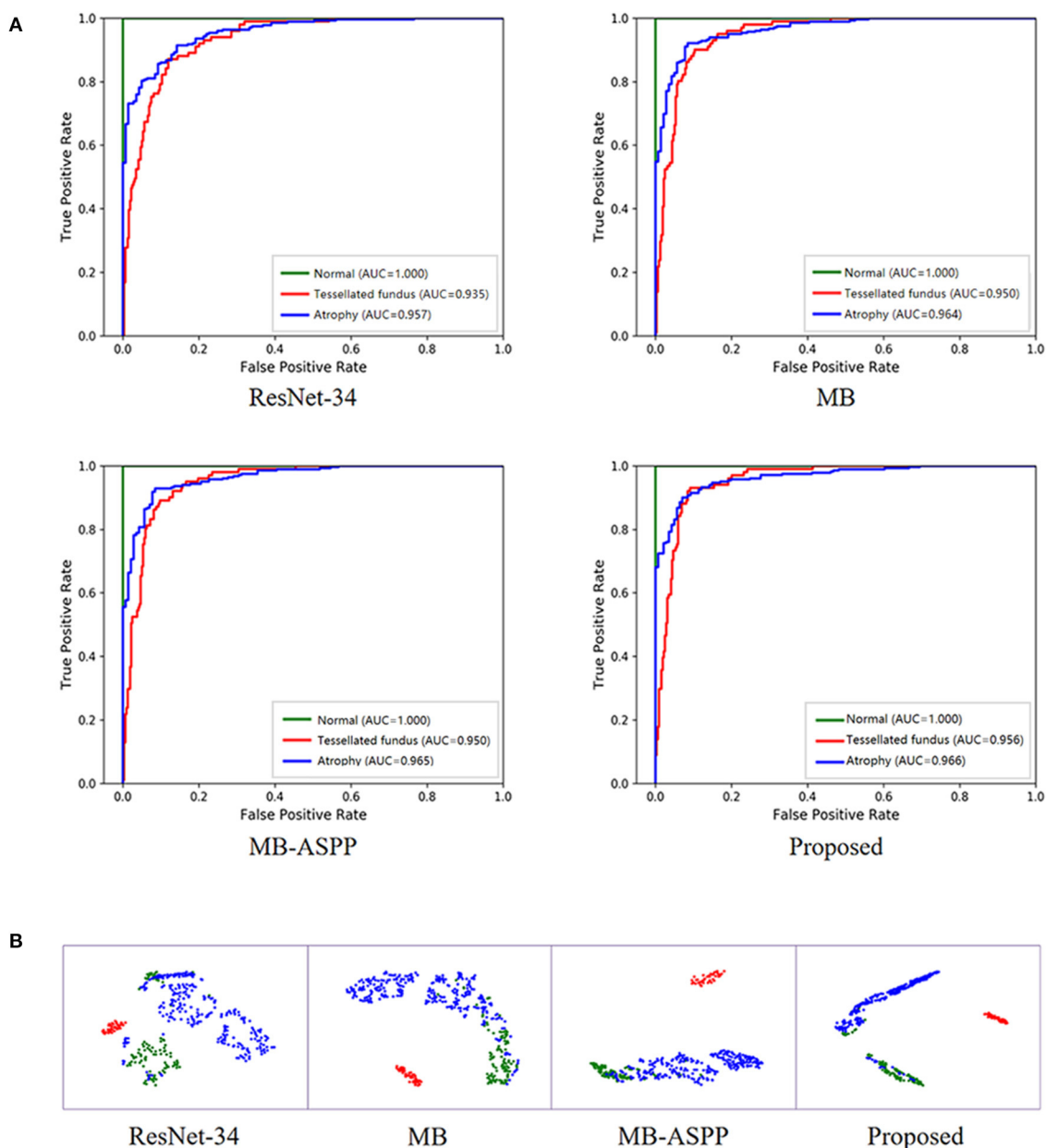


**FIGURE 6 |** Performance of AI system in category A with three sub-grades. **(A)** The ROC curves of different methods for category A with three sub-grades. AUC, area under the curve; ROC, receiver operating characteristic. **(B)** The t-SNE visualization of different methods for category A with three sub-grades. Red, blue, and green points represent the normal fundus (no myopic retinal lesions), tessellated fundus, and retinal atrophy, respectively.

## DATA AVAILABILITY STATEMENT

The raw data supporting the conclusions of this article will be made available by the authors, without undue reservation.

## ETHICS STATEMENT

The studies involving human participants were reviewed and approved by the Ethics Committee of Zhongshan

Ophthalmic Center (ZOC, Guangzhou, China) (ID: 2021KYPJ175). Written informed consent was not required for this study, in accordance with the local legislation and institutional requirements.

## AUTHOR CONTRIBUTIONS

ZW, WC, and SC: conception and design. LL: funding obtainment and provision of data. ZW,

SC, and YW: collection and assembly of data. HX and BL: data analysis and interpretation. YZ, LL, and SC: manuscript revision. All authors wrote the manuscript and approved the final version of the manuscript.

## REFERENCES

- Dolgin E. The myopia boom. *Nature*. (2015) 519:276–8. doi: 10.1038/519276a
- Holden BA, Fricke TR, Wilson DA, Jong M, Naidoo KS, Sankaridurg P, et al. Global prevalence of myopia and high myopia and temporal trends from 2000 through 2050. *Ophthalmology*. (2016) 123:1036–42. doi: 10.1016/j.ophtha.2016.01.006
- Ruiz-Medrano J, Montero JA, Flores-Moreno I, Arias L, García-Layana A, Ruiz-Moreno JM. Myopic maculopathy: current status and proposal for a new classification and grading system (ATN). *Prog Retin Eye Res*. (2019) 69:80–115. doi: 10.1016/j.preteyeres.2018.01.005
- Fricke TR, Jong M, Naidoo KS, Sankaridurg P, Naduvilath TJ, Ho SM, et al. Global prevalence of visual impairment associated with myopic macular degeneration and temporal trends from 2000 through 2050: systematic review, meta-analysis and modelling. *Br J Ophthalmol*. (2018) 102:855–62. doi: 10.1136/bjophthalmol-2017-311266
- Morgan IG, French AN, Ashby RS, Guo X, Ding X, He M, et al. The epidemics of myopia: aetiology and prevention. *Prog Retin Eye Res*. (2018) 62:134–49. doi: 10.1016/j.preteyeres.2017.09.004
- Wong TY, Ohno-Matsui K, Leveziel N, Holz FG, Lai TY, Yu HG, et al. Myopic choroidal neovascularisation: current concepts and update on clinical management. *Br J Ophthalmol*. (2015) 99:289–96. doi: 10.1136/bjophthalmol-2014-305131
- Zhao X, Ma W, Lian P, Tanumiharjo S, Lin Y, Ding X, et al. Three-year outcomes of macular buckling for macular holes and foveoschisis in highly myopic eyes. *Acta Ophthalmol*. (2020) 98:e470–e8. doi: 10.1111/aos.14305
- Saw SM, Gazzard G, Shih-Yen EC, Chua WH. Myopia and associated pathological complications. *Ophthalmic Physiol Opt*. (2005) 25:381–91. doi: 10.1111/j.1475-1313.2005.00298.x
- Matheny ME, Whicher D, Thadaneys Israni S. Artificial intelligence in health care: a report from the national academy of medicine. *JAMA*. (2020) 323:509–10. doi: 10.1001/jama.2019.21579
- Schwalbe N, Wahl B. Artificial intelligence and the future of global health. *Lancet*. (2020) 395:1579–86. doi: 10.1016/S0140-6736(20)30226-9
- Hosny A, Aerts H. Artificial intelligence for global health. *Science*. (2019) 366:955–6. doi: 10.1126/science.aay5189
- Long E, Lin H, Liu Z, Wu X, Wang L, Jiang J, et al. An artificial intelligence platform for the multihospital collaborative management of congenital cataracts. *Nat Biomed Eng*. (2017) 1:0024. doi: 10.1038/s41551-016-0024
- Li Z, He Y, Keel S, Meng W, Chang RT, He M. Efficacy of a deep learning system for detecting glaucomatous optic neuropathy based on color fundus photographs. *Ophthalmology*. (2018) 125:1199–206. doi: 10.1016/j.ophtha.2018.01.023
- Gargeya R, Leng T. Automated identification of diabetic retinopathy using deep learning. *Ophthalmology*. (2017) 124:962–9. doi: 10.1016/j.ophtha.2017.02.008
- Grassmann F, Mengelkamp J, Brandl C, Harsch S, Zimmermann ME, Linkohr B, et al. A deep learning algorithm for prediction of age-related eye disease study severity scale for age-related macular degeneration from color fundus photography. *Ophthalmology*. (2018) 125:1410–20. doi: 10.1016/j.ophtha.2018.02.037
- Brown JM, Campbell JP, Beers A, Chang K, Ostmo S, Chan RVP, et al. Automated diagnosis of plus disease in retinopathy of prematurity using deep convolutional neural networks. *JAMA Ophthalmol*. (2018) 136:803–10. doi: 10.1001/jamaophthalmol.2018.1934
- Varadarajan AV, Poplin R, Blumer K, Angermueller C, Ledsam J, Chopra R, et al. Deep learning for predicting refractive error from retinal fundus images. *Invest Ophthalmol Vis Sci*. (2018) 59:2861–8. doi: 10.1167/iops.18-23887
- Poplin R, Varadarajan AV, Blumer K, Liu Y, McConnell MV, Corrado GS, et al. Prediction of cardiovascular risk factors from retinal fundus photographs via deep learning. *Nat Biomed Eng*. (2018) 2:158–64. doi: 10.1038/s41551-018-0195-0
- Varadarajan AV, Bavishi P, Ruamviboonsuk P, Chotcomwongse P, Venugopalan S, Narayanaswamy A, et al. Predicting optical coherence tomography-derived diabetic macular edema grades from fundus photographs using deep learning. *Nat Commun*. (2020) 11:130. doi: 10.1038/s41467-019-13922-8
- Sogawa T, Tabuchi H, Nagasato D, Masumoto H, Ikuno Y, Ohsugi H, et al. Accuracy of a deep convolutional neural network in the detection of myopic macular diseases using swept-source optical coherence tomography. *PLoS ONE*. (2020) 15:e0227240. doi: 10.1371/journal.pone.0227240
- Dai S, Chen L, Lei T, Zhou C, Wen Y. Automatic detection of pathological myopia and high myopia on fundus images. In: 2020 IEEE International Conference on Multimedia and Expo (ICME). London: IEEE (2020).
- Xie H, Zeng X, Lei H, Du J, Wang J, Zhang G, et al. Cross-attention multi-branch network for fundus diseases classification using SLO images. *Med Image Anal*. (2021) 71:102031. doi: 10.1016/j.media.2021.102031
- Xie H, Lei H, Zeng X, He Y, Chen G, Elazab A, et al. AMD-GAN: attention encoder and multi-branch structure based generative adversarial networks for fundus disease detection from scanning laser ophthalmoscopy images. *Neural Netw*. (2020) 132:477–90. doi: 10.1016/j.neunet.2020.09.005
- Li Y, Feng W, Zhao X, Liu B, Zhang Y, Chi W, et al. Development and validation of a deep learning system to screen vision-threatening conditions in high myopia using optical coherence tomography images. *Br J Ophthalmol*. (2020). doi: 10.1136/bjophthalmol-2020-317825 (accessed December 21, 2020).
- Hemelings R, Elen B, Blaschko MB, Jacob J, Stalmans I, De Boever P. Pathological myopia classification with simultaneous lesion segmentation using deep learning. *Comput Methods Programs Biomed*. (2021) 199:105920. doi: 10.1016/j.cmpb.2020.105920
- Tan TE, Anees A, Chen C, Li S, Xu X, Li Z, et al. Retinal photograph-based deep learning algorithms for myopia and a blockchain platform to facilitate artificial intelligence medical research: a retrospective multicohort study. *Lancet Digit Health*. (2021) 3:e317–29. doi: 10.1016/S2589-7500(21)00055-8
- Guo Y, Wang R, Zhou X, Liu Y, Wang L, Lv C, et al. Lesion-aware segmentation network for atrophy and detachment of pathological myopia on fundus images. In: 2020 IEEE 17th International Symposium on Biomedical Imaging (ISBI) Iowa City, IA: IEEE (2020).
- Baid U, Baheti B, Dutande P, Talbar S. Detection of pathological myopia and optic disc segmentation with deep convolutional neural networks. In: *TENCON 2019 - 2019 IEEE Region 10 Conference (TENCON)* (2019).
- Vongphanit J, Mitchell P, Wang JJ. Prevalence and progression of myopic retinopathy in an older population. *Ophthalmology*. (2002) 109:704–11. doi: 10.1016/S0161-6420(01)01024-7

## FUNDING

This work was supported by National Natural Science Foundation of China (No.62106153) and Guangdong Province Science and Technology Projects (No.3030901010066).

**Conflict of Interest:** The authors declare that the research was conducted in the absence of any commercial or financial relationships that could be construed as a potential conflict of interest.

**Publisher's Note:** All claims expressed in this article are solely those of the authors and do not necessarily represent those of their affiliated organizations, or those of the publisher, the editors and the reviewers. Any product that may be evaluated in this article, or claim that may be made by its manufacturer, is not guaranteed or endorsed by the publisher.

Copyright © 2022 Wu, Cai, Xie, Chen, Wang, Lei, Zheng and Lu. This is an open-access article distributed under the terms of the Creative Commons Attribution License (CC BY). The use, distribution or reproduction in other forums is permitted, provided the original author(s) and the copyright owner(s) are credited and that the original publication in this journal is cited, in accordance with accepted academic practice. No use, distribution or reproduction is permitted which does not comply with these terms.





# Air Tamponade for Rhegmatogenous Retinal Detachment With Inferior Breaks After 25-Gauge Pars Plana Vitrectomy: Technique and Outcome

Peiyang Shen<sup>1,2</sup>, Xiangbin Kong<sup>2\*</sup>, Lijun Zhou<sup>2</sup>, Peng Su<sup>2</sup>, Xiaohe Lu<sup>1\*</sup> and Mingguang He<sup>3,4\*</sup>

<sup>1</sup> Department of Ophthalmology, Zhujiang Hospital, Southern Medical University, Guangzhou, China, <sup>2</sup> Department of Ophthalmology, The Second People's Hospital of Foshan, Affiliated Foshan Hospital of Southern Medical University, Foshan, China, <sup>3</sup> Department of Surgery, Centre for Eye Research Australia, Ophthalmology, University of Melbourne, Melbourne, VIC, Australia, <sup>4</sup> State Key Laboratory of Ophthalmology, Zhongshan Ophthalmic Center, Sun Yat-sen University, Guangzhou, China

## OPEN ACCESS

### Edited by:

Shaochong Zhang,  
Shenzhen Eye Hospital, China

### Reviewed by:

Wei Chen,  
Shantou University, The Chinese  
University of Hong Kong, China  
Muhammad Amer Awan,  
Shifa Tameer-e-Millat University,  
Pakistan

### \*Correspondence:

Xiaohe Lu  
luxh63@163.com  
Xiangbin Kong  
xiangbin\_kong@sina.com  
Mingguang He  
mingguang.he@unimelb.edu.au

### Specialty section:

This article was submitted to  
Ophthalmology,  
a section of the journal  
Frontiers in Medicine

**Received:** 12 June 2021

**Accepted:** 18 February 2022

**Published:** 07 April 2022

### Citation:

Shen P, Kong X, Zhou L, Su P,  
Lu X and He M (2022) Air Tamponade  
for Rhegmatogenous Retinal  
Detachment With Inferior Breaks After  
25-Gauge Pars Plana Vitrectomy:  
Technique and Outcome.  
Front. Med. 9:724234.  
doi: 10.3389/fmed.2022.724234

To evaluate the outcomes of 25-gauge (G) pars plana vitrectomy (PPV) with air tamponade for rhegmatogenous retinal detachment (RRD) with inferior breaks. This retrospective consecutive case series included fifty-two eyes of fifty-two RRD patients with inferior breaks who underwent 25-G PPV with air tamponade. These patients were followed up for at least 6 months following surgery. Primary and final anatomical success rates and postoperative complications were the main outcome measures. The mean age of the patients (39 men and 13 women) was  $51.8 \pm 11.8$  years. There were 49 primary RRDs (94.2%) and three recurrent RRDs (5.8%). The mean follow-up period was  $8.2 \pm 1.6$  months (range: 6–13 months). Sixteen eyes (30.8%) presented with high myopia, and six eyes (11.5%) were pseudophakic. Proliferative vitreous retinopathy grade was C1 in four eyes (7.7%). Of the 52 eyes, two (3.8%) were complicated with choroidal detachment, and forty (76.9%) had the macula detached. The single- and final-operation success rates were 96.2% and 100%, respectively. During follow-up, secondary cataract surgery was performed in eight eyes (17.4%) of the 46 phakic eyes. 25-G PPV with air tamponade is effective in treating selected RRD patients with inferior breaks. Patients can benefit from early visual recovery and less complications.

**Keywords:** air tamponade, inferior breaks, 25-gauge, pars plana vitrectomy, rhegmatogenous retinal detachment

## INTRODUCTION

Rhegmatogenous retinal detachment (RRD) is a severe vision-threatening disease, defined as the separation of the inner neurosensory retina and the outer retinal pigment epithelium (RPE) due to retinal breaks formation caused by abnormal vitreoretinal traction (1). At present, pars plana vitrectomy (PPV) gains popularity in treating RRD due to its low invasiveness and adequate visualization of the peripheral retina via the wide-angle viewing system (2–5). After removing the vitreous, long-acting gas, such as 14% perfluoropropane ( $C_3F_8$ ) and 18% sulfur hexafluoride ( $SF_6$ ), or silicone oil are injected into the vitreous cavity to support retinal breaks closure and assure chorioretinal adhesion establishment.

Since April 2016, long-acting gases were no longer commercially available in China because of legislation changes. Silicone oil carries potential complications such as elevated intraocular pressure (IOP) and the necessity of secondary removal surgery (6). The current preference includes using air as a reasonable alternative for the tamponade (5, 7, 8). The air has a shorter half-life and a lower risk of elevated IOP and cataract development or progression compared to other agents. Previous studies have suggested that air can perform on par with long-acting gas in terms of surgical outcome (5, 9). However, air tamponade is generally indicated for RRDs with superior breaks; yet, the inferior breaks always pose a challenge for air tamponade (10–13). Therefore, we conduct this retrospective study to evaluate the surgical outcomes of RRD patients with inferior retinal breaks treated with 25-gauge (G) PPV using air tamponade only.

## MATERIALS AND METHODS

We reviewed medical records of all RRD patients from April 2018 to April 2021 who underwent 25-G PPV with air tamponade. These patients had at least one causative break located in the inferior retina (between 4 and 8 o'clock meridian). The exclusion criteria included giant retinal tears, proliferative vitreous retinopathy (PVR) grade C2 or greater, myopic macular hole-associated retinal detachments, traumatic RRDs, pediatric RRDs (birth to 18 years of age), other serious eye diseases, and less than 6 months of follow-up. The Ethics Committee of the Second People's Hospital of Foshan approved the study. It was performed following the Tenets of the World Medical Association's Declaration of Helsinki. Written consent for surgical treatment was obtained from each patient.

All eligible patients underwent comprehensive ophthalmic examinations, including Snellen best-corrected visual acuity (BCVA) measurement, non-contact tonometry, fundus examination, B-ultrasonography, and optical coherence tomography (OCT). The characteristics (number, size, type, and location) of retinal breaks and other procedures details (e.g., combined lens extraction and drainage retinotomy) were extracted from surgical records. PVR diagnosis was made according to the classification of the American Retina Society Terminology Committee, United States (14).

Two surgeons conducted all surgeries under retrobulbar anesthesia (PSh and XK). After proper conjunctival sac disinfection using povidone-iodine, a standard three-port 25-G PPV was performed using the Alcon Constellation Vision System (Alcon Laboratories, Fort Worth, TX, United States) and a non-contact wide-angle viewing system (the RESIGHT 700, Carl Zeiss Meditec AG, Jena, Germany). The vitrectomy was conducted using a cut rate of 5,000 cuts per minutes (cpm) with proportional vacuum settings and a maximum vacuum of 450 mmHg. Phacoemulsification and intraocular lens (IOL) implantation were performed simultaneously if lens opacification was visually significant.

After removing the core vitreous, the manual posterior vitreous detachment (if absent) was induced using vitreous cutter

near the optic disc. Careful inspection was performed routinely with the assistance of triamcinolone and soft tip of the flute needle to detect vitreoschisis. The peripheral vitreous base was shaved up to ora serrata under 360° scleral indentation. All visible PVR membranes were peeled cautiously. After complete vitrectomy and meticulously searching for all existing breaks, the retina was flatten using fluid-air exchange (air pressure = 30 mmHg). The subretinal fluid (SRF) was drained out through existing breaks or drainage retinotomy. Retinal breaks and degenerative areas were treated by endolaser photocoagulation. Prophylactic 360° laser cerclage, perfluorocarbon liquid (PFCL), or cryopexy was not used in any eyes. At the end, the residual fluid was drained off with the flute needle to ensure complete air-fill of the vitreous cavity. Sclerotomies were carefully closed in case of air leakage.

Patients were required to maintain an alternative supine or lateral position at least 12 h/day for no less than 5 days. Follow-up examinations were scheduled at 1 day, 1 and 2 weeks, and 1, 3, and 6 months after surgery. Two weeks after surgery, axial length (AL) measurement for the highly myopic eyes was performed using Lenstar LS 900 (Haag-Streit AG, Koeniz, Switzerland, software version 1.1). If necessary, extra visits were scheduled. We prescribed dexamethasone eyedrops and ophthalmic ointment (TobraDex, Alcon) for each patient after the surgery for 2 weeks. Primary and final anatomical success rates and postoperative complications were the main outcome measures.

## Statistical Analysis

For statistical analysis, BCVA in the Snellen value was converted to the logarithm of the minimum angle of resolution (logMAR). Visual acuity of light perception, hand movements, and counting fingers were assigned as 2.9, 2.6, and 2.3, respectively (15). Mann-Whitney *U* test was employed to compare BCVA. All continuous data were expressed as mean  $\pm$  standard deviation. *P* values < 0.05 were considered significant. Analyses were performed using SPSS for windows 21.0 (SPSS Inc., Chicago, IL, United States).

## RESULTS

### Baseline Characteristics

Fifty-two eyes of 52 consecutive patients (39 men and 13 women) with causative inferior breaks were recruited. Baseline characteristics are summarized in **Table 1**. Supplementary Material showed the clinical characteristics and treatment outcomes of each patient. The mean age was  $51.8 \pm 11.8$  years (range: 28–79), and the mean follow-up was  $8.2 \pm 1.6$  months (range: 6–13 months). Sixteen patients (30.8%) presented with high myopia, with a mean AL of  $28.21 \pm 1.66$  mm (range: 26.15–31.12, measured 2 weeks after surgery). There were 46 phakic eyes (88.5%) and six pseudophakic eyes (11.5%). The posterior lens capsule was intact in three eyes (50.0%). Yttrium–aluminum–garnet laser capsulotomy was performed in the other three eyes (50.0%). PVR grade was C1 in four eyes (7.7%), with the numeral one referring to the number of quadrants with visible PVR membrane formation.

**TABLE 1 |** Clinical characteristics of 52 eyes undergone 25-G PPV with air tamponade for RRD with inferior breaks.

Characteristic	
Gender (male: female)	39 (75.0%): 13 (25.0%)
Age (years)	51.8 ± 11.8 (range: 28–79)
Disease course (days)	15.2 ± 15.1 (median:10, range: 2–90)
Preoperative logMAR BCVA (Snellen equivalent)	1.59 ± 0.93 (20/778)
Lens status (phakic: pseudophakic)	46 (88.5%): 6 (11.5%)
Vitreous status (transparent: haze: hemorrhage)	20 (38.5%): 22 (42.3%): 10 (19.2%)
High myopia (eyes)	16 (30.8%)
Axial length of highly myopic eyes (mm)	28.21 ± 1.66 (range:26.15–31.12)
PVR grade (A or none: B: C1)	22 (42.3%): 26 (50.0%): 4 (7.7%)
RRD extent (clock hours)	6.5 ± 2.3 (range: 2–12)
Macular involved (on: off)	12 (23.1%): 40 (76.9%)
Drainage retinotomy (no: yes)	25 (48.1%): 27 (51.9%)

PPV, pars plana vitrectomy; RRD, rhegmatogenous retinal detachment; LogMAR, the logarithm of the minimum angle of resolution; BCVA, best corrected visual acuity; PVR, proliferative vitreous retinopathy.

This series included forty-nine primary RRDs (94.2%) and three recurrent RRDs (5.8%). Of the three eyes, two were vitrectomized eyes (Case 20 underwent lens extraction and intraocular lens (IOL) implantation and silicone oil removal 7 years ago; Case 24 underwent lens extraction and IOL implantation and silicone oil removal 8 months ago). Yttrium–aluminum–garnet laser capsulotomy was performed for both patients. Another patient (Case 25) underwent scleral buckling for primary detachment 1 year ago.

Intraoperatively, we found the mean detachment extent was  $6.5 \pm 2.3$  clock hours (range: 2–12). There was a total of 150 breaks, of which 76 (50.7%) were located in the superior retina (between 8 and 4 o'clock meridian, including the 8 and 4 o'clock meridian), and the other 74 (49.3%) were located in the inferior retina (between 4 and 8 o'clock meridian). One hundred and one breaks (67.3%) were horseshoe tears, and forty-nine breaks (32.7%) were atrophic holes. Thirteen eyes (25.0%) had inferior breaks only, and thirty-nine eyes (75.0%) had both superior and inferior breaks. **Table 2** illustrates the characteristics of retinal breaks. Two eyes (3.8%) were complicated with choroidal detachment. Four patients who had lens opacification with visual significance underwent PPV combined with cataract surgery.

## Anatomical Outcome

Retinal reattachment after single surgery was achieved in 50 of the 52 patients (96.2%). The other two patients received vitrectomy with silicone oil tamponade as a salvage treatment, and no one had redetachment after silicone oil removal until the last follow-up. **Table 3** shows the clinical characteristics of the two patients. Both eyes were attributed to new breaks, and Case 49 was related to the newly developed macular hole.

## Visual Acuity Outcome

Mean preoperative logMAR BCVA (Snellen equivalent 20/796) was  $1.60 \pm 0.93$  (range: 0–2.6, median: 1.7). The mean

**TABLE 2 |** Clinical characteristics of retinal breaks.

Characteristic	
<b>No. of breaks</b>	
Mean no.	2.9 ± 2.1 (range: 1–12)
Single: two: three or more (eyes)	9 (17.3%): 18 (34.6%): 25 (48.1%)
<b>Type of breaks</b>	
Horseshoe tears	29 (55.8%)
Atrophic holes	8 (15.4%)
Horseshoe tears + atrophic holes	15 (28.8%)
<b>Size of breaks</b>	
Small breaks ( $\leq 2$ PD)	38 (73.1%)
Medium breaks ( $> 2$ PD, and $\leq 5$ PD)	14 (26.9%)
<b>Location of breaks</b>	
Inferior	13 (25.0%)
Superior + inferior	39 (75.0%)

**TABLE 3 |** Clinical characteristics of patients with primary reattachment failure.

Characteristics	Case 35	Case 49
Gender	Male	Male
Age (years)	49	44
Disease course (days)	10	4
Myopia	Yes	High myopia (AL: 29.55 mm)
<b>Preoperatively</b>		
Number of quadrants involved	5	6
Number of retinal breaks	4	3
Location of retinal breaks	Two in 7 o' clock, one in 8 o' clock, and one in 9 o' clock	One in 7 o' clock, one in 8 o' clock, and one in 9 o' clock
Type of retinal breaks	Horseshoe tears	Horseshoe tears and atrophic hole
Size of retinal breaks (PD)	1	1
Macular involved	Off	Off
PVR	None or A	None or A
Final success	Yes	Yes

postoperative logMAR BCVA (Snellen equivalent 20/55) was  $0.44 \pm 0.24$  (range: 0–1.1, median: 0.45), showing a significant improvement ( $P < 0.001$ ).

## Complications

The air was completely absorbed 9–12 days following surgery. Temporary IOP elevation ( $> 21$  mmHg) occurred in seven highly myopic patients 1 week after the surgery and was controlled well using topical medications without any permanent damage. Ocular hypotony, endophthalmitis, and other serious complications were not observed. During follow-up, eight eyes (17.4%) of the 46 phakic eyes underwent secondary cataract surgery.

## DISCUSSION

This retrospective consecutive case series included fifty-two eyes of fifty-two RRD patients, demonstrating that inferior breaks

in RRDs can be effectively managed with 25-G PPV combined with air tamponade. After a follow-up of at least 6 months, fifty patients (96.2%) achieved successful retinal reattachment after a single surgery, with corresponding improvements in BCVA. This technique demonstrated favorable surgical outcomes and fewer complications.

Conventionally, long-term tamponades, such as  $C_3F_8$  and silicone oil, are commonly used. However, long-acting gas significantly affects postoperative visual rehabilitation and requires a prolonged prone position. Silicone oil can also lead to many potential complications, such as secondary glaucoma and cataract. Moreover, these patients require additional surgery to remove silicone oil. Therefore, attempts have been made to shorten the prone positioning period and minimize complications by using air.

Using air tamponade has several important advantages. Air, with a much shorter half-life and the non-expansile property, usually remains in the eye for less than 1 week (16), allows much quicker visual rehabilitation, and reduces postoperative complications, such as elevated IOP and PVR (11, 17). Like the long-acting gas, air provides buoyant force and great surface tension to seal retinal breaks, preventing fluid accumulation in the subretinal space. A previous study showed that the retina-RPE adhesion occurs within 24 h in situations without SRF (18). After that time, fluid will not enter the subretinal space through

breaks. Therefore, the long-term tamponade may be unnecessary for retinal detachment. Moreover, the shorter duration of air in the eye may mitigate against postoperative PVR or epiretinal membrane formation (19).

The locations of retinal breaks and quadrants involved are important and clinically relevant factors that may affect surgical outcomes (5). Inferior breaks always pose a challenge to intraocular air tamponade. Previous studies showed conflicting results. Tan et al. (10) found that RRDs that involved the inferior quadrants had significantly lower primary success rates when using air tamponade, compared to  $SF_6$  tamponade. They suggested that air tamponade should only be used in superior RRDs. Nevertheless, in their study, shaving of the vitreous base was only performed around retinal breaks, and cryocoagulation was used in all cases, which is known to require longer time to induce chorioretinal adhesion than laser coagulation. A prospective randomized study by Zhou et al. (11) indicated that air had equivalent tamponade effects to  $C_3F_8$  for RRDs with inferior breaks (single-operation success rate: 84 and 78% in air and  $C_3F_8$  groups, respectively). Martínez-Castillo et al. (12, 13) reported that PPV with air tamponade was effective in the treatment of pseudophakic RRDs with inferior breaks without facedown position postoperatively (primary success rate: 90–93.3%). Consistent with previously reported results, this case series, with single and final operation success rates of 96.2 and

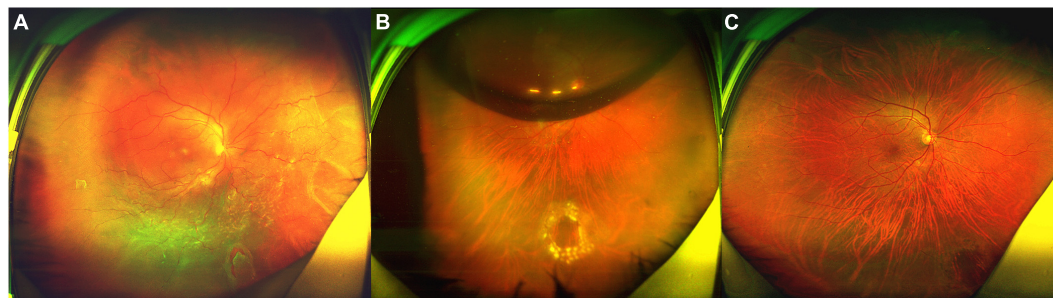


**FIGURE 1 |** Fundus photograph taken preoperatively and postoperatively of the patient (No. 15) undergoing 25-G PPV with air tamponade. **(A)** A total RRD (range: 12 clock hours) with an inferonasal horseshoe tear (2.5 PD) and posterior PVR. **(B)** Postoperative 6-day follow-up: the retina reattached. There was an air bubble in the vitreous cavity. **(C)** Postoperative 6-month follow-up: the retina reattached, with the firm chorioretinal adhesion induced by laser coagulation.

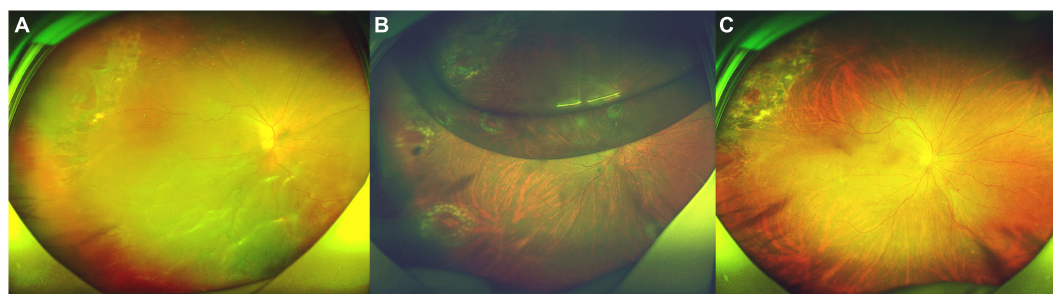


**FIGURE 2 |** Fundus photograph taken preoperatively and postoperatively of the patient (No. 27) undergoing 25-G PPV with air tamponade. **(A)** A macular-off RRD (range: 11 clock hours) with nine horseshoe tears in superotemporal, inferotemporal, and inferonasal quadrants and posterior PVR. **(B)** Postoperative 5-day follow-up: the retina reattached. There was an air bubble in the vitreous cavity. **(C)** Postoperative 4-month follow-up: the retina reattached, with the firm chorioretinal adhesion induced by laser coagulation.



100%, respectively, provides further evidence that air tamponade is sufficient to establish a stable chorioretinal adhesion and achieve retinal reattachment in RRDs with inferior breaks.

For RRDs with inferior breaks, it may be challenging to maintain the retinal breaks attached until the chorioretinal adhesion developed. For RRDs with superior breaks, air in the vitreous cavity can seal the breaks easily because of buoyant force and great surface tension. Regarding RRDs with inferior breaks, air may be unlikely to provide effective tamponade for the breaks for a sufficient duration postoperatively, as the residual SRF tends to fall to the inferior quadrant and may seep around edge of the inferior breaks due to gravity. Thus, it is assumed that air tamponade may be insufficient for the treatment of RRDs with inferior breaks. However, Martínez-Castillo et al. (12, 20) reported that 20-G PPV with air tamponade could adequately treat RRDs with inferior breaks, if complete drainage of SRF was performed. Tetsumoto et al. (9) inferred that short-term tamponade may sufficiently reduce the risk of redetachment if the SRF does not reach the original break. In present study, we adjusted the head position appropriately during the fluid-air exchange, allowing the SRF to flow out easily. In patients with a tiny break in the far periphery, a drainage retinotomy can be created to fully drain the SRF. A peripheral drainage retinotomy should be attempted in a superior quadrant, whenever possible, to avoid complications. Moreover, postoperative supine positioning could prevent the SRF from collecting around the inferior breaks, giving sufficient duration for the establishment of stable chorioretinal adhesion. A recent study by Gozawa et al. (21) observed intraocular gas contact rates of the retina using MRI. They found that the gas could adequately support and seal superior and inferior parts of the retina in the supine position, with a gas contact rate exceeding 90%. Therefore, the patients in this study were instructed to maintain an alternative supine or lateral position, implying that intraocular air bubble can effectively seal inferior breaks and enhance SRF absorption. In addition, the supine position is less demanding and easier for the patients to maintain.

Previous literature demonstrated that the primary anatomical success rates of air tamponade varied from 73 to 94.5% (11, 12, 20, 22–24). This discrepancy may be due to different patient selection criteria, varied sample sizes, and diverse vitreoretinal surgical techniques. It should be noted that surgical techniques are essential for a successful RRD repair. The pathogenesis of RRD involves vitreoretinal tractional forces that result in a full-thickness break (1). Therefore, our technique highlights complete vitreous removal. The vitreous around retinal breaks and vitreous base were removed as completely as possible under 360° scleral indentation. A wide-angle viewing system and scleral indentation are critical for a successful shaving of the vitreous base. In addition, advanced vitreous cutter and directional endolaser probe have greatly facilitated the management of retinal breaks in peripheral, reducing complications such as iatrogenic breaks and posterior capsular damage. Triamcinolone was also used routinely to detect the residual vitreous gel in case of insufficient vitreous liquefaction. In addition, excessive interventions should be avoided to prevent unnecessary complications. PFCL is usually used during vitrectomy to facilitate the peripheral vitreous

shaving and SRF drainage. However, subretinal migration of PFCL is a common complication. Li et al. (5) reported that a 360° prophylactic laser coagulation could improve anatomical success rate. It is essential to identify and treat all retinal breaks. Nevertheless, excessive laser may cause retinal necrosis and small, difficult-to-find retinal holes, leading to a redetachment. These holes are difficult to identify within the patches of chorioretinal atrophy. In present study, most patients had severe vitreous liquefaction or horseshoe tears with strong vitreoretinal traction, or a combination of these factors. Therefore, we did not choose scleral buckling as the primary treatment. Our experience with this case series provides further evidence that the complete vitrectomy with air tamponade could be effective in repairing RRDs with inferior breaks. After a follow-up of at least 6 months, the retina of fifty eyes completely reattached after a single surgery, obtaining a primary success rate of 96.2%.

No serious adverse events occurred during the procedure, which indicated the safety of the current surgical technique. As previously demonstrated (10, 11, 20), the leading cause of redetachment is new breaks, which occurred in both recurrent patients. One patient (Case 49) complicated with high myopia developed a myopic macular hole-associated retinal detachments 2 weeks after surgery. As a small amount of submacular fluid would be left at the end of surgery, a potential explanation may be that the great surface tension of air presses against the fovea and the submacular fluid. Previous literature disclosed that exposure of the lens to abnormally high oxygen levels can lead to nuclear sclerosis in vitrectomized eyes (25). In this case series, eight eyes (17.4%) underwent secondary cataract surgery during follow-up. The air usually remains in the eye for about 1 week. The shorter duration of intraocular air contacting with the lens may reduce the risk of cataract development or progression. This study has several limitations, including its retrospective design and the lack of a control group. The retrospective design has an inherent risk of selection bias. In addition, all patients were enrolled from a single tertiary institution, which may cause selection bias.

In conclusion, we observed a satisfactory success rate using 25-G PPV with air tamponade in repairing RRDs with inferior breaks. This technique has a faster visual rehabilitation, a shorter positioning period, fewer complications, and reduced medical costs. The high success rate of this study suggests that air has emerged as a reasonable alternative for tamponade in the management of RRDs with inferior breaks. Prospective comparative studies to assess the efficacy of this technique for complex RRDs are required in the future work.

## Typical Case Presentation

Patient No. 15 (Figure 1).

A 46-year-old highly myopic man was referred to our clinic. He complained of decreased vision in the right eye, which had persisted for about 40 days prior to his initial visit to our clinic. His BCVA was 1.7 logMAR (Snellen equivalent 20/1,000). The AL was 26.29 mm in the right eye, which was measured by Lenstar 2 weeks after surgery. Fundoscopy revealed a total RRD (range: 12 clock hours) with posterior PVR and an inferonasal horseshoe tear (2.5 PD) (Figure 1A). Six days after surgery, the retina

reattached (**Figure 1B**). Six months after surgery, the BCVA in right eye was 0.6 logMAR (Snellen equivalent 20/80, **Figure 1C**).

Patient No. 27 (**Figure 2**).

A 61-year-old man presented with darkness and decreased vision in the right eye that developed over 1 month. He was previously treated by laser retinopexy for superotemporal tears and localized detachment 20 days ago, but developed a macular-off retinal detachment with nine horseshoe tears and posterior PVR. Intraoperatively, he was found to have multiple horseshoe tears along the attachment of the posterior hyaloid to the posterior vitreous base. His BCVA was 1.7 logMAR (Snellen equivalent 20/1000). Fundoscopy revealed a macular-off RRD (range: 11 clock hours) with nine horseshoe tears (**Figure 2A**). Five days after surgery, the retina reattached (**Figure 2B**). Four months after surgery, the BCVA in right eye was 0.6 logMAR (Snellen equivalent 20/80, **Figure 2C**).

## DATA AVAILABILITY STATEMENT

The data can be obtained with a request to the corresponding authors. There is no confidential data or any restriction on accession to the original data.

## ETHICS STATEMENT

The studies involving human participants were reviewed and approved by Ethics Committee of the Second People's Hospital of Foshan. The patients/participants provided their written informed consent to participate in this study. Written informed consent was obtained from the individual(s) for the publication of any potentially identifiable images or data included in this article.

## REFERENCES

1. D'Amico DJ. Clinical practice. primary retinal detachment. *N Engl J Med*. (2008) 359:2346–54. doi: 10.1056/NEJMc0804591
2. Hwang JC. Regional practice patterns for retinal detachment repair in the United States. *Am J Ophthalmol*. (2012) 153:1125–8. doi: 10.1016/j.ajo.2011.11.034
3. Antoun J, Azar G, Jabbour E, Kourie HR, Slim E, Schakal A, et al. Vitreoretinal surgery with silicone oil tamponade in primary uncomplicated rhegmatogenous retinal detachment: clinical outcomes and complications. *Retina*. (2016) 36:1906–12. doi: 10.1097/IAE.0000000000001008
4. Znaor L, Medic A, Binder S, Vucinovic A, Marin J, Puljak L. Pars plana vitrectomy versus scleral buckling for repairing simple rhegmatogenous retinal detachments. *Cochrane Database Syst Rev*. (2019) 3:CD009562. doi: 10.1002/14651858.CD009562.pub2
5. Li Y, Cheung N, Jia L, Zhang H, Liu N. Surgical outcomes of 25-gauge pars plana vitrectomy using air as an internal tamponade for primary rhegmatogenous retinal detachment. *Retina*. (2020) 40:2077–82. doi: 10.1097/IAE.0000000000002744
6. Al-Jazzaf AM, Netland PA, Charles S. Incidence and management of elevated intraocular pressure after silicone oil injection. *J Glaucoma*. (2005) 14:40–6. doi: 10.1097/01.jgg.0000145811.62095.5a
7. Zhang Z, Peng M, Wei Y, Jiang X, Zhang S. Pars plana vitrectomy with partial tamponade of filtered air in rhegmatogenous retinal detachment caused by superior retinal breaks. *BMC Ophthalmol*. (2017) 17:64. doi: 10.1186/s12886-017-0459-6

## AUTHOR CONTRIBUTIONS

PSh and XK designed the study. PSh, XK, and XL had full access to all data in the study and take responsibility for the integrity of the data and the accuracy of the data analysis. PSh, XK, LZ, and PSu had roles in the clinical management, patient recruitment, and clinical data collection. PSh had roles in data collection and statistical analysis. PSh wrote the manuscript. XL and MH contributed to critical revision of the report. All authors reviewed and approved the final version of the manuscript.

## FUNDING

This work was supported by Basic and Applied Basic Research Foundation of Guangdong Province, China (2019B1515120011); Science and Technology Planning Project of Foshan, Guangdong (1920001001336); Guangdong Medical Research Foundation, China (B2019079); Postdoctoral Program of International Training Project for Young Talents in Guangdong Province, 2020; and Clinical Research Project of Bethune-Merck Diabetes Foundation, 2017.

## SUPPLEMENTARY MATERIAL

The Supplementary Material for this article can be found online at: <https://www.frontiersin.org/articles/10.3389/fmed.2022.724234/full#supplementary-material>

8. Lin Z, Liang QH, Lin K, Hu ZX, Chen TY, Wu RH, et al. Air tamponade and without heavy liquid usage in pars plana vitrectomy for rhegmatogenous retinal detachment repair. *Int J Ophthalmol*. (2018) 11:1779–83. doi: 10.18240/ijo.2018.11.08
9. Tetsumoto A, Imai H, Hayashida M, Otsuka K, Matsumiya W, Miki A, et al. The comparison of the surgical outcome of 27-gauge pars plana vitrectomy for primary rhegmatogenous retinal detachment between air and SF6 gas tamponade. *Eye (Lond)*. (2020) 34:299–306. doi: 10.1038/s41433-019-0726-2
10. Tan HS, Oberstein SY, Mura M, Bijl HM. Air versus gas tamponade in retinal detachment surgery. *Br J Ophthalmol*. (2013) 97:80–2. doi: 10.1136/bjophthalmol-2012-302140
11. Zhou C, Qiu Q, Zheng Z. AIR versus gas tamponade in rhegmatogenous retinal detachment with inferior breaks after 23-gauge pars plana vitrectomy: a prospective, randomized comparative interventional study. *Retina*. (2015) 35:886–91. doi: 10.1097/IAE.0000000000000416
12. Martinez-Castillo V, Boixadera A, Verdugo A, Garcia-Arumi J. Pars plana vitrectomy alone for the management of inferior breaks in pseudophakic retinal detachment without facedown position. *Ophthalmology*. (2005) 112:1222–6. doi: 10.1016/j.ophtha.2004.12.046
13. Martinez-Castillo V, Verdugo A, Boixadera A, Garcia-Arumi J, Corcostegui B. Management of inferior breaks in pseudophakic rhegmatogenous retinal detachment with pars plana vitrectomy and air. *Arch Ophthalmol*. (2005) 123:1078–81. doi: 10.1001/archophth.123.8.1078
14. The Retina Society Terminology Committee. The classification of retinal detachment with proliferative vitreoretinopathy. *Ophthalmology*. (1983) 90:121–5. doi: 10.1016/s0161-6420(83)34588-7

15. Holladay JT. Visual acuity measurements. *J Cataract Refract Surg.* (2004) 30:287–90. doi: 10.1016/j.jcrs.2004.01.014
16. Thompson JT. Kinetics of intraocular gases. Disappearance of air, sulfur hexafluoride, and perfluoropropane after pars plana vitrectomy. *Arch Ophthalmol.* (1989) 107:687–91. doi: 10.1001/archophth.1989.01070010705031
17. Sigler EJ, Randolph JC, Calzada JI, Charles S. Pars plana vitrectomy with medium-term postoperative perfluoro-N-octane for recurrent inferior retinal detachment complicated by advanced proliferative vitreoretinopathy. *Retina.* (2013) 33:791–7. doi: 10.1097/IAE.0b013e31826a6978
18. Folk JC, Sneed SR, Folberg R, Coonan P, Pulido JS. Early retinal adhesion from laser photocoagulation. *Ophthalmology.* (1989) 96:1523–5. doi: 10.1016/s0161-6420(89)32696-0
19. Sebag J, Tang M. Pneumatic retinopexy using only air. *Retina.* (1993) 13:8–12. doi: 10.1097/00006982-199313010-00003
20. Martinez-Castillo VJ, Garcia-Arumi J, Boixadera A. Pars plana vitrectomy alone for the management of pseudophakic rhegmatogenous retinal detachment with only inferior breaks. *Ophthalmology.* (2016) 123:1563–9. doi: 10.1016/j.ophtha.2016.03.032
21. Gozawa M, Kanamoto M, Ishida S, Takamura Y, Iwasaki K, Kimura H, et al. Evaluation of intraocular gas using magnetic resonance imaging after pars plana vitrectomy with gas tamponade for rhegmatogenous retinal detachment. *Sci Rep.* (2020) 10:1521. doi: 10.1038/s41598-020-58508-3
22. Wickham L, Connor M, Aylward GW. Vitrectomy and gas for inferior break retinal detachments: are the results comparable to vitrectomy, gas, and scleral buckle? *Br J Ophthalmol.* (2004) 88:1376–9. doi: 10.1136/bjo.2004.043687
23. Colyer MH, Barazi MK, von Fricken MA. Retrospective comparison of 25-gauge transconjunctival sutureless vitrectomy to 20-gauge vitrectomy for the repair of pseudophakic primary inferior rhegmatogenous retinal detachment. *Retina.* (2010) 30:1678–84. doi: 10.1097/IAE.0b013e3181dd6da1
24. Dell'Omo R, Barca F, Tan HS, Bijl HM, Oberstein SY, Mura M. Pars plana vitrectomy for the repair of primary, inferior rhegmatogenous retinal detachment associated to inferior breaks. A comparison of a 25-gauge versus a 20-gauge system. *Graefes Arch Clin Exp Ophthalmol.* (2013) 251:485–90. doi: 10.1007/s00417-012-2059-8
25. Holekamp NM, Shui YB, Beebe DC. Vitrectomy surgery increases oxygen exposure to the lens: a possible mechanism for nuclear cataract formation. *Am J Ophthalmol.* (2005) 139:302–10. doi: 10.1016/j.ajo.2004.09.046

**Conflict of Interest:** The authors declare that the research was conducted in the absence of any commercial or financial relationships that could be construed as a potential conflict of interest.

**Publisher's Note:** All claims expressed in this article are solely those of the authors and do not necessarily represent those of their affiliated organizations, or those of the publisher, the editors and the reviewers. Any product that may be evaluated in this article, or claim that may be made by its manufacturer, is not guaranteed or endorsed by the publisher.

Copyright © 2022 Shen, Kong, Zhou, Su, Lu and He. This is an open-access article distributed under the terms of the Creative Commons Attribution License (CC BY). The use, distribution or reproduction in other forums is permitted, provided the original author(s) and the copyright owner(s) are credited and that the original publication in this journal is cited, in accordance with accepted academic practice. No use, distribution or reproduction is permitted which does not comply with these terms.



# Clinical Relevance of Body Fluid Volume Status in Diabetic Patients With Macular Edema

Jie Yao<sup>1,2†</sup>, Qingsheng Peng<sup>1†</sup>, Yuanhong Li<sup>3†</sup>, Anyi Liang<sup>1</sup>, Jianteng Xie<sup>4</sup>, Xuenan Zhuang<sup>1,5</sup>, Ruoyu Chen<sup>1,6</sup>, Yesheng Chen<sup>1,6,7</sup>, Zicheng Wang<sup>1,8</sup>, Liang Zhang<sup>1,2,6\*</sup> and Dan Cao<sup>1,6,7\*</sup>

<sup>1</sup> Department of Ophthalmology, Guangdong Provincial People's Hospital, Guangdong Academy of Medical Sciences, Guangzhou, China, <sup>2</sup> Shantou University Medical College, Shantou, China, <sup>3</sup> Department of Nutrition, Guangdong Provincial People's Hospital, Guangdong Academy of Medical Sciences, Guangzhou, China, <sup>4</sup> Department of Nephrology, Guangdong Provincial People's Hospital, Guangdong Academy of Medical Sciences, Guangzhou, China, <sup>5</sup> State Key Laboratory of Ophthalmology, Zhongshan Ophthalmic Center, Sun Yat-sen University, Guangzhou, China, <sup>6</sup> Southern Medical University, Guangzhou, China, <sup>7</sup> Department of Cardiology, Guangdong Cardiovascular Institute, Guangdong Provincial People's Hospital, Guangdong Academy of Medical Sciences, Guangzhou, China, <sup>8</sup> School of Medicine, South China University of Technology, Guangzhou, China

## OPEN ACCESS

### Edited by:

Shaochong Zhang,  
Shenzhen Eye Hospital, China

### Reviewed by:

Veena Rao Rajji,  
Rush University, United States  
Embrong Zunaina,  
Universiti Sains Malaysia, Malaysia

### \*Correspondence:

Dan Cao  
dancao5413@163.com  
Liang Zhang  
zhangliang5413@163.com

<sup>†</sup>These authors have contributed  
equally to this work and share first  
authorship

### Specialty section:

This article was submitted to  
Ophthalmology,  
a section of the journal  
Frontiers in Medicine

**Received:** 18 January 2022

**Accepted:** 21 March 2022

**Published:** 12 April 2022

### Citation:

Yao J, Peng Q, Li Y, Liang A, Xie J,  
Zhuang X, Chen R, Chen Y, Wang Z,  
Zhang L and Cao D (2022) Clinical  
Relevance of Body Fluid Volume  
Status in Diabetic Patients With  
Macular Edema.  
Front. Med. 9:857532.  
doi: 10.3389/fmed.2022.857532

**Objective:** To investigate body fluid status in diabetic macular edema (DME) patients and the extent to which it is affected by renal function.

**Methods:** One hundred and thirty-two eyes from 132 patients with diabetes mellitus (DM) were prospectively collected in this cross-sectional, observational study. Thirty-five were DM patients without diabetic retinopathy (DR), 31 were DR patients without DME, and 66 were DME patients. The fluid status of each participant was quantified with extracellular water-to-total body water ratio (ECW/TBW) using a body composition monitor. Central subfield thickness (CST) and macular volume (MV) were obtained using optical coherence tomography (OCT). Urine albumin-to-creatinine ratio (UACR), estimated glomerular filtration rate (eGFR), and albumin was obtained using serum and urine laboratory data.

**Results:** ECW/TBW was significantly increased in DME patients ( $39.2 \pm 0.9$ , %) compared to DM ( $38.1 \pm 0.7$ , %,  $P = 0.003$ ) and DR patients without DME ( $38.7 \pm 0.9$ , %,  $P < 0.001$ ). In multilinear regression, fluid overload was positively related to DME and UACR (DME vs. DM:  $\beta = 2.418$ ,  $P < 0.001$ ; DME vs. DR:  $\beta = 1.641$ ,  $P = 0.001$ ; UACR, per  $10^2$ ,  $\beta = 1.017$ ,  $P = 0.01$ ). In the binary logistic regression for DME risk, the area under the receiver operating characteristic curve (AUROC) increased significantly by adding ECW/TBW along with UACR and age (AUC: 0.826 vs. 0.768).

**Conclusion:** DME patients had elevated body fluid volume independent of kidney functions. The assessment of extracellular fluid status may help in the management of DME.

**Keywords:** diabetic macular edema (DME), optical coherence tomography, body composition measurement, fluid status, albuminuria



## INTRODUCTION

The burden of diabetes mellitus (DM) is growing globally, with a worldwide estimated prevalence of 4.1% in 2010 expected to increase to 7.7% by 2030 (1, 2). In China, up to 11.6% of the population aged 18 years and older has diabetes (3). Diabetic microvascular complications such as retinopathy (DR) and macular edema (DME) are the major causes of blindness in DM patients in China (4). Diabetic kidney disease (DKD) is another common microvascular complication that leads to kidney failure in approximately 40% of diabetic patients (5). Our group found that the elevation of urine albumin-to-creatinine ratio (UACR) or the worsening in UACR stages, a signature change for renal function in DKD, was correlated with DME (6) and macular thickening (7). Clinical evidence also supports this connection. DME patients with better renal function had greater chances of better prognoses, especially in refractory DME (8, 9). DKD and DR share similar pathogenesis (10). Hyperglycemia-induced inflammation and oxidative stress lead to loss of endothelial cells, pericytes, and disruption of cell junctions, which contribute to the breakdown of vascular barrier in both the kidney and retina (10). For DME, hyperglycemia-linked pathways also contribute to dysfunction of retinal pigment epithelium (RPE) cells and glial cells such as Müller cells, which normally drain the fluid in the retina to the systemic circulation and keep the retina dehydrated (11, 12). Increased entry of fluid through the damaged blood-retinal barrier (BRB) and decreased drainage result in accumulation of fluid, especially in the macula (13).

Interestingly, while DKD has been proven associated with the elevation in extracellular fluid volume (14), a recent study discovered that fluid overload also appeared in DME patients (15). Imbalance of hydrostatic and oncotic pressure explained by Starling equation could account for the phenomenon. The fluid status was monitored by body composition measurement (BCM) objectively and non-invasively, which is widely assumed credible assessing the fluid status of patients with chronic kidney diseases in clinical practice (16, 17). DME characterized by exudative fluid accumulation in the macula was speculated as a focal manifestation of extracellular fluid overload. The accessibility of extracellular water to total body water (ECW/TBW) ratio

makes it the perfect systemic fluid marker for DME studies and a potential biomarker for DME treatments (18). Still, the confounding effect between DKD and fluid overload has not been discussed deeply regarding the relationship with DME. There lacked evidence of whether the fluid expansion came up through DME pathophysiological alterations along or shared pathogenesis between DME and DKD.

In this paper, the fluid statuses among different DM patients, including DR patients with or without DME and diabetic patients with or without DR, were investigated. By further exploiting associated changes of fluid status and renal function parameters in DME, this study proposed a novel hypothesis for the role of body fluid status in DME mechanisms. It provided significant clinical evidence to guide future DME management and treatments.

## METHODS

This was a cross-sectional observational study. Diabetic patients diagnosed with or without DR and DME by a multi-disciplinary team at Guangdong Provincial People's Hospital were prospectively included from May 2020 to February 2021. Medical records were reviewed by a chief-resident doctor from the department of ophthalmology and a chief-resident doctor from the department of endocrine of Guangdong Provincial People's Hospital. All patients included were informed of the study contents and signed written consent. This study was conducted following the Declaration of Helsinki and under the supervision of the Research Ethics Committee of Guangdong Provincial People's Hospital, Guangdong Academy of Medical Sciences (registration number: GDREC2018380H).

### Participant

Patients aged 18 years or older, diagnosed with DM, with or without DR and DME, and capable of going through funduscopic examination, optical coherence tomography (OCT) scans, and BCM were included in the study. Exclusion criteria were receiving pan-retinal photocoagulation, intravitreal injection or pars-planar vitrectomy within 3 months, other retinal diseases including age-related macular disease, retinal vascular occlusion, retinal vasculitis, macular hole, and epiretinal membrane, significant cataract affecting fundus examination, and severe systemic diseases including myocardial infarction, stroke, CKD at end-stage, and under hemodialysis or peritoneal dialysis.

### Clinical Parameters

All patients were examined for the following characteristics and parameters: age, sex, height, body weight, systolic blood pressure (SBP), diastolic blood pressure (DBP), history of hypertension, DM duration. Hypertension was defined as SBP  $\geq 140$  mmHg or DBP  $\geq 90$  mmHg (19). Diagnosis and duration of DM were obtained from medical records. Each participant's DM duration was labeled as those diagnosed for 10 years or more and those who were not. Laboratory parameters included glycated hemoglobin (HbA1c), complete blood count, renal functions such as serum creatinine, urea, UACR, lipid profile including cholesterol, triglyceride, low-density lipoprotein (LDL), and

**Abbreviations:** DM, diabetes mellitus; DR, diabetic retinopathy; DME, diabetic macular edema; SBP, systolic blood pressure; DBP, diastolic blood pressure; BMI, body mass index; LogMAR, logarithm of minimal angle of resolution; BCVA, best-corrected visual acuity; IOP, intraocular pressure; CST, central subfield thickness; MV, macular volume; UACR, urine albumin-to-creatinine ratio; eGFR, estimated glomerular filtration rate; HbA1c, glycated hemoglobin; TP, total protein; HDL, high-density lipoprotein; LDL, low-density lipoprotein; NLR, neutrophil-to-lymphocyte ratio; MLR, monocyte-to-lymphocyte ratio; PLR, platelet-to-lymphocyte ratio; PBF, percentage of body fat; ECW/TBW, extracellular water-to-total body water ratio; VFA, visceral fat area; BMR, basic metabolic rate; SMI, skeletal muscle index; DKD, diabetic kidney disease; VEGF, vascular endothelial growth factor; BIA, bioimpedance analysis; BCM, body composition measurement; CKD, chronic kidney disease; OCT, optical coherence tomography; ART, automatic real time; DSM-BIA, direct segmental multi-frequency bioelectrical impedance analysis; ECW, Extracellular water; ICW, intracellular water; PhA, phase angle; CKD-EPI, Chronic Kidney Disease Epidemiology Collaboration; ESL, endothelial surface layer; IVI, intravitreal injection; RPE, retinal pigment epithelium; BRB, blood-retinal barrier.

high-density lipoprotein (HDL). Other factors included albumin, total protein (TP), and 25-hydroxyvitamin D. Body mass index (BMI) was calculated using the formula of weight in kilograms divided by height in meters squared (20). The estimated glomerular filtration rate (eGFR) was calculated from serum creatinine using the formula of Chronic Kidney Disease Epidemiology Collaboration (CKD-EPI) equation (21). All blood samples and urine samples were collected in the morning after 8-h fasting before patients taking breakfast.

The eGFR value of all participants was labeled as normal ( $\geq 60$  mL/min/1.73 m<sup>2</sup>) and impaired ( $< 60$  mL/min/1.73 m<sup>2</sup>) according to the definition of CKD (22). The stages of albuminuria was classified with the definition of the USA National Kidney Foundation (23) as normoalbuminuria (UACR  $< 30$  mg/g), microalbuminuria (UACR  $\geq 30$  mg/g,  $< 300$  mg/g), and macroalbuminuria (UACR  $\geq 300$  mg/g).

## Ophthalmic Examinations

All patients received comprehensive baseline ophthalmic examination, including best-corrected visual acuity (BCVA), intraocular pressure (IOP), dilated fundus examination, fundus photography, and OCT. BCVA was examined with the Snellen chart and converted into the logarithm of minimal angle of resolution (logMAR) (24). IOP was investigated with non-contact tonometry (TX-20 Full Auto Tonometer; Canon, Inc., Tokyo, Japan). All patients received slit lamp fundus examination and fundus photography (TRC-NW8 non-mydratic) retinal camera, Topcon, Tokyo, Japan; D7500 DSLR camera, Nikon, Tokyo, Japan) to obtained one fovea-centered and one optic nerve head-centered photo after mydriasis. OCT examination (Spectralis; Heidelberg Engineering, Heidelberg, Germany) was conduct to capture the image of the macula, which was composed of 61 B-scans at an automatic real-time (ART) setting (10 images averaged) in the central  $30 \times 25^\circ$  area. Central subfield thickness (CST), which was defined as the mean retinal thickness of the 1 mm fovea-centered area, and macular volume (MV), which was the volume of the nine subfields of the Early Treatment Diabetic Retinopathy Study (ETDRS) grid, were obtained automatically from the integrated software. The manual adjustments were performed when there were obvious segmenting or fovea locating errors. Diagnosis and staging of DR and DME were based on the fundus examination, fundus photography, and OCT images follow the International Clinical Diabetic Retinopathy Disease Severity Scale and International Clinical Diabetic Macular Edema Disease Severity Scale by two experienced ophthalmologists specialized in retinal disease (PDR,  $\kappa = 0.897$ ; DME,  $\kappa = 0.918$ ) (25). Differing diagnoses were reassessed and diagnosed by a senior chief ophthalmologist.

## Body Composition Measurement

All patients underwent BCM examination (InBody S10; InBody CO., LTD., Seoul, Korea), which measured different body compositions via direct segmental multi-frequency bioelectrical impedance analysis (DSM-BIA). An eight-electrode system connecting to the ankles and two fingertips of each patient's hand segments the human body into five parts, including the right arm,

left arm, right leg, left leg, and trunk, and measures different body parts compartments. The instrument uses a current of 6 frequencies, including 1 kHz, 5 kHz, 50 kHz, 250 kHz, 500 kHz, and 1 MHz, the varied cell membrane conductivities from high-frequency to low-frequency current are therefore translated into extracellular water (ECW) and intracellular water (ICW) with different impedance (26). In the in-built software, other data including ECW/TBW of the whole body and separate body compartments, including right arm, left arm, trunk, right leg and left leg, and percentage of body fat (PBF), visceral fat area (VFA), skeletal muscle index (SKI) and phase angle (PhA) were calculated. All patients went through the examination in a supine position after 8-h fasting before breakfast, right before the OCT examination.

## Statistical Analysis

Participants were divided into three groups, including DM group (without DR), DR group (diagnosed with DR but no DME), and DME group (diagnosed with DR and DME) according to their diagnosis. Normally distributed continuous variables were shown as mean  $\pm$  standard deviation in **Table 1**;  $\chi^2$  tests were carried out to compare non-parametric variables among the three groups. Tests for homogeneity of variance were conducted on the general characteristics, BCM parameters, and renal function parameters, and no variate was found significant. For each participant, the one eye with higher CST, MV, and more severe DR stage was included in the data analysis. Analysis of variance (ANOVA) was applied to compare the quantitative characteristics, including age, SBP, DBP, BMI, BCVA, IOP, blood test parameters, and BCM results among three groups. Two multivariate linear models were carried out to estimate the effect of renal functions on body fluid status among three diabetic groups after adjusting for significant covariates identified in the univariate linear model. Step-by-step multivariate binary logistic regressions with a backward method were conducted to predict DME risk. The models' receiver operating characteristic (ROC) curves were then drawn to demonstrate their predictive power quantified by the area under the curves (AUC). All statistical analysis was performed using SPSS software (version 26.0, IBM Corp., Armonk, NY, USA). A  $P < 0.05$  indicates statistical significance.

## RESULTS

One hundred thirty-two patients (73 male and 59 female) with 132 eyes were enrolled in the study. **Table 1** shows the details of general characteristics, systemic factors, ocular parameters and BCM parameters among the DM group ( $n = 35$ ), DR group ( $n = 31$ ), and DME group ( $n = 66$ ). As for general characteristics, there was no statistically significant difference in sex, age, hypertension, blood pressure, weight among the three groups (all  $P > 0.05$ ), and there were significant differences in DM duration ( $P < 0.001$ ) and BMI ( $P = 0.013$ ). BCVA, CST and MV were significantly different among three groups (all  $P < 0.001$ ) while IOP was not ( $P = 0.942$ ).

**TABLE 1** | General characteristics, systemic parameters and ocular parameters of patients among three groups.

Characteristics	DM, <i>n</i> = 35	DR, <i>n</i> = 31	DME, <i>n</i> = 66	<i>P</i> <sup>a</sup>	<i>P</i> <sup>b</sup>	<i>P</i> <sup>c</sup>	<i>P</i> <sup>d</sup>
Female, <i>n</i> (%)	19 (54.3)	17 (54.8)	23 (34.8)	0.075 <sup>e</sup>	-	-	-
Hypertension, <i>n</i> (%)	11 (31.4)	14 (45.2)	31 (47.0)	0.303 <sup>e</sup>	-	-	-
DM duration <10 years, <i>n</i> (%)	25 (71.4)	7 (22.6)	27 (40.9)	<0.001 <sup>e</sup>	-	-	-
Age, years	56.3 ± 15.5	60.6 ± 8.8	57.7 ± 9.3	0.293	0.380	1.000	0.707
SBP, mmHg	131.8 ± 24.7	133.3 ± 20.7	137.6 ± 18.5	0.358	1.000	0.551	1.000
DBP, mmHg	82.5 ± 14.8	78.6 ± 11.4	81.5 ± 11.6	0.406	0.606	1.000	0.820
MAP, mmHg	98.9 ± 16.7	96.8 ± 13.2	100.2 ± 12.0	0.516	1.000	1.000	0.755
BMI, kg/m <sup>2</sup>	24.9 ± 3.0	24.1 ± 3.4	23.1 ± 2.7	0.013*	0.885	0.012*	0.324
HbA1c, %	8.5 ± 3.1	8.7 ± 2.0	8.1 ± 1.8	0.620	1.000	1.000	0.572
Hemoglobin, g/L	135.2 ± 15.3	121.8 ± 21.6	120.1 ± 17.5	0.387	0.009*	<0.001*	1.000
TP, mg/L	69.2 ± 7.4	71.9 ± 5.8	71.6 ± 8.9	0.281	0.525	0.445	1.000
Albumin, g/L	39.8 ± 3.2	40.0 ± 4.7	38.7 ± 5.4	0.381	1.000	0.897	0.673
Urea, mmol/L	5.6 ± 2.1	8.3 ± 4.5	9.1 ± 4.4	<0.001*	0.016*	<0.001*	1.000
Creatinine, μmol/L	68.3 ± 20.0	134.8 ± 166.3	116.4 ± 77.7	0.016*	0.020*	0.061	1.000
eGFR, mL/min/1.73 m <sup>2</sup>	95.6 ± 24.0	67.3 ± 25.5	68.8 ± 28.4	<0.001*	<0.001*	<0.001*	1.000
UACR, mg/gCr	21.6 ± 29.9	785.3 ± 1640.8	1265.7 ± 1381.4	<0.001*	0.057	<0.001*	0.271
UACR stage, median (range) <sup>f</sup>	1 (1–2)	2 (1–3)	3 (1–3)	<0.001 <sup>e</sup>	-	-	-
25-hydroxyvitamin D, ng/mL	24.7 ± 7.8	17.5 ± 6.9	18.7 ± 7.0	0.023*	0.029*	0.038*	1.000
NLR	2.2 ± 1.2	2.7 ± 1.3	2.9 ± 1.2	0.056	0.422	0.050	1.000
MLR, 10 <sup>-1</sup>	2.4 ± 1.2	2.7 ± 1.3	2.9 ± 1.2	0.021*	0.515	0.017*	0.767
PLR	112.2 ± 43.2	145.4 ± 50.5	149.1 ± 51.1	0.001*	0.021*	0.001*	1.000
<b>Ocular parameters</b>							
LogMAR	0.1 ± 0.2	0.4 ± 0.5	0.6 ± 0.4	<0.001*	0.085	<0.001*	0.010*
IOP, mmHg	14.0 ± 3.0	14.0 ± 3.4	13.8 ± 3.8	0.942	1.000	1.000	1.000
<b>OCT values</b>							
CST, μm	264.9 ± 20.6	268.0 ± 29.6	417.5 ± 168.1	<0.001*	1.000	<0.001*	<0.001*
MV, mm <sup>3</sup>	8.5 ± 0.4	8.7 ± 0.5	10.9 ± 2.6	<0.001*	1.000	<0.001*	<0.001*
<b>BCM parameters</b>							
ECW/TBW, %	38.1 ± 0.7	38.7 ± 0.9	39.2 ± 0.9	<0.001*	0.008*	<0.001*	0.019*
PBF, %	29.3 ± 7.3	27.7 ± 5.8	26.3 ± 7.8	0.125	1.000	0.130	1.000
VFA, cm <sup>2</sup>	91.8 ± 35.6	87.9 ± 28.9	78.8 ± 28.5	0.101	1.000	0.131	0.546
BMR, kcal	1386.3 ± 184.2	1336.7 ± 212.2	1354.3 ± 213.9	0.604	0.991	1.000	1.000
SMI, kg/m <sup>2</sup>	7.1 ± 1.1	6.8 ± 1.1	6.9 ± 1.2	0.467	0.766	0.913	1.000
Phase angle	5.7 ± 0.8	5.3 ± 0.8	4.9 ± 0.8	<0.001*	0.231	<0.001*	0.014*

DM, diabetes mellitus; DR, diabetic retinopathy; DME, diabetic macular edema; SBP, systolic blood pressure; DBP, diastolic blood pressure; MAP, mean arterial pressure; BMI, body mass index; HbA1c, glycated hemoglobin; TP, total protein; eGFR, estimated glomerular filtration rate; UACR, urine albumin-to-creatinine ratio; NLR, neutrophil-to-lymphocyte ratio; MLR, monocyte-to-lymphocyte ratio; PLR, platelet-to-lymphocyte ratio; LogMAR, the logarithm of minimal angle of resolution, for best-corrected visual acuity; IOP, intraocular pressure; CST, central subfield thickness; MV, macular volume; ECW/TBW, extracellular water-to-total body water ratio; PBF, percentage of body fat; VFA, visceral fat area; BMR, basal metabolic rate; SMI, skeletal muscle index.

<sup>a,b,c,d</sup>were acquired using one-way ANOVA; <sup>e</sup> was acquired using  $\chi^2$  tests.

<sup>a,e</sup>*P*-value among three group.

<sup>b</sup>*P*-value between DM group and DR group.

<sup>c</sup>*P*-value between DM group and DME group.

<sup>d</sup>*P*-value between DR group vs DME group.

<sup>f</sup>UACR stage including normoalbuminuria, microalbuminuria and macroalbuminuria were denoted as stage 1 to 3.

\*Stand for *P* < 0.05.

## Systemic Factors and BCM Parameters Among Three Groups

All parameters of blood test and BCM parameters were found normally distributed. In the test of homogeneity, PhA and ECW/TBW showed a high level of collinearity. Hence PhA was excluded in further analysis. In the *post-hoc* analysis, systemic parameters including urea and PLR in both the DME group and

DR group were significantly higher than the DM groups (all *P* < 0.05), while hemoglobin, 25-hydroxyvitamin D, eGFR were significantly lower than the DM group (all *P* < 0.05). UACR (DME group: 1265.7 ± 1381.4 mg/gCr; DM group: 21.6 ± 29.9 mg/gCr, *P* < 0.001) and MLR (DME group: 2.9 ± 1.2 × 10<sup>-1</sup>; DM group: 2.4 ± 1.2 × 10<sup>-1</sup>, *P* = 0.017) was found elevated in the DME group compared to DM group. As for BCM parameters, the

**TABLE 2 |** Influence factors of ECW/TBW with univariate and multivariate linear models.

	Model 1				Model 2				Model 3			
	$\beta$	95%CI	Exp $\beta$	P	$\beta$	95%CI	Exp $\beta$	P	$\beta$	95%CI	Exp $\beta$	P
<b>Groups</b>												
DM	Reference	–	–	–	Reference	–	–	–	Reference	–	–	–
DR	0.627	0.229–1.026	1.873	0.002*	0.526	0.123–0.929	1.692	0.011*	0.387	0.036–0.809	1.472	0.073
DME	1.131	0.793–1.469	3.099	<0.001*	1.095	0.765–1.425	2.989	<0.001*	0.883	0.530–1.236	2.418	<0.001*
<b>Groups</b>												
DR	Reference	–	–	–	Reference	–	–	–	Reference	–	–	–
DME	0.504	0.152–0.855	1.656	<0.001*	0.569	0.268–0.869	1.767	<0.001*	0.496	0.196–0.796	1.642	0.001*
Age	0.037	0.024–0.05	1.038	<0.001*	0.038	0.026–0.049	1.038	<0.001*	0.038	0.027–0.048	1.039	<0.001*
DM Duration	0.160	0.005–0.315	1.173	0.043*	–0.057	–0.185–0.072	0.945	0.389	–0.006	–0.137–0.125	0.994	0.926
MAP	–0.008	–0.02–0.004	0.992	0.188	–0.011	–0.019 to –0.002	0.990	0.017*	–0.012	–0.021 to –0.004	0.988	0.005*
Albumin	–0.051	–0.084–0.018	0.950	0.003*	–0.046	–0.073 to –0.02	0.955	0.001*	–0.018	–0.052–0.016	0.982	0.296
eGFR	–0.013	–0.018–0.008	0.987	<0.001*	–0.001	–0.006–0.004	0.999	0.620	–	–	–	–
UACR	0.030	0.019–0.041	1.031	<0.001*	–	–	–	–	0.017	0.004–0.029	1.017	0.010*

DM, diabetes mellitus; DR, diabetic retinopathy; DME, diabetic macular edema; MAP, mean arterial pressure; eGFR, estimated glomerular filtration rate; UACR, urine albumin-to-creatinine ratio.

DM duration, every 5 years; MAP, per mmHg; Albumin, per g/L; eGFR, per mL/min/1.73 m<sup>2</sup>; UACR, per 10<sup>–2</sup> mg/g.

Model 1: univariate analysis; Model 2: multivariate model adjusted for systemic covariates and eGFR; Model 3: multivariate model adjusted for systemic covariates and UACR.

P was acquired using generalized linear model.

\*Stands for  $P < 0.05$ .

DME group had significantly higher ECW/TBW than both the DM group and DR group ( $P < 0.001$ ). No significant differences of PBF, VFA, BMR, and SMI were detected among three groups (all  $P > 0.05$ ).

## Association Between DME and Fluid Overload

**Table 2** demonstrates the association between DME and fluid overload. Univariate linear model (Model 1) shows that DME (compared to both DR and DM), age, DM duration, and UACR were positively associated with fluid overload, while albumin level and eGFR were negatively associated with fluid overload (all  $P < 0.05$ ). No significant association was found between MAP and ECW/TBW ( $P = 0.188$ ). In the multivariate linear model, DME, DR, age, MAP, and albumin showed significant impact on ECW/TBW (all  $P < 0.05$ ; Model 2), while eGFR was not significantly associated with ECW/TBW ( $P = 0.620$ ; Model 2). In the multivariate model focusing on UACR, only DME, age, and UACR were positively associated with ECW/TBW (all  $P < 0.05$ ), while MAP showed a negative association with ECW/TBW ( $P = 0.005$ ).

## Fluid Overload and Its Related Influence Factors of DME

In the binary logistic regression analysis with backward method of the risk of DME, age (per 1 year, OR = 0.941,  $P = 0.009$ ), UACR stage (microalbuminuria, OR = 5.16,  $P = 0.005$ ; macroalbuminuria, OR = 5.198,  $P = 0.003$ ), and ECW/TBW (per 10<sup>–2</sup>, OR = 2.814,  $P = 0.002$ ) entered the model under the probability for removal at 0.05. Details were shown in **Table 3**. The predictive power of the multivariate regression

**TABLE 3 |** Multivariate binary logistic regression for DME risk.

	$\beta$	S.E.	P	Exp ( $\beta$ )
ECW/TBW	1.035	0.327	0.002*	2.814
Age	–0.06	0.023	0.009*	0.941
Normoalbuminuria	Reference	–	–	–
Microalbuminuria	1.641	0.588	0.005*	5.16
Macroalbuminuria	1.648	0.55	0.003*	5.198

DME, diabetic macular edema; ECW/TBW, extracellular water-to-total body water ratio.

Adjusted  $r^2$  of logistic regression model = 0.401.

Exp ( $\beta$ ) stands for standardized regression coefficient.

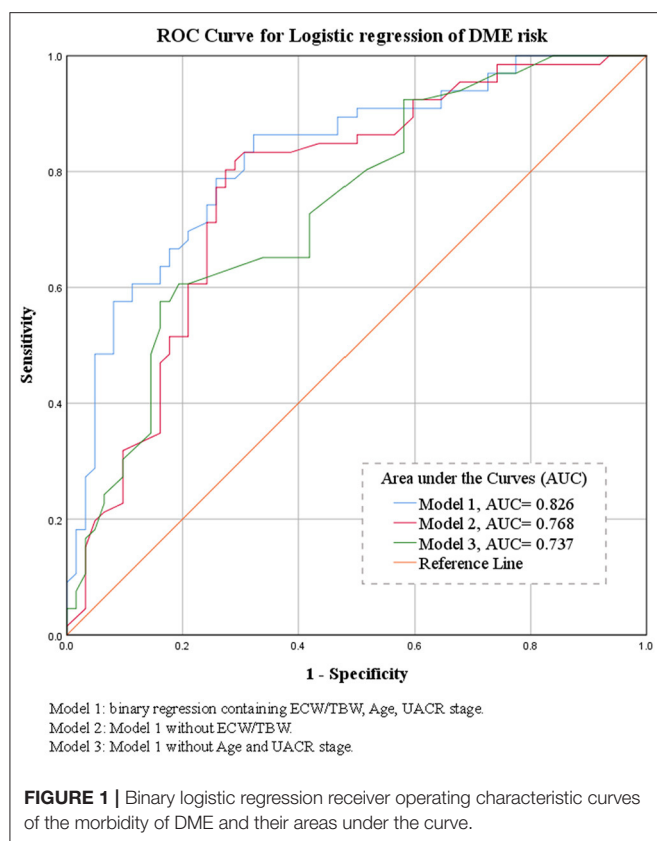
\*Stands for  $P < 0.05$ .

models was demonstrated as ROC curves shown in **Figure 1** (Model 1: ECW/TBW, UACR, and Age: AUC = 0.826; Model 2: UACR and Age: AUC = 0.768; Model 3: ECW/TBW: AUC = 0.737).

## DISCUSSION

This study provided new evidence to demonstrate the role of fluid overload in DME. As previously described, the relationship between barrier dysfunction and macular edema, impaired renal function and fluid overload have been investigated, respectively (10, 15). However, the complicated interaction between barrier dysfunction and fluid overload has not been elucidated yet, which make it intricate to explain whether the fluid overload is the mediator between barrier dysfunction and macular edema, or it can lead to DME without the impact from BRB breakdown, as fluid overload also had other influencing factors (27–29).





Our study corroborated that fluid overload existed in patients with DME. Furthermore, we were the first to discover that the relationship between fluid retention and DME is independent of renal functions, especially UACR and eGFR. ECW/TBW was proven to be a risk factor for DME, suggesting that fluid overload is a contributing factor to DME apart from BRB disruption.

Tsai et al. (15) had found that the level of fluid overload was correlated with CST in patients with DR, and volume overload was the influence factor of DME. Our study also found a significant difference in fluid status between DME patients and DM patients without DME, either with or without DR. These results suggested that volume expansion might contribute to DME development. Meanwhile, we did not find significant differences in fluid overload status between the DR and DM groups, indicating that fluid overload could be a risk factor for DME but not DR.

A recent study found that fluid overload was correlated with the stages of UACR in T2DM patients with DKD (14). DKD was regarded as a sign of endothelial dysfunction due to oxidative stress and inflammation (30). Also, multiple studies confirmed that UACR levels were significantly associated with DME (6, 7, 31). Hsieh et al. (32) found patients with higher baseline UACR levels to have higher risks for developing DME during the follow-up period than those with lower UACR levels. Nephropathy and retinopathy co-existed in diabetic patients (33). Hemodynamic and structural changes due to inflammatory cytokines and oxidative stress under high blood glucose have

been speculated as the cause (31). The increased UACR level suggests albumin leakage in the glomerulus and indicates the vascular barrier breakdown systemically. Even though the BRB was formed predominantly with tight junctions different to peripheral capillaries (34), in our study, the UACR stages were associated with ECW/TBW after adjustment, indicating that UACR is a significant influence factor for fluid overload. Therefore, it was of great importance to consider the role of DKD presented by albuminuria in the process of fluid retention in DME.

As ECW/TBW was reported to be affectable by multiple factors (14, 35, 36), we gradually adjusted for systemic factors, eGFR, and albuminuria, when analyzing fluid status among all participants. DME and ECW/TBW were still positively related after adjusting for confounders, suggesting that in DM patients, DME happens simultaneously with the presence of fluid overload, which was not affected by apparent inner BRB breakdown. Our results confirmed that the two parameters, ECW/TBW and UACR, are independent risk factors for DME. Hence, it could be speculated that the role of systemic fluid overload in DME development may collaborate with other mechanisms than deteriorated BRB function.

Throughout the body, fluid volume, hydrostatic and oncotic pressure, levels of albumin, and capillary permeability are the keys to maintaining the fluid balance between the intracellular and extracellular spaces, which is also true in the retina case. One of the popular theories for DME development was explicated by the starling equation (13). The hydrostatic pressure and oncotic pressure in different compartments govern the movement direction of fluid, which maintain homeostasis under normal circumstances (37). For example, the water transport of RPE cells was proved coupling with lactate, which provide a positive oncotic pressure to drive the water flow (38). It can be speculated that when hydrostatic pressure increases in the capillaries under volume expansion, fluid in the capillaries tends to move to the extravascular space (13). Therefore, high fluid volume can lead to peripheral edema and macular edema in the eyes. Recently, the revised starling equation has risen to make up for the shortcoming of the traditional one (37). The vascular barrier was composed of not only endothelial cells but also a layer which is known as the endothelial surface layer (ESL). ESL is the inner surface of the vascular wall, a semi-permeable layer composed of the glycocalyx and plasma protein such as albumin. Especially, albumin plays a vital role in its filtration function. ESL is usually impaired under systemic inflammation, including DM. The increased production of acute-phase protein suppresses albumin synthesis in the liver due to the limited synthesis capacity. Moreover, increased excretion of albumin from the kidney in the long run in patients with impaired kidney function further decreases the albumin level, leading to the dysfunction of ESL and leakage of fluid and protein. While on the retina, the damaged Müller cells no longer sustain neovascular coupling with DR progression, creating a focal high permeable environment for the albumin (39). Taking together, both fluid overload and impaired blood-retinal barrier can lead to leakage of fluid into the retinal interstitial space, resulting in macular edema.

As retinal thickness decreases with aging (40), we found the model consisting of ECW/TBW, UACR, and age achieved high accuracy in predicting DME risk. This result tally with the hypothesis that fluid overload could be a systemic fluid marker, parallel to the barrier dysfunction represented by albuminuria in the development of DME, in addition to focal VEGF elevation and inflammation.

In clinical practice, anti-VEGF agents are considered the first-line treatment for DME. However, non-responders exits at a considerable percentage (41). Some cases are even refractory to both anti-VEGF treatment and corticosteroid (42), demonstrating the need for additional therapies to treat this disease more comprehensively. Also, it is known that DME does not necessarily fit the regular course of DR progression. It may occur at any stage of DR (43). Therefore, beyond ischemia and inflammation, increased fluid volume may be another critical component in the pathophysiology of DME that has not been given sufficient attention. Several researchers also reported cases in which patients with DME improved, both central retinal thickness reduced and visual acuity improved, after diuretic therapy and restricting salt intake (44, 45), some of whom were even resistant to ophthalmic intervention anti-VEGF and grid laser treatment (46). Considering our findings in this study, we propose that, on the one hand, fluid overload can be one of the mechanisms that cause DME. In this point, treatment to ameliorate extracellular volume expansion such as diuretics and sodium-glucose cotransporter 2 inhibitors may have a role in treating DME patients with high ECW/TBW. On the other hand, in cases of DME who inadequately respond to anti-VEGF therapies and anti-inflammatory drugs, the underlying disease pathology may be mediated by fluid retention. Hence, further study with longitudinal design to observe the treatment response of DME patients with different fluid statuses would be pivotal to confirm the hypothesis.

There were some limitations of the study. The sample size was calculated with preliminary study data. Still, more substantial statistical power might reveal more significant systemic influence factors. Also, the assessment of the risk of DME was to be tested prospectively, and further cohort studies should be conducted to collaborate with our results.

In conclusion, systemic fluid status elevated significantly in patients with DME compared with diabetic patients

without DME. Fluid overload and albuminuria were independent risk factors for DME. Fluid overload might have initiated the extravasation in macula edema in addition to barrier dysfunction.

## DATA AVAILABILITY STATEMENT

The raw data supporting the conclusions of this article will be made available by the authors, without undue reservation.

## ETHICS STATEMENT

The studies involving human participants were reviewed and approved by Research Ethics Committee of the Guangdong General Hospital (GDREC2018380H). The patients/participants provided their written informed consent to participate in this study.

## AUTHOR CONTRIBUTIONS

JY, QP, and YL contributed to the study conception and design. Material preparation and data collection were performed by AL, JX, XZ, RC, YC, and ZW. Data analysis was conducted and the first draft of the manuscript was written by JY and QP. DC and LZ contributed to the manuscript reviewing and editing and funding acquisition. All authors read and approved the final manuscript.

## FUNDING

This work was funded by Guangzhou Municipal Science and Technology Bureau (grant 202102080008) and Bethune-Merck Diabetes Research Fund (G2018030).

## ACKNOWLEDGMENTS

The authors would like to thank DC and LZ for their administrative support, technical support, critical revision, and supervision. The authors would also like to thank the staff of the ophthalmology clinic of Guangdong Provincial People's Hospital for their assistance in the recruitment of the participants.

## REFERENCES

- Chen L, Magliano DJ, Zimmet PZ. The worldwide epidemiology of type 2 diabetes mellitus—present and future perspectives. *Nat Rev Endocrinol.* (2011) 8:228–36. doi: 10.1038/nrendo.2011.183
- Shaw JE, Sicree RA, Zimmet PZ. Global estimates of the prevalence of diabetes for 2010 and 2030. *Diabetes Res Clin Pract.* (2010) 87:4–14. doi: 10.1016/j.diabres.2009.10.007
- Zheng Y, Ley SH, Hu FB. Global aetiology and epidemiology of type 2 diabetes mellitus and its complications. *Nat Rev Endocrinol.* (2018) 14:88–98. doi: 10.1038/nrendo.2017.151
- Song P, Yu J, Chan KY, Theodoratou E, Rudan I. Prevalence, risk factors and burden of diabetic retinopathy in China: a systematic review and meta-analysis. *J Glob Health.* (2018) 8:010803. doi: 10.7189/jogh.08.010803
- Doshi SM, Friedman AN. Diagnosis and management of type 2 diabetic kidney disease. *Clin J Am Soc Nephrol.* (2017) 12:1366–73. doi: 10.2215/CJN.11111016
- Zhuang X, Cao D, Yang D, Zeng Y, Yu H, Wang J, et al. Association of diabetic retinopathy and diabetic macular oedema with renal function in southern Chinese patients with type 2 diabetes mellitus: a single-centre observational study. *BMJ Open.* (2019) 9:e031194. doi: 10.1136/bmjopen-2019-031194
- Zhuang X, Cao D, Zeng Y, Yang D, Yao J, Kuang J, et al. Associations between retinal microvasculature/microstructure and renal function in type 2 diabetes patients with early chronic kidney disease. *Diabetes Res Clin Pract.* (2020) 168:108373. doi: 10.1016/j.diabres.2020.108373
- Lai IP, Huang WL, Yang CM, Yang CH, Ho TC, Hsieh YT. Renal biomarkers for treatment effect of ranibizumab for diabetic macular edema. *J Diabetes Res.* (2020) 2020:7239570. doi: 10.1155/2020/7239570

9. Warid Al-Laftah FA, Elshafie M, Alhashimi M, Pai A, Farouq M. Pretreatment clinical variables associated with the response to intravitreal bevacizumab (Avastin) injection in patients with persistent diabetic macular edema. *Saudi J Ophthalmol.* (2010) 24:133–8. doi: 10.1016/j.sjopt.2010.05.001
10. Barrett EJ, Liu Z, Khamaisi M, King GL, Klein R, Klein BEK, et al. Diabetic microvascular disease: an endocrine society scientific statement. *J Clin Endocrinol Metab.* (2017) 102:4343–410. doi: 10.1210/jc.2017-01922
11. Reichhart N, Strauss O. Ion channels and transporters of the retinal pigment epithelium. *Exp Eye Res.* (2014) 126:27–37. doi: 10.1016/j.exer.2014.05.005
12. Reichenbach A, Bringmann A. Glia of the human retina. *Glia.* (2020) 68:768–96. doi: 10.1002/glia.23727
13. Daruich A, Matet A, Moulin A, Kowalczyk L, Nicolas M, Sellam A, et al. Mechanisms of macular edema: beyond the surface. *Prog Retin Eye Res.* (2018) 63:20–68. doi: 10.1016/j.pretyeres.2017.10.006
14. Nakajima H, Hashimoto Y, Kaji A, Sakai R, Takahashi F, Yoshimura Y, et al. Impact of extracellular-to-intracellular fluid volume ratio on albuminuria in patients with type 2 diabetes: a cross-sectional and longitudinal cohort study. *J Diabetes Investig.* (2020) 12:1202–11. doi: 10.1111/jdi.13459
15. Tsai MJ, Cheng CK, Wang YC. Association of body fluid expansion with optical coherence tomography measurements in diabetic retinopathy and diabetic macular edema. *Invest Ophthalmol Vis Sci.* (2019) 60:3606–12. doi: 10.1167/iov.19-27044
16. Fiedler R, Jehle PM, Osten B, Dorligschaw O, Girndt M. Clinical nutrition scores are superior for the prognosis of haemodialysis patients compared to lab markers and bioelectrical impedance. *Nephrol Dial Transplant.* (2009) 24:3812–7. doi: 10.1093/ndt/gfp346
17. Kraemer M, Rode C, Wizemann V. Detection limit of methods to assess fluid status changes in dialysis patients. *Kidney Int.* (2006) 69:1609–20. doi: 10.1038/sj.ki.5000286
18. Sukackiene D, Laucyte-Cibulskiene A, Vickiene A, Rimsevicius L, Miglinas M. Risk stratification for patients awaiting kidney transplantation: role of bioimpedance derived edema index and nutrition status. *Clin Nutr.* (2020) 39:2759–63. doi: 10.1016/j.clnu.2019.12.001
19. Giles TD, Materson BJ, Cohn JN, Kostis JB. Definition and classification of hypertension: an update. *J Clin Hypertens.* (2009) 11:611–4. doi: 10.1111/j.1751-7176.2009.00179.x
20. Nuttall FQ. Body mass index: obesity, BMI, and health: a critical review. *Nutr Today.* (2015) 50:117–28. doi: 10.1097/NT.0000000000000092
21. Levey AS, Stevens LA, Schmid CH, Zhang YL, Castro AF 3rd, Feldman HI, et al. A new equation to estimate glomerular filtration rate. *Ann Intern Med.* (2009) 150:604–12. doi: 10.7326/0003-4819-150-9-200905050-00006
22. Glasscock RJ, Warnock DG, Delanaye P. The global burden of chronic kidney disease: estimates, variability and pitfalls. *Nat Rev Nephrol.* (2017) 13:104–14. doi: 10.1038/nrneph.2016.163
23. Johnson DW, Jones GR, Mathew TH, Ludlow MJ, Chadban SJ, Usherwood T, et al. Chronic kidney disease and measurement of albuminuria or proteinuria: a position statement. *Med J Aust.* (2012) 197:224–5. doi: 10.5694/mja11.11468
24. Elliott DB. The good (logMAR), the bad (Snellen) and the ugly (BCVA, number of letters read) of visual acuity measurement. *Ophthalmic Physiol Opt.* (2016) 36:355–8. doi: 10.1111/opo.12310
25. Early treatment diabetic retinopathy study design and baseline patient characteristics. *Ophthalmology.* (1991) 98:741–56. doi: 10.1016/S0161-6420(13)38009-9
26. Ling CH, de Craen AJ, Slagboom PE, Gunn DA, Stokkel MP, Westendorp RG, et al. Accuracy of direct segmental multi-frequency bioimpedance analysis in the assessment of total body and segmental body composition in middle-aged adult population. *Clin Nutr.* (2011) 30:610–5. doi: 10.1016/j.clnu.2011.04.001
27. Taniguchi M, Yamada Y, Fukumoto Y, Sawano S, Minami S, Ikezoe T, et al. Increase in echo intensity and extracellular-to-intracellular water ratio is independently associated with muscle weakness in elderly women. *Eur J Appl Physiol.* (2017) 117:2001–7. doi: 10.1007/s00421-017-3686-x
28. Ohashi Y, Joki N, Yamazaki K, Kawamura T, Tai R, Oguchi H, et al. Changes in the fluid volume balance between intra- and extracellular water in a sample of Japanese adults aged 15–88 yr old: a cross-sectional study. *Am J Physiol Renal Physiol.* (2018) 314:F614–22. doi: 10.1152/ajprenal.00477.2017
29. Booth J, Pinney J, Davenport A. N-terminal proBNP—marker of cardiac dysfunction, fluid overload, or malnutrition in hemodialysis patients? *Clin J Am Soc Nephrol.* (2010) 5:1036–40. doi: 10.2215/CJN.09001209
30. Satoh M. Endothelial dysfunction as an underlying pathophysiological condition of chronic kidney disease. *Clin Exp Nephrol.* (2012) 16:518–21. doi: 10.1007/s10157-012-0646-y
31. Knudsen ST, Bek T, Poulsen PL, Hove MN, Rehling M, Mogensen CE. Macular edema reflects generalized vascular hyperpermeability in type 2 diabetic patients with retinopathy. *Diabetes Care.* (2002) 25:2328–34. doi: 10.2337/diacare.25.12.2328
32. Hsieh YT, Tsai MJ, Tu ST, Hsieh MC. Association of abnormal renal profiles and proliferative diabetic retinopathy and diabetic macular edema in an Asian population with type 2 diabetes. *JAMA Ophthalmol.* (2018) 136:68–74. doi: 10.1001/jamaophthalmol.2017.5202
33. Faselis C, Katsimardou A, Imprialos K, Deligkaris P, Kallistratos M, Dimitriadis K. Microvascular complications of type 2 diabetes mellitus. *Curr Vasc Pharmacol.* (2020) 18:117–24. doi: 10.2174/1570161117666190502103733
34. Naylor A, Hopkins A, Hudson N, Campbell M. Tight junctions of the outer blood retina barrier. *Int J Mol Sci.* (2019) 21:211. doi: 10.3390/ijms21010211
35. Park S, Lee CJ, Jhee JH, Yun HR, Kim H, Jung SY, et al. Extracellular fluid excess is significantly associated with coronary artery calcification in patients with chronic kidney disease. *J Am Heart Assoc.* (2018) 7:e008935. doi: 10.1161/JAHA.118.008935
36. Tai R, Ohashi Y, Mizuiri S, Aikawa A, Sakai K. Association between ratio of measured extracellular volume to expected body fluid volume and renal outcomes in patients with chronic kidney disease: a retrospective single-center cohort study. *BMC Nephrol.* (2014) 15:189. doi: 10.1186/1471-2369-15-189
37. Woodcock TE, Woodcock TM. Revised Starling equation and the glycolyx model of transvascular fluid exchange: an improved paradigm for prescribing intravenous fluid therapy. *Br J Anaesth.* (2012) 108:384–94. doi: 10.1093/bja/aer515
38. Hamann S, Kiilgaard JF, la Cour M, Prause JU, Zeuthen T. Cotransport of H<sup>+</sup>, lactate, and H<sub>2</sub>O in porcine retinal pigment epithelial cells. *Exp Eye Res.* (2003) 76:493–504. doi: 10.1016/S0014-4835(02)00329-9
39. Coughlin BA, Feenstra DJ, Mohr S. Muller cells and diabetic retinopathy. *Vision Res.* (2017) 139:93–100. doi: 10.1016/j.visres.2017.03.013
40. Duan XR, Liang YB, Friedman DS, Sun LP, Wong TY, Tao QS, et al. Normal macular thickness measurements using optical coherence tomography in healthy eyes of adult Chinese persons: the Handan Eye Study. *Ophthalmology.* (2010) 117:1585–94. doi: 10.1016/j.ophtha.2009.12.036
41. Bressler NM, Beaulieu WT, Glassman AR, Blinder KJ, Bressler SB, Jampol LM, et al. Persistent macular thickening following intravitreal aflibercept, bevacizumab, or ranibizumab for central-involved diabetic macular edema with vision impairment: a secondary analysis of a randomized clinical trial. *JAMA Ophthalmol.* (2018) 136:257–69. doi: 10.1001/jamaophthalmol.2017.6565
42. Maturi RK, Glassman AR, Liu D, Beck RW, Bhavsar AR, Bressler NM, et al. Effect of adding dexamethasone to continued ranibizumab treatment in patients with persistent diabetic macular edema: A DRCR network phase 2 randomized clinical trial. *JAMA Ophthalmol.* (2018) 136:29–38. doi: 10.1001/jamaophthalmol.2017.4914
43. Flaxel CJ, Adelman RA, Bailey ST, Fawzi A, Lim JJ, Vemulakonda GA, et al. Diabetic retinopathy preferred practice pattern(R). *Ophthalmology.* (2020) 127:P66–145. doi: 10.1016/j.ophtha.2019.09.025
44. Ciardella AP. Partial resolution of diabetic macular oedema after systemic treatment with furosemide. *Br J Ophthalmol.* (2004) 88:1224–5. doi: 10.1136/bjo.2004.042580
45. Samanta R, Puthalath AS, Saraswat N, Agrawal A, Singh A, Mittal S. Rapidly reversing bilateral macular edema associated with fluid overload in a young type 1 diabetic. *Indian J Ophthalmol.* (2019) 67:1221–3. doi: 10.4103/ijo.IJO\_1805\_18

46. Kahtani ES. Diabetic glomerulosclerosis can be the pathogenesis of refractory diabetic macular edema. *Clin Ophthalmol.* (2015) 9:929–33. doi: 10.2147/OPTH.S80850

**Conflict of Interest:** The authors declare that the research was conducted in the absence of any commercial or financial relationships that could be construed as a potential conflict of interest.

**Publisher's Note:** All claims expressed in this article are solely those of the authors and do not necessarily represent those of their affiliated organizations, or those of the publisher, the editors and the reviewers. Any product that may be evaluated in

this article, or claim that may be made by its manufacturer, is not guaranteed or endorsed by the publisher.

Copyright © 2022 Yao, Peng, Li, Liang, Xie, Zhuang, Chen, Chen, Wang, Zhang and Cao. This is an open-access article distributed under the terms of the Creative Commons Attribution License (CC BY). The use, distribution or reproduction in other forums is permitted, provided the original author(s) and the copyright owner(s) are credited and that the original publication in this journal is cited, in accordance with accepted academic practice. No use, distribution or reproduction is permitted which does not comply with these terms.





# Chaperonin-Containing TCP1 Subunit 5 Protects Against the Effect of Mer Receptor Tyrosine Kinase Knockdown in Retinal Pigment Epithelial Cells by Interacting With Filamentous Actin and Activating the LIM-Kinase 1/Cofilin Pathway

## OPEN ACCESS

### Edited by:

Hetian Lei,  
Shenzhen Eye Hospital, China

### Reviewed by:

Tsz Kin Ng,  
Shantou University and the Chinese  
University of Hong Kong, China  
Guoxing Xu,  
First Affiliated Hospital of Fujian  
Medical University, China

### \*Correspondence:

Yehong Zhuo  
zhuoyh@mail.sysu.edu.cn

<sup>†</sup>These authors have contributed  
equally to this work

### Specialty section:

This article was submitted to  
Ophthalmology,  
a section of the journal  
Frontiers in Medicine

Received: 24 January 2022

Accepted: 09 March 2022

Published: 13 April 2022

### Citation:

Feng L, Li H, Du Y, Zhang T,  
Zhu Y, Li Z, Zhao L, Wang X, Wang G,  
Zhou L, Jiang Z, Liu Z, Ou Z, Wen Y  
and Zhuo Y (2022)  
Chaperonin-Containing TCP1 Subunit  
5 Protects Against the Effect of Mer  
Receptor Tyrosine Kinase Knockdown  
in Retinal Pigment Epithelial Cells by  
Interacting With Filamentous Actin  
and Activating the LIM-Kinase  
1/Cofilin Pathway.  
Front. Med. 9:861371.  
doi: 10.3389/fmed.2022.861371

Lujia Feng<sup>1†</sup>, Haichun Li<sup>1†</sup>, Yong Du<sup>2†</sup>, Ting Zhang<sup>1</sup>, Yingting Zhu<sup>1</sup>, Zhidong Li<sup>1</sup>,  
Ling Zhao<sup>1</sup>, Xing Wang<sup>1</sup>, Gongpei Wang<sup>1</sup>, Linbin Zhou<sup>1</sup>, Zhaorong Jiang<sup>3</sup>, Zheng Liu<sup>1</sup>,  
Zhancong Ou<sup>1</sup>, Yuwen Wen<sup>1</sup> and Yehong Zhuo<sup>1\*</sup>

<sup>1</sup> State Key Laboratory of Ophthalmology, Zhongshan Ophthalmic Center, Guangdong Provincial Key Laboratory of Ophthalmology and Visual Science, Guangdong Provincial Clinical Research Center for Ocular Diseases, Sun Yat-sen University, Guangzhou, China, <sup>2</sup> Guizhou Provincial People's Hospital, Guizhou University, Guiyang, China, <sup>3</sup> Ophthalmology Department of Zhuhai Integrated Traditional Chinese and Western Medicine Hospital, Zhuhai, China

Retinitis pigmentosa (RP), characterized by the gradual loss of rod and cone photoreceptors that eventually leads to blindness, is the most common inherited retinal disorder, affecting more than 2.5 million people worldwide. However, the underlying pathogenesis of RP remains unclear and there is no effective cure for RP. Mutations in the Mer receptor tyrosine kinase (*MERTK*) gene induce the phagocytic dysfunction of retinal pigment epithelium (RPE) cells, leading to RP. Studies have indicated that filamentous actin (F-actin)—which is regulated by chaperonin-containing TCP1 subunit 5 (CCT5)—plays a vital role in phagocytosis in RPE cells. However, whether CCT5/F-actin signaling is involved in *MERTK*-associated RP remains largely unknown. In the present study, we specifically knocked down *MERTK* and CCT5 through siRNA transfection and examined the expression of CCT5 and F-actin in human primary RPE (HsRPE) cells. We found that *MERTK* downregulation inhibited cell proliferation, migration, and phagocytic function; significantly decreased the expression of F-actin; and disrupted the regular arrangement of F-actin. Importantly, our findings firstly indicate that CCT5 interacts with F-actin and is inhibited by *MERTK* siRNA in HsRPE cells. Upregulating CCT5 using CCT5-specific lentiviral vectors (CCT5-Le) rescued the cell proliferation, migration, and phagocytic function of HsRPE cells under the *MERTK* knockdown condition by increasing the expression of F-actin and restoring its regular arrangement via the LIMK1/cofilin, but not the SSH1/cofilin, pathway. In conclusion, CCT5 protects against the effect of *MERTK* knockdown in HsRPE cells and demonstrates the potential for effective treatment of *MERTK*-associated RP.

**Keywords:** retinitis pigmentosa, *MERTK*, CCT5, f-actin, phagocytosis

## INTRODUCTION

Retinitis pigmentosa (RP) is the most common inherited retinal disease that affected tens of millions of people worldwide and is caused by a series of gene mutations that eventually lead to progressive retinal degeneration (1). As the most common inherited retinal disease, RP affects more than 2.5 million people worldwide (2, 3). However, the pathogenesis of RP remains unclear, and there is currently no effective treatment (4). Studies have shown that the Mer receptor tyrosine kinase (*MERTK*) gene mutation can lead to RP in humans (5). In the Royal College of Surgeons (RCS) rat, which is a typical animal model of human autosomal recessive inherited RP, the disease was found to be caused by the *Mertk* gene mutation (6). The *MERTK* gene encodes the Mer receptor tyrosine kinase, which belongs to the TAM receptor kinase family and participates in the phagocytic process (5). Retinal pigment epithelium (RPE) can constantly phagocytize the shed photoreceptor outer segment (POS), which plays a vital role in maintaining retinal homeostasis, as POS renewal is essential for visual function (7). The phagocytic dysfunction of RPE is an important aspect of the pathogenesis of RP (8). According to previous studies, a mutation in the *MERTK* gene leads to the phagocytic dysfunction of RPE cells, which is responsible for *MERTK*-associated RP (5). However, the mechanism underlying the *MERTK* gene mutation leading to phagocytic dysfunction remains largely unknown.

The process of POS phagocytosis is based on the rigorous control of the distribution and expression of the actin cytoskeleton (9). Actin, as a major component of the cytoskeleton, plays a vital role in the POS phagocytosis process. A previous study showed alphavbeta5 binding POS which is the first step of the POS phagocytosis process is required actin (10). However, nearly decades after the phenomenon was first described, much remains unknown regarding the role of the actin cytoskeleton in this process. Recent studies have emphasized that the rearrangement of RPE cytoskeletal filamentous actin (F-actin) is essential for POS internalization (11). The formation of phagocytic cups *via* the early recruitment of F-actin lays the foundation for phagocytosis, which means any factor that obstructs the expression of F-actin or disrupts the arrangement of F-actin will lead to phagocytic dysfunction, as the phagocytic cup formed by the orderly aggregation of F-actin combined with POS is the key to phagocytosis initiation (12). Previous studies demonstrated that the F-actin arrangement is abnormal in RPE cells with low phagocytotic activity (13). Recent studies also indicated that phagocytes formed by the recruitment of F-actin and the binding of POS must be combined with *MERTK* (14). In other words, the *MERTK* gene mutation may impair the recruitment of F-actin. However, the involvement of abnormal

epithelial F-actin cytoskeleton in *MERTK*-associated RP remains largely unknown.

The TCP-1 cyclic complex, also known as the chaperonin-containing TCP-1 (CCT), is composed of eight parallel subunits (CCT1–8) (15–17). Assisted by ATP binding and hydrolysis, the main function of CCT is to help refold misfolded or unfolded proteins. Between 5% and 10% of the proteins in mammalian cells interact with CCT (18). In *S. cerevisiae*, CCT deficiency mutations lead to death, demonstrating the importance of CCT function (19). Actin is one of the main substrates of CCT; however, the exact mechanism by which CCT promotes actin folding is not yet understood (20, 21). A recent study found that CCT was required for efficient actin myofilament assembly (22) and that CCT5-specific ATP binding was required for efficient actin folding (23). Additionally, CCT5 controls lysosome biogenesis *via* the actin cytoskeleton (24). The actin/CCT5 pathway is implicated in multiple diseases—including hereditary sensory neuropathies (23), legionella pneumophila infection (25), muscle atrophy (26), and Alzheimer's disease (24)—suggesting that CCT5 is associated with various cellular physiological processes in different tissues. Nonetheless, whether the F-actin/CCT5 pathway plays a vital role in *MERTK*-associated RP remains to be elucidated. Therefore, the present study explored the relationship between CCT5, F-actin, and RP, and the potential molecular mechanism underlying this disease.

## RESULTS

### Mer Receptor Tyrosine Kinase siRNA Inhibited Cell Proliferation and Induced Morphological Changes and Phagocytic Dysfunction in Human Primary RPE Cells

On the 7 days after the HsRPE cells were extracted and cultured in DMEM medium, we observed cultured cells with an inverted phase-contrast microscope, we found each cell contains abundant brownish-yellow pigments which is the characterization of the HsRPE cell. This result suggests that we're extracting the HsRPE cells, not other nerve cells, fibroblasts, blood vessel cells, etc (Figure 1A). To further verify that the cells we extracted were HsRPE cells, we stained the cultured cells with RPE65, an RPE cell-specific protein. The result showed every cultured cell is stained with RPE65 (green) (Figure 1B). These results indicate that we have successfully extracted and cultured HsRPE cells. To establish a model of *MERTK*-associated RP *in vitro*, *MERTK* siRNA was applied to HsRPE cells. To test the target-specific efficacy of the *MERTK* siRNA, two types of *MERTK* siRNA (*MERTK* siRNA1 and *MERTK* siRNA2) were used. Both the mRNA and protein expression of *MERTK* in the siRNA groups were significantly reduced compared with those in the negative control (NC) siRNA groups (Figures 1C,D). Since *MERTK* siRNA2 more effectively downregulated *MERTK* than *MERTK* siRNA1, we applied *MERTK* siRNA2 in the subsequent experiments. A Cell Counting Kit-8 (CCK8) assay was used to determine the viability of HsRPE cells. Compared with the NC siRNA group, the group with knocked down *MERTK*

**Abbreviations:** CCK8 Cell Counting Kit-8, CCT chaperonin-containing TCP-1, CCT5 chaperonin-containing TCP1 subunit 5, CCT5-Le CCT5-specific lentiviral vectors, Co-IP co-immunoprecipitation, F-actin filamentous actin, HsRPE human primary RPE, LIMK1 LIM-kinase 1, *MERTK* Mer receptor tyrosine kinase, NC negative control, OD optical density, p-cofilin Phosphorylated cofilin, POS photoreceptor outer segment, RCS Royal College of Surgeons, RP retinitis pigmentosa, RPE retinal pigment epithelium, RT-PCR quantitative real-time PCR, SSH1 slingshot 1, TESK1 testicular protein kinase 1.

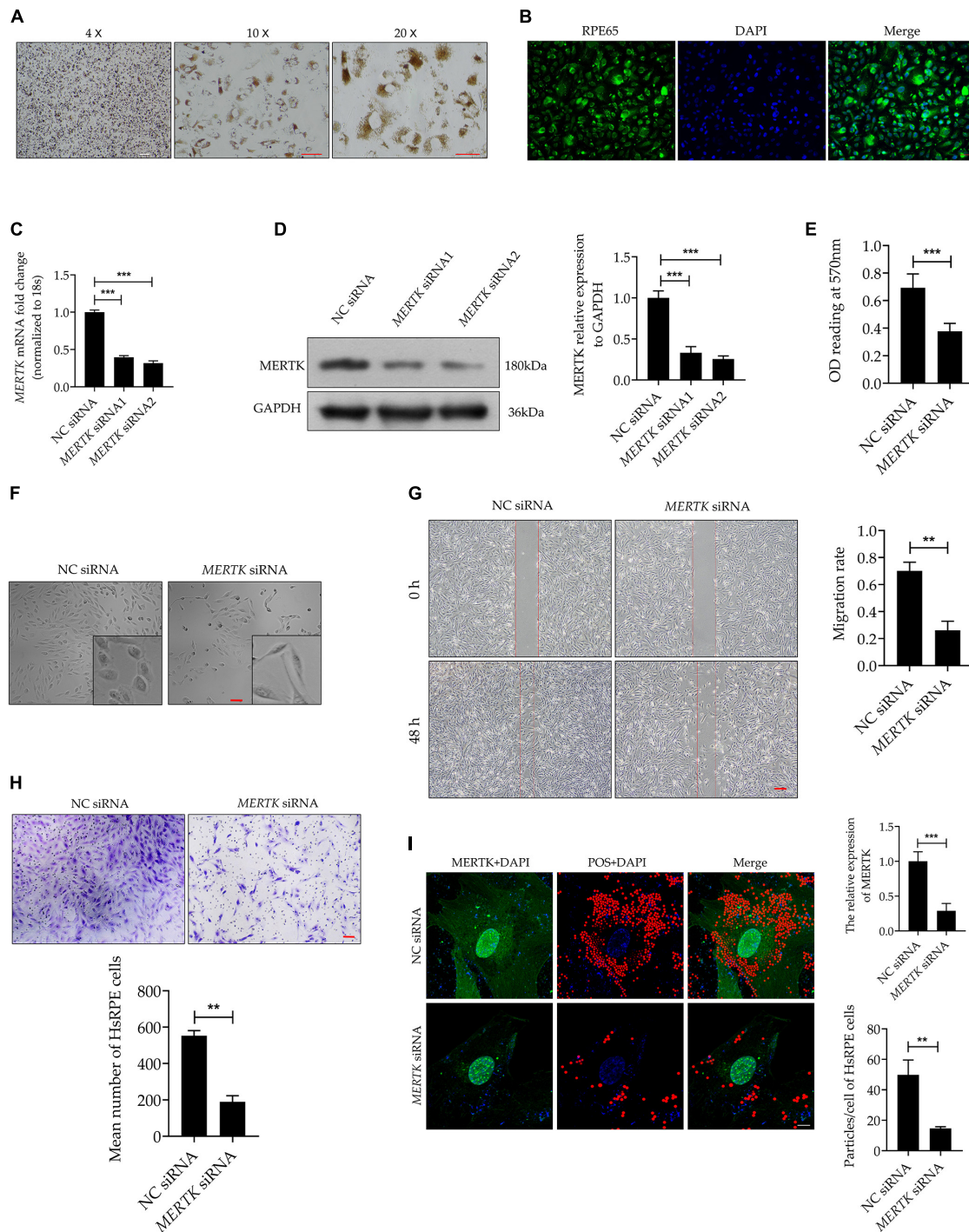


**FIGURE 1 |** *MERTK* siRNA inhibited cell proliferation and induced morphological changes and phagocytic dysfunction in HsRPE cells. **(A)** The primary cultured HsRPE cells were observed with an inverted microscope at different magnifications (4X, 10X, and 20X). Scale bars: white bar 100  $\mu$ m; red bars 10  $\mu$ m. **(B)** The HsRPE cells were identified by immunofluorescence staining with RPE65 antibody. Scale bars: 50  $\mu$ m. **(C)** HsRPE cells were treated with NC, *MERTK* siRNA1, or *MERTK* siRNA2 (20 nM) for 24 h, and the expression of *MERTK* was analyzed by RT-PCR. **(D)** HsRPE cells were treated with NC, *MERTK* siRNA1, or *MERTK* siRNA2 (20 nM) for 24 h, and *MERTK* expression was determined by Western blotting. **(E)** HsRPE cells were treated with NC or *MERTK* siRNA2 (*MERTK* siRNA) for 48 h, and cell proliferation was analyzed by CCK8. **(F)** HsRPE cells were treated the same as in (E), and cell morphology was observed with an inverted microscope. Scale bars: 100  $\mu$ m. **(G)** HsRPE cells were treated the same as in (E), and wound-healing assays were performed to assess the wound-healing capabilities of HsRPE cells. Scale bars: 200  $\mu$ m. **(H)** HsRPE cells were treated the same as in (E), and Transwell assays were performed to evaluate the migration activity of HsRPE cells (purple). Scale bars: 100  $\mu$ m. **(I)** HsRPE cells were treated the same as in (E), and their phagocytic ability was examined using phagocytosis assays. The red dots represent the particles and the green dye represents the *MERTK* protein. Scale bars: 5  $\mu$ m. \*\* $P < 0.01$ ; \*\*\* $P < 0.001$ .



exhibited suppressed cell proliferation, as the optical density (OD) value of the NC siRNA group was higher than that of the *MERTK* siRNA group (**Figure 1E**). We then observed the changes in cell morphology using an inverted microscope and found that the cellular morphologies of the HsRPE cells were very different between the NC siRNA group and the *MERTK* siRNA group. The cells of the NC siRNA group had a typical polygonal appearance; however, the *MERTK* siRNA-transfected cells became elongated in shape (**Figure 1F**). Wound-healing assays and Transwell migration assays were performed to assess the wound-healing ability and migration of HsRPE cells. The results demonstrated that the number of migrated HsRPE cells and their migration distance was significantly decreased in the *MERTK* siRNA group compared with the NC siRNA group (**Figures 1G,H**). We performed the phagocytosis assay combined with the immunofluorescence assay to evaluate the effect of *MERTK* siRNA on the phagocytic function of HsRPE cells. For the phagocytosis assay, Nile red-labeled particles and *MERTK* immunofluorescent staining were used. In the NC siRNA group, the expression of MerTK (green) is significantly higher than *MERTK* siRNA group, and massive red particles were phagocytized into the HsRPE cells, while the number of red particles that were phagocytized into the HsRPE cells was significantly decreased in the *MERTK* siRNA group (**Figure 1I**). These results indicate that *MERTK*-specific siRNA inhibited cell proliferation and induced morphological changes and phagocytic dysfunction in HsRPE cells.

### Mer Receptor Tyrosine Kinase siRNA Downregulated the Expression of Chaperonin-Containing TCP1 Subunit 5, Which Interacted and Co-localized With Filamentous Actin in Human Primary RPE Cells

Filamentous actin plays a vital role in phagocytosis. To determine whether F-actin was involved in *MERTK*-associated RP, we detected F-actin by quantitative real-time PCR (RT-PCR) and Western blot assays separately. Both the RT-PCR and Western blot assays demonstrated that *MERTK* siRNA significantly inhibited F-actin at both the mRNA and protein levels, as compared with the NC group (**Figures 2A,B**). Furthermore, to detect the distribution and arrangement of F-actin, we performed the immunofluorescence analysis. The results indicated that F-actin demonstrated a highly regular radial distribution of filamentous order in the NC group. However, in the *MERTK* siRNA group, the F-actin clumped together in a disorderly arrangement around the nucleus (**Figure 2C**). CCT5 plays an important role in actin regulation; therefore, to determine whether CCT5 was involved in the regulation of F-actin in *MERTK*-associated RP, CCT5 expression at the mRNA and protein levels was assessed. The RT-PCR results indicated that the downregulation of *MERTK* significantly suppressed the expression of CCT5 at the mRNA level, compared with that in the NC group, in HsRPE cells (**Figure 2D**). In line with the mRNA-level results, the Western blotting

results demonstrated that CCT5 expression was significantly suppressed by *MERTK* siRNA in HsRPE cells (**Figure 2E**). To analyze whether CCT5 and F-actin directly interacted, we performed immunolocalization and co-immunoprecipitation (Co-IP) assays. Immunofluorescence analysis demonstrated that CCT5 and F-actin co-localized in the cytoplasm of HsRPE cells (**Figure 2F**), and Co-IP analysis demonstrated that CCT5 proteins could directly bind with F-actin proteins, but could not directly bind with *MERTK* proteins in HsRPE cells (**Figures 2G,H**). These results indicate that CCT5 interacts and co-localizes with F-actin but not *MERTK* and that *MERTK* siRNA can decrease F-actin expression *via* the regulation of CCT5 expression in HsRPE cells.

### Upregulation of Chaperonin-Containing TCP1 Subunit 5 Expression Recovered the Morphology and Migration Function Destroyed by Mer Receptor Tyrosine Kinase siRNA in Human Primary RPE Cells

For a better insight into the involvement of CCT5 in RP, CCT5-specific siRNA and lentiviral vectors were used to downregulate and upregulate CCT5 expression separately. We tested two siRNAs (*CCT5* siRNA1 and *CCT5* siRNA2) and selected *CCT5* siRNA2, showing the best downregulation efficiency, for the subsequent experiments (**Figure 3A**). After the *CCT5* siRNA was transfected into HsRPE cells, the expression of CCT5 was significantly downregulated. On the other hand, treatment with *CCT5*-specific lentiviral vectors (*CCT5*-Le) significantly upregulated the expression of CCT5, compared with that in the *MERTK* siRNA group, at both the mRNA and protein levels (**Figures 3B,C**). CCK8 assays were used to detect the viability of HsRPE cells. Compared with the *MERTK* siRNA group, the *MERTK* siRNA + *CCT5* siRNA group demonstrated significant further suppression of cell proliferation, as the optical density (OD) value of the *MERTK* siRNA + *CCT5* siRNA group was lower than that of the *MERTK* siRNA groups. However, the viability of HsRPE cells in the *MERTK* siRNA + *CCT5*-Le group was significantly higher than that seen in the *MERTK* siRNA group (**Figure 3D**). These results demonstrate that the upregulation of CCT5 expression enhanced the viability of HsRPE cells, which was inhibited by *MERTK* siRNA. Next, we observed changes in cell morphology using an inverted microscope. In the *MERTK* siRNA + *CCT5* siRNA group, the shape of the HsRPE cells became more elongated than in the *MERTK* siRNA group. However, in the *MERTK* siRNA + *CCT5*-Le group, the shape of the HsRPE cells became typically polygonal, as in the NC group (**Figure 3E**). These results indicate that upregulating CCT5 expression restored the morphological dysfunction induced by *MERTK* siRNA. Wound-healing and Transwell-migration assays demonstrated that the migration distance and the number of migrated HsRPE cells were significantly suppressed in the *MERTK* siRNA group compared with the control group and that *CCT5* siRNA further suppressed these parameters. However,



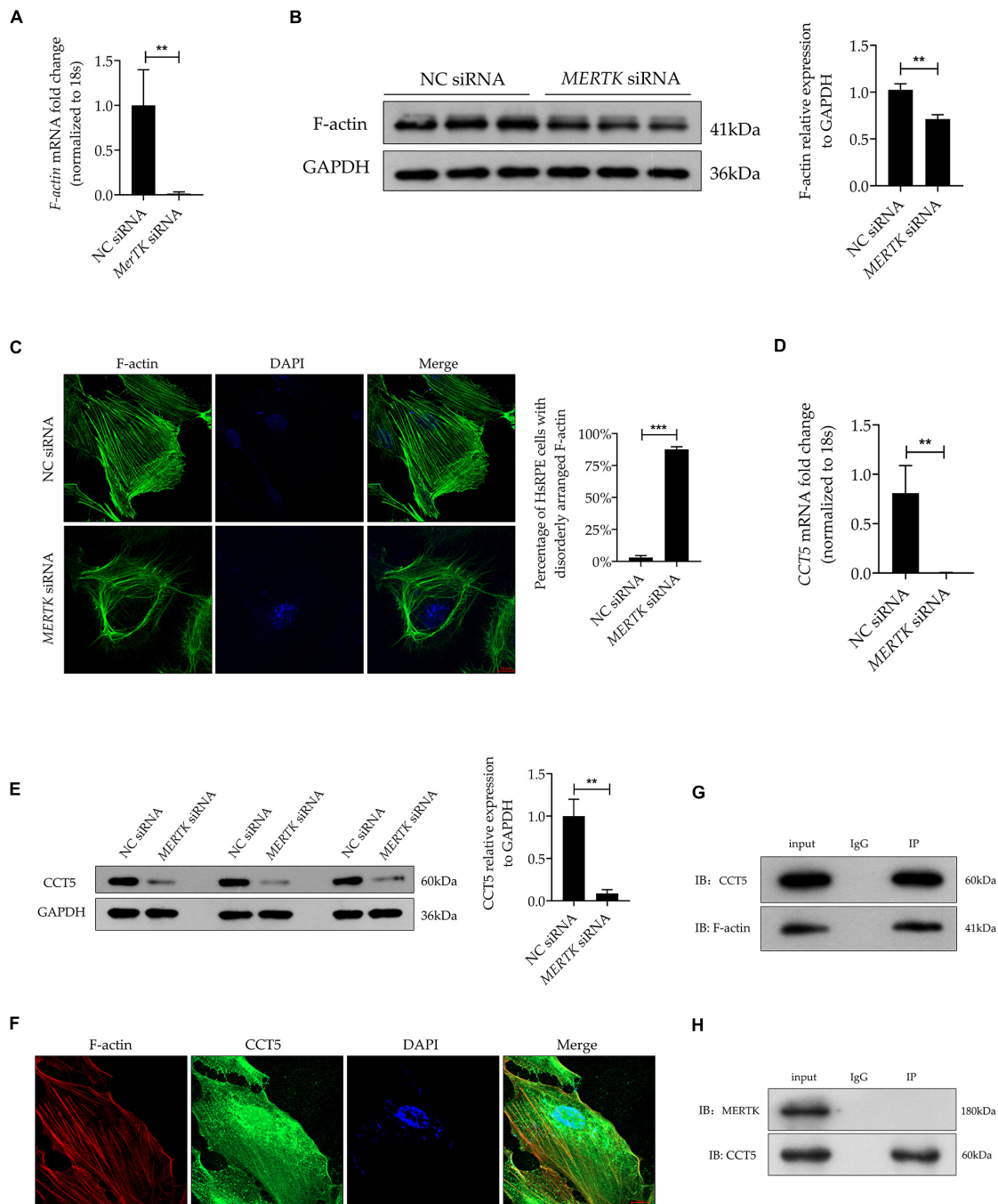


**FIGURE 2 |** *MERTK* siRNA downregulated the expression of CCT5, which interacted and co-localized with F-actin in HsRPE cells. **(A)** HsRPE cells were treated with NC or *MERTK* siRNA for 24 h, and the expression of *F-actin* was analyzed by RT-PCR. **(B)** HsRPE cells were treated with NC or *MERTK* siRNA for 48 h, and the expression of F-actin was analyzed by Western blotting. **(C)** HsRPE cells were treated the same as in **(B)**, and the distribution and organization of F-actin (green) were detected by immunofluorescence analysis. Scale bars: 10  $\mu$ m. **(D)** HsRPE cells were treated the same as in **(A)**, and *CCT5* expression was analyzed by RT-PCR. **(E)** HsRPE cells were treated the same as in **(B)**, and *CCT5* expression was analyzed by Western blotting. **(F)** The co-localization (yellow) of F-actin (red) and CCT5 (green) in HsRPE cells was assessed by immunolocalization analysis. Scale bars: 10  $\mu$ m. **(G)** The binding between F-actin and CCT5 in HsRPE cells was verified by co-immunoprecipitation. **(H)** The binding between *MERTK* and CCT5 in HsRPE cells was verified by co-immunoprecipitation. \*\* $P < 0.01$ ; \*\*\* $P < 0.001$ .

*CCT5*-Le significantly increased the migration distance and the number of migrated HsRPE cells, which were suppressed by *MERTK* siRNA (Figures 3F,G). These results indicate that

upregulation of *CCT5* expression restored the morphology and migration function, which were disrupted in HsRPE cells with *MERTK* siRNA.

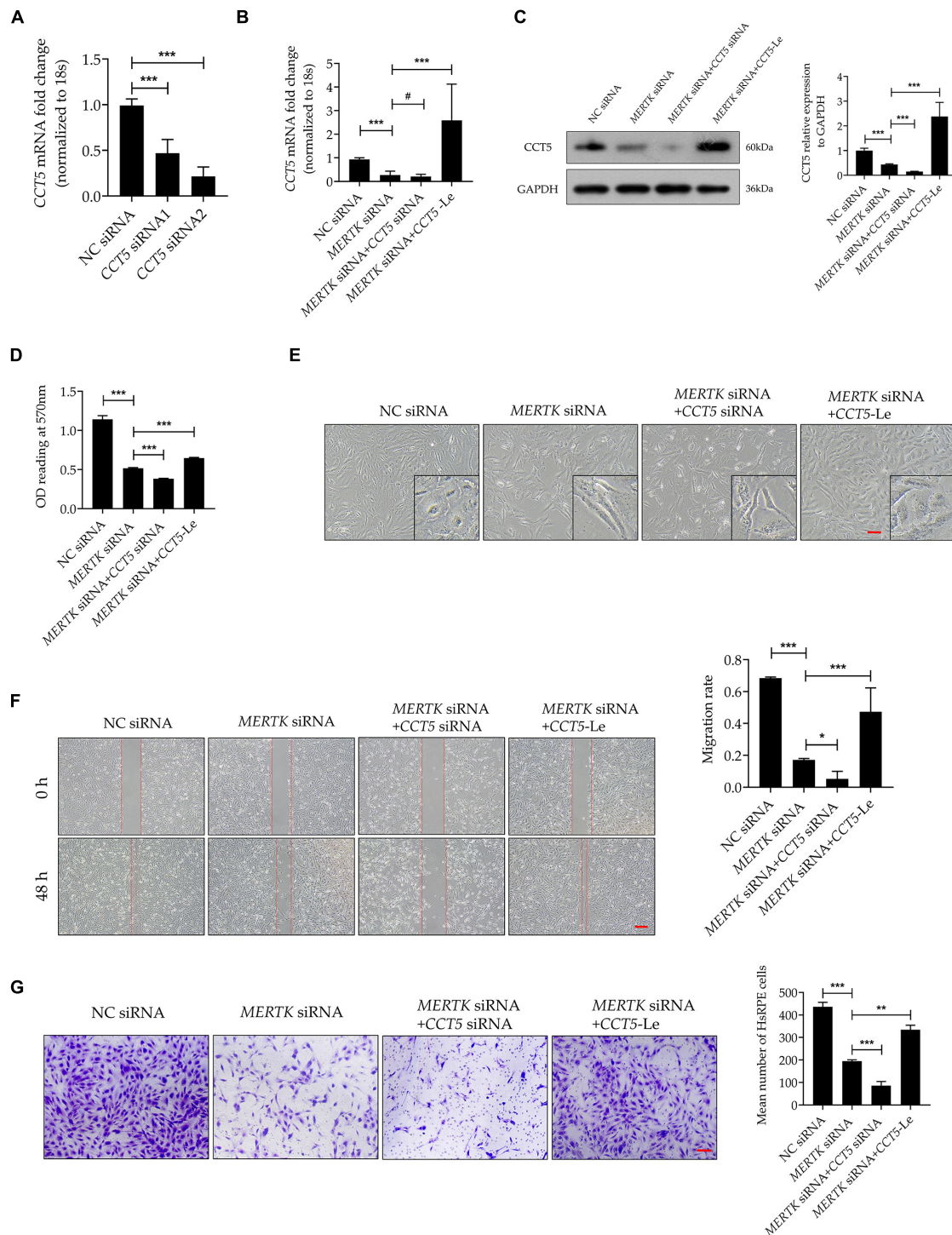


**FIGURE 3 |** Upregulation of CCT5 expression recovered the morphology and migration function disrupted by *MERTK* siRNA in HsRPE cells. **(A)** HsRPE cells were treated with NC, CCT5 siRNA1, or CCT5 siRNA2 (20 nM) for 24 h, and CCT5 expression was analyzed by RT-PCR. **(B)** HsRPE cells were treated with or without CCT5 siRNA or CCT5-specific lentiviral vectors (CCT5-Le) after exposure to NC or *MERTK* siRNA for 24 h, and the expression of CCT5 was analyzed by RT-PCR. **(C)** HsRPE cells were treated with or without CCT5 siRNA or CCT5-specific lentiviral vectors (CCT5-Le) after exposure to NC or *MERTK* siRNA for 48 h, and CCT5 expression was analyzed by Western blotting. **(D)** HsRPE cells were treated the same as in (C), and cell proliferation was determined by CCK8 assay. **(E)** HsRPE cells were treated the same as in (C), and morphological changes were observed using an inverted microscope. Scale bars: 100  $\mu$ m. **(F)** HsRPE cells were treated the same as in (C), and wound-healing assays were performed to assess the wound-healing capabilities of HsRPE cells. Scale bars: 200  $\mu$ m. **(G)** HsRPE cells were treated the same as in (C), and Transwell assays were performed to evaluate the migration activity of HsRPE cells (purple). Scale bars: 100  $\mu$ m. #  $P > 0.05$ ; \* $P < 0.05$ ; \*\* $P < 0.01$ ; \*\*\* $P < 0.001$ .

## Upregulating Chaperonin-Containing TCP1 Subunit 5 Expression Rescued the Phagocytic Function Disrupted by Mer Receptor Tyrosine Kinase siRNA by Restoring the Expression and Organization of Filamentous Actin in Human Primary RPE Cells

To investigate the function of *CCT5*-Le in the phagocytic process of HsRPE cells, we performed the phagocytosis assay combined with the immunofluorescence assay. The *MERTK* siRNA group exhibited a significantly decreased expression of *CCT5* (green) and a significantly decreased quantity of red particles that were phagocytized into the HsRPE cells, as compared with the NC siRNA group. In the *MERTK* siRNA + *CCT5* siRNA group, the expression of *CCT5* was further decreased and the number of red particles phagocytized into HsRPE cells was further reduced compared with that in the *MERTK* siRNA group. By contrast, the *MERTK* siRNA + *CCT5*-Le group exhibited a significantly increased *CCT5* expression and quantity of red particles phagocytized into HsRPE cells compared with the *MERTK* siRNA group (**Figure 4A**). To investigate whether *CCT5*-Le rescued the phagocytic function *via* the regulation of F-actin, the expression of F-actin was then examined. Our results indicate that *MERTK* siRNA significantly decreased the expression of F-actin at both the mRNA and protein levels, as compared with that in the NC group. In the *MERTK* siRNA + *CCT5* siRNA group, the expression of F-actin was decreased further compared with that in the *MERTK* siRNA group. However, in the *MERTK* siRNA + *CCT5*-Le group, F-actin expression was significantly increased, compared with that in the *MERTK* siRNA and *MERTK* siRNA + *CCT5* siRNA groups (**Figures 4B,C**). Furthermore, to detect whether *CCT5*-Le restored the distribution and arrangement of F-actin, we performed the immunofluorescence analysis. In the *MERTK* siRNA + *CCT5* siRNA group, the distribution and arrangement of F-actin became more irregular than that in the *MERTK* siRNA group. However, in the *MERTK* siRNA + *CCT5*-Le group, the distribution and arrangement of F-actin were recovered, as seen in the NC group (**Figure 4D**). These results indicate that the upregulation of *CCT5* expression rescued the phagocytic function, which was disrupted by *MERTK* siRNA, by restoring the expression and organization of F-actin in HsRPE cells.

## Chaperonin-Containing TCP1 Subunit 5 Rescued Human Primary RPE Cells With Mer Receptor Tyrosine Kinase-Associated Retinitis Pigmentosa via the LIM-Kinase 1/Cofilin, but Not the SSH1/Cofilin, Pathway

Phosphorylated cofilin (p-cofilin) and cofilin are essential regulators of F-actin dynamics, regulating the polymerization and depolymerization of F-actin in the processes of phagocytosis and migration. To determine whether cofilin and p-cofilin were involved in *CCT5*-Le's rescue of the phagocytosis and migration

function of HsRPE cells with *MERTK*-associated RP, we next determined their levels of expression. Notably, we found that the expression of both cofilin and p-cofilin was suppressed in the *MERTK* siRNA group compared with that in the NC group. In the *MERTK* siRNA + *CCT5* siRNA group, the expression of both cofilin and p-cofilin was decreased further when compared with that in the *MERTK* siRNA group. However, in the *MERTK* siRNA + *CCT5*-Le group, the expression of both cofilin and p-cofilin was increased compared with that in the *MERTK* siRNA and *MERTK* siRNA + *CCT5* siRNA groups (**Figure 5A**). Cofilin is inactivated *via* phosphorylation by LIM-kinase 1 (LIMK1) and testicular protein kinase 1 (TESK1) and reactivated *via* dephosphorylation by slingshot 1 (SSH1). Therefore, to investigate whether LIMK1, TSK1, and SSH1 regulated the activity of cofilin in the process of *CCT5*-Le's rescue of the phagocytosis and migration function of HsRPE cells under *MERTK*-associated RP, we detected the expression of LIMK1, TSK1, and SSH1. The results indicate that the expression of LIMK1, TSK1, and SSH1 was decreased in the *MERTK* siRNA group, compared with that in the NC group. However, in the *MERTK* siRNA + *CCT5* siRNA group, only the expression of LIMK1 and TSK1, and not SSH1, was further decreased compared with that in the *MERTK* siRNA group. In the *MERTK* siRNA + *CCT5*-Le group, the expression of LIMK1 and TSK1 was increased, but the expression of SSH1 again demonstrated no significant change compared with that in the *MERTK* siRNA and *MERTK* siRNA + *CCT5* siRNA groups (**Figure 5B**). These results indicate that *CCT5*-Le rescued the phagocytosis and migration function which were destroyed by *MERTK* siRNA *via* the LIMK1/cofilin, but not the SSH1/cofilin, pathway.

## DISCUSSION

Retinitis pigmentosa is caused by multiple molecular interactions, of which the phagocytic dysfunction induced by a *MERTK* mutation in RPE cells is one of the most vital (1). As a cytoskeleton actin protein, F-actin plays an important role in cellular motility and phagocytosis (27). *CCT5* acts as a chaperone protein and plays a vital role in maintaining the normal function and structure of actin proteins (28). Recently, numerous studies have demonstrated the role that F-actin plays in the phagocytosis of RPE cells (29). However, to date, studies have failed to determine whether *CCT5* is associated with F-actin regulation or whether it plays an essential role in the progression of RP. Therefore, in this study, we focused on the role of *CCT5*'s regulation of F-actin in the pathogenesis of RP and the molecular mechanism of such.

We found that downregulating *MERTK* inhibited cell proliferation, migration, and phagocytic function. Additionally, knocking down *MERTK* significantly inhibited F-actin's expression and disrupted its regular arrangement. Importantly, our study revealed, for the first time, that *CCT5* interacts with F-actin and that *CCT5* expression is inhibited by *MERTK* siRNA in HsRPE cells. Upregulating *CCT5* rescued the cell proliferation, migration, and phagocytic function which were destroyed by *MERTK* siRNA *via* an increase in the expression of F-actin, as



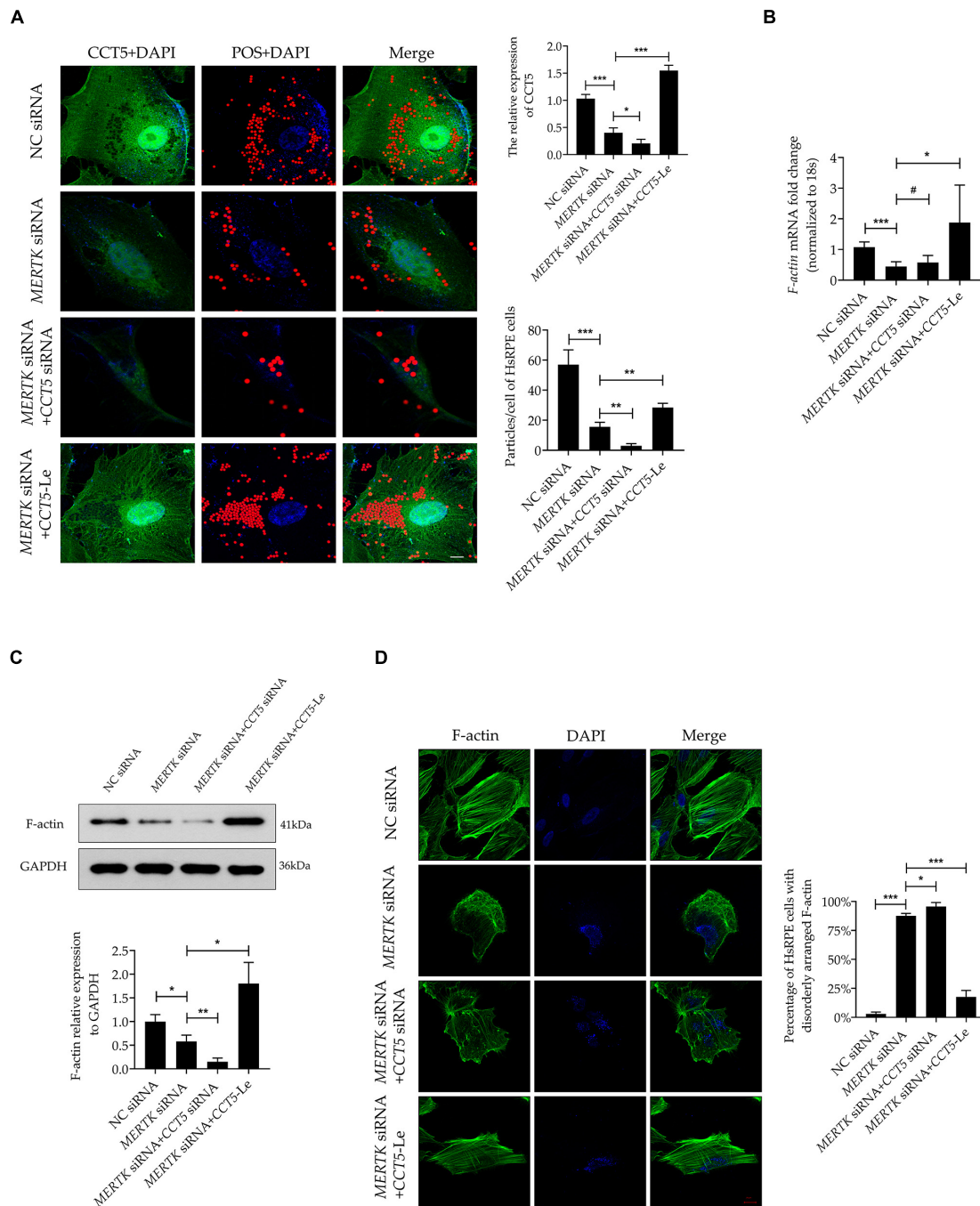


**FIGURE 4 |** CCT5 rescued the phagocytic function disrupted by *MERTK* siRNA by restoring the expression and organization of F-actin in HsRPE cells. **(A)** HsRPE cells were treated with or without *CCT5* siRNA or *CCT5*-Le after exposure to NC or *MERTK* siRNA for 48 h, and the phagocytic ability of HsRPE cells was examined by phagocytosis assay. The red dots represent the particles and the green dye represents the *CCT5* protein. Scale bars: 5  $\mu$ m. **(B)** HsRPE cells were treated with or without *CCT5* siRNA or *CCT5*-Le after exposure to NC or *MERTK* siRNA for 24 h, and *F-actin* expression was analyzed by RT-PCR. **(C)** HsRPE cells were treated the same as in (A), and *F-actin* expression was analyzed by Western blotting. **(D)** HsRPE cells were treated the same as in (A), and the distribution and organization of *F-actin* (green) were detected by immunofluorescence analysis. Scale bars: 10  $\mu$ m. #  $P > 0.05$ ; \* $P < 0.05$ ; \*\* $P < 0.01$ ; \*\*\* $P < 0.001$ .

well as the remodeling of its regular arrangement. Moreover, we discovered that *CCT5* promoted the remodeling of *F-actin*'s arrangement *via* the LIMK1/cofilin, but not the SSH1/cofilin, pathway (Figure 6).

Phagocytosis in RPE cells is a highly conserved, complex process that has evolved to counter the constant shedding of POS (30). To maintain the healthy photoreceptor–RPE interface of the retina, RPE cells constantly phagocytize the POS; however,



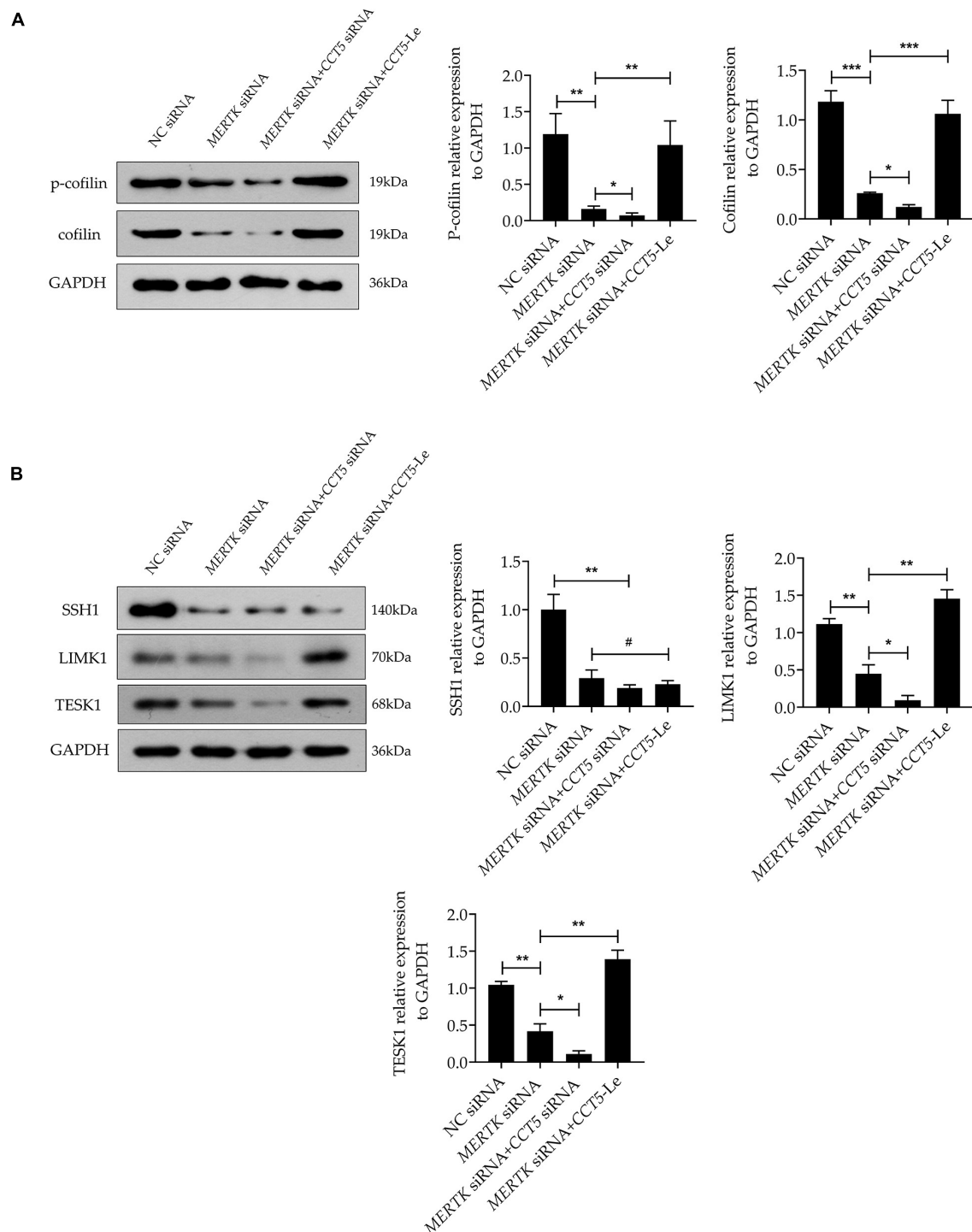


**FIGURE 5 |** CCT5 rescued HsRPE cells with *MERTK*-associated RP via the LIMK1/cofilin, but not the SSH1/cofilin, pathway. **(A)** HsRPE cells were treated with or without CCT5 siRNA or CCT5-Le after exposure to NC or *MERTK* siRNA for 48 h, and the cofilin and p-cofilin expression was analyzed by Western blotting. **(B)** HsRPE cells were treated the same as in **(A)**, and the expression of LIMK1, TESK1, and SSH1 was analyzed by Western blotting. \* $P < 0.05$ ; \*\* $P < 0.01$ ; \*\*\* $P < 0.001$ .

the mutation of *MERTK* results in phagocytic dysfunction in RPE cells, leading to RP. However, which part of the phagocytic process is disrupted in RPE cells with the *MERTK*

mutation remains to be elucidated. Ensheathment is required for POS fragmentation before internalization. The *MERTK* ligands Gas6 and Protein S contribute to the initiation of POS

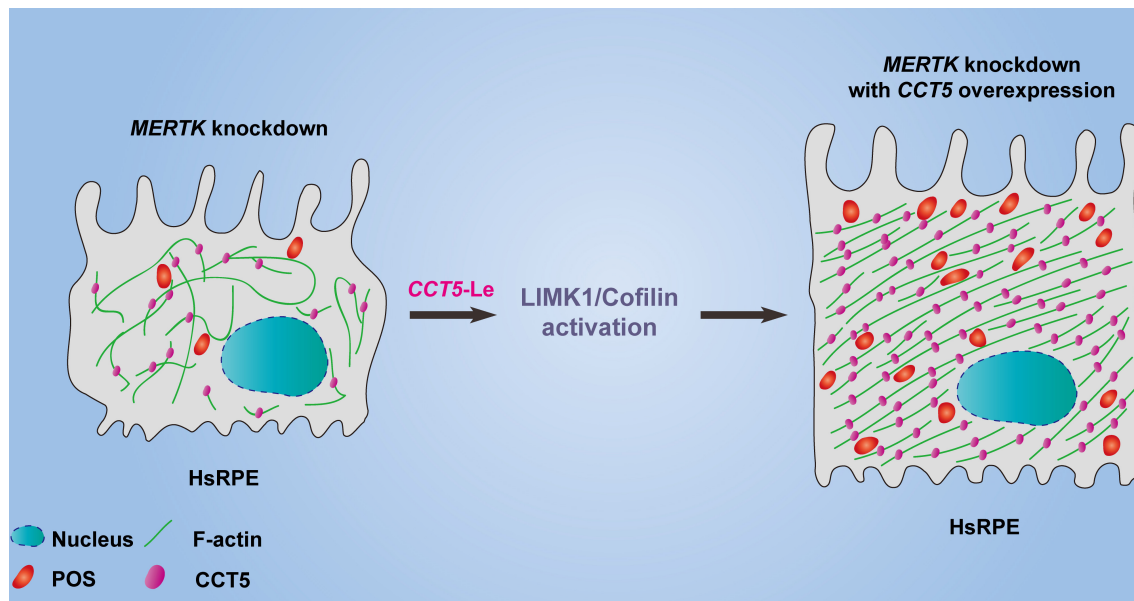


**FIGURE 6 |** The model diagram of *CCT5*-specific lentiviral vectors (*CCT5-Le*) rescued the cell phagocytic function of HsRPE cells under *MERTK* siRNA condition by increasing the expression of F-actin and restoring its regular arrangement via the LIMK1/cofilin pathway.

ensheathed by RPE (31). Abnormalities in the ensheathment, fragmentation, and internalization process in POS phagocytosis were found to occur in *MERTK*-mutated RPE while restoring *MERTK* expression in the RPE cells of RP patients reversed these abnormalities (32). The ensheathment, fragmentation, and internalization process require an appropriate F-actin distribution and arrangement (33). Therefore, the appropriate expression and correct spatial organization of F-actin filaments are essential for normal proliferation, migration, and phagocytic function (34–36). A recent study reported that, due to the lack of *Mertk*, the RPE cells of RCS rats could not aggregate F-actin and bind POS, even in the presence of protein S (14). Additionally, a previous study revealed that hypophagocytic RPE cells contain F-actin stress fibers but lack adjacent lateral circumferential F-actin (13). Together, these studies indicate that F-actin is involved in *MERTK*-associated RP. In line with these findings, our *MERTK*-associated RP model in HsRPE cells demonstrated that knocking down *MERTK* significantly inhibited the expression of F-actin and disrupted its regular arrangement. Moreover, we found that downregulating *MERTK* expression inhibited proliferation, migration, and phagocytic function.

Filamentous actin is regulated by various actin-binding proteins (37). Cofilin is a ubiquitous actin-binding protein that binds to F-actin only in its dephosphorylated state. When dephosphorylated cofilin binds to actin, it depolymerizes F-actin; however, phosphorylation at Ser 3 inactivates cofilin which then separates from, and thereby repolymerizes, F-actin (38). The recombination of the actin cytoskeleton *via* polymerization and depolymerization of F-actin by cofilin is indispensable for various cellular activities, such as phagocytosis, cytokinesis, and cell migration (39). The balance between F-actin and

cofilin is vital for preserving the normal physiological function of cells. Once this balance is disturbed, many diseases can result—including Alzheimer's disease (40, 41), mitotic disorder (42), cancers (43), optic nerve injury (44), migration disorder (35), immune dysfunction (45), and more. However, whether cofilin takes part in *MERTK*-associated RP retains a veil of mystery. First, we revealed that knocking down *MERTK* significantly inhibited the expression of both cofilin and p-cofilin in HsRPE cells. These results are consistent with the abnormal expression and arrangement of F-actin in our *MERTK*-associated RP model in HsRPE cells. The phosphorylation of cofilin is controlled by the LIMK1/TESK1 pathway (46–48). LIMK1 and TESK1 are, therefore, two key components of the signal transduction pathways that link extracellular stimulation to changes in cytoskeletal structure (49, 50). It was reported that the N-terminal kinase of TESK1 may be a putative candidate accounting for LIMK-independent cofilin phosphorylation, as it shows approximately 50% amino-acid identity with LIMK (51, 52). On the other hand, cofilin is activated by dephosphorylation by the phosphatase SSH1. SSH1's activity is strongly increased by its binding to F-actin (53). According to previous studies, the overexpression of LIMK1 and TESK1 in cultured cells results in the accumulation of F-actin, and the overexpression of SSH1 leads to the depolymerization of F-actin (49, 50, 53). However, no currently available research indicates a regulatory relationship between LIMK1, TESK1, SSH1, cofilin, and F-actin in RP. In our study, we revealed that the expression of LIMK1, TESK1, and SSH1 was inhibited after *MERTK* expression was downregulated. These results explain why knocking down *MERTK* significantly inhibited the expression of both cofilin and p-cofilin in HsRPE cells.

As a chaperonin, CCT5 assists in the folding of the unfolding or misfolded proteins, and actin is reported to be a natural substrate for CCT5 (21). It is reported that the effect of CCT5 on the z-disk of sarcomere cells is required for the efficient assembly of actin filaments, and CCT5-specific ATP binding is required for the efficient folding of actin *in vivo*. In addition, the mutant A-actin subtype that causes linear myopathy in patients acquires its pathogenic conformation through this function of CCT5 (22). Julie et al. found that CCT depletion did not affect actin-polypeptide synthesis but led to a decrease in natural actin levels and a disturbance of actin-based cell motility (54). McCormack et al. found that actin appeared to fold in association with chaperonin and that actin site II—located at the apex of actin subdomain 4—was the main binding site for CCT binding (55). Llorca et al. produced a three-dimensional reconstruction of the CCT and  $\alpha$ -actin complex, which demonstrated that  $\alpha$ -actin interacts with the apical domain of one of the two CCT subunits. Furthermore, they found that actin's binding to CCT is subunit-specific and geometrically dependent (21). CCT5's interactions in HsRPE cells with the *MERTK* mutation have not yet been reported. In our study, we discovered that CCT5 interacted with F-actin and that CCT5's expression was inhibited by *MERTK* siRNA in HsRPE cells. To verify that F-actin was regulated by CCT5, we downregulated and upregulated CCT5 separately in HsRPE cells. We found that upregulating the expression of CCT5 using *CCT5-Le* increased the expression of F-actin and remodeled its distribution and arrangement in our *MERTK*-associated RP model in HsRPE cells. When the expression of CCT5 was decreased using CCT siRNA, the effect was exactly opposite to that of *CCT5-Le*. In addition to its effect on actin, CCT5 has been reported to be connected to multiple cellular processes including proliferation, migration, and apoptosis *via* its relation with numerous proteins such as cyclin D1, polymerase basic protein, cell-division cycle protein 20, and P53 (56–59). In our study, we found that CCT5 regulated the expression of LIMK1 and TESK1 but not SSH1. Moreover, upregulating CCT5 rescued the cell proliferation, migration, and phagocytic function of HsRPE cells under *MERTK*-associated RP. These results indicate that CCT5 protects against *MERTK*-associated RP in RPE cells through interactions with F-actin and the activation of the LIMK1/cofilin pathway.

However, there are several limitations to our study. First, we only performed *in vitro* experiments in an RPE cell model established using *MERTK* siRNA. *In vivo* experiments should be performed in RCS rats to verify the role of CCT5 in *MERTK*-associated RP. Many questions remain to be answered in RCS rats, including whether the expression of CCT5 is abnormal in the RPE cells of RCS rats and whether regulating the expression of CCT5 can rescue the RP. Second, although CCT consists of eight subunits, we only detected the function of CCT5 in HsRPE cells. Thus, whether other paralogous subunits are involved in RP requires further exploration. Third, we found that the expression of cofilin, p-cofilin, LIMK1, and TESK1 was upregulated by *CCT5-Le*, but how CCT5 increases their expression—whether by increasing their transcription or by decreasing their degradation—remains to be determined. Although LIMK1 and TESK1 control the phosphorylation of

cofilin, no studies have demonstrated that they control the expression of cofilin. Therefore, whether CCT5 directly increases total cofilin expression or indirectly increases cofilin levels *via* other signals requires further study. We will attempt to find answers to these questions in future research.

In summary, despite the abovementioned limitations, our results demonstrate, for the first time, that the cell proliferation, migration, and phagocytic function of RPE cells are inhibited by *MERTK*-associated RP due to the abnormal expression of F-actin and disruption of its regular arrangement. Importantly, our findings reveal that CCT5 interacts with F-actin and regulates its expression and arrangement. Upregulating CCT5 protects against the effect of *MERTK* knockdown in RPE cells through its interactions with F-actin and activation of the LIMK1/cofilin pathway. These findings provide a new perspective for research into the mechanisms underlying *MERTK*-associated RP and provide a new direction for future studies of the molecular mechanisms of RP pathogenesis.

## MATERIALS AND METHODS

### Cell Culture

Human donor eyes were obtained from the Guangdong Eye Bank in accordance with the 2013 Declaration of Helsinki. Written consent was obtained from the donor or the donor's family for the eye to be used in medical research. The study was approved by the Ethics Committee of Zhongshan Eye Center, Sun Yat-sen University. The human primary RPE (HsRPE) cells were separated from human donor eyes as previously described (60). All the HsRPE cells were cultured in DMEM containing 4.5 g/L glucose, which was supplemented with 1% penicillin/streptomycin and 10% FBS, in a humidified incubator with a 5% CO<sub>2</sub> atmosphere at 37°C.

### siRNA Transfections

The siRNAs for *MERTK* and *CCT5* were designed and synthesized by RiboBio Inc. (Guangzhou, China). The sequences of the *MERTK* siRNA and *CCT5* siRNA are listed in **Table 1**. Transient transfections of the siRNAs for human *MERTK* (20 nM) and *CCT5* (20 nM) were conducted using Lipofectamine RNAiMAX (Invitrogen, New York, NY, United States), according to the manufacturer's protocol. Morphological changes in the cells were investigated using an inverted microscope (Carle ZEISS Axio Observer 7, Oberkochen, Baden-wuerttemberg, Germany), 48 h after siRNA transfection.

**TABLE 1** | List of siRNA sequences.

Gene	Sequences (5'–3')
<i>MERTK</i> siRNA1	GGATGAAGCCTCCGACTAA
<i>MERTK</i> siRNA2	GGTGACCTCTGTCCGAATCA
<i>CCT5</i> siRNA1	GGAGAGACGTTGACTTTGA
<i>CCT5</i> siRNA2	GCGATAGCGTCCTTGTGTA
NC siRNA	TTCTCCGAACGTGTACAGT

**TABLE 2 |** Sequences of PCR primers.

Gene	Forward sequence (5'-3')	Reverse sequence (5'-3')
<i>MERTK</i>	GGAAATAGCTACGCGGGGAA	TTCCGAACGTCAGGCAGAACT
<i>CCT5</i>	AGTATGCCATGAGAGCGTTT	GCAGGGTTCATCTCCTTCAC
<i>F-actin</i>	TGATGTTAGGCCTGCAAGA	GTAGTGCTGCATCAATTCC
<i>18s</i>	GTAACCCGTTGAACCCCA	CCATCCAATCGGTAGTAG

## Real-Time PCR

The RNA of the HsRPE samples was extracted using Trizol reagent (Invitrogen, New York, NY, United States). After cDNA was synthesized by reverse transcribing the RNA, the RT-PCR assay was performed using a LightCycler 480 SYBR Green I Master (Roche, Indianapolis, IN, United States). The values for each gene were normalized to the levels of tubulin or 18S mRNA. The sequences of the primers used for RT-PCR are listed in Table 2.

## Western Blot Assay

Cell lysis buffer was used to extract the total protein of the HsRPE cell samples before it was separated by sodium dodecyl sulfate polyacrylamide gel electrophoresis (SDS-PAGE). The total protein was then transferred onto polyvinylidene difluoride (PVDF) membranes (Millipore, Bedford, MA, United States). The PVDF membranes were incubated with different primary antibodies: anti-MERTK (Cell Signaling Technology, 4319S), anti-F-actin (Abcam, ab130935), anti-CCT5 (Proteintech, 11603-1-AP), anti-cofilin (Abcam, ab54532), anti-phosphorylated cofilin (p-cofilin, Abcam, ab12866), anti-LIMK1 (Affinity, AF6345), anti-TESK1 (Affinity, DF4012), anti-SSH1 (Abcam, ab76943), and anti-GAPDH (Abcam, ab8245). The membranes were incubated with the corresponding secondary antibody for 1 h at room temperature. The binding of specific antibodies was visualized using Chemiluminescent fluid (Millipore, WBKLS0500).

## Cell Counting Kit-8 Assay

A CCK8 kit (Beyotime, Shanghai, China) was used to determine the cell viability. The HsRPE cells were cultured at a density of  $7 \times 10^3$  cells/well in 96-well plates, after exposure to MERTK siRNA with or without the interference of CCT5 expression for 48 h. The CCT8 assay was performed as previously described in Zhou et al. (61), and the absorption values at a wavelength of 570 nm were evaluated.

## Wound-Healing and Transwell-Migration Assays

Wound-healing assays were performed as previously described in Qi et al. (62). Briefly, HsRPE cells from all the groups were seeded into 24-well plates until 100% confluence was attained. Wounds were scratched in the confluent cell layers using 200  $\mu$ L pipette tips, and the samples were cultured for a further 24 h. The Transwell assays were performed in 24-well plates with a chamber insert (8  $\mu$ m pore size) (Corning, 3422, Corning, NY, United States). After 24 h of incubation with transfected MERTK siRNAs, CCT5 siRNAs, or CCT5 lentiviral vectors (CCT5-Le), the underlying HsRPE cells were stained with crystal violet before the number of migrated cells was determined using an inverted microscope (Carle ZEISS Axio Observer 7, Oberkochen, Baden-wurttemberg, German).

## Phagocytosis Assay

Phagocytosis assays were performed as previously described in Irschick et al. (63). To assess the phagocytosis of HsRPE cells, Nile red-labeled Fluospheres (Sigma-Aldrich, F8825) were used. HsRPE cells from all the groups were cultured until the cell confluence reached 80%. Then, the medium was replaced and 10  $\mu$ L/mL of diluted 2  $\mu$ m-diameter particles were added. HsRPE cells were phagocytized with microspheres in a 5% CO<sub>2</sub> atmosphere at 37°C for 6 h and then washed with PBS three times to remove the unphagocytized particles before being stained with

**TABLE 3 |** Sequences of the lentiviral vectors of CCT5.

Name	Sequence
Lentiviral vectors of CCT5	ATGAACCTCCTCTGGGACCCACTATCGAGAACTATCAGTGTCTCATATAATGGCAGCAAAGGCTGTAGCAAATACAATGAGAACAT CACTTGGACCAAATGGGCTTGATAAGATGATGGTGGATAAGGATGGAGATGTGACTGTAACTAATGATGGGGCCACCATCTTAAGCA TGATGGATGTTGATCATCAGATTGCCAAGCTGATGGTGGAACTGTCCAAGTCTCAGGATGATGAAATTGGAGATGGAACACAGGAG TGGTTGTCTGGCTGGTGCCTTGTTAGAAGAAGCGGAGCAATTGCTAGACCGAGGCATTACCCCAATCAGAATAGCCGATGGCTAT GAGCAGGCTGCTCGTGTGCTATTGAACACCTGGACAAGATCAGCGATAGCGTCTTGTGACATAAAGGACACCGAACCCTGTAT TCAGACAGCAAAAACCGCTGGGCTCCAAAGTGGTCAACAGTTGTCACCGACAGATGGCTGAGATTGCTGTGAATGCCGTCTCTC ACTGTAGCAGATATGGAGCGGAGAGACGTTGACTTTGAGCTTATCAAAGTAGAAGGCAAAGTGGGCGGCAGGCTGGAGGACACTA AACTGATTAAAGGGCGTGATTGTGGACAAGGATTCAGTCACCCACAGATGCCAAAAAAGTGAAGATGCGAAGATTGCAATTCTC ACATGTCCATTTGAACACCCCAACCAAAAACAAAGCATAAGCTGGATGTGACCTCTGTGCAAGATTATAAAGCCCTTCAGAAATAC GAAAAGGAGAAATTTGAAGAGATGATTCAACAAATTAAGAGACTGGTGCTAACCTAGCAATTTGTCAGTGGGGCTTTGATGATGAA GCAAATCACTTACTTCTTCAGAACAACTTGCTGCGGTTGCTGGGTAGGAGGACCTGAAATTGAGCTGATTGCCATCGCAACAGG AGGGCGGATCGTCCCCAGGTTCTCAGAGCTCAGACCGAGAGAGCTGGGCTTTGCTGGTCTTGACAGGAGATCTCATTTGGGACA ACTAAGGATAAATGCTGGTCATCGAGCAGTGAAGAACTCCAGAGCTGTAACCATTTTATTAGAGGAGGAAATAAGATGATCATTGA GGAGCGCAACGATCCCTTCACGATGCTTTGTGTGTCATCCGGAACCTCATCCGCGATAATCGTGTGGTGTATGGAGGAGGGGCT GCTGAGATATCCTGTGCCCTGGCAGTTAGCCAAAGAGGCGGATAAGTGCCCCACCTTAGAACAGTATGCCATGAGAGCGTTTGGCG ACGCACCTGGAGGTCATCCCATGGCCCTCTCTGAAAACAGTGGCATGAATCCCATCCAGACTATGACCGAAGTCCGAGCCAGACA GGTGAAGGAGATGAACCCTGCTCTTGGCATCGACTGTTTGACAAGGGGACAAATGATATGAAGCAACAGCATGTGCATAGAAACCT TGATTGGCAAAAAGCAACAGATATCTCTTGAACACAAATGGTTAGATGATTTTGAAGATTGATGACATTGTAAGCCTGGAGAATCT GAAGAATGA



4',6-diamidino-2-phenylindole (DAPI) for 10 min. Finally, the number of microspheres was quantified by measuring the total fluorescence present using a confocal microscope (Carle ZEISS Axio Imager Z2, Oberkochen, Germany).

## Immunofluorescence

The immunofluorescence assays were performed as previously described in Feng et al. (64). HsRPE cells were fixed with 4% paraformaldehyde for 15 min, followed by blocking with 5% BSA at room temperature for 1 h. The cell samples were incubated with RPE65 (Abcam, ab235950), F-actin (Abcam, ab130935), CCT5 (Proteintech, 11603-1-AP), and *MERTK* (Cell Signaling Technology, 4319S) antibodies. Cell samples were then incubated with secondary antibodies for 1 h at room temperature. Subsequently, the nuclei of the cells were stained using DAPI for 7 min. All the images were taken using a confocal microscope (Carle ZEISS LSM 980, Oberkochen, Germany).

## Co-immunoprecipitation

The total protein of the HsRPE cell samples was extracted using cell lysis buffer, leaving 100  $\mu$ L of cell lysate as the input group. Two 1.5 EP tubes were filled with 400  $\mu$ L of HsPRE cell lysis solution, and 100  $\mu$ L of RIPA lysis buffer was added to each. One tube was incubated under rotation with 5  $\mu$ g of anti-CCT5 (Proteintech, 11603-1-AP), while the other tube was incubated under rotation with 5  $\mu$ g of rabbit anti-IgG (Cell Signaling Technology, 2729) at 4°C overnight. Fifty microliters of Protein A/G Magnetic Beads (Bimake Ferromagnetic Bead, B23202) were added to two additional 1.5 mL EP tubes. The magnetic beads were washed twice with 1 ml of precooled PBS and centrifuged at 3000 rpm for 1 min. Next, the magnetic beads were rotated and blocked with 3% BSA at 4°C for 30 min, followed by centrifugation at 3000 rpm for 1 min, absorbing the blocking solution, adding the antibody-protein complexes into the magnetic beads, and incubating under rotation at room temperature for 1 h. After incubation, the magnetic beads were washed with washing buffer. After the centrifugation of the proteins at 12,000 rpm and 4°C for 1 min, the supernatant was discarded carefully. Next, the proteins were separated by SDS-PAGE and transferred onto PVDF membranes. The membranes were probed with anti-F-actin (Abcam, ab130935) and anti-CCT5 (Proteintech, 11603-1-AP), and their corresponding secondary antibodies. Specific antibody binding was visualized using chemiluminescent fluid (Millipore, WBKLS0500).

## Transfection and Expression of Chaperonin-Containing TCP1 Subunit 5-Le

Lentiviral vectors were used to upregulate the expression of CCT5. The recombinant plasmid, contained pLV-CMV.hCCT5.EF1.CopGFP-T2A-Puro.Wpre, was used to produce the lentivirus. The 293 T cells were then transfected with the lentivirus. After 72 h, the 293 T cells were collected, the concentrated virus was extracted by centrifugation, and the virus titer was detected. The HsRPE cells were then inoculated in 6-well plates and incubated until their confluence was about

30%, and 50  $\mu$ L of virus was added (titer:  $2 \times 10^8$  TU/mL). After another 48 h of culture, the expression of the target gene in the lentivirus was observed by measuring the green fluorescent protein (GFP), and the mRNA and protein levels were detected. The sequences of the lentiviral vectors of CCT5 are listed in Table 3.

## Statistical Analysis

Statistical analysis was performed using SPSS 26.0. An unpaired *t*-test and one-way ANOVA were used to analyze and compare the differences between groups. The data are expressed as the means  $\pm$  standard deviations (SD) of at least three independent trials. A *p*-value less than 0.05 was considered statistically significant.

## DATA AVAILABILITY STATEMENT

The raw data supporting the conclusions of this article will be made available by the authors, without undue reservation.

## ETHICS STATEMENT

The studies involving human participants were reviewed and approved by the Ethics Committee of Zhongshan Eye Center, Sun Yat-sen University. The patients/participants provided their written informed consent to participate in this study.

## AUTHOR CONTRIBUTIONS

LF designed the experiments and wrote the manuscript. HL performed the experiments. YD performed the literature search and provided experimental support. TZ, YtZ, ZdL, LZ, and XW collected the data. GW, LbZ, ZJ, and ZL analyzed the data. ZO and YW performed the extraction of HsRPE cells. YhZ supervised the project and reviewed the manuscript. LF, HL, and YD have made equal contributions to the study and should therefore be regarded as equal authors. All authors have read and approved the published version of the manuscript.

## FUNDING

Our study was funded by the Science and Technology Program of Guangzhou, China (202102010216); the National Key Research and Development Project of China (2020YFA0112701); the National Natural Science Foundation of China (82171057).

## ACKNOWLEDGMENTS

We are grateful to Caibin Deng for his helpful suggestions, to Jing Chen for her help in the culture of the HsRPE cells, and to Jiangna Chen for her help regarding the Western blot analysis. We thank the members of the Zhongshan Ophthalmic Center at Sun Yat-sen University for their helpful comments and suggestions during this study.

## REFERENCES

- Hartong DT, Berson EL, Dryja TP. Retinitis pigmentosa. *Lancet*. (2006) 368:1795–809. doi: 10.1016/s0140-6736(06)69740-7
- Humphries P, Kenna P, Farrar GJ. On the molecular genetics of retinitis pigmentosa. *Science*. (1992) 256:804–8. doi: 10.1126/science.1589761
- Dias MF, Joo K, Kemp JA, Fialho S, Cunha ADS, Woo SJ, et al. Molecular genetics and emerging therapies for retinitis pigmentosa: basic research and clinical perspectives. *Prog Retin Eye Res*. (2018) 63:107–31. doi: 10.1016/j.preteyeres.2017.10.004
- Ducloyer J-B, Le Meur G, Cronin T, Adjali O, Weber M. Gene therapy for retinitis pigmentosa. *Med Sci*. (2020) 36:607–15. doi: 10.1051/medsci/2020095
- Gal A, Li Y, Thompson D, Weir J, Orth U, Jacobson S, et al. Mutations in MERTK, the human orthologue of the RCS rat retinal dystrophy gene, cause retinitis pigmentosa. *Nat Genet*. (2000) 26:270–1. doi: 10.1038/81555
- D'Cruz PM, Yasumura D, Weir J, Matthes MT, Abderrahim H, Lavail MM, et al. Mutation of the receptor tyrosine kinase gene MERTK in the retinal dystrophic RCS rat. *Hum Mol Genet*. (2000) 9:645–51. doi: 10.1093/hmg/9.4.645
- Kwon W, Freeman SA. Phagocytosis by the retinal pigment epithelium: recognition, resolution, recycling. *Front Immunol*. (2020) 11:604205. doi: 10.3389/fimmu.2020.604205
- Essner E, Pino RM, Griewski RA. Distribution of anionic sites on the surface of retinal pigment epithelial and rod photo-receptor cells. *Curr Eye Res*. (1981) 1:381–9. doi: 10.3109/02713688109019975
- Bullock A, Duan W, Finnemann SC. PI 3-kinase independent role for AKT in F-actin regulation during outer segment phagocytosis by RPE cells. *Exp Eye Res*. (2013) 113:9–18. doi: 10.1016/j.exer.2013.05.002
- Finnemann SC, Rodriguez-Boulton E. Macrophage and retinal pigment epithelium phagocytosis: apoptotic cells and photoreceptors compete for  $\alpha$ v $\beta$ 3 and  $\alpha$ v $\beta$ 5 integrins, and protein kinase C regulates  $\alpha$ v $\beta$ 5 binding and cytoskeletal linkage. *J Exp Med*. (1999) 190:861–74. doi: 10.1084/jem.190.6.861
- Bullock A, Maminishkis A, Mizui M, Finnemann SC. Semaphorin4D-PlexinB1 Signaling Attenuates Photoreceptor Outer Segment Phagocytosis by Reducing Rac1 Activity of RPE Cells. *Mol Neurobiol*. (2018) 55:4320–32. doi: 10.1007/s12035-017-0649-5
- Freeman SA, Goyette J, Furuya W, Woods EC, Bertozzi CR, Bergmeier W, et al. Integrins form an expanding diffusional barrier that coordinates phagocytosis. *Cell*. (2016) 164:128–40. doi: 10.1016/j.cell.2015.11.048
- Müller C, Charniga C, Temple S, Finnemann SC. Quantified F-actin morphology is predictive of phagocytic capacity of stem cell-derived retinal pigment epithelium. *Stem Cell Rep*. (2018) 10:1075–87. doi: 10.1016/j.stemcr.2018.01.017
- Mao Y, Finnemann SC. Acute RhoA/Rho kinase inhibition is sufficient to restore phagocytic capacity to retinal pigment epithelium lacking the engulfment receptor MERTK. *Cells*. (2021) 10:1927. doi: 10.3390/cells10081927
- Frydman J, Nimmegern E, Erdjument-Bromage H, Wall JS, Tempst P, Hartl FU. Function in protein folding of TRiC, a cytosolic ring complex containing TCP-1 and structurally related subunits. *Embo J*. (1992) 11:4767–78. doi: 10.1002/j.1460-2075.1992.tb05582.x
- Cong Y, Baker ML, Jakana J, Woolford D, Miller EJ, Reissmann S, et al. A 4.0-Å resolution cryo-EM structure of the mammalian chaperonin TRiC/CCT reveals its unique subunit arrangement. *Proc Natl Acad Sci USA*. (2010) 107:4967–72. doi: 10.1073/pnas.0913774107
- Rommelaere H, Van Troys M, Gao Y, Melki R, Cowan NJ, Vandekerckhove J, et al. Eukaryotic cytosolic chaperonin contains t-complex polypeptide 1 and seven related subunits. *Proc Natl Acad Sci USA*. (1993) 90:11975–9. doi: 10.1073/pnas.90.24.11975
- Frydman J, Hartl FU. Principles of chaperone-assisted protein folding: differences between in vitro and in vivo mechanisms. *Science*. (1996) 272:1497–502. doi: 10.1126/science.272.5267.1497
- Dekker C, Stirling P, McCormack EA, Filmore H, Paul A, Brost RL, et al. The interaction network of the chaperonin CCT. *Embo J*. (2008) 27:1827–39. doi: 10.1038/emboj.2008.108
- Llorca O, Martín-Benito J, Grantham J, Ritco-Vonsovici M, Willison KR, Carrascosa JL, et al. The 'sequential allosteric ring' mechanism in the eukaryotic chaperonin-assisted folding of actin and tubulin. *Embo J*. (2001) 20:4065–75. doi: 10.1093/emboj/20.15.4065
- Llorca O, McCormack EA, Hynes GM, Grantham JJ, Cordell J, Carrascosa JL, et al. Eukaryotic type II chaperonin CCT interacts with actin through specific subunits. *Nature*. (1999) 402:693–6. doi: 10.1038/45294
- Berger J, Berger S, Li M, Jacoby AS, Arner A, Bavi N, et al. In vivo function of the chaperonin TRiC in  $\alpha$ -actin folding during sarcomere assembly. *Cell Rep*. (2018) 22:313–22. doi: 10.1016/j.celrep.2017.12.069
- Sergeeva O, Tran MT, Haase-Pettingell C, King JA. Biochemical characterization of mutants in chaperonin proteins CCT4 and CCT5 associated with hereditary sensory neuropathy. *J Biol Chem*. (2014) 289:27470–80. doi: 10.1074/jbc.M114.576033
- Pavel M, Imarisio S, Menzies FM, Jimenez-Sanchez M, Siddiqi FH, Wu X, et al. CCT complex restricts neurodegenerative protein aggregation via autophagy. *Nat Commun*. (2016) 7:13821. doi: 10.1038/ncomms13821
- Levanova N, Steinemann M, Böhmer KE, Schneider S, Belyi Y, Schlosser A, et al. Characterization of the glucosyltransferase activity of *Legionella pneumophila* effector SetA. *Naunyn-Schmiedeberg Arch Pharmacol*. (2018) 392:69–79. doi: 10.1007/s00210-018-1562-9
- Ogneva IV, Biryukov NS. Lecithin prevents cortical cytoskeleton reorganization in rat soleus muscle fibers under short-term gravitational disuse. *PLoS One*. (2016) 11:e0153650. doi: 10.1371/journal.pone.0153650
- Grunheid S, Finlay BB. Microbial pathogenesis and cytoskeletal function. *Nature*. (2003) 422:775–81. doi: 10.1038/nature01603
- Mádi A, Mikkat S, Ringel B, Thiesen HJ, Glocker MO. Profiling stage-dependent changes of protein expression in *Caenorhabditis elegans* by mass spectrometric proteome analysis leads to the identification of stage-specific marker proteins. *Electrophoresis*. (2003) 24:1809–17. doi: 10.1002/elps.200305390
- Czuczman MA, Fattouh R, van Rijn J, Canadien V, Osborne S, Muise AM, et al. Listeria monocytogenes exploits efferocytosis to promote cell-to-cell spread. *Nature*. (2014) 509:230–4. doi: 10.1038/nature13168
- Kim J-Y, Zhao H, Martinez J, Doggett TA, Kolesnikov AV, Tang PH, et al. Noncanonical Autophagy Promotes the Visual Cycle. *Cell*. (2013) 154:365–76. doi: 10.1016/j.cell.2013.06.012
- Nandrot EF. Opposite roles of MERTK ligands Gas6 and protein s during retinal phagocytosis. *Adv Exp Med Biol*. (2018) 1074:577–83. doi: 10.1007/978-3-319-75402-4\_70
- Almedawar S, Vafia K, Schreier S, Neumann K, Khattak S, Kurth T, et al. MERTK-dependent ensheathment of photoreceptor outer segments by human pluripotent stem cell-derived retinal pigment epithelium. *Stem Cell Rep*. (2020) 14:374–89. doi: 10.1016/j.stemcr.2020.02.004
- Hayes MJ, Shao D, Bailly M, Moss SE. Regulation of actin dynamics by annexin 2. *Embo J*. (2006) 25:1816–26. doi: 10.1038/sj.emboj.7601078
- Haralambiev L, Nitsch A, Jacoby JM, Strakeljahn S, Bekeschus S, Mustea A, et al. Cold atmospheric plasma treatment of chondrosarcoma cells affects proliferation and cell membrane permeability. *Int J Mol Sci*. (2020) 21:2291. doi: 10.3390/ijms21072291
- Bisaria A, Hayer A, Garbett D, Cohen D, Meyer T. Membrane-proximal F-actin restricts local membrane protrusions and directs cell migration. *Science*. (2020) 368:1205–10. doi: 10.1126/science.aay7794
- Kitano M, Nakaya M, Nakamura T, Nagata S, Matsuda M. Imaging of Rab5 activity identifies essential regulators for phagosome maturation. *Nature*. (2008) 453:241–5. doi: 10.1038/nature06857
- McGough A. F-actin-binding proteins. *Curr Opin Struct Biol*. (1998) 8:166–76. doi: 10.1016/s0959-440x(98)80034-1
- Hirayama A, Adachi R, Otani S, Kasahara T, Suzuki K. Cofilin plays a critical role in IL-8-dependent chemotaxis of neutrophilic HL-60 cells through changes in phosphorylation. *J Leukoc Biol*. (2006) 81:720–8. doi: 10.1189/jlb.0506314
- Shiozaki N, Nakano K, Kushida Y, Noguchi TQP, Uyeda TQP, Wloga D, et al. ADF/Cofilin Is Not Essential but Is Critically Important for Actin Activities during Phagocytosis in *Tetrahymena thermophila*. *Eukaryot Cell*. (2013) 12:1080–6. doi: 10.1128/ec.00074-13
- Bamburg JR, Bernstein BW. Actin dynamics and cofilin-actin rods in Alzheimer disease. *Cytoskeleton*. (2016) 73:477–97. doi: 10.1002/cm.21282

41. Kang DE, Woo JA. Cofilin, a master node regulating cytoskeletal pathogenesis in alzheimer's disease. *J Alzheimer's Dis.* (2019) 72:S131–44. doi: 10.3233/JAD-190585
42. Jin Z, Yao X, Wen L, Hao G, Kwon J, Hao J, et al. AIP1 and Cofilin control the actin dynamics to modulate the asymmetric division and cytokinesis in mouse oocytes. *Faseb J.* (2020) 34:11292–306. doi: 10.1096/fj.20200093r
43. Chang C-Y, Leu J-D, Lee Y-J. The actin depolymerizing factor (ADF)/cofilin signaling pathway and DNA damage responses in cancer. *Int J Mol Sci.* (2015) 16:4095–120. doi: 10.3390/ijms16024095
44. Hao Q, Zhang Y, Li X, Liang L, Shi H, Cui Z, et al. Upregulated neuregulin-1 protects against optic nerve injury by regulating the RhoA/cofilin/F-actin axis. *Life Sci.* (2020) 264:118283. doi: 10.1016/j.lfs.2020.118283
45. Burkhardt JK, Carrizosa E, Shaffer MH. The Actin Cytoskeleton in T Cell Activation. *Annu Rev Immunol.* (2008) 26:233–59. doi: 10.1146/annurev.immunol.26.021607.090347
46. Yang N, Higuchi O, Ohashi K, Nagata K, Wada A, Kangawa K, et al. Cofilin phosphorylation by LIM-kinase 1 and its role in Rac-mediated actin reorganization. *Nature.* (1998) 393:809–12. doi: 10.1038/31735
47. Sakurai K, Talukdar I, Patil VS, Dang J, Li Z, Chang K-Y, et al. Kinome-wide Functional Analysis Highlights the Role of Cytoskeletal Remodeling in Somatic Cell Reprogramming. *Cell Stem Cell.* (2014) 14:523–34. doi: 10.1016/j.stem.2014.03.001
48. Rösok O, Pedetour F, Ree AH, Aasheim H-C. Identification and Characterization of TESK2, a Novel Member of the LIMK/TESK Family of Protein Kinases, Predominantly Expressed in Testis. *Genomics.* (1999) 61:44–54. doi: 10.1006/geno.1999.5922
49. Arber S, Barbayannis FA, Hanser H, Schneider C, Stanyon C, Bernard O, et al. Regulation of actin dynamics through phosphorylation of cofilin by LIM-kinase. *Nat Cell Biol.* (1998) 393:805–9. doi: 10.1038/31729
50. Wang L, Buckley AF, Spurney RF. Regulation of cofilin phosphorylation in glomerular podocytes by testis specific kinase 1 (TESK1). *Sci Rep.* (2018) 8:12286. doi: 10.1038/s41598-018-30115-3
51. Sarmiere PD, Bamberg JR. Regulation of the neuronal actin cytoskeleton by ADF/cofilin. *J Neurobiol.* (2003) 58:103–17. doi: 10.1002/neu.10267
52. Yu Q, Wu C, Chen Y, Li B, Wang R, Huang R, et al. Inhibition of LIM kinase reduces contraction and proliferation in bladder smooth muscle. *Acta Pharm Sin B.* (2021) 11:1914–30. doi: 10.1016/j.apsb.2021.01.005
53. Eiseler T, Döppler H, Yan IK, Kitatani K, Mizuno K, Storz P. Protein kinase D1 regulates cofilin-mediated F-actin reorganization and cell motility through slingshot. *Nat Cell Biol.* (2009) 11:545–56. doi: 10.1038/ncb1861
54. Grantham J, Brackley KI, Willison KR. Substantial CCT activity is required for cell cycle progression and cytoskeletal organization in mammalian cells. *Exp Cell Res.* (2006) 312:2309–24. doi: 10.1016/j.yexcr.2006.03.028
55. McCormack EA, Rohman MJ, Willison KR. Mutational screen identifies critical amino acid residues of beta-actin mediating interaction between its folding intermediates and eukaryotic cytosolic chaperonin CCT. *J Struct Biol.* (2001) 135:185–97. doi: 10.1006/jsbi.2001.4389
56. Meng Y, Yang L, Wei X, Luo H, Hu Y, Tao X, et al. CCT5 interacts with cyclin D1 promoting lung adenocarcinoma cell migration and invasion. *Biochem Biophys Res Commun.* (2021) 567:222–9. doi: 10.1016/j.bbrc.2021.04.105
57. Zhang X, Lin X, Qin C, Huang K, Sun X, Zhao L, et al. Avian Chaperonin Containing TCP1 Subunit 5 Supports Influenza A Virus Replication by Interacting With Viral Nucleoprotein, PB1, and PB2 Proteins. *Front Microbiol.* (2020) 11:538355. doi: 10.3389/fmicb.2020.538355
58. Ooe A, Kato K, Noguchi S. Possible involvement of CCT5, RGS3, and YKT6 genes up-regulated in p53-mutated tumors in resistance to docetaxel in human breast cancers. *Breast Cancer Res Treat.* (2006) 101:305–15. doi: 10.1007/s10549-006-9293-x
59. Wang Q, Huang W-R, Chih W-Y, Chuang K-P, Chang C-D, Wu Y, et al. Cdc20 and molecular chaperone CCT2 and CCT5 are required for the Muscovy duck reovirus p10.8-induced cell cycle arrest and apoptosis. *Veter Microbiol.* (2019) 235:151–63. doi: 10.1016/j.vetmic.2019.06.017
60. Terluk MR, Ebeling MC, Fisher CR, Kapphahn RJ, Yuan C, Kartha RV, et al. N-Acetyl-L-cysteine Protects Human Retinal Pigment Epithelial Cells from Oxidative Damage: Implications for Age-Related Macular Degeneration. *Oxidative Med Cell Longev.* (2019) 2019:1–14. doi: 10.1155/2019/5174957
61. Zhou J, Jiang Y, Chen H, Wu Y, Zhang L. Tanshinone I attenuates the malignant biological properties of ovarian cancer by inducing apoptosis and autophagy via the inactivation of PI3K/AKT/mTOR pathway. *Cell Prolif.* (2019) 53:e12739. doi: 10.1111/cpr.12739
62. Qi T, Jing R, Wen C, Hu C, Wang Y, Pei C, et al. Interleukin-6 promotes migration and extracellular matrix synthesis in retinal pigment epithelial cells. *Histochem Cell Biol.* (2020) 154:629–38. doi: 10.1007/s00418-020-01923-4
63. Irschick EU, Sgonc R, Böck G, Wolf H, Fuchs D, Nussbaumer W, et al. Retinal pigment epithelial phagocytosis and metabolism differ from those of macrophages. *Ophthalmic Res.* (2004) 36:200–10. doi: 10.1159/000078778
64. Feng L, Liang L, Zhang S, Yang J, Yue Y, Zhang X. HMGB1 downregulation in retinal pigment epithelial cells protects against diabetic retinopathy through the autophagy-lysosome pathway. *Autophagy.* (2021) 2021:1–20. doi: 10.1080/15548627.2021.1926655

**Conflict of Interest:** The authors declare that the research was conducted in the absence of any commercial or financial relationships that could be construed as a potential conflict of interest.

**Publisher's Note:** All claims expressed in this article are solely those of the authors and do not necessarily represent those of their affiliated organizations, or those of the publisher, the editors and the reviewers. Any product that may be evaluated in this article, or claim that may be made by its manufacturer, is not guaranteed or endorsed by the publisher.

Copyright © 2022 Feng, Li, Du, Zhang, Zhu, Li, Zhao, Wang, Wang, Zhou, Jiang, Liu, Ou, Wen and Zhuo. This is an open-access article distributed under the terms of the Creative Commons Attribution License (CC BY). The use, distribution or reproduction in other forums is permitted, provided the original author(s) and the copyright owner(s) are credited and that the original publication in this journal is cited, in accordance with accepted academic practice. No use, distribution or reproduction is permitted which does not comply with these terms.



# Blue Light Induces RPE Cell Necroptosis, Which Can Be Inhibited by Minocycline

Weilin Song, Ruilin Zhu, Wenna Gao, Chen Xing and Liu Yang\*

Department of Ophthalmology, Peking University First Hospital, Beijing, China

**Purpose:** Damage to and death of the retinal pigment epithelium (RPE) are closely related to retinal degeneration. Blue light is a high-energy light that causes RPE damage and triggers inflammatory responses. This study investigates whether blue light induces RPE necroptosis, explores pharmacologic therapy and specific mechanisms, and provides hints for research on retinal degeneration.

**Methods:** The human RPE cell line ARPE-19 was cultured and subjected to blue light insult *in vitro*. Annexin V/PI was used to evaluate RPE survival. Minocycline was applied to inhibit the death of RPE. Proteomic measurement was used to analyze protein expression. Inhibitors of necroptosis and apoptosis were applied to assess the death mode. Immunofluorescence of protein markers was detected to analyze the mechanism of cell death. Subcellular structural changes were detected by transmission electron microscopy. Reactive oxygen species (ROS) was tested by DCFH-DA. Mitochondrial membrane potential ( $\Delta\psi_m$ ) was detected by JC-1. BALB/c mice received blue light exposure, and RPE flatmounts were stained for verification *in vivo*.

**Results:** Blue light illumination induced RPE death, and minocycline significantly diminished RPE death. Proteomic measurement showed that minocycline effectively mitigated protein hydrolysis and protein synthesis disorders. Necroptosis inhibitors (Nec-1s, GSK-872) increased the survival of RPE cells, but apoptosis inhibitors (Z-VAD-FMK) did not. After blue light illumination, high-mobility group box-1 (HMGB1) was released from the nucleus, receptor-interacting protein kinase 3 (RIPK3) aggregated, and mixed-lineage kinase domain-like protein (MLKL) increased in the RPE. The application of minocycline alleviated the above phenomena. After blue light illumination, RPE cells exhibited necrotic characteristics accompanied by destruction of cell membranes and vacuole formation, but nuclear membranes remained intact. Minocycline improved the morphology of RPE. Blue light increased ROS and decreased  $\Delta\psi_m$  of RPE, minocycline did not reduce ROS but kept  $\Delta\psi_m$  stable. *In vivo*, HMGB1 release and RIPK3 aggregation appeared in the RPE of BALB/c mice after blue light illumination, and minocycline alleviated this effect.

**Conclusions:** Blue light exposure causes RPE necroptosis. Minocycline reduces the death of RPE by keeping  $\Delta\psi_m$  stable, inhibiting necroptosis, and preventing HMGB1 release. These results provide new ideas for the pathogenesis and treatment of retinal degeneration.

**Keywords:** necroptosis, cell death, retinal pigment epithelium, minocycline, blue light, retinal degeneration

## OPEN ACCESS

### Edited by:

Haijiang Lin,  
Massachusetts Eye and Ear Infirmary  
and Harvard Medical School,  
United States

### Reviewed by:

Haiwei Xu,  
Army Medical University, China  
Weihong Yu,  
Peking Union Medical College  
Hospital (CAMS), China

### \*Correspondence:

Liu Yang  
liu\_yang@bjmu.edu.cn

### Specialty section:

This article was submitted to  
Ophthalmology,  
a section of the journal  
Frontiers in Medicine

**Received:** 08 December 2021

**Accepted:** 04 April 2022

**Published:** 26 April 2022

### Citation:

Song W, Zhu R, Gao W, Xing C and  
Yang L (2022) Blue Light Induces RPE  
Cell Necroptosis, Which Can Be  
Inhibited by Minocycline.  
Front. Med. 9:831463.  
doi: 10.3389/fmed.2022.831463



## INTRODUCTION

RPE is a special epithelial cell located between the neuroretina and choroid that plays a crucial role in maintaining normal visual function. RPE cells can absorb light, protect against photooxidation, exchange heat, phagocytize the outer segment of the photoreceptor, participate in vitamin-A metabolism, secrete vascular endothelial growth factors, participate in the formation of the blood–retina outer barrier, and provide oxygen and nutrients from the choroid to the outer retina (1–3). Owing to the complex physiological functions of RPE cells, damage to and death of RPE cells are closely related to retinal degeneration such as retinitis pigmentosa (RP), Best disease, age-related macular degeneration (AMD), and Stargardt disease.

The structures of the eyes, including the cornea, aqueous humor, lens, and vitreous humor, absorb photons of different wavelengths sequentially. The visible light component (380–780 nm) of optical radiation can reach the retina, and the blue light component (400–500 nm) is particularly important because of its high energy (4, 5). The blue light part of 400 to 460 nm is considered to cause potential phototoxic retinal damage (4, 6). A wavelength of approximately 440 nm has been shown to be an excitation peak that damages photoreceptors and RPE function (6). In rhesus, 441 nm blue light-induced photochemical lesions originate in the RPE (7). Light-emitting diodes (LEDs) are widely used in daily life. Compared with traditional light sources, LED light sources emit more blue light, peaking at 435 to 460 nm (4, 8). This condition can lead to a range of health problems including retinal photochemical damage and disorder of circadian rhythms (4, 9, 10). In this study, we used blue light to induce RPE cell damage, studied the mode of RPE death, and explored therapeutic strategies and specific mechanisms.

Cell death is now divided into two categories: accidental cell death (ACD) and regulated cell death (RCD) (11). ACD is caused by severe lesions such as a consequence of burns and is immediate and insensitive to pharmacologic treatment (11). RCD means that cell death can be genetically regulated and modified by pharmacologic or genetic intervention (11–13). Apoptosis is a type of traditional RCD. Necrosis used to be considered passive cell death that could not be regulated. Currently, some types of cell death possess necrotic manifestations, such as necroptosis, which is regulated by RIPK1/3 and is a member of RCD. In the process of necroptosis, RIPK1 recruits RIPK3 to form the necrosome. MLKL is then recruited and activated by RIPK3 and ultimately executes necroptosis (14). Research of Murakami et al. (15) showed that in dsRNA-induced retinal degeneration, necroptosis of RPE cells was crucial and participated in damage-associated molecular patterns (DAMPs)-mediated inflammation. The dysfunction and death mode of RPE in retinal degenerations needs further study.

As a second-generation semisynthetic tetracycline, minocycline has antibiotic properties and can cross the blood–brain barrier. In addition to its antibiotic properties, minocycline has been found to exhibit neuroprotective and anti-inflammatory properties (16–18). Minocycline has been proven to be neuroprotective in various disease models. These disease models contain hemorrhagic and ischemic stroke, spinal cord

injury, neuropathic pain, multiple sclerosis (MS), Alzheimer's disease (AD), Huntington's disease, Parkinson's disease, and amyotrophic lateral sclerosis (ALS) (17, 19).

In this study, we adopted blue light exposure to induce human RPE cell damage and death, assessed the death mode of RPE cells induced by the blue light, and sought corresponding pharmacologic treatment. We applied minocycline to inhibit necroptosis of RPE cells and explored the mechanism, demonstrating that minocycline had an excellent rescue effect on dying RPE cells.

## MATERIALS AND METHODS

### Reagents and Antibodies

Minocycline hydrochloride, Nec-1s, GSK-872, and Z-VAD-FMK were purchased from MedChemExpress (Monmouth Junction, NJ, USA). Anti-HMGB1 antibody and anti-rabbit IgG (H+L), F(ab')<sub>2</sub> fragment (Alexa Fluor 488 Conjugate) were purchased from Cell Signaling Technology (Danvers, MA, USA). Anti-ZO-1, anti-RIPK3 and anti-MLKL antibodies were purchased from Proteintech (Rosemont, IL, USA). Mitochondrial membrane potential assay kit with JC-1 and ROS assay kit were purchased from Beyotime Biotechnology (Shanghai, China). DMEM/F12 and DMSO were purchased from Sigma-Aldrich (St. Louis, MO, USA). Fetal bovine serum was purchased from Gibco (Logan, UT, USA). Dead cell apoptosis kit with Annexin V Alexa Fluor 488 & Propidium Iodide (PI), goat anti-rabbit IgG (H+L) (Alexa Fluor 488), and goat anti-mouse IgG (H+L) (Alexa Fluor 568) were purchased from Invitrogen (Carlsbad, CA, USA).

### Cell Culture and Blue Light Illumination

ARPE-19 cells were cultured in DMEM/F12 supplemented with 10% FBS and 1% penicillin-streptomycin at 37°C in 5% CO<sub>2</sub>. After the medium was replaced, the corresponding drugs (minocycline, Nec-1s, GSK-872, and Z-VAD-FMK) were added to the medium and preincubated for 30 min at 37°C in 5% CO<sub>2</sub>. Then, the cells were exposed to 2200 lux blue light (440–445 nm wavelength) at 37°C in 5% CO<sub>2</sub>. The time of blue light exposure was determined according to the experimental needs.

### Annexin V/PI Staining

ARPE-19 cells were harvested and washed in cold PBS. Then, the cells were resuspended in 1X annexin-binding buffer. The cell density was  $1 \times 10^6$  cells/ml. Afterward, 5  $\mu$ l Alexa Fluor 488 annexin V and 1  $\mu$ l 100  $\mu$ g/ml PI working solution were added to each 100  $\mu$ l of cell suspension. The cells were incubated at room temperature for 15 min. Then, 400  $\mu$ l of 1X annexin-binding buffer was added to the cell suspension. Next, stained cells were analyzed by flow cytometry (Calibur, BD, USA).

### Mass Spectrometry-Based Proteomic Measurement

For each group of cells, three biological replicates were prepared. Proteins were extracted from each group of cells. One hundred micrograms of protein sample were mixed with 100  $\mu$ l of 8 M urea 0.1 M Tris/HCl solution, centrifuged for 15 min at 14,000 g, and repeated twice. Then, 100  $\mu$ l 8 M urea 0.1 M Tris/HCl

solution was added, and 10  $\mu$ l 0.05 M TCEP solution was added, incubated at 37°C for 1 h. Then, 10  $\mu$ l of 0.1 M IAA was added and incubated at 37°C for 1 h. The sample was centrifuged for 15 min at 14,000 g. The sample was washed twice with 50 mM ammonium bicarbonate. Trypsin (1  $\mu$ g) was dissolved in 100  $\mu$ l of 50 mM ammonium bicarbonate, and then the mixed liquid was added. The sample was incubated at 37°C overnight, and the peptide fragments were collected by centrifugation. LC-MS/MS analysis was performed with a mass spectrometer (Q-Exactive HF, Thermo Scientific, USA). MaxQuant software (version 1.4.1.2) was used for data analysis.

## Transmission Electron Microscopy

ARPE-19 cells were trypsinized and washed by PBS. Then, the cells were fixed in 2.5% glutaraldehyde. The cells were postfixed in  $\text{OsO}_4$ , dehydrated in ethanol, and embedded in epoxy resin. Ultrathin sections were made and then stained with uranium acetate and lead citrate double staining. These specimens were observed with transmission electron microscopy (JEM1400PLUS, JEOL, Japan).

## ROS Measurement

The culture medium was removed, and 10  $\mu$ M DCFH-DA (diluted in serum-free culture medium) was added. ARPE-19 cells were incubated at 37°C in 5%  $\text{CO}_2$  for 25 min. Then, the cells were washed with serum-free cell culture medium three times to fully remove the non-intracellular DCFH-DA. The cells were collected, and the fluorescence intensity was detected by flow cytometry (Calibur, BD, USA).

## Mitochondrial Membrane Potential Detection

The supernatant was removed, and JC-1 dye solution (1 $\times$ ) was added and incubated at 37°C in 5%  $\text{CO}_2$  for 20 min. Then, the cells were washed twice with JC-1 buffer solution. The cell culture medium was added again, and fluorescence images were taken via laser confocal microscopy (TCS-SP8 STED 3X, Leica, Germany).

## Immunofluorescence

ARPE-19 cells of different groups were fixed with 4% paraformaldehyde for 20 min and blocked with 0.3% Triton X-100 and 5% goat serum for 30 min. Primary antibody was added and incubated at 4°C overnight. After washing with PBS, the cells were incubated with secondary antibodies for 1 h at room temperature. Next, the cells were stained with DAPI and mounted in antifade mounting medium. Fluorescence images were acquired via laser confocal microscopy (TCS-SP8 STED 3X, Leica, Germany).

## Animals and Blue Light Illumination

BALB/c mice (8 to 10 weeks, male) were used in this study. Mice received 24 h dark adaptation before blue light exposure. The minocycline group received intraperitoneal injection of minocycline 50 mg/kg 1 h before blue light exposure, and 12 h after blue light exposure. The blue light group received intraperitoneal injection of PBS as a control. Their pupils were dilated with eye drops containing 0.5%

tropicamide and 0.5% phenylephrine (Santen Pharmaceutical, Osaka, Japan) before blue light exposure. The mice were exposed to 4500 lux blue light (440–445 nm wavelength) for 1 h.

## RPE Flatmount Staining

The eyes of the mice were enucleated 24 h after blue light illumination. The anterior segment and the neuroretina were removed and fixed in 4% PFA for 1 h. After washing with PBS, the eyecup was blocked with 0.3% Triton X-100 and 5% goat serum for 30 min, and primary antibody was added and incubated at 4°C overnight. The flatmounts were incubated with secondary antibodies for 1 h at room temperature after washing with PBS. Next, the flatmounts were stained with DAPI and mounted in antifade mounting medium. Fluorescence images were acquired via laser confocal microscopy (TCS-SP8 STED 3X, Leica, Germany).

## RESULTS

### Blue Light Induces Death of RPE Cells, Which Can Be Inhibited by Minocycline

In this study, we used blue light at 440–445 nm to damage ARPE-19 cells. As a cell line derived from human RPE, ARPE-19 has excellent RPE characteristics. ZO-1 immunofluorescence staining of ARPE-19 cells was positive, which indicated the formation of tight junctions among the cells (**Figure 1A**). In addition to antibiotic properties, minocycline has been confirmed to have neuroprotective effects in various injury and neurodegenerative models. Minocycline has not been reported to be used to protect RPE cells from light damage. After the addition of minocycline, the ARPE-19 cellular state improved significantly. Flow cytometry confirmed that a large number of cells died after exposure to blue light. Most of the dead cells were located in the upper right quadrant of the flowchart, indicating that the cells were Annexin V/PI double-staining positive (**Figure 1B**). After application of minocycline, the number of Annexin V/PI double-stained positive cells decreased dramatically, and the cell survival percentage increased. As the dose of minocycline increased, the cell survival percentage rose successively (**Figure 1B**). The application of 20 or 30  $\mu$ M minocycline substantially increased the percentage of surviving cells, indicating the protective effect of minocycline on blue-light-damaged RPE cells (**Figure 1C**).

To further investigate the death caused by blue light and the protective effect of minocycline, we used mass spectrometry. After exposure to blue light, the expression of a large amount of protein decreased due to protein hydrolysis and protein synthesis disorder. Compared with the control group, 444 proteins were downregulated and 33 proteins were upregulated in the blue light group. However, the number of downregulated proteins in the minocycline group was obviously less than that in the light group (**Figures 2A–F**). With the application of minocycline, the expression of proteins representing normal cell activities was upregulated, including cellular processes, environmental information processing, and genetic information processing (**Figures 2G–I**). Compared with the blue light group, 78 proteins

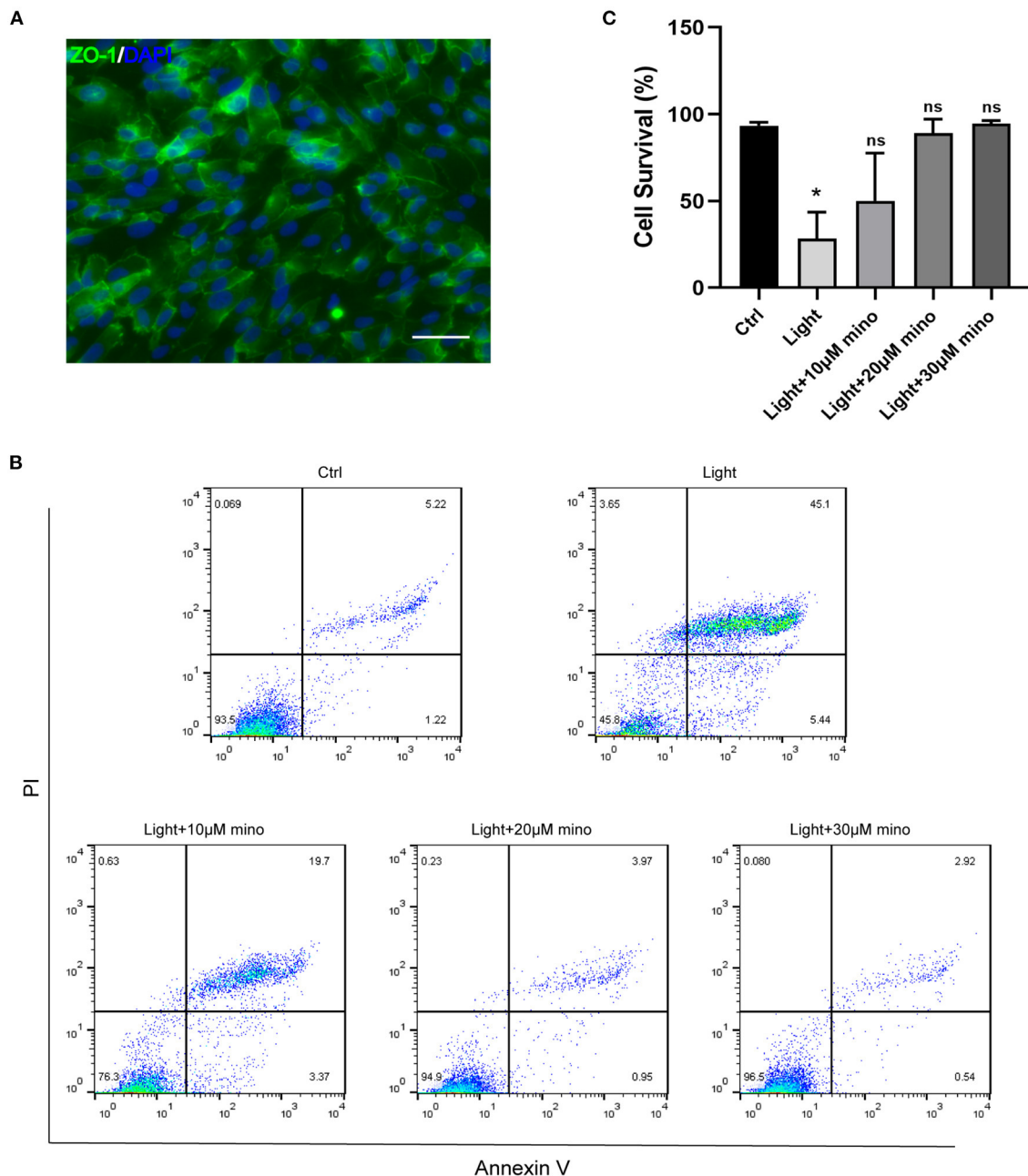


**FIGURE 1 |** Blue light causes death of RPE cells, and minocycline protects RPE cells from blue light-induced death. **(A)** ZO-1 immunofluorescence staining of ARPE-19 cells indicated formation of tight junctions. Scale bar: 50 μm. **(B)** Detection of ARPE-19 cell viability with Annexin V/PI. With increasing minocycline doses, death of ARPE-19 cells induced by blue light decreased significantly. ARPE-19 cells received blue light exposure for 2 h and were further cultured for 2 h before Annexin V/PI detection. **(C)** Quantitative analysis of **(B)** ( $n = 3$ ). \* $p < 0.05$ .

were upregulated and 9 proteins were downregulated in the blue light with minocycline group (Figure 2J). Venn diagram showed differences and commonalities of proteins among groups (Figure 2K). In general, blue light exposure induces RPE cell death, and minocycline can protect RPE cells from blue light-induced death.

## Death of RPE Cells Induced by Blue Light Is Necroptosis, and Minocycline Inhibits the Process of Necroptosis

The pattern of cell death caused by blue light needs further study. Combined with the previous results of Annexin V/PI double staining, we experimentally verified the ARPE-19 cell

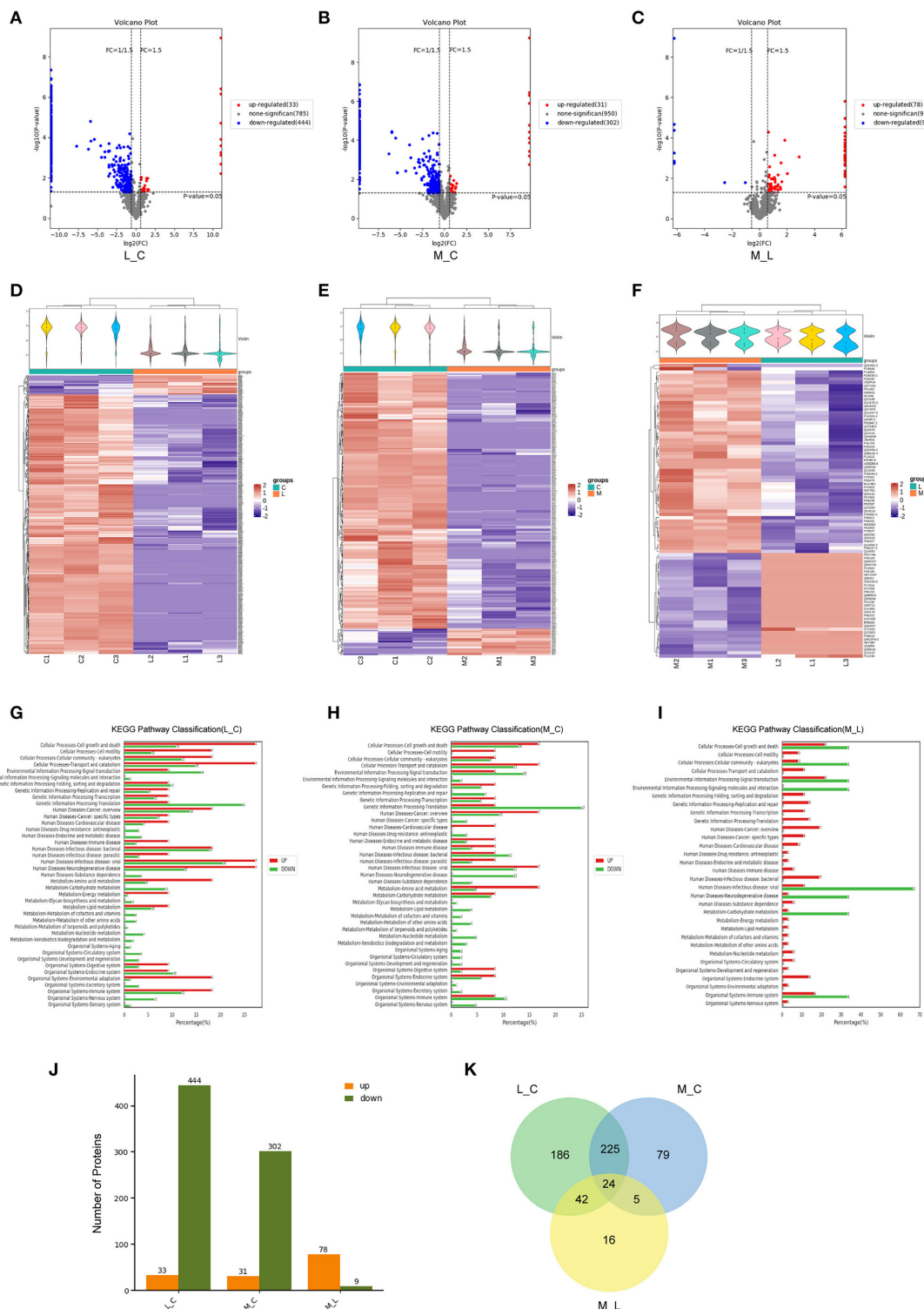
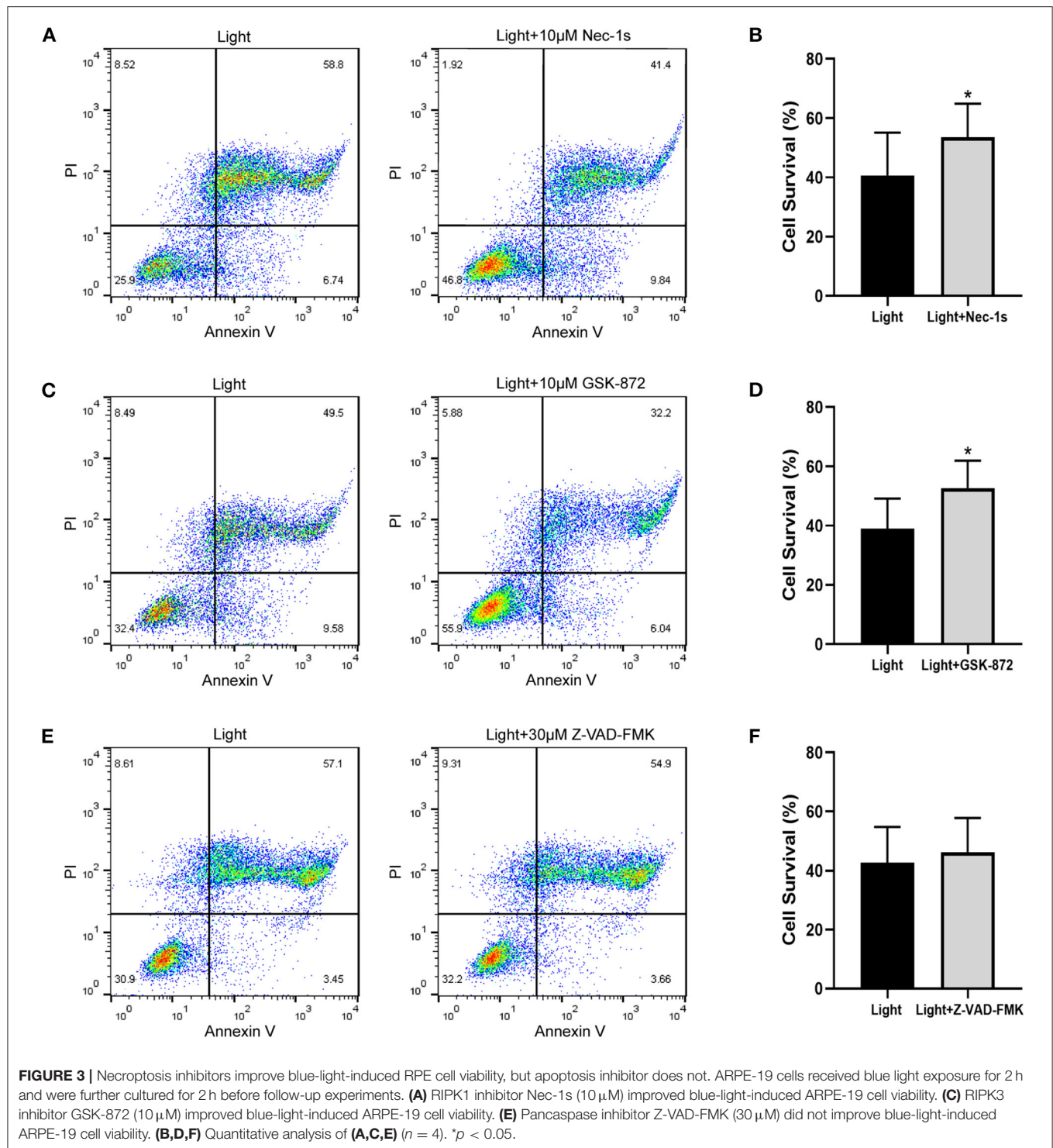


**FIGURE 2 |** Mass spectrometry-based proteomic analysis of cell damage caused by blue light and rescue effect of minocycline *in vitro*. ARPE-19 cells received blue light exposure for 2 h and were further cultured for 2 h before follow-up experiments. **(A–C)** Volcano plots of different groups. Light damage led to decrease in expression of large number of proteins, which was alleviated by minocycline. **(D–F)** Violin plot and clustering heatmap. Cluster analysis of protein expression in different groups. **(G–I)** Distribution map of upregulated and downregulated proteins at KEGG Level 2 in three groups. **(J)** Number of upregulated and downregulated proteins in different groups. **(K)** Venn analysis of characteristics and commonality of different proteins in each group. L\_C, blue light group vs. control group; M\_C, Blue light with minocycline group vs. control group; M\_L, blue light with minocycline group vs. blue light group.





death mode. As an inhibitor of RIPK1, Nec-1s is a more stable variant of Nec-1 and a more specific inhibitor of RIPK1 without the IDO-targeting effect (20). GSK-872 is the RIPK3 inhibitor. Both Nec-1s ( $p = 0.027$ ) and GSK-872 ( $p = 0.025$ ) improved cell survival (Figures 3A–D).

On the other hand, the pannicaspase inhibitor Z-VAD-FMK ( $p = 0.068$ ) did not improve cell survival, which meant that the cells did not die from apoptosis but necroptosis (Figures 3E,F). Immunofluorescence experiments confirmed this point.

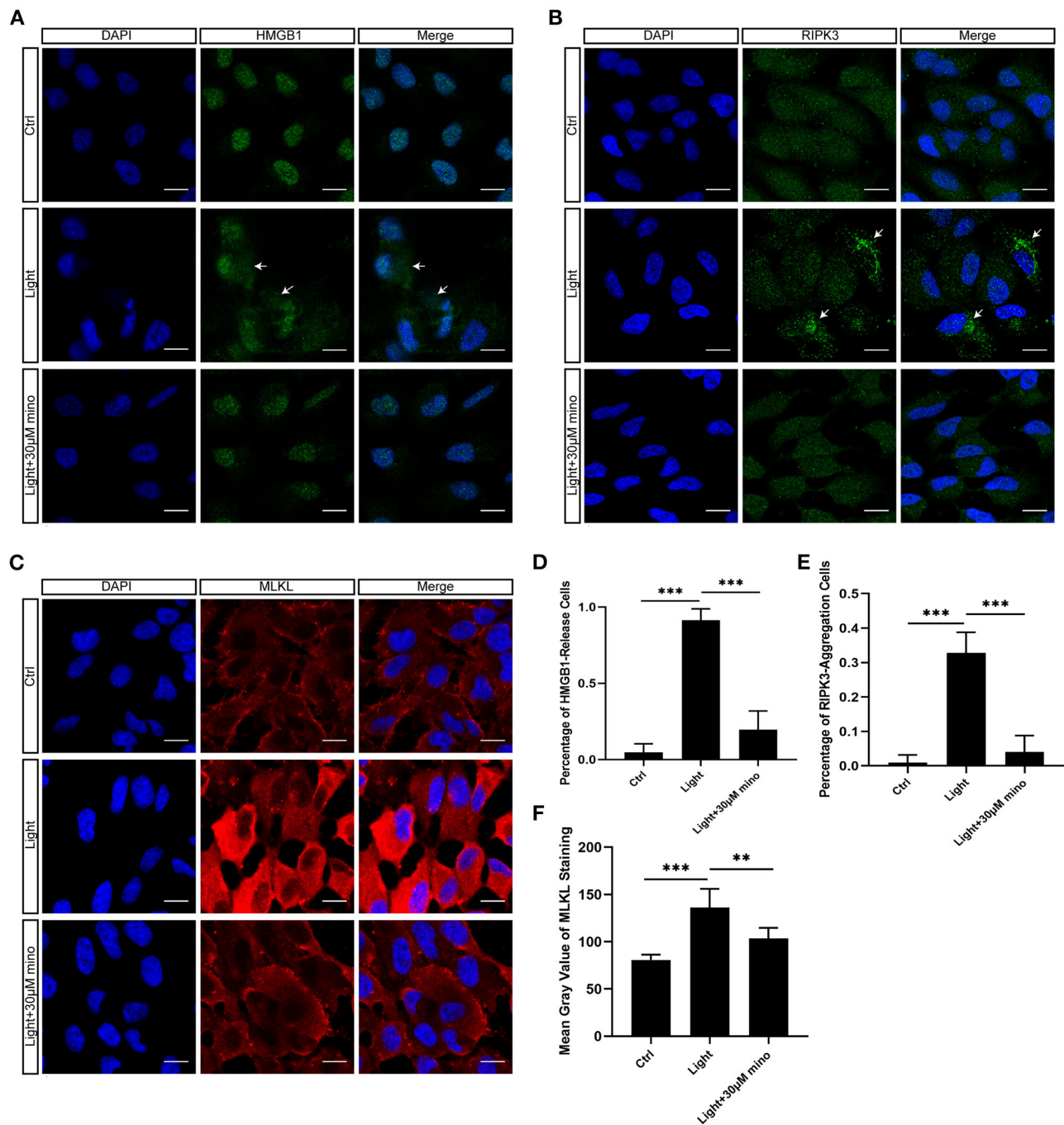


**FIGURE 4 |** Immunofluorescence verification of necroptosis molecular hallmarks in blue-light-induced RPE *in vitro*. ARPE-19 cells were exposed to blue light for 2 h and further cultured for 2 h before immunofluorescence experiments. **(A)** Blue light caused release of HMGB1 from nuclei of ARPE-19 cells. White arrows indicated release of HMGB1 from nuclei. Minocycline treatment significantly reduced release of HMGB1 from nucleus. Scale bar: 15  $\mu$ m. **(B)** Blue light caused aggregation of RIPK3 and enhancement of local fluorescence intensity in ARPE-19 cells. White arrows indicated aggregation of RIPK3. RIPK3 aggregation was evidently alleviated in light with minocycline group cells. Scale bar: 15  $\mu$ m. **(C)** Compared with blue light-induced cells, MLKL staining was light in normal APRE-19 cells and slightly obvious at cell edge. After blue light exposure, fluorescence of MLKL staining was obvious and homogeneous. In blue light with minocycline group cells, fluorescence characteristics were between control group and blue light exposure group. Scale bar: 15  $\mu$ m. **(D)** Quantitative fluorescence analysis of **(A)** ( $n = 6$ ). **(E)** Quantitative fluorescence analysis of **(B)** ( $n = 6$ ). **(F)** Quantitative fluorescence analysis of **(C)** ( $n = 6$ ).  $^{**}p < 0.01$ ,  $^{***}p < 0.001$ .

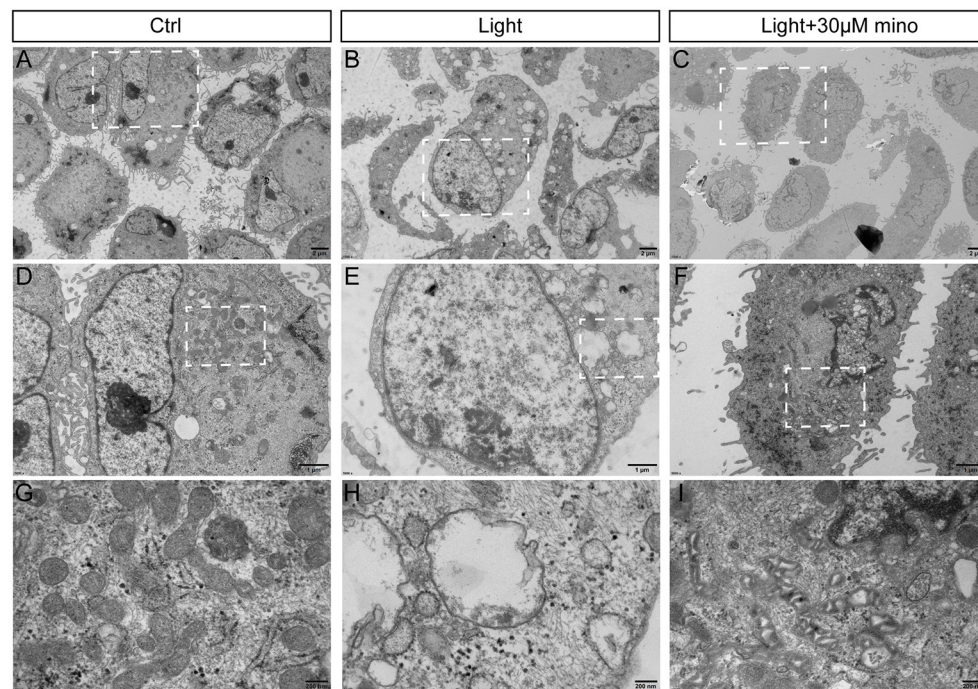


**FIGURE 5 |** Ultrastructure of RPE cells to show blue light damage and protective effects of minocycline via transmission electron microscopy. ARPE-19 cells were exposed to blue light for 2 h and were further cultured for 2 h. **(A)** Photomicrograph of normal ARPE-19 cells. **(B)** Photomicrograph of ARPE-19 cells exposed to blue light. **(C)** Photomicrograph of ARPE-19 cells with blue light exposure and minocycline treatment. **(D–F)** Enlarged parts of white dotted boxes in **(A–C)**. In cells of blue light group, many cytoplasmic vacuoles were observed, cell membranes were damaged, and nuclear membranes were intact. **(G–I)** Enlarged views of mitochondria in white dotted boxes in **(D–F)**. Note large number of mitochondria in normal ARPE-19 cells. In blue light group, mitochondria disappeared, and vacuoles remained. Under blue light with minocycline, mitochondria existed, but mitochondrial intermembrane space was enlarged. **(A–C)** Scale bar: 2  $\mu\text{m}$ . **(D–F)** Scale bar: 1  $\mu\text{m}$ . **(G–I)** Scale bar: 200 nm.

As a DNA-binding nuclear protein, HMGB1 is highly conserved. HMGB1 is also a major DAMPs that is released from necrotic cells. In necrosis, HMGB1 is passively released from the nucleus into the extracellular matrix to promote inflammation (21). In apoptotic cells, HMGB1 is firmly bound to chromatin and isolated into apoptotic bodies (21, 22). We analyzed the percentage of HMGB1-release cells in different groups, and there was significant difference between groups. After exposure to blue light, HMGB1 located in the nucleus of RPE cells was released in large quantities ( $p = 0.000$ ). This release of HMGB1 was effectively weakened with the application of minocycline ( $p = 0.000$ ) (**Figures 4A,D**). In normal RPE cells, the fluorescence of RIPK3 was homogeneous. After blue light exposure, RIPK3 aggregated ( $p = 0.000$ ), characterized by local punctiform fluorescence, suggesting the formation of necrosomes. Within the minocycline treatment, the fluorescence of RPE was similar to that of control cells (**Figures 4B,E**). MLKL staining was light in normal APRE-19 cells and slightly obvious at the cell edge. After blue light exposure, the fluorescence of MLKL staining was obvious and homogeneous ( $p = 0.000$ ), indicating the recruitment and activation of MLKL. Along with the application of minocycline, the MLKL fluorescence intensity of RPE cell decreased ( $p = 0.006$ ) (**Figures 4C,F**). These findings indicate

that blue light can induce RPE cell necroptosis and that minocycline inhibits necroptosis and DAMPs release in RPE cells *in vitro*.

### The Mechanism of Inhibition Necroptosis by Minocycline Is Related to Mitochondria Protection

Taken together, the results of flow cytometry and immunofluorescence indicated that the effect of minocycline on RPE rescue was better than that of the necroptosis inhibitors Nec-1s and GSK-872. To further explore the mechanism by which minocycline inhibits necroptosis in RPE cells, transmission electron microscopy was applied. Compared with the control group and blue light with minocycline group, the morphological changes of RPE cells of the blue light group were obvious (**Figures 5A–C**). RPE cells in the blue light group exhibited necrotic characteristics accompanied by microvillus disappearance, destruction of cell membranes, organelle disintegration, and vacuoles formation (**Figures 5B,E**). After the addition of minocycline, the illuminated cells retained some microvilli, and the cell morphology was similar to that of the control group (**Figures 5D,F**). Further enlarged pictures show the details of mitochondria in the three groups



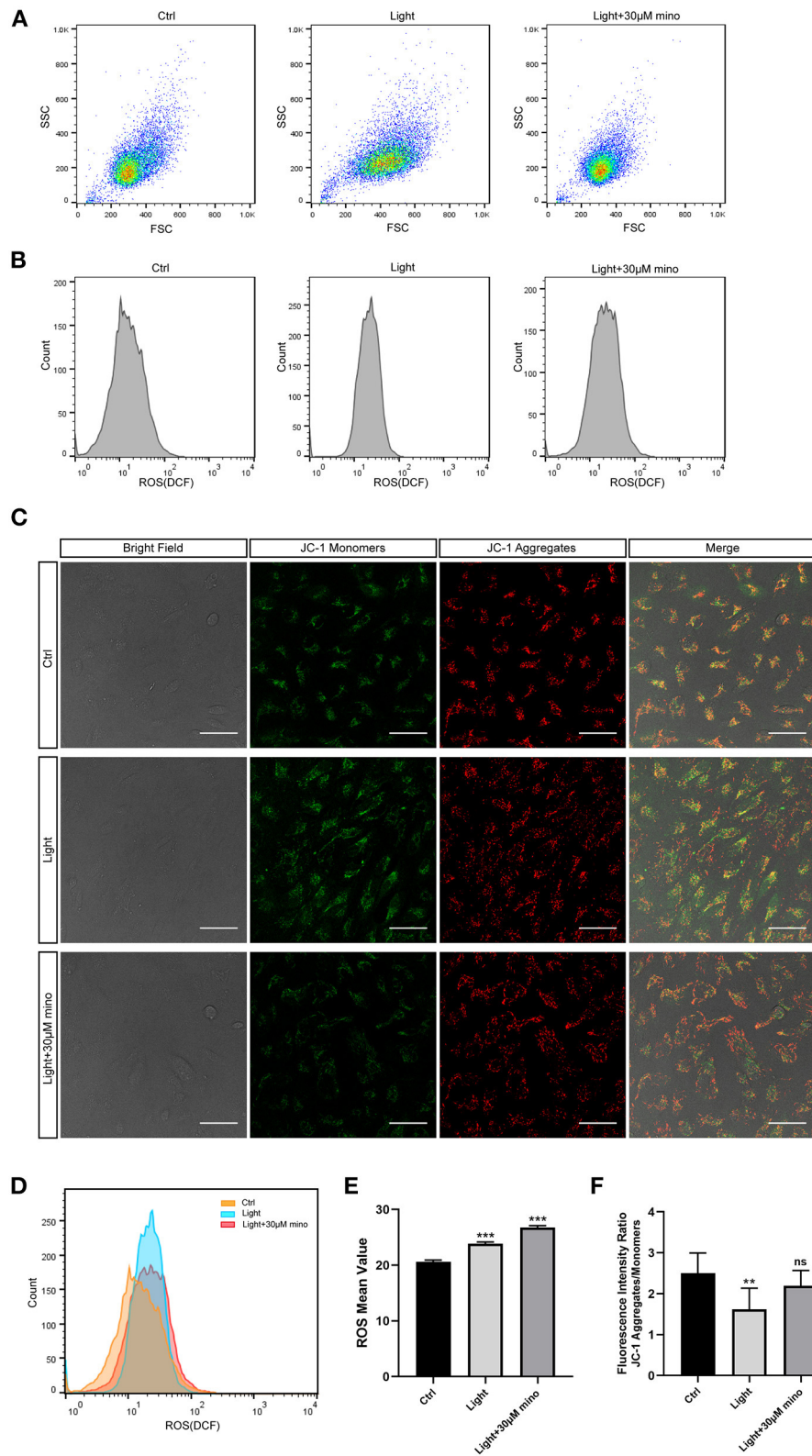


**FIGURE 6 |** Mechanisms by which minocycline reduces light-induced RPE death. **(A)** Variations in FSCs and SSCs in ARPE-19 cells in different groups in ROS experiment. Blue light exposure time was 30 min. In blue light group, cell mass became elliptical, and FSC value moved right. In blue light with minocycline group, ARPE-19 cells were preincubated with 30  $\mu$ M minocycline for 30 min before blue light exposure, and cell mass was aggregated and similar to that of control group. **(B)** ROS of ARPE-19 cells in different groups. Blue light exposure time was 30 min. **(C)** Bright field and JC-1 fluorescence images of different groups. Blue light

(Continued)



**FIGURE 6** | exposure time was 1 h. Scale bar: 50  $\mu\text{m}$ . **(D)** Superposition of three groups ROS diagrams in **(B)**. Curve of blue light group became sharp and moved right. Curve of blue light with minocycline group moved right. **(E)** Quantitative analysis of **(B)**. ROS in both blue light group and blue light with minocycline group was increased ( $n = 3$ ). **(F)** Quantitative analysis of **(C)**. In blue light group, decrease in fluorescence intensity ratio suggested decrease in  $\Delta\psi_m$  ( $n = 10$ ).  $**p < 0.01$ ,  $***p < 0.001$ .

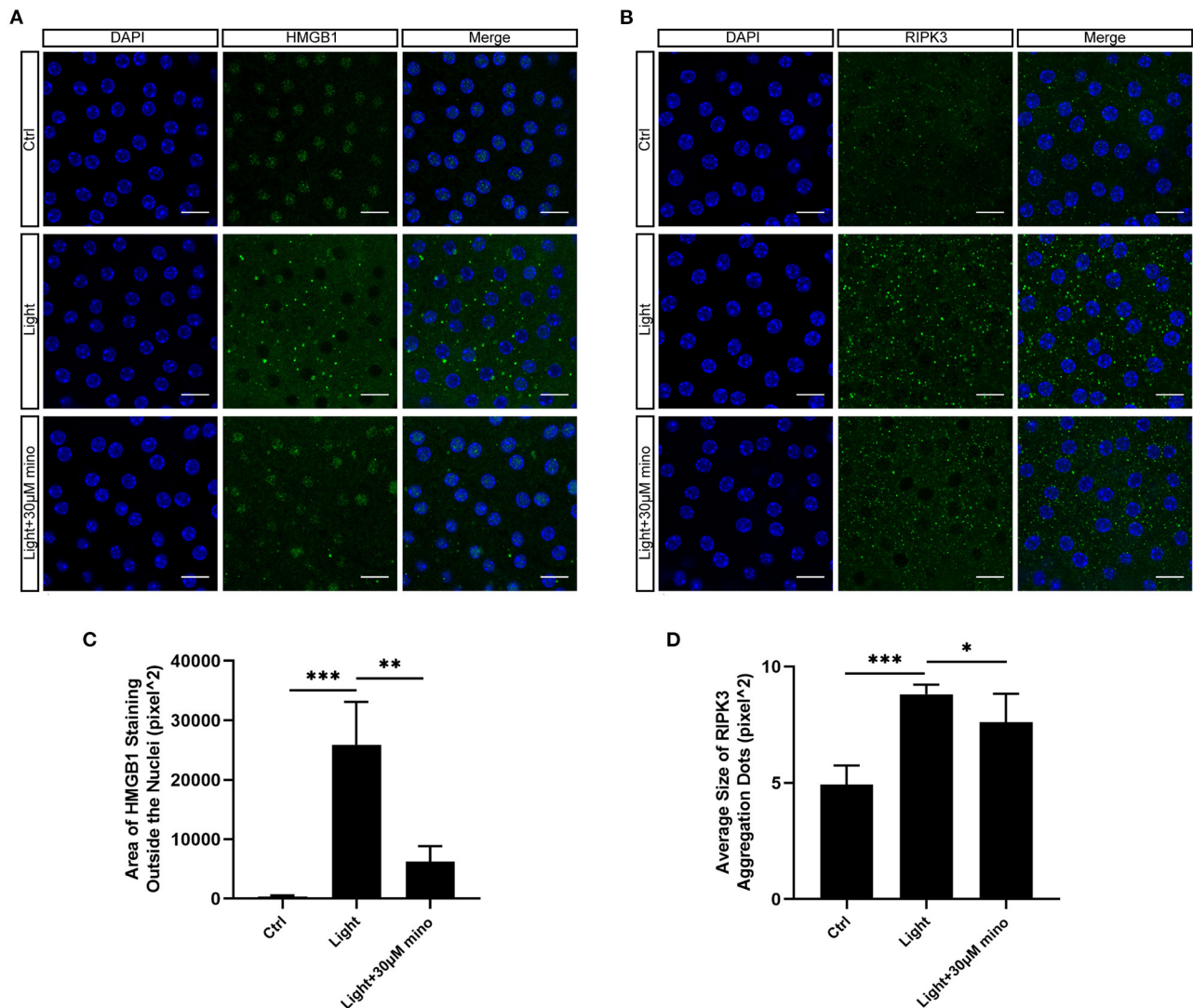


**FIGURE 7** | Expression of necroptosis-related proteins in RPE flatmount staining *in vivo*. **(A)** Blue light caused release of HMGB1 from nuclei of RPE cells. Minocycline treatment significantly reduced release of HMGB1 from nuclei. Scale bar: 15  $\mu\text{m}$ . **(B)** Blue light caused aggregation of RIPK3 in RPE cells. Minocycline treatment alleviated aggregation. Scale bar: 15  $\mu\text{m}$ . **(C)** Quantitative fluorescence analysis of **(A)** ( $n = 6$ ). **(D)** Quantitative fluorescence analysis of **(B)** ( $n = 6$ ).  $*p < 0.05$ ,  $**p < 0.01$ ,  $***p < 0.001$ .

of cells. There were a large number of mitochondria in normal ARPE-19 cells. In the blue light group, mitochondria disappeared with vacuoles remaining. Under blue light with minocycline, the mitochondrial intermembrane space was enlarged, suggesting that mitochondrial oxidative respiration was active (Figures 5G–I). This might be why cells resisted blue light damage and avoided the formation of necroptosis.

Reactive oxygen species (ROS) contain oxygen free radicals such as superoxide anion radical ( $\text{O}_2^{\bullet-}$ ) and hydroxyl radical ( $^{\bullet}\text{OH}$ ) and non-radical oxidants such as hydrogen peroxide ( $\text{H}_2\text{O}_2$ ) and singlet oxygen ( $^1\text{O}_2$ ) (23). ROS are mainly produced by mitochondria as byproducts of aerobic metabolism. High levels of ROS result in oxidative stress, and low levels of ROS regulate signaling pathways (24, 25). In the ROS experiment, after 30 min of blue light exposure, the RPE cell mass spread

out and became elliptical in the FSC/SSC diagram, suggesting that the RPE cells were swollen and that ROS in the RPE cells increased (**Figures 6A,B**). The cell mass of the blue light with the minocycline group was similar to the control group, and the cell state was even better according to FSC/SSC diagram, although ROS of the RPE cells was also elevated (**Figures 6A,B**). In the ROS experiment, the ROS levels of the blue light group were elevated ( $p = 0.000$ ), and minocycline did not lower the ROS levels ( $p = 0.000$ ) (**Figures 6B,D,E**). Minocycline could not prevent the blue light-induced ROS increase, but the RPE cells treated with minocycline remained in good condition. This suggests that RPE cells here have a good tolerance to ROS, and ROS may not be as threatening as previously thought.

Mitochondria are the potential targets of blue light and the regulatory centers of cell death. The synthesis of ATP, uptake and storage of  $\text{Ca}^{2+}$ , and generation and detoxification of ROS are inseparable from  $\Delta\psi_m$  (26). The collapse of  $\Delta\psi_m$  implies cell death. After 1 h of blue light exposure, RPE cells exhibited a decrease in  $\Delta\psi_m$ , as quantitated by the JC-1 aggregates and monomers fluorescence intensity ratio ( $p = 0.001$ ). In the blue light with minocycline group,  $\Delta\psi_m$  of RPE cells remained relatively stable ( $p = 0.133$ ) (**Figures 6C,F**). The utilization of minocycline was conducive to maintaining the stabilization of  $\Delta\psi_m$  and the normal physiological function of cells exposed to blue light.

In conclusion, blue light exposure can lead to an increase in ROS. However, the protective effect of minocycline does not occur by reducing ROS but stabilizing  $\Delta\psi_m$ . This protects the mitochondrial structure and function to maintain the normal physiological function of RPE cells and to avoid death.

## Minocycline Suppresses Necroptosis Signs in RPE Cells Caused by Blue Light *in vivo*

To analyze the influence of blue light exposure on the RPE *in vivo*, BALB/c mice were exposed to blue light. Mice that received minocycline treatment were intraperitoneally injected with minocycline. In the control group, HMGB1 was only expressed in the nucleus. In the blue light group, a large amount of HMGB1 was released from the nucleus ( $p = 0.000$ ). In the blue light with minocycline group, minocycline reduced the release of HMGB1 from the nucleus ( $p = 0.001$ ), although part of HMGB1 was still released into the cytoplasm (**Figures 7A,C**). After blue light exposure, RIPK3 staining showed punctate fluorescence enhancement, indicating the aggregation of RIPK3 ( $p = 0.000$ ). With the application of minocycline, the aggregation of RIPK3 was slightly weakened ( $p = 0.046$ ) (**Figures 7B,D**). These results indicate that DAMPs and inflammation play important roles in the process of blue light-induced RPE degeneration. Necroptosis is involved in blue light-induced RPE degeneration *in vivo*. Minocycline can alleviate necroptosis and inhibit DAMPs release.

## DISCUSSION

In our current research, we demonstrated that blue light exposure can lead to RPE cell necroptosis and HMGB1 release and that minocycline can reduce the death of RPE cells, inhibit

necroptosis, and prevent the release of HMGB1 by keeping  $\Delta\psi_m$  stable.

There is significant evidence about inflammation in the process of retinal degeneration. Apoptosis is generally considered to be anti-inflammatory by withholding the signal broadcast of damaged cells. Previous studies showed that light induces the apoptosis of RPE cells (27, 28). However, different wavelengths, irradiation durations, and intensities of light can cause different levels of damage to RPE cells. At the same time, the methods to distinguish apoptosis and necrosis are limited, so the two cell death modes cannot be well-distinguished. For instance, the TUNEL assay is traditionally considered to identify apoptotic cells, but necrotic cells can also be TUNEL positive due to DNA strand breakage. Annexin V/PI staining cannot adequately distinguish between necrosis and apoptosis. Apoptosis is an ATP-dependent death mode, intracellular ATP levels keep largely unvaried until the end of the death, whereas necrosis happens under intracellular ATP depletion (29). The modes of cell death are switchable. Caspase-8 is a switch between apoptosis and necroptosis. In apoptosis, Caspase-8 suppresses necroptosis by cleaving RIPK3 (30). Study of Yang et al. showed that RPE cells presented low levels of Caspase-8 expression (31). This means that RPE cells are more prone to necroptosis when suffer damage. In addition, autophagy has been studied in blue light-induced RPE injury. Autophagy might be a protective mechanism against blue light-induced RPE damage at an early stage (32, 33) because of its homeostatic mechanism by removing faulty cellular components. Nevertheless, abnormal autophagy at the late stage of blue light-induced RPE damage might aggravate cell degeneration (32).

Necroptosis has been implicated in many human neurodegenerative diseases. Cell death and neuroinflammation motivated by necroptosis mediate the pathogenesis of these diseases (34) including ALS (35), MS (36), AD (37), and Parkinson's disease (38). In retinal neurodegenerative diseases such as RP and AMD, oxidative stress and mitochondrial dysfunction of RPE cells are observed (39–41). Hanus et al. (42, 43) found that oxidants could induce RPE cell necroptosis. This indicates that research on necroptosis is crucial for relevant pathophysiology exploration in retinal degeneration.

Necrotic cells release DAMPs, and DAMPs can cause an inflammatory response. Murakami et al. (15) showed that RIPK3 deficiency suppressed the release of DAMPs from necrotic cells and cytokine production. HMGB1 is a major DAMPs. As a prototypical alarmin, extracellular HMGB1 can activate innate immunity, and TLR4 and RAGE are the main HMGB1 receptors (44). The release of HMGB1 into the extracellular matrix can be induced by various cell stresses and diseases such as trauma, hemorrhagic shock, and sepsis (45, 46). Our study proved that blue light exposure induced HMGB1 release from RPE cell nuclei, once again proving that blue light excited RPE cell inflammation and necroptosis.

The experimental results showed that direct blue light exposure could cause necroptosis of RPE cells by damaging mitochondria, thus emphasizing the link between blue light exposure and RPE degeneration. Blue light, mitochondria, RPE

necroptosis, and cell death pathways around these three factors need to be further studied.

The rescue effect of minocycline on necroptosis is much better than that of Nec-1s and GSK-872 because the rescue effect of minocycline is multifaceted. The first point is the protective function of minocycline on mitochondria. As we have proven, within minocycline, even under blue light exposure,  $\Delta\psi_m$  remained relatively stable so that mitochondria could provide ATP continuously. Multiple studies have confirmed that minocycline can play an effective therapeutic role in different neurodegenerative diseases. The therapeutic properties may be due to the antiapoptotic effects of minocycline (47, 48), inhibition of key enzymes activities such as matrix metalloproteinases (MMPs) (49), inducible nitric oxide synthase (iNOS) (50), phospholipase A2 (PLA<sub>2</sub>) (51), inhibition of microglial activation (52), calcium chelation, and other mechanisms (17, 19). Obviously mitochondrial Ca<sup>2+</sup> accumulation leads to the opening of mitochondrial permeability transition pore. It is followed by the mitochondrial swelling and the mitochondrial membrane rupture, which results in the liberation of mitochondrial proteins, including cytochrome c (53). Overload of Ca<sup>2+</sup> concentration exists at the early stage of necroptosis. Minocycline can decrease intracellular levels of Ca<sup>2+</sup> and prevent the release of cytochrome c (54). Necroptosis is involved in the pathogenesis of several neurodegenerative diseases such as MS, AD, Parkinson's disease, and ALS, and it is possible that minocycline inhibits necroptosis in these neurodegenerative diseases and thus alleviates these diseases. In summary, the protective effect of minocycline may be the result of multilayered synthesis, and mitochondrial conservation is a priority in blue-light-induced RPE cell death.

The conventional view is that ROS are toxic to cells because of their high chemical reactivity. As signaling molecules and enhancing immunologic defense, ROS are also considered to be beneficial for biosystems (55, 56). This biological contradiction underlies mechanisms by which ROS are significant for the normal activities of living organisms and their senescence (55). Therefore, homeostasis of ROS is crucial to normal cell activities. The retina is a high-energy demand and highly oxygen-consuming tissue (57). The highest oxygen levels are in the choroid, whereas this descends sharply across the outer retina, forming a large gradient of oxygen (58). RPE cells perform complex and important biological functions including transporting oxygen to the outer retina, and are rich in

mitochondria. Upon continuous exposure to light with intensive oxygen metabolism, RPE cells are more tolerant to oxidative stress than other cells. In our results for RPE cells in the blue light with minocycline group, although ROS of the cells were elevated, the cell state was even better, which indicated that transient ROS elevation might not lead to the death of RPE cells. In the process of blue light damage, mitochondria serve as death regulation centers, and a decrease in  $\Delta\psi_m$  leads to the obstruction of ATP synthesis, which is more fatal. Long-term oxidative stress can lead to the degeneration of RPE cells; however, brief strong light exposure is more dangerous than continuous weak light stimulation.

In conclusion, our results demonstrate that blue light can induce RPE cell necroptosis and DAMPs release. Minocycline has excellent effects on inhibiting the necroptosis and DAMPs release of RPE cells under blue light illumination and can improve the survival of RPE cells remarkably by stabilizing  $\Delta\psi_m$ . This study provides new clues regarding the pathogenesis and treatment of retinal degeneration.

## DATA AVAILABILITY STATEMENT

The original contributions presented in the study are included in the article/supplementary materials, further inquiries can be directed to the corresponding author/s.

## ETHICS STATEMENT

The animal study was reviewed and approved by Animal Care and Use Committee of Peking University First Hospital.

## AUTHOR CONTRIBUTIONS

WS designed and implemented the experiments and drafted the manuscript. RZ participated in the model construction of blue light damage. WG and CX participated in cell experiments. LY directed the experimental design, revised the article, and provided financial support. All authors contributed to the article and approved the submitted version.

## FUNDING

This work was supported by the National Natural Science Foundation of China (Nos. 81470650 and 81670841).

## REFERENCES

1. Saint-Geniez M, Kurihara T, Sekiyama E, Maldonado AE, D'Amore PA. An essential role for RPE-derived soluble VEGF in the maintenance of the choriocapillaris. *Proc Natl Acad Sci USA*. (2009) 106:18751–6. doi: 10.1073/pnas.0905010106
2. Strauss O. The retinal pigment epithelium in visual function. *Physiol Rev*. (2005) 85:845–81. doi: 10.1152/physrev.00021.2004
3. Datta S, Cano M, Ebrahimi K, Wang L, Handa JT. The impact of oxidative stress and inflammation on RPE degeneration in non-neovascular AMD. *Prog Retin Eye Res*. (2017) 60:201–18. doi: 10.1016/j.preteyeres.2017.03.002
4. Behar-Cohen F, Martinsons C, Viénot F, Zissis G, Barlier-Salsi A, Cesarini JP, et al. Light-emitting diodes (LED) for domestic lighting: any risks for the eye? *Prog Retin Eye Res*. (2011) 30:239–57. doi: 10.1016/j.preteyeres.2011.04.002
5. Godley BF, Shamsi FA, Liang FQ, Jarrett SG, Davies S, Boulton M. Blue light induces mitochondrial DNA damage and free radical production in epithelial cells. *J Biol Chem*. (2005) 280:21061–6. doi: 10.1074/jbc.M502194200
6. Alverve PV, Marshall J, Seregard S. Age-related maculopathy and the impact of blue light hazard. *Acta Ophthalmol Scand*. (2006) 84:4–15. doi: 10.1111/j.1600-0420.2005.00627.x
7. Ham WJ, Ruffolo JJ, Mueller HA, Clarke AM, Moon ME. Histologic analysis of photochemical lesions produced in rhesus retina by short-wave-length light. *Invest Ophthalmol Vis Sci*. (1978) 17:1029–35.



8. Liu X, Zhou Q, Lin H, Wu J, Wu Z, Qu S, et al. The protective effects of blue light-blocking films with different shielding rates: a rat model study. *Transl Vis Sci Technol.* (2019) 8:19. doi: 10.1167/tvst.8.3.19
9. Revell VL, Barrett DC, Schlangen LJ, Skene DJ. Predicting human nocturnal nonvisual responses to monochromatic and polychromatic light with a melanopsin photosensitivity function. *Chronobiol Int.* (2010) 27:1762–77. doi: 10.3109/07420528.2010.516048
10. Shang YM, Wang GS, Sliney D, Yang CH, Lee LL. White light-emitting diodes (LEDs) at domestic lighting levels and retinal injury in a rat model. *Environ Health Perspect.* (2014) 122:269–76. doi: 10.1289/ehp.1307294
11. Galluzzi L, Bravo-San PJ, Vitale I, Aaronson SA, Abrams JM, Adam D, et al. Essential versus accessory aspects of cell death: recommendations of the NCCD 2015. *Cell Death Differ.* (2015) 22:58–73. doi: 10.1038/cdd.2015.54
12. Galluzzi L, Vitale I, Abrams JM, Alnemri ES, Baehrecke EH, Blagosklonny MV, et al. Molecular definitions of cell death subroutines: recommendations of the Nomenclature Committee on Cell Death 2012. *Cell Death Differ.* (2012) 19:107–20. doi: 10.1038/cdd.2011.96
13. Galluzzi L, Kepp O, Krautwald S, Kroemer G, Linkermann A. Molecular mechanisms of regulated necrosis. *Semin Cell Dev Biol.* (2014) 35:24–32. doi: 10.1016/j.semcdb.2014.02.006
14. Weinlich R, Oberst A, Beere HM, Green DR. Necroptosis in development, inflammation and disease. *Nat Rev Mol Cell Biol.* (2017) 18:127–36. doi: 10.1038/nrm.2016.149
15. Murakami Y, Matsumoto H, Roh M, Giani A, Kataoka K, Morizane Y, et al. Programmed necrosis, not apoptosis, is a key mediator of cell loss and DAMP-mediated inflammation in dsRNA-induced retinal degeneration. *Cell Death Differ.* (2014) 21:270–7. doi: 10.1038/cdd.2013.109
16. Hughes EH, Schlichtenbrede FC, Murphy CC, Broderick C, van Rooijen N, Ali RR, et al. Minocycline delays photoreceptor death in the rds mouse through a microglia-independent mechanism. *Exp Eye Res.* (2004) 78:1077–84. doi: 10.1016/j.exer.2004.02.002
17. Garrido-Mesa N, Zarzuelo A, Gálvez J. Minocycline: far beyond an antibiotic. *Br J Pharmacol.* (2013) 169:337–52. doi: 10.1111/bph.12139
18. Romero-Miguel D, Lamanna-Rama N, Casquero-Veiga M, Gómez-Rangel V, Desco M, Soto-Montenegro ML. Minocycline in neurodegenerative and psychiatric diseases: an update. *Eur J Neurol.* (2021) 28:1056–81. doi: 10.1111/ene.14642
19. Yong VW, Wells J, Giuliani F, Casha S, Power C, Metz LM. The promise of minocycline in neurology. *Lancet Neurol.* (2004) 3:744–51. doi: 10.1016/S1474-4422(04)00937-8
20. Takahashi N, Duprez L, Grootjans S, Cauwels A, Nerinckx W, DuHadaway JB, et al. Necrostatin-1 analogues: critical issues on the specificity, activity and *in vivo* use in experimental disease models. *Cell Death Dis.* (2012) 3:e437. doi: 10.1038/cddis.2012.176
21. Scaffidi P, Misteli T, Bianchi ME. Release of chromatin protein HMGB1 by necrotic cells triggers inflammation. *Nature.* (2002) 418:191–5. doi: 10.1038/nature00858
22. Ellerman JE, Brown CK, de Vera M, Zeh HJ, Billiar T, Rubartelli A, et al. Masquerader: high mobility group box-1 and cancer. *Clin Cancer Res.* (2007) 13:2836–48. doi: 10.1158/1078-0432.CCR-06-1953
23. Zorov DB, Juhaszova M, Sollott SJ. Mitochondrial reactive oxygen species (ROS) and ROS-induced ROS release. *Physiol Rev.* (2014) 94:909–50. doi: 10.1152/physrev.00026.2013
24. Blaser H, Dostert C, Mak TW, Brenner D. TNF and ROS crosstalk in inflammation. *Trends Cell Biol.* (2016) 26:249–61. doi: 10.1016/j.tcb.2015.12.002
25. Mittler R. ROS are good. *Trends Plant Sci.* (2017) 22:11–9. doi: 10.1016/j.tplants.2016.08.002
26. Nicholls DG. Mitochondrial membrane potential and aging. *Aging Cell.* (2004) 3:35–40. doi: 10.1111/j.1474-9728.2003.00079.x
27. Lin CH, Wu MR, Li CH, Cheng HW, Huang SH, Tsai CH, et al. Editor's highlight: periodic exposure to Smartphone-Mimic Low-Luminance blue light induces retina damage through Bcl-2/BAX-Dependent apoptosis. *Toxicol Sci.* (2017) 157:196–210. doi: 10.1093/toxsci/kfx030
28. Hafezi F, Marti A, Munz K, Remé CE. Light-induced apoptosis: differential timing in the retina and pigment epithelium. *Exp Eye Res.* (1997) 64:963–70. doi: 10.1006/exer.1997.0288
29. Hanus J, Anderson C, Wang S. RPE necroptosis in response to oxidative stress and in AMD. *Ageing Res Rev.* (2015) 24:286–98. doi: 10.1016/j.arr.2015.09.002
30. O'Donnell MA, Perez-Jimenez E, Oberst A, Ng A, Massoumi R, Xavier R, et al. Caspase 8 inhibits programmed necrosis by processing CYLD. *Nat Cell Biol.* (2011) 13:1437–42. doi: 10.1038/ncb2362
31. Yang P, Peairs JJ, Tano R, Zhang N, Tyrell J, Jaffe GJ. Caspase-8-mediated apoptosis in human RPE cells. *Invest Ophthalmol Vis Sci.* (2007) 48:3341–9. doi: 10.1167/iovs.06-1340
32. Cheng KC, Hsu YT, Liu W, Huang HL, Chen LY, He CX, et al. The role of oxidative stress and autophagy in Blue-Light-Induced damage to the retinal pigment epithelium in zebrafish *in vitro* and *in vivo*. *Int J Mol Sci.* (2021) 22:1338. doi: 10.3390/ijms22031338
33. Yang PM, Cheng KC, Huang JY, Wang SY, Lin YN, Tseng YT, et al. Sulforaphane inhibits blue light-induced inflammation and apoptosis by upregulating the SIRT1/PGC-1 $\alpha$ /Nrf2 pathway and autophagy in retinal pigment epithelial cells. *Toxicol Appl Pharmacol.* (2021) 421:115545. doi: 10.1016/j.taap.2021.115545
34. Yuan J, Amin P, Ofengeim D. Necroptosis and RIPK1-mediated neuroinflammation in CNS diseases. *Nat Rev Neurosci.* (2019) 20:19–33. doi: 10.1038/s41583-018-0093-1
35. Re DB, Le Verche V, Yu C, Amoroso MW, Politi KA, Phani S, et al. Necroptosis drives motor neuron death in models of both sporadic and familial ALS. *Neuron.* (2014) 81:1001–8. doi: 10.1016/j.neuron.2014.01.011
36. Ofengeim D, Ito Y, Najafav A, Zhang Y, Shan B, DeWitt JP, et al. Activation of necroptosis in multiple sclerosis. *Cell Rep.* (2015) 10:1836–49. doi: 10.1016/j.celrep.2015.02.051
37. Caccamo A, Branca C, Piras IS, Ferreira E, Huentelman MJ, Liang WS, et al. Necroptosis activation in Alzheimer's disease. *Nat Neurosci.* (2017) 20:1236–46. doi: 10.1038/nn.4608
38. Iannielli A, Bido S, Folladori L, Segnali A, Cancellieri C, Maresca A, et al. Pharmacological inhibition of necroptosis protects from dopaminergic neuronal cell death in parkinson's disease models. *Cell Rep.* (2018) 22:2066–79. doi: 10.1016/j.celrep.2018.01.089
39. Kaarniranta K, Pawlowska E, Szczepanska J, Jablkowska A, Blasiak J. Role of mitochondrial DNA damage in ROS-mediated pathogenesis of Age-Related Macular Degeneration (AMD). *Int J Mol Sci.* (2019) 20:2374. doi: 10.3390/ijms20102374
40. Zhou B, Liu J, Kang R, Klionsky DJ, Kroemer G, Tang D. Ferroptosis is a type of autophagy-dependent cell death. *Semin Cancer Biol.* (2020) 66:89–100. doi: 10.1016/j.semcancer.2019.03.002
41. Yumnamcha T, Devi TS, Singh LP. Auranofin mediates mitochondrial dysregulation and inflammatory cell death in human retinal pigment epithelial cells: implications of retinal neurodegenerative diseases. *Front Neurosci.* (2019) 13:1065. doi: 10.3389/fnins.2019.01065
42. Hanus J, Anderson C, Sarraf D, Ma J, Wang S. Retinal pigment epithelial cell necroptosis in response to sodium iodate. *Cell Death Discov.* (2016) 2:16054. doi: 10.1038/cddiscovery.2016.54
43. Hanus J, Zhang H, Wang Z, Liu Q, Zhou Q, Wang S. Induction of necrotic cell death by oxidative stress in retinal pigment epithelial cells. *Cell Death Dis.* (2013) 4:e965. doi: 10.1038/cddis.2013.478
44. Yang H, Wang H, Andersson U. Targeting inflammation driven by HMGB1. *Front Immunol.* (2020) 11:484. doi: 10.3389/fimmu.2020.00484
45. Deng M, Scott MJ, Fan J, Billiar TR. Location is the key to function: HMGB1 in sepsis and trauma-induced inflammation. *J Leukoc Biol.* (2019) 106:161–9. doi: 10.1002/JLB.3MIR1218-497R
46. Okamoto K, Tamura T, Sawatsubashi Y. Sepsis and disseminated intravascular coagulation. *J Intensive Care.* (2016) 4:23. doi: 10.1186/s40560-016-0149-0
47. Chen M, Ona VO, Li M, Ferrante RJ, Fink KB, Zhu S, et al. Minocycline inhibits caspase-1 and caspase-3 expression and delays mortality in a transgenic mouse model of Huntington disease. *Nat Med.* (2000) 6:797–801. doi: 10.1038/77528
48. Garrido-Mesa N, Zarzuelo A, Gálvez J. What is behind the non-antibiotic properties of minocycline? *Pharmacol Res.* (2013) 67:18–30. doi: 10.1016/j.phrs.2012.10.006
49. Golub LM, Ramamurthy NS, McNamara TF, Greenwald RA, Rifkin BR. Tetracyclines inhibit connective tissue breakdown: new therapeutic implications for an old family of drugs. *Crit Rev Oral Biol Med.* (1991) 2:297–321. doi: 10.1177/10454411910020030201



50. Amin AR, Patel RN, Thakker GD, Lowenstein CJ, Attur MG, Abramson SB. Post-transcriptional regulation of inducible nitric oxide synthase mRNA in murine macrophages by doxycycline and chemically modified tetracyclines. *Febs Lett.* (1997) 410:259–64. doi: 10.1016/S0014-5793(97)00605-4
51. Pruzanski W, Greenwald RA, Street IP, Laliberte F, Stefanski E, Vadas P. Inhibition of enzymatic activity of phospholipases A2 by minocycline and doxycycline. *Biochem Pharmacol.* (1992) 44:1165–70. doi: 10.1016/0006-2952(92)90381-R
52. Liu B, Hong JS. Role of microglia in inflammation-mediated neurodegenerative diseases: mechanisms and strategies for therapeutic intervention. *J Pharmacol Exp Ther.* (2003) 304:1–7. doi: 10.1124/jpet.102.035048
53. Orrenius S, Gogvadze V, Zhivotovsky B. Calcium and mitochondria in the regulation of cell death. *Biochem Biophys Res Commun.* (2015) 460:72–81. doi: 10.1016/j.bbrc.2015.01.137
54. Garcia-Martinez EM, Sanz-Blasco S, Karachitos A, Bandez MJ, Fernandez-Gomez FJ, Perez-Alvarez S, et al. Mitochondria and calcium flux as targets of neuroprotection caused by minocycline in cerebellar granule cells. *Biochem Pharmacol.* (2010) 79:239–50. doi: 10.1016/j.bcp.2009.07.028
55. D'Autréaux B, Toledano MB. ROS as signalling molecules: mechanisms that generate specificity in ROS homeostasis. *Nat Rev Mol Cell Biol.* (2007) 8:813–24. doi: 10.1038/nrm2256
56. Yang S, Lian G. ROS and diseases: role in metabolism and energy supply. *Mol Cell Biochem.* (2020) 467:1–12. doi: 10.1007/s11010-019-03667-9
57. Yu DY, Cringle SJ. Retinal degeneration and local oxygen metabolism. *Exp Eye Res.* (2005) 80:745–51. doi: 10.1016/j.exer.2005.01.018
58. Jarrett SG, Boulton ME. Consequences of oxidative stress in age-related macular degeneration. *Mol Aspects Med.* (2012) 33:399–417. doi: 10.1016/j.mam.2012.03.009

**Conflict of Interest:** The authors declare that the research was conducted in the absence of any commercial or financial relationships that could be construed as a potential conflict of interest.

**Publisher's Note:** All claims expressed in this article are solely those of the authors and do not necessarily represent those of their affiliated organizations, or those of the publisher, the editors and the reviewers. Any product that may be evaluated in this article, or claim that may be made by its manufacturer, is not guaranteed or endorsed by the publisher.

Copyright © 2022 Song, Zhu, Gao, Xing and Yang. This is an open-access article distributed under the terms of the Creative Commons Attribution License (CC BY). The use, distribution or reproduction in other forums is permitted, provided the original author(s) and the copyright owner(s) are credited and that the original publication in this journal is cited, in accordance with accepted academic practice. No use, distribution or reproduction is permitted which does not comply with these terms.



# Cytomegalovirus-Immune Recovery Retinitis After Initiation of Highly Active Antiretroviral Therapy: A Case Series

Yiwen Qian<sup>1†</sup>, Luoziyi Wang<sup>1†</sup>, Jing Jiang<sup>1</sup>, Jinshan Suo<sup>1</sup>, Huan Weng<sup>1</sup>, Xin Che<sup>1</sup>, Hongzhou Lu<sup>2\*†</sup> and Zhiliang Wang<sup>1\*†</sup>

<sup>1</sup> Department of Ophthalmology, Huashan Hospital of Fudan University, Shanghai, China, <sup>2</sup> Department of Infectious Disease, Shenzhen Third People's Hospital, Shenzhen, China

## OPEN ACCESS

### Edited by:

Alessandro Meduri,  
University of Messina, Italy

### Reviewed by:

Giovanni William Oliverio,  
University of Messina, Italy  
Somayeh Shatizadeh Malekshahi,  
Tarbiat Modares University, Iran  
Riwanti Estiasari,  
University of Indonesia, Indonesia

### \*Correspondence:

Zhiliang Wang  
ophwzl@163.com  
Hongzhou Lu  
luhongzhou@fudan.edu.cn

<sup>†</sup>These authors have contributed  
equally to this work

### Specialty section:

This article was submitted to  
Ophthalmology,  
a section of the journal  
Frontiers in Medicine

Received: 01 November 2021

Accepted: 14 March 2022

Published: 27 April 2022

### Citation:

Qian Y, Wang L, Jiang J, Suo J, Weng H, Che X, Lu H and Wang Z (2022) Cytomegalovirus-Immune Recovery Retinitis After Initiation of Highly Active Antiretroviral Therapy: A Case Series. *Front. Med.* 9:807013. doi: 10.3389/fmed.2022.807013

**Purpose:** To delineate the characteristics and treatment of cytomegalovirus-immune recovery retinitis (CMV-IRR) in human immunodeficiency virus (HIV) patients with immune recovery under effective highly active antiretroviral therapy (HAART) regimen.

**Methods:** We reported four patients with HIV who were diagnosed with CMV-IRR soon after effective HAART. Plasma levels of CD4 T cells, HAART regimen, and other clinical and laboratory characteristics of the four patients were described. Patients were monitored for ocular manifestations and clinical signs under effective ocular and systemic anti-cytomegalovirus (CMV) and corticosteroid treatment for 12 months.

**Results:** With HAART, plasma levels of CD4 T cell counts rose remarkably. The mean baseline CD4 count of the four patients was 14.5 (range from 7 to 33) cells/ $\mu$ l before HAART and 183.25 (range from 153 to 220) cells/ $\mu$ l when diagnosed with CMV-IRR. Ophthalmic examination demonstrated severe vitreous opacities and necrotizing retinitis, intraretinal hemorrhages, and vasculitis. A large number of CMV sequencing was detected by DNA sequencing of vitreous samples. All four patients were recovered from CMV-IRR with anti-CMV and corticosteroid treatment.

**Conclusions:** Cytomegalovirus-immune recovery retinitis is a new diagnosis of HIV-associated ocular complication under HAART. These findings suggest that the immunological effects of HAART may accelerate the CMV retinitis in patients with very low initial CD4 T cell counts. HIV patients are recommended to have a thorough fundus examination before HAART initiation and a close follow-up especially in those with low CD4 counts to avoid the progression of CMV retinitis.

**Keywords:** cytomegalovirus retinitis, human immunodeficiency virus, highly active antiretroviral therapy, cytomegalovirus-immune recovery retinitis, case series

## INTRODUCTION

In the pre-highly active antiretroviral therapy (HAART) era, cytomegalovirus retinitis (CMVR) is the most common intraocular opportunistic infection in patients with Acquired Immune Deficiency Syndrome (AIDS) and occurs primarily in patients with an absolute CD4 counts <50 cells/ $\mu$ l. HAART was introduced in 1996 to treat HIV-infected patients by reducing HIV viral load

and increasing CD4 T cell counts. The most commonly used combination of HAART consists of one protease inhibitor and two reverse transcriptase inhibitors, resulting in increased life survival and a decrease in the incidence of CMVR.

Over the past 20 years, the HAART-mediated improvement of immune function in patients with AIDS may also alter the way in which the eye responds to cytomegalovirus (CMV), resulting in a change in the clinical manifestations of ocular CMV retinitis.

Immune reconstitution inflammatory syndromes (IRIS) represent an inflammatory response to an opportunistic pathogen in the context of immune recovery after initiating HAART (1). Immune recovery uveitis (IRU) is characterized by anterior segment and vitreous inflammatory reactions that are directed toward CMV antigens in ocular tissues, accompanied by cystoid macular edema (CME) and epiretinal membrane formation (2).

Immune recovery uveitis occurs in some patients with pre-existing CMVR due to the improved immune function associated with new potent antiretroviral. It has been described in the context of inactive retinitis several months to years after HAART initiation (3). In contrast, active CMV retinitis in immune reconstitution subjects had only been documented in a few case series with complex and severe retinal lesions and was postulated as an IRIS phenomenon, called “immune recovery retinitis” (4).

Therefore, in this retrospective study, we reported four patients with active CMV retinitis and severe vitritis in the context of a successful HAART regimen. They all had very low CD4 T cells before HAART initiation and were then developed to CMV-IRR within 8 weeks in good response to HAART. We depicted the clinical signs and the DNA sequencing of the vitreous body and followed up with them for 12 months with effective treatment.

## METHODS

### Patients and Methods

We reviewed four patients who attended our department and were diagnosed with active CMV-IRR with high CD4 counts under effective HAART from May 2019 to January 2021. We retrospectively studied the medical records of the four patients including clinical manifestations, ophthalmic examinations, and treatments. The study was approved by the institutional ethics committee of Huashan Hospital affiliated with Fudan University (protocol number: KY2021-837), and the treatment was performed under the tenets of the Declaration of Helsinki. The patients enrolled in the study signed the written informed consent for the publication of their data and examinations. Demographic data, CD4 cell counts, and current HAART regimen were all recorded. The CD4 counts were done using flow cytometry in all four patients. Ophthalmological examinations were performed using a slit lamp, fundoscopic investigation, fundus photographs, ocular B-ultrasound, and optic coherent tomography (OCT) (ZEISS, CIRRUS HD-OCT 4000, Germany).

## Signs and Symptoms of CMV-IRR

Diagnosis of IRIS was specified as follows: (1) good response to ART; (2) deterioration of an infectious condition related to ART initiation; and (3) inability to explain the symptoms.

Cytomegalovirus retinitis was defined by necrotizing retinitis, intraretinal hemorrhages, and vasculitis (manifested as yellow-white retinal lesions with granular border and hemorrhage along with vessels). Retinitis improvement was defined as the replacement of hemorrhages with atrophic scar (5). The location of the CMVR lesion was categorized into three zones. Zone 1 consisted of the area within 1,500  $\mu\text{m}$  of the edge of the optic nerve or within 3,000  $\mu\text{m}$  of the center of the fovea. Zone 2 was extended from the limits of zone 1 to a circle defined by the ampullae of the vortex veins. Zone 3 was extended from the limits of zone 2 to the ora serrata.

Patients with CMV-IRR were defined as those who developed CMV retinitis or worsening CMV retinitis with vitritis on successful HAART (4). The CMV-IRR was diagnosed by an experienced ophthalmologist by fundoscopic exploration and vitreous sample DNA sequencing (BGI, China).

Immune recovery uveitis was defined by completely healed CMV retinitis with any of the following types of ocular inflammation under successful ART: anterior uveitis, vitritis, papillitis, cystoid macular edema, or epiretinal membrane (6).

Moreover, HIV retinopathy, toxoplasmosis retinitis, acute retinal necrosis, progressive outer retinal necrosis, and syphilitic retinochoroiditis were excluded by laboratory assessment and fundus manifestations.

## Treatment of CMV-IRR

All four patients underwent three-port pars plana vitrectomy (PPV) for vitreous samples DNA sequencing with or without silicone oil tamponades. They all received appropriate anti-CMV therapy during the follow-up that includes oral ganciclovir (2 g/tid) and intravitreal injections. Intravitreal treatment regimen included ganciclovir (2 mg/0.1 ml) and dexamethasone (0.4 mg) injections (once a week for the first months and transferred once every other week until the lesion border was stable). All four patients received oral ganciclovir treatment for 6 months and the mean intravitreal injection was 7.25 times for an eye (range from 6 to 10).

## RESULTS

In our study, all four patients were progressed with active CMVR lesions with immune recovery within 8 weeks of HAART initiation. Characteristics of the four CMV-IRR patients with HIV positive are summarized in **Table 1**. Among the four patients, the mean CD4 T cells were 14.5/ $\mu\text{l}$  at the HIV diagnosis and 183.25/ $\mu\text{l}$  at the CMV-IRR diagnosis. All four patients had an obvious increase of CD4 T cells over 100/ $\mu\text{l}$  from a very low baseline ( $<40/\mu\text{l}$ ). They came to our ophthalmology department and presented with progressed blurred vision without any ophthalmological examination or treatment. The slit lamp showed vitritis and retinitis without anterior segment abnormalities. The vitreous activity was evaluated according to

**TABLE 1** | Characteristics of the four cytomegalovirus-immune recovery retinitis (CMV-IRR) patients with human immunodeficiency virus (HIV) positive.

	Patient			
	1	2	3	4
Age	54	40	50	40
Gender	Male	Male	Male	Male
AIDS diagnosis				
Eye with CMV-IRR	Right	Both	Both	Left
CD4 counts/ $\mu$ l				
Baseline	10	8	33	7
CVMR diagnosis	200	160	220	153
HAART				
Drug	AZT,3TC,EFV	3TC,DTG	3TC,EFV,TDF	3TC,EFV,TDF
Week	8	7	4	8
Visual acuity	R 20/166 L 20/25	R 20/50 L 20/40	R 20/25 L 20/50	R NLP L 20/66
IOP	R15 L16	R20 L17	R8 L8	L14
Vitreous	+++	++	++	++
CVMR region	Zone 2,3	Zone 2,3	Zone 2,3	Zone 1,2,3
Surgery	PPV+silicone oil tamponades	PPV+silicone oil tamponades	PPV	PPV
Intravitreal injection				
Drugs	Ganciclovir+TA	Ganciclovir+TA	Ganciclovir+TA	Ganciclovir+TA
Times	10	8	6	6
Surgery complications	NO	Retinal detachment	No	Vitreous hemorrhage
CMV copies	66,544	446,072	60,527	206,679
Outcomes after 12 months	R 20/100 L 20/25	R 20/20 L 20/20	R 20/25 L 20/40	R NLP L 20/50

3TC, Lamivudine; DTG, Dolutegravir; EFV, Efavirenz; TDF, Tenofovir; TA, dexamethasone; NLP, no light perception.

the grading system (1+ to 4+) proposed by Nussenblatt et al. (7). Fundus examination including mydriasis fundus examinations, ultrasound B scans, and OCT scans was performed in the four patients. The fundus showed typical necrotizing retinitis, intraretinal hemorrhages, and vasculitis (**Figure 1**, patient four). Three patients had retina lesions in zones 2 and 3, while the other patient had retina involvement in zones 1–3. OCT showed normal in one patient and a slight epiretinal membrane in macular in two patients. The other patient had a minor retinal neurosensory layer detachment in the macular (**Figures 2A–D**). Ultrasound B scans demonstrated obvious vitritis in all four patients (**Figures 3A–D**). PPV was done and vitreous samples were aspirated for next-generation sequencing. The results demonstrated a high copy of the CMV sequence ranging from 60,527 to 445,532.

Then, the patients underwent weekly intravitreal injection of ganciclovir 2 mg/0.1 ml plus steroids/dexamethasone 0.4 mg for the first month and shifted to biweekly till the lesion was stable. Oral use of ganciclovir was administered as 2 g tid for 6 months.

## Patient 1

A 54-year-old male experienced blurred vision in the right eye 2 months after HAART initiation (Zidovudine [AZT], Lamivudine [3TC], and Efavirenz [EFV]). CD4 counts were 200/ $\mu$ l. Visual Acuity (VA) was 20/166 in the right eye. Ophthalmic examination

showed retinal necrosis and hemorrhages with severe vitritis (++) in zones 2 and 3. OCT showed a slight epiretinal membrane in the macular of the right eye. He underwent PPV and silicone oil tamponades, and silicone oil removal was conducted 6 months later. Vitreous DNA sequencing showed CMV sequence of 66,544 copies. A total of 10 intravitreal injections were performed until the lesions were stable. His VA of the right eye was 20/100 at the last follow-up.

## Patient 2

A 40-year-old male experienced blurred vision and black shadows in both eyes 2 months after HAART initiation (3TC and Dolutegravir [DTG]). CD4 counts were 160/ $\mu$ l. VA was 20/50 in the right eye and 20/40 in the left eye. Ophthalmic examination showed retinal necrosis and hemorrhages with vitritis (++) in zones 2 and 3. OCT was normal in the macular. He underwent PPV and silicone oil tamponades in the left eye and ganciclovir and steroid intravitreal injections for both eyes. Afterward, immediate PPV and silicone oil tamponades were conducted in the opposite eye for secondary retinal detachment 1 month later. Vitreous DNA sequencing showed a CMV sequence of 446,072 copies. Silicone oil removal was conducted 4 months later for both eyes. Intravitreal injections were conducted eight times separately for both eyes. VA of the patient was 20/20 in both eyes at the last follow-up.



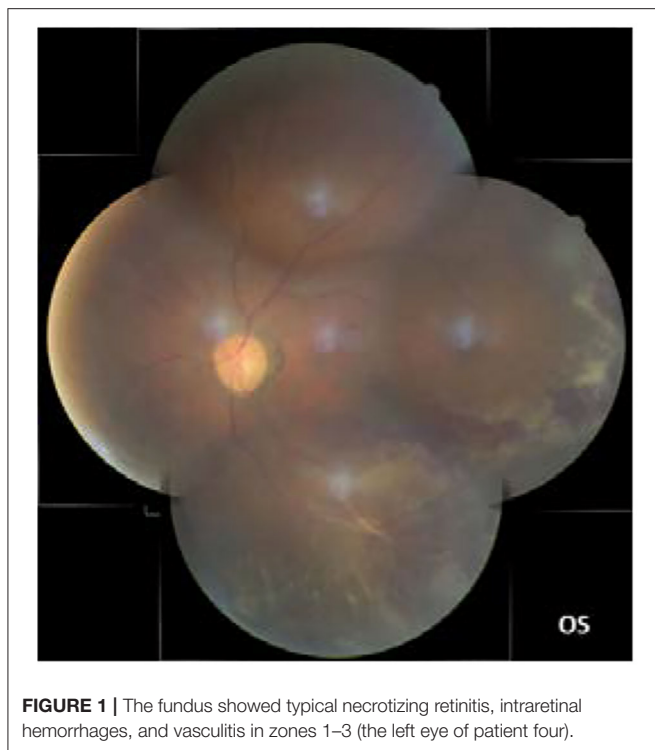


**FIGURE 1 |** The fundus showed typical necrotizing retinitis, intraretinal hemorrhages, and vasculitis in zones 1–3 (the left eye of patient four).

### Patient 3

A 50-year-old male experienced blurred vision for both eyes 4 weeks after HAART initiation (3TC, EFV, and TDF). He had the herpes zoster infection three times since 2014. CD4 counts were 220/ $\mu$ l. VA was 20/25 in the right eye and 20/50 in the left eye. Ophthalmic examination showed retinal necrosis with vitritis (++) in both eyes in zones 2 and 3. He underwent PPV and silicone oil tamponades in both eyes and intravitreal injections six times in total. Vitreous DNA sequencing showed a CMV sequence of 60,527 copies. Silicone oil removal was conducted 4 months later. VA of the patient was 20/25 in the right eye and 20/40 in the left eye at the last follow-up.

### Patient 4

A 40-year-old male experienced blurred vision in the left eye 6 weeks after HAART initiation (3TC, EFV, and TDF). CD4 counts were 153/ $\mu$ l. VA was 20/66 in the left eye. His right eye has no light perception since his youth for an unknown reason. Ophthalmic examination showed retinal necrosis and hemorrhages with vitritis (++) in zones 1–3. He underwent PPV and intravitreal injection for the left eye. Afterward, immediate PPV and silicone oil tamponades were operated on due to vitreous hemorrhage for retinal holes 1 week after surgery. Moreover, regular intravitreal injections were performed six times in total. Vitreous DNA sequencing showed a CMV sequence of 206,679 copies. Silicone oil removal was conducted 6 months later. His VA of the left eye was 20/50 at the last follow-up.

## DISCUSSION

In general, CMV retinitis was a severe opportunistic infection due to immunodeficiency with minimal intraocular inflammation, which has been extensively described in patients with HIV under ineffective treatment. We found that a small number of patients with CMV retinitis suffered retinitis progression and vitritis rapidly with HAART initiation. The results of this case series suggested that the pattern of CMVR of HIV patients might have changed by the introduction of HAART.

Traditionally, vitritis has not previously been associated with AIDS-related CMV retinitis. In 1997, Jacobson et al. firstly reported 5 cases of CMV retinitis with immune response 4–7 weeks after HAART (8). In their report, two patients had vitritis that was noted early in the course of the retinitis, and the vitritis occurred in patients who have a history of very low CD4 counts before HAART initiation. All 5 patients had recovered from the retinitis after a 7-month follow-up.

In 2014, Ruiz-Cruz et al. described a case series of patients with either new-onset CMV retinitis or CMV retinitis relapse (increasing border activity) soon after initiating HAART. They named it CMV-IRR, which could be described as a HAART-induced inflammatory immune response to subclinical CMV ocular infection (4). Most of them showed immune recovery, manifested as a rise of CD4 T cells and occurred within 2 months after HAART. Moreover, they suggested a hypothesis that active CMV retinitis might be an initial stage of a continual process leading to healed CMV retinitis observed in IRU.

However, some studies provided no evidence for the proposed “immune recovery retinitis.” The long-term result of CMVR in patients with HIV indicated that immune recovery with HAART can inactivate CMV retinitis lesions, even without anti-CMV drugs (9). The recent large-scale study by Gary et al. indicated that severe opacity was associated with lower CD4T-lymphocyte count and CMVR lesions were getting inactive after immune recovery with HAART (10). Tural et al. and MacDonald et al. demonstrated that some patients who responded to combined antiretroviral treatment with an increase in CD4 T-lymphocyte levels regained the ability to suppress CMV without specific anti-CMV therapy (11, 12).

Cytomegalovirus retinitis activity (indicated by the corresponding surface area) is accurately reflected by the presence and level of CMV DNA in aqueous humor and vitreous humor (13). In our study, among the thirty patients with CMV retinitis, four (13.3%) were progressed with active CMVR lesions with immune recovery within 8 weeks of HAART initiation. They all had a history of low CD4T cells and a subsequent good immunological response, indicating the immune recovery retinitis caused by the immune response of CMV infection. Furthermore, they suffered from severe vitritis and a high copy of CMV in the vitreous body, which demonstrated that an effective HAART regimen might fail to inactivate the CMV retinitis lesions.

Immune recovery uveitis emerges as a cause of visual morbidity in AIDS patients with pre-existing CMVR several months to years of initiation of HAART (14–17). Patients

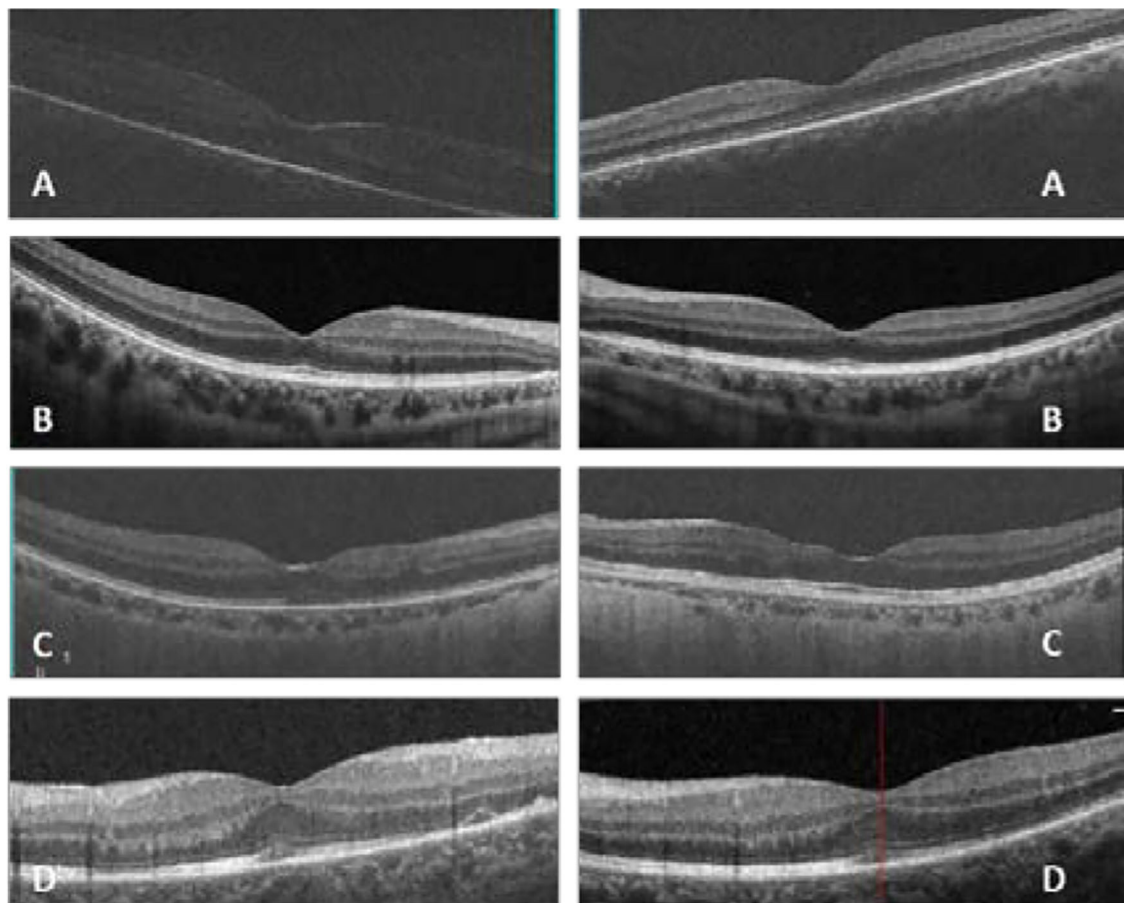


**FIGURE 2 |** In patient one (A), optic coherent tomography (OCT) showed an epiretinal membrane in macular in the right eye; in patient two (B), OCT was normal in macular in both eyes; in patient three (C), OCT showed a slight epiretinal membrane and inner retina disorder in macular in both eyes; in patient four (D), OCT showed a slight epiretinal membrane and a minor retinal neurosensory layer detachment in the left eye (Left: the right eye, right: the left eye, (D) shows only the left eye for the atrophy of the right eye).

with IRU were reported in the literature to have no active retinitis or detectable CMV DNA in peripheral blood (14). It is associated with the presence of inactive CMV retinitis, combination antiretroviral therapy with protease inhibitors, and evidence of at least partial immune reconstitution suggested by increased CD4<sup>+</sup> cell counts. The study by Robinson et al. showed that patients with IRU had a 10-fold increase in the mean CD4 T cell at the time of examination when compared with the mean CD4 T cell count at the time of diagnosis of CMV retinitis (18).

The reason for some patients showing CMV-IRR was still unknown. CMV-IRR may be caused by an immune response against persistent CMV antigen in the eye, while the immune response to CMV antigens varies a lot in patients (18). The possible mechanisms of CMV-IRR development could be summarized as follows: CMV retinitis causes a breakdown in the blood-ocular barrier and may allow migration of inflammatory cells into the eye. Patients with IRU might suffer from CMV retinitis or systemic CMV infection at a very low level of CD4 counts before HAART initiation. The good

immunological response and increased CD4 counts with HAART treatment activated the immune response to CMV antigens. The inflammation could be activated by CMV antigens expressed on latently infected cells, near the areas of previously active CMV retinitis. Schrier et al. previously have shown that this may be related to the predisposition to CMV retinitis (6). Further studies are necessary to evaluate the incidence and pathogenesis of this newly described syndrome.

Treatment of CMV-IRR has faced rigorous challenge with limited experience and severe retina inflammation and high intraocular CMV copies. Regular treatment of CMV retinitis includes systemic and ocular ganciclovir (topical and intravitreal). Traditionally, weekly injections are advised until active CMV retinitis lesions are resolved (19). The concentration of intravitreal ganciclovir varies from 0.4 to 4 mg/0.1 ml in different research studies (20–24). A successful approach in South Africa gave biweekly injections of 2 mg of ganciclovir for the first 2 weeks followed by weekly injections until immune reconstitution, and the patient has received systematic anti-CMV

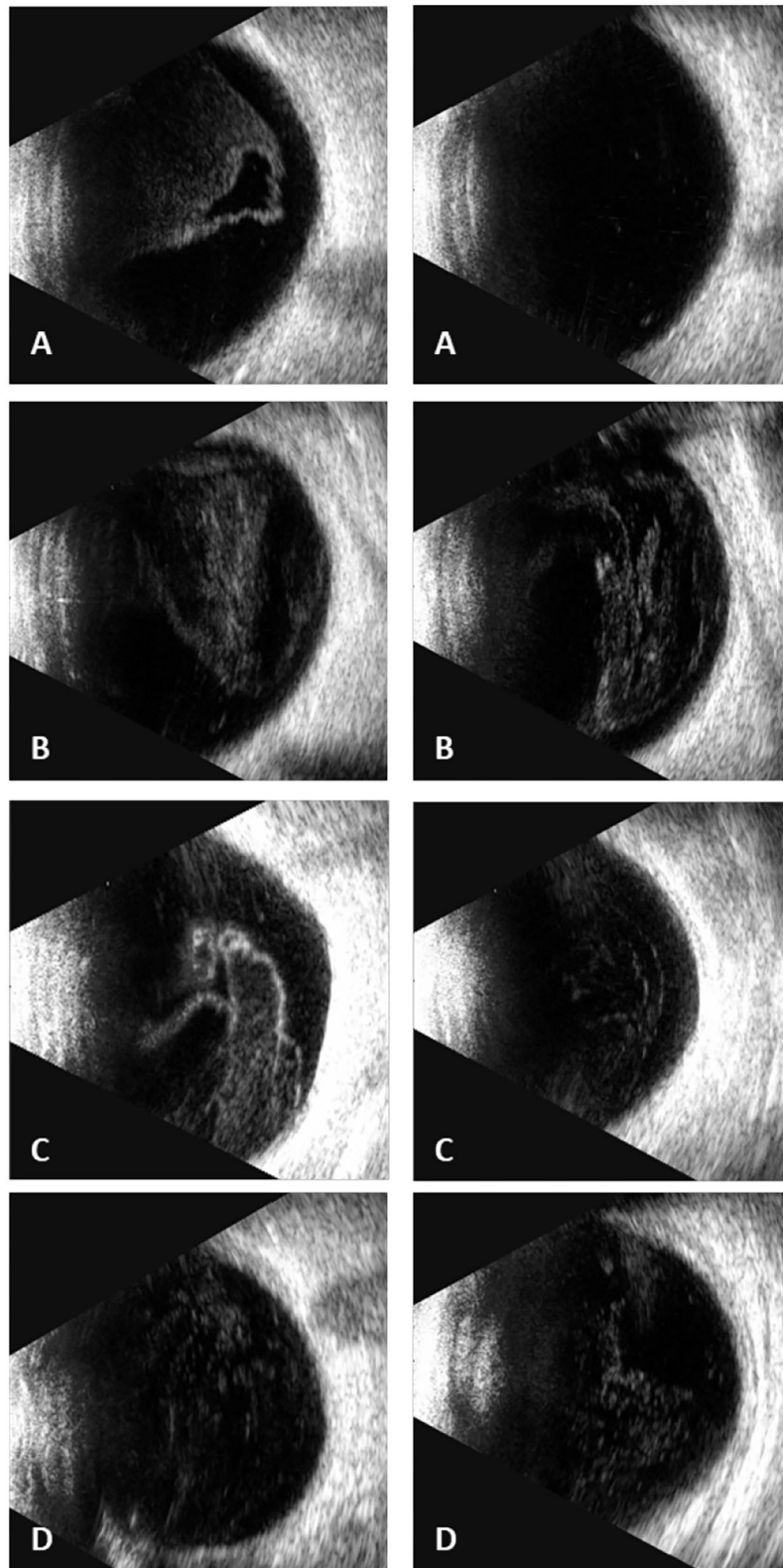


**FIGURE 3 |** Ultrasound B scans demonstrated severe vitritis in all four patients [(A) patient one, (B) patient two, (C) patient three, (D) patient four] (Left: the right eye; right: the left eye) [(D) shows only the left eye for the atrophy of the right eye].

treatment for at least 3 months (25). IRU with severe vitreous inflammation and/or CME typically was treated with periocular corticosteroids (triamcinolone acetonide 40 mg) or intravitreal corticosteroids without complications (26–28). Furthermore, some authors recommend restarting anti-CMV therapy to prevent CMV reactivation following corticosteroid treatment (3, 29). In our study, we combined intravitreal injection of ganciclovir with dexamethasone to suppress the high copies of CMV and severe vitritis and retinitis. Systemic corticosteroids and non-steroidal anti-inflammatory agents were not utilized because of relative immune compromise (30).

Ganciclovir is one of the optimal strategies in treating CMV retinitis. After diffusing into CMV-infected cells, ganciclovir is phosphorylated by the viral kinase UL97 and then further phosphorylated by cellular kinases to ganciclovir triphosphate, which inhibits the viral DNA polymerase UL54. To inhibit the replication of wild-type strains of CMV *in vitro*, the inhibitory concentration IC50 of Ganciclovir is 0.25–1.22 mg/l (31). Based on our experience and previous reports about CMV retinitis (22, 23), weekly intravitreal injection of 2 mg ganciclovir was effective and safe in most cases. The average intravitreal injections were 7.5 times (range from 6 to 10 times) in the four patients until retinal lesions were stable.

The presence of silicone oil in the vitreous cavity might have been a protective factor (26). It is fairly safe to assume that the ERM seen in our three patients was the result of vitritis inflammation (15). Recently, ERM formation has been recognized as an inflammatory complication of IRU by Studies of the Ocular Complications of AIDS and is being used as a diagnostic criterion in the definition of IRU (15, 26).

All four patients had immediate PPV with or without silicone oil tamponades due to severe retinal complications even under effective treatment. One patient with bilateral CMV-IRR had a retinal detachment in the non-PPV eye with routine intravitreal injections 1 month after the CMV-IRR diagnosis. Another patient suffered from vitreous hemorrhage because of retinal holes 1 week after PPV surgery (without silicone oil tamponades). They all had silicone oil removal 4–6 months after the surgery. Future studies with a larger sample size are needed to clarify the treatment and prognosis of the diseases. Regular ophthalmologic follow-up has been recommended at 3-month intervals for patients with HIV. Our patients had the incident of CMV-IRR within 2 months after HIV initiation. CMV-IRR was a newly diagnosed ocular complication with progressive retinitis and vitritis under effective HAART. Two of our patients developed vitreous hemorrhage or retinal detachment

during treatment. Thus, we suggested a closer ophthalmologic examination especially for those patients with CD4 counts less than 50 cells/ $\mu$ l. Pupil dilation and fundus examination should be performed to avoid missing the peripheral lesions.

## CONCLUSIONS

In conclusion, patients with HIV are recommended to have a thorough ophthalmic examination before HAART. Vitreous DNA sequencing should be adopted in patients with possible CMV retinitis lesions. Intravitreal ganciclovir and corticosteroids are safe and effective in CMV-IRR patients. PPV with silicone oil tamponades may be essential to avoid the complications of retinal detachment and vitreous hemorrhage.

## DATA AVAILABILITY STATEMENT

The original contributions presented in the study are included in the article/supplementary material, further inquiries can be directed to the corresponding author/s.

## ETHICS STATEMENT

The studies involving human participants were reviewed and approved by Huashan Hospital affiliated to Fudan University. The patients/participants provided their written informed consent to participate in this study. Written informed consent was obtained from the individual(s) for the publication of any potentially identifiable images or data included in this article.

## AUTHOR CONTRIBUTIONS

Research design was conducted by ZW, YQ, and HL. Data collection was undertaken by LW, YQ, and JJ. Data analysis and interpretation were performed by XC, YQ, and LW. The manuscript was finished by YQ, LW, JJ, JS, HW, XC, HL, and ZW and revised by ZW and HL. All authors contributed to the article and approved the submitted version.

## FUNDING

This study was supported by the National Natural Science Foundation of China NSFC, no. 81900897 and Shanghai Science and Technology 20Y11910800. The sponsor or funding organization had no role in the design or conduct of this research.

## REFERENCES

- Walker NF, Scriven J, Meintjes G, Wilkinson RJ. Immune reconstitution inflammatory syndrome in HIV-infected patients. *HIV AIDS*. (2015) 7:49–64. doi: 10.2147/HIV.S42328
- Dujic M, Jevtovic D. [Immune recovery vitritis]. *Srp Arh Celok Lek*. (2007) 135:513–5. doi: 10.2298/SARH0710513D
- Urban B, Bakunowicz-Lazarczyk A, Michalczyk M. Immune recovery uveitis: pathogenesis, clinical symptoms, and treatment. *Mediat Inflamm*. (2014) 2014:971417. doi: 10.1155/2014/971417
- Ruiz-Cruz M, Alvarado-de la Barrera C, Ablanedo-Terrazas Y, Reyes-Teran G. Proposed clinical case definition for cytomegalovirus-immune recovery retinitis. *Clin Infect Dis*. (2014) 59:298–303. doi: 10.1093/cid/ciu291
- Zambarakji HJ, Newson RB, Mitchell SM. CMVR diagnoses and progression of CD4 cell counts and HIV viral load measurements in HIV patients on HAART. *Brit J Ophthalmol*. (2001) 85:837–41. doi: 10.1136/bjo.85.7.837



6. Schrier RD, Song MK, Smith IL, Karavellas MP, Bartsch DU, Torriani FJ, et al. Intraocular viral and immune pathogenesis of immune recovery uveitis in patients with healed cytomegalovirus retinitis. *Retina*. (2006) 26:165–9. doi: 10.1097/00006982-200602000-00007
7. Nussenblatt RB, Palestine AG, Chan CC, Roberge F. Standardization of vitreal inflammatory activity in intermediate and posterior uveitis. *Ophthalmology*. (1985) 92:467–71. doi: 10.1016/S0161-6420(85)34001-0
8. Stein DS. Cytomegalovirus retinitis after initiation of highly active antiretroviral therapy. *Lancet*. (1997) 350:589–90. doi: 10.1016/S0140-6736(05)63176-5
9. Reed JB, Briggs JW, McDonald JC, Freeman WR, Morse LS. Highly active antiretroviral therapy-associated regression of cytomegalovirus retinitis: long-term results in a small case series. *Retina*. (2001) 21:339–43. doi: 10.1097/00006982-200108000-00007
10. Holland GN, Van Natta ML, Goldenberg DT, Ritts R Jr, Danis RP, et al. Relationship between opacity of cytomegalovirus retinitis lesion borders and severity of immunodeficiency among people with AIDS. *Invest Ophthalmol Vis Sci*. (2019) 60:1853–62. doi: 10.1167/iov.18-26517
11. Macdonald JC, Karavellas MP, Torriani FJ, Morse LS, Smith IL, Reed JB, et al. Highly active antiretroviral therapy-related immune recovery in AIDS patients with cytomegalovirus retinitis. *Ophthalmology*. (2000) 107:877–81; discussion: 881–3. doi: 10.1016/S0161-6420(00)0023-3
12. Tural C, Romeu J, Sirera G, Andreu D, Conejero M, Ruiz S, et al. Long-lasting remission of cytomegalovirus retinitis without maintenance therapy in human immunodeficiency virus-infected patients. *J Infect Dis*. (1998) 177:1080–3. doi: 10.1086/517399
13. Smith IL, Macdonald JC, Freeman WR, Shapiro AM, Spector SA. Cytomegalovirus (CMV) retinitis activity is accurately reflected by the presence and level of CMV DNA in aqueous humor and vitreous. *J Infect Dis*. (1999) 179:1249–53. doi: 10.1086/314710
14. Kempen JH, Min YI, Freeman WR, Holland GN, Friedberg DN, Dietherich DT, et al. Risk of immune recovery uveitis in patients with AIDS and cytomegalovirus retinitis. *Ophthalmology*. (2006) 113:684–94. doi: 10.1016/j.opthta.2005.10.067
15. Karavellas MP, Lowder CY, Macdonald C, Avila CP Jr, Freeman WR. Immune recovery vitritis associated with inactive cytomegalovirus retinitis: a new syndrome. *Arch Ophthalmol*. (1998) 116:169–75. doi: 10.1001/archophth.116.2.169
16. Karavellas MP, Plummer DJ, Macdonald JC, Torriani FJ, Shufelt CL, Azen SP, et al. Incidence of immune recovery vitritis in cytomegalovirus retinitis patients following institution of successful highly active antiretroviral therapy. *J Infect Dis*. (1999) 179:697–700. doi: 10.1086/314639
17. Sudharshan S, Kaleemunnisha S, Banu AA, Shrikrishna S, George AE, Babu BR, et al. Ocular lesions in 1,000 consecutive HIV-positive patients in India: a long-term study. *J Ophthalmic Inflamm Infect*. (2013) 3:2. doi: 10.1186/1869-5760-3-2
18. Robinson MR, Reed G, Csaky KG, Polis MA, Whitcup SM. Immune-recovery uveitis in patients with cytomegalovirus retinitis taking highly active antiretroviral therapy. *Am J Ophthalmol*. (2000) 130:49–56. doi: 10.1016/S0002-9394(00)00530-4
19. Ausayakhun S, Yuvaves P, Ngamtiphakom S, Prasitsilp J. Treatment of cytomegalovirus retinitis in AIDS patients with intravitreal ganciclovir. *J Med Assoc Thai*. (2005) 88(Suppl. 9):S15–20.
20. Agarwal A, Kumari N, Trehan A, Khadwal A, Dogra MR, Gupta V, et al. Outcome of cytomegalovirus retinitis in immunocompromised patients without Human Immunodeficiency Virus treated with intravitreal ganciclovir injection. *Graefes Arch Clin Exp Ophthalmol*. (2014) 252:1393–401. doi: 10.1007/s00417-014-2587-5
21. Ociecek P, Barnacle JR, Gumulira J, Phiri S, Heller T, Grabska-Liberek I. Cytomegalovirus retinitis screening and treatment in human immunodeficiency virus patients in Malawi: a feasibility study. *Open Forum Infect Dis*. (2019) 6:ofz439. doi: 10.1093/ofid/ofz439
22. Choopong P, Vivittaworn K, Konlakij D, Thoongsuwan S, Pitukung A, Tesavibul N. Treatment outcomes of reduced-dose intravitreal ganciclovir for cytomegalovirus retinitis. *BMC Infect Dis*. (2016) 16:164. doi: 10.1186/s12879-016-1490-6
23. Xie LY, Chen C, Kong WJ, Du KF, Guo CG, Dong HW, et al. Effect of individualized therapy for AIDS patients with cytomegalovirus retinitis in intravitreal ganciclovir injections. *Int J Ophthalmol*. (2019) 12:1351–5. doi: 10.18240/ijo.2019.08.19
24. Yutthitham K, Ruamviboonsuk P. The high-dose, alternate-week intravitreal ganciclovir injections for cytomegalovirus retinitis in acquired immune deficiency syndrome patients on highly active antiretroviral therapy. *J Med Assoc Thai*. (2005) 88(Suppl. 9):S63–8.
25. Visser L. Managing CMV retinitis in the developing world. *Community Eye Health*. (2003) 16:38–9.
26. Karavellas MP, Azen SP, Macdonald JC, Shufelt CL, Lowder CY, Plummer DJ, et al. Immune recovery vitritis and uveitis in AIDS: clinical predictors, sequelae, treatment outcomes. *Retina*. (2001) 21:1–9. doi: 10.1097/00006982-200102000-00001
27. El-Bradey MH, Cheng L, Song MK, Torriani FJ, Freeman WR. Long-term results of treatment of macular complications in eyes with immune recovery uveitis using a graded treatment approach. *Retina*. (2004) 24:376–82. doi: 10.1097/00006982-200406000-00007
28. Henderson HW, Mitchell SM. Treatment of immune recovery vitritis with local steroids. *Brit J Ophthalmol*. (1999) 83:540–5. doi: 10.1136/bjo.83.5.540
29. Holland GN. AIDS and ophthalmology: the first quarter century. *Am J Ophthalmol*. (2008) 145:397–408. doi: 10.1016/j.ajo.2007.12.001
30. Jabs DA, Ahuja A, Van Natta M, Lyon A, Srivastava S, Gangaputra S, et al. Course of cytomegalovirus retinitis in the era of highly active antiretroviral therapy: five-year outcomes. *Ophthalmology*. (2010) 117:2152–61.e1–2. doi: 10.1016/j.opthta.2010.03.031
31. Carmichael A. Cytomegalovirus and the eye. *Eye*. (2012) 26:237–40. doi: 10.1038/eye.2011.327

**Conflict of Interest:** The authors declare that the research was conducted in the absence of any commercial or financial relationships that could be construed as a potential conflict of interest.

**Publisher's Note:** All claims expressed in this article are solely those of the authors and do not necessarily represent those of their affiliated organizations, or those of the publisher, the editors and the reviewers. Any product that may be evaluated in this article, or claim that may be made by its manufacturer, is not guaranteed or endorsed by the publisher.

Copyright © 2022 Qian, Wang, Jiang, Suo, Weng, Che, Lu and Wang. This is an open-access article distributed under the terms of the Creative Commons Attribution License (CC BY). The use, distribution or reproduction in other forums is permitted, provided the original author(s) and the copyright owner(s) are credited and that the original publication in this journal is cited, in accordance with accepted academic practice. No use, distribution or reproduction is permitted which does not comply with these terms.



# Differences in Vitreous Protein Profiles in Patients With Proliferative Diabetic Retinopathy Before and After Ranibizumab Treatment

Xinping She<sup>1†‡</sup>, Chen Zou<sup>2‡</sup> and Zhi Zheng<sup>1\*</sup>

<sup>1</sup> Shanghai Key Laboratory of Ocular Fundus Diseases, Department of Ophthalmology, Shanghai General Hospital, Shanghai Jiao Tong University School of Medicine, National Clinical Research Center for Eye Diseases, Shanghai Engineering Center for Visual Science and Photomedicine, Shanghai Engineering Center for Precise Diagnosis and Treatment of Eye Diseases, Shanghai, China, <sup>2</sup> Eye Institute, Eye and ENT Hospital, Shanghai Medical College, Fudan University, Shanghai, China

## OPEN ACCESS

### Edited by:

Hetian Lei,  
Shenzhen Eye Hospital, China

### Reviewed by:

Matthew P. Simunovic,  
The University of Sydney, Australia  
Katelyn Swindle-Reilly,  
The Ohio State University,  
United States

### \*Correspondence:

Zhi Zheng  
zzheng88@sjtu.edu.cn

### †ORCID:

Xinping She  
orcid.org/0000-0001-7803-2246

‡These authors have contributed  
equally to this work

### Specialty section:

This article was submitted to  
Ophthalmology,  
a section of the journal  
Frontiers in Medicine

Received: 14 September 2021

Accepted: 29 April 2022

Published: 27 May 2022

### Citation:

She X, Zou C and Zheng Z (2022)  
Differences in Vitreous Protein Profiles  
in Patients With Proliferative Diabetic  
Retinopathy Before and After  
Ranibizumab Treatment.  
Front. Med. 9:776855.  
doi: 10.3389/fmed.2022.776855

Proliferative diabetic retinopathy (PDR) accounts for severe impact on vision, its mechanism is still poorly understood. To compare the differences of vitreous protein profiles in PDR patients before and after a complete anti-vascular endothelial growth factor (VEGF) loading dose with ranibizumab treatment. Twelve vitreous humor (VH) samples were collected from six PDR patients before (set as pre group) and after (set as post group) intravitreal injection of ranibizumab (IVR) treatment. LC-MS/MS and bioinformatics analysis were performed to identify differentially expressed proteins. Proteins were validated with targeted proteomics using parallel reaction monitoring (PRM) in a validation set consisting of samples from the above patients. A total of 2680 vitreous proteins were identified. Differentially expressed proteins were filtrated with fold change  $\geq 2.0$  (post group/ pre group protein abundance ratio  $\geq 2$  or  $\leq 0.5$ ) and  $p$ -value  $< 0.05$ . 11 proteins were up-regulated and 17 proteins were down-regulated, while consistent presence/absence expression profile group contains one elevated protein and nine reduced proteins, among which seven proteins were identified as potential biomarkers for IVR treatment through PRM assays. Bioinformatics analysis indicated the up-regulated proteins were significantly enriched in “GnRH secretion” and “Circadian rhythm” signaling pathway. This report represents the first description of combined label-free quantitative proteomics and PRM analysis of targeted proteins for discovery of different proteins before and after IVR treatment in the same patient. IVR treatment may protect against PDR by promoting SPP1 expression through “GnRH secretion” and “Circadian rhythm” signaling pathway.

**Keywords:** proliferative diabetic retinopathy, proteomics, ranibizumab, label-free, LC-MS/MS, PRM

## BACKGROUND

Diabetic retinopathy (DR) is the leading cause of blindness among working age people (1–4). The worldwide prevalence of DR has been estimated to be 34.6% in patients with diabetes, and the prevalence of vision-threatening DR, such as proliferative diabetic retinopathy (PDR) has been estimated to be 6.96% (5). PDR is the worst

stage of DR, it may lead to devastating complications, such as vitreous hemorrhage or tractional retinal detachment.

Several studies have shown that vascular endothelial growth factor (VEGF) is a crucial causative factor of PDR (6, 7). Ranibizumab is a specific anti-VEGF drug, it is an engineered, humanized and recombinant antibody fragment binding closely to all VEGF-A isoforms. Preoperative intravitreal injection of ranibizumab (IVR) treatment significantly reduces the occurrence of intraoperative and postoperative complications (8). A meta-analysis of 14 randomized controlled trials indicated that anti-VEGF pretreatment before vitrectomy greatly facilitated surgery (9). Another network meta-analysis revealed that preoperative anti-VEGF pretreatment showed the best treatment effect (10). However, the molecular mechanism is not completely clear. We previously reported that preoperative IVR treatment in patients with severe PDR contributes to a decreased risk of postoperative neovascular glaucoma (11), and found further changes in vitreous protein profiles of PDR patients treated with and without IVR (12). While there have been no reports on the changes in vitreous humor (VH) protein profile before and after IVR treatment in the same patient. Taking the influence of individual differences into account, the VH samples of the same patient before and after IVR treatment were tested, then the identified differences can be considered to be entirely caused by IVR. This is a research topic worthy of further study. Thus, it is of interest to study differences of vitreous protein profile in PDR patients before and after ranibizumab treatment.

Proteomics have been widely applied for global analysis of proteins (13), and it has great value for studying the effects of DR (14, 15). Label-free quantification is a type of quantitative mass spectrometry method. This technology does not require expensive isotope labels as internal standards, but it improves the detection efficiency of low-abundance proteins and the accuracy of protein quantification. Using label-free quantification technology, the sample loading volume is small. In recent years, label-free quantification has been commonly applied for the study of DR (16–18). Parallel reaction monitoring (PRM) is an ion monitoring technology based on high-resolution and high-precision MS. Compared with western blotting and ELISA, it has higher sensitivity and higher resolution and unlike these other methods, it can be used for the simultaneous detection of multiple target proteins without the need for antibodies (19). Therefore, it is often used as a verification method.

In this study, 12 vitreous samples were collected from six PDR patients before and after IVR treatment, and label-free technology combined with PRM target validation was used to conduct proteomic analysis of and assess the VH samples. This study aimed to identify differences in vitreous protein profiles in patients with PDR before and after IVR treatment and to

further reveal the potential therapeutic targets of ranibizumab in PDR patients.

## MATERIALS AND METHODS

### Patients and Sample Collection

Six PDR patients who required vitrectomy were recruited from the department of ophthalmology, Shanghai General Hospital. The protocol was approved by the Research Ethics Committee of Shanghai General Hospital (Ethical approval number: 2021KY031). Signed informed consent was obtained from all patients, and the experimental procedures followed the tenets of the declaration of Helsinki. Patients' rights to privacy were protected in this study. All of the PDR participants were screened according to the expert consensus for the prevention and treatment of DR. Examinations were carried out by a professional ophthalmologist after pupil dilation. Clinical characteristics of the study population are shown in **Table 1**.

The inclusion and exclusion criteria were as follows. Patients who met the diagnostic criteria of PDR with vitreous hemorrhage were eligible for inclusion in the study. Eyes that received laser or intraocular injection therapy within 3 months were excluded; patients with retinal vein occlusion, retinopathy of prematurity, sickle cell retinopathy, familial exudative retinopathy and other retinal vascular diseases were excluded.

Before IVR treatment, we used 25G vitreous cutter (Constellation; Alcon Instruments, Inc., Fort Worth, TX, USA) to collect 0.25–0.3 mL VH without any infusion, and these VH samples were used as the pre group. A portion of the VH was extracted to make room for the injection of ranibizumab, and 0.5 mg/0.05 mL ranibizumab (Lucentis; Novartis Pharma Schweiz AG Inc., Schaffhauserstrasse 4332 Stein, Switzerland) was injected. Three days later, we used 25G vitreous cutter to collect 0.25–0.3 mL VH without any infusion before pars plana vitrectomy (PPV), and which were used as the post group. After obtaining the vitreous sample, we immediately performed a centrifugation. 0.25–0.3 mL of undiluted VH was centrifuged for 10 min at 4 °C and 15000 rpm; then the supernatant was stored in liquid nitrogen and analyzed later. Sample processing refers to the method in our previous publication (12).

### Sample Processing

VH samples were lysed according to the FASP procedure (20), and proteins were extracted by using buffer 1 (4% SDS, 100 mM Tris-HCl, 1 mM DTT; pH 7.6). The concentration of protein was quantified with the BCA Protein Assay Kit (Bio-Rad, USA). A filter-aided sample preparation procedure (20) was used for protein digestion. 200 µg of protein from each sample was added to 30 µL buffer 2 [4% SDS, 100 mM DTT, 150 mM Tris-HCl (pH 8.0)]. Protein suspensions were digested with 4 µg trypsin (Promega) in 40 µL 25 mM NH<sub>4</sub>HCO<sub>3</sub> buffer overnight at 37°C. The peptides were desalted on C18 cartridges [Empore™ SPE Cartridges C18 (Sigma)], concentrated by vacuum centrifugation and reconstituted in 40 µL of 0.1% (v/v) formic acid. UV light spectral density at 280 nm was used to estimate the peptide content.

**Abbreviations:** DR, Diabetic retinopathy; PDR, Proliferative DR; IVR, Intravitreal injection of ranibizumab; VH, Vitreous humor; PRM Parallel reaction monitoring; PPV Pars plana vitrectomy; GO, Gene ontology; KEGG, Kyoto Encyclopedia of Genes and Genomes; PPI, Protein–protein interaction; FC, Fold change; BP, Biological processes; MF, Molecular functions; CC Cellular components; TIMS, trapped ion mobility spectrometry.

**TABLE 1** | Clinical characteristics of the patients.

Patient	Gender	Age(years)	Diabetes course(years)	Surgical eye	Vision	IOP(mmHg)
5	M	33	2	OS	HM	17.4
6	M	31	13	OS	0.4	16.2
7	M	46	13	OD	HM	12.3
8	F	60	5	OD	0.25	12.5
9	M	53	20	OD	0.01	16.5
10	F	27	8	OD	0.04	12.1

IOP, intraocular pressure.

**TABLE 2** | Maxquant identification and quantification parameter table.

Item	Value
Enzyme	Trypsin
Max missed cleavages	2
Main search	6 ppm
First search	20 ppm
MS/MS tolerance	20 ppm
Fixed modifications	Carbamidomethyl (C)
Variable modifications	Oxidation (M)
Database	Swissprot_Homo_sapiens_20395_20210106.fasta
Database pattern	Reverse
Include contaminants	TRUE
Protein FDR	≤0.01
Peptide FDR	≤0.01
Peptides used for protein quantification	Use razor and unique peptides
Time window (match between runs)	2 min
protein quantification	LFQ
min. ratio count	1

Label-free quantification analysis was performed on a trapping ion mobility mass spectrometer (Bruker, timsTOF™ Pro). The mass spectrometer was operated in positive ion mode. A Pierce high pH reversed-phase fractionation kit (Thermo Scientific) was used to fractionate samples into six fractions by increasing acetonitrile step-gradient elution according to the instructions. MS data were acquired using a data-dependent top 10 method by dynamically choosing the most abundant precursor ions from the survey scan (100–1700 m/z) for higher-energy C-trap dissociation fragmentation. The raw MS data for each sample were combined and searched using MaxQuant 1.5.3.17 software. Parameters and instructions are shown in **Table 2**.

## Bioinformatics Analysis

Hierarchical clustering analysis was performed by using Cluster 3.0 and Java TreeView software. The protein sequences of the selected differentially expressed proteins were locally searched using NCBI BLAST and InterProScan to find homologous

sequences. Gene Ontology (GO) terms were mapped, and the sequences were annotated using the software program Blast2GO (<https://www.blast2go.com/>). The GO annotation results were plotted by R scripts. Proteins were blasted against the online Kyoto Encyclopedia of Genes and Genomes (KEGG) database (<http://geneontology.org/>) to retrieve their KEGG orthology identifications. Enrichment analysis was performed based on Fisher's exact test. Protein–protein interactions (PPIs) were retrieved from the IntAct molecular interaction database using gene symbols or STRING software, and *P*-values <0.05 were considered significant.

## Validation of Proteomic Analysis

To further verify the LC-MS/MS results, PRM analysis was performed for the same samples used in the MS discovery phase ( $n = 6$  in both the post group and pre group) by using a high-resolution Q-Exactive HF mass spectrometer (Thermo Scientific, USA). The isotope relabeling peptide (PRTC:GLILVGGYGTR) was spiked in each sample and used as a standard internal reference. The original PRM files were analyzed using SKYLINE 3.5.0 software.

## Statistics

IBM SPSS 20.0 (SPSS, Inc., USA) and SAS (version 9.4) were used for statistical analysis. The Venn diagram was generated using an online tool developed by the Van de Peer Laboratory (Bioinformatics & Evolutionary Genomics). Comparisons among groups were conducted using paired sample *t*-test. Definition of proteins with present or absent expression was that, two or more times in one set of samples are not null values, and all the data in the other set are null values. Quantifiable proteins can be defined as more than half of the biological replicates have quantitative information. When screening differentially expressed proteins, the criterion of fold change (FC) >2 times or FC <0.5 times, and *P*-value <0.05 was applied.

## RESULTS

### Identification and Quantification of Protein Profiles

A total of 2680 VH proteins were identified in this study (**Supplementary Table S1**). Among these proteins, 13 were found solely in the post group, 101 were found solely in the pre



group, and the other 2566 proteins were found in both the pre group and post group (Figure 1A). Venn diagrams were used to analyze the overlap of proteins between the pre group and post group (Figures S1A,B).

A total of 38 proteins were differentially expressed in the post group compared with the pre group, including 11 up-regulated and 17 down-regulated, one only found in POST-group and nine excluded to PRE-group (Figure 1B). Significantly down-regulated proteins are marked in blue ( $FC < 0.5$  and  $P < 0.05$ ), while significantly up-regulated proteins are marked in red ( $FC > 2.0$  and  $P < 0.05$ ) in the volcano plot in Figure 1C. The database species used was Swissprot\_Homo\_sapiens\_20395\_20210106.fasta.

## GO Function Analysis of Differentially Expressed Proteins

A total of 1874 GO terms related to all 38 differentially expressed proteins were identified using Blast2GO software (Supplementary Table S2). Furthermore, the number of differentially expressed proteins was determined according to GO secondary function annotation. Among the GO secondary functions, 20 subcategories were in the biological process (BP) category, 7 were in the molecular function (MF) category and 13 were in the cellular component (CC) category. The top GO terms from each category were selected (Figure 2A). The predominant term in the BP category was “cellular process” (33 proteins), followed by “biological regulation” (29 proteins), “regulation of biological process” (28 proteins), “metabolic process” (28 proteins), “response to stimulus” (25 proteins), and “positive regulation of biological process” (21 proteins). The largest number of proteins were involved in the MF “binding” (30 proteins), followed by “catalytic activity” (17 proteins). The largest number of proteins were enriched in the CCs “cell part” (37 proteins) and “cell” (37 proteins), followed by “organelle” (28 proteins).

To reveal the overall functional enrichment characteristics of all differentially expressed proteins and to identify the most important significantly enriched GO terms, Fisher’s exact test ( $P < 0.05$ ) was applied to perform enrichment analysis of the differentially expressed proteins. The BP term that exhibited the most significant change in enrichment was “phagocytosis, recognition,” the MF term that exhibited the most significant change in enrichment was “intramolecular oxidoreductase activity,” and the CC term that exhibited the most significant change in enrichment was “DSIF complex” (Fig 2B–D). The main proteins involved were immunoglobulin heavy variable 3–23 (IGHV3-23), RNA-splicing ligase RtcB homolog (RTCB), osteopontin (SPP1), thymidine phosphorylase (TYMP), proactivator polypeptide-like 1 (PSAPL1), puromycin-sensitive aminopeptidase (NPEPPS), and complement C1q subcomponent subunit A (C1QA).

## KEGG Pathway Analysis

All 38 differentially expressed proteins were blasted against the online KEGG database and were subsequently mapped to KEGG pathways.

As shown in Figure 3A, the most notable pathway was “Protein processing in endoplasmic reticulum” (four proteins), followed by “Prion disease” (three proteins), “GnRH secretion” (two proteins), “NF-kappa B signaling pathway” (two proteins), and “Wnt signaling pathway” (two proteins). Furthermore, we used Fisher’s exact test ( $P < 0.05$ ) to perform KEGG pathway enrichment analysis of the 38 differentially expressed proteins. The results showed that “GnRH secretion” exhibited the most significant change in enrichment followed by “NF-kappa B signaling pathway” and “Protein processing in endoplasmic reticulum” (Figure 3B).

To better investigate the significance of the differences in the pathways for which the differentially expressed proteins were enriched, we performed KEGG pathway and pathway enrichment analyses of the up-regulated and down-regulated proteins separately (Figure 3C). The down-regulated proteins were significantly enriched in “Prion disease” (three proteins,  $P = 0.0417$ ), while the up-regulated proteins were significantly enriched in “GnRH secretion” (two proteins,  $P = 0.0020$ ), “Circadian rhythm” (one protein,  $P = 0.0461$ ).

## Protein Interaction Network Analysis

The PPI network diagram showed that 28 of the 38 differentially expressed proteins were involved in the interactive network (Figure 4). According to intergroup analysis and comparison, the proteins ACTB (Actin, cytoplasmic 1), SPP1 and PTGES3 (Prostaglandin E synthase 3) had larger circles than the other proteins, indicating that they might be the key points that affect the metabolic or signal transduction pathways of the entire system.

## Verification of Candidate Proteins by PRM

Seven proteins that showed significant changes in expression, including IGHV3-23, RTCB, SPP1, TYMP, PSAPL1, NPEPPS, C1QA, were examined by PRM. These proteins had larger FC values and are associated with potentially important biological functions related to angiogenesis, proliferation, and fibrosis. The expression of three of the proteins (IGHV3-23, RTCB, SPP1) was up-regulated in the post group compared with the pre group, and the expression of four proteins (TYMP, PSAPL1, NPEPPS, C1QA) was down-regulated in the post group compared with the pre group. We found that the overall trends of the label-free quantification and PRM results were consistent (Figure 5, Supplementary Table S4). The consistency of the PRM and label-free quantification results indicated the reliability of our proteomic data. Information such as peptide, precursor Mz, fragment ion, areas and other original data are shown in Supplementary Table S3. Targeted peptide Skyline analysis results were shown in Supplementary Figure S2.

## DISCUSSION

In our present study, a total of 38 significant differentially expressed proteins were identified in the VH of PDR patients collected before and after IVR treatment. In our previous study, we identified differentially expressed proteins between PDR patients who received anti-VEGF therapy and those who did

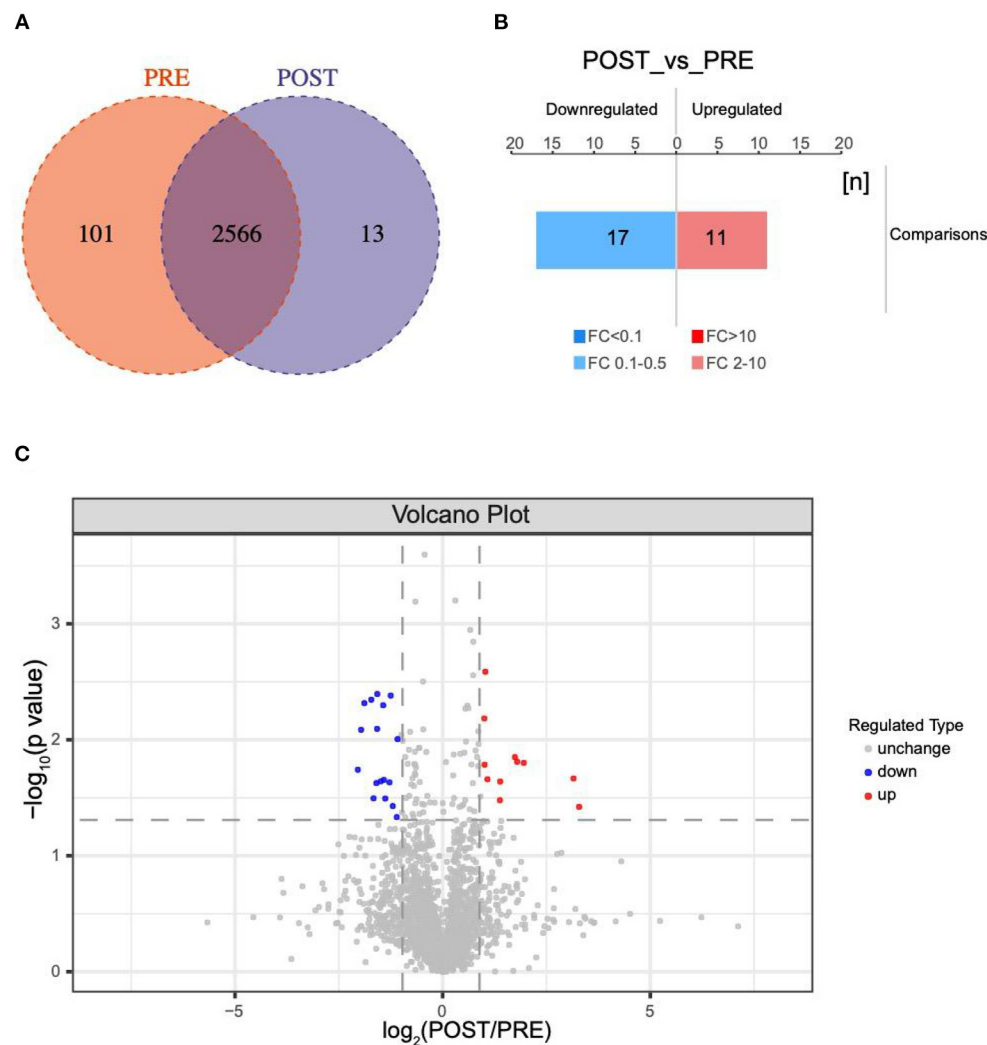


**FIGURE 1 |** Changes in protein profiles before and after IVR treatment. **(A)** Venn diagram of differentially expressed proteins between the post group and pre group; **(B)** Histogram showing quantitative differences in protein expression between the post group and pre group. Significantly down-regulated proteins are marked in blue ( $FC < 0.5$  and  $P < 0.05$ ), and significantly up-regulated proteins are marked in red ( $FC > 2$  and  $P < 0.05$ ); **(C)** Volcano plot showing the significant differences in protein expression between the post group and pre group ( $P < 0.05$ ).

not (12, 21). However, in those two studies, the treated samples and untreated samples were collected from different patients. The design of our study is a paired sample, which compares the preoperative and postoperative samples of the same person.

Bioinformatics analysis indicated that the most significantly enriched BP was “phagocytosis, recognition.” The signaling pathway that most significantly enriched was “protein processing in endoplasmic reticulum.”

We further analyzed the up-regulated proteins and down-regulated proteins among the 38 differentially expressed proteins separately using the database. The up-regulated proteins were significantly enriched in “GnRH secretion” and “Circadian rhythm” signaling pathway.

Among the differentially expressed proteins identified by LC-MS/MS, we were particularly interested in seven proteins

(IGHV3-23, RTCB, SPP1, TYMP, PSAPL1, NPEPPS, C1QA). These proteins play critical roles in angiogenesis, proliferation, and fibrosis, which are all closely associated with the development of PDR. However, the role of these proteins in the pathogenesis of DR is unclear. In our study, we verified the differential expression of these candidate proteins by PRM, and the results were generally consistent with those obtained by LC-MS/MS. These results suggest that these proteins may be important in the pathogenesis of DR.

IGHV3-23 belongs to a group of approximately 40 functional variable (V) genes in the immunoglobulin heavy chain locus on chromosome 14, and the variable domain participates in antigen recognition. IGHV3-23 may play a pathologically relevant role in the occurrence or progression of thymic MALT lymphoma (22). In chronic lymphocytic leukemia, IGHV3 gene is being

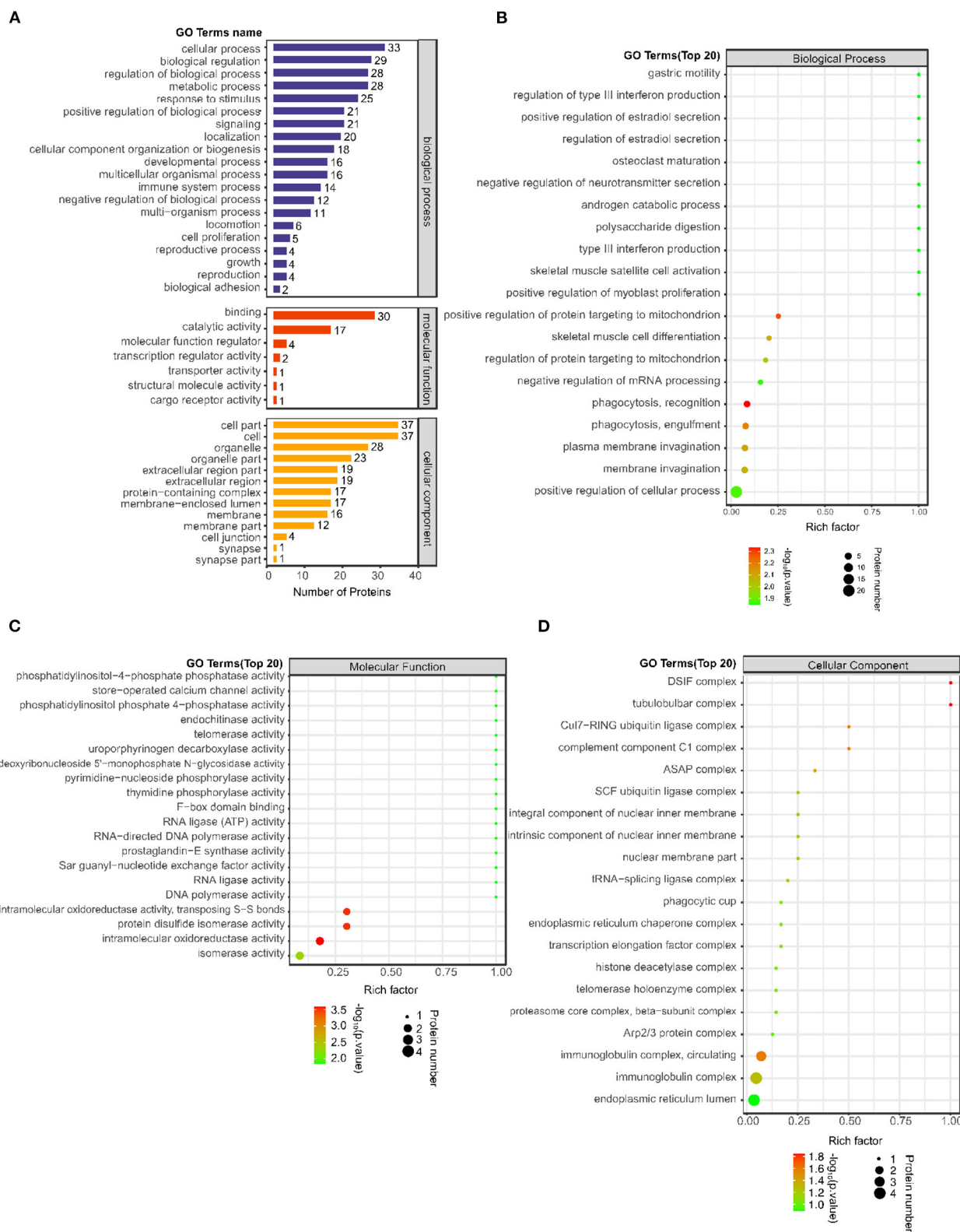


**FIGURE 2 |** Number of differentially expressed proteins on the GO secondary function annotation level and Top 20 GO terms between the post IVR group and pre IVR group. **(A)** Graph of GO annotation of the differentially expressed proteins according to GO secondary function annotation. BPs, MFs and CCs are shown in blue, red and orange, respectively; **(B–D)** Bubble charts showing the results of enrichment analysis of BPs, MFs, and CCs for the differentially expressed proteins using Fisher's exact test ( $P < 0.05$ ). The color represents the  $P$ -value (take  $-\log_{10}$ ); the closer the color is to red, the smaller the  $P$ -value and the higher the significance of the enrichment of the corresponding.

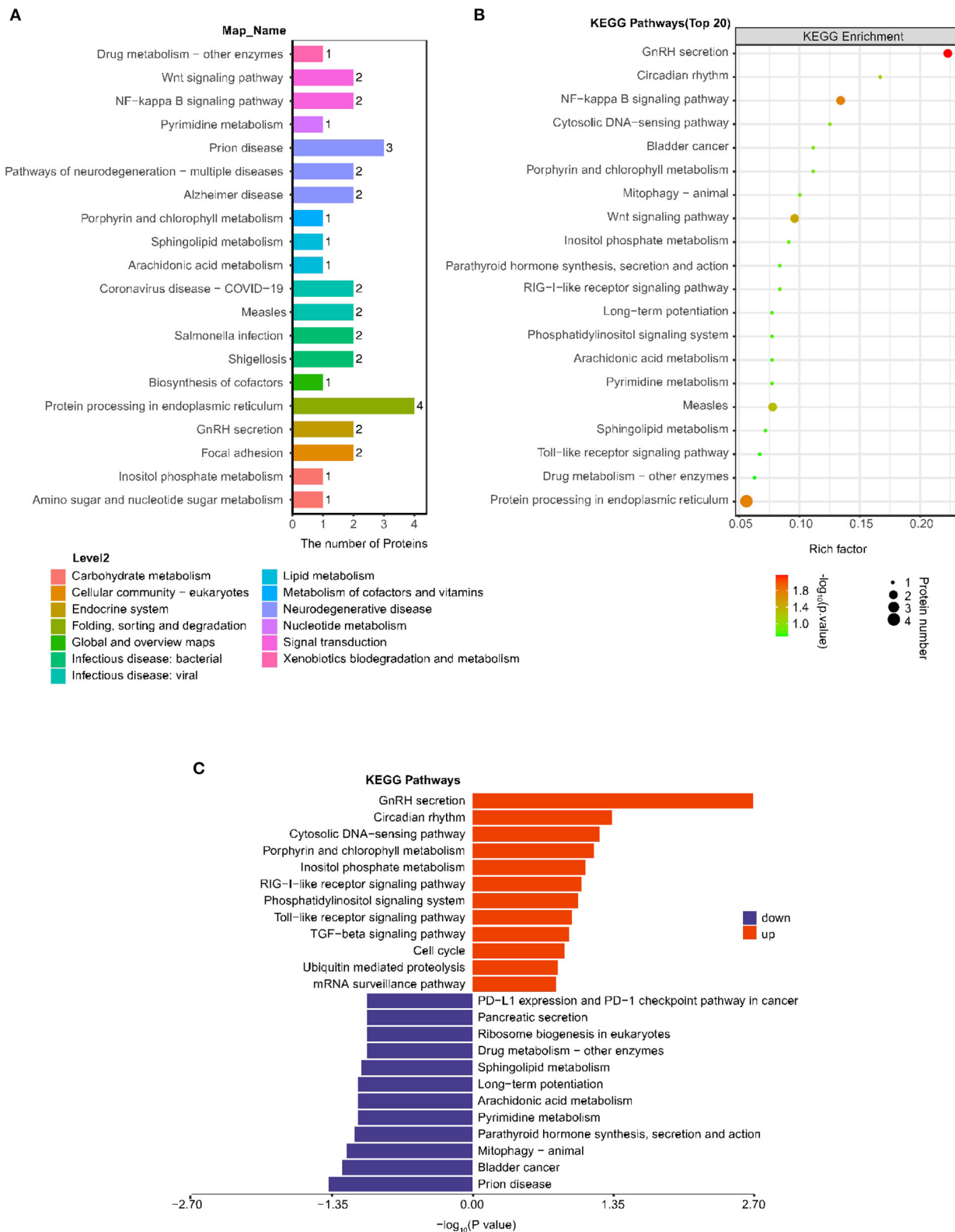
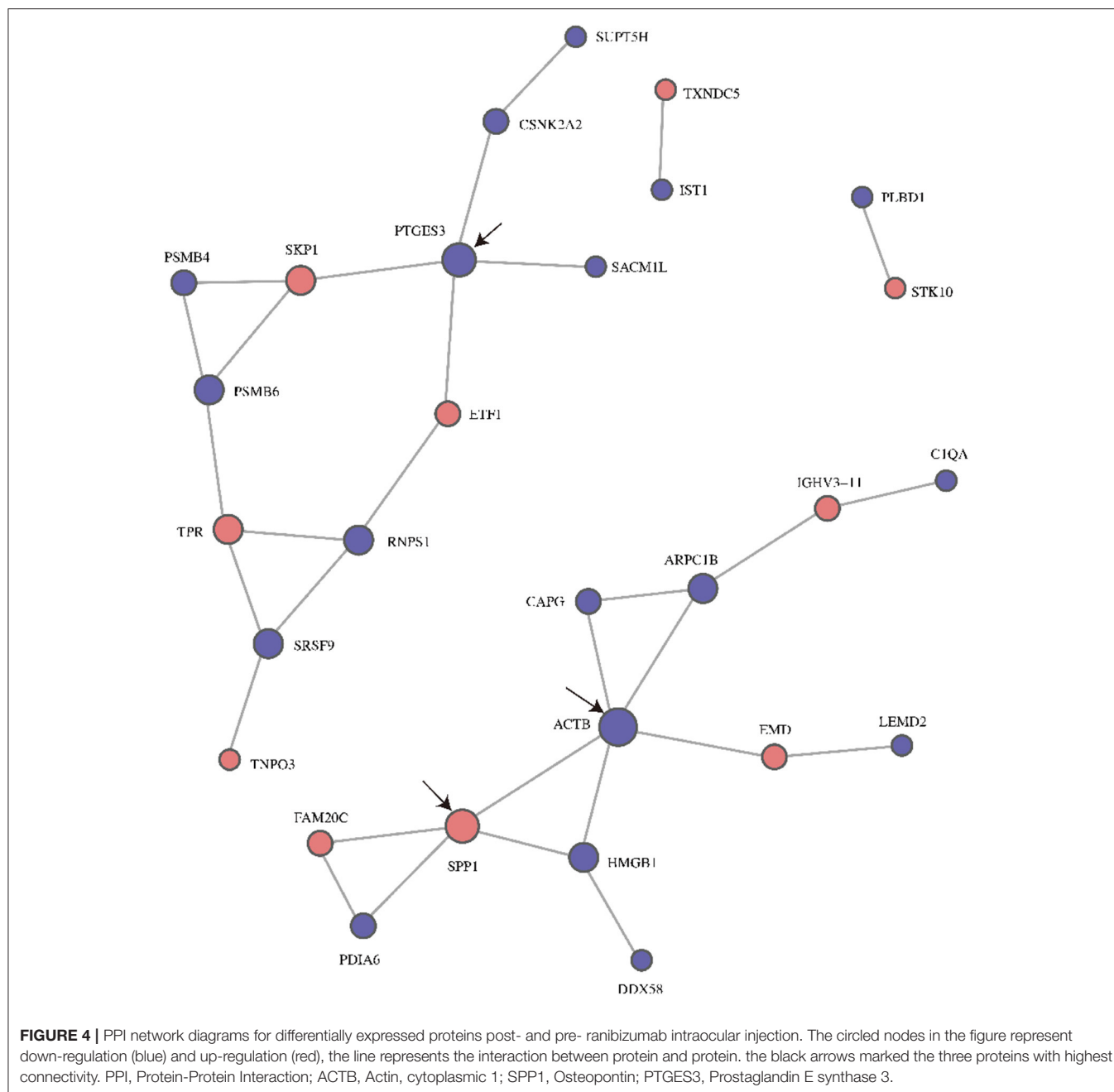


**FIGURE 3 |** Analysis of changes in KEGG pathway between the post IVR group and pre IVR group. **(A)** Histogram showing the top 20 KEGG pathways in which the differentially expressed proteins between the post and pre group; **(B)** Bubble chart showing the enrichment of the top 20 KEGG pathways, as determined by Fisher's exact test ( $P < 0.05$ ); **(C)** Pathways in which the up-regulated and down-regulated differentially expressed proteins were enriched.





highly utilized and with high mutational load, it has been shown to that display a bad prognosis (23). A relatively large Taiwanese cohort of chronic lymphocytic leukemia showed the most frequent usage of IGHV3-23 gene (24). In COVID-19 patients, IGHV3-23 was over-represented and was identified as novel B-cell-receptor (25). RTCB is a catalytic subunit of the tRNA-splicing ligase complex that acts as an RNA ligase with broad substrate specificity and may act on RNAs. Recent studies on Parkinson's disease have shown that RTCB-1 can play a neuroprotective effect by splicing XBP-1 mRNA (26). Another instance of a nonsplicing function for a tRNA processing factor

is the discovery that, following axonal injury, RtcB mutants in *C. elegans* exhibit axon regeneration times that are faster than those of wild-type nematodes (27). This role for RtcB depends on its ligase activity and appears to be specific to neurons. SPP1 (synonym osteopontin), is a glycosylated protein. It is the main adhesion and chemotactic factor for vascular cells. As an angiogenic and fibrogenic factor, SPP1 has been reported to be expressed in patients with DR (28). Plasma SPP1 levels are associated with the presence and severity of DR, suggesting that SPP1 may be a potential biomarker for DR. Ang II upregulated SPP1 expression in adult rat cardiac

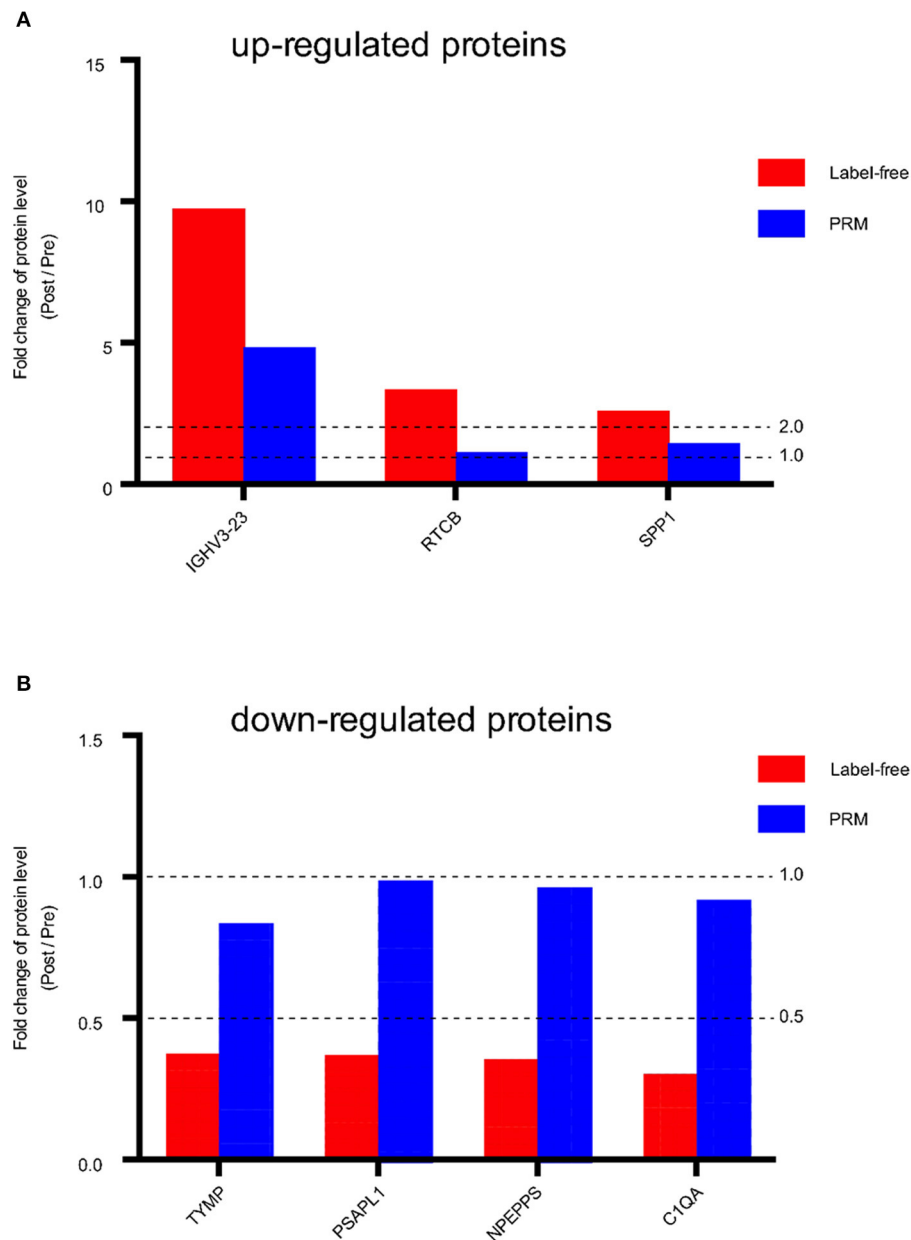


**FIGURE 5 |** Fold change of protein level (Post / Pre) in Label-free and PRM verification. **(A)** Up-regulated proteins between the post IVR group and pre IVR group. **(B)** Down-regulated proteins between the post IVR group and pre IVR group. Fold change (FC) >2 times or FC <0.5 times, and  $P$ -value <0.05.

fibroblasts by ROS-mediated activation of ERK1/2 and JNK pathways (29). A recent study demonstrated that S100A4 induces NF- $\kappa$ B-dependent expressions and secretions of SPP1 in osteosarcoma cell lines (30). These findings suggest that SPP1 may be a molecular mechanism related to S100A4 signaling. The increases in IGHV3-23, RTCB, and SPP1 expression indicated that ranibizumab may play an immune-activating and neuroprotective role in PDR patients.

TYMP has a role in inducing chemotaxis of ECs and angiogenesis. Through its enzymatic activity, TYMP produces

2-deoxy-d-ribose-1-phosphate from thymidine; subsequent hydrolysis generates 2-deoxy-d-ribose, which is the molecule that exerts chemotactic and angiogenic effects (31). A clinical study identified PSAPL1 genes to be enriched in the patients with face and neck atopic dermatitis(AD), suggesting that innate immune system is potentially associated with the pathophysiology of face and neck AD (32). PSAPL1 was associated with breast cancer grade and involved in the epithelial cell differentiation pathways and the sphingolipid metabolic process (33). Protein PSAPL1 was different in non-lesional and

lesional samples compared to healthy skin and might represent proteins that contribute to maintaining the non-lesional state (34).

NPEPPS is involved in proteolytic events essential for cell growth and viability. It is required for the proliferation of myoblasts in the growth phase (35). C1QA associates with the proenzymes C1r and C1s to yield C1, the first component of the serum complement system. A study identified C1qA as a novel AGE-binding protein in human serum and found that it participates in stimulating the classical complement pathway (36). The decrease in the expression of these four proteins, TYMP, PSAPL1, NPEPPS, C1QA, indicates that ranibizumab may have a protective effect in PDR patients by reducing angiogenesis, inhibiting cell proliferation, inhibiting complement activation, etc.

The choice of ranibizumab is based on our previous research (12). Ranibizumab inhibits all isoforms of VEGF-A to block the activation of the VEGFR-1 and VEGFR-2 receptors, which prevents subsequent neovascularization due to receptor activation (37). Compared with bevacizumab, ranibizumab has a higher VEGF165 binding affinity (38) and achieves robust DR regression. Ranibizumab is a chimeric molecule that includes a nonbinding human sequence which makes it less antigenic in primates and a high affinity epitope that binds to VEGF-A (39). Ranibizumab appears to have some benefits in terms of systemic adverse events than other anti-VEGF agents (40). We used a Bruker timsTOF<sup>TM</sup> Pro mass spectrometer to analyze the VH. This instrument couples trapped ion mobility spectrometry (TIMS) to high-resolution time-of-flight MS. Use of the ion mobility parameter added a dimension of separation and increased overall system peak capacity in the gas phase. Ultimately, this resulted in better coverage of the proteome (41, 42).

However, there were some limitations to this study. First, the sample size of each group was small. Second, we did not conduct in-depth research on the results of this experiment at the animal or cell level. Large-scale clinical studies and *in vitro* experiments are necessary to investigate the molecular mechanisms of IVR in PDR. At the same time, we should also study the therapeutic effects of other anti-VEGF drugs on PDR in further study.

## CONCLUSIONS

In conclusion, this study demonstrated that VH protein profiles differed in response to ranibizumab treatment. Proteins that showed increased expression after IVR treatment were significantly enriched in “GnRH secretion” and “Circadian rhythm” pathway. This report reveals IVR treatment may protect against PDR by promoting SPP1 expression through “GnRH secretion” and “Circadian rhythm” signaling pathway, providing a new perspective on the mechanism of ranibizumab treatment to PDR.

## DATA AVAILABILITY STATEMENT

The datasets presented in this study can be found in online repositories. The names of the repository/repositories and accession number(s) can be found below. The mass spectrometry proteomics data have been deposited to the ProteomeXchange Consortium via the PRIDE (<http://www.ebi.ac.uk/pride>) partner repository with the dataset identifier PXD027592; Username: reviewer\_pxd027592@ebi.ac.uk; Password: b7I8VHZMs.

## ETHICS STATEMENT

The studies involving human participants were reviewed and approved by Ethics Committee of Shanghai General Hospital (Ethical approval number: 2021KY031). The patients/participants provided their written informed consent to participate in this study. Written informed consent was obtained from the individual(s) for the publication of any potentially identifiable images or data included in this article.

## AUTHOR CONTRIBUTIONS

XS and ZZ: Conceptualization. XS and CZ: Formal analysis. XS: Methodology, data curation, and writing original draft. ZZ: Writing review and editing. All authors read and approved the final manuscript.

## FUNDING

Research reported in this publication was supported by the Program of the National Natural Science Foundation of China (81770947); National Key R&D Program of China (2016YFC0904800, 2019YFC0840607; National Science and Technology Major Project of China (2017ZX09304010).

## ACKNOWLEDGMENTS

We thank Shanghai Applied Protein Technology Co. Ltd. for technical assistance in proteomic analysis. The manuscript was edited for proper English language, grammar, punctuation, spelling, and overall style by highly qualified native English-speaking editors at AJE.

## SUPPLEMENTARY MATERIAL

The Supplementary Material for this article can be found online at: <https://www.frontiersin.org/articles/10.3389/fmed.2022.776855/full#supplementary-material>

**Supplementary Figure S1** | Protein overlap analysis in the pre group and post group.

**Supplementary Figure S2** | Targeted peptide PRM<sub>1</sub> Skyline analysis results.

**Supplementary Table S1** | Protein identification and quantification, a total of 2680 vitreous proteins were identified.

**Supplementary Table S2** | A total of 1874 GO terms related to all 38 differentially expressed proteins were identified.

**Supplementary Table S3** | Information of peptide, precursor Mz, fragment ion, areas and other original data for PRM quantitative Skyline data.

**Supplementary Table S4** | Fold change of protein level in Label-free and PRM (Post / Pre).

## REFERENCES

- Benoit SR, Swenor B, Geiss LS, Gregg EW, Saaddine JB. Eye care utilization among insured people with diabetes in the U.S., 2010-2014. *Diabetes Care*. (2019) 42:427–33. doi: 10.2337/dc18-0828
- Kang EY, Chen TH, Garg SJ, Sun CC, Kang JH, Wu WC, et al. Association of statin therapy with prevention of vision-threatening diabetic retinopathy. *JAMA Ophthalmol*. (2019) 137:363–71. doi: 10.1001/jamaophthalmol.2018.6399
- Hou XW, Wang Y, Pan CW. Metabolomics in diabetic retinopathy: a systematic review. *Invest Ophthalmol Vis Sci*. (2021) 62:4. doi: 10.1167/iov.62.10.4
- Malechka VV, Chen J, Cheng R, Ma JX, Moiseyev G. The single administration of a chromophore alleviates neural defects in diabetic retinopathy. *Am J Pathol*. (2020) 190:1505–12. doi: 10.1016/j.ajpath.2020.03.009
- Yau JW, Rogers SL, Kawasaki R, Lamoureux EL, Kowalski JW, Bek T, et al. Global prevalence and major risk factors of diabetic retinopathy. *Diabetes Care*. (2012) 35:556–64. doi: 10.2337/dc11-1909
- Rezzola S, Loda A, Corsini M, Semeraro F, Annese T, Presta M, et al. Angiogenesis-inflammation cross talk in diabetic retinopathy: novel insights from the chick embryo chorioallantoic membrane/human vitreous platform. *Front Immunol*. (2020) 11:581288. doi: 10.3389/fimmu.2020.581288
- Forbes JM, Cooper ME. Mechanisms of diabetic complications. *Physiol Rev*. (2013) 93:137–88. doi: 10.1152/physrev.00045.2011
- Hu L, Chen Q, Du Z, Wang W, Zhao G. Evaluation of vitrectomy combined preoperative intravitreal ranibizumab and postoperative intravitreal triamcinolone acetonide for proliferative diabetic retinopathy. *Int Ophthalmol*. (2021) 41:1635–42. doi: 10.1007/s10792-021-01703-6
- Zhao XY, Xia S, Chen YX. Antivascular endothelial growth factor agents pretreatment before vitrectomy for complicated proliferative diabetic retinopathy: a meta-analysis of randomised controlled trials. *Br J Ophthalmol*. (2018) 102:1077–85. doi: 10.1136/bjophthalmol-2017-311344
- Wang DY, Zhao XY, Zhang WF, Meng LH, Chen YX. Perioperative anti-vascular endothelial growth factor agents treatment in patients undergoing vitrectomy for complicated proliferative diabetic retinopathy: a network meta-analysis. *Sci Rep*. (2020) 10:18880. doi: 10.1038/s41598-020-75896-8
- Lu Q, Zou C, Cao H, Zhao M, Yu S, Qiu Q, et al. Preoperative intravitreal injection of ranibizumab for patients with severe proliferative diabetic retinopathy contributes to a decreased risk of postoperative neovascular glaucoma. *Acta ophthalmologica*. (2016) 94:414–5. doi: 10.1111/aos.13019
- Zou C, Han C, Zhao M, Yu J, Bai L, Yao Y, et al. Change of ranibizumab-induced human vitreous protein profile in patients with proliferative diabetic retinopathy based on proteomics analysis. *Clin Proteomics*. (2018) 15:12. doi: 10.1186/s12014-018-9187-z
- Leitner A. A review of the role of chemical modification methods in contemporary mass spectrometry-based proteomics research. *Anal Chim Acta*. (2018) 1000:2–19. doi: 10.1016/j.aca.2017.08.026
- Csosz É, Deák E, Kalló G, Csutak A, Tozsér J. Diabetic retinopathy: proteomic approaches to help the differential diagnosis and to understand the underlying molecular mechanisms. *J Proteomics*. (2017) 150:351–8. doi: 10.1016/j.jprot.2016.06.034
- Kim HJ, Kim PK, Yoo HS, Kim CW. Comparison of tear proteins between healthy and early diabetic retinopathy patients. *Clin Biochem*. (2012) 45:60–7. doi: 10.1016/j.clinbiochem.2011.10.006
- Yokomizo H, Maeda Y, Park K, Clermont AC, Hernandez SL, Fickweiler W, et al. Retinol binding protein 3 is increased in the retina of patients with diabetes resistant to diabetic retinopathy. *Sci Transl Med*. (2019) 11:eau6627. doi: 10.1126/scitranslmed.aau6627
- Shahulhameed S, Vishwakarma S, Chhablani J, Tyagi M, Pappuru RR, Jakati S, et al. A systematic investigation on complement pathway activation in diabetic retinopathy. *Front Immunol*. (2020) 11:154. doi: 10.3389/fimmu.2020.00154
- Youngblood H, Robinson R, Sharma A, Sharma S. Proteomic biomarkers of retinal inflammation in diabetic retinopathy. *Int J Mol Sci*. (2019) 20:4755. doi: 10.3390/ijms20194755
- Juocevičius A, Oral A, Lukmann A, Takáč P, Tederko P, Häzner I, et al. Evidence-based position paper on Physical and Rehabilitation Medicine (PRM) professional practice for people with cardiovascular conditions. The European PRM position (UEMS PRM Section). *Eur J Phys Rehabil Med*. (2018) 54:634–43. doi: 10.23736/S1973-9087.18.05310-8
- Wiśniewski JR, Zougman A, Nagaraj N, Mann M. Universal sample preparation method for proteome analysis. *Nat Methods*. (2009) 6:359–62. doi: 10.1038/nmeth.1322
- Zou C, Zhao M, Yu J, Zhu D, Wang Y, She X, et al. Difference in the vitreal protein profiles of patients with proliferative diabetic retinopathy with and without intravitreal conbercept injection. *J Ophthalmol*. (2018) 2018:7397610. doi: 10.1155/2018/7397610
- Yoshida M, Okabe M, Eimoto T, Shimizu S, Ueda-Otsuka K, Okamoto M, et al. Immunoglobulin VH genes in thymic MALT lymphoma are biased toward a restricted repertoire and are frequently unmutated. *J Pathol*. (2006) 208:415–22. doi: 10.1002/path.1889
- Messmer BT, Raphael BJ, Aerni SJ, Widhopf GF, Rassenti LZ, Gribben JG, et al. Computational identification of CDR3 sequence archetypes among immunoglobulin sequences in chronic lymphocytic leukemia. *Leuk Res*. (2009) 33:368–76. doi: 10.1016/j.leukres.2008.05.022
- Huang YJ, Kuo MC, Chang H, Wang PN, Wu JH, Huang YM, et al. Distinct immunoglobulin heavy chain variable region gene repertoire and lower frequency of del(11q) in Taiwanese patients with chronic lymphocytic leukaemia. *Br J Haematol*. (2019) 187:82–92. doi: 10.1111/bjh.16051
- Wen W, Su W, Tang H, Le W, Zhang X, Zheng Y, et al. Immune cell profiling of COVID-19 patients in the recovery stage by single-cell sequencing. *Cell Discov*. (2020) 6:31. doi: 10.1038/s41421-020-00187-5
- Ray A, Zhang S, Rentas C, Caldwell KA, Caldwell GA. RTCB-1 mediates neuroprotection via XBP-1 mRNA splicing in the unfolded protein response pathway. *J Neurosci*. (2014) 34:16076–85. doi: 10.1523/JNEUROSCI.1945-14.2014
- Kosmaczewski SG, Han SM, Han B, Irving Meyer B, Baig HS, Athar W, et al. RNA ligation in neurons by RtcB inhibits axon regeneration. *Proc Natl Acad Sci*. (2015) 112:8451–6. doi: 10.1073/pnas.1502948112
- Abu El-Asrar AM, Imtiaz Nawaz M, Kangave D, Siddiquei MM, Geboes K. Osteopontin and other regulators of angiogenesis and fibrogenesis in the vitreous from patients with proliferative vitreoretinal disorders. *Mediators Inflamm*. (2012) 2012:493043. doi: 10.1155/2012/493043
- Xie Z, Pimental DR, Lohan S, Vasertriger A, Pligavko C, Colucci WS, et al. Regulation of angiotensin II-stimulated osteopontin expression in cardiac microvascular endothelial cells: role of p42/44 mitogen-activated protein kinase and reactive oxygen species. *J Cell Physiol*. (2001) 188:132–8. doi: 10.1002/jcp.1104
- Berge G, Pettersen S, Grotterød I, Bettum IJ, Boye K, Mølandsmo GM. Osteopontin—an important downstream effector of S100A4-mediated invasion and metastasis. *Int J Cancer*. (2011) 129:780–90. doi: 10.1002/ijc.25735
- Cherrington JM, Strawn LM, Shawver LK. New paradigms for the treatment of cancer: the role of anti-angiogenesis agents. *Adv Cancer Res*. (2000) 79:1–38. doi: 10.1016/S0065-230X(00)79001-4
- Yasuda-Sekiguchi F, Shiohama A, Fukushima A, Obata S, Mochimaru N, Honda A, et al. Single nucleotide variations in genes associated with innate immunity are enriched in Japanese adult cases of face and neck type atopic dermatitis. *J Dermatol Sci*. (2021) 101:93–100. doi: 10.1016/j.jdermsci.2020.11.005
- Rakha EA, Alsalem M, ElSharawy KA, Toss MS, Raafat S, Mihai R, et al. Visual histological assessment of morphological features reflects the underlying molecular profile in invasive breast cancer: a morphomolecular study. *Histopathology*. (2020) 77:631–45. doi: 10.1111/his.14199



34. Szél E, Bozó R, Hunyadi-Gulyás É, Manczinger M, Szabó K, Kemény L, et al. Comprehensive proteomic analysis reveals intermediate stage of non-lesional psoriatic skin and points out the importance of proteins outside this trend. *Sci Rep.* (2019) 9:11382. doi: 10.1038/s41598-019-47774-5
35. Osana S, Kitajima Y, Suzuki N, Nunomiya A, Takada H, Kubota T, et al. Puromycin-sensitive aminopeptidase is required for C2C12 myoblast proliferation and differentiation. *J Cell Physiol.* (2021) 236:5293–305. doi: 10.1002/jcp.30237
36. Chikazawa M, Shibata T, Hatasa Y, Hirose S, Otaki N, Nakashima F, et al. Identification of C1q as a binding protein for advanced glycation end products. *Biochemistry.* (2016) 55:435–46. doi: 10.1021/acs.biochem.5b00777
37. Ferrara N, Damico L, Shams N, Lowman H, Kim R. Development of ranibizumab, an anti-vascular endothelial growth factor antigen binding fragment, as therapy for neovascular age-related macular degeneration. *Retina.* (2006) 26:859–70. doi: 10.1097/01.iae.0000242842.14624.e7
38. Papadopoulos N, Martin J, Ruan Q, Rafique A, Rosconi MP, Shi E, et al. Binding and neutralization of vascular endothelial growth factor (VEGF) and related ligands by VEGF Trap, ranibizumab and bevacizumab. *Angiogenesis.* (2012) 15:171–85. doi: 10.1007/s10456-011-9249-6
39. Hussain N, Ghanekar Y, Kaur I. The future implications and indications of anti-vascular endothelial growth factor therapy in ophthalmic practice. *Indian J Ophthalmol.* (2007) 55:445–50. doi: 10.4103/0301-4738.36480
40. Plyukhova AA, Budzinskaya MV, Starostin KM, Rejdak R, Bucolo C, Reibaldi M, et al. Comparative safety of Bevacizumab, Ranibizumab, and Aflibercept for treatment of neovascular Age-Related Macular Degeneration (AMD): a systematic review and network meta-analysis of direct comparative studies. *J Clin Med.* (2020) 9:1522. doi: 10.3390/jcm9051522
41. Meier F, Brunner AD, Frank M, Ha A, Bludau I, Voytik E, et al. diaPASEF: parallel accumulation-serial fragmentation combined with data-independent acquisition. *Nat Methods.* (2020) 17:1229–36. doi: 10.1038/s41592-020-00998-0
42. Distler U, Kuharev J, Navarro P, Tenzer S. Label-free quantification in ion mobility-enhanced data-independent acquisition proteomics. *Nat Protoc.* (2016) 11:795–812. doi: 10.1038/nprot.2016.042

**Conflict of Interest:** The authors declare that the research was conducted in the absence of any commercial or financial relationships that could be construed as a potential conflict of interest.

**Publisher's Note:** All claims expressed in this article are solely those of the authors and do not necessarily represent those of their affiliated organizations, or those of the publisher, the editors and the reviewers. Any product that may be evaluated in this article, or claim that may be made by its manufacturer, is not guaranteed or endorsed by the publisher.

Copyright © 2022 She, Zou and Zheng. This is an open-access article distributed under the terms of the Creative Commons Attribution License (CC BY). The use, distribution or reproduction in other forums is permitted, provided the original author(s) and the copyright owner(s) are credited and that the original publication in this journal is cited, in accordance with accepted academic practice. No use, distribution or reproduction is permitted which does not comply with these terms.



# Optical Coherence Tomography Biomarkers in Predicting Treatment Outcomes of Diabetic Macular Edema After Dexamethasone Implants

Yu-Te Huang<sup>1</sup>, Yen-Chieh Chang<sup>1</sup>, Ping-Ping Meng<sup>1</sup>, Chun-Ju Lin<sup>1,2,3\*</sup>, Chun-Ting Lai<sup>1\*</sup>, Ning-Yi Hsia<sup>1</sup>, Huan-Sheng Chen<sup>4</sup>, Peng-Tai Tien<sup>1,5</sup>, Henry Bair<sup>1,6</sup>, Jane-Ming Lin<sup>1,3</sup>, Wen-Lu Chen<sup>1,3</sup> and Yi-Yu Tsai<sup>1,2,3</sup>

<sup>1</sup> Department of Ophthalmology, China Medical University Hospital, China Medical University, Taichung, Taiwan, <sup>2</sup> School of Medicine, College of Medicine, China Medical University, Taichung, Taiwan, <sup>3</sup> Department of Optometry, Asia University, Taichung, Taiwan, <sup>4</sup> An-Shin Dialysis Center, NephroCare Ltd., Fresenius Medical Care, Taichung, Taiwan, <sup>5</sup> Graduate Institute of Clinical Medical Science, College of Medicine, China Medical University, Taichung, Taiwan, <sup>6</sup> Byers Eye Institute, Stanford University School of Medicine, Stanford, CA, United States

## OPEN ACCESS

### Edited by:

Shaochong Zhang,  
Shenzhen Eye Hospital, China

### Reviewed by:

Giovanni William Oliverio,  
University of Messina, Italy  
Qingshan Chen,  
Jinan University, China

### \*Correspondence:

Chun-Ju Lin  
doctoraga@gmail.com  
Chun-Ting Lai  
withwind037@yahoo.com.tw

<sup>†</sup>These authors have contributed  
equally to this work

### Specialty section:

This article was submitted to  
Ophthalmology,  
a section of the journal  
Frontiers in Medicine

Received: 10 January 2022

Accepted: 23 May 2022

Published: 09 June 2022

### Citation:

Huang Y-T, Chang Y-C, Meng P-P,  
Lin C-J, Lai C-T, Hsia N-Y, Chen H-S,  
Tien P-T, Bair H, Lin J-M, Chen W-L  
and Tsai Y-Y (2022) Optical  
Coherence Tomography Biomarkers  
in Predicting Treatment Outcomes  
of Diabetic Macular Edema After  
Dexamethasone Implants.  
Front. Med. 9:852022.  
doi: 10.3389/fmed.2022.852022

**Purpose:** To identify optical coherence tomography (OCT) biomarkers that may predict functional and anatomical outcomes in diabetic macular edema (DME) patients treated with intravitreal dexamethasone (DEX) implant.

**Materials and Methods:** Sixty-four eyes from 50 patients with DME were enrolled. Best-corrected visual acuity (BCVA) and OCT biomarkers including central retinal thickness (CRT), subretinal fluid (SRF), intraretinal cysts (IRC), ellipsoid zone disruption (EZD), disorganization of retinal inner layers (DRIL), hard exudate (HE), hyperreflective foci (HRF), epiretinal membrane (ERM), and vitreomacular interface (VMI) changes were evaluated at baseline and at 3, 6, and 12 months after treatment. Multiple logistic analysis was performed to evaluate each OCT biomarker as a predictive factor for functional and anatomical improvement at the end of treatment.

**Results:** The presence of SRF at baseline was associated with a favorable outcome, with CRT improving by more than 100  $\mu\text{m}$  after treatment from multivariate logistic regression analysis [odds ratio 6.16 (1.75–21.6)]. In addition, baseline SRF predicted a greater CRT improvement from multiple regression analysis (model R-square 0.11,  $p = 0.006$ ). The reduction of DRIL, SRF, LONLC, IRC, and EZD were correlated with better CRT improvement (more than 100  $\mu\text{m}$ ) ( $P < 0.05$ ). SRF and EZD recovery can also predict better visual prognosis ( $P < 0.05$ ).

**Conclusion:** OCT biomarkers can be used to predict who may benefit the most after DEX treatment. We suggest that the DEX implant should be considered as a first line treatment in DME patients with SRF.

**Keywords:** diabetic macular edema (DME), disorganization of retinal inner layers, hyperreflective foci, intravitreal dexamethasone implant, optical coherence tomography biomarkers, subretinal fluid

## INTRODUCTION

Diabetes mellitus (DM) is one of the most important global health issues, with an estimated 425 million patients suffering from DM worldwide (1). Among the complications of DM, diabetic macular edema (DME) is the most frequent cause of visual impairment, with prevalence rates ranging from 7 to 12.8% among those with diabetes from different population-based studies (2–4). DME is also one of the leading complications among those with retinal vascular disorders (5).

Antivascular endothelial growth factor (anti-VEGF) injections are generally considered over focal grid laser photocoagulation as the gold standard and first-line therapy for clinically significant DME (6, 7). Nonetheless, up to 40% of patients do not respond optimally, with half of that classified as non-responder after monthly injections for 1 year (8).

Besides anti-VEGFs, there are other available treatments for DME including laser, surgery, and corticosteroids, with each targeting different pathogenic mechanisms of the disease. The biodegradable intravitreal dexamethasone (DEX) implant (Ozurdex®, Allergan, Inc., Irvine, CA, United States) has been identified as an effective treatment of DME and is approved by the US Food and Drug Administration (FDA) (9). In addition, the beneficial effects of DEX implant in anti-VEGF non-responders are well-established in several studies (9, 10).

As it is crucial to identify which DME patients may most benefit from DEX implant, spectral domain optical coherence tomography (SD-OCT) may serve as non-invasive, rapid, safe, and cost-effective predictive tool. Quantitative measurements in OCT such as central retinal thickness (CRT) and qualitative data i.e., different space of fluid distribution, disorganization of the retinal inner layers (DRIL), ellipsoid zone disruption (EZD), hard exudate (HE), hyperreflective foci (HRF) may serve as OCT biomarkers (11–13). The aim of this study is to investigate whether these OCT biomarkers can serve as predictors to identify which DME patients will most benefit from DEX implants.

## MATERIALS AND METHODS

This retrospective, interventional case series study was conducted at China Medical University Hospital (CMUH) between January 2018 and January 2021. The study was performed in accordance with the World Medical Association's Declaration of Helsinki and the study design was approved by the Institutional Review Board of CMUH (IRB number: CMUH109-REC3-158). Owing to the retrospective design of the study, the review board waived the need for written informed consent.

### Population and Study Design

Inclusion criteria were as follows: (1) age older than 18 years; (2) history of type 1 or 2 diabetes mellitus; (3) presence of severe NPDR (non-proliferative diabetic retinopathy) and PDR (proliferative diabetic retinopathy) confirmed by widefield fluorescein angiography; (4) DME with central retinal

thickness more than 250  $\mu$ m; (5) treatment with at least one DEX implant; (6) follow-up lasting at least 3 months. For patients who received bilateral treatment with DEX, both eyes could be included.

The main exclusion criteria were as follows: (1) a history of pars plana vitrectomy in the study eye; (2) concomitant glaucoma; (3) another concomitant retinal disease that causes macular edema including retinal vein occlusion, neovascular age-related macular degeneration or uveitis; (4) previous treatment with intraocular anti-VEGF within 3 months or corticosteroids within 6 months prior to treatment with DEX implant; (5) any other ocular condition that can influence visual acuity.

Each patient's demographic data, medical history (including diabetes and hypertension), best-corrected visual acuity (BCVA), IOP, and CRT, as well as the occurrence of any complications, prior to and 3, 6, and 12 months after the DEX implant were retrieved from the electronic medical record. Any patients whose IOP exceeded 25 mmHg at any visit was evaluated and treated accordingly. Patients were eligible for retreatment with DEX implant if their retinal thickness increased by 50  $\mu$ m from the lowest recorded level, and further doses of DEX implant were also given if the patient experienced a recurrence of ME as determined by OCT.

### Outcome Measurement

The OCT scans were all obtained by SD-OCT (Heidelberg Spectralis, Heidelberg, Germany). In each patient, SD-OCT was used to record 25 6-mm radial scans across the retina centered on the fovea ( $6 \times 6$  mm area) (Figure 1). Grading of OCT images was all performed by two evaluators manually (YTH and PPM), masked to details of clinical findings and systemic parameters. When disagreement occurred, a third senior retina specialist would determine the final grading (CJL). OCT images were graded for the following parameters at each visit (baseline, 3, 6, and 12 months): EZD, DRIL, presence of HE, presence of HRF, its quantity (average number in one cut), and location (between the ILM and the INL; between the OPL and the ELM; in all retinal layers), SRF, intraretinal cyst (IRC), presence of an epiretinal membrane (ERM), presence of large outer nuclear layer cyst (more than 100  $\mu$ m) (LONLC) and vitreomacular interface (VMI) [posterior vitreous detachment (PVD), vitreomacular adhesion (VMA), and vitreomacular traction (VMT)].

### Statistical Analysis

All analyses were computed by using PASW Statistics 18 software (Version 18.0. Chicago: SPSS Inc.). The numerical data are expressed as mean and standard deviation and the categorical variables as absolute frequency and percentage. The baseline characteristic of patients and changes in CRT were analyzed by using Chi-square and one-way ANOVA. Multiple regression analysis was performed to evaluate the possible OCT biomarker (EZD, DRIL, HE, HRF, SRF, IRC, ERM, and VMI) as predictive factors for final visual acuity improvement at the end of

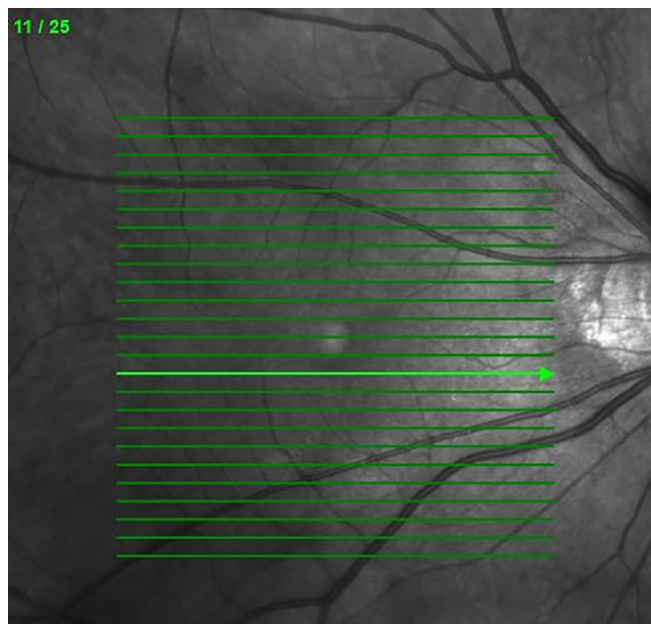


**FIGURE 1** | The 25 6-mm radial scans across the retina centered on the fovea in SD-OCT.

treatment. A  $p$ -value smaller than 0.05 was considered to be statistically significant.

## RESULTS

### Study Population

A total of 64 eyes from 50 participants were ultimately included in this study. Demographic and baseline characteristics are detailed in **Table 1**. Of the included eyes with DME, 37 (58.8%) were naïve and 27 (42.2%) were refractory to previous anti-VEGF injections; 59 (92.2%) of patients had severe NPDR and 5 (7.81%) patients had PDR. Thirty patients (60%) were female, 20 (40%) were male, and mean age was  $66.22 \pm 10.17$  years old. Mean duration of follow-up was  $9.89 \pm 3.24$  months and 92.2% of the cases were followed up more than 6 months. A total of 38 eyes (59.4%) were phakic and 26 eyes (40.6%) were pseudophakic. HbA1c levels were available for 29 patients; the mean value was  $7.47 \pm 1.34\%$ .

### Anatomical and Functional Outcome

The mean final change in CRT for all 64 eyes after the DEX implant treatments reached a statistically significant level (decreased from a mean initial CRT of  $411.17 \pm 119.50 \mu\text{m}$  to a mean final CRT of  $333.00 \pm 103.89 \mu\text{m}$ ,  $p < 0.05$ ) (**Figure 2A**). During the follow-up period, CRT showed rapid improvement in the first 3 months, then fluctuated within a stable range (**Figure 2B**). The mean change in LogMAR BCVA of all 64 eyes after the DEX implant treatments showed statistical significance ( $0.81 \pm 0.46$ – $0.67 \pm 0.49$ ,  $p < 0.05$ ). The BCVA improved gradually but significantly after 12 months (**Figure 3**),

taking slightly longer to reach the level of significance than the CRT changes.

During the follow-up period, 21 (32.8%) eyes received one injection, 23 (35.9%) eyes received two injections, and 20 (31.3%) eyes received three injections (mean injection number:  $1.98 \pm 0.81$ ). IOP elevation is an important concern in patients

**TABLE 1** | Baseline clinical data and status of OCT biomarkers.

Baseline clinical data	50 patients, 64 eyes
Age	$66.22 \pm 10.17$
Gender (female)	30/50 (60.0%)
Lens (pseudophakic)	26/64 (40.6%)
Side (OD)	30/64 (46.9%)
HbA1c	$7.47 \pm 1.34$
CRT <i>initial</i>	$411.17 \pm 119.50$
LogMAR <i>initial</i>	$0.81 \pm 0.46$
IOP <i>initial</i>	$15.66 \pm 3.40$
s/p IVI	27/64 (42.2%)
s/p PST	28/64 (43.8%)
s/p PRP	37/64 (57.8%)
<b>Follow-up months</b>	
3	5/64 (7.8%)
6	15/64 (23.4%)
12	44/64 (68.8%)
Mean	$9.89 \pm 3.24$
<b>Injection times</b>	
1	21/64 (32.8%)
2	23/64 (35.9%)
3	20/64 (31.3%)
Mean	$1.98 \pm 0.81$



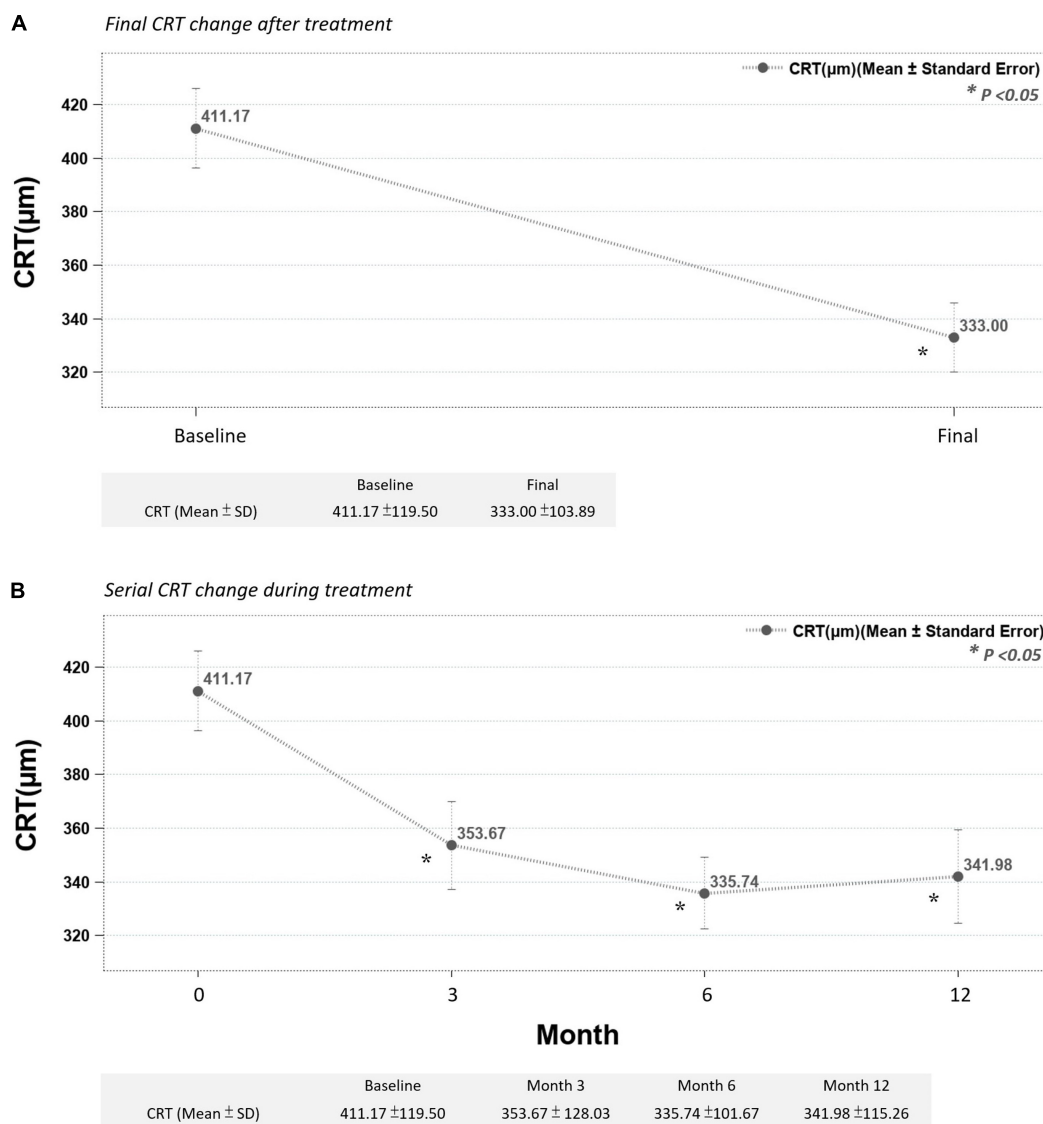


**FIGURE 2 | (A)** Final CRT significantly improved after treatment. **(B)** Mean CRT improved significantly after the third month and continuously improved up to the end of the study (month 12) (\* $p < 0.05$  compared to before-treatment data).

receiving DEX implant. The mean change IOP of all the eyes were from  $15.66 \pm 3.40$  to  $15.89 \pm 4.83$  mmHg, which showed no statistically significant difference ( $p > 0.05$ ). Serial IOP measurements during treatment also revealed no obvious elevation (Figure 4).

## Optical Coherence Tomography Biomarker Analysis

In our study group, baseline OCT biomarker characteristics showed high prevalence of HRF (92.2%), IRC (82.8%), DRIL (79.7%), and HE (71.9%); and lower prevalence of SRF (23.4%) and LONLC (31.3%) (Table 2).

Multiple regression analysis was used for evaluating possible OCT biomarkers that predict improvement of CRT at the end of

treatment. The presence of SRF at baseline was correlated with CRT improvement of more than  $100\mu\text{m}$  after treatment from multivariate logistic regression analysis [with SRF vs. without SRF: odds ratio 6.16 (1.75–21.6)] (Figure 5). Also, in Table 3, positive baseline SRF predicted a greater CRT improvement from multiple regression analysis (model R-square 0.11,  $p = 0.006$ ).

No single OCT biomarker at baseline was associated with BCVA improvement to a statistically significant degree (all  $p > 0.05$ ). However, trends of BCVA improvements were more prominent in eyes without DRIL (69.2% eye without DRIL displayed BCVA improvement vs. 47.1% of eyes with DRIL.), and with HRF (54.2 vs. 20%) and PVD (56.3 vs. 37.5%) (Table 4).

The DEX implant treatment significantly decreased the proportion of DRIL, SRF, LONLC, IRC and EZD ( $p < 0.05$ ). In subgroup analyses, we investigated OCT biomarker changes

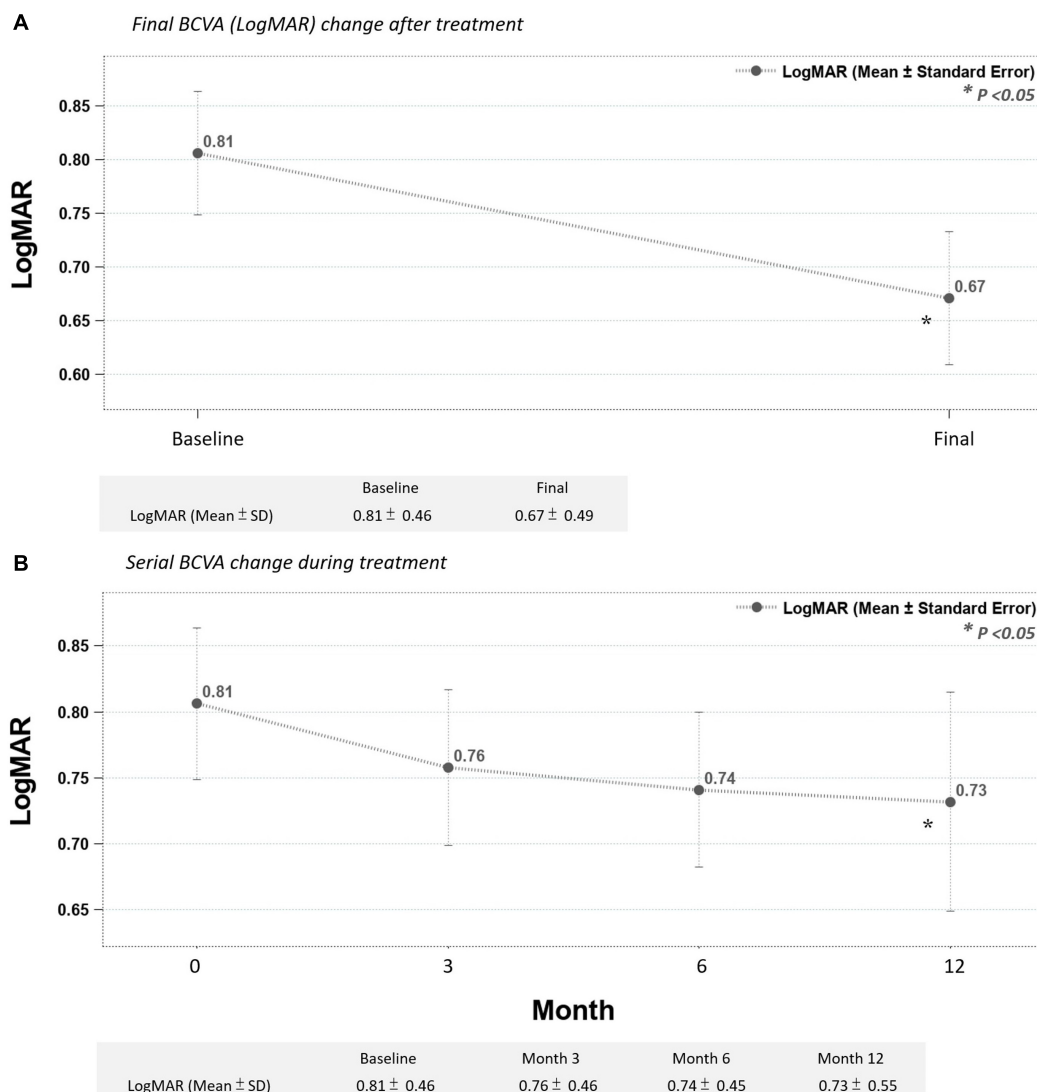


**FIGURE 3 | (A)** Final BCVA (LogMAR) significantly improved after treatment. **(B)** Mean BCVA improved gradually after the third month, reaching statistical significance in month 12 (\* $p < 0.05$  compared to before-treatment data).

correlated with final CRT improvements (greater than 100  $\mu\text{m}$  or less than 100  $\mu\text{m}$ ) and final BCVA (VA improved group vs. VA not improved group). In the group with final CRT improvements greater than 100  $\mu\text{m}$ , DRIL, SRF, LONLC, IRC, and EZD all significantly decreased while none of these OCT biomarkers significantly changed in groups with CRT improvements less than 100  $\mu\text{m}$  (Table 5). In groups stratified by BCVA improvements, DRIL decreased regardless of VA status, while BCVA improvements were correlated with SRF and EZD resolution ( $p < 0.05$ ) (Table 6).

## DISCUSSION

In the present study, we found the presence of SRF as the best OCT biomarker to predict CRT improvement. Also,

the reduction of DRIL, SRF, LONLC, IRC, and EZD were correlated with better CRT improvement (more than 100  $\mu\text{m}$ ) ( $P < 0.05$ ). SRF and EZD recovery can also predict better visual improvement.

Also, we demonstrated that under real-world conditions, DEX implant served as an effective and efficient strategy in treating DME, both anatomically and functionally. With an average of fewer than two injections, the treatment effect was sustained during the 1-year follow-up in most of the cases.

In practice, most clinicians consider anti-VEGF as a first-line treatment with laser photocoagulation as adjuvant therapy (14). DEX implant is mainly used as a second line therapy in most clinical situations due to the side effects of glaucoma and cataract progression (9, 15). Several guidelines recommend of DEX implant usage in patients with history of major cardiovascular event, vitrectomized eye, anti-VEGF

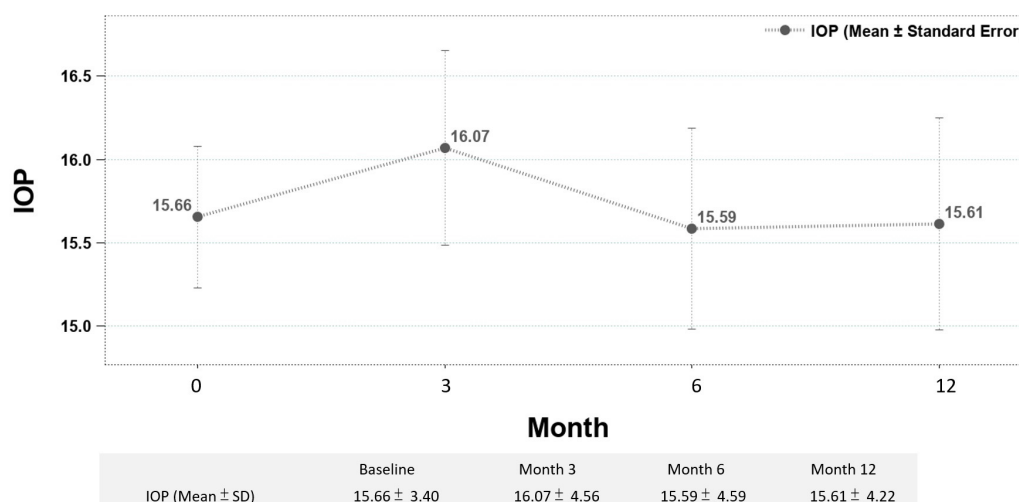


**FIGURE 4 |** Serial IOP change during treatment, revealing no obvious elevation.

non-responder, and pseudophakia (15–17). In the current study, we proposed qualitative OCT biomarkers in DME could provide important information to guide the treatment choice.

To date, there is limited literature focusing on the relationship between DEX implant efficacy, baseline OCT characteristics, and changes of OCT biomarkers in DME patients. Most studies focus on baseline OCT biomarkers as predictors of functional outcome. Zur et al. demonstrated that baseline continuous IS-OS layer and submacular fluid responded better to DEX implants. Also, treatment response was not different among treatment-naïve and refractory group (13). Meduri et al. proposed similar conclusions that the presence of SRF and the integrity of EZ were positive biomarkers in predicting the efficacy of DEX implant in treatment-naïve DME patients (18). Vujosevic et al. showed that treatment-naïve DME patients with baseline SRF had a better response to intravitreal dexamethasone rather than to anti-VEGF (19).

The presence of SRF in DME is associated with active inflammation and higher levels of IL-6 in vitreous cavity (20). Corticosteroids are well-known for its efficient anti-inflammation effects, with strong inhibition of TNF- $\alpha$ , VEGF, and ICAM-1, and upregulation of anti-inflammatory agents such as adenosine and IL-10 (21). Therefore, as expected, the presence of baseline SRF served as a good indicator for response to DEX implant treatment.

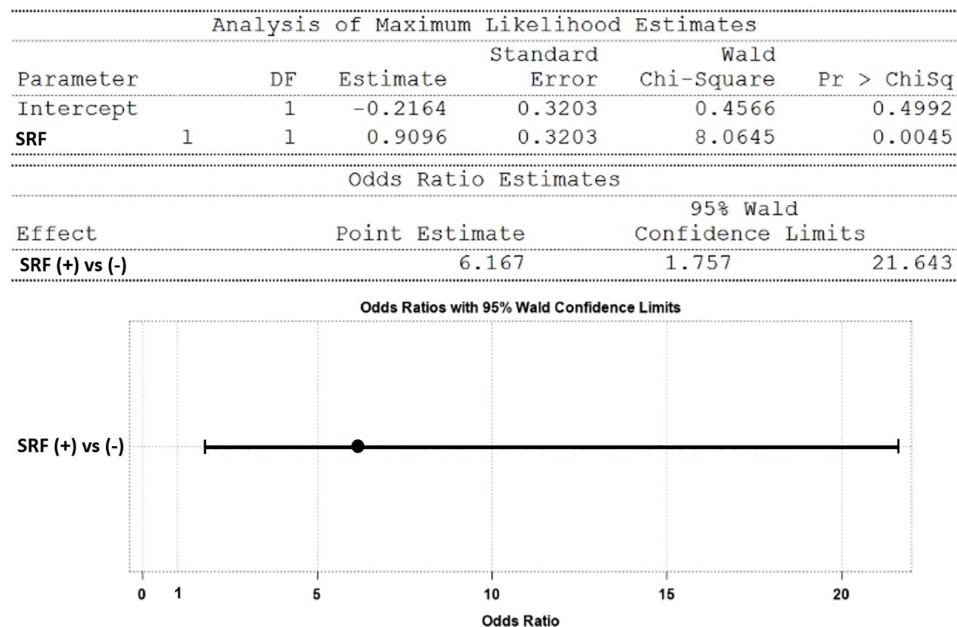
In contrast, the role of baseline HRF is less clear, with some studies considering it as a biomarker for improved DEX implant treatment response (19, 22) and other studies coming to the opposite conclusion, considering the lack of HRF as a better prognostic factor (15, 23). In our current study, the baseline HRF is a neutral OCT biomarker, with no statistically significant prediction of functional and anatomical outcomes, which is similar to the study by Ahn et al. (24). Pathology studies have suggested HRF to be lipoprotein extravasation after breakdown of the inner blood retinal barrier in the initial stages of the development of intraretinal

hard exudates (25). Further studies are needed to identify its role in DME. In our study, higher DR severity may be another reason that baseline HRF had less predictive power for functional and anatomical outcomes. Also, the high percentage of HRF at baseline can be another evidence of high severity (92.2%). In fact, 56.25% (36/64) of the cases showed decreasing amounts of HRF.

In the present study, the reduction of DRIL, LONLC, IRC, and EZD was correlated with more than 100  $\mu$ m CRT improvement. The presence of DRIL in DME was thought of as a sign of chronicity of macular edema and dysfunction of Muller cells (11). We hypothesized that reduction of DRIL after DEX implant might be related to its anti-inflammatory effect on Muller cells, correlating with more CRT improvement. The reduction of other parameters like LONLC and IRC was more apparently related to better anatomical outcome with less space occupied fluid inside the retina. In addition, EZD indicated the breakdown of photoreceptors cells, hindered the normal visual phototransduction and was related to the worse functional outcome (26). We did not find other parameters like ERM, VMI, and the quality and quantity of HRF to be related the visual and anatomical prognosis in the present study.

**TABLE 2 |** Baseline OCT Biomarkers.

Baseline OCT biomarkers	
DRIL (+)	51/64 (79.7%)
ERM (+)	35/64 (54.7%)
EZD (+)	34/64 (53.1%)
HE (+)	46/64 (71.9%)
HRF (+)	59/64 (92.2%)
IRC (+)	53/64 (82.8%)
LONLC (+)	20/64 (31.3%)
SRF (+)	15/64 (23.4%)
VMI (VMA or VMT)	16/64 (25.0%)



\* Variables included before model selection: gender, age, lens status and all baseline OCT biomarkers

**FIGURE 5 |** Model using OCT biomarkers as predictors of CRT improvement greater than 100  $\mu\text{m}$  after treatment (multivariate logistic regression): the presence of SRF at baseline favored an outcome with CRT improvement > 100  $\mu\text{m}$  [SRF (+) vs. (-): odds ratio 6.16 (1.75–21.6)].

**TABLE 3 |** Model using OCT biomarkers as predictors to predict extent of CRT improvement ( $\Delta\text{CRT}$ ) after treatment (multiple regression).

Analysis of variance						
Source	DF	Sum of squares	Mean square	AIC	F-value	Pr > F
Model	1	122,153	122,153	-151.4508	8.01	0.0063
Error	62	945,646	15,252	-165.4669		
Corrected Total	63	1,067,799	0.4375	-201.8591		

Variable	Parameter estimate	Standard error	Type II SS	F-value	Pr > F
Intercept	-54.00000	17.64292	142,884	9.37	0.0033
SRF	-103.13333	36.44305	122,153	8.01	0.0063

\*Variables included before model selection: gender, age, lens status, and all baseline OCT biomarkers.

Central macular thickness is a well-established proxy for treatment outcome in several studies (14–19). However, in our study, there are some gaps between anatomical and functional outcomes. There are some possible explanations. First, we only enrolled DME patients who were confirmed by OCT, with severity indicated by the high presence of IRC, HRF, and DRIL (all near 80%). Also, the use of a DEX implant was considered as second choice in most clinical situations, with 57.8, 43.8, and 42.2% cases having been previously treated with panretinal photocoagulation (PRP), posterior subtenon triamcinolone injection (PST), and anti-VEGF respectively. Combined with the chronicity and high severity of our DME patients, limited visual recovery may occur despite an improved foveal contour. As a results, the findings of our study are still valid if DEX implants are used in an earlier stage or in treatment-naïve patients.

The progression of cataract might bias visual acuity improvement despite successful treatment with DEX implant. Indeed, there would be some cataract progression in patients who received more than one DEX implant. But we are convinced the outcomes are valid for several reasons. First, there was no significant cataract progression that required operation during the follow-up period. More importantly, we performed multivariate analysis and lens status was not significantly associated with outcomes. Previous studies have found similar conclusions that the lens status was not significantly associated with differences in BCVA (10, 27). Lastly, if we had divided our subjects into two groups, the smaller case number in each group would make the outcomes less reliable.

About sample size, because this is a retrospective study, we have collected all the available and eligible cases as many as possible. In the meantime, we did not set up a



**TABLE 4 |** Treatment results of BCVA grouped by baseline OCT biomarker status.

Baseline biomarker	Percentage of eyes with BCVA improvement		Final BCVA response ( $\Delta$ LogMAR, mean $\pm$ SD)	
	(+)	(-)	(+)	(-)
DRIL	24/51 (47.1%)	9/13 (69.2%)	-0.11 $\pm$ 0.43	-0.22 $\pm$ 0.21
ERM	19/35 (54.3%)	14/29 (48.3%)	-0.12 $\pm$ 0.43	-0.15 $\pm$ 0.35
EZD	17/34 (50.0%)	16/30 (53.3%)	-0.20 $\pm$ 0.44	-0.06 $\pm$ 0.33
HE	24/46 (52.2%)	9/18 (50.0%)	-0.14 $\pm$ 0.43	-0.11 $\pm$ 0.28
HRF	32/59 (54.2%)	1/5 (20.0%)	-0.15 $\pm$ 0.41	-0.00 $\pm$ 0.06
IRC	28/53 (52.8%)	5/11 (45.5%)	-0.14 $\pm$ 0.43	-0.09 $\pm$ 0.16
LONLC	9/20 (45.0%)	24/44 (54.5%)	-0.14 $\pm$ 0.52	-0.13 $\pm$ 0.33
SRF	6/15 (40.0%)	27/49 (55.1%)	-0.16 $\pm$ 0.44	-0.13 $\pm$ 0.38
VMI	6/16 (37.5%)	27/48 (56.3%)	-0.09 $\pm$ 0.33	-0.15 $\pm$ 0.41

Comparing positive baseline biomarker status to negative baseline biomarker status, by Chi-Square and Student *t*-test.

**TABLE 5 |** Changes of OCT biomarkers presentation pre (baseline) and after study in whole group and by final CRT response.

	Whole group		Group by final CRT response			
	Pre	After	CRT improved > 100 $\mu$ m		CRT improved $\leq$ 100 $\mu$ m	
			Pre	After	Pre	After
DRIL	51/64 (79.7%)	33/64 (51.6%)*	20/22 (90.9%)	10/22 (45.5%)*	31/42 (73.8%)	23/42 (54.8%)
SRF	15/64 (23.4%)	5/64 (7.8%)*	10/22 (45.5%)	0/22 (0.0%)*	5/42 (11.9%)	5/42 (11.9%)
LONLC	20/64 (31.3%)	7/64 (10.9%)*	10/22 (45.5%)	0/22 (0.0%)*	10/42 (23.8%)	7/42 (16.7%)
IRC	53/64 (82.8%)	42/64 (65.6%)*	21/22 (95.5%)	16/22 (72.7%)*	32/42 (76.2%)	26/42 (61.9%)
EZD	34/64 (53.1%)	25/64 (39.1%)	17/22 (77.3%)	10/22 (45.5%)*	17/42 (40.5%)	15/42 (35.7%)

\**p* < 0.05, compared to pre-study, by Chi-Square test.

**TABLE 6 |** Changes of OCT biomarkers presentation in groups and by final BCVA response.

	Group by final BCVA response			
	VA improved ( $\Delta$ LogMAR < 0)		VA not improved ( $\Delta$ LogMAR $\geq$ 0)	
	Pre	After	Pre	After
DRIL	22/33 (72.7%)	15/33 (45.5%)*	27/31 (87.1%)	18/31 (58.1%)*
SRF	6/33 (18.2%)	1/33 (3.0%)*	9/31 (29.0%)	4/31 (12.9%)
LONLC	9/33 (27.3%)	3/33 (9.1%)	11/31 (35.5%)	4/31 (12.9%)*
IRC	28/33 (84.9%)	22/33 (66.7%)	25/31 (80.7%)	20/31 (64.5%)
EZD	17/33 (51.5%)	9/33 (27.3%)*	17/31 (54.8%)	16/31 (51.6%)

\**p* < 0.05, compared to pre-study, by Chi-Square test.

minimally required sample size because the main purpose of this study is not to compare outcomes between exposure and non-exposure groups for which sample size is crucial in the study design to make sure the power of the study is enough to confirm the value of intervention. Instead, the nature of our study is an exploratory one, which focused on the presentation of OCT biomarkers in patients with different characteristics, their changes during the treatment process, their role of prediction to treatment response and so on.

Most of the limitations of this study came from its retrospective nature. And the clinical decision to initiate DEX

implant was based on the physician's choice. Moreover, due to the strict inclusion and exclusion criteria, there were a relatively low number of study subjects. Also, we could not separately treat naïve patient from the non-naïve patients. However, we provided the wash-out period (intraocular anti-VEGF within 3 months or corticosteroids within 6 months). Wide field fluorescein angiographies were not analyzed, therefore information regarding macular perfusion and peripheral non-ischemia area was not available.

In conclusion, OCT biomarkers can be used to guide selection of DME patients who may most benefit from DEX implants. We furthermore suggest that DEX implant should be considered as

a first-line treatment in patient with SRF at baseline. Changes of DRIL, SRF, LONLC, IRC, and EZD can also help predict the treatment response in DEX implant. Further head-to-head large-scale clinical trial between anti-VEGF agents and DEX implant is needed to identify the role of these OCT biomarkers to optimized current treatment of DME patients.

## DATA AVAILABILITY STATEMENT

The raw data supporting the conclusions of this article will be made available by the authors, without undue reservation.

## REFERENCES

- International Diabetes Federation. *IDF Diabetes Atlas*. 8th ed. Brussels: International Diabetes Federation (2017).
- Kempner JH, O'Colmain BJ, Leske MC, Haffner SM, Klein R, Moss SE, et al. The prevalence of diabetic retinopathy among adults in the United States. *Arch Ophthalmol.* (2004) 122:552–63. doi: 10.1001/archophth.122.4.552
- Yau JWY, Rogers SL, Kawasaki R, Lamoureux EL, Kowalski JW, Bek T, et al. Global prevalence and major risk factors of diabetic retinopathy. *Diabetes Care.* (2012) 35:556–64.
- Lee R, Wong TY, Sabanayagam C. Epidemiology of diabetic retinopathy, diabetic macular edema and related vision loss. *Eye Vis (Lond).* (2015) 2:17. doi: 10.1186/s40662-015-0026-2
- Jaulim A, Ahmed B, Khanam T, Chatziralli I. Branch retinal vein occlusion: epidemiology, pathogenesis, risk factors, clinical features, diagnosis, and complications. An update of the literature. *Retina.* (2013) 33:901–10. doi: 10.1097/IAE.0b013e3182870c15
- Bressler SB, Glassman AR, Almukhtar T, Bressler NM, Ferris FL, Googe JM Jr., et al. Five-year outcomes of ranibizumab with prompt or deferred laser versus laser or triamcinolone plus deferred ranibizumab for diabetic macular edema. *Am J Ophthalmol.* (2016) 164:57–68. doi: 10.1016/j.ajo.2015.12.025
- Heier JS, Korobelnik JF, Brown DM, Schmidt-Erfurth U, Do DV, Midena E, et al. Intravitreal aflibercept for diabetic macular edema: 148-week results from the VISTA and VIVID studies. *Ophthalmology.* (2016) 123:2376–85. doi: 10.1016/j.ophtha.2016.07.032
- Busch C, Fraser-Bell S, Iglicki M, Lupidi M, Couturier A, Chaikitmongkol V, et al. Real-world outcomes of non-responding diabetic macular edema treated with continued anti-VEGF therapy versus early switch to dexamethasone implant: 2-year results. *Acta Diabetol.* (2019) 56:1341–50. doi: 10.1007/s00592-019-01416-4
- Haller JA, Kuppermann BD, Blumenkranz MS, Williams GA, Weinberg DV, Chou C, et al. Randomized controlled trial of an intravitreal dexamethasone drug delivery system in patients with diabetic macular edema. *Arch Ophthalmol.* (2010) 128:289–96. doi: 10.1001/archophth.128.10.289
- Hsia NY, Lin CJ, Chen HS, Chang CH, Bair H, Lai CT, et al. Short-term outcomes of refractory diabetic macular edema switch from ranibizumab to dexamethasone implant and the influential factors: a retrospective real world experience. *Front Med (Lausanne).* (2021) 8:649979. doi: 10.3389/fmed.2021.649979
- Zur D, Iglicki M, Sala-Puigdollers A, Chhablani J, Lupidi M, Fraser-Bell S, et al. Disorganization of retinal inner layers as a biomarker in patients with diabetic macular oedema treated with dexamethasone implant. *Acta Ophthalmol.* (2020) 98:e217–23. doi: 10.1111/aos.14230
- Murakami T, Yoshimura N. Structural changes in individual retinal layers in diabetic macular edema. *J Diabetes Res.* (2013) 2013:920713. doi: 10.1155/2013/920713
- Zur D, Iglicki M, Busch C, Invernizzi A, Mariuzzi M, Loewenstein A, et al. OCT biomarkers as functional outcome predictors in diabetic macular edema treated with dexamethasone implant. *Ophthalmology.* (2018) 125:267–75. doi: 10.1016/j.ophtha.2017.08.031

## ETHICS STATEMENT

The studies involving human participants were reviewed and approved by the China Medical University Hospital. The ethics committee waived the requirement of written informed consent for participation.

## AUTHOR CONTRIBUTIONS

All authors listed have made a substantial, direct, and intellectual contribution to the work, and approved it for publication.

- Schmidt-Erfurth U, Garcia-Arumi J, Bandello F, Berg K, Chakravarthy U, Gerendas BS, et al. Guidelines for the management of diabetic macular edema by the European society of retina specialists (EURETINA). *Ophthalmologica.* (2017) 237:185–222. doi: 10.1159/000458539
- Boyer DS, Yoon YH, Belfort R Jr., Bandello F, Maturi RK, Augustin AJ, et al. Three-year, randomized, sham-controlled trial of dexamethasone intravitreal implant in patients with diabetic macular edema. *Ophthalmology.* (2014) 121:1905–14. doi: 10.1016/j.ophtha.2014.04.024
- Chhablani J, Wong K, Tan GS, Sudhakar A, Laude A, Cheung CMG, et al. Diabetic macular edema management in asian population: expert panel consensus guidelines. *Asia Pac J Ophthalmol (Phila).* (2020) 9:426–34. doi: 10.1097/APO.0000000000000312
- Das T, Aurora A, Chhablani J, Giridhar A, Kumar A, Raman R, et al. Evidence-based review of diabetic macular edema management: consensus statement on Indian treatment guidelines. *Indian J Ophthalmol.* (2016) 64:14–25. doi: 10.4103/0301-4738.178142
- Meduri A, Oliverio GW, Trombetta L, Giordano M, Inferrera L, Trombetta CJ. Optical coherence tomography predictors of favorable functional response in naïve diabetic macular edema eyes treated with dexamethasone implants as a first-line agent. *J Ophthalmol.* (2021) 2021:6639418. doi: 10.1155/2021/6639418
- Vujosevic S, Toma C, Villani E, Muraca A, Torti E, Florimbi G, et al. Diabetic macular edema with neuroretinal detachment: OCT and OCT-angiography biomarkers of treatment response to anti-VEGF and steroids. *Acta Diabetol.* (2020) 57:287–96. doi: 10.1007/s00592-019-01424-4
- Sonoda S, Sakamoto T, Yamashita T, Shirasawa M, Otsuka H, Sonoda Y. Retinal morphologic changes and concentrations of cytokines in eyes with diabetic macular edema. *Retina.* (2014) 34:741–8. doi: 10.1097/IAE.0b013e3182a48917
- Lupo G, Motta C, Giurdanella G, Anfuso CD, Alberghina M, Drago F, et al. Role of phospholipases A2 in diabetic retinopathy: in vitro and in vivo studies. *Biochem Pharmacol.* (2013) 86:1603–13. doi: 10.1016/j.bcp.2013.09.008
- Ceravolo I, Oliverio GW, Alibrandi A, Bhatti A, Trombetta L, Rejdak RT, et al. The Application of Structural Retinal Biomarkers to Evaluate the Effect of Intravitreal Ranibizumab and Dexamethasone Intravitreal Implant on Treatment of Diabetic Macular Edema. *Diagnostics (Basel).* (2020) 10:413. doi: 10.3390/diagnostics10060413
- Chatziralli I, Santarelli M, Patrao N, Nicholson L, Zola M, Rajendram R, et al. Identification of time point to best define 'sub-optimal response' following intravitreal ranibizumab therapy for diabetic macular edema based on real-life data. *Eye (Lond).* (2017) 31:1594–9. doi: 10.1038/eye.2017.111
- Ahn J, Han S, Ahn SM, Kim SW, Oh J. Clinical implications of suspended scattering particles in motion observed by optical coherence tomography angiography. *Sci Rep.* (2020) 10:15. doi: 10.1038/s41598-019-55606-9
- Bolz M, Schmidt-Erfurth U, Deak G, Mylonas G, Kriechbaum K, Scholda C. Diabetic retinopathy research group Vienna. Optical coherence tomographic hyperreflective foci: a morphologic sign of lipid extravasation in diabetic macular edema. *Ophthalmology.* (2009) 116:914–20. doi: 10.1016/j.ophtha.2008.12.039
- Santos AR, Alves D, Santos T, Figueira J, Silva R, Cunha-Vaz JG. Measurements of retinal fluid by optical coherence tomography leakage in diabetic macular

- edema: a biomarker of visual acuity response to treatment. *Retina*. (2019) 39:52–60. doi: 10.1097/IAE.0000000000001905
27. Pinto M, Mathis T, Massin P, Akesbi J, Lereuil T, Voirin N, et al. Visual acuity gain profiles and anatomical prognosis factors in patients with drug-naïve diabetic macular edema treated with dexamethasone implant: the NAVEDEX study. *Pharmaceutics*. (2021) 13:194. doi: 10.3390/pharmaceutics13020194

**Conflict of Interest:** H-SC was employed by NephroCare Ltd.

The remaining authors declare that the research was conducted in the absence of any commercial or financial relationships that could be construed as a potential conflict of interest.

**Publisher's Note:** All claims expressed in this article are solely those of the authors and do not necessarily represent those of their affiliated organizations, or those of the publisher, the editors and the reviewers. Any product that may be evaluated in this article, or claim that may be made by its manufacturer, is not guaranteed or endorsed by the publisher.

Copyright © 2022 Huang, Chang, Meng, Lin, Lai, Hsia, Chen, Tien, Bair, Lin, Chen and Tsai. This is an open-access article distributed under the terms of the Creative Commons Attribution License (CC BY). The use, distribution or reproduction in other forums is permitted, provided the original author(s) and the copyright owner(s) are credited and that the original publication in this journal is cited, in accordance with accepted academic practice. No use, distribution or reproduction is permitted which does not comply with these terms.



# Uveal Effusion Syndrome: Clinical Characteristics, Outcome of Surgical Treatment, and Histopathological Examination of the Sclera

Nan Zhou, Lihong Yang, Xiaolin Xu and Wenbin Wei\*

Beijing Tongren Eye Center, Beijing Key Laboratory of Intraocular Tumor Diagnosis and Treatment, Medical Artificial Intelligence Research and Verification Laboratory of the Ministry of Industry and Information Technology, Beijing Tongren Hospital, Capital Medical University, Beijing, China

## OPEN ACCESS

### Edited by:

Haijiang Lin,  
Harvard Medical School,  
United States

### Reviewed by:

Carlos Pavesio,  
Moorfields Eye Hospital NHS  
Foundation Trust, United Kingdom  
Liu Yang,  
Peking University First Hospital, China

### \*Correspondence:

Wenbin Wei  
weiwenbintr@163.com

### Specialty section:

This article was submitted to  
Ophthalmology,  
a section of the journal  
Frontiers in Medicine

**Received:** 29 September 2021

**Accepted:** 17 January 2022

**Published:** 09 June 2022

### Citation:

Zhou N, Yang L, Xu X and Wei W  
(2022) Uveal Effusion Syndrome:  
Clinical Characteristics, Outcome of  
Surgical Treatment, and  
Histopathological Examination of the  
Sclera. *Front. Med.* 9:785444.  
doi: 10.3389/fmed.2022.785444

**Purpose:** In this study, we aimed to investigate clinical characteristics and histopathology and evaluate surgical outcomes of quadrant lamellar sclerectomy with sclerostomy for uveal effusion syndrome (UES).

**Design:** Retrospective, cohort study.

**Participants:** Overall, 106 eyes of 66 patients diagnosed with UES were treated at the Beijing Tongren Hospital between January 1, 2001 and June 26, 2021.

**Methods:** Patients were examined by routine ophthalmologic examinations, fluorescein and indocyanine green angiography (FFA/ICGA); axial length determination; color Doppler ultrasound (CDU); ultrasound biomicroscopy (UBM), optical coherence tomography (OCT), and optical coherence tomographic angiography (SD/SS-OCTA). Quadrant lamellar sclerectomy with sclerostomy was performed at the equator in all patients and histopathological examination of the excised sclera was analyzed in all samples.

**Main Outcome Measures:** The reattachment of the choroid and retina with resolution of the serous fluid, best corrected visual acuity (BCVA), choroidal thickness, and recurrence of ciliochoroidal detachment were the main outcome measures.

**Results:** Two subgroups were identified: (1) type 1 (nanophthalmic eye), wherein the eyeball was small (average axial length  $15.83 \pm 1.45$  mm) with high hypermetropia (average 12.6 diopters) and (2) type 2 (non-nanophthalmic eye), wherein the eyeball size was normal (average axial length  $23.45 \pm 1.68$  mm) with or without refractive error, combined with or without systemic symptoms. Histopathologically, types 1 and 2 demonstrated similarly abnormal sclera with the disorganization of collagen fiber bundles and deposits of proteoglycans in the matrix. Quadrant lamellar sclerectomy with sclerostomy was effective in both types 1 and 2, inducing post-operative resolution of the subretinal fluid accumulation and increasing the useful BCVA. The choroidal thickness was significantly different before and after surgery ( $P < 0.05$ ). Approximately 98.1% of cases attained permanent reattachment within 6 months after one operation through this procedure. The single operation success rate was 96.2%, and success with one or two operations was 100%.



**Conclusions:** UES is caused by abnormalities of the sclera and increased resistance to transscleral fluid outflow, combined with increased choroidal thickness. Quadrantic lamellar-sclerectomy with sclerostomy is an effective treatment for UES that can rescue correct the useful visual acuity.

**Keywords:** uveal effusion syndrome, nanophthalmic eye, idiopathic ciliochoroidal detachment, clinical characteristics, outcomes of surgical treatment

## INTRODUCTION

The term “uveal effusion syndrome” was first described by Schepens and Brockhurst in 1963 (1). Subsequently, in 1975, Brockhurst (2) reported that this entity condition was associated with nanophthalmos and scleral abnormality and that the congestion of the choroidal venous system caused by the compression of vortex veins by a thick sclera was the cause of subretinal fluid accumulation. He then proposed a novel surgical procedure involving vortex vein decompression (3). Based on these studies, the nanophthalmos and abnormality of the sclera were considered the pathogenic factors associated with UES.

In 1982, Gass and Jallow (4) reported idiopathic serous detachment of the retina, ciliary body, and choroid, and termed it idiopathic uveal effusion syndrome (IUES). They conjectured that this disorder was caused by scleral abnormality with enhanced resistance to the outflow of transscleral intraocular protein; they introduced (5, 6) a surgical procedure comprising scleral resection without vortex vein decompression. Trelstad et al. (7) revealed that a sclera with UES demonstrated histochemical abnormalities and their findings were supported by subsequent studies (8–12). Forrester (13) believed that IUES was a type of ocular mucopolysaccharidosis, with the initial defect resting in the proteodermatan synthesis and/or degradation by the scleral fibroblasts. Additional evidence also showed that abnormal mucopolysaccharides of the sclera played an important role in IUES pathogenesis.

These reports indicated that in UES, scleral abnormality impedes transscleral outflow of intraocular protein and fluid and compresses the vortex veins, resulting in choroidal vein congestion. Intraocular fluid accumulates in the choroidal space, leading to ciliochoroidal detachment (14–18).

However, optimum treatment methods for UES have been debated. Vortex vein decompression with scleral resection was initially advocated for the treatment of uveal effusion associated with nanophthalmos. Gass (17) believed that the treatment effect had less to do with vortex vein decompression than with scleral resection to facilitate protein and fluid drainage through the sclera. The effectiveness of scleral resection and sclerostomy were also reported in subsequent studies (19–22).

In our study, we describe the clinical characteristics of UES and classify UES eyes into two subgroups based on axial length, refractive error, and systemic symptoms. In addition, to further explore the therapeutic effectiveness for UES in Asian patients, we performed a minimum volume quadrantic surgical procedure and followed up for a long time for detecting

the resolution of the ciliochoroidal detachment and the useful final vision.

## PATIENTS AND METHODS

We retrospectively analyzed 106 eyes of 66 consecutive Asian patients diagnosed with primary UES treated from January 1, 2001 to June 26, 2021 at the Beijing Tongren Hospital. The study and data collection were in compliance with the principles of the Declaration of Helsinki, and written informed consent was obtained from all participants. The operative procedure was performed by senior ophthalmologists (WB, W).

Cases that met the following inclusion criteria were included: (1) the fundus showed bullous retinal detachment in the periphery without any evidence of rhegmatogenous retinal detachment; (2) retinal detachment was accompanied by annular peripheral flat or bullous ciliochoroidal detachment; (3) FA/ICGA demonstrated a leopard-spot pigmentation sign without leakage from the choroid into the subretinal space; (4) the ora serrata was easily observed without scleral depression; (5) subretinal fluid was easily shifted from its position, and (6) other causes of ciliochoroidal detachment such as prolonged hypotony, intraocular tumor, dural arteriovenous fistula, and intraocular inflammation were excluded.

The clinical data concerning patient demographics, associated ocular and systemic disease, treatment history, ocular symptoms, BCVA, and intraocular pressure (IOP), axial length (by A-scan or IOL-master), standard ocular CDU (since 2010), UBM (since 2013), FFA/ICGA, choroidal thickness (by EDI-OCT/OCTA [ $\mu\text{m}$ ], since 2010), as well as OCT and SD/SS-OCTA (since 2010) were collected. The surgical findings including intraoperative and post-operative period were noted. A record of the histopathological features was listed. Long-term outcomes, in terms of reattachment of the choroid and retina, BCVA, choroidal thickness, surgical side effects, and recurrence of UES, were assessed.

## Operative Procedure

Surgical treatment was performed in all eyes included in this study, the main surgical procedure was as Gass described previously (5), but we modified and adopted minimum volume standards for surgical procedures. We performed lamellar-sclerectomy with sclerostomy at two sites in the temporoinferior and nasoinferior quadrants during the initial surgery; if recurrence occurred, we

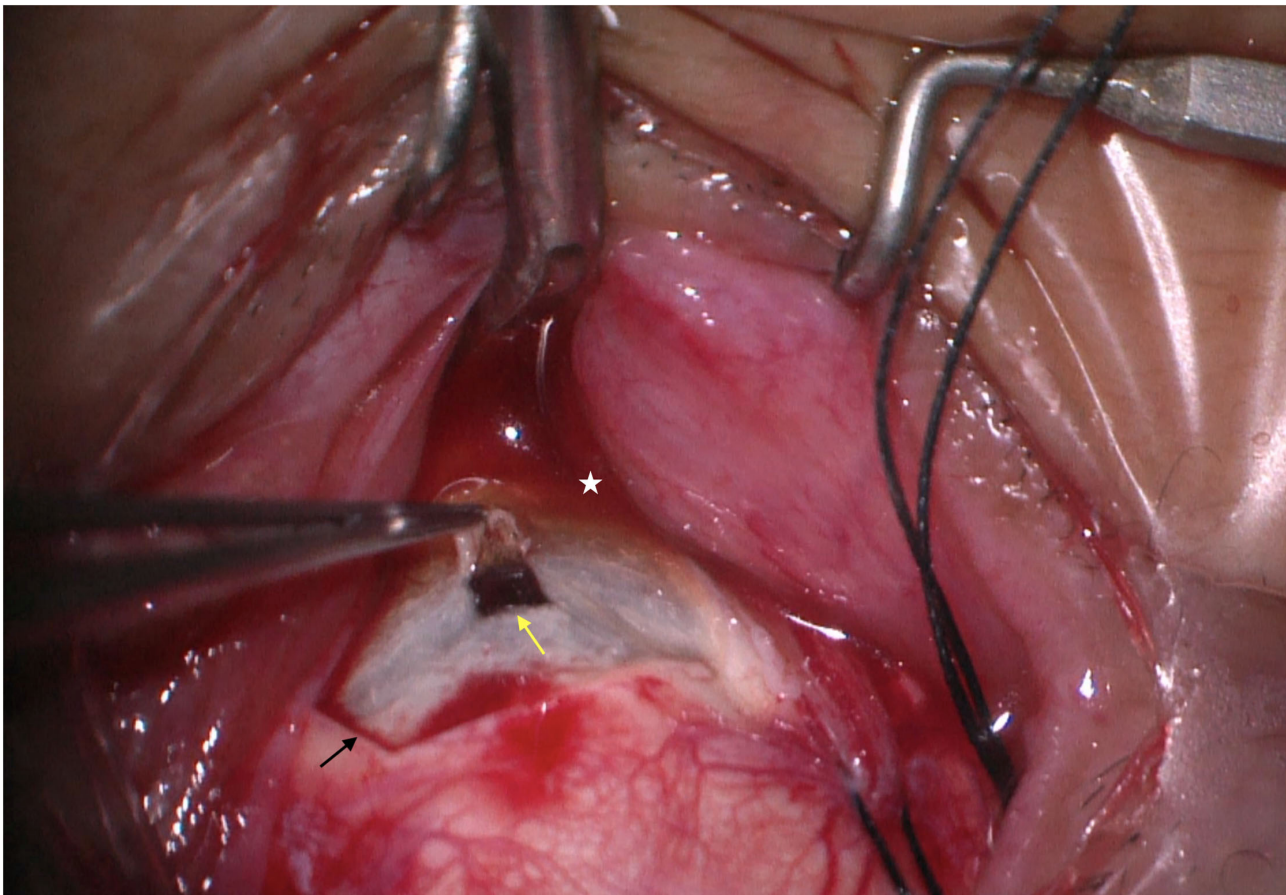


**FIGURE 1 |** Quadrantic lamellar-sclerectomy with sclerostomy. At the equator of each quadrant, we created a two-thirds thickness scleral incision measuring 6 mm × 4 mm (black arrow), on the center of each sclerectomy bed, the sclerostomy was excised in pieces measuring 2 mm × 2 mm (yellow arrow), and the choroid was exposed. The image was taken immediately after the sclerostomy was completed. Note that the choroid is exposed and abundant yellow serous suprachoroidal fluid was spontaneously released (white star).

performed additional surgeries at the equator in the supratemporal and supranasal quadrants following a similar procedure.

At the equator of these two quadrants, extending from immediately behind the extraocular muscle insertions to the vortex veins, we created a two-third thickness of scleral incision measuring ~5–6 mm × 3–4 mm (**Figure 1**) and performed sclerectomies in each quadrant. On the center of each sclerectomy bed, the sclerostomy that was excised in pieces measuring ~2 mm × 2 mm and the choroid were exposed. When sclerectomy was performed and the choroid was exposed, abundant serous suprachoroidal fluid was spontaneously released. If IOP was decreased during choroidal drainage, a small amount of balanced salt solution (BSS) (0.5–1.5 ml) was injected with a 30-gauge needle at a site 3.0 to 3.5 mm from the limbus into the eyeball to maintain the IOP. Tenon's capsule and the bulbar conjunctiva were closely sutured using 8-0 Vicryl sutures. We did not perform the vortex vein decompression. All excised scleral pieces were analyzed via histopathological examinations.

Patients were followed up regularly by previously described ophthalmologic examinations on months 1, 2, and 3 after surgery, and then every 6 months thereafter during the follow-up visits. In addition, FA/ICGA and EDI-OCT/OCTA were repeatedly examined.

### Statistical Analysis

Data collected on continuous scale, including age (years), axial length (millimeters) and choroidal thickness (μm), were expressed as mean, median, minimum, and maximum. Student's *t*-test was performed to compare the choroidal thickness and BCVA measurements pre- and post-operation. *P*-value <0.05 was considered to be significantly different. All analyses were performed using Stata version 15.0 (StataCorp. LLC, College Station, TX, USA).

### RESULTS

In all, 106 eyes of 66 patients (Asian/Chinese) with UES were included in this study and underwent quadrant

lamellar-sclerectomy with sclerostomy. The mean patient age was  $36.08 \pm 12.67$  years (median, 43; range, 26–62). To evaluate the effect of surgical management on the affected eyes, we divided patients with UES into two subgroups according to the following criteria: type 1, nanophthalmic eye, axial length  $<19.0$  mm, with high grade of hypermetropia in refraction; type 2, non-nanophthalmic eye with abnormal sclera, normal axial length ( $\geq 21.0$  mm), with or without accompanied systemic symptoms. During the time of surgery, types 1 and 2 demonstrated rigid and thickened sclera. CDU showed the highest scleral thickness of 2.1–3.2 mm.

Among the 106 eyes in 66 patients with UES, type 1 was found in 62 eyes (31 patients) and type 2 in 44 eyes (35 patients). Among them, 30 eyes (29%) were previously treated with periocular corticosteroids (triamcinolone acetonide or methylprednisolone) and showed no effective response. The median follow-up duration was 65.3 months (range, 12–122 months). Clinical data of the patients and eyes are listed in Table 1.

**TABLE 1 |** Descriptive characteristics of patients with UES of type 1 and type 2.

Characteristics	Type 1 (nanophthalmic eye) $n1 = 31$ patients, $n2 = 62$ eyes	Type 2 (non-nanophthalmic eye) $n1 = 35$ ; $n2 = 44$ eyes
Age (yes)		
Mean	$35.86 \pm 12.22$	$44.68 \pm 8.18$
Median (range)	31 (26–62)	43 (32–62)
Sex, No. (%)		
Female (%)	42 (13/31)	57 (20/35)
Male (%)	58 (18/31)	43 (15/35)
Laterality	100%	26 (9/35)
Right eye (%)	/	40 (21/52)
Left eye (%)	/	60 (31/52)
Axial length (mm)		
Mean	$15.83 \pm 1.45$	$23.45 \pm 1.68$
Median (range)	15.16 (13.85–18.03)	24.03 (21.4–26.20)
Average refractive error (D)	+12.6	<1.00
Closed angle glaucoma (%)	97 (60/62)	None
Systemic symptoms ( $n$ , %)	None	polyarteritis nodosa (1, 2.8%), psoriasis (2, 5.7%), demyelinating disease (1, 2.8%), rheumatoid arthritis (2, 5.7%), Sjogren Syndrome (1, 2.8%), chronic dermatitis (1, 2.8%), vasculitis (2, 5.7%), facial nevus flammeus (port-wine stain) (1, 2.8%)
Episcleral vessel dilation (%)	None	81.8% (36/44)
Recurrences during follow-up (%)	6 (4/62)	None

UES, uveal effusion syndrome; yes, years; D, diopter.

## Clinical Characteristics of UES Patients

### Type 1 (Nanophthalmic Eye)

There were 62 eyes in 31 patients in this group and all patients presented with bilateral nanophthalmos eyes (Figure 2A). The mean age was  $35.86 \pm 12.22$  years (median, 31; range, 26–62 years), with 18 males and 13 females (Table 1). All patients were in good health systemically. Axial length was  $15.83 \pm 1.45$  mm (median, 15.16, ranged, 13.85–18.03 mm), and the axial lengths showed  $<1$  mm difference between both eyes of a single patient. Both eyes demonstrated high hypermetropia, with an average of +12.6 D (ranging, +8.9 to +18.0 D).

Further, 60 eyes (97%) of 30 patients showed a peripheral shallow anterior chamber because of a swollen iris, and underwent YAG laser iridectomy, and IOP was within normal limits in all eyes post-operatively. Exudative bullous retinal detachment accompanied by annular peripheral ciliochoroidal detachment was observed in the unilateral eye (Figure 2B); and slight annular ciliochoroidal detachment and choroidal folds that were not significant were seen in the contralateral eye.

Both eyes demonstrated a small optic disc with slight papilledema, which was commonly observed in the highly hypermetropic eye. FFA did not reveal any abnormality except retinal vein dilation in 33 eyes; however, a leopard-spot sign of granular hyperfluorescence of the retinal pigment epithelium (RPE) was observed in the posterior pole and inferior quadrants in all eyes (Figure 3A). ICGA revealed diffusely granular marked choroidal hyperfluorescence at an early stage, which increased with time and persisted until the late stage as diffuse intense choroidal hyperfluorescence (Figure 3B). The abnormal ICGA findings in the affected eye were the same as those observed in the fellow eye. UBM showed the presence of ciliary body edema and detachment in all eyes, which led to an anterior rotation of the ciliary body. CDU clearly demonstrated small eye sizes and remarkably thickened sclera (mean 2.5 mm), with the accumulation of subretinal fluid.

### Type 2 (Non-nanophthalmic Eye)

There were 44 eyes of 35 patients in this group; most of the patients (26/35, 74.3%) showed unilateral UES. The mean age was  $44.68 \pm 8.18$  years (median, 43; range, 32–62 years), with 15 males and 20 females (Table 1). Axial length was  $23.45 \pm 1.68$  mm (median, 24.03, range, 21.4–26.20 mm). Both eyes of a single patient revealed almost the same normal axial lengths. The difference in the axial length in both eyes was within 1.0 mm. Refractive errors of these eyes were  $<1.00$  D, without any high hyperopia.

The accompanying systemic symptoms were polyarteritis nodosa in 1 patient, psoriasis in 2 patients, demyelinating disease in 1 patient, rheumatoid arthritis in 2 patients, Sjogren Syndrome in 1 patient, chronic dermatitis in 1 patient, vasculitis in 2 patients, and facial nevus flammeus (port-wine stain) in 1 patient (Figure 4A). External eye examination revealed episcleral vessel dilation (36/44, 81.8%) (Figure 4B); anterior chamber was free of cells; IOP was normal in all eyes. Fundus examination demonstrated typical manifestations of exudative retinal detachment associated with ciliochoroidal detachment similar to those observed in type 1, except that there was no



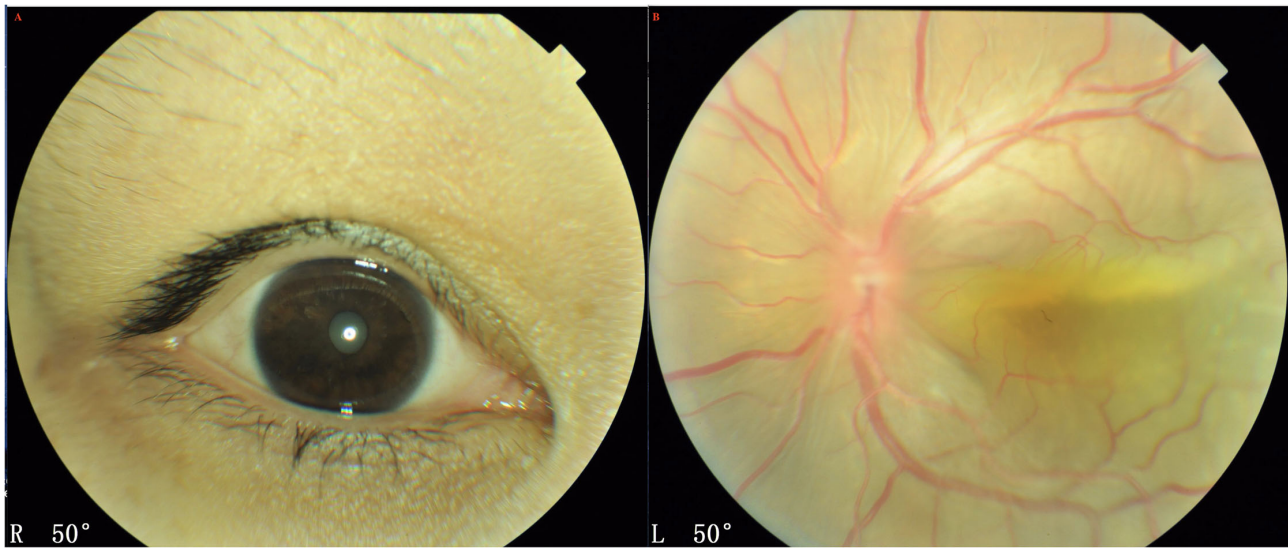


**FIGURE 2** | A 27-year- women with UES type 1. **(A)** Patients presented with nanophthalmos eyes. **(B)** Exudative retinal detachment accompanied by annular peripheral ciliochoroidal detachment was observed (Imagenet 6, Topcon, Japan).

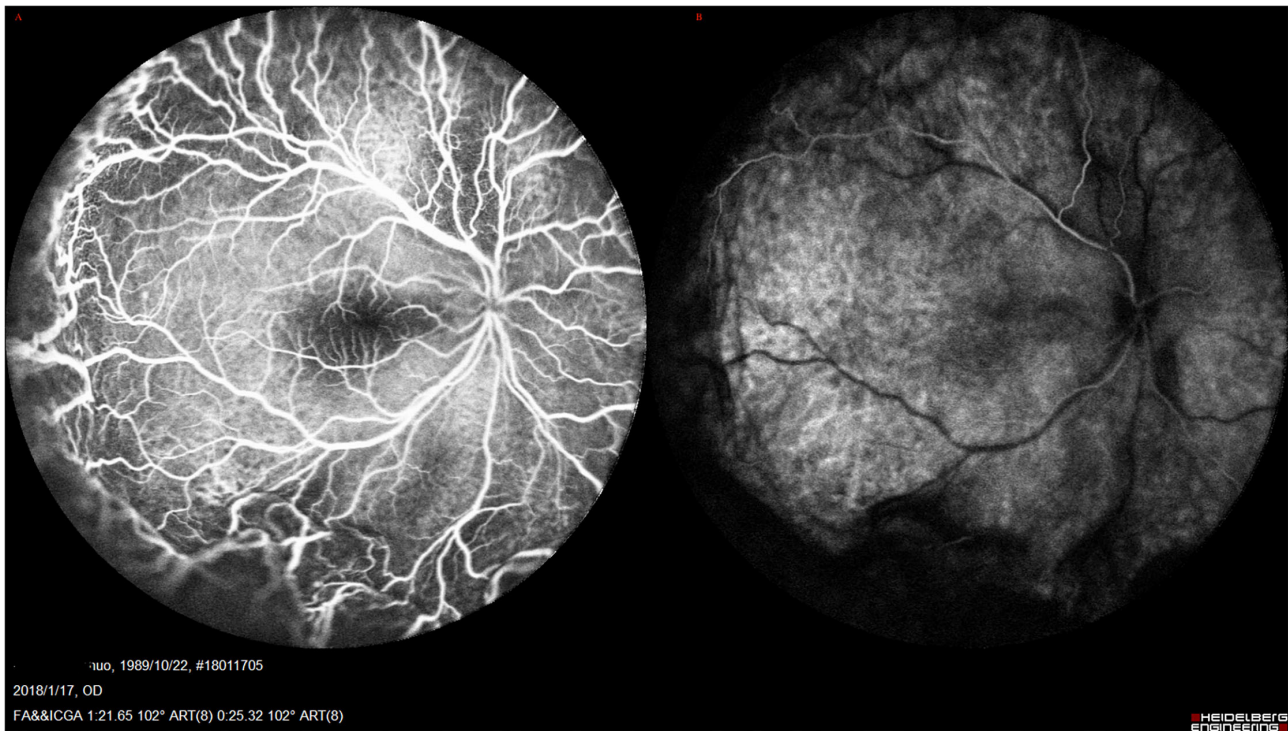
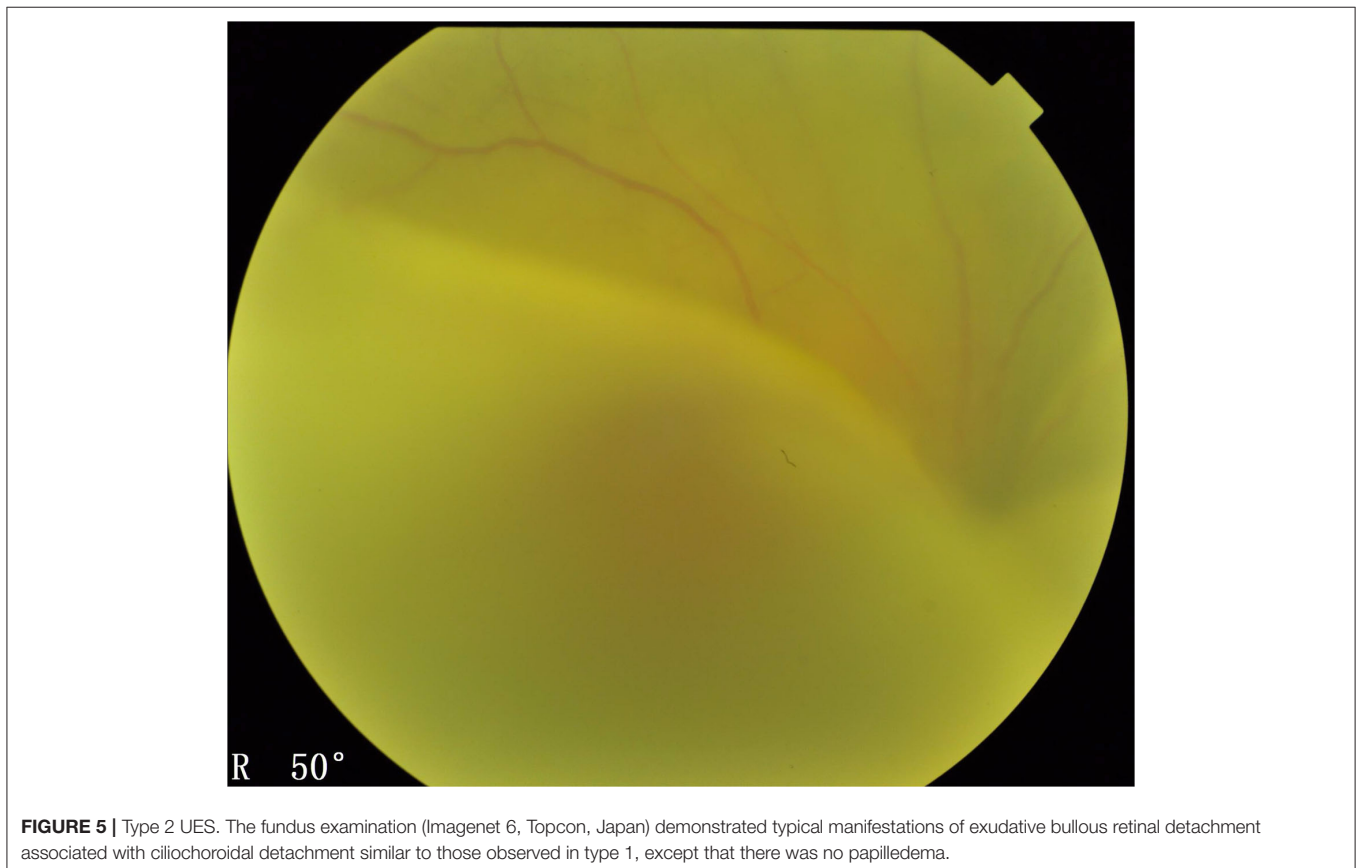
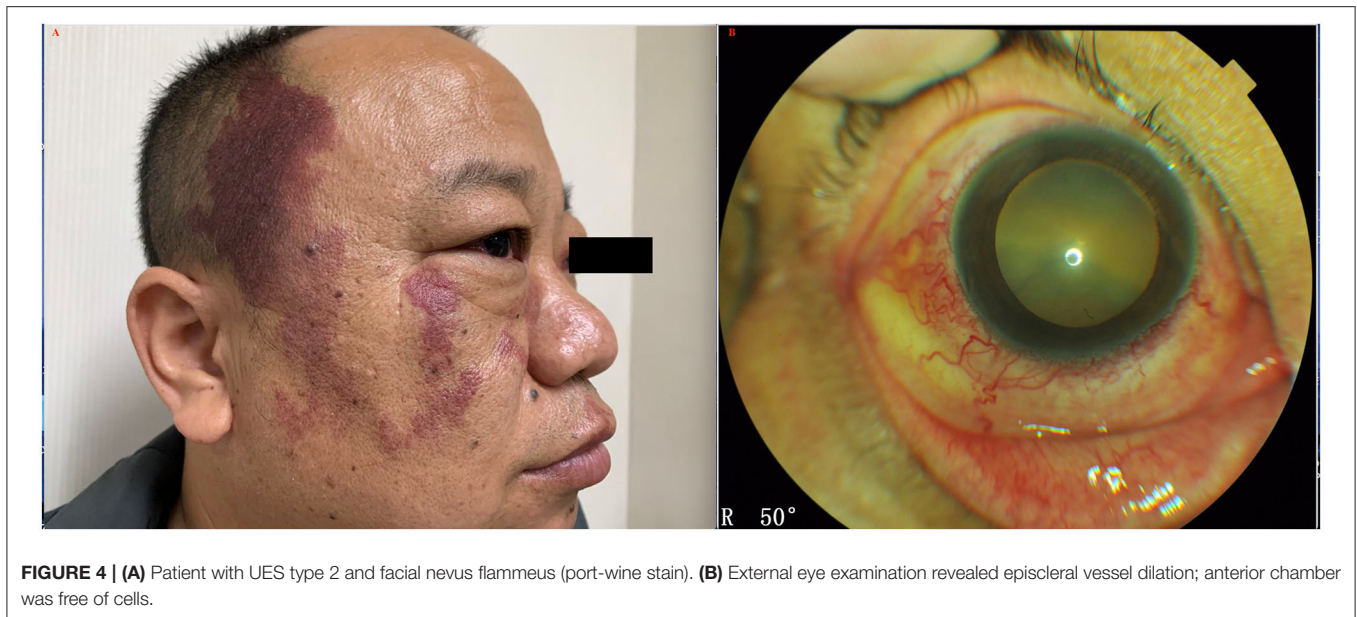


**FIGURE 3** | UES in Type 1. **(A)** FFA (Spectralis; Heidelberg Engineering, Inc.) revealed the retinal vein dilation with leopard-spot sign of granular hyperfluorescence of the retinal pigment epithelium (RPE) was observed in the posterior pole and inferior quadrants. **(B)** ICGA revealed diffusely granular marked choroidal hyperfluorescence at the early stage, which increased with time and persisted until the late stage as diffuse intense choroidal hyperfluorescence.

papilledema (**Figure 5**). FA/ICGA findings showed diffuse patchy hyperfluorescence and leopard-spot signs, which were almost similar to those observed in type 1, without dye leakage in any eye (**Figures 6A,B**). UBM showed the presence of a ciliochoroidal

effusion and ciliary body detachment, similar to type 1, in the affected eyes. In all patients, CDU showed normal-sized eyes, with marked thickening of the sclera (mean 2.7 mm) and choroidal and retinal detachment in all eyes (**Figure 7**).





## OCT and OCTA

The choroidal thickness and macular areas in both eyes of UES patients were evaluated via OCT and OCTA. All eyes (type 1 and type 2) showed pachychoroid.

In type 1, EDI-OCT was performed in 42 eyes of 21 patients and a choroidal thickness of  $869.46 \pm 8.33 \mu\text{m}$  (range,  $381.20\text{--}878.58 \mu\text{m}$ ) was observed (**Figure 8**); both eyes of the same patient showed almost the same choroidal thickness

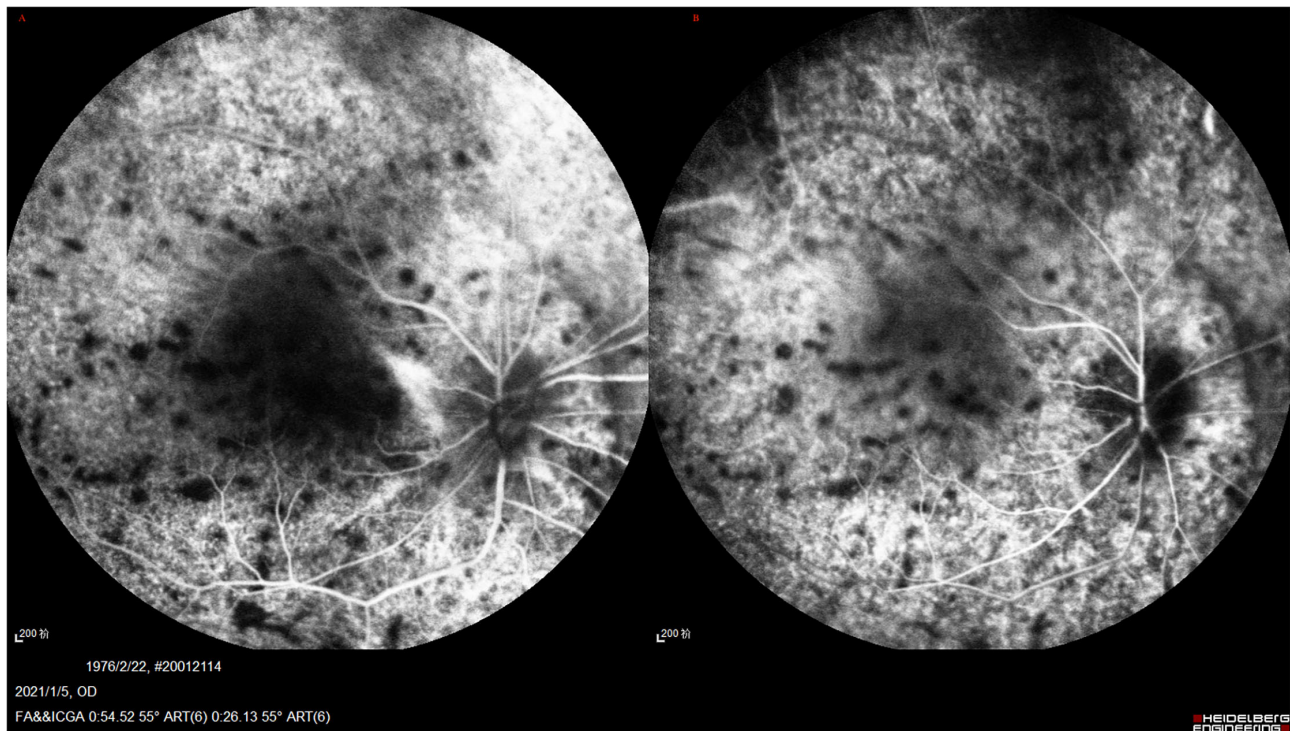


**FIGURE 6 | (A,B)** UES in type 2. FA/ICGA (Spectralis; Heidelberg Engineering, Inc) findings showed diffused patchy hyperfluorescence and leopard-spot sign, which were almost similarly observed in type 1, without dye leakage in any eye.

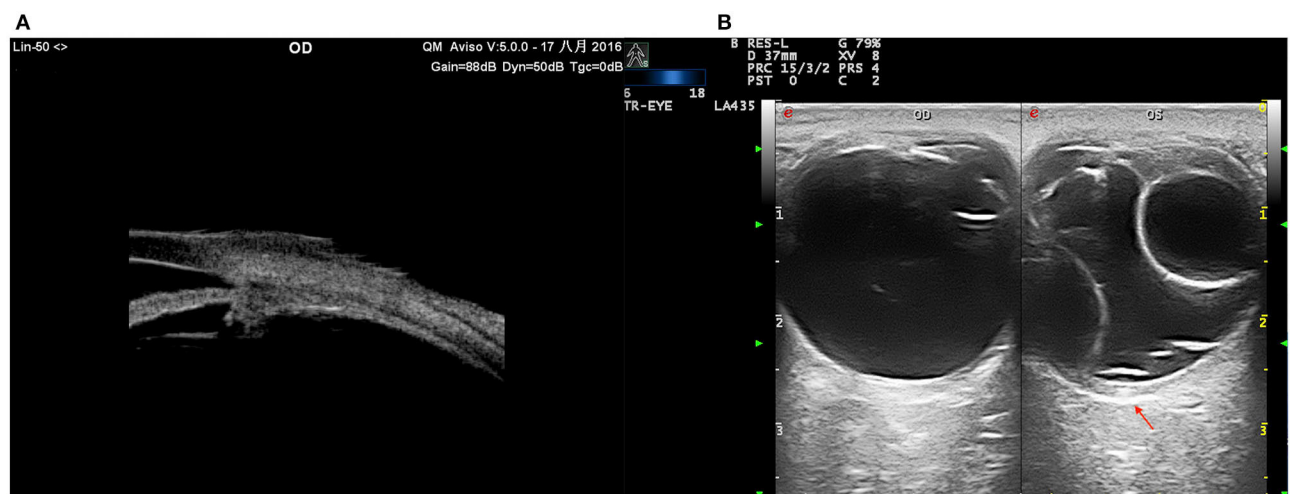


**FIGURE 7 | UES in type 2. (A)** UBM examination showing effusion of the ciliary body and thickened sclera. **(B)** CDU (TomTec Imaging System, Germany): annular bullous choroidal detachment, remarkably thickened sclera (red arrow).

(Figure 7B); in type 2, EDI-OCT was performed in 38 eyes of 19 patients; a choroidal thickness of  $816.56 \pm 10.21 \mu\text{m}$  (range, 589.63–1075.61  $\mu\text{m}$ ) was observed in the affected eye and  $781.23 \pm 9.33 \mu\text{m}$  (range, 692.42–1104.15  $\mu\text{m}$ ) in the fellow eye (Figure 9). Both eyes of the same patient showed almost the same choroidal thickness.

SD-OCT showed that each retinal layer was uneven and wavy; leopard spots were observed in the fundus corresponding to

the accumulation of outer retinal material, which presented as focal thickening of the RPE layer. B-scan of SS-OCT showed the scleral thickness of  $\sim 3 \text{ mm}$  (Figure 8), consistent with the CDU measurements.

SD/SS-OCTA was performed in 18 type 1 eyes and revealed capillary tortuosity, thickened subfoveal choroid, crowded macular morphology, and macular dysplasia with attenuation of foveal avascular zone (FAZ) (Figure 10). The restoration of



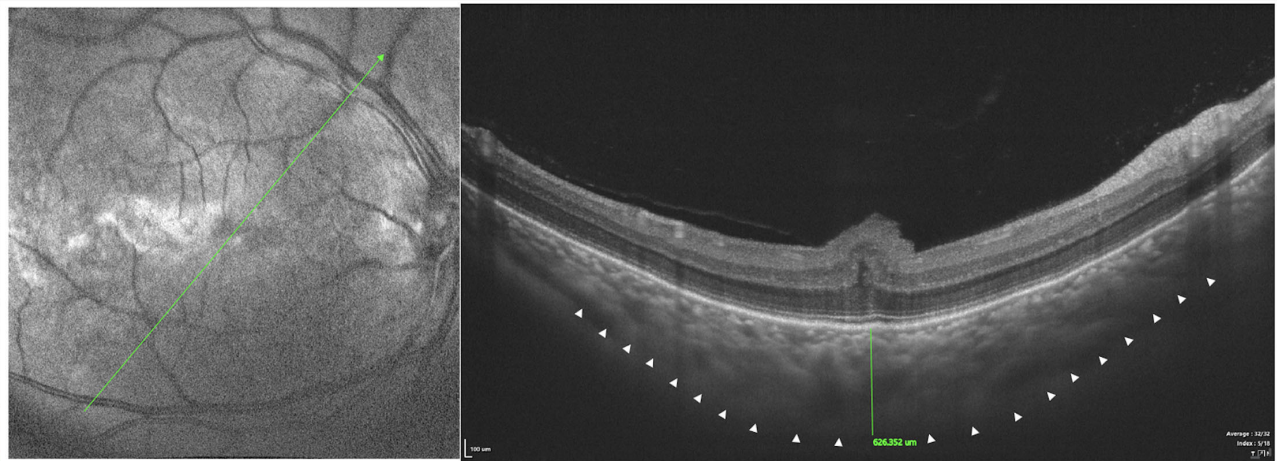


**FIGURE 8 |** SS-OCT (SS-OCT, VG200D, SVision Imaging, Ltd., China) in type 1 showed that each retinal layer was uneven and wavy with pachychoroid, leopard-sign spots in the fundus corresponding to accumulation of outer retinal material, which presented as focal thickening of the RPE layer.

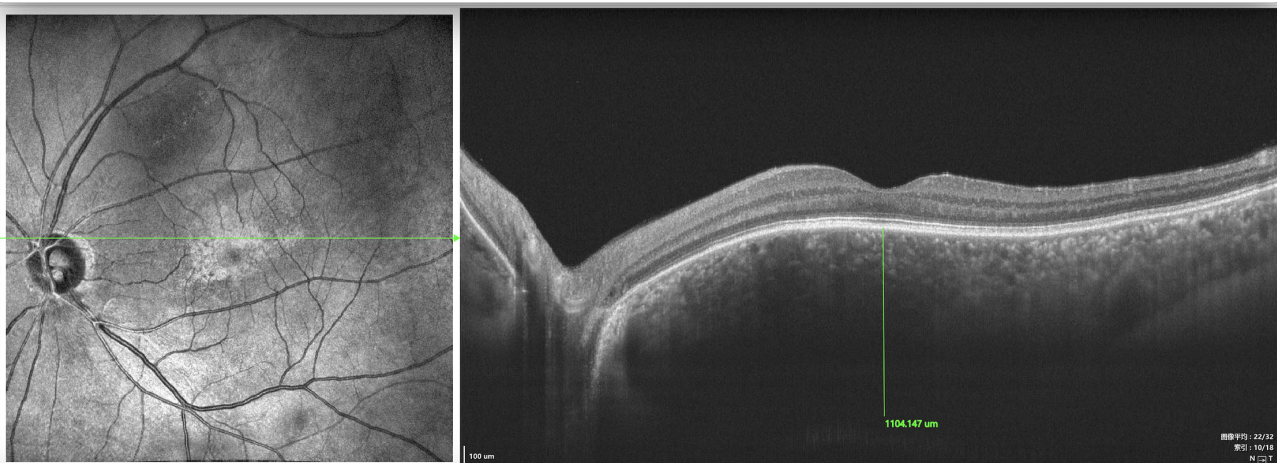


**FIGURE 9 |** SS-OCT (SS-OCT, VG200D, SVision Imaging, Ltd., China) in type 2 showed that each retinal layer was even with the pachychoroid, leopard-sign spots in the fundus corresponding to accumulation of outer retinal material, which presented as focal thickening of the RPE layer.

photoreceptor and RPE damage, flattening of crowded macular morphology, and expansion of attenuation of FAZ were observed by SS-OCT/OCTA with time during follow-up post-operatively (**Supplementary Figures 1, 2**).

SD/SS-OCTA was performed in 16 eyes in type 2 and revealed the normal FAZ size and retinal layers (**Figure 11**); however, pachychoroid was seen in both eyes.

## Surgical Management and Outcome

We performed quadrant lamellar-sclerectomy with sclerostomy at two sites at the equator in the inferior quadrants in all eyes and the procedure was as described above (**Figure 1**). There were no surgical side effects, such as hemorrhage, infection, iatrogenic retinal tear, and aggravation of cataract, during

the intraoperative or post-operative period. Of the eyes that underwent one scleral thinning surgery, complete resolution of subretinal and suprachoroidal fluid was observed within 6 months in 98.1% of eyes, and the mean time of retinal flattening was 1.2 months (range: 0.5–2.5 months).

## Type 1

We performed surgery in 62 eyes. During surgery, we noted that the eyeballs were small sized, with insertions of the rectus muscles and the equator located unusually anteriorly; the equator located 8 to 10 mm posterior to the limbus. The sclera were abnormally rigid and thick. Thickness of the sclera at the equator was more than 2.0 mm, which was consistent with the CDU results.



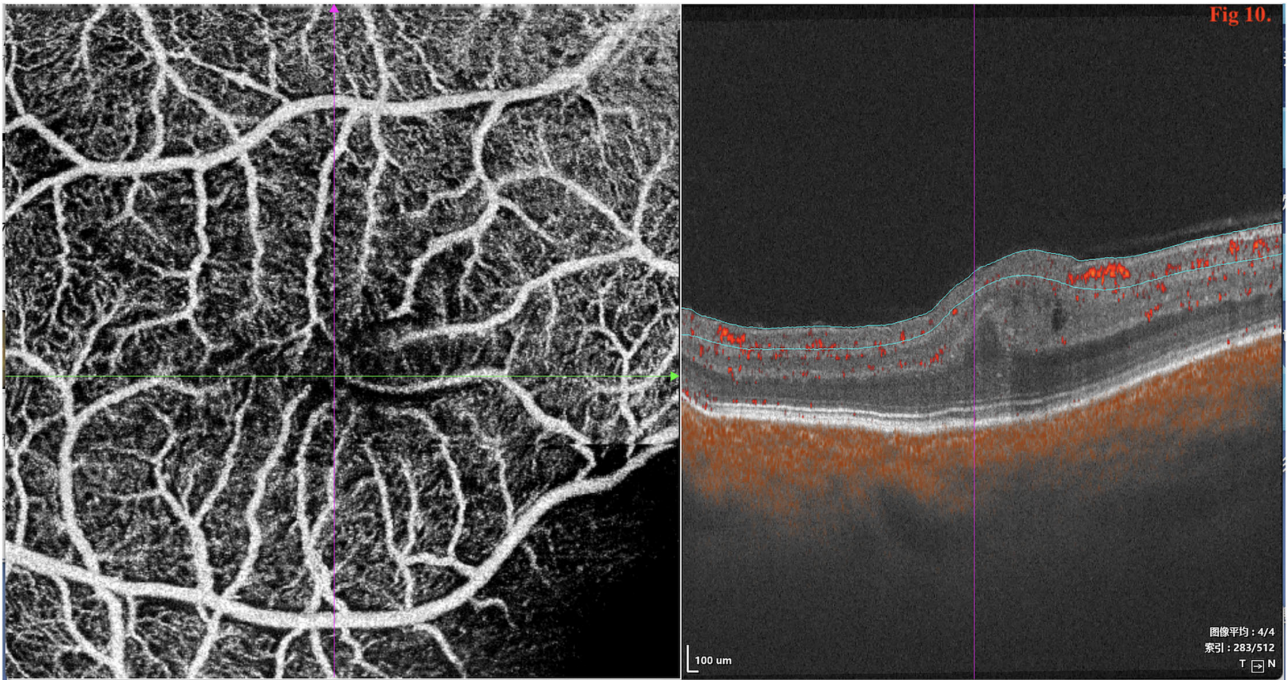


**FIGURE 10 |** SD/SS-OCTA (SS-OCT, VG200D, SVision Imaging, Ltd., China) in type 1 revealed that the macular morphology was crowded and showed macular dysplasia with decreased size of foveal avascular zone (FAZ).

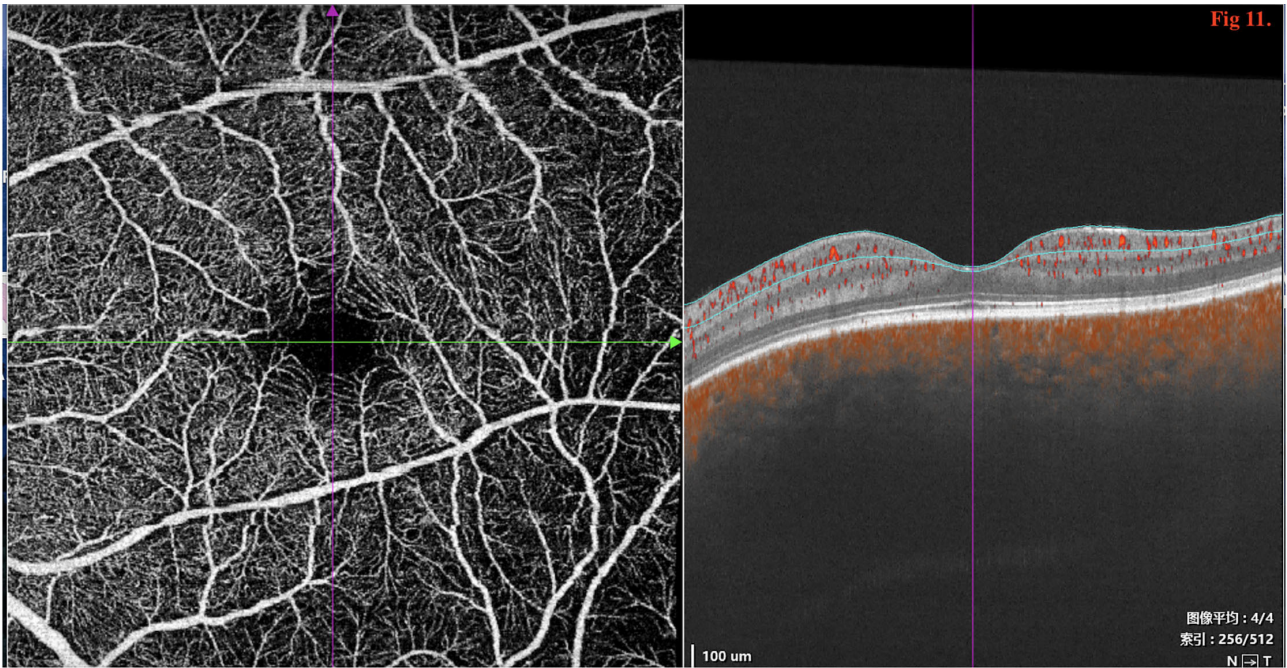


**FIGURE 11 |** SD/SS-OCTA (SS-OCT, VG200D, SVision Imaging, Ltd., China) revealed that the macular morphology was normal with no decrease in the size of foveal avascular zone (FAZ).



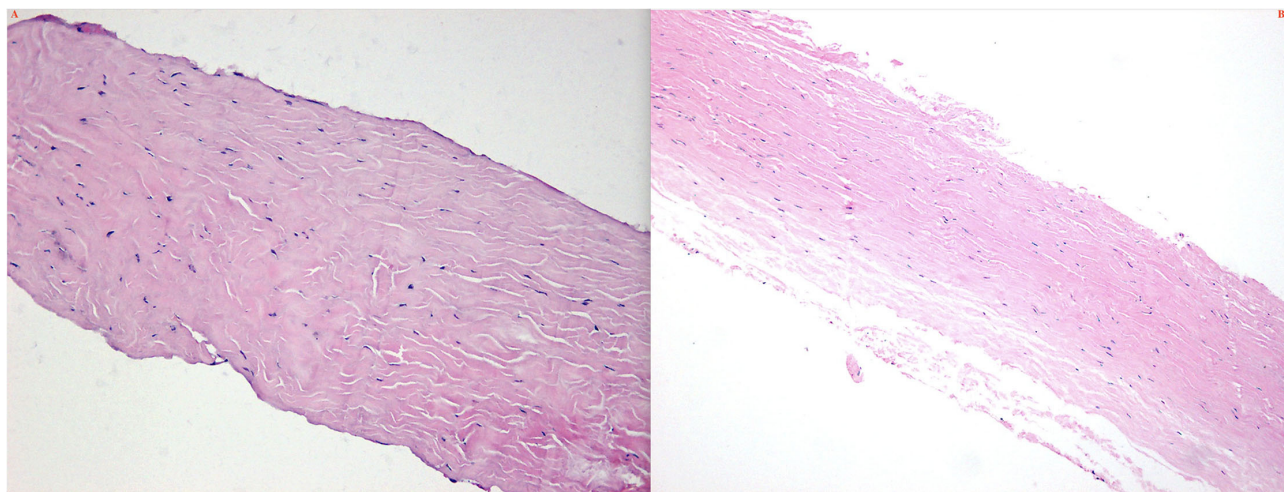


**FIGURE 12 |** Histochemical features of the scleras in type 1 (A) and type 2 (B). Note the collagen fibers bundles was variable diameters, arranged irregularly; spaces between collagen fibers bundles were enlarged.

After surgery, ciliochoroidal and retinal detachment resolved with complete resolution of subretinal fluid within 1.0 to 2.5 months in all nanophthalmic eyes (**Figure 12**).

Among patients who underwent bilateral surgery, the mean interval between surgeries for the two eyes was  $9.85 \pm 11.50$  months (median 8, range 1–36 months).

Two eyes of 2 patients showed recurrence of UES 2 years later and 2 eyes of 2 patients showed recurrence 3 years later; we performed the same surgery at two sites at the equator in the upper quadrants. After reoperation, the choroidal and retinal detachment were completely resolved without any signs of recurrence at the last follow-up. In addition, 3 eyes (5%) of 2 patients in type 1 group showed reattachment spontaneously without surgery (follow-up duration, 11 months to 8 years).

One year after surgery, FA/ICGA was performed in all patients in whom the retina was completely reattached. Angiography demonstrated marked hyperfluorescence in the choroidal background fluorescence during the early to late phase in both the affected and unaffected eyes. These findings were similar to those observed before the surgery.

In the type 1 group, BCVA at presentation was 20/100 to 20/200 in 20 (32.2%) eyes, and  $\leq 20/200$  in 42 (67.7%) eyes; final BCVA was 20/80 in 22 (35.5%) eyes, 20/100 to 20/200 in 33 (53.2%) eyes (**Table 2**).

## Type 2

In 44 eyes, we performed quadrant lamellar-sclerectomy with sclerostomy at two sites at the equator in the lower quadrants. During surgery, the eyeball was normal in size; however, the sclera was abnormally rigid and thickened in all eyes. The sclera at the equator was more than 2.5 mm thick.

All procedures were successful and no recurrence of UES was observed at the last follow-up. In 2 patients, the unaffected eyes showed retinal and choroidal detachment caused by UES, 9 and 11 months after the affected eye was operated, respectively. The

surgery was performed and was successful in these two patients (**Figure 13**).

In the type 2 group, BCVA at presentation was 20/100 to 20/200 in 8 (18.1%) eyes, and  $\leq 20/200$  in 36 (86.4%) eyes; final BCVA was 20/80 in 5 (11.4%) of eyes, 20/100 to 20/200 in 35 (79.5%) (**Table 2**).

In type 2, we disclosed that 26 patients had a monocular disease and 9 had a bilateral disease. A total of 9 patients who had monocular involvement at initial examination developed disease of the contralateral eye at a mean interval of 9.0 months (range, 8–12 months).

There was no difference in choroidal thickness and BCVA between the two groups ( $P > 0.05$ ) post-operatively. The final BCVA was not related to the time of retinal choroidal detachment, but related to the early subretinal fluid removal and photoreceptor damage.

At the 6-month follow-up, the choroidal thickness in both groups after operation was lower than that before operation ( $P < 0.05$ ). At the last follow-up, the mean choroidal thickness in the type 1 group before and after operation was  $869.46 \pm 8.33 \mu\text{m}$  and  $599.53 \pm 9.16 \mu\text{m}$ , respectively; in the type 2 group, the mean choroidal thickness of the affected eyes before and after operation was  $836.56 \pm 10.21 \mu\text{m}$  and  $713.32 \pm 8.43 \mu\text{m}$ , respectively (**Table 3**). There was significant difference in the before and after operation values between these two groups ( $P < 0.05$ ). After age and gender matching, there were no significant differences in the choroidal thickness of affected eyes between type 1 and type 2 UES patients ( $P > 0.05$ ).

## Histopathological Examination of the Sclera

Surgically excised scleral pieces of type 1 and type 2 were examined histopathologically. Pathologically, collagen fiber bundles in the thickened sclera demonstrated markedly irregular arrangement and the widths of

**TABLE 2 |** Change in best corrected visual acuity (BCVA) of patients with UES before- and post-surgery to the last follow-up visit available.

BCVA-before surgery (%)	Type 1 (nanophthalmic eye) n1 = 31 patients, n2 = 62 eyes	Type 2 (non-nanophthalmic eye) n1 = 35; n2 = 44 eyes
<20/200	42 (67.7%)	36 (86.4%)
20/100–20/200	20 (32.2%)	8 (18.1%)
BCVA-post surgery		
<20/200	7 (11.3%)	4 (9.0%)
20/200–20/133	33 (53.2%)	35 (79.5%)
20/80	22 (35.5%)	5 (11.4%)

BCVA, best corrected visual acuity.

the bundles varied (Figures 14A,B). Deposits of matrix between the bundles were remarkable in all eyes.

Histochemical features of the sclera showed that collagen fiber bundles were of variable diameters and arranged irregularly and spaces between collagen fibers bundles were enlarged; however, the Alcian blue staining (glycosaminoglycans) of the matrix in type 1 and type 2 eyes was negative.

## DISCUSSION

To the best of our knowledge, our study, 106 eyes of 66 patients with UES, reports the largest case series concerning UES including nanophthalmos and non-nanophthalmos (idiopathic). After undergoing one scleral thinning surgery, complete resolution of subretinal and supraciliochoroidal fluid was observed within a mean time of 1.2 months in 98.1% of eyes. During a mean follow-up duration of 65.3 months, the final BCVA improved or stabilized in 89.6% of eyes; however, OCT/OCTA imaging revealed that the extent of improvement was limited by photoreceptor and pigment epithelial damage resulting from macular dysplasia or chronic retinal detachment. The OCTA role in defining macular status and visual potential is consistent with Mansour's (23) findings in nanophthalmos. In addition, in our nanophthalmos group, secondary glaucoma combined with optic atrophy was also the main reason for poor final vision.

In the present study, we divided the eyes of patients with primary UES into two groups mainly according to the axial length: type 1 and type 2 UES. Type 1 and 2 UES showed incompletely same clinical characteristics but similar histologic appearance, except for the axial length and refractive error (Table 1). These results indicate that both types are subtypes in the same category.

In incomplete conformity with previous studies (1, 2, 4), several special clinical features were noted in a large proportion of our Asian patients: type 1 showed bilateral involvement, protracted course, elevated IOP accompany closer of anterior chamber, and absence of known systemic disorders; type 2: male sex and unilateral involvement, middle age at onset, normal

IOP, dilated episcleral veins, and no vitreous cells, but may be accompanied with different systemic symptoms. Ancillary testing typically revealed characteristic FFA abnormalities consistent with leopard-spot RPE alterations. CDU showed evidence of diffuse choroidal thickening, and similarly, OCT/OCTA showed pachychoroid in type 1 and type 2 UES. The choroidal thickness significantly changed before and after surgery.

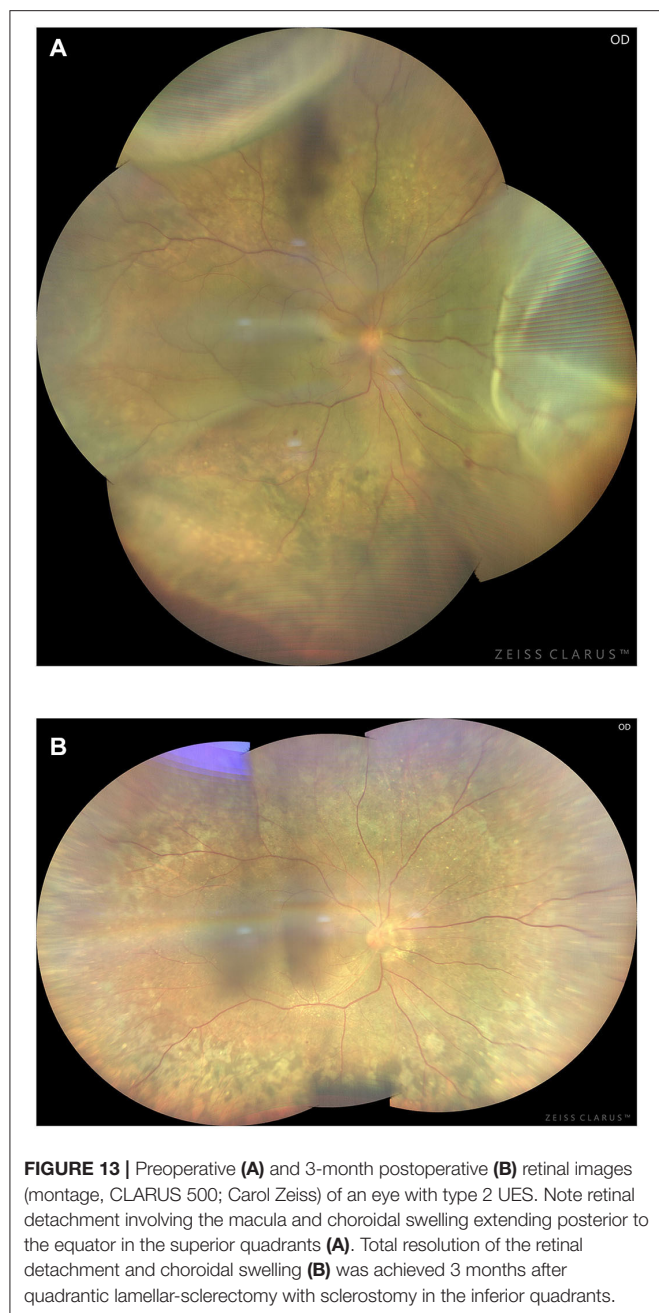
Subsequent single recurrences in 0.4% of eyes in type 1 over a mean follow-up duration of 65.3 months responded to reoperation. No recurrence was observed in type 2. Only 3 eyes of 2 patients (0.3%) in type 1 occurred reattachment spontaneously without surgery (range of follow-up, 3 months to 2 years). However, in the absence of an unoperated control group with similar disease severity, we cannot entirely confirm whether the reattachments observed in our cases were spontaneous and unrelated to the surgical procedure; alternatively, this may be a phase in the natural history of the disorder.

The pathogenesis of UES is unclear, possibly related to congenital anomaly of the sclera and vortex vein hypoplasia, and the secondary block of transscleral fluid outflow.

In types 1 and 2 UES, OCT/OCTA revealed marked thickening of the choroid and sclera (Figure 1), and at surgery, the sclera was abnormally rigid and unusually thickened to more than 2.5 mm. Histopathological studies showed disorganization of collagen fiber bundles and variation in size of collagen fibrils. These findings were consistent with previous studies (7–13, 17). Because of the histopathological abnormalities in the rigid and thickened sclera, fluid drainage was also compromised from the decreased function of uveoscleral outflow pathways, leading to excessive protein and fluid accumulation in the suprachoroidal space.

Previous studies have demonstrated excessive glycosaminoglycans accumulation in the matrix of the sclera, combined with defective vortex veins, resulting in decreased drainage of extravasated protein through channels of the transscleral outflow pathway (5, 24–26). However, in the present study, the histochemical examination showed the Alcian blue staining (glycosaminoglycans) in the matrix was negative in all eyes. These findings were not consistent with previous studies. Therefore, we believe that the theory of glycosaminoglycan deposition in the sclera of patients with UES needs further research and interpretation with caution.

Along with the main proposed mechanism which results in subretinal fluid accumulation, a second mechanism is the choroidal vein congestion caused by vortex vein compression by the thickened sclera (4). ICGA in types 1 and 2 demonstrated markedly diffuse choroidal hyperfluorescence during the early stage, and this finding persisted and increased in the late stage (Figures 3, 6). OCT/OCTA showed pachychoroid in type 1 and type 2, and the choroidal thickness was significantly increased. These findings suggest that there is marked hyperpermeability in the choroidal vessels and massive accumulation of fluid in the choroidal stroma. However, the choroidal thickness decreased with time during follow-up post-operatively, indicating that the speculation on the pathological mechanism of the disease is reasonable and indicating the effectiveness of this surgical treatment.



Ciliochoroidal detachment is manifested by the accumulation of fluid in the choroid, particularly in the suprachoroid, observed at the periphery for almost 360 degrees, even before the fundus changes detectably. During this period, the eye is asymptomatic and in the subclinical stage of UES. The condition usually occurs in the fellow eye in type 1, and is proven by OCT/OCTA, UBM, and ICGA. Following the development of the disease, long-term accumulation of the choroidal fluid decompensates the RPE and prevents inward to outward trans-RPE fluid flow through the pump mechanism of RPE (27). Subsequently, subretinal fluid accumulated and exudative retinal detachment occurred. In the

**TABLE 3 |** Change in choroidal thickness of patients with UES before- and post-surgery to the last follow-up visit available.

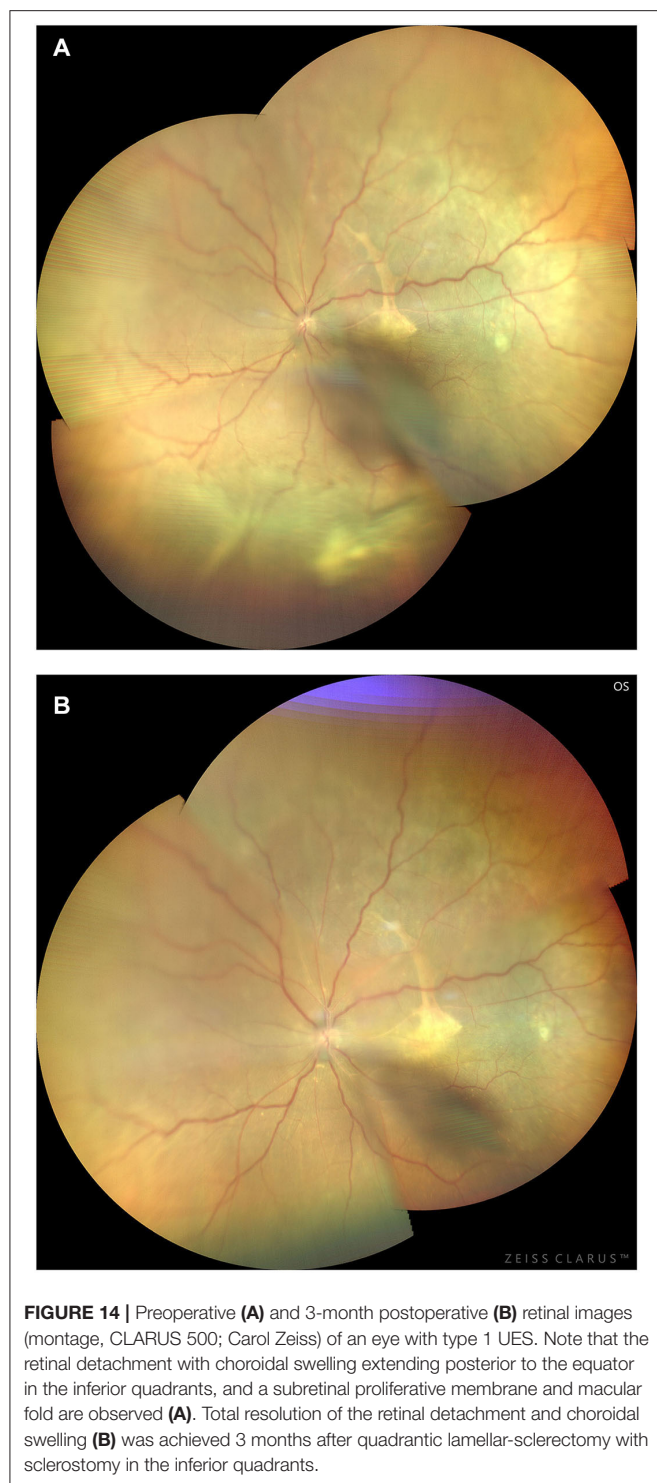
	Type 1 (nanophthalmic eye) <i>n</i> 1 = 21 patients, <i>n</i> 2 = 42 eyes	Type 2(non-nanophthalmic eye) <i>n</i> 1 = 19; <i>n</i> 2 = 38 eyes	
Choroidal thickness ( $\mu$ m)	Affected eyes	Affected eyes	Fellow eyes
Before- surgery	869.46 $\pm$ 8.33	816.56 $\pm$ 10.21	781.23 $\pm$ 9.33
Post-surgery	599.53 $\pm$ 9.16	713.32 $\pm$ 8.43	/

clinical stage of UES, the ocular manifestations became apparent and symptomatic in eyes with both unilateral and bilateral involvement. These processes suggest that scleral abnormality is a major cause of the UES (Figure 8), and our study confirmed initial hypothesis (5) by Gass again.

Given the development of the disorder, surgical management of the sclera is reasonable (2, 3, 5, 6). In 1975, Shaffe (28) proposed that the cause of ciliochoroidal effusion associated with nanophthalmos is choroidal engorgement caused by impaired drainage of vortex veins because of the thick sclera characteristic of this disease. Brockhurst (3) subsequently reported the successful use of vortex vein decompression as a surgical remedy of nanophthalmic uveal effusions. However, the surgery was challenging to perform because considerable bleeding occurred during the removal of the sclera around the vortex vein. In 1983, Gass (5) suggested partial-thickness sclerectomies without vortex vein decompression in UES with nanophthalmos and reported successful effectiveness. Uyama (29) subsequently performed subscleral sclerectomy (sclerectomy under the scleral flap) without vortex vein decompression. This procedure preserved the scleral flap and the procedure was relatively complicated, and this may be related to recurrence post-operatively. In recent years, in Mansour's (29) small series of type 1 UES, faster resolution of subretinal fluid was reported with extensive circumferential scleral resection (90% thickness) without unroofing the choroid, allowing the removal of the scleral barrier to diffusion. They described the effectiveness with speed of resolution [within an average ( $\pm$ SD) of 13.9 ( $\pm$ 8.7) days]; however, we still believe with this procedure, there may be a risk of developing scleral staphyloma after resection because of the large-scale scleral removal. Therefore, we attempted to modify the Gass's techniques and performed minimum volume quadrant lamellar-sclerectomy with sclerostomy without decompression of the vortex vein, retaining the stable IOP and avoiding hemorrhage during the surgery. The rationale for abovementioned procedures were similar to that of trabeculectomy to create a bypass outflow route for the aqueous humor.

The nature of the scleral abnormality in IUES has not been clarified. There is evidence that vortex vein obstruction also plays a role in the pathogenesis of UES in normal-sized eyes (7). In our





series, signs of increased uveal venous pressure, such as dilated episcleral veins, were obviously present in most type 2 patients, which may be associated with the sclera and increased resistance to transscleral outflow of the intraocular fluid. Uyama (30) found blood in Schlemm's canal, and on intraoperative examination, the vortex veins were thought to be reduced in number and/or

caliber in 68% of eyes. Furthermore, signs of uveal congestion observed in type 2 patients in our study decreased or disappeared after scleral surgery. This implies that vortex vein obstruction is at least partially a secondary change, resulting possibly from scleral swelling induced by high protein concentration (5). In addition, in our series, type 2 patients had bilateral disease, which may imply the associated systemic factors.

Based on the previous reports indicating that the proteoglycan composition of the surrounding matrix controlled the size and organization of collagen fibers (31, 32), several reports speculate that a defect in mucopolysaccharide metabolism may be the cause of abnormalities such as thickened sclera or permeability in this disorder (7, 9, 33, 34). Of interest, in this regard, was the occurrence and successful treatment of ciliochoroidal effusion by combined sclerectomies and sclerostomies in a patient with systemic mucopolysaccharidosis type II (Hunter's syndrome), a disorder in which the sclera is thickened by the deposition of mucopolysaccharide (8). This type previously was categorized as IUES and was treated in the same manner as nanophthalmos. Interestingly, in our series, the type 2 UES accompanied different systemic symptoms, which may be categorized as the systemic disease-associated factors to UES; thus, "idiopathic/primary UES" in the true sense is still controversial.

Thus, in IUES, transscleral protein transport impairment seems to be the primary pathophysiologic factor and uveal congestion plays a secondary role. Based on the successful use of Gass's technique in patients with nanophthalmic uveal effusion (19, 20, 35), Allen (20) and Johnson (21) suggested that the same pathophysiology and surgery may be applied in IUES.

ICGA revealed that a subclinical condition in the choroid lasts for a long period after surgery. Recurrence of retinal and ciliochoroidal detachment sometimes occurs. When the effects of draining choroidal fluid cease, reoperation is necessary and can be performed easily without complications. In our small number of patients with recurrence, reoperation was favorable. Thereafter, the suprachoroidal fluid spontaneously drained and retinal detachment gradually resolved.

In this study, we achieved a successful outcome with this procedure without any complication in all eyes with types 1 or 2 UES. This procedure was easy to perform, and the outcomes were excellent. For type 1 nanophthalmos, secondary angle closure caused by uveal effusion occurs because of fluid accumulation in the supraciliary space extending anteriorly from the suprachoroidal space (36). UBM demonstrated that the ciliary body is anatomically hinged to the eye wall at the scleral spur, and accumulation of supraciliary fluid leads to detachment and anterior rotation of the ciliary body. The mass effect causes forward displacement of the lens-iris diaphragm, leading to a shallow anterior chamber, aqueous misdirection, appositional angle closure, and elevated IOP. In our experience, it is necessary to perform YAG laser iridectomy before scleral surgery to reduce IOP and avoid intraoperative complications, such as suprachoroidal hemorrhage.

In conclusion, our results revealed that abnormal sclera and increased resistance to transscleral outflow of intraocular fluid is the primary cause of types 1 and 2 UES, and creation of a bypass outflow route for intraocular fluid by lamellar-sclerectomy with



sclerostomy is the rationale for surgical treatment of this condition. Minimum volume quadrantic lamellar-sclerectomy with sclerostomy is highly recommended as the first-choice treatment and is effective. Although we found no significant correlation between the lasting term of pre-operative RD and final BCVA, the excellent results with the modified surgical technique performed in our cases and the visual recovery seen in many patients indicates that surgical intervention as soon as macular function is threatened by subretinal fluid accumulation is the key to successful treatment. Further systemic and genetic studies associated with scleral abnormality should be helpful in understanding the precise cause of primary UES.

## DATA AVAILABILITY STATEMENT

The raw data supporting the conclusions of this article will be made available by the authors, without undue reservation.

## ETHICS STATEMENT

The studies involving human participants were reviewed and approved by Medical Ethics Committee of the Beijing Tongren Hospital. The patients/participants provided their written informed consent to participate in this study. Written informed consent was obtained from the individual(s) for the

publication of any potentially identifiable images or data included in this article.

## AUTHOR CONTRIBUTIONS

WW and LY: examination of the patient and interpretation of results. NZ and XX: interpretation of results, writing, and reviewing of the manuscript. All authors read and approved the final manuscript.

## FUNDING

This study was funded by the National Natural Science Foundation of China (No. 81272981) and the Beijing Natural Science Foundation (No. 7151003) provided financial support.

## SUPPLEMENTARY MATERIAL

The Supplementary Material for this article can be found online at: <https://www.frontiersin.org/articles/10.3389/fmed.2022.785444/full#supplementary-material>

**Supplementary Figures 1, 2** | UES in type 1. The restoration of photoreceptor and RPE damage, flattening of crowded macular morphology, and expansion of attenuation of FAZ were observed by SS-OCT/OCTA with time during follow-up post-operatively.

## REFERENCES

- Schepens CL, Brockhurst RJ. Uveal effusion. I. Clinical picture. *Arch Ophthalmol.* (1963) 70:189–201. doi: 10.1001/archopht.1963.00960050191010
- Brockhurst RJ. Nanophthalmos with uveal effusion: a new clinical entity. *Arch Ophthalmol.* (1975) 93:1289–99. doi: 10.1001/archopht.1975.01010020923001
- Brockhurst RJ. Vortex vein decompression for nanophthalmic uveal effusion. *Arch Ophthalmol.* (1980) 98:1987–90. doi: 10.1001/archopht.1980.01020040839008
- Gass JDM, Jallow S. Idiopathic serous detachment of the choroid, ciliary body, and retina (uveal effusion syndrome). *Ophthalmology.* (1982) 89:1018–32. doi: 10.1016/S0161-6420(82)34685-0
- Gass JDM. Uveal effusion syndrome: a new hypothesis concerning pathogenesis and technique of surgical treatment. *Trans Am Ophthalmol Soc.* (1983) 81:246–60.
- Gass JDM. Uveal effusion syndrome. A new hypothesis concerning pathogenesis and technique of surgical treatment. *Retina.* (1983) 3:159–63. doi: 10.1097/00006982-198300330-00003
- Trelstad RL, Silberman NN, Brockhurst RJ. Nanophthalmic sclera: ultrastructural, histochemical, and biochemical observations. *Arch Ophthalmol.* (1982) 100:1935–8. doi: 10.1001/archopht.1982.01030040915009
- Vine AK. Uveal effusion in Hunter's syndrome: evidence that abnormal sclera is responsible for the uveal effusion syndrome. *Retina.* (1986) 6:57–60. doi: 10.1097/00006982-198600610-00005
- Ward RC, Gragoudas ES, Pon DM, Albert DM. Abnormal scleral findings in uveal effusion syndrome. *Am J Ophthalmol.* (1988) 106:139–46. doi: 10.1016/0002-9394(88)90825-2
- Fukuchi T, Sawaguchi S, Honda T, Saito T, Iizuka Y, Iwata K, et al. Proteoglycan abnormality in a nanophthalmos sclera. *Nippon Ganka Gakkai Zasshi.* (1993) 97:260–7.
- Stewart DH III, Streeten BW, Brockhurst RJ, Anderson DR, Hirose T, Gass DM. Abnormal scleral collagen in nanophthalmos: an ultrastructural study. *Arch Ophthalmol.* (1991) 109:1017–25. doi: 10.1001/archopht.1991.01080070129050
- Tagami N, Uyama M, Yamada K, Kosaki J, Ohkuma H, Tomoda T. Histological observations on the sclera in uveal effusion. *Nippon Ganka Gakkai Zasshi.* (1993) 97:268–74.
- Forrester JV, Lee WR, Kerr PR, Dua HS. The uveal effusion syndrome and trans-scleral flow. *Eye.* (1990) 4:354–65. doi: 10.1038/eye.1990.48
- Brockhurst RJ. Ciliochoroidal (uveal) effusion. In: Ryan SJ, editor. *Retina*. 2nd ed. St. Louis, MO: Mosby (1994). vol. 2, ch. 112.
- Brockhurst RJ. Uveal effusion. In: Albert DM, Jakobiec FA, editors. *Principles and Practice of Ophthalmology: Clinical Practice*. Philadelphia, PA: Saunders (1994). vol. 1, ch. 37.
- Johnson MW. Uveal effusion. In: Guyer DR, Yannuzzi LA, Chang S, editors. *Retina, Vitreous, Macula*. Philadelphia, PA: Saunders (1999). p. 658–68.
- Gass JDM. *Stereoscopic Atlas of Macular Diseases: Diagnosis and Treatment*. 4th ed. St. Louis, MO: Mosby (1997). vol. 1, p. 200–5.
- Ryan EA, Zwaan J, Chylack LT Jr. Nanophthalmos with uveal effusion. Clinical and embryologic considerations. *Ophthalmology.* (1982) 89:1013–17. doi: 10.1016/S0161-6420(82)34686-2
- Casswell AG, Gregor ZJ, Bird AC. The surgical management of uveal effusion syndrome. *Eye.* (1987) 1:115–9. doi: 10.1038/eye.1987.17
- Allen KM, Meyers SM, Zegarra H. Nanophthalmic uveal effusion. *Retina.* (1988) 8:145–7. doi: 10.1097/00006982-198808020-00012
- Johnson MW, Gass JDM. Surgical management of the idiopathic uveal effusion syndrome. *Ophthalmology.* (1990) 97:778–85. doi: 10.1016/S0161-6420(90)32511-3
- Schneiderman TE, Johnson MW. A new approach to the surgical management of idiopathic uveal effusion syndrome. *Am J Ophthalmol.* (1997) 123:262–3. doi: 10.1016/S0002-9394(14)71049-9
- Mansour AM, Stewart MW, Yassine SW, Mehanna CZ, Casella AMB, Hamam RN, et al. Unmeasurable small size superficial and deep foveal avascular zone in nanophthalmos: the Collaborative Nanophthalmos OCTA Study. *Br J Ophthalmol.* (2019) 103:1173–8. doi: 10.1136/bjophthalmol-2018-312781

24. Young RD. The ultrastructural organization of proteoglycans and collagen in human and rabbit scleral matrix. *J Cell Sci.* (1985) 74:95–104. doi: 10.1242/jcs.74.1.95
25. Scott JE, Hughes EW. Proteoglycan-collagen relationships in developing chick and bovine tendons. Influence of the physiological environment. *Connect Tissue Res.* (1986) 14: 267–78. doi: 10.3109/03008208609017470
26. Jackson TL, Hussain A, Morley AMS, Sullivan PM, Hodgetts A, El-Osta A, et al. Scleral hydraulic conductivity and macromolecular diffusion in patients with uveal effusion syndrome. *Invest Ophthalmol Vis Sci.* (2008) 49:5033–40. doi: 10.1167/iovs.08-1980
27. Marmor MF. Control of subretinal fluid and mechanisms of serous detachment. In: Marmor MF, Wolfensberger TJ, editors. *The Retinal Pigment Epithelium: Function and Disease*. New York, NY: Oxford University Press (1998). p. 420–38.
28. Shaffer RN. Discussion, 119–20, of: Calhoun FP. The management of glaucoma in nanophthalmos. *Trans Am Ophthalmol Soc.* (1975) 73:97–122.
29. Mansour A, Stewart MW, Shields CL, Hamam R, Abdul Fattah M, Sheheitli H, et al. Extensive circumferential partial-thickness sclerectomy in eyes with extreme nanophthalmos and spontaneous uveal effusion. *Br J Ophthalmol.* (2019) 103:1862–7. doi: 10.1136/bjophthalmol-2018-313702
30. Uyama M, Takahashi K, Kozaki J, Tagami N, Takada Y, Ohkuma H, et al. Uveal effusion syndrome: clinical features, surgical treatment, histologic examination of the sclera, and pathophysiology. *Ophthalmology.* (2000) 107:441–9. doi: 10.1016/S0161-6420(99)00141-4
31. Myers DB, Highton TC, Rayns DG. Ruthemium red-positive filaments interconnecting collagen fibrils. *J Ultrastruct Res.* (1973) 42:87–92. doi: 10.1016/S0022-5320(73)80008-5
32. Borcharding MS, Blacik LJ, Sittig RA, Bizzell JW, Breen M, Weinstein HG. Proteoglycans and collagen fiber organization in human comeoscleral tissue. *Exp Eye Res.* (1975) 21:59–70. doi: 10.1016/0014-4835(75)90057-3
33. Yue BYJT, Duvall J, Goldberg ME, Puck A, Tso MO, Sugar J. Nanophthalmic sclera: morphologic and tissue culture studies. *Ophthalmology.* (1986) 93:534–41.
34. Ghazi NG, Richards CP, Abazari A. A modified ultrasound-guided surgical technique for the management of the uveal effusion syndrome in patients with normal axial length and scleral thickness. *Retina.* (2013) 33:1211–9. doi: 10.1097/IAE.0b013e3182790eb8
35. Good WV, Stem WH. Recurrent nanophthalmic uveal effusion syndrome following laser trabeculoplasty. *Am J Ophthalmol.* (1988) 106:234–5.
36. Shah PR, Yohendran J, Hunyor AP, Grigg JR, McCluskey PJ. Uveal effusion: clinical features, management, and visual outcomes in a retrospective case series. *J Glaucoma.* (2016) 25:329–35. doi: 10.1097/IJG.0000000000000329

**Conflict of Interest:** The authors declare that the research was conducted in the absence of any commercial or financial relationships that could be construed as a potential conflict of interest.

**Publisher's Note:** All claims expressed in this article are solely those of the authors and do not necessarily represent those of their affiliated organizations, or those of the publisher, the editors and the reviewers. Any product that may be evaluated in this article, or claim that may be made by its manufacturer, is not guaranteed or endorsed by the publisher.

Copyright © 2022 Zhou, Yang, Xu and Wei. This is an open-access article distributed under the terms of the Creative Commons Attribution License (CC BY). The use, distribution or reproduction in other forums is permitted, provided the original author(s) and the copyright owner(s) are credited and that the original publication in this journal is cited, in accordance with accepted academic practice. No use, distribution or reproduction is permitted which does not comply with these terms.



# A Novel Role of IL13R $\alpha$ 2 in the Pathogenesis of Proliferative Vitreoretinopathy

Hui Qi<sup>1</sup>, Lijun Dong<sup>1</sup>, Dong Fang<sup>1</sup>, Lu Chen<sup>1</sup>, Yun Wang<sup>1</sup>, Ning Fan<sup>1</sup>, Xingxing Mao<sup>1</sup>, Wenyi Wu<sup>2</sup>, Xiaohu Yan<sup>1</sup>, Guoming Zhang<sup>1</sup>, Shaochong Zhang<sup>1\*</sup> and Hetian Lei<sup>1\*</sup>

<sup>1</sup> Shenzhen Eye Hospital, Shenzhen Eye Institute, Jinan University, Shenzhen, China, <sup>2</sup> Department of Ophthalmology, Hunan Key Laboratory, National Clinical Research Center for Geriatric Disorders, Xiangya Hospital, Central South University, Changsha, China

## OPEN ACCESS

### Edited by:

Jorge M. Barcia,  
Catholic University of Valencia  
San Vicente Mártir, Spain

### Reviewed by:

Xiaoqing Guo,  
Harvard Medical School,  
United States  
Teng Teng,  
Capital Medical University, China  
Maryada Sharma,  
Postgraduate Institute of Medical  
Education and Research, India

### \*Correspondence:

Shaochong Zhang  
zhangshaochong@gzoc.com  
Hetian Lei  
leihetian18@hotmail.com

### Specialty section:

This article was submitted to  
Ophthalmology,  
a section of the journal  
Frontiers in Medicine

**Received:** 08 December 2021

**Accepted:** 28 April 2022

**Published:** 13 June 2022

### Citation:

Qi H, Dong L, Fang D, Chen L,  
Wang Y, Fan N, Mao X, Wu W, Yan X,  
Zhang G, Zhang S and Lei H (2022) A  
Novel Role of IL13R $\alpha$ 2  
in the Pathogenesis of Proliferative  
Vitreoretinopathy.  
Front. Med. 9:831436.  
doi: 10.3389/fmed.2022.831436

Proliferative vitreoretinopathy (PVR), an inflammatory and fibrotic blinding disease, is still a therapeutic challenge. Retinal pigment epithelial (RPE) cells dislodged in the vitreous play a central role in the PVR pathogenesis. To identify potential novel contributors to the pathogenesis of PVR, we investigated a profile of vitreous-induced changes in ARPE-19 cells by RNA sequencing. Bioinformatics analysis of the sequencing data showed that there were 258 genes up-regulated and 835 genes down-regulated in the ARPE-19 cells treated with human vitreous. Among these genes, there were three genes related to eye disease with more than threefold changes. In particular, quantitative PCR and western blot results showed that interleukin 13 receptor (IL13R) $\alpha$ 2 that is over-expressed in a variety of cancers was up-regulated more than three times in the vitreous-treated ARPE-19 cells. Immunofluorescence analysis indicated that interleukin-13 receptor subunit  $\alpha$ 2 (IL13R $\alpha$ 2) was highly expressed in ARPE-19 cells within epiretinal membranes from patients with PVR. Importantly, blocking IL13R $\alpha$ 2 with its neutralizing antibody significantly inhibited vitreous-induced contraction of ARPE-19 cells, suggesting a novel role of IL13R $\alpha$ 2 in the PVR pathogenesis. These findings will improve our understanding of the molecular mechanisms by which PVR develops and provides potential targets for PVR therapeutics.

**Keywords:** vitreous, retinal pigment epithelial cells, RNA sequencing, IL13R $\alpha$ 2, proliferative vitreoretinopathy

## INTRODUCTION

Proliferative vitreoretinopathy (PVR) refers to the retinal re-detachment caused by extensive contraction and traction of the proliferative membrane on the surface of the retina and behind the vitreous after reattachment of rhegmatogenous retinal detachment (RRD) (1–4). It is the most common cause of failure to repair RRD (2). The growth and contraction of cell membranes in

**Abbreviations:** ARPE-19, a human retinal pigment epithelial cell line; CLL, chronic lymphocytic leukemia; DEG, differentially expressed genes; EGFR, epidermal growth factor receptor; EMT, epithelial–mesenchymal transition; ERM, epiretinal membranes; HPRRE, human primary RPE; IL13RA2, Interleukin 13 receptor alpha-2; MAPK, mitogen-activated protein kinase; PDGFR, platelet-derived growth factor receptor; PVR, proliferative vitreoretinopathy; RPE, retinal pigment epithelial cells; TGF- $\beta$ , transforming growth factor beta; TNF- $\alpha$ , tumor necrosis factor alpha; VEGF, vascular endothelial growth factor.

the vitreous cavity and on both sides of the surface of the retina, and intraretinal fibrosis are characteristics of PVR. PVR occurs in 8–10% of patients undergoing primary retinal detachment correction surgery, and in 40–60% of patients with open global injury (5, 6). At present, repeated surgery is the only option for patients with PVR (3, 7). But recurrent detachment and retinal damage caused by the PVR process itself lead to poor visual effects of the surgery. In the past period of continuous development of vitreous surgery technology, the incidence of PVR in prospective studies has remained unchanged (8, 9).

Fibrotic epiretinal membranes (ERMs) are composed of extracellular matrix such as collagen and fibronectin and cells such as retinal pigment epithelial (RPE) cells, fibroblasts, glial cells, and macrophages (3, 10–12). Almost all risk factors for PVR are related to the diffusion of RPE cells in the vitreous or the destruction of the blood–eye barrier (6). In the process of retinal tear in PVR patients, the detached RPE cells will contact the vitreous, causing the vitreous to stimulate the migration of RPE cells on the surface of the retina. At the same time, the inflammatory mediators and blood released by the retinal tear promote the production of collagen by RPE cells, which further lead to the formation and contraction of ERM (13). Due to the role of RPE cells and glial cells in the vitreous membrane in the pathogenesis of PVR, RPE cells have been widely used in the study of the pathogenesis of PVR (14, 15).

The purpose of this study was to investigate the differentially expressed genes (DEGs) of human RPE cells induced by vitreous and thereby to identify potential therapeutic targets.

## MATERIALS AND METHODS

### Major Reagents

Primary antibodies against  $\beta$ -actin (Cat. 4970 1:2,000), pan Keratin (Cat. 4545S, 1:200), and interleukin13 receptor subunit  $\alpha 2$  (IL13R $\alpha 2$ ) (Cat. 85677S 1:1,000) were bought from the Cell Signaling Technology (Danvers, MA, United States), a neutralizing antibody for IL13R $\alpha 2$  was purchased from the R&D Systems (Cat. AF146), and a primary antibody against Ki67 (Cat. ab243878, 1:200) was purchased from the Abcam (Danvers, MA, United States). Horseradish peroxidase-conjugated goat anti-rabbit IgG (Cat. SA00001-2, 1:5,000) was ordered from the Proteintech (Danvers, MA, United States). Fluorescent labeled secondary antibodies of rabbit (Cat. A21206) or mouse (Cat. WA316324) were bought from the Thermo Fisher Scientific (Waltham, MA, United States).

### Patient Vitreous and ARPE-19 Cells Culture

Before launching the project, the ethics approval of the clinical research ethics committee of Jinan University was obtained. A written informed consent was signed by each patient before vitreous samples were harvested from patients with or without PVR (HV).

ARPE-19 purchased from American Type Culture Collection (Manassas, VA, United States), and was cultured in the DMEM/F12 medium with 10% fetal bovine serum (FBS) and

1% penicillin G sodium (100 units/ml) and streptomycin (100 mg/ml) in a humidified incubator at 37°C with 5% CO<sub>2</sub> (16).

### Porcine Vitreous

Porcine vitreous was taken from fresh porcine eyes, frozen at a –80°C freezer. The eyeballs were dissected on ice and the isolated vitreous was diluted at 1:3 in DMEM/F12 and filtered for sterilization (17).

### Cell Proliferation Assay

Cells were cultured a 6-well plate with slides in the DMEM/F12 supplemented with 10% FBS. After the cells were completely attached to the slide, the medium was changed to DMEM/F12 only. Then the cells were treated with vitreous with Ki67 for a proliferation assay. The Ki67 primary antibody was incubated at 4°C overnight, and the fluorescent secondary antibody was incubated for 1 h in the dark at room temperature. Finally, the cells were stained with 4',6-diamidino-2-phenylindole (DAPI) for 10 min, and the slides were mounted for photographs in a NIKON Ti2-E fluorescence microscope (18, 19).

### Cell Migration Assay

Cells were grown to confluence in a 24-well plate before the cell monolayer was scratched with a 200- $\mu$ l-pipet tip to create a wound. After washing the cells twice with phosphate-buffered saline (PBS), either DMEM/F12, or vitreous (1:3 dilution in DMEM/F12) was added. Photographs were taken to record the width of the wounds at the beginning of the experiment, and then they were taken again 24 h later. After at least three independent experiments were conducted, Adobe Photoshop CC 2018 software was used to analyze the wound healing areas (20, 21).

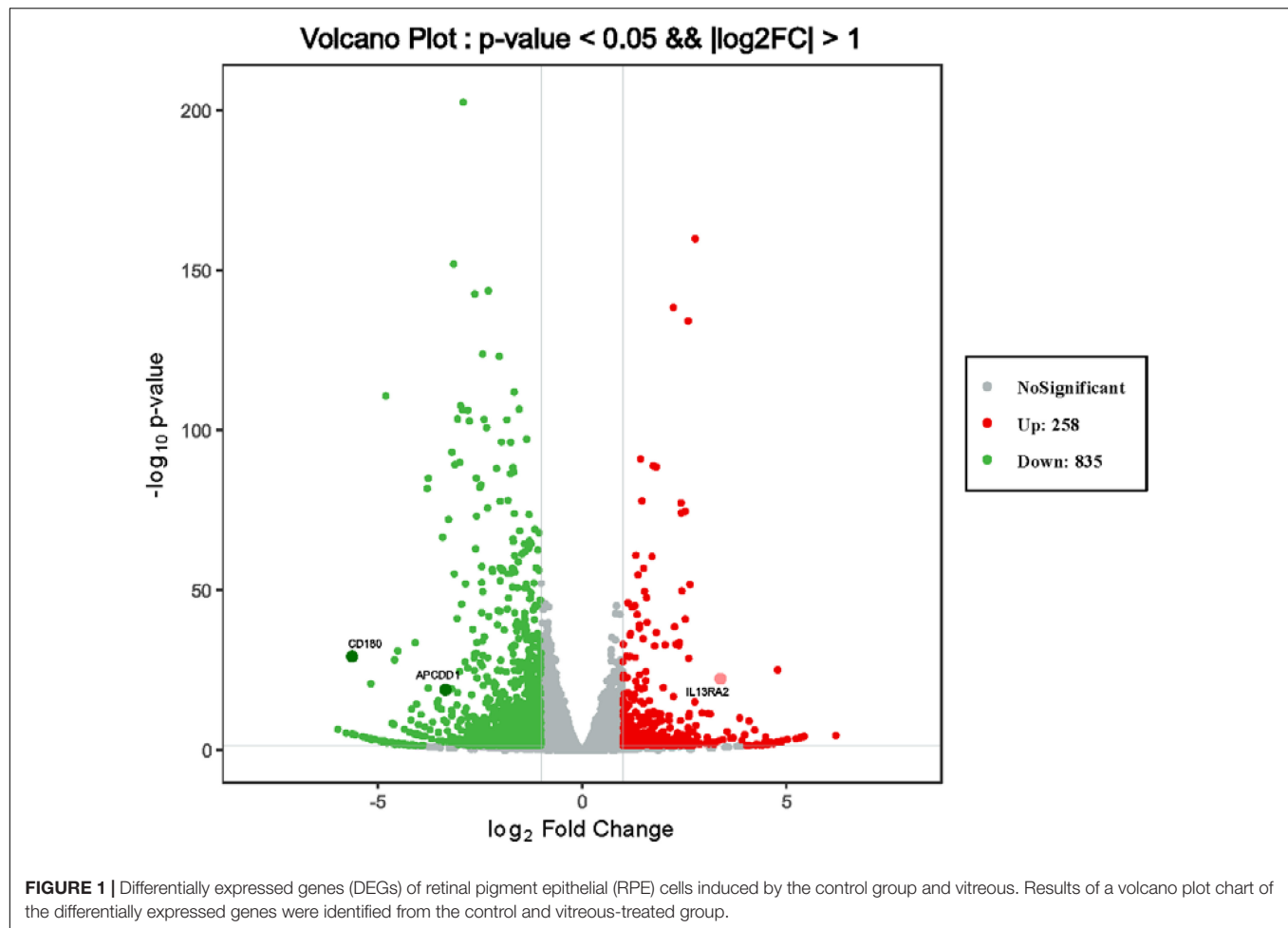
### Contraction Assay

Cells were trypsinized, counted, and centrifuged at 800 rpm for 5 min. The cell pellets were re-suspended in a collagen I solution (Cat. A10483, Gibco, United States) (pH 7.2) on ice, and the collected cells were diluted to  $1 \times 10^6$  cells/ml in the collagen solution, which were transferred to the wells (300  $\mu$ l/well) in a 24-well plate that had been incubated with 5 mg/ml bovine serum albumin (BSA)/PBS overnight. The plates were moved into a 37°C incubator for 90 min to allow the collagen to solidify, where upon the collagen gel was overlaid with 0.5 ml of either DMEM/F12, vitreous (1:3 dilution in DMEM/F12), or vitreous plus a neutralizing antibody against IL13R $\alpha 2$  (1  $\mu$ g/well). After 48 h, the diameter of the gel was measured and calculated. The data of three independent experiments were used for statistical analysis (21–23). Neutralizing the IL13R $\alpha 2$  receptor using neutralizing antibodies in collagen gel contraction is the same as the contraction assay.

### RNA Sequencing

Serum starved ARPE-19 cells at 70–80% confluence were treated with human vitreous diluted at a ratio of 1:3 in the DMEM/F12 medium for 24 h. The treated cells were then harvested by Trizol for RNA isolation using an OMEGA kit (R6834). Subsequently,





a Complementary DNA (cDNA) library was established and the quality and integrity of the RNA were examined by a NanoDrop analysis. RNA sequencing was performed by NovaSeq 6000. The differential genes were screened to satisfy  $|\log_2\text{FC}| \geq 1$  and  $p < 0.05$ , and genes were further screened to identify significantly differentially expressed genes related to eye diseases (24, 25).

Notably, Gene Ontology (GO) and Kyoto Encyclopedia of Genes and Genomes (KEGG) are two databases, and enrichment analysis is an integrated calculation of the functional information in the database. The full name of GO database analysis is Gene Ontology, and it divides the function of genes into three parts: cellular component (CC), molecular function (MF), and biological process (BP). Using the GO database, we can get the disease correlation of the target gene at the three levels of CC, MF, and BP. KEGG database analysis is a kind of pathway-related database to study the various pathways of the human body that genes participate in (24, 25).

### Quantitative PCR (qPCR) Analysis

Total RNA in the RPE cells treated by vitreous was extracted using an OMEGA kit (R6834), and then reverse transcribed to construct a cDNA library using a kit (RR036A, Takara). The differential expression of eye

disease-related genes was analyzed by qPCR using a kit (RR820A, Takara). Primer sequences: IL13RA2 forward (F): 5'-GGGCATTGAAGCGAAGATACA-3'; IL13RA2 reverse (R): 5'-GCCCAGGAACCTTTGAACTTCTG-3' (26); APCDD1 forward (F): 5'-TCCTGCTCAGATACCTGTTCC-3'; APCDD1 reverse (R): 5'-GTGATGGCACTGTGACTCCT-3'; CD180 forward (F): 5'-AACCTAAGCCTGAACTTCAATGG-3'; CD180 reverse (R): 5'-GCCAGAGAGACTGAGTAGTAGAG-3'.

### Western Blot

When cells reached 70–80% confluence, they were serum-starved for 24 h, and then treated with or without vitreous from patients (diluted 1:3 in DMEM/F12) for 24 h. After two washes with ice-cold PBS, cells were lysed in a cell lysis buffer for 30 min. The cell lysates were then clarified by centrifugation at 13,000 rpm for 10 min at 4°C. The total proteins were quantitated using a BCA kit (Cat. KGP250, keyGen, China), and the samples were boiled for 5 min. Proteins were separated by 10% sodium dodecyl-sulfate-polyacrylamide gel electrophoresis (SDS-PAGE), transferred to polyvinylidene difluoride (PVDF) membranes, and then subjected to western blot analysis using desired antibodies. Signal intensity was determined by densitometry using the Image J Software (22).

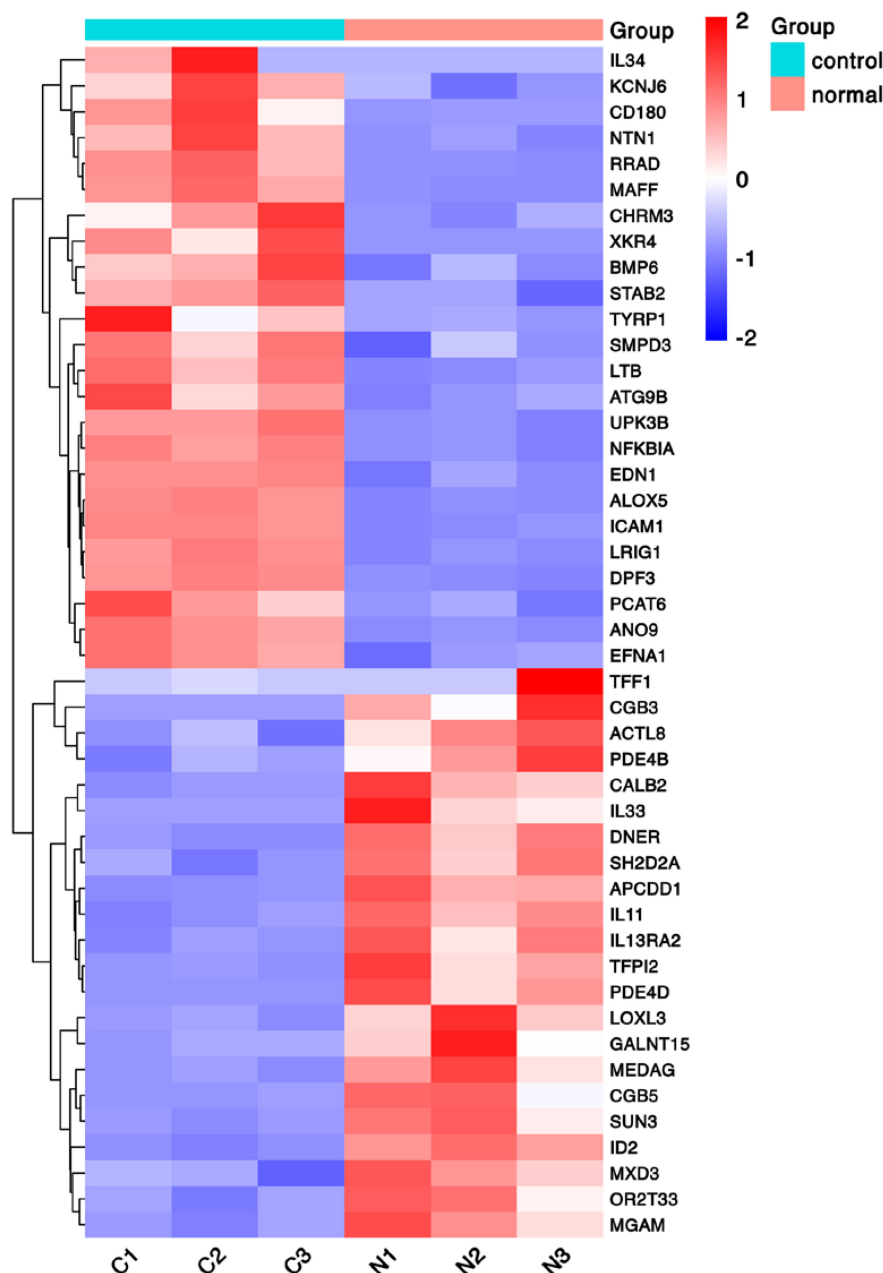


**FIGURE 2 |** Heat map of hierarchical clustered genes. A heat map of hierarchical clustered genes. In total, there were 46 genes from the genomics data showing a significantly aberrant expression (at least two-fold change),  $p < 0.05$ . In the clustering analysis, red and blue regions indicate the up-regulated and down-regulated genes, respectively. C1, C2, C3, and N1, N2, N3 represent the three independent repetitions of the control group and the vitreous induction group, respectively.

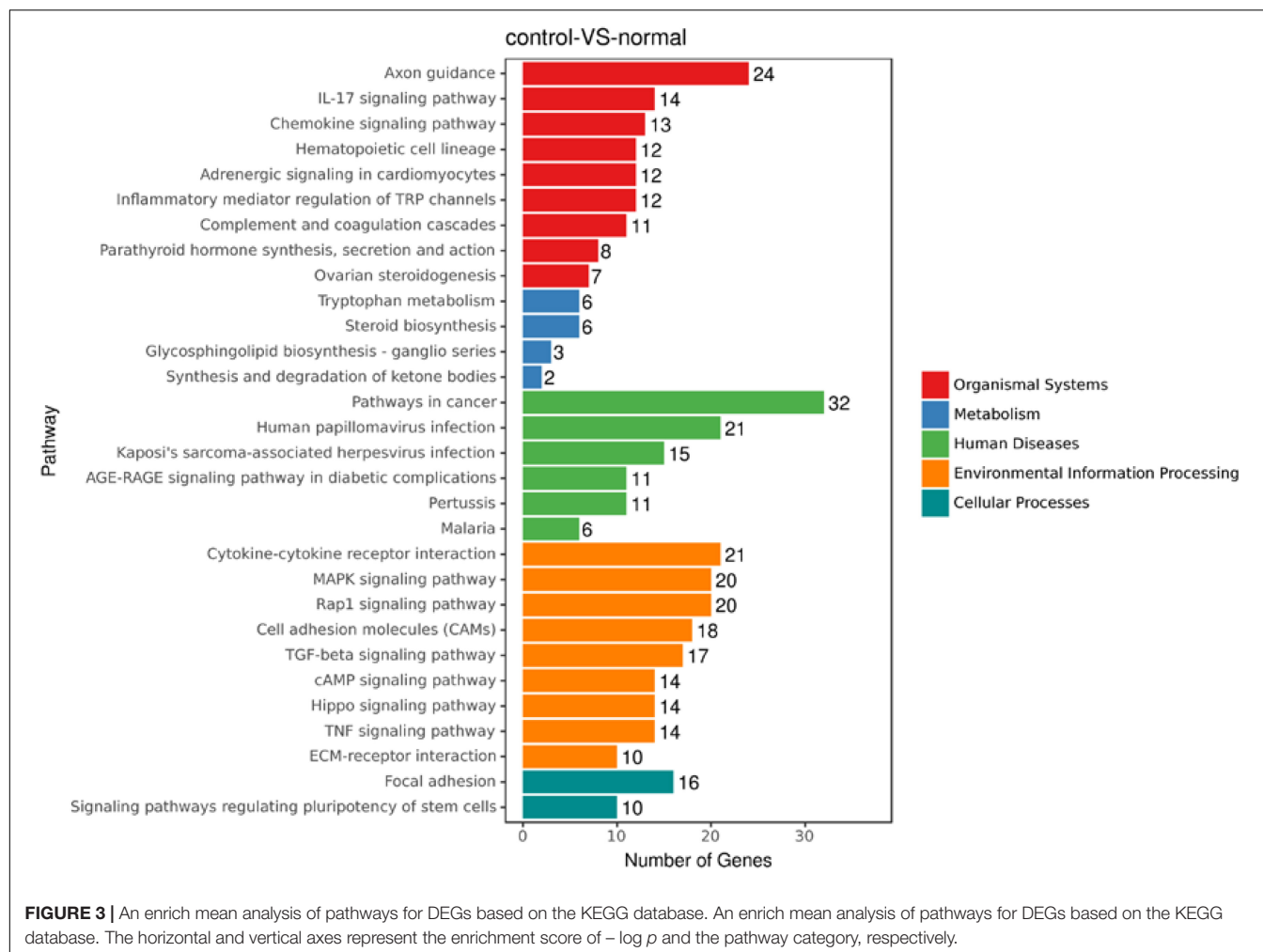
## Immunofluorescence

This experiment was performed as described previously (27, 28). Briefly, the tissues on slides were fixed with 4% paraformaldehyde (PFA) for 10 min at room temperature, blocked with 3% FBS for 30 min at room temperature, and then incubated with primary antibodies (anti-IL13R $\alpha$ 2 antibody or non-immune IgG at 1:200 dilution) at 4°C overnight. After thorough washes, the secondary antibody at a ratio of 1:1,000 was incubated at room temperature for 1 h in the dark. Next, the DAPI staining at a ratio of

1:1,000 was performed in the dark for additional 10 min. Finally, after the slides were washed thoroughly, they were mounted for photograph in a NIKON Ti2-E fluorescence microscope (27, 28).

## Statistics

Data from three independent experiments were used for statistical analysis with ordinary one-way ANOVA. The  $p$  value less than 0.05 was considered to be a significant difference (29).



## RESULTS

### RNA Sequencing Analysis Reveals That There Are 258 Genes Up-Regulated and 835 Genes Down-Regulated in Vitreous-Treated Retinal Pigment Epithelial Cells

Treatment of RPE cells with vitreous *in vitro* was to mimic PVR pathogenesis *in vivo*, and vitreous from human, bovine, and experimental rabbits is able to enhance cell proliferation, survival, and contraction (23, 30, 31). We then tested if vitreous from porcine could also have a similar bioactivity. Results showed that porcine vitreous was also capable of enhancing cell proliferation as shown in **Supplementary Figures 1–3**. These data are consistent with our previous findings that vitreous enhances PVR-related cellular events (13).

To discover novel genes contributing to PVR pathogenesis, we next treated ARPE-19 cells with human vitreous for transcriptional profiling. The quality of the RNA extracted from ARPE-19 cells treated with human vitreous reached the requirements for RNA sequencing (data not shown). Significant

DEGs between the control and the vitreous-treated groups were identified based on the criteria of a  $\log_2$ -fold change of  $>2$ . The results showed that in the RPE cells treated with human vitreous there were 1,093 differential genes, of which there were 258 genes up-regulated (23.6%) and 835 genes were down-regulated (76.4%). Among them, there are three genes related to eye diseases (**Figure 1**). Cluster analysis was performed on 46 of the differentially expressed genes in the genomics data. In the cluster heatmap, the red and blue regions represent the up-regulated and down-regulated expression of genes, respectively (**Figure 2**); KEGG enrichment analysis revealed that nearly half of the differential genes were mainly concentrated in pathways related to cellular components such as the mitogen-activated protein kinase (MAPK) pathway (**Figure 3**).

**TABLE 1 |** Main DEGs after vitreous induced.

Gene	Description	logFC	P value
CD180	CD180 molecule	−5.6276	0.0000
APCDD	APC down-regulated 1	−3.3411	0.0000
IL13RA2	interleukin 13 receptor subunit alpha 2	3.3898	0.0000

## Vitreous Induces Changes in *IL13RA2* Expression of mRNA and Protein

Among the 1,093 differential genes induced by vitreous, there were three genes with more than threefold changes (Table 1), which were confirmed by qPCR analysis (Figure 4). Noticeably, PVR is an inflammatory eye disease (12), IL13 is present in the vitreous (32); in addition, IL13R $\alpha$ 2 can bind to IL13 with high affinity to enhance cell proliferation and migration in the carcinogenesis (33, 34), and these cellular events are related to PVR pathogenesis. Thereby, we next investigated whether a vitreous-induced change in *IL13RA2* revealed by RNA sequencing was indeed the case. To this end, we treated ARPE-19 cells again with human vitreous and analyzed them with qPCR. The results showed that the vitreous treatments dramatically heightened the IL13RA2 expression in the RPE cells as shown in Figure 4.

Since vitreous induced changes in mRNA expression of *IL13RA2*, we next examined if its protein levels were also changed with the vitreous stimulation. As expected, Western blot analysis showed that vitreous augmented IL13R $\alpha$ 2 expression in the ARPE-19 cells (Figure 5). This Western blotting data are consistent with those obtained from RNA sequencing and qPCR.

## IL13R $\alpha$ 2 Is Highly Expressed in Epiretinal Membranes From Patients With Proliferative Vitreoretinopathy

We next investigated whether IL13R $\alpha$ 2 was expressed in RPE cells within the epiretinal membranes from PVR patients. To this end, we stained epiretinal membranes with antibodies against keratin specific for epithelial cells and IL13R $\alpha$ 2. The immunofluorescence results showed that IL13R $\alpha$ 2 was highly expressed in RPE cells in epiretinal membranes from PVR patients (Figure 6).

## Neutralization of IL13R $\alpha$ 2 Prevents Vitreous-Induced Contraction of Retinal Pigment Epithelial Cells

One of important events in the PVR pathogenesis is the contraction of epiretinal membranes, leading to the retinal detachment. Thereby we assessed if neutralization of IL13R $\alpha$ 2 could prevent vitreous-induced contraction of ARPE-19 cells in a collagen gel contraction assay, one of cellular models for PVR. As expected, vitreous stimulated the contraction of the collagen gel, and the antibody neutralizing IL13R $\alpha$ 2 significantly prevented the contraction induced by the vitreous (Figure 7), suggesting that this antibody is promising for PVR therapeutics.

## DISCUSSION

In this article, we report that vitreous induced a large increase in IL13R $\alpha$ 2 in ARPE-19 cells and blocking IL13R $\alpha$ 2 with its neutralizing antibody prevents contraction of ARPE-19 cells, implicating a novel role of IL13R $\alpha$ 2 in the PVR pathogenesis. The clinical manifestations of PVR are related to a series of inflammatory and fibrotic changes (12, 35–37). When the retina

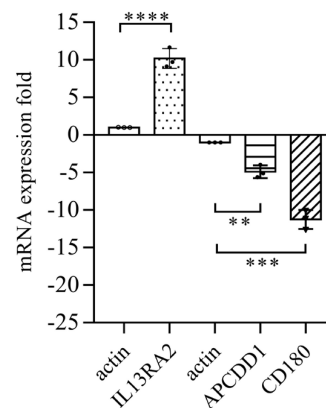


**FIGURE 4 |** Vitreous induced changes in the mRNA expression. The qPCR analysis of mRNA expression in ARPE-19 cells induced by vitreous. The mean  $\pm$  SD of three independent experiments is shown; \*\*\*\* denotes 0.0001, using paired *t* test; \*\*\* denotes 0.001, using paired *t* test; \*\* denotes 0.01, using paired *t* test. Positive values indicate a fold increase in expression of the target gene relative to the internal reference, and negative values are opposite.

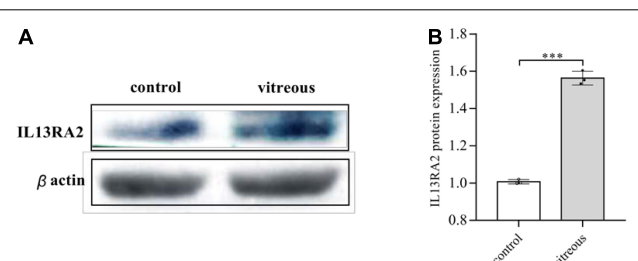


**FIGURE 5 |** Vitreous induced the protein expression of IL13R $\alpha$ 2. Western blot analysis of the vitreous-induced protein expression of IL13RA2 in ARPE-19 cells. One of three representative experiments is shown. Bar graphs showed the Western blot band intensity, and the mean  $\pm$  SD of three independent experiments is shown; \*\*\* denotes 0.001, using paired *t* test. **(A)** The protein expression of IL13RA2 in ARPE-19 cells. **(B)** Histogram of protein expression gray value. The mean  $\pm$  SD of three independent experiments is shown; \*\*\* denotes 0.001, using paired *t* test. Control: ARPE-19 cells treated with DMEM/F12 only. Vitreous: ARPE-19 cells treated with vitreous diluted in DMEM/F12.

of a patient ruptures, RPE cells exposed in the vitreous cavity respond to the vitreal growth factors and cytokines, leading to forward feedback to secrete these factors more (38), mediating wound repair responses such as matrix synthesis, cell migration, proliferation, and epithelial–mesenchymal transition (EMT), leading to the formation of epiretinal membranes, an essential process of PVR (39).

So far, the pathogenesis of PVR has not been completely understood. Hypotheses for PVR formation have been proposed for the essential roles of multiple growth factors and cytokines, such as transforming growth factor beta (TGF- $\beta$ ), platelet-derived growth factor (PDGF), vascular endothelial growth factors (VEGF), interleukins (ILs), tumor necrosis factor alpha (TNF- $\alpha$ ) (12, 38, 40). ILs can be secreted by a variety of cells in response to a variety of stimulation including tissue damage. In



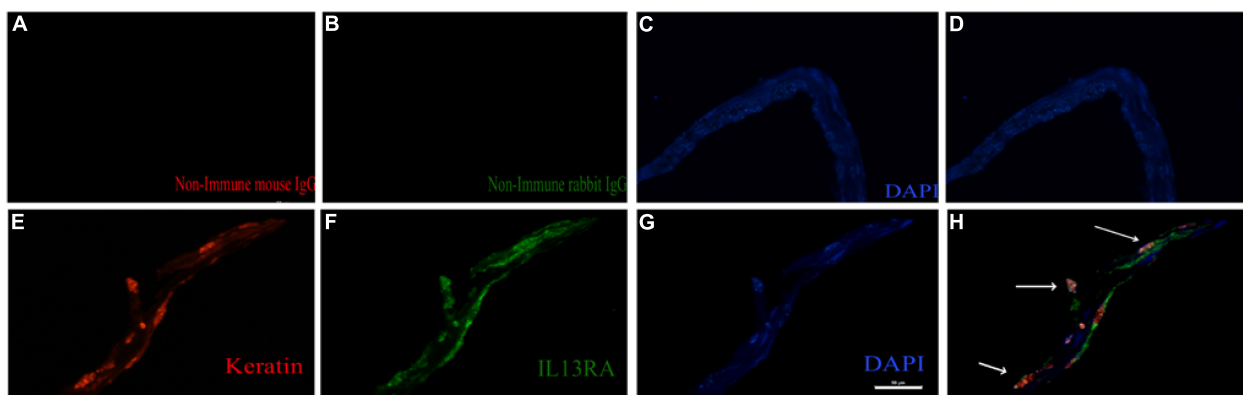


**FIGURE 6** | IL13R $\alpha$ 2 is highly expressed in RPE cells within epiretinal membranes from patients with proliferative vitreoretinopathy (PVR). Fibrotic epiretinal membranes from patients with PVR were first incubated with primary antibodies: a mixture of non-immune mouse and rabbit IgGs (**A–D**), or of anti-IL13R $\alpha$ 2 and pan keratin antibodies (**E–H**) at 4°C overnight, and then with fluorescently labeled secondary antibodies at 1 h in room temperature. Co-staining of IL13R $\alpha$ 2 with pan keratin in H indicates IL13R $\alpha$ 2 expression in RPE cells in the ERMs from patients with PVR. Scale bar: 50  $\mu$ m.

recent years, studies have revealed that ILs are closely related to the occurrence and development of PVR. For instance, IL-6, a marker of acute inflammation (41), is up-regulated in the vitreous and subretinal fluid of the PVR group, and is positively correlated with the degree and duration of RRD and PVR grades (42, 43). IL-8, playing a key role in regulating inflammation and mediating angiogenesis, is elevated in PVR patients (44).

We herein report that IL13R $\alpha$ 2 is heightened in the vitreous-treated RPE cells. IL13R $\alpha$ 2, one of the high-affinity membrane receptors of IL-13, is highly expressed in tumors, such as liver cancer (45), glioblastoma (46), colon cancer (47), and pancreatic cancer (48). IL13R $\alpha$ 2 has two forms: transmembrane form and extracellular soluble form (49–51). The transmembrane form is related to the signal transduction of ligands and the binding of

other membrane receptors to form different functional subunits; soluble IL13R $\alpha$ 2 seems to inhibit the function of IL13 (51, 52). It is speculated that the functions of the two forms of IL13R $\alpha$ 2 may be antagonistic to each other. The previous studies on tumors reported that the overexpression of IL13R $\alpha$ 2 endows tumors with the ability to invade and metastasize. IL-13 plays a key role in many pathological processes, such as asthma, pulmonary fibrosis, and ulcerative colitis (53, 54), and IL13 as an inflammatory

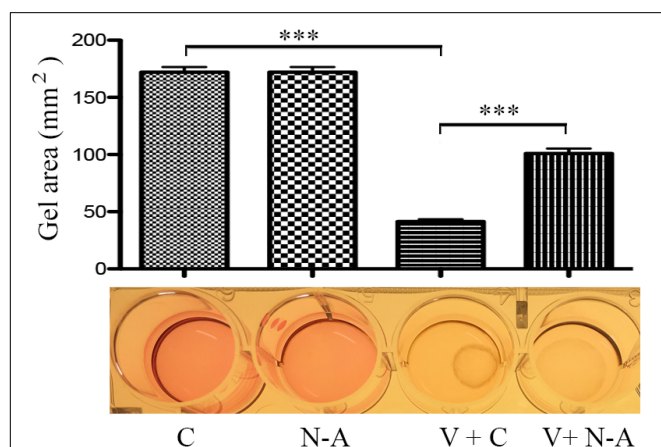


**FIGURE 7** | Blocking IL13R $\alpha$ 2 prevents vitreous-induced contraction of RPE cells. After the mixtures of ARPE-19 cells with collagen I solution formed a collagen gel, they were treated with DMEM/F12 + an antibody or vitreous + an antibody for 48 h. C, control antibody; N-A: neutralizing antibody against IL13R $\alpha$ 2; V + C, vitreous + control antibody; V + N-A, vitreous + neutralizing antibody against IL13R $\alpha$ 2. \*\*\* denotes 0.001, using paired *t* test.

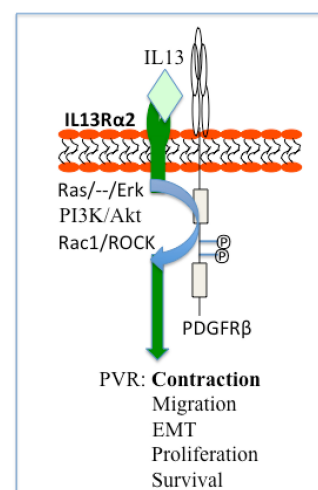


**FIGURE 8** | Schematic of a hypothesis: a role of IL13R $\alpha$ 2 cooperates with PDGFR $\beta$  in the PVR pathogenesis. Based on current literatures (13, 55) IL13R $\alpha$ 2 cooperates with PDGFR $\beta$  to initiate signaling pathways of Ras/Raf/MEK/ERK, PI3K/Akt, Rac1/ROCK, and thereby enhance cellular responses (survival, proliferation, EMT, migration, and contraction) intrinsic to PVR. ERK, extracellular signal-regulated kinases; PI3K, phosphoinositide 3 kinase; Rac1, Ras-related C3 botulinum toxin substrate 1; ROCK, Rho-associated protein kinase; EMT, epithelial–mesenchymal transition; PVR, proliferative vitreoretinopathy.

factor plays an important part in various inflammatory reactions, suggesting IL13RA2 may play an important role in PVR.

Noticeably, IL13R $\alpha$ 2 cooperates with epidermal growth factor receptor (EGFR) VIII signaling to promote glioblastoma multiforme (46), whereas PDGF receptor (PDGFR) $\beta$  plays an essential role in vitreous-induced cellular responses related to PVR (13). Thereby we hypothesize that in ARPE-19 cells, IL13R $\alpha$ 2 interacts with PDGFR $\beta$  signaling to boost vitreous-stimulated cellular events intrinsic to PVR as illustrated in **Figure 8**, and this hypothesis is being tested in our research group.

In this study, we employed RNA sequencing to discover changes in vitreous-treated ARPE-19 cells, leading to our findings that IL13R $\alpha$ 2 was up-regulated significantly, and blockade of IL13R $\alpha$ 2 prevented contraction of ARPE-19 cells, suggesting that IL13R $\alpha$ 2 be a novel therapeutic target for PVR.

## DATA AVAILABILITY STATEMENT

HL is the guarantor of this work, has full access to all the data in the study, and takes responsibility for the integrity of the data and the accuracy of the data analysis. The datasets generated during and/or analyzed during the current study are available from the corresponding author upon reasonable request.

## ETHICS STATEMENT

The studies involving human participants were reviewed and approved by the Jinan University Research Ethics Board. The

patients/participants provided their written informed consent to participate in this study.

## AUTHOR CONTRIBUTIONS

HQ, LD, and DF performed most of the experiments and analyzed the results. YW, NF, XM, GZ, and WW performed some experiments and managed projects. SZ and HL conceived the experiments, analyzed the data, and wrote the manuscript. All authors contributed to the article and approved the submitted version.

## FUNDING

This work was supported by the National Natural Science Foundation of China (82070989) to HL, and Sanming Project of Medicine in Shenzhen (No. SZSM202011015) to XY, GZ, SZ, and HL. No funding bodies had any role in study design, data collection and analysis, and decision to publish, or preparation of the manuscript.

## SUPPLEMENTARY MATERIAL

The Supplementary Material for this article can be found online at: <https://www.frontiersin.org/articles/10.3389/fmed.2022.831436/full#supplementary-material>

## REFERENCES

- Das V, Bhattacharya S, Chikputtaiah C, Hazra S, Pal M. The basics of epithelial-mesenchymal transition (EMT): a study from a structure, dynamics, and functional perspective. *J Cell Physiol.* (2019) 234: 14535–55. doi: 10.1002/jcp.28160
- Lin YC, Shen ZR, Song XH, Liu X, Yao K. Comparative transcriptomic analysis reveals adriamycin-induced apoptosis via p53 signaling pathway in retinal pigment epithelial cells. *J Zhejiang Univ Sci B.* (2018) 19:895–909. doi: 10.1631/jzus.B1800408
- Asato R, Yoshida S, Ogura A, Nakama T, Ishikawa K, Nakao S, et al. Comparison of gene expression profile of epiretinal membranes obtained from eyes with proliferative vitreoretinopathy to that of secondary epiretinal membranes. *PLoS One.* (2013) 8:e54191. doi: 10.1371/journal.pone.0054191
- Roybal CN, Velez G, Toral MA, Tsang SH, Bassuk AG, Mahajan VB. Personalized proteomics in proliferative vitreoretinopathy implicate hematopoietic cell recruitment and mTOR as a therapeutic target. *Am J Ophthalmol.* (2018) 186:152–63. doi: 10.1016/j.ajo.2017.11.025
- Andre F, Ciruelos E, Rubovszky G, Campone M, Loibl S, Rugo HS, et al. Alpelisib for PIK3CA-mutated, hormone receptor-positive advanced breast cancer. *N Engl J Med.* (2019) 380:1929–40.
- Pastor JC, Rojas J, Pastor-Idoate S, Lauro S, Di, Gonzalez-Buendia L, Delgado-Tirado S. Proliferative vitreoretinopathy: a new concept of disease pathogenesis and practical consequences. *Prog Retin Eye Res.* (2016) 51:125–55. doi: 10.1016/j.preteyeres.2015.07.005
- Schiff L, Boles C, Fernandes M, Nachmani B, Gentile R, Blenkinsop TA. P38 inhibition reverses TGF $\beta$ 1 and TNF $\alpha$ -induced contraction in a model of proliferative vitreoretinopathy. *Commun. Biol.* (2019) 2:162.
- Zhou RM, Wang XQ, Yao J, Shen Y, Chen SN, Yang H, et al. Identification and characterization of proliferative retinopathy-related long noncoding RNAs. *Biochem Biophys Res Commun.* (2015) 465:324–30. doi: 10.1016/j.bbrc.2015.07.120
- Rojas JI, Fernandez JC, Pastor R, MacLaren E, Ramkissoon Y, Harsum S, et al. Predicting proliferative vitreoretinopathy: temporal and external validation of models based on genetic and clinical variables. *Br J Ophthalmol.* (2015) 99:41–8. doi: 10.1136/bjophthalmol-2014-305263
- Bastiaans J, van Meurs JC, Mulder VC, Nagtzaam NM, Smits-te Nijenhuis M, Dufour-van den Goorbergh DC, et al. The role of thrombin in proliferative vitreoretinopathy. *Invest Ophthalmol Vis Sci.* (2014) 55:4659–66. doi: 10.1167/iovs.14-14818
- Garweg JG, Tappeiner C, Halberstadt M. Pathophysiology of proliferative vitreoretinopathy in retinal detachment. *Surv Ophthalmol.* (2013) 58:321–9. doi: 10.1016/j.survophthal.2012.12.004
- Moysidis SN, Thanos A, Vavvas DG. Mechanisms of inflammation in proliferative vitreoretinopathy: from bench to bedside. *Mediat Inflamm.* (2012) 2012:1–11. doi: 10.1155/2012/815937
- Yang Y, Huang X, Ma G, Cui J, Matsubara JA, Kazlauskas A, et al. PDGFR $\beta$  plays an essential role in patient vitreous-stimulated contraction of retinal pigment epithelial cells from epiretinal membranes. *Exp Eye Res.* (2020) 197:108116. doi: 10.1016/j.exer.2020.108116
- Oberstein SY, Byun J, Herrera D, Chapin EA, Fisher SK, Lewis GP. Cell proliferation in human epiretinal membranes: characterization of cell types

- and correlation with disease condition and duration. *Mol Vis.* (2011) 17:1794–805.
15. Umazume K, Tsukahara R, Liu L, Fernandez de Castro JP, McDonald K, Kaplan HJ, et al. Role of retinal pigment epithelial cell beta-catenin signaling in experimental proliferative vitreoretinopathy. *Am J Pathol.* (2014) 184:1419–28. doi: 10.1016/j.ajpath.2014.01.022
  16. Sant DW, Camarena V, Mustafi S, Li Y, Wilkes Z, Van Booven D, et al. Ascorbate Suppresses VEGF expression in retinal pigment epithelial cells. *Invest Ophthalmol Vis Sci.* (2018) 59:3608–18. doi: 10.1167/iov.18-24101
  17. Rimpela AK, Reunanen S, Hagstrom M, Kidron H, Urtti A. Binding of small molecule drugs to porcine vitreous humor. *Mol Pharm.* (2018) 15:2174–9. doi: 10.1021/acs.molpharmaceut.8b00038
  18. Graefe C, Eichhorn L, Wurst P, Kleiner J, Heine A, Panetas I, et al. Optimized Ki-67 staining in murine cells: a tool to determine cell proliferation. *Mol Biol Rep.* (2019) 46:4631–43. doi: 10.1007/s11033-019-04851-2
  19. Meng S, Zhu Y, Li J-F, Wang X. Apigenin inhibits renal cell carcinoma cell proliferation. *Oncotarget.* (2017) 8:19834–42.
  20. Huang X, Zhou G, Wu W, Ma G, D'Amore PA, Mukai S, et al. Editing VEGFR2 Blocks VEGF-Induced Activation of Akt and Tube Formation. *Invest Ophthalmol Vis Sci.* (2017) 58:1228–36. doi: 10.1167/iov.16-20537
  21. Chen N, Hu Z, Yang Y, Han H, Lei H. Inactive Cas9 blocks vitreous-induced expression of Mdm2 and proliferation and survival of retinal pigment epithelial cells. *Exp Eye Res.* (2019) 186:107716. doi: 10.1016/j.exer.2019.107716
  22. Lei H, Velez G, Hovland P, Hirose T, Gilbertson D, Kazlauskas A. Growth factors outside the PDGF family drive experimental PVR. *Invest Ophthalmol Vis Sci.* (2009) 50:3394–403. doi: 10.1167/iov.08-3042
  23. Lei H, Velez G, Cui J, Samad A, Maberley D, Matsubara J, et al. N-acetylcysteine suppresses retinal detachment in an experimental model of proliferative vitreoretinopathy. *Am J Pathol.* (2010) 177:132–40. doi: 10.2353/ajpath.2010.090604
  24. Zhang H, He L, Cai L. Transcriptome sequencing: RNA-Seq. *Methods Mol Biol.* (2018) 1754:15–27.
  25. Schumacker ST, Coppage KR, Enke RA. RNA sequencing analysis of the human retina and associated ocular tissues. *Sci Data.* (2020) 7:199. doi: 10.1038/s41597-020-0541-4
  26. Wagner EM. Monitoring gene expression: quantitative real-time rt-PCR. *Methods Mol Biol.* (2013) 1027:19–45. doi: 10.1007/978-1-60327-369-5\_2
  27. Ding X, Bai Y, Zhu X, Li T, Jin E, Huang L, et al. The effects of pleiotrophin in proliferative vitreoretinopathy. *Graefes Arch Clin Exp Ophthalmol.* (2017) 255:873–84. doi: 10.1007/s00417-016-3582-9
  28. Diercks GF, Pas HH, Jonkman MF. Immunofluorescence of autoimmune bullous diseases. *Surg Pathol Clin.* (2017) 10:505–12.
  29. Huang X, Zhou G, Wu W, Duan Y, Ma G, Song J, et al. Genome editing abrogates angiogenesis in vivo. *Nat Commun.* (2017) 8:112. doi: 10.1038/s41467-017-00140-3
  30. Lei H, Velez G, Kazlauskas A. Pathological signaling via platelet-derived growth factor receptor  $\alpha$  involves chronic activation of Akt and suppression of p53. *Mol Cell Biol.* (2011) 31:1788–99.
  31. Han H, Yang Y, Liu B, Tian J, Dong L, Qi H, et al. Chalconoracin prevents vitreous-induced activation of AKT and migration of retinal pigment epithelial cells. *J Cell Mol Med.* (2021) 25:9102–11. doi: 10.1111/jcmm.16590
  32. Yoshida S, Kobayashi Y, Nakama T, Zhou Y, Ishikawa K, Arita R, et al. Increased expression of M-CSF and IL-13 in vitreous of patients with proliferative diabetic retinopathy: implications for M2 macrophage-involving fibrovascular membrane formation. *Br J Ophthalmol.* (2015) 99:629–34. doi: 10.1136/bjophthalmol-2014-305860
  33. Fujisawa T, Joshi B, Nakajima A, Puri RK. A novel role of interleukin-13 receptor  $\alpha$ 2 in pancreatic cancer invasion and metastasis. *Cancer Res.* (2009) 69:8678–85. doi: 10.1158/0008-5472.CAN-09-2100
  34. Marquez-Ortiz RA, Contreras-Zarate MJ, Tesic V, Alvarez-Eraso KLF, Kwak G, Littrell Z, et al. IL13R $\alpha$ 2 promotes proliferation and outgrowth of breast cancer brain metastases. *Clin Cancer Res.* (2021) 27:6209–21. doi: 10.1158/1078-0432.CCR-21-0361
  35. Chaudhary R, Scott RAH, Wallace G, Berry M, Logan A, Blanch RJ. Inflammatory and fibrogenic factors in proliferative vitreoretinopathy development. *Transl Vis Sci Technol.* (2020) 9:23. doi: 10.1167/tvst.9.3.23
  36. Ni Y, Qin Y, Huang Z, Liu F, Zhang S, Zhang Z. Distinct serum and vitreous inflammation-related factor profiles in patients with proliferative vitreoretinopathy. *Adv Ther.* (2020) 37:2550–9. doi: 10.1007/s12325-020-01325-x
  37. Dai Y, Dai C, Sun T. Inflammatory mediators of proliferative vitreoretinopathy: hypothesis and review. *Int Ophthalmol.* (2020) 40:1587–601. doi: 10.1007/s10792-020-01325-4
  38. Pennock S, Haddock LJ, Elliott D, Mukai S, Kazlauskas A. Is neutralizing vitreal growth factors a viable strategy to prevent proliferative vitreoretinopathy? *Prog Retin Eye Res.* (2014) 40:16–34. doi: 10.1016/j.preteyeres.2013.12.006
  39. Rouberol F, Chiquet C. [Proliferative vitreoretinopathy: pathophysiology and clinical diagnosis]. *J Fr Ophtalmol.* (2014) 37:557–65. doi: 10.1016/j.jfo.2014.04.001
  40. Morescalchi F, Duse S, Gambicorti E, Romano MR, Costagliola C, Semeraro F. Proliferative vitreoretinopathy after eye injuries: an overexpression of growth factors and cytokines leading to a retinal keloid. *Mediat Inflamm.* (2013) 2013:269787. doi: 10.1155/2013/269787
  41. Ricker LJ, Kijlstra A, Kessels AG, de Jager W, Liem AT, Hendrikse F, et al. Interleukin and growth factor levels in subretinal fluid in rhegmatogenous retinal detachment: a case-control study. *PLoS One.* (2011) 6:e19141. doi: 10.1371/journal.pone.0019141
  42. Symeonidis C, Papakonstantinou E, Androudi S, Georgalas I, Rotsos T, Karakiulakis G, et al. Comparison of interleukin-6 and matrix metalloproteinase expression in the subretinal fluid and the vitreous during proliferative vitreoretinopathy: Correlations with extent, duration of RRD and PVR grade. *Cytokine.* (2014) 67:71–6. doi: 10.1016/j.cyto.2014.02.012
  43. Kon CH, Occlleston NL, Aylward GW, Khaw PT. Expression of vitreous cytokines in proliferative vitreoretinopathy: a prospective study. *Invest Ophthalmol Vis.* (1999) 40:705–12.
  44. Rasier R, Gormus U, Artunay O, Yuzbasioglu E, Oncel M, Bahcecioglu H. Vitreous levels of VEGF, IL-8, and TNF- $\alpha$  in retinal detachment. *Curr Eye Res.* (2010) 35:505–9. doi: 10.3109/02713681003597248
  45. Wang M, Yao R, Wang Y. Silencing of IL13RA2 promotes partial epithelial-mesenchymal transition in hepatocellular carcinoma via ERK signaling pathway activation. *FEBS Open Bio.* (2020) 10:229–36. doi: 10.1002/2211-5463.12774
  46. Newman JP, Wang GY, Arima K, Guan SP, Waters MR, Cavenee WK, et al. Interleukin-13 receptor  $\alpha$ 2 cooperates with EGFRvIII signaling to promote glioblastoma multiforme. *Nat Commun.* (2017) 8:1913.
  47. Song X, Traub B, Shi J, Kornmann M. Possible roles of interleukin-4 and -13 and their receptors in gastric and colon cancer. *Int J Mol Sci.* (2021) 22:727.
  48. Barderas R, Bartolome RA, Fernandez-Acenero MJ, Torres S, Casal JI. High expression of IL-13 receptor  $\alpha$ 2 in colorectal cancer is associated with invasion, liver metastasis, and poor prognosis. *Cancer Res.* (2012) 72:2780–90. doi: 10.1158/0008-5472.CAN-11-4090
  49. Tabata Y, Khurana HGK. IL-13 receptor isoforms: breaking through the complexity. *Curr Allergy Asthma.* (2007) 7:338–45. doi: 10.1007/s11882-007-0051-x
  50. Wills-Karp M, Finkelman FD. Untangling the complex web of IL-4- and IL-13-mediated signaling pathways. *Sci Signal.* (2008) 1:e55. doi: 10.1126/scisignal.1.51.pe55
  51. McKenzie AN, Fallon PG. Decoy receptors in the regulation of T helper cell type 2 responses. *J Exp Med.* (2003) 197:675–9. doi: 10.1084/jem.20030096
  52. Mm M-K. Opposing roles for IL-13 and IL-13 receptor  $\alpha$ 2 in health and disease. *Immunol Rev.* (2004) 202:191–202. doi: 10.1111/j.0105-2896.2004.00210.x
  53. Chung SI, Horton JA, Ramalingam TR, White AO, Chung EJ, Hudak KE, et al. IL-13 is a therapeutic target in radiation lung injury. *Sci Rep.* (2016) 6:39714. doi: 10.1038/srep39714
  54. Rosen MJ, Frey MR, Washington MK, Chaturvedi R, Kuhnlein LA, Matta P, et al. STAT6 activation in ulcerative colitis: a new target for prevention of IL-13-induced colon epithelial cell dysfunction. *Inflamm Bowel Dis.* (2011) 17:2224–34. doi: 10.1002/ibd.21628

55. Newman JP, Wang GY, Arima K. Interleukin-13 receptor alpha 2 cooperates with EGFRvIII signaling to promote glioblastoma multiforme. *Nat Commun.* (2017) 1:1913.

**Conflict of Interest:** The authors declare that the research was conducted in the absence of any commercial or financial relationships that could be construed as a potential conflict of interest.

**Publisher's Note:** All claims expressed in this article are solely those of the authors and do not necessarily represent those of their affiliated organizations, or those of the publisher, the editors and the reviewers. Any product that may be evaluated in

this article, or claim that may be made by its manufacturer, is not guaranteed or endorsed by the publisher.

Copyright © 2022 Qi, Dong, Fang, Chen, Wang, Fan, Mao, Wu, Yan, Zhang, Zhang and Lei. This is an open-access article distributed under the terms of the Creative Commons Attribution License (CC BY). The use, distribution or reproduction in other forums is permitted, provided the original author(s) and the copyright owner(s) are credited and that the original publication in this journal is cited, in accordance with accepted academic practice. No use, distribution or reproduction is permitted which does not comply with these terms.





# Inner Retinal Layer Hyperreflectivity Is an Early Biomarker for Acute Central Retinal Artery Occlusion

Daniel A. Wenzel<sup>1,2</sup>, Sven Poli<sup>3,4</sup>, Maria Casagrande<sup>2</sup>, Vasyl Druchkiv<sup>2</sup>, Martin S. Spitzer<sup>2</sup>, Karl Ulrich Bartz-Schmidt<sup>1</sup>, Carsten Grohmann<sup>2†</sup> and Maximilian Schultheiss<sup>2\*†</sup>

<sup>1</sup> University Eye Hospital, Centre for Ophthalmology, University Hospital Tübingen, Tübingen, Germany, <sup>2</sup> Department of Ophthalmology, University Medical Center Hamburg-Eppendorf, Hamburg, Germany, <sup>3</sup> Department of Neurology and Stroke, University Hospital Tübingen, Tübingen, Germany, <sup>4</sup> Hertie Institute for Clinical Brain Research, University Hospital Tübingen, Tübingen, Germany

## OPEN ACCESS

### Edited by:

Jodhbir Mehta,  
Singapore National Eye Centre,  
Singapore

### Reviewed by:

Peng Xiao,  
Sun Yat-sen University, China  
Yan Yan,  
Shanghai Jiao Tong University, China

### \*Correspondence:

Maximilian Schultheiss  
maximilianschultheiss@gmail.com

<sup>†</sup>These authors have contributed  
equally to this work and share last  
authorship

### Specialty section:

This article was submitted to  
Ophthalmology,  
a section of the journal  
Frontiers in Medicine

**Received:** 13 January 2022

**Accepted:** 20 June 2022

**Published:** 06 July 2022

### Citation:

Wenzel DA, Poli S,  
Casagrande M, Druchkiv V,  
Spitzer MS, Bartz-Schmidt KU,  
Grohmann C and Schultheiss M  
(2022) Inner Retinal Layer  
Hyperreflectivity Is an Early Biomarker  
for Acute Central Retinal Artery  
Occlusion. *Front. Med.* 9:854288.  
doi: 10.3389/fmed.2022.854288

**Purpose:** To investigate inner retinal hyperreflectivity on optical coherence tomography (OCT) as a potential biomarker indicating acute central retinal artery occlusion (CRAO).

**Methods:** A total of 56 patients at two university hospitals with acute CRAO (symptom onset  $\leq 48$  h) were included in this retrospective study. The optical intensity of the inner retinal layers was determined in both eyes and the relationship between symptom onset and inner retinal layer optical intensity in OCT scans compared to the unaffected fellow eye was analyzed. Several differential diagnoses [central retinal vein occlusion, anterior ischemic optic neuropathy, diabetic macular edema, and subretinal fibrosis/disciform scar (Junius-Kuhnt)] served as controls to validate optical intensity-based diagnosis of CRAO.

**Results:** CRAO strongly correlated with an increased inner retinal layer hyperreflectivity in this cohort with acute CRAO with a time since symptom onset ranging from 1.1 to 48.0 h. Receiver operating characteristic (ROC) analysis showed an area under the curve of 0.99 to confirm CRAO with a true positive rate of 0.93 and a false positive rate of 0.02. No correlation between optical intensity and time since symptom onset was noticeable. None of the differential diagnoses did show an elevated optical intensity of the inner retinal layers as it was detectable in CRAO.

**Conclusion:** OCT-based determination of inner retinal layer hyperreflectivity is a very promising biomarker for a prompt diagnosis of CRAO in an emergency setting. This may be of major interest to speed up the administration of a possible thrombolytic treatment.

**Keywords:** central retinal artery occlusion (CRAO), optical coherence tomography, retinal ischemia, retinal imaging biomarkers, ischemia biomarker

**Abbreviations:** CRAO, central retinal artery occlusion; CRVO, central retinal vein occlusion; DME, diabetic macular edema; JK, Junius-Kuhnt, age related macular degeneration with subretinal fibrosis/disciform scar; (NA-)AION, (non-)arteritic anterior ischemic optic neuropathy; OCT, optical coherence tomography; RRTI, relative retinal thickness increase.

## INTRODUCTION

Acute central retinal artery occlusion (CRAO) causes sudden monocular vision loss. Early intravenous thrombolysis (IVT) within 4.5 h is currently subject of ongoing prospective randomized trials. However, established algorithms and strategies for a rapid and accurate diagnosis and to triage patients do not yet exist. Most patients do not reach appropriate medical facilities in time to potentially initiate IVT, which illustrates the urgent need for retinal ischemia biomarkers in order to quickly and safely diagnose CRAO and provide therapy within a therapeutic time window of 4.5 h (1–7).

Typically, CRAO is a clinical diagnosis, though funduscopy changes, such as a cherry red spot or retinal pallor, may be lacking within the IVT-relevant very early phase, while ischemic signs may already become apparent on optical coherence tomography (OCT) scans (8). OCT provides high resolution non-invasive microstructural retinal images and has been shown to be a valuable diagnostic instrument for CRAO (9–16). Several retinal ischemia biomarkers can be visualized early, using OCT imaging within the acute phase of CRAO. Besides a loss of structure of the retinal layers, ischemic intracellular edema causes a time-dependent increase in retinal thickness, which eventually resolves and is followed by severe inner retinal atrophy in the chronic phase (9, 10, 12, 14–18). The relative retinal thickness increase (RRTI, retinal thickness increase at the thickest portion of the papillomacular bundle of the affected compared to unaffected eye) may provide information about the onset of ischemia with high accuracy (16). The ischemic edema is accompanied by hyperreflective inner retinal layers (ganglion cell layer to outer plexiform layer) and hyporeflexive outer retinal layers (11, 19). Whereas the hyperreflectivity of the inner retinal layers is discussed to be most likely due to an increased intracellular ischemic edema, whereas consequently hyporeflexivity of the outer layers is caused by the decreased signal permeability of the edematous inner retinal layers (19, 20). However, as the retinal thickness often is normal or only mildly increased within the first hours (8, 10, 16), we hypothesized that the ischemia-induced increase in optical intensity may potentially be visible as the first ischemic sign anteceding retinal edema. This study therefore investigated the optical intensity of the inner retinal layers as a diagnostic criterium of CRAO and as a discriminator between potential differential diagnoses of CRAO with (sub-)acute vision loss.

## MATERIALS AND METHODS

### Study Design and Patient Selection

The retrospective analysis included 56 patients (35 male, 21 female; age  $73.1 \pm 10.9$ , range 42–93) with acute CRAO who presented at two tertiary care facilities (University Eye Hospital Tübingen, Germany and Department of Ophthalmology, University Medical Center Hamburg-Eppendorf, Germany). All included patients were able to reliably report the time of symptom onset ( $\leq 48$  h) of sudden, painless and persistent monocular vision loss and received an OCT scan of both eyes within 48 h [mean (SD) time-to-OCT (TTO):  $13.2 \pm 10.5$  h

(range 1.1–48.0 h)]. Visual acuity was  $\leq 20/400$ . CRAO was diagnosed by an ophthalmologist. Inner retinal layer reflectivity of the affected and unaffected eye was compared. Patients with high picture noise or poor OCT image quality had to be excluded prior to analysis. Mean OCT quality index (signal-to-noise ratio, higher index indicates better quality) was  $26.4 \pm 5.1$  in CRAO eyes and  $27.4 \pm 4.7$  in healthy fellow eyes. Also lens status was analyzed, as potentially opacities can decrease image quality: lens status was symmetric in 55 patients. Lens status was according to age (no cataract) in 14 patients, 15 patients had incipient cataract, 7 patients presented with advanced cataract and pseudophakia was recorded in 15 patients. In four patients lens status was not recorded. One patient was pseudophakic in the healthy eye and had incipient cataract on the opposite eye affected by CRAO. Patients with retinal/macular pathologies other than CRAO (reperfused/transient CRAO, arteritic CRAO, cilioretinal artery, age-related macular degeneration, epiretinal gliosis, etc.) were also excluded.

In addition, the optical intensity of the inner retinal layers was analyzed and compared to the fellow eye in 40 patients with manifest potential differential diagnoses of possibly causing subjective acute vision loss, such as central retinal vein occlusion (CRVO;  $n = 10$ ), diabetic macular edema (DME;  $n = 10$ ), subretinal fibrosis/disciform scar (Junius-Kuhnt, JK;  $n = 10$ ), or non-arteritic anterior ischemic optic neuropathy (NA-AION;  $n = 10$ ). The inner retinal optical intensity of the eyes with CRAO was compared to the more severely affected fellow eyes of the other differential diagnoses.

### Data Collection and Statistics

Optical coherence tomography scans were performed with a Spectral-Domain OCT (Spectralis OCT, Heidelberg Engineering, Germany). Horizontal scans and the “white-on-black” mode through the fovea of both eyes were processed, saved as grayscale JPEG images and then further analyzed with ImageJ (National Institutes of Health, Bethesda, MD, United States) similar to the study of Chen et al. (11). The fovea centralis was identified and the four scans around the central scan (two below and two above) and the central scan were used for segmentation. After manual segmentation of the inner retinal layers (see **Figure 1**; retinal nerve fiber layer, ganglion cell layer, inner plexiform layer, inner nuclear layer, and outer plexiform layer) the raw scores of optical intensity that were inside the segmentation [gray scale, 0 (black) to 255 (white)] were extracted and analyzed using the software R (21). Only the inner retinal layer reflectivity was included into our analysis. Receiver operating characteristic (ROC) analysis was performed to classify between the eye affected and unaffected eye given the optical intensity. For each value of optical intensity sensitivity and specificity was calculated. The optimal cut-off was found by maximizing the sum of sensitivity and specificity.

Analysis of variance (ANOVA) and *post hoc t*-test adjusted for multiple comparisons with Bonferroni method were used to compare the optical intensity between the potential differential diagnoses of CRAO and test for significance. The residuals from the linear model were verified for normal distribution using Shapiro–Wilk test ( $p > 0.05$ ). Variances were equal (Levene test  $p > 0.05$ ).

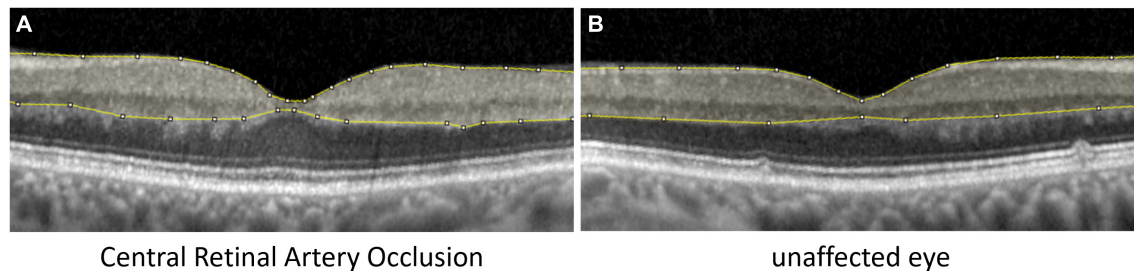


**FIGURE 1** | Analysis of inner retinal layer reflectivity. Segmentation of the inner retinal layers, where the optical intensity was analyzed in eyes with **(A)** central retinal artery occlusion and **(B)** the unaffected fellow eye.

## RESULTS

In the analyzed patient cohort of 56 patients the time between known symptom onset and OCT scan (TTO) ranged from 1.1 to 48.0 h ( $13.2 \pm 10.5$  h (mean  $\pm$  SD; see **Table 1** for data overview). The optical intensity of the study eye group affected by CRAO ranged from 134 to 219 (mean  $177 \pm 19$ ) compared to 85 to 153 ( $123 \pm 14$ ) in the group of healthy fellow eyes (see **Figure 2**), and, without exception, was higher in all of the patients' eyes with CRAO compared to their fellow eye (see **Figure 3**). The optical intensity was normally distributed and showed a statistically highly significant difference ( $p < 0.001$ ) between both groups. A temporal correlation of the increase in optical intensity could not be observed ( $R^2_{\text{adj}} = 0.009$ ), as a distinct difference in optical intensity could be seen from the very beginning (within the first hours) (see **Figure 3**). The mean relative increase in optical intensity of the affected compared to the fellow eye was  $46.8 \pm 25.5\%$  (95% confidence interval 39.4–52.6%). ROC-analysis (see **Figure 4**) of the classification by inner retinal layer optical intensity revealed the optimal cut-off with the highest sum of sensitivity and specificity at a raw score of 149.46 with an area under the curve (AUC) of 0.99 and a true positive rate (sensitivity) of 0.93 and false positive rate (1-specificity) of 0.02. Using the optimal cut-off, only four CRAO retinas showed an optical intensity, which was located in the range of the healthy eyes and vice versa even only one healthy retina above 149.46 respectively in the range of CRAO retinas.

**TABLE 1** | Data overview.

	Range	Mean (SD)	Median (Q1, Q3)
Time-to-oct (h)	1.1–48.0	13.2 (10.5)	9.0 (5.2, 20.1)
Mean optical intensity (CRAO)	134–219	177 (19)	177 (165, 193)
Mean optical intensity (fellow eye)	85–153	123 (14)	124 (118, 130)
Absolute difference	5.1–130.1	54.8 (23.6)	53.6 (38.3, 68.8)
Relative increase (%)	3.7–152.5	46.8 (25.5)	43.9 (29.7, 57.1)

*Time-to-OCT in hours (time from symptom onset to the time of OCT scan), mean optical intensity in the eyes with central retinal artery occlusion and the unaffected fellow eye and the absolute and relative difference between both groups.*

The comparison of optical intensity between possible differential diagnoses of CRAO showed a significant difference (see **Table 2**;  $p < 0.001$  in all pairwise comparisons with CRAO) between CRAO and AION, JK, CRVO, and DME, whereas there were no significant differences between these groups (see **Table 2**; AION vs. JK,  $p_{\text{adj}} = 1.000$ ; AION vs. CRVO,  $p_{\text{adj}} = 1.000$ ; AION vs. DME,  $p_{\text{adj}} = 0.770$ ; JK vs. CRVO,  $p_{\text{adj}} = 1.000$ ; JK vs. DME,  $p_{\text{adj}} = 1.000$ ; and CRVO vs. DME,  $p_{\text{adj}} = 1.000$ ) or between the fellow eyes ( $p_{\text{adj}} > 0.05$ ) (see **Figure 5**).

## DISCUSSION

Optical coherence tomography is a non-invasive high resolution *in vivo* retinal imaging method and is likely to become the key diagnostic instrument in the acute management of CRAO. Typically, CRAO is a clinical diagnosis, but as unfortunately clinical signs such as retinal edema and a cherry red spot may have not evolved in the very early phase, pathognomonic signs on OCT scans can provide valuable information about CRAO. An increase in retinal thickness for example is a characteristic feature, for which a temporal correlation has been shown recently (16, 17). Similarly, a rise in optical intensity in the affected eye can be observed (9, 11, 12, 19), but the temporal dynamics have yet been unknown. In CRAO the inner retinal layers appear as a hyperreflective demarcated and mostly edematous band. Consequently, the light signal is attenuated by edematous inner retinal layers and the outer retinal layers appear hyporeflective. Possibly, the optical intensity is correlated to the final visual outcome (11).

In this study we retrospectively analyzed the optical intensity of the inner retinal layers (analyzed collectively) compared to the healthy fellow eye in patients that had suffered from CRAO. The optical intensity in the CRAO group was statistically highly significant higher compared to the healthy fellow eye group ( $p < 0.001$ ; AUC 0.99, true positive rate 0.93, and false positive rate 0.02), which can therefore be interpreted as reliable parameter to diagnose CRAO in the acute phase. The absolute values in our study of the measured optical intensity of the inner retinal layers are comparable to the data of previously published studies (11, 12). Another study reported that the increase in optical intensity of the inner nuclear layer was most indicative for CRAO among all retinal layers (19). However, in

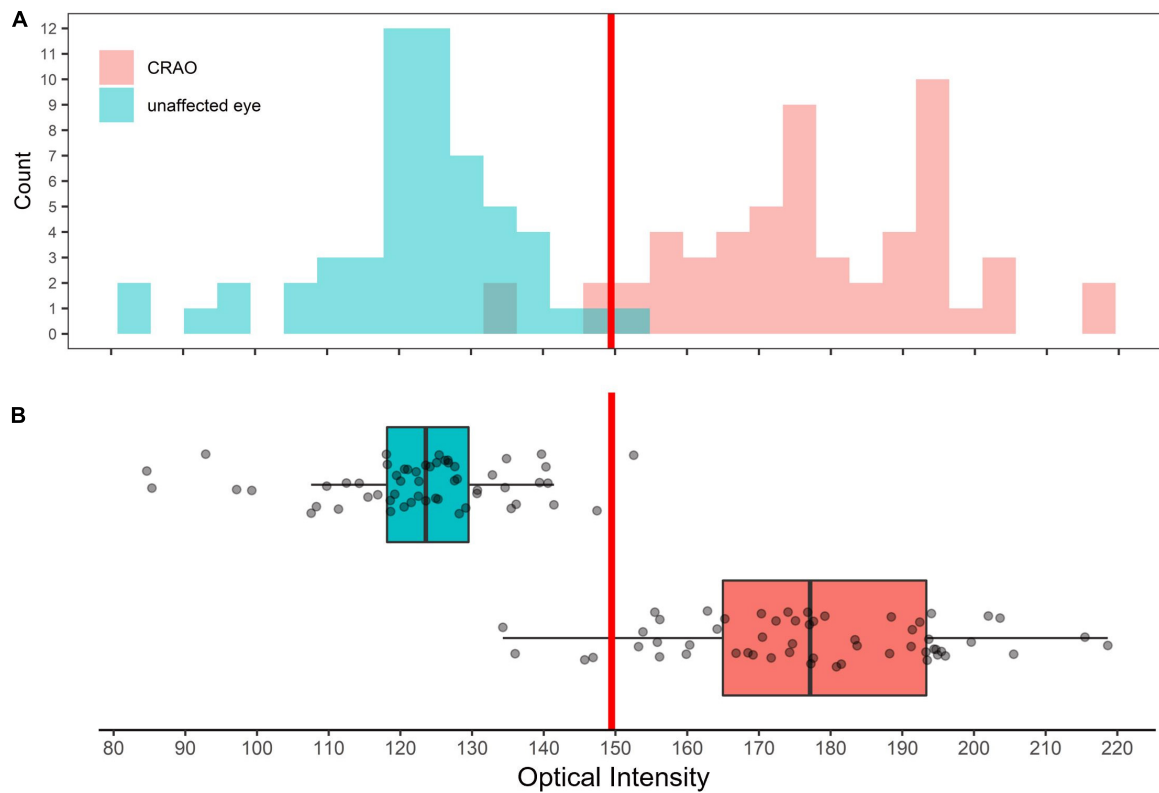


**FIGURE 2 |** Distribution of optical intensity of in eye with central retinal artery occlusion and unaffected fellow eyes. Histogram (A) and box plot (B) showing the distribution of optical intensity in the eyes with CRAO (red) and in the unaffected fellow eyes (cyan). Differences in optical intensity were highly significant ( $p < 0.001$ ).

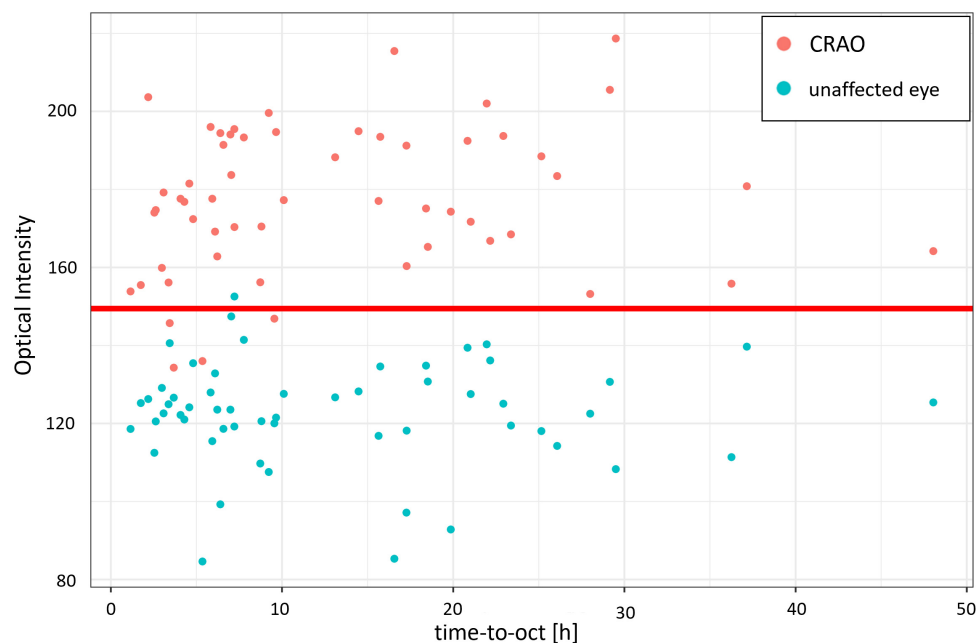


**FIGURE 3 |** Optical intensity over time of the affected and unaffected fellow eye. Optical intensity of the inner retinal layers differs significantly in acute central retinal artery occlusion between the affected (red) and the unaffected fellow eye (cyan). Time did not have an impact or correlation on the optical intensity increase of the inner retinal layers ( $R^2_{\text{adj}} = 0.009$ ). The red line marks the optimal cut-off value estimated with the ROC analysis.



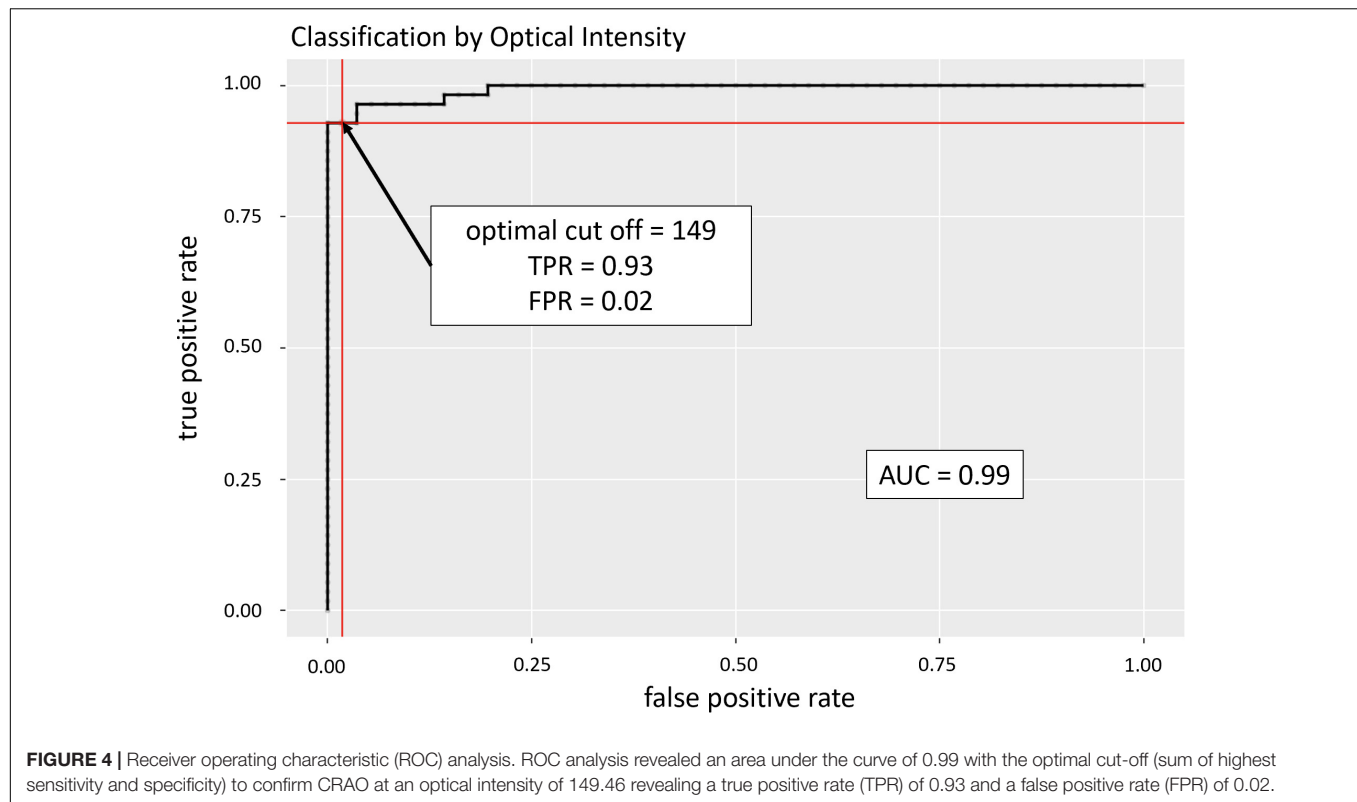


**TABLE 2 |** Optical intensity data of all included groups.

	CRAO	AION	JK	CRVO	DME	<i>p</i> -Value
<b>Study eye</b>						<0.001 <sup>a</sup>
<i>n</i>	56	9	10	9	9	
Range	134–219	108–171	104–157	91–159	79–136	
Mean (SD)	177 (19)	134 (22)	129 (19)	128 (25)	112 (19)	
Median (Q1, Q3)	177 (165, 193)	131 (120, 140)	125 (117, 147)	123 (107, 148)	112 (99, 126)	
<b>Fellow eye</b>						0.248 <sup>a</sup>
<i>n</i>	56	9	10	9	9	
Range	85–153	106–145	96–164	119–137	93–143	
Mean (SD)	123 (14)	121 (13)	128 (20)	129 (6)	115 (15)	
Median (Q1, Q3)	124 (118, 130)	118 (112, 127)	125 (119, 132)	132 (123, 133)	116 (109, 121)	

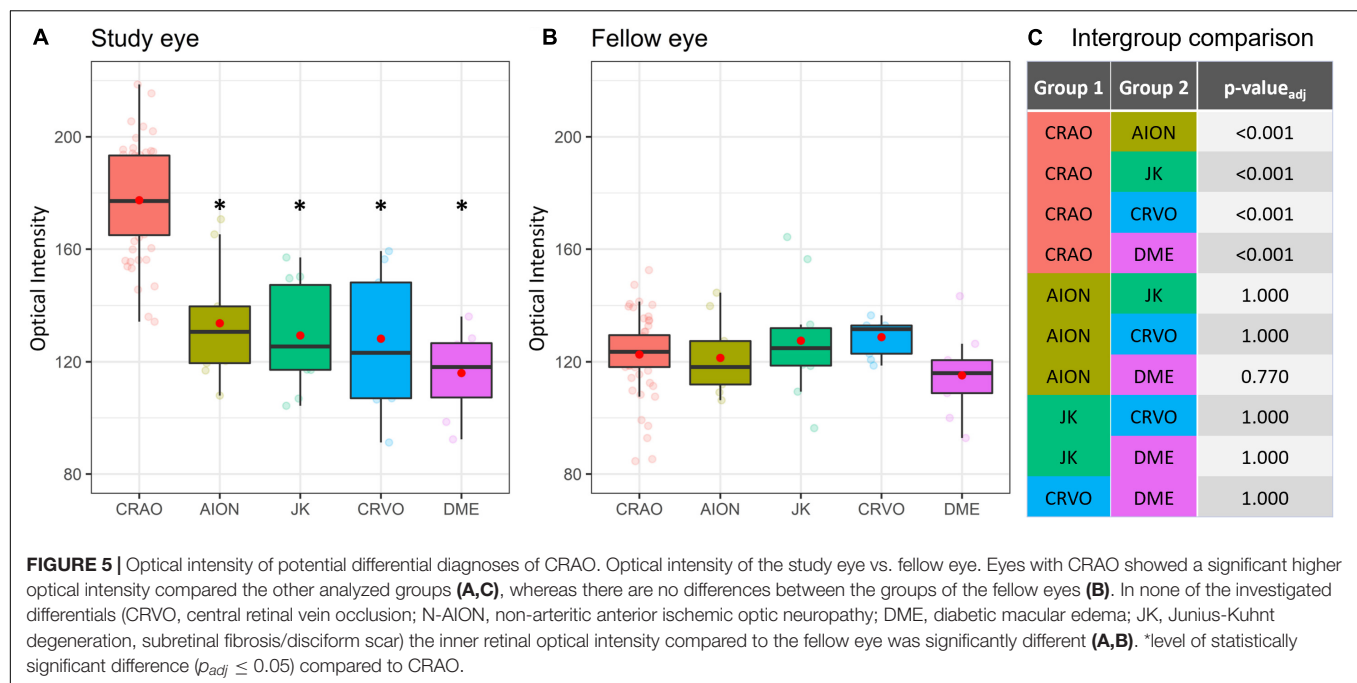
SD, standard deviation; Q1, first quartile that corresponds to 25%; Q3, third quartile that corresponds to 75%.

<sup>a</sup>ANOVA.

our opinion defining single layers of the inner retina can be quite challenging in the acute situation as they become hard to distinguish in the ischemic retina. We therefore preferred the summarized analysis of the optical intensity of the inner retina as a whole.

The first 4.5 h after ischemia onset are critical for the prognosis of every therapeutic approach. Administration of IVT within 4.5 h shows a superior visual prognosis compared to the untreated natural course (4, 6, 7). The RRTI, the change of retinal thickness in the affected compared to the healthy fellow eye, is a parameter showing temporal changes and therefore allowing a highly accurate estimate of ischemia duration, which can be essential when the exact onset of symptoms cannot be

reported reliably (10, 16, 17). Furthermore, the RRTI might reveal the amount ischemia induced retinal damage (higher RRTI represents more severe damage). Nevertheless, since significant retinal edema develops over time and may be lacking in the very early phase of CRAO, the RRTI might not be suitable to diagnose CRAO within the first few hours (16, 17). Moreover, retinal edema is not a specific sign of ischemia and can be apparent in other retinal vascular disorders such as DME or retinal vein occlusion. Vice versa, this is where the optical intensity comes in to the picture as the optical intensity allows quick diagnosis of CRAO and may therefore enhance the diagnostic algorithm as an early biomarker – even in the absence or before the development of significant retinal edema. In contrast to



the time-dependent RRTI, the optical intensity did not show a significant temporal increase or correlation (16, 17). The increase in optical intensity was already visible in patients with a very short time since symptom onset (1–4 h) and hyperreflectivity did not change significantly over time (up to 48 h). Consequently, optical intensity comes with the great potential to be used as an early diagnostic discriminator in patients with acute vision loss in order to decide whether the underlying cause is CRAO, and thus requires an immediate neurovascular workup. Potential differential diagnoses coming with a possible monocular loss or reduction of vision, such as CRVO, DME, JK, or NA-AION can be ruled out safely. Vitreous hemorrhage, another potential differential, can be easily confirmed by funduscopy or sonography, as OCT typically is not possible due to limited light signal penetration.

Among the limitations of this study is the retrospective character including a possible selection bias, as only patients with known symptom onset and available OCT scans of both eyes were included in our analysis. The central scan through the fovea as well the two scans above and below were used for segmentation, which could be a possible bias but enables an automatized workflow for the future detection of CRAO, because the central scan is usually detected automatically by OCT imaging machines. Also, the relatively low number of patients within the first 3 h limit the validity of the optical intensity increase within the acute phase, as it remains unknown when exactly and how fast the optical intensity increases, but nonetheless there was no significant increase with time in our cohort. Moreover, quality parameters of OCT imaging need to be established for a valid optical intensity analysis as image noise may reduce the reliability of optical intensity. For example, a lower limit of the signal-noise-ratio to warrant valid use of optical intensity needs to be established. Opacities of the optical axis such as

cataract or corneal opacities, vitreous hemorrhage can decrease the light signal and therefore it needs to be kept in mind that this may potentially influence the measured optical intensity. This is especially relevant in patients with asymmetrical lens status. Although we could differentiate CRAO from healthy eyes accurately in almost all, there are a few patients that have not matched perfectly: one patient with asymmetrical lens status was included in our study: the eye with CRAO had incipient cataract, the healthy fellow eye was pseudophakic and showed increased optical intensity compared to the other healthy eyes. However, there we found no particular reason why this was not the case in other pseudophakic eyes. Other eyes with an optical intensity out of line were found in three CRAO eyes, in which the optical intensity was too low compared to the other eyes with CRAO: one patient had a relatively low RRTI of only 7% 3.5 h after ischemia onset and therefore could somewhat influence the optical intensity. The two other patients (one with both eye having incipient cataract, one with both eyes having advanced cataract) had a high image noise as a possible confounder, although signal-to-noise ratio reached a decent quality level in these patients. OCT enables a fast visualization of characteristic microstructural changes in the ischemic retina in CRAO (9, 14, 20). This study revealed that the diagnosis of CRAO on the basis of an optical intensity increase in the inner retinal layers is reliable, even in the acute phase where other clinical signs may only be visible faintly. Further research with a higher number of patients is required to confirm this studies results and the clinical use in order to implement optical intensity-based diagnosis of CRAO in an emergency algorithm. Included in an emergency algorithm, the optical intensity should be used to decide on whether the diagnosis is CRAO or not and the RRTI to define or confirm the time since ischemia onset. Altogether, both parameters support patient-reported

information with objectifiable information, that potentially could be decisive in the further management and visual prognosis. Moreover, an automatic determination of these parameters by an automated OCT software or machine learning algorithms would greatly accelerate the ophthalmological diagnosis and further neurovascular referral to promptly initiate IVT within 4.5 h of ischemia onset and/or to start with a comprehensive neurovascular work-up. Additional imaging modalities could potentially enhance the diagnostic workflow. There is evidence that a positive retrobulbar spot sign visualized by ultrasound could be associated with a poor response to IVT and could therefore be a contraindication (15, 22, 23). Retinal diffusion restriction visualized by diffusion-weighted magnetic resonance imaging (DWI-MRI) may provide additional information (24). Further studies are needed to explore the possibilities offered by different diagnostic tools. Conclusively, a hyperreflectivity of the inner retinal layers may confirm acute CRAO. Particularly, when determined in the very early phase, the optical intensity may serve as a diagnostic biomarker, also in the absence of obvious fundus changes or before retinal edema can be detected.

## DATA AVAILABILITY STATEMENT

The raw data supporting the conclusions of this article will be made available by the authors, without undue reservation.

## REFERENCES

- Chan W, Flowers AM, Meyer BI, Bruce BB, Newman NJ, Biousse V. acute central retinal artery occlusion seen within 24 hours at a tertiary institution. *J Stroke Cerebrovasc Dis.* (2021) 30:105988. doi: 10.1016/j.jstrokecerebrovasdis.2021.105988
- Flowers AM, Chan W, Meyer BI, Bruce BB, Newman NJ, Biousse V. Referral Patterns of central retinal artery occlusion to an academic center affiliated with a stroke center. *J Neuroophthalmol.* (2021) 41:480–7. doi: 10.1097/WNO.0000000000001409
- Hoyer C, Kahlert C, Schlichtenbrede F, Platten M, Szabo K, Faculty M, et al. Central retinal artery occlusion as a neuro-ophthalmological emergency: the need for raising public awareness. *Eur J Neurol.* (2021) 28:2111–4. doi: 10.1111/ene.14735
- Mac Grory B, Nackenoff A, Poli S, Spitzer MS, Nedelmann M, Guillon B, et al. Intravenous fibrinolysis for central retinal artery occlusion: a cohort study and updated patient-level meta-analysis. *Stroke.* (2020) 51:2018–25. doi: 10.1161/STROKEAHA.119.028743
- Schmidt D, Schumacher M, Feltgen N. Circadian incidence of non-inflammatory retinal artery occlusions. *Graefes Arch Clin Exp Ophthalmol.* (2009) 247:491–4. doi: 10.1007/s00417-008-0989-y
- Schrag M, Youn T, Schindler J, Kirshner H, Greer D. Intravenous fibrinolytic therapy in central retinal artery occlusion a patient-level meta-analysis. *JAMA Neurol.* (2015) 72:1148–54. doi: 10.1001/jamaneurol.2015.1578
- Schultheiss M, Härtig F, Spitzer MS, Feltgen N, Spitzer B, Hüsing J, et al. Intravenous thrombolysis in acute central retinal artery occlusion – a prospective interventional case series. *PLoS One.* (2018) 13:e0198114. doi: 10.1371/journal.pone.0198114
- Balal S, J'Bari AS, Hassan A, Sharma A, Wagner SK, Pasu S. Capturing the occult central retinal artery occlusion using optical coherence tomography. *Curr Eye Res.* (2021) 46:1762–7. doi: 10.1080/02713683.2021.1921219
- Ahn SJ, Woo SJ, Park KH, Jung C, Hong JH, Han MK. Retinal and choroidal changes and visual outcome in central retinal artery occlusion: an optical

## ETHICS STATEMENT

Ethical review and approval was not required for the study on human participants in accordance with the local legislation and institutional requirements. Written informed consent for participation was not required for this study in accordance with the national legislation and the institutional requirements.

## AUTHOR CONTRIBUTIONS

DW, MSS, KB-S, CG, and MS contributed to the conception and design of the study. DW, MC, CG, and MS performed the data collection. VD and CG performed the statistical analysis. DW, SP, MSS, CG, and MS interpreted the data. DW and MS searched literature. DW wrote the first draft of the manuscript. VD, CG, and MS wrote sections of the manuscript. DW, SP, MC, VD, MSS, KB-S, CG, and MS performed the manuscript revision and approved for submission and publication. All authors contributed to the article and approved the submitted version.

## ACKNOWLEDGMENTS

This study was partly presented at the annual meeting 2021 of the German Ophthalmological Society Deutsche Ophthalmologische Gesellschaft (DOG).

- coherence tomography study. *Am J Ophthalmol.* (2015) 159:667–76. doi: 10.1016/j.ajo.2015.01.001
- Casagrande M, Kromer R, Wenzel DA, Poli S, Spitzer MS, Druchkiv V, et al. Determination of ischemia onset based on automatically generated spectralis SD-OCT values in acute central retinal artery occlusion. *J Ophthalmol.* (2021) 2021:5527292. doi: 10.1155/2021/5527292
- Chen H, Xia H, Qiu Z, Chen W, Chen X. Correlation of optical intensity on optical coherence tomography and visual outcome in central retinal artery occlusion. *Retina.* (2016) 36:1964–70. doi: 10.1097/IAE.0000000000000107
- Furashova O, Matthé E. Retinal changes in different grades of retinal artery occlusion: an optical coherence tomography study. *Invest Ophthalmol Vis Sci.* (2017) 58:5209–16. doi: 10.1167/iov.17-22411
- Mac Grory B, Schrag M, Poli S, Boisvert CJ, Spitzer MS, Schultheiss M, et al. Structural and functional imaging of the retina in central retinal artery occlusion – current approaches and future directions. *J Stroke Cerebrovasc Dis.* (2021) 30:105828. doi: 10.1016/j.jstrokecerebrovasdis.2021.105999
- Matthé E, Eulitz P, Furashova O. ACUTE RETINAL ISCHEMIA IN CENTRAL VERSUS BRANCH RETINAL ARTERY OCCLUSION: changes in retinal layers' thickness on spectral-domain optical coherence tomography in different grades of retinal ischemia. *Retina.* (2020) 40:1118–23. doi: 10.1097/IAE.0000000000002527
- Schneider M, Fischer-wedi CV, Bemme S, Kortleben M, Feltgen N, Liman J. The Retrobulbar spot sign and prominent middle limiting membrane as prognostic markers in non-arteritic retinal artery occlusion. *J Clin Med.* (2021) 18:2. doi: 10.3390/jcm10020338
- Wenzel DA, Kromer R, Poli S, Steinhorst NA, Casagrande MK, Spitzer MS, et al. Optical coherence tomography-based determination of ischaemia onset – the temporal dynamics of retinal thickness increase in acute central retinal artery occlusion. *Acta Ophthalmol.* (2021) 99:e247–52. doi: 10.1111/aos.14563
- Ochakovski GA, Wenzel DA, Spitzer MS, Poli S, Härtig F, Fischer MD, et al. Retinal oedema in central retinal artery occlusion develops as a

- function of time. *Acta Ophthalmol.* (2020) 98:e680–4. doi: 10.1111/aos.14375
18. Schmidt D, Kube T, Feltgen N. Central retinal artery occlusion - findings in optical coherence tomography and functional correlations. *Eur J Med Res.* (2006) 11:250–2.
  19. Chen H, Chen X, Qiu Z, Xiang D, Chen W, Shi F, et al. Quantitative analysis of retinal layers' optical intensities on 3D optical coherence tomography for central retinal artery occlusion. *Sci Rep.* (2015) 5:1–6. doi: 10.1038/srep09269
  20. Chu YK, Hong YT, Byeon SH, Kwon OW. In vivo detection of acute ischemic damages in retinal arterial occlusion with optical coherence tomography: a "prominent middle limiting membrane sign.". *Retina.* (2013) 33:2110–7. doi: 10.1097/IAE.0b013e3182899205
  21. R Core Team. *R: A Language and Environment for Statistical Computing.* [Internet]. Vienna: R Foundation for Statistical Computing (2021).
  22. Czihal M, Lottspeich C, Köhler A, Prearo I, Hoffmann U, Priglinger SG, et al. Transocular sonography in acute arterial occlusions of the eye in elderly patients: diagnostic value of the spot sign. *PLoS One.* (2021) 16:e0247072. doi: 10.1371/journal.pone.0247072
  23. Nedelmann M, Graef M, Weinand F, Wassill KH, Kaps M, Lorenz B, et al. Retrobulbar spot sign predicts thrombolytic treatment effects and etiology in central retinal artery occlusion. *Stroke.* (2015) 46:2322–4. doi: 10.1161/STROKEAHA.115.009839
  24. Danyel LA, Böhner G, Connolly F, Siebert E. Standard diffusion-weighted mri for the diagnosis of central retinal artery occlusion: a case-control study. *Clin Neuroradiol.* (2021) 31:619–26. doi: 10.1007/s00062-020-00955-6

**Conflict of Interest:** MS, MSS, and SP are initiators of the REVISION trial on early intravenous thrombolysis in central retinal artery occlusion (NCT04965038), study medication (verum and placebo) is supplied by Boehringer Ingelheim Pharma GmbH & Co. KG.

The remaining authors declare that the research was conducted in the absence of any commercial or financial relationships that could be construed as a potential conflict of interest.

**Publisher's Note:** All claims expressed in this article are solely those of the authors and do not necessarily represent those of their affiliated organizations, or those of the publisher, the editors and the reviewers. Any product that may be evaluated in this article, or claim that may be made by its manufacturer, is not guaranteed or endorsed by the publisher.

Copyright © 2022 Wenzel, Poli, Casagrande, Druchkiv, Spitzer, Bartz-Schmidt, Grohmann and Schultheiss. This is an open-access article distributed under the terms of the Creative Commons Attribution License (CC BY). The use, distribution or reproduction in other forums is permitted, provided the original author(s) and the copyright owner(s) are credited and that the original publication in this journal is cited, in accordance with accepted academic practice. No use, distribution or reproduction is permitted which does not comply with these terms.



# Advantages of publishing in Frontiers



## OPEN ACCESS

Articles are free to read  
for greatest visibility  
and readership



## FAST PUBLICATION

Around 90 days  
from submission  
to decision



## HIGH QUALITY PEER-REVIEW

Rigorous, collaborative,  
and constructive  
peer-review



## TRANSPARENT PEER-REVIEW

Editors and reviewers  
acknowledged by name  
on published articles

## Frontiers

Avenue du Tribunal-Fédéral 34  
1005 Lausanne | Switzerland

Visit us: [www.frontiersin.org](http://www.frontiersin.org)

Contact us: [frontiersin.org/about/contact](http://frontiersin.org/about/contact)



## REPRODUCIBILITY OF RESEARCH

Support open data  
and methods to enhance  
research reproducibility



## DIGITAL PUBLISHING

Articles designed  
for optimal readership  
across devices



## FOLLOW US

@frontiersin



## IMPACT METRICS

Advanced article metrics  
track visibility across  
digital media



## EXTENSIVE PROMOTION

Marketing  
and promotion  
of impactful research



## LOOP RESEARCH NETWORK

Our network  
increases your  
article's readership